



IAEA FEC 2016

26th IAEA Fusion Energy Conference

26TH IAEA FUSION ENERGY CONFERENCE

17–22 October 2016
Kyoto, Japan

Programme, Abstracts and Conference Material

Organized by the



IAEA

International Atomic Energy Agency

Hosted by the Government of Japan



through the
Ministry of Education,
Culture, Sports, Science
and Technology (MEXT)



and the
National Institute for
Fusion Science (NIFS)



CN-234
www.iaea.org/meetings

Organized by the:



60 Years

IAEA

Atoms for Peace and Development

26th IAEA

Fusion Energy Conference

17–22 October 2016 Kyoto, Japan

Programme & Book of Abstracts &
Conference Material

Scan relevant QR to download the
“Conference 4me” application.



Android



iPhone



Windows

Mobile Conference App for smartphones and tablets

Participants may wish to download the conference application (app) available at Google Play and the iTunes Store. Use the above QR code, or, once in the app store, simply search for “Conference 4me”, and install the app. Once installed and running, search and download the FEC–2016 conference. The application provides a digital, mobile copy of the conference agenda and timetables, venue information, social network updates, and more.

The app allows you to:

- customise your own schedule and view last-minute programme changes;
- view powerpoint presentations of those speakers who have permitted their release after the presentation;

Colophon

This book has been assembled from the abstract sources submitted by the contributing authors via the [Indico](#) conference management platform. Layout, editing, and typesetting of the book, including customized \TeX & \LaTeX macros, was done by Dr. P. Knowles, LogrusData, Vienna, Austria.

This book is PDF hyperlinked: activating coloured text will, in general, move you throughout the book.

Introduction

The International Atomic Energy Agency (IAEA) fosters the exchange of scientific and technical results in nuclear fusion research and development through its series of Fusion Energy Conferences. The 26th IAEA Fusion Energy Conference (FEC 2016) aims to provide a forum for the discussion of key physics and technology issues as well as innovative concepts of direct relevance to the use of nuclear fusion as a source of energy.

With the International Thermonuclear Experimental Reactor (ITER) being built in Cadarache, France as next-step fusion device, and a number of major new fusion experiments becoming operational such as Wendelstein 7X (Germany) and JT60-SA (Japan) and in view of the concomitant need to demonstrate the technological feasibility of fusion power plants as well as the economic viability of this method of energy production, the fusion community is now facing new challenges. The way these challenges are addressed will dictate research orientations in the present and coming decades.

The scientific scope of FEC 2016 is, therefore, intended to reflect the priorities of this new era in fusion energy research. The conference aims to serve as a platform for sharing the results of research and development efforts in both national and international fusion experiments that have been shaped by these new priorities, and to thereby help in pinpointing worldwide advances in fusion theory, experiments, technology, engineering, safety and socio-economics. Furthermore, the conference will also set these results against the backdrop of the requirements for a net energy producing fusion device and a fusion power plant in general, and will thus help in defining the way forward.

With the participation of international organizations such as the ITER Organization and the European Atomic Energy Community (Euratom), as well as the collaboration of more than forty countries and several research institutes, including those working on smaller plasma devices, it is expected that this conference will, as in the past, serve to identify possibilities and means for continuous and effective international collaboration in this area.

The 26th IAEA Fusion Energy Conference is being organized by the IAEA in cooperation with the National Institute for Fusion Science, Japan. Previous conferences in this series were held in Salzburg (1961), Culham (1965), Novosibirsk (1968), Madison (1971), Tokyo (1974), Berchtesgaden (1976), Innsbruck (1978), Brussels (1980), Baltimore (1982), London (1984), Kyoto (1986), Nice (1988), Washington DC (1990), Würzburg (1992), Seville (1994), Montreal (1996), [Yokohama \(1998\)](#), [Sorrento \(2000\)](#), [Lyon \(2002\)](#), [Vilamoura \(2004\)](#), [Chengdu \(2006\)](#), [Geneva \(2008\)](#), [Daejeon \(2010\)](#), [San Diego \(2012\)](#) and [Saint Petersburg \(2014\)](#).

	Name	Country/International Organization
Chair:	Alain Bécoulet	France
Vice Chair:	Boris V. Kuteev	Russian Federation
	Clemente Angioni	Germany
	Dhiraj Bora	India
	Richard Buttery	United States of America
	Arun Chakraborty	India
	Mark Foster	United States of America
	David Gates	United States of America
	Carlos Hidalgo	Spain
	Matthew Hole	Australia
	Yong Seok Hwang	Korea, Republic of
	Victor Ilgisonis	Russian Federation
	Takashi Inoue	Japan
	Sylvie Jacquemot	France
	Yutaka Kamada	Japan
	Yasuaki Kishimoto	Japan
	Sergei Lebedev	Russian Federation
	Darren McDonald	EU
	Harry McLean	United States of America
	Tomohiro Morisaki	Japan
	Hyeon Park	Korea, Republic of
	Hiroyuki Shiraga	Japan
	Joseph Snipes	ITER
	Yuntao Song	China
	Don Spong	United States of America
	Elizabeth Surrey	United Kingdom
	Yuhong Xu	China

Conference Secretariat

IAEA Scientific Secretaries:

Mr Ralf Kaiser

Ms Sehila M. González de Vicente

Mr Richard Kamendje

Division of Physical and Chemical Sciences
International Atomic Energy Agency
Vienna International Centre, PO Box 100
1400 Vienna, Austria
tel: +43 1 2600 21756 (Kaiser)
tel: +43 1 2600 21753 (González)
tel: +43 1 2600 21707 (Kamendje)

physics@iaea.org

IAEA Administration and Organization:

Ms Martina Khaelss

Division of Conference and Document Services
International Atomic Energy Agency
Vienna International Centre, PO Box 100
1400 Vienna, Austria
tel: +43 1 2600 21315
fax: +43 1 26007

M.Khaelss@iaea.org

Local Organization

Host Government Officials:

Mr Shigekazu Matsuura

International Nuclear and
Fusion Energy Affairs Division
Ministry of Education, Culture, Sports,
Science and Technology (MEXT)
3-2-2, Kasumigaseki, Chiyoda-ku
Tokyo, 100-8959
Japan
tel: +81 3 6734 4163

Mr Hiroshi Yamada

National Institute for
Fusion Science (NIFS)
322-6 Oroshi
Toki, Gifu Prefecture, 509-5292
Japan
tel: +81 572 58 2342
yamada.hiroshi@fec2016.jp

Presentation and Abstract Book

This book contains all abstracts accepted for the conference. Abstracts have been edited for style uniformity. The views expressed remain the responsibility of the named authors. No responsibility is held by the organizers for any material reproduced, or linked, in this book.

IAEA Publications

All IAEA publications may be ordered from the
Sales and Promotion Unit,
International Atomic Energy Agency,
P.O. Box 100, A-1400 Vienna, Austria
Fax: +43 1 2600-29302

sales.publications@iaea.org

www.iaea.org/Publications/index.html

Nuclear Fusion Journal

Participants have been invited to submit their paper for possible publication in the IAEA journal, [Nuclear Fusion](#). If your institution does not have access to the journal, pdfs of these FEC derived articles can be requested from nf@iaea.org.

Note that contributed papers will be made available as preprints via the IAEA Fusion Portal (<https://nucleus.iaea.org/sites/fusionportal>). Links on the abstract pages direct the reader to both the pre-print and the Nuclear Fusion journal, respectively.

Participation in an IAEA Scientific Meeting

Governments of Member States and those organizations whose activities are relevant to the meeting subject matter are invited to designate participants in the IAEA scientific conferences and symposia. In addition, the IAEA itself may invite a limited number of scientists as invited speakers. Only participants designated or invited in this way are entitled to present papers and take part in the discussions.

Representatives of the press, radio, television or other information media and members of the public, the latter as “observers”, may also be authorized to attend, but without the right to take part in the proceedings.

Scientists interested in participating in any of the IAEA meetings should request information from the Government authorities of their own countries, in most cases the Ministry of Foreign Affairs or national atomic energy authority.

Working Language & Resolutions

Working Language: English. No simultaneous translation will be provided.

Resolutions: No resolutions may be submitted for consideration on any subject; no votes will be taken.

Satellite Meetings

Satellite meetings can be held. Meeting rooms and times can be reserved via the [conference website](#).

Information for Participants

The [conference website](#) contains links to many helpful guides. Notably, the [Indico](#) conference system is used for all correspondence concerning contributions.

This book contains all abstracts accepted by the FEC programme committee. Note that abstracts have been edited for style uniformity.

Overview of Contributions (as of May 3, 2018)

2	Keynote presentations
23	Overview talks
88	Regular talks
20	Rapporteured papers
12	Overview poster presentations
582	Regular poster presentations
2	Post deadline talks
—	Post deadline poster presentations
5	Summary talks

Overview posters will be exhibited during the entire conference. All oral presentations will also be displayed as posters according to the programme.

The duration of oral presentations indicated in the programme already includes discussion time. Speakers are requested to make available the following times for discussions:

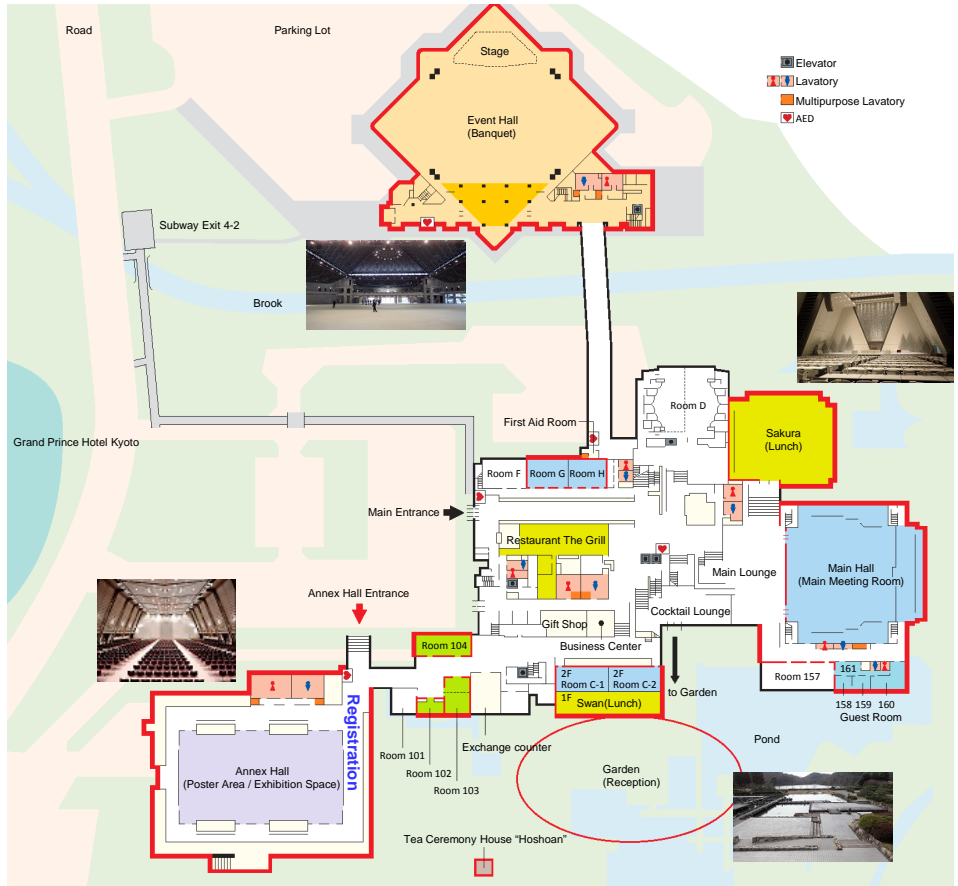
- 4' for overview presentation (total 25')
- 3' for regular oral presentation (total 20')

Rapporteur papers are identified by the letter "a" after the paper number. Rapporteured papers are identified by the letters "b" or "c" after the paper number.

Explanation of Abbreviations

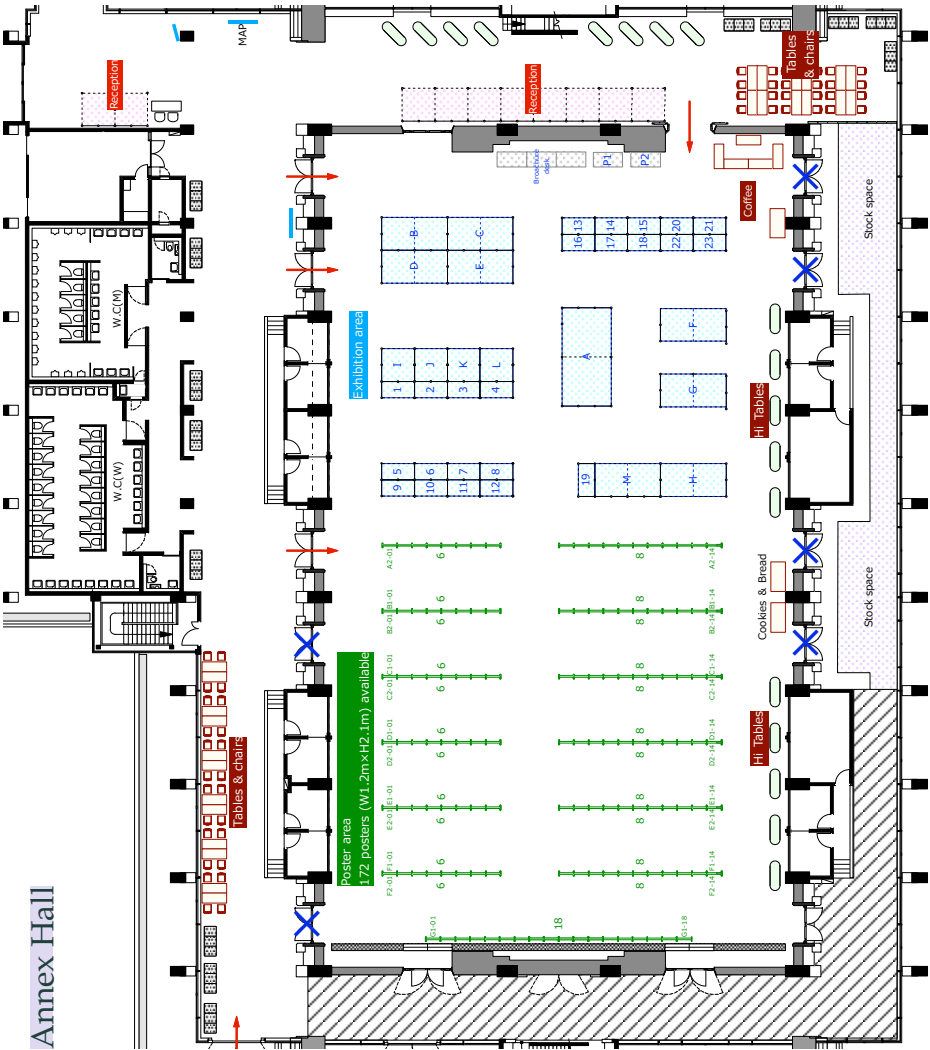
O	Opening
S	Summary
OV	Overviews
OVP	Overview Posters
EX	Magnetic Confinement Experiments
TH	Magnetic Confinement Theory and Modeling
FIP	Fusion Engineering, Integration and Power Plant Design
FNS	Fusion Nuclear Physics and Technology
ICC	Innovative Confinement Concepts
IFE	Inertial Fusion Experiments and Theory
MPT	Materials Physics and Technology
PD	Post-Deadline Contributions
PPC	Plasma Overall Performance and Control
SEE	Safety, Environmental and Economic Aspects of Fusion

Kyoto International Conference Center
 Takaragaike, Sakyo-ku
 Kyoto 606-0001, Japan



- Main Meeting Room : Main Hall
- Briefing Room : Room 161
- Room for Satellite Meetings : Rooms C-1, C-2, G and H
- Poster Area / Exhibition Space : Annex Hall
- Reception : Garden
- Banquet : Event Hall
- Lunch Restaurants : Sakura, Swan
- IAEA Conference Secretariat : Room 103
- IAEA Nuclear Fusion Office : Room 103
- Local Organizers' Office : Room 104

- a ITER Organization
- b Toshiba Corp.
- c Hitachi
- d Mitsubishi Electric Corp.
- e Mitsubishi Heavy Industries, Ltd.
- f JADA
- g QST-Rokkasho
- h NIFS/Sokendai
- i SGI Japan, Ltd.
- j Toshiba Electron Tubes & Device
- k National Instruments
- l Tayo Corp., Chuo Ltd.
- m IHL Corp.
- n Toyo Tanso Co., Ltd.
- 1 Teletyne LeCroy
- 2 Techno AP Co., Ltd.
- 3 TOYAMA
- 4 NGC Corp.
- 5 ULVAC Cryonics, Inc.
- 6 Hamamatsu Photonics K.K.
- 7 Bunkoukeiki Co., Ltd.
- 8 COSMOTECH, Inc.
- 9 COMSOL, by KESCO
- 10 General Engineering Co., Ltd.
- 11 Fujikura Ltd.
- 12 Japan Laser Corp.
- 13 MISH Intl.
- 14 Anritsu Corp.
- 15 Seiko EG&G/CAEN S.p.A
- 16 UKAEA
- 17 General Atomics
- 18 Sigmakoki Co., Ltd.
- 19 Panasonic Corp.
- 20 Metal Technology, Co., Ltd.
- 21 Nord-Lock
- 22 IRIE KOKEN Co., Ltd.
- 23 Airframe Aerodesign Pvt. Ltd.
- P1 Springer Nature
- P2 Jpn. Soc. Plasma Science & Nuclear Fusion Research



Annex Hall

Day Date	Monday Oct. 17, 2016	Tuesday Oct. 18, 2016	Wednesday Oct. 19, 2016	Thursday Oct. 20, 2016	Friday Oct. 21, 2016	Saturday Oct. 22, 2016					
08:30 — 10:15	<i>O/1</i> Opening —&— Keynote p. 10	<i>OV/3</i> Overview: Magnetic Fusion p. 14	<i>P1</i> Posters p. 14	<i>FIP/2</i> In-Vessel Components p. 22	<i>P3</i> Posters p. 23	<i>EX/5, TH/3, PPC/2</i> Transport & LH Transition p. 38	<i>P5</i> Posters p. 39	<i>EX/7–TH/5</i> RF & SOL Physics p. 53	<i>P7</i> Posters p. 54	<i>FIP/3</i> DEMO Technology p. 68	
Coffee Break: 10:15 — 10:45											
10:45 — 12:30	<i>OV/1</i> Overview: Magnetic Fusion p. 10	<i>EX/1–TH/1</i> 3D Physics p. 14	<i>P1</i> Posters p. 14	<i>EX/2–TH/2</i> Divertor & SOL Physics p. 22	<i>P3</i> Posters p. 23	<i>EX/6–TH/4</i> Energetic Particle Physics p. 38	<i>P5</i> Posters p. 39	<i>EX/8–TH/6</i> Turbulence & Transport p. 53	<i>P7</i> Posters p. 54	<i>EX/11, TH/9, FIP/4, PD</i> Transport, Construction & PD p. 68	
Lunch: 12:30 — 14:00											
14:00 — 16:10	<i>OV/2</i> Overview: Magnetic Fusion p. 10	<i>OVP</i> Posters p. 11	<i>OV/4</i> Overview: Magnetic Fusion p. 18	<i>P2</i> Posters p. 18	<i>EX/3</i> Pedestal & ELM Physics p. 28	<i>P4</i> Posters p. 29	<i>IFE/1</i> Inertial Fusion Experiments & Theory p. 46	<i>P6</i> Posters p. 47	<i>EX/9–TH/7</i> Disruptions p. 61	<i>P8</i> Posters p. 62	Summary (14:00 – 16:00) p. 69
Coffee Break: 16:10 — 16:40											
16:40 — 18:45	<i>FIP/1</i> ITER Technology p. 11	<i>OVP</i> Posters p. 11	<i>OV/5</i> Overview: Magnetic Fusion p. 18	<i>P2</i> Posters p. 18	<i>EX/4–PPC/1</i> Steady State & Hybrid Scenarios p. 29	<i>P4</i> Posters p. 29	<i>MPT/1–FNS/1</i> Materials & Fusion Nuclear Science p. 46	<i>P6</i> Posters p. 47	<i>EX/10–TH/8</i> ELMs Suppression & Dynamics p. 61	<i>P8</i> Posters p. 62	Summary (16:30 – 18:00) p. 69
19:30 — 22:00	Reception	Nuclear Fusion Board Meeting		Banquet							

08:00 – 16:00: **Conference Registration**

O/1 **Opening Plenary**
 Chair: Hiroshi Yamada (Japan) **(08:30 – 10:15)**
Main Hall

Time Id	Presenter		Title
08:30 O/1-1	Y. Amano	IAEA	Opening Address
08:40 O/1-2	Host Country Representative	Japan	Welcome Address
08:55 O/1-3	M. Venkatesh	IAEA	Opening Remarks
09:10 O/1-4	A. Iiyoshi	Japan	Fusion for Sustainable World Development
09:40 O/1-5	F. Portero	Spain	The Strategic Dimensions of the Fusion Energy Challenge

OV/1 **Overviews 1: Magnetic Fusion**
 Chair: Kenichi Kurihara (Japan) **(10:45 – 12:30)**
Main Hall

Time Id	Presenter		Title
10:45 OV/1-1	Y. Takeiri	Japan	Extension of Operational Regime of LHD towards Deuterium Experiment
11:10 OV/1-2	B. Bigot	ITER	Progress in ITER Construction, Manufacturing and R&D
11:35 OV/1-3	W. M. Solomon	USA	DIII-D Research Advancing the Scientific Basis for Burning Plasmas and Fusion Energy
12:00 OV/1-4	X. Litaudon	EC	Overview of the JET Results in Support to ITER

OV/2 **Overviews 2: Magnetic Fusion**
 Chair: Predhiman Kaw (India) **(14:00 – 16:10)**
Main Hall

Time Id	Presenter		Title
14:00 OV/2-1	A. Kallenbach	Germany	Overview of ASDEX-Upgrade Results
14:25 OV/2-2	Y. Liang	China	Overview of EAST Experiments on the Development of High-Performance Steady-State Scenario
14:50 OV/2-3	B. N. Breizman	USA	Kinetics of Relativistic Runaway Electrons
15:15 OV/2-4	Y.-K. Oh	Korea, Rep. of	Overview of the KSTAR Research in Support of ITER and DEMO
15:40 OV/2-5	E. S. Marmor	USA	Overview of High-Field Divertor Tokamak Results from Alcator C-Mod

Summary



Fusion Engineering, Integration and Power Plant Design

FIP/1

Chair: Jérôme Paméla (France)

Main Hall

(16:40 – 18:45)

Time Id	Presenter		Title
16:40 FIP/1-1	P. Fu	China	Recent Progress of ITER Package in ASIPP
17:00 FIP/1-2	J. Smith	USA	ITER Central Solenoid Module Fabrication
17:20 FIP/1-3Ra	J. Hiratsuka	Japan	Long-Pulse Acceleration of 1 MeV Negative Ion Beams toward ITER and JT-60SA Neutral Beam Injectors
FIP/1-3Rb			Towards Powerful Negative Ion Beams at the Test Facility ELISE for the ITER and DEMO NBI System
17:40 FIP/1-4	M. Kasaki	Japan	Progress of Experimental Study on Negative Hydrogen Ion Production and Extraction
18:00 FIP/1-5	A. Mukherjee	India	Progress in High Power Test of R&D Source for ITER ICRF System
18:20 FIP/1-6Ra	G. Denisov	Russian Fed.	New Results of Development of Gyrotrons for Plasma Fusion Installations
FIP/1-6Rb			Development of Multifrequency Megawatt Gyrotrons for Fusion Devices in JAEA
FIP/1-6Rc			Development of over-MW Gyrotrons for Fusion at Frequencies from 14 GHz to Sub-THz

Break: 14:45 – 15:15

OVP

Overview Posters

Annex Hall

(14:00 – 18:45)

Id	Presenter		Title
OV/1-1	Y. Takeiri	Japan	Extension of Operational Regime of LHD towards Deuterium Experiment
OV/1-2	B. Bigot	ITER	Progress in ITER Construction, Manufacturing and R&D
OV/1-3	W. M. Solomon	USA	DIII-D Research Advancing the Scientific Basis for Burning Plasmas and Fusion Energy
OV/1-4	X. Litaudon	EC	Overview of the JET Results in Support to ITER

Id	Presenter	Title
OV/2-1	A. Kallenbach	Germany Overview of ASDEX-Upgrade Results
OV/2-2	B. N. Wan	China Overview of EAST Experiments on the Development of High-performance Steady-State Scenario
OV/2-3	B. N. Breizman	USA Kinetics of Relativistic Runaway Electrons
OV/2-4	Y.-K. Oh	Korea, Rep. of Overview of the KSTAR Research in Support of ITER and DEMO
OV/2-5	E. S. Marmor	USA Overview of High-Field Divertor Tokamak Results from Alcator C-Mod
OV/3-1	R. C. Wolf	Germany First Plasma Operation of Wendelstein 7-X
OV/3-2	M. J. Edwards	USA The Quest for Laboratory Inertial Fusion Ignition in the US
OV/3-3	H. Shirai	Japan Recent Progress of JT-60SA Project
OV/3-4	Y. Wan	China Overview of the Present Progresses and Activities on the Chinese Fusion Engineering Test Reactor
OV/4-1	J. Knaster	Japan Overview of the IFMIF/EVEDA Project
OV/4-2	H. Azechi	Japan A Pathway to Laser Fusion Energy: Fast Ignition Realization Experiment (FIREX)
OV/4-3Ra	S. Pradhan	India Overview of SST-1 Upgrade & Recent Experiments in SST-1
OV/4-3Rb	R. Tanna	India Overview of Recent Experimental Results from ADITYA Tokamak
OV/4-4	X. Duan	China Overview of Recent Experiments on HL-2A Tokamak
OV/4-5	D. Sarychev	Russian Fed. Review of Recent Experiments on the T-10 Tokamak with All Metal Wall
OV/5-1	F. Castejón	Spain 3D Effects on Transport and Plasma Control in the TJ-II Stellarator
OV/5-2	J. Menard	USA Overview of First Results from NSTX-U and Analysis Highlights from NSTX
OV/5-3	A. Kirk	UK Overview of Recent Physics Results from MAST
OV/5-4	R. Fonck	USA H-Mode and Nonsolenoidal Startup in the Pegasus Ultralow-A Tokamak
OV/5-5	Y. Takase	Japan Overview of Spherical Tokamak Research in Japan
OV/P-1	S. Coda	Switzerland Overview of the TCV Tokamak Programme: Scientific Progress and Facility Upgrades
OV/P-2	M. Zuin	Italy Overview of the RFX-Mod Fusion Science Activity

Id	Presenter		Title
OV/P-3	R. Dejarnac	Czech Republic	Overview of Recent COMPASS Activities
OV/P-4	G. Pucella	Italy	Overview of the FTU Results
OV/P-5	J. S. Sarff	USA	Overview of MST Reversed Field Pinch Research in Advancing Fusion Science
OV/P-6	G. Zhuang	China	Progress of the Recent Experimental Research on the J-TEXT Tokamak
OV/P-7	S. Krasheninnikov	USA	Edge and Divertor Plasma: Detachment, Stability, and Plasma-Wall Interactions
OV/P-8	K. Itoh	Japan	Hysteresis and Fast Timescale in Transport Relation of Toroidal Plasmas
OV/P-9	D. Borba	UK	Overview of Simulation Results Using Computation Resources in the Framework of IFERC-CSC
OV/P-10	Y. Wu	China	Overview of DEMO Safety R&D and the Potential Future Role of IEA ESEFP IA
OV/P-11	P. Wouters	EC	Implementation within the European Domestic Agency of the French Nuclear Safety Order of 2012, Concerning Basic Nuclear Installation, Applicable to ITER Project
OV/P-12	H. Meyer	UK	Overview of Progress in European Medium Sized Tokamaks towards an Integrated Plasma-Edge/Wall Solution

19:30 – 22:00: **Welcome Reception, Garden**

OV/3

Summary



Overviews 3: Magnetic Fusion

Chair: Kwang-Wook Kim (Rep. Korea)

Main Hall

(08:30 – 10:15)

Time Id	Presenter		Title
08:30 OV/3-1	R. C. Wolf	Germany	First Plasma Operation of Wendelstein 7-X
08:55 OV/3-2	M. J. Edwards	USA	The Quest for Laboratory Inertial Fusion Ignition in the US
09:20 OV/3-3	H. Shirai	Japan	Recent Progress of JT-60SA Project
09:45 OV/3-4	Y. Wan	China	Overview of the Present Progresses and Activities on the Chinese Fusion Engineering Test Reactor

EX/1 and TH/1

Summary



3D Physics

Chair: Saskia Mordijck (USA)

Main Hall

(10:45 – 12:30)

Time Id	Presenter		Title
10:45 EX/1-1	P. Piovesan	Italy	Role of MHD Dynamo in the Formation of 3D Equilibria in Fusion Plasmas
11:05 EX/1-2	C. Paz-Soldan	USA	Optimization of the Plasma Response for the Control of Edge-Localized Modes with 3D Fields
11:25 TH/1-1	S. Hudson	USA	Penetration and Amplification of Resonant Perturbations in 3D Ideal-MHD Equilibria
11:45 EX/1-3	Y. In	Korea, Rep. of	Enhanced Understanding of Nonaxisymmetric Intrinsic and Controlled Field Impacts in Tokamaks
12:05 EX/1-4	O. Schmitz	USA	Enhancement of Helium Exhaust by Resonant Magnetic Perturbation Fields

P1

Posters 1

Annex Hall

(08:30 – 12:30)

Id	Presenter		Title
FIP/1-1	P. Fu	China	Recent Progress of ITER Package in ASIPP
FIP/1-2	J. Smith	USA	ITER Central Solenoid Module Fabrication
FIP/1-3Ra	J. Hiratsuka	Japan	Long-pulse Acceleration of 1 MeV Negative Ion Beams toward ITER and JT-60SA Neutral Beam Injectors

Id	Presenter		Title
FIP/1-3Rb	U. Fantz	Germany	Towards Powerful Negative Ion Beams at the Test Facility ELISE for the ITER and DEMO NBI System
FIP/1-4	M. Kasaki	Japan	Progress of Experimental Study on Negative Hydrogen Ion Production and Extraction
FIP/1-5	A. Mukherjee	India	Progress in High Power Test of R&D Source for ITER ICRF System
FIP/1-6Ra	G. Denisov	Russian Fed.	New Results of Development of Gyrotrons for Plasma Fusion Installations
FIP/1-6Rb	R. Ikeda	Japan	Development of Multifrequency Megawatt Gyrotrons for Fusion Devices in JAEA
FIP/1-6Rc	T. Kariya	Japan	Development of over-MW Gyrotrons for Fusion at Frequencies from 14 GHz to Sub-THz
TH/P1-1	J. Geiger	Germany	Plasma Effects in Full-Field MHD-Equilibrium Calculations for W7-X
TH/P1-2	F. Ebrahimi	USA	Physics of Flux Closure during Plasmoid-Mediated Reconnection in Coaxial Helicity Injection
TH/P1-3	A. Reiman	USA	Pressure Driven Currents Near Magnetic Islands in 3D MHD Equilibria: Effects of Pressure Variation within Flux Surfaces and of Symmetry
TH/P1-4	K. Ichiguchi	Japan	Three-Dimensional Numerical Analysis of Interaction between Plasma Rotation and Interchange Modes
TH/P1-5	H. Miura	Japan	Two-Fluid Subgrid-Scale Viscosity in Nonlinear Simulation of Ballooning Modes in a Heliotron Device
TH/P1-6	J.-K. Park	USA	Self-Consistent Optimization of Neoclassical Toroidal Torque with Anisotropic Perturbed Equilibrium in Tokamaks
TH/P1-7	S. C. Jardin	USA	Nonlinear 3D M3D-C1 Simulations of Tokamak Plasmas Crossing a MHD Linear Stability Boundary
TH/P1-8	J. R. King	USA	Nonlinear Extended-MHD Modelling by the NIMROD Code of Broadband-MHD Turbulence during DIII-D QH-Mode Discharges
TH/P1-9	F. Liu	France	Nonlinear MHD Simulations of Quiescent H-Mode Pedestal in DIII-D and Implications for ITER

Id	Presenter		Title
TH/P1-10	A. Fil	USA	Modelling and Simulation of Pedestal Control Techniques for NSTX-U
TH/P1-11	P. Maget	France	First Principle Fluid Modelling of Neoclassical Tearing Modes and of their Control
TH/P1-12	E. Poli	Germany	Toroidal Gyrokinetic Studies of the Tearing Mode in Tokamak Plasmas
TH/P1-13	S. Inoue	Japan	Active Control and Stabilization of Locked Mode in Tokamaks at High Magnetic Reynolds Number
TH/P1-14	M. Furukawa	Japan	Extension of Numerical Matching Method to Weakly Nonlinear Regime: Beyond the Rutherford Theory of Magnetic Island Evolution
TH/P1-15	N. Ivanov	Russian Fed.	Magnetic Island Behaviour under Nonaxisymmetric Halo Current at Vertical Displacement Event
TH/P1-16	V. E. Lukash	Russian Fed.	Advances in Numerical Modelling of MGI Mitigated Disruptions in ITER
TH/P1-17	A. Y. Aydemir	Korea, Rep. of	Role of Explosive Instabilities in High- β Disruptions in Tokamaks
TH/P1-18	T. Bolzonella	Italy	Securing High- β_N JT-60SA Operational Space by MHD Stability and Active Control Modelling
TH/P1-19	I. Bandyopadhyay	India	Plasma Disruption and VDE Modelling in Support of ITER
TH/P1-20	J. Shiraishi	Japan	Impact of Kinetic Effects of Energetic Particles on Resistive Wall Mode Stability in Rotating High- β Plasmas
TH/P1-21	Z. R. Wang	USA	Nyquist Analysis of Kinetic Effects on the Plasma Response in NSTX and DIII-D Experiments
TH/P1-22	J. P. Lee	USA	An Analytic Scaling Relation for the Maximum Tokamak Elongation against $n = 0$ MHD Resistive Wall Modes
TH/P1-23	V. Pustovitov	Russian Fed.	Pfirsch-Tasso Versus Standard Approaches in the Plasma Stability Theory
TH/P1-24	M. Bécoulet	France	Nonlinear MHD Modelling of Edge Localized Modes Dynamics
TH/P1-25	S. Futatani	Spain	Nonlinear MHD Simulations of Pellet Triggered ELMs

Id	Presenter		Title
TH/P1-26	F.Orain	Germany	Nonlinear Modelling of the Edge Localized Mode Control by Resonant Magnetic Perturbations in ASDEX-Upgrade
TH/P1-27	A. Sen	India	Nonlinear Simulation of ELM Dynamics in the Presence of RMPs and Pellet Injection
TH/P1-28	J. Kim	Korea, Rep. of	Numerical Calculations of Plasma Response to External Magnetic Perturbations
TH/P1-29	V. S. Mykhaylenko	Korea, Rep. of	Drift-Alfvén Instabilities and Turbulence of Magnetic Field Aligned Shear Flows
TH/P1-30	L. Zheng	USA	MHD Stability of ITER H-Mode Confinement with Pedestal Bootstrap Current and Diamagnetic Effects Taken into Account
TH/P1-31	R. Shurygin	Russian Fed.	Equilibrium Solutions of MHD Equations for GAMs in the Edge Tokamak Plasma
TH/P1-32	H. Feng	China	Excitation of Frequency Jump by Barely Passing Electrons
TH/P1-33	B. Coppi	USA	Magneto-Thermal Reconnection Processes, Related Angular Momentum Transport Issues and Formation of High Energy Particle Populations
TH/P1-34	A. Matsuyama	Japan	Simulation Study of Interaction between Runaway Electron Generation and Resistive MHD Modes over Avalanche Timescale
TH/P1-35	D. Brennan	USA	Collisional Generation of Runaway Electron Seed Distributions Leading to Subcriticality, Avalanche, or Fast Transfer
TH/P1-36	J. R. Martín-Solís	Spain	Current Profile Shape Effects on the Formation and Termination of Runaway Beams in Tokamak Disruptions and Implications for ITER
TH/P1-37	H. Nuga	Japan	Simulations of Runaway Electron Generation including Hot-Tail Effect
TH/P1-38	Z. Guo	USA	Phase Locking, Phase Slips and Turbulence: A New Approach to Mechanisms for Quiescent H-Mode

OV/4

Summary



Overviews 4: Magnetic Fusion

Chair: Dennis Whyte (USA)

Main Hall

(14:00 – 16:10)

Time Id	Presenter		Title
14:00 OV/4-1	J. Knaster	Japan	Overview of the IFMIF/EVEDA Project
14:25 OV/4-2	H. Azechi	Japan	A Pathway to Laser Fusion Energy: Fast Ignition Realization Experiment (FIREX)
14:50 OV/4-3Ra	S. Pradhan	India	Overview of SST-1 Upgrade & Recent Experiments in SST-1
OV/4-3Rb			Overview of Recent Experimental Results from ADITYA Tokamak
15:15 OV/4-4	X. Duan	China	Overview of Recent Experiments on HL-2A Tokamak
15:40 OV/4-5	D. Sarychev	Russian Fed.	Review of Recent Experiments on the T-10 Tokamak with All Metal Wall

OV/5

Summary



Overviews 5: Magnetic Fusion

Chair: Sergei Lebedev (Russian Fed.)

Main Hall

(16:40 – 18:45)

Time Id	Presenter		Title
16:40 OV/5-1	F. Castejón	Spain	3D Effects on Transport and Plasma Control in the TJ-II Stellarator
17:05 OV/5-2	J. Menard	USA	Overview of First Results from NSTX-U and Analysis Highlights from NSTX
17:30 OV/5-3	A. Kirk	UK	Overview of Recent Physics Results from MAST
17:55 OV/5-4	R. Fonck	USA	H-Mode and Nonsolenoidal Startup in the Pegasus Ultralow-A Tokamak
18:20 OV/5-5	Y. Takase	Japan	Overview of Spherical Tokamak Research in Japan

P2

Posters 2

Annex Hall

(14:00 – 18:45)

Id	Presenter		Title
TH/1-1	S. Hudson	USA	Penetration and Amplification of Resonant Perturbations in 3D Ideal-MHD Equilibria
EX/1-1	P. Piovesan	Italy	Role of MHD Dynamo in the Formation of 3D Equilibria in Fusion Plasmas
EX/1-4	O. Schmitz	USA	Enhancement of Helium Exhaust by Resonant Magnetic Perturbation Fields

Id	Presenter	Country	Title
EX/1-2	C. Paz-Soldan	USA	Optimization of the Plasma Response for the Control of Edge-Localized Modes with 3D Fields
EX/1-3	Y. In	Korea, Rep. of	Enhanced Understanding of Nonaxisymmetric Intrinsic and Controlled Field Impacts in Tokamaks
TH/P2-1	S. Maeyama	Japan	Gyrokinetic Analysis of the Effects of Electron-Scale Turbulence on Ion-Scale Microinstabilities
TH/P2-2	M. Nakata	Japan	Multispecies ITG-TEM Driven Turbulent Transport of DT Ions and He-ash in ITER Burning Plasmas
TH/P2-3	M. Nunami	Japan	Anomalous and Neoclassical Transport of Hydrogen Isotope and Impurity Ions in LHD Plasmas
TH/P2-4	S. Kobayashi	France	Direct Identification of Predator-Prey Dynamics in Gyrokinetic Simulations
TH/P2-5	S. Yi	Korea, Rep. of	Gyrokinetic Simulations of an Electron Temperature Gradient Turbulence-Driven Current in Tokamak Plasmas
TH/P2-6	C. Angioni	Germany	Progress in the Theoretical Description and the Experimental Characterization of Tungsten Transport in Tokamaks
TH/P2-7	J. Candy	USA	Crucial Role of Zonal Flows and Electromagnetic Effects in ITER Turbulence Simulations Near Threshold
TH/P2-8	G. M. Staebler	USA	A Model of the Saturation of Coupled Electron and Ion Scale Gyrokinetic Turbulence
TH/P2-9	T. Rafiq	USA	New Nonlinear Microtearing Mode Transport Model for Tokamak Plasmas
TH/P2-10	A. Y. Pankin	USA	Extending the Validation of Multimode Model for Anomalous Transport to High Poloidal β DIII-D Discharges
TH/P2-11	S. Suwanna	Thailand	Evaluation of Predictive Capability for Hydrogenic and Impurity Density in L- and H-Mode Tokamak Plasma Using Multimode Transport Model
TH/P2-12	I. Voitsekhovitch	UK	Recent EUROfusion Achievements in Support to Computationally Demanding Multiscale Fusion Physics Simulations and Integrated Modelling

Id	Presenter		Title
TH/P2-13	G. Falchetto	France	EUROfusion Integrated Modelling (EU-IM) Capabilities and Selected Physics Applications
TH/P2-14	S. D. Pinches	ITER	Progress in the ITER Integrated Modelling Programme and the Use and Validation of IMAS within the ITER Members
TH/P2-15	A. Wisitsorasak	Thailand	The Development of SOL Transport Model for Integrated Core-SOL Simulation of L-Mode Plasma
TH/P2-16	R. Budny	USA	Alpha Heating and Isotopic Mass Scaling in JET DT Plasmas
TH/P2-17	H.-T. Kim	EC	Statistical Validation of Transport Models on Baseline Discharges in Preparation for the Extrapolation to JET DT
TH/P2-18	N. Poolyarat	Thailand	Simulation of Neoclassical Tearing Modes in JET
TH/P2-19	N. Hayashi	Japan	Core-Edge Coupled Predictive Modelling of JT-60SA High- β Steady-State Plasma with Impurity Accumulation
TH/P2-20	M. Romanelli	UK	Investigation of Sustainable Reduced-Power Noninductive Scenarios on JT-60SA
TH/P2-21	S. Murakami	Japan	Integrated Simulation of Deuterium Experiment Plasma in LHD
TH/P2-22	S. H. Kim	ITER	Development of ITER Nonactivation Phase Operation Scenarios
TH/P2-23	E. Militello Asp	UK	ITER Fuelling Requirements and Scenario Development for H, He and DT through JINTRAC Integrated Modelling
TH/P2-24	Y.-S. Na	Korea, Rep. of	On Benchmarking of Simulations of Particle Transport in ITER
TH/P2-25	J. Y. Kim	Korea, Rep. of	Physics-Based Integrated Modelling of the Energy Confinement Time Scaling Laws in Tokamaks
TH/P2-26	T. Onjun	Thailand	Predicted Fusion Performance for ITER and DEMO Plasmas Using a BALDUR Code with Predictive Tritium Influx Model
TH/P2-27	R. Hager	USA	A New Understanding of the Bootstrap Current in Steep Edge Pedestal and its Effect on the Pedestal Stability
TH/P2-28	Z. Liu	USA	Analysis of Weakly Coherent Mode in I-Mode with the BOUT++ Code
TH/P2-29	M. Francisquez	USA	Global 3D Braginskii Simulations of the Tokamak Edge Region

Id	Presenter	Title
TH/P2-30	M. Kotschenreuther USA	Gyrokinetic Simulations of Tokamak Pedestals: Present Experiments and Extrapolation to Burning Plasmas
TH/P2-31	I. Holod USA	Gyrokinetic Simulations of Microturbulence in DIII-D Pedestal
TH/P2-32	Y. Xiao China	Gyrokinetic Simulation of Tokamak Edge Plasmas
TH/P2-33	M. M. Tsventoukh Russian Fed.	Steep Gradients in Plasma Confined at Convex-Concave Magnetic Field Lines

FIP/2


**Fusion Engineering, Integration and
Power Plant Design**

Chair: Anatoli Krasilnikov (Russian Fed.)

Main Hall

(08:30 – 10:15)

Wed

Time Id	Presenter		Title
08:30 FIP/2-1Ra	Y. Seki	Japan	Progress of Qualification Testing for Full-Scale Plasma-Facing Unit Prototype of Full Tungsten ITER Divertor in Japan
FIP/2-1Rb			Progresses on WEST Platform Construction towards First Plasmas
08:50 FIP/2-2	K. Feng	China	Design and R&D Progress of Chinese HCCB TBS Programme
09:10 FIP/2-3	I. Ricapito	EC	Lessons Learned for the Breeding Blanket Designers from the Design Development of the European Test Blanket Module Systems (He, Tritium, Liquid Metal Systems)
09:30 FIP/2-4	A. Saraswat	India	Development of Sensors for High-Temperature High-Pressure Liquid Pb/Pb-16Li Applications
09:50 FIP/2-5	M. Ono	USA	Liquid Lithium Loop System to Solve Challenging Technology Issues for Fusion Power Plant

EX/2 and TH/2

Divertor & SOL Physics

Chair: Ulrich Stroth (Germany)

Main Hall

(10:45 – 12:30)

Time Id	Presenter		Title
10:45 EX/2-1	A. McLean	USA	The Role of Drifts and Radiating Species in Detached Divertor Operation at DIII-D
11:05 EX/2-2	D. Carralero	Germany	Recent Progress towards a Quantitative Description of Filamentary SOL Transport
11:25 TH/2-1	C.-S. Chang	USA	Gyrokinetic Projection of the Divertor Heat-flux Width from Present Tokamaks to ITER
11:45 EX/2-3	H. Reimerdes	Switzerland	TCV Experiments towards the Development of a Plasma Exhaust Solution
12:05 TH/2-2	I. Senichenkov	Russian Fed.	Study of Detached H-Modes in Full Tungsten ASDEX-Upgrade with N Seeding by SOLPS-ITER Modelling

P3

Posters 3

Annex Hall

(08:30 – 12:30)

Id	Presenter	Title
EX/P3-1	M. Porkolab	USA Studies of Turbulence and Transport in the Alcator C-Mod and DIII-D Tokamaks with Phase Contrast Imaging and Gyrokinetic Modelling
EX/P3-2	J. E. Rice	USA Effects of the q Profile on Toroidal Rotation in Alcator C-Mod LHCD Plasmas
EX/P3-3	M. L. Reinke	USA Investigations of Radial High- Z Transport Mechanisms in ICRF-Heated Alcator C-Mod H-Mode Plasmas
EX/P3-5	J. C. Wright	USA Experimental Results from Three-Ion Species Heating Scenario on Alcator C-Mod
EX/P3-6	B. LaBombard	USA Plasma Profiles and Impurity Screening Behaviour of the High-Field Side Scrape-Off Layer in Near-Double-Null Configurations: Prospect for Mitigating Plasma-Material Interactions on RF Actuators and First-Wall Components
EX/P3-7	D. Brunner	USA Divertor and Core Plasma Performance Optimization Enabled by Direct Feedback Control of Surface Heat Flux on Alcator C-Mod's High- Z Vertical Target Plate Divertor
EX/P3-8	R. S. Granetz	USA Developing Disruption Warning Algorithms Using Large Databases on Alcator C-Mod and EAST Tokamaks
EX/P3-9	S. Mordijck	USA Dominant Role of Turbulence in Determining Particle Transport and Confinement
EX/P3-10	G. R. McKee	USA Turbulence Evolution and Transport Behaviour during Current Ramp-Up in ITER-Like Plasmas on DIII-D
EX/P3-11	L. Schmitz	USA Turbulence-Flow Coupling and Poloidal Main-Ion Flow Acceleration Preceding the L-H Transition
EX/P3-12	R. S. Wilcox	USA Toroidally Localized Turbulence with Applied 3D Fields in the DIII-D Tokamak
EX/P3-13	J. deGrassie	USA Dimensionless Size Scaling of Intrinsic Rotation
EX/P3-14	F. Turco	USA Confinement and Stability of the ITER Baseline Scenario in DIII-D

Wed

Id	Presenter		Title
EX/P3-15	J. D. Hanson	USA	Stability of High-Performance, Negative Central Shear Discharges
EX/P3-16	M. Okabayashi	USA	Physics of Unlocked Tearing Modes and Disruption Avoidance by Feedback-Based Electromagnetic Torque Injection
EX/P3-18	M. Shafer	USA	Validating Extended MHD Models of Plasma Response against Measurements of Islands in DIII-D
EX/P3-19	D. Orlov	USA	The Contribution of Perturbation Coil Geometry Induced Sidebands and MHD Response in KSTAR and DIII-D
EX/P3-20	D. Shirakid	USA	Disruption Mitigation in the Presence of Pre-Existing MHD Instabilities
EX/P3-21	E. Kolemen	USA	Adaptive Real-Time Pedestal Control for DIII-D and Prospects for ITER
EX/P3-22	R. I. Pinsker	USA	Experiments on Helicons in DIII-D: Investigation of the Physics of a Reactor-Relevant Noninductive Current Drive Technology
EX/P3-23	E. Schuster	USA	Improved Reproducibility of Plasma Discharges via Physics-Model-Based q -Profile Feedback Control in DIII-D
EX/P3-24	M. A. Van Zeeland	USA	Electron Cyclotron Heating Modification of Alfvén Eigenmode Activity in DIII-D
EX/P3-25	A. W. Leonard	USA	Robust H-Mode Pedestal Compatibility with SOL and Divertor Plasma Constraints
EX/P3-26	A. Sontag	USA	SOL Effects on the Pedestal Structure in DIII-D Discharges
EX/P3-27	T. W. Petrie	USA	Edge, Divertor and Plasma Behaviour in High-Power High-Performance Double-Null Plasmas
EX/P3-28	B. Covele	USA	X-Divertors for Facilitating Detachment without Degrading the DIII-D H-Mode
EX/P3-29	D. Eldon	USA	Controlling Marginally Detached Divertor Plasmas
EX/P3-30	V. Soukhanovskii	USA	Snowflake Divertor Configuration Effects on Pedestal Stability and Edge Localized Modes in NSTX and DIII-D
EX/P3-31	G. Verdoolaege	Belgium	Robust Estimation of Tokamak Energy Confinement Scaling through Geodesic Least Squares Regression
EX/P3-32	U. Shumlak	USA	Results from the Sheared-Flow Stabilized Z-Pinch and Scaling to Fusion Conditions

Id	Presenter		Title
EX/P3-33	T. Jarboe	USA	Applying the New Principles of Plasma Self-Organization to Tokamak
EX/P3-34	R. P. Majeski	USA	Observation of an Isothermal Electron Temperature Profile with Low Recycling Lithium Walls in LTX
EX/P3-36	A. Costley	UK	Compact Fusion Energy Based on the Spherical Tokamak
EX/P3-37	T. Asai	Japan	Compact Toroid Injection Fuelling on a Large-sized Field-Reversed Configuration
EX/P3-38	Y. Ono	Japan	Reconnection Heating Experiments and Simulations for Torus Plasma Merging Startup
EX/P3-39	D. Gates	USA	Recent Advances in Stellarator Optimization
EX/P3-40	J. P. Levesque	USA	Ferritic Wall and Scrape-Off-Layer Current Effects on Kink Mode Dynamics
EX/P3-41	H. Gota	USA	Achievement of Field-Reversed Configuration Plasma Sustainment via 10 MW Neutral-Beam Injection on the C-2U Device
EX/P3-42	A. Hossack	USA	Plasma Response to Sustainment with Imposed-dynamo Current Drive in HIT-SI and HIT-SI3
EX/P3-46	M. Nishiura	Japan	Ion Heating in Magnetosphere Plasma Device RT-1
EX/P3-47	S. Medvedev	Russian Fed.	Single Null Divertor in Negative Triangularity Tokamak
TH/P3-1	Y. Idomura	Japan	Full-f Gyrokinetic Simulation including Kinetic Electrons
TH/P3-2	Y. Kishimoto	Japan	Characteristics of Turbulent Transport in Flux-Driven Toroidal Plasmas
TH/P3-3	K. Imadera	Japan	ITB Formation in Gyrokinetic Flux-Driven ITG Turbulence
TH/P3-4	L. Qi	Korea, Rep. of	Gyrokinetic Simulations of Electrostatic Microinstabilities with Bounce-Averaged Kinetic Electrons for Shaped Tokamak Plasmas
TH/P3-5	G. Dif-Pradalier	France	Validation of Self-Organization Dynamics in Fusion Plasmas
TH/P3-6	S. Leerink	Finland	Coupling Full-f Gyrokinetic Studies to Experimental Measurements of the Isotope Effect for FT-2 Tokamak Plasmas

Id	Presenter		Title
TH/P3-7	R. Ganesh	India	Effect of Magnetic Shear and Equilibrium Flows on Collisionless Microtearing and Mixed Parity Modes in Hot Tokamak Plasmas
TH/P3-8	K. C. Shaing	USA	Neoclassical Toroidal Plasma Viscosity with Effects of Finite Banana Width in Finite Aspect Ratio Tokamaks
TH/P3-9	M. Honda	Japan	Predictions of Toroidal Rotation and Torque Sources Arising in Nonaxisymmetric Perturbed Magnetic Fields in Tokamaks
TH/P3-10	S. Matsuoka	Japan	Global Kinetic Effect on the Collisionality Dependence of the Neoclassical Toroidal Viscosity in the Superbanana-Plateau Regime
TH/P3-11	J. Seol	Korea, Rep. of	Effects of Localized Neoclassical Toroidal Viscosity Effects on the Toroidal Rotation Profile in KSTAR
TH/P3-12	W. W. Wang	USA	Understanding and Predicting Profile Structure and Parametric Scaling of Intrinsic Rotation
TH/P3-13	H. H. Kaang	Korea, Rep. of	Residual Stress and Momentum Transport in Electromagnetic ITG Turbulence
TH/P3-14	W. Guttenfelder	USA	Analysis and Prediction of Momentum Transport in Spherical Tokamaks
TH/P3-15	C. Fenzi	France	Co- and Countercurrent Rotation in Tore Supra LHCD Plasmas: Neoclassical and Turbulent Transport Processes
TH/P3-16	S. Nowak	Italy	Effect of the EC Torque on Slow Plasma Rotation under Central ECH/ECCD for NTM Onset
TH/P3-17	L. Garcia	Spain	Relation of Plasma Flow Structures to Particle Tracer Orbits
TH/P3-18	J. Omotani	Sweden	Edge Flow from Momentum Transport by Neutrals
TH/P3-19	P. H. Diamond	USA	New Results in Negative Viscosity Models for Fusion Plasma Dynamics
TH/P3-20	Y. Kosuga	Japan	Transport of Parallel Momentum by the Triplet Correlation in Drift Wave Turbulence
TH/P3-21	M. Yagi	Japan	Nonlocal Plasma Response to Edge Perturbation in Tokamak
TH/P3-22	D. del-Castillo-Negrete	USA	Modulated Heat Pulse Propagation and Partial Transport Barriers in 3D Chaotic Magnetic Fields

Id	Presenter	Country	Title
TH/P3-23	M. Malkov	USA	L-H Transition Threshold Physics at Low Collisionality
TH/P3-24	T. Onjun	Thailand	Effects of Heat and Particle Sources Perturbations on L-H-L Transitions Based on Bifurcation Concept
TH/P3-25	T. S. Hahm	Korea, Rep. of	$E \times B$ Shear and Precession Shear Induced Turbulence Suppression
TH/P3-26	K. Hallatschek	Germany	Zonal Flows and GAMs in Comparative Gyrokinetic and Two-Fluid Tokamak Turbulence Simulations
TH/P3-27	M. Leconte	Korea, Rep. of	Helical Electric Potential Modulation via Zonal Flow Coupling to Resonant Magnetic Perturbations
TH/P3-29	S. S. Kim	Korea, Rep. of	Tokamak Turbulence Simulations Using BOUT++ in Core Region
TH/P3-30	W. Horton	USA	Steady State Turbulent ITER-Like Plasmas with RF Drivers
TH/P3-31	C. McDevitt	USA	Turbulent Current Drive Mechanisms
TH/P3-32	C.-Y. An	Korea, Rep. of	Effect of Energy-Nontransporting Nonlinear Flux on the Turbulent Plasma Transport
TH/P3-33	N. Kasuya	Japan	Numerical Diagnostics of Turbulent Transport in Three-Dimensional Magnetic Configurations
TH/P3-34	R. Chahine	France	The Effect of Shaping on Reversed Field Pinch Dynamics
TH/P3-35	D. Bonfiglio	Italy	Progress in Theoretical RFP Studies: New Stimulated Helical Regimes and Similarities with Tokamak and Stellarator
TH/P3-36	L. Sugiyama	USA	Solar Coronal Loops as Magnetically Confined Tori with Gravity
TH/P3-37	J. Martinell	Mexico	Studies of Magnetic Islands in the TJ-II Helic and the Related Transport
TH/P3-38	M. Rajković	Serbia	Predicting Cross-Scale Self-Organization in Turbulent Magnetically Confined Plasmas
TH/P3-39	A. Beklemishev	Russian Fed.	Diamagnetic Plasma Confinement in Linear Traps

EX/3



Pedestal & ELM Physics

Chair: Philip B. Snyder (USA)

Main Hall

(14:00 – 16:10)

Wed

Time Id	Presenter		Title
14:00 EX/3-1	A. E. Hubbard	USA	Advances in Physics and Performance of the I-Mode Regime over an Expanded Operating Space on Alcator C-Mod
14:20 EX/3-2	X. Chen	USA	Bifurcation of Quiescent H-Mode to a Wide Pedestal Regime in DIII-D and Advances in the Understanding of Edge Harmonic Oscillations
14:40 EX/3-3	C. Maggi	UK	Studies of the Pedestal Structure in JET with the ITER-Like Wall
15:00 EX/3-4	H. Urano	Japan	Global Stabilization Effect of Shafranov Shift on the Edge Pedestal Plasmas in JET and JT-60U
15:20 EX/3-5	M. Dunne	Germany	The Role of the Density Profile Location on Pedestal Stability in ASDEX-Upgrade
15:40 EX/3-6	I. Chapman	UK	Joint Experiments Tailoring the Plasma Evolution to Maximize Pedestal Performance

Summary

EX/4 and PPC/1



Steady State and Hybrid Scenarios

Chair: Li Jiangang (China)

Main Hall

(16:40 – 18:45)

Time Id	Presenter		Title
16:40 EX/4-1	C. C. Petty	USA	Advances in the Steady-State Hybrid Regime in DIII-D: A Fully-Noninductive, ELM-Suppressed Scenario for ITER
17:00 EX/4-2	J. Qian	China	Advances in the High Bootstrap Fraction Regime on DIII-D towards the $Q = 5$ Mission of ITER Steady State
17:20 EX/4-3	A. M. Garofalo	USA	Development of High Poloidal β , Steady-State Scenario with ITER-Like W Divertor on EAST
17:40 PPC/1-1	H. Takahashi	Japan	Extension of Operational Regime in High-Temperature Plasmas and Effect of ECRH on Ion Thermal Transport in the LHD
18:00 EX/4-4	S. Sakakibara	Japan	Extension of High- β Plasma Operation to Low Collisional Regime
18:20 EX/4-5	M. Hirsch	Germany	Confinement in Wendelstein 7-X Limiter Plasmas

Wed

P4

Posters 4

Annex Hall

(14:00 – 18:45)

Id	Presenter		Title
EX/2-1	A. McLean	USA	The Role of Drifts and Radiating Species in Detached Divertor Operation at DIII-D
EX/2-2	D. Carralero	Germany	Recent Progress towards a Quantitative Description of Filamentary SOL Transport
EX/2-3	H. Reimerdes	Switzerland	TCV Experiments towards the Development of a Plasma Exhaust Solution
FIP/2-1Ra	Y. Seki	Japan	Progress of Qualification Testing for Full-Scale Plasma-Facing Unit Prototype of Full Tungsten ITER Divertor in Japan
FIP/2-1Rb	J. Bucalossi	France	Progresses on WEST Platform Construction towards First Plasmas
FIP/2-2	K. Feng	China	Design and R&D Progress of Chinese HCCB TBS Programme
FIP/2-3	I. Ricapito	EC	Lessons Learned for the Breeding Blanket Designers from the Design Development of the European Test Blanket Module Systems (He, Tritium, Liquid Metal Systems)

Id	Presenter		Title
FIP/2-4	A. Saraswat	India	Development of Sensors for High-Temperature High-Pressure Liquid Pb/Pb-16Li Applications
FIP/2-5	M. Ono	USA	Liquid Lithium Loop System to Solve Challenging Technology Issues for Fusion Power Plant
TH/2-1	C.-S. Chang	USA	Gyrokinetic Projection of the Divertor Heat-flux Width from Present Tokamaks to ITER
TH/2-2	I. Senichenkov	Russian Fed.	Study of Detached H-Modes in Full Tungsten ASDEX-Upgrade with N Seeding by SOLPS-ITER Modelling
EX/P4-1	S.-W. Yoon	Korea, Rep. of	Extension of Operational Boundary of High- β Long-pulse Operation at KSTAR
EX/P4-2	Y.-S. Park	USA	Investigation of MHD Stability in KSTAR High- β_N Plasmas
EX/P4-3	H. Park	Korea, Rep. of	Validation of $q_0 \geq 1.0$ in the MHD Quiescent Time after Crash of the Sawtooth Instability in KSTAR
EX/P4-4	W. H. Ko	Korea, Rep. of	Influences of Nonaxisymmetric Field on H-Mode Power Threshold and Pedestal Rotation in KSTAR
EX/P4-5	J. Kim	Korea, Rep. of	Direct Destabilizations of Macro/Micro Edge Instabilities by Magnetic Perturbations
EX/P4-6	Y. In	Korea, Rep. of	Study of the Locked Mode Disruption with the 3D Imaging Data in KSTAR
EX/P4-7	M. Kim	Korea, Rep. of	Study of Nonlinear Phase of the ELMs by Comparison between ECEI ELM Observation and Nonlinear MHD Simulations
EX/P4-8	J. G. Bak	Korea, Rep. of	Characteristics of Halo Current in the KSTAR Tokamak
EX/P4-9	K. Kim	Korea, Rep. of	Characteristics of Magnetic Braking Depending on 3D Field Configuration in KSTAR
EX/P4-10	S. G. Lee	Korea, Rep. of	Long-Lived Pressure-Driven MHD Mode in KSTAR Plasmas
EX/P4-12	S.-H. Hahn	Korea, Rep. of	Measuring and Extending Vertical Stabilization Controllability of KSTAR
EX/P4-13	H.-S. Kim	Korea, Rep. of	Application of Physics-Based Profile Control Approach to KSTAR

Id	Presenter	Title	Title
EX/P4-14	J. Lee	Korea, Rep. of	ECH-assisted Plasma Startup Experiment Using Trapped Particle Configuration in KSTAR
EX/P4-15	J. Lee	Korea, Rep. of	ELM, Edge Turbulence and their Interaction in the ELM-crash Suppression Phase under the $n = 1$ RMP
EX/P4-16	S. Ko	Korea, Rep. of	Study of Toroidal Rotation and Ion Temperature Pedestals between ELM Bursts on KSTAR H-Mode Plasmas
EX/P4-17	Y. Shi	Korea, Rep. of	Fluctuation Signatures of Rotation Reversals and Nonlocal Transport Events in KSTAR L-Mode Plasmas
EX/P4-18	J. Hong	Korea, Rep. of	Effects of ECH and RMP on Argon Impurity Transport in KSTAR Plasmas
EX/P4-19	D. H. Na	Korea, Rep. of	Rotation Reversal in KSTAR and its Turbulence and Transport Characteristics
EX/P4-20	W. Lee	Korea, Rep. of	Ion-Scale Turbulence Study in KSTAR L-Mode Plasmas
EX/P4-21	S.-H. Hong	Korea, Rep. of	Comprehensive Study on Deposition inside the Gap of Castellated Tungsten Blocks of Different Shapes
EX/P4-22	J.-G. Kwak	Korea, Rep. of	The Assessment of the Neutron Yield and the Toroidal Distribution of Neutron Emission on Deuterium Beam-Plasma Interaction Dominated KSTAR Operation
EX/P4-23	K. C. Lee	Korea, Rep. of	Measurements of SOL Density Increase and Poloidal Asymmetry on KSTAR ELMs
EX/P4-24	H. Lee	Korea, Rep. of	H-Mode Divertor Target Heat Load Measurements on KSTAR
EX/P4-25	M.-K. Bae	Korea, Rep. of	Comparative Study of KSTAR and DiPS-2 on the Heat Flux to the First Wall
EX/P4-26	J. Kim	Korea, Rep. of	Experimental Observations of Beam-Driven Alfvén Eigenmodes in KSTAR
EX/P4-27	J. Ko	Korea, Rep. of	Current Profile Evolutions with External Current Drive for KSTAR
EX/P4-28	M. Cheon	Korea, Rep. of	Loss of Predisruptive Runaway Electrons by Magnetic Perturbation and its Effect on Plasma Disruption
EX/P4-29	C.-M. Ryu	Korea, Rep. of	Observation and Simulation of TAEs in KSTAR Plasmas

Id	Presenter		Title
EX/P4-30	J.-W. Ahn	USA	Shielding and Amplification of Nonaxisymmetric Divertor Heat Flux by Plasma Response to Applied 3D Fields in NSTX and KSTAR
EX/P4-31	F. Militello	UK	Scrape-Off Layer and Divertor Physics Advances in MAST
EX/P4-32	H. Tanabe	Japan	Investigation of Merging/Reconnection Heating during Solenoid-Free Startup of Plasmas in the MAST Spherical Tokamak
EX/P4-33	S. A. Sabbagh	USA	Isolation of Neoclassical Toroidal Viscosity Profile under Varied Plasma and 3D Field Conditions in Low and Medium Aspect Ratio Tokamaks
EX/P4-34	J. W. Berkery	USA	Characterization and Forecasting of Unstable Resistive Wall Modes in NSTX and NSTX-U
EX/P4-35	Y. Ren	USA	Exploring the Regime of Validity of Global Gyrokinetic Simulations with Spherical Tokamak Plasmas
EX/P4-36	F. Scotti	USA	Kinetic Profiles and Impurity Transport Response to 3D-Field Triggered ELMs in NSTX
EX/P4-38	R. Maingi	USA	Comparison of Helium Glow and Lithium Evaporation Wall Conditioning Techniques in Achieving High Performance H-Mode Discharges in NSTX
EX/P4-39	L. F. Delgado-Aparicio	USA	Locked-Mode Avoidance and Recovery without External Momentum Input Using ICRH
EX/P4-40	D. Smith	USA	Identification of Characteristic ELM Evolution Patterns with Alfvén-Scale Measurements and Unsupervised Machine Learning Analysis
EX/P4-41	E. Fredrickson	USA	Parametric Dependence of EPMS in NSTX
EX/P4-42	R. Perkins	USA	Large RF Field Amplitudes in the SOL and Far-Field RF Sheaths: A Proposed Mechanism for the Anomalous Loss of RF Power to the SOL of NSTX
EX/P4-43	M. D. Boyer	USA	Feedback Control Design for Noninductively Sustained Scenarios in NSTX-U Using TRANSP
EX/P4-44	N. Bakharev	Russian Fed.	Counter-NBI Experiments on Globus-M

Id	Presenter	Country	Title
EX/P4-45	H. Tanaka	Japan	Noninductive Production of Extremely Overdense Spherical Tokamak Plasma by Electron Bernstein Wave Excited via O-X-B Method in LATE
EX/P4-47	I. Vargas-Blanco	Costa Rica	Recommissioning of the Spherical Tokamak MEDUSA in Costa Rica
EX/P4-48	A. Ejiri	Japan	Plasma Startup Experiments on the TST-2 Spherical Tokamak
EX/P4-49	K. Hanada	Japan	Investigation of Hydrogen Recycling Property and its Control with Hot Wall in Long Duration Discharges on QUEST
EX/P4-50	H. Idei	Japan	Noninductive Electron Cyclotron Heating and Current Drive with Dual Frequency (8.2/28 GHz) Waves in QUEST
EX/P4-51	M. Bongard	USA	ELM Characterization and Dynamics at Near-Unity A in the Pegasus ST
EX/P4-52	Y. Tan	China	TAE during Minor Disruptions in the SUNIST Spherical Tokamak
EX/P4-53	H. Lee	Korea, Rep. of	Study on EBW Assisted Startup and Heating Experiments via Direct XB Mode Conversion from Low Field Side Injection in VEST
FIP/P4-2	M. Nocente	Italy	Conceptual Design of the Radial Gamma-Ray Spectrometers System for Alpha Particle and Runaway Electron Measurements at ITER
FIP/P4-3	C. Hellesen	Sweden	Conceptual Design of the Best TOF Neutron Spectrometer for Fuel-Ion Ratio Measurements at ITER
FIP/P4-4	L. R. Baylor	USA	Pellet Injection Technology and Application to Mitigate Transient Events on ITER
FIP/P4-5	R. Imazawa	Japan	Progress on Integrated Design of ITER Poloidal Polarimeter for Current Profile Measurement
FIP/P4-6	F. Poli	USA	Electron Cyclotron Power Management in ITER, the Path from the Commissioning Phase to Demonstration Discharges
FIP/P4-7	H. Nakanishi	Japan	High-Performance Data Transfer for Full Data Replication between ITER and the Remote Experimentation Centre
FIP/P4-8	K. Itami	Japan	Design Development of the ITER Divertor Diagnostic Systems in Japan

Wed

Id	Presenter		Title
FIP/P4-9	K. Takahashi	Japan	Development of ITER Poloidal Steering Equatorial EC Launcher Enhancing ECCD Performance
FIP/P4-10	N. Umeda	Japan	Development of Ultrahigh Voltage Insulation Technology for the Power Supply Components in Neutral Beam System on ITER
FIP/P4-11	Y. Kawano	Japan	Overview of ITPA R&D Activities for Improvement of ITER Diagnostic Performance
FIP/P4-12	A. K. Chakraborty	India	Electro-Mechanical Design and Experimental Validation of Post Insulators for Beam Source for ITER Diagnostic Neutral Beam
FIP/P4-13	S. M. Manoah	India	Concept Design of the Heavy Duty Multipurpose Deployer for ITER
FIP/P4-14	S. Kajita	Japan	Effect of Wall Light Reflection in ITER Diagnostics
FIP/P4-15	D. Gin	Russian Fed.	On Fast Ions Diagnostics with Gamma-Ray Spectrometry in ITER
FIP/P4-16	D. Marocco	Italy	System Level Design and Performances of the ITER Radial Neutron Camera
FIP/P4-17	A. Zvonkov	Russian Fed.	CXRS-edge Diagnostic in the Harsh ITER Environment
FIP/P4-18	L. Hu	China	Progress on Design and R&D of ITER Diagnostic-Radial X-ray Camera
FIP/P4-20	J. K. Anderson	USA	High Power Testing of Water-Cooled Waveguide for ITER ECH Transmission Lines
FIP/P4-21	Z. Song	China	Research and Development Progress of the ITER PF Converter System
FIP/P4-22	J. Chen	China	Technical Preparation for Series Production of ITER Enhance Heat Flux FW Panels
FIP/P4-27	E. E. Mukhin	Russian Fed.	ITER Core Thomson Scattering: Objectives and Error Analysis
FIP/P4-28	V. Toigo	Italy	The ITER Neutral Beam Test Facility toward SPIDER Operation
FIP/P4-29	F. Albajar	EC	The Development of the European 1 MW, 170 GHz CW Gyrotron for the ITER Electron Cyclotron Heating System

Id	Presenter	Country	Title
FIP/P4-31	G. Serianni	Italy	Synergy of Numerical Simulations and Experimental Measurements to Improve the Interpretation of Negative Ion Beam Properties
FIP/P4-33	J. A. González Guevara	Mexico	60 GHz–300 kW Gyrotron General Design for the Mexican Tokamak “T”
FIP/P4-36	A. K. Chakraborty	India	Manufacturing and Commissioning of Large Size UHV Class Vacuum Vessel for Indian Test Facility (INTF) for Neutral Beams
FIP/P4-37	M. Tokitani	Japan	Fabrication of Divertor Mock-Up with ODS-Cu and W by Improved Brazing Technique
FIP/P4-38	M. Modestov	USA	Liquid Metal Flow Control Simulation at Liquid Metal Experiment
FIP/P4-39	R. Zanino	Italy	Modelling the Lithium Loop in a Liquid Metal Divertor for Future Fusion Reactors
FIP/P4-40	A. Fasoli	Switzerland	TCV Divertor and Heating Upgrades for Contributing to DEMO Physics Basis
FIP/P4-41	Y. Hatano	Japan	Japan-US Joint Research Project PHENIX (2013–2018); Heat Transfer Tests, Neutron Irradiation and Postirradiation Examinations for Development of He-Cooled Tungsten Divertor
FIP/P4-42	C. Day	Germany	Assessment of the Operational Window for JT-60SA Divertor Pumping under Consideration of the Effects from Neutral-Neutral Collisions
FIP/P4-43	A. Sergis	UK	Flow Characteristics in HyperVapotron Elements Operating with Nanofluids
FIP/P4-44	F. Bonelli	Germany	Self-Consistent Coupling of DSMC Method and SOLPS Code for Modelling Tokamak Particle Exhaust
FIP/P4-45	P. K. Domalapally	Czech Republic	Computational Fluid Dynamic Analysis of Screw Tube Relevant for Fusion Applications
FIP/P4-46	J. Ghosh	India	Upgrade of ADITYA Tokamak with Limiter Configuration to ADITYA Upgrade Tokamak with Divertor Configuration
TH/P4-1	T. Fülöp	Sweden	Kinetic Modelling of Runaways in Fusion Plasmas
TH/P4-2	P. Aleynikov	Germany	Generation of Runaway Electrons during the Thermal Quench in Tokamaks

Id	Presenter		Title
TH/P4-3	T. Kurki-Suonio	Finland	The Effect of Plasma Response on Losses of Energetic Ions in the Presence of 3D Perturbations in Different ITER Scenarios
TH/P4-4	R. Farengo	Argentina	Diffusion of Energetic Particles Due to Charge Changes and Neoclassical Tearing Modes
TH/P4-5	G. J. Kramer	USA	Improving Fast-Ion Confinement in High-Performance Discharges by Suppressing Alfvén Eigenmodes
TH/P4-6	G. Vlad	Italy	Linear and Nonlinear Dynamics of Electron Fishbones
TH/P4-7	Z. Lin	USA	Nonlinear Interactions of Low-Frequency Alfvén Eigenmodes
TH/P4-8	W. Zhang	China	Gyrokinetic Particle Simulation of Fast-Electron Driven β -Induced Alfvén Eigenmodes
TH/P4-10	D. Spong	USA	Global Gyrokinetic Simulation of Energetic Particle-Driven Instabilities in 3D Systems
TH/P4-11	H. Wang	Japan	Simulations of Energetic Particle Driven Geodesic Acoustic Mode and Global Alfvén Eigenmode in 3D LHD Equilibrium
TH/P4-12	M. Sasaki	Japan	A New Branch of Geodesic Acoustic Modes Driven by Fast Ions
TH/P4-14	R. E. Waltz	USA	A Critical Gradient Model for Energetic Particle Transport from Alfvén Eigenmodes: GYRO Verification, DIII-D Validation, and ITER Projection
TH/P4-16	G. Fu	USA	Hybrid Simulations of Beam-Driven Fishbone and TAEs in NSTX
TH/P4-17	E. Belova	USA	Coupling of Neutral-Beam-Driven Compressional Alfvén Eigenmodes to Kinetic Alfvén Waves in NSTX and Energy Channelling
TH/P4-18	M. Lesur	France	Nonlinear Excitation of Subcritical Fast Ion-Driven Modes
TH/P4-19	X. Wang	Germany	On the Structure of Wave-Particle Interactions and Nonlinear Alfvénic Fluctuation Dynamics
TH/P4-20	L. Chen	China	On Excitation of Zonal Structures by Kinetic Alfvén Waves
TH/P4-21	Z. Qiu	China	Nonlinear Excitation of Fine-Structure Zonal Flow by Alfvén Eigenmodes

Id	Presenter	USA	Title
TH/P4-23	N. Bertelli	USA	Towards a Self Consistent Evaluation of the RF Wave-Field and the Ion Distribution Functions in Tokamak Plasmas
TH/P4-24	Y. Petrov	USA	A Fully-Neoclassical Finite-Orbit-Width Version of the CQL3D Fokker-Planck Code
TH/P4-25	J. Bao	China	Nonlinear Particle Simulation of Radio Frequency Waves in Tokamak
TH/P4-26	A. V. Arefiev	USA	Kinetic Simulations of the Full O-X-B Mode Conversion Process and the Deteriorating Effect of High Power Levels
TH/P4-27	S. Shiraiwa	USA	Integration of Core/Edge Plasmas in Fullwave RF Simulation
TH/P4-28	J. Lin	China	Toroidal Electromagnetic Particle-in-Cell Code with Gyro-kinetic Election and Fully-kinetic Ion
TH/P4-29	A. Ram	USA	Scattering of Radio Frequency Waves by Density Fluctuations in Tokamak Plasmas
TH/P4-30	D. Green	USA	Verification of a Configuration Space Method for Evaluating the All-Orders Linear Kinetic Plasma Response to RF Power
TH/P4-31	J. Myra	USA	An Improved RF-Sheath Boundary Condition and Implications for ICRF Modelling
TH/P4-32	E. Z. Gusakov	Russian Fed.	Low-Threshold Two-UH-Plasmon Decay as a Reason for Anomalous Backscattering and Absorption in Second Harmonic ECRH Experiments
TH/P4-34	T. Jenkins	USA	High-Performance Computational Modelling of Plasma-Surface Interactions and RF Antennas
TH/P4-35	Z. Gao	China	Parallel Momentum Transport Induced by RF Waves and by Plasma Turbulence
TH/P4-36	A. Zhao	China	Isotopic Effect of Parametric Instabilities during Lower Hybrid Waves Injection into Hydrogen/Deuterium Plasmas
TH/P4-37	A. Sid	Algeria	Temperature Anisotropy in Magnetized Fusion Plasma

Wed

EX/5, TH/3, PPC/2**Transport & LH Transition**

Chair: Sibylle Guenter (Germany)

*Main Hall***(08:30 – 10:15)**

Time Id	Presenter		Title
08:30 PPC/2-1	A. Loarte	ITER	Evaluation of Tungsten Transport and Concentration Control in ITER Scenarios
08:50 TH/3-1	X. Garbet	France	Synergetic Effects of Collisions, Turbulence and Sawtooth Crashes on Impurity Transport
09:10 EX/5-1	Z. Yan	USA	Turbulence and Sheared Flow Structures Behind the Isotopic Dependence of the L-H Power Threshold and H-L Back Transition on DIII-D
09:30 EX/5-2	J. Hillesheim	UK	Role of Stationary Zonal Flows and Momentum Transport for L-H Transitions in JET
09:50 EX/5-3	A. Diallo	USA	Energy Exchange Dynamics across L-H Transitions in NSTX

EX/6 and TH/4**Energetic Particles Physics**

Chair: Ritoku Horiuchi (Japan)

*Main Hall***(10:45 – 12:30)**

Time Id	Presenter		Title
10:45 EX/6-1	M. Garcia-Munoz	Spain	The Role of Plasma Response on Fast-Ion Losses Induced by Edge 3D Fields in the ASDEX-Upgrade and DIII-D Tokamaks
11:05 TH/4-1	R. Akers	UK	High Fidelity Simulations of Fast Ion Power Flux Driven by 3D Field Perturbations on ITER
11:25 EX/6-2	C. Collins	USA	Critical Gradient Behaviour of Fast-Ion Transport from Alfvén Eigenmodes Guides Predictive Models for Burning Plasmas
11:45 TH/4-2	A. Biancalani	Germany	Gyrokinetic Investigation of the Nonlinear Interplay of Alfvén Instabilities and Energetic Particles in Tokamaks
12:05 TH/4-3	A. Bierwage	Japan	First-Principle Simulations Reproduce Multiple Cycles of Abrupt Large Relaxation Events in Beam-Driven JT-60 Plasmas

P5

Posters 5

Annex Hall

(08:30 – 12:30)

Id	Presenter	Title
EX/3-1	A. E. Hubbard	USA Advances in Physics and Performance of the I-Mode Regime over an Expanded Operating Space on Alcator C-Mod
EX/3-2	X. Chen	USA Bifurcation of Quiescent H-Mode to a Wide Pedestal Regime in DIII-D and Advances in the Understanding of Edge Harmonic Oscillations
EX/3-3	C. Maggi	UK Studies of the Pedestal Structure in JET with the ITER-Like Wall
EX/3-4	H. Urano	Japan Global Stabilization Effect of Shafranov Shift on the Edge Pedestal Plasmas in JET and JT-60U
EX/3-5	M. Dunne	Germany The Role of the Density Profile Location on Pedestal Stability in ASDEX-Upgrade
EX/3-6	I. Chapman	UK Joint Experiments Tailoring the Plasma Evolution to Maximize Pedestal Performance
EX/4-1	C. C. Petty	USA Advances in the Steady-State Hybrid Regime in DIII-D: A Fully-Noninductive, ELM-Suppressed Scenario for ITER
EX/4-2	J. Qian	China Advances in the High Bootstrap Fraction Regime on DIII-D towards the $Q = 5$ Mission of ITER Steady State
EX/4-3	A. M. Garofalo	USA Development of High Poloidal β , Steady-State Scenario with ITER-Like W Divertor on EAST
EX/4-4	S. Sakakibara	Japan Extension of High- β Plasma Operation to Low Collisional Regime
EX/4-5	M. Hirsch	Germany Confinement in Wendelstein 7-X Limiter Plasmas
PPC/1-1	H. Takahashi	Japan Extension of Operational Regime in High-Temperature Plasmas and Effect of ECRH on Ion Thermal Transport in the LHD
EX/P5-1	A. Dinklage	Germany The Effect of Transient Density Profile Shaping on Transport in Large Stellarators and Heliotrons
EX/P5-2	M. Hirsch	Germany Initial Observations on Core Electron Heat Transport in W7-X

Thu

Id	Presenter		Title
EX/P5-3	A. Langenberg	Germany	Minerva Bayesian Analysis of X-ray Imaging Spectrometer Data for Temperature and Density Profile Inference at Wendelstein 7-X
EX/P5-4	A. Krämer-Flecken	Germany	Investigation of Turbulence Rotation in Limiter Plasmas at W7-X with a New Installed Poloidal Correlation Reflectometry
EX/P5-5	S. Lazerson	USA	Error Field Measurement, Correction and Heat Flux Balancing on Wendelstein 7-X
EX/P5-6	N. Pablant	USA	Investigation of Initial Plasma Parameters on the Wendelstein 7-X Stellarator Using the X-ray Imaging Crystal Spectrometer
EX/P5-7	G. A. Wurden	USA	Limiter Observations during W7-X First Plasmas
EX/P5-8	S. A. Bozhakov	Germany	Enhancement of W7-X Performance by Symmetrization of Limiter Loads with Error Field Correction Coils
EX/P5-9	P. Drews	Germany	Measurement of the Plasma Edge Profiles Using the Combined Probe on W7-X
EX/P5-10	Y. Liang	Germany	Diagnostic Setup and Modelling for Investigation of Synergy between 3D Edge Physics and Plasma-Wall Interactions on Wendelstein 7-X
EX/P5-11	D. Moseev	Germany	Application of the ECRH Radiation for Plasma Diagnosis in Wendelstein 7-X
EX/P5-12	J. Ongena	Belgium	Physics and Applications of ICRH on W7-X
EX/P5-13	S. Marsen	Germany	First Results from Protective ECRH Diagnostics for Wendelstein 7-X
EX/P5-14	O. Grulke	Germany	Transport Studies during the First Campaign of Wendelstein 7-X
EX/P5-15	D. Den Hartog	USA	Enhanced Measurements for MHD Validation Using Integrated Data Analysis on the MST Fusion Research Experiment
EX/P5-16	J. K. Anderson	USA	An Island-Induced Alfvén Eigenmode and Effects of Nonaxisymmetry on Fast Ions in the RFP
EX/P5-17	D. L. Brower	USA	Evidence for Trapped Electron Mode Turbulence in MST Improved Confinement RFP Plasmas
EX/P5-18	L. Frassinetti	Sweden	Effect of External Magnetic Perturbations on the EXTRAP T2R Reversed-Field Pinch Plasma
EX/P5-19	W. Liu	China	Overview of Keda Torus Experiment Initial Results

Id	Presenter	Country	Title
EX/P5-20	T. Lan	China	Initial Operation Results from KTX
EX/P5-21	M. Nagata	Japan	Investigations of Plasmoid Formation and Flux Closure in Transient Coaxial Helicity Injection on HIST
EX/P5-22	S. Masamune	Japan	Improved Low-Aspect-Ratio RFP Performance with Active MHD Control and Associated Change in Magnetic Topology in RELAX
EX/P5-23	M. E. Puiatti	Italy	Extended Scenarios Opened by the Upgrades of the RFX-Mod Experiment
EX/P5-24	M. Spolaore	Italy	H-Mode Achievement and Edge Features in RFX-Mod Tokamak Operation
EX/P5-25	M. Agostini	Italy	Kinetic Properties of Edge Plasma with 3D Magnetic Perturbations in RFX-Mod
EX/P5-26	R. Lorenzini	Italy	Transport Studies with Magnetic Islands in Fusion Plasmas
EX/P5-28	S. Banerjee	India	Observation of Large Filaments during the Disruptive Phase of ADITYA Tokamak Plasma
EX/P5-29	D. C. Raval	India	Plasma Startup Studies and Electromagnetic Field Computation for SST-1 Tokamak
EX/P5-30	J. R. Dhongde	India	MHD Phenomena and Disruption Characteristics in SST-1 Early Plasma
EX/P5-31	J. R. Dhongde	India	Observation and Study of Lock Mode Characteristics in SST-1 Plasma
EX/P5-32	S. Pradhan	India	Low Density Plasma Regimes in SST-1 with and without Suprathermal Electrons
EX/P5-33	D. C. Raval	India	Plasma Facing Components Technologies in SST-1
FNS/P5-1	I. Palermo	Spain	Optimization Process for the Design of the DCLL Blanket for the European Demonstration Fusion Reactor According to its Nuclear Performances
FNS/P5-2	J. Rapp	USA	Developing the Science and Technology for the Material Plasma Exposure Experiment (MPEX)
FNS/P5-3	S. Şahin	Turkey	First Wall Lifetime Extension with Flowing Liquid Zone for Fusion Reactors
FNS/P5-5	S. Sato	Japan	New Integral Experiments for a Variety of Fusion Reactor Materials with DT Neutron Source at JAEA/FNS
FNS/P5-6	T. Fujita	Japan	Optimization Study of Normal Conductor Tokamak for Commercial Neutron Source

Thu

Id	Presenter		Title
FNS/P5-8	K. Ogawa	Japan	Investigation on Irradiation Effects on Highly Integrated Leading Edge Electronic Components of Diagnostics and Control Systems for the LHD Deuterium Operation
FNS/P5-9	S. M. Manoah	India	Design and Analysis of SST-2 Vacuum Vessel
FNS/P5-10	U. Fischer	Germany	Advanced Neutronics Simulation Tools and Data for Fusion Applications
FNS/P5-11	A. Zhirkin	Russian Fed.	Fusion Neutron Source Blanket: Requirements on Calculation Accuracy and Benchmark Experiment Precision
FNS/P5-12	J. Yu	China	Design and R&D Activities of Fusion Breeder Blankets in China
FNS/P5-13	C. Velasquez	Brazil	Temperature Sensitivity Analysis of Nuclear Cross Section Using FENDL for Fusion-Fission System
IFE/P5-2	R. Khaydarov	Uzbekistan	Improvement of Characteristics of Laser Source of Ions by Changing the Parameters of the Target and External Parameters
IFE/P5-4	N. Ding	China	Recent Advances in Theoretical and Numerical Studies of Z-Pinch Driven Inertial Confinement Fusion in the IAPCM
IFE/P5-5	T. Kikuchi	Japan	Recent Activities on Heavy Ion Inertial Fusion in Japan
IFE/P5-6	K. W. Hill	USA	Adapting High Resolution X-ray Spectroscopy from MFE to Temperature and Density Measurements in ICF
IFE/P5-7	A. N. Simakov	USA	The Role of Beryllium Ablators in Inertial Confinement Fusion
IFE/P5-8	J. Liu	China	Spherical Convergent Plasma Fusion (SCPF) Neutron Generator by Laser Drive: Theory and Experiment
IFE/P5-9	Y. Mori	Japan	Fast Heating of an Imploded Core under Counter Beam Irradiation by Using a Repetitive IFE Driver HAMA
IFE/P5-10	Y. Kitagawa	Japan	Unified Studies of Fast-Ignition Scheme Fusion with Counterbeam Configuration
IFE/P5-11	Y. Arikawa	Japan	Improvement in the Heating Efficiency of Fast Ignition Inertial Confinement Fusion by Suppressing the Preformed Plasma
IFE/P5-12	H. Nagatomo	Japan	Compression and Electron Beam Heating of Solid Target under the External Magnetic Field for Fast Ignition

Id	Presenter		Title
IFE/P5-13	A. Morace	Japan	Plasma Mirror Implementation on LFEX Laser for Ion and Fast Electron Fast Ignition
IFE/P5-14	H. J. Kong	Korea, Rep. of	Coherent Beam Combination for Laser Fusion Driver Design Using Rotation Wedge Self-Phase-Controlled Stimulated Brillouin Scattering Phase Conjugation Mirrors
IFE/P5-17	K. Ishii	Japan	Present Operation Status of Target Injection System
IFE/P5-18	R. C. Issac	India	Suitability of Nano-Structured Materials for Inertial Fusion Reactor Inner Walls
IFE/P5-19	T. Norimatsu	Japan	Conceptual Design and Issue Analysis of Laser Fusion Experiment Reactor (LIFT)
MPT/P5-1	G. Tynan	USA	Experimental Study of Deuterium Retention and Thermo-Mechanical Properties in Ion-Beam Displacement-Damaged Tungsten
MPT/P5-2	S. Rogozhkin	Russian Fed.	ODS Steels: Nanostructure Evolution under Irradiation
MPT/P5-3	J. W. Coenen	Germany	Tungsten Composite Materials for Fusion First Wall Applications
MPT/P5-4	C. Linsmeier	Germany	Advanced Tungsten-Based Materials as an Option for a Fusion Reactor
MPT/P5-5	A. Kreter	Germany	Overview of Recent Plasma-Material Interaction Studies in the Linear Plasma Device PSI-2
MPT/P5-6	A. Litnovsky	Germany	Smart Tungsten Alloys as First Wall Material for a Future Fusion Power Plant
MPT/P5-7	I. Tazhibayeva	Kazakhstan	Study of Properties of Tungsten Irradiated in Hydrogen Atmosphere
MPT/P5-9	A. Kimura	Japan	Structural Material Innovation for Advanced Blanket Design: Current Status and Future Prospect of ODS Steels R&D
MPT/P5-11	H. Kondo	Japan	Validation of Liquid Lithium Target Stability for Intense Neutron Source
MPT/P5-12	X. Liu	China	Design and Fabrication of the Active Cooling Divertor Components for HL-2M Tokamak
MPT/P5-13	A. Kasugai	Japan	Progress on the Development of Linear IFMIF Prototype Accelerator and the Beam Commissioning
MPT/P5-14	M. Sakamoto	Japan	Hydrogen Isotope Retention in Tungsten Surface-Modified by Heavy Ion Irradiation, Helium Bubbles and Tungsten Deposition

Thu

Id	Presenter		Title
MPT/P5-15	M. Wirtz	Germany	Material Properties and their Influence on the Behaviour of Tungsten as Plasma Facing Material
MPT/P5-16	M. Nakajima	Japan	Assessment of Corrosion Behaviour of Reduced Activation Ferritic/Martensitic Steel, F82H in High Temperature Water
MPT/P5-17	N. Nemati	Iran	Investigation of W/Cu Functionally Graded Material with CMA Particles as Plasma Facing for First Wall Components
MPT/P5-18	T. Shimizu	Japan	Investigation of Lanthanoid-Doped APLF Scintillators for Neutron Detection
MPT/P5-19	Y. Nobuta	Japan	Effects of Modified Surfaces Produced at Plasma-Facing Surface on Hydrogen Isotopes and Helium Release Behaviour in the LHD
MPT/P5-21	T. Nagasaka	Japan	Development of Dissimilar-Metals Joint of Oxide-Dispersion-Strengthened (ODS) and Non-ODS Reduced-Activation Ferritic Steels
MPT/P5-23	A. Ito	Japan	BCA-KMC Hybrid Simulation with Meta-Modelling for Hydrogen Dynamic Retention in Tungsten Material
MPT/P5-24	Q. Huang	China	Status and Strategy of CLAM Steel for Fusion Application in China
MPT/P5-25	E. Wakai	Japan	Small Specimen Test Technology Development towards Design of Fusion DEMO Reactors and Future Direction Plan
MPT/P5-26	K. B. Woller	USA	Impact of Helium Ion Energy Modulation on Tungsten Surface Morphology and Nano-Tendrils Growth
MPT/P5-27	M. Oya	Japan	Deuterium Retention and Melting Behaviour in Toughened, Fine-Grained Recrystallized Tungsten
MPT/P5-29	H. T. Lee	Japan	Modelling Fuel Retention in Tungsten Plasma-Facing Materials under Realistic Tokamak Operation including Plasma Impurities
MPT/P5-30	M. A. Jaworski	USA	High-Temperature, Liquid Metal Plasma-Facing Component Research and Development for the NSTX-U
MPT/P5-31	Y. Oya	Japan	Effect of Defect Concentration and Distribution on Hydrogen Isotope Retention and Diffusion in Damaged W for Fusion First Wall

Id	Presenter	Country	Title
MPT/P5-32	I. E. Garkusha	Ukraine	Novel Test Bed Facility for PSI Issues in Fusion Reactor Conditions on the Base of Next Generation QSPA Plasma Accelerator
MPT/P5-33	J. M. Perlado	Spain	Multiscale Modelling of Materials: Light Species Dynamics in Nano-W and EOS of Hydrogen
MPT/P5-35	B. M. Sorbom	USA	Determination of Radiation Damage Limits to High-Temperature Superconductors in Reactor-Relevant Conditions to Inform Compact Fusion Reactor Design
MPT/P5-38	A. V. Spitsyn	Russian Fed.	Deuterium Permeation through Candidate Structural Materials for a Fusion Reactor
MPT/P5-39	L. Avotina	Latvia	Activities for Fusion Energy Functional and Plasma Facing Material Research at the University of Latvia
MPT/P5-41	F. Arbeiter	Germany	The Accomplishments of Lithium Target and Test Facility Validation Activities in the IFMIF/EVEDA Phase
MPT/P5-42	R. S. Rawat	Singapore	Investigations of Tungsten as Candidate Plasma Facing Material under High Repetition and Intense Fusion-Relevant Pulses
PDP-12	S. Jacquemot	France	Overview of some key achievements on the route to IFE

IFE/1

Inertial Fusion Experiments &
Theory

Chair: Jose Manuel Perlado (Spain)

Main Hall

(14:00 – 16:10)

Time Id	Presenter		Title
14:00 IFE/1-1	J.-L. Miquel	France	Overview of the Laser Megajoule First Experiments
14:20 IFE/1-2	S. Fujioka	Japan	Fast Ignition Inertial Confinement Fusion with Kilo-Tesla Magnetic Field
14:40 IFE/1-3	J. Frenje	USA	Observations of Residual Bulk-Fluid Motion and Low-Mode Areal-Density Asymmetries at Peak Convergence in NIF Implosions through Spectral Measurements of DD and DT Neutrons
15:00 IFE/1-4	A. Yogo	Japan	Laser-Driven Ion Acceleration on LFEX for Fast Ignition: State of the Art and Applications
15:20 IFE/1-5	H. G. Rinderknecht	USA	Ion Kinetic Dynamics in Strongly-Shocked Plasmas Relevant to ICF
15:40 IFE/1-6	J. Kawanaka	Japan	LFEX-Laser: A Multi-Kilojoule, Multi-Petawatt Heating Laser for Fast Ignition

MPT/1 and FNS/1

Summary



Materials & Fusion Nuclear Science

Chair: Takeo Muroga (Japan)

Main Hall

(16:40 – 18:45)

Time Id	Presenter		Title
16:40 MPT/1-1	R. Stoller	USA	Recent Advances in Radiation Materials Science from the US Fusion Reactor Materials Programme
17:00 MPT/1-2Ra MPT/1-2Rb	G.-N. Luo	China	Overview on Decade Development of Plasma-Facing Components at ASIPP Advances in Understanding of High-Z Material Erosion and Redeposition in Low-Z Wall Environment in DIII-D
17:20 MPT/1-3	A. Widdowson	UK	Overview of Fuel Inventory in JET with the ITER-Like Wall
17:40 FNS/1-1	Y. Shpanskiy	Russian Fed.	Status of DEMO-FNS Development
18:00 FNS/1-2	M. Gilbert	UK	Activation, Decay Heat, and Waste Classification Studies of the European DEMO Concept
18:20 FNS/1-3	Z. Xu	China	Optimizing Full-coverage Free Surface Flow for Liquid Metal PFCs

P6

Posters 6

Annex Hall

(14:00 – 18:45)

Id	Presenter	Title
EX/5-1	Z. Yan	USA Turbulence and Sheared Flow Structures Behind the Isotopic Dependence of the L-H Power Threshold and H-L Back Transition on DIII-D
EX/5-2	J. Hillesheim	UK Role of Stationary Zonal Flows and Momentum Transport for L-H Transitions in JET
EX/5-3	A. Diallo	USA Energy Exchange Dynamics across L-H Transitions in NSTX
EX/6-1	M. Garcia-Munoz	Spain The Role of Plasma Response on Fast-Ion Losses Induced by Edge 3D Fields in the ASDEX-Upgrade and DIII-D Tokamaks
EX/6-2	C. Collins	USA Critical Gradient Behaviour of Fast-Ion Transport from Alfvén Eigenmodes Guides Predictive Models for Burning Plasmas
PPC/2-1	A. Loarte	ITER Evaluation of Tungsten Transport and Concentration Control in ITER Scenarios
TH/3-1	X. Garbet	France Synergetic Effects of Collisions, Turbulence and Sawtooth Crashes on Impurity Transport
TH/4-1	R. Akers	UK High Fidelity Simulations of Fast Ion Power Flux Driven by 3D Field Perturbations on ITER
TH/4-2	A. Biancalani	Germany Gyrokinetic Investigation of the Nonlinear Interplay of Alfvén Instabilities and Energetic Particles in Tokamaks
TH/4-3	A. Bierwage	Japan First-Principle Simulations Reproduce Multiple Cycles of Abrupt Large Relaxation Events in Beam-Driven JT-60 Plasmas
EX/P6-1	M. Rubel	Sweden Fuel Inventory and Deposition in Castellated Beryllium Structures in JET
EX/P6-2	K. Heinola	Finland Long-Term Fuel Retention and Release in JET ITER-Like Wall at ITER-Relevant Baking Temperatures
EX/P6-3	D. Borodin	Germany ERO Modelling of Be Erosion in JET and Extrapolation of the Data for ITER
EX/P6-5	Y. Corre	France Thermal Analysis of Transient Tungsten Melting Experiments at JET
EX/P6-6	S. Wiesen	Germany Impact of the JET ITER-Like Wall on H-Mode Plasma Fuelling

Thu

Id	Presenter	Title
EX/P6-8	S. E. Sharapov	UK Studies of Alfvén Eigenmodes in the ITER Baseline Scenario, Sawtoothed JET Plasmas, and MAST Hydrogen-Deuterium Plasmas
EX/P6-9	R. D'Inca	Germany Multimachine Experimental Investigation of Ion Cyclotron Emission
Thu EX/P6-10	D. Van Eester	Belgium Recent Ion Cyclotron Resonance Heating Experiments in JET in Preparation of a DT Campaign
EX/P6-11	E. de la Luna	Spain Recent Results on High-Triangularity H-Mode Studies in JET-ILW
EX/P6-12	T. Tala	Finland Density Peaking in JET: Driven by Fuelling or Transport?
EX/P6-13	C. Giroud	UK Progress in Understanding the Role of Low- Z Impurity in the Confinement in JET-ILW and in JET-C Plasmas
EX/P6-14	P. Mantica	Italy Electron Heat Transport in JET from Ion to Electron Scales: Experimental Investigation and Gyro-kinetic Simulations
EX/P6-15	F. Koechl	Austria Evolution and Control of Tungsten Transport in the Termination Phase of JET H-Mode Discharges and Implications for ITER
EX/P6-16	M. Goniche	France Ion Cyclotron Resonance Heating for Tungsten Control in JET H-Mode Scenarios
EX/P6-17	M. Valisa	Italy The Role of ELMs and Inter-ELM Phases in the Transport of Heavy Impurities in JET
EX/P6-18	H. Weisen	Switzerland Neutron Yield Studies in JET H-Modes
EX/P6-19	N. Ashikawa	Japan Comprehensive Analysis of Metal Dust Particles in JET-ILW, and Impact on Fusion Reactor
EX/P6-20	J. Grzonka	Poland Detailed Survey of Dust Particles from JET with the ITER-Like Wall: Origin, Composition and Internal Structure
EX/P6-21	A. Hakola	Finland Plasma-Wall Interaction Studies in the Full-W ASDEX-Upgrade during Helium Plasma Discharges
EX/P6-22	F. Reimold	Germany Analysis of the Impact of Nitrogen- & Neon-Seeding on ASDEX-Upgrade H-Modes with SOLPS Simulations
EX/P6-23	P. Martin	Italy Physics, Control and Mitigation of Disruptions and Runaway Electrons in the EUROfusion Medium Size Tokamaks Science Programme

Id	Presenter		Title
EX/P6-24	V. Igochine	Germany	MHD Limits and Plasma Response in High- β Hybrid Operations in ASDEX-Upgrade
EX/P6-25	M. Willensdorfer	Germany	Plasma Response of External Magnetic Perturbations at the Edge: Comparisons between Measurements and 3D MHD Models
EX/P6-26	J.-M. Noterdaeme	Germany	Ion Cyclotron Range of Frequency Power Challenges and Solutions
EX/P6-27	M. Weiland	Germany	Phase-Space Resolved Measurements of the Influence of RF Heating and MHD Instabilities on the Fast-Ion Distribution in ASDEX-Upgrade
EX/P6-28	C. Hopf	Germany	Advances in Neutral Beam Current Drive Experiments on ASDEX-Upgrade
EX/P6-29	T. Pütterich	Germany	The Role of the Neoclassical E_r for the L-H Transition in ASDEX-Upgrade
EX/P6-30	E. Viezzer	Germany	Ion Heat and Toroidal Momentum Transport Studies in the H-Mode Transport Barrier of ASDEX-Upgrade
EX/P6-31	F. Clairet	France	Pedestal and Core Turbulence Dynamics Using 1 μ s Sweeping Profile Reflectometry
EX/P6-32	P. Manz	Germany	Turbulence Characteristics of the I-Mode Confinement Regime in ASDEX-Upgrade
EX/P6-33	V. V. Plyusnin	Portugal	Comparison of Runaway Electron Generation Parameters in Small, Medium-sized and Large Tokamaks: A Survey of Experiments in COMPASS, TCV, ASDEX-Upgrade and JET
EX/P6-34	J. Mlynář	Czech Republic	Losses of Runaway Electrons in MHD-Active Plasmas of the COMPASS Tokamak
EX/P6-35	M. Komm	Czech Republic	Contribution to the Multimachine Pedestal Scaling from COMPASS Tokamak
EX/P6-36	J. A. Snipes	ITER	Overview of the Preliminary Design of the ITER Plasma Control System
EX/P6-37	D. A. Humphreys	USA	Plasma Control Studies Using DIII-D Design Tools in Support of ITER
EX/P6-38	G. Pautasso	Germany	Generation of the Disruption Mitigation Trigger: Developing a Preliminary Design for ITER
EX/P6-39	M. Lehnen	ITER	Plasma Disruption Management in ITER
EX/P6-40	R. Roccella	ITER	Modelling ITER Asymmetric VDEs through Asymmetries of Toroidal Eddy Currents

Id	Presenter		Title
EX/P6-41	P. de Vries	ITER	Multimachine Analysis of Termination Scenarios, Providing the Specifications for Controlled Shutdown of ITER Discharges
EX/P6-42	A. Sips	EC	Assessment of the Baseline Scenario at $q_{95} \sim 3$ for ITER
EX/P6-44	A. Polevoi	ITER	Integrated Simulations of H-Mode Operation in ITER including Core Fuelling, Divertor Detachment and ELM Control
EX/P6-45	J. Citrin	Netherlands	Real-Time Tokamak Simulation with a First-Principle-Based Neural Network Turbulent Transport Model
EX/P6-46	C. Myers	USA	A Multimachine Analysis of Nonaxisymmetric and Rotating Halo Currents
EX/P6-47	W. Tang	USA	Big Data Machine Learning for Disruption Predictions
EX/P6-48	K. Crombe	Belgium	IShTAR: A Dedicated Facility to Characterize the Interactions between ICRF Waves and Plasma
EX/P6-49	Y. Hamada	Japan	Observation of KBM and MTM in JIPPT-IIU Tokamak Plasmas Using a Heavy Ion Beam Probe
EX/P6-50	A. Vertkov	Russian Fed.	Corrosion Compatibility of Capillary-Porous System Solid Base with Low Melting Metals Applied as Plasma Facing Materials for Tokamak
EX/P6-51	J. Mora-Meléndez	Costa Rica	First Results of the Stellarator of Costa Rica 1 (SCR-1)
EX/P6-52	A. Arakcheev	Russian Fed.	Dynamics of Tungsten Erosion under ELM-Like Intense Heat Loads
EX/P6-53	I. Furno	Switzerland	Basic Studies of Blob Dynamics in X-Point Configurations and Interaction with Suprathermal Ions in the TORPEX Device
TH/P6-1	P. Tamain	France	Progress towards Self-Consistent Treatment of Turbulence in Edge Plasma Modelling Codes
TH/P6-2	A. Hakim	USA	Scrape-Off-Layer Turbulence in Tokamaks Simulated with a Continuum Gyrokinetic Code
TH/P6-3	J. P. S. Bizarro	Portugal	Growth Estimates, Control and Structures in a Two-Field Model of the Scrape-Off Layer

Id	Presenter	Country	Title
TH/P6-4	Y. Marandet	France	The Role of Statistical Noise in Edge Plasma Transport Codes Based on Kinetic Monte Carlo Solvers for Neutrals: an Analogy with Turbulent Fluctuations
TH/P6-5	W. Choe	Korea, Rep. of	Comparison of Divertor Heat Flux Splitting by 3D Fields with Field Line Tracing Simulation in KSTAR
TH/P6-6	A. Stegmeir	Germany	The Field Line Map Approach for Simulations of Plasma Edge/SOL Turbulence
TH/P6-7	D. P. Stotler	USA	Neutral Recycling Effect on Edge ITG Turbulence and Transport
TH/P6-8	P. Ricci	Switzerland	Progress in First-Principles Simulation of SOL Plasma Turbulence and Neutral Atom Dynamics with the GBS Code
TH/P6-9	N. Mellet	France	Multiscale Modelling of Sheath Physics in Edge Transport Codes
TH/P6-10	R. Churchill	USA	Kinetic Understanding of Neoclassical Scrape-Off Layer Physics, Comparison with Fluid Modelling, and Experimental Validation
TH/P6-11	F. Effenberg	Germany	Numerical Investigation of 3D Plasma Edge Transport and Heat Fluxes including Impurity Effects in Wendelstein 7-X Startup Plasmas with EMC3-EIRENE
TH/P6-12	J. Lore	USA	Pedestal-to-Wall 3D Fluid Transport Simulations on DIII-D and NSTX
TH/P6-15	I. Katanuma	Japan	Particle Simulation on Blob Formation and Propagation in an Open System
TH/P6-16	S.-H. Ku	USA	Understanding the Blobby Turbulence in Edge Plasma from Gyrokinetic Simulation
TH/P6-17	H. Hasegawa	Japan	Impurity Transport Caused by Blob and Hole Propagations
TH/P6-18	X. Xu	USA	Nonlinear Dynamics of ELMs with E_r Shear and Collisionality Trends
TH/P6-19	T. Y. Xia	China	Divertor Heat Flux Simulations in ELMy H-Mode Discharges of EAST and Other Tokamaks
TH/P6-20	J. Huang	China	EMC3-EIRENE Simulations for the Impact of External Magnetic Perturbations on EAST Edge Plasma
TH/P6-22	A. Kirschner	Germany	Modelling of Prompt Deposition of Tungsten under Fusion Relevant Conditions

Thu

Id	Presenter	Country	Title
TH/P6-23	S. Yamoto	Japan	Kinetic Modelling of Tungsten Impurity Transport Using the IMPGYRO Code
TH/P6-24	R. Zagorski	Poland	Numerical Analyses of Baseline JT-60SA Design Concepts with the COREDIV Code
TH/P6-25	X. Tang	USA	Plasma Particle and Energy Exhaust to and Recycling at a Tungsten Surface
TH/P6-26	R. Bisson	France	Retention and Release of Hydrogen Isotopes in Tungsten Plasma Facing Components: Understanding and Controlling with an Integrated Approach
TH/P6-27	K. Ibano	Japan	Particle Simulation of Plasma Heat-Flux Dissipation by Evaporated Wall Materials
TH/P6-28	M. Campanell	USA	Strong Electron Emission Could Enable a New Plasma-Surface Interaction Regime in Divertors
TH/P6-29	S. Sangaroon	Thailand	A Model for Predicting Tritium Flux from Blanket Mock-Up in Tokamak Fusion Reactors
TH/P6-30	J. Ghosh	India	Investigation of Neutral Particle Dynamics in ADITYA Tokamak Plasma with DEGAS2 Code
TH/P6-31	M. M. Tsventoukh	Russian Fed.	Plasma-Surface Interactions Leading to Self-Sustained Discharges at the First Wall
TH/P6-32	B. LaBombard	USA	Assessment of X-Point Target Divertor Configuration for Power Handling and Detachment Front Control

Summary

EX/7 and TH/5**RF & SOL Physics**

Chair: Yong Liu (China)

Main Hall

(08:30 – 10:15)

Time Id	Presenter		Title
08:30 TH/5-1	P. T. Bonoli	USA	Novel Reactor Relevant RF Actuator Schemes for the Lower Hybrid and the Ion Cyclotron Range of Frequencies
08:50 EX/7-1	G. M. Wallace	USA	Influence of the Scrape-Off Layer on RF Actuator Performance
09:10 EX/7-2	T. Oishi	Japan	Observation of Carbon Impurity Flow in the Edge Stochastic Magnetic Field Layer of Large Helical Device and its Impact on the Edge Impurity Control
09:30 EX/7-3Ra	B. Sieglin	Germany	Assessment of Divertor Heat Load with and without External Magnetic Perturbation
EX/7-3Rb			Elimination of the Nonaxisymmetric Inter-ELM Heat Flux Generated by Resonant Magnetic Perturbations in Detached Divertor Conditions
09:50 TH/5-2	N. K. Bisai	India	Role of Neutral Gas in Scrape-Off Layer of Tokamak Plasmas

Summary

EX/8 and TH/6**Turbulence & Transport**

Chair: Gary M. Staebler (USA)

Main Hall

(10:45 – 12:30)

Time Id	Presenter		Title
10:45 EX/8-1	M. Yoshida	Japan	Magnetic Shear Effects on Plasma Transport and Turbulence at High Electron to Ion Temperature Ratio in DIII-D and JT-60U Plasmas
11:05 TH/6-1	C. Holland	USA	Demonstrating the Multiscale Nature of Electron Transport through Experimentally Validated Simulations
11:25 TH/6-2	A. Ishizawa	Japan	Multimachine Analysis of Turbulent Transport in Helical Systems via Gyrokinetic Simulation
11:45 TH/6-3	J. Garcia	France	Electromagnetic Gyrokinetic Analysis of the Isotope Effect
12:05 EX/8-2	D. Yu	China	Ion Internal Transport Barrier in Neutral Beam Heated Plasmas on HL-2A

P7		Posters 7	
		<i>Annex Hall</i>	(08:30 – 12:30)
Id	Presenter		Title
EX/9-1	E. Joffrin	France	Disruption Study Advances in the JET Metallic Wall
EX/9-2	N. Commaux	USA	Shattered Pellet Injection as the Primary Disruption Mitigation Technique for ITER
EX/9-3	Y. Liu	China	Mitigation of Runaway Current with Supersonic Molecular Beam Injection on HL-2A Tokamak
EX/9-4	G. Papp	Germany	Runaway Electron Generation and Mitigation on the European Medium Sized Tokamaks ASDEX-Upgrade and TCV
EX/10-1	A. Bortolon	USA	Effectiveness of High-Frequency ELM Pacing with D ₂ and Nonfuel Pellets in DIII-D
EX/10-2	G. Xu	China	ELM Pace-Making and Long-Pulse ELM-Stable H-Mode Operation with LHCD in EAST
EX/10-3	G. Yun	Korea, Rep. of	Edge-Localized Modes on KSTAR: Global Structure and Distinct Evolution Stages Involving Quasi-Steady State and Phase Transitions
FNS/1-1	Y. Shpanskiy	Russian Fed.	Status of DEMO-FNS Development
FNS/1-2	M. Gilbert	UK	Activation, Decay Heat, and Waste Classification Studies of the European DEMO Concept
FNS/1-3	Z. Xu	China	Optimizing Full-coverage Free Surface Flow for Liquid Metal PFCs
IFE/1-1	J.-L. Miquel	France	Overview of the Laser Megajoule First Experiments
IFE/1-2	S. Fujioka	Japan	Fast Ignition Inertial Confinement Fusion with Kilo-Tesla Magnetic Field
IFE/1-3	J. Frenje	USA	Observations of Residual Bulk-Fluid Motion and Low-Mode Areal-Density Asymmetries at Peak Convergence in NIF Implosions through Spectral Measurements of DD and DT Neutrons
IFE/1-4	A. Yogo	Japan	Laser-Driven Ion Acceleration on LFEX for Fast Ignition: State of the Art and Applications
IFE/1-5	H. G. Rinderknecht	USA	Ion Kinetic Dynamics in Strongly-Shocked Plasmas Relevant to ICF

Id	Presenter	Country	Title
IFE/1-6	J. Kawanaka	Japan	LFEX-Laser: A Multi-Kilojoule, Multi-Petawatt Heating Laser for Fast Ignition
MPT/1-1	R. Stoller	USA	Recent Advances in Radiation Materials Science from the US Fusion Reactor Materials Programme
MPT/1-2Ra	G. N. Luo	China	Overview on Decade Development of Plasma-Facing Components at ASIPP
MPT/1-2Rb	R. Ding	USA	Advances in Understanding of High-Z Material Erosion and Redeposition in Low-Z Wall Environment in DIII-D
MPT/1-3	A. Widdowson	UK	Overview of Fuel Inventory in JET with the ITER-Like Wall
TH/7-1	S. Konovalov	Russian Fed.	Assessment of the Runaway Electron Energy Dissipation in ITER
TH/7-2	L. Xue	China	Effect of the Second X-Point on the Hot VDE for HL-2M
TH/8-1	N. Aiba	Japan	Diamagnetic MHD Equations for Plasmas with Fast Flow and its Application to ELM Analysis in JT-60U and JET-ILW
TH/8-2	S. Pamela	UK	Multimachine Modelling of ELMs and Pedestal Confinement: From Validation to Prediction
TH/8-3	H. Jhang	Korea, Rep. of	Excitation of Zonal Flows and their Impact on Dynamics of Edge Pedestal Collapse
EX/P7-1	Y. Peysson	France	Experiments and Modelling towards Long Pulse High Confinement Operation with Radiofrequency Heating and Current Drive in EAST
EX/P7-2	X. Gao	China	Key Issues towards Long Pulse High β_N Operation on EAST Tokamak
EX/P7-4	Y. Sun	China	ELM Suppression Using Resonant Magnetic Perturbation in EAST
EX/P7-5	B. J. Ding	China	Recent Experimental and Modelling Advances in the Understanding of Lower Hybrid Current Drive in ITER-Relevant Regimes
EX/P7-7	B. Lyu	China	Experimental Study of Radio-Frequency Driven Spontaneous Rotation for High-Performance Plasmas on EAST
EX/P7-8	X. J. Zhang	China	Heating and Confinements by the Waves in the Ion Cyclotron Range of Frequencies on EAST

Id	Presenter		Title
EX/P7-9	X. Y. Gong	China	Current Drive with Combined Electron Cyclotron Wave and High Harmonic Fast Wave in Tokamak Plasmas
EX/P7-10	L. Wang	China	Evidence and Modelling of 3D Divertor Footprint Induced by Lower Hybrid Waves on EAST with Tungsten Divertor Operations
EX/P7-12	X. D. Zhang	China	Fishtail Divertor: A New Divertor Concept on EAST for Active Control of Heat Load on Divertor Plate
EX/P7-15	G. Li	China	Predictions of the Baseline Operation Scenario in Chinese Fusion Engineering Test Reactor
EX/P7-16	W. X. Ding	USA	Current Transport and Density Fluctuations at L-H Transition on EAST
EX/P7-17	W. Chen	China	Kinetic Alfvén-Ballooning Instabilities in Tokamak Plasmas with Weak Magnetic Shears and Low-Pressure Gradients
EX/P7-19	X. Q. Ji	China	Experimental Investigation of Interaction between Turbulence and Large-Scale Mode Structures in HL-2A
EX/P7-21	Z. Y. Cui	China	Study of Impurity Transport in the HL-2A ECRH Plasmas with MHD Instabilities
EX/P7-22	Z. B. Shi	China	Role of SMBI Deposition in ELM Mitigation and the Underlying Turbulence Characteristics
EX/P7-24	J. Dong	China	Roles of an Inward Particle Flux Inducing Quasi-Mode in Pedestal Dynamics on HL-2A Tokamak
EX/P7-25	M. Xu	China	Direct Measurement of ELM Related Momentum Transport in the Edge of HL-2A H-Mode Plasmas
EX/P7-27	L. W. Yan	China	Synchronization of GAMs and Magnetic Fluctuations on HL-2A Tokamak
EX/P7-29	Y. Xu	China	Investigation of Mechanisms for the Generation of Blobs/Holes at the Boundary of the HL-2A Tokamak
EX/P7-30	M. Xu	China	Experimental Evaluation of Langmuir Probe Sheath Potential Coefficient
EX/P7-34	A. Ekedahl	France	First Experiments in H-Mode Plasmas with the Passive-Active Multijunction LHCD Launcher in HL-2A and Impact on Pedestal Instabilities

Id	Presenter		Title
EX/P7-35	F. Deeba	Pakistan	Spectroscopic Studies on GLAST-III Tokamak by Varying the Inductance and Charging Voltage of Vertical Field Coils
EX/P7-36	A. Malaquias	Portugal	Studies on ISTTOK during Edge Electrode Biasing Assisted AC Operation
EX/P7-38	J. Stockel	Czech Republic	Contribution of Joint Experiments on Small Tokamaks in the Framework of IAEA Coordinated Research Projects to Mainstream Fusion Research
EX/P7-39	C. Xiao	Canada	Modification of Toroidal Flow Velocity through Momentum Injection by Compact Torus Injection into the STOR-M Tokamak Discharge
EX/P7-40	S. Lebedev	Russian Fed.	High Frequency Magnetic Oscillations in the TUMAN-3M Ohmically Heated Plasmas
EX/P7-41	S. I. Lashkul	Russian Fed.	Effect of the Transition to Improved Core Confinement Observed in the LHCD Experiment at FT-2 Tokamak
EX/P7-42	A. Shevelev	Russian Fed.	Runaway Electrons Studies with Hard X-Ray and Microwave Diagnostics in the FT-2 Low-Hybrid Current Drive Discharges
EX/P7-43	D. A. Maurer	USA	Control of Sawtooth Oscillation Dynamics Using Externally Applied Stellarator Transform
EX/P7-44	C. Hidalgo	Spain	On the Influence of ECRH on Neoclassical and Anomalous Mechanisms Using a Dual Heavy Ion Beam Probe Diagnostic in the TJ-II Stellarator
EX/P7-45	T. Estrada	Spain	Plasma Flow, Turbulence and Magnetic Islands in TJ-II
EX/P7-47	K. J. McCarthy	Spain	Plasma Core Fuelling by Cryogenic Pellet Injection in the TJ-II Stellarator
EX/P7-48	D. López-Bruna	Spain	Confinement Modes and Magnetic-Island Driven Modes in the TJ-II Stellarator
FIP/P7-1	T. Brown	USA	Development of a 3 m HTS FNSF Device and the Qualifying Design and Engineering R&D Needed to Meet the Low AR Design Point
FIP/P7-2	J. Miyazawa	Japan	REVOLVER-D: The Ergodic Limiter/Divertor Consisting of Molten Tin Shower Jets Stabilized by Chains

Id	Presenter		Title
FIP/P7-3	G. Neilson	USA	Progress in K-DEMO Heating/Current Drive and Tokamak Configuration Development
FIP/P7-4	G. Grossetti	Germany	DEMO Port Plug Design and Integration Studies
FIP/P7-5	P. Sonato	Italy	Conceptual Design of the DEMO NBIs: Main Developments and R&D Achievements
FIP/P7-6	D. G. Whyte	USA	Smaller & Sooner: Exploiting High Magnetic Fields from New Superconductors for a More Attractive Fusion Energy Development Path
FIP/7-7	M. Q. Tran	Switzerland	EU DEMO Heating and Current Drive: Physics and Technology
FIP/P7-8	G. Granucci	Italy	Conceptual Design of the DEMO EC-System: Main Developments and R&D Achievements
FIP/P7-9	F. Warmer	Germany	Integrated Concept Development of Next-Step Helical-Axis Advanced Stellarators
FIP/P7-10	L. Zani	France	Evolutions of EU DEMO Reactor Magnet System Design Along the Recent Years and Lessons Learned for the Future
FIP/P7-11	N. Yanagi	Japan	Helical Coil Design and Development with 100 kA HTS STARS Conductor for FFHR-d1
FIP/P7-12	F. Crisanti	Italy	DTT: An Integrated Bulk and Edge Plasma Experiment to Tackle the Power Exhaust Problem in View of DEMO
FIP/P7-13	J.-M. Noterdaeme	Germany	Ion Cyclotron Range of Frequency Power for DEMO
FIP/P7-14	R. Wenninger	Germany	Power Handling and Plasma Protection Aspects that Affect the Design of the DEMO Divertor and First Wall
FIP/P7-15	J. Park	Korea, Rep. of	Nuclear Analysis of Structural Damage and Nuclear Heating on Enhanced K-DEMO Divertor Model
FIP/P7-16	M. Rozenkevich	Russian Fed.	Concept of Tritium Processing and Confinement in Fuel Cycle of Ignitor
FIP/P7-17	C. Danani	India	Zero D and 1.5D Transport Analysis of SST-2
FIP/P7-18	M. Velarde	Spain	Multiscale Integral Analysis of Tritium Leakages in Fusion Power Plants
FIP/P7-19	M. Gryaznevich	UK	Overview and Status of Construction of ST40

Id	Presenter		Title
FIP/P7-20	W. Morris	UK	Approaches for the Qualification of Exhaust Solutions for DEMO-Class Devices
FIP/P7-21	C. Reux	France	DEMO Design Using the SYCOMORE System Code: Conservative Designs and Pathways towards the Reactor
FIP/P7-22	N. Asakura	Japan	Physics and Engineering Design Studies on Power Exhaust and Divertor for a 1.5 GW Fusion Power DEMO
FIP/P7-24	J. Agarwal	India	Progress towards Achieving Large Pumping Speed for Exhaust from Fusion Grade Machines
FIP/P7-25	C. Danani	India	Nuclear Design Analyses of SST-2
FIP/P7-26	G. Stankunas	Lithuania	Comparative Analysis of WCLL to Different European DEMO Blanket Concepts in Terms of Activation and Decay Heat after Exposure to Neutron Irradiation
FIP/P7-27	M. Ferrari	F4E	How Tokamak Interface Requirements Are Driving the Design of TBM Systems in ITER towards Breeding Blanket Design in DEMO
FIP/P7-29	G. Aiello	France	Design of the Helium-Cooled Lithium-Lead Breeding Blanket in CEA: From TBM to DEMO
FIP/P7-31	A. Saraswat	India	Overview of Indian LLCB TBM Programme and Status of R&D Activities
FIP/P7-33	S. S. Ananyev	Russian Fed.	DT Fuel System of DEMO-FNS Tokamak with Tritium Breeding Blanket
FIP/P7-34	D. Schissel	USA	Remote Third Shift EAST Operation: A New Paradigm
FIP/P7-35	M. Yokoyama	Japan	Extended Capability of the Integrated Transport Analysis Suite, TASK3D-a, for LHD Experiment, and its Impacts on Facilitating Stellarator-Heliotron Research
FIP/P7-36	R. Lunsford	USA	ELM Pacing with High Frequency Multispecies Impurity Granule Injection in NSTX-U H-Mode Discharges
FIP/P7-37	J.-C. Vallet	France	Towards the Completion of the CEA Contributions to the Broader Approach Projects
FIP/P7-38	S. Pradhan	India	Techno-Economic Aspects of High Current Leads for Fusion Devices
FIP/P7-39	E. Villedieu	France	The Articulated Inspection Arm Development
FIP/P7-40	P. Khvostenko	Russian Fed.	Status of Tokamak T-15MD

Id	Presenter		Title
FIP/P7-41	V. Minaev	Russian Fed.	Spherical Tokamak Globus-M2: Design, Integration, Construction
FIP/P7-42	R. Raman	USA	NSTX-U Contributions to Disruption Mitigation Studies in Support of ITER
FIP/P7-43	R. R. Khayrutdinov	Russian Fed.	Development of Regulators Synthesis Method for Magnetic Plasma Control System of the T-15 Tokamak
FIP/P7-44	O. A. Muñoz Ovalle	Mexico	Reciprocating Langmuir Probes Set Design for the Mexican Tokamak "T"
FIP/P7-45	Q. Zhang	China	Upgrade and Operational Performance of EAST Cryogenic System
FIP/P7-46	J. Agarwal	India	India's Pellet Fuelling Programme
FIP/P7-47	S. Banerjee	India	Design of Charge Exchange Recombination Spectroscopy (CXRS) on SST-1 Tokamak
SEE/P7-1	K. Gi	Japan	Assessment of Potential and Breakeven Prices of Fusion Power Plants under Low-Carbon Development Scenarios
SEE/P7-2	X. Z. Jin	Germany	Proposal of the Confinement Strategy for EU DEMO
SEE/P7-3	A. Prades	Spain	Social Research on Fusion
SEE/P7-4	H. Cabal	Spain	Exploration of Fusion Power Penetration under Different Global Energy Scenarios Using the EFDA Times Energy Optimization Model
SEE/P7-5	Y. Someya	Japan	Safety and Waste Management Studies as Design Feedback for a Fusion DEMO Reactor in Japan
SEE/P7-6	S. Konishi	Japan	Future Electric Market and Fusion Deployment Strategy with Electricity Storage Systems

[Summary](#)**EX/9 and TH/7****Disruptions**

Chair: Abhijit Sen (India)

*Main Hall***(14:00 – 16:10)**

Time Id	Presenter		Title
14:00 EX/9-1	E. Joffrin	France	Disruption Study Advances in the JET Metallic Wall
14:20 EX/9-2	N. Commaux	USA	Shattered Pellet Injection as the Primary Disruption Mitigation Technique for ITER
14:40 EX/9-3	Y. Liu	China	Mitigation of Runaway Current with Supersonic Molecular Beam Injection on HL-2A Tokamak
15:00 TH/7-1	S. Konovalov	Russian Fed.	Assessment of the Runaway Electron Energy Dissipation in ITER
15:20 EX/9-4	G. Papp	Germany	Runaway Electron Generation and Mitigation on the European Medium Sized Tokamaks ASDEX-Upgrade and TCV
15:40 TH/7-2	L. Xue	China	Effect of the Second X-Point on the Hot VDE for HL-2M

[Summary](#)**EX/10 and TH/8****ELMs Suppression & Dynamics**

Chair: Hyeon K. Park (Rep. Korea)

*Main Hall***(16:40 – 18:45)**

Time Id	Presenter		Title
16:40 EX/10-1	A. Bortolon	USA	Effectiveness of High-Frequency ELM Pacing with D ₂ and Nonfuel Pellets in DIII-D
17:00 EX/10-2	G. Xu	China	ELM Pace-Making and Long-Pulse ELM-Stable H-Mode Operation with LHCD in EAST
17:20 EX/10-3	G. S. Yun	Korea, Rep. of	Edge-Localized Modes on KSTAR: Global Structure and Distinct Evolution Stages Involving Quasi-Steady State and Phase Transitions
17:40 TH/8-1	N. Aiba	Japan	Diamagnetic MHD Equations for Plasmas with Fast Flow and its Application to ELM Analysis in JT-60U and JET-ILW
18:00 TH/8-2	S. Pamela	UK	Multimachine Modelling of ELMs and Pedestal Confinement: From Validation to Prediction
18:20 TH/8-3	H. Jhang	Korea, Rep. of	Excitation of Zonal Flows and their Impact on Dynamics of Edge Pedestal Collapse

Fri

P8 **Posters 8** *Annex Hall* **(14:00 – 18:45)**

Id	Presenter		Title
EX/7-1	G. M. Wallace	USA	Influence of the Scrape-Off Layer on RF Actuator Performance
EX/7-2	T. Oishi	Japan	Observation of Carbon Impurity Flow in the Edge Stochastic Magnetic Field Layer of Large Helical Device and its Impact on the Edge Impurity Control
EX/7-3Ra	B. Sieglin	Germany	Assessment of Divertor Heat Load with and without External Magnetic Perturbation
EX/7-3Rb	A. Briesemeister	USA	Elimination of the Nonaxisymmetric Inter-ELM Heat Flux Generated by Resonant Magnetic Perturbations in Detached Divertor Conditions
EX/8-1	M. Yoshida	Japan	Magnetic Shear Effects on Plasma Transport and Turbulence at High Electron to Ion Temperature Ratio in DIII-D and JT-60U Plasmas
EX/8-2	D. Yu	China	Ion Internal Transport Barrier in Neutral Beam Heated Plasmas on HL-2A
EX/11-1	B. A. Grierson	USA	Validation of Theoretical Models of Intrinsic Torque in DIII-D and Projection to ITER by Dimensionless Scaling
FIP/3-1Ra	H. Tanigawa	Japan	Accomplishment of DEMO R&D Activity of IFERC Project in BA Activity and Strategy toward DEMO
FIP/3-1Rb	R. Hiwatari	Japan	Progress of Conceptual Design Study on Japanese DEMO
FIP/3-2	R. Kemp	UK	Dealing with Uncertainties in Fusion Power Plant Conceptual Development
FIP/3-3	J. Kang	Korea, Rep. of	Development of a Systematic, Self-Consistent Algorithm for K-DEMO Steady-State Operation Scenario
FIP/3-4Ra	A. Sagara	Japan	Two Conceptual Designs of Helical Fusion Reactor FFHR-d1A Based on ITER Technologies and Challenging Ideas
FIP/3-4Rb	H. Hashizume	Japan	Development of Remountable Joints and Heat Removable Techniques for High-temperature Superconducting Magnets

Id	Presenter	Country	Title
FIP/3-4Rc	K. Takahata	Japan	Lessons Learned from the Eighteen-Year Operation of the LHD Poloidal Coils Made from CIC Conductors
FIP/3-5	P. Bruzzone	Switzerland	High Temperature Superconductors for Fusion at the Swiss Plasma Center
FIP/4-1Ra	Y. Shibama	Japan	Assembly Technologies of the Superconducting Tokamak on JT-60SA
FIP/4-1Rb	P. Decool	France	JT-60SA TF Coil Manufacture, Test and Preassembly by CEA
TH/6-1	C. Holland	USA	Demonstrating the Multiscale Nature of Electron Transport through Experimentally Validated Simulations
TH/6-2	A. Ishizawa	Japan	Multimachine Analysis of Turbulent Transport in Helical Systems via Gyrokinetic Simulation
TH/6-3	J. Garcia	France	Electromagnetic Gyrokinetic Analysis of the Isotope Effect
TH/9-1	O. Meneghini	USA	Development of a First-Principles Self-Consistent Core-Pedestal Model and its Application to ITER
TH/5-1	P. T. Bonoli	USA	Novel Reactor Relevant RF Actuator Schemes for the Lower Hybrid and the Ion Cyclotron Range of Frequencies
TH/5-2	N. K. Bisai	India	Role of Neutral Gas in Scrape-Off Layer of Tokamak Plasmas
EX/P8-1	Y. Yoshimura	Japan	Progress of Steady State Operation Using RF Heating in the LHD
EX/P8-2	T. I. Tsujimura	Japan	Impact of the LHD Peripheral Region and the Magnetic Axis Shift on Optimal On-Axis ECRH Injection for High-Electron-Temperature Plasmas
EX/P8-3	G. Motojima	Japan	Global Particle Balance and its Relationship with the Plasma Wall Interaction Emerging in Long Pulse Discharges on the Large Helical Device
EX/P8-4	Y. Nakamura	Japan	Strong Suppression of Impurity Accumulation in Steady-State Hydrogen Discharges with High Power NBI Heating on LHD
EX/P8-5	X. Huang	Japan	Formation of Impurity Transport Barrier in LHD Plasmas with Hollow Density Profile

Id	Presenter		Title
EX/P8-6	B. Peterson	Japan	Experimental Observations and Modelling of Poloidal Asymmetries in Radiation Profiles during N ₂ Seeding Compared with Ne Seeding in LHD
EX/P8-7	K. Ida	Japan	Flow Damping Due to the Stochastization of Magnetic Field in Large Helical Device
EX/P8-8	Y. Narushima	Japan	Observations of Sustained Phase Shifted Magnetic Islands from Externally Imposed $m/n = 1/1$ RMP in LHD
EX/P8-9	T. Tokuzawa	Japan	Magnetic Island Formation in Locked-Like Mode in Helical Plasmas
EX/P8-10	S. Ohdachi	Japan	Observation of the Ballooning Mode that Limits the Operation Space of the High-Density Superdense-Core Plasma in the LHD
EX/P8-11	K. Tanaka	Japan	Improvements of Ion Energy Confinement in Helium Rich Plasma of LHD
EX/P8-12	X. D. Du	Japan	Stabilization of the Helically Trapped Energetic Ions Driven Resistive Interchange Mode by On-Axis Electron-Cyclotron Heating in a Helical Plasma
EX/P8-13	T. Ido	Japan	Abrupt Excitation of Intense Geodesic Acoustic Mode in the LHD
EX/P8-14	D. Kato	Japan	Observation of Visible Forbidden Lines of Tungsten Highly Charged Ions in LHD Core Plasmas and its Application to Ion Distribution Analysis
EX/P8-16	T. Minami	Japan	Role of Magnetic Topology to Form Electron Internal Transport Barrier on Heliotron J
EX/P8-17	S. Kobayashi	Japan	Study of H-Mode Transition Triggered by High-Intensity Gas Puffing in NBI Plasmas of Heliotron J
EX/P8-18	H. Okada	Japan	Fast Ion Generation by Combination Heating of ICRF and NBI in Heliotron J
EX/P8-19	K. Nagasaki	Japan	Suppression of Alfvén Eigenmodes by ECH/ECCD in Heliotron J
EX/P8-20	S. Ohshima	Japan	Isotope Effects on Long Range Correlation and the Nonlinear Coupling with Turbulence in Heliotron J
EX/P8-21	G. Mazzitelli	Italy	Liquid Metal Experiments on FTU
EX/P8-22	D. Carnevale	Italy	Analysis of Runaway Beam Suppression Experiments in FTU

Id	Presenter		Title
EX/P8-23	A. Bruschi	Italy	Observation of Short Time-Scale Spectral Emissions at Millimetre Wavelengths with the New CTS Diagnostic on the FTU Tokamak
EX/P8-24	O. Tudisco	Italy	Evidence of Thermo-Diffusive Pinch in Particle Transport
EX/P8-25	B. Labit	Switzerland	The Physics of the Heat Flux Narrow Decay Length in the TCV Scrape-Off Layer: Experiments and Simulations
EX/P8-26	N. Vianello	Italy	On Filamentary Transport in the TCV Tokamak: Addressing the Role of the Parallel Connection Length
EX/P8-27	B. Esposito	Italy	First Experimental Results of Runaway Beam Control in TCV
EX/P8-28	T. P. Goodman	Switzerland	Scattering of EC Waves by Edge Turbulence: Measurements and Modelling in TCV and TORPEX
EX/P8-29	B. Duval	Switzerland	Neutral Beam Heating on the TCV Tokamak
EX/P8-30	B. Geiger	Germany	Study of the Fast-Ion Distribution Function in the TCV Tokamak Based on FIDA Spectroscopy and the TRANSP Code
EX/P8-31	D. Douai	France	Development of Helium Electron Cyclotron Wall Conditioning on TCV for the Operation of JT-60SA
EX/P8-32	C. Galperti	Switzerland	Distributed Digital Real-Time Control System for the TCV Tokamak and its Applications
EX/P8-33	F. Felici	Netherlands	Real-Time Model-Based Plasma State Estimation, Monitoring and Integrated Control in TCV, ASDEX-Upgrade and ITER
EX/P8-34	A. Melnikov	Russian Fed.	Study of Interactions between GAMs and Broadband Turbulence in the T-10 Tokamak
EX/P8-35	P. Savrukhin	Russian Fed.	Disruptions and Runaway Mitigation Using ECRH and Inductive Power Supply Systems in the T-10 Tokamak
EX/P8-36	M. Nurgaliev	Russian Fed.	Study of Light and Heavy Impurities Transport in OH and ECRH Plasmas on the T-10 Tokamak
EX/P8-37	I. Lyublinski	Russian Fed.	Lithium and Tungsten Limiters for 3 MW of ECR Plasma Heating in T-10 Tokamak: Design, First Results

Id	Presenter		Title
EX/P8-38	T. Wakatsuki	Japan	Reduction of CS Flux Consumption during Plasma Current Ramp-Up on DEMO Reactor
EX/P8-39	T. Goto	Japan	Development of a Real-Time Simulation Tool towards Self-Consistent Scenario of Plasma Startup and Sustainment on Helical Fusion Reactor FFHR-d1
EX/P8-40	G. Giruzzi	France	Physics and Operation Oriented Activities in Preparation of the JT-60SA Tokamak Exploitation
EX/P8-41	S. Brezinsek	Germany	Preparation of PFCs for the Efficient Use in ITER and DEMO: Plasma-Wall Interaction Studies within the EUROfusion Consortium
EX/P8-42	Y. Nakashima	Japan	Recent Progress of Divertor Simulation Research Using the GAMMA 10/PDX Tandem Mirror
EX/P8-43	R. Ikezoe	Japan	Spatial Structure of Spontaneously Excited ICRF Waves and Relevant High-Energy Ion Loss in the GAMMA 10 Tandem Mirror
EX/P8-44	Y. Hayashi	Japan	Investigation of Detached Recombining Plasmas in a Linear Device Pilot-PSI and its Impact on Plasma Detachment in Fusion Devices
EX/P8-45	A. Burdakov	Russian Fed.	Development of Experiment on Multiple-Mirror Trap for Fusion in Budker INP
EX/P8-46	P. Bagryansky	Russian Fed.	Progress of Plasma Confinement Studies in the Gas Dynamic Trap
PDP-02	I. M. Ferreira Nunes	Portugal	First Results from Recent JET Experiments in Hydrogen and Hydrogen-Deuterium Plasmas
PDP-03	N. Gorelenkov	USA	Suppression of Alfvén modes through additional beam heating
PDP-04	J. Stober	Germany	Advanced Tokamak Experiments in Full-W ASDEX Upgrade
PDP-05	M. J. Hole	Australia	Fluid Models for Burning and 3D Plasmas: Challenging the Kinetic Paradigm
PDP-07	S. Takamura	Japan	Microwrinkle Structure on Refractory Metal Surfaces Irradiated by Noble Gas Plasma Species
PDP-08	S. Wiesen	Germany	The Effect of the Isotope on the H-Mode Density Limit

Id	Presenter	Country	Title
PDP-09	R. Goldston	USA	Recent Advances towards a Lithium Vapor Box Divertor
PDP-10	B. Breizman	USA	Chirping in Plasmas; Test of Criterion for Chirping Onset and Simulation of Explosive Chirping
PDP-11	M. Inomoto	Japan	Formation of Closed Flux Surfaces in Reconnection Current Layer by Accelerated Electrons during Merging Start-up of Spherical Tokamak
PDP-13	J. Anderson	Sweden	Statistical Description of Turbulent Transport for Flux Driven Toroidal Plasmas
PDP-14	M. Wischmeier	Germany	Facing the Challenge of Power Exhaust on the way to a Future Power Plant with Experiments in the JET and ASDEX Upgrade Tokamaks
PDP-15	S. Newton	Sweden	Impurity Transport and Plasma Flow in a Mixed Collisionality Stellarator Plasma
PDP-16	N. Fukumoto	Japan	Advanced Fuelling in Spherical Tokamak by Compact Toroid Injection on QUEST
PDP-18	N. Kargin	Russian Fed.	Metal Hall Sensors for the New Generation Reactors of the DEMO Scale
PDP-19	Y. Igitkhanov	Germany	Effect of Divertor Performance on the Pumping Efficiency in DEMO
PDP-21	C. Corr	Australia	Helium Ion Energy Threshold for Helium Retention and Nano-bubble Formation in Tungsten
PDP-23	A. Portone	Fusion For Energy (European Commission)	Active and Passive Stabilization of $n = 0$ RWMs in Future Tokamak Devices
PDP-24	R. Srivastava	India	Collisional Radiative Model Using the Fully Relativistic Cross-sections for the Hydrogen-cesium Plasma Relevant to ITER Negative Ion Based NBI System
PDP-25	V. Kornev	Russian Fed.	DD Neutron Emission Measurement in the Compact Tokamak TUMAN-3M
PDP-26	M. Probst	Austria	Electron-Impact Ionization Cross Sections of Molecules and Ions in Fusion Plasma

Summary

**DEMO Technology****FIP/3**

Chair: Elizabeth Surrey (UK)

*Main Hall***(08:30 – 10:15)**

Time Id	Presenter		Title
08:30 FIP/3-1Ra	H. Tanigawa	Japan	Accomplishment of DEMO R&D Activity of IFERC Project in BA Activity and Strategy toward DEMO
	FIP/3-1Rb		Progress of Conceptual Design Study on Japanese DEMO
08:50 FIP/3-2	R. Kemp	UK	Dealing with Uncertainties in Fusion Power Plant Conceptual Development
09:10 FIP/3-3	J. Kang	Korea, Rep. of	Development of a Systematic, Self-Consistent Algorithm for K-DEMO Steady-State Operation Scenario
09:30 FIP/3-4Ra	A. Sagara	Japan	Two Conceptual Designs of Helical Fusion Reactor FFHR-d1A Based on ITER Technologies and Challenging Ideas
	FIP/3-4Rb		Development of Remountable Joints and Heat Removable Techniques for High-Temperature Superconducting Magnets
	FIP/3-4Rc		Lessons Learned from the Eighteen-Year Operation of the LHD Poloidal Coils Made from CIC Conductors
09:50 FIP/3-5	P. Bruzzone	Switzerland	High Temperature Superconductors for Fusion at the Swiss Plasma Center

Summary

**EX/11, TH/9, FIP/4, PD****Transport, Construction and PD**

Chair: Richard Hawryluk (USA)

*Main Hall***(10:45 – 12:30)**

Time Id	Presenter		Title
10:45 TH/9-1	O. Meneghini	USA	Development of a First-Principles Self-Consistent Core-Pedestal Model and its Application to ITER
11:05 EX/11-1	B. A. Grierson	USA	Validation of Theoretical Models of Intrinsic Torque in DIII-D and Projection to ITER by Dimensionless Scaling

Time Id	Presenter		Title
11:25 FIP/4-1Ra	Y. Shibama	Japan	Assembly Technologies of the Superconducting Tokamak on JT-60SA
FIP/4-1Rb			JT-60SA TF Coil Manufacture, Test and Preassembly by CEA
11:45 PD/1-1	R. Nazikian	USA	First Observation of ELM Suppression in ASDEX-Upgrade in a Similarity Experiment with DIII-D
12:05 PD/1-2	H.-S. Bosch	Germany	Final Integration, Commissioning and Start of the Wendelstein 7-X Stellarator Operation

Sat

S/1

Summary 1

Chair: Boris Kuteev (Russian. Fed.)

Main Hall

(14:00 – 16:00)

Time Id	Presenter		Title
14:00 NF	S. Le Masurier	IAEA	The Nuclear Fusion Prize
14:20 S/1-1	Y. Kamada	Japan	Summary EX/C, EX/S & PPC
14:50 S/1-2	D. Hill	USA	Summary EX/D, EX/W & ICC
15:20 S/1-3	S. Konovalov	Russian Fed.	Summary Magnetic Confinement Theory

S/2

Summary 2

Chair: Alain Bécoulet (France)

Main Hall

(16:30 – 18:00)

Time Id	Presenter		Title
16:30 S/2-1	S. Jacquemot	France	Summary Inertial Fusion Experiments and Theory
17:00 S/2-1	J. Li	China	Summary FIP, FNS, MPT & SEE
17:30 S/2-3	IAEA Representative	IAEA	Closing Address
17:50 S/2-4	Host Country Representative	Japan	Conference Closing

Contents

Introduction	1
Programme Committee	2
Conference Secretariat	3
Overview of Contributions	6
Explanation of Abbreviations	6
Timetable	9
Monday 17 October 2016	10
Tuesday 18 October 2016	14
Wednesday 19 October 2016	22
Thursday 20 October 2016	38
Friday 21 October 2016	53
Saturday 22 October 2016	68
Abstracts	123
O/1: Opening Plenary	123
O/1-4 A. Iiyoshi, Fusion for Sustainable World Development	124
O/1-5 F. Portero, The Strategic Dimensions of the Fusion Energy Challenge	125
OV: Overviews	127
OV/1-1 Y. Takeiri, Extension of Operational Regime of LHD towards Deuterium Experiment	128
OV/1-2 B. Bigot, Progress in ITER Construction, Manufacturing and R&D	129
OV/1-3 W. M. Solomon, DIII-D Research Advancing the Scientific Basis for Burning Plasmas and Fusion Energy	130
OV/1-4 X. Litaudon, Overview of the JET Results in Support to ITER	131
OV/2-1 A. Kallenbach, Overview of ASDEX-Upgrade Results	132
OV/2-2 B. N. Wan, et al., Overview of EAST Experiments on the Development of High- Performance Steady-State Scenario	133

OV/2-3	B. N. Breizman, <i>et al.</i>, Kinetics of Relativistic Runaway Electrons	134
OV/2-4	Y.-K. Oh, <i>et al.</i>, Overview of the KSTAR Research in Support of ITER and DEMO	135
OV/2-5	E. S. Marmor, Overview of High-Field Divertor Tokamak Results from Al- cator C-Mod	136
OV/3-1	R. C. Wolf, First Plasma Operation of Wendelstein 7-X	137
OV/3-2	M. J. Edwards, <i>et al.</i>, The Quest for Laboratory Inertial Fusion Ignition in the US .	138
OV/3-3	H. Shirai, <i>et al.</i>, Recent Progress of JT-60SA Project	139
OV/3-4	Y. Wan, <i>et al.</i>, Overview of the Present Progresses and Activities on the Chinese Fusion Engineering Test Reactor	140
OV/4-1	J. Knaster, <i>et al.</i>, Overview of the IFMIF/EVEDA Project	141
OV/4-2	H. Azechi, A Pathway to Laser Fusion Energy: Fast Ignition Realization Experiment (FIREX)	142
OV/4-3Ra	S. Pradhan, <i>et al.</i>, Overview of SST-1 Upgrade & Recent Experiments in SST-1	143
OV/4-3Rb	R. Tanna, <i>et al.</i>, Overview of Recent Experimental Results from ADITYA Tokamak	145
OV/4-4	X. Duan, Overview of Recent Experiments on HL-2A Tokamak	146
OV/4-5	D. Sarychev, <i>et al.</i>, Review of Recent Experiments on the T-10 Tokamak with All Metal Wall	147
OV/5-1	F. Castejón, 3D Effects on Transport and Plasma Control in the TJ-II Stel- larator	148
OV/5-2	J. Menard, Overview of First Results from NSTX-U and Analysis High- lights from NSTX	149
OV/5-3	A. Kirk, Overview of Recent Physics Results from MAST	150
OV/5-4	R. Fonck, <i>et al.</i>, H-Mode and Nonsolenoidal Startup in the Pegasus Ultralow- A Tokamak	151

OV/5-5	Y. Takase, <i>et al.</i>, Overview of Spherical Tokamak Research in Japan	152
OV/P-1	S. Coda, Overview of the TCV Tokamak Programme: Scientific Progress and Facility Upgrades	153
OV/P-2	M. Zuin, <i>et al.</i>, Overview of the RFX-Mod Fusion Science Activity	154
OV/P-3	R. Dejarnac, Overview of Recent COMPASS Activities	155
OV/P-4	G. Pucella, Overview of the FTU Results	156
OV/P-5	J. S. Sarff, <i>et al.</i>, Overview of MST Reversed Field Pinch Research in Advanc- ing Fusion Science	157
OV/P-6	G. Zhuang, Progress of the Recent Experimental Research on the J-TEXT Tokamak	159
OV/P-7	S. Krasheninnikov, <i>et al.</i>, Edge and Divertor Plasma: Detachment, Stability, and Plasma- Wall Interactions	160
OV/P-8	K. Itoh, <i>et al.</i>, Hysteresis and Fast Timescale in Transport Relation of Toroidal Plasmas	161
OV/P-9	D. Borba, <i>et al.</i>, Overview of Simulation Results Using Computation Resources in the Framework of IFERC-CSC	162
OV/P-10	Y. Wu, <i>et al.</i>, Overview of DEMO Safety R&D and the Potential Future Role of IEA ESEFP IA	163
OV/P-11	P. Wouters, <i>et al.</i>, Implementation within the European Domestic Agency of the French Nuclear Safety Order of 2012, Concerning Basic Nuclear Installation, Applicable to ITER Project	164
OV/P-12	H. Meyer, <i>et al.</i>, Overview of Progress in European Medium Sized Tokamaks towards an Integrated Plasma-Edge/Wall Solution	165
EX:	Magnetic Confinement Experiments	167
EX/1-1	P. Piovesan, <i>et al.</i>, Role of MHD Dynamo in the Formation of 3D Equilibria in Fusion Plasmas	168

EX/1-2	C. Paz-Soldan, et al., Optimization of the Plasma Response for the Control of Edge-Localized Modes with 3D Fields	169
EX/1-3	Y. In, et al., Enhanced Understanding of Nonaxisymmetric Intrinsic and Controlled Field Impacts in Tokamaks	170
EX/1-4	O. Schmitz, et al., Enhancement of Helium Exhaust by Resonant Magnetic Perturbation Fields	171
EX/2-1	A. McLean, et al., The Role of Drifts and Radiating Species in Detached Divertor Operation at DIII-D	172
EX/2-2	D. Carralero, et al., Recent Progress towards a Quantitative Description of Filamentary SOL Transport	173
EX/2-3	H. Reimerdes, et al., TCV Experiments towards the Development of a Plasma Exhaust Solution	174
EX/3-1	A. E. Hubbard, et al., Advances in Physics and Performance of the I-Mode Regime over an Expanded Operating Space on Alcator C-Mod	175
EX/3-2	X. Chen, et al., Bifurcation of Quiescent H-Mode to a Wide Pedestal Regime in DIII-D and Advances in the Understanding of Edge Harmonic Oscillations	176
EX/3-3	C. Maggi, et al., Studies of the Pedestal Structure in JET with the ITER-Like Wall	177
EX/3-4	H. Urano, et al., Global Stabilization Effect of Shafranov Shift on the Edge Pedestal Plasmas in JET and JT-60U	178
EX/3-5	M. Dunne, et al., The Role of the Density Profile Location on Pedestal Stability in ASDEX-Upgrade	179
EX/3-6	I. Chapman, et al., Joint Experiments Tailoring the Plasma Evolution to Maximize Pedestal Performance	180
EX/4-1	C. C. Petty, et al., Advances in the Steady-State Hybrid Regime in DIII-D: A Fully-Noninductive, ELM-Suppressed Scenario for ITER	181
EX/4-2	J. Qian, et al., Advances in the High Bootstrap Fraction Regime on DIII-D towards the $Q = 5$ Mission of ITER Steady State	182

EX/4-3	A. M. Garofalo, et al., Development of High Poloidal β , Steady-State Scenario with ITER-Like W Divertor on EAST	183
EX/4-4	S. Sakakibara, et al., Extension of High- β Plasma Operation to Low Collisional Regime	184
EX/4-5	M. Hirsch, et al., Confinement in Wendelstein 7-X Limiter Plasmas	185
EX/5-1	Z. Yan, et al., Turbulence and Sheared Flow Structures Behind the Isotopic Dependence of the L-H Power Threshold and H-L Back Tran- sition on DIII-D	187
EX/5-2	J. Hillesheim, et al., Role of Stationary Zonal Flows and Momentum Transport for L-H Transitions in JET	188
EX/5-3	A. Diallo, et al., Energy Exchange Dynamics across L-H Transitions in NSTX	189
EX/6-1	M. Garcia-Munoz, et al., The Role of Plasma Response on Fast-Ion Losses Induced by Edge 3D Fields in the ASDEX-Upgrade and DIII-D Tokamaks	190
EX/6-2	C. Collins, et al., Critical Gradient Behaviour of Fast-Ion Transport from Alfvén Eigenmodes Guides Predictive Models for Burning Plasmas	191
EX/7-1	G. M. Wallace, et al., Influence of the Scrape-Off Layer on RF Actuator Performance	192
EX/7-2	T. Oishi, et al., Observation of Carbon Impurity Flow in the Edge Stochastic Magnetic Field Layer of Large Helical Device and its Impact on the Edge Impurity Control	193
EX/7-3Ra	B. Sieglin, et al., Assessment of Divertor Heat Load with and without External Magnetic Perturbation	194
EX/7-3Rb	A. Briesemeister, et al., Elimination of the Nonaxisymmetric Inter-ELM Heat Flux Generated by Resonant Magnetic Perturbations in Detached Divertor Conditions	195
EX/8-1	M. Yoshida, et al., Magnetic Shear Effects on Plasma Transport and Turbulence at High Electron to Ion Temperature Ratio in DIII-D and JT-60U Plasmas	196
EX/8-2	D. Yu, et al., Ion Internal Transport Barrier in Neutral Beam Heated Plas- mas on HL-2A	197

EX/9-1	E. Joffrin, <i>et al.</i>, Disruption Study Advances in the JET Metallic Wall	198
EX/9-2	N. Commaux, <i>et al.</i>, Shattered Pellet Injection as the Primary Disruption Mitigation Technique for ITER	199
EX/9-3	Y. Liu, <i>et al.</i>, Mitigation of Runaway Current with Supersonic Molecular Beam Injection on HL-2A Tokamak	200
EX/9-4	G. Papp, <i>et al.</i>, Runaway Electron Generation and Mitigation on the European Medium Sized Tokamaks ASDEX-Upgrade and TCV	201
EX/10-1	A. Bortolon, <i>et al.</i>, Effectiveness of High-Frequency ELM Pacing with D ₂ and Nonfuel Pellets in DIII-D	202
EX/10-2	G. Xu, <i>et al.</i>, ELM Pace-Making and Long-Pulse ELM-Stable H-Mode Operation with LHCD in EAST	203
EX/10-3	G. S. Yun, <i>et al.</i>, Edge-Localized Modes on KSTAR: Global Structure and Distinct Evolution Stages Involving Quasi-Steady State and Phase Transitions	204
EX/11-1	B. A. Grierson, <i>et al.</i>, Validation of Theoretical Models of Intrinsic Torque in DIII-D and Projection to ITER by Dimensionless Scaling	205
EX/P3-1	M. Porkolab, <i>et al.</i>, Studies of Turbulence and Transport in the Alcator C-Mod and DIII-D Tokamaks with Phase Contrast Imaging and Gyrokinetic Modelling	206
EX/P3-2	J. E. Rice, <i>et al.</i>, Effects of the q Profile on Toroidal Rotation in Alcator C-Mod LHCD Plasmas	207
EX/P3-3	M. L. Reinke, <i>et al.</i>, Investigations of Radial High- Z Transport Mechanisms in ICRF-Heated Alcator C-Mod H-Mode Plasmas	208
EX/P3-5	J. C. Wright, <i>et al.</i>, Experimental Results from Three-Ion Species Heating Scenario on Alcator C-Mod	209
EX/P3-6	B. LaBombard, <i>et al.</i>, Plasma Profiles and Impurity Screening Behaviour of the High-Field Side Scrape-Off Layer in Near-Double-Null Configurations: Prospect for Mitigating Plasma-Material Interactions on RF Actuators and First-Wall Components	210

EX/P3-7	D. Brunner, et al., Divertor and Core Plasma Performance Optimization Enabled by Direct Feedback Control of Surface Heat Flux on Alcator C-Mod's High-Z Vertical Target Plate Divertor . . .	211
EX/P3-8	R. S. Granetz, et al., Developing Disruption Warning Algorithms Using Large Databases on Alcator C-Mod and EAST Tokamaks	212
EX/P3-9	S. Mordijck, et al., Dominant Role of Turbulence in Determining Particle Transport and Confinement	213
EX/P3-10	G. R. McKee, et al., Turbulence Evolution and Transport Behaviour during Current Ramp-Up in ITER-Like Plasmas on DIII-D	214
EX/P3-11	L. Schmitz, et al., Turbulence-Flow Coupling and Poloidal Main-Ion Flow Acceleration Preceding the L-H Transition	215
EX/P3-12	R. S. Wilcox, et al., Toroidally Localized Turbulence with Applied 3D Fields in the DIII-D Tokamak	216
EX/P3-13	J. deGrassie, et al., Dimensionless Size Scaling of Intrinsic Rotation	217
EX/P3-14	F. Turco, Confinement and Stability of the ITER Baseline Scenario in DIII-D	218
EX/P3-15	J. D. Hanson, Stability of High-Performance, Negative Central Shear Discharges	219
EX/P3-16	M. Okabayashi, Physics of Unlocked Tearing Modes and Disruption Avoidance by Feedback-Based Electromagnetic Torque Injection .	220
EX/P3-18	M. Shafer, et al., Validating Extended MHD Models of Plasma Response against Measurements of Islands in DIII-D	221
EX/P3-19	D. Orlov, et al., The Contribution of Perturbation Coil Geometry Induced Sidebands and MHD Response in KSTAR and DIII-D	222
EX/P3-20	D. Shirakid, et al., Disruption Mitigation in the Presence of Pre-Existing MHD Instabilities	223
EX/P3-21	E. Kolemen, et al., Adaptive Real-Time Pedestal Control for DIII-D and Prospects for ITER	224

EX/P3-22	R. I. Pinsker, <i>et al.</i>, Experiments on Helicons in DIII-D: Investigation of the Physics of a Reactor-Relevant Noninductive Current Drive Technology	225
EX/P3-23	E. Schuster, <i>et al.</i>, Improved Reproducibility of Plasma Discharges via Physics- Model-Based q -Profile Feedback Control in DIII-D	226
EX/P3-24	M. A. Van Zeeland, <i>et al.</i>, Electron Cyclotron Heating Modification of Alfvén Eigen- mode Activity in DIII-D	227
EX/P3-25	A. W. Leonard, <i>et al.</i>, Robust H-Mode Pedestal Compatibility with SOL and Diver- tor Plasma Constraints	228
EX/P3-26	A. Sontag, <i>et al.</i>, SOL Effects on the Pedestal Structure in DIII-D Discharges	229
EX/P3-27	T. W. Petrie, <i>et al.</i>, Edge, Divertor and Plasma Behaviour in High-Power High- Performance Double-Null Plasmas	230
EX/P3-28	B. Covele, <i>et al.</i>, X-Divertors for Facilitating Detachment without Degrading the DIII-D H-Mode	231
EX/P3-29	D. Eldon, <i>et al.</i>, Controlling Marginally Detached Divertor Plasmas	232
EX/P3-30	V. Soukhanovskii, <i>et al.</i>, Snowflake Divertor Configuration Effects on Pedestal Stabili- ty and Edge Localized Modes in NSTX and DIII-D	233
EX/P3-31	G. Verdoolaege, Robust Estimation of Tokamak Energy Confinement Scaling through Geodesic Least Squares Regression	234
EX/P3-32	U. Shumlak, <i>et al.</i>, Results from the Sheared-Flow Stabilized Z-Pinch and Scal- ing to Fusion Conditions	235
EX/P3-33	T. Jarboe, <i>et al.</i>, Applying the New Principles of Plasma Self-Organization to Tokamak	236
EX/P3-34	R. P. Majeski, Observation of an Isothermal Electron Temperature Profile with Low Recycling Lithium Walls in LTX	237
EX/P3-36	A. Sykes, <i>et al.</i>, Compact Fusion Energy Based on the Spherical Tokamak	238
EX/P3-37	T. Asai, <i>et al.</i>, Compact Toroid Injection Fuelling on a Large-sized Field- Reversed Configuration	239

EX/P3-38	Y. Ono, et al., Reconnection Heating Experiments and Simulations for Torus Plasma Merging Startup	240
EX/P3-39	D. Gates, et al., Recent Advances in Stellarator Optimization	241
EX/P3-40	J. P. Levesque, et al., Ferritic Wall and Scrape-Off-Layer Current Effects on Kink Mode Dynamics	242
EX/P3-41	H. Gota, et al., Achievement of Field-Reversed Configuration Plasma Sus- tainment via 10 MW Neutral-Beam Injection on the C-2U Device	243
EX/P3-42	A. Hossack, et al., Plasma Response to Sustainment with Imposed-dynamo Current Drive in HIT-SI and HIT-SI3	244
EX/P3-46	M. Nishiura, et al., Ion Heating in Magnetosphere Plasma Device RT-1	245
EX/P3-47	S. Medvedev, et al., Single Null Divertor in Negative Triangularity Tokamak . .	246
EX/P4-1	S.-W. Yoon, et al., Extension of Operational Boundary of High- β Long-pulse Operation at KSTAR	247
EX/P4-2	Y.-S. Park, et al., Investigation of MHD Stability in KSTAR High- β_N Plasmas	248
EX/P4-3	H. Park, et al., Validation of $q_0 \geq 1.0$ in the MHD Quiescent Time after Crash of the Sawtooth Instability in KSTAR	249
EX/P4-4	W. H. Ko, et al., Influences of Nonaxisymmetric Field on H-Mode Power Threshold and Pedestal Rotation in KSTAR	250
EX/P4-5	J. Kim, et al., Direct Destabilizations of Macro/Micro Edge Instabilities by Magnetic Perturbations	251
EX/P4-6	M. J. Choi, et al., Study of the Locked Mode Disruption with the 3D Imaging Data in KSTAR	252
EX/P4-7	M. Kim, et al., Study of Nonlinear Phase of the ELMs by Comparison be- tween ECEI ELM Observation and Nonlinear MHD Simula- tions	253
EX/P4-8	J. G. Bak, et al., Characteristics of Halo Current in the KSTAR Tokamak . . .	254

EX/P4-9	K. Kim, et al., Characteristics of Magnetic Braking Depending on 3D Field Configuration in KSTAR	255
EX/P4-10	S. G. Lee, et al., Long-Lived Pressure-Driven MHD Mode in KSTAR Plasmas	256
EX/P4-12	S.-H. Hahn, et al., Measuring and Extending Vertical Stabilization Controllability of KSTAR	257
EX/P4-13	H.-S. Kim, et al., Application of Physics-Based Profile Control Approach to KSTAR	258
EX/P4-14	J. Lee, et al., ECH-assisted Plasma Startup Experiment Using Trapped Particle Configuration in KSTAR	259
EX/P4-15	J. Lee, et al., ELM, Edge Turbulence and their Interaction in the ELM-crash Suppression Phase under the $n = 1$ RMP	260
EX/P4-16	S. Ko, et al., Study of Toroidal Rotation and Ion Temperature Pedestals between ELM Bursts on KSTAR H-Mode Plasmas	261
EX/P4-17	Y. Shi, et al., Fluctuation Signatures of Rotation Reversals and Nonlocal Transport Events in KSTAR L-Mode Plasmas	262
EX/P4-18	J. Hong, et al., Effects of ECH and RMP on Argon Impurity Transport in KSTAR Plasmas	263
EX/P4-19	D. H. Na, et al., Rotation Reversal in KSTAR and its Turbulence and Transport Characteristics	264
EX/P4-20	W. Lee, et al., Ion-Scale Turbulence Study in KSTAR L-Mode Plasmas . . .	265
EX/P4-21	S.-H. Hong, et al., Comprehensive Study on Deposition inside the Gap of Castellated Tungsten Blocks of Different Shapes	266
EX/P4-22	J.-G. Kwak, et al., The Assessment of the Neutron Yield and the Toroidal Distribution of Neutron Emission on Deuterium Beam-Plasma Interaction Dominated KSTAR Operation	267
EX/P4-23	K. C. Lee, et al., Measurements of SOL Density Increase and Poloidal Asymmetry on KSTAR ELMs	268
EX/P4-24	H. Lee, et al., H-Mode Divertor Target Heat Load Measurements on KSTAR	269

EX/P4-25	M.-K. Bae, et al., Comparative Study of KSTAR and DiPS-2 on the Heat Flux to the First Wall	270
EX/P4-26	J. Kim, et al., Experimental Observations of Beam-Driven Alfvén Eigen- modes in KSTAR	271
EX/P4-27	J. Ko, et al., Current Profile Evolutions with External Current Drive for KSTAR	272
EX/P4-28	M. Cheon, et al., Loss of Predisruptive Runaway Electrons by Magnetic Per- turbation and its Effect on Plasma Disruption	273
EX/P4-29	C.-M. Ryu, et al., Observation and Simulation of TAEs in KSTAR Plasmas	274
EX/P4-30	J.-W. Ahn, et al., Shielding and Amplification of Nonaxisymmetric Divertor Heat Flux by Plasma Response to Applied 3D Fields in NSTX and KSTAR	275
EX/P4-31	F. Militello, et al., Scrape-Off Layer and Divertor Physics Advances in MAST	276
EX/P4-32	H. Tanabe, et al., Investigation of Merging/Reconnection Heating during Solenoid- Free Startup of Plasmas in the MAST Spherical Tokamak	277
EX/P4-33	S. A. Sabbagh, et al., Isolation of Neoclassical Toroidal Viscosity Profile under Varied Plasma and 3D Field Conditions in Low and Medium Aspect Ratio Tokamaks	278
EX/P4-34	J. W. Berkery, et al., Characterization and Forecasting of Unstable Resistive Wall Modes in NSTX and NSTX-U	279
EX/P4-35	Y. Ren, et al., Exploring the Regime of Validity of Global Gyrokinetic Sim- ulations with Spherical Tokamak Plasmas	280
EX/P4-36	F. Scotti, et al., Kinetic Profiles and Impurity Transport Response to 3D-Field Triggered ELMs in NSTX	281
EX/P4-38	R. Maingi, et al., Comparison of Helium Glow and Lithium Evaporation Wall Conditioning Techniques in Achieving High Performance H-Mode Discharges in NSTX	282
EX/P4-39	L. F. Delgado-Aparicio, et al., Locked-Mode Avoidance and Recovery without External Momentum Input Using ICRH	283

EX/P4-40	D. Smith, et al., Identification of Characteristic ELM Evolution Patterns with Alfvén-Scale Measurements and Unsupervised Machine Learning Analysis	284
EX/P4-41	E. Fredrickson, et al., Parametric Dependence of EPs in NSTX	285
EX/P4-42	R. Perkins, et al., Large RF Field Amplitudes in the SOL and Far-Field RF Sheaths: A Proposed Mechanism for the Anomalous Loss of RF Power to the SOL of NSTX	286
EX/P4-43	M. D. Boyer, et al., Feedback Control Design for Noninductively Sustained Scenarios in NSTX-U Using TRANSP	287
EX/P4-44	N. Bakharev, et al., Counter-NBI Experiments on Globus-M	288
EX/P4-45	H. Tanaka, et al., Noninductive Production of Extremely Overdense Spherical Tokamak Plasma by Electron Bernstein Wave Excited via O-X-B Method in LATE	289
EX/P4-47	I. Vargas-Blanco, et al., Recommissioning of the Spherical Tokamak MEDUSA in Costa Rica	290
EX/P4-48	A. Ejiri, et al., Plasma Startup Experiments on the TST-2 Spherical Tokamak	291
EX/P4-49	K. Hanada, et al., Investigation of Hydrogen Recycling Property and its Control with Hot Wall in Long Duration Discharges on QUEST .	292
EX/P4-50	H. Idei, et al., Noninductive Electron Cyclotron Heating and Current Drive with Dual Frequency (8.2/28 GHz) Waves in QUEST	293
EX/P4-51	M. Bongard, et al., ELM Characterization and Dynamics at Near-Unity A in the Pegasus ST	294
EX/P4-52	Y. Tan, et al., TAE during Minor Disruptions in the SUNIST Spherical Tokamak	295
EX/P4-53	H. Lee, et al., Study on EBW Assisted Startup and Heating Experiments via Direct XB Mode Conversion from Low Field Side Injection in VEST	296
EX/P5-1	A. Dinklage, et al., The Effect of Transient Density Profile Shaping on Transport in Large Stellarators and Heliotrons	297

EX/P5-2	U. Höfel, et al., Initial Observations on Core Electron Heat Transport in W7-X298	
EX/P5-3	A. Langenberg, et al., Minerva Bayesian Analysis of X-ray Imaging Spectrometer Data for Temperature and Density Profile Inference at Wen- delstein 7-X	299
EX/P5-4	A. Krämer-Flecken, et al., Investigation of Turbulence Rotation in Limiter Plasmas at W7-X with a New Installed Poloidal Correlation Reflectometry	300
EX/P5-5	S. Lazerson, et al., Error Field Measurement, Correction and Heat Flux Balanc- ing on Wendelstein 7-X	301
EX/P5-6	N. Pablant, et al., Investigation of Initial Plasma Parameters on the Wendelstein 7-X Stellarator Using the X-ray Imaging Crystal Spectrometer	302
EX/P5-7	G. A. Wurden, et al., Limiter Observations during W7-X First Plasmas	303
EX/P5-8	S. A. Bozhnikov, et al., Enhancement of W7-X Performance by Symmetrization of Limiter Loads with Error Field Correction Coils	304
EX/P5-9	P. Drews, et al., Measurement of the Plasma Edge Profiles Using the Com- bined Probe on W7-X	305
EX/P5-10	Y. Liang, et al., Diagnostic Setup and Modelling for Investigation of Synergy between 3D Edge Physics and Plasma-Wall Interactions on Wendelstein 7-X	306
EX/P5-11	D. Moseev, et al., Application of the ECRH Radiation for Plasma Diagnosis in Wendelstein 7-X	307
EX/P5-12	J. Ongena, et al., Physics and Applications of ICRH on W7-X	308
EX/P5-13	S. Marsen, et al., First Results from Protective ECRH Diagnostics for Wendel- stein 7-X	309
EX/P5-14	O. Grulke, Transport Studies during the First Campaign of Wendelstein 7-X	310
EX/P5-15	D. Den Hartog, et al., Enhanced Measurements for MHD Validation Using Inte- grated Data Analysis on the MST Fusion Research Experiment	311

EX/P5-16	J. K. Anderson, et al., An Island-Induced Alfvén Eigenmode and Effects of Nonax- isymmetry on Fast Ions in the RFP	312
EX/P5-17	D. L. Brower, et al., Evidence for Trapped Electron Mode Turbulence in MST Improved Confinement RFP Plasmas	313
EX/P5-18	L. Frassinetti, et al., Effect of External Magnetic Perturbations on the EXTRAP T2R Reversed-Field Pinch Plasma	314
EX/P5-19	W. Liu, et al., Overview of Keda Torus Experiment Initial Results	315
EX/P5-20	T. Lan, et al., Initial Operation Results from KTX	316
EX/P5-21	M. Nagata, Investigations of Plasmoid Formation and Flux Closure in Transient Coaxial Helicity Injection on HIST	317
EX/P5-22	S. Masamune, et al., Improved Low-Aspect-Ratio RFP Performance with Active MHD Control and Associated Change in Magnetic Topology in RELAX	318
EX/P5-23	M. E. Puiatti, et al., Extended Scenarios Opened by the Upgrades of the RFX- Mod Experiment	319
EX/P5-24	M. Spolaore, H-Mode Achievement and Edge Features in RFX-Mod Toka- mak Operation	320
EX/P5-25	M. Agostini, et al., Kinetic Properties of Edge Plasma with 3D Magnetic Pertur- bations in RFX-Mod	321
EX/P5-26	R. Lorenzini, Transport Studies with Magnetic Islands in Fusion Plasmas	322
EX/P5-28	S. Banerjee, et al., Observation of Large Filaments during the Disruptive Phase of ADITYA Tokamak Plasma	323
EX/P5-29	S. Jana, et al., Plasma Startup Studies and Electromagnetic Field Computa- tion for SST-1 Tokamak	324
EX/P5-30	J. R. Dhongde, et al., MHD Phenomena and Disruption Characteristics in SST-1 Early Plasma	325
EX/P5-31	M. K. Bhandarkar, et al., Observation and Study of Lock Mode Characteristics in SST-1 Plasma	326

EX/P5-32	K. Patel, et al., Low Density Plasma Regimes in SST-1 with and without Suprathermal Electrons	327
EX/P5-33	D. C. Raval, et al., Plasma Facing Components Technologies in SST-1	328
EX/P6-1	M. Rubel, et al., Fuel Inventory and Deposition in Castellated Beryllium Structures in JET	329
EX/P6-2	K. Heinola, et al., Long-Term Fuel Retention and Release in JET ITER-Like Wall at ITER-Relevant Baking Temperatures	330
EX/P6-3	D. Borodin, et al., ERO Modelling of Be Erosion in JET and Extrapolation of the Data for ITER	331
EX/P6-5	Y. Corre, et al., Thermal Analysis of Transient Tungsten Melting Experiments at JET	332
EX/P6-6	S. Wiesen, et al., Impact of the JET ITER-Like Wall on H-Mode Plasma Fuelling	333
EX/P6-8	S. E. Sharapov, et al., Studies of Alfvén Eigenmodes in the ITER Baseline Scenario, Sawtoothed JET Plasmas, and MAST Hydrogen-Deuterium Plasmas	334
EX/P6-9	R. D’Inca, et al., Multimachine Experimental Investigation of Ion Cyclotron Emission	335
EX/P6-10	D. Van Eester, et al., Recent Ion Cyclotron Resonance Heating Experiments in JET in Preparation of a DT Campaign	336
EX/P6-11	E. de la Luna, et al., Recent Results on High-Triangularity H-Mode Studies in JET-ILW	337
EX/P6-12	T. Tala, et al., Density Peaking in JET: Driven by Fuelling or Transport? . .	338
EX/P6-13	C. Giroud, et al., Progress in Understanding the Role of Low-Z Impurity in the Confinement in JET-ILW and in JET-C Plasmas	339
EX/P6-14	P. Mantica, et al., Electron Heat Transport in JET from Ion to Electron Scales: Experimental Investigation and Gyro-kinetic Simulations . .	340

EX/P6-15	F. Koechl, et al., Evolution and Control of Tungsten Transport in the Termination Phase of JET H-Mode Discharges and Implications for ITER	341
EX/P6-16	M. Goniche, et al., Ion Cyclotron Resonance Heating for Tungsten Control in JET H-Mode Scenarios	342
EX/P6-17	M. Valisa, et al., The Role of ELMs and Inter-ELM Phases in the Transport of Heavy Impurities in JET	343
EX/P6-18	H. Weisen, et al., Neutron Yield Studies in JET H-Modes	344
EX/P6-19	N. Ashikawa, et al., Comprehensive Analysis of Metal Dust Particles in JET-ILW, and Impact on Fusion Reactor	345
EX/P6-20	E. Fortuna-Zalesna, et al., Detailed Survey of Dust Particles from JET with the ITER-Like Wall: Origin, Composition and Internal Structure	346
EX/P6-21	A. Hakola, et al., Plasma-Wall Interaction Studies in the Full-W ASDEX-Upgrade during Helium Plasma Discharges	347
EX/P6-22	F. Reimold, et al., Analysis of the Impact of Nitrogen- & Neon-Seeding on ASDEX-Upgrade H-Modes with SOLPS Simulations	348
EX/P6-23	P. Martin, et al., Physics, Control and Mitigation of Disruptions and Runaway Electrons in the EUROfusion Medium Size Tokamaks Science Programme	349
EX/P6-24	V. Igochine, et al., MHD Limits and Plasma Response in High- β Hybrid Operations in ASDEX-Upgrade	351
EX/P6-25	M. Willensdorfer, et al., Plasma Response of External Magnetic Perturbations at the Edge: Comparisons between Measurements and 3D MHD Models	352
EX/P6-26	J.-M. Noterdaeme, et al., Ion Cyclotron Range of Frequency Power Challenges and Solutions	353
EX/P6-27	M. Weiland, et al., Phase-Space Resolved Measurements of the Influence of RF Heating and MHD Instabilities on the Fast-Ion Distribution in ASDEX-Upgrade	354

EX/P6-28	C. Hopf, et al., Advances in Neutral Beam Current Drive Experiments on ASDEX-Upgrade	355
EX/P6-29	T. Pütterich, et al., The Role of the Neoclassical E_r for the L-H Transition in ASDEX-Upgrade	356
EX/P6-30	E. Viezzer, et al., Ion Heat and Toroidal Momentum Transport Studies in the H-Mode Transport Barrier of ASDEX-Upgrade	357
EX/P6-31	F. Clairet, et al., Pedestal and Core Turbulence Dynamics Using 1 μ s Sweeping Profile Reflectometry	358
EX/P6-32	P. Manz, et al., Turbulence Characteristics of the I-Mode Confinement Regime in ASDEX-Upgrade	359
EX/P6-33	V. V. Plyusnin, et al., Comparison of Runaway Electron Generation Parameters in Small, Medium-sized and Large Tokamaks: A Survey of Experiments in COMPASS, TCV, ASDEX-Upgrade and JET .	360
EX/P6-34	J. Mlynář, et al., Losses of Runaway Electrons in MHD-Active Plasmas of the COMPASS Tokamak	361
EX/P6-35	M. Komm, et al., Contribution to the Multimachine Pedestal Scaling from COMPASS Tokamak	362
EX/P6-36	J. A. Snipes, et al., Overview of the Preliminary Design of the ITER Plasma Control System	363
EX/P6-37	D. A. Humphreys, et al., Plasma Control Studies Using DIII-D Design Tools in Support of ITER	364
EX/P6-38	G. Pautasso, et al., Generation of the Disruption Mitigation Trigger: Developing a Preliminary Design for ITER	365
EX/P6-39	M. Lehnen, et al., Plasma Disruption Management in ITER	366
EX/P6-40	R. Roccella, et al., Modelling ITER Asymmetric VDEs through Asymmetries of Toroidal Eddy Currents	367
EX/P6-41	P. de Vries, et al., Multimachine Analysis of Termination Scenarios, Providing the Specifications for Controlled Shutdown of ITER Discharges	368

EX/P6-42	A. Sips, et al., Assessment of the Baseline Scenario at $q_{95} \sim 3$ for ITER . . .	369
EX/P6-44	A. Polevoi, et al., Integrated Simulations of H-Mode Operation in ITER including Core Fuelling, Divertor Detachment and ELM Control .	370
EX/P6-45	J. Citrin, et al., Real-Time Tokamak Simulation with a First-Principle-Based Neural Network Turbulent Transport Model	371
EX/P6-46	C. Myers, et al., A Multimachine Analysis of Nonaxisymmetric and Rotating Halo Currents	372
EX/P6-47	W. Tang, et al., Big Data Machine Learning for Disruption Predictions . . .	373
EX/P6-48	K. Crombe, et al., IShTAR: A Dedicated Facility to Characterize the Interactions between ICRF Waves and Plasma	374
EX/P6-49	T. Watari, et al., Observation of KBM and MTM in JIPPT-IIU Tokamak Plasmas Using a Heavy Ion Beam Probe	375
EX/P6-50	A. Vertkov, et al., Corrosion Compatibility of Capillary-Porous System Solid Base with Low Melting Metals Applied as Plasma Facing Materials for Tokamak	376
EX/P6-51	J. Mora-Meléndez, et al., First Results of the Stellarator of Costa Rica 1 (SCR-1)	377
EX/P6-52	L. Vyacheslavov, et al., Dynamics of Tungsten Erosion under ELM-Like Intense Heat Loads	378
EX/P6-53	I. Furno, et al., Basic Studies of Blob Dynamics in X-Point Configurations and Interaction with Suprathermal Ions in the TORPEX Device	379
EX/P7-1	Y. Peysson, et al., Experiments and Modelling towards Long Pulse High Confinement Operation with Radiofrequency Heating and Current Drive in EAST	380
EX/P7-2	X. Gao, et al., Key Issues towards Long Pulse High β_N Operation on EAST Tokamak	381
EX/P7-4	Y. Sun, et al., ELM Suppression Using Resonant Magnetic Perturbation in EAST	382

EX/P7-5	B. J. Ding, et al., Recent Experimental and Modelling Advances in the Understanding of Lower Hybrid Current Drive in ITER-Relevant Regimes	383
EX/P7-7	B. Lyu, et al., Experimental Study of Radio-Frequency Driven Spontaneous Rotation for High-Performance Plasmas on EAST	384
EX/P7-8	X. J. Zhang, et al., Heating and Confinements by the Waves in the Ion Cyclotron Range of Frequencies on EAST	385
EX/P7-9	X. Y. Gong, et al., Current Drive with Combined Electron Cyclotron Wave and High Harmonic Fast Wave in Tokamak Plasmas	386
EX/P7-10	L. Wang, et al., Evidence and Modelling of 3D Divertor Footprint Induced by Lower Hybrid Waves on EAST with Tungsten Divertor Operations	387
EX/P7-12	X. D. Zhang, et al., Fishtail Divertor: A New Divertor Concept on EAST for Active Control of Heat Load on Divertor Plate	388
EX/P7-15	G. Li, et al., Predictions of the Baseline Operation Scenario in Chinese Fusion Engineering Test Reactor	389
EX/P7-16	W. X. Ding, et al., Current Transport and Density Fluctuations at L-H Transition on EAST	390
EX/P7-17	W. Chen, et al., Kinetic Alfvén-Ballooning Instabilities in Tokamak Plasmas with Weak Magnetic Shears and Low-Pressure Gradients . .	391
EX/P7-19	X. Q. Ji, et al., Experimental Investigation of Interaction between Turbulence and Large-Scale Mode Structures in HL-2A	392
EX/P7-21	Z. Y. Cui, et al., Study of Impurity Transport in the HL-2A ECRH Plasmas with MHD Instabilities	393
EX/P7-22	Z. B. Shi, et al., Role of SMBI Deposition in ELM Mitigation and the Underlying Turbulence Characteristics	394
EX/P7-24	J. Dong, et al., Roles of an Inward Particle Flux Inducing Quasi-Mode in Pedestal Dynamics on HL-2A Tokamak	395

EX/P7-25	M. Xu, et al., Direct Measurement of ELM Related Momentum Transport in the Edge of HL-2A H-Mode Plasmas	396
EX/P7-27	L. W. Yan, et al., Synchronization of GAMs and Magnetic Fluctuations on HL-2A Tokamak	397
EX/P7-29	O. Pan, et al., Investigation of Mechanisms for the Generation of Blobs/Holes at the Boundary of the HL-2A Tokamak	398
EX/P7-30	L. Nie, et al., Experimental Evaluation of Langmuir Probe Sheath Potential Coefficient	399
EX/P7-34	A. Ekedahl, et al., First Experiments in H-Mode Plasmas with the Passive-Active Multijunction LHCD Launcher in HL-2A and Impact on Pedestal Instabilities	400
EX/P7-35	F. Deeba, et al., Spectroscopic Studies on GLAST-III Tokamak by Varying the Inductance and Charging Voltage of Vertical Field Coils . . .	401
EX/P7-36	A. Malaquias, et al., Studies on ISTTOK during Edge Electrode Biasing Assisted AC Operation	402
EX/P7-38	J. Stockel, et al., Contribution of Joint Experiments on Small Tokamaks in the Framework of IAEA Coordinated Research Projects to Mainstream Fusion Research	403
EX/P7-39	C. Xiao, et al., Modification of Toroidal Flow Velocity through Momentum Injection by Compact Torus Injection into the STOR-M Toka- mak Discharge	404
EX/P7-40	S. Lebedev, et al., High Frequency Magnetic Oscillations in the TUMAN-3M Ohmically Heated Plasmas	405
EX/P7-41	S. I. Lashkul, et al., Effect of the Transition to Improved Core Confinement Ob- served in the LHCD Experiment at FT-2 Tokamak	406
EX/P7-42	A. Shevelev, et al., Runaway Electrons Studies with Hard X-Ray and Microwave Diagnostics in the FT-2 Low-Hybrid Current Drive Discharges	407
EX/P7-43	D. A. Maurer, et al., Control of Sawtooth Oscillation Dynamics Using Externally Applied Stellarator Transform	408

EX/P7-44	C. Hidalgo, et al., On the Influence of ECRH on Neoclassical and Anomalous Mechanisms Using a Dual Heavy Ion Beam Probe Diagnostic in the TJ-II Stellarator	409
EX/P7-45	T. Estrada, et al., Plasma Flow, Turbulence and Magnetic Islands in TJ-II . . .	410
EX/P7-47	K. J. McCarthy, et al., Plasma Core Fuelling by Cryogenic Pellet Injection in the TJ-II Stellarator	411
EX/P7-48	D. López-Bruna, et al., Confinement Modes and Magnetic-Island Driven Modes in the TJ-II Stellarator	412
EX/P8-1	Y. Yoshimura, et al., Progress of Steady State Operation Using RF Heating in the LHD	413
EX/P8-2	T. I. Tsujimura, et al., Impact of the LHD Peripheral Region and the Magnetic Axis Shift on Optimal On-Axis ECRH Injection for High-Electron-Temperature Plasmas	414
EX/P8-3	G. Motojima, et al., Global Particle Balance and its Relationship with the Plasma Wall Interaction Emerging in Long Pulse Discharges on the Large Helical Device	415
EX/P8-4	Y. Nakamura, et al., Strong Suppression of Impurity Accumulation in Steady-State Hydrogen Discharges with High Power NBI Heating on LHD	416
EX/P8-5	X. Huang, et al., Formation of Impurity Transport Barrier in LHD Plasmas with Hollow Density Profile	417
EX/P8-6	B. Peterson, et al., Experimental Observations and Modelling of Poloidal Asymmetries in Radiation Profiles during N ₂ Seeding Compared with Ne Seeding in LHD	418
EX/P8-7	K. Ida, et al., Flow Damping Due to the Stochastization of Magnetic Field in Large Helical Device	419
EX/P8-8	Y. Narushima, et al., Observations of Sustained Phase Shifted Magnetic Islands from Externally Imposed $m/n = 1/1$ RMP in LHD	420
EX/P8-9	T. Tokuzawa, et al., Magnetic Island Formation in Locked-Like Mode in Helical Plasmas	421

EX/P8-10	S. Ohdachi, et al., Observation of the Ballooning Mode that Limits the Operation Space of the High-Density Superdense-Core Plasma in the LHD	422
EX/P8-11	K. Tanaka, et al., Improvements of Ion Energy Confinement in Helium Rich Plasma of LHD	423
EX/P8-12	X. D. Du, et al., Stabilization of the Helically Trapped Energetic Ions Driven Resistive Interchange Mode by On-Axis Electron-Cyclotron Heating in a Helical Plasma	424
EX/P8-13	T. Ido, et al., Abrupt Excitation of Intense Geodesic Acoustic Mode in the LHD	425
EX/P8-14	D. Kato, et al., Observation of Visible Forbidden Lines of Tungsten Highly Charged Ions in LHD Core Plasmas and its Application to Ion Distribution Analysis	426
EX/P8-16	T. Minami, et al., Role of Magnetic Topology to Form Electron Internal Transport Barrier on Heliotron J	427
EX/P8-17	S. Kobayashi, et al., Study of H-Mode Transition Triggered by High-Intensity Gas Puffing in NBI Plasmas of Heliotron J	428
EX/P8-18	H. Okada, et al., Fast Ion Generation by Combination Heating of ICRF and NBI in Heliotron J	429
EX/P8-19	K. Nagasaki, et al., Suppression of Alfvén Eigenmodes by ECH/ECCD in Heliotron J	430
EX/P8-20	S. Ohshima, et al., Isotope Effects on Long Range Correlation and the Nonlinear Coupling with Turbulence in Heliotron J	431
EX/P8-21	G. Mazzitelli, et al., Liquid Metal Experiments on FTU	432
EX/P8-22	D. Carnevale, et al., Analysis of Runaway Beam Suppression Experiments in FTU	433
EX/P8-23	A. Bruschi, et al., Observation of Short Time-Scale Spectral Emissions at Millimetre Wavelengths with the New CTS Diagnostic on the FTU Tokamak	434
EX/P8-24	O. Tudisco, et al., Evidence of Thermo-Diffusive Pinch in Particle Transport .	435

EX/P8-25	B. Labit, <i>et al.</i>, The Physics of the Heat Flux Narrow Decay Length in the TCV Scrape-Off Layer: Experiments and Simulations	436
EX/P8-26	N. Vianello, <i>et al.</i>, On Filamentary Transport in the TCV Tokamak: Addressing the Role of the Parallel Connection Length	437
EX/P8-27	B. Esposito, <i>et al.</i>, First Experimental Results of Runaway Beam Control in TCV	438
EX/P8-28	T. P. Goodman, <i>et al.</i>, Scattering of EC Waves by Edge Turbulence: Measurements and Modelling in TCV and TORPEX	439
EX/P8-29	B. Duval, <i>et al.</i>, Neutral Beam Heating on the TCV Tokamak	440
EX/P8-30	B. Geiger, <i>et al.</i>, Study of the Fast-Ion Distribution Function in the TCV Toka- mak Based on FIDA Spectroscopy and the TRANSP Code .	441
EX/P8-31	D. Douai, <i>et al.</i>, Development of Helium Electron Cyclotron Wall Condition- ing on TCV for the Operation of JT-60SA	442
EX/P8-32	H. Anand, <i>et al.</i>, Distributed Digital Real-Time Control System for the TCV Tokamak and its Applications	443
EX/P8-33	F. Felici, <i>et al.</i>, Real-Time Model-Based Plasma State Estimation, Monitoring and Integrated Control in TCV, ASDEX-Upgrade and ITER .	444
EX/P8-34	A. Melnikov, <i>et al.</i>, Study of Interactions between GAMs and Broadband Turbu- lence in the T-10 Tokamak	445
EX/P8-35	P. Savrukhin, <i>et al.</i>, Disruptions and Runaway Mitigation Using ECRH and In- ductive Power Supply Systems in the T-10 Tokamak	446
EX/P8-36	M. Nurgaliev, <i>et al.</i>, Study of Light and Heavy Impurities Transport in OH and ECRH Plasmas on the T-10 Tokamak	447
EX/P8-37	I. Lyublinski, <i>et al.</i>, Lithium and Tungsten Limiters for 3 MW of ECR Plasma Heating in T-10 Tokamak: Design, First Results	448
EX/P8-38	T. Wakatsuki, <i>et al.</i>, Reduction of CS Flux Consumption during Plasma Current Ramp-Up on DEMO Reactor	449

EX/P8-39	T. Goto, <i>et al.</i>, Development of a Real-Time Simulation Tool towards Self-Consistent Scenario of Plasma Startup and Sustainment on Helical Fusion Reactor FFHR-d1	450
EX/P8-40	G. Giruzzi, <i>et al.</i>, Physics and Operation Oriented Activities in Preparation of the JT-60SA Tokamak Exploitation	451
EX/P8-41	S. Brezinsek, <i>et al.</i>, Preparation of PFCs for the Efficient Use in ITER and DEMO: Plasma-Wall Interaction Studies within the EUROfusion Consortium	453
EX/P8-42	Y. Nakashima, <i>et al.</i>, Recent Progress of Divertor Simulation Research Using the GAMMA 10/PDX Tandem Mirror	454
EX/P8-43	R. Ikezoe, <i>et al.</i>, Spatial Structure of Spontaneously Excited ICRF Waves and Relevant High-Energy Ion Loss in the GAMMA 10 Tandem Mirror	456
EX/P8-44	Y. Hayashi, <i>et al.</i>, Investigation of Detached Recombining Plasmas in a Linear Device Pilot-PSI and its Impact on Plasma Detachment in Fusion Devices	457
EX/P8-45	A. Burdakov, <i>et al.</i>, Development of Experiment on Multiple-Mirror Trap for Fusion in Budker INP	458
EX/P8-46	P. Bagryansky, <i>et al.</i>, Progress of Plasma Confinement Studies in the Gas Dynamic Trap	459
TH:	Magnetic Confinement Theory and Modeling	461
TH/1-1	S. Hudson, <i>et al.</i>, Penetration and Amplification of Resonant Perturbations in 3D Ideal-MHD Equilibria	462
TH/2-1	C.-S. Chang, <i>et al.</i>, Gyrokinetic Projection of the Divertor Heat-flux Width from Present Tokamaks to ITER	463
TH/2-2	I. Senichenkov, <i>et al.</i>, Study of Detached H-Modes in Full Tungsten ASDEX-Upgrade with N Seeding by SOLPS-ITER Modelling	464
TH/3-1	X. Garbet, <i>et al.</i>, Synergetic Effects of Collisions, Turbulence and Sawtooth Crashes on Impurity Transport	465

TH/4-1	R. Akers, et al., High Fidelity Simulations of Fast Ion Power Flux Driven by 3D Field Perturbations on ITER	466
TH/4-2	A. Biancalani, et al., Gyrokinetic Investigation of the Nonlinear Interplay of Alfvén Instabilities and Energetic Particles in Tokamaks	467
TH/4-3	A. Bierwage, et al., First-Principle Simulations Reproduce Multiple Cycles of Abrupt Large Relaxation Events in Beam-Driven JT-60 Plasmas	468
TH/5-1	P. T. Bonoli, et al., Novel Reactor Relevant RF Actuator Schemes for the Lower Hybrid and the Ion Cyclotron Range of Frequencies	469
TH/5-2	N. K. Bisai, et al., Role of Neutral Gas in Scrape-Off Layer of Tokamak Plasmas	470
TH/6-1	C. Holland, et al., Demonstrating the Multiscale Nature of Electron Transport through Experimentally Validated Simulations	471
TH/6-2	A. Ishizawa, et al., Multimachine Analysis of Turbulent Transport in Helical Systems via Gyrokinetic Simulation	472
TH/6-3	J. Garcia, et al., Electromagnetic Gyrokinetic Analysis of the Isotope Effect .	473
TH/7-1	S. Konovalov, et al., Assessment of the Runaway Electron Energy Dissipation in ITER	474
TH/7-2	L. Xue, et al., Effect of the Second X-Point on the Hot VDE for HL-2M . .	475
TH/8-1	N. Aiba, et al., Diamagnetic MHD Equations for Plasmas with Fast Flow and its Application to ELM Analysis in JT-60U and JET-ILW	476
TH/8-2	S. Pamela, et al., Multimachine Modelling of ELMs and Pedestal Confinement: From Validation to Prediction	477
TH/8-3	H. Jhang, et al., Excitation of Zonal Flows and their Impact on Dynamics of Edge Pedestal Collapse	478
TH/9-1	O. Meneghini, et al., Development of a First-Principles Self-Consistent Core-Pedestal Model and its Application to ITER	479
TH/P1-1	J. Geiger, et al., Plasma Effects in Full-Field MHD-Equilibrium Calculations for W7-X	480

TH/P1-2	F. Ebrahimi, <i>et al.</i>, Physics of Flux Closure during Plasmoid-Mediated Reconnection in Coaxial Helicity Injection	481
TH/P1-3	A. Reiman, Pressure Driven Currents Near Magnetic Islands in 3D MHD Equilibria: Effects of Pressure Variation within Flux Surfaces and of Symmetry	482
TH/P1-4	K. Ichiguchi, <i>et al.</i>, Three-Dimensional Numerical Analysis of Interaction between Plasma Rotation and Interchange Modes	483
TH/P1-5	H. Miura, <i>et al.</i>, Two-Fluid Subgrid-Scale Viscosity in Nonlinear Simulation of Ballooning Modes in a Heliotron Device	484
TH/P1-6	J.-K. Park, <i>et al.</i>, Self-Consistent Optimization of Neoclassical Toroidal Torque with Anisotropic Perturbed Equilibrium in Tokamaks	485
TH/P1-7	S. C. Jardin, <i>et al.</i>, Nonlinear 3D M3D-C1 Simulations of Tokamak Plasmas Crossing a MHD Linear Stability Boundary	486
TH/P1-8	J. R. King, <i>et al.</i>, Nonlinear Extended-MHD Modelling by the NIMROD Code of Broadband-MHD Turbulence during DIII-D QH-Mode Discharges	487
TH/P1-9	F. Liu, <i>et al.</i>, Nonlinear MHD Simulations of Quiescent H-Mode Pedestal in DIII-D and Implications for ITER	488
TH/P1-10	A. Fil, <i>et al.</i>, Modelling and Simulation of Pedestal Control Techniques for NSTX-U	489
TH/P1-11	P. Maget, <i>et al.</i>, First Principle Fluid Modelling of Neoclassical Tearing Modes and of their Control	490
TH/P1-12	E. Poli, <i>et al.</i>, Toroidal Gyrokinetic Studies of the Tearing Mode in Tokamak Plasmas	491
TH/P1-13	S. Inoue, <i>et al.</i>, Active Control and Stabilization of Locked Mode in Tokamaks at High Magnetic Reynolds Number	492
TH/P1-14	M. Furukawa, <i>et al.</i>, Extension of Numerical Matching Method to Weakly Non-linear Regime: Beyond the Rutherford Theory of Magnetic Island Evolution	493

TH/P1-15	N. Ivanov, et al., Magnetic Island Behaviour under Nonaxisymmetric Halo Current at Vertical Displacement Event	494
TH/P1-16	V. E. Lukash, et al., Advances in Numerical Modelling of MGI Mitigated Disrup- tions in ITER	495
TH/P1-17	A. Y. Aydemir, et al., Role of Explosive Instabilities in High- β Disruptions in Toka- maks	496
TH/P1-18	T. Bolzonella, et al., Securing High- β_N JT-60SA Operational Space by MHD Sta- bility and Active Control Modelling	497
TH/P1-19	I. Bandyopadhyay, et al., Plasma Disruption and VDE Modelling in Support of ITER .	498
TH/P1-20	J. Shiraishi, et al., Impact of Kinetic Effects of Energetic Particles on Resistive Wall Mode Stability in Rotating High- β Plasmas	499
TH/P1-21	Z. R. Wang, et al., Nyquist Analysis of Kinetic Effects on the Plasma Response in NSTX and DIII-D Experiments	500
TH/P1-22	J. P. Lee, et al., An Analytic Scaling Relation for the Maximum Tokamak Elongation against $n = 0$ MHD Resistive Wall Modes	501
TH/P1-23	V. Pustovitov, et al., Pfirsch-Tasso Versus Standard Approaches in the Plasma Stability Theory	502
TH/P1-24	M. Bécoulet, et al., Nonlinear MHD Modelling of Edge Localized Modes Dy- namics	503
TH/P1-25	S. Futatani, et al., Nonlinear MHD Simulations of Pellet Triggered ELMs . . .	504
TH/P1-26	F. Orain, et al., Nonlinear Modelling of the Edge Localized Mode Control by Resonant Magnetic Perturbations in ASDEX-Upgrade . .	505
TH/P1-27	D. Chandra, et al., Nonlinear Simulation of ELM Dynamics in the Presence of RMPs and Pellet Injection	506
TH/P1-28	J. Kim, et al., Numerical Calculations of Plasma Response to External Mag- netic Perturbations	507
TH/P1-29	V. S. Mykhaylenko, et al., Drift-Alfvén Instabilities and Turbulence of Magnetic Field Aligned Shear Flows	508

TH/P1-30	L. Zheng, et al., MHD Stability of ITER H-Mode Confinement with Pedestal Bootstrap Current and Diamagnetic Effects Taken into Account	509
TH/P1-31	R. Shurygin, et al., Equilibrium Solutions of MHD Equations for GAMs in the Edge Tokamak Plasma	510
TH/P1-32	H. Feng, et al., Excitation of Frequency Jump by Barely Passing Electrons	511
TH/P1-33	B. Coppi, et al., Magneto-Thermal Reconnection Processes, Related Angular Momentum Transport Issues and Formation of High Energy Particle Populations	512
TH/P1-34	A. Matsuyama, et al., Simulation Study of Interaction between Runaway Electron Generation and Resistive MHD Modes over Avalanche Timescale	513
TH/P1-35	D. Brennan, et al., Collisional Generation of Runaway Electron Seed Distribu- tions Leading to Subcriticality, Avalanche, or Fast Transfer	514
TH/P1-36	J. R. Martín-Solís, et al., Current Profile Shape Effects on the Formation and Termi- nation of Runaway Beams in Tokamak Disruptions and Im- plications for ITER	515
TH/P1-37	H. Nuga, et al., Simulations of Runaway Electron Generation including Hot- Tail Effect	516
TH/P1-38	Z. Guo, et al., Phase Locking, Phase Slips and Turbulence: A New Ap- proach to Mechanisms for Quiescent H-Mode	517
TH/P2-1	S. Maeyama, et al., Gyrokinetic Analysis of the Effects of Electron-Scale Turbu- lence on Ion-Scale Microinstabilities	518
TH/P2-2	M. Nakata, et al., Multispecies ITG-TEM Driven Turbulent Transport of DT Ions and He-ash in ITER Burning Plasmas	519
TH/P2-3	M. Nunami, et al., Anomalous and Neoclassical Transport of Hydrogen Isotope and Impurity Ions in LHD Plasmas	520
TH/P2-4	S. Kobayashi, et al., Direct Identification of Predator-Prey Dynamics in Gyroki- netic Simulations	521
TH/P2-5	S. Yi, et al., Gyrokinetic Simulations of an Electron Temperature Gradi- ent Turbulence-Driven Current in Tokamak Plasmas	522

TH/P2-6	C. Angioni, et al., Progress in the Theoretical Description and the Experimental Characterization of Tungsten Transport in Tokamaks	523
TH/P2-7	J. Candy, et al., Crucial Role of Zonal Flows and Electromagnetic Effects in ITER Turbulence Simulations Near Threshold	524
TH/P2-8	G. M. Staebler, A Model of the Saturation of Coupled Electron and Ion Scale Gyrokinetic Turbulence	525
TH/P2-9	T. Rafiq, et al., New Nonlinear Microtearing Mode Transport Model for Tokamak Plasmas	526
TH/P2-10	A. Y. Pankin, et al., Extending the Validation of Multimode Model for Anoma- lous Transport to High Poloidal β DIII-D Discharges	527
TH/P2-11	S. Suwanna, et al., Evaluation of Predictive Capability for Hydrogenic and Im- purity Density in L- and H-Mode Tokamak Plasma Using Multimode Transport Model	528
TH/P2-12	I. Voitsekhovitch, et al., Recent EUROfusion Achievements in Support to Computa- tionally Demanding Multiscale Fusion Physics Simulations and Integrated Modelling	529
TH/P2-13	G. Falchetto, et al., EUROfusion Integrated Modelling (EU-IM) Capabilities and Selected Physics Applications	531
TH/P2-14	S. D. Pinches, et al., Progress in the ITER Integrated Modelling Programme and the Use and Validation of IMAS within the ITER Members .	534
TH/P2-15	A. Wisitsorasak, et al., The Development of SOL Transport Model for Integrated Core-SOL Simulation of L-Mode Plasma	536
TH/P2-16	R. Budny, Alpha Heating and Isotopic Mass Scaling in JET DT Plasmas	537
TH/P2-17	H.-T. Kim, et al., Statistical Validation of Transport Models on Baseline Dis- charges in Preparation for the Extrapolation to JET DT . . .	538
TH/P2-18	N. Poolyarat, et al., Simulation of Neoclassical Tearing Modes in JET	539
TH/P2-19	N. Hayashi, et al., Core-Edge Coupled Predictive Modelling of JT-60SA High- β Steady-State Plasma with Impurity Accumulation	540

TH/P2-20	M. Romanelli, et al., Investigation of Sustainable Reduced-Power Noninductive Scenarios on JT-60SA	541
TH/P2-21	S. Murakami, et al., Integrated Simulation of Deuterium Experiment Plasma in LHD	542
TH/P2-22	S. H. Kim, et al., Development of ITER Nonactivation Phase Operation Scenarios	543
TH/P2-23	E. Militello Asp, et al., ITER Fuelling Requirements and Scenario Development for H, He and DT through JINTRAC Integrated Modelling . . .	544
TH/P2-24	Y.-S. Na, et al., On Benchmarking of Simulations of Particle Transport in ITER	545
TH/P2-25	J. Y. Kim, et al., Physics-Based Integrated Modelling of the Energy Confinement Time Scaling Laws in Tokamaks	546
TH/P2-26	T. Onjun, et al., Predicted Fusion Performance for ITER and DEMO Plasmas Using a BALDUR Code with Predictive Tritium Influx Model	547
TH/P2-27	R. Hager, et al., A New Understanding of the Bootstrap Current in Steep Edge Pedestal and its Effect on the Pedestal Stability	548
TH/P2-28	Z. Liu, et al., Analysis of Weakly Coherent Mode in I-Mode with the BOUT++ Code	549
TH/P2-29	M. Francisquez, et al., Global 3D Braginskii Simulations of the Tokamak Edge Region	550
TH/P2-30	M. Kotschenreuther, et al., Gyrokinetic Simulations of Tokamak Pedestals: Present Experiments and Extrapolation to Burning Plasmas	551
TH/P2-31	I. Holod, et al., Gyrokinetic Simulations of Microturbulence in DIII-D Pedestal	552
TH/P2-32	Y. Xiao, et al., Gyrokinetic Simulation of Tokamak Edge Plasmas	553
TH/P2-33	M. M. Tsvetoukh, et al., Steep Gradients in Plasma Confined at Convex-Concave Magnetic Field Lines	554
TH/P3-1	Y. Idomura, et al., Full-f Gyrokinetic Simulation including Kinetic Electrons . .	555
TH/P3-2	Y. Kishimoto, et al., Characteristics of Turbulent Transport in Flux-Driven Toroidal Plasmas	556

TH/P3-3	K. Imadera, et al., ITB Formation in Gyrokinetic Flux-Driven ITG Turbulence .	557
TH/P3-4	L. Qi, et al., Gyrokinetic Simulations of Electrostatic Microinstabilities with Bounce-Averaged Kinetic Electrons for Shaped Toka- mak Plasmas	558
TH/P3-5	G. Dif-Pradalier, et al., Validation of Self-Organization Dynamics in Fusion Plasmas	559
TH/P3-6	S. Leerink, et al., Coupling Full-f Gyrokinetic Studies to Experimental Mea- surements of the Isotope Effect for FT-2 Tokamak Plasmas .	560
TH/P3-7	D. Verma, et al., Effect of Magnetic Shear and Equilibrium Flows on Collision- less Microtearing and Mixed Parity Modes in Hot Tokamak Plasmas	561
TH/P3-8	K. C. Shaing, et al., Neoclassical Toroidal Plasma Viscosity with Effects of Finite Banana Width in Finite Aspect Ratio Tokamaks	562
TH/P3-9	M. Honda, et al., Predictions of Toroidal Rotation and Torque Sources Arising in Nonaxisymmetric Perturbed Magnetic Fields in Tokamaks	563
TH/P3-10	S. Matsuoka, et al., Global Kinetic Effect on the Collisionality Dependence of the Neoclassical Toroidal Viscosity in the Superbanana-Plateau Regime	564
TH/P3-11	J. Seol, et al., Effects of Localized Neoclassical Toroidal Viscosity Effects on the Toroidal Rotation Profile in KSTAR	565
TH/P3-12	W. W. Wang, et al., Understanding and Predicting Profile Structure and Para- metric Scaling of Intrinsic Rotation	566
TH/P3-13	H. H. Kaang, et al., Residual Stress and Momentum Transport in Electromag- netic ITG Turbulence	567
TH/P3-14	W. Guttentfeller, et al., Analysis and Prediction of Momentum Transport in Spheri- cal Tokamaks	568
TH/P3-15	C. Fenzi, et al., Co- and Countercurrent Rotation in Tore Supra LHCD Plas- mas: Neoclassical and Turbulent Transport Processes	569
TH/P3-16	S. Nowak, et al., Effect of the EC Torque on Slow Plasma Rotation under Cen- tral ECH/ECCD for NTM Onset	570

TH/P3-17	L. Garcia, et al., Relation of Plasma Flow Structures to Particle Tracer Orbits	571
TH/P3-18	J. Omotani, et al., Edge Flow from Momentum Transport by Neutrals	572
TH/P3-19	P. H. Diamond, et al., New Results in Negative Viscosity Models for Fusion Plasma Dynamics	573
TH/P3-20	Y. Kosuga, et al., Transport of Parallel Momentum by the Triplet Correlation in Drift Wave Turbulence	574
TH/P3-21	M. Yagi, et al., Nonlocal Plasma Response to Edge Perturbation in Tokamak	575
TH/P3-22	D. del-Castillo-Negrete, et al., Modulated Heat Pulse Propagation and Partial Transport Barriers in 3D Chaotic Magnetic Fields	576
TH/P3-23	M. Malkov, et al., L-H Transition Threshold Physics at Low Collisionality . . .	577
TH/P3-24	B. Chatthong, et al., Effects of Heat and Particle Sources Perturbations on L-H-L Transitions Based on Bifurcation Concept	578
TH/P3-25	T. S. Hahm, et al., $E \times B$ Shear and Precession Shear Induced Turbulence Sup- pression	579
TH/P3-26	K. Hallatschek, Zonal Flows and GAMs in Comparative Gyrokinetic and Two-Fluid Tokamak Turbulence Simulations	580
TH/P3-27	M. Leconte, Helical Electric Potential Modulation via Zonal Flow Cou- pling to Resonant Magnetic Perturbations	581
TH/P3-29	S. S. Kim, et al., Tokamak Turbulence Simulations Using BOUT++ in Core Region	582
TH/P3-30	W. Horton, et al., Steady State Turbulent ITER-Like Plasmas with RF Drivers .	583
TH/P3-31	C. McDevitt, et al., Turbulent Current Drive Mechanisms	584
TH/P3-32	C.-B. Kim, et al., Effect of Energy-Nontransporting Nonlinear Flux on the Tur- bulent Plasma Transport	585
TH/P3-33	N. Kasuya, et al., Numerical Diagnostics of Turbulent Transport in Three-Dimensional Magnetic Configurations	586

TH/P3-34	R. Chahine, et al., The Effect of Shaping on Reversed Field Pinch Dynamics . . .	587
TH/P3-35	D. Bonfiglio, et al., Progress in Theoretical RFP Studies: New Stimulated Helical Regimes and Similarities with Tokamak and Stellarator . . .	588
TH/P3-36	L. Sugiyama, et al., Solar Coronal Loops as Magnetically Confined Tori with Gravity	589
TH/P3-37	J. Martinell, et al., Studies of Magnetic Islands in the TJ-II Helic and the Re- lated Transport	590
TH/P3-38	M. Rajković, et al., Predicting Cross-Scale Self-Organization in Turbulent Mag- netically Confined Plasmas	591
TH/P3-39	A. Beklemishev, Diamagnetic Plasma Confinement in Linear Traps	592
TH/P4-1	T. Fülöp, et al., Kinetic Modelling of Runaways in Fusion Plasmas	593
TH/P4-2	P. Aleynikov, et al., Generation of Runaway Electrons during the Thermal Quench in Tokamaks	594
TH/P4-3	T. Kurki-Suonio, et al., The Effect of Plasma Response on Losses of Energetic Ions in the Presence of 3D Perturbations in Different ITER Scenarios	595
TH/P4-4	R. Farengo, et al., Diffusion of Energetic Particles Due to Charge Changes and Neoclassical Tearing Modes	596
TH/P4-5	G. J. Kramer, et al., Improving Fast-Ion Confinement in High-Performance Dis- charges by Suppressing Alfvén Eigenmodes	597
TH/P4-6	G. Vlad, et al., Linear and Nonlinear Dynamics of Electron Fishbones . . .	598
TH/P4-7	Z. Lin, et al., Nonlinear Interactions of Low-Frequency Alfvén Eigenmodes	599
TH/P4-8	W. Zhang, et al., Gyrokinetic Particle Simulation of Fast-Electron Driven β - Induced Alfvén Eigenmodes	600
TH/P4-10	D. Spong, et al., Global Gyrokinetic Simulation of Energetic Particle-Driven Instabilities in 3D Systems	601
TH/P4-11	H. Wang, et al., Simulations of Energetic Particle Driven Geodesic Acoustic Mode and Global Alfvén Eigenmode in 3D LHD Equilibrium	602

TH/P4-12	M. Sasaki, <i>et al.</i>, A New Branch of Geodesic Acoustic Modes Driven by Fast Ions	603
TH/P4-14	R. E. Waltz, <i>et al.</i>, A Critical Gradient Model for Energetic Particle Transport from Alfvén Eigenmodes: GYRO Verification, DIII-D Validation, and ITER Projection	604
TH/P4-16	G. Fu, <i>et al.</i>, Hybrid Simulations of Beam-Driven Fishbone and TAEs in NSTX	605
TH/P4-17	E. Belova, <i>et al.</i>, Coupling of Neutral-Beam-Driven Compressional Alfvén Eigenmodes to Kinetic Alfvén Waves in NSTX and Energy Channelling	606
TH/P4-18	M. Lesur, <i>et al.</i>, Nonlinear Excitation of Subcritical Fast Ion-Driven Modes	607
TH/P4-19	X. Wang, <i>et al.</i>, On the Structure of Wave-Particle Interactions and Nonlinear Alfvénic Fluctuation Dynamics	608
TH/P4-20	L. Chen, <i>et al.</i>, On Excitation of Zonal Structures by Kinetic Alfvén Waves	609
TH/P4-21	Z. Qiu, <i>et al.</i>, Nonlinear Excitation of Fine-Structure Zonal Flow by Alfvén Eigenmodes	610
TH/P4-23	N. Bertelli, <i>et al.</i>, Towards a Self Consistent Evaluation of the RF Wave-Field and the Ion Distribution Functions in Tokamak Plasmas	611
TH/P4-24	Y. Petrov, <i>et al.</i>, A Fully-Neoclassical Finite-Orbit-Width Version of the CQL3D Fokker-Planck Code	612
TH/P4-25	J. Bao, <i>et al.</i>, Nonlinear Particle Simulation of Radio Frequency Waves in Tokamak	613
TH/P4-26	A. V. Arefiev, <i>et al.</i>, Kinetic Simulations of the Full O-X-B Mode Conversion Process and the Deteriorating Effect of High Power Levels	614
TH/P4-27	S. Shiraiwa, <i>et al.</i>, Integration of Core/Edge Plasmas in Fullwave RF Simulation	615
TH/P4-28	J. Lin, <i>et al.</i>, Toroidal Electromagnetic Particle-in-Cell Code with Gyro-kinetic Election and Fully-kinetic Ion	616

TH/P4-29	A. Ram, et al., Scattering of Radio Frequency Waves by Density Fluctuations in Tokamak Plasmas	617
TH/P4-30	D. Green, et al., Verification of a Configuration Space Method for Evaluating the All-Orders Linear Kinetic Plasma Response to RF Power	618
TH/P4-31	J. Myra, et al., An Improved RF-Sheath Boundary Condition and Implications for ICRF Modelling	619
TH/P4-32	E. Z. Gusakov, et al., Low-Threshold Two-UH-Plasmon Decay as a Reason for Anomalous Backscattering and Absorption in Second Harmonic ECRH Experiments	620
TH/P4-34	T. Jenkins, et al., High-Performance Computational Modelling of Plasma-Surface Interactions and RF Antennas	621
TH/P4-35	Z. Gao, et al., Parallel Momentum Transport Induced by RF Waves and by Plasma Turbulence	622
TH/P4-36	A. Zhao, et al., Isotopic Effect of Parametric Instabilities during Lower Hybrid Waves Injection into Hydrogen/Deuterium Plasmas	623
TH/P4-37	A. Sid, et al., Temperature Anisotropy in Magnetized Fusion Plasma	624
TH/P6-1	P. Tamain, et al., Progress towards Self-Consistent Treatment of Turbulence in Edge Plasma Modelling Codes	625
TH/P6-2	A. Hakim, et al., Scrape-Off-Layer Turbulence in Tokamaks Simulated with a Continuum Gyrokinetic Code	626
TH/P6-3	J. P. S. Bizarro, et al., Growth Estimates, Control and Structures in a Two-Field Model of the Scrape-Off Layer	627
TH/P6-4	Y. Marandet, et al., The Role of Statistical Noise in Edge Plasma Transport Codes Based on Kinetic Monte Carlo Solvers for Neutrals: an Analogy with Turbulent Fluctuations	628
TH/P6-5	W. Choe, et al., Comparison of Divertor Heat Flux Splitting by 3D Fields with Field Line Tracing Simulation in KSTAR	629
TH/P6-6	A. Stegmeir, et al., The Field Line Map Approach for Simulations of Plasma Edge/SOL Turbulence	630

TH/P6-7	D. P. Stotler, et al., Neutral Recycling Effect on Edge ITG Turbulence and Transport	631
TH/P6-8	P. Ricci, et al., Progress in First-Principles Simulation of SOL Plasma Turbulence and Neutral Atom Dynamics with the GBS Code . . .	632
TH/P6-9	N. Mellet, et al., Multiscale Modelling of Sheath Physics in Edge Transport Codes	633
TH/P6-10	R. Churchill, et al., Kinetic Understanding of Neoclassical Scrape-Off Layer Physics, Comparison with Fluid Modelling, and Experimental Validation	634
TH/P6-11	F. Effenberg, et al., Numerical Investigation of 3D Plasma Edge Transport and Heat Fluxes including Impurity Effects in Wendelstein 7-X Startup Plasmas with EMC3-EIRENE	635
TH/P6-12	J. Lore, et al., Pedestal-to-Wall 3D Fluid Transport Simulations on DIII-D and NSTX	636
TH/P6-15	I. Katanuma, et al., Particle Simulation on Blob Formation and Propagation in an Open System	637
TH/P6-16	S.-H. Ku, et al., Understanding the Blobby Turbulence in Edge Plasma from Gyrokinetic Simulation	638
TH/P6-17	H. Hasegawa, et al., Impurity Transport Caused by Blob and Hole Propagations	639
TH/P6-18	X. Xu, et al., Nonlinear Dynamics of ELMs with E_r Shear and Collisionality Trends	640
TH/P6-19	T. Y. Xia, et al., Divertor Heat Flux Simulations in ELMy H-Mode Discharges of EAST and Other Tokamaks	641
TH/P6-20	J. Huang, et al., EMC3-EIRENE Simulations for the Impact of External Magnetic Perturbations on EAST Edge Plasma	642
TH/P6-22	A. Kirschner, et al., Modelling of Prompt Deposition of Tungsten under Fusion Relevant Conditions	643
TH/P6-23	S. Yamoto, et al., Kinetic Modelling of Tungsten Impurity Transport Using the IMPGYRO Code	644

TH/P6-24	R. Zagorski, et al., Numerical Analyses of Baseline JT-60SA Design Concepts with the COREDIV Code	645
TH/P6-25	X. Tang, et al., Plasma Particle and Energy Exhaust to and Recycling at a Tungsten Surface	646
TH/P6-26	R. Bisson, et al., Retention and Release of Hydrogen Isotopes in Tungsten Plasma Facing Components: Understanding and Controlling with an Integrated Approach	647
TH/P6-27	K. Ibano, et al., Particle Simulation of Plasma Heat-Flux Dissipation by Evap- orated Wall Materials	648
TH/P6-28	M. Campanell, et al., Strong Electron Emission Could Enable a New Plasma-Surface Interaction Regime in Divertors	649
TH/P6-29	S. Sangaroon, et al., A Model for Predicting Tritium Flux from Blanket Mock-Up in Tokamak Fusion Reactors	650
TH/P6-30	R. Dey, et al., Investigation of Neutral Particle Dynamics in ADITYA Toka- mak Plasma with DEGAS2 Code	651
TH/P6-31	M. M. Tsvetoukh, et al., Plasma-Surface Interactions Leading to Self-Sustained Dis- charges at the First Wall	652
TH/P6-32	M. Umansky, et al., Assessment of X-Point Target Divertor Configuration for Power Handling and Detachment Front Control	653
FIP:	Fusion Engineering, Integration and Power Plant Design	655
FIP/1-1	P. Fu, et al., Recent Progress of ITER Package in ASIPP	656
FIP/1-2	J. Smith, et al., ITER Central Solenoid Module Fabrication	657
FIP/1-3Ra	J. Hiratsuka, et al., Long-Pulse Acceleration of 1 MeV Negative Ion Beams to- ward ITER and JT-60SA Neutral Beam Injectors	658
FIP/1-3Rb	U. Fantz, et al., Towards Powerful Negative Ion Beams at the Test Facility ELISE for the ITER and DEMO NBI System	659
FIP/1-4	M. Kisaki, et al., Progress of Experimental Study on Negative Hydrogen Ion Production and Extraction	660

FIP/1-5	A. Mukherjee, et al., Progress in High Power Test of R&D Source for ITER ICRF System	661
FIP/1-6Ra	G. Denisov, et al., New Results of Development of Gyrotrons for Plasma Fusion Installations	662
FIP/1-6Rb	R. Ikeda, et al., Development of Multifrequency Megawatt Gyrotrons for Fusion Devices in JAEA	663
FIP/1-6Rc	T. Kariya, et al., Development of over-MW Gyrotrons for Fusion at Frequencies from 14 GHz to Sub-THz	664
FIP/2-1Ra	Y. Seki, et al., Progress of Qualification Testing for Full-Scale Plasma-Facing Unit Prototype of Full Tungsten ITER Divertor in Japan . . .	665
FIP/2-1Rb	J. Bucalossi, et al., Progresses on WEST Platform Construction towards First Plasmas	666
FIP/2-2	K. Feng, et al., Design and R&D Progress of Chinese HCCB TBS Programme	668
FIP/2-3	I. Ricapito, et al., Lessons Learned for the Breeding Blanket Designers from the Design Development of the European Test Blanket Module Systems (He, Tritium, Liquid Metal Systems)	669
FIP/2-4	A. Saraswat, et al., Development of Sensors for High-Temperature High-Pressure Liquid Pb/Pb-16Li Applications	670
FIP/2-5	M. Ono, et al., Liquid Lithium Loop System to Solve Challenging Technology Issues for Fusion Power Plant	671
FIP/3-1Ra	H. Tanigawa, et al., Accomplishment of DEMO R&D Activity of IFERC Project in BA Activity and Strategy toward DEMO	672
FIP/3-1Rb	R. Hiwatari, et al., Progress of Conceptual Design Study on Japanese DEMO .	673
FIP/3-2	R. Kemp, et al., Dealing with Uncertainties in Fusion Power Plant Conceptual Development	674
FIP/3-3	J. Kang, et al., Development of a Systematic, Self-Consistent Algorithm for K-DEMO Steady-State Operation Scenario	675

FIP/3-4Ra	A. Sagara, et al., Two Conceptual Designs of Helical Fusion Reactor FFHR- d1A Based on ITER Technologies and Challenging Ideas . . .	676
FIP/3-4Rb	H. Hashizume, et al., Development of Remountable Joints and Heat Removable Techniques for High-Temperature Superconducting Magnets	677
FIP/3-4Rc	K. Takahata, et al., Lessons Learned from the Eighteen-Year Operation of the LHD Poloidal Coils Made from CIC Conductors	678
FIP/3-5	P. Bruzzone, et al., High Temperature Superconductors for Fusion at the Swiss Plasma Center	679
FIP/4-1Ra	Y. Shibama, et al., Assembly Technologies of the Superconducting Tokamak on JT-60SA	680
FIP/4-1Rb	P. Decool, et al., JT-60SA TF Coil Manufacture, Test and Preassembly by CEA	681
FIP/P4-2	M. Nocente, et al., Conceptual Design of the Radial Gamma-Ray Spectrometers System for Alpha Particle and Runaway Electron Measure- ments at ITER	682
FIP/P4-3	C. Hellesen, Conceptual Design of the Best TOF Neutron Spectrometer for Fuel-Ion Ratio Measurements at ITER	683
FIP/P4-4	L. R. Baylor, et al., Pellet Injection Technology and Application to Mitigate Tran- sient Events on ITER	684
FIP/P4-5	R. Imazawa, et al., Progress on Integrated Design of ITER Poloidal Polarimeter for Current Profile Measurement	685
FIP/P4-6	F. Poli, et al., Electron Cyclotron Power Management in ITER, the Path from the Commissioning Phase to Demonstration Discharges	686
FIP/P4-7	H. Nakanishi, et al., High-Performance Data Transfer for Full Data Replication between ITER and the Remote Experimentation Centre . . .	687
FIP/P4-8	K. Itami, et al., Design Development of the ITER Divertor Diagnostic Sys- tems in Japan	688
FIP/P4-9	K. Takahashi, et al., Development of ITER Poloidal Steering Equatorial EC Launcher Enhancing ECCD Performance	689

FIP/P4-10	N. Umeda, <i>et al.</i>, Development of Ultrahigh Voltage Insulation Technology for the Power Supply Components in Neutral Beam System on ITER	690
FIP/P4-11	Y. Kawano, <i>et al.</i>, Overview of ITPA R&D Activities for Improvement of ITER Diagnostic Performance	691
FIP/P4-12	V. N. Muvvala, <i>et al.</i>, Electro-Mechanical Design and Experimental Validation of Post Insulators for Beam Source for ITER Diagnostic Neutral Beam	692
FIP/P4-13	K. K. Gotewal, <i>et al.</i>, Concept Design of the Heavy Duty Multipurpose Deployer for ITER	693
FIP/P4-14	S. Kajita, <i>et al.</i>, Effect of Wall Light Reflection in ITER Diagnostics	694
FIP/P4-15	D. Gin, <i>et al.</i>, On Fast Ions Diagnostics with Gamma-Ray Spectrometry in ITER	695
FIP/P4-16	D. Marocco, <i>et al.</i>, System Level Design and Performances of the ITER Radial Neutron Camera	696
FIP/P4-17	A. Zvonkov, <i>et al.</i>, CXRS-edge Diagnostic in the Harsh ITER Environment	697
FIP/P4-18	L. Hu, <i>et al.</i>, Progress on Design and R&D of ITER Diagnostic-Radial X-ray Camera	698
FIP/P4-20	J. K. Anderson, <i>et al.</i>, High Power Testing of Water-Cooled Waveguide for ITER ECH Transmission Lines	699
FIP/P4-21	Z. Song, <i>et al.</i>, Research and Development Progress of the ITER PF Con- verter System	700
FIP/P4-22	J. Chen, <i>et al.</i>, Technical Preparation for Series Production of ITER Enhance Heat Flux FW Panels	701
FIP/P4-27	G. S. Kurskiev, <i>et al.</i>, ITER Core Thomson Scattering: Objectives and Error Analysis	702
FIP/P4-28	V. Toigo, <i>et al.</i>, The ITER Neutral Beam Test Facility toward SPIDER Operation	703
FIP/P4-29	F. Albajar, <i>et al.</i>, The Development of the European 1 MW, 170 GHz CW Gy- rotron for the ITER Electron Cyclotron Heating System	704

FIP/P4-31	G. Serianni, et al., Synergy of Numerical Simulations and Experimental Measurements to Improve the Interpretation of Negative Ion Beam Properties	705
FIP/P4-33	J. A. González Guevara, et al., 60 GHz–300 kW Gyrotron General Design for the Mexican Tokamak “T”	706
FIP/P4-36	J. Joshi, et al., Manufacturing and Commissioning of Large Size UHV Class Vacuum Vessel for Indian Test Facility (INTF) for Neutral Beams	707
FIP/P4-37	M. Tokitani, et al., Fabrication of Divertor Mock-Up with ODS-Cu and W by Improved Brazing Technique	708
FIP/P4-38	M. Modestov, et al., Liquid Metal Flow Control Simulation at Liquid Metal Experiment	709
FIP/P4-39	R. Zanino, et al., Modelling the Lithium Loop in a Liquid Metal Divertor for Future Fusion Reactors	710
FIP/P4-40	A. Fasoli, TCV Divertor and Heating Upgrades for Contributing to DEMO Physics Basis	711
FIP/P4-41	Y. Hatano, et al., Japan-US Joint Research Project PHENIX (2013–2018); Heat Transfer Tests, Neutron Irradiation and Postirradiation Examinations for Development of He-Cooled Tungsten Divertor	712
FIP/P4-42	C. Day, et al., Assessment of the Operational Window for JT-60SA Divertor Pumping under Consideration of the Effects from Neutral-Neutral Collisions	713
FIP/P4-43	A. Sergis, et al., Flow Characteristics in HyperVapotron Elements Operating with Nanofluids	714
FIP/P4-44	F. Bonelli, et al., Self-Consistent Coupling of DSMC Method and SOLPS Code for Modelling Tokamak Particle Exhaust	715
FIP/P4-45	P. K. Domalpalay, et al., Computational Fluid Dynamic Analysis of Screw Tube Relevant for Fusion Applications	716
FIP/P4-46	J. Ghosh, et al., Upgrade of ADITYA Tokamak with Limiter Configuration to ADITYA Upgrade Tokamak with Divertor Configuration	717

FIP/P7-1	T. Brown, et al., Development of a 3 m HTS FNSF Device and the Qualifying Design and Engineering R&D Needed to Meet the Low AR Design Point	718
FIP/P7-2	J. Miyazawa, et al., REVOLVER-D: The Ergodic Limiter/Divertor Consisting of Molten Tin Shower Jets Stabilized by Chains	719
FIP/P7-3	G. Neilson, et al., Progress in K-DEMO Heating/Current Drive and Tokamak Configuration Development	720
FIP/P7-4	G. Grossetti, et al., DEMO Port Plug Design and Integration Studies	721
FIP/P7-5	P. Sonato, et al., Conceptual Design of the DEMO NBIs: Main Developments and R&D Achievements	722
FIP/P7-6	D. G. Whyte, et al., Smaller & Sooner: Exploiting High Magnetic Fields from New Superconductors for a More Attractive Fusion Energy Development Path	723
FIP/7-7	M. Q. Tran, et al., EU DEMO Heating and Current Drive: Physics and Technology	724
FIP/P7-8	G. Granucci, et al., Conceptual Design of the DEMO EC-System: Main Developments and R&D Achievements	725
FIP/P7-9	F. Warmer, et al., Integrated Concept Development of Next-Step Helical-Axis Advanced Stellarators	726
FIP/P7-10	L. Zani, et al., Evolutions of EU DEMO Reactor Magnet System Design Along the Recent Years and Lessons Learned for the Future	727
FIP/P7-11	N. Yanagi, et al., Helical Coil Design and Development with 100 kA HTS STARS Conductor for FFHR-d1	728
FIP/P7-12	F. Crisanti, DTT: An Integrated Bulk and Edge Plasma Experiment to Tackle the Power Exhaust Problem in View of DEMO	729
FIP/P7-13	A. Bader, et al., Ion Cyclotron Range of Frequency Power for DEMO	730
FIP/P7-14	R. Wenninger, et al., Power Handling and Plasma Protection Aspects that Affect the Design of the DEMO Divertor and First Wall	731

FIP/P7-15	J. Park, et al., Nuclear Analysis of Structural Damage and Nuclear Heating on Enhanced K-DEMO Divertor Model	732
FIP/P7-16	M. Rozenkevich, et al., Concept of Tritium Processing and Confinement in Fuel Cy- cle of Ignitor	733
FIP/P7-17	V. Menon, et al., Zero D and 1.5D Transport Analysis of SST-2	734
FIP/P7-18	M. Velarde, et al., Multiscale Integral Analysis of Tritium Leakages in Fusion Power Plants	735
FIP/P7-19	M. Gryaznevich, et al., Overview and Status of Construction of ST40	736
FIP/P7-20	W. Morris, et al., Approaches for the Qualification of Exhaust Solutions for DEMO-Class Devices	737
FIP/P7-21	C. Reux, et al., DEMO Design Using the SYCOMORE System Code: Con- servative Designs and Pathways towards the Reactor	738
FIP/P7-22	N. Asakura, et al., Physics and Engineering Design Studies on Power Exhaust and Divertor for a 1.5 GW Fusion Power DEMO	739
FIP/P7-24	R. Gangradey, et al., Progress towards Achieving Large Pumping Speed for Ex- haust from Fusion Grade Machines	740
FIP/P7-25	C. Danani, et al., Nuclear Design Analyses of SST-2	741
FIP/P7-26	G. Stankunas, et al., Comparative Analysis of WCLL to Different European DEMO Blanket Concepts in Terms of Activation and Decay Heat after Exposure to Neutron Irradiation	742
FIP/P7-27	M. Ferrari, et al., How Tokamak Interface Requirements Are Driving the De- sign of TBM Systems in ITER towards Breeding Blanket De- sign in DEMO	743
FIP/P7-29	G. Aiello, et al., Design of the Helium-Cooled Lithium-Lead Breeding Blan- ket in CEA: From TBM to DEMO	744
FIP/P7-31	R. Bhattacharyay, et al., Overview of Indian LLCB TBM Programme and Status of R&D Activities	745

FIP/P7-33	S. S. Ananyev, et al., DT Fuel System of DEMO-FNS Tokamak with Tritium Breeding Blanket	746
FIP/P7-34	D. Schissel, et al., Remote Third Shift EAST Operation: A New Paradigm . . .	747
FIP/P7-35	M. Yokoyama, et al., Extended Capability of the Integrated Transport Analysis Suite, TASK3D-a, for LHD Experiment, and its Impacts on Facilitating Stellarator-Heliotron Research	748
FIP/P7-36	R. Lunsford, et al., ELM Pacing with High Frequency Multispecies Impurity Granule Injection in NSTX-U H-Mode Discharges	749
FIP/P7-37	J.-C. Vallet, et al., Towards the Completion of the CEA Contributions to the Broader Approach Projects	750
FIP/P7-38	V. L. Tanna, et al., Techno-Economic Aspects of High Current Leads for Fusion Devices	751
FIP/P7-39	E. Villedieu, et al., The Articulated Inspection Arm Development	752
FIP/P7-40	P. Khvostenko, et al., Status of Tokamak T-15MD	753
FIP/P7-41	V. Minaev, et al., Spherical Tokamak Globus-M2: Design, Integration, Construction	754
FIP/P7-42	R. Raman, et al., NSTX-U Contributions to Disruption Mitigation Studies in Support of ITER	755
FIP/P7-43	R. R. Khayrutdinov, et al., Development of Regulators Synthesis Method for Magnetic Plasma Control System of the T-15 Tokamak	756
FIP/P7-44	O. A. Muñoz Ovalle, et al., Reciprocating Langmuir Probes Set Design for the Mexican Tokamak "T"	757
FIP/P7-45	Q. Zhang, et al., Upgrade and Operational Performance of EAST Cryogenic System	758
FIP/P7-46	J. Mishra, et al., India's Pellet Fuelling Programme	759
FIP/P7-47	M. B. Chowdhuri, et al., Design of Charge Exchange Recombination Spectroscopy (CXRS) on SST-1 Tokamak	760

FNS: Fusion Nuclear Physics and Technology	761
FNS/1-1 Y. Shpanskiy, et al., Status of DEMO-FNS Development	762
FNS/1-2 M. Gilbert, et al., Activation, Decay Heat, and Waste Classification Studies of the European DEMO Concept	763
FNS/1-3 Z. Xu, et al., Optimizing Full-coverage Free Surface Flow for Liquid Metal PFCs	764
FNS/P5-1 I. Palermo, et al., Optimization Process for the Design of the DCLL Blanket for the European Demonstration Fusion Reactor According to its Nuclear Performances	765
FNS/P5-2 J. Rapp, et al., Developing the Science and Technology for the Material Plasma Exposure Experiment (MPEX)	766
FNS/P5-3 S. Şahin, First Wall Lifetime Extension with Flowing Liquid Zone for Fusion Reactors	767
FNS/P5-5 S. Sato, et al., New Integral Experiments for a Variety of Fusion Reactor Materials with DT Neutron Source at JAEA/FNS	768
FNS/P5-6 T. Fujita, et al., Optimization Study of Normal Conductor Tokamak for Com- mercial Neutron Source	769
FNS/P5-8 K. Ogawa, et al., Investigation on Irradiation Effects on Highly Integrated Leading Edge Electronic Components of Diagnostics and Control Systems for the LHD Deuterium Operation	770
FNS/P5-9 S. M. Manoah, et al., Design and Analysis of SST-2 Vacuum Vessel	771
FNS/P5-10 U. Fischer, et al., Advanced Neutronics Simulation Tools and Data for Fusion Applications	772
FNS/P5-11 A. Zhirkin, et al., Fusion Neutron Source Blanket: Requirements on Calcula- tion Accuracy and Benchmark Experiment Precision	773
FNS/P5-12 J. Yu, Design and R&D Activities of Fusion Breeder Blankets in China	774
FNS/P5-13 C. Velasquez, et al., Temperature Sensitivity Analysis of Nuclear Cross Section Using FENDL for Fusion-Fission System	775

IFE: Inertial Fusion Experiments and Theory	777
IFE/1-1 J.-L. Miquel, et al., Overview of the Laser Megajoule First Experiments	778
IFE/1-2 S. Fujioka, et al., Fast Ignition Inertial Confinement Fusion with Kilo-Tesla Magnetic Field	779
IFE/1-3 J. Frenje, et al., Observations of Residual Bulk-Fluid Motion and Low-Mode Areal-Density Asymmetries at Peak Convergence in NIF Implosions through Spectral Measurements of DD and DT Neutrons	780
IFE/1-4 A. Yogo, et al., Laser-Driven Ion Acceleration on LFEX for Fast Ignition: State of the Art and Applications	781
IFE/1-5 H. G. Rinderknecht, et al., Ion Kinetic Dynamics in Strongly-Shocked Plasmas Relevant to ICF	782
IFE/1-6 J. Kawanaka, et al., LFEX-Laser: A Multi-Kilojoule, Multi-Petawatt Heating Laser for Fast Ignition	783
IFE/P5-2 R. Khaydarov, et al., Improvement of Characteristics of Laser Source of Ions by Changing the Parameters of the Target and External Parameters	784
IFE/P5-4 N. Ding, et al., Recent Advances in Theoretical and Numerical Studies of Z-Pinch Driven Inertial Confinement Fusion in the IAPCM .	785
IFE/P5-5 T. Kikuchi, et al., Recent Activities on Heavy Ion Inertial Fusion in Japan	786
IFE/P5-6 K. W. Hill, et al., Adapting High Resolution X-ray Spectroscopy from MFE to Temperature and Density Measurements in ICF	787
IFE/P5-7 A. N. Simakov, et al., The Role of Beryllium Ablators in Inertial Confinement Fusion	788
IFE/P5-8 J. Liu, et al., Spherical Convergent Plasma Fusion (SCPF) Neutron Gener- ator by Laser Drive: Theory and Experiment	789
IFE/P5-9 Y. Mori, et al., Fast Heating of an Imploded Core under Counter Beam Irra- diation by Using a Repetitive IFE Driver HAMA	790
IFE/P5-10 Y. Kitagawa, et al., Unified Studies of Fast-Ignition Scheme Fusion with Coun- terbeam Configuration	791

IFE/P5-11	Y. Arikawa, et al., Improvement in the Heating Efficiency of Fast Ignition Inertial Confinement Fusion by Suppressing the Preformed Plasma	792
IFE/P5-12	H. Nagatomo, et al., Compression and Electron Beam Heating of Solid Target under the External Magnetic Field for Fast Ignition	793
IFE/P5-13	A. Morace, et al., Plasma Mirror Implementation on LFEX Laser for Ion and Fast Electron Fast Ignition	794
IFE/P5-14	H. J. Kong, et al., Coherent Beam Combination for Laser Fusion Driver Design Using Rotation Wedge Self-Phase-Controlled Stimulated Brillouin Scattering Phase Conjugation Mirrors	795
IFE/P5-17	K. Ishii, et al., Present Operation Status of Target Injection System	796
IFE/P5-18	R. C. Issac, et al., Suitability of Nano-Structured Materials for Inertial Fusion Reactor Inner Walls	797
IFE/P5-19	T. Norimatsu, et al., Conceptual Design and Issue Analysis of Laser Fusion Experiment Reactor (LIFT)	798
MPT:	Materials Physics and Technology	799
MPT/1-1	R. Stoller, et al., Recent Advances in Radiation Materials Science from the US Fusion Reactor Materials Programme	800
MPT/1-2Ra	G.-N. Luo, et al., Overview on Decade Development of Plasma-Facing Components at ASIPP	801
MPT/1-2Rb	R. Ding, et al., Advances in Understanding of High-Z Material Erosion and Redeposition in Low-Z Wall Environment in DIII-D	802
MPT/1-3	A. Widdowson, et al., Overview of Fuel Inventory in JET with the ITER-Like Wall	803
MPT/P5-1	G. Tynan, et al., Experimental Study of Deuterium Retention and Thermo-Mechanical Properties in Ion-Beam Displacement-Damaged Tungsten	804
MPT/P5-2	S. Rogozhkin, et al., ODS Steels: Nanostructure Evolution under Irradiation	805

MPT/P5-3	J. W. Coenen, <i>et al.</i>, Tungsten Composite Materials for Fusion First Wall Applications	806
MPT/P5-4	C. Linsmeier, <i>et al.</i>, Advanced Tungsten-Based Materials as an Option for a Fusion Reactor	807
MPT/P5-5	A. Kreter, <i>et al.</i>, Overview of Recent Plasma-Material Interaction Studies in the Linear Plasma Device PSI-2	808
MPT/P5-6	A. Litnovsky, <i>et al.</i>, Smart Tungsten Alloys as First Wall Material for a Future Fusion Power Plant	809
MPT/P5-7	I. Tazhibayeva, <i>et al.</i>, Study of Properties of Tungsten Irradiated in Hydrogen Atmosphere	810
MPT/P5-9	A. Kimura, <i>et al.</i>, Structural Material Innovation for Advanced Blanket Design: Current Status and Future Prospect of ODS Steels R&D	811
MPT/P5-11	H. Kondo, <i>et al.</i>, Validation of Liquid Lithium Target Stability for Intense Neutron Source	812
MPT/P5-12	X. Liu, <i>et al.</i>, Design and Fabrication of the Active Cooling Divertor Components for HL-2M Tokamak	813
MPT/P5-13	A. Kasugai, <i>et al.</i>, Progress on the Development of Linear IFMIF Prototype Accelerator and the Beam Commissioning	814
MPT/P5-14	M. Sakamoto, <i>et al.</i>, Hydrogen Isotope Retention in Tungsten Surface-Modified by Heavy Ion Irradiation, Helium Bubbles and Tungsten Deposition	815
MPT/P5-15	M. Wirtz, <i>et al.</i>, Material Properties and their Influence on the Behaviour of Tungsten as Plasma Facing Material	816
MPT/P5-16	M. Nakajima, <i>et al.</i>, Assessment of Corrosion Behaviour of Reduced Activation Ferritic/Martensitic Steel, F82H in High Temperature Water	817
MPT/P5-17	N. Nemati, <i>et al.</i>, Investigation of W/Cu Functionally Graded Material with CMA Particles as Plasma Facing for First Wall Components	818
MPT/P5-18	T. Shimizu, <i>et al.</i>, Investigation of Lanthanoid-Doped APLF Scintillators for Neutron Detection	819

MPT/P5-19	Y. Nobuta, <i>et al.</i>, Effects of Modified Surfaces Produced at Plasma-Facing Surface on Hydrogen Isotopes and Helium Release Behaviour in the LHD	820
MPT/P5-21	T. Nagasaka, <i>et al.</i>, Development of Dissimilar-Metals Joint of Oxide-Dispersion-Strengthened (ODS) and Non-ODS Reduced-Activation Ferritic Steels	821
MPT/P5-23	A. Ito, <i>et al.</i>, BCA-KMC Hybrid Simulation with Meta-Modelling for Hydrogen Dynamic Retention in Tungsten Material	822
MPT/P5-24	Q. Huang, Status and Strategy of CLAM Steel for Fusion Application in China	823
MPT/P5-25	E. Wakai, <i>et al.</i>, Small Specimen Test Technology Development towards Design of Fusion DEMO Reactors and Future Direction Plan	824
MPT/P5-26	K. B. Woller, <i>et al.</i>, Impact of Helium Ion Energy Modulation on Tungsten Surface Morphology and Nano-Tendrils Growth	825
MPT/P5-27	M. Oya, <i>et al.</i>, Deuterium Retention and Melting Behaviour in Toughened, Fine-Grained Recrystallized Tungsten	826
MPT/P5-29	H. T. Lee, <i>et al.</i>, Modelling Fuel Retention in Tungsten Plasma-Facing Materials under Realistic Tokamak Operation including Plasma Impurities	827
MPT/P5-30	M. A. Jaworski, <i>et al.</i>, High-Temperature, Liquid Metal Plasma-Facing Component Research and Development for the NSTX-U	828
MPT/P5-31	Y. Oya, <i>et al.</i>, Effect of Defect Concentration and Distribution on Hydrogen Isotope Retention and Diffusion in Damaged W for Fusion First Wall	829
MPT/P5-32	I. E. Garkusha, <i>et al.</i>, Novel Test Bed Facility for PSI Issues in Fusion Reactor Conditions on the Base of Next Generation QSPA Plasma Accelerator830	
MPT/P5-33	J. M. Perlado, <i>et al.</i>, Multiscale Modelling of Materials: Light Species Dynamics in Nano-W and EOS of Hydrogen	831

MPT/P5-35	B. M. Sorbom, <i>et al.</i>, Determination of Radiation Damage Limits to High-Temperature Superconductors in Reactor-Relevant Conditions to Inform Compact Fusion Reactor Design	832
MPT/P5-38	A. V. Spitsyn, <i>et al.</i>, Deuterium Permeation through Candidate Structural Materials for a Fusion Reactor	833
MPT/P5-39	L. Avotina, <i>et al.</i>, Activities for Fusion Energy Functional and Plasma Facing Material Research at the University of Latvia	834
MPT/P5-41	F. Arbeiter, <i>et al.</i>, The Accomplishments of Lithium Target and Test Facility Validation Activities in the IFMIF/EVEDA Phase	835
MPT/P5-42	R. S. Rawat, <i>et al.</i>, Investigations of Tungsten as Candidate Plasma Facing Material under High Repetition and Intense Fusion-Relevant Pulses	836
PPC:	Plasma Overall Performance and Control	837
PPC/1-1	H. Takahashi, <i>et al.</i>, Extension of Operational Regime in High-Temperature Plasmas and Effect of ECRH on Ion Thermal Transport in the LHD	838
PPC/2-1	A. Loarte, <i>et al.</i>, Evaluation of Tungsten Transport and Concentration Control in ITER Scenarios	839
SEE:	Safety, Environmental and Economic Aspects of Fusion	841
SEE/P7-1	K. Gi, <i>et al.</i>, Assessment of Potential and Breakeven Prices of Fusion Power Plants under Low-Carbon Development Scenarios	842
SEE/P7-2	X. Z. Jin, <i>et al.</i>, Proposal of the Confinement Strategy for EU DEMO	843
SEE/P7-3	A. Prades, <i>et al.</i>, Social Research on Fusion	844
SEE/P7-4	H. Cabal, <i>et al.</i>, Exploration of Fusion Power Penetration under Different Global Energy Scenarios Using the EFDA Times Energy Optimization Model	845
SEE/P7-5	Y. Someya, <i>et al.</i>, Safety and Waste Management Studies as Design Feedback for a Fusion DEMO Reactor in Japan	846

SEE/P7-6	S. Konishi, et al., Future Electric Market and Fusion Deployment Strategy with Electricity Storage Systems	847
PD:	Post-Deadline Contributions	849
PD/1-1	R. Nazikian, et al., First Observation of ELM Suppression in ASDEX-Upgrade in a Similarity Experiment with DIII-D	850
PD/1-2	H.-S. Bosch, et al., Final Integration, Commissioning and Start of the Wendel- stein 7-X Stellarator Operation	851
PDP-02	I. M. Ferreira Nunes, et al., First Results from Recent JET Experiments in Hydrogen and Hydrogen-Deuterium Plasmas	852
PDP-03	N. Gorelenkov, et al., Suppression of Alfvén modes through additional beam heating	853
PDP-04	J. Stober, et al., Advanced Tokamak Experiments in Full-W ASDEX Upgrade	854
PDP-05	M. J. Hole, et al., Fluid Models for Burning and 3D Plasmas: Challenging the Kinetic Paradigm	855
PDP-07	S. Takamura, Microwrinkle Structure on Refractory Metal Surfaces Irradi- ated by Noble Gas Plasma Species	856
PDP-08	A. Huber, et al., The Effect of the Isotope on the H-Mode Density Limit . . .	857
PDP-09	R. Goldston, et al., Recent Advances towards a Lithium Vapor Box Divertor . .	858
PDP-10	H. Berk, et al., Chirping in Plasmas; Test of Criterion for Chirping Onset and Simulation of Explosive Chirping	859
PDP-11	M. Inomoto, et al., Formation of Closed Flux Surfaces in Reconnection Current Layer by Accelerated Electrons during Merging Start-up of Spherical Tokamak	860
PDP-12	S. Jacquemot, Overview of some key achievements on the route to IFE . .	861
PDP-13	J. Anderson, Statistical Description of Turbulent Transport for Flux Driven Toroidal Plasmas	862

PDP-14	M. Wischmeier, et al., Facing the Challenge of Power Exhaust on the way to a Future Power Plant with Experiments in the JET and ASDEX Upgrade Tokamaks	863
PDP-15	S. Newton, et al., Impurity Transport and Plasma Flow in a Mixed Collisionality Stellarator Plasma	865
PDP-16	N. Fukumoto, et al., Advanced Fuelling in Spherical Tokamak by Compact Toroid Injection on QUEST	866
PDP-18	N. Kargin, et al., Metal Hall Sensors for the New Generation Reactors of the DEMO Scale	867
PDP-19	Y. Igitkhanov, et al., Effect of Divertor Performance on the Pumping Efficiency in DEMO	868
PDP-21	C. Corr, et al., Helium Ion Energy Threshold for Helium Retention and Nano-bubble Formation in Tungsten	869
PDP-23	A. Portone, Active and Passive Stabilization of $n = 0$ RWMs in Future Tokamak Devices	870
PDP-24	R. Srivastava, et al., Collisional Radiative Model Using the Fully Relativistic Cross-sections for the Hydrogen-cesium Plasma Relevant to ITER Negative Ion Based NBI System	871
PDP-25	V. Kornev, et al., DD Neutron Emission Measurement in the Compact Tokamak TUMAN-3M	872
PDP-26	M. Probst, et al., Electron-Impact Ionization Cross Sections of Molecules and Ions in Fusion Plasma	873
Indexes		875

O/1: Opening Plenary

O/1

Fusion for Sustainable World Development

A. Iiyoshi¹

¹*Chubu University, Kasugai, Aichi, Japan*

Corresponding Author: A. Iiyoshi, iiyoshi@isc.chubu.ac.jp

It has been more than half a century since fusion energy research was disclosed at the 2nd Atoms for Peace conference, held in September 1958, in Geneva. During the course of this period, DT-burning experiments were actually conducted in TFTR and in JET, both intended for energy breakeven: $Q = 1$. This is a tremendous achievement of mankind, wishing to create a self-burning star on the Earth.

The IAEA fusion energy conference was once held in Kyoto in 1986, so that this is the second time hosted in Kyoto. In the meantime, another IAEA-FEC was held in October, 1998 in Yokohama, which happened to be right after the DT-burning experiments, mentioned above. Interestingly, it was around that time the ITER-EDA came to a critical phase.

As opposed to the rest of the world, from the beginning the Japanese fusion research community chose to explore multiple possibilities, including magnetic confinement by tokamak, helical and mirror configurations, and also laser-driven inertial confinement, each having made remarkable progress. In addition to achieving burning plasmas in tokamaks, LHD built at NIFS has been a unique effort in helical plasma studies, until recently W7-X in Germany has been put in operation.

It is remarkable to find that these confinement facilities are making progress in their respective missions towards, the integration of which will hopefully lead to the realization of fusion energy. On its way, however, an experimental reactor, ITER being constructed in France, must be successful in sustaining the energy break even condition with $Q > 10$, which will no doubt affect the design of the first DEMO reactor.

For the rest of the process before fusion energy can be realized, all the governments in the fusion research community will hopefully provide continuous support for these confinement experiments, but basic research conducted in laboratory-scale facilities as well, which could end up with unexpected “spin-off” products, valuable for other communities. For example, the technology developed for superconducting magnets can be used for the long-distance DC-power transmission of solar energy.

As such, one must remember that although the public acceptance of it may vary due to the socio-technical situation, fusion energy research and development can always contribute in many ways to the sustainable global development.



The Strategic Dimensions of the Fusion Energy Challenge

F. Portero¹

¹*Universidad Francisco de Vitoria, Madrid, Spain*

Corresponding Author: F. Portero, f.portero@ufv.es

Human beings have a short history in universe terms. Just 200 000 years old and no more than 100 000 years old out of Africa. As a consequence of climate changes those men decided to leave the continent looking for new land and new opportunities to prosper. It is impossible to understand the history of the humankind without keeping in mind its effort to understand the reality and to overcome the challenge to transform it. No other species has been able to advance so much in the knowledge of the environment; but those advances resulted, at the end, in radical changes in the environment, in our cultures and in our identity. Our civilization is built on the idea of permanent economic progress. We need to generate wealth as a premise to guarantee welfare, education, health, research, social cohesion... , and economic activity requires energy. Our history shows a constant effort to improve our ability to generate more and more energy at minor possible cost. Economic revolutions are at the origin of social and political revolutions, but in many cases they are themselves a consequence of previous energy revolutions. If the capacity to generate energy is the precondition of economic progress and social welfare, we have to conclude that energy independence is a key goal for all the states. In advanced societies we have to face with growing demands of secure and clean energy sources at the same time. As a consequence nuclear fission, one of the cheapest and easiest ways to generate energy in large quantities, has been called into question. Without fission energy, a large number of countries would have to largely depend on others to access necessary energy resources. Every day we see how energy dependence implies political dependence. A sovereign but energy dependent country has to condition its policy to the supplier's interests.

Free access to an unlimited and cheaper energy is the basis of political independence and equal opportunities in the global market. Research and production costs are conditioned by the price of energy. Political leaders try to confront these challenges through a diversification strategy. They are eventually succeeding in reducing the strategic limitations, but not the high costs of the energy generation and its effects. In some cases, like hydraulic fracturing (fracking), environmental impact remains a serious problem. In others, alternative ways of generating energy like solar or eolic power plants involve in many occasions a serious impact on the landscape and the environment. If we want a clean and cheap energy that guarantees not only respect for nature but also independence of states and enterprises, we need to direct our attention to fusion power. Nowadays fusion power is a major scientific challenge that requires the effort of everyone. A joint action is required to overcome the challenges posed by its generation and this implies the involvement of states, the support of society and the determination of the scientific community. Success is just a matter of time and resources, and the consequences promise to be extraordinary.

As a carbon-free energy source based on abundant fuels with no particular geographic distribution, controlled thermonuclear Fusion would eventually represent a breakthrough in the history of the mankind. Deuterium can be extracted from water and tritium is produced from lithium, which is found in the earth's crust. Significant progress is being done in making fusion energy production a reality. ITER will be the biggest fusion reactor on

earth, but science and technology gaps still remain and need to be closed. Researchers and engineers together with policy makers require all needed tools to accomplish this new revolution in the history of the mankind, bringing the energy of the sun and all other stars to the earth to be used for peaceful purposes. Fusion power will give way to a new era where access to a clean, safe and unlimited energy will be a reality, an era with new challenges, such as the conquest of space. We will leave behind many of the problems that characterized 19th and 20th centuries. At last we will have at our disposal the power source required to navigate beyond our solar system.

OV: Overviews



Extension of Operational Regime of LHD towards Deuterium Experiment

Y. Takeiri¹

LHD Experiment Group

¹National Institute for Fusion Science (NIFS), Toki, Gifu, Japan

Corresponding Author: Y. Takeiri, takeiri@nifs.ac.jp

The final goal of the LHD project is to obtain the high performance helical plasma relevant to the fusion reactor, i.e., ion and electron temperature $T_i > 10$ keV, volume averaged $\beta > 5\%$, fusion triple product $n_e n_T T_i > 10^{20}$ keV s/m³, and long pulse length of more than 3600 s with heating power of 3 MW. In order to achieve this objective, the deuterium plasma is expected to have better energy and particle confinement than the hydrogen plasma, which is clearly seen in tokamaks, but is not always obvious in helical devices.

As the finalization of the hydrogen experiment towards the deuterium phase, the exploration of the best performance of the hydrogen plasma was intensively performed in the Large Helical Device (LHD). High T_i , T_e , of more than 6 keV were simultaneously achieved by superimposing the high power electron cyclotron resonance heating (ECH) on the neutral beam injection (NBI) heated plasma. It was also demonstrated in hydrogen/helium discharges that experimental and numerical results imply the existence of the confinement improvement for heavier ions than proton. Another key parameter to present plasma performance is an averaged β value. The high- β regime around 4% was extended to an order of magnitude lower collisional regime than before. The pulse length has also become longer. In the last experimental campaign, the high performance plasma with e-ITB could successfully be maintained for more than 5 minutes. In such a long pulse discharge, it was found that the mixed-material deposition layer plays a key role in the wall retention and the particle recycling. These three results assured the start of the deuterium experiment from March 2017.



Progress in ITER Construction, Manufacturing and R&D

B. Bigot¹

¹*International Thermonuclear Experimental Reactor (ITER),
Cadarache Centre, 13108 Saint-Paul-lès-Durance, France*

Corresponding Author: B. Bigot, bernard.bigot@iter.org

The ITER project is a critical step in the development of fusion energy: its role is to confirm the feasibility of exploiting magnetic confinement fusion for the production of energy for peaceful purposes by providing an integrated demonstration of the physics and technology required for a fusion power plant. Rapid progress is being made in the design, manufacturing, construction and R&D activities, and the facility is now taking shape at Saint-Paul-lès-Durance.

Supported by impressive achievements in fusion technology R&D, manufacturing of ITER components is in full swing. The international collaboration formed around the production of superconducting magnets for ITER has produced over 600 t of Nb₃Sn and almost 250 t of NbTi superconducting strand. 80% of the superconductors required for the ITER magnets are complete, and coil fabrication activities are underway in six of the seven partners factories. Fabrication of the vacuum vessel is moving forward, with structures being manufactured under the responsibility of four contributing Domestic Agencies, manufacturing of the thermal shield is also in progress, and the first elements of the cryostat (~29 m diameter × ~29 m height) have been delivered to the ITER site.

Substantial progress has also been achieved in prototyping and R&D activities in areas such as plasma facing components, in-vessel coils, H&CD systems, remote handling and power supplies in preparation for manufacturing. A wide-ranging physics R&D programme, closely integrated with the ITPA and the major fusion facilities in the ITER Members, is also addressing key issues impacting on finalization of the ITER design and preparations for operation. These R&D activities encompass studies of disruption mitigation, analysis of ELM control by magnetic perturbations, characterization of heat loads in stationary and transient plasma phases, plasma-wall interactions with all-metal PFCs, and studies of plasma scenarios for nonactive and nuclear phases of the ITER experimental programme.

The paper will review the progress made in developing the advanced technologies required for ITER and in the manufacturing activities for major tokamak components, discuss advances made in experimental and modelling studies of key physics issues, detail measures taken to establish a more effective project organization and present the status of construction of the ITER facility.



DIII-D Research Advancing the Scientific Basis for Burning Plasmas and Fusion Energy

W. M. Solomon¹

¹Princeton Plasma Physics Laboratory (PPPL), Princeton, NJ 08540, USA

Corresponding Author: W. M. Solomon, solomon@fusion.gat.com

The DIII-D tokamak has addressed key issues to advance the physics basis for burning plasmas for ITER and future steady-state fusion devices. Developments on ITER scenarios include the discovery of a new wide-pedestal variant of QH-mode where increased edge transport is found to allow higher pedestal pressure, consistent with peeling-ballooning theory, and complete ELM suppression in steady-state “hybrid” plasmas that is relatively insensitive to q_{95} , having weak effect on the pedestal. Shattered pellet injection (SPI) has been shown an effective technique for runaway electron (RE) plateau dissipation. Mixed species shattered pellet injection (SPI) enabled control of disruption characteristics, while keeping the radiation fraction, divertor heat loads, and current quench times within ITER requirements. Reduced transport models such as TGLF reproduce the reduced confinement associated with additional electron heating in DIII-D ITER baseline plasmas. Density peaking can recover the performance, as can raising the pedestal density, which increases the pedestal pressure and can even give access to Super H-mode for ITER. Both high- q_{\min} and hybrid steady-state plasmas have avoided fast ion instabilities and achieved increased performance by control of the fast ion pressure gradient and magnetic, and use of external control tools such as ECH. In the boundary, $E \times B$ drifts are found important for simulating observed asymmetries in divertor detachment, and the erosion rate of high- Z materials is found to be reduced through control of the electric field in the presheath. Between-ELM heat flux asymmetries in the presence of RMP fields are eliminated in detached divertor conditions. Higher low- Z impurity concentrations in the background plasma are also found to reduce the net erosion rate of high- Z targets, even to the point of net deposition. These small-sample studies are being used to investigate high- Z impurity contamination efficiency from different divertor locations and impact on the core plasma performance, which in-turn inform the forthcoming metal divertor tile experiments.

AO

Overview of the JET Results in Support to ITER

X. Litaudon¹

The JET contributors

¹EUROfusion

Corresponding Author: X. Litaudon, xavier.litaudon@euro-fusion.org

Europe has elaborated a Roadmap to the realization of fusion energy in which “ITER is the key facility and its success is the most important overarching objective of the programme”. We review the contribution of the recent JET experiments with the ITER first wall materials mix, and, the underlying physics understanding to mitigate the scientific risks identified in the ITER research plan. Indeed, together with the ITER scenario development, a strong focus on JET is pursued for addressing ITER needs and developing a sound physics basis for the extrapolation through first principle and integrated modelling: plasma wall interaction, disruption mitigation (installation of a third mitigation valve), H-mode access, W-control with higher electron heating (ICRH ITER-like antenna reinstated), pellet ELMs pacing with the optimized vertical high field side track. The JET ITER-like wall (ILW) experiment provides an insight in the coupling between tokamak-plasma operation and plasma-surface interaction in the unique Be/W material environment and acts as test-bed to verify models and modelling tools for ITER. Disruptions are considered as the highest programmatic risk in the ITER Research Plan and experimental and modelling effort in Europe and JET are reviewed. High spatial resolution Doppler backscattering measurements have revealed novel insights into the development of the edge transport barrier. The operational constraints of a metal wall can prevent reaching plasma energy confinement required for $Q_{DT} = 10$ on ITER. Progress on JET to mitigate this risk is reported aiming at maximizing the core and pedestal performance in stationary condition with the W divertor constrain. The measured DD neutron fluence and gamma dose rates have been successfully compared with simulations performed with the codes used for ITER nuclear safety analyzes. Finally, the benefit to further use JET beyond 2020 to train the international ITER team with an upgrade tungsten divertor and with the ITER control tools will be discussed.

This work has been carried out within the framework of the EUROfusion Consortium and has received funding from the Euratom research and training programme 2014–2018 under grant agreement No. 633053. The views and opinions expressed herein do not necessarily reflect those of the European Commission.



Overview of ASDEX-Upgrade Results

A. Kallenbach¹

¹Max-Planck-Institut für Plasmaphysik, Garching, Germany

Corresponding Author: A. Kallenbach, arne.kallenbach@ipp.mpg.de

The ASDEX-Upgrade programme is devoted to the preparation of ITER operation and the development of plasma scenarios and physics understanding for a future DEMO. Different scenario lines adapted to critical research tasks are developed and naturally integrated with the metallic, high- Z plasma facing components environment. The scenarios can be mainly divided into low core collisionality and high divertor collisionality conditions, which can be achieved simultaneously only in devices of ITER size.

The development of noninductive scenarios relies on low core collisionality and is performed with low neutral divertor pressure and an attached divertor. Fully noninductive operation with a combination of NBCD and ECCD has been achieved at $I_p = 0.8$ MA and a safety factor $q_{95} = 5.4$. The core W concentration is quite high as a consequence of the hot SOL and divertor which result in high W sputtering yields.

A normalized exhaust power P_{sep}/R of 10 MW/m has been achieved with nitrogen (N) seeding and a partially detached outer divertor at a total heating power of 25 MW. A high neutral deuterium divertor pressure was found to be essential for efficient divertor cooling. Confinement degradation connected to a high neutral pressure is partly compensated by improvement due to the effects of N. Investigations of the cause for the improved energy confinement with N seeding suggest that an inward shift of the pedestal density profile in relation to the temperature profile is the main driver for an enhanced pedestal stability which is associated with the improved confinement. The inward shift is attributed to a shrinking of a high density region on the high field side SOL due to the power reduction caused by the N radiation, which effects the fuelling in the X-point region.

The new pair of ICRF antennas with three straps has fulfilled the predicted reduction of tungsten release from connected limiters. The tungsten influx during antenna operation is similar or even slightly smaller compared to the two-strap antenna pair with boron coated limiters. With the three-strap antennas operated for central heating, generally a reduction of the central tungsten concentration is observed despite a still moderately increased W influx. A high local density in front of the antenna, achieved by well-tailored gas puffing, further optimizes ICRF operation with regard to coupling and low W release.



Overview of EAST Experiments on the Development of High-Performance Steady-State Scenario

B. N. Wan¹, Y. Liang², X. Gong¹, N. Xiang¹, G. Xu¹, Y. Sun¹, L. Wang¹, J. Qian¹, H. Liu¹, L. Zeng¹, L. Zhang¹, X. Zhang¹, J. Huang¹, B. J. Ding¹, Q. Zang¹, M. Li¹, F. Ding¹, S. Ding¹, T. Zhang¹, Y. Zhang¹, and G. Li¹

¹*Institute of Plasma Physics, Chinese Academy of Sciences, Hefei, Anhui, People's Republic of China*

²*Forschungszentrum Jülich, Jülich, Germany*

Corresponding Author: B. N. Wan, bnwan@ipp.ac.cn

EAST aims to demonstrate steady-state advanced high-performance H-mode plasmas with ITER-like configuration, plasma control and heating schemes. Since 2015, EAST has been equipped with all ITER-related auxiliary heating and current drive systems. Two NBI systems injected from co- and countercurrent directions, have been installed on EAST and allow the flexible study of the plasma rotation effect. A flexible in-vessel RMP coil system was installed in 2014 for active MHD instability control in order to achieve long-pulse steady-state operation in the EAST tokamak. Since then, EAST has been capable of investigating ELM control with most existing methods, including RMP, pellet-pacing, SMBI, LHW and Li-pellet injection.

The exploration of fully noninductive, high performance, upper single-null discharges with the tungsten divertor has been successfully demonstrated with upgrades of heating and current drive capabilities on EAST. A higher β regime has been achieved with the 4.6 GHz LHCD and NBI. Experimental results show that LHWs at 4.6 GHz exhibit stronger current drive capability than at 2.45 GHz, in agreement with less pronounced parametric instability behaviour with the 4.6 GHz LH wave. By means of the 4.6 GHz and 2.45 GHz LHCD systems, H-mode is obtained at relatively high density.

A stationary ELM-stable H-mode regime has been achieved in EAST with 4.6 GHz LHCD. This regime allows nearly fully noninductive long-pulse operations, exhibiting a relatively high pedestal and good global energy confinement with $H_{98}(y, 2)$ near 1.2, good impurity control, and the capability of operation at relatively high density.

Complete suppression of ELMs has been observed during the application of $n = 1$ and 2 RMPs on EAST. The experimental results show that the plasma response plays an important role in ELM control. Critical thresholds for the amplitude of the RMPs and the plasma rotation for this transition have been observed for the first time on EAST.

The 3D edge magnetic topology has been applied for active control of heat and particle fluxes deposited on the divertor targets in steady-state operation on EAST. The impacts of the 3D magnetic topology on the edge plasma transport and heat flux distribution have been investigated using the EMC3-EIRENE code and found to be consistent with the experimental observation of strike-line splitting.



Kinetics of Relativistic Runaway Electrons

B. N. Breizman¹, P. Aleynikov²

¹*Institute for Fusion Studies (IFS), University of Texas at Austin, Austin, TX 78712, USA*

²*Max-Planck-Institut für Plasmaphysik, Greifswald, Germany*

Corresponding Author: B. N. Breizman, breizman@mail.utexas.edu

This overview talk covers recent developments in the theory of runaway electrons in tokamaks. Such electrons are known to be of serious concern with regard to safe operation of large-scale tokamaks in general and ITER in particular. They can quickly replace a large part of the bulk electron current during disruptions, and the corresponding magnetic energy exceeds the particle kinetic energy. This feature separates the time-scale of the runaway production from the time-scale of the current decay. The talk deals with the following physics aspects of the runaway evolution: 1) survival and acceleration of initially hot electrons during thermal quench, 2) effect of magnetic perturbations on runaway confinement, 3) multiplication of the runaways via knock-on collisions with the bulk electrons, 4) slow decay of the runaway current, and 5) runaway-driven microinstabilities. Several theory groups internationally are currently addressing these aspects. The recent progress includes a first-principle description of the primary runaway electron production during the thermal quench, estimates of the runaway losses through partially destroyed magnetic flux surfaces, an improved description of fast electron collisions with heavy impurities within a Thomas-Fermi model for screening, a rigorous kinetic theory for relativistic runaways in the electric field that is close to the avalanche threshold, refined evaluation of the critical field for avalanche onset with a systematic description of knock-on collisions and radiative losses, demonstration of phase-space attractor that supports a peaked distribution function of the runaways, a model for current damping in a self-sustained regime of marginal criticality for the runaways, and reassessment of thresholds for the runaway-driven microinstabilities. Some of these new theoretical findings are directly relevant to current experiments on DIII-D, ASDEX-U, and JET. They also provide an important input for ITER disruption modelling and runaway mitigation strategy.

Work supported by the U.S. Department of Energy, Contract No. DE-FG02-04ER54742 and by ITER Contract No. ITER/CT/15/4300001178.



Overview of the KSTAR Research in Support of ITER and DEMO

Y.-K. Oh¹, S.-W. Yoon¹, J.-G. Kwak¹, Y. In¹, Y. Jeon¹, S. Wang¹, Y.-U. Nam¹, S.-H. Hong¹, J.-M. Kwon¹, Y. Chu¹, K.-R. Park¹, H. K. Park², W. Choe³, G. Yun⁴, Y.-S. Na⁵, J.-K. Park⁶, S. A. Sabbagh⁷, J.-W. Ahn⁸, and D. A. Humphreys⁹

¹National Fusion Research Institute (NFRI), Daejeon, Republic of Korea

²Ulsan National Institute of Science and Technology (UNIST), Ulsan, Republic of Korea

³Korea Advanced Institute of Science and Technology (KAIST), Daejeon, Republic of Korea

⁴Pohang University of Science and Technology (POSTECH), Pohang, Gyeongbuk 790-784, Republic of Korea

⁵Seoul National University, Seoul, Republic of Korea

⁶Princeton Plasma Physics Laboratory (PPPL), Princeton, NJ 08540, USA

⁷Columbia University, New York, NY 10027, USA

⁸Oak Ridge National Laboratory (ORNL), Oak Ridge, TN 37831, USA

⁹General Atomics, San Diego, CA 92186, USA

Corresponding Author: Y.-K. Oh, ykoh@nfri.re.kr

The KSTAR device has been operated since the first plasma in 2008 with the mission of exploring the physics and technologies of high performance steady-state operation that are essential for ITER and fusion reactor. KSTAR has been focussing on maximizing performance and extending pulse length targeting H-mode discharge up to 300 s at higher plasma current up to 2 MA, and at higher normalized β (β_N) up to ~ 5 .

In the 2015 campaign, various long-pulse H-mode discharges have been operated after the improved plasma shape control, and a longest H-mode discharge was achieved up to 55 s at 0.6 MA in plasma current and 2.9 T in toroidal field utilizing 4.2 MW neutral beam and 0.65 MW ECCD systems. This will be the longest H-mode discharge in tokamak devices. Fully noninductive discharges have been carried out at the reduced plasma current of 0.4 MA to access the steady-state operation condition. The first fully noninductive operation was achieved with relatively high plasma performances ($\beta_N \sim 2.1$ and $\beta_P \sim 3.0$). However the shot was terminated at about 16 s due to excessive heat in the poloidal limiter.

The KSTAR device could be an ideal device to investigate the basics of the stability limits and confinement improvements utilizing unique features of KSTAR such as extremely low error field, versatile in-vessel control coils (IVCC), and advanced 2D/3D imaging diagnostics. In this paper, the progress of the KSTAR research to support ITER and DEMO will be reported.



Overview of High-Field Divertor Tokamak Results from Alcator C-Mod

E. S. Marmar¹

Alcator C-Mod Team, MIT

¹Massachusetts Institute of Technology (MIT), Cambridge, MA 02139, USA

Corresponding Author: E. S. Marmar, marmar@psfc.mit.edu

C-Mod is the only divertor tokamak in the world capable of operating at B fields up to 8 T, equalling and exceeding that planned for ITER. C-Mod is compact, thus accessing regimes of extreme edge power density (1 MW/m² average through the plasma surface). Scrape-off layer (SOL) power widths are of order of a few mm, with measured parallel power flows > 1 GW/m² at the divertor, surpassing the design for ITER, and approaching the levels envisioned in power plants. C-Mod results are particularly important for providing the physics basis of the high-field, compact tokamak approach, which can lead to a faster path in the development of fusion energy [1]. Results of experiments and related modelling, obtained since the last IAEA FEC meeting, span the topics of core transport and turbulence, RF heating and current drive, pedestal physics, scrape-off layer, divertor and plasma-wall interactions. ICRF has been successfully applied to control and reverse accumulation of high- Z impurities in the core plasma. ICRF has also been employed to control and mitigate locked-modes induced by error fields. For the first time ever, feedback of low- Z seeding for divertor power dissipation has been tied directly to real-time plasma power fluxes measured on the high- Z metal PFCs in the divertor, and used to mitigate those fluxes with no degradation of the pedestal pressure or core confinement. The naturally ELM-free I-mode regime has been up to $B_t = 8$ T, and to double-null topology. I-mode threshold scalings show a weak dependence on B , yielding a significantly broader window for I-mode operation at high field. Quiescence of the high-field side scrape-off layer makes this a potentially attractive location for placement of RF actuators to ameliorate plasma interactions with launchers; the wave physics for penetration and damping, for both ICRF and LHRF appears very favourable for high-field side launch. BOUT++ edge plasma simulations are shedding important light on the nature of I-mode pedestal fluctuations which regulate impurity transport in this regime. LHRF has been employed as an actuator for controlling plasma rotation and rotation shear, critical parameters for turbulence control. A new disruption database has been populated, and used to identify key variables that could be used for disruption prediction and avoidance.

References

[1] B. Sorbom, *et al.*, Fusion Eng. Des. **100**, 378 (2015).



First Plasma Operation of Wendelstein 7-X

R. C. Wolf¹

¹*Max-Planck-Institut für Plasmaphysik, Garching, Germany*

Corresponding Author: R. C. Wolf, robert.wolf@ipp.mpg.de

The main objective of the optimized stellarator Wendelstein 7-X (W7-X) is the demonstration of steady-state plasma operation at fusion relevant plasma parameters thereby verifying that the stellarator is a viable fusion power plant concept. The design of W7-X is based on an elaborate optimization procedure to overcome the shortcomings of the concept. After completing the main construction phase of W7-X and successfully commissioning the device, first plasma operation started in December 2015. Plasma operation of W7-X follows a staged approach according to the successive completion of the in-vessel components. During the first operational phase five inboard limiters defined the last closed flux surface. Subsequently, W7-X will be equipped with a test divertor unit and eventually with a steady-state capable high heat flux divertor including active water cooling of all in-vessel components. Integral commissioning of plasma start-up and operation using an electron cyclotron resonance heating (ECRH) and an extensive set of plasma diagnostics, and initial physics studies during the first operational campaign have been successfully completed. Both in helium and hydrogen, plasma break-down was easily achieved. Gaining experience with plasma vessel conditioning, discharge lengths could be continuously extended. Eventually, discharges lasted up to 6 s, reaching an injected energy of 4 MJ which is twice the limit originally agreed for the limiter configuration. At higher powers of 4 MW and central electron densities of $4.5 \times 10^{19}/\text{m}^3$, central temperatures reached values of 7 keV for the electrons and just above 2 keV for the ions. Important physics studies during this first operational phase include the assessment of the heat load distribution over the inboard limiters changing the toroidal phase and amplitude of deliberately applied error fields, impurity injection and confinement experiments including the effect of the rotational transform, and ECRH power deposition and heat pulse propagation experiments. Also a first assessment of the central electron root confinement, 2nd harmonic O-mode ECRH using multipass absorption, and the investigation of confinement and stability of discharges with co- and counter-current drive (ECCD) have been achieved. This paper will give an overview of the results of the first experimental campaign of W7-X.

OV



The Quest for Laboratory Inertial Fusion Ignition in the US

M. J. Edwards¹, T. C. Sangster², and D. B. Sinars³

¹Lawrence Livermore National Laboratory (LLNL), Livermore, CA 94550, USA

²Laboratory for Laser Energetics, University of Rochester, Rochester, NY 14627, USA

³Sandia National Laboratories (SNL), Albuquerque, NM 87185, USA

Corresponding Author: M. J. Edwards, edwards39@llnl.gov

Ignition and significant fusion yield from Inertial Confinement Fusion (ICF) remains a grand scientific challenge. The ICF community in the US, together with international collaborators, is executing a coordinated effort exploring three approaches to ignition each with different risks and advantages: laser driven X-ray drive, laser direct drive, and magnetic direct drive. This talk presents the status and future focus of these approaches in the US.

X-ray drive is pursued at the National Ignition Facility (NIF). In this approach ~ 1.8 MJ of laser light illuminates a cylindrical gold hohlraum to produce a highly uniform X-ray field to implode a spherical capsule containing DT fuel. The original ignition target design gave fusion yields (~ 2 kJ or $\sim 5 \times 10^{14}$ neutrons) far from ignition because of the challenging hydrodynamics associated with the high ($\sim 35\times$) convergence ratio (CR) compounded by laser plasma instabilities (LPI) in the hohlraum introducing strong time dependent drive asymmetry. A more stable, lower CR variation of that design resulted in yields approaching 10^{16} neutrons (~ 26 kJ) and for the first time demonstrated significant alpha self-heating that roughly doubled the fusion yield. It has become clear that further improvements in performance will require better control of the implosion shape by reducing the LPI that currently prevents the precision drive symmetry needed for ignition as well as improved capsule mounting schemes that perturb the implosion less.

In laser direct drive (LDD) the capsule is directly irradiated spherically with laser light. This couples more energy to the fuel than in X-ray drive reducing the capsule convergence ratio needed for ignition to ~ 20 at NIF's energy. However, the proximity of the laser to the capsule places stringent demands on the laser target coupling uniformity and the allowable levels of LPI. The laser coupling and hydrodynamics of LDD are being refined at the LLE's Omega laser in hydro-scaled targets with laser imprinting and LPI mitigation being studied in collaboration with NRL.



Recent Progress of JT-60SA Project

H. Shirai¹, P. Barabaschi², and Y. Kamada¹

¹Japan Atomic Energy Agency (JAEA), Naka, Japan

²F4E: Fusion for Energy, ITER EU Centre, 08019 Barcelona, Spain

Corresponding Author: H. Shirai, shirai.hiroshi@jaea.go.jp

The JT-60SA project has been promoted since June 2007 under the framework of the Broader Approach (BA) agreement and Japanese national fusion programme for an early realization of fusion energy by conducting supportive and complementary work for the ITER project and directing DEMO design activity. With the powerful and varied deposition profile of heating and current drive system, flexible plasma shaping capability and various kinds of in-vessel coils to suppress MHD instabilities, JT-60SA is sure to play an essential role to address essential issues to achieve long sustainment of high- β_N burning plasmas expected in DEMO. Components and systems of JT-60SA are procured by the implementing agencies (IAs): Fusion for Energy in EU and JAEA in Japan. Their design, fabrication, installation and commissioning have been actively directed and supervised by the IAs. As of the end of 2015, twenty-seven procurement arrangement (PAs) have been concluded covering 95% of the values of in-kind contribution for JT-60SA. In spite of the size, components of JT-60SA have been manufactured well within the tolerance of 1 mm order. EU procures TF coils, most of the power supply systems, cryogenic system, cryostat and so on. The cold test of the first TF coil with a nominal current of 25.7 kA at 4.5–7.0 K was successfully completed. JA procures EF coils, Central Solenoids, Vacuum Vessel, thermal shields, heating system, diagnostics system and so on. Vacuum Vessel sectors were welded on the cryostat base forming a 340° torus. The heating systems (P-NBI, N-NBI and ECRF) have been conditioned to operate at their full power (41 MW in total) for 100 s. The first plasma of JT-60SA is scheduled in 2019. Wide range of operational region of JT-60SA kept in mind, the JT-60SA research plan (SARP) has been regularly updated on the basis of intensive discussion among European and Japanese researchers. The latest SARP (version 3.3) open to the public in March 2016 shows that wide operational region of JT-60SA covers that of recent European and Japanese DEMO designs. DEMO oriented researches such as study of ECRF assisted startup, investigation of noninductive current overdrive scenario using TOPICS code were added. This paper summarize the recent progress of JT-60SA Project pushed forward by close collaboration of EU and Japan.

OV



Overview of the Present Progresses and Activities on the Chinese Fusion Engineering Test Reactor

Y. Wan¹, J. Li¹, Y. Liu², X. Wang³, V. Chan⁴, and M. Ye⁴

¹*Institute of Plasma Physics, Chinese Academy of Sciences, Hefei, Anhui, People's Republic of China*

²*Southwestern Institute of Physics, Chengdu, Sichuan, People's Republic of China*

³*China Academy of Engineering Physics, Mianyang, People's Republic of China*

⁴*University of Science and Technology of China, Hefei, Anhui, People's Republic of China*

Corresponding Author: Y. Wan, wanyx@ustc.edu.cn

The Chinese Fusion Engineering Testing Reactor (CFETR) is the next device for the Chinese magnetic confinement fusion (MCF) programme which aims to bridge the gaps between the fusion experiment ITER and the demonstration reactor DEMO. CFETR will be operated in two phases: Steady-state operation and tritium self-sustainment will be the two key issues for the first phase with a modest fusion power up to 200 MW. The second phase aims for DEMO validation with a fusion power over 1 GW. Advanced H-mode physics, high magnetic fields up to 7 T, high frequency electron cyclotron resonance heating (230 GHz) and lower hybrid current drive (7.5 GHz) together with off-axis negative-ion neutral beam injection will be used for achieving steady-state advanced operation. The detailed design, research and development activities including integrated modelling, R&D on high field magnet, material, T plant, remote handling, physical validation on EAST tokamak to demonstrate feasibility of high performance steady state operation, and future MCF road map will be introduced in this paper.

OV

Overview of the IFMIF/EVEDA Project

J. Knaster¹, R. Heidinger², and S. O'hira³

¹International Fusion Materials Irradiation Facility (IFMIF/EVEDA), Rokkasho, Aomori, Japan

²F4E: Fusion for Energy, ITER EU Centre, 08019 Barcelona, Spain

³Japan Atomic Energy Agency (JAEA), Naka, Japan

Corresponding Author: J. Knaster, juan.knaster@ifmif.org

IFMIF, the International Fusion Materials Irradiation Facility, presently in its Engineering Validation and Engineering Design Activities (EVEDA) phase under the Broader Approach Agreement, will allow accelerated testing of structural materials with fusion relevant neutrons at > 20 dpa/year in 500 cm^3 .

IFMIF consists of two 125 mA and 40 MeV D^+ linear accelerators operating in CW mode. The concurrent beam lines impact on a liquid lithium target with a $200 \text{ mm} \times 50 \text{ mm}$ beam cross section. The target consists of a $25 \text{ mm} \pm 1 \text{ mm}$ thick liquid lithium screen flowing at 15 m/s and 250°C channelled by a $R = 250 \text{ mm}$ concave RAFM backplate. The suitable neutron flux generated in the forward direction will irradiate 12 test capsules housing around 1000 small specimens independently cooled with helium gas.

The Engineering Design Activity (EDA) phase of IFMIF was successfully accomplished within the allocated time. The Engineering Validation Activity (EVA) phase has focussed on validating the Accelerator Facility, the Target Facility and the Test Facility with the construction of various prototypes. The ELTL has successfully demonstrated the long term stability of a lithium flow under IFMIF nominal operational conditions with 25 days continuous operation in Oarai (JAEA) at 250°C and 15 m/s within $\pm 1 \text{ mm}$ free surface fluctuations. A full-scale prototype of the High Flux Test Module has been successfully tested in the HELOKA loop (KIT Karlsruhe) demonstrating the feasibility of the uniformity in the temperature selected for the specimen set irradiated in each capsule. LIPAc, presently under installation and commissioning, will validate the concept of IFMIF Accelerators with a D^+ beam of 125 mA and 9 MeV. The commissioning of the H^+/D^+ beams in Rokkasho Fusion Institute at 100 keV was concluded early 2016; the commissioning of the 5 MeV beam is to follow till early 2017. The 9 MeV D^+ beam will be achieved with a superconducting cryomodule during 2018.

The realization of a fusion relevant neutron source is a necessary step for the successful development of fusion. The stable progress achieved in this final EVEDA phase has ruled out technical concerns and potential showstoppers raised in the past. In the light of costs, which are unquestionably marginal to those of a fusion plant, a situation has emerged where soon steps towards constructing a Li(d,xn) fusion relevant neutron source could be taken.



A Pathway to Laser Fusion Energy: Fast Ignition Realization Experiment (FIREX)

H. Azechi¹

¹*Institute of Laser Engineering, Osaka University, Osaka, Japan*

Corresponding Author: H. Azechi, azechi@ile.osaka-u.ac.jp

Here we report recent progress of the fast ignition inertial confinement fusion demonstration. Fraction of low energy (< 1 MeV) component of the relativistic electron beam (REB), which efficiently heats the fuel core, increases by the factor of 4 by enhancing pulse contrast of heating laser and removing preformed plasma sources. Kilo-tesla magnetic field is studied to guide the diverging REB to the fuel core. The transport simulation of the REB accelerated by the heating laser in the externally applied and compressed magnetic field indicates that the REB can be guided efficiently to the fuel core. The integrated simulation shows $> 4\%$ of the heating efficiency and > 4 keV of ion temperature are achievable by using GEKKO-XII and LFEX, properly designed cone-fuel and the external magnetic field.



Overview of SST-1 Upgrade & Recent Experiments in SST-1

S. Pradhan¹, Z. Khan¹, V. L. Tanna¹, U. Prasad¹, Y. Paravastu¹, D. C. Raval¹, H. Masand¹, A. Kumar¹, J. R. Dhongde¹, K. B. Patel¹, M. K. Bhandarkar¹, B. K. Shukla¹, S. Jana¹, D. Ghosh¹, H. S. Patel¹, T. J. Parekh¹, I. A. Mansuri¹, K. R. Dhanani¹, A. Varadharajulu¹, Y. S. Khristi¹, P. Biswas¹, C. N. Gupta¹, S. George¹, P. Semwal¹, D. K. Sharma¹, H. K. Gulati¹, K. Mahajan¹, B. R. Praghi¹, M. Banauddha¹, A. R. Makwana¹, H. H. Chudasma¹, M. Kumar¹, R. Manchanda¹, Y. S. Joisa¹, K. Asudani¹, S. N. Pandya¹, S. K. Pathak¹, P. J. Patel¹, P. Santra¹, F. S. Pathan¹, P. K. Chauhan¹, M. S. Khan¹, P. L. Thankey¹, A. Prakash A¹, P. N. Panchal¹, R. N. Panchal¹, R. J. Patel¹, G. I. Mahsuria¹, D. P. Sonara¹, K. M. Patel¹, S. P. Jayaswal¹, M. Sharma¹, J. C. Patel¹, P. Varmora¹, G. L. N. Srikanth¹, D. R. Christian¹, A. Garg¹, N. Bairagi¹, G. R. Babu¹, A. G. Panchal¹, M. M. Vora¹, A. K. Singh¹, R. Sharma¹, H. D. Nimavat¹, P. Shah¹, T. Y. Raval¹, A. L. Sharma¹, A. Ojha¹, S. Kumar¹, N. K. Ramaiya¹, V. Siju¹, M. V. Gopalakrishna¹, A. Kumar¹, P. K. Sharma¹, P. K. Atrey¹, S. V. Kulkarni¹, K. K. Ambulkar¹, P. R. Parmar¹, A. L. Thakur¹, J. V. Raval¹, S. Purohit¹, P. K. Mishra¹, A. N. Adhiya¹, U. C. Nagora¹, J. Thomas¹, V. K. Chaudhari¹, K. G. Patel¹, S. Dalakoti¹, C. G. Virani¹, S. Gupta¹, A. Kumar¹, B. Chaudhari¹, R. Kaur¹, R. Srinivasan¹, A. N. Sharma¹, K. J. Doshi¹, D. Raju¹, D. H. Kanabar¹, R. Jha¹, A. Das¹, and D. Bora¹

The IPR SST-1 Team

¹*Institute for Plasma Research (IPR), Bhat, Gandhinagar, India*

Corresponding Author: S. Pradhan, pradhan@ipr.res.in

Steady State Superconducting Tokamak (SST-1) is an “operational” experimental superconducting device since late 2013. Since last IAEA-FEC; SST-1 has been upgraded with plasma facing components being installed and integrated in the vacuum vessel and is getting prepared towards long pulse operations in both circular and elongated configurations. The PFC integration has been completed in August 2015 and initial experiments have begun in SST-1 with circular plasma configurations. SST-1 offers a unique possibility of investigating long pulse discharges with large aspect ratio (> 5.5) compared to contemporary devices. Presently, SST-1 standard ohmic discharges are in excess of 100 kA with typical core density $\sim 2 \times 10^{19}/\text{m}^3$ and core electron temperatures ~ 500 eV having duration in excess of 300 ms. A 42 GHz ECR preionization source at ~ 150 kW in 1.5 T central field breaks down the gas, the current starts up at ~ 1.3 MA/s in 60–80 ms in an induced field of ~ 0.3 V/m. These standard discharges demonstrate copious saw teething and MHD activities as the pulse progresses including NTM, mode locking and MHD characteristics. PFC equipped SST-1 has completed these basic experimental studies confirmed with simulations. These includes eddy currents influencing the NULL dynamics, field errors, equilibrium index evolutions, wall influencing plasma characteristics, plasma positions, plasma rotational and tearing mode characteristics including the island width and island growths, etc. Presently, SST-1 is attempting at multi second long high aspect ratio plasma discharges by coupling the lower hybrid with the Ohmic plasma as well as with robust real time position and density controls.

Continued...

The SST-1 device has been upgraded with a pair of internal coil aimed at effective fast plasma control and a pair of segmented coil aimed at controlling some of the rotational aspects of plasma including the RMPs and ELMs. Supersonic molecular beam injection (SMBI) from both high field and low field sides and pellets injection systems have also been added with several edge plasma diagnostics aimed at both density control and edge plasma turbulence studies. The upgrade details including the planned ones, salient early plasma characteristics in large aspect ratio PFC equipped SST-1 plasma and future experimental plans towards long pulse operations in SST-1 will be elaborated in this paper.

Overview of Recent Experimental Results from ADITYA Tokamak

R. Tanna¹, J. Ghosh¹, P. K. Chattopadhyay¹, H. Raj¹, S. Patel¹, C. Gupta¹, P. Dhyani², K. A. Jadeja¹, K. M. Patel¹, S. B. Bhatt¹, V. K. Panchal¹, N. C. Patel¹, C. Chavda¹, E. V. Praveenlal¹, K. S. Shah¹, M. N. Makwana¹, S. K. Jha¹, M. V. Gopalakrishna¹, K. Tahiliani¹, D. Sangwan¹, D. Raju¹, U. C. Nagora¹, S. K. Pathak¹, P. K. Atrey¹, S. Purohit¹, Y. S. Joisa¹, J. V. Raval¹, C. V. S. Rao¹, M. B. Chowdhuri¹, S. Banerjee¹, J. Thomas¹, N. K. Ramaiya¹, R. Manchanda¹, A. Kumar¹, P. K. Sharma¹, S. V. Kulkarni¹, K. Sathyanarayana¹, B. K. Shukla¹, A. Das¹, R. Jha¹, Y. C. Saxena¹, A. Sen¹, P. K. Kaw¹, and D. Bora¹

Rapporteured by: **S. Pradhan**

¹*Institute for Plasma Research (IPR), Bhat, Gandhinagar, India*

²*Ulsan National Institute of Science and Technology (UNIST), Ulsan, Republic of Korea*

Corresponding Author: R. Tanna, rtan.ipr@gmail.com

Several experiments, related to controlled thermonuclear fusion research and highly relevant for large size tokamaks including ITER, have been carried out in ADITYA, an ohmically heated circular limiter tokamak. Repeatable plasma discharges of maximum plasma current of ~ 160 kA and discharge duration beyond ~ 250 ms with plasma current flattop duration of ~ 140 ms has been obtained for the first time in ADITYA. The discharge reproducibility has been improved considerably with Lithium wall conditioning and improved plasma discharges are obtained by precisely controlling the plasma position. In these discharges, chord-averaged electron density $\sim 3.0\text{--}4.0 \times 10^{19}/\text{m}^3$ using multiple hydrogen gas puffs, electron temperature of the order of $\sim 500\text{--}700$ eV have been achieved.

Novel experiments related to disruption control are carried out and disruptions, induced by hydrogen gas puffing are successfully mitigated using biased electrode and ICR pulse techniques. Runaway electrons are successfully mitigated by applying a short local vertical field (LVF) pulse. A thorough disruption database has been generated by identifying the different categories of disruption. Detailed analysis of several hundred disrupted discharges showed that the current quench time is inversely proportional to q_{edge} . Formation of current filaments are observed during most of the disruptions, which helps in identifying the cause of disruption. Apart from this, for volt-sec recovery during the plasma formation phase, low loop voltage start-up and current ramp-up experiments have been carried out using ECRH and ICRH. Successful recovery of volt-sec leads to achievement of longer plasma discharge durations. In order to achieve better coupling of lower hybrid waves to the plasma, multiple gas puffs are injected prior to the launch of lower hybrid waves. The experiments showed considerable reduction in the reflection coefficient indicating better absorption of LH waves in plasma. In addition to that neon gas puff assisted radiative improved confinement mode has also been achieved in ADITYA. Further, the electrode biasing experiments have shown that during transition to better confinement mode, the Drift-Alfvén fluctuations are suppressed and the current profile gets modified near the edge plasma region. In this paper, all the above mentioned experiments will be discussed.



Overview of Recent Experiments on HL-2A Tokamak

X. Duan¹

¹*Southwestern Institute of Physics, Chengdu, Sichuan, People's Republic of China*

Corresponding Author: X. Duan, duanxr@swip.ac.cn

Recent experiments on the HL-2A tokamak have been aimed at the major challenges relevant to ITER operation and fusion energy development. Significant progress has been achieved in many areas, including the first demonstration of high coupling efficiency of LHCD passive-active multijunction (PAM) antenna in H-mode discharges, pedestal instability and dynamics, ITB formation mechanism, energetic particle physics, ELM and disruption mitigation, real-time control of tearing modes with ECRH, etc.

A new PAM antenna as an LHCD launcher was designed and installed on the HL-2A tokamak. A high coupling efficiency was demonstrated under NBI heated ELMy H-mode plasmas. This was the first time that PAM antenna was applied in H-mode. The effects of LHCD on ELM mitigation and control of heat load on divertor plate were also observed. It was found that impurity accumulation and relaxation in the edge could trigger a series of I-H-I transitions through the excitation of a broadband (50–150 kHz) electromagnetic (EM) turbulence. EM turbulence could also be excited by impurity injection via laser blow-off. An improved confinement with complete suppression of ELMs was achieved by this technique. These findings reveal the underlying physics of how impurity affects the pedestal evolution, and suggest an important method to actively control pedestal via impurity-excited EM turbulence. An inward particle flux induced by a quasi-coherent mode at frequency 40–60 kHz was found to be responsible for the dramatic changes of the gradients in pedestal and the triggering of ELMs. Dependence of the correlation of resistive ballooning modes and trapped electron modes on electron temperature increase was observed experimentally. Formation of the ion ITB was found to be closely related to the T_e/T_i ratio. A new nonlocal transport phenomenon triggered by the fishbone was observed and demonstrated to be caused by electromagnetic fluctuations. High-frequency RSAE and resonant kinetic ballooning mode were confirmed in experiments, and found to cause energetic ions losses. Low- n Alfvénic ITG were observed and identified in Ohmic and NBI plasmas. For the first time, nonresonant internal kink modes destabilized by energetic electrons with ECRH+ECCD were found in current ramp-up phases.

OV



Review of Recent Experiments on the T-10 Tokamak with All Metal Wall

D. Sarychev¹, G. Notkin¹, V. Vershkov¹, D. Shelukhin¹, M. Buldakov¹, A. Melnikov¹, S. Grashin¹, Y. Dnestrovskiy¹, P. Savrukhin¹, V. Krupin¹, and S. Neudatchin¹

¹National Research Centre "Kurchatov Institute", Moscow, Russian Federation

Corresponding Author: D. Sarychev, dmvsar@yandex.ru

A review of the recent experimental results obtained on the T-10 tokamak is presented. To decrease the level of light impurities in 2015 both the rail and circular limiters were replaced with ones made of tungsten. The used tungsten type "POLEMA" as well as the technology of its soldering to the bronze substrate are similar to those applied for the production of the ITER divertor tiles. In the same time a movable lithium limiter was installed in the upper port. This limiter based on capillary-porous structure was made by JSC "Red Star". With the tungsten limiter a considerable increase of the core radiation losses was obtained. Results on prevention of tungsten penetration in the core plasma by central ECRH and by insertion of the lithium limiter are presented in the paper. The efficiency of heavier iron impurity removal depending on the discharge parameters and the power of the central ECRH was investigated. The maximal decrease of the heavier impurities concentrations is 5. Performed using the canonical profiles model analysis of the experiments on the density profile dynamic upon variation of the ECRH power showed that the density profile stiffness rises linearly with the heating power, while the peaking of the pressure profile in the core plasma asymptotically approaches to the canonical value. Using of bispectral analysis applied to the fluctuations of potential, density and poloidal magnetic field measured with heavy ion beam probe diagnostic showed an existence of three-wave interaction between GAM and broad-band turbulence. Also shown that the GAM amplitude declines with the mean density growth. The investigations of density fluctuation characteristics with correlation reflectometry confirmed a considerable decrease of the fluctuation amplitude together with disappearance of the quasicohherent modes on the inner side of the torus. Modelling showed that this effect can be, to a great extent, explained by nonlocality of reflectometry. Experiments with tangential X-ray detector indicated that abrupt restructuring of the low- m MHD modes and inward plasma shift during an energy quench are accompanied by bursts of the fast-scale (~ 0.5 MHz) magnetic fields oscillations. Plasma discharge recovery after an energy quench is demonstrated in the T-10 high density plasma using ECRH auxiliary heating and controllable operation of the plasma current.

OV



3D Effects on Transport and Plasma Control in the TJ-II Stellarator

F. Castejón¹

¹*Centro de Investigaciones Energéticas, Medioambientales y Tecnológicas (CIEMAT), Madrid, Spain*

Corresponding Author: F. Castejón, francisco.castejon@ciemat.es

Recent improvements in diagnostics and operation have led to better understanding of 3D effects on transport and plasma control in the TJ-II stellarator. Impurity transport: Direct measurements of electrostatic potential variations within the same magnetic flux surface in ECRH plasmas are presented. Calculations show that such asymmetries affect impurity accumulation. The asymmetry value and its observed dependency on the electric field are reproduced by neoclassical MC calculations. The dependence of the impurity confinement time on charge and mass has also been studied. Experiments have shown evidence of the influence of ECRH on turbulent mechanisms, increasing both the fluctuation level and the amplitude of Long-Range-Correlations as proxy of Zonal Flows (ZF), as well as affecting NC radial electric fields. Momentum transport and electromagnetic effects: Radial electric fields, ZF-like structures, time memory and radial correlations are modulated by low order rationals. It is shown that magnetic oscillations associated with rational surfaces play an key role in confinement transitions. Furthermore, evidence of the mutual interaction of NC and turbulent mechanisms in qualitative agreement with GK simulations is presented. Innovative power-exhaust scenarios using liquid metals: Novel solutions for plasma facing components based on liquid metals like Li and Sn/Li alloys have been developed. Biasing of Li limiters with respect to carbon ones has evidenced the role of the secondary electron emission of plasma exposed surfaces. Plasma stability studies: It has been shown that a reduction of magnetic well has a direct impact on fluctuations without reducing plasma confinement drastically, suggesting that Mercier stability calculations are missing some stabilization mechanisms. Plasma fuelling experiments and neutral dynamics: First core plasma fuelling experiments using a cryogenic pellet injector system are presented. The radial redistribution of particles can be understood qualitatively from NC predictions. First results on the impact of neutral fluctuations on the observed turbulent structures will be reported. Role of ECRH and iota profile on fast ion confinement: Results show that ECRH and iota-profile are potential tools for AE control. Coherent modes in NBI-heated plasmas are explained as global (GAE) and discrete shear-AEs induced by magnetic islands.

AO



Overview of First Results from NSTX-U and Analysis Highlights from NSTX

J. Menard¹

¹*Princeton Plasma Physics Laboratory (PPPL), Princeton, NJ 08540, USA*

Corresponding Author: J. Menard, jmenard@pppl.gov

The National Spherical Torus Experiment (NSTX) has undergone a major upgrade, and NSTX Upgrade (NSTX-U) is now the most capable Spherical Torus/Tokamak (ST) in the world programme. NSTX-U mission elements include: exploring unique ST parameter regimes to advance predictive capability for ITER and beyond, developing solutions for the plasma-material interface challenge, and advancing the ST as a possible Fusion Nuclear Science Facility or Pilot Plant. NSTX-U has two major new tools including a new central magnet and new 2nd more tangential neutral beam injector (NBI). Plasma control commissioning and scenario development has proceeded rapidly on NSTX-U. Diverted plasmas with $IP = 0.8$ MA, $B_t = 0.6$ T, and pulse-length $\tau_p \sim 1$ s are obtained routinely, and sustained H-mode plasmas have been accessed with 2.5 MW of NBI heating power. Peak parameters achieved during the first run-month of NSTX-U plasma operation include: NBI power ~ 4 MW, $IP = 1$ MA, stored energy ~ 200 kJ, $\beta_N \sim 4$, $\kappa \sim 2.2$, $\tau_{Etot} > 50$ ms, $\tau_p \sim 1.7$ s, and a 50% increase in pulse-length from $n = 1$ error field correction. Expected results from the first run campaign include assessments of: core and pedestal confinement at lower collisionality via 60% higher field and current than NSTX, fast-ion confinement and current drive from the new 2nd NBI, and stability and control of high- κ and high- β_N plasmas. Extensive analysis of NSTX results continued including novel analysis of: edge turbulence data during the L-to-H-mode transition, heat flux footprint narrowing with increasing amplitude of edge-localized modes, and gyrokinetic modelling of core turbulence from dissipative trapped electron mode and electron temperature gradient modes. Further, a unified kinetic resistive wall mode physics model has been developed, and Massive Gas Injection valves similar to proposed ITER valves will be tested on NSTX-U. Lastly, a new method for determining the saturation level for Alfvén Eigenmodes has been developed, and SOL power losses for RF heating modelled and interpreted with the AORSA code. Results from the first research campaign of NSTX-U will be presented, initial comparisons between NSTX-U and NSTX results described, and NSTX analysis highlights presented.

OV



Overview of Recent Physics Results from MAST

A. Kirk¹

¹*Culham Centre for Fusion Energy (CCFE), Culham Science Centre, Abingdon, UK*

Corresponding Author: A. Kirk, andrew.kirk@ccfe.ac.uk

New results from MAST will be presented that focus on validating models in order to extrapolate to future devices. Particular attention will be given to the areas of scenario development, fast particle physics and plasma exhaust.

Understanding filamentary transport across the scrape-off layer is a key issue for the design and operation of future devices as it is crucial in determining the power loadings to the divertor and first wall of the machine. A detailed characterization of the MAST scrape-off layer has been performed including results from new diagnostics giving plasma potential and ion temperature measurements. Detailed studies have revealed how filament characteristic are responsible for the broadening of the midplane density profile. These measurements have been compared to extensive modelling, including 3D effects on filaments dynamics with the BOUT++ code, and benchmarking the SOLPS code. Impurity transport studies have shown how the balance between neoclassical and anomalous transport leads to carbon and nitrogen being screened from the core plasma compared to helium which is peaked at the centre. These results, combined with SOLPS modelling, suggest that a stable detachment region can be produced if the impurity puffing is localized.

Measurements from a Doppler Backscattering system combined with GS2 simulations have shown that both microtearing modes (MTMs) and electron temperature gradient (ETG) modes can be unstable at the top of the pedestal, along with kinetic ballooning modes at the bottom of the steep gradient region. The experimental observations of the relative amplitudes and wavelengths of the density and magnetic field fluctuations at the top of the pedestal are more similar to the linear characteristics of the ETG than the MTM.

Comprehensive measurements from a suite of diagnostics on MAST have shown the effect that core MHD modes and resonant magnetic perturbations (RMPs) have on the confinement and redistribution of fast ions arising from neutral beam injection (NBI). Subsequent experiments on MAST demonstrated that by vertically displacing the plasma to achieve off-axis NBI fast ion injection or by changing plasma density or NBI power to vary the fast ion pressure gradient the redistribution could be mitigated.



H-Mode and Nonsolenoidal Startup in the Pegasus Ultralow-A Tokamak

R. Fonck¹, J. Barr¹, G. Bodner¹, M. Bongard¹, M. Burke¹, D. Kriete¹, J. Perry¹, J. Reusch¹,
D. Schlossberg¹, C. Sovinec¹, and K. Thome¹

¹University of Wisconsin-Madison, Madison, WI 53706, USA

Corresponding Author: R. Fonck, rjfonck@wisc.edu

Studies at near-unity aspect ratio offer unique insights into the high confinement (H-mode) regime and support development of novel startup scenarios. Ohmic H-mode operation has been attained at $A < 1.3$. Edge plasma parameters permit probe measurements of the edge pedestal, including the local current density profile, with high spatial and temporal resolution. H-mode plasmas have standard L-H transition phenomena: a drop in D_α radiation; the formation of pressure and current pedestals; field-aligned filament ejection during ELMs; and a doubling of energy confinement time from $H_{98} \sim 0.5$ to ~ 1 . The L-H power threshold P_{LH} increases monotonically with n_e , consistent with the ITPA08 empirical scaling used for ITER and the theoretical FM3 model. Unlike at high A , P_{LH} is comparable in limited and single-null diverted topologies at $A \sim 1.2$, consistent with FM3 predictions. The magnitude of P_{LH} exceeds ITPA scalings by an order of magnitude, with P_{LH}/P_{ITPA08} increasing as A approaches 1. Multiple n modes are observed during two classes of ELMs, consistent with excitation of multiple peeling-ballooning modes. Small, type-III-like ELMs occur at $P_{OH} \sim P_{LH}$ with $n \leq 4$. Large, type-I-like ELMs occur with $P_{OH} > P_{LH}$ and intermediate $5 < n < 15$. Helical edge current injection appears to suppress type-III ELM activity. $J_{edge}(R, t)$ measurements across single ELMs show the nonlinear generation and expulsion of current-carrying filaments during the ELM crash. Local Helicity Injection (LHI) offers a nonsolenoidal tokamak startup technique. Helicity is injected via current sources at the plasma edge. A circuit model that treats the plasma as a resistive element with time-varying inductance reasonably predicts $I_p(t)$. The electron confinement governs the power balance. Initial measurements show peaked T_e and pressure profiles, which are comparable to Ohmic-like transport or moderately stochastic confinement. Extrapolation suggests $I_p \sim 1$ MA may be achievable in NSTX-U. Resistive MHD simulations suggest I_p is built from current rings injected during reconnection between unstable helical current streams. Several experimental observations support this model: imaging of the merging current streams; $n = 1$ MHD activity and discrete current stream localized in the plasma edge; and anomalously high impurity ion heating in the edge region.

OV



Overview of Spherical Tokamak Research in Japan

Y. Takase¹, A. Ejiri², T. Fujita³, K. Hanada⁴, H. Idei⁴, M. Nagata⁵, Y. Ono¹, H. Tanaka⁶, A. Fukuyama⁶, Y. Kamada⁷, N. Fukumoto⁵, R. Horiuchi⁸, Y. Nagayama⁸, Y. Takeiri⁸, and S. Tsuji-Iio⁹

¹University of Tokyo, Tokyo, Japan

²Graduate School of Frontier Science, University of Tokyo, Tokyo, Japan

³Nagoya University, Nagoya, Japan

⁴Research Institute for Applied Mechanics (RIAM), Kyushu University, Kasuga, Japan

⁵University of Hyogo, Kobe, Japan

⁶Kyoto University, Nishikyo-ku, Kyoto 615-8540, Japan

⁷Japan Atomic Energy Agency (JAEA), Naka, Japan

⁸National Institute for Fusion Science (NIFS), Toki, Gifu, Japan

⁹Tokyo Institute of Technology, Tokyo, Japan

Corresponding Author: Y. Takase, takase@k.u-tokyo.ac.jp

Nationally coordinated research on spherical tokamak (ST) is being conducted in Japan, to strengthen the scientific basis and to broaden future options of ST applications. The research themes to concentrate on are 1) the physics of very high- β plasmas, 2) development of start-up, current drive, and control techniques without the use of the central solenoid (CS), and 3) demonstration of very long pulse operation and the study of steady-state issues. Research elements are developed on several devices optimized for each objective. The basic mechanism of tokamak plasma formation by ECW/EBW was investigated on LATE. The tokamak configuration with closed flux surfaces is formed spontaneously when the equilibrium current changes from the vertical charge separation current to the toroidal return current. Highly over-dense plasmas have been produced, indicating mode conversion to EBW. A maximum plasma current of 66 kA was achieved using 28 GHz on QUEST. Plasma current start-up by LHW is being investigated on TST-2. The most efficient ramp-up was achieved by the capacitively-coupled combline antenna, which excites a travelling LHW with a sharp wavenumber spectrum and high directionality. Experiments with a top-launch antenna, expected to improve single-pass absorption and increase current drive efficiency, have started. The formation of closed flux surfaces by transient coaxial helicity injection (CHI) was verified by internal magnetic probe measurements on HIST. A stable closed flux formation was achieved by high bias flux operation, and the validity of helicity balance was confirmed. CHI electrodes were installed on QUEST under US-Japan collaboration. An RF-driven long pulse discharge of up to 810 s has been achieved on QUEST. Operation with hot metal wall has started, with the aim to control particle recycling by active wall temperature control. Compact toroid injection is being developed as an advanced fuelling method. High-power reconnection heating of ST plasmas using axial merging of two ST plasmas was demonstrated in TS-3, TS-4 and UTST. Collaboration on the MAST device has demonstrated that reconnection heating can be extended successfully to larger scale and higher magnetic field. ST plasma stability improvement was accomplished by applying a helical field in TOKASTAR-2, an ST-helical hybrid device equipped with helical field coils.

Overview of the TCV Tokamak Programme: Scientific Progress and Facility Upgrades

S. Coda¹

EUROfusion MST1 Team, EUROfusion, and TCV Team, Switzerland

¹*Swiss Plasma Center (SPC), École polytechnique fédérale de Lausanne (EPFL), 1015 Lausanne, Switzerland*

Corresponding Author: S. Coda, stefano.coda@epfl.ch

A broad upgrade programme is underway at the TCV tokamak. A historic first step is the present commissioning of the first neutral beam injector (NBI), delivering 1 MW of power at energies in the 15–30 keV range. Four gyrotrons are also being added in 2016–2018 to bring the total ECRH power to 6 MW. A second, counterinjected, 1 MW neutral beam is also planned, in addition to the introduction of variable-configuration divertor baffles, to expand the role of TCV in preparing the grounds for both ITER and DEMO. TCV is now operating partly as a European Medium-Size Tokamak (MST) facility within the EUROfusion consortium.

In the realm of edge and exhaust physics, access to divertor detachment has been investigated through density ramps and nitrogen puffing, first revisiting the conventional single-null divertor, then proceeding through the variety of alternative geometrical divertor configurations that TCV can sustain, including the X-divertor, X-point target, and the snowflake minus and plus. Studies of scrape-off layer (SOL) transport are focussing especially on the enhanced convection that leads to profile broadening at high density and is generally attributed to intermittent filamentary structures; through a large scan in parallel connection length, no evidence for far SOL profile broadening is found. The double heat-flux scale length measured in limited L-modes in the TCV SOL, a possible concern for reactor start-up, has been reproduced by the 3D turbulent-transport GBS code. A wall cleaning solution based on ECRH-sustained, current-less helium discharges was recently tested on TCV for JT-60SA.

In the area of control, a generalized plasma shape and position controller, based on real-time, sub-ms equilibrium reconstruction was recently tested successfully. Considerable attention has been given to disruptions. In addition to exploring techniques for disruption mitigation or avoidance (by massive gas injection or ECCD, and with assistance from real-time modelling), the related problems of runaway electron generation, mitigation, and control, are also being tackled. Investigations of the density disruption limit are ongoing, in particular to explore its dependence on gas puffing and plasma shape. The possible “seedless” excitation of NTMs, mediated by neoclassical toroidal viscosity, has been successfully studied by modifying the rotation profile with ECRH.

OVP

Overview of the RFX-Mod Fusion Science Activity

M. Zuin¹, M. E. Puiatti¹, L. Marrelli¹, and S. Dal Bello¹

¹*Consorzio RFX, Associazione EURATOM-ENEA sulla Fusione, Padova, Italy*

Corresponding Author: M. Zuin, matteo.zuin@igi.cnr.it

Thanks to its flexibility and unique control capability, the RFX-Mod device has been operated in the last two years to investigate a wide range of experimental conditions. Reversed-Field Pinch (RFP), Tokamak and the full range of magnetic configurations in between the two, the ultralow q , have been produced to contribute to physics common topics highlighting both similarities and peculiarities. The experiments have been inspired and complemented by an intense theoretical modelling activity, based on 3D nonlinear visco-resistive MHD, advanced nonlocal transport simulation, Hamiltonian guiding centre and nonlinear gyrokinetic codes. The RFX-Mod scientific programme thus provides contribution to magnetically confined plasma physics on various fundamental aspects: 3D effects, transport barriers and MHD control.

OV-P The effect of spontaneous or externally-induced 3D (helical) equilibria on high current RFP plasmas has been deeply investigated, with particular emphasis on the role of the isotopic effect. An enhancement of confinement in deuterium plasmas has been observed and reproduced by simulations. The role of 3D effects on transport and small scale turbulence in the presence of magnetic islands has been studied, as well as the role of a helical boundary in the formation of 3D core equilibria, relevant for the dynamo effect in hybrid regimes in Tokamaks.

Physics issues associated to the density limit phenomenon have been addressed in all magnetic configurations. The analysis of the locking-unlocking threshold for the spontaneous rotation of the tearing in the RFP has shown the absence of hysteresis in the presence of feedback control. The results are well reproduced by a code, reliable for Tokamak plasmas as well in the investigation of the feedback control of the $(2, 1)$ mode, successfully experimented in RFX-Mod. The application of 3D perturbations has demonstrated to be effective in deconfining runaway electrons in Tokamak plasmas. Long lasting H-modes have been attained in both circular and shaped (single null) plasmas thanks to the exploitation of an edge polarized electrode. Indications of the first L-H transitions in $q(a) < 2$ circular plasmas have been obtained. In order to enhance the confinement properties in RFP and to extend the operational scenarios both in RFP and Tokamak, a series of modifications for the RFX-Mod device has been proposed.



Overview of Recent COMPASS Activities

R. Dejarnac¹

¹*Institute of Plasma Physics AS CR v.v.i., Prague, Czech Republic*

Corresponding Author: R. Dejarnac, dejarnac@ipp.cas.cz

The COMPASS tokamak is one of the present devices operating with an ITER-like plasma shape. Its flexibility combined to an extensive set of diagnostics and NBI heating allow to address a broad range of key areas in support of the worldwide fusion programme such as H-mode, MHD, RAE, disruptions, PWI. The recent results obtained in COMPASS addressing these key issues are reviewed here.

The control and characterization of the L-H transition and the pedestal physics represent a large part of the COMPASS scientific programme. Recycling and actuators such as the X-point height play a significant role in accessing H-mode. GAMs oscillating at frequencies 25–40 kHz are observed in L-mode discharges, increasing with the ion mass and with a decreasing amplitude from D to H plasmas. COMPASS also contributes to multimachine databases with pedestal and SOL width scalings studies. Using perturbation coils, the influence of 3D fields on the strike-points splitting, ELM control and transport is reported.

The MHD modes studies mainly concern the plasma interaction with RMPs, the characterization of Alfvén-like modes and disruption/mitigation experiments. High frequency quasi-coherent oscillations (ranging from 200 kHz to above 1 MHz) that follow Alfvénic frequency scaling are observed in ohmic discharges. An extensive experimental study of MHD effects in losses of runaway electrons has been performed. In the field of disruptions, an intermachine empirical scaling of critical magnetic disruption precursors has been developed, as well as the study of the disruptions toroidal asymmetry.

The exhaust and plasma-material interaction studies in COMPASS contributed to the ITER divertor monoblocks design as part of the ITPA. Power deposition on leading edge was investigated both experimentally (inner-wall limiters with gaps and leading edges viewed by a high-resolution IR camera) and numerically (PIC simulations), with the latter reproducing well this experiment and the recent lamella melting experiment on JET. The ITER monoblocks shaping was also investigated in the frame of an ITER contract. Comparison with the deposited power from ion orbit calculations are consistent and confirm results presented at the previous IAEA FEC. However, the role of the E -field and the contribution from the electrons on the total power flux accounted in PIC calculations predict marginally lower power.

OVP

Overview of the FTU Results

G. Pucella¹

¹*Agenzia nazionale per le nuove tecnologie, l'energia e lo sviluppo economico sostenibile (ENEA), Rome, Italy*

Corresponding Author: G. Pucella, gianluca.pucella@enea.it

Experiments of electron cyclotron (EC) assisted breakdown have shown the presence of runaway electrons (RE) also below the Dreicer electric field threshold, indicating that the RF power acts as seeding for fast electrons, and a large database of postdisruption generated RE beams has been analyzed in order to identify linear dynamical models for new position and current RE beam controllers. A linear microstability analysis of neon doped pulses has been carried out to investigate the mechanisms leading to the observed density peaking. A study of the $E \times B$ drift effect on the MARFE instability has been performed and the peaking of density profile has been well reproduced using a particle pinch term of the form $D_T n d(\ln T)/dr$. The 2/1 tearing mode (TM) observed in high density plasmas has shown a final phase characterized by limit cycles on the amplitude/frequency plane. The analysis of the linear stability has highlighted a destabilization with increasing peaking of the current profile during the density ramp-up, and experiments of real-time control of such a TM, by means of EC heating of the magnetic islands, have shown a considerable stabilizing effect. A cooled lithium limiter with thermal load capability up to 10 MW/m^2 has been tested. The pulse duration has been extended up to 4.5 s and elongated configurations have been obtained for 3.5 s, with the X-point just outside the plasma chamber. W/Fe samples have been exposed in the SOL in order to study the sputtering of Fe and the W enrichment of the surface layer. Dust has been collected and analyzed, showing that the metallic population exhibits a high fraction of magnetic grains. A new diagnostic for in-flight RE studies has provided simultaneously the image and the visible/infrared spectrum of the forward and backward radiation. A fast infrared camera for thermo-graphic analysis has provided the pattern of the toroidal limiter heating by disruption heat loads, and a triple-GEM detector has been mounted on one equatorial port for soft-X-rays diagnostics. The collective Thomson scattering diagnostic has been upgraded and used for investigations on parametric decay instability excitation by EC beams correlated with magnetic islands, and new capabilities of the Cherenkov probe have been explored in the presence of Beta-induced Alfvén Eigenmodes associated to high-amplitude magnetic islands.

OV/P



Overview of MST Reversed Field Pinch Research in Advancing Fusion Science

J. S. Sarff¹, J. K. Anderson¹, P. Brunzell², D. L. Brower³, B. E. Chapman¹, D. Den Hartog¹, W. X. Ding³, L. Frassinetti², R. W. Harvey⁴, V. Mirnov¹, M. Nornberg¹, S. Polosatkin⁵, C. Sovinec¹, D. Spong⁶, P. W. Terry¹, A. F. Almagri¹, J. Boguski¹, P. Bonofiglio¹, M. Borchardt¹, W. Capecchi¹, C. Cook¹, D. Craig⁷, J. Egedal¹, A. DuBois¹, J. Duff¹, X. Feng¹, D. Demers⁸, P. Fimognari⁸, C. Forest¹, M. Galante¹, J. Goetz¹, C. C. Hegna¹, D. Holly¹, C. Jacobson¹, J. Johnson¹, J. Kim¹, S. Kubala¹, L. Lin³, K. McCollam¹, M. McGarry¹, L. Morton¹, S. Munaretto¹, T. Nishizawa¹, R. Norval¹, P. Nonn¹, S. Oliva¹, M. J. Pueschel¹, J. Reusch¹, L. Reusch¹, J. Sauppe¹, S. Sears¹, A. Seltzman¹, J. Triana¹, D. Thuecks¹, G. Whelan¹, Z. Williams¹, A. Xing¹, O. Schmitz¹, T. Crowley⁸, V. Belykh⁵, V. Davydenko⁵, A. A. Ivanov⁵, R. Fridström², P. Franz⁹, S. Hirshman⁶, E. Parke³, H. Stephens¹⁰, M. Tan¹¹, and J. Titus¹²

¹University of Wisconsin-Madison, Madison, WI 53706, USA

²KTH Royal Institute of Technology, Stockholm, Sweden

³University of California Los Angeles, CA 90095, USA

⁴CompX, Del Mar, CA 92014, USA

⁵Budker Institute of Nuclear Physics (BINP), Novosibirsk, Russian Federation

⁶Oak Ridge National Laboratory (ORNL), Oak Ridge, TN 37831, USA

⁷Wheaton College, Wheaton, IL 60187, USA

⁸Xantho Technologies, LLC, Madison, WI 53705, USA

⁹Consorzio RFX, Associazione EURATOM-ENEA sulla Fusione, Padova, Italy

¹⁰Pierce College, Los Angeles, CA 91371, USA

¹¹University of Science and Technology of China, Hefei, Anhui, People's Republic of China

¹²Florida A&M University, Tallahassee, FL 32307, USA

Corresponding Author: J. S. Sarff, jssarff@wisc.edu

The reversed field pinch (RFP) offers unique capabilities that could be essential to closing gaps to fusion power. The RFP has large plasma current and small toroidal field, with $q(r) < 1$. Two key benefits arise: 1) the possibility for ohmic heating to ignition and 2) minimization of the field strength at the magnets. The material boundary can be made invisible to an inductive electric field, and the first-wall need not accommodate power injection ports or antennas. These features could help achieve a maintainable and reliable fusion power source.

This overview summarizes MST results important for the advancement of the RFP as well as for improved understanding of toroidal confinement generally. Evidence for first observations of trapped-electron mode (TEM) turbulence in the RFP is obtained. Short-wavelength density fluctuations exhibit a density-gradient threshold, and GENE modelling predicts unstable TEM's. Core-localized neutral beam injection stimulates bursty modes with both Alfvénic and EPM scaling. One mode agrees with a new analytic theory for the magnetic-island-induced Alfvén eigenmode (MIAE), which conspires with an EPM to affect fast ion transport.

Continued...

At high current, the RFP transitions to the quasi-single-helicity (QSH) state. A method to control the locked phase of QSH has been developed using resonant magnetic perturbations (RMP). Runaway electrons that appear without RMP are suppressed. An improved model for simultaneous interactions of multiple tearing modes and error fields has been developed. The RFP's tearing-relaxation behaviour together with well-developed theory and computation create a ripe opportunity for rigorous validation of MHD models.

Integrated data analysis (IDA) complements validation by maximizing the information embedded in multiple diagnostics, which is essential for future fusion development steps having limited diagnostics. Using IDA methods, meta-diagnostics that combine charge-exchange recombination spectroscopy, X-ray tomography, and Thomson scattering yield more robust measurements of Z_{eff} and T_e , critical parameters for MHD. Nonlinear studies using an extended MHD model including drift and two-fluid physics in NIMROD show features similar to MST observations, including a tendency for the MHD and Hall emf terms to oppose each other in Ohm's law, and opposition of the Maxwell and Reynolds stresses in momentum balance.

Progress of the Recent Experimental Research on the J-TEXT Tokamak

G. Zhuang¹

¹Huazhong University of Science and Technology, Hubei, People's Republic of China

Corresponding Author: G. Zhuang, ge-zhuang@hust.edu.cn

The progress of experimental research over last two years on the J-TEXT tokamak is reviewed, the most significant results including: the investigation of the effect of resonant magnetic perturbations (RMPs) on the J-TEXT operation region, impurity transport and confinement, and runaway electrons suppression; study of the threshold for runaway current generation; and identification of the quasi-coherent characteristics in spectra of density fluctuations. The effect of RMPs on the J-TEXT ohmically heated operation region is studied on J-TEXT by applying RMPs in high density limit and low- q limit discharges. It is found that moderate amplitude of applied RMPs either increases the density limit from less than $0.7n_{GW}$ to $0.85n_{GW}$ or lowers edge safety factor q_a from 2.15 to nearly 2.0. As a result, the disruption precursor is suppressed and the disruption is delayed by about 30–150 ms. The influence of RMPs on impurity behaviour is also studied by applied RMP with $m/n = 2/1$ dominant component. It is found that the CV decay time after methane injection decreases as the RMP amplitude increases. When the RMP penetration occurs, the emission of CIII (464.7 nm) from the edge region develops a gradually increasing asymmetry. Stronger emission occurs at the high-field-side (HFS) edge. The potential suppression of runaway electrons by RMP is also investigated on J-TEXT. The experimental result indicates that the magnetic perturbation enhanced the runaway loss rate by the formation of magnetic islands rather than by the magnetic perturbation itself. Both the amplitude and the length of runaway current can be reduced by applying the RMP before the disruption. Regarding the threshold for runaway current generation, it is found that the key parameter affecting runaway generation is the edge safety factor q_a , not B_t , on J-TEXT. The threshold of q_a decreases with increasing B_t . The electrostatic turbulence exhibited quasi-coherent characteristics in the spectra of density fluctuations observed in the J-TEXT ohmic confinement regime. These quasi-coherent modes (QCMs) are detectable in a large plasma region ($r/a \sim 0.3-0.8$) with frequency of 30–140 kHz. The mode rotates in the electron diamagnetic direction. The combined experimental results indicate that the QCMs survive in the linear ohmic confinement regime of the plasma, where the TEM is predicted to be unstable.

OVP

Edge and Divertor Plasma: Detachment, Stability, and Plasma-Wall Interactions

S. Krasheninnikov¹, A. Pigarob¹, R. Smirnov¹, and W. Lee¹

¹University of California San Diego, CA 92093, USA

Corresponding Author: S. Krasheninnikov, skrash@mae.ucsd.edu

The processes involving edge plasma and plasma-material interactions in magnetic fusion devices are very multifaceted and include a wide spectrum of phenomena ranging from plasma turbulence and meso-scale stability, recycling and transport processes of hydrogen species in the wall material, to the modification of wall material properties. In many cases these processes are strongly coupled and exhibit synergistic effects. Here we present the results of our studies of a wide range of edge plasma related issues: Our numerical simulations solve a long standing dispute on the roles of impurity radiation loss, plasma volumetric recombination, and ion-neutral friction in the rollover of the plasma flux to the target, which is the manifestation of detachment. We show that the rollover is caused by the increase of the impurity radiation loss and volumetric plasma recombination while the ion-neutral friction, although important for establishing necessary edge plasma conditions, does not contribute per se. With numerical modelling and theoretical analysis we consider stability of detachment and show that the absorption and desorption of hydrogen and impurity species from the wall can be crucial for a global stability of detached plasma. We also identify different mechanisms of meso-scale thermal instabilities driven by impurity radiation and resulting in a self-sustained oscillations of edge plasma parameters. We consider a trapping of He, which is an intrinsic impurity of fusion plasmas, in the first wall tungsten material. Our newly developed model, accounting for the generation of additional He traps caused by He bubble growth, fits all available experimental data on the layer of nano-bubbles observed in W under irradiation of low energy He plasma. Finally, we report on an impact of sheared magnetic field on the dynamics of blobs and ELM filaments playing an important role in edge and SOL plasma transport.

Work supported by the U.S. Department of Energy, Office of Science, Office of Fusion Energy Sciences under Award Numbers DE-FG02-04ER54739, DE-FG02-06ER54852, DE-SC0010413, and through the Scientific Discovery through Advanced Computing (SciDAC) programme on Plasma Surface Interactions, funded by U.S. Department of Energy, Office of Science, Advanced Scientific Computing Research and Fusion Energy Sciences under Award Number DE-SC0008660.



Hysteresis and Fast Timescale in Transport Relation of Toroidal Plasmas

K. Itoh¹, S.-I. Itoh², K. Ida¹, S. Inagaki³, Y. Kamada⁴, K. Kamiya⁴, J. Dong⁵, C. Hidalgo⁶, T. E. Evans⁷, W. H. Ko⁸, H. K. Park⁹, T. Tokuzawa¹, S. Kubo¹, T. Kobayashi³, Y. Kosuga¹⁰, G. Yun¹¹, S. Song⁵, N. Kasuya³, Y. Nagashima², C. Moon¹, M. Yoshinuma¹, R. Makino¹, T. I. Tsujimura¹, H. Tsuchiya¹, and U. Stroth¹²

¹National Institute for Fusion Science (NIFS), Toki, Gifu, Japan

²Research Institute for Applied Mechanics (RIAM), Kyushu University, Kasuga, Japan

³Kyushu University, Kasuga, Japan

⁴Japan Atomic Energy Agency (JAEA), Naka, Japan

⁵Southwestern Institute of Physics, Chengdu, Sichuan, People's Republic of China

⁶Centro de Investigaciones Energéticas, Medioambientales y Tecnológicas (CIEMAT), Madrid, Spain

⁷General Atomics, San Diego, CA 92186, USA

⁸National Fusion Research Institute (NFRI), Daejeon, Republic of Korea

⁹Ulsan National Institute of Science and Technology (UNIST), Ulsan, Republic of Korea

¹⁰Institute for Advanced Study, Kyushu University, Kasuga, Japan

¹¹Pohang University of Science and Technology (POSTECH), Pohang, Gyeongbuk 790-784, Republic of Korea

¹²Max-Planck-Institut für Plasmaphysik, Garching, Germany

Corresponding Author: K. Itoh, itoh@nifs.ac.jp

This article assesses the understanding of, and impacts by, the hysteresis of transport relation. The rapid changes of fluxes compared to slow changes of plasma parameters are presented for both edge barrier and core plasmas. The theoretical approaches to understand the direct influence of heating power on turbulent transport are addressed. The advanced data analysis method to search the hysteresis in gradient-flux relation is explained. Finally, the importance of transport hysteresis on the control system of fusion device is discussed. The modulation ECH experiment, in which the heating power repeats on-and-off periodically, revealed hysteresis and fast changes in gradient-flux relation. The decisive progress is that both the hysteresees in the gradient-flux and gradient-fluctuation relations were observed simultaneously. Analyses of observations that can be interpreted as the hysteresis have been undertaken on various experiments: LHD, ASDXE-U, DIII-D, HL-2A, JFT-2M, JT-60U, KSTAR, TJ-II, and W7-AS. Hysteresis with rapid timescale exists in the channels of energy, electron and impurity, and plausibly in momentum.

The causes of hysteresis and fast timescale are discussed. The nonlocal-in-space coupling works here, but does not suffice. One mechanism for “the heating heats turbulence” is that the external source S in phase space for heating has its fluctuation in turbulent plasma: $S(f) = S(f_0) + (dS/df)\delta f$, where δf is the perturbation of distribution function. This coupling can induce the direct input of heating power into fluctuations. The height of the jump in transport hysteresis is smaller for heavier hydrogen isotope, and is one of origins of isotope effect on confinement. Advanced methods of data analysis are presented. The transport hysteresis can be studied by observing the higher harmonics of temperature perturbation δT_m in heating modulation experiments. The hysteresis introduces the term δT_m , which depends on the harmonic number m in algebraic manner (not exponential decay). The impacts of transport hysteresis on the control system are assessed. The control system must be designed so as to protect the system from sudden plasma loss. Thermonuclear instability due to fusion power is also discussed.



Overview of Simulation Results Using Computation Resources in the Framework of IFERC-CSC

D. Borba¹, A. Fukuyama², N. Nakajima³, and Y. Ishii³

¹*EUROfusion/JET, Culham Science Centre, Abingdon, Oxfordshire, OX14 3DB, UK*

²*Kyoto University, Nishikyo-ku, Kyoto 615-8540, Japan*

³*Japan Atomic Energy Agency (JAEA), Naka, Japan*

Corresponding Author: D. Borba, duarte.borba@euro-fusion.org

Following the successful operation of a European High Performance Computer For Fusion applications (HPC-FF) in Jülich, Germany, from 2009 to 2013, a new supercomputer dedicated to magnetic fusion research was procured within the Broader Approach agreement between Europe and Japan. The new platform, “Helios”, was installed in the International Fusion Energy Research Centre – Computational Simulation Centre (IFERC-CSC) in Rokkasho, Japan and it started operations in January 2012 and is expected to serve until the end of 2016. The use of the Helios computer has been rather successful with a large scientific output expressed in the number of peer-reviewed publications of around one per project per year. In the 5th cycle of operation of Helios, over 120 projects have been selected, corresponding to over 300 users. In this paper, the main scientific and technical results obtained in the Helios numerical simulations projects are described with emphasis on the impact in developing fusion science and related technologies. At the end of its life cycle the use of Helios will be replaced in Europe with a new EUROfusion supercomputer, allowing further development of fusion technologies based on computer modelling and simulations. Collaborations between Japan and Europe will continue with new opportunities for joint projects like Helios.

OV-P

Overview of DEMO Safety R&D and the Potential Future Role of IEA ESEFP IA

Y. Wu¹, Z. Chen¹, M. Jin¹, Y. Li¹, J. Jiang¹, L. Hu¹, C. Alejaldre², E. Stevens³, K. Kim⁴, D. Maisonnier⁵, A. Kalashnikov⁶, K. Tobita⁷, and D. Jackson⁸

¹*Institute of Nuclear Energy Safety Technology, CAS, Anhui, People's Republic of China*

²*Former ITER Deputy Director-General, ITER Organization*

³*Fusion Energy Sciences, U.S. Department of Energy, Washington, DC 20585, USA*

⁴*National Fusion Research Institute (NFRDI), Daejeon, Republic of Korea*

⁵*European Commission*

⁶*ROSATOM State Atomic Energy Corporation, Moscow, Russian Federation*

⁷*Japan Atomic Energy Agency (JAEA), Naka, Japan*

⁸*Dept of Engineering Physics, McMaster University, Hamilton, ON L8S-4L8, Canada*

Corresponding Author: Y. Wu, yican.wu@fds.org.cn

A fusion DEMO reactor, like other advanced nuclear energy systems, must satisfy several goals including a high level of public and worker safety, low environmental impact, high reactor availability, a closed fuel cycle, and the potential to be economically competitive. The experience of the ITER project will facilitate DEMO programmes in developing a safety approach and a safety design, performing safety analyzes under the scrutiny of a nuclear regulator, ensuring device availability, managing the radioactive waste, and conducting economic assessments. However, there are still large scientific and technological gaps between the current ITER and DEMO reactors. In this paper international fusion safety research relevant to DEMO will be summarized following the lessons learned from ITER. The main scientific and technological challenges will be presented by considering the differences between fission and fusion reactors as well as the corresponding implications on DEMO design and operation, with perspectives not only from fusion energy development but also from the development of Generation-IV fission reactors. Potential research topics for international collaboration will also be addressed with emphasis on the International Energy Agency (IEA) implementing agreement (IA) on a cooperative programme on Environmental, Safety and Economic aspects of Fusion Power (ESEFP).

Implementation within the European Domestic Agency of the French Nuclear Safety Order of 2012, Concerning Basic Nuclear Installation, Applicable to ITER Project

P. Wouters¹, J. Furlan¹, G. Serra¹, and P. Jucker¹

¹F4E: Fusion for Energy, ITER EU Centre, 08019 Barcelona, Spain

Corresponding Author: P. Wouters, paul.wouters@f4e.europa.eu

The ITER project is being undertaken at Cadarache, France, to construct and operate an experimental nuclear fusion facility. The aim of this paper is the description of the implementation of the French Order of February 7, 2012, concerning Nuclear Installation (called Installation Nuclear de Base, INB) in France within the European Domestic Agency (EU-DA). For protection of Public Safety, Health and Salubrity, and of Nature and Environment, the French order (INB Order 07/02/2012) establishes general rules relating to the Design, Construction, Operation, Final shutdown, Dismantling, Surveillance and Maintenance of Nuclear facilities during their full life cycle.

OV-P The INB Order applies namely to the operator (ITER Organization) and involves the whole supply chain. The EU-DA, as a tier 1 supplier, has duties regarding the compliance with the requirements propagated from the INB Order, mainly the dispositions to be propagated from the nuclear operator to the chain of suppliers performing Protection Important Activities (PIA), called external interveners in the INB order, in the contracts. Among other nuclear regulations in force in France, presently encoded in the French Environmental Code as, the Nuclear Pressurized Equipment regulation (ESPN), the INB Order addresses domains where the EU-DA shall play a prime role in providing to the nuclear operator reliable evidences and sound demonstration in organization and responsibilities, nuclear safety demonstration, traceability, validation of methods, qualifications, calculations and modelling, and so on.

The EU-DA applies a Requirements Management and Verification (RMV) process in order to track, control and verify all technical requirements applicable to ITER components under the EU-DA responsibility. This process is applied to the nuclear safety defined requirements in a way that allows all defined requirements on ITER components to be recorded and controlled at all the different levels of the supply chain in a systematic way.

Finally the communication performed within the EU-DA organization and the supply chain to continuously improve the nuclear safety culture, which is a first priority of the ITER project, will be presented.

Overview of Progress in European Medium Sized Tokamaks towards an Integrated Plasma-Edge/Wall Solution

H. Meyer¹, T. Eich², M. Beurskens², S. Coda³, A. Hakola⁴, and P. Martin⁵

¹*Culham Centre for Fusion Energy (CCFE), Culham Science Centre, Abingdon, UK*

²*Max-Planck-Institut für Plasmaphysik, Greifswald, Germany*

³*Swiss Plasma Center (SPC), École polytechnique fédérale de Lausanne (EPFL), 1015 Lausanne, Switzerland*

⁴*VTT Technical Research Centre of Finland Ltd., Espoo, Finland*

⁵*Consorzio RFX, Associazione EURATOM-ENEA sulla Fusione, Padova, Italy*

Corresponding Author: H. Meyer, hendrik.meyer@ukaea.uk

Progress in tackling the edge challenge within the new European Medium Size Tokamak Task Force (EU-MST) will be reported. EU-MST coordinates research on ASDEX-Upgrade, MAST and TCV supported by the local teams. The challenge is approached from two directions. On the one hand plasma regimes reducing the transient heat loads whilst trying to maintain high confinement are developed with active ELM control techniques and natural small ELM scenarios. On the other hand divertor solutions with detachment control and advanced magnetic configurations are studied. The type-I ELM energy flux is found to never exceed a value proportional to the pedestal top pressure times the minor radius and is never lower than 1/3 of this maximum value. Interestingly, the actively controlled type-I ELMs with resonant magnetic perturbations on MAST and AUG also fit well into this operational band and so to reduce heat loads well below the ITER material limits a change of ELM regime is likely required. Such RMP aided small ELM regimes have been found at low and high density, although the low density, low collisionality regimes are often accompanied by an unacceptable drop in confinement. For the high-density regimes, also accessed without RMPs, evidence is mounting that a high scrape-off layer (SOL) density is a key parameter. The RMP ELM control has been found to be transferable to He plasmas. New data from TCV on ELM control with vertical kicks and edge ECRH will also be presented. Partial detachment of the divertor and its control is also a part of the integrated solution. The X-point radiation in N seeded discharges at high P/R has now been identified as a suitable control parameter. The studies of detachment have been extended to advanced divertor configurations experimentally on TCV and theoretically on MAST. Here target heat loads are reduced by geometrical means as well as by volumetric processes. Predicted impurity trapping between the two X-points of a snowflake configuration could further aid the heat flux reduction. SOL flows and filamentary transport become important in understanding the power distribution between the different strike zones. With RMPs, lobe structures form that locally increase the heat load and may influence the divertor radiation. The access to a wide parameter space, new concepts and integration within EU-MST is instrumental for progress in this area.

EAO

EX: Magnetic Confinement Experiments

EX



Role of MHD Dynamo in the Formation of 3D Equilibria in Fusion Plasmas

P. Piovesan¹, D. Bonfiglio¹, S. Cappello¹, L. Chacón², C. Chrystal³, D. Escande⁴, P. Franz¹, C. T. Holcomb⁵, V. Igochine⁶, T. C. Luce⁷, L. Marrelli¹, M. Nornberg⁸, C. Paz-Soldan⁷, L. Piron⁹, J. S. Sarff⁸, N. Taylor³, D. Terranova¹, F. Turco¹⁰, P. Zanca¹, and B. Zaniol¹

¹Consorzio RFX, Associazione EURATOM-ENEA sulla Fusione, Padova, Italy

²Los Alamos National Laboratory (LANL), Los Alamos, NM 87545, USA

³Oak Ridge Associated Universities (ORAU), Oak Ridge, TN 37831, USA

⁴Physique des Interactions Ioniques et Moléculaires (PIIM), CNRS, Aix-Marseille Université, France

⁵Lawrence Livermore National Laboratory (LLNL), Livermore, CA 94550, USA

⁶Max-Planck-Institut für Plasmaphysik, Garching, Germany

⁷General Atomics, San Diego, CA 92186, USA

⁸University of Wisconsin-Madison, Madison, WI 53706, USA

⁹Culham Centre for Fusion Energy (CCFE), Culham Science Centre, Abingdon, UK

¹⁰Columbia University, New York, NY 10027, USA

Corresponding Author: P. Piovesan, paolo.piovesan@igi.cnr.it

This work investigates the formation of helical core equilibria in toroidal fusion plasmas, focussing on the role of dynamo, or magnetic flux pumping mechanisms in determining the equilibrium current profile. Dynamo effects determine the safety factor profile of the final 3D equilibrium, with important consequences on MHD stability and transport. We compare experimental results from multiple machines (RFX-Mod, MST, AUG, DIII-D) and nonlinear MHD modelling. Two paradigmatic cases of helical state formation are considered and common physics is identified, by direct measurements of dynamo effects and MHD simulations: spontaneous formation in high-current reversed-field pinch (RFP) plasmas [1] and the hybrid scenario in high- β tokamak plasmas [2]. Helical cores form in both cases, either spontaneously via saturation of MHD modes, or due to the marginally-stable ideal MHD response to external 3D fields. Direct measurements of the dynamo emf associated to 3D plasma distortions will be presented for a database of helical RFP plasmas from RFX-Mod and MST, covering a wide range of plasma parameters. Similar measurements were also done in helical states forming in response to external 3D fields in Ohmic RFX-Mod tokamak plasmas and in DIII-D high- β hybrid plasmas. Experimental results qualitatively agree with nonlinear MHD modelling performed with the codes SpeCyl [3], PIXIE3D [4], and NIMROD [5]. They indicate that central current is redistributed by a dominantly electrostatic MHD dynamo. The underlying physics common to RFP and tokamak is thus revealed: a helical core displacement modulates parallel current density along flux tubes, which requires a helical electrostatic potential to build up, giving rise to a helical dynamo flow. Similar results were also recently obtained with the M3D-C1 code [6].

References

- [1] R. Lorenzini, *et al.*, *Nature Phys.* **5**, 570 (2009).
- [2] T. C. Luce, *et al.*, *Nucl. Fusion* **54**, 013015 (2014).
- [3] D. Bonfiglio, *et al.*, *Phys. Rev. Lett.* **94**, 145001 (2005).
- [4] D. Bonfiglio, *et al.*, *Plasma Phys. Control. Fusion* **57**, 044001 (2015).
- [5] J. R. King, C. R. Sovinec, V. V. Mirnov, *Phys. Plasmas* **19**, 055905 (2012).
- [6] S. C. Jardin, *et al.*, *Phys. Rev. Lett.* **115**, 215001 (2015).



Optimization of the Plasma Response for the Control of Edge-Localized Modes with 3D Fields

C. Paz-Soldan¹, R. Nazikian², R. A. Moyer³, T. E. Evans⁴, N. M. Ferraro², N. C. Logan², J. Callen⁵, X. Chen⁴, D. Eldon⁶, M. Fenstermacher⁷, A. M. Garofalo⁴, B. A. Grierson², R. Groebner⁴, C. C. Hegna⁵, S. Haskey², M. J. Lanctot⁴, C. J. Lasnier⁷, T. C. Luce⁴, B. Lyons⁴, G. R. McKee⁵, D. Orlov³, T. L. Rhodes⁸, M. Shafer⁹, P. B. Snyder⁴, W. M. Solomon⁴, E. Strait⁴, R. S. Wilcox⁹, and A. Wingen⁹

¹Oak Ridge Institute for Science Education (ORISE), Oak Ridge, TN 37831, USA

²Princeton Plasma Physics Laboratory (PPPL), Princeton, NJ 08540, USA

³University of California San Diego, CA 92093, USA

⁴General Atomics, San Diego, CA 92186, USA

⁵University of Wisconsin-Madison, Madison, WI 53706, USA

⁶Princeton University, Princeton, NJ 08544, USA

⁷Lawrence Livermore National Laboratory (LLNL), Livermore, CA 94550, USA

⁸University of California Los Angeles, CA 90095, USA

⁹Oak Ridge National Laboratory (ORNL), Oak Ridge, TN 37831, USA

Corresponding Author: C. Paz-Soldan, paz-soldan@fusion.gat.com

Measurements and modelling of the plasma response to applied 3D magnetic perturbations — specifically its dependence on collisionality, β , and rotation — yield new insight into the physics of edge-localized mode (ELM) control and better define the criteria needed to achieve ELM suppression in ITER. ELM control depends on the coupling of the applied field to a stable edge mode that drives resonant fields on edge rational surfaces and is directly observed on high-field side (HFS) magnetic sensors. The edge mode amplitude is inversely proportional to pedestal collisionality yet is insensitive to global β , consistent with a current-driven mode as opposed to a pressure-driven kink, and reinforcing the importance of ITER-like collisionality to resonant field drive [1]. Advances in ideal MHD modelling have identified highly stable, β -independent plasma response modes that nonetheless drive strong resonant fields — showing a path to ELM control with minimal impact on global stability [2, 3]. Onset of ELM-suppression is consistent with a transport bifurcation driven by the penetration of resonant fields, evidenced by sudden changes in: boundary heat flux, visible helical striations, pedestal-top rotation and fluctuations, and HFS magnetic effects [4]. Systematic torque and β scans reveal a loss of ELM suppression consistent with two-fluid modelling predictions of a reduction in the penetrated field [5]. These results further the development of quantitative models for the conditions necessary to achieve ELM suppression, emphasizing both edge mode coupling for resonant field drive, and low pedestal-top electron rotation for resonant field penetration. Optimization of the equilibrium conditions and discharge evolution, in addition to the applied field structure, will be required to successfully achieve ELM suppression in ITER.

References

- [1] C. Paz-Soldan, *et al.*, Nucl. Fusion, 2016 (in press).
- [2] C. Paz-Soldan, *et al.*, Phys. Rev. Lett. **114**, 105001 (2015).
- [3] N. Logan, *et al.*, Phys. Plasmas 2016 (in review).
- [4] R. Nazikian, *et al.*, Phys. Rev. Lett. **114**, 105002 (2015).
- [5] R. Moyer, *et al.*, Nucl. Fusion, 2016 (in preparation).



Enhanced Understanding of Nonaxisymmetric Intrinsic and Controlled Field Impacts in Tokamaks

Y. In¹, J.-K. Park², Y. Jeon¹, J. Kim¹, G. Park¹, W. H. Ko¹, H. Lee¹, J.-W. Juhn¹, S.-W. Yoon¹,
and H. K. Park^{3,1}

3D Physics Task Force in KSTAR

¹National Fusion Research Institute (NFRI), Daejeon, Republic of Korea

²Princeton Plasma Physics Laboratory (PPPL), Princeton, NJ 08540, USA

³Ulsan National Institute of Science and Technology (UNIST), Ulsan, Republic of Korea

Corresponding Author: Y. In, yongkyoon@nfri.re.kr

An extensive study of intrinsic and controlled nonaxisymmetric field impacts in KSTAR has enhanced the understanding about nonaxisymmetric field physics and its implications, as well as demonstrating the importance of optimal 3D configurations in resonant magnetic perturbation (RMP)-driven control on edge localized modes (ELMs) in tokamaks. The $n = 1$ intrinsic nonaxisymmetric field was measured to remain as low as $\langle \delta B/B_0 \rangle_{m/n=2/1} \sim 4 \times 10^{-5}$ at high- β plasmas ($\beta_N \sim 2$), which corresponds to approximately 20% below the targeted ITER tolerance level. A systematic survey of $n = 1$ controlled resonant field has revealed that KSTAR has a lower power threshold for L-H transition (at least 10%) than DIII-D (configured with $n = 3$ RMP) with similar plasma densities of $n_e = (2-2.6) \times 10^{19}/\text{m}^3$, possibly benefiting from a low level of intrinsic error field and toroidal field ripple. As for the RMP ELM control, a high-quality $n = 1$ RMP ELM suppression (duration of $\sim 40\tau_E$) was achieved using an operationally “reproducible” approach. Throughout this investigation, we diagnosed edge activities using 3D ECE imaging diagnostics (ECEI) on both high-field-side (HFS) and low-field-side (LFS) simultaneously for the first time. According to ECEIs, the RMP ELM suppression was full of lively edge activities, which appears quite challenging to a prevailing theory that “peeling–ballooning” stability boundary is crossed from unstable to stable regimes due to RMP. While exploring the most favourable 3D configuration ($n = 1$, +90 deg. phasing), we discovered that midplane IVCC coils played a major role in mitigating the ELMs, while two off-midplane IVCCs ($n = 1$ odd-parity) appeared insignificant on ELM behaviour change. In contrast, when the off-midplane IVCCs are configured with $n = 1$ even-parity, strong plasma response was observed, even triggering mode-locking at high RMP currents. Considering that the ITER RMP coils are composed of 3-rows, just like in KSTAR, further 3D physics study in KSTAR is expected to help us minimize the uncertainties of the ITER RMP coils, as well as establish an optimal 3D configuration for ITER and beyond.



Enhancement of Helium Exhaust by Resonant Magnetic Perturbation Fields

O. Schmitz¹, K. Ida², M. Kobayashi², A. Bader¹, S. Brezinsek³, T. E. Evans⁴, Y. Feng⁵, H. Funaba², M. Goto², C. C. Hegna¹, O. Mitarai⁶, T. Morisaki², G. Motojima², Y. Narushima², D. Nicolai⁶, U. Samm⁶, G. Spizzo⁷, H. Tanaka⁸, M. Yoshinuma², and Y. Xu⁹

¹Department of Engineering Physics, University of Wisconsin-Madison, Madison, WI 53706, USA

²National Institute for Fusion Science (NIFS), Toki, Gifu, Japan

³Forschungszentrum Jülich, Jülich, Germany

⁴General Atomics, San Diego, CA 92186, USA

⁵Max-Planck-Institut für Plasmaphysik, Greifswald, Germany

⁶Liberal Arts Education Center, Tokai University, 9-1-1 Toroku, Kumamoto 862-8652, Japan

⁶Forschungszentrum Jülich, Jülich, Germany

⁷Consorzio RFX, Associazione EURATOM-ENEA sulla Fusione, Padova, Italy

⁸Kyoto University, Nishikyo-ku, Kyoto 615-8540, Japan

⁹Southwestern Institute of Physics, Chengdu, Sichuan, People's Republic of China

Corresponding Author: O. Schmitz, oschmitz@wisc.edu

Exhaust of helium as a fusion born plasma impurity is a critical requirement for future burning plasmas. We demonstrate in this paper that resonant magnetic perturbation (RMP) fields can be used to actively improve helium exhaust features. We present results from the TEXTOR tokamak with a pumped limiter and from the LHD heliotron with the closed helical divertor. The results show an important additional functionality of the ITER RMP ELM control coils and dedicated experiments on present day devices like DIII-D, EAST or KSTAR which obtained full ELM suppression by RMP field application are motivated. In both devices RMP fields are applied to generate a magnetic island located in the very plasma edge and this magnetic island has a noticeable impact on the helium exhaust. At the TEXTOR tokamak, the effective helium confinement time τ_{p,He^*} is reduced by up to 43% and the actual reduction depends on the coupling of the magnetic island to the pump device. The LHD heliotron device, in contrast, features intrinsically a 3D boundary and the closed helical divertor was designed for optimal pumping in this geometry. Without RMP field applied, τ_{p,He^*} is a factor of ~ 4 higher for LHD compared to TEXTOR discharges in a comparable plasma density range. Ion root transport — one out of several different impurity transport regimes at LHD — is the most likely inward transport driver causing the high τ_{p,He^*} . When a magnetic island is seeded into the intrinsic edge stochastic layer, a decrease of τ_{p,He^*} by up to 30% and hence values closer to the tokamak situation are established. This shows that RMP fields are a fine-tuning actuator for the exhaust of helium, which is an attractive additional functionality for the ITER ELM control coils. 3D fluid plasma edge transport and kinetic neutral gas modelling with the EMC3-EIRENE code shows for LHD that the actual helium concentration in the plasma core is dominated by wall recycling of helium. This points out that the back-fuelling of the plasma by helium emitted from the plasma and recycled at the wall elements needs to be controlled. The edge magnetic island induced is shown to be an effective actuator to retain the recycled helium in the plasma periphery where it can be pumped away.



The Role of Drifts and Radiating Species in Detached Divertor Operation at DIII-D

A. McLean¹, T. Rognlien¹, J. Canik², S. Allen¹, A. W. Leonard³, P. C. Stangeby⁴, T. Abrams³, J. A. Boedo⁵, I. Bykov⁵, A. Briesemeister², R. Ding⁶, J. D. Elder⁴, D. Eldon⁷, M. Fenstermacher¹, M. Groth⁸, H. Guo³, J. Guterl³, D. Hill³, E. Kolemen⁷, C. J. Lasnier¹, M. A. Makowski¹, W. H. Meyer¹, A. Moser³, T. H. Osborne³, T. W. Petrie³, G. Porter¹, D. L. Rudakov⁵, C. Samuell¹, C. Sang⁶, D. M. Thomas³, E. A. Unterberg², H. Wang², and J. G. Watkins⁹

¹Lawrence Livermore National Laboratory (LLNL), Livermore, CA 94550, USA

²Oak Ridge National Laboratory (ORNL), Oak Ridge, TN 37831, USA

³General Atomics, San Diego, CA 92186, USA

⁴Institute for Aerospace Studies, University of Toronto, Toronto, ON M5S-1A1, Canada

⁵University of California San Diego, CA 92093, USA

⁶Institute of Plasma Physics, Chinese Academy of Sciences, Hefei, Anhui, People's Republic of China

⁷Princeton Plasma Physics Laboratory (PPPL), Princeton, NJ 08540, USA

⁸Aalto University, Espoo, Finland

⁹Sandia National Laboratories (SNL), Albuquerque, NM 87185, USA

Corresponding Author: A. McLean, mclean@fusion.gat.com

EX

A comprehensive experimental campaign at DIII-D has advanced understanding and modelling of the effects of drifts and radiating species in diverted plasma up to ITER-relevant collisionality. Unique diagnostic capabilities are employed to show directly that plasma drifts lead to in/out asymmetries as well as shifts in radial parameter profiles throughout the divertor legs, and are a critical factor for predicting detachment onset, and particle and heat fluxes for a detached divertor. These results are reproduced by first-of-its-kind boundary modelling of H-mode discharges with a full physics description of drifts using UEDGE in both toroidal field directions, confirming that the interplay of radial and poloidal $E \times B$ drifts are primarily responsible for target asymmetries and localization of high density/low temperature plasma in the scrape-off layer. SOLPS modelling of L-mode helium discharges with negligible carbon emission suggests that molecules and atomic contributions may play a role in explaining a consistent shortfall in divertor radiation observed in boundary modelling of multiple tokamaks. These and future planned studies of detachment provide valuable physics insight informing the implementation of high- Z plasma facing components at key locations poloidally in DIII-D in 2016.



Recent Progress towards a Quantitative Description of Filamentary SOL Transport

D. Carralero¹, H. W. Müller², M. Groth³, J. Adamek⁴, L. Aho-Mantila⁵, S. Artene¹, G. Birkenmeier¹, M. Brix⁶, G. Fuchert⁷, P. Manz¹, J. Madsen⁸, S. Marsen⁷, U. Stroth¹, H. J. Sun¹, N. Vianello⁹, M. Wischmeier¹, and E. Wolfrum¹

¹Max-Planck-Institut für Plasmaphysik, Garching, Germany

²University of Vienna, 1010 Vienna, Austria

³Aalto University, Espoo, Finland

⁴Institute of Plasma Physics AS CR v.v.i., Prague, Czech Republic

⁵VTT Technical Research Centre of Finland Ltd., Espoo, Finland

⁶Culham Science Centre, Abingdon, UK

⁷Max-Planck-Institut für Plasmaphysik, Greifswald, Germany

⁸Technical University of Denmark (DTU), Copenhagen, Denmark

⁹Consorzio RFX, Associazione EURATOM-ENEA sulla Fusione, Padova, Italy

Corresponding Author: D. Carralero, daniel.carralero@ipp.mpg.de

Heat and particle transport onto plasma-facing components is a key issue for next generation tokamaks, as it will determine the erosion levels and the heat loads at the main chamber first wall. In the scrape-off layer (SOL), this transport is thought to be dominated by the perpendicular convection of filaments. In this work, we present recent experiments which have led to an improved picture of filamentary transport, and its role on the onset of a density profile flattening, known in the literature as the density “shoulder” [1]. First, L-mode experiments carried out in the three tokamaks of the ITER stepladder (COMPASS, AUG and JET) showed how normalized divertor collisionality [2] can be used to scale both filament size and the density e-folding length in the far SOL. Furthermore, a transition in the filament regime is found to be the reason for the formation of the density shoulder, as it coincided with a change in the scaling of filament size with propagation velocity from Sheath Limited regime to Inertial regime [3]. This result was later confirmed in AUG by independent experiments which showed how the polarization term in the charge conservation equation became dominant after the onset of the shoulder and how the transition was reversed as filaments propagate radially across regions of decreasing collisionality. Besides, measurements carried out in AUG with a Retarding Field Analyzer in equivalent discharges have led to the discovery of a strong reduction of T_i in the far SOL after the onset of the shoulder, both in filaments and background plasmas, which can not be explained by the minor reduction of T_i at the separatrix. Finally, equivalent experiments in H-mode carried out in AUG have shown how inter-ELM filaments follow the same general behaviour as L-mode filaments, and how a density profile flattening reminiscent of the density shoulder is observed when collisionality is increased over a similar threshold. Besides, Thomson Scattering data indicate the same sharp increase on the e-folding length of density and electron temperature in the near SOL above a critical collisionality.

References

- [1] B. LaBombard, *et al.*, Phys. Plasmas **8**, 2107 (2001).
- [2] J. R. Myra, *et al.*, Phys. Plasmas **13**, 092509 (2006).
- [3] D. Carralero, *et al.*, Phys. Rev. Lett. **115**, 215002 (2015).



TCV Experiments towards the Development of a Plasma Exhaust Solution

H. Reimerdes¹, J. Harrison², P. Innocente³, B. Lipschultz⁴, M. Spolaore³, C. Theiler¹, C. Tsui⁵, W. Vijvers⁶, J. A. Boedo⁵, G. Calabrò⁶, F. Crisanti⁶, B. Duval¹, B. Labit¹, T. Lunt⁷, R. Maurizio¹, V. Pericoli⁸, U. Sheikh¹, K. Verhaegh⁴, and N. Vianello³

¹Swiss Plasma Center (SPC), École polytechnique fédérale de Lausanne (EPFL), 1015 Lausanne, Switzerland

²Culham Centre for Fusion Energy (CCFE), Culham Science Centre, Abingdon, UK

³Consorzio RFX, Associazione EURATOM-ENEA sulla Fusione, Padova, Italy

⁴University of York, Heslington, UK

⁵University of California San Diego, CA 92093, USA

⁶Agenzia nazionale per le nuove tecnologie, l'energia e lo sviluppo economico sostenibile (ENEA), Rome, Italy

⁶FOM Institute DIFFER, Association EURATOM-FOM, Nieuwegein, Netherlands

⁷Max-Planck-Institut für Plasmaphysik, Garching, Germany

⁸CREATE/ENEA/EURATOM Association, Università di Napoli, Naples, Italy

Corresponding Author: H. Reimerdes, holger.reimerdes@epfl.ch

Present research towards a plasma exhaust solution for a fusion power plant aims at validating edge physics models to strengthen the predictive capabilities and improving the operating regime and the divertor configuration. The TCV tokamak is used in particular to investigate to what extent geometric modifications of the configuration can affect the plasma exhaust performance by decreasing the peak heat loads, improving the control of the detached condition and enhancing the compatibility of the divertor solution with core performance. Detachment experiments in TCV have so far been restricted to Ohmically heated L-mode plasmas. Recent TCV experiments connect to previous detachment studies using standard single-null configurations, where the onset of detachment is best observed at sufficiently high density when the direction of the magnetic field results in an ion ∇B drift away from the X-point. The studies were extended to nitrogen seeding and to an entire suite of alternative magnetic configurations, including the variation of the poloidal flux expansion at the outer target, the introduction of flux flaring towards the target (X divertor), the movement of the secondary X-point inside the vessel (X-point target) as well as various snowflake configurations. The snowflake minus configuration has attracted particular interest as recent EMC3-EIRENE simulations predict a large region of radiation between two X-points. In addition to the detachment characteristics the effect of the altered connection length and magnetic shear on turbulent transport is investigated. The recent experiments benefited from a range of improved diagnostic capabilities including a new divertor spectroscopy system, an upgraded infrared thermography system, an extended set of wall-mounted Langmuir probes and a newly installed reciprocating probe. Experiments in 2016 will also be able to take advantage of the newly installed neutral beam injection (NBI) heating system, which allows for auxiliary heating of high density plasmas and thereby for testing of potential solutions under higher heat fluxes and in regimes with a higher SOL pressure.

EX



Advances in Physics and Performance of the I-Mode Regime over an Expanded Operating Space on Alcator C-Mod

A. E. Hubbard¹, D. Brunner¹, I. Cziegler², E. M. Edlund³, J. W. Hughes¹, B. LaBombard¹, Y. Lin¹, Z. Liu⁴, E. S. Marmor³, M. L. Reinke⁵, J. E. Rice¹, B. M. Sorbom¹, J. Terry¹, J. R. Walk¹, A. White¹, D. G. Whyte¹, S. M. Wolfe¹, S. Wukitch¹, and X. Xu⁶

¹Plasma Science & Fusion Center, MIT, Cambridge, MA 02139, USA

²York Plasma Institute, University of York, Heslington, UK

³Massachusetts Institute of Technology (MIT), Cambridge, MA 02139, USA

⁴Institute of Plasma Physics, Chinese Academy of Sciences, Hefei, Anhui, People's Republic of China

⁵Oak Ridge National Laboratory (ORNL), Oak Ridge, TN 37831, USA

⁶Lawrence Livermore National Laboratory (LLNL), Livermore, CA 94550, USA

Corresponding Author: A. E. Hubbard, hubbard@psfc.mit.edu

Significant progress has been made on Alcator C-Mod in expanding the configurations and conditions for which the I-mode regime can be accessed and maintained and understanding the physics which underlies the transport improvement. An important result from multidevice studies is that the power threshold for I-mode has only a weak dependence on B_t , while the upper power limit increases with B_t , making I-modes more robust at higher field [1]. Experiments in 2015 have extended this trend, achieving clear I-modes at up to 8.0 T. The I-mode regime is naturally stable to ELMs, and combines high τ_E with low particle confinement [2]. This has benefits for fusion reactors, eliminating damaging ELM heat pulses and avoiding impurity accumulation.

The τ_E in I-mode is in the H-mode range and has weak power degradation $\sim P^{-0.3}$. ELITE analysis shows the pedestal to be stable, consistent with this lack of saturation and the absence of ELMs. Nonlinear GYRO simulations show that I-mode core T_i and T_e profiles are stiffer than in L-mode, resembling H-mode with regards to marginal ITG stability. I-mode pedestal physics is also advancing, through measurements of fluctuations and flows and using simulations. Both a GAM and a high frequency fluctuation termed the Weakly Coherent Mode are present and strongly interact. Nonlinear BOUT++ simulations agree with many observed features of the WCM.

The C-Mod team has been exploring prospects for extrapolation of I-mode to larger fusion devices. We predict ITER would need about 70 MW to enter I-mode. It should be possible to remain in I-mode and to produce high fusion power, provided that density can be sufficiently increased. Accessibility for compact, high- B fusion reactors such as ARC is even more favourable. We are also investigating integration with divertor solutions. Mitigating heat flux using low- Z impurity seeding has been demonstrated, and we have begun to investigate divertor detachment strategies. While robust I-mode operation is typically achieved with ion $B \times \nabla B$ drift away from the X-point, new experiments show that after the L-I transition, the regime can be maintained in a DN configuration. This may help to reduce peak heat flux. Further I-mode experiments will be a priority in 2016.

References

- [1] A. E. Hubbard, *et al.*, IAEA FEC-2014. EX/P6-22, (2014).
- [2] D. G. Whyte, *et al.*, Nucl. Fusion **50**, 105005 (2010).

Work supported by the U.S. Department of Energy.



Bifurcation of Quiescent H-Mode to a Wide Pedestal Regime in DIII-D and Advances in the Understanding of Edge Harmonic Oscillations

X. Chen¹, K. H. Burrell¹, T. H. Osborne¹, K. K. Barada², N. M. Ferraro³, A. M. Garofalo¹, B. A. Grierson³, R. Groebner¹, N. C. Luhmann, Jr.⁴, G. R. McKee⁵, C. Muscatello¹, R. Nazikian³, M. Ono⁶, C. C. Petty¹, X. Ren⁴, T. L. Rhodes², C. J. Rost⁷, P. B. Snyder¹, W. M. Solomon³, B. Tobias³, Z. Yan⁵, and L. Zeng²

¹General Atomics, San Diego, CA 92186, USA

²University of California Los Angeles, CA 90095, USA

³Princeton Plasma Physics Laboratory (PPPL), Princeton, NJ 08540, USA

⁴University of California Davis, CA 95616, USA

⁵University of Wisconsin-Madison, Madison, WI 53706, USA

⁶Graduate University for Advanced Studies (SOKENDAI), Hayama, Kanagawa, Japan

⁷Massachusetts Institute of Technology (MIT), Cambridge, MA 02139, USA

Corresponding Author: X. Chen, chenxi@fusion.gat.com

In a recent discovery, the Quiescent H-mode (QH-mode) regime in DIII-D has been found to bifurcate into a new state at low torque in double-null shaped plasmas, characterized by increased pedestal height, width and global confinement [1, 2]. This provides an alternate path for achieving high performance ELM-stable operation at low torque, in addition to the conventional QH-mode operation sustained at low-torque with applied 3D fields [3]. Measurements and simulation indicate that in the wide pedestal state, the decreased $E \times B$ shear destabilizes broadband turbulence, which relaxes edge pressure gradients, improves peeling-ballooning stability and enables a wider and thus higher pedestal and enhanced confinement. In parallel, new experimental study and modelling [4] of low, experimentally-relevant toroidal mode number ($n \leq 5$) Edge Harmonic Oscillation (EHO), which regulates the standard QH edge, validate the proposed importance of rotational shear in exciting the EHO. The ability to accurately simulate the EHO and maintain high performance QH-mode at low torque is an essential requirement for projecting QH-mode operation to ITER.

References

- [1] K. H. Burrell, *et al.*, Plasma Phys. (in press).
- [2] X. Chen, *et al.*, Nucl. Fusion (H-mode workshop, 2015).
- [3] A. M. Garofalo, *et al.*, Nucl. Fusion **51**, 083018(2011).
- [4] X. Chen, *et al.*, Nucl. Fusion (submitted).



Studies of the Pedestal Structure in JET with the ITER-Like Wall

C. Maggi¹, E. Delabie², L. Frassinetti³, L. Horvath⁴, A. Lunniss⁴, I. Lupelli¹, S. Saarelma¹, F. J. Casson¹, M. Leyland⁴, P. Stanislas¹, H. Urano⁵, and H. Wilson⁴

¹Culham Centre for Fusion Energy (CCFE), Culham Science Centre, Abingdon, UK

²Oak Ridge National Laboratory (ORNL), Oak Ridge, TN 37831, USA

³KTH Royal Institute of Technology, Stockholm, Sweden

⁴York Plasma Institute, University of York, Heslington, UK

⁵Japan Atomic Energy Agency (JAEA), Naka, Japan

Corresponding Author: C. Maggi, costanza.maggi@ukaea.uk

The H-mode pedestal structure is characterized in JET-ILW plasmas limited by type-I ELMs. The pre-ELM pressure width Δ_p increases with the square root of $\beta_{\text{pol,PED}}$, as assumed in EPED, in H-modes with low D gas injection. In dimensionless experiments Δ_p broadens at constant $\beta_{\text{pol,PED}}$ with increasing ν_{PED}^* . In power and gas scans $\Delta_p/\sqrt{\beta_{\text{pol,PED}}}$ is constant with ν_{PED}^* , but is systematically wider at higher, than at lower, D rates. Δ_p may therefore depend also on other parameters, directly or indirectly connected with the D neutral content in the plasma, implying that atomic physics could contribute in setting the pedestal width. The pedestal evolution during the ELM cycle is more complex than what would be expected if KBMs were to control the inter-ELM pressure gradient evolution. At high- β and low D gas injection rates $p_{e,\text{PED}}$ increases due to narrowing of the width and steepening of the gradient. The n_e width narrows and the gradient increases until the ELM, suggesting qualitative consistency with the neutral penetration model. The n_e pedestal structure evolves similarly at low and high D gas rates. At high- β , $T_{e,\text{PED}}$ saturates half way through the ELM cycle at high D gas rates. This causes the reduction in $p_{e,\text{PED}}$ in higher- β plasmas when the D gas rate is increased at constant net input power. The edge bootstrap current J_{BS} , derived with NEO from the measured kinetic profiles and Z_{eff} , increases throughout the ELM cycle at low- β , while it saturates well in advance of the ELM crash at high- β . Initial isotope experiments have investigated pedestal formation in H versus D. In the high density branch, $P_{L-H}(H) = 2P_{L-H}(D)$. H and D plasmas have matched stored energy and diamagnetic edge E_r . The higher power in H required to achieve the same stored energy as in D is consistent with the lower L-mode energy confinement in H. Assuming that the L-H transition requires an $E_r \times B$ shearing rate similar to the growth rate of the most unstable mode, $\gamma_{E,\text{crit}} \sim \gamma_{\text{turb}}$, the above result suggests γ_{turb} independent of mass in the high n_e branch. In the low n_e branch $P_{L-H}(H) \gg 2P_{L-H}(D)$. Similar edge n_e profiles are observed in H and D, but H plasmas have a stronger T_e gradient, indicating the need for a larger $\gamma_{E,\text{crit}}$ to trigger the L-H transition and suggesting an isotope effect on γ_{turb} .

EX



Global Stabilization Effect of Shafranov Shift on the Edge Pedestal Plasmas in JET and JT-60U

H. Urano¹, S. Saarelma², L. Frassinetti³, N. Aiba¹, C. Maggi², I. Chapman², I. Lupelli², C. Challis², M. Leyland⁴, M. Beurskens², K. Kamiya¹, C. Giroud², and S. Pamela^{2,5}

¹Japan Atomic Energy Agency (JAEA), Naka, Japan

²Culham Centre for Fusion Energy (CCFE), Culham Science Centre, Abingdon, UK

³KTH Royal Institute of Technology, Stockholm, Sweden

⁴University of York, Heslington, UK

⁵United Kingdom Atomic Energy Authority, Culham Science Centre, Abingdon, UK

Corresponding Author: H. Urano, urano.hajime@jaea.go.jp

Here we report the global stabilization effect of Shafranov shift on the edge pedestal plasmas. Experimental observations show that i) the increased Shafranov shift stabilizes the ballooning component of the peeling-ballooning mode (PBM) so that the edge pressure gradient is raised together with the expansion of the edge transport barrier (ETB) and ii) when the Shafranov shift is fixed the increased collisionality reduces the edge pressure gradient whereas the ETB expands. This physics process has been examined using JET and JT-60U, in both of which the Shafranov shift stabilizes the pedestal most effectively because the pedestal plasmas in these devices are constraint systematically by the ballooning component of the PBM instability. The results will give a physics picture of H-mode edge and core interplay which contributes to an accurate prediction of the ETB structure in ITER.

EX



The Role of the Density Profile Location on Pedestal Stability in ASDEX-Upgrade

M. Dunne¹, L. Frassinetti², S. Potzel¹, F. Reimold³, M. Wischmeier¹, E. Wolfrum¹, M. Bernert¹, M. Beurskens⁴, M. Cavedon¹, E. Fable¹, R. Fischer¹, B. Kurzan¹, F. Laggner⁵, R. McDermott¹, G. Tardini¹, and M. Willensdorfer¹

¹Max-Planck-Institut für Plasmaphysik, Garching, Germany

²KTH Royal Institute of Technology, Stockholm, Sweden

³Forschungszentrum Jülich, Jülich, Germany

⁴Culham Centre for Fusion Energy (CCFE), Culham Science Centre, Abingdon, UK

⁵Institute for Applied Physics, Technische Universität Wien, 1040 Vienna, Austria

Corresponding Author: M. Dunne, mike.dunne@ipp.mpg.de

Scrape-off layer (SOL) properties are controlled by a number of parameters, such as heating power, main ion fuelling, and impurity seeding. The high field side high density (HFSHD) is a region of high density ($\sim 10\times$ higher than the separatrix density) localized to the HFS SOL and is observed in both ASDEX-Upgrade (AUG) and JET when a gas puff at sufficient heating power is applied. It can be mitigated by either reducing the input power to the main plasma or by radiating this power, via, for example, nitrogen seeding, before it reaches the HFS SOL.

Observations of the density profile and the HFSHD show that the presence of the HFSHD is linked with an outward shift of the density profile. Conversely, when it is mitigated, the profile shifts radially inwards. At the same time, nitrogen seeding has been observed to increase pedestal and global confinement in fuelled discharges on AUG by up to 40%.

Interpretive pedestal modelling is used to validate the peeling-ballooning hypothesis of pedestal limiting ELM behaviour. While this is a valuable tool, it is limited since only final plasma states involving a variety of changes in impurity content, SOL characteristics, and global β can be analyzed. As such, a predictive pedestal tool (iPED) was developed using similar assumptions to the EPED model to vary each parameter independently.

In addition to the standard inputs of predictive pedestal models, an ad-hoc shift of the density profile, based on experimental measurements, is included. An inward shift (of up to $0.01 \rho_{\text{poloidal}}$) has a dramatic impact on the predicted pedestal stability, increasing it by $\sim 30\%$ in a typical AUG scenario and is the dominant factor determining the eventual pedestal top. Increased Z_{eff} and global β also contribute to pedestal stabilization, but have a smaller impact.

To determine the final global plasma state, iPED is combined with the ASTRA transport model. ASTRA and iPED are iterated in a step-wise manner until convergence of the core and pedestal plasmas is reached. This allows the evolution of the global plasma in response to small changes at the separatrix to be modelled, and offers a demonstration of how SOL properties can impact both the pedestal and global confinement.

EX



Joint Experiments Tailoring the Plasma Evolution to Maximize Pedestal Performance

I. Chapman¹, S. Saarelma¹, R. Cesario², S. Coda³, E. de la Luna⁴, A. Kirk¹, C. Maggi¹, A. Merle³, R. Scannell¹, H. Urano⁵, J. Connor¹, M. Dunne⁶, R. Fisher⁷, C. Ham¹, J. Hastie¹, J. Hobirk⁶, O. McCormack⁸, M. Peterka⁹, O. Sauter³, J. Simpson¹, E. R. Solano¹⁰, and W. Wright¹¹

¹Culham Centre for Fusion Energy (CCFE), Culham Science Centre, Abingdon, UK

²Associazione EURATOM-ENEA Unità Tecnica Fusione, Frascati, Italy

³Swiss Plasma Center (SPC), École polytechnique fédérale de Lausanne (EPFL), 1015 Lausanne, Switzerland

⁴EFDA-CSU, Culham Science Centre, Abingdon, UK

⁵Japan Atomic Energy Agency (JAEA), Naka, Japan

⁶Max-Planck-Institut für Plasmaphysik, Garching, Germany

⁷University of Bath, Bath, UK

⁸Consorzio RFX, Associazione EURATOM-ENEA sulla Fusione, Padova, Italy

⁹Institute of Plasma Physics AS CR v.v.i., Prague, Czech Republic

¹⁰Centro de Investigaciones Energéticas, Medioambientales y Tecnológicas (CIEMAT), Madrid, Spain

¹¹Durham University, Durham, England

Corresponding Author: I. Chapman, ian.chapman@ccfe.ac.uk

EX

The pedestal height has been significantly increased by optimizing the plasma conditions at H-mode access in joint experiments in JET, ASDEX Upgrade, MAST and TCV. A predictive pedestal model has been developed negating the need to specify the global β and core density peaking. This model predicted that doubling the core pressure during the L-mode phase in JET would increase the pedestal height by 20%. Experiments on JET therefore tailored the plasma evolution to increase the core pressure before the pedestal is formed to stabilize ballooning modes. Small changes to the magnetic geometry coupled with early impurity seeding increased the H-mode threshold power by a factor of two. The resultant 70% increase in core pressure before pedestal formation resulted in an 18% increase in pedestal height, in excellent agreement with ab initio EUROPEd predictions.

We have demonstrated causality that an increased core pressure stabilizes ballooning modes allowing hotter pedestals using the flexibility in magnetic configuration in the medium-sized devices MAST and TCV. By shifting a double-null configuration upwards by 2 cm in MAST, it is possible to increase the L-H transition threshold power significantly. On returning to a balanced configuration, an immediate L-H transition is triggered, allowing a systematic variation of the core plasma pressure upon pedestal formation. It is observed that the pedestal top electron pressure before the first ELM is increased by 100% when the global β at the moment of the L-H transition is increased by 25%. Pedestal performance with variation in core pressure has also been tested on TCV by switching configuration rapidly from unfavourable ∇B drift and long divertor connection length to favourable ∇B configuration with shorter divertor legs. Stability analysis confirms that the enhanced Shafranov shift stabilizes the ballooning modes, allowing the pedestal to reach higher pressures before the ELM crash. Furthermore, a self-consistent averaged ballooning equation has been derived at low shear to explicate succinctly the benefit of increasing global β in s-alpha stability space from the enhanced Shafranov shift and plasma shaping. Finally, we test an ITER-relevant method to increase the core pressure prior to pedestal formation by suppressing the L-H transition using nonaxisymmetric perturbations in ASDEX-Upgrade.



Advances in the Steady-State Hybrid Regime in DIII-D: A Fully-Noninductive, ELM-Suppressed Scenario for ITER

C. C. Petty¹, R. Nazikian², F. Turco³, X. Chen¹, E. J. Doyle⁴, T. E. Evans¹, J. R. Ferron¹,
A. M. Garofalo¹, B. A. Grierson², C. T. Holcomb⁵, A. W. Hyatt¹, G. L. Jackson¹,
E. Kolemen², R. J. La Haye¹, C. J. Lasnier⁵, N. C. Logan², T. C. Luce¹, D. Orlov⁶,
T. H. Osborne¹, D. C. Pace¹, C. Paz-Soldan¹, T. W. Petrie¹, P. B. Snyder¹, W. M. Solomon²,
N. Z. Taylor¹, and M. A. Van Zeeland¹

¹General Atomics, San Diego, CA 92186, USA

²Princeton Plasma Physics Laboratory (PPPL), Princeton, NJ 08540, USA

³Columbia University, New York, NY 10027, USA

⁴University of California Los Angeles, CA 90095, USA

⁵Lawrence Livermore National Laboratory (LLNL), Livermore, CA 94550, USA

⁶University of California San Diego, CA 92093, USA

Corresponding Author: C. C. Petty, petty@fusion.gat.com

A new regime with β , collisionality and plasma shape relevant to the ITER steady-state mission has been attained in DIII-D using the fully noninductive hybrid scenario, including complete ELM suppression over a wide q_{95} window (between 5.9 and 7.1) and with little confinement degradation using resonant magnetic perturbation (RMP) coils. Furthermore, high- β hybrid plasmas have been integrated with an argon-based radiative divertor to advance divertor heat flux dissipation towards reactor relevance. Fully noninductive hybrids with simultaneous high- β ($\beta_N \leq 3.1$) and high confinement ($H_{98}(y, 2) \leq 1.4$) in the ITER similar shape have achieved zero surface loop voltage for up to two current relaxation times using efficient central current drive from ECCD and NBCD. This steady-state regime has been successfully integrated with ELM suppression by applying an odd parity $n = 3$ RMP, which has only a minor impact on the pedestal pressure ($\sim 15\%$) and $H_{98}(y, 2) \sim 10\%$. The odd parity RMP couples well to the high- q_{95} ITER steady-state case discussed here, whereas the even parity RMP couples better to the low- q_{95} ITER baseline scenario. The achieved $\beta_N (= 3.1)$ equals the no-wall limit while remaining below the ideal with-wall limit ($= 4.1$). Central ECCD is found to be effective in suppressing Alfvén eigenmodes (AE) and although the thermal transport increases during ECCD, this is mostly offset by the improved fast ion transport from AE suppression. Scaling these DIII-D hybrids to ITER's major radius and magnetic field while keeping the dimensionless parameters fixed except ρ^* yields a 9 MA plasma with 500 MW of fusion power and a required current drive power of 130 MW; this gives $Q_{\text{fus}} \approx 4$, close to the desired value of $Q_{\text{fus}} = 5$. In additional experiments that integrated the hybrid scenario with a radiating divertor, the combination of argon seeding and strong deuterium puffing more than doubles the plasma radiative power, up to 55% of the input power, with less than 10% increase in Z_{eff} and less than 5% reduction in $H_{98}(y, 2)$. IR camera measurements find that the peak heat flux in the upper, outer divertor falls by a factor of 2 (from 4.6 to 2.3 MW/m²) for the argon-based radiative divertor.

Work supported in part by the U.S. Department of Energy under DE-FC02-04ER54698, DE-AC02-09CH11466, DE-FG02-04ER54761, DE-FG02-08ER54984, DE-AC52-07N27344 and DE-FG02-05ER54809.



Advances in the High Bootstrap Fraction Regime on DIII-D towards the $Q = 5$ Mission of ITER Steady State

J. Qian¹, A. M. Garofalo², X. Gong¹, Q. Ren¹, W. M. Solomon³, G. Xu¹, B. A. Grierson³, W. Guo¹, C. T. Holcomb⁴, S. Ding¹, J. McClenaghan⁵, G. R. McKee⁶, C. Pan¹, G. M. Staebler², and B. N. Wan¹

¹*Institute of Plasma Physics, Chinese Academy of Sciences, Hefei, Anhui, People's Republic of China*

²*General Atomics, San Diego, CA 92186, USA*

³*Princeton Plasma Physics Laboratory (PPPL), Princeton, NJ 08540, USA*

⁴*Lawrence Livermore National Laboratory (LLNL), Livermore, CA 94550, USA*

⁵*Oak Ridge Associated Universities (ORAU), Oak Ridge, TN 37831, USA*

⁶*University of Wisconsin-Madison, Madison, WI 53706, USA*

Corresponding Author: J. Qian, jqqian@ipp.ac.cn

Extension of large radius internal transport barrier (ITB), high bootstrap current fraction scenario toward low plasma rotation and q_{95} relevant to steady state operation at $Q = 5$ in ITER has been successfully demonstrated in DIII-D. New DIII-D experiments have shown that the key feature of large radius ITB and excellent energy confinement when the scenario is extended inductively to higher plasma current, for lower q_{95} , and more balanced neutral beam injection (NBI), for lower plasma rotation. Large radius ITBs can be maintained at significantly reduced values of q_{95} and of the plasma rotation, compared to earlier experiments. The weak sensitivity of confinement on rotation by energy transport modelling indicates that $E \times B$ shear does not play a major role in the turbulence suppression. Neoclassical transport is predicted to be the dominant transport mechanism for the main ion energy. Experimental fluctuation measurements show no long wavelength turbulence at both high and low torque conditions. Experiments also show that a flat carbon density profile is observed inside the ITB and there is no obvious accumulation of impurities despite the excellent energy confinement quality. TGLF-SAT1 modelling indicates that the impurity transport is indeed much stronger than neoclassical. Experimental results and ideal MHD stability analysis show how wall stabilization can enable a high- β_N limit even in presence of strong ITBs. The larger ITB radius improves the wall-stabilization effect, enabling a higher β_N . The experimentally measured maximum stable β_N agrees well with the ideal MHD, ideal wall limit predictions. Extrapolating the DIII-D results using a 0D model shows that with the improved confinement of the scenario, the high bootstrap fraction regime could achieve $Q = 5$ in ITER at $\beta_N \sim 2.9$ and $q_{95} \sim 7$. Results from self-consistent, 1.5D modelling of ITER steady state using TGLF-SAT1 will also be presented.

EX



Development of High Poloidal β , Steady-State Scenario with ITER-Like W Divertor on EAST

A. M. Garofalo¹, X. Gong², L. Cui³, S. Ding², C. T. Holcomb⁴, A. W. Hyatt¹, M. J. Lanctot¹, B. Lyu², J. McClenaghan⁵, J. Qian², Q. Ren², W. M. Solomon³, and G. Xu²

¹General Atomics, San Diego, CA 92186, USA

²Institute of Plasma Physics, Chinese Academy of Sciences, Hefei, Anhui, People's Republic of China

³Princeton Plasma Physics Laboratory (PPPL), Princeton, NJ 08540, USA

⁴Lawrence Livermore National Laboratory (LLNL), Livermore, CA 94550, USA

⁵Oak Ridge Associated Universities (ORAU), Oak Ridge, TN 37831, USA

Corresponding Author: A. M. Garofalo, garofalo@fusion.gat.com

Experiments on EAST [1] have started to adapt the fully-noninductive high poloidal β scenario developed on DIII-D [2, 3], in order to demonstrate, in principle, steady state tokamak operation at high performance on metal walls. The electron density is systematically varied in order to vary the deposition profile of the external lower hybrid current drive (LHCD), while keeping the plasma in fully-noninductive conditions to achieve a broad current profile that could enable improved core confinement, similar to the scenario on DIII-D. On DIII-D, a broad current profile is sustained by a large fraction of the off-axis bootstrap current, obtained with $\beta_p \geq 3$. On EAST, a broad current profile can be sustained at lower $\beta_p \geq 2$ using a large fraction of current drive from LH. The LHCD profile is expected to become more off-axis with higher density. With only LHCD and bootstrap as sources of plasma current (keeping the loop voltage near zero for several current relaxation times effectively removes the Ohmic current), the total current profile should become broader at higher density. As expected, at higher density the experimental results showed broader current profiles indicated by lower values of the internal inductance. Using the newly commissioned POINT (polarimeter-interferometer) diagnostic coupled with the EFIT algorithm that uses the POINT data for q -profile reconstruction, these experiments will enable strict tests of LHCD deposition models, and will strengthen the physics basis for achieving high performance, steady state discharges in future burning plasmas.

References

- [1] B. Wan, *et al.*, Nucl. Fusion **55**, 104015 (2015).
- [2] A. M. Garofalo, *et al.*, Nucl. Fusion **55**, 123025 (2015).
- [3] Q. Ren, *et al.*, *Bull. Am. Phys. Soc.*, **60** (2015), submitted to Phys. Plasmas.

Work supported by the U.S. Department of Energy under DE-SC0010685, DE-AC02-09-CH11466, DE-AC52-07NA27344, DE-AC05-06OR23100, and by the National Magnetic Confinement Fusion Programme of China (No. 2015GB102000, 2015GB101000, 2015GB110001 and 2015GB103001)



Extension of High- β Plasma Operation to Low Collisional Regime

S. Sakakibara¹, K. Watanabe¹, S. Ohdachi¹, Y. Suzuki¹, H. Funaba¹, K. Tanaka¹, K. Ida¹,
T. Tokuzawa¹, and I. Yamada¹

¹National Institute for Fusion Science (NIFS), Toki, Gifu, Japan

Corresponding Author: S. Sakakibara, sakakis@lhd.nifs.ac.jp

Previous experiments in LHD show that high- β plasma with more than 5% was successfully achieved in the high collisional regime because of low magnetic field operation at 0.425 T. To investigate the collisionality dependence of plasma confinement property, we have made high- β experiments in relatively high-field configurations at 1 T to increase the electron temperature. As a result, high- β plasma with more than 4% was successfully produced by multipellet injections in one order lower collisional regime than that of previous high- β operations. A peaked plasma pressure is formed after the pellet injection, which causes large Shafranov shift and core instability, whereas no confinement degradation is observed then. An improvement of particle confinement was observed during a high- β discharge produced by gas-puff, and then particle flux to divertor was reduced by more than 40%. Strong instabilities with $m/n = 1/2$ and/or $2/3$ at plasma edge appeared then and suppressed an increment of averaged β to 3.4%. Spontaneous change of the magnetic topology contributes to the increase in averaged β value, while it triggers excitation of edge MHD instabilities.

EX

**Confinement in Wendelstein 7-X Limiter Plasmas**

M. Hirsch¹, A. Dinklage¹, A. Alonso², T. Andreeva³, M. Beurskens³, H.-S. Bosch¹, C. D. Beidler³, C. Biedermann³, E. Blanco⁴, S. A. Bozhakov¹, R. Brakel⁴, R. Burhenn⁴, B. Buttenschön³, Á. Cappa², A. Czarnecka⁵, M. Endler³, T. Estrada⁴, T. Fornal⁵, G. Fuchert³, J. Geiger³, O. Grulke³, D. Hartmann³, J. Balduhn³, U. Höfel³, M. Jakubowski¹, T. Klinger³, S. Klose³, J. Knauer³, G. Kocsis⁶, R. König³, P. Kornejew³, A. Krämer-Flecken⁷, N. Krawczyk⁵, M. Krychowiak³, M. Kubkowska⁵, I. Ksiązek⁸, A. Langenberg³, H. P. Laqua³, S. Lazerson⁹, H. Maaßberg³, N. Marushchenko³, S. Marsen³, V. Moncada¹⁰, D. Moseev¹, D. Naujoks³, M. Otte³, N. Pablant⁹, E. Pasch³, F. Pisano¹¹, K. Rahbarnia³, T. Schröder³, T. Stange³, L. Stephey¹², T. Szepesi⁶, T. Sunn Pedersen³, H. Trimino-Mora³, H. Thomsen³, H. Tsuchiya¹³, Y. Turkin³, T. Wauters¹⁴, U. Wenzel³, A. Werner³, R. C. Wolf¹, G. A. Wurden¹⁵, D. Zhang³, and J. H. Harris¹⁶

¹Max-Planck-Institut für Plasmaphysik, Garching, Germany

²Laboratorio Nacional de Fusión (LNF),

Centro de Investigaciones Energéticas, Medioambientales y Tecnológicas (CIEMAT), Madrid, Spain

³Max-Planck-Institut für Plasmaphysik, Greifswald, Germany

⁴Centro de Investigaciones Energéticas, Medioambientales y Tecnológicas (CIEMAT), Madrid, Spain

⁵Institute of Plasma Physics and Laser Microfusion, Warsaw, Poland

⁶Wigner Research Center, Association EURATOM, Budapest, Hungary

⁷Forschungszentrum Jülich, Jülich, Germany

⁸Opole University, Opole, Poland

⁹Princeton Plasma Physics Laboratory (PPPL), Princeton, NJ 08540, USA

¹⁰Commissariat à l'énergie atomique (CEA), 91400 Gif-sur-Yvette, France

¹¹University of Cagliari, Cagliari, Italy

¹²University of Wisconsin-Madison, Madison, WI 53706, USA

¹³National Institute for Fusion Science (NIFS), Toki, Gifu, Japan

¹⁴Laboratory for Plasma Physics, ERM/KMS, Brussels, Belgium

¹⁵Los Alamos National Laboratory (LANL), Los Alamos, NM 87545, USA

¹⁶Oak Ridge National Laboratory (ORNL), Oak Ridge, TN 37831, USA

Corresponding Author: M. Hirsch, matthias.hirsch@ipp.mpg.de

Wendelstein 7-X (W7-X) is built to assess the concept of optimized stellarators at reactor-relevant values of both collisionality and the plasma β .

In its first operation phase (started in the end of 2015 for 10 weeks of plasma experiments), the device is equipped with five uncooled, inboard carbon limiters. This phase of the project is dedicated to integrated operation, commissioning and tests of components, diagnostics and device control performed under plasma conditions. In addition a physics programme has been conducted as far as the machine conditions allowed.

Continued...

The experimental programme started with the optimization of the ECH induced plasma break-down. Sequences of ECH pulses have been performed for wall conditioning as well as helium glow discharge conditioning (in periods without magnetic field). The device is operated with helium and hydrogen gas puffs but yet without feedback density control. Pulses are limited by technical margins and machine capabilities. For example, the discharge length is restricted by the maximum allowed energy for a single discharge which has been set to 4 MJ per pulse to avoid uncontrolled overheating of unprotected in-vessel components.

At the time this abstract is being prepared, stationary discharges over 6 s have been achieved, however, due to the described energy limit, with reduced heating power. High performance discharges with 4 MW heating power and an overall duration of around a second reach stationary electron temperature profiles with about 8 keV in the core surrounded by steep temperature gradients at around half minor radius. The density ramped up in successive gas pulses reaches $\sim 2.5 \times 10^{19}/\text{m}^3$; beyond that the discharges degrade and are terminated by radiation. The central ion temperature increases continuously unto the discharge end due to the increasing electron ion coupling and reached up to 2 keV in the best cases.

The paper gives an overview of the energy and particle confinement in the first phase of W7-X in line with findings on transport.



Turbulence and Sheared Flow Structures Behind the Isotopic Dependence of the L-H Power Threshold and H-L Back Transition on DIII-D

Z. Yan¹, P. Gohil², G. R. McKee¹, D. Eldon³, B. A. Grierson⁴, T. L. Rhodes⁵, and C. C. Petty²

¹University of Wisconsin-Madison, Madison, WI 53706, USA

²General Atomics, San Diego, CA 92186, USA

³Princeton University, Princeton, NJ 08544, USA

⁴Princeton Plasma Physics Laboratory (PPPL), Princeton, NJ 08540, USA

⁵University of California Los Angeles, CA 90095, USA

Corresponding Author: Z. Yan, zyan5@wisc.edu

Measurements of long wavelength ($K_{\perp}\rho_I < 1$) density fluctuation characteristics in the edge of both deuterium (D) and hydrogen (H) plasmas across the L-H transition on DIII-D demonstrate the existence of single or double bands of low-wavenumber turbulence observed near the edge of H and D plasmas, which are strongly correlated with the L to H-mode transition power threshold (P_{L-H}) and can help explain the isotopic and density dependence of P_{L-H} , and how the P_{L-H} difference is reduced at higher density. Understanding and accurately predicting the L-H power threshold is critical to operating and achieving high confinement in burning plasmas such as ITER. Above about $n_e \sim 4 \times 10^{19}/\text{m}^3$, P_{L-H} is seen to converge for the H and D, and increases for both with higher density. Surprisingly, the P_{L-H} increases significantly at low density in H but not in D plasmas. Two distinct frequency bands of density fluctuations are observed in the D plasmas at low density, $n_e \sim 1.2\text{--}1.5 \times 10^{19}/\text{m}^3$, but not in H plasmas with similar density, which appears to be connected to the much lower power threshold in D at low density. Consistently, $E \times B$ shear near region of $r/a \sim 0.95\text{--}1.0$ is larger in D plasmas than in H plasmas at low density; as the P_{L-H} increases with increasing density, the dual mode structure disappears while $E \times B$ shear becomes similar and small for both D and H plasmas at higher density, $n_e \sim 5 \times 10^{19}/\text{m}^3$, where P_{L-H} is similar for both D and H plasmas. In the H-L back transition, the ELM like bursts preceding the back transition can eliminate the large transient heat load to the divertor. The size of the bursts is reduced with lower rotation. The power difference ($\Delta_P = P_{L-H} - P_{H-L}$) between the L-H transition and H-L back transition increases with increasing density in D plasmas, but reduces in H plasmas, indicating stronger hysteresis in D plasmas as density is increased. The increased edge fluctuations, increased flow shear, and the dual-band nature of edge turbulence correlating with lower P_{L-H} can explain the strong isotope and density dependencies of P_{L-H} and support current L-H transition theories but suggest a complex behaviour that can inform a more complete model of the L-H transition threshold.

EX



Role of Stationary Zonal Flows and Momentum Transport for L-H Transitions in JET

J. Hillesheim¹, E. Delabie², C. Maggi¹, H. Meyer¹, and L. Meneses³

¹Culham Centre for Fusion Energy (CCFE), Culham Science Centre, Abingdon, UK

²Oak Ridge National Laboratory (ORNL), Oak Ridge, TN 37831, USA

³Institute of Plasmas and Nuclear Fusion (IPNF), Association EURATOM/IST, Lisbon, Portugal

Corresponding Author: J. Hillesheim, jon.hillesheim@ukaea.uk

Unravelling the conditions that permit access to H-mode continues to be an unresolved physics issue for tokamaks. The scaling of the L-H transition power threshold, P_{L-H} , to future devices has considerable uncertainty. Experiments have been performed in JET, with the ITER-like W/Be wall, to investigate the dependencies of P_{L-H} and also to probe the underlying physics of the transition including newly available Doppler Backscattering (DBS) measurements of turbulence and flows. We report results from experiments characterizing P_{L-H} , turbulence, and edge flows as a function of density, both above and below the minimum of the dependence of P_{L-H} on density. Result from new experiments characterizing dependencies of P_{L-H} on I_p in both the high and low density branch of the transition will be reported, at high B_t (3.0–3.4 T) and I_p (2.2–3.2 MA), with scans keeping either I_p or q_{95} constant.

EX

We observe fine-scale structure in the radial electric field inferred from DBS, with observations consistent with zonal flows (ZFs). The zonal flows are observed at the bottom of the edge E_r well before the L-H transition. In the low density branch of the transition the ZFs disappear after NBI heating is added, well before the L-H transition, while in the high density branch they disappear only following the L-H transition. Also in the high density branch, the E_r profile builds up after NBI is added into the core at a constant gradient, concomitant with a suppression of density fluctuation levels before the L-H transition. Fluctuation levels are then suppressed further following the transition. These observations point to the need to understand the role of momentum transport for the transition and not just heat transport, and also separate necessary conditions for sustaining the H-mode pedestal from the causes of the L-H transition and its effects, and aid in discriminating between models for the transition.



Energy Exchange Dynamics across L-H Transitions in NSTX

A. Diallo¹, S. Banerjee², S. Zweben¹, and T. Stoltzfus-Dueck¹

¹Princeton Plasma Physics Laboratory (PPPL), Princeton, NJ 08540, USA

²Institute for Plasma Research (IPR), Bhat, Gandhinagar, India

Corresponding Author: A. Diallo, adiallo@pppl.gov

The physical mechanism governing the L-H transition has been a long standing theoretical and experimental challenge. Understanding its trigger mechanism is critical for the operation of future fusion devices and ITER. This work is motivated by the need to test L-H transition models (e.g., predator-prey, and $E \times B$ flow suppression) and explore possible new L-H transition dynamics. This paper presents detailed analysis of the L-H transition on three sets (NBI, RF, and Ohmic) of NSTX discharges using the gas-puff-imaging diagnostics for high temporal and spatial resolutions. The analysis studies the edge velocities and energy dynamics across the L-H transition using an implementation of the orthogonal decomposition programming for high temporal resolution velocity fields. One motivation is recent work [1] on C-Mod, where a time sequence was suggested for the L-H transition, namely, the peaking of the Reynolds power and then a collapse of the turbulence and finally the rise of the diamagnetic electric field. In contrast, in all the investigated NSTX discharges, the production term (computed 1 cm inside the separatrix) is negative, pointing to transfer from the DC flows to the fluctuations, even immediately before the L-H transition. This suggests that depletion of turbulent fluctuation energy via transfer to the mean flow may not play a key role in the L-H transition. In addition, for the three sets of discharges, we observe that the thermal free energy is consistently much larger than the kinetic energy produced by the mean poloidal flow across the L-H transitions. These observations are inconsistent with the predator-prey model. The paper will describe the analysis including error estimations. Furthermore, analysis of the radial correlation dynamics across the L-H transition will be discussed.

References

[1] I. Cziegler, *et al.*, Plasma Phys. Control. Fusion **56** 075013 (2014).

Work supported by the U.S. Department of Energy contract DE-AC02-09CH11466.



The Role of Plasma Response on Fast-Ion Losses Induced by Edge 3D Fields in the ASDEX-Upgrade and DIII-D Tokamaks

M. Garcia-Munoz¹, X. Chen², N. M. Ferraro², W. W. Heidbrink³, M. Hoelzl¹, P. de Marne¹, M. Dunne¹, J. Galdon⁴, C. Jimenez-Ramos⁴, M. Nocente⁵, D. C. Pace², M. Rodriguez-Ramos⁴, L. Sanchis-Sanchez⁴, A. Snicker⁶, W. Suttrop¹, and M. A. Van Zeeland²

¹Max-Planck-Institut für Plasmaphysik, Garching, Germany

²General Atomics, San Diego, CA 92186, USA

³University of California Irvine, CA 92697, USA

⁴Universidad de Sevilla, Seville, Spain

⁵Università degli Studi di Milano-Bicocca, 20126 Milano, Italy

⁶Aalto University, Espoo, Finland

Corresponding Author: M. Garcia-Munoz, manuel.garcia-munoz@ipp.mpg.de

A joint experimental effort on the DIII-D and ASDEX-Upgrade (AUG) tokamaks shows that fast-ion confinement is quite sensitive to both edge localized modes (ELMs) and the externally imposed magnetic perturbations (MPs) used to mitigate ELMs.

In DIII-D, the role of plasma response to externally applied MPs, and its impact on fast ion loss, is studied by varying the relative phase between the upper and lower I-coils across shots in ELMy H-mode plasmas with rotating $n = 1$ perturbations. A large perturbation is observed on a magnetic probe for 0° relative phasing, while a much smaller response is measured for 240° phasing. These changes are caused by changes in the plasma response associated with coupling to resonant and nonresonant internal kinks. When the MP is applied, the oscillating $n = 1$ fast-ion loss signal more than doubles for the phasing that couples to the resonant internal kink. Companion experiments conducted at AUG similarly show that fast-ion losses increase with plasma response. As in DIII-D, changes in the poloidal phase of the MP have a strong effect on the plasma response and, consequently, the fast-ion losses. The calculated losses are largest when the phase is resonant for fast-ions.

Unmitigated ELMs are observed to cause significant fast-ion losses in a bursting fashion that resemble the filamentary structure of the intra ELM perturbation. Time-dependent full orbit simulations have been carried out during an ELM crash in 3D fields calculated with JOREK. The dominant (for this case) $n = 8$ ELM structure is clearly visible on the simulated first wall heat load. The time-scale of the simulated losses is consistent with the observed ELM induced filamentary losses. Simulations further indicate that the large fast-ion bursts observed in low collisionality plasmas appear correlated with ELM perturbations that are radially extended.

The results presented here prove that the plasma response plays an important role in determining the impact externally applied 3D fields have on the fast-ion population and ultimately on the interaction between fast-ions and edge perturbations in general. The ability to tune the perturbation poloidal spectra (and coupling to internal modes) may help finding a coils configuration that maximize the ELM mitigation while keeping the associated fast-ion losses under acceptable levels.



Critical Gradient Behaviour of Fast-Ion Transport from Alfvén Eigenmodes Guides Predictive Models for Burning Plasmas

C. Collins¹, W. W. Heidbrink², G. J. Kramer³, D. C. Pace¹, C. C. Petty¹, M. Podestá³,
M. A. Van Zeeland¹, and R. B. White³

¹General Atomics, San Diego, CA 92186, USA

²University of California Irvine, CA 92697, USA

³Princeton Plasma Physics Laboratory (PPPL), Princeton, NJ 08540, USA

Corresponding Author: C. Collins, collinscs@fusion.gat.com

Recent experiments in the DIII-D tokamak show that many overlapping small-amplitude Alfvén eigenmodes (AEs) cause stiff fast-ion transport above a critical threshold. This result suggests that reduced models can be used to effectively predict alpha profiles, beam ion profiles, and losses to aid in the design of optimized scenarios for future burning plasma devices. Three key features of critical gradient behaviour have been observed; 1) a sudden increase in incremental transport occurs above the AE linear stability threshold, 2) fast-ion losses become intermittent above threshold, and 3) stiff transport causes the fast-ion density profiles to become fixed despite increased source. Comparison with theoretical analysis using the NOVA and ORBIT codes shows that the threshold corresponds to when particle orbits become stochastic due to wave-particle resonances with AEs in the region of phase space measured by the diagnostic [1]. The measured threshold changes as beam deposition shifts AE induced stochasticity to different regions of phase space. For the first time, intermittent fast ion loss activity was observed, which peaked at the simultaneous occurrence of nearly constant frequency Toroidal Alfvén Eigenmodes (TAE) and frequency sweeping Reverse Shear Alfvén Eigenmodes. Intermittency was largely reduced when the types of AEs were altered by applying electron cyclotron heating (ECH) near the minimum in the magnetic safety factor profile, resulting in a TAE dominant spectrum. The fast-ion deuterium alpha diagnostic shows that in the stiff transport regime, incremental transport is localized to midcore radii, and the fast-ion density gradient becomes fixed at a critical value. These measurements can be used to quantitatively validate AE critical gradient transport models, giving greater confidence when applied to ITER.

References

[1] C. S. Collins, *et al.*, Phys. Rev. Lett. **116**, 095001 (2016).



Influence of the Scrape-Off Layer on RF Actuator Performance

G. M. Wallace¹, I. Faust¹, R. Perkins², S. Shiraiwa¹, S. G. Baek¹, N. Bertelli², P. T. Bonoli¹, J. C. Hosea², R. Mumgaard¹, R. R. Parker¹, S. D. Scott², T. Shinya³, G. Taylor², J. R. Wilson², and S. Wukitch¹

¹Plasma Science & Fusion Center, MIT, Cambridge, MA 02139, USA

²Princeton Plasma Physics Laboratory (PPPL), Princeton, NJ 08540, USA

³University of Tokyo, Tokyo, Japan

Corresponding Author: G. M. Wallace, wallaceg@mit.edu

Experimental and modelling results from Alcator C-Mod and NSTX show that details of the scrape-off layer (SOL) can significantly impact the effectiveness of radio frequency (RF) heating and current drive actuators. C-Mod experiments show that cold, dense conditions in the SOL lead to significant collisional absorption of lower hybrid (LH) waves outside the last closed flux surface (LCFS), reducing lower hybrid current drive (LHCD) efficiency in the multipass regime common in high density diverted experiments to date. Measurements of the fast electron tail are in close agreement with ray tracing/Fokker-Planck modelling including a realistic 2-point SOL model. On NSTX, high-harmonic fast-wave power is trapped in the SOL by [1] the righthand cutoff [2] and thought to be dissipated in divertor RF sheaths [3].

This paper will present new measurements from a unique suite of diagnostics that show how LH wave power is absorbed in the SOL on C-Mod. While LHCD is a leading method for driving noninductive current off-axis, there is a so-called “density limit” for efficient current drive observed in experiments on limited tokamaks. A more restrictive density limit was later discovered in diverted topologies. Recovering high current drive efficiency at densities in excess of $10^{20}/\text{m}^3$ is critical for steady state tokamak reactors, and is a primary research thrust of C-Mod.

Recent LH power modulation experiments on C-Mod show that the LH waves are absorbed near the LCFS at high density [4]. Power flux diagnostics looking at the edge show a prompt response to LH power modulation, ruling out absorption of the LH waves in the confined plasma. The toroidally symmetric nature of the edge response indicates that the LH wave absorption is distributed around the torus outside the LCFS due to ray stochasticity in the multipass regime. Ray tracing/Fokker-Planck simulations including a realistic SOL model improve agreement with experimental fast electron measurements. The cold, dense regions of the SOL near the divertors strongly absorb rays through collisional absorption according to the model.

References

- [1] S. Shiraiwa, AIP Conf. Proc. **1689**, 030016 (2015).
- [2] N. Bertelli, Nucl. Fusion **54**, 083004 (2014).
- [3] R. J. Perkins, Phys. Plas. **22**, 042506 (2015).
- [4] I. C. Faust, submitted to Phys. Plas. (2016).

Work supported by the U.S. Department of Energy, Contract No. DE-FC02-99ER54512 on Alcator C-Mod, a Department of Energy Office of Science user facility.



Observation of Carbon Impurity Flow in the Edge Stochastic Magnetic Field Layer of Large Helical Device and its Impact on the Edge Impurity Control

T. Oishi¹, S. Morita¹, S. Dai¹, M. Kobayashi¹, G. Kawamura¹, X. Huang¹, H. Zhang², Y. Liu², and M. Goto¹

¹National Institute for Fusion Science (NIFS), Toki, Gifu, Japan

²Graduate University for Advanced Studies (SOKENDAI), Hayama, Kanagawa, Japan

Corresponding Author: T. Oishi, oishi@lhd.nifs.ac.jp

Stochastization of edge magnetic fields has been extensively studied not only for the ELM mitigation but also for the plasma detachment and the impurity transport. Large Helical Device (LHD) has a thick stochastic magnetic field layer called “ergodic layer” located at the edge plasma with three-dimensional structure intrinsically formed by helical coils. Recently, reduction of the parallel impurity transport, so called “impurity screening”, has been studied in LHD. The theoretical modelling explains that the parallel momentum balance on impurity ions in the ergodic layer determines the direction and quantity of the impurity flow, which can be the key mechanism driving the impurity screening. Therefore, precise profile measurements of the impurity flow are required to examine the validity of the theoretical modelling on the impurity transport in stochastic magnetic field layer.

Space-resolved VUV spectroscopy using a 3 m normal incidence spectrometer has been developed to measure the impurity emission profile in a wavelength range of 300–3200 Å. A full vertical profile of C³⁺ impurity flow is evaluated from Doppler shift of the second order of CIV line emission (2×1548.20 Å) at a horizontally-elongated plasma position of LHD for a hydrogen discharge with $R_{ax} = 3.6$ m, $B_t = 2.75$ T, $n_e = 6.0 \times 10^{13}/\text{cm}^3$ and $P_{in} = 10$ MW. It is found that the carbon flow at the top and bottom edges in the ergodic layer has the same direction toward outboard side along the major radius direction. The flow velocity increases with the density at both the top and bottom edges of the ergodic layer.

The simulation result of C³⁺ impurity flow parallel to the magnetic field lines calculated with a 3D simulation code, EMC3-EIRENE, indicates that the major radius component of the flow has the same direction toward outboard side at the top and bottom edges in the ergodic layer. The experiment and the simulation agree with each other quantitatively, which concludes that the parallel flow in the ergodic layer can be well explained by the presently used theoretical modelling. In particular, the impurity screening driven by the friction force between impurity and bulk ions can be more effective at higher electron density range. The density dependence of the flow in the modelling can be also clarified by the experimental result.

EX



Assessment of Divertor Heat Load with and without External Magnetic Perturbation

B. Sieglin¹, T. Eich¹, M. Faitsch¹, A. Herrmann¹, A. Kirk², A. Scarabosio¹, W. Suttrop¹, and A. Thornton²

¹Max-Planck-Institut für Plasmaphysik, Garching, Germany

²Culham Centre for Fusion Energy (CCFE), Culham Science Centre, Abingdon, UK

Corresponding Author: B. Sieglin, bernhard.sieglin@ipp.mpg.de

Studies of the steady state scrape-off layer heat transport with and without external magnetic perturbation in ASDEX-Upgrade L-Mode are shown. It is found that the heat transport perpendicular to the magnetic field is within the uncertainty unaffected by external magnetic perturbation. The observed heat flux pattern is explained by heat flux calculations using the vacuum field of the external magnetic perturbation. It is seen that the intensity of the lobes to generate a toroidally nonuniform power deposition pattern is largely reduced with increasing divertor broadening S .

For type-I ELMs a multimachine scaling using data from three devices based on the pedestal pressure prior to the ELM crash is presented. The presented multi machine scaling for the ELM induced thermal load onto the target includes data from JET, ASDEX-Upgrade and MAST with unmitigated and mitigated ELMs. The mitigation techniques used are external magnetic perturbation (MP) and kicks which is a fast vertical movement of the plasma column. The leading quantity detected in the scaling is the pedestal pressure prior to the ELM crash.

An approach to scale the thermal load of ELMs without the need to scale the ELM wetted area is presented. An approximately linear dependence of the peak ELM energy density with the pedestal top electron pressure and minor radius and a square root dependence on the relative ELM loss energy, is found in JET operating with CFC and ILW, ASDEX-Upgrade operating with carbon and tungsten plasma facing components and MAST.

Results from ELM mitigation experiments using magnetic perturbation in JET, ASDEX-Upgrade and MAST and aiming to induce higher ELM frequencies as well as experiments using kicks in JET are in agreement with the scaling. Here it is observed that the reduced thermal load due to ELMs is correlated to the loss of pedestal pressure. These new findings will be discussed for the operation of ITER and the access to ELM divertor heat load mitigation.

EX

Elimination of the Nonaxisymmetric Inter-ELM Heat Flux Generated by Resonant Magnetic Perturbations in Detached Divertor Conditions

A. Briesemeister¹, J.-W. Ahn¹, J. Canik¹, M. Fenstermacher², H. G. Frerichs³, E. Hinson³, C. J. Lasnier¹, J. Lore¹, A. W. Leonard⁴, M. A. Makowski², A. McLean², W. H. Meyer², O. Schmitz³, M. Shafer¹, E. A. Unterberg¹, J. G. Watkins⁵, and R. S. Wilcox¹

Rapporteur by: **B. Sieglin**

¹Oak Ridge National Laboratory (ORNL), Oak Ridge, TN 37831, USA

²Lawrence Livermore National Laboratory (LLNL), Livermore, CA 94550, USA

³University of Wisconsin-Madison, Madison, WI 53706, USA

⁴General Atomics, San Diego, CA 92186, USA

⁵Sandia National Laboratories (SNL), Albuquerque, NM 87185, USA

Corresponding Author: A. Briesemeister, briesemeister@fusion.gat.com

In DIII-D, measurements show that at high densities, above the onset of divertor detachment, the nonaxisymmetric heat flux striations between ELMs created by resonant magnetic perturbation (RMP) fields are eliminated and the heat flux profile is nearly identical to that measured without RMPs. Measurements show that the RMPs continue to affect the particle balance even when there were no measurable perturbations to the heat flux structure. ELM mitigation was seen when the RMPs were applied, but not ELM suppression.

Previous results from DIII-D showing that increasing density can cause heat flux to the striations to increase, [1] as well as results from NSTX showing that heat flux in the striations can remain high during detachment [2], have caused concerns about the compatibility of RMPs and the divertor operation in ITER. In this work, density has been raised beyond that previously used to study RMP effects in DIII-D. It is shown that above the onset of detachment, striations in the heat flux gradually decreased with increasing density and are effectively eliminated at 90% of the Greenwald density. Eliminating these striations could dispense with the requirement that RMP fields on ITER rotate to distribute the nonaxisymmetric heat flux.

When RMPs are applied, the density in the main plasma drops and the peak inter-ELM heat flux to the divertor is observed. Peak heat flux generally scales inversely with the plasma density even without RMPs. When gas puffing is used to increase the main plasma density to pre-RMP levels the peak inter-ELM heat flux returns to a value at or below the pre-RMP value. The 3D edge code EMC3-EIRENE [3] is used to explore the relative contributions of changes in particle transport, source and sink effects. Measurements of electron temperature made using divertor Thomson scattering show that a structure similar to that predicted by EMC3-EIRENE appears when RMPs are applied. The structure in the electron temperature generated by the RMPs does not extend to the floor tiles in detached conditions where striations in the heat flux profile were also eliminated.

References

- [1] M. W. Jakuboski, *et al.*, Nucl. Fusion **49**, 095013 (2009).
- [2] J. W. Ahn, *et al.*, Plasma Phys. Control. Fusion **56**, 015005 (2014).
- [3] Y. Feng, *et al.*, J. Nucl. Mater. **241–243**, 930–934, (1997).



Magnetic Shear Effects on Plasma Transport and Turbulence at High Electron to Ion Temperature Ratio in DIII-D and JT-60U Plasmas

M. Yoshida¹, G. R. McKee², M. Murakami³, J. R. Ferron⁴, C. T. Holcomb⁵, F. Turco⁶, C. C. Petty⁴, A. M. Garofalo⁴, T. L. Rhodes⁷, L. Schmitz⁷, E. M. Davis⁸, M. Ono^{2,9}, C. Sung⁷, M. Nakata¹⁰, W. M. Solomon¹¹, B. A. Grierson¹¹, and C. M. Collins⁴

¹Japan Atomic Energy Agency (JAEA), Naka, Japan

²University of Wisconsin-Madison, Madison, WI 53706, USA

³Oak Ridge National Laboratory (ORNL), Oak Ridge, TN 37831, USA

⁴General Atomics, San Diego, CA 92186, USA

⁵Lawrence Livermore National Laboratory (LLNL), Livermore, CA 94550, USA

⁶Columbia University, New York, NY 10027, USA

⁷University of California Los Angeles, CA 90095, USA

⁸Massachusetts Institute of Technology (MIT), Cambridge, MA 02139, USA

⁹Graduate University for Advanced Studies (SOKENDAI), Hayama, Kanagawa, Japan

¹⁰National Institute for Fusion Science (NIFS), Toki, Gifu, Japan

¹¹Princeton Plasma Physics Laboratory (PPPL), Princeton, NJ 08540, USA

Corresponding Author: M. Yoshida, yoshida.maiko@jaea.go.jp

EX Negative magnetic shear has been demonstrated to mitigate the confinement degradation typically observed with increasing the electron to ion temperature ratio (T_e/T_i), and the mechanisms are now understood in terms of fluctuation measurements and gyrokinetic (GK) simulations in DIII-D steady-state plasmas. The impact of T_e/T_i on plasma transport and confinement is a critical issue for ITER and DEMO, where electron heating by alpha particles will be dominant. In the new experiments in DIII-D negative magnetic shear (NS) discharges, the T_i profile was maintained as T_e/T_i increased through electron cyclotron range of frequency (ECRF) heating, while in positive magnetic shear (PS) plasmas, a large reduction in T_i was observed at increased T_e/T_i . The different transport behaviour has been explained by the turbulence measurements and GK simulations; the increase in T_e/T_i had less impact on broadband turbulent fluctuations in the NS plasmas compared with that in the PS plasmas. The difference reflects changes in thermal energy confinement; the ion thermal diffusivity remained constant in the NS plasma but increased in the PS plasma when ECRF was applied. The reduced confinement degradation at high T_e/T_i with NS has been commonly observed in DIII-D and JT-60U.



Ion Internal Transport Barrier in Neutral Beam Heated Plasmas on HL-2A

D. Yu¹, Y. Wei¹, L. Liu¹, J. Dong¹, K. Ida², K. Itoh², A. Sun¹, J. Cao¹, Z. Shi¹, Z. Wang³, H. Du³, S.-I. Itoh⁴, X. He¹, W. Chen¹, Q. Ma¹, K. Zhao¹, Y. Zhou¹, J. Wang¹, X. Ji¹, W. Zhong¹, Y. Li¹, J. M. Gao¹, Y. Liu¹, Y. Xu¹, L. Yan¹, Q. Yang¹, X. Ding¹, X. Duan¹, and Y. Liu¹

¹*Southwestern Institute of Physics, Chengdu, Sichuan, People's Republic of China*

²*National Institute for Fusion Science (NIFS), Toki, Gifu, Japan*

³*Dalian University of Technology, Dalian City, Liaoning, People's Republic of China*

⁴*Research Institute for Applied Mechanics (RIAM), Kyushu University, Kasuga, Japan*

Corresponding Author: D. Yu, yudl@swip.ac.cn

Ion internal transport barriers (iITBs) are first observed in neutral beam injection (NBI) heated plasmas at the HL-2A tokamak. The position of the barrier foot, in the stationary state, coincides with the $q = 1$ surface within its uncertainty of measurement. iITBs can develop more easily at the beginning of NBI heating. Also, iITBs are unstable for the sawtooth plasma. Simulations reveal that the thermal diffusivity of ions inside the barrier can be as low as the neoclassical level. It is observed that the toroidal flow shear in the stationary iITB state reaches the level required for suppressing the ion temperature gradient mode (ITG) instability, which indicates the important role of flow shear in sustaining the iITB.

EX



Disruption Study Advances in the JET Metallic Wall

E. Joffrin¹, P. Drewelow², P. de Vries³, S. Gerasimov⁴, M. Lehnen⁵, P. Martin⁶, G. Matthews⁴, A. Murari⁶, E. Nardon¹, D. Paccagnella^{6,7}, C. Reux⁸, G. Pautasso², R. Rocella³, C. Sozzi⁹, H. Strauss¹⁰, M. Barruzo⁴, A. Fil¹¹, T. Hender⁴, S. Jachmich¹², U. Kruezi⁴, B. N'Konga¹³, R. Moreno¹⁴, A. Pau¹⁵, V. Riccardo⁴, F. Rimini⁴, J. Vega¹⁴, and F. Villone¹⁶

¹Commissariat à l'énergie atomique (CEA), 91400 Gif-sur-Yvette, France

²Max-Planck-Institut für Plasmaphysik, Garching, Germany

³International Thermonuclear Experimental Reactor (ITER),

Cadarache Centre, 13108 Saint-Paul-lès-Durance, France

⁴Culham Centre for Fusion Energy (CCFE), Culham Science Centre, Abingdon, UK

⁵Forschungszentrum Jülich, Jülich, Germany

⁶Consorzio RFX, Associazione EURATOM-ENEA sulla Fusione, Padova, Italy

⁷Consiglio Nazionale delle Ricerche (CNR), Rome, Italy

⁸Institut de Recherche sur la Fusion par confinement Magnétique (IRFM),

Commissariat à l'énergie atomique (CEA/Cadarache), 13108 Saint-Paul-lès-Durance, France

⁹Associazione EURATOM-ENEA, Istituto di Fisica del Plasma (IFP),

Consiglio Nazionale delle Ricerche (CNR), 20125 Milan, Italy

¹⁰HRS Fusion, West Orange, NJ 07052, USA

¹¹Princeton University, Princeton, NJ 08544, USA

¹²Laboratory for Plasma Physics, ERM/KMS, Brussels, Belgium

¹³Lab. J.A. Dieudonné, Université Nice Sophia Antipolis, Nice, France

¹⁴Centro de Investigaciones Energéticas, Medioambientales y Tecnológicas (CIEMAT), Madrid, Spain

¹⁵University of Cagliari, Cagliari, Italy

¹⁶CREATE/ENEA/EURATOM Association, Università di Napoli, Naples, Italy

Corresponding Author: E. Joffrin, emmanuel.joffrin@cea.fr

Disruption remains the major risk for the operation of ITER and fusion reactors. JET is now equipped with three fast disruption mitigation valves (DMVs) located at different poloidal and toroidal locations mimicking the ITER set-up of DMVs. In JET, massive gas injection (MGI) from one DMV is systematically applied with 90% deuterium and 10% argon when a disruption event is detected for plasma current above 2 MA or energy content in excess of 5 MJ total energy. Using the JET disruption mitigation system, the vessel forces during vertical displacement of disruptions could be reduced by 40% and the asymmetric forces fully mitigated.

In the past two years JET has developed a comprehensive scientific programme in view of understanding and controlling disruptions in the metallic environment. In particular, using the set of DMVs, important advances have been achieved in understanding the efficiency of massive gas injection, the impact of the electro-magnetic loads and radiation asymmetry. The need to mitigate disruptions up to high plasma current (4.5 MA) has prompted pragmatic approaches to disruption prediction. Modelling efforts has also been carried out for a better understanding of the electromagnetic loads (halo currents) and massive gas injection physics.



Shattered Pellet Injection as the Primary Disruption Mitigation Technique for ITER

N. Commaux¹, D. Shiraki¹, L. R. Baylor¹, N. W. Eidietis², E. M. Hollmann³, V. Izzo³, C. J. Lasnier⁴, R. A. Moyer³, T. Jernigan¹, S. Combs¹, and S. Meitner¹

¹*Oak Ridge National Laboratory (ORNL), Oak Ridge, TN 37831, USA*

²*General Atomics, San Diego, CA 92186, USA*

³*University of California San Diego, CA 92093, USA*

⁴*Lawrence Livermore National Laboratory (LLNL), Livermore, CA 94550, USA*

Corresponding Author: N. Commaux, commaux@fusion.gat.com

The shattered pellet injection (SPI) technique has demonstrated disruption thermal quench (TQ) and current quench (CQ) control that scale to meet ITER disruption mitigation requirements. This innovative technique was tested for the last few years on DIII-D and showed improved results when compared to massive gas injection (MGI) technique in comparable conditions. Major disruptions on large tokamaks such as ITER are expected to generate deleterious heat loads during the TQ, mechanical stress during the CQ and multi-MeV runaway electron (RE) beams. Thus the mitigation of these disruptions is critical to reliable operations of ITER. SPI showed significant improvements on DIII-D when compared to equivalent MGI in identical plasma targets. The particle delivery efficiency to the plasma characterizes the potential effect of SPI and MGI on RE formation since the RE formation by avalanche is expected to be mitigated if the electron density is high enough. The fraction of injected particles observed in the plasma was doubled for SPI and observed to be significantly faster. The fast delivery of radiative impurities by SPI is expected to reduce the peak heat load by radiating the thermal energy on the entire surface of the wall instead of being funnelled by conduction to the divertor. SPI shutdowns yielded 20% lower divertor heat load than equivalent MGI shutdowns on DIII-D. The compatibility between TQ mitigation and acceptable CQ timescale was tested through a new technique using mixed D₂/neon SPI on DIII-D. This technique enabled the demonstration that the mitigation of the TQ heat loads improves continuously for small neon contents on DIII-D and that acceptable TQ mitigation and CQ decay time on ITER may be compatible in a limited range of D₂/neon fraction. Although early SPI injections could have an effect on RE avalanche during the CQ, the formation of RE beam may occur. Thus this technique was studied for the mitigation of existing RE beam on DIII-D. The SPI was compared to equivalent MGI. These results showed that both neon SPI and MGI dissipate part or all of the RE current. The effect of pure D₂ SPI on RE was opposite to neon with a significant drop in the effective resistivity of the RE beam and background plasma electron density.

Work supported by the U.S. Department of Energy under DE-AC05-00OR22725, DE-FC02-04ER54698, DE-FG02-07ER54917 and DE-AC52-07NA27344.



Mitigation of Runaway Current with Supersonic Molecular Beam Injection on HL-2A Tokamak

Y. Liu¹, Y. Dong¹

¹*Southwestern Institute of Physics, Chengdu, Sichuan, People's Republic of China*

Corresponding Author: Y. Liu, yiliu@swip.ac.cn

EX Disruption mitigation experiments with MGI have been carried out on HL-2A with a rapid (~ 1 ms), massive ($\sim 10^{21}$ particles) injection of helium/neon/argon to study various injection scenarios. The behaviours of runaway currents in MGI induced disruptions have been investigated. A long-lasting RE plateau is achieved after argon injection by MGI even at $B_t = 1.28$ T, much lower than previous B_t threshold found in other tokamaks. It was found that argon injection can cause the generation of runaways carrying up to 30% of the initial plasma current, while disruptions triggered by injection of helium or neon are runaway free. Furthermore, the runaway current caused by argon injection with MGI was successfully suppressed by SMBI with a number of injected atoms of about 1.0×10^{21} . Light gases, such as helium, are selected in this experiment for its high efficiency in increasing the density. These experiments suggest that SMBI might be viable for runaway suppression in future tokamaks even though core penetration of jet neutrals is not achieved. An understanding of this paradox is obtained by modelling, which shows that the initial cooling of the plasma periphery triggers a very rapid growth of low-order tearing mode, resulting in a stochastic region over much of the plasma. This allows rapid transport across the entire plasma, and could explain the effectiveness of SMBI mitigation in HL-2A in spite of the shallow penetration of the neutral gas jet. In addition, a toroidal Alfvén eigenmode (TAE) was observed during disruptions deliberately triggered by the massive gas injection (MGI) of argon. This mode occurs at the beginning of the current quench and lasts about 1–2 ms. These instabilities appears to be favourable in limiting the RE beam formation. It has been found that the runaway plateau is easy to obtain on the condition of high normalized magnetic fluctuation level ($\delta B/B_t$), the runaway plateau is even invisible when $\delta B/B_t$ the exceeds the threshold of about 7.8×10^{-4} , indicating that this magnetic mode plays a scattering role on the RE beam strength.



Runaway Electron Generation and Mitigation on the European Medium Sized Tokamaks ASDEX-Upgrade and TCV

G. Papp¹, G. Pautasso¹, J. Decker², M. Gobbin³, P. J. McCarthy⁴, D. Choi², S. Coda², B. Duval², R. Dux¹, B. Erdos⁵, O. Ficker⁶, C. Fuchs¹, L. Giannone¹, G. Anja¹, K. Lackner¹, L. Marelli³, A. Mlynek¹, M. Maraschek¹, M. Nocente⁷, P. Piovesan³, V. V. Plyusnin⁸, I. P. Gergo⁵, P. Z. Poloskei⁵, S. Potzel¹, C. Reux⁹, B. Sieglin¹, C. Sommariva⁹, W. Suttrop¹, G. Tardini¹, W. Treutterer¹, and M. Valisa³

¹Max-Planck-Institut für Plasmaphysik, Garching, Germany

²Swiss Plasma Center (SPC), École polytechnique fédérale de Lausanne (EPFL), 1015 Lausanne, Switzerland

³Consorzio RFX, Associazione EURATOM-ENEA sulla Fusione, Padova, Italy

⁴University College Cork, Cork, Republic of Ireland

⁵University of Technology and Economics (BME), Budapest, Hungary

⁶Institute of Plasma Physics AS CR v.v.i., Prague, Czech Republic

⁷Università degli Studi di Milano-Bicocca, 20126 Milano, Italy

⁸Institute of Plasmas and Nuclear Fusion (IPNF), Association EURATOM/IST, Lisbon, Portugal

⁹Institut de Recherche sur la Fusion par confinement Magnétique (IRFM),

Commissariat à l'énergie atomique (CEA/Cadarache), 13108 Saint-Paul-lès-Durance, France

Corresponding Author: G. Papp, ppg@ipp.mpg.de

Disruptions in tokamaks can lead to the generation of a relativistic runaway electron (RE) beam that may cause serious damage to the first wall. The uncontrolled loss of such a high energy electron beam is intolerable and therefore the issue of how to avoid or mitigate the beam generation is of prime importance for ITER. The European medium sized tokamaks ASDEX-Upgrade (AUG) and TCV have recently joined the international effort of better understanding runaway electron generation and dissipation, aiding the development of the future ITER disruption and runaway electron mitigation system.

The AUG RE scenario is a 2.5 T, circular, low density, limiter discharge with 2.5 MW of Electron Cyclotron Resonance Heating. The injection of 0.05–0.2 bar·ℓ (1.2–5 × 10²¹ particles) of argon produces a well reproducible disruption and leads to the generation of 100–400 kA of runaway electron beam that can last up to 400 ms. The main goal on AUG was to study the interaction of REs with partially ionized high-*Z* materials. Suppression of REs was achieved with 0.17 bar·ℓ of argon or 0.7 bar·ℓ of neon using the in-vessel piezo valves. Injection from ex-vessel valves requires ~10× more gas to achieve suppression. We identified a (1, 1) mode surviving the disruption for several ms, indicating a partial survival of the plasma core, which was also indicated by the survival of ECRH-introduced seed particles. A resonant magnetic perturbation configuration was developed that leads to up to a factor 2 decrease in the RE current by changing the disruption dynamics.

The main goal of experiments carried out on TCV is to utilize TCV's flexible plasma shape and position control to determine the direct and indirect effects of plasma shaping on RE generation and dissipation. The base scenario is a 1.4 T, low density, circular, limiter discharge. Using multichord HXR spectrometers we have determined the effective critical field for RE generation and detection. The value found is higher than the Dreicer value by about an order of magnitude, in agreement with previous experimental findings. These quasisteady discharges also provide a dataset for validating time-dependent Fokker–Planck simulations. Further discharges, including postdisruptive studies are ongoing, and the results of these experiments are also going to be presented in this contribution.



Effectiveness of High-Frequency ELM Pacing with D₂ and Nonfuel Pellets in DIII-D

A. Bortolon¹, L. R. Baylor², R. Maingi¹, D. Mansfield¹, A. L. Roquemore¹, R. Lunsford¹, A. Nagy¹, G. L. Jackson³, T. H. Osborne³, N. Commaux², D. Shirakid², C. J. Lasnier⁴, M. A. Makowski⁴, P. B. Parks³, R. Groebner³, and R. Nazikian¹

¹Princeton Plasma Physics Laboratory (PPPL), Princeton, NJ 08540, USA

²Oak Ridge National Laboratory (ORNL), Oak Ridge, TN 37831, USA

³General Atomics, San Diego, CA 92186, USA

⁴Lawrence Livermore National Laboratory (LLNL), Livermore, CA 94550, USA

Corresponding Author: A. Bortolon, abortolon@pppl.gov

DIII-D studies of high-frequency ELM pacing by pellet injection were extended to ITER scenarios at low beam torque, demonstrating ELM peak heat flux mitigation with D₂ pellets, and also with Li spheres, proving the concept of ELM pacing with nonfuel pellets, a technique that could potentially reduce the throughput to the pumping and fuel reprocessing systems in ITER.

Injection of D₂ pellets at frequencies up to 90 Hz was performed in low-torque ITER baseline scenarios ($q_{95} = 3.1$, $\beta_N = 1.7$, $n_e = 4 \times 10^{19}/\text{m}^3$, $T_{\text{inj}} = 0.1 \text{ N}\cdot\text{m}$). High frequency injection resulted in ELM pacing at frequencies as much as $8 \times$ the natural ELM frequency (10 Hz). The resulting inner divertor peak heat flux was reduced by more than a factor of 10. During the high frequency injection, confinement remained similar to the reference discharge ($H_{98}(y, 2) \sim 0.8$) with reduced concentration of metal impurities (Fe, Ni, Mo).

Injection frequencies up to 200 Hz were obtained with new Impurity Granule Injector (IGI), capable of injecting spherical pellets of nonfuel materials (e.g., Li, C, B4C), with controllable speed (60–120 m/s) and selectable pellet size. By using the IGI with Li spheres (0.3–1.0 mm) in ITER shaped plasmas at moderate torque of 3.0 N·m, ELM pacing was demonstrated for the full discharge length, with constant $H_{98}(y, 2) \approx 1.0$, effective density control and reduced high-Z impurities. In this scenario the ELM frequency was increased by $3\text{--}5 \times$ over the natural ELM frequency (12 Hz), but the maximum ELM frequency appears to be limited only by the injection frequency of the larger granules. The increase of paced ELM frequency resulted in a lower q_{ELM} , at the outer strike point, where $q_{\text{ELM}} \sim 1/f_{\text{ELM}}$. Measurements of q_{ELM} at the inner strike point found q_{ELM} often higher than expected at high frequency of ELM pacing. Li spheres of 0.7–1.0 mm diameter were also used to pace ELMs in the low torque ITER baseline scenario ($\beta_N = 1.9$, $T_{\text{inj}} = 0.75 \text{ N}\cdot\text{m}$), achieving 100% pacing efficiency at $f_{\text{inj}} \leq 200 \text{ Hz}$. A broad distribution of triggered ELM size was observed, where 5% paced ELMs had q_{ELM} similar to natural ELMs.

The combined dataset provides unique support of ITER mitigation research, both in terms of operational demonstrations and understanding of the physics of ELM pacing and mitigation.



ELM Pace-Making and Long-Pulse ELM-Stable H-Mode Operation with LHCD in EAST

G. Xu¹, M. Wang¹, Q. Yang¹, Y. Ye¹, T. H. Osborne², M. Jia¹, G. Li¹, Y. Wang¹, H. Wang², H. Guo², Y. Liang¹, X. Gong¹, and B. N. Wan¹

¹*Institute of Plasma Physics, Chinese Academy of Sciences, Hefei, Anhui, People's Republic of China*

²*General Atomics, San Diego, CA 92186, USA*

Corresponding Author: G. Xu, gsxu@ipp.ac.cn

A new control technique for the edge-localized modes (ELMs) by pace-making with low-hybrid current drive (LHCD) power modulation has been demonstrated, for the first time, in the EAST superconducting tokamak. The achievable pace-making frequency is up to 120 Hz, which appears to be limited only by the pedestal recovery time. LHCD leads to the density pump-out and local flattening of the density gradient near the separatrix, associated with the LHCD-induced edge stochastic magnetic region by driving helical current filaments along the magnetic field lines in the scrape-off layer, similar to the effect generated by the RMPs. The density and pressure gradients just inside the stochastic region (near the pedestal top) are steepened, which destabilizes the ELMs. High pedestal and good global energy confinement have been achieved due to the expansion of ballooning boundary with increasing pedestal width and the shift of peak gradient region radially inward. The triggered ELMs are mostly small ELMs since the ELM collapses occur mainly in the steep gradient region near the pedestal top. In addition, a stationary ELM-stable H-mode regime has been achieved in EAST with 4.6 GHz LHCD. This regime allows near fully noninductive long-pulse (>20 s) operations, which exhibits relatively high pedestal and good global energy confinement with $H_{98}(y, 2)$ near 1.2, good impurity control, and capability of operation at relatively high density ($\langle n_e \rangle / n_{GW} \sim 0.5$). The enhanced pedestal height and global energy confinement are the result of an expansion of the ballooning stability boundary brought about by the local flattening of the density gradient near the separatrix, increase of the pedestal width and shift of the peak gradient region radially inward. These profile changes are resulted from the combined effect of LHCD-induced edge plasma ergodization and edge-coherent-mode-induced density pump-out. Such a stationary ELM-stable H-mode regime transitions into a steady small-ELM region with divertor peak heat flux less than 5 MW/m^2 , when additional heating power from NBI, ICRF or 2.45 GHz LHCD is applied. This small-ELM regime offers a suitable candidate for high-performance steady-state H-mode operations. Nearly fully noninductive (loop voltage <math><0.1 \text{ V}</math>) long-pulse (>20 s) small-ELM H-mode plasmas have been achieved with bootstrap current fraction of $\sim 35\%$ and density of $\langle n_e \rangle / n_{GW} \sim 0.7$.

EX



Edge-Localized Modes on KSTAR: Global Structure and Distinct Evolution Stages Involving Quasi-Steady State and Phase Transitions

G. S. Yun¹, J. Lee², J. E. Lee¹, S. Thatipamula¹, M. H. Kim¹, M. J. Choi², W. Lee², and H. K. Park²

¹Pohang University of Science and Technology (POSTECH), Pohang, Gyeongbuk 790-784, Republic of Korea

²Ulsan National Institute of Science and Technology (UNIST), Ulsan, Republic of Korea

Corresponding Author: G. S. Yun, gunsu@postech.ac.kr

Edge-localized modes (ELMs) in the KSTAR tokamak appear substantially different from the conventional picture of ELMs as an explosive transport event in the plasma edge triggered by exponentially growing ballooning and external kink modes on the low field side of the plasma. The 2D images of ELMs visualized by an advanced imaging diagnostics [1] with microsecond time resolution revealed that the modes evolve in three distinctive stages: 1) quasi-steady (saturated) filamentary mode [2] with long life time (up to ~ 100 ms), 2) abrupt structural transformation near the onset of crash into irregular-shaped filaments [2] or in the middle of the intercrash period [3], and 3) multiple filament bursts during the crash phase [2]. Perhaps the most astonishing finding is the clear existence of filamentary modes exist on the high field side as well as on the low field side [4], suggesting that the ELM dynamics in the KSTAR involve other driving forces such as d'Angelo instability besides ballooning and external kink. In addition, we demonstrate that the ELM evolution stages are associated with distinct changes of RF emission spectra [5] (100–1000 MHz), suggesting the RF signal as a better alternative to the conventional D_α signal which represents only the aftermath of the collapse of the edge confinement.

References

[1] G. S. Yun, *et al.*, *Rev. Sci. Instrum.* **85**, 11D820 (2014).

[2] G. S. Yun, *et al.*, *Phys. Rev. Lett.* **107**, 045004 (2011).

[3] J. E. Lee, *et al.*, *Nucl. Fusion* **55**, 113035 (2015).

[4] J. Lee, *et al.*, submitted.

[5] S. Thatipamula, *et al.*, submitted.

Work supported by the NRF of Korea under grant No. NRF-2014M1A7A1A03029881, BK+ programme, and A3 Foresight programme.



Validation of Theoretical Models of Intrinsic Torque in DIII-D and Projection to ITER by Dimensionless Scaling

B. A. Grierson¹, X. Wang¹, C. Chrystal², J. deGrassie³, J. A. Boedo⁴, W. M. Solomon¹, G. M. Staebler³, and D. Battaglia¹

¹Princeton Plasma Physics Laboratory (PPPL), Princeton, NJ 08540, USA

²Oak Ridge Associated Universities (ORAU), Oak Ridge, TN 37831, USA

³General Atomics, San Diego, CA 92186, USA

⁴University of California San Diego, CA 92093, USA

Corresponding Author: B. A. Grierson, bgriers@pppl.gov

Experiments in DIII-D have validated advanced models of main-ion intrinsic rotation and used dimensionless parameter scans to predict a significant amount of intrinsic torque in ITER. Recent measurements of deuterium toroidal rotation using main ion spectroscopy in DIII-D have validated predictions of Reynolds stress induced toroidal flow in the plasma core and rotation induced by ion orbit losses in the plasma edge. In the core of dominantly electron heated plasmas with $T_e = T_i$, the main-ion intrinsic toroidal rotation undergoes a reversal. Above a critical ECH heating power the core rotation reversal correlates with the critical gradient for ITG turbulence. Residual stress from zonal-flow $E \times B$ shear and turbulence intensity gradient are the dominant symmetry breaking mechanisms producing residual stress intrinsic torque, balanced by momentum diffusion, creating the hollow profile. Quantitative agreement is obtained for the first time between the measured main-ion toroidal rotation and the profile predicted by nonlinear GTS gyrokinetic simulations. In dimensionless scaling experiments that vary only ρ^* the intrinsic torque in the plasma is found to scale in a favourable way to ITER, projecting to increased intrinsic torque at lower ρ^* . The intrinsic torque projected for the high current H-mode phase of ITER is approximately 85 N·m, exceeding the neutral beam torque of 35 N·m. This intrinsic torque is expected to drive an average intrinsic rotation of approximately 60 km/s. The total angular momentum scales with the boundary condition near the separatrix, and in the edge of plasmas with high and low collisionality and either sign of plasma current main-ion intrinsic rotation measurements are consistent with an orbit-loss model. Edge plasma rotation increases as collisionality decreases, projecting favourably to ITER. First-principles based prediction of the ITER rotation profile requires validated models of both turbulent transport that determine the core profile shape, as well as the neoclassical kinetic processes that determine the boundary condition. Experiments at DIII-D are combining the validation of turbulent momentum transport in the plasma core with the intrinsic rotation at the boundary and made significant advancements in our predictive capability for ITER.

Work supported by the U.S. Department of Energy under DE-AC02-09CH11466, DE-FC02-04ER54698, and DE-FG02-07ER54917.



Studies of Turbulence and Transport in the Alcator C-Mod and DIII-D Tokamaks with Phase Contrast Imaging and Gyrokinetic Modelling

M. Porkolab¹, P. C. Ennever², A. Marinoni², C. J. Rost², S. G. Baek², E. M. Davis², E. M. Edlund², D. R. Ernst², J. W. Hughes², J. E. Rice², K. H. Burrell³, J. Candy³, R. I. Pinsker³, G. M. Staebler³, G. R. McKee⁴, B. A. Grierson⁵, M. L. Reinke⁶, and T. L. Rhodes⁷

¹Massachusetts Institute of Technology (MIT), Cambridge, MA 02139, USA

²Plasma Science & Fusion Center, MIT, Cambridge, MA 02139, USA

³General Atomics, San Diego, CA 92186, USA

⁴University of Wisconsin-Madison, Madison, WI 53706, USA

⁵Princeton Plasma Physics Laboratory (PPPL), Princeton, NJ 08540, USA

⁶Oak Ridge National Laboratory (ORNL), Oak Ridge, TN 37831, USA

⁷University of California Los Angeles, CA 90095, USA

Corresponding Author: M. Porkolab, porkolab@psfc.mit.edu

EX Experimental results are presented where the macroscopic plasma conditions were manipulated by external actuators, such as injection of medium to low Z_i impurity gases with ohmic heating (Alcator C-Mod) to dilute the main deuterium ion species, or deploy a different mix of NBI and ECH heating methods (DIII-D), thus enabling us to study the resulting changes in transport and turbulence. Subsequently, we were able to carry out quantitative comparisons between gyrokinetic code predictions (GYRO and GS2) and compare them with measurements of the fluctuating density spectrum based on a calibrated Phase Contrast Imaging (PCI) technique. In Alcator C-Mod, dilution by nitrogen seeding was found to decrease the ion temperature gradient scale lengths in the outer regions of the plasma where ITG modes were dominant. GYRO simulations reproduced the observed change in the energy transport with the seeding as a reduction in ITG driven transport. The PCI measured density fluctuation amplitudes also decreased substantially with nitrogen seeding. Simulations of these plasmas with the nonlinear gyrokinetic code GYRO were performed and the density fluctuations from nonlinear GYRO simulations were found to agree with the experimental PCI measurements. On the DIII-D tokamak experiments simulating the NBI heated ITER Baseline Scenario showed that added electron cyclotron heating (ECH) affected turbulent fluctuations at different scales, as measured by Phase Contrast Imaging (PCI) diagnostic. After turning off the ECH power, the intensity of fluctuations at frequencies higher than 200 kHz increased within 20 ms, due to electron modes that were enhanced by the prompt response of the electron temperature inverse scale length in the outer third of the minor radius. Such modes were observed in nonlinear gyro-kinetic simulations to generate a significant transient heat flux and an inward particle pinch. In contrast, the behaviour of fluctuations at lower frequencies was dictated by the slower time evolution of other equilibrium quantities such as density and flow shear. In particular, the intensity of fluctuations was observed to decrease with the mean flow shear exceeding the maximum linear growth rate of ITG modes.

Work supported by the U.S. Department of Energy contracts DE-FC02-99ER54512 on Alcator C-Mod, DE-FC02-04ER54698 on DIII-D, both DOE FES User Facilities, and Grant DE-FG02-94ER54235 at MIT.



Effects of the q Profile on Toroidal Rotation in Alcator C-Mod LHCD Plasmas

J. E. Rice¹, C. Gao², R. Mumgaard², R. R. Parker¹, S. D. Scott³, S. Shiraiwa¹, G. M. Wallace¹, P. T. Bonoli², L. F. Delgado-Aparicio³, C. Fenzi⁴, R. S. Granetz², M. J. Greenwald², A. E. Hubbard¹, J. W. Hughes¹, J. H. Irby¹, J. P. Lee¹, E. S. Marmar², M. L. Reinke⁵, and S. M. Wolfe¹

¹Plasma Science & Fusion Center, MIT, Cambridge, MA 02139, USA

²Massachusetts Institute of Technology (MIT), Cambridge, MA 02139, USA

³Princeton Plasma Physics Laboratory (PPPL), Princeton, NJ 08540, USA

⁵Oak Ridge Institute for Science Education (ORISE), Oak Ridge, TN 37831, USA

⁴Institut de Recherche sur la Fusion par confinement Magnétique (IRFM), Commissariat à l'énergie atomique (CEA/Cadarache), 13108 Saint-Paul-lès-Durance, France

Corresponding Author: J. E. Rice, rice@psfc.mit.edu

In future magnetic fusion devices, external momentum input from neutral beam injection will be low, and to reap the benefits of rotation, such as stabilization of deleterious MHD modes and shear suppression of turbulence, utilizing radio frequency drive and understanding self-generated flow would be prudent. Changes in the core toroidal rotation profiles following injection of lower hybrid (LH) waves have been documented in Alcator C-Mod plasmas. Shot by shot scans of LH input power have been performed at fixed magnetic field and electron density for several plasma currents. For sawtooth target plasmas, if the input power is low enough that the central safety factor q_0 remains below 1, the change in the core rotation is in the countercurrent direction, consistent in sign, magnitude and LH power scaling with direct momentum input from the LH waves. If the power level is high enough that there are significant changes to the q profile, including the termination of sawtooth oscillations, the change in the toroidal rotation is in the cocurrent direction, consistent with changes in sign of the momentum flux through the residual stress and its dependence on the current density profile. The direction of the rotation changes depends on whether q_0 is below or above unity, and seemingly not on the magnetic shear, nor the Ohmic confinement regime of the target plasma.

EX



Investigations of Radial High- Z Transport Mechanisms in ICRF-Heated Alcator C-Mod H-Mode Plasmas

M. L. Reinke¹, A. Loarte², J. E. Rice³, F. J. Casson⁴, M. Chilenski³, N. Howard³, A. E. Hubbard³, J. W. Hughes³, S. M. Wolfe³, and S. Wukitch³

¹*Oak Ridge National Laboratory (ORNL), Oak Ridge, TN 37831, USA*

²*International Thermonuclear Experimental Reactor (ITER), Cadarache Centre, 13108 Saint-Paul-lès-Durance, France*

³*Plasma Science & Fusion Center, MIT, Cambridge, MA 02139, USA*

⁴*Culham Centre for Fusion Energy (CCFE), Culham Science Centre, Abingdon, UK*

Corresponding Author: M. L. Reinke, mlreinke@psfc.mit.edu

Recent Alcator C-Mod research investigates mechanisms by which ion cyclotron range of frequency (ICRF) heating can effectively mitigate on-axis accumulation of high- Z impurities and explores new techniques to study their interaction with edge transport barriers (ETB). In C-Mod EDA H-modes using D(H) minority heating, modifying the minority concentration and the major radius of the minority resonance layer results in substantive changes in core high- Z impurity transport. Raising the minority fraction is linked to enhanced core peaking of tungsten injected via laser ablation. When the minority resonance layer is moved off-axis to the low-field side (LFS), bridging the $q = 1$ surface, core accumulation is avoided similar to when heating on-axis. In contrast, off-axis heating on the high field side (HFS) at similar minor radii resulted in tungsten accumulation, uncontrolled radiation rise and core electron temperature collapse. These observations differ from recent JET results showing a weak difference in tungsten-driven soft X-ray peaking between LFS and HFS heating. Diffusive and convective transport of high- Z impurities in C-Mod are constrained by STRAHL simulations. Using TORIC in TRANSP to model the minority species and NEO and GKW to model the neoclassical and turbulent transport, a range mechanisms are investigated by which minority heating can impact the core radial impurity transport. While minority heating may modify the core peaking, volume averaged impurity content is controlled by radial flux at the ETB. Modelling suggests that for opaque scrape-off layers as expected in ITER, kinetic profiles will combine to result in outward neoclassical impurity flux between edge localized modes (ELMs). This important result stands in contrast to the widely observed behaviour of quasi-stationary impurity flux between ELMs or in ELM-free H-modes to be directed inward, building up core impurity content. Experimental results from Alcator C-Mod suggest that this condition of outward impurity flux may be transiently accessed following a transition from I-mode to ELM-free H-mode. By tracking the time evolution impurities introduced prior to the H-mode transition, the direction of the impurity flux can be estimated from time-evolving STRAHL simulations of impurity spectroscopy. Initial results using this novel pedestal transport analysis technique are presented.

EX



Experimental Results from Three-Ion Species Heating Scenario on Alcator C-Mod

J. C. Wright¹, Y. Lin¹, M. Porkolab², S. Wukitch¹, Ye. O. Kazakov³, D. Van Eester³, and J. Ongena³

¹Plasma Science & Fusion Center, MIT, Cambridge, MA 02139, USA

²Massachusetts Institute of Technology (MIT), Cambridge, MA 02139, USA

³Laboratory for Plasma Physics, ERM/KMS, Brussels, Belgium

Corresponding Author: J. C. Wright, jcwright@mit.edu

Recent experiments on Alcator C-Mod using a small fraction of ³He added to a H(D) plasma have demonstrated efficient ion cyclotron radio frequency (ICRF) heating and indications of MeV ³He tail temperatures. For high toroidal magnetic field $B_0 = 8$ T discharges with D majority, ³He minority absorption is typically used and has low single pass absorption compared to the H minority absorption scenario. We have observed strong toroidal rotation that is correlated with RF power absorption on thermal ³He ions via mode converted waves. ICRF can also generate high energy ions and this provides a tool to study fast ion dynamics and optimize the quality of plasma confinement. This new scenario has much higher absorption and works by adjusting concentrations of the majority and two minority species to arrange that the polarization of the ICRF wave is favourable for ion heating at the location of the cyclotron resonance of a third trace species.

Experiments using a H:D:(³He) three-ion scenario were carried out on C-Mod with an 8 T field and an H:D ratio of approximately 2 : 1. The ³He fraction was varied from 0.4% to 2%. A strong increase in toroidal Alfvén eigenmode (TAE) activity coincided with the addition of ³He to the H(D) plasmas. TAE activity is indicative of the formation of fast ions with a energy on the order of 1 MeV. Increased heating localized around the ³He fundamental cyclotron layer was also observed. We will present analysis of the minority ion temperature using Fokker–Planck calculations coupled with a full wave code over a range of ³He fractions. These temperatures will be compared with theoretical calculations of TAE thresholds. A synthetic PCI diagnostic using the modelled 3D RF fields will be compared to the experimental PCI to determine the breakdown between the two competing absorption mechanisms present in mode conversion layer. These mechanisms can either heat electrons or ions or drive momentum in the ion channel. We will conclude with a discussion of the applicability of this scenario to the upcoming DT campaign on JET, operations on ITER and as a source of pseudo-alphas on W7-X.

Work supported by the U.S. Department of Energy grants for SciDAC Center for Simulation of Wave Plasma Interactions DOE DE-FC02-01ER54648, Alcator C-Mod Science user facility DE-FC02-99ER54512, and the Phase Contrast Imaging Diagnostic on C-Mod, DE-FG02-94-ER54235.

Plasma Profiles and Impurity Screening Behaviour of the High-Field Side Scrape-Off Layer in Near-Double-Null Configurations: Prospect for Mitigating Plasma-Material Interactions on RF Actuators and First-Wall Components

B. LaBombard¹, A. Kuang¹, D. Brunner¹, B. Mumgaard¹, M. L. Reinke², J. Terry¹, J. W. Hughes¹, J. R. Walk¹, M. Chilenski¹, Y. Lin¹, E. S. Marmor¹, G. M. Wallace¹, D. G. Whyte¹, S. M. Wolfe¹, and S. Wukitch¹

¹Plasma Science & Fusion Center, MIT, Cambridge, MA 02139, USA

²Oak Ridge National Laboratory (ORNL), Oak Ridge, TN 37831, USA

Corresponding Author: B. LaBombard, labombard@psfc.mit.edu

EX The improved impurity screening characteristics of the high-field side scrape-off layer to local impurity sources, previously reported for single null geometries, is found to be retained in double null configurations — strengthening the argument for locating current drive and heating actuators on the high-field side. The high-field-side (HFS) scrape-off layer (SOL) is known to exhibit extremely low levels of cross-field transport [1] and excellent impurity screening characteristics [2] in single-null magnetic configurations. It has been proposed that future tokamaks should exploit these remarkable HFS characteristics to solve critical plasma-material interaction (PMI) and sustainment challenges: relocate all RF actuators and close-fitting wall structures to the HFS and employ near-double-null magnetic topologies, to precisely control plasma conditions at the antenna/plasma interface and mitigate the impact of PMI [3]. Dedicated experiments were performed on Alcator C-Mod during the 2015 experimental campaign to quantify impurity screening characteristics and scrape-off layer profiles in near-double-null configurations. Nitrogen screening by the HFS SOL is found to be a factor of 2.5 better than LFS in balanced double-null discharges, despite an extremely thin scrape-off layer. Impurity screening is found to be insensitive to current and Greenwald fraction. HFS impurity screening is least effective (only a factor of 1.5 improvement) in unbalanced double-null discharges that favour the active divertor in the direction of $B \times \nabla B$. Unbalanced discharges that favour the most active divertor opposite the direction of $B \times \nabla B$ have excellent HFS screening characteristics, a factor of 5 better than LFS. The latter situation is particularly promising for the use of HFS RF actuators in I-mode plasmas: a high confinement, steady state, ELM-free regime that is accessible at high magnetic field to a large range of input power for this magnetic topology [4].

References

- [1] N. Smick, *et al.*, Nucl. Fusion **53**, 02300 (2013).
- [2] G. McCracken, *et al.*, Phys. Plasmas **4**, 1681 (1997).
- [3] B. LaBombard, *et al.*, Nucl. Fusion **55**, 053020 (2015).
- [4] A. Hubbard, *et al.*, IAEA FEC-2014, EX/P6-22, (2014).

Work supported by the U.S. Department of Energy, Office of Fusion Energy Sciences under Award Number DE-FC02-99ER54512 on Alcator C-Mod, a DOE Office of Science User Facility.

Divertor and Core Plasma Performance Optimization Enabled by Direct Feedback Control of Surface Heat Flux on Alcator C-Mod's High-Z Vertical Target Plate Divertor

D. Brunner¹, S. M. Wolfe¹, B. LaBombard¹, A. Kuang¹, B. Lipschultz², M. L. Reinke³, S. G. Baek¹, S. Ballinger⁴, W. Burke¹, E. M. Edlund¹, P. C. Ennever¹, I. Faust¹, T. Golfinopoulos¹, A. E. Hubbard¹, J. W. Hughes¹, J. H. Irby¹, B. Mumgaard¹, J. Terry¹, S. Shiraiwa¹, J. R. Walk¹, and S. Wukitch¹

¹Plasma Science & Fusion Center, MIT, Cambridge, MA 02139, USA

²University of York, Heslington, UK

³Oak Ridge National Laboratory (ORNL), Oak Ridge, TN 37831, USA

⁴Columbia University, New York, NY 10027, USA

Corresponding Author: D. Brunner, brunner@mit.edu

The C-Mod team has developed a new tool for control of plasma conditions at the divertor target. It is the first heat flux mitigation system to employ real-time measurements of surface heat flux to control impurity seeding. Control of the conditions at the divertor surface is one of the remaining challenges to tokamak fusion energy. Active cooling technology limits the surface heat flux to $\sim 10 \text{ MW/m}^2$ or less and erosion of solid, high-Z targets limits the incident plasma temperature $< 5 \text{ eV}$. Yet, plasma entering the divertor will be intense: The scrape-off layer heat flux width scales inversely with the poloidal magnetic field and is independent of machine size [1]. This results in a parallel heat flux that scales as $q_{\parallel} \sim P_{\text{SOL}} B/R$. Projecting this to ITER results in an unmitigated parallel heat flux of $\sim 5 \text{ GW/m}^2$ and $> 10 \text{ GW/m}^2$ in a DEMO-class device [2]. Seeding of low-Z impurities (N_2 and Ne) into the divertor to mitigate the focussed plasma heat flux into a uniform photon heat flux is viewed as a necessity. Yet excessive seeding comes at a cost, lowering pedestal pressures and increasing core dilution.

C-Mod is an excellent test of reactor-relevant plasma control solutions: it has an ITER-like high-Z, vertical target plate and is the only experiment with demonstrated heat fluxes in excess of 1 GW/m^2 . During FY15 a system for real-time control of heat flux was deployed [3]. The system uses surface thermocouples and an analog computer to output accurate signals of heat flux, which are used to control the injection rate of nitrogen into the private flux region. It has been used to reduce the surface heat flux from $> 25 \text{ MW/m}^2$ (corresponding to an unmitigated parallel heat flux $q_{\parallel} \sim 500 \text{ MW/m}^2$) to less than 5 MW/m^2 while avoiding degradation of energy confinement, i.e., H_{98} . Yet, even at nearly zero surface heat flux, the divertor Langmuir probes still indicate a plasma temperature too high ($> 5 \text{ eV}$) to suppress sputtering. In the FY16 campaign a divertor mirror Langmuir probe system [4], which outputs real-time measurements of electron temperature, will be used in an attempt to feedback on the plasma temperature at the divertor target.

References

- [1] T. Eich, *et al.*, Nucl. Fusion **53**, 093031 (2013).
- [2] B. LaBombard, *et al.*, Nucl. Fusion **55**, 053020 (2015).
- [3] D. Brunner, *et al.*, Rev. Sci. Instrum. **87**, 023504 (2016).
- [4] B. LaBombard and L. Lyons, Rev. Sci. Instrum. **78**, 073501 (2007).



Developing Disruption Warning Algorithms Using Large Databases on Alcator C-Mod and EAST Tokamaks

R. S. Granetz¹, R. A. Tinguely¹, B. Wang², B. J. Xiao², and Z. P. Luo²

¹*Massachusetts Institute of Technology (MIT), Cambridge, MA 02139, USA*

²*Institute of Plasma Physics, Chinese Academy of Sciences, Hefei, Anhui, People's Republic of China*

Corresponding Author: R. S. Granetz, granetz@mit.edu

To address the challenge of disruption prediction, we have created large disruption warning databases for both Alcator C-Mod and EAST by compiling values for a number of proposed disruption-relevant parameters sampled at many different times throughout all plasma discharges, disruptive and nondisruptive, during the 2015 campaigns on the respective machines. The disruption-relevant parameters include such intuitive quantities as I_p error [= $I_p - I_p(\text{programmed})$], radiated power fraction [= $P_{\text{rad}}/P_{\text{input}}$], $n/n_{\text{Greenwald}}$, $n = 1$ mode amplitude, as well as a number of equilibrium parameters derived from EFIT reconstructions (q_{95} , elongation, etc.). Examples of the evolution of these parameters prior to disruptions on C-Mod and EAST, will be shown.

The disruption warning databases for C-Mod and EAST each contain parameter values from well over 100,000 time slices. This allows one to provide quantitative answers to such questions as: 1) Is parameter “X” (e.g., I_p error or n/n_G or $n = 1$ mode amplitude) correlated with impending disruptions? If yes, 2) What fraction of disruptions do not show a correlation (i.e., missed disruptions)? 3) What is an appropriate trigger level for each correlated parameter, and how does the number of “false positives” vary with the trigger level? 4) What is the typical warning time, and how does the warning time vary with trigger level? This fundamental quantitative characterization of disruption-relevant parameters is absolutely crucial for developing any credible real-time disruption warning algorithms.

These databases are also amenable to the application of advanced “machine learning” techniques to discern more complicated dependencies on parameters, and the development of more advanced warning algorithms.

In principle, the disruption-relevant parameters in the C-Mod and EAST disruption warning databases could be available in real-time, and their plasma control systems could implement a disruption prediction algorithm based on the analysis of these large databases to provide a warning with sufficient lead time that could be used to move the plasma to a less unstable state to avoid a disruption, or to trigger a disruption mitigation system.

This work supported in part by: U.S. Department of Energy Grants DE-FC02-99ER54512, DE-SC0010720 and DE-SC0010492, using Alcator C-Mod, a DOE Office of Science User Facility

EX

Dominant Role of Turbulence in Determining Particle Transport and Confinement

S. Mordijck¹, X. Wang¹, L. Zeng², E. J. Doyle², T. L. Rhodes², L. Schmitz², C. Chrystal³, Z. Yan⁴, and G. R. McKee⁴

¹College of William & Mary, Williamsburg, VA 23185, USA

²University of California Los Angeles, CA 90095, USA

³Oak Ridge Associated Universities (ORAU), Oak Ridge, TN 37831, USA

⁴University of Wisconsin-Madison, Madison, WI 53706, USA

Corresponding Author: S. Mordijck, mordijck@cs.wm.edu

In this paper we will show that particle confinement is determined by changes in turbulence characteristic outside midradius up to the top of the pedestal in DIII-D H-mode plasmas. We find that the Electron Cyclotron Heating (ECH) density pump-out at low collisionality is the result of an increase in turbulence drive from $\rho = 0.7$ – 0.9 . The frequency of the mode and thus the turbulence type changes from the Ion Gradient Temperature (ITG) to Trapped Electron Mode (TEM) on a much longer time scale. Secondly, we find that particle confinement is strongly reduced in balanced torque injected plasmas, where the $E \times B$ shear close to the top of the pedestal drops below the linear growth rate of long wavelength turbulence [1, 2]. Both these observations have a strong impact on predictions for ITER, where most of the plasma heating is deposited in the electron channel and the Neutral Beams (NBI) inject relatively low momentum.

One option to counter effects of reduced particle confinement at the plasma edge is to increase peaking of the core density profile. An experimental database has shown that density peaking is influenced by collisionality, and the dominant unstable mode, while theory predicts the q -profile should be inversely proportional with the density gradient [3]. We do find, similar as on AUG, that at midradius the frequency of the most unstable mode correlates with the inverse density scale length. Experimentally we observe that $1/q \sim \nabla n_e$, as predicted by theory. The correlation is stronger when $T_e = T_i$ and the plasma is in the ITG regime. When we increase the electron temperature with ECH, the correlation becomes weaker.

From these results we can conclude that turbulence plays a dominant role in determining the density profile and particle confinement. However, the predictive capability of particle transport is not well validated and the density profile is assumed to be flat in ITER scenarios [4]. Through comparisons with quasi-linear gyro-kinetic simulations we plan to validate existing codes in order to make better predictions for ITER.

References

- [1] X. Wang, *et al.*, Plasma Phys. Control. Fusion, In review, (2015).
- [2] S. Mordijck, *et al.*, Phys. Plasmas **19**, 056503 (2012).
- [3] C. Angioni, *et al.*, Nucl. Fusion **52**, 114003 (2012).
- [4] L. Garzotti, *et al.*, Nucl. Fusion **52**, 013002 (2012).

Turbulence Evolution and Transport Behaviour during Current Ramp-Up in ITER-Like Plasmas on DIII-D

G. R. McKee¹, M. Austin², J. A. Boedo³, R. Bravenec⁴, C. Holland³, G. L. Jackson⁵, T. C. Luce⁵, T. L. Rhodes⁶, D. L. Rudakov³, G. Wang⁶, Z. Yan¹, L. Zeng⁶, and Y. Zhao^{1,7}

¹University of Wisconsin-Madison, Madison, WI 53706, USA

²University of Texas at Austin, Austin, TX 78712, USA

³University of California San Diego, CA 92093, USA

⁴Fourth State Research, Austin, TX 78704, USA

⁵General Atomics, San Diego, CA 92186, USA

⁶University of California Los Angeles, CA 90095, USA

⁷Suzhou University, Suzhou, People's Republic of China

Corresponding Author: G. R. McKee, george.mckee@wisc.edu

EX Low-wavenumber density fluctuations exhibit rapidly changing characteristics during the current ramp-up phase of ITER-like discharges that reflect a complex interaction between evolving electron transport, safety factor (q) and kinetic profiles and low-order rational surfaces. These measurements and analysis can explain discrepancies between various transport models and measurements during the critical ramp-up phase. ITER similar shape plasmas were performed on DIII-D to characterize performance and measure comprehensive turbulence characteristics. Comparison of these fluctuations, transport and profiles with simulations is aimed at developing a validated transport model that incorporates the unique characteristics of the ramp-up phase. Transient windows of suppressed fluctuations are observed during ramp-up, which correspond to low-order-rational q -surfaces entering the plasma that are associated with regions and times of improved transport; the local electron temperature exhibits transient increases during these periods of reduced fluctuations. Measurements of the 2D fluctuation properties, obtained across the outer half-radius with Beam Emission Spectroscopy, illustrate the complex behaviour of turbulence during current ramp-up. Density fluctuations at $\rho = 0.55$ exhibit fluctuations that decrease in amplitude with time. At $\rho = 0.82$, a very large amplitude burst of low-frequency turbulence occurs early in the current ramp, simultaneously with a set of Reversed-Shear Alfvén Eigenmodes (RSAEs). A Geodesic Acoustic Mode (GAM) is evident with a frequency that increases with time as T_e increases. The scrape-off layer T_e profile cools and narrows during the ramp-up as the core heats, consistent with increased energy confinement time at lower q_{95} . The amplitude profile of low- k fluctuations exhibits a strong reduction in turbulence with reduced q_{95} ; thermal energy confinement likewise increases with decreasing q_{95} . Comparison of turbulence properties with time-varying linear growth rates with GYRO and GENE will allow for the development of a more complete and accurate model of transport properties during the current ramp phase.



Turbulence-Flow Coupling and Poloidal Main-Ion Flow Acceleration Preceding the L-H Transition

L. Schmitz¹, B. A. Grierson², T. L. Rhodes¹, Z. Yan³, G. R. McKee³, P. Gohil⁴, L. Zeng¹, L. Bardoczi¹, D. Eldon², C. Chrystal⁵, P. H. Diamond⁶, W. Peebles¹, R. Groebner⁴, K. H. Burrell⁴, and C. C. Petty⁴

¹University of California Los Angeles, CA 90095, USA

²Princeton Plasma Physics Laboratory (PPPL), Princeton, NJ 08540, USA

³University of Wisconsin-Madison, Madison, WI 53706, USA

⁴General Atomics, San Diego, CA 92186, USA

⁵Oak Ridge Associated Universities (ORAU), Oak Ridge, TN 37831, USA

⁶University of California San Diego, CA 92093, USA

Corresponding Author: L. Schmitz, lschmitz@ucla.edu

Understanding flow drive and damping across the relevant ion collisionality range is crucial for connecting the L-H transition trigger physics to the macroscopic L-H power threshold scaling. This is of utmost importance for minimizing the auxiliary heating power required for H-mode access in burning plasmas. It is shown here for the first time that the main-ion poloidal flow acceleration is quantitatively consistent with Reynolds-stress-driven shear flow amplification across the entire edge shear layer, leading to the observed dipolar shear layer structure inside the last closed flux surface (LCFS). The poloidal flow damping rate is found to be consistent with the neoclassical plateau regime at intermediate density $n = 3 \times 10^{19}/\text{m}^3$. This work in He plasmas substantially extends previous work on L-H transitions induced by limit cycle oscillations (LCO), and on fast (regular) L-H transitions, [1–3]. We present direct, high resolution measurements of the poloidal and toroidal main ion flow during the trigger phase of the L-H transition, using He main-ion CER. The measured $E \times B$ velocity modulation at the start of the LCO is in phase with the local ion poloidal velocity modulation, indicating flow in opposite directions just inside the LCFS and near the bottom of the E_r well. In contrast, the laboratory frame toroidal velocity is not significantly modulated during LCO. It is demonstrated that i) the Reynolds stress gradient changes sign across the shear layer, consistent with the observed poloidal flow propagation in opposite directions; ii) the measured Reynolds stress drive is quantitatively balanced by the ion flow acceleration and damping terms. This data presents compelling quantitative evidence that the L-mode-LCO transition is triggered via $E \times B$ shear flow amplification mediated by the perpendicular Reynolds stress gradient. Long-range toroidal $E \times B$ flow correlation in the LCO peaks at intermediate plasma density around the L-H power threshold minimum.

References

- [1] L. Schmitz, *et al.*, Phys. Rev. Lett. **108**, 155002 (2012).
- [2] G. Tynan, *et al.*, Nucl. Fusion **53**, 073053 (2013).
- [3] Z. Yan, *et al.*, Phys. Rev. Lett. **107**, 055004 (2014).

Work supported by the U.S. Department of Energy, Contracts DE-FG02-08ER54984, DE-AC02-09CH11466, DE-FG02-89ER53296, DE-FG02-08ER54999, DE-FC02-04ER54698, DE-AC05-06OR23100 and DE-FG02-06ER54871.

Toroidally Localized Turbulence with Applied 3D Fields in the DIII-D Tokamak

R. S. Wilcox¹, M. Shafer¹, N. M. Ferraro², G. R. McKee³, L. Zeng⁴, T. L. Rhodes⁴, J. Canik¹, C. Paz-Soldan⁵, R. Nazikian², and E. A. Unterberg¹

¹Oak Ridge National Laboratory (ORNL), Oak Ridge, TN 37831, USA

²Princeton Plasma Physics Laboratory (PPPL), Princeton, NJ 08540, USA

³University of Wisconsin-Madison, Madison, WI 53706, USA

⁴University of California Los Angeles, CA 90095, USA

⁵General Atomics, San Diego, CA 92186, USA

Corresponding Author: R. S. Wilcox, wilcoxr@fusion.gat.com

EX When resonant magnetic perturbations are applied to suppress edge localized modes using the internal coil set in the DIII-D tokamak with toroidal mode number $n = 3$, measurements of density fluctuations at toroidally separate locations using beam emission spectroscopy (BES) and Doppler back-scattering show larger fluctuation amplitudes in one toroidal phasing than the other. This relationship is consistent regardless of the amplitude of the applied $n = 3$ field, whereas the global density confinement characteristics change, demonstrating a decoupling of the locally measured density fluctuations from the globally observed density pumpout. Plasma rotation and E_r scale with the amplitude of the applied field and with density pumpout, indicating that changes in rotation shearing are not responsible for the observed changes to the turbulence. Although changes to the magnetic flux surface shaping are small, changes to the density within a surface based on 2-fluid M3D-C1 simulations are large enough to significantly alter the density gradient scale length. Flux bundles with modelled increases to the density gradient scale length correspond to those with increased fluctuation amplitudes. Reflectometer measurements in a geometrically similar location as BES observe an increase in the gradient scale length in the same phases that BES observes larger amplitude fluctuations, in qualitative agreement with the M3D-C1 modelling, suggesting a possible mechanism for turbulence destabilization in toroidally localized flux tubes.

Work supported in part by the U.S. Department of Energy under contracts DE-AC05-00OR22725, DE-AC02-09CH11466, DE-FG02-08ER54999, DE-FG02-08ER54984, DE-FC02-04ER54698.



Dimensionless Size Scaling of Intrinsic Rotation

J. deGrassie¹, W. M. Solomon², J. E. Rice³, and J.-M. Noterdaeme⁴

¹General Atomics, San Diego, CA 92186, USA

²Princeton Plasma Physics Laboratory (PPPL), Princeton, NJ 08540, USA

³Plasma Science & Fusion Center, MIT, Cambridge, MA 02139, USA

⁴Max-Planck-Institut für Plasmaphysik, Garching, Germany

Corresponding Author: J. deGrassie, degrassie@fusion.gat.com

A dimensionless empirical scaling for intrinsic toroidal rotation is given; $M_A \sim \beta_N \rho^*$, where M_A is the toroidal velocity divided by the Alfvén velocity, β_N the usual normalized β value, and ρ^* is the ion gyroradius divided by the minor radius. This scaling is in agreement with experimental data from DIII-D, and also incorporates some published data from C-Mod and JET. The velocity used in this scaling is in an outer location in minor radius, outside of the interior core and inside of the large gradient edge region in H-mode conditions, although the scaling result is not very sensitive to the chosen location in H-mode. This scaling establishes the basic magnitude of the intrinsic toroidal rotation and we discuss its relation to the rich variety of rotation profiles that can be realized for intrinsic conditions, that is, minimal injected torque. This scaling has some similarities to existing dimensioned scalings, both the Rice scaling [1] and the scaling of Parra *et al.* [2].

References

[1] J. E. Rice, *et al.*, Phys. Plasmas **7**, 1825 (2000).

[2] F. I. Parra, *et al.*, Phys. Rev. Lett. **108**, 095001 (2012).

EX



Confinement and Stability of the ITER Baseline Scenario in DIII-D

F. Turco¹

¹*Columbia University, New York, NY 10027, USA*

Corresponding Author: F. Turco, turcof@fusion.gat.com

Analysis of ~180 ITER Baseline Scenario (IBS) demonstration discharges in DIII-D provides insight into the cause of the 2/1 disruptive instabilities that limit the duration of these plasmas. Raw MSE data and detailed equilibrium reconstructions show that a larger current profile gradient in the region of the $q = 2$ surface characterizes the unstable cases, providing the drive for the 2/1 tearing mode onset. Rotation measurements indicate that lower differential rotation at the marginal stability point constitutes the additional separating factor for part of the unstable shots at low injected torque. The current profile is observed to evolve with the plasma rotation, due to modifications in the pedestal transport, and initial transport modelling shows that time dependent predictive simulations can capture these changes. The approach to the instability at low rotation is observed in Active MHD Spectroscopy (AMS) measurements of the plasma response. Drift-kinetic modelling of these measurements indicates that nonideal effects are significant despite the relatively low β_N of these plasmas. The inclusion of collisionality and resistivity is crucial to capture the nature of the modes and ensure predictive capability for ITER plasmas. A combination of the real-time AMS amplitude and phase measurements can be used to detect the onset of the relevant modes, potentially in time for a disruption avoidance or mitigation system to be deployed.

EX

Stability of High-Performance, Negative Central Shear Discharges

J. D. Hanson¹

¹*Columbia University, New York, NY 10027, USA*

Corresponding Author: J. D. Hanson, jmh2130@columbia.edu

DIII-D experiments demonstrate high-performance, negative central shear (NCS) equilibria with enhanced stability when the minimum safety factor q_{\min} exceeds 2, qualitatively confirming theoretical predictions of favourable stability in the NCS regime. The discharges exhibit good confinement and performance ($H_{89} = 2.5$, $H_{98}(y, 2) = 1.5$, $\beta_N = 4$), and are ultimately limited by the ideal-wall stability boundary predicted by ideal MHD theory, as long as tearing mode (TM) locking events, resistive wall modes (RWMs), and internal kink modes are properly avoided or controlled. Although the discharges exhibit rotating TMs, locking events are avoided as long as a threshold minimum safety factor value $q_{\min} > 2$ is maintained. Fast timescale magnetic feedback control ameliorates RWM activity, expanding the stable operating space and allowing access to β_N values approaching the ideal-wall limit. Quickly growing and rotating instabilities consistent with internal kink mode dynamics are encountered when the ideal wall limit is reached. Ideal MHD stability analysis predicts that the ideal-wall limit can be further increased to $\beta_N > 4$ by broadening the current profile. This path toward improved stability has the potential advantage of being compatible with the bootstrap-dominated equilibria envisioned for advanced tokamak (AT) fusion reactors.

EX



Physics of Unlocked Tearing Modes and Disruption Avoidance by Feedback-Based Electromagnetic Torque Injection

M. Okabayashi¹

¹Princeton Plasma Physics Laboratory (PPPL), Princeton, NJ 08540, USA

Corresponding Author: M. Okabayashi, mokabaya@pppl.gov

Resistive and quasilinear 3D modelling is improving the understanding of recent experiments [1] carried out in DIII-D and RFX-Mod, in which disruptions were prevented by means of electromagnetic torque applied by nonaxisymmetric (3D) coils. We will report the 3D aspects of experimental observations in comparison with finite resistivity (tearing) response by MARS-F and a time dependent torque balance simulation by MARS-Q [2]. Even though these codes are based on linear perturbation theory, many experimental observations are consistent with these 3D model predictions. One is the discovery of stable formation of a multilayered tearing structure just after avoiding the tearing mode locking. According to magnetic sensors and the internal profile perturbed signals such as toroidal rotation and ion temperature, the mode's maximum perturbation is poloidally and radially concentrated toward the poloidal angle of the control coil location. This is completely different from the ideal-MHD based RWM response, which is nearly independent of the poloidal structure of the applied 3D fields. But, the resistive (tearing) plasma response by MARS-F in the presence of finite plasma resistivity predicts precisely this type of unique poloidal features. The large flow shear observed in experiments is considered as a possible mechanism to stably sustain the multilayer structure for long duration. This flow shear buildup seems to be qualitatively consistent with the initial results of time dependent torque balance simulation with MARS-Q. The experimental results and their consistency with 3D MHD models suggest that the use of electromagnetic torque, applied by error field coils or ELM control coils, could help to avoid locked-mode disruptions in ITER.

References

- [1] M. Okabayashi, *et al.*, IAEA FEC-2014, [EX/P2-42](#) (in progress).
[2] Y. Q. Liu, *et al.*, Phys. Plasmas **20**, 042503 (2013).

Work supported in part by the U.S. Department of Energy under DE-AC02-09CH114661, DE-FC02-04ER546984, DE-FG02-04ER547615, DE-AC05-06OR231006, and DE-AC05-00OR227257.

Validating Extended MHD Models of Plasma Response against Measurements of Islands in DIII-D

M. Shafer¹, J. Canik¹, T. E. Evans², N. M. Ferraro³, S. Hirshman¹, J. Lore¹, and M. Austin⁴

¹Oak Ridge National Laboratory (ORNL), Oak Ridge, TN 37831, USA

²General Atomics, San Diego, CA 92186, USA

³Princeton Plasma Physics Laboratory (PPPL), Princeton, NJ 08540, USA

⁴University of Texas at Austin, Austin, TX 78712, USA

Corresponding Author: M. Shafer, shafermw@ornl.gov

Measurements of islands induced by resonant magnetic perturbations (RMP) in the core of a L-mode DIII-D plasma are used to challenge predicted screening trends from linearized extended MHD and to examine modelling of the nonlinearly saturated island state. In these plasmas, fine torque scans reveal that large $n = 1$ RMP-induced islands are present at multiple mode-rational surfaces at low rotation, but are completely screened at higher rotation. Understanding trends of rotational screening is crucial for predictive capability of RMP ELM control solutions. At sufficiently low torque (< 0.2 N·m), the fields form $n = 1$ island chains at $m = 2, 3, 4$. There is an observed nonlinear threshold for this torque, where small torque increments lead to a completely screened plasma response. Island formation correlates best with near-zero perpendicular electron flow, $\Omega_{e,\perp}$, at the $q = 2$ surface. These measurements are compared to linearized single-fluid and two-fluid extended MHD modelling to examine rotational screening. Simulations using the linearized extended MHD code, M3D-C1, do not find clear agreement between calculated resonant fields and observations of island dependent on $\Omega_{e,\perp}$ in contrast to previous expectations; these L-mode plasmas are predicted to have strong screening even at these values of low rotation. However, single-fluid simulations show better agreement with strong resonant field penetration at low rotation. New nonlinear resistive 3D modelling of the saturated island state is validated against these experimental island measurements. These MHD simulations in the absence of rotation are performed with the SIESTA code. A series of meta-stable equilibria are modelled with an increasing helical $2/1$ perturbation until the modelled island width matches experiment. These meta-stable equilibria demonstrate the transition from even-parity screening currents at the rational surface at low perturbation levels to odd-parity Pfirsch-Schlüter currents when a large island is present. Basic plasma response experiments challenge current modelling capability used in understanding 3D fields and also more specifically for predicting ELM control capabilities.

EX



The Contribution of Perturbation Coil Geometry Induced Sidebands and MHD Response in KSTAR and DIII-D

D. Orlov¹, T. E. Evans², R. A. Moyer¹, B. Lyons^{2,3}, N. M. Ferraro⁴, L. Sugiyama⁵, and G. Park⁶

¹University of California San Diego, CA 92093, USA

²General Atomics, San Diego, CA 92186, USA

³Oak Ridge Institute for Science Education (ORISE), Oak Ridge, TN 37831, USA

⁴Princeton Plasma Physics Laboratory (PPPL), Princeton, NJ 08540, USA

⁵Massachusetts Institute of Technology (MIT), Cambridge, MA 02139, USA

⁶National Fusion Research Institute (NFRI), Daejeon, Republic of Korea

Corresponding Author: D. Orlov, orlov@fusion.gat.com

In this work we show that the application of a “square wave” $n = 1$ toroidal perturbation on DIII-D and KSTAR leads to significant $n = 3$ toroidal sidebands. In the vacuum model, these $n = 3$ sidebands assist in creation of wide stochastic field in the edge of the plasma. In KSTAR, the $n = 3$ sideband fields create vacuum islands in the right places to extend the vacuum island overlap width to more than 25%. We have also shown that these $n = 3$ sidebands are screened less by the plasma response, and the “rational surface resonant” fields are of similar size with the main $n = 1$ fields in KSTAR. The effect of these sidebands in the RMP ELM suppression should be studied more carefully both experimentally and numerically as these sidebands may play an important role. Recent studies on DIII-D [1] have shown that RMP ELM suppression may be achieved with a reduced number of RMP coils and less total injected magnetic flux due to the increasing role of toroidal sidebands. Application of “square wave” $n = 4$ and “discretized cosine” $n = 3$ waveforms in ITER RMP coils has also shown some advantages of “square wave” waveforms as they are naturally capable to generate multiple toroidal sidebands [2]. The modelling results suggest the importance of self-consistent, nonlinear modelling of the plasma response including the full toroidal mode spectrum that is applied, since interactions among the toroidal sidebands may be important. These results also provide a hypothesis for why RMP ELM suppression with an $n = 1$ spectrum has been more difficult to achieve in DIII-D than either $n = 2$ and $n = 3$, since the kink-driven screening of the applied RMP field is more complete at $n = 1$ than $n = 2$ or 3. Finally, the direct implication for ELM suppression in ITER is that the number of coils (and hence larger toroidal mode number) should be preserved to maintain the highest margin for success.

References

- [1] D. M. Orlov, *et al.*, Nucl. Fusion **56**, 036020, (2016).
 [2] T. E. Evans, *et al.*, Nucl. Fusion **53**, 093029, (2013).



Disruption Mitigation in the Presence of Pre-Existing MHD Instabilities

D. Shirakid¹, R. S. Granetz², N. Commaux¹, L. R. Baylor¹, D. Brunner², C. M. Cooper³, N. W. Eidietis⁴, E. M. Hollmann⁵, A. Kuang², C. J. Lasnier⁶, R. A. Moyer⁵, C. Paz-Soldan⁴, R. Raman⁷, M. L. Reinke¹, R. A. Tinguely², and I. Bykov⁵

¹Oak Ridge National Laboratory (ORNL), Oak Ridge, TN 37831, USA

²Massachusetts Institute of Technology (MIT), Cambridge, MA 02139, USA

³Oak Ridge Associated Universities (ORAU), Oak Ridge, TN 37831, USA

⁴General Atomics, San Diego, CA 92186, USA

⁵University of California San Diego, CA 92093, USA

⁶Lawrence Livermore National Laboratory (LLNL), Livermore, CA 94550, USA

⁷University of Washington, Seattle, WA 98195, USA

Corresponding Author: D. Shirakid, shirakid@fusion.gat.com

Experiments on the DIII-D and Alcator C-Mod tokamaks show that disruption mitigation by massive gas injection (MGI) and shattered pellet injection (SPI) of high- Z impurities remain effective in the presence of large preexisting MHD instabilities. Rotating and locked magnetic islands will precede a large fraction of disruptions in ITER, making their impact on disruption mitigation a critical concern. Experiments on both machines show that such instabilities do not significantly impede the ability of massive impurity injection to mitigate thermal quench (TQ) and current quench (CQ) loads. On DIII-D, SPI significantly increases peak densities relative to unmitigated disruptions, indicating efficient assimilation of the injected impurities, with or without the presence of the modes. Similar results are found for MGI, on both DIII-D and C-Mod. This efficient assimilation of injected high- Z radiating impurities allows effective TQ mitigation, with enhanced radiation fractions and corresponding decreases in divertor heating, as measured by infrared imaging. MGI and SPI are able to accelerate the CQ even in the presence of preexisting MHD precursors. Reconstructions of the plasma geometry during the CQ show that vertical displacements of the plasma are reduced relative to unmitigated disruptions, for all cases with MGI or SPI, while halo current impulses and resulting vacuum vessel displacements are also significantly reduced. Peak electron density during the CQ, which is an important metric for runaway electron mitigation, is enhanced in the case of impurity injection and do not differ between stable and MHD unstable discharges. Toroidally distributed measurements of the radiated power on C-Mod indicate that radiation asymmetries during the disruption are not significantly higher in plasmas with locked modes. This result implies that measured radiation asymmetries are likely driven by MHD activity which is initiated by the impurity injection process itself, rather than by the predisruption instabilities. Overall, these results on DIII-D and C-Mod increase confidence in the existing physics basis for disruption mitigation, and the resulting design of the ITER disruption mitigation system.

Work supported by the U.S. Department of Energy under DE-AC05-00OR22725, DE-FC02-99ER54512, DE-FC02-04ER54698, DE-FG01-07ER54917, DE-AC52-07NA27344 and DE-SC0006757.



Adaptive Real-Time Pedestal Control for DIII-D and Prospects for ITER

E. Kolemen¹, D. Eldon¹, A. Bortolon², T. E. Evans³, M. Fenstermacher⁴, B. A. Grierson², D. A. Humphreys³, O. Meneghini³, C. Paz-Soldan³, and E. A. Unterberg⁵

¹Princeton University, Princeton, NJ 08544, USA

²Princeton Plasma Physics Laboratory (PPPL), Princeton, NJ 08540, USA

³General Atomics, San Diego, CA 92186, USA

⁴Lawrence Livermore National Laboratory (LLNL), Livermore, CA 94550, USA

⁵Oak Ridge National Laboratory (ORNL), Oak Ridge, TN 37831, USA

Corresponding Author: E. Kolemen, ekolemen@princeton.edu

EX A comprehensive adaptive real-time (rt) ELM control system that exploits key properties of ELM physics, Resonant Magnetic Perturbation (RMP) ELM suppression physics, and an extensive set of diagnostic inputs to make rt decisions about the control of multiple actuators to sustain ELM suppression/mitigation is demonstrated at DIII-D. The control experiments showed the path dependence and hysteresis of plasma recovery: even for the same final perturbing 3D currents, starting with higher initial 3D currents leads to lower recovery down the path. This demonstrates the need for a control system to keep the ITER RMP perturbations close to the ELM suppression threshold at all times. The development at DIII-D initiates progress toward adaptive pedestal control, and includes pedestal profile control as well as ELM suppression or mitigation. The 3D coil configuration and phasing for RMP ELM suppression is adjusted in real-time based on SURFMN calculations of the vacuum edge pitch-resonant, and kink-resonant harmonics of the applied 3D magnetic perturbation and offline IPEC data. The amplitude of the 3D coils is regulated to achieve a given ELM frequency (or none) using ELM detection based on the D_α measurements from the divertor region. For pedestal control, the plasma control system (PCS) acquires rt Thomson scattering diagnostic data and fits the pedestal width and height for temperature and density profiles. Based on the Thomson fits, PCS regulates the pedestal density by adjusting the gas-puffing rate to increase particle source and RMP density “pump-out” to reduce it. Real-time pedestal stability boundary calculation using a neural network based on EPED1 runs, and a real-time pellet injection control for turn-on and turn-off timing and ELM frequency are under development. These developments at DIII-D pave the way for ITER adaptive pedestal control.



Experiments on Helicons in DIII-D: Investigation of the Physics of a Reactor-Relevant Noninductive Current Drive Technology

R. I. Pinsker¹, R. Prater¹, C. P. Moeller¹, J. deGrassie¹, C. C. Petty¹, M. Porkolab², J. K. Anderson¹, J. A. Boedo³, X. Chen¹, A. M. Garofalo¹, C. Lau⁴, A. Nagy⁵, D. C. Pace¹, H. Torreblanca¹, J. G. Watkins⁶, and L. Zeng⁷

¹General Atomics, San Diego, CA 92186, USA

²Massachusetts Institute of Technology (MIT), Cambridge, MA 02139, USA

³University of California San Diego, CA 92093, USA

⁴Oak Ridge National Laboratory (ORNL), Oak Ridge, TN 37831, USA

⁵Princeton Plasma Physics Laboratory (PPPL), Princeton, NJ 08540, USA

⁶Sandia National Laboratories (SNL), Albuquerque, NM 87185, USA

⁷University of California Los Angeles, CA 90095, USA

Corresponding Author: R. I. Pinsker, pinsker@fusion.gat.com

Experiments have begun in DIII-D to evaluate noninductive current drive by the Landau absorption of a toroidally-directive spectrum of helicon waves (also known as “very high harmonic fast waves”, “fast waves in the lower hybrid range of frequencies”, or “whistlers”). Modelling has shown [1] that noninductive current drive at midradius ($\rho \sim 0.5$) should be achievable in DIII-D with fast waves at 0.5 GHz, with an efficiency twice as high as with noninductive current drive tools currently available on DIII-D (neutral beams and electron cyclotron current drive) in high- β conditions. An innovative Travelling Wave Antenna (TWA) of the “comb-line” type with 12 radiating modules has been constructed, installed in DIII-D, and is currently being tested at very low power (< 1 kW) to evaluate the antenna coupling in the linear regime, and to prototype technological aspects of such structures in the tokamak environment. Preliminary results indicate strong antenna-plasma coupling, with detailed 3D modelling underway to quantitatively compare the measurements with theoretical expectations. A key input to this model is the edge and far SOL electron density profile, which is being measured with a microwave reflectometer and with fixed and movable Langmuir probes. An important issue for wave coupling in this regime is the degree to which (undesired) quasi-electrostatic slow waves are excited by the structure; evaluation of this is a point of emphasis in the ongoing work. A high-power system is presently being prepared for installation later in 2016 in which a single 1.2 MW klystron at 476 MHz will be used to power a TWA with ~ 36 radiating elements in a structure 2 m wide. The goals of the high-power experiments include evaluation of nonlinear effects on excitation of the desired waves (ponderomotive effects, parametric decay) and measurements of the deposition profile and of the current drive efficiency. Ray-tracing predicts [1] an RF-driven current of ~ 60 kA per coupled MW of helicon power, which should result in an easily measurable driven current in DIII-D in high- β discharges.

References

[1] R. Prater, *et al.*, Nucl. Fusion **54**, 083024 (2014).

Work supported in part by the U.S. Department of Energy under DE-FC02-04ER54698, DE-FG02-94ER54084, DE-FG02-07ER54917, DE-AC05-00OR22725, DE-AC02-09CH11466, DE-AC04-94AL85000, DE-FG02-08ER54984.

Improved Reproducibility of Plasma Discharges via Physics-Model-Based q -Profile Feedback Control in DIII-D

E. Schuster¹, J. E. Barton¹, W. P. Wehner¹, M. D. Boyer¹, T. C. Luce², J. R. Ferron², C. T. Holcomb³, M. L. Walker², D. A. Humphreys², W. M. Solomon⁴, B. G. Penaflor², and R. D. Johnson²

¹Lehigh University, Bethlehem, PA 18015, USA

²General Atomics, San Diego, CA 92186, USA

³Lawrence Livermore National Laboratory (LLNL), Livermore, CA 94550, USA

⁴Princeton Plasma Physics Laboratory (PPPL), Princeton, NJ 08540, USA

Corresponding Author: E. Schuster, schuster@lehigh.edu

Recent experiments on DIII-D demonstrate the potential of physics-model-based q -profile control to improve reproducibility of plasma discharges. A combined feedforward+feedback control scheme was employed to optimize the current ramp-up phase by consistently achieving target q profiles (Target 1: $q_{\min} = 1.3$, $q_{95} = 4.4$; Target 2: $q_{\min} = 1.65$, $q_{95} = 5.0$; Target 3: $q_{\min} = 2.1$, $q_{95} = 6.2$) at prescribed times during the plasma formation phase (Target 1: $t = 1.5$ s; Target 2: $t = 1.3$ s; Target 3: $t = 1.0$ s). At the core of the control scheme is a nonlinear, first-principles-driven, physics-based, control-oriented model of the plasma dynamics valid for low confinement (L-mode) scenarios. A partial-differential-equation model of the q -profile dynamics combines the poloidal magnetic flux diffusion equation with physics-based models of the electron density and temperature profiles, the plasma resistivity, and the noninductive current sources (auxiliary and bootstrap). Firstly, a nonlinear, constrained optimization algorithm to design feedforward actuator trajectories is developed with the objective of numerically complementing the traditional trial-and-error experimental effort of advanced scenario planning. The goal of the optimization algorithm is to design actuator trajectories that steer the plasma to the target q profile at a predefined time subject to the plasma dynamics and practical plasma state and actuator constraints, such as the minimum q value and the maximum available auxiliary heating and current-drive (H&CD) power. To prevent undesired L-H transitions, a constraint on the maximum allowable total auxiliary power is imposed in addition to the maximum powers for the individual H&CD actuators. Secondly, integrated feedback control algorithms are designed to keep the q -profile evolution on track by countering the effects of external plasma disturbances, thereby adding robustness to the control scheme. The H&CD system and the total plasma current are the actuators utilized by the feedback controllers to control the plasma dynamics. Experimental results are presented to demonstrate the effectiveness of the combined feedforward+feedback control scheme to consistently achieve the desired target profiles at the predefined times. These results also show how the addition of feedback control significantly improves upon the feedforward-only solution by reducing the matching error.



Electron Cyclotron Heating Modification of Alfvén Eigenmode Activity in DIII-D

M. A. Van Zeeland¹, W. W. Heidbrink², S. E. Sharapov³, D. Spong⁴, Á. Cappa⁵, X. Chen¹, C. Collins², M. Garcia-Munoz⁶, N. N. Gorelenkov⁷, G. J. Kramer⁷, P. Lauber⁶, Z. Lin², D. C. Pace¹, and C. C. Petty¹

¹General Atomics, San Diego, CA 92186, USA

²University of California Irvine, CA 92697, USA

³Culham Centre for Fusion Energy (CCFE), Culham Science Centre, Abingdon, UK

⁴Oak Ridge National Laboratory (ORNL), Oak Ridge, TN 37831, USA

⁵Laboratorio Nacional de Fusión (LNF),

Centro de Investigaciones Energéticas, Medioambientales y Tecnológicas (CIEMAT), Madrid, Spain

⁶Max-Planck-Institut für Plasmaphysik, Garching, Germany

⁷Princeton Plasma Physics Laboratory (PPPL), Princeton, NJ 08540, USA

Corresponding Author: M. A. Van Zeeland, vanzeeland@fusion.gat.com

Localized electron cyclotron heating (ECH) can have a dramatic impact on neutral beam driven Alfvén eigenmode (AE) activity in DIII-D plasmas. The most common effect, which is explained here for the first time, is a shift in the dominant observed modes from a mix of reversed shear Alfvén eigenmodes (RSAEs) and toroidicity induced Alfvén eigenmodes (TAEs) to a spectrum of weaker TAEs when ECH is deposited near the shear reversal point, q_{\min} . Discharges with weaker RSAE activity also have reduced fast ion transport. A recent experiment to understand the physical mechanisms responsible for this shift in AE stability included variations of ECH steering, power, and timing as well as current ramp rate, beam injection geometry, and beam power. All variations were observed to change the impact of ECH on AE activity significantly. In some cases, RSAE activity was enhanced with ECH near q_{\min} as opposed to near the axis, in contrast to the original DIII-D experiments [1]. It is found that during intervals when the geodesic acoustic mode (GAM) frequency at q_{\min} is elevated and the calculated RSAE minimum frequency is very near or above the nominal TAE frequency (f_{TAE}), RSAE activity is not observed or RSAEs with a much reduced frequency sweep range are found. This condition is primarily brought about by ECH modification of the local electron temperature (T_e) which can raise both the local T_e at q_{\min} as well as its gradient. A q -evolution model that incorporates this reduction in RSAE frequency sweep range is in agreement with the observed spectra and appears to capture the relative balance of TAE or RSAE-like modes throughout the current ramp phase of over 38 DIII-D discharges. Detailed ideal MHD calculations using the NOVA code show both modification of plasma pressure and pressure gradient at q_{\min} play an important role in modifying the RSAE activity. Analysis of a case with ECH near q_{\min} , and no observable RSAE activity, shows the traditional RSAE is no longer an eigenmode of the system. Calculations with the nonperturbative gyro fluid code TAEFL confirms this change in RSAE activity and also shows a large drop in the resultant mode growth rates.

References

[1] M. A. Van Zeeland, *et al.*, Plasma Phys. Control. Fusion **50**, 035009 (2008).

Work supported by the U.S. Department of Energy under DE-FC02-04ER54698, SC-G903402, DE-AC05-00OR22725, and DE-AC02-09CH11466.

Robust H-Mode Pedestal Compatibility with SOL and Divertor Plasma Constraints

A. W. Leonard¹, R. Groebner¹, M. A. Makowski², A. McLean², A. Moser¹, T. H. Osborne¹, and P. C. Stangeby³

¹General Atomics, San Diego, CA 92186, USA

²Lawrence Livermore National Laboratory (LLNL), Livermore, CA 94550, USA

³Institute for Aerospace Studies, University of Toronto, Toronto, ON M5S-1A1, Canada

Corresponding Author: A. W. Leonard, leonard@fusion.gat.com

EX Experiments on DIII-D have advanced the physics basis for simultaneously achieving a high pressure H-mode pedestal for high core plasma confinement with a highly dissipative divertor for protection of plasma facing components in future reactor tokamaks. These studies show achievement of this goal is governed by the coupling of several pedestal and divertor processes including: 1) the pedestal density profile dependence on the recycling neutral ionization source, 2) the separatrix density required to achieve strong divertor dissipation for high power exhaust, 3) the direct effect of dissipative divertor operation on pedestal performance, and 4) maintaining adequate power flux across the separatrix for robust H-mode confinement. A closed divertor configuration is shown to reduce the core plasma density, even for divertor detachment onset, due to a reduction in the pedestal ionization source. The separatrix density is found to increase with power, resulting in a variation in the accessible ratio of separatrix to pedestal top density. Robust pedestal pressure is found compatible with dissipative divertor operation, as long as collisionality remains low enough for optimal MHD stability, and core radiation from impurity seeding is limited to maintain sufficient power flux across the separatrix. The results suggest that a robust pedestal may be compatible with highly dissipative divertor operation for the lower core collisionality expected in future larger tokamaks. Taken together the pedestal requirements imply that innovative divertor solutions will be required to obtain dissipative operation at lower core density as future tokamaks scale to larger size and higher field.

Work supported by the U.S. Department of Energy under DE-FC02-04ER546981, DE-AC52-07NA273442.

SOL Effects on the Pedestal Structure in DIII-D Discharges

A. Sontag¹, X. Chen², J. Canik¹, A. W. Leonard², J. Lore¹, A. Moser², M. Murakami¹,
J. Park¹, and C. C. Petty²

¹Oak Ridge National Laboratory (ORNL), Oak Ridge, TN 37831, USA

²General Atomics, San Diego, CA 92186, USA

Corresponding Author: A. Sontag, sontagac@ornl.gov

Core transport models predict that fusion power scales roughly as the square of the pressure at the top of the pedestal, so understanding the effects that determine pedestal structure in steady-state operational scenarios is important to project steady-state tokamak operational scenarios developed in DIII-D to ITER and other devices. Both experiments and modelling indicate that SOL conditions are important in optimizing the pedestal structure for high- β steady-state scenarios. The SOLPS code [1] is used to provide interpretive analysis of the pedestal and SOL to examine the impact of flows and fuelling on the pedestal structure, including the effects of drifts in the fluid model. This analysis shows that flows driven by the ∇B drift are outward when this drift is toward the X-point (favourable ∇B direction) and inward when the drift is away from the X-point (unfavourable ∇B direction). It is hypothesized that these flows will decrease the density gradient in the pedestal in the favourable direction, thereby stabilizing the KBM and increasing the pedestal width. Comparisons of pedestal structures in similarly shaped DIII-D steady-state plasmas confirm this change, showing increased density pedestal width but lower peak density with favourable drift direction. The pedestal temperature is higher in the lower density case, indicating that the change in particle confinement does not impact energy confinement. Modelling of cases with constant ∇B drift but changing between the more open lower divertor and more closed upper divertor show that there is increased fuelling inside the pedestal with the more open geometry. The cases with increased pedestal fuelling show increased pedestal height with similar pedestal width. The pedestal fuelling rate for both attached and detached cases is always lower with more closed divertor geometry than in any cases with more open geometry.

References

[1] R. Schneider, *et al.*, *Contrib. Plasma Phys.* **46**, 3 (2006).

Work supported by the U.S. Department of Energy under DE-AC05-00OR22725, and DE-FC02-04ER54698.

Edge, Divertor and Plasma Behaviour in High-Power High-Performance Double-Null Plasmas

T. W. Petrie¹, S. Allen², M. Fenstermacher², H. Guo¹, J. R. Ferron¹, R. Groebner¹, C. T. Holcomb², C. J. Lasnier², A. W. Leonard¹, T. C. Luce¹, A. McLean², M. A. Makowski², T. H. Osborne¹, D. C. Pace¹, W. M. Solomon³, F. Turco⁴, M. A. Van Zeeland¹, and J. G. Watkins⁵

¹General Atomics, San Diego, CA 92186, USA

²Lawrence Livermore National Laboratory (LLNL), Livermore, CA 94550, USA

³Princeton Plasma Physics Laboratory (PPPL), Princeton, NJ 08540, USA

⁴Columbia University, New York, NY 10027, USA

⁵Sandia National Laboratories (SNL), Albuquerque, NM 87185, USA

Corresponding Author: T. W. Petrie, petrie@fusion.gat.com

We identify major challenges to reducing divertor heat flux in high power, high performance near-double null DIII-D plasmas, while still maintaining sufficiently low density to allow for application of RF heating. The plasmas discussed here are characterized by: $\beta_N \approx 3-4$, $H_{98} \approx 1.5-1.7$, $dR_{SEP} \approx -5$ mm, and P_{IN} up to 20 MW. The scaling of the peak heat flux ($q_{\perp p}$) at the outer target of the primary divertor was proportional to $P_{SOL}^{0.92}$ and $I_p^{0.92}$ in the range $P_{SOL} = 8-19$ MW and $I_p = 1.0-1.4$ MA and is consistent with standard ITPA scaling for single null configurations.

Three distinct divertor heat flux reduction techniques were tested. First, the puff-and-pump radiating divertor was less effective in reducing divertor heat flux when β_N was raised to 3.7 than occurred for lower values of β_N and P_{IN} . In the higher β_N case, gas puffing during puff-and-pump resulted in an increase in τ_E and τ_p and led to more rapid fuelling of the core. This set an upper limit on the D₂ injection rate that can be tolerated without losing density control, thereby undermining the effectiveness of puff-and-pump. We are investigating how a decrease in ELMing frequency during D₂ injection at higher power and β_N may drive this process. Second, increasing the poloidal flux expansion at the outer target of the primary divertor did not produce the expected reduction in $q_{\perp p}$ that would have been expected from geometrical arguments, e.g., almost doubling the poloidal flux expansion reduced $q_{\perp p}$ by only $\sim 20\%$. Preliminary analysis suggests that cross-field diffusion effects appear to counteract poloidal flux expansion. Third, we show how $q_{\perp p}$ was reduced by 25-50% when an open divertor is closed on the common flux side of the outer divertor target ("semislot" divertor). Steady carbon buildup in the main plasma became significant during higher P_{IN} operation, and was largely due to sputtered carbon from graphite tiles on the horizontal surface above the pumping plenum entrance (and not from the "divertor" floor). Our results strongly suggest the necessity of further study before relying on either radiating divertor or poloidal flux expansion to adequately control divertor heat flux in high power, high performance DN plasmas.

Work supported by the U.S. Department of Energy under DE-FC02-04ER54698, DE-AC52-007NA27344, DE-AC02-09CH11466, DE-FG02-04ER54761, and DE-AC04-94AL85000.

X-Divertors for Facilitating Detachment without Degrading the DIII-D H-Mode

B. Covele¹, M. Kotschenreuther², P. Valanju³, S. Mahajan³, A. W. Leonard¹, H. Guo¹,
D. Hill⁴, M. Fenstermacher⁴, A. McLean⁴, and J. G. Watkins⁵

¹General Atomics, San Diego, CA 92186, USA

²Institute for Fusion Studies (IFS), University of Texas at Austin, Austin, TX 78712, USA

³University of Texas at Austin, Austin, TX 78712, USA

⁴Lawrence Livermore National Laboratory (LLNL), Livermore, CA 94550, USA

⁵Sandia National Laboratories (SNL), Albuquerque, NM 87185, USA

Corresponding Author: B. Covele, covelebm@utexas.edu

Highly flared, highly flux-expanded X-Divertors (XDs) on DIII-D detached at a lower Greenwald fraction and higher pedestal pressure than standard divertors (SDs), strongly reducing problematic plasma exhaust at the target, allowing for improved control of the detachment front, and maintaining a higher-confinement H-mode necessary for a future fusion reactor. XDs exhibit lower parallel ion fluxes to the target than the SD, as evidenced by probe ion saturation currents. Because the fluxes calculated are field-parallel fluxes, their reduction in the XD cannot be explained by projection due to flux expansion alone. C-III emission images illustrate the differences in detachment evolution between XDs and SDs, where the XD temperature front is seen moving away from the target for lower pedestal densities and higher pedestal pressures. SOLPS models support the notion of an XD-stabilized detachment front. Poloidal profiles of model electron temperatures show that XDs achieve very low temperatures at the target, while still maintaining high temperatures near the X-point, “insulating” the core from the target. This temperature gradient indicates resistance to upstream migration of the detachment front, preventing core confinement loss and X-point MARFEs. Achieving stable detachment for less gas puffing, lower Greenwald fraction, and higher H-mode pedestal pressure will be critical to satisfy simultaneously the needs for good core performance and effective divertor heat load mitigation, in ITER and a future reactor. X-Divertors lower the puffing threshold for stable detachment magnetically, by increasing the electron/ion path length through the neutral-dense region at the target, and increasing plasma-neutral dissipative reaction rates. In this way, X-Divertors may offer a simple, magnetic solution to the problem of robust, detached divertor operation.

EX

Controlling Marginally Detached Divertor Plasmas

D. Eldon¹, E. Kolemen¹, D. A. Humphreys², A. W. Leonard², A. McLean³, A. Moser², and P. C. Stangeby⁴

¹Princeton University, Princeton, NJ 08544, USA

²General Atomics, San Diego, CA 92186, USA

³Lawrence Livermore National Laboratory (LLNL), Livermore, CA 94550, USA

⁴Institute for Aerospace Studies, University of Toronto, Toronto, ON M5S-1A1, Canada

Corresponding Author: D. Eldon, deldon@princeton.edu

EX A new control system at DIII-D has stabilized the detached divertor plasma state in close proximity to the threshold for reattachment, thus demonstrating ability to maintain detachment with minimum gas puffing. When the same control system was instead ordered to hold the plasma at the threshold, the resulting T_e profiles separated into two groups with one group consistent with marginal detachment, and the other with marginal reattachment. This shows that a physical bifurcation is taking place, and the plasma dithers between the attached and detached states when the control system attempts to hold to the threshold. The control system is upgraded from the one described by Kolemen, *et al.* [1], and it handles ELMing plasmas by using real time D_α measurements to remove during-ELM slices from real time T_e measurements derived from Thomson scattering. The difference between measured and requested inter-ELM T_e is passed to a PID controller to determine gas puff commands. While some degree of detachment is essential for the health of ITER's divertor, more detached plasmas come at higher density with more radiation and excessive loss in confinement, making it desirable to limit detachment to the minimum level needed to protect the strike point [1]. However, the observed bifurcation in plasma conditions at the outer strike point with ion $B \times \nabla B$ into the divertor makes this a significant challenge. The ideal solution without local impurity puffing lies within a narrow (3%) range in upstream density with a steep penalty for going out of bounds; if the divertor plasma were to reattach, there could be a long (depending on delays in the gas puff system) window of high heat flux before detachment could be re-established. Thus, good understanding of detachment behaviour near the threshold for reattachment is required to properly tune an active control system to maintain ideal divertor performance without reattaching. The top-of-pedestal electron densities during dithering across the bifurcation and during stable marginally detached operation are the same within uncertainty, showing the need for local real-time measurements of the divertor conditions.

References

[1] E. Kolemen, *et al.*, J. Nucl. Mater. **463**, 1186 (2014).

Snowflake Divertor Configuration Effects on Pedestal Stability and Edge Localized Modes in NSTX and DIII-D

V. Soukhanovskii¹, S. Allen¹, M. Fenstermacher¹, C. J. Lasnier¹, M. A. Makowski¹, A. McLean¹, D. Ryutov¹, F. Scotti¹, E. Kolemen², R. E. Bell², A. Diallo², S. P. Gerhardt², R. Kaita², S. Kaye², B. LeBlanc², R. Maingi², J. Menard², M. Podestá², R. Groebner³, A. W. Hyatt³, A. W. Leonard³, T. H. Osborne³, T. W. Petrie³, R. Raman⁴, and J. G. Watkins⁵

¹Lawrence Livermore National Laboratory (LLNL), Livermore, CA 94550, USA

²Princeton Plasma Physics Laboratory (PPPL), Princeton, NJ 08540, USA

³General Atomics, San Diego, CA 92186, USA

⁴University of Washington, Seattle, WA 98195, USA

⁵Sandia National Laboratories (SNL), Albuquerque, NM 87185, USA

Corresponding Author: V. Soukhanovskii, vlad@llnl.gov

Analyses of snowflake (SF) divertor experiments in NSTX and DIII-D show that the SF divertor can increase edge magnetic shear and modify pressure profiles of the H-mode pedestal enabling pedestal stability control while maintaining good H-mode confinement ($H_{98}(y, 2) \sim 1$). The scrape-off layer (SOL) geometry modifications lead to reduced peak temperature of plasma-facing components (PFC) via significant additional dissipation and partitioning of ELM heat fluxes between additional strike points. In NSTX, where pedestal stability operating condition was close to the kink/peeling boundary with the standard divertor and lithium conditioning, the SF divertor formation led to destabilization of large ELMs and a concomitant reduction of carbon concentration by 30–50% in the pedestal. In DIII-D, kinetic profiles were weakly affected by the SF configuration; a reduction in energy lost per ELM was observed and the ELM frequency was slightly increased. Planned linear MHD stability calculations will help understand the SF effects that appeared to depend on pedestal stability operating point. A reduction of ELM-induced divertor peak temperature T_{surf} (and heat flux) in the SF divertor (cf., standard divertor) was observed in both NSTX and DIII-D experiments. The divertor ELM energy density in the SF configuration (cf., standard divertor) is reduced due to a combination of increased ELM ion transit time, power splitting between additional SF strike points, and additional dissipative losses, which are especially large in the high-density radiative SF divertor. The observed pedestal and SOL modifications are generally beneficial, and can be further developed into ELM control scenarios and ELM mitigation techniques.

Work performed under the auspices of the U.S. Department of Energy under DE-AC52-07NA27344.



Robust Estimation of Tokamak Energy Confinement Scaling through Geodesic Least Squares Regression

G. Verdoolaege¹

¹*Ghent University, 9000 Ghent, Belgium*

Corresponding Author: G. Verdoolaege, geert.verdoolaege@ugent.be

The standard scaling law for the global energy confinement in H-mode tokamak plasmas provides a guideline for machine design and planning of operational scenarios. In addition, it is used as a benchmark to assess the quality of confinement in present experiments. However, owing to the complexity of the multimachine data sets from which the scaling is derived, the coefficient estimates may vary considerably, depending on the regression method used to establish the fit. This necessitates a robust analysis of the confinement scaling law. For this purpose we have developed a new regression technique that is robust in the presence of significant uncertainty on all variables as well as the regression model, and that can handle outliers in the data. The technique, called geodesic least squares regression (GLS), is shown to yield consistent results in estimating the confinement scaling, in contrast to standard ordinary least squares (OLS). Furthermore, some of the coefficients estimated by GLS are significantly different from those given by OLS, particularly those corresponding to the geometrical properties of the plasma. Furthermore, the method is shown to enable direct estimation of the scaling in terms of physical dimensionless variables. Hence, GLS is a powerful regression method that is able to deliver the level of robustness required for scaling in multimachine databases, and in general in situations with limited knowledge about the regression model or substantial measurement uncertainty on all variables. The method is easily implemented and is hoped to be also of use in many other applications involving regression analysis in fusion science.

EX



Results from the Sheared-Flow Stabilized Z-Pinch and Scaling to Fusion Conditions

U. Shumlak¹, H. McLean², B. Nelson¹, A. Schmidt², R. Golingo¹, E. Claveau¹, M. Hughes¹, M. Ross¹, J. Barhydt¹, D. Caudle¹, E. Forbes¹, B. Kim¹, L. Su¹, R. Townsend¹, K. Tummel², and T. Weber¹

¹University of Washington, Seattle, WA 98195, USA

²Lawrence Livermore National Laboratory (LLNL), Livermore, CA 94550, USA

Corresponding Author: U. Shumlak, shumlak@uw.edu

The sheared-flow stabilized Z-pinch has been experimentally demonstrated to produce long-lived plasmas that satisfy radial force balance and are stable for thousands of exponential growth times. The sheared-flow stabilized Z-pinch has the potential to lead to a compact plasma confinement device that scales to fusion conditions. The stabilizing effect of a sheared axial flow on the $m = 1$ kink instability in Z-pinch has been studied using ideal MHD theory to reveal that a sheared axial flow stabilizes the kink mode when the shear exceeds a threshold value. Following these theoretical results, the ZaP Flow Z-Pinch group at the University of Washington has been experimentally investigating the connection between flow shear and gross plasma stability. Plasma stability is diagnosed with azimuthal arrays of magnetic probes that measure the plasma's magnetic structure. Large magnetic fluctuations occur during pinch assembly, after which the amplitude and frequency of the magnetic fluctuations diminish. This stable behaviour continues for an extended quiescent period. Plasma flow profiles are measured from the Doppler shift of plasma impurity lines. The experimental flow shear exceeds the theoretical threshold during the quiescent period. Scaling relations suggest that high energy density plasma and fusion conditions are possible in a compact design. Recent experiments with the upgraded ZaP-HD device have demonstrated the ability to increase the plasma parameters by compressing the plasma radius to smaller values than achieved with the ZaP device. Based on the successful results of ZaP and ZaP-HD, a new experiment FuZE is designed to scale the plasma parameters to fusion conditions. The project will focus on furthering our understanding of the physics with specific emphasis on the limitations of sheared flow stabilization and on the importance of kinetic effects at large drift speeds.

EX

Applying the New Principles of Plasma Self-Organization to Tokamak

T. Jarboe¹, D. Sutherland¹

¹*University of Washington, Seattle, WA 98195, USA*

Corresponding Author: T. Jarboe, jarboe@aa.washington.edu

Understanding sustainment of stable equilibria with helicity injection in HIT-SI has led to a simple picture of several tokamak features. Perturbations cause a viscous-like force on the current that flattens the j/B profile, which sustains and stabilizes the equilibrium. An explanation of the mechanism is based on the two properties of stable, ideal, two-fluid, magnetized plasma. First, the electron fluid is frozen to magnetic fields and, therefore, current flow is also magnetic field flow. Second, for a stable equilibrium the structure perpendicular to the flux surface resists deformation. This mechanism provides an explanation for the level of field error that spoils tokamak performance, the rate of poloidal flux loss in argon-induced disruptions in DIII-D, why transport barriers depend on the $E \times B$ shearing rate, and why a divertor may help in forming a pedestal.

Work supported by the U.S. Department of Energy Office of Science, Office of Fusion Energy Sciences under Award No. DE-FG02-96ER54361.



Observation of an Isothermal Electron Temperature Profile with Low Recycling Lithium Walls in LTX

R. P. Majeski¹

¹*Princeton Plasma Physics Laboratory (PPPL), Princeton, NJ 08540, USA*

Corresponding Author: R. P. Majeski, rmajeski@pppl.gov

Discharges with high edge electron temperatures and flat radial electron temperature profiles, extending to the last closed flux surface, and into the low field side scrape-off layer, have now been achieved in the Lithium Tokamak eXperiment (LTX), with lithium-coated walls. Flat temperature profiles are a long-predicted consequence of low recycling boundary conditions [1]. Temperature profiles are measured in repeated discharges with Thomson scattering; data from several discharges is averaged at each time point to improve accuracy at low density. Modelling indicates that the ion temperature profiles are also flat, which should eliminate temperature gradient-driven instabilities. The confined plasma therefore appears to be (separately) isothermal in the electron and ion populations. The edge density is very low, with a density profile which decreases approximately linearly with the poloidal flux. So far experiments are transient. Gas puffing is used to increase the plasma density. After gas injection stops, the discharge density is allowed to drop, and the edge is pumped by the low recycling lithium wall. The core impurity content, even in low density plasmas without fuelling, and edge electron temperatures of 200 eV, remains low. Z_{eff} is approximately 1.5, with most of the increase from oxygen, followed by carbon. The smallest fraction of the Z_{eff} increase, especially in the core, is from lithium. An upgrade to LTX, which includes a 35 A, 20 kV neutral beam injector to provide core fuelling and auxiliary heating, is underway. Two beam systems have been loaned to LTX by Tri Alpha Energy. With core fuelling provided by the neutral beam, an equilibrium similar to the “Isomak” [2] — a tokamak discharge in thermodynamic equilibrium — may be accessible in LTX, for the first time. A widened operational window, in both toroidal field and plasma current, is also planned, as well as eventual operation in diverted geometry. Results from the most recent experimental campaign will be described, as well as the upgraded configuration of LTX.

References

- [1] S. Krasheninnikov, L. Zakharov, G. Pereverzev, *Phys. Plasmas* **10**, 1678 (2003).
- [2] P. Catto and R. Hazeltine, *Phys. Plasmas* **13**, 122508 (2006).

Work supported by the U.S. Department of Energy contracts DE-AC02-09CH11466 and DE-AC05-00OR22725.

Compact Fusion Energy Based on the Spherical Tokamak

A. Sykes¹, A. Costley¹, M. Gryaznevich¹, P. Buxton¹, V. Chuyanov¹, J. Connor¹,
B. Huang¹, J. Hugill¹, D. Kingham¹, Y. Krivchenkov¹, G. Morgan², P. Noonan¹,
V. Shevchenko¹, G. Smith³, and C. Windsor¹

¹Tokamak Energy Ltd, Abingdon, UK

²Culham Electromagnetics Ltd., Abingdon OX14 3DB, UK

³Department of Materials, University of Oxford, Oxford, UK

Corresponding Author: A. Sykes, alan.sykes@tokamakenergy.co.uk

Tokamak Energy Ltd., UK, is developing spherical tokamaks (STs) using High Temperature Superconductor (HTS) magnets as a route to fusion power based on high gain, small size power plants. The paper presents an overview of the continuing advances in technology and modelling, which, together with key engineering developments, support this concept. The ST achieved recognition as a high- β plasma research device with many desirable properties. To date it has been shown to be viable as a compact fusion neutron source and component test facility, but not as a viable route to fusion power because of the inefficiency of driving high current in a slender copper centre column. However, significant new advances change the situation substantially. In particular the latest YBCO high temperature superconductors (HTS) are now proven to be able to carry large currents in strong magnetic fields in a very compact centre post. Innovative designs of neutron shielding indicate that relatively thin shields could give sufficient protection to an HTS core under significant neutron bombardment, and new engineering designs of the HTS centre column indicate tolerable stresses. Further, recent modelling has shown that, under reasonable operating conditions, tokamak pilot plants and reactors have a power gain Q_{fus} that is only weakly dependent on size, but depends on fusion power as $Q_{\text{fus}} \sim P_{\text{fus}} H^2$ where H is the confinement factor relative to ITER empirical scalings. For several reasons — including use of a β -independent confinement scaling demonstrated as being more appropriate than the IPB₀₈(y , 2) scaling — STs should achieve a specified Q_{fus} at considerably reduced P_{fus} , reducing wall and divertor loading. These innovations introduce the possibility of a superconducting ST Pilot Plant which can be much smaller than the designs previously considered. An example is given of a low-cost compact fusion pilot plant based on an ST of major radius 1.35 m and fusion power 150–200 MW with $Q_{\text{fus}} = 1$ –10, dependent on the confinement achieved. Higher gain versions would be developed from the insight gained and a fusion power plant would then consist of 10 or so of these modules. This approach offers significant advantages, not least that the small scale of the prototype modules should lead to rapid development at relatively low cost.

Compact Toroid Injection Fuelling on a Large-sized Field-Reversed Configuration

T. Asai¹, T. Matsumoto¹, T. Roche², I. Allfrey², H. Gota², J. Sekiguchi¹, T. Edo¹, E. Garate², T. Takahashi¹, M. Binderbauer², and T. Tajima³

¹*Nihon University, Tokyo, Japan*

²*Tri Alpha Energy, Foothill Ranch, CA 92688, USA*

³*University of California Irvine, CA 92697, USA*

Corresponding Author: T. Asai, asai.tomohiko@nihon-u.ac.jp

A repetitively driven compact toroid (CT) injector has been developed for large-sized field-reversed configuration (FRC) facility of the C-2/C-2U primarily for refuelling. Pursuit of the FRC as fusion reactor is motivated by highly favourable technological features: extremely high- β ($> 50\%$), a natural divertor, and axial mobility allowing separation of start-up and confinement functions. Recently, high confinement performance of FRC has been achieved on the C-2/C-2U facility by neutral beam injection (NBI). However, development of effective fuelling method remains as a significant task of FRC fusion reactor core. A CT is formed and injected by a magnetized coaxial plasma gun (MCPG) exclusively developed for the C-2/C-2U FRC. It consists of a set of coaxial cylindrical electrodes, a bias coil and four gas injection ports which are arranged tangentially on the outer electrode. The inner electrode is coated by tungsten to reduce impurity influx. A plasma ring is generated within a gap between the electrodes and is accelerated by Lorentz self-force. During this acceleration process, toroidal current is induced by a poloidal flux interlinked with the plasma ring. Then, the magnetized spheromak-like CT is ejected from the MCPG. To refuel the particles of long-lived FRCs, multiple CT injection is required. Thus, a multistage discharge circuit has been developed for multipulsed CT injection. Drive frequency of this system can be adjusted up to 1 kHz and the number of CT shots per injector is 2; the system can be further upgraded for larger number of injection pulses. The developed MCPG has achieved supersonic ejection velocity in the range of ~ 100 km/s. Key plasma parameters of electron density, electron temperature and the number of particles are $\sim 5 \times 10^{21}/\text{m}^3$, ~ 40 eV, and $0.5\text{--}1.0 \times 10^{19}$, respectively. In this project, single and double pulsed CT injection fuelling have been conducted on the C-2/C-2U facility by two CT injectors. The CT injectors are mounted 1 m apart on the vicinity of midplane. To avoid disruptive perturbation on the FRC, the CT injectors have been operated at the lower limit of particle inventory. The experiments demonstrated successful fuelling with significant density build-up of 20–30% of the FRC particle inventory per single CT injection without any deleterious effects on the C-2/C-2U FRC.

EX



Reconnection Heating Experiments and Simulations for Torus Plasma Merging Startup

Y. Ono¹, T. Yamada², S. Inoue¹, M. Inomoto¹, C.-Z. Cheng¹, M. Gryaznevich³, R. Scannell³, N. Conway³, B. J. Crowley³, C. Michael³, H. Hara⁴, S. Usami⁵, and R. Horiuchi⁵

¹University of Tokyo, Tokyo, Japan

²Kyushu University, Kasuga, Japan

³Culham Centre for Fusion Energy (CCFE), Culham Science Centre, Abingdon, UK

⁴National Astronomical Observatory of Japan (NAOJ), Mitaka-shi, Tokyo, Japan

⁵National Institute for Fusion Science (NIFS), Toki, Gifu, Japan

Corresponding Author: Y. Ono, ono@k.u-tokyo.ac.jp

A series of merging experiments: TS-3, TS-4 and MAST made clear the promising characteristics of reconnection heating for merging formation of high- β spherical tokamak (ST) and field-reversed configuration (FRC). We found the reconnection outflow produces MW-class (< 30 MW in TS-3) ion heating power based on the findings:

- i) its ion heating energy that scales with square of the reconnecting magnetic field B_{rec} ,
- ii) its energy loss lower than 10%,
- iii) its ion heating energy in the downstream $10\times$ larger than its electron heating energy at around X-point, and,
- iv) low dependence of ion heating on the guide (toroidal) field B_g .

Based on UK-Japan collaboration, we made the upscaled merging experiment in MAST and documented significant ion heating $T_i \sim 1.2$ keV by increasing B_{rec} to 0.2 T. Its ion heating ~ 1.2 keV and heating time 3–5 ms are about four times higher and 50 times shorter than the conventional ion heating ~ 0.3 keV and heating time ~ 200 ms by the CS startup. An important finding is that the B_{rec}^2 scaling law of reconnection heating energy was successfully extended over 1.2 keV under $n_e \sim 1.5 \times 10^{19}/\text{m}^3$. It depends just on B_{rec} and with little dependence on the guide (toroidal) magnetic field B_g . During the ST merging, B_{rec} and B_g are almost equal to poloidal field B_p and toroidal field B_t , respectively but both components of B_p and B_t reconnect during the two spheromak merging with opposing B_t for FRC formation. Since the reconnection accelerated ions up to 70% of the Alfvén speed, the ion velocity scales with B_{rec} , so that the T_i increment and the reconnection heating energy scale with B_{rec}^2 under constant n_e . It is noted that the reconnection heating does not depend on plasma size as long as the reconnection time is shorter than the plasma confinement time. This extended scaling law suggests that the merging startup will possibly realize the burning plasma temperature $T_i > 10$ keV just by increasing B_{rec} over 0.6 T. The merging and reconnection heating will possibly provide a new direct route to burning plasma regimes without using any additional heating. This promising scaling leads us to new reconnection heating experiments for future direct access to burning plasma regime: TS-U in U. Tokyo and ST-40 in Tokamak Energy.

Recent Advances in Stellarator Optimization

D. Gates¹, T. Brown¹, J. Breslau¹, M. Landreman², S. Lazerson¹, H. Mynick¹, G. Neilson¹,
N. Pomphrey¹, P. Xanthopoulos³, and A. Zolfaghari¹

¹Princeton Plasma Physics Laboratory (PPPL), Princeton, NJ 08540, USA

²University of Maryland, College Park, MD 20742, USA

³Max-Planck-Institut für Plasmaphysik, Greifswald, Germany

Corresponding Author: D. Gates, dgates@pppl.gov

Computational optimization has revolutionized the field of stellarator design. To date, optimizations have focussed primarily on optimization of neoclassical confinement and ideal MHD stability, although limited optimization of other parameters has also been performed. One of the criticisms that has been levelled at this method of design is the complexity of the resultant field coils. Recently, a new coil optimization code, COILOPT++, — which uses a spline instead of a Fourier representation of the coils — was written and included in the STELLOPT suite of codes. The advantage of this method is that it allows the addition of real space constraints on the locations of the coils. The code has been tested by generating coil designs for optimized quasi-axisymmetric stellarator plasma configurations of different aspect ratios. As an initial exercise, a constraint that the windings be vertical was placed on large major radius half of the nonplanar coils. Further constraints were also imposed that guaranteed that sector blanket modules could be removed from between the coils, enabling a sector maintenance scheme. Results of this exercise will be presented. New ideas on methods for the optimization of turbulent transport have garnered much attention since these methods have led to design concepts that are calculated to have reduced turbulent heat loss. We have explored possibilities for generating an experimental database to test whether the reduction in transport that is predicted is consistent with experimental observations. To this end, a series of equilibria that can be made in the now latent QUASAR experiment have been identified that will test the predicted transport scalings. Fast particle confinement studies aimed at developing a generalized optimization algorithm will also be discussed.

EX

Ferritic Wall and Scrape-Off-Layer Current Effects on Kink Mode Dynamics

J. P. Levesque¹, M. C. Ablter¹, J. Bialek¹, J. W. Brooks¹, P. J. Byrne¹, P. E. Hughes¹, C. J. Hansen², M. E. Mauel¹, G. A. Navratil¹, Q. Peng¹, D. J. Rhodes¹, and C. C. Stoafer¹

²University of Washington, Seattle, WA 98195, USA

¹Columbia University, New York, NY 10027, USA

Corresponding Author: J. P. Levesque, jpl2131@columbia.edu

The HBT-EP research programme aims to: i) quantify wall-stabilized kink mode dynamics and multimode response to applied magnetic perturbations, ii) understand the relationship between control coil configuration, conducting and ferromagnetic wall effects, and active feedback control, and iii) explore advanced feedback algorithms. We present an overview of planned research activities for the next three years, along with ongoing experiments in support of upcoming research. Multiple simultaneous kink modes are measured by over 200 local magnetic sensors. We observe that modulation of $n = 1$ halo current depends on phase and amplitude of rotating kink modes and applied RMPs. A low latency (14 μ s) control system uses 96 inputs and 64 outputs for adaptive control of kinks, via a 512-core graphics processing unit. An in-vessel adjustable ferromagnetic wall is used to study ferritic resistive wall modes, and produces increased mode growth rates, RMP response, and disruptivity. Magnetic feedback suppression of modes requires higher actuator gain with the nearby ferritic wall. A biased electrode in the plasma is coupled to the feedback system, and is used to control the rotation of kinks and evaluate error fields. At strong positive bias, the electrode induces a fast plasma rotation state with enhanced poloidal flow shear. A quasi-linear sharp-boundary model of the plasma's multimode response to error fields, including resistive and ferromagnetic effects, is developed to determine harmful error-field structures. Machine upgrades will allow improved measurements and control of scrape-off layer (SOL) currents. Movable tiles positioned around limiting surfaces will measure SOL and vessel currents during mode activity and disruptions. Biasable plates at divertor strike points will allow control of field-aligned SOL currents for feedback studies. An extreme ultraviolet diagnostic including i) four sets of 16 poloidal views and ii) a two-colour 16-chord tangential system will allow tomographic reconstruction of the plasma's optical emission and internal structure of kink modes, along with temperature profiles versus time. These measurements will enable feedback on kink modes using only optical sensors and both magnetic and edge-current actuators.

EX

Achievement of Field-Reversed Configuration Plasma Sustainment via 10 MW Neutral-Beam Injection on the C-2U Device

H. Gota¹, M. Binderbauer¹, T. Tajima¹, S. Putvinski¹, M. Tuszewski¹, D. Barnes¹, S. Dettrick¹, E. Garate¹, S. Korepanov¹, A. Smirnov¹, M. C. Thompson¹, X. Yang¹, S. Schmitz², Z. Lin³, A. A. Ivanov⁴, and T. Asai⁵

¹Tri Alpha Energy, Foothill Ranch, CA 92688, USA

²University of California Los Angeles, CA 90095, USA

³University of California Irvine, CA 92697, USA

⁴Budker Institute of Nuclear Physics (BINP), Novosibirsk, Russian Federation

⁵Nihon University, Tokyo, Japan

Corresponding Author: H. Gota, hgota@trialphaenergy.com

The world's largest compact-toroid device, C-2, has been upgraded to C-2U at Tri Alpha Energy to achieve sustainment of field-reversed configuration (FRC) plasmas by neutral-beam (NB) injection (NBI) and edge biasing [1, 2], and the C-2U experiment is characterized by the following key system upgrades: increased total NB input power from ~4 MW (20 keV hydrogen) to 10+ MW (15 keV hydrogen) with tilted injection angle; enhanced edge-biasing capability inside of each end-divertor for boundary and stability control. C-2U experiments with those upgraded systems have successfully demonstrated dramatic improvements in FRC performance. As anticipated, there are strong effects of the upgraded NB injectors on FRC performance such as: i) rapid and strong accumulation of fast ions (about a half of initial thermal pressure replaced by fast-ion pressure); ii) fast-ion footprint largely determines FRC dimensions; iii) double-humped electron density and temperature profiles; iv) FRC lifetime and global plasma stability scale strongly with NBI power; and v) plasma performance correlates with NB pulse duration in which diamagnetism persists several milliseconds after NB termination due to accumulated fast ions. The key accomplishment on C-2U is sustainment of advanced beam-driven FRCs with a macroscopically stable and hot plasma state for up to 5+ ms, limited only by hardware and stored energy constraints such as the NBs' pulse duration (flat-top ~8 ms) and current sourcing capability of end-on plasma guns. Furthermore, plasma diamagnetism in the best discharges has reached record lifetimes of over 11 ms, timescales twice as long as C-2. In this regime fast ions are well trapped and nearly classically confined, suppressing broadband magnetic turbulence as well as enhancing fusion reactivity via beam driven collective effects. Density fluctuations near the separatrix and in the scrape-off layer have also been dramatically suppressed by a combination of NBI and $E \times B$ shearing via plasma-gun edge biasing, thereby improving confinement properties. The demonstrated sustainment of beam-driven FRCs in C-2U is an extraordinary achievement for the FRC and innovative confinement concepts communities, and may lead to intriguing possibilities for fusion reactors.

References

- [1] M. Tuszewski, *et al.*, Phys. Rev. Lett. **108**, 255008 (2012).
- [2] M. W. Binderbauer, *et al.*, Phys. Plasmas **22**, 056110 (2015).

Plasma Response to Sustainment with Imposed-dynamo Current Drive in HIT-SI and HIT-SI3

A. Hossack¹, T. Jarboe¹, K. Morgan¹, D. Sutherland¹, C. J. Hansen¹, C. Everson¹, and B. Nelson¹

¹University of Washington, Seattle, WA 98195, USA

Corresponding Author: A. Hossack, saracen@uw.edu

The Helicity Injected Torus – Steady Inductive (HIT-SI) program studies efficient, steady-state current drive for magnetic confinement plasmas using a novel experimental method. Stable, high- β spheromaks have been sustained using steady, inductive current drive which is significantly more efficient than RF or neutral beams when scaled to a reactor. Externally induced loop voltage and magnetic flux are oscillated together so that helicity and power injection are always positive, sustaining the edge plasma current indefinitely. Imposed-dynamo Current Drive (IDCD) theory further shows that the entire plasma current is sustained. The method is ideal for low aspect ratio, toroidal geometries and is compatible with closed flux surfaces. Experimental studies of spheromak plasmas sustained with IDCD have shown stable magnetic profiles with evidence of pressure confinement. New measurements show coherent motion of a stable spheromak in response to the imposed perturbations. On the original device two helicity injectors were mounted on either side of the spheromak and the injected mode spectrum was predominantly $n = 1$ due to the geometry. Coherent, rigid motion indicates that the spheromak is stable and a lack of plasma-generated $n = 1$ energy indicates that the maximum q is maintained below 1 during sustainment. Results from the HIT-SI3 device are also presented. Three inductive helicity injectors are mounted on one side of the spheromak flux conserver. Varying the relative injector phasing changes the injected mode spectrum which includes $n = 2, 3$, and higher modes. Spheromaks have been sustained with toroidal current three times greater than the quadrature sum of injector currents.

Work supported by the U.S. Department of Energy, Office of Science, Office of Fusion Energy Sciences, under Award Number DE-FG02-96ER54361.

Ion Heating in Magnetosphere Plasma Device RT-1

M. Nishiura¹, Y. Kawazura¹, Z. Yoshida¹, Y. Yano¹, H. Saitoh¹, M. Yamasaki¹,
T. Mushiake¹, A. Kashyap¹, N. Takahashi¹, M. Nakatsuka¹, and A. Fukuyama²

¹University of Tokyo, Tokyo, Japan

²Kyoto University, Nishikyo-ku, Kyoto 615-8540, Japan

Corresponding Author: M. Nishiura, nishiura@ppl.k.u-tokyo.ac.jp

While the stable high- β (~ 1) confinement by a dipole magnetic field was successfully demonstrated with high-temperature electrons ($T_e > 10$ keV) [1, 2], the heating of ions was a challenge. We have made two major progresses in this direction. i) We developed a system for ion cyclotron resonance of frequency (ICRF) heating, and demonstrated the active heating of ions by launching a slow wave. The ion temperatures in the core region are increased in hydrogen, helium and deuterium plasmas. The differences of temperatures among ion species suggest a strong influence of the charge-exchange loss by which the bulk ions remain relatively cold (< 20 eV) in comparison with impurity ions. ii) We also found a spontaneous heating mechanism concomitantly occurring with the up-hill diffusion [3, 4].

References

- [1] H. Saitoh, *et al.*, Phys. Plasmas **21**, 082511 (2014).
- [2] M. Nishiura, *et al.*, Nucl. Fusion **55**, 053019 (2015).
- [3] N. Sato, *et al.*, [Self-Organization and Heating by Inward Diffusion in Magnetospheric Plasmas](#), (2015).
- [4] Y. Kawazura, *et al.*, Phys. Plasmas **22**, 112503 (2015).



Single Null Divertor in Negative Triangularity Tokamak

S. Medvedev¹, A. Merle², M. Kikuchi³, A. A. Ivanov¹, A. Martynov¹, Y. Poshekhonov¹,
O. Sauter², and L. Villard²

¹*Keldysh Institute of Applied Mathematics, RAS, Moscow, Russian Federation*

²*Swiss Plasma Center (SPC), École polytechnique fédérale de Lausanne (EPFL), 1015 Lausanne, Switzerland*

³*National Institutes for Quantum and Radiological Science and Technology (QST), Chiba-shi, Japan*

Corresponding Author: S. Medvedev, medvedev@a5.kiam.ru

Fusion research has to solve the power handling problem toward fusion demonstration reactor (DEMO). Tokamak plasma with negative triangularity and an outboard divertor X-point may offer such an opportunity as an innovative concept. The present paper extends this concept investigating single-null negative-triangularity tokamak (SN-NTT). Double-null negative-triangularity tokamak (DN-NTT) configurations feature quite high stable pedestals in the 1st region of ballooning stability but the vertical stability is an issue for the DN-NTT. Already with one outboard X-point in the SN-NTT, internal modes set the pedestal height limit. The changes in ELM regime, pedestal structure and Mercier mode driven turbulence are major issues yet to be investigated for the negative triangularity tokamak concept. Studying such phenomena from first principles would require nonlinear, electromagnetic gyrokinetic simulations. While negative triangularity plasma has some favourable MHD property with respect to ELMs, the β limit is relatively low. That is connected with the absence of a magnetic well for elongated plasma cross-sections. However, negative triangularity tokamak configurations with optimized pressure gradient profiles can be stable for $\beta_N > 3$ at elongation $\kappa = 1.8$ and internal inductance $l_i = 0.9$, even in the absence of the magnetic well, with Mercier modes stabilized by magnetic shear in the SN-NTT with the optimal upper triangularity value close to zero. Apart from the ELM mitigation and satisfactory level of β limits, negative triangularity tokamaks feature other possibilities for power handling such as naturally increased separatrix wetted area due to divertor location at larger radii and more flexible divertor configuration using PF coils inside the TF coil made of NbTi superconductor in the low field region. Negative triangularity experiments in TCV show a reduction in electron heat transport by a factor two compared with positive triangularity D-shaped configurations, which is partly explained by nonlinear gyrokinetic simulations. This configuration also allows better pumping accessibility due to larger conductance. Engineering restrictions on toroidal field (TF) coils at the high field side may not allow the TF shape conformal to negative triangularity plasma: more realistic race-track shaped TF coils are better compatible with the SN-NTT configuration.



Extension of Operational Boundary of High- β Long-pulse Operation at KSTAR

S.-W. Yoon¹, Y.-S. Bae¹, Y.-M. Jeon¹, W. H. Ko¹, J.-Y. Kim¹, M.-H. Woo¹, H. S. Kim¹,
H. H. Lee¹, S. H. Lee¹, S. H. Han¹, J. M. Park², M. J. Lanctot³, and Y.-K. Oh¹

¹National Fusion Research Institute (NFRI), Daejeon, Republic of Korea

²Oak Ridge National Laboratory (ORNL), Oak Ridge, TN 37831, USA

³General Atomics, San Diego, CA 92186, USA

Corresponding Author: S.-W. Yoon, swyoon@nfri.re.kr

For the realization of the fusion reactor, solving issues for high- β steady-state operation is one of the essential research topics for the present superconducting tokamaks and in this regard KSTAR has been focussing on maximizing performance and increasing pulse length addressing scientific and technical issues. Typically, previous study on high- β operation has been focussing on advanced scenario in relatively short pulse discharge at KSTAR and partial success has been reported [1]. However, it must be stressed that it is also essential to verify compatibility of developed high- β scenario to long-pulse and stable long-pulse operation is possible only with reduced level of performance compared with that of the short-pulse. In this work, the results of recent experimental approaches in long-pulse operation are presented focussing respectively on high- β_N , high- β_p and high l_i scenario. For high- β_N experiments, conditions of the maximum β_N is investigated mainly by parametric scans of toroidal magnetic field ($B_t = 1.4$ – 2.0 T) and neutral beam injection power (3–5 MW). The achieved β_N is close to 3 with $I_p = 0.4$ MA, $B_t = 1.4$ T and $P_{\text{ext}} \sim 6$ MW and it is found to be limited by $m/n = 2/1$ tearing mode and is sensitive on the internal inductance. For high- β_p experiments, conditions of the maximum β_N is investigated mainly by parametric scans of plasma current ($I_p = 0.4$ – 0.7 MA) and also neutral beam injection power (3–5 MW). The achieved β_p is also close to 3 with $I_p = 0.4$ MA, $B_t = 2.9$ T and $P_{\text{ext}} \sim 6$ MW and it is found to be limited by heating power and without indication of MHD activities. In addition, high- β_p discharge is due to high bootstrap fraction, closed to the state of fully noninductive current drive though pulse length is limited to 12 s by excessive heat-load on the protection limiters which is probably due to NBI prompt loss. Finally, attempt for high l_i will be addressed briefly on scenario development and transient results.

References

[1] S.-W. Yoon, *et al.*, IAEA FEC–2014, [OV/3-4](#)



Investigation of MHD Stability in KSTAR High- β_N Plasmas

Y.-S. Park¹, S. A. Sabbagh¹, J. W. Berkery¹, J. Bialek¹, J. Kim², W. H. Ko², Y. Jeon², S.-H. Hahn², S.-W. Yoon², Y. In², Y.-S. Bae², J. G. Bak², M. J. Choi², S. G. Lee², S. C. Jardin³, J.-G. Kwak², G. Yun⁴, Y.-K. Oh², and H. K. Park⁵

¹Columbia University, New York, NY 10027, USA

²National Fusion Research Institute (NFRI), Daejeon, Republic of Korea

³Princeton Plasma Physics Laboratory (PPPL), Princeton, NJ 08540, USA

⁴Pohang University of Science and Technology (POSTECH), Pohang, Gyeongbuk 790-784, Republic of Korea

⁵Ulsan National Institute of Science and Technology (UNIST), Ulsan, Republic of Korea

Corresponding Author: Y.-S. Park, ypark@pppl.gov

H-mode plasma operation in KSTAR reached high normalized β , β_N , up to 4.3 with reduced plasma internal inductance, l_i , to near 0.7. This significantly surpassed the computed $n = 1$ ideal no-wall β_N limit by a factor of 1.6. The high- β_N above 4 has been achieved in discharges having lowered B_t in the range 0.9–1.3 T with plasma current of 0.35–0.43 MA. The l_i was maintained at low values which resulted in high ratios of β_N/l_i up to 6.3. Pulse lengths at maximum β_N were initially limited by a loss of equilibrium radial control but were extended to longer pulses in 2015 by new, more rapid control resulting in β_N greater than 3 sustained for ~ 1 s. A significant conclusion of the analysis of these plasmas having $\beta_N > \beta_N^{\text{no-wall}}$ is that low- n global kink/ballooning or RWMs were not detected, and therefore were not that cause of the plasma termination. Kinetic modification of the ideal MHD $n = 1$ stability criterion, computed by the MISK code, has been used to analyze kinetic RWM stability in the achieved high- β_N equilibria with measured density, temperature and rotation profiles. This first examination of kinetic RWM stability for experimental KSTAR equilibria shows the kinetic RWM to be stable, which is consistent with the observation. The analysis is under active development and will soon examine reconstructed equilibria that include internal profile measurements. A $m/n = 2/1$ tearing mode onsets at the achieved high- $\beta_N > 3$ and experimentally reduces β_N by more than 30%. The stability of the observed 2/1 tearing mode at high- β_N is examined by using the M3D-C1 code solving the linearized single fluid, resistive MHD equations coupled with the EFIT reconstruction. The linear stability calculation shows a stable 2/1 mode while the equilibrium is experimentally unstable to the 2/1 mode. The mode eigenfunction shows a clear tearing parity at $q = 2$ but the mode growth rates are negative. The negative linear growth rate implies that the mode is classically stable, and the pressure driven neoclassical terms dominate over the current gradient term in the target equilibrium expected to have a nonnegligible bootstrap current. Further calculations including the pressure driven terms and toroidal rotation effect are presently underway to better understand tearing stability with near steady-state plasma profiles.

EX



Validation of $q_0 \geq 1.0$ in the MHD Quiescent Time after Crash of the Sawtooth Instability in KSTAR

H. Park¹, J. Ko¹, Y. Nam², Y.-S. Bae¹, W. Lee³, G. H. Choe², G. Yun², and S. C. Jardin⁴

¹National Fusion Research Institute (NFRI), Daejeon, Republic of Korea

²Pohang University of Science and Technology (POSTECH), Pohang, Gyeongbuk 790-784, Republic of Korea

³Ulsan National Institute of Science and Technology (UNIST), Ulsan, Republic of Korea

⁴Princeton Plasma Physics Laboratory (PPPL), Princeton, NJ 08540, USA

Corresponding Author: H. Park, hyeonpark@unist.ac.kr

Long standing issue of full versus partial reconnection model of the sawtooth instability is revisited in Korean Superconducting Tokamak Advanced Research (KSTAR). The measured central safety factor, q_0 by Motional Stark Effect (MSE) is ~ 1.0 and this measurement alone cannot validate the sawtooth instability model definitively due to nontrivial off-set error. Study of controlled experiment of the tearing modes ($m > 1$) sensitive to magnetic shear with the resistive magnetohydrodynamic (MHD) theory supports the full reconnection model. Here, the radial position of the excited tearing modes ($m/n > 1/1$) and their time evolution into the $1/1$ kink mode before the crash in sawtooth plasma suggests that $q_0 \geq 1.0$ in the MHD quiescent period after the crash and $q_0 < 1.0$ before the crash. Experimental observation of long lived tearing modes with constant mode number in nonsawtooth discharge (presumably $q_0 \geq 1.0$) further supports the fact that $q_0 \geq 1.0$ in the MHD quiescent period after crash in sawtooth discharge and hence the complete reconnection model.

EX



Influences of Nonaxisymmetric Field on H-Mode Power Threshold and Pedestal Rotation in KSTAR

W. H. Ko¹, H. S. Kim¹, Y. In¹, J. H. Lee¹, H. H. Lee¹, J. Seol¹, K. Ida², Y. M. Jeon¹, S.-W. Yoon¹, and H. K. Park³

¹National Fusion Research Institute (NFRI), Daejeon, Republic of Korea

²National Institute for Fusion Science (NIFS), Toki, Gifu, Japan

³Ulsan National Institute of Science and Technology (UNIST), Ulsan, Republic of Korea

Corresponding Author: W. H. Ko, whko@nfri.re.kr

EX Significant reduction of H-mode power threshold (P_{th}) has been identified in KSTAR. Such a favourable finding is attributable to low intrinsic error field [1] and toroidal field ripple [2], which has been corroborated by high pedestal rotation. According to a preliminary comparison, KSTAR has at least 10% lower P_{th} during L to H-mode transition than DIII-D which have similar size but with different error-field and with $n = 3$ nonaxisymmetric fields [3]. Since KSTAR has been diagnosed with an order of magnitude lower intrinsic error field ($\langle \delta B/B_0 \rangle_{m/n=2/1} \sim 1 \times 10^{-5}$ [1]) compared with the DIII-D at the low background and toroidal field ripple ($\delta_{TF} = 0.05\%$ [2]), it allows us to rigorously control nonaxisymmetric field without intrinsic error field impacts. In particular, we are keen on the influences of nonaxisymmetric fields on pedestal transport, which may regulate pedestal profiles to stay below the thresholds for the peeling-ballooning instabilities. A systematic study has been in progress to clarify the underlying physical mechanisms of ELM suppression and mitigation by nonaxisymmetric fields. At the same time, since the L-H power threshold is known to be greatly affected by nonaxisymmetric fields, a systematic scan has been conducted with the most influence nonaxisymmetric component, $n = 1$ in KSTAR. Despite various differences between DIII-D and KSTAR, both studies suggest the reduction of δB has a linear dependence on P_{th} . Considering that P_{th} is very important to determine the power requirements for future devices and that further reduction of P_{th} is also feasible in terms of various plasma parameters. Nonaxisymmetric fields reduced the both pedestal of toroidal rotation and ion temperature [4]. Overall, lower level of intrinsic error field and toroidal field ripple in KSTAR is attributable to higher pedestal rotation, leading to the increase of radial electric field near the separatrix. The ongoing 3D transport study focusses on H-mode threshold power and pedestal transport with controlled nonaxisymmetric fields. Based on the preliminary investigation, we are cautiously predicting that the lowest P_{th} would be found from the lowest intrinsic error field device.

References

- [1] Y. In, *et al.*, Nucl. Fusion **55**, 043004 (2015).
- [2] S.-W. Yoon, *et al.*, IAEA FEC-2014, [OV/3-4](#).
- [3] P. Gohil, *et al.*, Nucl. Fusion **51**, 103020 (2011).
- [4] W. H. Ko, *et al.*, Nucl. Fusion **55**, 083013 (2015).



Direct Destabilizations of Macro/Micro Edge Instabilities by Magnetic Perturbations

J. Kim¹, M. J. Choi¹, J. Lee², J. Kwon¹, Y.-M. Jeon¹, and S.-W. Yoon¹

¹*National Fusion Research Institute (NFRI), Daejeon, Republic of Korea*

²*Ulsan National Institute of Science and Technology (UNIST), Ulsan, Republic of Korea*

Corresponding Author: J. Kim, jayhyunkim@nfri.re.kr

It has been regarded that magnetic perturbation (MP) by nonaxisymmetric fields is the most promising technique in controlling edge-localized mode (ELM) crashes that are potentially harmful to the lifetime of first wall in reactor scale devices. However, the exact mechanism of MP has not been fully understood in both ELM crash mitigation and suppression. Here, we investigated the characteristics of macro and micro edge instabilities in relation to MP during ELM crash controlled discharges of KSTAR. Especially, the MP turning-off periods were focussed in order to rule out the effect of pedestal evolution. As a result, it was found that the response of macro and micro edge instabilities is very prompt against the applied MP. It suggests that the MP could directly drive macro and also micro instabilities of edge plasmas otherwise the discharge was stable against them. The detailed analyzes are still on-going with local fluctuation measurements and both numerical and theoretical efforts to reveal the underlying features of MP-driven edge instabilities.

EX



Study of the Locked Mode Disruption with the 3D Imaging Data in KSTAR

M. J. Choi¹, H. K. Park², G. Yun³, J. Kim¹, M.-H. Woo¹, W. Lee², K. Lee¹, W. H. Ko¹,
Y.-S. Park⁴, Y. In¹, J. Ko¹, B. Park¹, N. C. Luhmann, Jr.⁵, and Y.-S. Na⁶

¹National Fusion Research Institute (NFRI), Daejeon, Republic of Korea

²Ulsan National Institute of Science and Technology (UNIST), Ulsan, Republic of Korea

³Pohang University of Science and Technology (POSTECH), Pohang, Gyeongbuk 790-784, Republic of Korea

⁴Columbia University, New York, NY 10027, USA

⁵University of California Davis, CA 95616, USA

⁶Seoul National University, Seoul, Republic of Korea

Corresponding Author: M. J. Choi, mjchoi@nfri.re.kr

Discharges on the Korea Superconducting Tokamak Advanced Research (KSTAR) device often have suffered from minor and major disruptions by a large growth of the $m/n = 2/1$ MHD instability. It requires 3D measurements to decipher the underlying physics of the complicated disruption dynamics. The electron cyclotron emission imaging (ECEI) system on KSTAR is used to measure quasi-3D electron temperature (T_e) fluctuations, and the measurements revealed the detailed process of the disruptions from the onset to the explosive growth of the instability. Onset mechanisms such as the pressure and current profile contraction with density increase and the penetration of the resonant magnetic field perturbation (RMP) are examined by the imaging data. On the other hand, minor and major disruptions triggered by the naturally formed $2/1$ magnetic island have been analyzed in detail and the characteristics of the island growth and electron heat transport are studied. In the KSTAR discharge #8999, three different types of disruptive events were identified during the locked mode phase. They are labelled as the small and large minor disruptions and the major disruption, respectively. The small minor disruption is characterized as a localized heat transport event near the $q = 2$ region with a single $2/1$ instability. As for a large minor disruption, the initial $2/1$ instability is followed by an additional core instability, which leads to a successive partial relaxation of the region with $q < 2$. During the major disruption, the quasi-3D imaging data demonstrate one possible mechanism of the explosive growth of the $m/n = 2/1$ magnetic island, i.e., a cold bubble convection. The observed cold bubble and its coupling with the $2/1$ island imply that a sufficiently low magnetic shear could be responsible for the explosive growth of the $2/1$ island and the major disruption.

Work supported by Korea Ministry of Science, ICT and Future Planning under Contract No. OR1509 and NRF Korea under Grant No. NRF-2014M1A7A1A03029865 and NRF-2014M1A7A1A03029881.



Study of Nonlinear Phase of the ELMs by Comparison between ECEI ELM Observation and Nonlinear MHD Simulations

M. Kim¹, J. Lee¹, J. E. Lee², H. K. Park^{1,3}, G. S. Yun², W. Lee¹, X. Xu⁴, S. C. Jardin⁵, and M. Bécoulet⁶

¹Ulsan National Institute of Science and Technology (UNIST), Ulsan, Republic of Korea

²Pohang University of Science and Technology (POSTECH), Pohang, Gyeongbuk 790-784, Republic of Korea

³National Fusion Research Institute (NFRI), Daejeon, Republic of Korea

⁴Lawrence Livermore National Laboratory (LLNL), Livermore, CA 94550, USA

⁵Princeton Plasma Physics Laboratory (PPPL), Princeton, NJ 08540, USA

⁶Institut de Recherche sur la Fusion par confinement Magnétique (IRFM), Commissariat à l'énergie atomique (CEA/Cadarache), 13108 Saint-Paul-lès-Durance, France

Corresponding Author: M. Kim, minwookim@unist.ac.kr

A control of the ELM-crash is required for a stable plasma operation in a fusion reactor if the H-mode is adapted as an operation scenario. In the KSTAR H-mode plasma, a comparative study between 2D ECEI images of ELMs and MHD simulations has been performed in order to study the underlying physics of the ELM necessary for establishing an effective and robust ELM control. As a first step, the BOUT++ linear simulation is used to generate a mode structure at the edge of the H-mode plasma. The simulation results are converted into the synthetic images and compared with the observed images. An excellent agreement between two images provides confidence on ECEI edge observation. With same set of equilibria, a linear stability is investigated using BOUT++ and M3D-C1. The results from two codes are qualitatively matched. In the JOREK simulation, an apparent poloidal rotation of the mode is studied. The reproduced rotation agrees well with the measured one by ECEI as ~ 5 km/s in ion diamagnetic drift direction. Since recently observed ELM dynamics in KSTAR, for example, saturation and transient phase before the crash, multiple mode excitation and mode number transition during inter-ELM-crash periods, are associated with the nonlinear phenomena, the nonlinear simulation should be considered in comparative study. Preliminary nonlinear BOUT++ simulation results were obtained and post analysis process was established. A post analysis process of other two codes will be also developed for the comparison with the ECEI observations. Ultimately the comparative study between the observation and the nonlinear simulations will make a possible to study the role of electron and ion during the ELM-cycle, effect of diffusion coefficient and rotation on ELM dynamics.

Work supported by NRF of Korea under contract No. NRF-2014M1A7A1A03029865.



Characteristics of Halo Current in the KSTAR Tokamak

J. G. Bak¹, H.-S. Kim¹, S.-H. Hahn¹, J. Kim¹, and I.-S. Choi¹

¹National Fusion Research Institute (NFRI), Daejeon, Republic of Korea

Corresponding Author: J. G. Bak, jgbak@nfri.re.kr

The investigation of poloidal halo current (HC) I_h flowing along the support structures for plasma facing components (PFCs) during the vertical displacement event (VDE) under the toroidal magnetic field B_t is required for the estimate of the $I_h \times B_t$ force on the structures in the KSTAR tokamak because it can be expected that the force will cause damages on the structures in the KSTAR when plasma current and toroidal field will become higher than 1.0 MA and 3.0 T, respectively, for achieving high performance. The characteristics of the HCs during VDEs in the KSTAR are investigated by using the HCM measurements in the experimental campaigns of 2014 and 2015. In the measurements, the growth rate of the VDE γ_z is 30–200/s, and the maximum magnitude of the HC $I_{h,\max}$ is up to 20% of the predischarged plasma current I_{p0} . In addition, the value of $I_{h,\max}$ increases as the maximum value of the current quenching rate $(dI_p/dt)_{\max}$ becomes higher. From the experimental investigation of parametric dependences of the HC, it is found that a higher value of $I_{h,\max}$ is obtained for larger values of κ in the case of downward VDE. Secondly, the value of $I_{h,\max}$ slightly decreases as q_{95} increases, and the value linearly depends upon I_p , n_e , W_{tot} and β_p . Thirdly, the upper limit of the HC can be estimated by using the relationship as $I_{h,\max} \sim 1.4I_{p0}/q_{95}$ from the investigation. Finally, the trend of the toroidal peaking factor (TPF) versus halo fraction $I_{h,\max}/I_{p0}$ in KSTAR is obtained, and the maximum value of TPF multiplied by $I_{h,\max}/I_{p0}$ is lower than 0.58. The magnitude of the HC can be decreased by adjusting the amount of gas-puff at the divertor region. The HC rotation can be observed in the KSTAR, and its rotation frequency is ~ 1 kHz during only one revolution in the counter I_p direction during a downward VDE. The toroidal distribution of local HC can be changed by applying the nonaxisymmetric magnetic perturbation (NMP) field ($n = 1$ and -90° phasing) due to resonant magnetic perturbation coil at the edge region in the KSTAR. In this work, the experimental investigations of the characteristics of the HC during the VDE and the HC rotation and effect of the NMP field on the toroidal distribution of the local HC in the KSTAR will be reported, and the preliminary results from analysis on toroidal variation of the local HC will be presented.

EX

Characteristics of Magnetic Braking Depending on 3D Field Configuration in KSTAR

K. Kim¹, W. Choe¹, Y. In², W. H. Ko², J. G. Bak², M. J. Choi², H. Kim², H. Lee¹, J.-K. Park³, Y. Jeon², J.-G. Kwak², S.-W. Yoon², and Y.-K. Oh²

¹*Korea Advanced Institute of Science and Technology (KAIST), Daejeon, Republic of Korea*

²*National Fusion Research Institute (NFRI), Daejeon, Republic of Korea*

³*Princeton Plasma Physics Laboratory (PPPL), Princeton, NJ 08540, USA*

Corresponding Author: K. Kim, kimk@kaist.ac.kr

Toroidal rotation braking by neoclassical toroidal viscosity driven by nonaxisymmetric (3D) magnetic fields, called magnetic braking, has great potential to control rotation profile, and thereby improve tokamak stability and performance. In order to characterize magnetic braking in various 3D field configurations, dedicated experiments have been carried out in 2015 campaign, applying a variety of static $n = 1$ 3D fields in the different phasing of -90° , 0° , and $+90^\circ$. The 0° phasing fields achieved quiescent magnetic braking without density pump-out, which is consistent with vacuum and ideal plasma response analysis predicting deeply penetrating 3D fields without significant plasma response. On the other hand, strong resonant-type magnetic braking was achieved by the -90° phasing fields, which is identified by strong density pump-out and confinement degradation, and explained by excitation of kink response captured by ideal plasma response calculation. Very strong resonant plasma response was observed under the $+90^\circ$ phasing at $q_{95} \sim 6.0$, leading to severe confinement degradation and eventual disruption by locked modes. The strong resonant transport was substantially modified to nonresonant-type transport at higher $q_{95} \sim 7.2$, as the resonant particle transport was significantly reduced, and global rotation braking was changed to localized braking. This is well explained by perturbed equilibrium calculations indicating the strong kink coupling at lower q_{95} is substantially shielded by ideal plasma response for higher q_{95} discharge. These experiments will be presented and discussed in detail with experimental and numerical analyzes for perturbed equilibrium, neoclassical and turbulent transport, and compared with $n = 2$ magnetic braking experiments that produced significant variations of the NTV torque profile depending on the phasing of $n = 2$ field coils. In particular, experiments in the 2016 campaign will explore potential utilization of the nonresonant magnetic braking to improve global confinement and performance through toroidal rotation profile control, which will be presented with various diagnostics and transport analyzes.

EX



Long-Lived Pressure-Driven MHD Mode in KSTAR Plasmas

S. G. Lee¹, J. Seol¹, H. H. Lee¹, A. Y. Aydemir¹, L. Terzolo¹, K. D. Lee¹, Y.-S. Bae¹,
J. G. Bak¹, G. H. Choe², G. S. Yun², and J. W. Yoo¹

¹National Fusion Research Institute (NFRI), Daejeon, Republic of Korea

²Pohang University of Science and Technology (POSTECH), Pohang, Gyeongbuk 790-784, Republic of Korea

Corresponding Author: S. G. Lee, sglee@nfri.re.kr

Highly coherent structures associated with an extremely long-lived saturated magnetohydrodynamic (MHD) instability have been observed in KSTAR tokamak under a long-pulse and steady-state operation. As the plasma performance is increased in advanced tokamak regimes, possible deleterious effects of MHD modes become more important, especially for steady-state burning plasmas in the next-step devices such as ITER and DEMO. One of the commonly seen modes is the $m/n = 2/1$ resistive kink mode that either leads to confinement degradation, or mode locking followed by a full disruption. In KSTAR, however, long-pulse discharges regularly exhibit a coherent structure in the form of a saturated pressure-driven MHD mode that can be sustained as long as 40 s, the full discharge duration, when the mode is located near the plasma core region with a broad safety factor profile with q_0 larger than 2.



Measuring and Extending Vertical Stabilization Controllability of KSTAR

S.-H. Hahn¹, D. A. Humphreys², D. Mueller³, N. W. Eidiotis², J. G. Bak¹, Y. Jeon¹,
M. J. Lanctot², J. Kim¹, A. W. Hyatt², and M. L. Walker²

¹*National Fusion Research Institute (NFRI), Daejeon, Republic of Korea*

²*General Atomics, San Diego, CA 92186, USA*

³*Princeton Plasma Physics Laboratory (PPPL), Princeton, NJ 08540, USA*

Corresponding Author: S.-H. Hahn, hahn76@nfri.re.kr

The paper summarizes a series of multi-year experimental activities done under the ITPA MHD stability TG from year 2012 to year 2015. The relevant activity, MDC-18, addresses many axisymmetric control issues needing resolution for ITER, which include 1) fundamental controllability of axisymmetric equilibria and relevant metrics, 2) noise effects in the principal diagnostics, and 3) evaluation of candidates of control algorithms/approach in operating devices. As the first step, a series of dedicated “release-and-catch” experiments are performed at KSTAR to measure the principal metrics for vertical stability — the stability margin and the maximum controllable vertical displacement ΔZ_{\max} . The dynamics of the vertical movement is measured and analyzed by magnetic reconstructions, validations against the nonmagnetic diagnostics, and an axisymmetric plasma response model which can simulate the experimental results in the appropriate time resolution. Through the year-by-year experiments, the effect of the outboard passive stabilizer structure changes on the VS characteristics has been quantitatively recorded.

Based on the plasma response model obtained in the experiment, relevant experimental approaches are described for extending controllability of the vertical stability feedback controls. The present scheme is briefly described and analyzed first. Effects of new diagnostics design are also analyzed, with real experimental demonstration. Finally, results of a new control approach using decoupling in the frequency domain are introduced, in order to reduce competition between the “fast” feedback for vertical displacement of the plasma centre and the “slow” feedback for the boundary control. The decoupling method has been demonstrated in a full shape as a prerequisite for the ITER similar shape (ISS) development research.

EX



Application of Physics-Based Profile Control Approach to KSTAR

H.-S. Kim¹, S. H. Kim², Y. M. Jeon¹, Y.-S. Na³, Y.-S. Bae¹, S.-H. Hahn¹, M. Joung¹, K. D. Lee¹, H. S. Han¹, M.-H. Woo¹, T. G. Lee¹, S. W. Yun², J. S. Ko¹, and S.-W. Yoon¹

¹National Fusion Research Institute (NFRI), Daejeon, Republic of Korea

²International Thermonuclear Experimental Reactor (ITER),

Cadarache Centre, 13108 Saint-Paul-lès-Durance, France

³Seoul National University, Seoul, Republic of Korea

Corresponding Author: H.-S. Kim, hskim0618@nfri.re.kr

Advanced tokamak operations, promising candidates for DEMO operations, require control of plasma profiles to establish and to sustain the enhanced energy confinement and the noninductive current fraction. The safety factor (q) profile and the electron temperature (T_e) profile control have to be controlled to access and maintain the advanced operation modes and to improve controllability of the q profile as well as to keep the high plasma pressure [1], respectively. The KSTAR experiments have been initiated aiming at establishing a real-time control system of multiple plasma profiles (T_e and q profiles) using multiple actuators (NBI and EC) and to validate applied physics-based control models [2]. The real-time T_e profile control has been firstly demonstrated in KSTAR experiments for four specific topics: application of the physics-based control models to the time-varying control target in a single discharge, simultaneous application of multiple actuators (NBI and EC), profile control demonstration in the presence of an external disturbance, and real-time update of the physics-based plasma response models. The q profile control system is currently being developed using real-time Motional Stark Effect (MSE) diagnostic in KSTAR. Implementation of the q profile response model and its validation has been conducted by performing off-line analysis of KSTAR discharges, prior to its application to real KSTAR experiments. Once the q profile control is additionally demonstrated, the combined control of multiple plasma profiles will contribute to exploring the advanced operation regimes in KSTAR and also for addressing the control issues on MHD instabilities.

References

- [1] H.-S. Kim, Ph. D. Dissertation, Seoul Nation. Univ. (2015).
[2] S. H. Kim, *et al.*, Nucl. Fusion **52**, 074002 (2012).

ECH-assisted Plasma Startup Experiment Using Trapped Particle Configuration in KSTAR

J. Lee¹, J. Kim², Y. An², M.-G. Yoo¹, Y. S. Hwang¹, and Y.-S. Na¹

¹*Seoul National University, Seoul, Republic of Korea*

²*National Fusion Research Institute (NFRI), Daejeon, Republic of Korea*

Corresponding Author: J. Lee, germine@snu.ac.kr

ECH-assisted plasma start-up using trapped particle configuration (TPC) is performed in KSTAR 2015 experiment campaign for feasibility study of TPC in superconducting, conventional tokamaks. It is widely known that ECH can significantly assist the start-up of tokamak plasmas with preionization. The dependency of the quality of the ECH preionization plasma on the magnetic configuration has been addressed in VEST systematically where it was found that TPC can achieve better confinement of the preionized plasma compared with the conventional field null configuration (FNC). In KSTAR, a plasma start-up scenario is developed for TPC based on the FNC scenario, by superimposing the TPC structure made by PF#5 onto FNC. As for preionization, 170 GHz, 2nd harmonic X-mode ECH/ECCD is applied. The injection power is up to 600 kW. Toroidal magnetic field is set to be 2.7 T at the major radius to match the resonance layer with the TPC region. Although no enhancement of the plasma start-up is observed under FNC, clear enhancement is shown under TPC. By adding the poloidal field strength of 36 gauss, a significant enhancement is achieved under TPC with the preionization plasma density of $4 \times 10^{18}/\text{m}^3$. The D_α signal indicates that a highly ionized plasma is formed under the TPC case. Based on these preionization plasmas, much earlier and faster plasma current formation is achieved. The loop voltage signal shows the highly improved plasma current initiation with the lower loop voltage and the higher plasma current ramp-up rate than the FNC case. The start-up experiment under the various poloidal field strength of TPC is performed which shows that the plasma start-up performance with TPC strongly depends on the vertical field strength so that the quality of the preionization is more important factor than the Lloyd condition for start-up of tokamak plasmas with preionization. Finally, the robust plasma start-up is achieved in 2015 KSTAR campaign, with contaminated wall condition after disruption experiments while continuous failure is observed with FNC. The results show that TPC can be applied to conventional tokamaks for enhanced plasma start-up performance. It is envisaged that TPC can improve the start-up of ITER where a low loop-voltage start-up is inevitable due to the limitation of superconducting solenoid coils.

EX



ELM, Edge Turbulence and their Interaction in the ELM-crash Suppression Phase under the $n = 1$ RMP

J. Lee¹, G. Yun², M. J. Choi³, W. Lee¹, H. K. Park¹, Y.-M. Jeon³, J.-M. Kwon³, and N. C. Luhmann, Jr.⁴

¹*Ulsan National Institute of Science and Technology (UNIST), Ulsan, Republic of Korea*

²*Pohang University of Science and Technology (POSTECH), Pohang, Gyeongbuk 790-784, Republic of Korea*

³*National Fusion Research Institute (NFRI), Daejeon, Republic of Korea*

⁴*University of California Davis, CA 95616, USA*

Corresponding Author: J. Lee, jaehyun@unist.ac.kr

The effect of static $n = 1$ resonant magnetic perturbation (RMP) on edge-localized mode (ELM) and edge turbulence has been investigated using electron cyclotron emission imaging (ECEI) system. The ECEI revealed that filamentary ELM is still present in the edge when the ELM crash is completely suppressed by $n = 1$ RMP. Correlation analysis showed the RMP enhances turbulent fluctuations in the edge toward the ELM-crash suppression phase. The spectral power distribution showed that edge turbulence has a linear dispersion for wide range of wavenumber and frequency. With velocimetry analysis, the turbulence has character of interchange mode which involves a net radial outward particle and heat transport. Bispectral analysis showed the nonlinear interaction between ELM and turbulent eddies, which implies that exchange of free energy between them may prevent the large ELM crashes.

EX



Study of Toroidal Rotation and Ion Temperature Pedestals between ELM Bursts on KSTAR H-Mode Plasmas

S. Ko¹, J. Kwon¹, W. H. Ko¹, S. Kim¹, H. Jhang¹, and L. Terzolo¹

¹National Fusion Research Institute (NFRI), Daejeon, Republic of Korea

Corresponding Author: S. Ko, shko@nfri.re.kr

Steep pedestal profiles of ion temperature (T_i) and toroidal rotation (V_ϕ) are routinely observed in neutral beam injection(NBI)-heated KSTAR H-mode plasmas [1]. In this work, we report a result of detailed analysis of pedestal characteristics. By analyzing a set of data with different experimental conditions, we show that T_i and V_ϕ pedestals are coupled to each other and whose correlation becomes stronger when NBI-power is low. This suggests the existence of intrinsic toroidal torque in the pedestal. To investigate further the magnitude and the role of intrinsic torque, we perform a 1D transport analysis and find that the prevalence of residual microturbulences is necessary to explain momentum transport in the pedestal. The estimated strength of intrinsic torque is shown to be comparable to that from a 2.7 MW NBI source. Finally, we show that nondiffusive momentum flux is indispensable to explain momentum transport in the pedestal and a residual stress model fits the observed momentum flux reasonably.

References

[1] W. H. Ko, *et al.*, Nucl. Fusion **55**, 083013 (2015).

EX

Fluctuation Signatures of Rotation Reversals and Nonlocal Transport Events in KSTAR L-Mode Plasmas

Y. Shi¹, J. Kwon², D. H. Na¹, and W. Ko²

¹Seoul National University, Seoul, Republic of Korea

²National Fusion Research Institute (NFRI), Daejeon, Republic of Korea

Corresponding Author: Y. Shi, yjshi@ipp.ac.cn

In KSTAR experiments, we found that nonlocal transport (NLT) is closely connected to the rotation reversal and impurity transport. We demonstrated that NLT can be controlled by ECH, and the intrinsic rotation and impurity dynamics follow the change in NLT. Supersonic molecular beam injection (SMBI) was used to induce the cooling of edge electrons. The cut-off density for NLT can be significantly extended by ECH. Without ECH, NLT disappears as the line averaged density n_e increases above $1.5 \times 10^{19}/\text{m}^3$. By applying ECH, NLT reappears with $n_e = 2.4 \times 10^{19}/\text{m}^3$. The ion temperature profiles show little changes, but the electron temperature profiles are significantly changed by ECH, and core toroidal rotation also changes from countercurrent in OH plasma to cocurrent direction in ECH plasma. The carbon impurity profile becomes hollow by ECH. We investigated the fluctuation characters of these ECH and OH plasmas by 2D diagnostics in KSTAR. Although sawtooth exists during NLT in the ECH plasma, 2D ECEI images show that the NLT pattern is not rotating in time. Poloidal flow of core plasma estimated from ECEI is in electron diamagnetic direction in ECH plasma. The ECEI results indicate that the correlation between NLT and conventional MHD activity is weak. The MIR and BES results show that the auto-power spectra of density fluctuation are almost the same in outer region for ECH and OH plasma. In the core region, the power spectra of the density fluctuation of ECH plasma are broader than those of OH plasma. The discrepancy in the density power spectra of ECH and OH plasma increases with frequency. All these observations in macroscopic parameters and micro fluctuations suggest a possible link between the macro phenomena and the structural changes in microfluctuations. One theoretical hypothesis to explain the cutoff density for NLT is the transition of dominant fluctuation mode from ion temperature gradient (ITG) mode to trapped electron mode (TEM). The rotation reversal can be also explained by the transition of fluctuation mode. The increase of the cut-off density for NLT by ECH supports this theoretical hypothesis. A preliminary gyrokinetic analysis indicates that the ECH drives strong TEM instabilities in the core region. These efforts will build a concrete physical picture to unify NLT and intrinsic rotation with the dynamics of microscopic turbulence.

EX



Effects of ECH and RMP on Argon Impurity Transport in KSTAR Plasmas

J. Hong¹, H. Y. Lee¹, S. Henderson², K. Kim¹, I. Song¹, S. H. Lee³, J. Kim³, J. Jang¹, C. R. Seon³, J. S. Park¹, J. G. Bak³, W. H. Ko³, S. G. Lee³, J. W. Yoo³, J. H. Lee³, J. H. Jeong³, H. S. Kim³, and W. Choe¹

¹Korea Advanced Institute of Science and Technology (KAIST), Daejeon, Republic of Korea

²University of Strathclyde, Glasgow, UK

³National Fusion Research Institute (NFRI), Daejeon, Republic of Korea

Corresponding Author: J. Hong, joochwanhong@kaist.ac.kr

Experiments were conducted in KSTAR plasmas by injecting a trace amount of Ar gas as a test particle while applying two different actuators: electron cyclotron resonance heating (ECH) and resonant magnetic perturbation (RMP). Effects of ECH was investigated in KSTAR L- and H-mode discharges. For L-mode discharges ($I_p = 400$ kA, $B_t = 2$ T), 110 GHz ECH of 350 kW was applied to heating positions varied in the vertical direction. The Ar radiation, measured by soft X-ray (SXR) array diagnostics showed significant reduction in the core impurity emissivity with the ECH. The reduction was the largest by on-axis ECH heating and became smaller as the heating was delivered at outer locations. For H-mode plasmas ($I_p = 600$ kA, $B_t = 2.8$ T, $P_{\text{NBI}} \sim 4.0$ MW), 170 GHz ECH of 800 and 600 kW was applied to the positions of $Z = 0$ at fixed $R = 1.66$ m. Emissivity measurements of 3.4 nm (Ar^{16+}) by X-ray (XICS) and 35.4 nm (Ar^{15+}) by VUV spectrometers indicate that the ECH reduced the peak emissivity of the Ar^{15+} ; however, the ECH increased the emissivity of the Ar^{16+} . It was observed that the ECH effects for reducing (Ar^{15+}) and increasing (Ar^{16+}) emissivity were stronger with higher heating power. Ar impurity transport experiments using $+90^\circ$ phasing of $n = 1$ RMP was also studied in the H-mode plasma ($I_p = 0.5$ MA, $B_t = 2.15$ T, $P_{\text{NBI}} \sim 3.0$ MW). The RMP coil current (I_{RMP}) was scanned from 0 to 2.5 kA and the trace Ar gas was puffed under the RMP. It was observed that the increase of I_{RMP} reduced line-averaged electron density by up to 15% and increased the ELM frequency from 52 Hz to 67 Hz. The peak divertor heat flux and stored energy loss during a single ELM burst were also decreased by the increase of I_{RMP} , along with mitigation of ELM by the RMP. The SXR radiation at the plasma core was decreased with the increase of I_{RMP} . These observations imply that the impurity accumulation can be controlled by the RMP application. A detailed discussion on the Ar transport coefficients, i.e., diffusion and convection coefficients, obtained by the ADAS-SANCO impurity transport code analysis will be presented. In addition, the analysis results from neoclassical and gyrokinetic simulation will also be discussed to provide theoretical understanding of the role of ECH and RMP on Ar transport in the KSTAR plasma.

Rotation Reversal in KSTAR and its Turbulence and Transport Characteristics

D. H. Na¹, S. M. Yang¹, S. G. Lee², C. Angioni³, J. A. Lee⁴, Y. Shi¹, J.-M. Kwon², H. Jhang², W. H. Ko², T. S. Hahm¹, and Y.-S. Na¹

¹Seoul National University, Seoul, Republic of Korea

²National Fusion Research Institute (NFRI), Daejeon, Republic of Korea

³Max-Planck-Institut für Plasmaphysik, Garching, Germany

⁴Pohang University of Science and Technology (POSTECH), Pohang, Gyeongbuk 790-784, Republic of Korea

Corresponding Author: D. H. Na, mania0020@snu.ac.kr

For several years, dedicated experiments have been performed in the KSTAR Ohmic L-mode plasmas to investigate the rotation reversal phenomena and it was finally observed in 2015. We found that the rotation reversal can be related to the rotation gradient change with respect to the electron density or the collisionality in the region $\rho \sim 0.3-0.6$. In KSTAR, its possible mechanism was investigated by perturbative experiments using the beam blip technique with two measurement systems, X-ray imaging crystal spectrometers (XICS) and charge exchange recombination spectroscopy (CES). The result of the momentum transport analysis implies that the rotation reversal with respect to the electron density or the collisionality mainly results from the change of the momentum transport rather than that of the intrinsic torque. For a better understanding of the underlying physics, linear and nonlinear gyrokinetic simulations are performed with GKW to analyze the turbulence and transport characteristics in the experiment. The results are compared with fluctuation characteristics measured by multichannel microwave imaging reflectometry (MIR) and electron cyclotron emission imaging (ECEI).

EX

Ion-Scale Turbulence Study in KSTAR L-Mode Plasmas

W. Lee¹, J.-E. Leem², G. S. Yun², H. K. Park³, S. H. Ko³, M. J. Choi³, Y.-S. Park⁴, T.-K. Kim⁵,
H. Park⁵, C. W. Domier⁶, and N. C. Luhmann, Jr.⁶

¹Ulsan National Institute of Science and Technology (UNIST), Ulsan, Republic of Korea

²Pohang University of Science and Technology (POSTECH), Pohang, Gyeongbuk 790-784, Republic of Korea

³National Fusion Research Institute (NFRI), Daejeon, Republic of Korea

⁴Columbia University, New York, NY 10027, USA

⁵Kyungpook National University (KNU), Daegu, Republic of Korea

⁶University of California Davis, CA 95616, USA

Corresponding Author: W. Lee, woochanglee@unist.ac.kr

In KSTAR L-mode discharges ($B_{t0} = 3\text{--}3.3$ T and $I_p = 600$ kA) heated by ~ 1.5 MW neutral beam injection (NBI), 200–400 kHz turbulent fluctuations were observed with a multichannel (4 radial and 16 poloidal) microwave imaging reflectometer system [1]. Linear gyrokinetic simulations with GYRO predicted that turbulence is most unstable at $k_\theta \sim 3/\text{cm}$ ($k_\theta \rho_s \sim 0.4$) and the most unstable mode frequencies in the plasma frame ($\omega_0/2\pi$) are a few tens of km in the NBI L-mode discharges. The most unstable mode frequencies were shifted by equilibrium $E \times B$ flow velocities ($U_{E \times B}$) and their frequencies in the laboratory frame, which are given by $\omega/2\pi = (k_\perp U_{E \times B} + \omega_0)/2\pi$ [2], were consistent with the measurements. Turbulence in a discharge #9010) was modelled with a nonlinear gyrokinetic code GTS and the result showed that the dominant wavenumber and apparent poloidal velocities of fluctuations were consistent with the GYRO simulation result and measurement. In order to study the measured turbulence structure scales and their dependence on the local equilibrium parameters, the temporal and spatial characteristic scales of the measured turbulence were evaluated with the cross correlation analysis and compared with equilibrium parameters relevant to the ion-scale turbulence.

References

- [1] W. Lee, *et al.*, Nucl. Fusion **54**, 023012 (2014).
- [2] R. A. Koch and W. Tang, Phys. Fluids **21**, 1236 (1978).

Work supported by the NRF of Korea under grant No. 2014M1A7A1A03029865 and the U.S. Department of Energy under grant No. DE-FG02-99ER54531.



Comprehensive Study on Deposition inside the Gap of Castellated Tungsten Blocks of Different Shapes

S.-H. Hong¹, E. Bang¹, S.-A. Park², H. S. So², Q. Xu³, H. Lee², and G.-N. Luo³

¹National Fusion Research Institute (NFRI), Daejeon, Republic of Korea

²Kyung Hee University, Dongdaemun, Seoul, Republic of Korea

³Institute of Plasma Physics, Chinese Academy of Sciences, Hefei, Anhui, People's Republic of China

Corresponding Author: S.-H. Hong, sukhhong@nfri.re.kr

In this paper, we report the results from a series of experiment using special tungsten block tiles performed in KSTAR on fuel retention inside the gap of castellated blocks of different shapes. Results presented in this paper suggest a comprehensive understanding on deposition procedure inside the gap and would give valuable information on the Be deposition inside the gap of castellated tungsten tiles in ITER. For the experiment, we have manufactured tiles consisting of five different shapes of tungsten blocks. These tungsten block tiles are exposed to L- and H-mode discharges during the 2014–2015 campaign, then removed from the vacuum vessel after the campaign for further analysis. PIC-EDDY code is employed to simulate the deposition inside the gaps. The surface density of gaps is in a range from 1.0×10^{15} C atom/cm² up to 7.0×10^{15} C atom/cm². Comparing the surface density of toroidal and poloidal gaps of different shapes, contribution of each species can be separated, since the contribution of neutrals is independent of the shape and depth of the gap (or height of the leading edge). At the gap entrance, neutral contribution is about 5.0×10^{15} atom/cm², decreases down to 2.0×10^{15} atom/cm² at a depth of 0.5 mm, and remain constant at 1.0×10^{15} atom/cm² afterwards down to the depth of 5 mm. The contribution of ions is concentrated on very narrow position within 0.6 mm from the entrance. Modelling of the deposition patterns by using PIC-EDDY code is underway. Raman spectra of deposited layers along the gap shows different chemical bonding structures. At the entrance, Raman spectra show typical feature of diamond-like carbon layers, while somewhat polymer-like carbon feature was identified at the bottom of the gap. From divertor IR measurements, the surface temperature of tungsten blocks has reached over 500°C, causing hydrogen reduction and graphitization. This can be also seen from the decrease of the intensity ratio I(D)/I(G) along the gap: sp³ sites in a-C:H films are bound to hydrogen, thus, highly sp³-bonded a-C:H are hydrogen-rich films (soft, low density, and polymeric).

EX



The Assessment of the Neutron Yield and the Toroidal Distribution of Neutron Emission on Deuterium Beam-Plasma Interaction Dominated KSTAR Operation

J.-G. Kwak¹, Y. Lee¹, M. Cheon¹, K. Shinohara², and J. Jo³

¹National Fusion Research Institute (NFRI), Daejeon, Republic of Korea

²Japan Atomic Energy Agency (JAEA), Naka, Japan

³Seoul National University, Seoul, Republic of Korea

Corresponding Author: J.-G. Kwak, jgkwak@nfri.re.kr

The importance of neutron emission measurements and modelling at present nuclear fusion devices relies on its usage for designing future reactor for shielding as well as the fact that it has the information about the plasma property. Especially a small amount of nuclear heating on SC magnet impacts heavily on safe operation of machine due to tight temperature margin of quenching. Since the successful first operation in 2008, the plasma performance of KSTAR has been enhanced and duration of H-mode for deuterium plasma is extended to over 50 s, surpassing the current conventional tokamak operation. In addition to long-pulse operation, the plasma performance is further extended on the high- β_p discharge characterizing the fully noninductive discharge over 10 s. So there is a lot of production of fast neutrons coming from $D(d,n)^3\text{He}$ reaction. It is found that most of neutrons are 2.45 MeV neutrons coming from deuterium beam plasma interaction and total fluence for a campaign is about 10^{19} . Especially, several Ni activation samples are installed in 2015 campaign inside the vacuum vessel and total accumulated neutron flux is calculated from gamma emission measurement after the campaign. The preliminary results show that the neutron activation both inside and outside the vacuum vessel has nonuniform distribution and it has larger neutron flux around poloidal limiter area. Considering the prompt ion loss at nominal KSTAR operation both with and without RMP, including the high- β_p operation, prompt loss ions from 100 keV neutral ion beams hit the specific position on three poloidal limiters, the resulting neutron emission is calculated and compared with the measurements. In addition, 14 MeV neutrons from DT reaction are analyzed by neutron activation analysis method using Si and Cu samples whose threshold energy is over 10 MeV. It is estimated that the amount of 14 MeV neutrons is less than 0.5% of that of 2.45 MeV neutrons for 2015 KSTAR campaign. Including above topics, the presentation will address the recent results on neutron energy spectra using neutron spectrometer based on proton telescope and post radioactive activation measure based on gamma analysis from neutron induced activation on SC tokamak including thermal shield and magnet.

EX

Measurements of SOL Density Increase and Poloidal Asymmetry on KSTAR ELMs

K. C. Lee¹, J.-W. Juhn¹, J. G. Park¹, Y.-U. Nam¹, S. H. Lee¹, J. H. Lee¹, S. Zoletnik², and M. Lampert²

¹National Fusion Research Institute (NFRI), Daejeon, Republic of Korea

²Wigner Research Center, Association EURATOM, Budapest, Hungary

Corresponding Author: K. C. Lee, kclee@nfri.re.kr

An analysis of edge density evolution during the large ELMs on KSTAR is developed by the measurements including two interferometer systems and the beam emission spectroscopy (BES). The vertical far infrared interferometer (FIRI) data of large ELM crashes for the high power heated plasma showed plasma density increase, which is a contrary tendency to the general plasma density change at the ELM crashes. The radial millimetre wave interferometer (MMWI) data showed smaller density increase than the vertical interferometer and 2D BES data showed poloidally upward flow of edge density during the ELMs, which implies poloidal asymmetry of edge density distribution. The order of diagnostics response in time is analyzed as: 1) midplane emission (filterscope), 2) SOL density increase (FIRI/MMWI), 3) divertor emission (D_α). The magnitude of density increase at the ELM crashes measured by FIRI for high power heated plasmas recorded up to 20% which is contrast to the response of low power heated plasma (5–10% decrease). A simple one dimensional model of plasma-neutral interaction including ionization and recombination will be presented with detail methods of diagnostics.

EX



H-Mode Divertor Target Heat Load Measurements on KSTAR

H. Lee¹, C. S. Kang¹, S. Oh¹, J. G. Bak¹, R. A. Pitts², S.-H. Hong¹, H. G. Frerichs³, J.-K. Park⁴, O. Schmitz³, H. Wi¹, Y. Kim¹, H. Kim¹, H. Kim¹, K. Kim¹, D. Seo¹, and W. Choe⁵

¹National Fusion Research Institute (NFRI), Daejeon, Republic of Korea

²International Thermonuclear Experimental Reactor (ITER),
Cadarache Centre, 13108 Saint-Paul-lès-Durance, France

³University of Wisconsin-Madison, Madison, WI 53706, USA

⁴Princeton Plasma Physics Laboratory (PPPL), Princeton, NJ 08540, USA

⁵Korea Advanced Institute of Science and Technology (KAIST), Daejeon, Republic of Korea

Corresponding Author: H. Lee, jdfm@nfri.re.kr

Divertor target heat loads in future long pulse, high power tokamak reactors such as ITER or DEMO will impose major operational constraints. Detached divertor operation and suppression or substantial mitigation of edge localized modes (ELMs) will be mandatory. One of the most promising ELM mitigation methods to be applied on ITER is the use of 3D magnetic perturbations (MPs). This technique substantially modifies the divertor SOL structure and can lead to nonaxisymmetric power loading on the targets [1]. The study of this 3D heat deposition under highly dissipative, H-mode conditions is a key research area for ITER. The KSTAR tokamak is equipped with an extensive set of in-vessel magnetic perturbation (MP) coils. A state-of-the-art infrared (IR) thermography system has also recently been installed, viewing the lower, outer divertor target from the top of the main chamber. The power density on the target is set by the scrape-off layer (SOL) power width, λ_q . A recent multimachine scaling for the H-mode λ_q based on high resolution IR finds an expected value of $\lambda_q \sim 1$ mm for the ITER H-mode baseline scenario [2]. It has been found that the first inter-ELM λ_q values obtained in the KSTAR H-mode plasmas are in good agreement with the multimachine scaling. Furthermore, ELM suppression and mitigation is a priority research area on KSTAR [3], but until the installation of the new thermography system, it has not been possible to observe the target heat loads during MP application. However, in the last year, it has been clearly observed that the application of the 3D MPs can induce the splitting of the outer divertor heat striking point. A clear evidence of different strike point splitting pattern seen on the target between the two different coil perturbations was also found. This paper presents an overview of the first experimental studies of divertor power loading, with emphasis on the characterization of inter-ELM heat load widths in the absence of MPs and on the nonaxisymmetric divertor heat loading arising from the application of MPs.

References

- [1] O. Schmitz, *et al.*, J. Nucl. Mater. **438**, S194 (2013).
- [2] T. Eich, *et al.*, Nucl. Fusion **53**, 09031 (2013).
- [3] Y. M. Jeon, *et al.*, Phys. Rev. Lett. **109**, 035004 (2012).



Comparative Study of KSTAR and DiPS-2 on the Heat Flux to the First Wall

M.-K. Bae¹, I. J. Kang¹, R. A. Pitts², J. G. Bak³, H.-S. Kim³, S.-H. Hong³, and K.-S. Chung¹

¹*Hanyang University, Seongdong-gu, Seoul, Republic of Korea*

²*International Thermonuclear Experimental Reactor (ITER),*

Cadarache Centre, 13108 Saint-Paul-lès-Durance, France

³*National Fusion Research Institute (NFRI), Daejeon, Republic of Korea*

Corresponding Author: M.-K. Bae, bmin999@gmail.com

Although type-I ELM heat flux mainly reaches the divertor plates, it would cause severe damage to the first wall in advanced tokamaks due to radial convective loss of ELM. Heat loads on the first wall is mostly caused by the fast radial convective propagation of ELM filaments. In this paper, heat fluxes toward the first wall of KSTAR device are investigated as a form of ELM filaments, and they are compared with those of Divertor Plasma Simulator-2 (DiPS-2) installed in Hanyang University. Plasma parameters are measured by a specially designed electric probe system composed of a set of eight probes, which are fixed on the outboard midplane wall. These are arranged in two, poloidally separated, triple probes and one Mach probe, which allow direct measurements of electron temperatures, particle and heat fluxes, and Mach numbers at the wall with enhanced time resolved acquisition rate of 2 MHz. During 2015 KSTAR campaign, type-I ELMing H-mode discharges have been performed with a lower single null magnetic geometry, where the outboard separatrix position is slowly scanned over a radial distance of 7 cm, reducing the wall probe-separatrix distance to a minimum of ~9 cm, which enables us to investigate parallel ELM filament energy loss in terms of radial distance. A separate fast reciprocating probe head is held at fixed position toroidally close and 4.7 cm radially in front of the wall probe. An average filament radial propagation speed is extracted as 100 m/s or so from those separated probes. Heat flux (q_{\parallel}) is observed to exponentially decay in the radial direction with the following typical range of parameters: $q_{\parallel} = 0.04\text{--}0.5 \text{ MW/m}^2$. The decay length of heat flux has been deduced as 26–34 mm. Along with the measured radial propagation speed and the calculated radial profile of the magnetic connection lengths across the SOL. To expand the case of pure plasma in KSTAR to the case of impure and dusty plasmas, we performed experiments on heat flux to the wall in a linear plasma device, called DiPS-2 which has relevant physical parameters and geometry to simulate both the edge plasmas and ELM phenomena of toroidal devices. Fixed azimuthal probes are installed which are to be simulated the poloidal probes of KSTAR.

EX



Experimental Observations of Beam-Driven Alfvén Eigenmodes in KSTAR

J. Kim¹, T. Rhee¹, J. Y. Kim², H.-S. Kim¹, M.-H. Woo¹, C.-S. Byun³, Y.-S. Na³, J. G. Bak¹,
H. Kim¹, K. Shinohara⁴, and C. Cheng⁵

¹*National Fusion Research Institute (NFRI), Daejeon, Republic of Korea*

²*University of Science & Technology, Daejeon, Republic of Korea*

³*Seoul National University, Seoul, Republic of Korea*

⁴*Japan Atomic Energy Agency (JAEA), Naka, Japan*

⁵*National Cheng Kung University, Tainan City, Taiwan, China*

Corresponding Author: J. Kim, kimju@nfri.re.kr

Energetic ions generated by auxiliary heating and fusion reactions are able to produce the characteristic Alfvénic activities such as excitation of Alfvén eigenmodes (AE) and high-frequency chirping modes through wave-particle interactions. In KSTAR, on-axis neutral beam injection (NBI) is a main supplier of the fast ions, and has two primary roles which are heating and current drive. Beam-ions produce radial fast-ion pressure profile that can drive the energetic particle modes including AEs. Neutral beam current drive (NBCD) could change the phase space of the fast-ion distribution, hence the excitation condition of the AE is varied. Most of high-performance/advanced discharges such as high- β_p or hybrid operation scenarios have shown the active Alfvénic modes, which may be caused by the enhanced fast-ion pressure gradient and the broad current density profile in the core region. Depending on the energy and the ion-source of the neutral beams, changes in frequency and amplitude of the AEs have been found and bursting energetic-particle continuum mode (EPM) can be excited or eliminated. It implies that NBI, utilized with the operation scenario, can be used as one of promising control tools to mitigate the AEs since fast-ion pressure and beam-driven current profiles have the primary role of exciting or mitigating the AEs. In addition, preliminary observations on the fast-ion losses, which seem to be associated with the multiple n -mode AEs or the fast-sweeping modes, are discussed in this presentation. Experimental observations of the AEs in the high-performance discharges are identified and categorized by the intensive modelling using the numerical codes such as CRONOS, NOVA and so on.

EX



Current Profile Evolutions with External Current Drive for KSTAR

J. Ko¹, J. Chung¹, M. Messmer², and S. Schenkelaars²

¹National Fusion Research Institute (NFRI), Daejeon, Republic of Korea

²Eindhoven University of Technology, Eindhoven, Netherlands

Corresponding Author: J. Ko, jinseok@nfri.re.kr

The current profile evolutions have been measured from the plasma discharges with the electron cyclotron current drive (ECCD) for the Korea Superconducting Tokamak Advanced Research (KSTAR) for the first time. This measurement has been possible by the newly-installed motional Stark effect (MSE) diagnostic system that utilizes the polarized Balmer-alpha emission from the energetic neutral deuterium atoms induced by the Stark effect under the Lorentz electric field. The 25-channel KSTAR MSE diagnostic is based on the conventional photoelastic modulator (PEM) approach with the spatial and temporal resolutions of < 2 cm (for the most of the channels except 2 to 3 channels inside the magnetic axis) and about 10 ms, respectively. The strong Faraday rotation imposed on the optical elements in the diagnostic system is calibrated out from a separate and well-designed polarization measurement procedure using an in-vessel reference polarizer during the toroidal-field ramp-up phase before the plasma experiment starts. The evolution of the pitch angle along with the modulated injection of the 170 GHz ECCD implies that the modulation frequency in the electron cyclotron wave injection is fast compared with the current relaxation time (about 1 s) at the KSTAR plasmas. According to the magnetic pitch angle profiles, it is conjectured that the wave energy is transported to the plasma with the time scale comparable to that of the modulation (about 0.1 s). The current density profile that can be inferred from the spatial gradient of the tokamak pitch angle is not drastically changed and instead, a significant shift of the whole profile including the location of the magnetic axis is clearly seen as a result of the energy transport. The measured pitch angle data can be used to constrain iterative equilibrium calculations in order to obtain current density and safety factor profiles consistent with the magnetic flux surfaces.

EX



Loss of Predisruptive Runaway Electrons by Magnetic Perturbation and its Effect on Plasma Disruption

M. Cheon¹, J. Kim¹, Y. An¹, and Y. In¹

¹*National Fusion Research Institute (NFRI), Daejeon, Republic of Korea*

Corresponding Author: M. Cheon, munseong@nfri.re.kr

Recently it is suggested that the loss of runaway electrons localized in the plasma triggers the plasma disruption by transferring their energy to the first wall generating massive impurities, based on the observation in KSTAR. In order to check the feasibility of the suggestion, localized magnetic perturbation was applied on the plasma edge to remove runaway electron beam from the plasma, utilizing the in-vessel field error correction coil installed at KSTAR. It is observed that sudden burst of photoneutrons was generated at certain level of the FEC coil current during a shot where a gradual increase of the perturbed field penetration was occurring by increasing the FEC coil current, indicating that the runaway electron beam localized on certain drift orbit were transported to the first wall by the magnetic perturbation reached the location. At the time of the neutron burst, typical disruptive behaviours such as the sudden decrease of the electron temperature, negative spike in the loop voltage, burst of D_α signal, fluctuation in Mirnov coil signal, and current decay with characteristic positive current excursion were observed, confirming the validity of the runaway-triggered plasma disruption model.

EX



Observation and Simulation of TAEs in KSTAR Plasmas

C.-M. Ryu¹, H. Rizvi¹

¹Pohang University of Science and Technology (POSTECH), Pohang, Gyeongbuk 790-784, Republic of Korea

Corresponding Author: C.-M. Ryu, ryu201@postech.ac.kr

Toroidicity induced Alfvén eigenmodes (TAE) [1–3] can be driven unstable by fast particles from neutral beam heating or fusion reactions and have been observed in different tokamaks [4–5]. We report the observation of TAEs in KSTAR plasmas during the 2013–2015 campaigns by the fast particles produced the neutral beam injection and global gyrokinetic simulations of them by using the GTC and GENE codes. Mode analysis indicates that the TAEs in KSTAR have low n numbers, mainly $n = 1$, differently from the cases of other tokamaks which showed rather high- n toroidal mode numbers. This seems to indicate that the finite Larmor radius (FLR) stabilizing effects are playing in KSTAR. To understand the TAE mode characteristics and finite orbit Larmor radius stabilization effects, we carried out linear simulations by using the GTC and GENE codes, which give results in agreement. The mode frequency, growth rate, poloidal and radial mode structures analyzed by using these two codes are presented.

References

- [1] F. Zonca, *et al.*, Plasma Phys. Control. Fusion **48**, B15 (2006).
- [2] W. W. Heidbrink, Phys. Plasmas **15**, 055501 (2008).
- [3] S. E. Sharapov, *et al.*, Nucl. Fusion **53**, 104022 (2013).
- [4] Ph. Lauber, Nucl. Fusion **52**, 094007 (2012).
- [5] S. da Graça, *et al.*, Plasma Phys. Control. Fusion **54**, 095014 (2012).

EX



Shielding and Amplification of Nonaxisymmetric Divertor Heat Flux by Plasma Response to Applied 3D Fields in NSTX and KSTAR

J.-W. Ahn¹, K. Kim², A. Briesemeister¹, G. Canal³, J. Canik¹, T. K. Gray¹, Y. In⁴, Y. Jeon⁴, C. S. Kang⁴, J. Kim⁴, W. H. Ko⁴, H. H. Lee⁴, A. Loarte⁵, R. Mainigi⁶, A. McLean⁷, J.-K. Park⁷, R. A. Pitts⁵, J. Lore¹, O. Schmitz⁸, F. Scotti⁷, and S.-W. Yoon⁴

¹Oak Ridge National Laboratory (ORNL), Oak Ridge, TN 37831, USA

²Korea Advanced Institute of Science and Technology (KAIST), Daejeon, Republic of Korea

³General Atomics, San Diego, CA 92186, USA

⁴National Fusion Research Institute (NFRI), Daejeon, Republic of Korea

⁵International Thermonuclear Experimental Reactor (ITER), Cadarache Centre, 13108 Saint-Paul-lès-Durance, France

⁶Princeton Plasma Physics Laboratory (PPPL), Princeton, NJ 08540, USA

⁷Lawrence Livermore National Laboratory (LLNL), Livermore, CA 94550, USA

⁸Department of Engineering Physics, University of Wisconsin-Madison, Madison, WI 53706, USA

Corresponding Author: J.-W. Ahn, jahn@pppl.gov

Understanding of underlying physics processes that determine nonaxisymmetric divertor footprints is crucial for ITER's long pulse operation scenario in the presence of 3D fields, as they will cause asymmetric erosion and redeposition of divertor material. It has been recently found that plasma response plays a key role in the formation of 3D lobe structure and divertor footprints by the applied 3D fields in NSTX and KSTAR. Work in NSTX showed that ideal plasma response from the IPEC modelling can significantly shield or amplify vacuum footprints from field line tracing. Comparison of footprint measurements by visible and IR cameras to the data from field line tracing reveals that $n = 1$ magnetic perturbations are significantly amplified while $n = 3$ perturbations are shielded. The mechanism of amplification and shielding is determined by the competition between shielding of resonant components and excitation of nonresonant components of applied 3D fields, demonstrated in the poloidal field spectrum when including plasma response in the modelling. Connection length (L_c) profile from the IPEC modelling for $n = 1$ case shows that L_c rapidly begins to decrease in a significantly deeper region, compared to the vacuum case where it only drops near the very plasma edge, corresponding to a dramatic amplification of vacuum footprint splitting. Shielding and amplification of applied 3D fields have been also observed in KSTAR by IPEC plasma response modelling. A full phase shift scan was conducted for $n = 1$ perturbations, while two distinctive phases (90° for resonant and 0° for nonresonant coil configuration) were closely examined for $n = 2$ perturbations. As in NSTX, nonresonant components of applied fields are amplified due to kink excitation while resonant components are strongly shielded, which produces net amplification (shielding) effect of applied fields that strengthens (weakens) footprint splitting, depending on which action is more dominant for a specific phase shift. Radial location of lobes in the measured heat flux profile shows better agreement with that from the field line tracing when plasma response is taken into account for calculation.

Work supported by the U.S. Department of Energy, contract numbers DE-AC05-00OR22725 (ORNL), DE-AC02-09CH11466 (PPPL), DE-FC02-04ER54698 (GA), and DE-AC52-07NA27344 (LLNL), and DE-SC0013911 (UW).



Scrape-Off Layer and Divertor Physics Advances in MAST

F. Militello¹, A. Kirk¹, S. Allan¹, B. Dudson², L. Easy^{2,1}, S. Elmore¹, T. Farley^{3,1}, L. Garzotti⁴, J. Harrison¹, E. Havlickova¹, B. Lipschultz^{2,1}, I. Lupelli¹, J. Omotani⁵, R. Scannell¹, A. Thornton¹, J. Young^{6,1}, and N. Walkden¹

¹Culham Centre for Fusion Energy (CCFE), Culham Science Centre, Abingdon, UK

²York Plasma Institute, University of York, Heslington, UK

³University of Liverpool, Liverpool, UK

⁴United Kingdom Atomic Energy Authority, Culham Science Centre, Abingdon, UK

⁵Chalmers University of Technology, Göteborg, Sweden

⁶University of Manchester, Manchester, UK

Corresponding Author: F. Militello, fulvio.militello@ukaea.uk

We review the recent MAST exhaust programme which focussed on the interplay between scrape-off layer (SOL) profiles and filaments, and on the physics of advanced divertors. MAST experiments demonstrated that the broadening of the SOL density profiles observed at high fuelling can occur in the absence of detachment and independently from ionization sources and that it is reduced at high I_p . At the midplane, Ball-pen and Retarding Field (RF) probes showed that E_r is sheared, peaks at ~ 1 kV/m and increases with I_p and that $T_i \sim 2-4 T_e$. A new binning technique of the High Resolution Thomson Scattering data showed that near SOL decay lengths decrease with I_p and increase with fuelling and that are well correlated with light emission, suggesting a role for the neutral particles in setting the profiles. A database of double-null inter-ELM target heat flux profiles was generated and their fall off length was extracted. The best scaling found utilizes the I_p and P_{SOL} but the quality of fit suggests that additional parameters might be required. Infrared thermography showed that L-mode filaments can account for the full target heat flux, and the RF probe that they carry significant ion energy to large distances. Fast visible imaging showed that their radial size (~ 2 cm) and velocity (~ 1 km/s) decrease as I_p increases. Measurements of individual blobs were compared to 3D simulations carried out with STORM to validate the code. An analytic model was developed to assess the effect of the observed ellipticity of the filaments. The effect of low divertor temperature, as expected when detached, was simulated by increasing the resistivity at the target, finding that blobs become electrically disconnected and speed up only for $T_e < 1$ eV. A theoretical framework was developed to interpret experimental density profiles using simple properties of the filaments. Each event is modelled with a wave function with amplitude and width distributed according to experimental observations and evolving according to fluid equations. Multifluid simulations of the MAST-U Super-X divertor show that it will detach at lower density ($\times 1/3$) or higher power ($\times 4$) with respect to the conventional divertor. The new divertor is predicted to reduce the target power load through magnetic geometry and baffling as the closure of the divertor leads to an increase in neutral density with concomitant power losses.

EX

Investigation of Merging/Reconnection Heating during Solenoid-Free Startup of Plasmas in the MAST Spherical Tokamak

H. Tanabe¹, T. Yamada², K. Gi¹, T. Watanabe¹, K. Kadowaki¹, M. Gryaznevich³, R. Scannell³, N. Conway³, C. Michael³, B. J. Crowley³, J. Harrison³, I. Fitzgerald³, A. Meakins³, N. Hawkes³, K. McClements³, T. O'Gorman³, and C.-Z. Cheng¹

¹University of Tokyo, Tokyo, Japan

²Kyushu University, Kasuga, Japan

³Culham Centre for Fusion Energy (CCFE), Culham Science Centre, Abingdon, UK

Corresponding Author: H. Tanabe, tanabe@ts.t.u-tokyo.ac.jp

We present results of recent studies of merging/reconnection heating during central solenoid (CS)-free plasma startup in the Mega-Amp Spherical Tokamak (MAST) which achieved major progress in the last three years through the use of new 32-chord ion-Doppler tomography, 130 channel YAG- and 300 channel Ruby-Thomson scattering diagnostics. In addition to the previously achieved ~ 1 keV heating without solenoid, detailed full temperature profile measurements including the diffusion region of magnetic reconnection have been achieved for the first time. 2D imaging measurements of ion and electron temperature profiles have revealed that magnetic reconnection mostly heats ions globally in the downstream region of outflow jet and electrons locally at the X-point. The electron temperature profile forms a characteristic peaked structure at the X-point on a scale length of typically 0.02 – 0.05 m $< c/\omega_{\pi}$. The higher toroidal field in MAST strongly inhibits cross-field thermal transport scaling as $1/B_t^2$ and the established profile is sustained on a millisecond time scale. In contrast, ions are mostly heated in the downstream region of outflow acceleration inside the current sheet width ($c/\omega_{\pi} \sim 0.1$ m) and around the stagnation point formed by reconnected flux mostly by viscosity dissipation and shock-like compressional damping of the outflow jet. Toroidal confinement also contributes to the characteristic profile, with a high temperature region arising from outflow heating, forming a ring structure aligned with the closed flux surface. There is an effective confinement of the downstream thermal energy due to a thick layer of reconnected flux. The characteristic structure is sustained for longer than an ion-electron energy relaxation time ($\tau_{ei}^E \sim 4$ – 11 ms) and the energy exchange between ions and electrons contributes to the bulk electron heating in the downstream region. The toroidal guide field mostly contributes to the formation of a localized electron heating structure at the X-point but not to bulk ion heating downstream; the latter determines the overall performance of the bulk startup heating. We have thus demonstrated that merging/reconnection heating can be achieved in plasmas with higher toroidal fields ($B_t > 0.3$ T) than those used in other experiments.

EX



Isolation of Neoclassical Toroidal Viscosity Profile under Varied Plasma and 3D Field Conditions in Low and Medium Aspect Ratio Tokamaks

S. A. Sabbagh¹, Y.-S. Park¹, R. E. Bell², Y. M. Jeon³, J. Kim³, J. Ko³, W. H. Ko³, B. LeBlanc², J. Lee³, K. C. Shaing⁴, Y. Sun⁵, J. W. Berkery¹, S. P. Gerhardt², S.-H. Hahn³, and Y. In³

¹*Columbia University, New York, NY 10027, USA*

²*Princeton Plasma Physics Laboratory (PPPL), Princeton, NJ 08540, USA*

³*National Fusion Research Institute (NFRI), Daejeon, Republic of Korea*

⁴*University of Wisconsin-Madison, Madison, WI 53706, USA*

⁵*Institute of Plasma Physics, Chinese Academy of Sciences, Hefei, Anhui, People's Republic of China*

Corresponding Author: S. A. Sabbagh, sabbagh@pppl.gov

Neoclassical Toroidal Viscosity (NTV) due to non-ambipolar particle diffusion occurs in tokamaks due to low magnitude ($\delta B/B_0 \sim 10^{-3}$) three-dimensional (3D) applied magnetic fields, used for positive purposes including alteration of the plasma rotation profile, V_t , to stabilize MHD modes and for ELM suppression. As ITER and future devices will use 3D fields for these purposes, it is important to accurately quantify NTV effects over key plasma and 3D field variations. The present work quantitatively analyzes and compares a formidable combination of NTV databases from two tokamak devices of significantly different aspect ratio. These data allows testing of NTV theory over a broad range of plasma variables including aspect ratio, q_{95} , collisionality, gyroradius, plasma rotation speed and profile, as well as 3D field strength and spectrum. Isolation of the NTV torque profile, T_{NTV} , is accomplished by applying the 3D field faster than the plasma momentum diffusion time. A dedicated international experiment was run in late 2015 to measure the NTV profile this way for the first time in the KSTAR superconducting tokamak at medium aspect ratio ($A = 3.5$). Over 360 variations of the parameters mentioned above were produced. These results are compared to new analysis of complementary experimental results from the extensive NTV database of low $A = 1.3$ NSTX plasmas. The NSTX experiments yield unique information in plasmas with computed displacements smaller than the ion banana width, showing that finite-orbit effects will average T_{NTV} over such spatial scales. In KSTAR, six different 3D field spectra were run, including dominantly $n = 2$, $n = 1$ field pitch-aligned, $n = 1$ field pitch nonaligned configurations, and their superposition. As expected by theory, the measured rotation profile change due to the 3D field, ∇V_t , does not change sign, and is close to zero near the plasma boundary. All cases show broader ∇V_t than found in NSTX. The change to the relative pitch alignment of the applied 3D field yielded a clear and unexpected result: the non-pitch-aligned field configuration produced a stronger change to the V_t profile than the pitch-aligned case. The ∇V_t is global and nonresonant, with no strong indication of localized resonant effects, similar to NSTX results in different field configurations.

Work supported by the U.S. Department of Energy contracts DE-FG02-99ER54524 and DE-AC02-09CH11466.



Characterization and Forecasting of Unstable Resistive Wall Modes in NSTX and NSTX-U

J. W. Berkery¹, S. A. Sabbagh¹, Y.-S. Park¹, R. E. Bell², S. P. Gerhardt², and C. Myers²

¹Columbia University, New York, NY 10027, USA

²Princeton Plasma Physics Laboratory (PPPL), Princeton, NJ 08540, USA

Corresponding Author: J. W. Berkery, jberkery@pppl.gov

A comprehensive approach to the prevention of disruption of fusion plasmas in tokamaks begins with identifying disruption event chains and the specific physics elements which comprise those chains. Then, if the events in the disruption chains can be forecast, cues can be provided to an avoidance system to break the chain. Within this framework, we examine the characterization and forecasting of unstable resistive wall modes (RWMs) in the NSTX tokamak and its upgrade NSTX-U. For forecasting purposes, one can examine when the plasma toroidal rotation profile falls into a weaker RWM stability region based upon kinetic stability theory. The MISK code solves for the growth rate of the RWM through a dispersion relation dependent on the changes in potential energy, δW . A model for the ideal no-wall δW term which depends on parameters that can be measured in real-time has been recently computed. For the kinetic δW_K term, full MISK calculations cannot be performed in real time, but a simplified model calculation based on physics insight from MISK takes a form that depends on $E \times B$ frequency, collisionality, and energetic particle fraction. The reduced model results are tested by analysis performed on a database of 44 NSTX discharges with unstable RWMs. For this analysis, we have created the Disruption Event Characterization and Forecasting (DECAF) code. For each discharge, the code finds the chain of events leading to a disruption by applying criteria that define each of the physical events. With a RWM poloidal sensor amplitude threshold of 30 G the RWM warning was found in each case, typically near the disruption limit. Other events detected in all discharges were failure to meet plasma current request, loss of wall proximity control, and low edge safety factor warnings. Loss of vertical stability control was present in most discharges, as was pressure peaking, which did not cause RWMs, typically occurring with or after them. In 59% of the cases, the RWM event occurred within 20 wall times of the disruption. Additionally, the RWM warnings that occurred earlier were not false positives; they caused significant temporary decreases in β_N . The DECAF code analysis of RWM-induced disruptions is under active development, including improved approaches in determining event causality.

Work supported by the U.S. Department of Energy Contracts DE-FG02-99ER54524 and DE-AC02-09CH11466.

EX



Exploring the Regime of Validity of Global Gyrokinetic Simulations with Spherical Tokamak Plasmas

Y. Ren¹, W. W. Wang¹, W. Guttenfelder¹, S. Kaye¹, S. Ethier¹, R. E. Bell¹, B. LeBlanc¹,
E. Mazzucato¹, D. Smith², C. W. Domier³, and H. Yuh⁴

¹Princeton Plasma Physics Laboratory (PPPL), Princeton, NJ 08540, USA

²University of Wisconsin-Madison, Madison, WI 53706, USA

³University of California Davis, CA 95616, USA

⁴Nova Photonics, Inc., Princeton, NJ 08540, USA

Corresponding Author: Y. Ren, yren@pppl.gov

EX Plasma turbulence is considered one of the main mechanisms for driving anomalous thermal transport in magnetic confinement fusion devices. Based on first-principle model, gradient-driven gyrokinetic simulations have often been used to explain turbulence-driven transport in present fusion devices, and in fact, many present predictive codes are based on the assumption that turbulence is gradient-driven. However, using the electrostatic global particle-in-cell Gyrokinetic Tokamak Simulation (GTS) code [1], we will show that while global gradient-driven gyrokinetic simulations provide decent agreement in ion thermal transport with a set of NBI-heated NSTX H-mode plasmas, they are not able to explain observed electron thermal transport variation in a set of RF-heated L-mode plasmas, where a factor of 2 decrease in electron heat flux is observed after the cessation of RF heating. Thus, identifying the regime of validity of the gradient-driven assumption is essential for first-principle gyrokinetic simulation. This understanding will help us more confidently predict the confinement performance of ITER and future magnetic confinement devices.

References

[1] W. X. Wang, *et al.*, Phys. Plasmas **17**, 072511 (2010).

Work supported by the U.S. Department of Energy and computational resource is provided by NERSC.



Kinetic Profiles and Impurity Transport Response to 3D-Field Triggered ELMs in NSTX

F. Scotti¹, V. Soukhanovskii¹, J. Canik², R. E. Bell³, A. Diallo³, S. Kaye³, B. LeBlanc³, and M. Podestà³

¹Lawrence Livermore National Laboratory (LLNL), Livermore, CA 94550, USA

²Oak Ridge National Laboratory (ORNL), Oak Ridge, TN 37831, USA

³Princeton Plasma Physics Laboratory (PPPL), Princeton, NJ 08540, USA

Corresponding Author: F. Scotti, fscotti@pppl.gov

The response of kinetic plasma profiles to 3D-field triggered edge localized modes (ELMs) and the inter-ELM carbon impurity transport were analyzed in lithium-conditioned H-mode discharges in NSTX. ELM-free lithium-conditioned H-mode discharges were characterized by core accumulation of impurities as a result of near-neoclassical impurity transport, an edge inward pinch and the absence of impurity flushing mechanisms. Nonaxisymmetric magnetic perturbations ($n = 3$) were applied to trigger ELMs (triggering frequency $f_{\text{ELM}} = 10\text{--}62.5$ Hz), and mitigate core impurity buildup maintaining the positive effects of lithium on energy confinement. Edge impurity flushing increased with f_{ELM} , with a progressive reduction in the carbon density n_C at the pedestal top. For ELMs triggered at 10 Hz, up to a 30% drop in n_C was observed, with comparable effects in the n_e , T_i , and toroidal velocity v_ϕ profiles. The increase in f_{ELM} led to a reduction in the core carbon inventory and progressively modified edge profiles. Inside the pedestal top, n_C and n_e were reduced by up to 60% and 40%, respectively, while being unaffected in the steep gradient region. T_i and v_ϕ normalized edge gradients increased by up to a factor of three. The ELM effect on the n_C profiles was reproduced in simulations with the impurity transport code MIST with an inward convective perturbation and an outward diffusive/convective perturbation to the steady state carbon transport coefficients (inside and outside normalized volumetric radii R_{VOL} of 0.6, respectively). The agreement of inter-ELM carbon transport with neoclassical estimates improved with the increase in f_{ELM} . The changes in T_i and n_D profiles due to triggered ELMs led to changes in carbon neoclassical transport coefficients comparable and opposite to those observed with the transition from ELMy boronized discharges to ELM-free lithium-conditioned discharges. In particular, the carbon neoclassical convective velocity (evaluated via NCLASS) at the top of the pedestal changed direction (from inward to outward). Concomitantly, better agreement between the neoclassical transport predictions and experimental inter-ELM n_C profile shapes was observed in lithium-conditioned discharges with triggered ELMs in a similar way to naturally ELMy discharges.

Work supported by the U.S. Department of Energy contracts DE-AC02-09CH11466, DE-AC05-00OR22725, DE-AC52-07NA27344.



Comparison of Helium Glow and Lithium Evaporation Wall Conditioning Techniques in Achieving High Performance H-Mode Discharges in NSTX

R. Maingi¹, J. Canik², R. E. Bell¹, A. Diallo¹, D. Boyle¹, R. Kaita¹, S. Kaye¹, B. LeBlanc¹, S. A. Sabbagh³, F. Scotti⁴, and V. Soukhanovskii⁴

¹Princeton Plasma Physics Laboratory (PPPL), Princeton, NJ 08540, USA

²Oak Ridge National Laboratory (ORNL), Oak Ridge, TN 37831, USA

³Columbia University, New York, NY 10027, USA

⁴Lawrence Livermore National Laboratory (LLNL), Livermore, CA 94550, USA

Corresponding Author: R. Maingi, rmaingi@pppl.gov

Experiments in NSTX demonstrated reproducible operation with interdischarge lithium evaporation, eliminating the need for interdischarge helium glow discharge cleaning (HeGDC), improving plasma confinement as well as the duty cycle. To assess the viability of operation without HeGDC and directly compare with interdischarge lithium evaporation, the interdischarge HeGDC duration was systematically reduced in four steps from the standard nine minutes to zero. Good discharge reproducibility without HeGDC was achieved with lithium evaporation doses of 100 mg or higher; evaporations of 200–300 mg typically resulted in very low ELM frequency or ELM-free operation, reduced recycling, and improved energy confinement. Similar results were obtained in the inverse experiment, i.e., when lithium evaporation was terminated, and intershot HeGDC was reinitiated, with a gradual increase in HeGDC duration and decrease in external fuelling. Finally, an experiment in which a large lithium dose (~ 25 g, ~ 100 times the typical intershot evaporation) prior to operations was conducted. In this case, about 100 plasma discharges over three run days were conducted with neither interdischarge Li evaporation nor HeGDC. Nearly all of these achieved H-mode, but the pulse lengths and performance were not reproducible.

While the discharges with longer interdischarge HeGDC times performed modestly better than those with shorter or no HeGDC durations, the discharge performance improved substantially in NSTX with increasing lithium dose in these strongly shaped plasmas, which were analyzed with SOLPS edge transport code. Data-constrained interpretive modelling with SOLPS quantified the edge transport change: the electron particle diffusivity decreased by 10–30 \times . The electron thermal diffusivity decreased by 4 \times just inside the top of the pedestal, but increased by up to 5 \times very near the separatrix. These results provide a baseline expectation for lithium benefits in NSTX-U, which is optimized for a boundary shape similar to the one used in this experiment. New results from upcoming wall conditioning experiments in NSTX-U will also be presented, when available.



Locked-Mode Avoidance and Recovery without External Momentum Input Using ICRH

L. F. Delgado-Aparicio¹, J. E. Rice², E. M. Edlund², I. Cziegler³, L. Sugiyama⁴, J. Terry², S. M. Wolfe², C. Gao², T. Golfinoopoulos², J. H. Irby², R. S. Granetz⁴, Y. Lin², S. Wukitch², M. J. Greenwald⁴, A. E. Hubbard², J. W. Hughes², E. S. Marmor², S. Houshmandyar⁵, P. Phillips⁵, and W. Rowan⁵

¹Princeton Plasma Physics Laboratory (PPPL), Princeton, NJ 08540, USA

²Plasma Science & Fusion Center, MIT, Cambridge, MA 02139, USA

³University of California San Diego, CA 92093, USA

⁴Massachusetts Institute of Technology (MIT), Cambridge, MA 02139, USA

⁵University of Texas at Austin, Austin, TX 78712, USA

Corresponding Author: L. F. Delgado-Aparicio, ldelgado@pppl.gov

A simple heating technique has been developed that could provide an actuator to circumvent error-field-induced locked-mode disruptions in tokamak plasmas. New observations of the formation and dynamics of error-field-induced locked-modes at ITER toroidal fields, without fuelling and external momentum input have recently been carried out on Alcator C-Mod. Locked-mode excitation is achieved by ramping-up a set of external control “A-coils” capable of producing nonaxisymmetric, predominantly $n = 1$, fields with different toroidal phase and a range of poloidal mode, m , spectra. Features of the locked-mode include significant braking of the core toroidal rotation, a strong density pump out due to interaction between the plasma and the resonant magnetic perturbation and a flattening of the temperature profiles at the $q = 2$ rational surface; the saturated island is approximately 6% of the minor radius. The density pump-out can also be the root for a reduction in the mode-locking thresholds, and is the main cause for a strong reduction in stored energy, confinement time and neutron production. Delay of the locked-mode onset and recovery from preexisting locked-modes has been successfully obtained using Ion Cyclotron Resonance Heating (ICRH). The use of external heating concomitant with the $n = 1$ error-field ramp-up resulted in a delay of the mode-onset avoiding the density pump-out and achieving high-confinement “H-modes”. Heating the low-density plasma after the mode-onset was not conducive to an L-H transition but resulted in unlocking the plasma without external torque and obtaining co/countercurrent flows at the edge/core.

Work performed at Alcator C-Mod, a DOE Office of Science User Facility under U.S. Department of Energy contracts, including DE-FC02-99ER54512 and others at MIT and DE-AC02-09CH11466 at PPPL.

EX



Identification of Characteristic ELM Evolution Patterns with Alfvén-Scale Measurements and Unsupervised Machine Learning Analysis

D. Smith¹, R. Fonck¹, G. R. McKee¹, A. Diallo², S. Kaye², B. LeBlanc², and S. A. Sabbagh³

¹University of Wisconsin-Madison, Madison, WI 53706, USA

²Princeton Plasma Physics Laboratory (PPPL), Princeton, NJ 08540, USA

³Columbia University, New York, NY 10027, USA

Corresponding Author: D. Smith, drsmith8@wisc.edu

Characteristic edge localized mode (ELM) evolution patterns are identified and measured at Alfvén timescales with a multipoint beam emission spectroscopy (BES) diagnostic on NSTX/NSTX-U, and parameter regimes corresponding to the characteristic ELM evolution patterns are identified. The linear peeling-ballooning stability boundary expresses an onset condition for ELMs, but ELM saturation mechanisms, filament dynamics, and multimode interactions require nonlinear models. Validation of nonlinear ELM models requires fast, localized measurements on Alfvén timescales. Recently, we investigated characteristic ELM evolution patterns with Alfvén-scale measurements from the NSTX-U beam emission spectroscopy (BES) system [1]. We applied clustering algorithms from the machine learning domain to ELM time-series data. The algorithms identified two or three groups of ELM events with distinct evolution patterns. In addition, we found that the identified ELM groups correspond to distinct parameter regimes for plasma current, shape, magnetic balance, and density pedestal profile [1]. The observed evolution patterns and corresponding parameter regimes suggest genuine variation in the underlying physical mechanisms that influence the evolution of ELM events and motivate nonlinear MHD simulations. Here, we review the previous results for ELM evolution patterns and parameter regimes, and we report on a new effort to explore the identified ELM groups with 2D BES measurements and nonlinear MHD simulations. Finally, we discuss opportunities to leverage machine learning tools in the data-rich fusion science field.

References

[1] D. R. Smith, *et al.*, Plasma Phys. Control. Fusion **58**, 045003 (2016).

Work supported by the U.S. Department of Energy, Office of Science, Office of Fusion Energy Sciences under Award Numbers DE-FG02-89ER53296, DE-SC0001288, and DE-AC02-09CH11466. This research used resources of the National Spherical Torus Experiment-Upgrade, which is a DOE Office of Science User Facility.



Parametric Dependence of EPMS in NSTX

E. Fredrickson¹, M. Podestá¹, S. P. Gerhardt¹, R. E. Bell¹, A. Diallo¹, B. LeBlanc¹,
F. Levinton², and H. Yuh²

¹*Princeton Plasma Physics Laboratory (PPPL), Princeton, NJ 08540, USA*

²*Nova Photonics, Inc., Princeton, NJ 08540, USA*

Corresponding Author: E. Fredrickson, efredrickson@pppl.gov

The International Tokamak Experimental Reactor (ITER) will have a large population of nonthermal, energetic ions consisting of fusion generated alphas and beam ions injected for current profile control. Potential redistribution and/or loss of those nonthermal ions is thus of concern as it will modify heating profiles, current profiles, and could lead to unacceptable levels of heating of plasma facing components. Redistribution and losses of fast ions have been documented as resulting from multiple Alfvénic modes, Toroidal Alfvén Eigenmodes and energetic particle modes (fishbones) on many smaller plasma devices. In this paper we present data and analysis of modes driven by neutral beam ions on the National Spherical Torus Experiment (NSTX). Fishbone-like EPMS are found predominantly in plasmas with $q_{\min} \approx 1$. The long-lived modes, beginning with a frequency chirp (EPM-LLM), typically appear for a broad range of q_{\min} with $1 < q_{\min} < 4$, and the frequency chirp is predominantly a result of a drop in the core toroidal rotation.

EX

Large RF Field Amplitudes in the SOL and Far-Field RF Sheaths: A Proposed Mechanism for the Anomalous Loss of RF Power to the SOL of NSTX

R. Perkins¹, J.-W. Ahn², R. E. Bell¹, N. Bertelli¹, A. Diallo¹, S. P. Gerhardt¹, T. K. Gray², M. A. Jaworski¹, J. C. Hosea¹, G. J. Kramer¹, B. LeBlanc¹, R. Maingi¹, A. McLean³, A. L. Roquemore¹, S. A. Sabbagh⁴, T. Gary¹, and J. R. Wilson¹

¹Princeton Plasma Physics Laboratory (PPPL), Princeton, NJ 08540, USA

²Oak Ridge National Laboratory (ORNL), Oak Ridge, TN 37831, USA

³Lawrence Livermore National Laboratory (LLNL), Livermore, CA 94550, USA

⁴Columbia University, New York, NY 10027, USA

Corresponding Author: R. Perkins, rperkins@pppl.gov

We propose a new model for the anomalous loss of high-harmonic fast-wave (HHFW) heating power to the scrape-off layer (SOL) of the National Spherical Torus eXperiment (NSTX). A significant fraction, up to 60%, of the coupled HHFW power can be lost along scrape-off layer field lines [1], creating bright spirals of heat deposition on the upper and lower divertor regions [2]. It is important to determine the underlying mechanism because, with 20 MW of ICRF power planned for ITER, a similar loss of ICRF power may erode the divertor and produce unacceptable impurity levels. We hypothesize that the SOL losses are caused by a two-step process. First, the radiofrequency (RF) field amplitude becomes quite high in the SOL when the right-hand fast-wave cutoff layer is positioned too close to the HHFW antenna [1–4]. Second, these RF fields setup far-field RF sheaths on the divertor tiles and drive an enhanced heat flux into the divertor [5]. We present results from a cylindrical cold-plasma model that demonstrate a class of modes that conduct a significant fraction of their wave power in the peripheral plasma [6]; these modes appear when roughly a quarter radial wavelength fits into the SOL. Experimental evidence for RF rectified voltages and currents is presented, and our analysis suggests that they could produce additional heat fluxes consistent with infrared camera measurements of the HHFW heat flux within the spirals. This suggests that the SOL losses can be minimized, and heating efficiency maximized, through tailoring of SOL density and antenna phasing, which will be an important consideration for high-power long-pulse ICRF heating on fusion devices, such as ITER.

References

- [1] J. C. Hosea, *et al.*, *Phys. Plasmas* **15**, 056104 (2008).
- [2] J. C. Hosea, *et al.*, *AIP Conf. Proc.* **1187**, 105 (2009).
- [3] D. L. Green, *et al.*, *Phys. Rev. Lett.* **107**, 145001 (2011).
- [4] N. Bertelli, *et al.*, *Nucl. Fusion* **54**, 083004 (2014).
- [5] R. J. Perkins, *et al.*, *Phys. Plasmas* **22**, 042506 (2015).
- [6] R. J. Perkins, *et al.*, 41st EPS Conference on Plasma Physics, P-1.011, (2015).

Work supported in part by the U.S. Department of Energy Contract No. DE-AC02-09CH11466.

Feedback Control Design for Noninductively Sustained Scenarios in NSTX-U Using TRANSP

M. D. Boyer¹, R. Andre¹, D. Gates¹, S. P. Gerhardt¹, J. Menard¹, and F. Poli¹

¹Princeton Plasma Physics Laboratory (PPPL), Princeton, NJ 08540, USA

Corresponding Author: M. D. Boyer, mboyer@pppl.gov

Spherical torus based designs for fusion nuclear science facilities [1] and pilot plants [2] have little to no room for a central solenoid, and require the plasma current to be generated noninductively. Recently completed upgrades to NSTX-U will enable the study of noninductive scenarios, including start-up, ramp-up, and flattop current sustainment. This paper examines active control of such scenarios using TRANSP simulations. TRANSP is a time-dependent integrated modelling code for prediction and interpretive analysis of tokamak experimental data. Its predictive mode has been used for scenario development on NSTX-U, including fully noninductive scenarios [3], and exploration of approaches to noninductive ramp-up [4]. Recently, the ability to include feedback control algorithms in TRANSP has been developed [5]. The actuators considered for control in this work are the six neutral beam sources and the plasma boundary shape. The neutral beam sources allow the current drive deposition and heating to be tailored in real-time. The primary plasma boundary shape parameter that is considered is the midplane outer gap. Increasing this gap leads to increased bootstrap current and moves the neutral beam deposition off axis, tending to increase the central safety factor. To understand the response of the plasma current, stored energy, and central safety factor to these actuators and to enable systematic design of control algorithms, simulations were run in which the actuators were modulated and a linearized dynamic response model was generated. The simplified model was used to design several PID control laws using different combinations of actuators and measurements. Closed loop simulations show that modest changes in the outer gap and heating power can improve the response time of the system, reject perturbations, and track target values of the controlled values. Strong coupling between the controlled quantities is observed, making multivariable control design an important next step.

References

- [1] Y. K. M. Peng, *et al.*, Plasma Phys. Control. Fusion **47**, B263 (2005).
- [2] J. E. Menard *et al.*, Nucl. Fusion **51**, 094011 (2011).
- [3] S. P. Gerhardt, *et al.*, Nucl. Fusion **52**, 083020 (2012).
- [4] F. Poli, *et al.*, Nucl. Fusion **55**, 123011 (2015).
- [5] M. D. Boyer *et al.*, Nucl. Fusion **55**, 053033 (2015).

Work supported by the U.S. Department of Energy Contract No. DE-AC02-09CH11466.



Counter-NBI Experiments on Globus-M

N. Bakharev¹, F. Chernyshev¹, P. Goncharov², V. Gusev¹, A. Iblyaminova¹,
G. S. Kurskiev¹, A. Melnik¹, V. Minaev¹, M. Mironov¹, M. Patrov¹, Y. Petrov¹,
N. Sakharov¹, P. Shchegolev¹, A. Telnova¹, S. Yu. Tolstyakov¹, and G. Zadvitskiy³

¹*Ioffe Institute, St. Petersburg, Russian Federation*

²*St. Petersburg State Polytechnical University, St. Petersburg, Russian Federation*

³*Université de Lorraine, Nancy, France*

Corresponding Author: N. Bakharev, bakharev@mail.ioffe.ru

For the first time a high energy counter-NBI was applied in the Globus-M spherical tokamak. The ELM-free H-mode was obtained. However, no significant increase in the ion temperature and plasma energy content as compared to ELMy H-mode was observed. This is due to a high level of fast ion losses (up to 97%), confirmed by modelling with NUBEAM and full 3D fast ion tracking algorithm. Increase in the plasma current from 120 to 200 kA as well as an increase in plasma-wall distance from 3 to 6 cm did not result in the increase of NB heating efficiency as it occurred during the co-NBI experiments. Modelling showed that in Globus-M2 counter-NBI experiments the power absorbed by plasma will be increased by more than an order of magnitude compared to the current experimental conditions.



Noninductive Production of Extremely Overdense Spherical Tokamak Plasma by Electron Bernstein Wave Excited via O-X-B Method in LATE

H. Tanaka¹, M. Uchida¹, T. Maekawa¹, K. Kuroda¹, Y. Nozawa¹, A. Yoshida¹,
D. Watanabe¹, K. Takamatsu¹, A. Hoshino¹, D. Honda¹, and T. Kawaharada¹

¹*Kyoto University, Nishikyo-ku, Kyoto 615-8540, Japan*

Corresponding Author: H. Tanaka, h-tanaka@energy.kyoto-u.ac.jp

Extremely overdense spherical tokamak plasmas are produced noninductively with electron Bernstein waves mode-converted via O-X-B scheme. When the fundamental electron cyclotron resonance (ECR) layer is located at the plasma core and the 2nd harmonic ECR layer is near the outboard vessel wall and the upper hybrid resonance layer is located between them, significant density rise is obtained with a strong gas puffing preventing hot spots and without intermittent plasma ejection phenomenon.

EX



Recommissioning of the Spherical Tokamak MEDUSA in Costa Rica

I. Vargas-Blanco¹, J. Mora¹, L. A. Araya-Solano¹, A. M. Rojas-Loaiza¹, J. M. Arias-Brenes¹, J. Rojas-Calderón¹, J. I. Monge-Colepicolo¹, A. Canizales¹, E. Acuña-Arias¹, and N. Piedra-Quesada¹

¹*Instituto Tecnológico de Costa Rica, Cartago, Costa Rica*

Corresponding Author: I. Vargas-Blanco, ivargas@itcr.ac.cr

The low aspect ratio spherical tokamak (ST) MEDUSA (Madison education small aspect ratio tokamak) is currently being recommissioned in Costa Rica and was donation to Costa Rica Institute of Technology by the University of Wisconsin–Madison, USA. The major characteristics of this device are [1]: plasma major radius $R_o < 0.14$ m, plasma minor radius $a < 0.10$ m, plasma vertical elongation 1.2, toroidal field at the geometric centre of the vessel $B_t < 0.5$ T, plasma current $I_p < 40$ kA, $n_e(0) < 2 \times 10^{20}/\text{m}^3$, central electron temperature $T_e(0) < 140$ eV, discharge duration is < 3 ms, top and bottom rail limiters, natural divertor D-shaped ohmic plasmas. In addition to training, the major objective of renamed device MEDUSA-CR is to address relevant physics for spherical and conventional tokamaks, taking advantage of the insulating vessel which allows plasma real time response to applied external electrical or magnetic fields.

EX

The major topics for the scientific programme are 1) Comparative studies of equilibrium and stability between natural divertor D and bean-shaped ST plasmas [2]; 2) Study of an ergodic magnetic limiter [2, 3, 4]; 3) Alfvén wave heating and current drive and; 4) Transport. Advances in some of these topics will be presented in this work, in addition to the technical tasks of machine recommissioning involving the redesign of energy, gas injection, vacuum system and control systems.

References

- [1] G. D. Garstka, PhD thesis, University of Wisconsin at Madison, September 1997.
- [2] C. Ribeiro, *et al.*, Proc. 25th Symposium on Fus. Eng., San Francisco, US, (2013).
- [3] C. Ribeiro, *et al.*, Proc. 39th EPS Conf. Contr. Fusion and Plasma Phys., **36F**, P1.091, Stockholm, Sweden, (2012).
- [4] J. J. E. Herrera-Velázquez, E. C. Alarcon, and C. Ribeiro, IAEA FEC–2012, San Diego, USA, (2012), [TH/P2-28](#).



Plasma Startup Experiments on the TST-2 Spherical Tokamak

A. Ejiri¹, Y. Takase², N. Tsujii¹, S. Yajima², T. Shinya¹, H. Yamazaki¹, C. P. Moeller³, H. Togashi¹, K. Toida¹, H. Homma¹, A. Ishida⁴, H. Furui¹, H. Kasahara⁵, T. Mutoh⁵, K. Nakamura¹, B. Roidl¹, K. Saito⁵, T. Seki⁵, M. Sonehara², W. Takahashi¹, T. Takeuchi², Y. Yoshida², and O. Mitarai⁶

¹Graduate School of Frontier Science, University of Tokyo, Tokyo, Japan

²University of Tokyo, Tokyo, Japan

³General Atomics, San Diego, CA 92186, USA

⁴Niigata University, Nishi-ku, Niigata, Japan

⁵National Institute for Fusion Science (NIFS), Toki, Gifu, Japan

⁶Kyushu Tokai University, Kumamoto, Japan

Corresponding Author: A. Ejiri, ejiri@k.u-tokyo.ac.jp

Plasma start-up without a large flux swing central solenoid (CS) is one of critical issues in fusion research. In the TST-2 spherical tokamak (ST), noninductive start-up by waves in the lower-hybrid frequency range (200 MHz) has been studied using three types of antennas. Presently a capacitively-coupled combline (CCC) antenna is used. The maximum sustained plasma current was increased from 16 kA to 25 kA by changing several conditions, such as a higher magnetic field strength and the installation of top and bottom limiters. This demonstrates that lower-hybrid wave (LHW) can be a powerful tool to start-up an ST plasma. Experiments suggested that the wave power is deposited mainly on the peripheral region. In order to improve the wave accessibility and to increase the signal pass absorption, we are preparing for a top-launch CCC antenna, by which a good core power deposition is expected due to the upshift of the n_{\parallel} during the propagation. In addition to the noninductive start-up experiments, AC Ohmic heating experiments with frequencies up to 10 kHz were performed. This is the first systematic experiments on the AC CS operation in tokamaks, and it can be an option to start-up an ST reactor with a small flux swing. It was demonstrated that it can drive a current with finite DC components (1.9 kA with a $|\text{flux swing}| < 2$ mVs) when the vertical field is applied. The ratio of the DC current to the flux swing is comparable to those in TST-2 standard Ohmic discharges. Furthermore, the plasma current can be ramped-up by superposing the AC Ohmic heating on a plasma sustained by EC wave power alone. The time averaged visible image of the plasma in this phase indicates the formation of an ST configuration. The minimum loop voltage for the breakdown was ± 0.5 V, which corresponds to ± 0.6 V/m at the inboard limiter. This value indicates potential application to superconducting CSs.

EX

Investigation of Hydrogen Recycling Property and its Control with Hot Wall in Long Duration Discharges on QUEST

K. Hanada¹, N. Yoshida¹, T. Honda¹, Z. Wang¹, A. Kuzmin¹, I. Takagi², T. Hirata², Y. Oya³, M. Miyamoto⁴, H. Zushi¹, M. Hasrgawa¹, K. Nakamura¹, A. Fujisawa¹, H. Idei¹, Y. Nagashima¹, O. Watanabe¹, T. Onchi¹, H. Watanabe¹, K. Tokunaga¹, A. Higashijima¹, S. Kawasaki¹, H. Nakashima¹, T. Nagata¹, Y. Takase⁵, A. Fukuyama², and O. Mitarai⁶

¹Research Institute for Applied Mechanics (RIAM), Kyushu University, Kasuga, Japan

²Graduate School of Engineering, Kyoto University, Nishikyo-ku, Kyoto 615-8540, Japan

³Shizuoka University, Shizuoka, Japan

⁴Shimane University, Matsue, Shimane, Japan

⁵University of Tokyo, Tokyo, Japan

⁶School of Industrial Engineering, Tokai University, Tokyo, Japan

Corresponding Author: K. Hanada, hanada@triam.kyushu-u.ac.jp

EX Hydrogen (H) recycling and wall pumping properties on a dynamic retention dominant wall (metal wall) have been investigated in a medium size spherical tokamak QUEST. The plasma facing wall on QUEST originally made of stainless steel type 316L (SS316L) and partially coated by atmosphere plasma splay tungsten has been already covered with redeposition layer of 5–100 nm in thickness due to plasma exposure. The redeposition layer is composed of carbon, tungsten, ferrite, chromium and nickel according to X-ray photoelectron spectroscopy (XPS) measurement. Nuclear reaction analysis (NRA) is applied to specimens exposed QUEST H plasmas with exposing deuterium (D) plasma of approximately 1 eV, and presence of H-isotope barrier (HB) between the redeposition layer and the substrate (SS316L) is confirmed due to little penetration to the substrate around 300–350 K of the sample holder temperature. The HB must give a significant impact to H dynamic retention and a surface-recombination limiting model with HB is proposed. The model predicts a typical time constant representing wall saturation, which is relating to H flux to the wall, surface recombination coefficient, and thickness of redeposition layer. In fact, the H storing capability on QUEST clearly depends on H flux and wall temperature experimentally. Especially time derivative wall stored H, that is wall pumping rate, has a clear relation to wall storing H and is well-fitted by the proposed model. Recently a hot wall is installed on QUEST to control H dynamic retention via modification of surface-recombination coefficient and its controllability of H dynamic retention in the range of 393–473 K is experimentally confirmed.



Noninductive Electron Cyclotron Heating and Current Drive with Dual Frequency (8.2/28 GHz) Waves in QUEST

H. Idei¹, T. Onchi², T. Kariya³, K. Hanada¹, T. Imai³, A. Ejiri⁴, O. Watanabe², K. Mishra², K. Nakamura², M. Hasegawa², S. Kawasaki², H. Nakashima², A. Higashijima², H. Zushi¹, Y. Takase⁵, and A. Fukuyama⁶

¹Research Institute for Applied Mechanics (RIAM), Kyushu University, Kasuga, Japan

²Kyushu University, Kasuga, Japan

³Plasma Research Center, University of Tsukuba, Tsukuba, Ibaraki, Japan

⁴Graduate School of Frontier Science, University of Tokyo, Tokyo, Japan

⁵University of Tokyo, Tokyo, Japan

⁶Kyoto University, Nishikyo-ku, Kyoto 615-8540, Japan

Corresponding Author: H. Idei, idei@triam.kyushu-u.ac.jp

By means of dual 8.2 GHz and 28 GHz waves, the over dense 25 kA plasma with central high energetic-electron pressure was noninductively built up and sustained for 0.4 s by Electron Bernstein Wave Heating (EBWH) effect between 8.2 GHz fundamental and 2nd harmonic electron cyclotron (EC) layers. Spontaneous Density Jumps (SDJs) have been clearly observed at a few times in a shot, and the electron density became over dense for the 8.2 GHz injection. The bulk electron temperature or pressure increased in the over dense region being fundamentally Doppler-shifted resonant with the parallel refractive index $N_{\parallel} > 4$ for the 8.2 GHz injection. Current-carrying energetic electrons with more than 200 keV were remarkably observed in the over dense region due to the 8.2 GHz EBWH effect.

EX



ELM Characterization and Dynamics at Near-Unity A in the Pegasus ST

M. Bongard¹, J. Barr¹, R. Fonck¹, D. Kriete¹, J. Reusch¹, and K. Thome¹

¹University of Wisconsin-Madison, Madison, WI 53706, USA

Corresponding Author: M. Bongard, mbongard@wisc.edu

Operation in the high confinement (H-mode) regime and mitigation of associated deleterious Edge Localized Mode (ELM) activity are necessary for the success of ITER and future reactors. H-mode studies at near-unity aspect ratio A can offer unique insights into these issues. Edge plasma parameters at low A permit unique measurements of the edge pedestal with high spatiotemporal resolution using probes. In particular, measurements of the current density profile J_{edge} of import to peeling-ballooning stability and its nonlinear dynamics during ELMs are presented. Two classes of ELMs have been identified to date by their proximity to P_{L-H} and measured n spectra provided by a near-edge Mirnov coil array. Both ELM types produce propagating, field-aligned filaments and have multiple n measured during the crash. These observations are consistent with the presence of a spectrum of simultaneously unstable peeling-ballooning modes anticipated by theory and nonlinear ELM simulations. Small, type-III-like ELMs occur at $P_{OH} \sim P_{L-H}$ with $n \leq 4$. Large, type-I-like ELMs occur with $P_{OH} P_{L-H}$ and intermediate $5 < n < 15$, similar to ELMs at $A \sim 1.3$ in NSTX. The type-III n ranges are opposite that reported at high A , and type-I n are in the low range of those reported at high A . These differences presumably reflect the strong peeling mode drive $\sim J_{\text{edge}}/B$ present in the ST. The dominant n component of a large ELM grows exponentially, whereas other n are nonlinearly driven and damped prior to the crash. Access to small and large ELMs are demonstrated in Ohmic H-mode plasmas by varying the applied input power. $J_{\text{edge}}(R, t)$ measurements have been obtained across single ELM events with sub-cm spatial and Alfvénic temporal resolution. Both ELM types feature the nonlinear generation of “current-hole” J_{edge} perturbations, similar to prior studies of nonlinear peeling mode dynamics in Pegasus. A type-I ELM is shown to additionally expel a current-carrying filament during the ELM crash. Initial experiments coupling small amounts of helical edge current injection to H-mode plasmas suggest suppression of type-III ELM activity and negligible macroscopic impact on the discharge. This occurs for injected currents $I_{\text{inj}} \lesssim 1$ kA. Above $I_{\text{inj}} \gtrsim 1$ kA the 3D field perturbation degrades the edge sufficiently to exit H-mode.

EX



TAE during Minor Disruptions in the SUNIST Spherical Tokamak

Y. Tan¹, Y. Liu¹, and Z. Gao¹

¹*Tsinghua University, Haidian, Beijing, People's Republic of China*

Corresponding Author: Y. Tan, tanyi@sunist.org

Toroidal Alfvén eigenmodes (TAEs) during minor disruptions have been identified in the ohmic plasmas of the SUNIST spherical tokamak. The TAE modes are observed in the frequency range of 150–400 kHz. The mode structure analysis indicates the existence of both $m/n = -3/-1$ and $-4/-1$ harmonics, propagating in the electron diamagnetic direction in the laboratory frame of reference. These TAEs appear simultaneously with the generation of REs in the current quench phase, followed by a RE current plateau.



Study on EBW Assisted Startup and Heating Experiments via Direct XB Mode Conversion from Low Field Side Injection in VEST

H. Lee¹, S.-H. Kim², Y. S. Hwang¹, J. Jo¹, J. Yang¹, and K. J. Chung¹

¹*Seoul National University, Seoul, Republic of Korea*

²*Korea Atomic Energy Research Institute (KAERI), Daejeon, Republic of Korea*

Corresponding Author: H. Lee, brbbebbero@snu.ac.kr

EBW is an effective heating method to generate over dense plasma in low magnetic field devices such as ST. The direct XB MC from LFS injection may be used effectively because the LFS X-mode can be easily transmitted to right hand (RH) polarized slow X wave or mode converted to highly damping Bernstein wave. In addition, it requires no injection angle adjustment and complicated hardware preparation like OXB MC. EBW heating experiments using direct XB MC from LFS injection has been performed in VEST and start-up schemes based on the EBW heating including trapped particle configuration (TPC) are suggested.

In the case of pure toroidal field, initial plasma is generated near the ECR when the MW power is lower, but density peak moves outward with higher heating power, by noting the collisional damping of EBW. Simulated results from 1D full wave code confirm the tunnelling and MC efficiencies of the injected X wave. As toroidal magnetic field decreases, plasma density decreases with low MC efficiency. But as the ECR layer moves toward the inboard side, density peak reappears where LB is lower. Therefore, high density plasmas can be generated both outboard and inboard sides with high XB MC efficiency due to small Ln and LB. By utilizing EBW collisional heating, two start-up schemes are suggested. In the case of the lower B_t which has the high density plasma near the inboard side, low loop voltage start-up can be realized with relatively high electric field. The other start-up scheme of the solenoid free start-up utilizing outer PF coils may be possible by utilizing high density plasmas toward the outboard region with the help of plasma evolution from the outboard to the inboard.

The density peak near the outboard side has the possibility of making higher EBW MC efficiency with short Ln, resulting in efficient plasma heating. More rapid plasma density increase with additional MW power from LFS X mode is observed near the core region. By noting that additional power is applied, abrupt density increase may be explained by the steep density profile due to plasma current. The EBW heating experiment with additional 10 kW MW power clearly shows density increase, but increase of T_e is still not observed. T_e increase via decrease of collisional damping will be pursued by decreasing operating pressure and impurity control as well as increasing ohmic heating power.



The Effect of Transient Density Profile Shaping on Transport in Large Stellarators and Heliotrons

A. Dinklage¹, R. Sakamoto², J. Baldzuhn¹, B. Craig¹, S. Cats³, K. J. McCarthy⁴, M. Henning¹, G. Motojima², M. Nakata⁵, M. Nunami², N. Pablant⁶, J. H. Proll¹, K. Tanaka², F. Warmer¹, R. C. Wolf¹, P. Xanthopoulos¹, H. Yamada², M. Yokoyama², M. Yoshinuma², and K. Ida²

¹Max-Planck-Institut für Plasmaphysik, Garching, Germany

²National Institute for Fusion Science (NIFS), Toki, Gifu, Japan

³FOM Institute DIFFER, Association EURATOM-FOM, Nieuwegein, Netherlands

⁴Centro de Investigaciones Energéticas, Medioambientales y Tecnológicas (CIEMAT), Madrid, Spain

⁵Japan Atomic Energy Agency (JAEA), Naka, Japan

⁶Princeton Plasma Physics Laboratory (PPPL), Princeton, NJ 08540, USA

Corresponding Author: A. Dinklage, dinklage@ipp.mpg.de

Continuous fuelling is a prerequisite for steady-state stellarator and heliotron fusion reactor operation. For 3D magnetic field configurations, outward directed thermodiffusion gives rise to density depletion in the hot plasma core which needs to be compensated by appropriate fuelling schemes. Pellet injection may generate particle sources relevant to the development of discharge scenarios applicable to reactor operation.

LHD and W7-X are sufficiently large to generate plasmas in transport regimes as anticipated for reactors, i.e., to allow studies in the long-mean-free-path collisionality regime at high plasma beta. Beyond the capability of allowing the study of reactor-grade 3D plasmas, the development of quasi steady-state operation scenarios is an objective of experimental strategies.

In 3D fields, transport processes after pellet injection shows characteristics of diffusive and convective contributions. The resulting thermodynamic forces also influence radial electric fields—both as a driving term but also by, e.g., affecting the E_r dependence of ion transport. Experiments have been conducted at different magnetic configurations on LHD. The spatiotemporal evaluation after the injection of a pellet in a LHD discharge showed cases with central density increase on the time scale of transport processes. The temperature gradient length and the density gradient length—and consequently the radial electric fields—change during the density relaxation and have impact on the fuelling efficacy. The time scale of the decay of the stored energy, however, follows the longer decay time of the particle time traces resembling the particle confinement time.

These experimental findings indicate a clear change of the thermodynamic forces, i.e., in particular the inverse density gradient length in the decay phase after pellet injection. The inverse temperature gradient lengths are varying much less, thereby the ratio of both shows a variation even changing its sign. Both measurements and estimates for the radial electric field indicate changes in E_r . The paper will discuss transport analysis for extended variations of the magnetic configuration ($R_{ax} = 3.6, 3.7, 3.9$ m) and the effect of pellet size and sequencing.

Initial Observations on Core Electron Heat Transport in W7-X

U. Höfel¹, M. Hirsch¹, M. Beurskens¹, S. A. Bozhnikov¹, A. Dinklage¹, G. Fuchert¹, J. Geiger¹, H.-J. Hartfuss¹, J. Knauer¹, P. Kornejew¹, A. Langenberg¹, H. P. Laqua¹, H. Maaßberg¹, N. Marushchenko¹, E. Pasch¹, N. Pablant², S. Schmuck³, T. Stange¹, H. Tsuchiya⁴, Y. Turkin¹, G. Weir¹, and R. C. Wolf¹

¹Max-Planck-Institut für Plasmaphysik, Greifswald, Germany

²Princeton Plasma Physics Laboratory (PPPL), Princeton, NJ 08540, USA

³Culham Centre for Fusion Energy (CCFE), Culham Science Centre, Abingdon, UK

⁴National Institute for Fusion Science (NIFS), Toki, Gifu, Japan

Corresponding Author: U. Höfel, udo.hoefel@ipp.mpg.de

The optimized stellarator Wendelstein 7-X aims at high-density steady-state discharges at reactor relevant collisionality regimes and β . The first test operation of W7-X (“OP1.1”) is dedicated to commissioning of the device, its periphery and its operation relevant diagnostics. For heating, ECRH with a total power of ~ 4 MW is available.

Electron heat transport studies use the flexibility of the ECRH system with the option for on- and off-axis heating, power steps and heatwaves. The electron temperature response is measured by ECE applying a 32-channel absolutely calibrated ECE radiometer supplemented with an additional 16 channel “zoom system” for higher spatial resolution in a suitable radial range. Further T_e and T_i profile information is obtained from an imaging X-ray spectrometer and Thomson scattering.

A maximum pulse length of 6 s has been reached in hydrogen discharges with central T_e values of ~ 8 keV while the density profiles remain flat reaching a line average electron density of about $\langle n_e \rangle < 2 \times 10^{19}/\text{m}^3$. The electron temperature profile from ECE shows a hot core surrounded by steep temperature gradients as it is expected for core electron root confinement scenarios where positive electric fields in the core reduce the neoclassical electron heat conductivity. The electron cyclotron emission profile is modelled with the TRAVIS code to disentangle thermal emission at the blackbody level, which can be used to derive the local T_e , from frequency shifted emission of suprathreshold core electrons. In these ECRH heated scenarios the ion temperature profile remains nearly flat throughout the discharge and increases continuously due to electron-ion coupling reaching up to $T_i = 2$ keV in the centre. Heatwave propagation is used to measure on- and off-axis location of the ECRH radial power deposition and its deposition profile as an input for power balance analysis. Power steps are used to derive transient decay times of the profile. The values from a first power balance are being compared with neoclassical expectations and assumptions on turbulent transport. Besides, from heatwave propagation dynamic electron heat transport coefficients are derived.

Next to the profile information the ECE time traces display a rich phenomenology of transport events or quasi coherent mode activity and by crashes some possibly related to rational surfaces.

Minerva Bayesian Analysis of X-ray Imaging Spectrometer Data for Temperature and Density Profile Inference at Wendelstein 7-X

A. Langenberg¹, N. Pablant², J. Svensson¹, O. Marchuk³, P. Valson¹, P. Traverso⁴,
D. Gates², and R. C. Wolf⁵

¹Max-Planck-Institut für Plasmaphysik, Greifswald, Germany

²Princeton Plasma Physics Laboratory (PPPL), Princeton, NJ 08540, USA

³Institute of Energy and Climate Research, Forschungszentrum Jülich, Jülich, Germany

⁴Auburn University, Auburn, AL 36849, USA

⁵Max-Planck-Institut für Plasmaphysik, Garching, Germany

Corresponding Author: A. Langenberg, andreas.langenberg@ipp.mpg.de

Starting from the first operation of the Wendelstein 7-X (W7-X) stellarator, the X-ray imaging crystal spectrometer system (XICS) routinely provides line of sight integrated measurements of electron, T_e , and ion temperatures, T_i , as well as Ar impurity densities, n_{Ar} , based on the spectral emission of an argon tracer impurity. In addition, XICS is capable to measure plasma flow velocities v that allows the determination of the radial electric field E_r as an essential observation for any transport analysis. With a view field covering a wide range of the plasma cross section and a time resolution of up to 5 ms, the temporal evolution of radial plasma parameter profiles has been studied in detail.

For the inference of the actual plasma parameter profiles from line of sight integrated measurements, an entire forward model of the XICS diagnostic has been created using the Minerva Bayesian Analysis framework. Other W7-X profile diagnostics, such as Thomson scattering and ECE, are also being developed within the Minerva framework, which in combination with the Bayesian approach makes it possible to analyze multiple diagnostics simultaneously, increasing accuracy and consistency.

First results on the performance of He and H plasmas at W7-X as well as the reliability of the inversion method will be discussed in detail.

EX

Investigation of Turbulence Rotation in Limiter Plasmas at W7-X with a New Installed Poloidal Correlation Reflectometry

A. Krämer-Flecken¹, T. Windisch², W. Behr¹, G. Czymek¹, P. Drews¹, O. Grulke²,
M. Hirsch², M. Knaup¹, Y. Liang¹, and O. Neubauer¹

¹Forschungszentrum Jülich, Jülich, Germany

²Max-Planck-Institut für Plasmaphysik, Greifswald, Germany

Corresponding Author: A. Krämer-Flecken, a.kraemer-flecken@fz-juelich.de

For the first operation phase of the optimized stellarator W7-X, a heterodyne poloidal correlation reflectometry (PCR) diagnostic is installed and in operation. The PCR system consists of an antennae array with one launching and four receiving antennae. The system is operated in a frequency range 22 GHz to 40 GHz. With the selected O-mode polarization of the system a density range of $0.6 \times 10^{19} \text{ m}^{-3}$ to $2.0 \times 10^{19} \text{ m}^{-3}$ is accessible. To achieve a fast scan of the full frequency range a microwave synthesizer is used where any switch in the frequency is performed in $< 100 \mu\text{s}$. The sight lines of all five antennae intersect at $R = 6 \text{ m}$ in the equatorial plane. The aim of the diagnostic is the measurement of the turbulence velocity in the gradient and edge region of the plasmas at W7-X. Therefore the delay time (Δt) of any antennae combination is calculated by means of cross correlation technique. With the knowledge of poloidal and toroidal separation at the cut off position in the plasma the velocity is calculated. The turbulence velocity is a sum of $E \times B$ velocity and phase velocity. The phase velocity is small compared to $E \times B$ velocity and can be neglected and allows the estimation of the radial electric field. Turbulence properties in the gradient and edge region are monitored with the PCR diagnostic as well. With respect to the local magnetic field the perpendicular correlation length and decorrelation time are calculated. The ratio of the delay times for equal poloidal and toroidal separation is used to calculate the magnetic field line pitch angle, assuming that turbulence structures are fully aligned along the magnetic field line. First measurements show the expected increase in Δt with increasing poloidal separation. Different Δt for the same poloidal and toroidal separation could be measured and allow to determine the magnetic pitch angle. With the density profiles from Thomson scattering the radial position of the measurement is estimated. The poloidal plasma velocity is studied in helium and hydrogen plasmas with different amounts of ECRH heating. A change in the direction of the velocity is observed at the plasma edge, indicating the existence of a shear layer in the plasma. First investigations of the underlying physics of this transition are studied and reported.

EX



Error Field Measurement, Correction and Heat Flux Balancing on Wendelstein 7-X

S. Lazerson¹, M. Otte², M. Jakubowski², G. A. Wurden³, U. Wenzel², T. Andreeva⁴, S. A. Bozhenkov², C. Biedermann², G. Kocsis⁵, T. Szepesi⁵, J. Geiger², T. Sunn Pedersen², and D. Gates¹

¹Princeton Plasma Physics Laboratory (PPPL), Princeton, NJ 08540, USA

²Max-Planck-Institut für Plasmaphysik, Garching, Germany

³Los Alamos National Laboratory (LANL), Los Alamos, NM 87545, USA

⁴Max-Planck-Institut für Plasmaphysik, Greifswald, Germany

⁵Wigner Research Center, Association EURATOM, Budapest, Hungary

Corresponding Author: S. Lazerson, lazerson@pppl.gov

The measurement and correction of error fields in Wendelstein 7-X (W7-X) is critical to long pulse high- β operation, as small error fields may cause overloading of divertor plates. Accordingly, as part of a broad collaborative effort, the detection and correction of error fields on the W7-X experiment has been performed using the US supplied trim coil system [1] in conjunction with the flux surface mapping diagnostic [2] and the US supplied high resolution infrared camera [3]. In the early commissioning phase of the experiment, the trim coils were used to open an $n/m = 1/2$ island chain in a specially designed magnetic configuration [3]. The flux surfacing mapping diagnostic was then able to directly image the magnetic topology of the experiment, allowing the inference of a small ~ 4 cm intrinsic island chain [4]. Scaled to the planned operating field (2.5 T), such error fields would be correctable using less than 10% the rated trim coil capacity. The suspected main source of the error field, slight misalignment of the superconducting coils, is then confirmed through a synthetic flux surface mapping diagnostic and detailed measurements of the coil positions. Confirmation of the error fields allows the assessment of magnetic fields which resonate with the $n/m = 5/5$ island chain. Predictions of the extent to which these error fields, if left uncorrected, could limit plasma performance are presented. Plasma experiments without applied correcting fields show a significant asymmetry in neutral pressure (centred in module 4) and light emission (visible, H_{α} , and carbon). Such pressure asymmetry is associated with divertor heat load asymmetries between the modules. Application of trim coil fields with $n = 1$ waveform correct the imbalance. Observations of the limiters temperatures in module 5 shows a clear dependence of the limiter heat flux pattern as the perturbing fields are rotated.

References

[1] T. Rummel, *et al.*, IEEE Trans. Appl. Supercond. **24(3)**, 1 (2014).

[2] M. Otte, *et al.*, "Setup and initial results from the magnetic flux surface diagnostics at Wendelstein 7-X", submitted to Plasma Phys. Control. Fusion.

[3] G. Wurden, *et al.*, EX/P5-7, This Conference.

[4] S. Lazerson, *et al.*, "First measurements of error fields on W7-X using flux surface mapping", submitted to Nucl. Fusion.



Investigation of Initial Plasma Parameters on the Wendelstein 7-X Stellarator Using the X-ray Imaging Crystal Spectrometer

N. Pablant¹, A. Langenberg², O. Marchuk³, D. Gates¹, S. Lazerson¹, A. Alonso⁴, M. Bitter¹, L. F. Delgado-Aparicio¹, K. W. Hill¹, S. Massidda⁵, G. H. Neilson¹, S. Satake⁶, J. Svensson⁷, P. Traverso⁵, P. Valson⁷, R. C. Wolf⁷, and M. Yokoyama⁶

¹Princeton Plasma Physics Laboratory (PPPL), Princeton, NJ 08540, USA

²Max-Planck-Institut für Plasmaphysik, Greifswald, Germany

³Institute of Energy and Climate Research, Forschungszentrum Jülich, Jülich, Germany

⁴Laboratorio Nacional de Fusión (LNF),

Centro de Investigaciones Energéticas, Medioambientales y Tecnológicas (CIEMAT), Madrid, Spain

⁵Auburn University, Auburn, AL 36849, USA

⁶National Institute for Fusion Science (NIFS), Toki, Gifu, Japan

⁷Max-Planck-Institut für Plasmaphysik, Garching, Germany

Corresponding Author: N. Pablant, npablant@pppl.gov

The performance of the Wendelstein 7-X (W7-X) stellarator during the first experimental campaign (OP1.1) is explored using measurements from the X-ray imaging crystal spectrometer (XICS) diagnostic. During OP1.1 plasmas have been produced in a limiter configuration, with up to 4 MW of ECH power. The properties of both helium and hydrogen plasmas are investigated.

The XICS system is designed to provide high-resolution profile measurements of the ion and electron temperatures (T_i , T_e), plasma flow velocity (v), and argon impurity density (n_{Ar}). Profile measurements of T_i and T_e are available with up to 5 ms time resolution and 2 cm spatial resolution with coverage of nearly the entire plasma radius. The diagnostic is based on spectroscopic analysis of emission from highly charged argon impurities that are added to the plasma in trace amounts. Routine measurements from the XICS system are available starting from the first week of W7-X operation.

Initial investigations of hydrogen plasmas from the first experimental campaign show thermalized distributions of the ion and electron temperatures. Ion temperatures of 2.1 keV and electron temperatures in excess of 6 keV have been achieved in plasmas with 4 MW of ECH heating and electron densities around a few times $10^{19}/m^3$.

The detailed evolution of the temperature profiles from these initial plasmas are reported along with argon impurity transport measurements and any recent results. Initial estimates of the ion heating and ion heat transport, which can be calculated from the temperature profiles and the plasma density, will also be discussed.

Limiter Observations during W7-X First Plasmas

G. A. Wurden¹, C. Biedermann², F. Effenberg³, M. Jakubowski⁴, L. Stephey³,
S. A. Bozhenkov², J. H. Harris⁵, H. Niemann², S. Klose², S. Marsen², H. P. Laqua²,
O. Schmitz³, E. A. Unterberg⁵, and R. König²

The W7-X Team

¹*Los Alamos National Laboratory (LANL), Los Alamos, NM 87545, USA*

²*Max-Planck-Institut für Plasmaphysik, Greifswald, Germany*

³*Department of Engineering Physics, University of Wisconsin-Madison, Madison, WI 53706, USA*

⁴*Max-Planck-Institut für Plasmaphysik, Garching, Germany*

⁵*Oak Ridge National Laboratory (ORNL), Oak Ridge, TN 37831, USA*

Corresponding Author: G. A. Wurden, wurden@lanl.gov

During the first operational phase (OP1.1) of the new W7-X stellarator, five poloidal graphite limiters serve as the main boundary for the plasma. For one of the limiters (Module 3) we have a common sight line for high resolution fast visible and midband infrared cameras, as well as filtered photomultipliers. Another limiter (Module 5) is instrumented with tangential view visible and near and long wavelength IR cameras, along with Langmuir probes. We will report on results from the first three months of operation. Dual heat stripes are seen for the first time on the limiters, and are consistent with diffusive and EMC3-EIRENE modelling [1, 2, 3] of the expected heat and particle flux patterns in a helical 3D magnetic field.

References

- [1] F. Effenberg, *et al.*, “Numerical investigation of edge transport and limiter heat loads in Wendelstein 7-X startup plasmas”, APS DPP Meeting, Savannah, GA, (2015), Submitted to Nucl. Fusion (2016).
- [2] S. A. Bozhenkov, F. Effenberg, *et al.*, 41st EPS Conference on Plasma Physics, P1.080, Berlin, (2014) [PDF link](#).
- [3] T. Sunn Pedersen, *et al.*, Nucl. Fusion **55**, 126001 (2015).

Enhancement of W7-X Performance by Symmetrization of Limiter Loads with Error Field Correction Coils

S. A. Bozhenkov¹, M. Jakubowski¹, S. Lazerson², H. Niemann¹, G. A. Wurden³,
U. Wenzel¹, L. Stephey⁴, R. König¹, C. Biedermann¹, G. Kocsis⁵, T. Szepesi⁵,
T. Sunn Pedersen¹, and R. C. Wolf¹

¹Max-Planck-Institut für Plasmaphysik, Garching, Germany

²Princeton Plasma Physics Laboratory (PPPL), Princeton, NJ 08540, USA

³Los Alamos National Laboratory (LANL), Los Alamos, NM 87545, USA

⁴University of Wisconsin-Madison, Madison, WI 53706, USA

⁵Wigner Research Center, Association EURATOM, Budapest, Hungary

Corresponding Author: S. A. Bozhenkov, boz@ipp.mpg.de

EX In the first Wendelstein 7-X operational campaign a dedicated limiter configuration was used for both helium and hydrogen plasmas. The achievable discharge duration and the heating power depend on the symmetry of power distribution between five limiters. Toroidally asymmetric loads appear due to misalignments and intrinsic error fields. It is found numerically that for misalignments of a few millimetres, one module receives about 10% higher power fraction. Error fields introduce helical deformations of flux surfaces and affect the power deposition even in a nonresonant case. An 1/1 error field of about 10^{-4} results in about 30% increase in the heat flux to one module. These findings are confirmed experimentally. Plasma-limiter interaction was studied with different amplitudes and phases of $n = 1$ perturbation produced by W7-X error field trim coils. A clear change in the heat and particle fluxes to the limiters is observed with the perturbation. The observed change is consistent with $n = 1$ structure. Without perturbation, the neutral pressure typically has a clear maximum in module 4. With a suitable perturbation phase and amplitude a toroidally symmetric neutral pressure is observed. This decreases the impurity accumulation and therefore extends the pulse duration. These results are of interest for the later steady state W7-X divertor operation, where a similar question will have to be addressed.

Measurement of the Plasma Edge Profiles Using the Combined Probe on W7-X

P. Drews¹, Y. Liang¹, O. Neubauer¹, P. Denner¹, M. Rack¹, S. Liu¹, N. Wang¹, D. Nicolai¹, A. Krämer-Flecken¹, O. Grulke², A. Charl¹, B. Schweer¹, Y. Gao³, K. P. Hollfeld¹, S. Guruparan¹, N. Sandri¹, and D. Höschel¹

¹Forschungszentrum Jülich, Jülich, Germany

²Max-Planck-Institut für Plasmaphysik, Greifswald, Germany

³Institute of Plasma Physics, Chinese Academy of Sciences, Hefei, Anhui, People's Republic of China

Corresponding Author: P. Drews, p.drews@fz-juelich.de

Wendelstein 7-X (W7-X), one of the world's largest stellarators, located at the IPP Greifswald, started operation recently with a limiter configuration. Edge plasma profile measurements, especially those of the electron temperature and density, will play a key role in validating the performance in comparison to the tokamak and hence the viability of a stellarator fusion reactor. The first operational phase (OP 1.1) is used primarily for setting up the diagnostics and testing the magnetic configuration.

In conjunction with the multipurpose manipulator, a fast reciprocating probe has been installed. There are currently two probe heads: the combined probe measuring the edge profiles and the sample station for plasma exposure studies, namely of tungsten. The combined probe includes i) two magnetic pick-up coil arrays, ii) Langmuir probes, and a Mach setup. This allows measuring at the same time and location, the edge radial profiles of the magnetic fields, the electron temperature and density, the electric fields; and the plasma flows. For good measurements, sufficient knowledge of the capabilities and limitations of the diagnostics concerning the frequency limits, noise and the possible sustainable heat loads is necessary. The capabilities of the probe system will be presented, including ongoing improvements. In this paper, the preliminary measurements of edge profiles using the combined probe in the limiter configuration will be presented. The power and density dependences of the edge transport will be discussed. The influence of magnetic perturbations induced by the trim coils on the edge profile of the electron density and temperature, and the magnetic topology will be investigated in the upcoming experiments. The turbulence will be measured and characterized using the Langmuir probe and the Mach probe. The edge intermittent events can be observed with the negatively biased Langmuir pin and compared with the results of the reflectometry measurements.

EX

Diagnostic Setup and Modelling for Investigation of Synergy between 3D Edge Physics and Plasma-Wall Interactions on Wendelstein 7-X

Y. Liang¹, O. Neubauer¹, R. König², P. Denner¹, M. Rack¹, S. Brezinsek¹, C. Linsmeier¹, and U. Samm¹

¹Forschungszentrum Jülich, Jülich, Germany

²Max-Planck-Institut für Plasmaphysik, Greifswald, Germany

Corresponding Author: Y. Liang, y.liang@fz-juelich.de

EX Plasma-wall interaction (PWI) in the divertor region of Wendelstein 7-X (W7-X) will be of great importance for operational phase OP1.2. While the erosion of the divertor will have an impact on its lifetime and is therefore a critical subject of investigation, fundamental PWI studies in the divertor region are in many ways equally significant. These plasma-wall interactions will be influenced by impurity transport, where the complex 3D magnetic geometry will play a crucial role, but this magnetic geometry could itself be influenced by plasma effects such as Pfirsch-Schlüter and bootstrap currents. Therefore, along with measurements of obvious quantities such as heat flux, PWI research in the divertor region will also require measurements of the temperature in the plasma edge and of the concentration and distribution of different impurities, in combination with modelling of impurity transport. In order to investigate systematically the synergy between 3D edge physics and PWI, a set of edge diagnostics has been developed for the upcoming W7-X experiments and the EMC3-EIRENE code is being extended to helium plasmas for OP1.1.

A set of endoscopes has been designed for visible and ultraviolet spectroscopy and tomography of the plasma edge, along with infrared thermography of the divertor tiles. Two-dimensional profiles of impurities (e.g., He, C) will be measured by two endoscopes viewing the island divertor region in the plasma edge with a spatial resolution of < 2 mm. A multipurpose manipulator, which is used as the carrier either of the probe head for measuring the plasma edge profiles or of samples for plasma exposure studies, was installed at the outside midplane on W7-X in 2015. A poloidal correlation reflectometer has also been installed. This system consists of an antenna array observing the propagation of turbulent phenomena in the midplane. The EMC3-EIRENE code package has been extended for plasma edge transport in helium plasma at Wendelstein 7-X using a hybrid fluid-kinetic approach by enabling EMC3 to treat non-hydrogen isotopes and extending the usage of EIRENE features within EMC3-EIRENE.

In this paper, a detailed physics concept of the diagnostic set-up and modelling for investigation of synergy between 3D edge physics and plasma-wall interactions will be presented.



Application of the ECRH Radiation for Plasma Diagnosis in Wendelstein 7-X

D. Moseev¹, H. P. Laqua¹, S. Marsen², T. Stange¹, I. Abramovic³, Á. Cappa⁴, H. Braune¹, F. Gellert¹, W. Kasperek⁵, J. W. Oostebeek³, and T. Wauters⁶

¹Max-Planck-Institut für Plasmaphysik, Garching, Germany

²Max-Planck-Institut für Plasmaphysik, Greifswald, Germany

³Eindhoven University of Technology, Eindhoven, Netherlands

⁴Laboratorio Nacional de Fusión (LNF),

Centro de Investigaciones Energéticas, Medioambientales y Tecnológicas (CIEMAT), Madrid, Spain

⁵University of Stuttgart, Stuttgart, Germany

⁶Laboratory for Plasma Physics, ERM/KMS, Brussels, Belgium

Corresponding Author: D. Moseev, dmitry.moseev@ipp.mpg.de

W7-X is an optimized stellarator with $n = 5$ toroidal symmetry. It is designed to produce high performance steady-state plasmas. The main heating mechanism is ECRH, which is capable of delivering continuously up to 5 MW with six gyrotrons at 140 GHz and in the next campaign the total power of the ECRH set-up will be increased to 9 MW and 10 gyrotrons. Such a powerful source of microwaves can also be used for diagnostic purposes. Investigation of the ECRH assisted plasma start-up is vital for large fusion devices, such as Wendelstein 7-X, ITER, and possibly DEMO. Here we present a systematic approach to the ECRH start-up studies in W7-X using stray radiation diagnostics.

W7-X is equipped with five absolutely calibrated sniffer probes distributed toroidally. They measure stray radiation which originates from unabsorbed microwaves used for heating. Temporal evolution of the sniffer probe signals is analyzed qualitatively and quantitatively. Quantitative inference of the first-pass plasma absorption is done by means of forward modelling using the multiresonator model applied to the actual W7-X geometry. The inference allows temporally resolved measurements of plasma absorption with good resolution, i.e., plasma startup and shutdown. It also makes possible to distinct between X-mode absorption and O-mode microwave absorption.

Collective Thomson scattering (CTS) is presently being designed for the W7-X stellarator. The goal of the system is to routinely diagnose temporally resolved ion temperature in the next experimental campaign. CTS has already proved to provide accurate T_i measurements in ASDEX Upgrade and TEXTOR. The diagnostic is relevant to future machines with high plasma density and, therefore, poor beam penetration which limits the use of charge exchange spectroscopy. The system is intended to use 140 GHz heating gyrotron as a source. The receiver part of the transmission line will share the quasi-optical transmission line with the heating system, which makes the shielding of the receiver from stray radiation challenging. An extra section of the transmission line in combination with a movable shutter mirror will be installed in quasi-optical transmission line in order to facilitate the receiver beam transmission from the additional measurement location.



Physics and Applications of ICRH on W7-X

J. Ongena¹, A. Messiaen¹, Ye. O. Kazakov¹, A. Krivska¹, F. Louche¹, B. Schweer¹, M. Vervier¹, D. Van Eester¹, M. Van Schoor¹, T. Wauters¹, V. Borsuk², K. P. Hollfeld², G. Offermans³, O. Neubauer², A. Dinklage⁴, D. Hartmann⁴, J.-P. Kallmeyer⁴, D. Birus⁴, and R. C. Wolf⁴

¹Laboratory for Plasma Physics, ERM/KMS, Brussels, Belgium

²Institute of Energy and Climate Research, Forschungszentrum Jülich, Jülich, Germany

³Forschungszentrum Jülich, Jülich, Germany

⁴Max-Planck-Institut für Plasmaphysik, Greifswald, Germany

Corresponding Author: J. Ongena, j.ongena@fz-juelich.de

An important aim of W7-X is to demonstrate fast ion confinement at volume averaged β values up to 5%, corresponding to plasma densities above $10^{20}/\text{m}^3$. Energetic H or D ions in W7-X with energies $50 < E < 100$ keV mimic alphas in a reactor. To this end, an ICRH system is prepared for W7-X, with RF power up to ~ 1.5 MW at frequencies between 25–38 MHz in pulses up to 10 s. For optimal coupling the antenna surface is carefully matched to the standard magnetic configuration of W7-X. A complex 3D antenna shape has thus to be made with state of the art CNC machines. The antenna can also be radially moved over 35 cm and a gas puffing system is implemented to improve local coupling whenever needed.

With minority heating, and despite better absorption of RF waves at high densities, the tail energy of RF-heated minority ions scales as $1/n_e^2$. The production efficiency of fast particles can be much improved using a new so-called three-ion heating ICRH scenario. Two majority gases (e.g., H and D) are used in a well chosen proportion to locate the maximum of the left-hand polarized electric field (E^+) of the magnetosonic wave at the resonance position of a third minority species (^3He). The new scheme allows for a low concentration of ^3He , ($< 1\%$) thus a large amount of RF power is absorbed per particle. We find that perpendicular energies between 50 and 100 keV or higher can be produced, even for $n_e > 2 \times 10^{20}/\text{m}^3$. The three-ion scheme will be used at $f \sim 25$ MHz. At $f \sim 38$ MHz also minority heating or second harmonic absorption can be used. If $n_{\text{H}}/n_e > 2\%$, H ions dominantly absorb RF power resulting in efficient plasma heating. If $n_{\text{H}}/n_e < 2\%$ fast second harmonic heating of D ions becomes the dominant power absorption channel, offering thus a second option to create fast D ions in high density W7-X plasmas.

With the permanent magnetic field of W7-X, ICRH can also be used for Ion Cyclotron Wall Conditioning (ICWC). The coupling of RF power to create a plasma is not limited to cyclotron resonance layers. Via collisional absorption homogeneous discharges can be created extending into the SOL which ensures an optimal plasma wetted wall area. The conditioning procedure consists of series of short ICRF pulses (2–5 s) with a duty cycle of 5 to 20%. The wall released hydrogen and impurities are efficiently evacuated in the interval between subsequent ICRF pulses.

First Results from Protective ECRH Diagnostics for Wendelstein 7-X

S. Marsen¹, D. Moseev², Y. Corre³, H. P. Laqua¹, V. Moncada³, M. Preynas¹, and T. Stange¹

¹Max-Planck-Institut für Plasmaphysik, Greifswald, Germany

²Max-Planck-Institut für Plasmaphysik, Garching, Germany

³Institut de Recherche sur la Fusion par confinement Magnétique (IRFM),

Commissariat à l'énergie atomique (CEA/Cadarache), 13108 Saint-Paul-lès-Durance, France

Corresponding Author: S. Marsen, stefan.marsen@ipp.mpg.de

W7-X is a steady-state capable optimized stellarator. The main heating system is electron cyclotron resonance heating (ECRH) operating at 140 GHz providing up to 9 MW microwave power. A set of diagnostics has been developed to protect the machine from nonabsorbed ECRH power which can easily damage in vessel components. The power is launched into the machine by front steerable quasi-optical launchers in X- or O-mode. While in X-mode the first pass absorption is ~99%, it is only 40–70% in O-mode. The nonabsorbed power hitting the inner wall is measured by waveguides embedded in the first wall (ECA diagnostic).

In order to prevent the inner wall from overheating or arcing, a near-infra red sensitive video diagnostic with a dynamic range of 450–1200°C was integrated in the ECRH launchers. Thermal calculations for the carbon tiles predict a temperature increase above the detection threshold for scenarios of plasma start-up failure or poor absorption on a time scale of ~100 ms and the risk of overheating after ~300 ms. However, no temperature rise above the detection threshold could be observed in experiments with failed break down, i.e., poor ECRH absorption for up to 100 ms. The stray radiation level inside the machine is measured by so called sniffer probes which were designed to collect all radiation approaching the probing surface independent of incident angle and polarization. Five sniffer probes are installed at different toroidal positions. They were absolutely calibrated.

The sniffer probes are integrated in the ECRH interlock system. During the first operational phase of W7-X this was the only available plasma interlock system. The signal quality proofed to be high enough for a reliable termination in case of poor absorption. After a breakdown phase of ~10 ms, the sniffer probe signals dropped by more than an order of magnitude. However, especially in the very first days of operation, most discharges died by a radiative collapse due to impurity influx. In this case the heating power was reliably switched off due to the increased level of stray radiation. A comparison with the ECA diagnostic clearly showed that the increased level of stray radiation was due to a decay of the plasma performance rather than approaching the cut-off density. In the latter case only the sniffer probe signal would have increased and not both ECA and sniffer probes.



Transport Studies during the First Campaign of Wendelstein 7-X

O. Grukke¹

¹Max-Planck-Institut für Plasmaphysik, Garching, Germany

Corresponding Author: O. Grukke, grukke@ipp.mpg.de

The understanding of cross-field transport of particles and energy represents one of the most important challenges on the verge towards magnetic confinement fusion and is indispensable to extrapolate to next-generation devices. The Wendelstein 7-X (W7-X) stellarator, designed to operate quasi steady-state (pulse lengths up to 30 minutes), has been optimized with respect to a reduction of neoclassical transport, low Shafranov-shift, and low bootstrap current to ensure viable divertor operation. The purpose of the first operation campaign, which started in December 2015, was the integral commissioning of the device and its components in helium and hydrogen plasmas in a limiter configuration using electron cyclotron resonance heating in X-mode polarization with heating powers $P_H \leq 4$ MW. The temporal evolution of the plasma density was monitored by a laser interferometer system and its profile via Thomson scattering. These profile information provide the basis for detailed comparison to neoclassical transport calculations. In preparation for long-pulse operation, dedicated plasma discharges have been devoted to impurity transport studies, using the X-ray imaging system and the HEXOS overview spectrometer to resolve the evolution of argon impurities injected into the plasma edge. Studies of turbulent transport were not the focus of the first experimental campaign. However, a number of fully-nonlinear turbulence simulation results exist for an entire flux-surface of W7-X. Fundamental characteristics are the influence of the unfavourable magnetic curvature region, which is poloidally highly localized in the W7-X magnetic field configuration, and the influence of local magnetic shear, which leads to an amplitude envelope following the five-fold magnetic field symmetry. Based on detailed profile measurements, fundamental considerations about instability growth rates can be made. In addition, an edge-localized correlation reflectometer system on W7-X measures fluctuation spectra and typical poloidal phase velocities, which are compared to the simulation results. This paper summarizes the results obtained in the first operation campaign of W7-X with respect to neoclassical and turbulent transport and its comparison to theoretical predictions.

EX



Enhanced Measurements for MHD Validation Using Integrated Data Analysis on the MST Fusion Research Experiment

D. Den Hartog¹, A. F. Almagri¹, D. Craig², P. Franz³, M. Galante¹, C. Jacobson¹, J. Johnson¹, K. McCollam¹, M. Meghan¹, L. Morton¹, M. Nornberg¹, E. Parke⁴, J. Reusch¹, L. Reusch¹, J. S. Sarff¹, J. Sauppe¹, C. Sovinec¹, H. Stephens⁵, and J. Triana¹

¹University of Wisconsin-Madison, Madison, WI 53706, USA

²Wheaton College, Wheaton, IL 60187, USA

³Consorzio RFX, Associazione EURATOM-ENEA sulla Fusione, Padova, Italy

⁴University of California Los Angeles, CA 90095, USA

⁵Pierce College Fort Steilacoom, Lakewood, WA, USA

Corresponding Author: D. Den Hartog, djdenhar@wisc.edu

Over the past several decades, numerical simulation has successfully described various dynamical phenomena in fusion research plasmas. Substantial effort is now being applied to enhance the quantitative predictive capability of numerical simulation. Two key tools for this effort are quantitative validation and integrated data analysis (IDA). To perform validation, results of a numerical simulation are globally tested against experimental measurements to identify areas of quantitative agreement and disagreement. As a platform for validation activities, MST is usually operated as a reversed-field pinch (RFP), which produces a complementary parameter space to tokamaks and stellarators. Validation efforts on MST are concentrated on simulation of processes within the scope of MHD, using the codes DEBS (nonlinear, single-fluid, visco-resistive MHD) and NIMROD (nonlinear, two-fluid, extended MHD). Specific effort is being applied to characterize how magnetic turbulence within the plasma scales with Lundquist number. Another validation effort underway is investigation of the spatial distribution and influence of fluctuation-induced Hall effect and Maxwell stress as represented by two-fluid models. The measurement needs for validation often cannot be met by single-instrument diagnostics considered in isolation. IDA provides a method to address this challenge by maximizing the usefulness of the information recorded by a set of diagnostics. The goal of IDA is to combine data from heterogeneous and complementary diagnostics, considering all dependencies within and between diagnostics, in order to obtain the most reliable measurements in a transparent and standardized way. IDA has been used on MST to combine information from two diagnostics (charge-exchange recombination spectroscopy and soft X-ray tomography) to produce a robust measurement of effective charge (Z_{eff}) with quantified uncertainty.

Work supported by the U.S. Department of Energy, Office of Science, Office of Fusion Energy Sciences under Award Number DE-FC02-05ER54814, and by the National Science Foundation under Award Number PHY-0821899.



An Island-Induced Alfvén Eigenmode and Effects of Nonaxisymmetry on Fast Ions in the RFP

J. K. Anderson¹, V. Belykh², J. Boguski¹, P. Bonfigli¹, W. Capecchi¹, C. Cook¹, V. Davydenko², C. C. Hegna¹, S. Hirshman³, A. A. Ivanov², J. Kim¹, K. McCollam¹, S. Polosatkin², J. S. Sarff¹, S. Sears¹, and D. Spong³

¹University of Wisconsin-Madison, Madison, WI 53706, USA

²Budker Institute of Nuclear Physics (BINP), Novosibirsk, Russian Federation

³Oak Ridge National Laboratory (ORNL), Oak Ridge, TN 37831, USA

Corresponding Author: J. K. Anderson, jkanders@wisc.edu

The existence of a magnetic-island induced gap in the shear Alfvén continuum was predicted numerically [1], but only recently have experimental observations of the MIAE been made in stellarator [2] and RFP plasmas [3]. As the role of 3D magnetic fields in tokamaks grows in prominence, associated changes in the Alfvénic spectral properties, including MIAEs, are anticipated. The core of the NBI-heated RFP plasma exhibits several unique variants of axisymmetry-breaking magnetic perturbations that impact fast ion confinement and stability. The appearance of magnetic islands and associated magnetic stochasticity is controllable. A well-formed core-localized island is adjustable in size, ideal for study of the MIAE. While the RFP is nominally axisymmetric, in the quasi-single-helicity limit the dominant island envelops the magnetic axis, producing a stellarator-like three dimensional geometry. Here we present observations of fast ion transport in the presence of MIAEs in a RFP plasma. We further show a relative insensitivity of fast ion confinement to magnetic stochasticity, but a strong response to a coherent, 3D core perturbation.

References

[1] A. Biancalani, *et al.*, Phys. Rev. Lett. **105**, 095002 (2010).

[2] H. J. Sun, *et al.*, Plasma Phys. Control. Fusion **57**, 125011 (2015).

[3] C. Cook, *et al.*, Submitted to Plasma Phys. Control. Fusion (2016).



Evidence for Trapped Electron Mode Turbulence in MST Improved Confinement RFP Plasmas

D. L. Brower¹, J. Duff², Z. Williams², B. E. Chapman², W. X. Ding¹, L. Lin¹, E. Parke¹, M. J. Pueschel², J. S. Sarff², and P. W. Terry²

¹University of California Los Angeles, CA 90095, USA

²University of Wisconsin-Madison, Madison, WI 53706, USA

Corresponding Author: D. L. Brower, brower@ucla.edu

Drift wave turbulence underlies key transport phenomena in toroidal, magnetically confined plasmas. While long-studied for the tokamak and stellarator configurations, the distinguishing features of the reversed field pinch (RFP) allow further development of gyrokinetic models that build on the RFP's features of high- β , large magnetic shear (tending to add stability), and relatively weak toroidal field. Since the RFP is poloidal-field-dominated, the role of ballooning is considerably weaker. Standard RFP behaviour tends to be governed by tearing magnetic fluctuations driven by the gradient in the current density. However, tokamak-like improved confinement occurs with inductive profile control (PPCD: pulsed poloidal current drive), and large-scale electromagnetic fluctuations are largely suppressed [1]. In this environment, gyro-scale instabilities are anticipated important and could ultimately limit confinement [2]. The role of drift waves is rapidly emerging for the RFP, and this provides a complementary environment to other configurations for exploring basic understanding of turbulent-driven-transport physics and improving confidence in predictive capability for future burning plasmas. Herein we describe detailed measurements of high-frequency density fluctuation spectral features and temporal-spatial dynamics in the MST-RFP. Comparison with modelling results from the gyrokinetic GENE code provide evidence that these fluctuations are consistent with expectations for TEM turbulence and may indeed be playing a role in governing the overall plasma confinement.

References

[1] J. S. Sarff, *et al.*, Nucl. Fusion **43**, 1684–1692 (2003).

[2] D. Carmody, *et al.*, Phys. Plasmas **22**, 012594 (2015).

Work supported by the U.S. Department of Energy, Office of Science, Office of Fusion Energy Sciences under Award Numbers DE-FC02-05ER54814, DE-FG02-85ER53212, and DE-FG02-01ER54615.



Effect of External Magnetic Perturbations on the EXTRAP T2R Reversed-Field Pinch Plasma

L. Frassinetti¹, R. Fridström¹, P. Brunzell¹, Y. Sun², A. C. Setiadi¹, and M. W. M. Kahn¹

¹KTH Royal Institute of Technology, Stockholm, Sweden

²Institute of Plasma Physics, Chinese Academy of Sciences, Hefei, Anhui, People's Republic of China

Corresponding Author: L. Frassinetti, lorenzo.frassinetti@ee.kth.se

The plasma braking due to resonant and nonresonant magnetic perturbations (MPs) is experimentally studied in the EXTRAP T2R [1] reversed-field pinch (RFP) and the results compared with theoretical models adapted to the RFP configuration. Resonant MP produces the tearing mode (TM) braking and, eventually, when the MP amplitude is above the locking threshold, TM locking. Unlocking is reached only by reducing the resonant MP amplitude below the locking threshold. The hysteresis is experimentally studied and the physical mechanisms that leads to an unlocking amplitude lower than the locking amplitude is ascribed to the relaxation of the velocity reduction profile. The experimental results are consistent with a localized electromagnetic torque that acts on the rotating TM island with a braking that spreads to the surrounding plasma via the viscous torque, in agreement with theoretical model described in reference [2].

EX Nonresonant MP produces a braking torque that affects the entire core region and is not localized to any specific position. This is in contrast to the braking produced by a resonant MP, where the torque is localized at the resonance. The experimental results show that the nonresonant MP torque is not simply related to the amplitude of the applied perturbation, but it is well correlated to the plasma displacement produced by the perturbation. This result is consistent with the prediction of a torque produced by neoclassical toroidal viscosity (NTV) effects. The NTV torque has been calculated by adapting the model described in reference [3] to EXTRAP T2R. The comparison between experimental braking torque and NTV torque shows a qualitatively good agreement both concerning the shape of the torque radial profile and the torque dependence on the plasma displacement.

The work shows that in EXTRAP T2R the braking induced by resonant and nonresonant MPs is produced by different physical mechanisms. The resonant MP torque is consistent with a braking electromagnetic torque that acts on the rotating TM. The nonresonant MP torque is consistent with a braking NTV torque that acts on the flow in the entire core region.

References

- [1] P. R. Brunzell, *et al.*, Plasma Phys. Control. Fusion **43**, 1457 (2001).
- [2] R. Fitzpatrick, *et al.*, Phys. Plasmas **8**, 4489 (2001).
- [3] Y. Sun, *et al.*, Nucl. Fusion **52**, 083007 (2012).

Overview of Keda Torus Experiment Initial Results

W. Liu¹, B. Xiao², A. Liu¹, H. Li¹, J. Xie¹, T. Lan¹, H. Zhou¹, C. Xiao³, X. Wen¹, L. Yang², S. Wan¹, H. Wang¹, W. You¹, M. Tan¹, W. Bai¹, C. Tu¹, B. Luo¹, P. Fu², Y. Song², Q. Yang², W. X. Ding⁴, and W. Mao¹

¹University of Science and Technology of China, Hefei, Anhui, People's Republic of China

²Institute of Plasma Physics, Chinese Academy of Sciences, Hefei, Anhui, People's Republic of China

³University of Saskatchewan, Saskatoon, SK S7N-5C9, Canada

⁴University of California Los Angeles, CA 90095, USA

Corresponding Author: W. Liu, wliu@ustc.edu.cn

The Keda Torus eXperiment (KTX) is a new reversed field pinch (RFP) device at the University of Science and Technology of China. KTX is complementary to the existing international Reversed Field Pinch (RFP) facilities. KTX includes the vacuum chamber, conducting shell, magnetic field windings, power supply, active control coils, vacuum pump, wall baking and data acquisition system. KTX construction and assembly were completed on August 1, 2015 and the first plasma was obtained on August 15, 2015. Intensive conditioning and optimization of the machine are underway to ramp up the plasma current towards full operation. An active feedback mode control system has been implemented. The pulsed power supply systems for poloidal field (PF) and toroidal field (TF), using thyristor and energy storage capacitors, have been tested and commissioned. In the first phase of KTX the total stored energy is 1.6 MJ for both PF and TF systems. The flexibility for the TF power supply enables both reversed toroidal field (RFP) and stable toroidal field (tokamak) operation modes. The probe arrays for electric and magnetic field measurement, 2D double-foil soft X-ray arrays, multichannel X-ray analyzers, middle plane H_α line detector, fast reciprocating Langmuir probes and 7-chord interferometry/polarimetry diagnostics are currently used in KTX for commission. KTX will be upgraded to the second phase after completion of the first operation phase. KTX programme will address some important RFP physics like the impact of 3D structure on plasma flow, and magnetic turbulence and plasma wall interaction, among other topics.

EX

Initial Operation Results from KTX

T. Lan¹, H. Li¹, J. Xie¹, H. Zhou¹, S. Wan¹, H. Wang¹, X. Wen¹, W. X. Ding², L. Yang³, C. Xiao⁴, M. Tan¹, P. Fu³, Y. Song³, Q. Yang³, W. Liu¹, B. Luo¹, C. Tu¹, B. Xiao³, W. Bai¹, A. Liu¹, and W. Mao¹

¹University of Science and Technology of China, Hefei, Anhui, People's Republic of China

²University of California Los Angeles, CA 90095, USA

³Institute of Plasma Physics, Chinese Academy of Sciences, Hefei, Anhui, People's Republic of China

⁴University of Saskatchewan, Saskatoon, SK S7N-5C9, Canada

Corresponding Author: T. Lan, lantao@ustc.edu.cn

Keda Torus eXperiment (KTX) is a medium size reversed field pinch (RFP) machine which has been constructed to study active feedback control of MHD modes, electromagnetic turbulences and plasma wall interaction under different magnetic configurations, such as low safety factor (q) tokamak and reversed field pinch. The variation of magnetic topology in the presence of both external and internal magnetic perturbations will impact on plasma performance. The first plasma of KTX was achieved on August 2015 shortly after the completion of the construction, suggesting sound physics and engineering design and proper fabrication and assembly. A low q tokamak and transient Reversed Field Pinch operation modes have been achieved with the same power supply system. For the tokamak mode, the maximum stored energy in the poloidal field reached 1.6 MJ, which correspond to a flux swing of about 1 Vs. The edge electron density and electron temperature are measured by Langmuir probes. For tokamak discharge, the measured edge electron density can reach $10^{19}/\text{m}^3$, and the electron temperature is around 10 eV. Magnetic fluctuations are measured by edge magnetic probes. The coherency spectra show coherent signal around 10 kHz with a dominant poloidal mode number $m = 3$. In RFP operation, effort was made to reverse the toroidal field quickly. RFP state on KTX is achieved for a short period of time. The stable RFP state operation mode is now being pursued on KTX.

EX



Investigations of Plasmoid Formation and Flux Closure in Transient Coaxial Helicity Injection on HIST

M. Nagata¹

¹*University of Hyogo, Kobe, Japan*

Corresponding Author: M. Nagata, nagata@eng.u-hyogo.ac.jp

Transient coaxial helicity injection (T-CHI) has been examined in the Helicity Injected Spherical Torus (HIST) device for solenoid-free plasma startup in a ST. Here, we report the formation process of T-CHI start-up plasma including flux-surface closure and fast magnetic reconnection. Experimental observation shows that i) two or three plasmoids or islands are generated in elongated toroidal current sheet; ii) For the stable discharges, the plasmoids merge and straightforwardly develop to a large-scale flux structure due to inward current diffusion during the decay phase; and iii) For discharges with the $n = 1$ kink instability, the distorted magnetic configuration relaxes back to an axisymmetric state during the decay phase, leading to generation of a sufficiently large closed flux. These findings could verify that the plasmoid instability in the elongated current layer and/or MHD relaxation with flux conversion during the nonlinear evolution of the kink mode in the presence of the strong toroidal (guide) field allows the formation of an X-point and the fast flux closure via magnetic reconnection in the T-CHI plasma start-up process.

EX



Improved Low-Aspect-Ratio RFP Performance with Active MHD Control and Associated Change in Magnetic Topology in RELAX

S. Masamune¹, A. Sanpei¹, Y. Aoki¹, T. Nagano¹, M. Higuchi¹, S. Nakanobo¹, R. Tsuboi¹, H. Himura¹, N. Mizuguchi², T. Akiyama², T. Mizuuchi³, K. McCollam⁴, D. Den Hartog⁴, and D. Paccagnella^{5,6}

¹*Kyoto Institute of Technology, Kyoto, Japan*

²*National Institute for Fusion Science (NIFS), Toki, Gifu, Japan*

³*Institute of Advanced Energy, Kyoto University, Nishikyo-ku, Kyoto 615-8540, Japan*

⁴*University of Wisconsin-Madison, Madison, WI 53706, USA*

⁵*Consorzio RFX, Associazione EURATOM-ENEA sulla Fusione, Padova, Italy*

⁶*Consiglio Nazionale delle Ricerche (CNR), Rome, Italy*

Corresponding Author: S. Masamune, masamune@kit.ac.jp

We have modified the active MHD control system in RELAX in order to compensate for the sideband effect arising from two poloidal gaps of the vacuum vessel. As a result, the discharge duration has reached iron-core-saturation-limited level with stabilization of the resistive wall mode (RWM). The plasma performance has also been improved; the central electron poloidal β , the ratio of central electron pressure to the edge poloidal magnetic field pressure, has reached $\sim 15\%$ from $\sim 10\%$ with the previous control system, where the electron poloidal β approximately equals the total electron β in the RFP. After the modification, self-organization to Quasi-Single Helicity (QSH) state has been observed even in deep-reversal discharges. Magnetic field line tracing with ORBIT code shows that helical flux surfaces recover during the QSH state in the core region, although the region is narrower than that in the conventional shallow-reversal case. The transition to QSH and associated change in magnetic topology may be related with improved axisymmetry of the magnetic boundary which is realized by stabilization of the RWM and the resultant improved RFP plasma performance in deep-reversal regime.

EX



Extended Scenarios Opened by the Upgrades of the RFX-Mod Experiment

M. E. Puiatti¹, M. Agostini¹, P. Bettini¹, A. Canton¹, R. Cavazzana¹, S. Dal Bello¹, M. Dalla Palma¹, R. S. Delogu¹, G. De Masi¹, A. Fassina¹, P. Innocente¹, L. Grandò¹, O. Kudlacek¹, G. Marchiori¹, L. Marrelli¹, N. Patel¹, S. Peruzzo¹, M. Siragusa¹, P. Sonato¹, M. Spolaore¹, M. Valisa¹, P. Zanca¹, and L. Zanotto¹

¹*Consorzio RFX, Associazione EURATOM-ENEA sulla Fusione, Padova, Italy*

Corresponding Author: M. E. Puiatti, mariaester.puiatti@igi.cnr.it

RFX-Mod is a flexible device capable of operating both as a Reversed Field Pinch and as a Tokamak, both circular and shaped. In both configurations the explored parameter range and the effectiveness in dealing with critical issues for magnetic confinement will be extended by some enhancements aiming at: a) reducing magnetic chaos by improving the performance of MHD control system; b) improving wall recycling and density control; c) favouring the L-H transition; d) developing new diagnostic systems, in particular increasing the number of magnetic sensors. The scientific motivations and perspectives of such upgrades are discussed in the paper.

In the Quasi Single Helicity helical regime, the performance improves when the magnetic chaos is reduced, i.e., at the lowest amplitudes of the $m = 1$ secondary modes and of the $m = 0$ modes. Moreover, operated as a tokamak, the exploitation of the feedback system allows the investigation of the $m/n = 2/1$ mode control, in particular exploring the $q(a) < 2$ scenario. Therefore, although the advanced MHD active control system allowed a progressive reduction of the field errors, the achievement of an even smoother magnetic boundary remains crucial for the RFP performance and also favours Tokamak operations. Simulations by the RFXLOCKING code show that by removing the inconel vacuum vessel, presently surrounding the plasma, the deformation of the last closed magnetic surface will be reduced (factor about 2). The same modification, combined with the optimization of the toroidal field winding power supply, will improve the $m = 0$ mode control. The improvement of density control relies on the change of the graphite tiles presently covering the first wall with higher conductivity ones, featuring lower temperature increase under high power loads. The deposition of a W layer on the graphite is also being evaluated, given the outward pinch observed after W LBO experiments, which prevents W core contamination. In tokamak configuration, to robustly exceed the L-H transition power threshold and exploit the feedback control system for ELM control studies, 1 MW neutral beam will be installed, whose shine-through has been evaluated to be ≈ 0.5 in the RFX-Mod operational conditions.

EX

H-Mode Achievement and Edge Features in RFX-Mod Tokamak Operation

M. Spolaore¹

¹*Consorzio RFX, Associazione EURATOM-ENEA sulla Fusione, Padova, Italy*

Corresponding Author: M. Spolaore, monica.spolaore@igi.cnr.it

The RFX-Mod experiment is a fusion device designed to operate as a Reversed Field Pinch (RFP), with a major radius $R = 2$ m and a minor radius $a = 0.459$ m. Its high versatility recently allowed operating also as an ohmic tokamak allowing comparative studies between the two configurations in the same device. The device is equipped with a state of the art MHD mode feedback control system, providing a magnetic boundary effective control and modulation, by applying resonant or nonresonant magnetic perturbations (MP) both in RFP and in tokamak configurations. In the fusion community the application of MPs is widely studied as a promising tool in particular to limit the impact of plasma filaments and ELMs, in particular on plasma facing components. An important issue is envisaged in the exploitation of the RFX-Mod active control system for ELM mitigation studies.

As a first step in this direction, this paper will focus on the most recent achievements in term of RFX-Mod tokamak explored scenarios, which allowed the first investigation of the ohmic and edge biasing induced H-mode. In particular the realization of D-shaped tokamak discharges and the design and deployment of an insertable polarized electrode were accomplished. Both operations took advantage of the implementation of a real-time feedback control system of the electron density and of a multivariable shape feedback control system designed on a full model-based approach. Indications of Ohmic H-mode were transiently observed during Single Null shaped plasmas. Stationary H-mode phases were instead obtained with insertable electrode biasing stimulation. The edge biasing is applied in new operation scenarios relatively unexplored with this technique in particular in plasma shaped Single Null discharges and in the very low- q circular plasma discharges, $q(a) < 2$, achievable in RFX-Mod. Important modification of the edge plasma density and flow properties are observed as well as, in some cases, a complex “dithering” phenomenology, characterized by very fast L-H and H-L transitions. These strong fluctuations appear associated to the onset of MHD activity, whose behaviour will be analyzed and discussed in the paper along with the filamentary structures observed in the fast turbulence electromagnetic fluctuations.

EX

Kinetic Properties of Edge Plasma with 3D Magnetic Perturbations in RFX-Mod

M. Agostini¹, P. Scarin¹

¹*Consorzio RFX, Associazione EURATOM-ENEA sulla Fusione, Padova, Italy*

Corresponding Author: M. Agostini, matteo.agostini@igi.cnr.it

Three-dimensional magnetic fields are commonly applied to the plasma edge of fusion devices in order to modify the plasma wall interaction, edge-localized modes (ELM) frequency, divertor loads and transport. However, the action of these magnetic perturbations (MPs) on the edge plasma is still not well understood, and to date there is no obvious relationship between the edge pressure gradient and the MP. This is an outstanding issue for control and suppression of (ELMs).

In this work the response of the kinetic properties of the edge plasma to 3D magnetic perturbations is studied in the RFX-Mod experiment, characterizing their toroidal and poloidal structure. The RFX-Mod experiment is particularly suited for these studies, since it can operate in reversed field pinch (RFP), ultralow q (ULQ) or tokamak configurations, all characterized by the presence of magnetic modes with different helicity. In RFP configuration different modes with $m = 1$ can develop spontaneously or applied externally; in ultralow q and tokamak discharges, modes with $m/n = 1/2, 1/3$ or $2/5$ develop in the edge, depending on the value of the safety factor.

A detailed study of the poloidal structure of the floating potential V_f and edge electron pressure P_e has been undertaken. The spatial structures of the floating potential and the P_e have been observed to be modulated according to the dominant magnetic topology. However, along the poloidal angle, the plasma configuration (characterized through V_f , P_e and neutral influxes), does not exactly reflect the helicity of the MP: more poloidal harmonics are present, and the rotation of the dominant $m = 1$ does not always follow the rotation of the MP. In particular, it is shown that in the equatorial midplane P_e and the magnetic deformation oscillate in phase; while at $\theta = 90^\circ$ there is a finite time shift between the two quantities.



Transport Studies with Magnetic Islands in Fusion Plasmas

R. Lorenzini¹

¹*Consorzio RFX, Associazione EURATOM-ENEA sulla Fusione, Padova, Italy*

Corresponding Author: R. Lorenzini, rita.lorenzini@igi.cnr.it

This work describes the development and the first applications of a new tool to study transport phenomena in fusion devices when magnetic islands are present. Whether as large islands or narrow chains, magnetic islands change drastically the topology of the transport problem and the consequent strong modification of transport has effects that depend on the configuration under examination. The conventional application of 1.5D transport codes need a monotonic coordinate, hence it cannot manage topologies with more than one magnetic axis. The broken nesting of magnetic surfaces demands a piecewise treatment where radial coordinates are defined in domains around their own magnetic axes. Furthermore island separatrices become shared boundaries that require careful treatment. As an example in the case of $m = 1$ island (m being the poloidal mode number) the domains are: the core enclosed by the island, the island itself, and the plasma external to the island.

This is called Multiple Domain scheme (MD): the MD scheme, which has been initially tested in a simple transport code, is included in the 1.5D code ASTRA. Here we present quantitative analysis of transport with magnetic islands in the following devices:

RFX-Mod: We investigated the role of separatrix disappearance, which is expected to increase the topology resilience to the magnetic chaos, in the behaviour of thermal conductivity found in the transport barriers and in the plasma bulk. The metrics elements that enter in the energy transport equation are provided by the SHEq code.

LHD: The metrics elements are obtained from Poincarè plots based on HINT2 calculations for a plasma with an externally imposed $n/m = 1/1$ "large" island. The MD scheme is used to perform an interpretative analysis of the experimental temperature profiles.

TJ-II: We have used TJ-II data to concentrate on the important topic of radial electric field modifications when a small island chain is present. A pseudo-cylindrical approximation is used to define the discontinuities in the metric coefficients around the separatrix. The modification of the unperturbed nonaxisymmetric fluxes in the island region is based on Shaing's formulation.

EX

Observation of Large Filaments during the Disruptive Phase of ADITYA Tokamak Plasma

S. Banerjee¹, N. K. Bisai¹, D. Chandra¹, P. Dhyani¹, R. Manchanda¹, M. B. Chowdhuri¹, N. K. Ramaiya¹, N. Parmar¹, J. Ghosh¹, R. Tanna¹, P. K. Chattopadhyay¹, D. Raju¹, P. K. Atrey¹, Y. Shankar Joisa¹, A. Sen¹, and P. K. Kaw¹

¹*Institute for Plasma Research (IPR), Bhat, Gandhinagar, India*

Corresponding Author: S. Banerjee, sbanerje@ipr.res.in

Study of the plasma dynamics during the termination phase of a tokamak discharge, particularly during a major disruption, is extremely important for gaining an understanding of essential processes that impact operation limits (e.g., the β limit), outward heat and particle flux and plasma control. Behaviour of the edge and scrape-off layer plasma during such an event is also vital since this region bridges the hot core plasma and the material wall of the device. We report on a detailed investigation of the edge dynamics during the discharge termination phase in ADITYA tokamak using fast visible imaging diagnostics and Langmuir probes.

A frequent observation during disruptions on the ADITYA tokamak is the occurrence of large filaments predominantly on the low field side. These filaments follow the enhanced interaction of the plasma column with the high field side (HFS) limiter surface almost at the end of the discharge. Just prior to the disruption, the plasma column shrinks considerably towards the HFS and the filaments evolve on a resistive diffusion time scale (~ 1 ms). In ADITYA, enhanced oscillations in the signals are observed just prior to the thermal quench. Oscillation amplitude peaks at the thermal quench. Similar phase chronology is observed during high and intermediate β disruptions in TFTR. Studies on gas puff induced disruptions followed by disruption mitigation using biased electrodes in ADITYA, had shown that the $m/n = 2/1, 3/1$ tearing modes were destabilized prior to the disruption sequence. These modes tend to lock and lead to field ergodization and subsequently cause a thermal quench, followed by the final current quench. For the TFTR observations resistive MHD simulations had concluded that the growth rate of plasma filaments did not depend on resistivity η_d but were influenced by the plasma β . Further, the number of fingers were shown to be inversely proportional to η_d . In contrast, our experimental observations show that the number of fingers is proportional to η_d in ADITYA. We will discuss the underlying physics of the formation of such filaments during disruptions in ADITYA and present model calculations supported by MHD simulations that are based on the growth of tearing modes and the mode locking scenario and that are consistent with the observed filament growth rates and the scaling of the number of filaments with η_d .

EX

Plasma Startup Studies and Electromagnetic Field Computation for SST-1 Tokamak

S. Jana¹, D. Ghosh¹, S. Pradhan¹, and D. C. Raval¹

The SST-1 Team

¹*Institute for Plasma Research (IPR), Bhat, Gandhinagar, India*

Corresponding Author: S. Jana, subrata.jana@ipr.res.in

The SST-1 start-up studies and development of appropriate model has been initiated using electromagnetic field computation for active current carrying conductor and SST-1 vacuum vessel eddy characteristics. This electromagnetic model has been employed to predict individual electromagnetic field for active electromagnet such as vertical field coil (VF), poloidal field coil (PF), radial control coil (RCC), central solenoid (CS) and other active current carrying coil. This model can be also useful to determine the some other break-down parameter such as connection length, ionization length and electric field etc.



MHD Phenomena and Disruption Characteristics in SST-1 Early Plasma

J. R. Dhongde¹, M. K. Bhandarkar¹, and S. Pradhan¹

¹*Institute for Plasma Research (IPR), Bhat, Gandhinagar, India*

Corresponding Author: J. R. Dhongde, jasraj@ipr.res.in

Steady State Superconducting Tokamak (SST-1) is a medium size tokamak ($R/a = 1.1/0.2$, $B_t \sim 1.5$ T to 3 T, $I_p \sim 102$ kA) in operation at the Institute for Plasma Research, India. SST-1 has been consistently producing plasma currents in excess of 100 kA, with plasma durations above 250 ms and a central magnetic field of 1.5 T in recent experimental campaigns of 2016. Investigation of experimental data measured using discrete in-vessel poloidal and toroidal Mirnov coils suggests the presence of MHD instabilities in SST-1 plasma. The Mirnov coil data have been analyzed using fast Fourier transform analysis, time resolved frequency analysis using wavelet spectrogram, singular value decomposition (SVD) and Mirnov phase comparison methods with an objective of investigating magnetohydrodynamic phenomena in large aspect ratio ($R/a > 5.5$) plasma columns such as formed in SST-1 plasmas. The analysis clearly explains the behaviour of MHD instabilities observed (i.e., tearing mode with $m/n = 2/1$), oscillation frequencies (in the range of ~ 5 –7 kHz), growth rate and the island width in SST-1 plasma, etc. Onsets of (minor, major) disruptions triggered by MHD instabilities have been correlated with other diagnostics such as soft-X-ray, ECE, H_α , and density, etc. The observations have been cross compared with the theoretical calculations based on Rutherford nonlinear theory and are found to be in good agreement. These new and novel results specific to high aspect ratio tokamak plasmas would be useful to future devices.

EX

Observation and Study of Lock Mode Characteristics in SST-1 Plasma

M. K. Bhandarkar¹, J. R. Dhongde¹, and S. Pradhan¹

The SST-1 Team

¹*Institute for Plasma Research (IPR), Bhat, Gandhinagar, India*

Corresponding Author: M. K. Bhandarkar, manisha@ipr.res.in

Steady State Superconducting Tokamak (SST-1) is a medium size operational Tokamak (major radius= 1.1 m, minor radius= 0.2 m) at the Institute for Plasma Research (IPR), India. In the recent experimental campaign, SST-1 has successfully achieved plasma currents in order of 100 kA and plasma duration in excess of ~330 ms at a central magnetic field of 1.5 T. An attempt has made to observe and study the behaviour of the magnetohydrodynamic (MHD) activity during different phases (Ramp-Up, Flat-Top and Ramp-down) of plasma pulse which leads to major/minor disruptions, its present mode (poloidal/toroidal mode number i.e., $m = 2, n = 1$) and impact on plasma confinement (i.e., confinement degrades or discharge terminates permanently) using experimental data from Mirnov probes. Statistical observation on mode lock instabilities encourages studying the characteristics of field errors influencing the mode rotations and its correlation with drift frequencies for plasmas at SST-1. Observed lock mode characteristics have also been correlated with diagnostics (i.e., ECE, density, X-ray systems, etc.) and heating system (ECRH) for prior and post PFC (plasma facing components) campaigns of SST-1.

EX

Low Density Plasma Regimes in SST-1 with and without Suprathermal Electrons

K. Patel¹, S. Pradhan¹

¹*Institute for Plasma Research (IPR), Bhat, Gandhinagar, India*

Corresponding Author: K. Patel, kpatel@ipr.res.in

Runaway dominated low density discharges are modelled for SST-1 using the model as proposed by I. El Chamaa Neto, *et al.*, for before plasma facing component installation and after plasma facing component installation. For both cases, modelled results are compared with measured data. It is found that the runaway generation takes place in the outer region of the plasma column and the effect of runaway generation is visible in the loop voltage signal, plasma current, H_{α} , bolometer and hard X-ray in the form of spikes. For both the cases plasma resistivity and electron temperature estimated using loop voltage spikes.



Plasma Facing Components Technologies in SST-1

D. C. Raval¹, Z. Khan¹, Y. Paravastu¹, K. R. Dhanani¹, P. Semwal¹, S. George¹,
A. Prakash A¹, G. R. Babu¹, M. S. Khan¹, P. L. Thankey¹, F. S. Pathan¹, and S. Pradhan¹

¹*Institute for Plasma Research (IPR), Bhat, Gandhinagar, India*

Corresponding Author: D. C. Raval, raval@ipr.res.in

SST-1 Tokamak was successfully commissioned in 2012 and the first plasma was achieved in June 2013 with poloidal limiters having SS 304L as vessel wall material. Due to plasma wall interactions, high-Z impurities released from the vessel wall which in turn cools the plasma by radiation loss. In order to reduce this effect, in 2nd phase of SST-1 refurbishment, PFC components were installed in the system. PFCs were integrated inside SST-1 vacuum vessel which is designed to withstand an input heat load of 1.0 MW/m^2 . Graphite was chosen as plasma facing material considering its good thermal properties and low atomic mass. Cu-Zr and Cu-Cr-Zr alloy plates embedded with SS 304L piping were used as back plate materials for proper heat conduction. Each and every component was tested at operating conditions to verify its functionality and to ensure conformity. Approximately 3800 tiles were mounted on 132 copper alloy back-plates. The total surface area of the installed PFCs exposed to plasma is about 40 m^2 which is nearly 50% of the total surface area of stainless steel vacuum chamber ($\sim 75 \text{ m}^2$). The volume of the vessel with the PFCs is $\sim 16 \text{ m}^3$. Gas-to-gas heat exchange method was adapted to heat nitrogen gas which was pressurized using a dedicated gas blower system to bake the PFC components. All PFC components passed through a temperature of 250°C for 8 hours flat top and working pressure of 4 bar under UHV conditions in validation tests. Strict metrology and QA/QC plans were structured and executed to integrate the PFC components inside the vacuum vessel. During pump down of the SST-1 main vacuum vessel, PFCs were baked at 250°C for nearly 10 days to remove the absorbed water vapours. At this condition, this main vacuum vessel was maintained at 150°C . In addition, initially hydrogen discharge cleaning was carried out followed with subsequent helium discharge cleaning to remove other surface impurities. With all PFCs and diagnostic integrated to the system, a base pressure of 4.5×10^{-8} mbar was achieved.

This paper represents SST-1 post PFC Plasma-scenario, PFC requirement inciting factors, PFC architecture and lay-out details, PFC components experimental validations, metrology plan with QA/QC and final installation of PFC with the vacuum vessel.

Fuel Inventory and Deposition in Castellated Beryllium Structures in JET

M. Rubel^{1,2}, P. Petersson¹, Y. Zhou¹, P. Coad², K. Heinola³, A. Widdowson², L. Cristian⁴,
C. Porosnicu⁴, S. Brezinsek⁵, A. Kirschner⁵, and D. Matveev⁵

¹KTH Royal Institute of Technology, Stockholm, Sweden

²Culham Centre for Fusion Energy (CCFE), Culham Science Centre, Abingdon, UK

³VTT Technical Research Centre of Finland Ltd., Espoo, Finland

⁴National Institute of Laser, Plasma and Radiation Physics (INFLPR), Bucharest, Romania

⁵Forschungszentrum Jülich, Jülich, Germany

Corresponding Author: M. Rubel, rubel@kth.se

All plasma-facing components in ITER will be castellated. A large scale test of castellated PFC is carried out at the JET tokamak which has been operated since year 2011 with the metal ITER-like wall (JET-ILW). This contribution is focussed on the morphology of beryllium castellated limiters and upper dump plates after experimental campaigns 2011–2012 and 2013–2014. The results of obtained with a set of complementary material research methods are summarized by the following points.

- The deposition in the 0.6 mm wide grooves of castellation is “shallow”. It reaches 1–4 mm into the 12 mm deep gap.
- Deuterium concentrations are small (maximum $4 \times 10^{18}/\text{cm}^2$). The estimated total amount of deuterium in all castellated limiters is around 9×10^{21} corresponding to less than 10% of the inventory on plasma-facing surfaces of limiters.
- There are only traces of Ni, Cr, and Fe deposited in the castellation gaps. The same applies to the carbon content.
- On plasma-facing surfaces, X-ray diffraction has clearly shown two distinct composition patterns: Be-W mixed intermetallic compounds (e.g., Be_{22}W) on the sides of limiters (deposition zone), whilst only pure Be is detected in the erosion zone. The lack of compound formation in the erosion zone indicates that no distinct changes in thermo-mechanical properties of Be PFC might be expected.

All data consistently show only small amounts of fuel and other elements (especially carbon) in the gaps. The results agree also with the earlier data on analyzes of the castellated Be structures used in JET-C when different gap width was used.

Long-Term Fuel Retention and Release in JET ITER-Like Wall at ITER-Relevant Baking Temperatures

K. Heinola¹, J. Likonen², T. Ahlgren¹, S. Brezinsek³, G. Matthews⁴, R. A. Pitts⁵,
G. De Temmerman⁵, and A. Widdowson⁶

¹University of Helsinki, 00100 Helsinki, Finland

²VTT Technical Research Centre of Finland Ltd., Espoo, Finland

³Forschungszentrum Jülich, Jülich, Germany

⁴Culham Centre for Fusion Energy (CCFE), Culham Science Centre, Abingdon, UK

⁵International Thermonuclear Experimental Reactor (ITER),

Cadarache Centre, 13108 Saint-Paul-lès-Durance, France

⁶United Kingdom Atomic Energy Authority, Culham Science Centre, Abingdon, UK

Corresponding Author: K. Heinola, kalle.heinola@helsinki.fi

JET with its ITER-like wall (ILW) material configuration is presently the only machine in which ITER-relevant plasma-material interactions, such as material erosion and migration and in-vessel fuel retention and removal, can be studied on the tokamak-scale. Especially the in-vessel tritium (T) retention in ITER has high safety importance. The ITER baseline to recover the trapped T is to perform baking of the plasma facing components (PFC), at 240°C for the Be first wall and at 350°C for the W divertor.

EX To study the fuel retention and release at ITER-relevant baking temperatures, a representative set of samples were cut from different ILW regions of selected divertor and main chamber PFCs for deuterium (D) outgassing studies using thermal desorption spectrometry (TDS). The prepared samples represent PFC locations with varying codeposit thicknesses (up to 15 μm). The TDS experiments were performed with different annealing rates (1 and 10 K/min) and dwell times (5 and 15 hrs) at the ITER-relevant bake temperatures. Finally, the sample temperature was raised up to 1000°C to empty the samples of any remaining D.

Results for the thickest ILW deposition indicate that more than 55% of the D is still retained after 15 h of baking at 350°C. A thinner deposited layer (5 μm) was found to have 40% retention after 5 h of annealing. A general feature to all of the ILW divertor samples was that annealing up to 1000°C showed the D₂ release maxima to take place at high temperatures above 330°C over a broad temperature range. For the Be main chamber samples, a relatively higher retention is observed after the ITER-relevant baking temperature at 240°C. The preliminary TDS result for a clean, deposit-free bulk Be sample shows over 60% retention after a 5 h baking at 240°C. Previous ILW postmortem results showed an order of magnitude less global retention in the main chamber as compared to the divertor. However, in ITER the much larger main chamber surface area compared to divertor and its low baking temperature 240°C may play an important role in assessing the accumulated T.



ERO Modelling of Be Erosion in JET and Extrapolation of the Data for ITER

D. Borodin¹, S. Brezinsek¹, I. Borodkina², M. Probst³, S. W. Lisgo⁴, R. A. Pitts⁴, M. Kocan⁴, C. Björkas⁵, A. Kirschner¹, J. Romazanov¹, J. Miettunen⁶, M. Groth⁶, and C. Linsmeier¹

¹Forschungszentrum Jülich, Jülich, Germany

²National Research Nuclear University "MEPhI", Moscow, Russian Federation

³University of Innsbruck, Innsbruck, Austria

⁴International Thermonuclear Experimental Reactor (ITER), Cadarache Centre, 13108 Saint-Paul-lès-Durance, France

⁵VTT Technical Research Centre of Finland Ltd., Espoo, Finland

⁶Aalto University, Espoo, Finland

Corresponding Author: D. Borodin, d.borodin@fz-juelich.de

Erosion will be one of the main factors determining the lifetime of the plasma-facing components (PFCs) in ITER, particularly the low- Z beryllium (Be) first wall (FW). This paper presents the tests of Be erosion data during experiments with the ITER-like wall (ILW) in JET and the corresponding revisiting of the predictive modelling for ITER. The key tool is the Monte Carlo 3D impurity transport and plasma-surface interaction ERO code.

In this paper two fits for Be sputtering data are used, both based on simulated data including the molecular dynamic (MD) approach. The factor 3–4 lower one called "ERO-min" implies large D content (50%) in a PFC surface. Chemically assisted sputtering (CAS) can contribute significantly (up to ~50%) to Be erosion. According to MD data used in ERO, CAS varies with energy of impinging ions and surface temperature T_s .

Benchmarking the ERO on results from the ILW is critical for gaining confidence in the modelling approach and the related data. Two Be erosion experiments have been performed in inner wall (IW) limited discharges. The T_s was found to have an influence on the molecular release fraction, which decreases to negligible values at 670 K. The plasma temperature in SOL (ion impact energies) was scanned whilst simultaneously monitoring the spectroscopic emission of BeI, BeII and BeD in the vicinity of the solid Be limiter. 3D ERO modelling allows the surface erosion to be characterized by the line-of-sight integrated emission. The "ERO-min" sputtering assumptions lead to the best match with experiments. ERO reproduces the BeD light emission trend and absolute value during the E_{imp} scan within 20%.

Earlier ERO erosion predictions for the ITER FW panels have been revisited. The ILW benchmark shows that the previously calculated upper limit (based on the "ERO-min" fit) of the FW panels lifetime estimation of ~4200 ITER discharges (steady state erosion) is the most appropriate. However, the improved (analytical) approach for calculating ion movement just before the surface impact leads to a decrease of the corresponding lifetime by 30% to ~3000 discharges. The CAS can lead to a further decrease, depending on T_s . However, these estimates are based on the most conservative assumptions regarding the background plasma and magnetic equilibrium expected for ITER. In reality, the Be FW panel lifetime is expected to be far greater.

Thermal Analysis of Transient Tungsten Melting Experiments at JET

Y. Corre¹, G. Matthews², J. W. Coenen³, R. Dejarnac⁴, I. Balboa², P. Bunting², I. Coffey², E. Gauthier¹, J. Gaspar⁵, D. Iglesias², S. Jachmich², K. Krieger³, R. A. Pitts⁶, M. Rack³, and S. Silburn²

¹*Institut de Recherche sur la Fusion par confinement Magnétique (IRFM), Commissariat à l'énergie atomique (CEA/Cadarache), 13108 Saint-Paul-lès-Durance, France*

²*Culham Centre for Fusion Energy (CCFE), Culham Science Centre, Abingdon, UK*

³*Forschungszentrum Jülich, Jülich, Germany*

⁴*Institute of Plasma Physics AS CR v.v.i., Prague, Czech Republic*

⁵*Aix-Marseille Université, Marseille, France*

⁶*International Thermonuclear Experimental Reactor (ITER)*

Corresponding Author: Y. Corre, yann.corre@cea.fr

Tungsten (W) melting by transient power loads, for example those delivered by edge localized modes (ELMs), is a major concern for next step fusion devices. By virtue of its size, the amplitude of unmitigated type-I ELMs on JET can be sufficient to induce transient flash melting at the divertor targets provided a deliberately misaligned element is introduced. A first experiment was performed in JET in 2013 using a special lamella with a sharp leading edge gradually varying from $h = 0.25$ mm to 2.5 mm in the poloidal direction towards the high field side in order to maximize the inter-ELM temperature rise. ELM-induced flash melting has been successively achieved allowing investigation of the resulting melt motion. However, using the available IR viewing geometry from top, it was not possible to directly discriminate between the top and leading edge power loads. To improve the experimental validation of heat load and melt motion modelling codes, a new protruding W lamella with a 15° slope in the toroidal direction has been installed for the 2015–16 campaigns, allowing direct, spatially resolved observation of the top surface and reduced sensitivity of the analysis to the surface incidence angle of the magnetic field. This paper reports on the results of these more recent experiments, with specific focus on IR data analysis and heat flux calculations during L-mode and ELMing H-mode discharges. It will demonstrate that, at least in L-mode, the assumption of optical heat flux projection is justified.

Reproducible L-mode discharges have been performed in the old and new experiments, providing, for a given parallel heat flux, IR surface temperature for three different geometries: protruding sharp leading edge, protruding 15° slope and standard shaped lamella. Thermal modelling based on the finite element method has been performed assuming an optical projection of the parallel heat flux, together with a specific IR sensor correction to simulate spatial resolution related effects. The amplitude of the parallel heat load is determined by iteration comparing synthetic with experimental IR data. Using the same model and underlying assumptions, good agreement is obtained for all three geometries, validating the assumption of optical heat load projection and providing a solid basis for the more complex H-mode conditions.

Impact of the JET ITER-Like Wall on H-Mode Plasma Fuelling

S. Wiesen¹, S. Brezinsek¹, M. Wischmeier², E. de la Luna³, M. Groth⁴, A. E. Järvinen⁵,
U. Losada³, and A. Martin³

¹Forschungszentrum Jülich, Jülich, Germany

²Max-Planck-Institut für Plasmaphysik, Garching, Germany

³Laboratorio Nacional de Fusión (LNF),

Centro de Investigaciones Energéticas, Medioambientales y Tecnológicas (CIEMAT), Madrid, Spain

⁴Aalto University, Espoo, Finland

⁵Lawrence Livermore National Laboratory (LLNL), Livermore, CA 94550, USA

Corresponding Author: S. Wiesen, s.wiesen@fz-juelich.de

JET ITER-like wall (ILW) experiments show that the edge density evolution is linked with the level of recycling as with increasing density a delay is observed before pedestal recovery after an ELM. Poor confinement in high-density baseline scenarios can be partially mitigated by choosing divertor plasma configurations with the strike-lines close to the divertor corners with enhanced pumping. The poloidal distribution of the ionization source and the fuelling profile is more delocalized as compared to JET-C (JET with C PFCs). The H-mode pedestal fuelling cycle is dynamically influenced by plasma-wall interactions, in particular:

- ELM induced energetic particles are kinetically reflected on W divertor PFCs leading to distributed refuelling away from the divertor depending on the divertor plasma configuration.
- Molecular re-emission can be delayed as particles are trapped in W PFCs (bulk-W and W-coated CFCs with different fuel content), resulting in retarded recycling after an ELM due to surface outgassing effects.
- Be is eroded from the main-chamber and migration leads to accumulation of Be deposits on the upper inner target plate. It is found that during the ELM outgassing does occur from these deposition areas leading to a localized fuelling effect on the high-field side.

Dedicated JET-ILW H-mode experiments have been executed to disentangle the aforementioned effects. A direct measurement of the particle flows in the SOL is not possible in JET. The poloidal fuelling profile is derived from 2D SOLPS-ITER simulations to allow comparison of H-mode fuelling efficiency between JET-ILW and JET-C.

Studies of Alfvén Eigenmodes in the ITER Baseline Scenario, Sawtoothing JET Plasmas, and MAST Hydrogen-Deuterium Plasmas

S. E. Sharapov¹, M. Fitzgerald¹, V. G. Kiptily¹, H. J. Oliver², C. Perez Von Thun³, Yu. V. Yakovenko⁴, B. N. Breizman⁵, J. Ferreira⁶, V. Goloborod'ko³, T. Johnson⁷, Ye. O. Kazakov⁸, M. Mantsinen^{9,10}, P. Rodrigues⁶, F. Rimini¹, M. Salewski¹¹, and M. Tsalas¹²

¹Culham Centre for Fusion Energy (CCFE), Culham Science Centre, Abingdon, UK

²Institute for Fusion Studies (IFS), University of Texas at Austin, Austin, TX 78712, USA

³Institute for Theoretical Physics, University of Innsbruck, Innsbruck, Austria

⁴Kiev Institute for Nuclear Research, Kiev, Ukraine

⁵University of Texas at Austin, Austin, TX 78712, USA

⁶Instituto Superior Técnico (IST), Lisbon, Portugal

⁷KTH Royal Institute of Technology, Stockholm, Sweden

⁸Laboratory for Plasma Physics, ERM/KMS, Brussels, Belgium

⁹Catalan Institution for Research and Advanced Studies (ICREA)

¹⁰Centro Nacional de Supercomputación (BSC), Barcelona, Spain

¹¹Technical University of Denmark (DTU), Lyngby, Denmark

¹²FOM Institute DIFFER, Association EURATOM-FOM, Nieuwegein, Netherlands

Corresponding Author: S. E. Sharapov, sergei.sharapov@ccfe.ac.uk

Good confinement of fusion-born alpha-particles is essential for the success of ITER. Modelling with the HAGIS code is performed to compute nonlinear stability of alpha-particle-driven TAEs and redistribution of alpha-particles in the 15 MA baseline ITER scenario. For this modelling, 129 TAEs with n 's from 1 to 35 were computed with the MISHKA code, and their damping effects were assessed with the CASTOR-K code. The self-consistent evolution of TAEs and alpha-particles results in TAE saturation amplitudes $dB_r/B_0 = 3 \times 10^{-4}$, with a stochastic transport of alpha-particles localized in a narrow core region, but with alpha-particle redistribution beyond $r/a = 0.5$ being minimal. Whilst these results are positive, their sensitivity to the shear raises the issue of the hierarchy of various alpha-particle-driven AEs throughout the sawtooth cycle. Experiments on fusion products performed recently on JET sawtoothing plasmas indicate on how AEs could vary throughout the sawtooth cycle in ITER. In these JET experiments, TAE, EAE, NAE, and Alfvén cascades (ACs) were observed throughout the sawtooth cycle. The difference in the time of excitation of these AEs is associated with the temporal evolution of the energetic particle profile, which also correlates with direct measurements of energetic particles with a suite of fast ion diagnostics. A correlation between sawtooth crash times and energy of most affected ions is investigated with ECE diagnostics is examined. Modelling of the cyclic AE excitation is performed for the JET data, and the study of alpha-driven AEs is then extended to the baseline ITER scenario. The planned D-T experiment on JET provides an important opportunity to validate the codes predicting alpha-particle effects on AEs. Preparation for AE studies in JET D-T plasma is proceeding along two avenues: i) development of JET scenarios for alpha-driven AEs. These scenarios are developed with q -profiles and β_{hot} values suitable for alpha-driven AEs, and ii) study of AEs in plasmas with mixed hydrogen isotopes. For this, D-H plasmas with NBI were obtained on MAST. A strong suppression effect of the D-H mixture was observed on Compressional AEs in the ion-ion hybrid frequency range.



Multimachine Experimental Investigation of Ion Cyclotron Emission

R. D’Inca¹, P. Jacquet², S. E. Sharapov², T. Akiyama³, G. Yun⁴, and D. C. Pace⁵

¹Max-Planck-Institut für Plasmaphysik, Garching, Germany

²Culham Centre for Fusion Energy (CCFE), Culham Science Centre, Abingdon, UK

³National Institute for Fusion Science (NIFS), Toki, Gifu, Japan

⁴Pohang University of Science and Technology (POSTECH), Pohang, Gyeongbuk 790–784, Republic of Korea

⁵General Atomics, San Diego, CA 92186, USA

Corresponding Author: R. D’Inca, rodolphe.dinca@ipp.mpg.de

Ion Cyclotron Emission (ICE) is an instability triggered by the resonant interaction between a population of fast ions and waves supported by the background plasma. The analysis of the signal passively measured with radio-frequency probes in time and frequency domains can provide information on the characteristics of the barely trapped and lost fusion alpha-particles in a machine such as ITER. ICE can exhibit very different features in time (steady state, transient, cyclic) and in frequency (presence of doublets or triplets at low frequency, continuum at high frequency, chirping, complicated mode structure) depending on the operational parameters, which makes it difficult to investigate it entirely on a single machine. A Joint Experiment was set up by the ITPA Energetic Particle Physics Topical Group to combine the experimental efforts of several machines (JET, DIII-D, ASDEX-Upgrade, KSTAR, LHD and MAST) which have installed or upgraded ICE diagnostics.

The qualification of ICE as a diagnostic requires several steps which involve experimentation. The first step is to characterize the nature (mode numbers, effect of background plasma composition) and evolution of the excited waves (in the linear, quasi-linear, fully nonlinear and decay phases). Second, the method to reconstruct the properties of the exciting ions from the emission spectrogram has to be tested for different heating scenarios (using different geometries and power profiles of neutral beam injectors and/or ion cyclotron resonant frequency heating) and benchmarked against other methods to characterize fast ion populations (⁴He, protons, beam ions), such as fast ion deuterium-alpha (FIDA) spectroscopy or fast ion loss detectors (FILDs) and then has to be applied to scenarios where instabilities such as ELMs (edge localized modes) or TAEs (toroidal Alfvén eigenmodes) are present and analyzed with methods like electron cyclotron emission imaging to check that ICE can indeed provide insights into the mechanism leading to fast ion losses. Finally, different diagnostic designs have to be tested to find the most flexible and least intrusive way of measuring the emission (using a Subharmonic Arc Detector like on JET), especially to determine the quality of signal that is attainable by using an RF probe in the ICRF transmission line, away from the harsh environment inside the vacuum vessel.

EX

Recent Ion Cyclotron Resonance Heating Experiments in JET in Preparation of a DT Campaign

D. Van Eester¹, E. A. Lerche¹, Ye. O. Kazakov¹, P. Jacquet², V. Bobkov³, A. Czarnecka⁴, C. Giroud², M. Goniche⁵, M. Nocente⁶, H. Weisen⁷, R. Dumont⁸, J. Eriksson⁹, L. Giacomelli¹⁰, C. Hellesen⁹, V. Kiptily², T. Koskela¹¹, M. Santala^{2,12}, and M. B. Schneider¹³

¹Laboratory for Plasma Physics, ERM/KMS, Brussels, Belgium

²Culham Centre for Fusion Energy (CCFE), Culham Science Centre, Abingdon, UK

³Max-Planck-Institut für Plasmaphysik, Garching, Germany

⁴Institute of Plasma Physics and Laser Microfusion, Warsaw, Poland

⁵Institut de Recherche sur la Fusion par confinement Magnétique (IRFM), Commissariat à l'énergie atomique (CEA/Cadarache), 13108 Saint-Paul-lès-Durance, France

⁶Università degli Studi di Milano-Bicocca, 20126 Milano, Italy

⁷EUROFusion (EFDA), Max-Planck-Institut für Plasmaphysik, Garching, Germany

⁸Commissariat à l'énergie atomique (CEA), 91400 Gif-sur-Yvette, France

⁹Uppsala University, Uppsala, Sweden

¹⁰Istituto di Fisica del Plasma (IFP), Consiglio Nazionale delle Ricerche (CNR), 20125 Milan, Italy

¹¹Aalto University, Espoo, Finland

¹²VTT Technical Research Centre of Finland Ltd., Espoo, Finland

¹³International Thermonuclear Experimental Reactor (ITER),

Cadarache Centre, 13108 Saint-Paul-lès-Durance, France

Corresponding Author: D. Van Eester, d.van.eester@fz-juelich.de

Ion cyclotron resonance heating (ICRH) is a powerful and flexible method, which can make a significant contribution to a future DT campaign on JET. It can be used for direct fuel ion heating or for minority ion heating, in the latter case leading to electron heating via Coulomb collisions of the fast minority ions with the electrons. Some ICRH schemes can also directly enhance nuclear reaction rates by accelerating fuel ions to energies near the maximum of the fusion cross sections, others allow performing tasks such as wall conditioning, controlling MHD instabilities and expelling heavy impurities from the plasma core. Since 2011 JET is equipped with an "ITER-like" beryllium wall and a tungsten divertor, making it prone to high- Z impurity accumulation, which frequently leads to a core radiation collapse. ICRH, using hydrogen minority heating at sufficiently high power (~ 4 MW in JET), is already well known to be an effective tool for preventing core impurity accumulation and the resulting radiation collapse, and is routinely used on JET. Here we report on initial successes of an important part of the JET work programme on ICRH applications, which is to investigate whether ICRH scenarios can be found that simultaneously achieve two or more of the above listed beneficial effects. In view of the demonstrated ability of ^3He minority heating of substantially increasing the fusion reactivity in DT plasmas, the potential of this heating scheme to also prevent impurity accumulation was evaluated. Anticipating that ^3He heating alone may not be suitably efficient for impurity control, a combination relying on using 2 distinct frequencies to simultaneously heat H and ^3He minorities was also tested. Sophisticated modelling tools are a key asset to optimally prepare for ITER. Various recent experiments provide a wealth of data to benchmark such codes. Modelling results highlighting the ICRH dynamics will be presented. It was e.g., also found that there is considerable potential in exploiting synergies between neutral beam heating and ICRH, due the favourable dependence of ICRH absorption on the resonating ion's Larmor radius, particularly at higher cyclotron harmonics.



Recent Results on High-Triangularity H-Mode Studies in JET-ILW

E. de la Luna¹, R. Fernanda², P. Lomas², A. Sips³, L. Frassinetti⁴, L. Amicucci⁵,
P. Drewelow⁶, J. Flanagan², I. M. Ferreira Nunes⁷, and S. Saarelma²

¹Centro de Investigaciones Energéticas, Medioambientales y Tecnológicas (CIEMAT), Madrid, Spain

²Culham Centre for Fusion Energy (CCFE), Culham Science Centre, Abingdon, UK

³JET Exploitation Unit, Culham Centre for Fusion Energy (CCFE), Culham Science Centre, Abingdon, UK

⁴KTH Royal Institute of Technology, Stockholm, Sweden

⁵Agenzia nazionale per le nuove tecnologie, l'energia e lo sviluppo economico sostenibile (ENEA), Rome, Italy

⁶Max-Planck-Institut für Plasmaphysik, Garching, Germany

⁷Institute of Plasmas and Nuclear Fusion (IPNF), Association EURATOM/IST, Lisbon, Portugal

Corresponding Author: E. de la Luna, elena.delaluna@ciemat.es

Recent experiments on JET with the ITER-like wall (ILW) show that divertor pumping is a key element to access good confinement at high triangularity in scenarios where high gas injection rates are required to keep W core radiation within acceptable limits (for plasma current above 1.5 MA). Similar to previously reported observations at low-triangularity, the use of a configuration where the divertor pumping is the most efficient (with both strike points in the divertor corners) makes low density operation more accessible, enabling access to higher pedestal temperatures and lower collisionalities. Higher pedestal temperature via profile stiffness lead to an increase of the total plasma pressure and stable discharges with $H_{98} = 0.9$ – 1 and global β of 1.8 – 2 are now routinely obtained for both plasma shapes (so far up to 2 MA). The density profile remains rather flat in the core with the change in divertor configuration, thus the improved confinement is clearly a pedestal effect. In comparison, discharges with the standard divertor geometry used in previous JET-ILW experiments, with the outer strike point in the horizontal target and the inner strike point on the vertical target, exhibit lower pedestal pressure (lower temperature) and reduced confinement in similar conditions. With the use of optimum pumping, higher pedestal temperatures and pressures (higher pedestal density at a given temperature) are obtained at higher triangularity in agreement with edge stability predictions. This highlights the importance of operating at higher pedestal temperature (high edge current at lower collisionality) to recover the beneficial effects of triangularity on pedestal stability. However, in contrast to results in JET-C, the confinement of high triangularity H-mode plasmas in JET-ILW degrades at higher densities, well before reaching the Greenwald limit, and no signature of the so-called type-I/type-II ELM regime (characterized by a decrease in ELM frequency with increasing gas injection rate) is found. The role of divertor conditions (recycling and radiation) on the ELMs dynamics, pedestal parameters and plasma confinement at high-triangularity in ILW scenarios will be investigated in order to better understand the different behaviour obtained in JET with the different wall materials.

EX



Density Peaking in JET: Driven by Fuelling or Transport?

T. Tala¹, A. Salmi¹, C. Bourdelle², L. Giacomelli³, C. Giroud⁴, R. Gomes⁵, J. Hillesheim⁴, A. E. Järvinen⁶, C. Maggi⁴, P. Mantica⁷, M. Maslov⁴, L. Meneses⁵, S. Menmuir⁴, S. Moradi⁸, S. Mordijck⁹, V. Naulin¹⁰, H. Nordman¹¹, J. J. Rasmussen¹⁰, A. Sips¹², J. Svensson¹³, M. Tsalas¹⁴, and H. Weisen¹⁵

¹VTT Technical Research Centre of Finland Ltd., Espoo, Finland

²Institut de Recherche sur la Fusion par confinement Magnétique (IRFM),

Commissariat à l'énergie atomique (CEA/Cadarache), 13108 Saint-Paul-lès-Durance, France

³Istituto di Fisica del Plasma CNR, EURATOM-ENEA-CNR Association, Milano, Italy

⁴Culham Centre for Fusion Energy (CCFE), Culham Science Centre, Abingdon, UK

⁵Institute of Plasmas and Nuclear Fusion (IPNF), Association EURATOM/IST, Lisbon, Portugal

⁶Lawrence Livermore National Laboratory (LLNL), Livermore, CA 94550, USA

⁷Istituto di Fisica del Plasma (IFP), Consiglio Nazionale delle Ricerche (CNR), 20125 Milan, Italy

⁸École Polytechnique, 91128 Palaiseau, France

⁹College of William & Mary, Williamsburg, VA 23185, USA

¹⁰Technical University of Denmark (DTU), Lyngby, Denmark

¹¹Chalmers University of Technology, Göteborg, Sweden

¹²JET Exploitation Unit, Culham Centre for Fusion Energy (CCFE), Culham Science Centre, Abingdon, UK

¹³Max-Planck-Institut für Plasmaphysik, Greifswald, Germany

¹⁴FOM Institute DIFFER, Association EURATOM-FOM, Nieuwegein, Netherlands

¹⁵EUROFusion (EFDA), Max-Planck-Institut für Plasmaphysik, Garching, Germany

Corresponding Author: T. Tala, tuomas.tala@vtt.fi

Particle transport and fuelling are a major open question in ITER physics. Core particle transport has been studied in JET by dimensionless collisionality scans both in H-mode and L-mode plasmas. Gas puff modulation was exploited to obtain particle transport coefficients and understand details of the neutral particle source. The dimensionless parameters, q , ρ^* , β_n and T_i/T_e are matched very well within the scan. The volume averaged density is very similar while the collisionality ν^* is varied simultaneously by a factor of 5. The density peaking factor, defined here as R/Ln_e , increases in the inner core ($r/a = 0.3$) from 1.2 to 2.5 and in the outer core ($r/a = 0.8$) from 1.5 to 3.9 when the volume averaged collisionality decreases from 0.47 to 0.09. In H-mode (executed with ITER-like wall), no change in R/Ln_e was observed in L-mode. The preliminary analysis shows that the NBI fuelling plays a major or even dominant role in contributing to the density peaking. In addition to core particle transport studies, several edge diagnostics were exploited to diagnose the neutral sources. Experimental analysis when fitting the amplitude, phase and source profile against the measured modulated density data suggests that particle source inside separatrix is fairly narrow and it does not contribute much inside the pedestal top. Inward convection of the order of 5 m/s at the plasma edge is needed to sustain the steep pedestal. This is also supported by time-dependent EDGE2D-EIRENE modelling that was performed for roughly over one modulation cycle. Nevertheless, one can notice that modelling suggests that ionization inside the separatrix is strongly concentrated on the low field side of the plasma. The width of the flux surface averaged ionization profile inside the separatrix is estimated to be roughly 1 cm on the outboard midplane being consistent with both the divertor camera and the experimental optimization analysis. The convection quickly drops to zero towards the core where small diffusion and NB source are responsible for the density peaking. But we also remind that as the error bars at the edge are large and potentially underestimated the wider source profiles cannot yet be ruled out with certainty.



Progress in Understanding the Role of Low- Z Impurity in the Confinement in JET-ILW and in JET-C Plasmas

C. Giroud¹, N. Aiba², S. Brezinsek³, A. Chankin³, E. Delabie⁴, L. Frassinetti⁵, J. Hillesheim¹, S. Pamela^{1,6}, S. Saarelma¹, S. Wiesen³, C. Maggi¹, H. Urano², P. Drewelow⁷, M. Leyland¹, D. Moulton¹, and S. Menmuir¹

¹Culham Centre for Fusion Energy (CCFE), Culham Science Centre, Abingdon, UK

²Japan Atomic Energy Agency (JAEA), Naka, Japan

³Forschungszentrum Jülich, Jülich, Germany

³Max-Planck-Institut für Plasmaphysik, Garching, Germany

⁴FOM Institute DIFFER, Association EURATOM-FOM, Nieuwegein, Netherlands

⁵KTH Royal Institute of Technology, Stockholm, Sweden

⁶United Kingdom Atomic Energy Authority, Culham Science Centre, Abingdon, UK

⁷Max-Planck-Institut für Plasmaphysik, Greifswald, Germany

Corresponding Author: C. Giroud, carine.giroud@ccfe.ac.uk

The pedestal confinement has significantly decreased in JET with its metallic ITER-like wall with reference to the carbon wall phase of JET (JET-C). In particular, a reduction in pedestal temperature is observed in all scenarios regardless of the level of D-gas injection or value of β_N . At low gas injection, excessive W radiation is not always the cause for this reduction. Unravelling the mechanisms that, in the absence of carbon in the plasma composition and/or as wall material, leads to a decrease in pedestal temperature is critical in predicting the pedestal pressure in ITER. This mechanism is most likely related to the observed increase in pedestal temperature with nitrogen (N) injection in JET-ILW4, and should also explain the lack of pedestal pressure improvement with neon (Ne) injection. This paper makes a synthesis of experimental observations made with extrinsic impurity injection since the first JET-ILW campaign and reviews our current understanding of the role of low- Z impurity on the pedestal pressure.

The first conjecture advocates that D-implantation and release in the W divertor target has been modified with respect to CFC divertor target during ELMy H-mode and could be reducing the pre-ELM pressure by reducing the power at the separatrix, via increased neutral losses or only the ELM-averaged pressure by impairing the pedestal recovery between two ELMs. The second conjecture proposes that improved pedestal stability would be caused by the pressure profile moving inward from the separatrix with impurity injection, either via a global shift or relative shift of the temperature and density profiles. The third conjecture points towards the recovery of pedestal pressure with N injection to an initial mechanism linked to the change in ELM energy losses which raises modestly the average global β by 10% but allows in return the virtuous cycle of an increased Shafranov shift, higher pedestal pressure allowing increased core pressure. This initial mechanism appear linked to the SOL temperature. It is becoming clear that to understand the mechanisms at play it is important to assess the plasma stability with inclusion of flows and resistivity.



Electron Heat Transport in JET from Ion to Electron Scales: Experimental Investigation and Gyro-kinetic Simulations

P. Mantica¹, N. Bonanomi², J. Citrin³, E. A. Lerche⁴, C. Sozzi¹, T. Görler⁵, N. Hawkes⁶, P. Migliano⁷, A. Peeters⁷, G. Szepesi⁶, M. Tsalas³, and D. Van Eester⁴

¹*Istituto di Fisica del Plasma (IFP), Consiglio Nazionale delle Ricerche (CNR), 20125 Milan, Italy*

²*Università degli Studi di Milano-Bicocca, 20126 Milano, Italy*

³*FOM Institute DIFFER, Association EURATOM-FOM, Nieuwegein, Netherlands*

⁴*Laboratory for Plasma Physics, ERM/KMS, Brussels, Belgium*

⁵*Max-Planck-Institut für Plasmaphysik, Garching, Germany*

⁶*Culham Centre for Fusion Energy (CCFE), Culham Science Centre, Abingdon, UK*

⁷*University of Bayreuth, 95447 Bayreuth, Germany*

Corresponding Author: P. Mantica, mantica@ifp.cnr.it

The TEM driven electron heat transport has been investigated experimentally in JET C-wall L-mode plasmas with dominant ICRH electron heating, by flux scans at constant total electron power and power modulation using ICRH in (³He)-D mode conversion scheme. The dependence of the TEM threshold on s and q has been studied by implementing ad hoc time waveforms of the plasma current in order to extend the range of s explored and to decouple it from q . Linear simulations have been made using the gyro-kinetic code GW. A strong dependence on s has been identified in the experiments and no dependence on q , in agreement with linear GW results. The experimental estimate of the electron stiffness in these plasmas is however significantly higher than predicted by nonlinear TEM gyro-kinetic simulations. This discrepancy is even worse in plasmas with comparable electron and ion heating (ICRH+NBI), in which the electron stiffness increases and a macroscopic drop of R/L_{T_e} is observed with respect to pure ICRH plasmas. Nonlinear simulations using GENE show that in both cases it is not possible to account for the experimental electron flux by just considering the ITG-TEM turbulence. Therefore, the idea that electron scale ETG turbulence could account for the missing flux has been explored, supported by the fact that the ETG threshold is predicted to decrease with the increasing T_i/T_e due to NBI heating. A first study of the ETG contribution to the heat flux, using linear and nonlinear local GENE simulations, was based on separate simulations of ion and electron scales. For the ETG saturation, either an ad hoc external flow shear or electron scale zonal flows were used. In both ICRH and ICRH+NBI cases it was found that a nonnegligible electron heat flux can be carried by the ETG modes, explaining the observations. However, a high sensitivity of the results on multiple parameters was found. In addition, recent studies show that multiscale simulations with real electron to ion mass ratio are needed for a proper ETG study. Computationally heavy multiscale simulations have then been started using GENE for these JET shots. The results will help to clarify if and when the electron scale instabilities can carry significant electron heat flux in JET plasmas, also in view of extrapolations to ITER scenarios, where the electron channel will be key for fusion performance.



Evolution and Control of Tungsten Transport in the Termination Phase of JET H-Mode Discharges and Implications for ITER

F. Koechl¹, A. Loarte², E. de la Luna³, I. M. Ferreira Nunes⁴, V. Parail⁵, C. Reux⁶, and F. Rimini⁵

¹*Institute of Atomic and Subatomic Physics, Technische Universität Wien, 1040 Vienna, Austria*

²*International Thermonuclear Experimental Reactor (ITER), Cadarache Centre, 13108 Saint-Paul-lès-Durance, France*

³*Centro de Investigaciones Energéticas, Medioambientales y Tecnológicas (CIEMAT), Madrid, Spain*

⁴*Institute of Plasmas and Nuclear Fusion (IPNF), Association EURATOM/IST, Lisbon, Portugal*

⁵*Culham Centre for Fusion Energy (CCFE), Culham Science Centre, Abingdon, UK*

⁶*Institut de Recherche sur la Fusion par confinement Magnétique (IRFM),*

Commissariat à l'énergie atomique (CEA/Cadarache), 13108 Saint-Paul-lès-Durance, France

Corresponding Author: F. Koechl, florian.koechl@ccfe.ac.uk

Operation of tokamaks with W PFCs presents specific challenges for impurity control. Lack of impurity control can lead to a radiative collapse due to W accumulation and increased disruptivity. W accumulation in stationary H-mode can be avoided by controlled ELM triggering and central RF heating. Such schemes are also expected to be effective in ITER. However, the control of W transport can be more challenging in the transition from stationary H-mode to L-mode. Long-ELM free phases could arise and lead to an uncontrolled increase of the edge W density and core density peaking causing W accumulation.

To address W control issues in the H-mode termination phase a series of dedicated experiments to be supported by JINTRAC modelling have been performed at JET including the variation of the decrease of the power ramp rate, gas fuelling and central ICRH, and applying active ELM control by vertical kicks and pellets. The experimental results obtained demonstrate the key role of maintaining ELM control and ICRH to control the W concentration in the exit phase of H-modes with slow (ITER-like) ramp-down of the NBI power in JET. Without ELM control, long ELM-free phases occur and W accumulation takes place even with central ICRH (~1 MW). The required level of ELM control can be achieved at JET through adjustment of gas fuelling or by active ELM control at levels of gas fuelling for which W accumulation occurs when kicks are not applied. The latter scenario provides an integrated solution regarding the control of W concentration and plasma energy evolution in the termination of H-modes that can be readily extrapolated to the corresponding phase of 15 MA $Q = 10$ plasmas in ITER.

Modelling studies performed with JINTRAC have shown that the existing models can appropriately reproduce the accumulation of W in the termination phase of JET H-modes. In this respect the lengthening of the H-mode termination phase by maintaining a low level of NBI heating, which provides a sizeable core particle source and peaks the core density profile, and ICRH are the key to differences in W behaviour found in the experiment.

The paper will describe the results of the JET experiments, the comparison with JINTRAC modelling and the adequacy of the models to reproduce the experimental results and draw conclusions regarding the extrapolation of the results and of the applied techniques to ITER.



Ion Cyclotron Resonance Heating for Tungsten Control in JET H-Mode Scenarios

M. Goniche¹, R. Dumont¹, V. Bobkov², P. Buratti³, S. Brezinsek⁴, C. Challis⁵, F. J. Casson⁵, L. Colas¹, A. Czarnecka⁶, N. Fedorczak¹, J. Garcia¹, C. Giroud⁵, M. Graham⁵, J. Graves⁷, P. Jacquet⁵, E. A. Lerche⁸, P. Mantica⁹, I. Monakhov⁵, P. Monier-Garbet¹, M. F. Nave¹⁰, I. M. Ferreira Nunes¹⁰, T. Pütterich², F. Rimini⁵, M. Valisa¹¹, and D. Van Eester⁸

¹Institut de Recherche sur la Fusion par confinement Magnétique (IRFM),

Commissariat à l'énergie atomique (CEA/Cadarache), 13108 Saint-Paul-lès-Durance, France

²Max-Planck-Institut für Plasmaphysik, Garching, Germany

³Agenzia nazionale per le nuove tecnologie, l'energia e lo sviluppo economico sostenibile (ENEA), Rome, Italy

⁴Forschungszentrum Jülich, Jülich, Germany

⁵Culham Centre for Fusion Energy (CCFE), Culham Science Centre, Abingdon, UK

⁶Institute of Plasma Physics and Laser Microfusion, Warsaw, Poland

⁷École polytechnique fédérale de Lausanne (EPFL), 1015 Lausanne, Switzerland

⁸Laboratory for Plasma Physics, ERM/KMS, Brussels, Belgium

⁹Istituto di Fisica del Plasma (IFP), Consiglio Nazionale delle Ricerche (CNR), 20125 Milan, Italy

¹⁰Institute of Plasmas and Nuclear Fusion (IPNF), Association EURATOM/IST, Lisbon, Portugal

¹¹Consorzio RFX, Associazione EURATOM-ENEA sulla Fusione, Padova, Italy

Corresponding Author: M. Goniche, marc.goniche@cea.fr

EX

Development of high performance plasma scenarios in high- Z metal plasma-facing environment is hampered by an unfavourable distribution of these particles across the plasma core, known as “core accumulation”. Tungsten core profiles have been analyzed in different JET scenarios ($I_p = 2.5\text{--}4.0$ MA, $P_{\text{tot}} = 18\text{--}30$ MW) with ICRH (0–6 MW, H minority heating) from the soft X-ray diagnostic. At a plasma current of 2.5 MA, the peaking of the tungsten radiation can be strongly reduced when ICRH power in excess of 4 MW is added to 15 MW of NBI power. At low gas rate ($\sim 5 \times 10^{21}$ el./s), more than 6 MW of ICRH power would be necessary to obtain flat W radiation profiles but the anisotropy of the W radiation profile is already strongly reduced with 4 MW. When the plasma current is raised, low tungsten peaking in quasi-stationary conditions (i.e., modulated between 1 and typically 3 with the sawtooth frequency) can still be obtained but with higher gas rate (typically, for 3.5 MA, 4×10^{22} el./s with strike point close to the pumping duct). In hybrid scenarios ($I_p = 2.5$ MA), strong peaking of the tungsten occurs 1.5–2 s after the start of the high power phase with slightly off-axis ICRH heating ($R_{\text{res}} - R_{\text{mag}} \sim 0.10$ m, $P_{\text{ICRH}} = 3\text{--}5$ MW). MHD activity plays a key role in tungsten transport and core W radiation is modulated with the sawtooth cycle. When at low plasma current ($I_p = 2.5$ MA), the tungsten peaking increases and saturates until the sawtooth crash, at higher I_p , the tungsten peaking generally starts decreasing well before the sawtooth crash. This is well correlated with fishbone activity generated by the fast ion pressure. Modelling of the temperature screening provided by the fast minority ions indicates that this screening is weak at low H concentration and experimental results suggests that even at high concentration ($n_{\text{H}}/n_e \sim 15\%$) this is not a major player for tungsten control.



The Role of ELMs and Inter-ELM Phases in the Transport of Heavy Impurities in JET

M. Valisa¹, L. Amicucci², C. Angioni³, R. Cesario⁴, L. Carraro¹, D. Coster³, F. J. Casson⁵, E. de la Luna⁶, I. Coffey⁵, P. Devynck⁷, P. Drewelow⁸, L. Frassinetti⁹, C. Giroud⁵, F. Koehl¹⁰, M. Leyland⁵, A. Loarte¹¹, M. Marinucci⁴, M. O'Mullane¹², V. Parail⁵, M. E. Puiatti¹, M. Romanelli⁵, and E. Stefanikova⁹

¹Consorzio RFX, Associazione EURATOM-ENEA sulla Fusione, Padova, Italy

²Agenzia nazionale per le nuove tecnologie, l'energia e lo sviluppo economico sostenibile (ENEA), Rome, Italy

³Max-Planck-Institut für Plasmaphysik, Garching, Germany

⁴Associazione EURATOM-ENEA Unità Tecnica Fusione, Frascati, Italy

⁵Culham Centre for Fusion Energy (CCFE), Culham Science Centre, Abingdon, UK

⁶Centro de Investigaciones Energéticas, Medioambientales y Tecnológicas (CIEMAT), Madrid, Spain

⁷Commissariat à l'énergie atomique (CEA/Cadarache), 13108 Saint-Paul-lès-Durance, France

⁸Max-Planck-Institut für Plasmaphysik, Greifswald, Germany

⁹KTH Royal Institute of Technology, Stockholm, Sweden

¹⁰Institute of Atomic and Subatomic Physics, Technische Universität Wien, 1040 Vienna, Austria

¹¹International Thermonuclear Experimental Reactor (ITER),

Cadarache Centre, 13108 Saint-Paul-lès-Durance, France

¹²University of Strathclyde, Glasgow, UK

Corresponding Author: M. Valisa, valisa@igi.cnr.it

Experimental and modelling activities have started at JET to assess the mechanisms controlling the penetration of high- Z impurities from the divertor into the core plasma and to provide a firm basis for the ELM-control requirements in ITER. The experiments are based on the injection of traces of extrinsic impurities in various ELMy plasmas, thus avoiding the variation of the impurity source with plasma conditions which complicates the interpretation of the data. Soft X-ray time traces of Mo injections show clear drops at each ELM events. The corresponding losses of Mo can be estimated by modelling the data and can be correlated to the ELM amplitude and to the main density losses. Emission lines of Li-like Ne reveal the dynamics of the region just inside the separatrix. Typical inverse proportionality is seen between the emissivity of the injected impurities and the ELM frequency, irrespective of the atomic number. A detailed comparison is made between natural ELMs and kick-triggered ELMs at the same frequency in 2 MA, 2.1 T, low triangularity discharges. Preliminary considerations indicate that small differences in the impurity behaviour may be attributed to the differences in the background plasmas. Modelling is based on the JINTRAC suite of codes that include 2D edge and 1D core transport descriptions of the ELM cycle, with the kinetic profiles from the experiment. The impurity transport in the SOL during ELMs involves complex mechanisms that affect directly impurities and the background plasma. Comparison with physics based MHD models is foreseen. The search for ITER-like conditions where an hollow W density profile develops at the edge of the JET plasma is driven by the observation that the proxy for the neoclassical convection at the edge barrier, based on the electron density and temperature normalized gradients, statistically decreases with increasing power suggesting that neoclassical convection could reverse and become outward directed for sufficiently high power. More in general, this work extends to the edge the effort that is being pursued in JET to understand the behaviour of heavy impurities in the plasma core and represents a step in the direction of an integrated and self-consistent approach to the problem of the heavy impurity study and control in present and future devices.

Neutron Yield Studies in JET H-Modes

H. Weisen¹, H.-T. Kim², J. Strachan³, S. D. Scott⁴, B. Yuriy², J. Buchanan², M. Fitzgerald², D. Keeling², K. Damian², L. Giacomelli⁵, T. Koskela⁶, M. Weisen⁷, C. Giroud⁸, and K.-D. Zastrow²

¹EUROFusion (EFDA), Max-Planck-Institut für Plasmaphysik, Garching, Germany

²United Kingdom Atomic Energy Authority, Culham Science Centre, Abingdon, UK

³Princeton Plasma Physics Laboratory (PPPL), Princeton, NJ 08540, USA

⁴Massachusetts Institute of Technology (MIT), Cambridge, MA 02139, USA

⁵Consiglio Nazionale delle Ricerche (CNR), Rome, Italy

⁶Aalto University, Espoo, Finland

⁷University of Strathclyde, Glasgow, UK

⁸Culham Centre for Fusion Energy (CCFE), Culham Science Centre, Abingdon, UK

Corresponding Author: H. Weisen, henri.weisen@epfl.ch

EX The ability to calculate and predict the neutron yield is essential for the planning of fusion experiments, such as the future deuterium/tritium experiment in JET. The fusion yield expected in JET from fast ion orbit calculations using NUBEAM/TRANSP has been systematically compared to the measurements from a set of three Uranium fission chambers, which were recalibrated in 2013. In many JET discharges the measured neutron rates fall short of the predicted ones by up to a factor 2, depending on plasma parameters. In JET, unlike ITER, neutrons are primarily from beam-thermal reactions and the causes of the neutron deficit are believed to be due to processes affecting the fast ion-thermal reactivity, such as fuel dilution, NBI deposition and fast ion transport. The study presented here is based on deuterium discharges, mostly from the JET carbon phase (until 2009) and cover a wide range of plasma conditions in H-mode, together with a few L-mode samples. NUBEAM/TRANSP simulations were produced for a set of 320 discharges which are representative of the entire JET operating domain. The deficit correlates with plasma parameters, being smallest or absent in discharges with highest toroidal rotation, T_e , T_i , and β_N , such as realized in “hybrid scenarios”, which provide the highest fusion yields in JET and are considered to be the best option for DT experiments. Contrary to widespread belief, Z_{eff} and dilution appear to play at best a minor role. Modelling of the neutron deficit assuming fast ion diffusion with $D_f = \chi_i$, is inconsistent with the observed parameter dependencies for the deficit, suggesting that fast ion transport and thermal heat transport are of different nature. MHD instabilities such as sawtooth crashes modelled by TRANSP and NTM’s modelled using ASCOT, appear to have too small an effect to explain the deficit. The fact that neutron rates at high- β_N (> 2.5) generally agree within errors with the measurements, gives confidence in our predictions of the fusion performance of high- β_N plasmas in the future DT campaign.



Comprehensive Analysis of Metal Dust Particles in JET-ILW, and Impact on Fusion Reactor

N. Ashikawa¹, N. Asakura², M. Oyaidzu², K. Isobe², A. Widdowson³, J. Grzonka⁴, M. Rubel⁵, M. Hara⁶, T. Otsuka⁷, D. Hamaguchi², H. Kurotaki², S. Nakano², J.-H. Kim², M. Miyamoto⁸, Y. Hatano⁶, Y. Torikai⁶, M. Tokitani¹, K. Heinola⁹, A. Baron-Wiechec³, S. Masuzaki¹, H. Tanigawa², M. Nakamichi², and T. Yamanishi²

¹National Institute for Fusion Science (NIFS), Toki, Gifu, Japan

²Japan Atomic Energy Agency (JAEA), Naka, Japan

³United Kingdom Atomic Energy Authority, Culham Science Centre, Abingdon, UK

⁴Warsaw University of Technology, Warsaw, Poland

⁵KTH Royal Institute of Technology, Stockholm, Sweden

⁶University of Toyama, Toyama, Japan

⁷Kyushu University, Kasuga, Japan

⁸Shimane University, Matsue, Shimane, Japan

⁹University of Helsinki, 00100 Helsinki, Finland

Corresponding Author: N. Ashikawa, ashikawa@lhd.nifs.ac.jp

Generation and accumulation of metal dust particles are important issues in material migration of the plasma facing components (PFCs) such as tungsten (W) and beryllium (Be) from viewpoints of the plasma operation, maintenance and safety in accidents for ITER and DEMO. On the other hand, analysis results of the material components and the internal structure of the dust particle are few because plasma experiment devices are limited and analysis procedures/devices are not well established. Analysis results of, in particular, Be dust particles are important for ITER, which have not been reported.

A comprehensive analysis of collected dust and divertor tiles in the Joint European Torus (JET) ITER-like wall (ILW) after the first campaign in 2011–2012 [1] has been carried out at the International Fusion Energy Research Centre (IFERC) in order to identify dust characteristics such as structures, material components and hydrogen isotope retention. After the first campaign of the JET-ILW operation in 2011–2012, dust particles were collected from 92% of the divertor surface area. Totally about 1 g was collected: 0.7 g and 0.3 g from the inner and outer divertors, respectively [1]. The analysis started from a large-size dust flake, i.e., 40–120 μm , to determine material components both on the surface and in the cross-section by cutting the dust particle using a focussed ion beam. For the flake-type Be-base dust particle, it was found that the damaged Be crystal structure contained a larger oxygen component near the surface ($\sim 2 \mu\text{m}$) measured by transmission electron microscopy and electron probe micro analyzer, respectively. Deuterium (D) retention in small weight of dust particles (4.4 mg) was evaluated to be 1.2×10^{21} atoms/g by thermal desorption spectrometry, which corresponds to 8.2×10^{20} atoms for all dust particles collected from the inner divertor (0.7 g). This result firstly suggests that contribution of dust particles to the total retention in experiment is small, i.e., less than 1% of the total retention in deposition layers of the inner divertor target.

In this paper, a detailed characterization, which is a relationship between retained hydrogen isotopes and compositions of JET-ILW dust particles, will be presented.

References

[1] A. Widdowson, *et al.*, Phys. Scr. **T159**, 014010 (2014).



Detailed Survey of Dust Particles from JET with the ITER-Like Wall: Origin, Composition and Internal Structure

E. Fortuna-Zaleśna¹, J. Grzonka¹, M. Rubel², A. Widdowson³, A. Garcia Carrasco⁴,
P. Petersson², and A. Baron-Wiechec³

¹Warsaw University of Technology, Warsaw, Poland

²KTH Royal Institute of Technology, Stockholm, Sweden

³United Kingdom Atomic Energy Authority, Culham Science Centre, Abingdon, UK

⁴Uppsala University, Uppsala, Sweden

Corresponding Author: E. Fortuna-Zaleśna, efortuna@inmat.pw.edu.pl

Comprehensive and systematic surveys of dust particles were performed at JET with the ITER-like wall (JET-ILW) after two experimental campaigns, ~19 h of plasma each. Though the total amounts removed were small (around 1 g) the study of dust categories is crucial for ITER because these are unique data from a full metal-wall (beryllium and tungsten) machine. The identification of various categories of particles allows conclusions on mechanisms underlying their generation and mobilization. This work deals with dust collected with sticky pads from the divertor tiles and, with metal splashes on erosion-deposition probes in the divertor and the main chamber wall. The local sampling is essential for: i) finding a correlation between the type of dust and the deposition pattern, and ii) comparison of dust identified in a given location after consecutive campaigns

The search has identified several forms. a) Flakes of Be-rich deposits (up to 800 μm) with embedded tiny metal particles: Ni, W. Irregular droplet-like W inclusions, up to 200 nm, are nearly uniformly distributed in the deposit with an exception of the bottom of the layer, i.e., film formed at the early commissioning phase without high power beam operation. There is also a significant content of nitrogen retained after plasma edge cooling. Films are crystalline, but the presence of amorphous regions cannot be fully excluded. b) Regular Be droplets, diameter 5–10 μm and — on probes — Be splashes with small bubbles thus indicating boiling of the droplet. c) Spherical W droplets, ~100 μm diameter, which could be formed in the experiment on tungsten melting. d) Droplets of Inconel. e) Irregular debris or flakes up to 300 μm containing W, Mo-W. f) Ceramics containing boron nitride, zirconium oxide, alumina.

In conclusion, the study clearly shows a correlation between the operation mode, material erosion, growth of codeposits and generation of dust.

Plasma-Wall Interaction Studies in the Full-W ASDEX-Upgrade during Helium Plasma Discharges

A. Hakola¹, S. Brezinsek², D. Douai³, V. Bobkov⁴, M. Balden⁴, D. Carralero⁴, H. Greuner⁴, A. Kallenbach⁴, K. Krieger⁴, G. Meisl⁴, M. Oberkofler⁴, V. Rohde⁴, P. A. Schneider⁴, A. Lahtinen⁵, G. De Temmerman⁶, R. Caniello⁷, F. Ghezzi⁷, T. Wauters⁸, A. Garcia Carrasco⁹, and P. Petersson¹⁰

¹VTT Technical Research Centre of Finland Ltd., Espoo, Finland

²Forschungszentrum Jülich, Jülich, Germany

³Institut de Recherche sur la Fusion par confinement Magnétique (IRFM), Commissariat à l'énergie atomique (CEA/Cadarache), 13108 Saint-Paul-lès-Durance, France

⁴Max-Planck-Institut für Plasmaphysik, Garching, Germany

⁵University of Helsinki, 00100 Helsinki, Finland

⁶International Thermonuclear Experimental Reactor (ITER), Cadarache Centre, 13108 Saint-Paul-lès-Durance, France

⁷Istituto di Fisica del Plasma (IFP), Consiglio Nazionale delle Ricerche (CNR), 20125 Milan, Italy

⁸Laboratory for Plasma Physics, ERM/KMS, Brussels, Belgium

⁹Uppsala University, Uppsala, Sweden

¹⁰KTH Royal Institute of Technology, Stockholm, Sweden

Corresponding Author: A. Hakola, antti.hakola@vtt.fi

The possible start-up phase of ITER with helium plasmas has set the need to understand in detail the interaction between tungsten plasma-facing components (PFCs) and helium. In addition, a smooth start of He plasma operations requires cleaning the vessel wall from residual fuel species and other impurities. To this end, ion cyclotron wall conditioning (ICWC) is a promising method. We have investigated these plasma-wall interaction topics in ASDEX-Upgrade (AUG) during its He campaign in 2015. First, the main-chamber components were cleaned from their D inventory by ICWC. The He content of the plasma increased from 30% to 80%, and bulk W samples exposed at the outer midplane of AUG were all measured to contain both He and D. Next, surface modifications and the formation of fuzz on virgin and predamaged (by He exposure) W surfaces as well as erosion and redeposition of W were studied. Tungsten samples were exposed to ELMy H-mode plasma discharges in He at the outer strike point of AUG. The fluence and ion energy were sufficient for inducing nanoscale modifications on the surface. The D content of the plasma remained at a constant level of ~10% during the experiment while the He content fluctuated around the average value of 80% due to H beams used for plasma heating. Surface analyzes showed that all the samples had been covered with deposits, mainly containing W, C, O, and B. In addition, the coral-like surface structures on the predamaged samples were intact and no signs of melting could be observed. The thickest deposits were observed in the private flux region and the rougher and the more modified the surface was, the more noticeable deposition was measured throughout the strike point region. Only little erosion, if anything at all, could be seen for W. The observed strong net deposition at the divertor is attributed to an influx of material from the main chamber and is qualitatively different from the behaviour during D operations in AUG. This could also be the case in ITER: nanoscale modifications of different W surfaces compete with the surface being eroded by plasma and with the growth of codeposited layers on PFCs by redeposited W, seeded impurities, and beryllium from the main chamber. Dedicated lab experiments and modelling efforts in the presence of impurity mixes are needed to enlighten the issue further.



Analysis of the Impact of Nitrogen- & Neon-Seeding on ASDEX-Upgrade H-Modes with SOLPS Simulations

F. Reimold¹, A. S. Kukushkin², M. Wischmeier³, M. Bernert³, and D. Reiter¹

¹Forschungszentrum Jülich, Jülich, Germany

²International Thermonuclear Experimental Reactor (ITER),

Cadarache Centre, 13108 Saint-Paul-lès-Durance, France

³Max-Planck-Institut für Plasmaphysik, Garching, Germany

Corresponding Author: F. Reimold, f.reimold@fz-juelich.de

Future fusion devices like ITER and DEMO will have to be operated with a detached divertor to meet material limits. Stable H-mode operation at high heating power $P_{\text{Heat}}/R = 5\text{--}12$ MW/m with both targets completely detached, confinement of $H_{98} = 0.8\text{--}0.95$ and Greenwald fraction of $f_{\text{GW}} = 0.7\text{--}0.9$ has been demonstrated with nitrogen seeding in the all-tungsten ASDEX Upgrade tokamak. In ITER gas handling would be simpler if neon could be used instead of nitrogen. Hence, neon seeding has been attempted in ASDEX-Upgrade for comparison. So far, detachment could not be achieved without provoking a radiative collapse due to tungsten accumulation. In order to still compare both radiative species, a series of H-modes with increasing seeding rates (high-recycling to detached outer divertor target) have been simulated. The simulations are based on input parameters and transport coefficients that are taken from closely validated SOLPS modelling of nitrogen seeded, medium heating power ($P_{\text{Heat}}/R = 5\text{--}7$ MW/m) discharges. The characteristic evolution of the radiation distribution and the impact on the upstream plasma parameters differ significantly for both seeding species. With nitrogen the divertor radiation increases and moves from the targets to the X-point and into the confined plasma, strongly localized in the direct proximity of the X-point. Similar to experiment, the upstream separatrix pressure varies only within 10% during this evolution. In contrast, neon mainly leads to an increase of main chamber radiation that strongly degrades the temperature pedestal. When the neon radiation finally condenses to the X-point, the separatrix pressure is reduced by about a factor of two. The differences for both seeding species seem to be due to at least two reasons. First, the radiation potential L_Z favours main chamber radiation for neon and divertor radiation for nitrogen. Second, divertor enrichment is strong for nitrogen and absent for neon in the simulations. The coherence with contrasting ITER simulations in which nitrogen and neon seeding to partial detachment show a similar impact on plasma performance will be discussed based on our findings.

EX



Physics, Control and Mitigation of Disruptions and Runaway Electrons in the EUROfusion Medium Size Tokamaks Science Programme

P. Martin¹, T. Blanken², D. Carnevale³, J. Decker⁴, B. Duval⁴, B. Esposito⁵, E. Fable⁶, F. Felici², A. Fil⁷, M. Gobbin¹, G. Granucci⁸, M. Hoelzl⁶, O. Kudlacek¹, M. Maraschek⁶, L. Marrelli¹, J. Mlynář⁹, E. Nardon¹⁰, M. Nocente¹¹, D. Paccagnella^{1,12}, G. Papp⁶, G. Pautasso⁶, P. Piovesan¹, C. Piron¹, V. V. Plyusnin¹³, C. Sommariva¹⁰, C. Sozzi⁸, M. Valisa¹, and P. Zanca¹

EUROfusion MST1, ASDEX-Upgrade, MAST, and TCX Teams

¹Consorzio RFX, Associazione EURATOM-ENEA sulla Fusione, Padova, Italy

²Eindhoven University of Technology, Eindhoven, Netherlands

³Università di Tor Vergata, 00173 Rome, Italy

⁴Swiss Plasma Center (SPC), École polytechnique fédérale de Lausanne (EPFL), 1015 Lausanne, Switzerland

⁵Agenzia nazionale per le nuove tecnologie, l'energia e lo sviluppo economico sostenibile (ENEA), Rome, Italy

⁶Max-Planck-Institut für Plasmaphysik, Garching, Germany

⁷Princeton University, Princeton, NJ 08544, USA

⁸Istituto di Fisica del Plasma (IFP), Consiglio Nazionale delle Ricerche (CNR), 20125 Milan, Italy

⁹Institute of Plasma Physics AS CR v.v.i., Prague, Czech Republic

¹⁰Commissariat à l'énergie atomique (CEA/Cadarache), 13108 Saint-Paul-lès-Durance, France

¹¹Università degli Studi di Milano-Bicocca, 20126 Milano, Italy

¹²Consiglio Nazionale delle Ricerche (CNR), Rome, Italy

¹³Institute of Plasmas and Nuclear Fusion (IPNF), Association EURATOM/IST, Lisbon, Portugal

Corresponding Author: P. Martin, piero.martin@igi.cnr.it

EUROfusion dedicates a significant effort to disruption and runaway electron (RE) research in its Medium Size Tokamaks (MST) Task Force, which coordinates the European activities in ASDEX-Upgrade (AUG), MAST-U and TCX. The MST disruption and RE programme addresses prediction, avoidance and mitigation.

Experiments on disruption mitigation utilize massive gas injection (MGI) systems in AUG and TCX. AUG focussed on the amount of injected gas and on the search for the minimum quantity for mitigation. The minimum amounts of gas used in the AUG MGI for successful mitigation is now two orders of magnitude smaller than the maximum values used before. The toroidal asymmetry of the radiation distribution in plasmas disrupting because of locked modes is being studied by exploiting the AUG active coil system, which allows for reproducible relative positioning of the locked mode with respect to the MGI valves. The JOEK code is presently being applied to AUG and extended to impurity MGI, as well as being complemented by a test particle module for RE studies.

Continued...

Scenarios for the reproducible generation of RE during disruptions have been developed both in AUG and TCV. In AUG, RE are produced by injecting argon in a 0.8 MA, ECRH heated circular plasma. A RE beam, carrying current up to 420 kA for 480 ms is formed. A second Ar injection, 70 ms after the first, is used to suppress the RE. The RE current decay rate grows with the amount of injected argon. RE control is attempted in AUG also by applying magnetic perturbation that could produce a stochastic magnetic field and eventually decorrelate RE, and by controlling the position of the RE beam via active ramp-down of the current. Disruption avoidance through MHD stabilization via localized injection of electron cyclotron waves is studied in AUG at high- β or close to the density limit, complemented by applied magnetic perturbations to control the locked mode position or to entrain it.

Indications of unexpected or “unhealthy” behaviour of the plasma that could be symptom of an incoming disruption are detected based on modelled plasma evolution and used as an input signal to a pulse supervision system. This is done with the RAPTOR code in AUG and TCV. The code gives detailed real-time information about profiles that are compared to known limits and to the expected plasma evolution providing an avoidance tool.



MHD Limits and Plasma Response in High- β Hybrid Operations in ASDEX-Upgrade

V. Igochine¹, P. Piovesan², P. Bettini², T. Bolzonella², I. Classen³, M. Dunne¹, A. Gude¹, P. Lauber¹, Y. Liu⁴, M. Maraschek¹, N. Marconato², L. Marelli², S. Mastrostefano⁵, P. J. McCarthy⁶, R. McDermott¹, M. Reich¹, D. Ryan⁴, M. Schneller¹, E. Strumberger¹, W. Suttrop¹, G. Tardini¹, F. Villone⁵, and D. Yadikin⁷

¹Max-Planck-Institut für Plasmaphysik, Garching, Germany

²Consorzio RFX, Associazione EURATOM-ENEA sulla Fusione, Padova, Italy

³FOM Institute DIFFER, Association EURATOM-FOM, Nieuwegein, Netherlands

⁴Culham Centre for Fusion Energy (CCFE), Culham Science Centre, Abingdon, UK

⁵Università degli Studi di Cassino e del Lazio Meridionale, Cassino, Italy

⁶University College Cork, Cork, Republic of Ireland

⁷Chalmers University of Technology, Göteborg, Sweden

Corresponding Author: V. Igochine, valentin.igochine@ipp.mpg.de

The improved H-mode scenario (or high- β hybrid operations) is one of the main candidates for high-fusion performance tokamak operation, which could potentially reach the steady-state condition. In this case, the normalized pressure β_N must be maximized and pressure driven instabilities limit the plasma performance. These instabilities could have either resistive ($m/n = 2/1$ and $3/2$ neoclassical tearing modes, NTMs), or ideal character ($n = 1$ ideal kink modes). In ASDEX-Upgrade (AUG), the first limit for maximum achievable β_N is set by NTMs. Application of preemptive electron cyclotron current drive at the $q = 2$ and $q = 1.5$ resonant surfaces reduces this problem, such that higher values of β_N can be reached. AUG experiments have shown that, in spite of the fact that hybrids are mainly limited by NTMs, proximity to the no-wall limit leads to amplification of external fields that strongly influences the plasma profiles: for example, rotation braking is observed throughout the plasma and peaks in the core. In this situation, even small external fields are amplified and their effect becomes visible. To quantify these effects, the plasma response to magnetic fields produced by B-coils is measured as β_N approaches the no-wall limit. These experiments and corresponding modelling allow identifying the main limiting factors which depend on the stabilizing influence of conducting components facing the plasma surface, existence of external actuators and kinetic interaction between the plasma and the marginally stable ideal modes. Analysis of the plasma reaction to external perturbations allowed us to identify optimal correction currents for compensating the intrinsic error field in the device. Such correction, together with analysis of kinetic effects, will help to increase β_N further in future experiments.

EX

Plasma Response of External Magnetic Perturbations at the Edge: Comparisons between Measurements and 3D MHD Models

M. Willensdorfer¹, W. Suttrop¹, A. Kirk², D. Brida¹, M. Cavedon¹, I. Classen³, S. Denk¹, M. Dunne¹, S. Fietz¹, R. Fischer¹, F. Laggner⁴, Y. Liu², T. Odstrčil¹, F. Orain¹, D. Ryan⁵, E. Strumberger¹, B. Vanovac³, E. Viezzer¹, and H. Zohm¹

¹Max-Planck-Institut für Plasmaphysik, Garching, Germany

²Culham Centre for Fusion Energy (CCFE), Culham Science Centre, Abingdon, UK

³FOM Institute DIFFER, Association EURATOM-FOM, Nieuwegein, Netherlands

⁴Institute for Applied Physics, Technische Universität Wien, 1040 Vienna, Austria

⁵York Plasma Institute, University of York, Heslington, UK

Corresponding Author: M. Willensdorfer, mwillens@ipp.mpg.de

At ASDEX-Upgrade ELM mitigation using external magnetic perturbations has been achieved at high plasma densities ($n_e/n_{GW} > 0.65$, corresponding to $\nu^* > 1.2$) and, more recently, at low pedestal collisionality ($\nu^* < 0.4$) accompanied with density pump-out. To investigate the interaction between the plasma response and ELM mitigation, comprehensive experiments using various plasma configurations have been conducted. These studies indicate that the optimum poloidal spectrum for ELM mitigation does not show a maximum of the magnetic field pitch-aligned component. Instead, it is aligned with the mode at the edge that is most strongly amplified by the plasma as calculated using magnetohydrodynamic (MHD) response codes. These experimental investigations in comparison with MARS-F are consistent with previous observations and underline the hypothesis that the plasma response around the X-point causes the ELM mitigation.

In order to measure the plasma response, we combined rigid rotating MP fields and measurements from toroidally localized high resolution diagnostics. Electron cyclotron emission (ECE) diagnostics, among others, have been used to determine the amplitude, the penetration and the poloidal mode structure of the flux surface displacements. To interpret the ECE measurements accurately, forward modelling of the radiation transport has been extended with ray tracing. The measurements are compared to synthetic data generated by combining the said forward model and a 3D ideal MHD equilibrium calculated by VMEC.

The measured penetration of the helical displacement is in good agreement with VMEC, whereas the measured amplitudes in the midplane are slightly larger. The measured amplitudes also exceed the vacuum field calculations, which indicates the presence of an amplified kink response at the edge. Although the calculated magnetic structure of this edge kink peaks at poloidal mode numbers larger than the resonant components $|m| > |nq|$, the displacement derived from ECE-imaging appears as mostly resonant. This is expected from ideal MHD in the proximity of rational surfaces. Both, VMEC and MARS-F calculations reproduce this experimental observation. Further rigid rotating field experiments using different poloidal spectra of the external MP suggests that the same least stable modes are excited by the MP-field.



Ion Cyclotron Range of Frequency Power Challenges and Solutions

J.-M. Noterdaeme¹, V. Bobkov¹, H. Fuenfgelder¹, R. D'Inca¹, R. Ochoukov¹, J. Jacquot¹, I. Stepanov², W. Zhang¹, H. Faugel¹, T. Vierle¹, I. Zammuto¹, K. Crombe³, R. Ragona², A. Messiaen², D. Van Eester², A. A. Tuccillo⁴, O. Tudisco⁴, G. Rocchi⁴, A. Mancini⁴, O. D'Arcangelo⁴, Q. Yang⁵, Q. Wang⁵, Y. Chen⁵, D. Milanese⁶, R. Maggiora⁶, L. Colas⁷, S. Heuraux⁸, E. Faudot⁸, J. Moritz⁸, A. Silva⁹, and D. Aguiam⁹

ASDEX-Upgrade and MST1 Teams

¹Max-Planck-Institut für Plasmaphysik, Garching, Germany

²Laboratory for Plasma Physics, ERM/KMS, Brussels, Belgium

³Ghent University, 9000 Ghent, Belgium

⁴Agenzia nazionale per le nuove tecnologie, l'energia e lo sviluppo economico sostenibile (ENEA), Rome, Italy

⁵Institute of Plasma Physics, Chinese Academy of Sciences, Hefei, Anhui, People's Republic of China

⁶Polytechnic University of Turin, Turin, Italy

⁷Institut de Recherche sur la Fusion par confinement Magnétique (IRFM),

Commissariat à l'énergie atomique (CEA/Cadarache), 13108 Saint-Paul-lès-Durance, France

⁹Instituto Superior Técnico (IST), Lisbon, Portugal

Corresponding Author: J.-M. Noterdaeme, noterdaeme@ipp.mpg.de

The coupling of power in the ion cyclotron range of frequency to the plasma has encountered challenges, which can be classified into two broad categories: the sensitivity to the plasma edge density profile with the difficulty to couple power to the plasma and the enhanced plasma-antenna interaction with, among others, the resulting impurity production. We report on the recent results obtained at the Max-Planck-Institut für Plasmaphysik, in cooperation with other partners, to address successfully those challenges.

In the category sensitivity to the plasma edge density profile, the problems encountered due to strong ELMs have long been solved with the use of 3-dB couplers. In recent experiments, local gas puffing helped to tailor the density profile and increase the coupling. Since a systematic study confirmed that the coupling can be calculated if the local density profile is known, we expect that the development of a theoretical approach to model the local density profile will develop into a predictive capability to calculate and optimize the coupling also for future machines. We will soon be able to benchmark this modelling with local density measurements, of which first results are available directly at the antenna. In the category enhanced plasma-antenna interaction, the hypothesis is that the enhanced interaction is due to RF sheaths, and that those sheaths are a consequence of induced current driven at inappropriate locations. New 3-strap antennas in ASDEX-Upgrade were designed to reduce those unwanted currents. This approach leads indeed to a strong reduction of impurity production. When the original W-coated 2-strap antennas were energized, the increase with ICRF of the W impurity concentration in the edge plasma is about twice the increase as when the B-coated 2-strap antennas were in operation. In contrast to this, when the new W-coated 3-strap antennas are energized the W concentration is not higher than when the B-coated 2-strap antennas are in operation. Direct measurements of the impurity production at the limiters of the W-coated antennas show a reduction by a factor of 2 between the 3-strap and the 2-strap antennas. Theoretical approaches to model in detail the formation of the sheaths are being developed and will be checked against measurements on ASDEX Upgrade and on IShTAR, a dedicated test stand.

Phase-Space Resolved Measurements of the Influence of RF Heating and MHD Instabilities on the Fast-Ion Distribution in ASDEX-Upgrade

M. Weiland¹, B. Geiger¹, R. Bilato¹, P. A. Schneider¹, G. Tardini¹, A. Jacobsen², S. K. Nielsen², F. Rytter¹, M. Salewski², and H. Zohm¹

¹Max-Planck-Institut für Plasmaphysik, Garching, Germany

²Technical University of Denmark (DTU), Copenhagen, Denmark

Corresponding Author: M. Weiland, markus.weiland@ipp.mpg.de

Fast, suprathermal ions provide a powerful mechanism to heat fusion plasmas and to drive plasma currents and rotation. It is therefore crucial for the success of future fusion devices (such as ITER and DEMO) to understand the physics of fast ions and ensure their safe confinement. In the presented work, experimental studies of the fast-ion phase space are carried out using a FIDA (fast-ion D_α) diagnostic at the ASDEX-Upgrade tokamak. Recent diagnostic upgrades allow the tomographic reconstruction of the 2D fast-ion velocity distribution at several radial positions on the low-field side.

The FIDA tomography is applied to study the velocity-space dependence of fast-ion redistribution during sawtooth crashes. It is found, that fast ions with high energies and pitches (v_{\parallel}/v) close to zero are less affected by the sawteeth. This can be explained by the fact that these ions have large drift velocities (compared to their parallel velocity) and are thus more weakly bound to the (reconnecting) magnetic field lines.

Moreover, we investigate the acceleration of fast deuterium ions by 2nd harmonic ion cyclotron resonance heating. In this ICRH scenario, hydrogen is resonant at the first harmonic, which is in competition with deuterium absorption and needs to be considered in the data analysis. We show that the FIDA tomography can be interpreted as sum of the D and H distribution function. In an NBI+ICRH phase, the tomographic reconstructions in the plasma centre yield two distinct high-energy tails above the NBI energy, which are not present in a NBI-only phase. Basic theoretical considerations suggest that these tails originate mainly from deuterium. In total, we calculate tomographic reconstructions at six radial positions spanning a broad range of the plasma radius. This is the first time that a radial profile $f(E, v_{\parallel}/v, \rho)$ of the fast-ion distribution function is reconstructed from FIDA measurements. The high-energy tails vanish in the outer-most radial positions, which is in agreement with the expected ICRH deposition position. A comparison to theoretical models reveals that the tails (above the NBI energy) are underestimated by TRANSP/TORIC in the very plasma centre and overestimated by TORIC-SSFPQL. These differences are discussed and compared to other fast-ion diagnostics. For lower energies (around and below the NBI energy) good agreement is found.



Advances in Neutral Beam Current Drive Experiments on ASDEX-Upgrade

C. Hopf¹, D. Rittich¹, B. Geiger¹, A. Bock¹, A. Burckhart¹, R. McDermott¹, A. Mlynek¹,
C. Rapson¹, M. Reich¹, F. Ryter¹, and M. Willensdorfer¹

¹Max-Planck-Institut für Plasmaphysik, Garching, Germany

Corresponding Author: C. Hopf, christian.hopf@ipp.mpg.de

Neutral beam current drive (NBCD) is an efficient option for noninductive tokamak operation. With its eight 2.5 MW neutral beams of different geometry ASDEX-Upgrade offers a versatile NBI system, well suited for current drive studies. Past studies comparing on- and off-axis NBCD at 5 MW gave contradictory results. To understand the current profiles constrained by MSE anomalous fast-ion transport needed to be assumed [1] while the fast-ion density profile constrained by fast-ion D_α (FIDA) spectroscopy appeared to be neoclassical [2]. To address this issue, new experiments were started in 2014 in which simultaneous MSE and FIDA measurements were achieved by adding an additional neutral beam on top of the 5 MW switched between radial on-axis and tangential off-axis beams. Remarkably constant T_e and n_e profiles were achieved by feedback-controlled ECRH. Despite the increased heating power NTMs and sawteeth were successfully mitigated by ECCD at two radial locations.

The MSE and FIDA data were compared with synthetic diagnostics data from postprocessed TRANSP output. Significant improvement was brought about by new measurements of the actual beam geometries, improved accuracy of the Z_{eff} profiles, and correction of TRANSP's radial electric field. While initial comparisons of the MSE angles suggested relatively strong fast-ion transport with diffusion coefficients $\geq 0.5 \text{ m}^2/\text{s}$ [2, 3], both MSE and FIDA are now in good agreement with the predictions with the much smaller ρ -, time- and energy-dependent microturbulent diffusion coefficients calculated according to [4]. These are on average below $0.2 \text{ m}^2/\text{s}$. Experimentally, the study was extended to 5 and 7.5 MW of total NBI, various beam geometries as well as varying Z_{eff} .

In view of steady-state tokamak operation, discharges with 800 MA plasma current, $q_{95} = 5.5$, $q_{\text{min}} > 1.5$, up to 12.5 MW NBI and 2.8 MW of ECRH recently achieved a two-seconds-long practically noninductive phase with $> 40\%$ NBCD, $> 40\%$ bootstrap current, and approximately 10% ECCD. These discharges are now extended in duration in order to approach a truly stationary current distribution.

References

- [1] S. Günter, *et al.*, Nucl. Fusion **47**, 920 (2007).
- [2] B. Geiger, *et al.*, Plasma Phys. Control. Fusion **57**, 014018 (2015).
- [3] B. Geiger, *et al.*, Nucl. Fusion **55**, 083001 (2015).
- [4] M. J. Pueschel, *et al.*, Nucl. Fusion **52**, 103018 (2012).



The Role of the Neoclassical E_r for the L-H Transition in ASDEX-Upgrade

T. Pütterich¹, M. Cavedon¹, E. Viezzer¹, G. Birkenmeier¹, R. Dux¹, T. Happel¹,
F. Laggner², P. Manz¹, R. McDermott¹, F. Ryter¹, U. Stroth¹, and E. Wolfrum¹

¹Max-Planck-Institut für Plasmaphysik, Garching, Germany

²Institute for Applied Physics, Technische Universität Wien, 1040 Vienna, Austria

Corresponding Author: T. Pütterich, thomas.puetterich@ipp.mpg.de

The radial electric field E_r at the plasma edge and its relation to plasma turbulence is investigated throughout the LH-transition and an ELM cycle. Various diagnostics are considered including an upgraded charge exchange recombination spectroscopy system. The latter is able to measure impurity temperature, flow and density profiles with a frequency of up to 20 kHz and a radial resolution of down to 3 mm. This enables the comparison of E_r with the one calculated from neoclassical theory ($E_{r,neo}$) taking toroidal flows into account. The events during which E_r is not explained by neoclassical theory are of special interest, as the difference indicates an additional mechanism such as turbulence driven zonal flows (ZF).

The occurrence of the latter is suggested by earlier investigations during the LH-transition performed at other tokamak experiments and also at ASDEX-Upgrade. For the present study, the I-phase at the LH-transition was investigated. In the I-phase regular turbulent bursts and profile changes occur with a frequency of a few kHz interrupted by more quiet phases. If the turbulence drives ZFs an increased E_r versus $E_{r,neo}$ is expected after the turbulent bursts, however, no significant discrepancies between E_r and $E_{r,neo}$ are found indicating negligible contributions of ZFs. Additionally, a correlation analysis shows a simultaneous evolution of the measured E_r , $E_{r,neo}$ and the turbulence and thus, a rise of the turbulence level prior to the flow generation as expected from predator-prey like turbulence-ZF interactions cannot be confirmed. Instead, the bursts during the I-phase show an ELM-type character. This observations suggest that $E_{r,neo}$ causes the required $E \times B$ shearing for the LH-transition along the lines in [1]. In addition, at the LH-transition, the well in the $E_{r,neo}$ -profile is found to deepen with increasing B_t , in agreement with $P_{L-H} \sim B_t$ while the $E \times B$ shear velocity ($\sim E_r/B$) is constant.

In order to better understand the observations at the LH-transition the same comparison of E_r and $E_{r,neo}$ is performed during a fully developed H-mode with type-I ELMs. It may be noted that during the I-phase the turbulence bursts do not reduce the E_r back to levels which are typical during L-mode, while during an H-mode the reduction of E_r during an ELM reduces E_r to levels which are observed in L-mode.

References

[1] P. Sauter, *et al.*, Nucl. Fusion **52**, 2012.



Ion Heat and Toroidal Momentum Transport Studies in the H-Mode Transport Barrier of ASDEX-Upgrade

E. Viezzler¹, M. Cavedon¹, E. Fable¹, A. Snicker¹, C. Angioni¹, R. Dux¹, S. Fietz¹, F. Laggner², R. McDermott¹, T. Pütterich¹, T. Odstrcil¹, F. Rytter¹, and E. Wolfrum¹

¹Max-Planck-Institut für Plasmaphysik, Garching, Germany

²Institute for Applied Physics, Technische Universität Wien, 1040 Vienna, Austria

Corresponding Author: E. Viezzler, eleonora.viezzler@ipp.mpg.de

The gradients in the ion and electron temperature profiles, T_i and T_e , are a key component for driving turbulent transport in plasmas. Since the 1980s, “profile resilience” has been observed on many tokamaks, which describes the fact that T_i and T_e are limited by a critical normalized temperature gradient. Beyond this critical R/LT the heat diffusivities increase drastically. Hence, with stiff profiles the edge temperature is a key to attaining higher core temperatures and higher plasma confinement. Understanding the transport processes in the H-mode transport barrier, where turbulence is strongly reduced, is essential for a reliable scaling to next step fusion devices. In this contribution we analyze the ion heat and momentum transport at the plasma edge of ASDEX-Upgrade (AUG) H-mode plasmas.

The experimentally determined ion heat diffusivities are compared to neoclassical theory and the impact of ELMs on the edge ion heat transport is studied in detail. During the inter-ELM phase the ion heat diffusivity in the pedestal region is close to the neoclassical level. High time-resolution CXRS measurements (100 μ s) enables detailed studies of the ion heat transport during the entire ELM cycle. The measurements show that during the ELM crash the radial ion temperature gradient flattens and the temperature close to the separatrix increases as a result of the ELM heat transport. The pre-ELM level in the ion heat transport is established approximately 2–3 ms after the ELM crash.

In order to study the edge momentum an H-mode edge rotation database was created at AUG. The data reveals a strong dependence of the impurity toroidal rotation on the ion collisionality. Below a certain collisionality threshold the impurity toroidal rotation switches sign from co- to counter-current. The edge rotation is modelled using ASTRA. Here, the toroidal torque balance equation including diffusion, pinch and external momentum sources is solved. Comparison between the experimental profiles and the simulations shows good agreement within the experimental uncertainties, indicating that diffusion and external momentum sources are the dominant players. The sign change of the impurity toroidal rotation observed at low collisionality can be explained by a negative edge torque combined with a large differential toroidal rotation, while the main ion toroidal rotation is almost unaffected.

EX



Pedestal and Core Turbulence Dynamics Using $1 \mu\text{s}$ Sweeping Profile Reflectometry

F. Clairet¹, R. Sabot², G. Conway³, U. Stroth³, A. Medvedeva³, C. Bottereau¹, D. Molina¹, S. Hacquin¹, and H. Arnichand¹

¹Commissariat à l'énergie atomique (CEA), 91400 Gif-sur-Yvette, France

²Institut de Recherche sur la Fusion par confinement Magnétique (IRFM),

Commissariat à l'énergie atomique (CEA/Cadarache), 13108 Saint-Paul-lès-Durance, France

³Max-Planck-Institut für Plasmaphysik, Garching, Germany

Corresponding Author: F. Clairet, frederic.clairet@cea.fr

Plasma turbulence is a key parameter governing the confinement quality of magnetically confined plasmas. It is responsible for a substantial particle and heat transport that affects the performance of a nuclear fusion device. More detailed knowledge and understanding are constantly needed and requires more and more precise measurements with, in turn, improved diagnostic performance. Swept frequency reflectometry, traditionally devoted to electron density profile measurements, have been constantly progressing in terms of sensitivity (S/N ratio) and sweeping rate. In this paper the symbolic limit of $1 \mu\text{s}$ sweep time with a dead time between sweeps of $0.25 \mu\text{s}$ has been recently reached by the Tore Supra (TS) reflectometers, which are today successfully experienced on the ASDEX-Upgrade (AUG) tokamak. Such a high sampling rate of 800 kHz improves the observation of the plasma temporal dynamic and high radial resolution from the edge to the plasma centre. They provide plasma measurements for a broad and continuous radial range, from the edge to the centre, at an acquisition rate which competes now with fixed frequency systems. In addition to fluctuation profiles or k_r spectra during L–I–H transition with high temporal resolution, it extends the observation to high frequency coherent modes and microinstabilities such as TEM and ITG over the entire plasma with a high radial resolution. We can follow the temporal evolution of an edge coherent oscillation around 100 kHz and see how at the ELM crash, this mode temporarily disappears and then rapidly recovers. The radial dependency of the spectra also provides an observation of the interplay between localized MHD neoclassical tearing modes and trapped electron modes (TEM). Comparisons with synthetic diagnostic simulations coupling a 2D reflectometry full-wave code with gyrokinetic (GENE) turbulence simulations have been performed. It has contributed to the assessment of the measurements as well as the numerical codes. It has pointed out the role of the plasma rotation and provided insights in the turbulence structure.

Turbulence Characteristics of the I-Mode Confinement Regime in ASDEX-Upgrade

P. Manz¹, T. Happel¹, F. Ryter¹, P. Hennequin², G. Birkenmeier¹, G. Conway¹, E. Viezzer¹, U. Stroth¹, A. Hetzenecker³, P. Lauber¹, D. Prisiazhniuk¹, V. Nikoleava¹, M. Maraschek¹, and C. Honore²

¹Max-Planck-Institut für Plasmaphysik, Garching, Germany

²École Polytechnique, 91128 Palaiseau, France

³Technische Universität München, Garching, Germany

Corresponding Author: P. Manz, peter.manz@ipp.mpg.de

The I-mode is an improved confinement regime of tokamak plasmas operating in the unfavourable ion ∇B -drift direction combining H-mode-like energy confinement with L-mode-like particle and impurity transport [1]. To qualify the I-mode as an operating scenario for ITER threshold and accessibility studies [2] also on a multimachine basis [3] are needed. Even if the I-mode might not be considered as a promising scenario for ITER, studies of turbulence in I-mode may offer a better understanding of the physics of the interaction of energy and particle transport barriers in general. The mechanism which selectively reduces only one of the transport channels is not understood. In the present contribution the turbulence characteristics of I-mode plasmas in ASDEX-Upgrade (AUG) have been studied in detail. In AUG the WCM appear at frequencies around 100 kHz with a width of a few 10 kHz [4]. The GAM advects the WCM and leads to the broadening through the Doppler effect [4]. In AUG magnetic fluctuations already present in L-mode close to the WCM frequency are amplified during the I-mode. Using the measured background profiles the gyrokinetic eigenvalue solver LIGKA is used to determine the kinetic continuum branches of the GAM and the geodesic Alfvénic mode (GAlf). The frequency of the magnetic fluctuations close to the WCM frequency coincides with the GAlf frequency [4]. Comparisons with the Mirnov coils show the characteristic toroidal and poloidal mode numbers of the GAlf of zero and one, respectively [4]. The origin of the WCM lies in the intermittent events, which exhibit a wavelet-like temporal structure where the characteristic frequency coincides with the centre-of-mass frequency of the WCM [5]. Possible generation scenarios for the bursts are discussed. The nonlinear interaction between GAM, WCM and the bursts will be discussed based on a detailed bispectral analysis of nonlocal interactions in frequency space of the experimental data. The importance of the solitary events for a selective density transport remains an open issue.

References

- [1] D. G. Whyte, *et al.*, Nucl. Fusion **50**, 105005 (2010).
- [2] F. Ryter, *et al.*, Nucl. Fusion (in preparation).
- [3] A. Hubbard, *et al.*, Nucl. Fusion (submitted).
- [4] P. Manz, *et al.*, Nucl. Fusion **55**, 083004 (2015).
- [5] T. Happel, *et al.*, Nucl. Fusion (submitted).

Comparison of Runaway Electron Generation Parameters in Small, Medium-sized and Large Tokamaks: A Survey of Experiments in COMPASS, TCV, ASDEX-Upgrade and JET

V. V. Plyusnin¹, C. Reux², V. Kiptily³, P. Lomas³, V. Riccardo³, G. Pautasso⁴, J. Decker⁵, G. Papp⁴, J. Mlynář⁶, S. Jachmich⁷, A. Shevelev⁸, E. Khilkevitch⁸, S. Coda⁵, B. Alper³, Y. M. Martin⁵, V. Weinzettl⁶, R. Dux⁴, B. Duval⁵, S. Gerasimov³, P. Martin⁹, M. Nocente¹⁰, and M. Vlaine¹¹

¹Institute of Plasmas and Nuclear Fusion (IPNF), Association EURATOM/IST, Lisbon, Portugal

²Institut de Recherche sur la Fusion par confinement Magnétique (IRFM),

Commissariat à l'énergie atomique (CEA/Cadarache), 13108 Saint-Paul-lès-Durance, France

³Culham Centre for Fusion Energy (CCFE), Culham Science Centre, Abingdon, UK

⁴Max-Planck-Institut für Plasmaphysik, Garching, Germany

⁵Swiss Plasma Center (SPC), École polytechnique fédérale de Lausanne (EPFL), 1015 Lausanne, Switzerland

⁶Institute of Plasma Physics AS CR v.v.i., Prague, Czech Republic

⁷Laboratory for Plasma Physics, ERM/KMS, Brussels, Belgium

⁸Ioffe Institute, St. Petersburg, Russian Federation

⁹Consorzio RFX, Associazione EURATOM-ENEA sulla Fusione, Padova, Italy

¹⁰Università degli Studi di Milano-Bicocca, 20126 Milano, Italy

¹¹Ghent University, 9000 Ghent, Belgium

Corresponding Author: V. V. Plyusnin, vladislav.plyusnin@ipfn.ist.utl.pt

EX Our report presents a survey of experiments on runaway electrons (RE) carried out recently in frames of EUROfusion Consortium in different tokamaks (COMPASS, ASDEX-Upgrade (AUG), TCV and JET). The increase of geometrical scale and physical parameters of plasma experiment on disruption generated RE has been studied. New data on disruption generated RE in COMPASS with carbon limiter and AUG with tungsten wall was collected and added to the database on RE in JET. Parameters of measured RE in different devices revealed similar trends on toroidal magnetic field fitting well into the JET database. Current values of RE beams demonstrated increasing trends with increase of geometrical size and parameters of plasma experiment from small and medium-sized tokamaks towards to JET. As well dissipation of RE beams in flattop discharges have been studied. Injections of impure gases into RE flattop discharges allowed distinguishing of two types of dissipative effect of such injections on RE populations in COMPASS and TCV. A description of diagnostics capable to characterize RE electrons and main measured parameters and values are given.

Losses of Runaway Electrons in MHD-Active Plasmas of the COMPASS Tokamak

J. Mlynář¹, O. Ficker¹, M. Vlainic², V. Weinzettl¹, S. Coda³, J. Decker³, P. Martin⁴, E. Nardon⁵, G. Papp⁶, V. V. Plyusnin⁷, C. Reux⁵, F. Saint-Laurent⁵, C. Sommariva⁵, J. Havlicek¹, O. Hronova¹, T. Markovic¹, R. Paprok¹, R. Panek¹, and J. Urban¹

¹Institute of Plasma Physics AS CR v.v.i., Prague, Czech Republic

²Ghent University, 9000 Ghent, Belgium

³Swiss Plasma Center (SPC), École polytechnique fédérale de Lausanne (EPFL), 1015 Lausanne, Switzerland

⁴Consorzio RFX, Associazione EURATOM-ENEA sulla Fusione, Padova, Italy

⁵Institut de Recherche sur la Fusion par confinement Magnétique (IRFM),

Commissariat à l'énergie atomique (CEA/Cadarache), 13108 Saint-Paul-lès-Durance, France

⁶Max-Planck-Institut für Plasmaphysik, Garching, Germany

⁷Institute of Plasmas and Nuclear Fusion (IPNF), Association EURATOM/IST, Lisbon, Portugal

Corresponding Author: J. Mlynář, mlynar@ipp.cas.cz

Significant role of MHD effects in mitigation and losses of runaway electrons (RE) was documented in dedicated experimental studies of RE at the COMPASS tokamak. The MHD activity analyzes were based on data from the extensive magnetic diagnostic system of COMPASS, while the RE losses were monitored by the hard X-ray (HXR) scintillation detectors.

RE in COMPASS are normally produced in the current ramp-up phase due to the increased toroidal electric field. Role of this RE seed on subsequent RE population proved significant. Robust control of the ramp-up RE seed via fuelling scenarios was achieved which allowed for systematic studies of RE confinement and loss in the current plateau phase [1]. Among others, recent experiments with complete suppression of the RE seed and decreasing plasma density in the current plateau resulted in the standard estimate of the critical field.

The contribution focusses on studies of periodic oscillations in the HXR intensity. We show that frequencies of the oscillations are clearly coherent with magnetic data oscillations in the presence of tearing modes. Second, a strong relation between the HXR intensity oscillations and the coil current noise due to the COMPASS power supply (the flywheel generator frequency) is described. Both observations demonstrate that perturbations of the magnetic field result in enhanced losses of runaway electrons. This conclusion corresponds well with previous observation in DIII-D [2]. Furthermore, our subsequent RE measurements at TCV tokamak show similar behaviour. The relevance of this work in respect of experiments on postdisruption RE confinement and mitigation will be discussed on the background of recent results from ASDEX-Upgrade and JET.

References

- [1] J. Mlynar, *et al.*, Europhys. Conf. Abs. **39E**, 4.102 (2015).
- [2] R. A. Moyer, *et al.*, General Atomics Report [GA-A27773](#) (2014).



Contribution to the Multimachine Pedestal Scaling from COMPASS Tokamak

M. Komm¹, P. Bilkova¹, M. Aftanas¹, M. Berta¹, P. Bohm¹, O. Bogar¹, L. Frassinetti², O. Grover¹, P. Hacek¹, J. Havlicek¹, M. Imrisek¹, J. Krbec¹, and E. Stefanikova¹

¹*Institute of Plasma Physics AS CR v.v.i., Prague, Czech Republic*

²*KTH Royal Institute of Technology, Stockholm, Sweden*

Corresponding Author: M. Komm, komm@ipp.cas.cz

The COMPASS tokamak is equipped with a set of high resolution diagnostics, which are capable of resolving the pedestal and hence contribute to the multimachine scaling of the pedestal parameters. The first results obtained for a series of shots at $q_{95} \sim 2.5$ in 2015 confirmed that typical pedestal dimensionless parameters obtained at COMPASS are close to those achieved in a multimachine matching experiments [1].

In order to approach the required values, the COMPASS tokamak [2] has recently enhanced its operational space by achieving a routine operation up to 2.1 T, i.e., Ohmic H-modes could be obtained also for $q_{95} \geq 3$, in addition to the NBI heated H-modes. At the same time, edge diagnostics were significantly upgraded. Particularly, the port for edge Thomson scattering observation system has been modified in order to improve the field of view and allow routine pedestal observation with the standard plasma size. In addition, the number of lasers for Thomson scattering has been doubled in order to increase the probability to obtain data for the pedestal profile in the last 20% of ELM cycle. A new experimental campaign collected the pedestal parameters in discharges at higher q_{95} for values of ν^* and ρ^* relevant to the multimachine matching experiment.

References

[1] M. Beurskens, *et al.*, Phys. Plasmas **18**, 056120 (2011).

[2] R. Panek, *et al.*, Plasma Phys. Control. Fusion **58**, 014015 (2015).

Overview of the Preliminary Design of the ITER Plasma Control System

J. A. Snipes¹, R. Albanese², G. Ambrosino³, R. Ambrosino², V. Amoskov⁴, S. Bremond⁵, M. Cinque², G. De Tommasi², P. de Vries¹, N. W. Eidietis⁶, R. Felton⁷, J. R. Ferron⁶, A. Formisano², Y. Gribov¹, M. Hosokawa¹, H. Alan⁶, D. A. Humphreys⁶, G. L. Jackson⁶, K. Andrey⁴, R. R. Khayrutdinov⁸, D. Kim¹, S. H. Kim¹, S. Konovalov⁸, E. Lamzin⁴, M. Lehnen¹, V. E. Lukash⁸, P. Lomas⁷, M. Mattei², A. Mineev⁴, P. Moreau⁵, G. Neu⁹, R. Nouaillletas⁵, G. Pautasso⁹, A. Pironti², C. Rapson⁹, G. Raupp⁹, T. Ravensbergen¹⁰, F. Rimini⁷, J.-M. Traveres⁵, W. Treutterer⁹, F. Villone², M. L. Walker⁶, A. S. Welander⁶, A. Winter¹, and L. Zabeo¹

¹International Thermonuclear Experimental Reactor (ITER),
Cadarache Centre, 13108 Saint-Paul-lès-Durance, France

²Consorzio CREATE, 80125 Napoli, Italy

³Università degli Studi di Napoli Federico II, 80138 Napoli, Italy

⁴D. V. Efremov Institute of Electrophysical Apparatus (JSC-NII-EFA), St. Petersburg, Russian Federation

⁵Commissariat à l'énergie atomique (CEA/Cadarache), 13108 Saint-Paul-lès-Durance, France

⁶General Atomics, San Diego, CA 92186, USA

⁷Culham Centre for Fusion Energy (CCFE), Culham Science Centre, Abingdon, UK

⁸National Research Centre "Kurchatov Institute", Moscow, Russian Federation

⁹Max-Planck-Institut für Plasmaphysik, Garching, Germany

¹⁰Eindhoven University of Technology, Eindhoven, Netherlands

Corresponding Author: J. A. Snipes, joseph.snipes@iter.org

The Preliminary Design of the ITER plasma control system (PCS) has been carried out since 2014 by members of the ITER Organization and a number of plasma control experts from CCFE, CEA-Cadarache, CREATE, Efremov, General Atomics, IPP-Garching, and Kurchatov as well as through a collaboration with Eindhoven University of Technology. This work builds on the PCS Conceptual Design that was approved in 2013 and focusses on the needs for 1st plasma and early plasma operation in H/He up to 15 MA operation with moderate auxiliary heating power in L-mode. Initial control schemes for plasma initiation, current rise, vertical stability, plasma position and shape, X-point formation, divertor operation, and density control with gas puffing and pellet injection are being developed. Commissioning of the electron cyclotron, ion cyclotron, and neutral beam heating systems are also included. Support functions for stray field topology and real-time plasma boundary reconstruction are included. In addition, initial event handling schemes for essential plant system faults and for disruption protection are being developed. The PCS architecture must also be capable of handling basic control for early plant system and plasma commissioning and the advanced control functions that will be needed for future high performance operation up to $Q = 10$ and for long pulse noninductive scenarios. A plasma control simulator is also being developed to test and validate control schemes. To handle the complexity of the ITER PCS, a systems engineering approach has been adopted with the development of a plasma control database to keep track of all control requirements including those of the associated diagnostics and actuators needed to carry out the control functions.

Plasma Control Studies Using DIII-D Design Tools in Support of ITER

D. A. Humphreys¹, N. W. Eidietis¹, J. R. Ferron¹, G. L. Jackson¹, M. J. Lanctot¹, M. L. Walker¹, A. S. Welander¹, G. Raupp², W. Treutterer², P. de Vries³, J. A. Snipes³, and A. Winter³

¹General Atomics, San Diego, CA 92186, USA

²Max-Planck-Institut für Plasmaphysik, Garching, Germany

³International Thermonuclear Experimental Reactor (ITER), Cadarache Centre, 13108 Saint-Paul-lès-Durance, France

Corresponding Author: D. A. Humphreys, humphreys@fusion.gat.com

Control analysis and design tools developed at DIII-D [1] have been applied to ITER in studies supporting design of the ITER plasma control system (PCS) [2] to prepare for the upcoming PCS preliminary design review (PDR). These studies include assessment of an extremum-seeking approach to real-time error field correction, advances in vertical controllability metrics, simulation of plasma initiation, evaluation of real-time equilibrium reconstruction effectiveness, and development of an integrated algorithmic approach to exception handling toward disruption-free operation of ITER. Integrated simulations have demonstrated the robustness and mutual compatibility of key control algorithms, as well as the effectiveness of critical exception handling algorithms in limiting the disruption frequency in ITER. The present studies follow the ITER PCS preliminary design focus on control requirements for the first plasma and early non-neutronic (H/He species) operating phases of ITER. Operating regimes are analyzed with plasma current ranging from several hundred kA to 15 MA and either full (5.3 T) or half (2.65 T) toroidal field, with corresponding machine operating limits and exception thresholds. These studies confirm the existence and consistency of control solutions with both device resources and PCS architecture.

References

[1] D. A. Humphreys, *et al.*, Nucl. Fusion **47**, 943 (2007).

[2] J. A. Snipes, *et al.*, Fusion Eng. Des. **89**, 507 (2014).

Generation of the Disruption Mitigation Trigger: Developing a Preliminary Design for ITER

G. Pautasso¹, P. de Vries², M. Lehnen², D. A. Humphreys³, C. Rapson¹, G. Raupp¹, J. A. Snipes², W. Treutterer¹, L. Zabeo², and A. Vergara-Fernandez²

¹Max-Planck-Institut für Plasmaphysik, Garching, Germany

²International Thermonuclear Experimental Reactor (ITER), Cadarache Centre, 13108 Saint-Paul-lès-Durance, France

³General Atomics, San Diego, CA 92186, USA

Corresponding Author: G. Pautasso, gap@ipp.mpg.de

Plasma disruptions, occurring above a given plasma current and thermal energy, will have to be mitigated in ITER, to avoid or suppress runaway electrons, reduce thermal and mechanical stresses on the machine components, and mitigate their damage. The necessary conditions for the fulfilment of, what is called here, the disruption mitigation function (DMF) are, firstly, the capability of recognizing that a disruption is going to occur, and secondly, the existence of a mitigation method and the technical feasibility of a mitigation system. Methods of “disruption prediction” and “disruption mitigation” are currently subject to R&D on the existing tokamaks and provide the know-how for the design of the DMF concept. The disruption mitigation system (DMS) will exploit impurity injection and is currently being designed [1].

The DMF is assigned in ITER to a cluster of systems. The central interlock system (CIS) is responsible for the ITER investment protection and may trigger the DMS as an ultimate tool to mitigate device damage. The plasma control system (PCS) is, however, the first line of defence and will assist CIS in performing the DMF. The PCS will have the responsibility of recognizing that a disruption is going to occur, of prescribing how an emergency and mitigated plasma shut-down should be executed, and of initiating its execution. The DMS executes the DMF. Each of these three systems involved is in an advanced design phase and the interfaces among them are being discussed and established.

This conference contribution presents the preliminary design for the generation of the trigger to the DMS, which has been developed during the PDR phase of the ITER PCS in collaboration between the ITER team and a consortium of external institutions [2]. The term “DMS trigger” indicates an array of signals, carrying the information that given DMS injectors must be fired at a given time, i.e., the DMS injection scheme. The generation of the DMS injection scheme requires processing sets of real time inputs with appropriate algorithms and therefore it will take place within the PCS. The trigger development will need to follow the plasma scenario evolution in ITER and the trigger reliability will have to increase along with the magnitude of the disruption loads.

References

- [1] M. Lehnen, *et al.*, J. Nucl. Mat. **463**, 39 (2015).
- [2] J. A. Snipes, *et al.*, EX/P6-36, This Conference.



Plasma Disruption Management in ITER

M. Lehnen¹, P. Aleynikov², B. Bazylev³, D. J. Campbell¹, S. Carpentier-Chouchana⁴, P. de Vries¹, F. Escourbiac¹, Y. Gribov¹, G. Huijsmans⁵, R. R. Khayrutdinov⁶, K. Dmitry⁶, K. Victor¹, S. Konovalov⁶, A. Loarte¹, J.-M. Martinez¹, J. R. Martín-Solís⁷, S. Maruyama¹, R. Mitteau¹, S. Pestchanyi³, R. A. Pitts¹, R. Roccella¹, G. Saibene⁸, and J. A. Snipes¹

¹International Thermonuclear Experimental Reactor (ITER),

Cadarache Centre, 13108 Saint-Paul-lès-Durance, France

²Max-Planck-Institut für Plasmaphysik, Garching, Germany

³Karlsruhe Institute of Technology (KIT), Karlsruhe, Germany

⁴EIRL S. Carpentier-Couchana, Meyrargues, France

⁵Institut de Recherche sur la Fusion par confinement Magnétique (IRFM),

Commissariat à l'énergie atomique (CEA/Cadarache), 13108 Saint-Paul-lès-Durance, France

⁶National Research Centre "Kurchatov Institute", Moscow, Russian Federation

⁷Universidad Carlos III de Madrid, Madrid, Spain

⁸F4E: Fusion for Energy, ITER EU Centre, 08019 Barcelona, Spain

Corresponding Author: M. Lehnen, michael.lehnen@iter.org

Successful operation of ITER and a timely achievement of its objectives require an accurate disruption management as the significant disruption loads can have severe impact on the availability of the device and the lifetime of the in-vessel components. Target values for the disruption rate and the mitigation success rate will have to be defined for each of the different operational phases. This paper will present a disruption management plan including such target values from the start of ITER operation at low current in H/He until the end of the first DT campaign. The loads that determine the target disruption and mitigation rates for the different phases of ITER operation are surface heat fluxes during the thermal quench, electromagnetic loads and halo driven thermal loads during the current quench, and runaway electron impact. To quantify the impact of these events, disruption budget consumption (DBC) will be associated with them for the individual operational phases with different plasma currents (magnetic energy) and thermal energies. The DBC is based on the allowable number of mitigated and unmitigated load cycles, which is limited by a) the fatigue lifetime of components, b) the impact of electro-magnetic loads on mechanical structures, c) the erosion of plasma facing components (PFCs) by heat fluxes from the thermal quench, from the radiation flash during mitigation, from the halo during vertical displacements and from runaway electrons, and d) the achievable mitigation success rate. The DBC used for the disruption plan presented here is based on present knowledge on the impact of loads and on the effectiveness of their mitigation. In particular, it is found that very high mitigation rates are required for current quenches during high current operation to avoid excessive heat loads and halo current amplitudes. The present ITER strategy with respect to runaways is two-fold: a) avoidance of runaway generation by an appropriate mitigation scheme resulting in very low runaway generation rates and b) mitigation by runaway energy dissipation through collisions with high-Z impurities before its deposition on PFCs. The paper will assess the ability of the present design of the ITER disruption mitigation system to provide the required efficiency and reliability.



Modelling ITER Asymmetric VDEs through Asymmetries of Toroidal Eddy Currents

R. Roccella¹, V. Riccardo², M. Roccella³, G. Janeschitz¹, M. Lehnen¹, G. Sannazzaro¹, and S. Chiochio¹

¹*International Thermonuclear Experimental Reactor (ITER),
Cadarache Centre, 13108 Saint-Paul-lès-Durance, France*

²*Culham Centre for Fusion Energy (CCFE), Culham Science Centre, Abingdon, UK*

³*L.T. Calcoli, Merate (LC), Italy*

Corresponding Author: R. Roccella, riccardo.roccella@iter.org

The causes of plasma asymmetries and rotation during disruptions are still an open issue even though their effects are clearly seen on present machines like JET where the vessel has been observed to move horizontally during asymmetric VDEs. Strong horizontal forces are then expected to be related to the plasma asymmetries. In ITER, loads caused by asymmetric VDEs are expected to be among the highest mechanical loads. A model consistent with most of JET measurements has been developed assuming that the asymmetric loads are caused not by a direct exchange of current between plasma and structure (as in the case of halo or surface currents) but to asymmetric conductive paths which arise, in the structures, when the plasma column asymmetrically wets the wall. This model of asymmetric toroidal eddy currents (ATEC) has been implemented in detailed finite element (FE) electromagnetic analyzes of locked and rotating AVDE experienced at JET. The results showed substantial match with all the main asymmetry related measurements done at JET. The same ATEC model is then used to assess loads on the ITER VV during asymmetric VDEs and detailed results are reported and discussed in this paper.

EX



Multimachine Analysis of Termination Scenarios, Providing the Specifications for Controlled Shutdown of ITER Discharges

P. de Vries¹, T. C. Luce², Y.-S. Bae³, J. Qian⁴, X. Gong⁴, D. A. Humphreys², A. Kavin⁵, C. Kessel⁶, R. R. Khayrutdinov⁷, E. de la Luna⁸, I. M. Ferreira Nunes⁹, F. Poli⁶, A. Sips¹⁰, J. A. Snipes¹, J. Stober¹¹, W. Treutterer¹¹, V. E. Lukash⁷, A. Loarte¹, S. H. Kim¹, I. Voitsekhovitch¹², M.-H. Woo³, and S. M. Wolfe¹³

¹International Thermonuclear Experimental Reactor (ITER),

Cadarache Centre, 13108 Saint-Paul-lès-Durance, France

²General Atomics, San Diego, CA 92186, USA

³Korea Atomic Energy Research Institute (KAERI), Daejeon, Republic of Korea

⁴Institute of Plasma Physics, Chinese Academy of Sciences, Hefei, Anhui, People's Republic of China

⁵D. V. Efremov Institute of Electrophysical Apparatus (JSC-NIIEFA), St. Petersburg, Russian Federation

⁶Princeton Plasma Physics Laboratory (PPPL), Princeton, NJ 08540, USA

⁷National Research Centre "Kurchatov Institute", Moscow, Russian Federation

⁸Centro de Investigaciones Energéticas, Medioambientales y Tecnológicas (CIEMAT), Madrid, Spain

⁹Institute of Plasmas and Nuclear Fusion (IPNF), Association EURATOM/IST, Lisbon, Portugal

¹⁰JET Exploitation Unit, Culham Centre for Fusion Energy (CCFE), Culham Science Centre, Abingdon, UK

¹¹Max-Planck-Institut für Plasmaphysik, Garching, Germany

¹²Culham Centre for Fusion Energy (CCFE), Culham Science Centre, Abingdon, UK

¹³Plasma Science & Fusion Center, MIT, Cambridge, MA 02139, USA

Corresponding Author: P. de Vries, peter.devries@iter.org

The controlled shutdown is an often overlooked, though important, phase of the tokamak discharge. The dynamics during this phase complicate control, making it difficult to avoid operational limits, which in the worst case, may lead to a disruption. This is exacerbated by the fact that at the end of the discharge the device is already operated close to many of its technical limits. For unplanned terminations, triggered by developing problems, the situation complicates further. To improve our understanding of the dynamics and control of ITER terminations, a study has been carried out on data from a large number of existing tokamaks. The aim of this joint analysis is to determine the specifications of ITER terminations. The study examined the parameter ranges in which present day devices operated during their terminations, as well as the dynamics of these parameters. The analysis addresses changes in internal inductance, l_i , during the plasma current ramp-down, relevant to vertical stability control, the energy (or, the poloidal β) decay, which relates to the radial position control, as well as the controllability of the density decay, and the H to L back transition. The results can be used to better prescribe the inputs for the modelling and preparation of ITER termination scenarios.



Assessment of the Baseline Scenario at $q_{95} \sim 3$ for ITER

A. Sips¹, J. Schweinzer², T. C. Luce³, S. M. Wolfe⁴, H. Urano⁵, J. Hobirk², S. Ide⁵, G. L. Jackson³, E. Joffrin⁶, C. Kessel⁷, P. Lomas¹, I. M. Ferreira Nunes⁸, T. Pütterich², F. Rimini¹, and J. Stober²

¹Culham Centre for Fusion Energy (CCFE), Culham Science Centre, Abingdon, UK

²Max-Planck-Institut für Plasmaphysik, Garching, Germany

³General Atomics, San Diego, CA 92186, USA

⁴Plasma Science & Fusion Center, MIT, Cambridge, MA 02139, USA

⁵Japan Atomic Energy Agency (JAEA), Naka, Japan

⁶Commissariat à l'énergie atomique (CEA), 91400 Gif-sur-Yvette, France

⁷Princeton Plasma Physics Laboratory (PPPL), Princeton, NJ 08540, USA

⁸Institute of Plasmas and Nuclear Fusion (IPNF), Association EURATOM/IST, Lisbon, Portugal

Corresponding Author: A. Sips, george.sips@jet.uk

In the last two years the Integrated Operation Scenarios Topical Group (IOS-TG) of the ITPA IOS-TG has combined results of joint experiments with other data available at $q_{95} \sim 3$ in a database of global parameters with ~ 3300 entries of stationary discharges from AUG, C-Mod, DIII-D, JET and JT-60U for both carbon wall and metal wall experiments. The analyzes focus on discharges that are stationary for ≥ 5 energy confinement times.

Compared to carbon wall data, experiments with metal walls (AUG, JET-ILW, and C-Mod) have (so-far) not found a way to access the low collision frequencies (as defined in [1]). No difference in performance is observed between carbon wall and metal wall discharges at high collisionality. Stationary discharges at $q_{95} \sim 3$ and $H_{98}(y, 2) \sim 1.0$ are typically obtained at $\beta_N \sim 2.0$, using predominantly cocurrent NBI heating (AUG, DIII-D and JET). In experiments using a metal walls in AUG, C-Mod H-mode and JET, the confinement is significantly reduced ($H_{98}(y, 2) \sim 0.8-0.9$) at $\beta_N \leq 1.8$. The figure of merit $G \equiv H_{89}\beta_n/q_{95}^2$ should be 0.42 for $Q = 10$ in ITER (note H89 is used here). For carbon wall data, G spans a range of 0.25 to 0.51 at the ITER reference beta of $\beta_N = 1.8$, while for data obtained with metal walls G varies from 0.23 to 0.36. More specifically, $G > 0.4$ has only been obtained at $\beta_N > 2.5$ for metal devices operating at $q_{95} \sim 3$, using dominant cocurrent NBI heating (AUG and JET). The ITER requirement for operation at $f_{GW} = 0.85$ can be obtained for triangularities (separatrix) in the range 0.2 to 0.45; an issue for ITER is that at the design value $\delta_x = 0.49$ or higher, DIII-D and C-mod (metal wall) have no data for $f_{GW} > 0.8$ and $H_{98}(y, 2) > 0.95$.

References

[1] T. C. Luce, *et al.*, Nucl. Fusion **54**, 013015 (2014).

Work supported by the U.S. Department of Energy, Awards DE-FC02-04ER546984 and DE-AC02-09CH114668. This work has been carried out within the framework of the EUROfusion Consortium and has received funding from the Euratom research and training programme 2014-2018 under grant agreement No. 633053. The views and opinions expressed herein do not necessarily reflect those of the European Commission.



Integrated Simulations of H-Mode Operation in ITER including Core Fuelling, Divertor Detachment and ELM Control

A. Polevoi¹, A. Loarte¹, R. Dux², T. Eich², E. Fable², S. Maruyama¹, S. Medvedev³, F. Koehl⁴, and V. Zhogolev⁵

¹*International Thermonuclear Experimental Reactor (ITER), Cadarache Centre, 13108 Saint-Paul-lès-Durance, France*

²*Max-Planck-Institut für Plasmaphysik, Garching, Germany*

³*Keldysh Institute of Applied Mathematics, RAS, Moscow, Russian Federation*

⁴*Institute of Atomic and Subatomic Physics, Technische Universität Wien, 1040 Vienna, Austria*

⁵*National Research Centre "Kurchatov Institute", Moscow, Russian Federation*

Corresponding Author: A. Polevoi, alexi.polevoi@iter.org

EX ELM mitigation for divertor protection is one of the main factors affecting plasma fuelling and detachment control at full current operation. Here we derive the scaling for the operational space, where the ELM mitigation for divertor protection is not required and parameters of ELM-pacing pellet injection are determined by the tungsten control. The scaling eliminates the uncertainty connected with the ELM affected area and enables definition of the operational space through global plasma parameters. It is based on the empirical scaling for ELM power load, and pedestal height based on the stability code predictions. The analysis revealed that in particular for the pedestal height, predicted by EPED1+SOLPS scaling, the ELM mitigation for divertor protection is not required in a rather wide range of plasma currents, $I_{p,max} < 7.5\text{--}15$ MA. The pellet and gas fuelling requirements compatible with control of plasma detachment, tungsten accumulation and the H-mode operation are assessed by 1.5D transport simulations for full tungsten redeposition and for the most conservative assumption of zero redeposition. The tungsten influx as a function of the ELM frequency is derived on the basis of consistent core-divertor simulations.



Real-Time Tokamak Simulation with a First-Principle-Based Neural Network Turbulent Transport Model

J. Citrin¹, S. Breton², F. Felici³, J. Redondo², T. Aniel², B. Baiocchi⁴, C. Bourdelle²,
Y. Camenen⁵, and F. Imbeaux²

¹FOM Institute DIFFER, Association EURATOM-FOM, Nieuwegein, Netherlands

²Institut de Recherche sur la Fusion par confinement Magnétique (IRFM),
Commissariat à l'énergie atomique (CEA/Cadarache), 13108 Saint-Paul-lès-Durance, France

³Eindhoven University of Technology, Eindhoven, Netherlands

⁴Istituto di Fisica del Plasma CNR, EURATOM-ENEA-CNR Association, Milano, Italy

⁵Centre national de la recherche scientifique (CNRS), 75016 Paris, France

Corresponding Author: J. Citrin, j.citrin@diffier.nl

A real-time capable core turbulence tokamak transport model is developed, extending a previous proof-of-principle [1]. This model emulates a quasilinear gyrokinetic turbulent transport code, via regularized nonlinear regression using neural networks. Calculation of transport fluxes for the entire radial profile is achieved at sub-millisecond timescales. Experimental validation is presented, including ion and electron heat transport, and particle transport. The unprecedented combination of computational speed and relative modelling accuracy provided by these methods opens up enormous potential for controller design, controller validation, discharge supervision, offline operational scenario development, and trajectory optimization using model-based predictive control techniques.

References

[1] J. Citrin, S. Breton, *et al.*, Nucl. Fusion **55**, 092001 (2015).

EX

A Multimachine Analysis of Nonaxisymmetric and Rotating Halo Currents

C. Myers¹, S. P. Gerhardt¹, N. W. Eidietis², R. S. Granetz³, and G. Pautasso⁴

¹Princeton Plasma Physics Laboratory (PPPL), Princeton, NJ 08540, USA

²General Atomics, San Diego, CA 92186, USA

³Massachusetts Institute of Technology (MIT), Cambridge, MA 02139, USA

⁴Max-Planck-Institut für Plasmaphysik, Garching, Germany

Corresponding Author: C. Myers, cmyers@pppl.gov

EX Halo currents are known to exhibit nonaxisymmetric and rotating features in several devices including JET, Alcator C-Mod, DIII-D, ASDEX-Upgrade, and NSTX. Such nonaxisymmetries are of great interest to ITER because they can increase mechanical stresses during a disruption, especially if the rotation resonates with the natural frequencies of the vessel. This paper presents an ITPA-initiated multimachine analysis of these phenomena. The ITPA nonaxisymmetric halo current database presently includes data from C-Mod, DIII-D, AUG, and NSTX. Measurements from JET will be added as they become available. The various contributions to the database are processed within a common analytical framework to facilitate direct comparisons between devices. Each entry in the database contains halo current measurements from toroidally resolved arrays of either shunt tiles or segmented Rogowski coils. Nonaxisymmetry is quantified in terms of the toroidal peaking factor, TPF, and rotation is quantified by integrating the phase of an $n = 1$ fit to the data. Significant nonaxisymmetries and rotation are observed across devices, and the collective database covers a broader parameter range than is covered by any single device. With regard to rotation, similar rotation frequencies are observed when the timebase is normalized to the characteristic “fast” quench timescale of each device. This indicates that the physics driving the rotation may be linked to the current quench. Additionally, the measured nonaxisymmetry (TPF) is compared to the “halo current magnitude.” Here, the halo current magnitude is defined as the peak measured halo current normalized to both the predisruption plasma current and the median halo current magnitude for a given device. With this normalization, the halo current magnitude and the toroidal peaking factor are found to be positively correlated. This runs counter to the published inverse correlation between the TPF and the “halo current fraction,” which is instead defined as the total inferred halo current normalized to the predisruption plasma current. If it is in fact the case that larger halo currents produce larger nonaxisymmetries, then it is even more imperative for the success of ITER to understand the physical processes that drive halo current nonaxisymmetries and rotation.

Work supported by the U.S. Department of Energy Contract D-AC02-09CH11466.



Big Data Machine Learning for Disruption Predictions

W. Tang¹, M. Parsons¹, E. Feibush¹, A. Murari², J. Vega², A. Pereira², I. M. Ferreira Nunes²,
T. Kurc³, and J. Choi⁴

¹Princeton Plasma Physics Laboratory (PPPL), Princeton, NJ 08540, USA

²EUROfusion/JET, Culham Science Centre, Abingdon, Oxfordshire, OX14 3DB, UK

³Stony Brook University, Stony Brook, NY 11794, USA

⁴Oak Ridge National Laboratory (ORNL), Oak Ridge, TN 37831, USA

Corresponding Author: W. Tang, wtang@pppl.gov

Building the scientific foundations needed to develop fusion power in a timely way can be facilitated not only by familiar “hypothesis-driven” or first principles approaches but also by engaging modern big-data-driven statistical methods featuring machine learning (ML). An especially time-urgent and very challenging problem facing the development of a fusion energy reactor today is the need to reliably mitigate and avoid large-scale major disruptions in magnetically-confined tokamak systems such as the Joint European Torus (JET) today and the burning plasma ITER device in the near future. These major macroscopic events lead to rapid termination of plasma discharges including severe impulsive heat loads damaging material components. Since they can damage the surfaces of the machine, which in turn can cost hundreds of millions of dollars to remediate, it is critical that the international fusion mission engage in multiple avenues to accelerate progress toward achieving the capability to reliably avoid such events with better than 95% predictive capability.

Accordingly, this paper will present results from the development and testing of ML-based-methodologies — an exciting R&D approach that is increasingly deployed in many scientific and industrial domains — to help provide much-needed guidance for disruption avoidance in JET. Working on this repository of the most important and largest (nearly a half petabyte and growing) database of fusion-grade plasmas, JET statistical scientists have successfully deployed ML software interfaced with the large JET data base over the course of the past six years. This has produced encouraging results involving primarily the application of the support vector machine (SVM) approach. The goals for the present investigations are to: i) achieve greater predictive reliability by improving the physics fidelity of the classifiers within the “supervised” ML workflow; and ii) establishing the portability of the associated software beyond JET to other current tokamak systems and to ITER in the future. This will necessitate more realistic multidimensional, time-dependent, and much larger complex data instead of the simpler zero-dimensional, temporal data considered at present in all of the JET ML studies. Current analysis (via MDS+ tree) of the JET disruption data base has been enabled by formal approval of EUROfusion/JET.

EX



IShTAR: A Dedicated Facility to Characterize the Interactions between ICRF Waves and Plasma

K. Crombe¹, R. D’Inca², J. Jacquot², R. Ochoukov², M. Usoltseva¹, A. Kostic¹, F. Louche³, D. Van Eester³, A. Nikiforov¹, J. Moreno¹, S. Heuroux⁴, S. Devaux⁴, E. Faudot⁴, J. Moritz⁴, H. Fuenfgelder², H. Faugel², and J.-M. Noterdaeme²

¹*Ghent University, 9000 Ghent, Belgium*

²*Max-Planck-Institut für Plasmaphysik, Garching, Germany*

³*Laboratory for Plasma Physics, ERM/KMS, Brussels, Belgium*

⁴*Institut Jean Lamour, Université de Lorraine, CNRS, Nancy, France*

Corresponding Author: K. Crombe, kristel.crombe@ugent.be

IShTAR (ion sheath test arrangement) is dedicated to the investigation of the interactions between an ICRF antenna and a plasma in the conditions (plasma temperature and density, magnetic configuration) representative of the plasma edge of a magnetic confinement fusion machine. The test bed is composed of a helicon plasma source and a main vessel, in which a dedicated single strap ICRF antenna is installed. Firstly, the optimization of the plasma source in order to get the highest density and most radially uniform plasma is presented (by changing of the position of the source and by scanning the operational parameters). In addition, the efficiency of the installed diagnostics (compensated and noncompensated Langmuir probes, B-dot probes, wideband spectrometer) is discussed. The second part addresses the effect of the ICRF operation on the generated plasma: the wave profiles in vacuum and plasma are recorded. The impact of the eigenmodes due to the small size of the vessel on the wave field at the interface between antenna and plasma is evaluated. The effect of the additional ionization on the density profile is also measured with the spatial variation of the plasma potential near and inside the RF sheath in front of the antenna strap. Finally, the feasibility of a diagnostic to directly measure the electrical field in the sheath by using the change in emission from energy levels modified by Stark effect and mixing is discussed.

EX

Observation of KBM and MTM in JIPPT-IIU Tokamak Plasmas Using a Heavy Ion Beam Probe

T. Watari¹, Y. Hamada¹, A. Nishizawa¹, K. Narihara¹, K. Ida¹, Y. Kawasumi¹, T. Ido¹, H. Nakanishi¹, and K. Toi¹

The JIPPT-IIU Group

¹National Institute for Fusion Science (NIFS), Toki, Gifu, Japan

Corresponding Author: T. Watari, watari.tetsuo@toki-fs.jp

There is a long history of research of magnetic fluctuations of low-frequency tearing mode using HIBP at TEXT tokamak. They succeeded to study tearing mode study, but abandoned the extension of their study into higher frequency above 10 kHz (typical tearing mode frequency). We invented metal-plate detector utilizing the secondary electron emission like a photomultiplier tube. Metal plates are hit by 0.5 MeV thallium secondary beam instead of light. With the higher detection efficiency, we are able to conduct the measurement with small diameter beam cross-section, leading to higher detection frequency of toroidal beam shift caused by poloidal magnetic fluctuations. Thus we were able to observe magnetic fluctuations of microtearing mode (MTM).

MTM is efficient both for breaking the magnetic surfaces and producing magnetic islands because of the even parity (perturbative magnetic field does not change its sign on the magnetic field line). Guttenfelder stated that about 90% of electron heat loss in high- β ST plasmas is estimated to be due to MTM. MTM has been studied theoretically for long time. MTM was considered to be induced by the resistivity, however, it is now considered to be caused by gradient B drift, therefore, collisionless instability. Accordingly, it may have large effect on ITER plasma. In addition, the numerical simulation requires very fine radial mesh, of the order of the electron gyroradius, and it is very difficult to estimate the effect on the transport by the global simulation of ITER plasmas in near future. In addition, the kinetic ballooning mode is not also studied experimentally because magnetic fluctuation measurement by CPS (cross-polarization scattering) using millimetre wave is not widely used.

Our experimental result is the first experimental finding of coexistence of MTM and KBM in the tokamak plasmas. Also we observe coexistence of KBM, ITG and TEM. In addition, we are able to observe ballooning effect of KBM predicted by Swarmy.



Corrosion Compatibility of Capillary-Porous System Solid Base with Low Melting Metals Applied as Plasma Facing Materials for Tokamak

A. Vertkov¹, I. Lyublinski¹

¹JSC "Red Star", Moscow, Russian Federation

Corresponding Author: A. Vertkov, avertkov@yandex.ru

EX Capillary-porous systems (CPS) with liquid Li, Ga, Sn and Sn-Li alloy is considered as an alternative decision under development for plasma facing elements (PFE) for DEMO-type fusion reactor and fusion neutron source. The main advantages of liquid low-melting metals in matrix of CPS with respect to solid materials are the possibility to provide surface self-restoration and high resistance to degradation of properties in tokamak conditions. The estimation of considered liquid metals application is carried out on the analysis of their corrosion compatibility with potential base materials of CPS and PFE: W, Nb, Mo, V and stainless steels. The experimental study of corrosion resistance are performed in static isothermal conditions in the temperature range of 400–1400°C. It is shown that the top temperature limit for operation of PFE based on the CPS with Ga does not exceed 400–500°C. Only W is compatible with Ga at higher temperatures. A similar situation is detected for structural materials in liquid Sn. Stainless steels are resistant at the temperatures not above 400–500°C and only W and Mo are compatible with Sn at $\geq 1000^\circ\text{C}$. In a contrast with Ga and Sn, the corrosive activity of Li is low and all considered structural materials are resistant at temperatures of $\leq 1000^\circ\text{C}$. The refractory metals and alloys are resistant to Li at higher temperature level.

In accordance with analysis, the operation window for PFE based on CPS with Ga and Sn is strongly limited on the level of 600°C by corrosion effects on structural materials. The only way to increase the operation temperature is by the application of W as PFE base material. For liquid Li the main limitation reason is its high vapour pressure at temperatures above 600°C.



First Results of the Stellarator of Costa Rica 1 (SCR-1)

J. Mora-Meléndez¹, I. Vargas-Blanco¹, L. Barillas-Mora¹, J. Sanchez-Castro¹,
E. Villalobos¹, F. Coto-Vílchez¹, A. Carmona¹, D. Morales Hidalgo¹, G. Madrigal Boza¹,
J. Fernández Vega¹, P. Mena Ceciliano¹, O. A. Gatica Valle¹, R. Esquivel Sancho¹,
J. Asenjo Castillo¹, R. Solano Piedra¹, M. G. Campos Fernández¹, and C. Otárola Zufüga¹

¹*Instituto Tecnológico de Costa Rica, Cartago, Costa Rica*

Corresponding Author: J. Mora-Meléndez, jamora@itcr.ac.cr

Since 2009, the Instituto Tecnológico de Costa Rica started a research project on stellarators which aims at designing, constructing and implementing the first device of this technology in Latin America. SCR-1 is a small-size, modular stellarator (Major radius= 0.238 m, plasma radius= 0.059 m, aspect ratio > 4.4, expected plasma volume $\approx 0.016 \text{ m}^3$, 10 mm thickness 6061-T6 aluminum vacuum vessel). The magnetic field strength at the centre is around 43.8 mT which will be produced by 12 copper modular coils with 4.6 kA-turn each. This field is EC resonant at R_o with a 2.45 GHz as 2nd harmonic, from 2 kW and 3 kW magnetrons. SCR-1 was redesigned from UST_1 stellarator.

The SCR-1 has several subsystems: vacuum system, coils system, high current system, EC heating system, gas injection system, control and acquisition system and diagnostics. The vacuum system is mainly composed by the vacuum vessel that was made of aluminum 6061-T6 and was constructed using 3-axis CNC milling machine, and welded with MIG technique. The coil system was made using 3D printing and casting moulds. It has 12 modular coils with 6 copper wire turns each, carrying a current of 767.8 A per turn. High current subsystem has two main parts: an industrial battery bank (150 A-h, 120 V), and an electric current regulator base on a buck converter that keep constant current on the coils. The EC heating system has two magnetrons, one of 2 kW and the other of 3 kW at a frequency of 2.45 GHz. Also, an antenna was designed to improve the microwave absorption. The main component of the gas injection system constitutes a mass flow controller of 20 SCCM. The control and acquisition system uses a NI PXIe-8135 2.3 GHz Core i7-3610QE Controller, Win7 (32-bit). The diagnostics included in the SCR-1 are a Langmuir probe (two removable heads, four tips each one), an iHR550 optical spectrometer and a heterodyne microwave interferometer (28 GHz).

Finally, we are going to show the magnetic mapping results using four different methods and local magnetic field measurements. Also, this work presents the results of the VMEC simulation and full-wave simulations using the IPF-FDMC code to develop different electron waves Bernstein heating scenarios. And the main reason is to present the first plasma shots, showing results of electron temperature and density using a Langmuir probe and an optical spectrometer.



Dynamics of Tungsten Erosion under ELM-Like Intense Heat Loads

L. Vyacheslavov¹, A. Arakcheev¹, A. Burdakov¹, I. Kandaurov¹, A. Kasatov¹,
V. Kurkuchekov¹, V. Popov¹, A. Shoshin¹, D. Skovorodin¹, Y. Trunev¹, and A. Vasilyev¹

¹*Budker Institute of Nuclear Physics (BINP), Novosibirsk, Russian Federation*

Corresponding Author: L. Vyacheslavov, vyachesl@gmail.com

Simulations of transient heat load corresponding to unmitigated ELMs type-I in ITER divertor are performed on novel material test facility developed at the Budker Institute of Nuclear Physics. Employing of intense long pulse (0.1–0.3 ms) electron beam as a heating source results in relative low light emission by the ablation plume hence facilitates imaging of the tungsten target during the entire heating process. Fast CCD cameras with minimal exposure time of 7 μ s are capable of producing a few 1.4 megapixel images in near infrared range during a single heating pulse. Crack formation is observed at the heat level near the tungsten melting threshold. At heat load well above the melting threshold the spatial structure and temporal behaviour of melt layer is imaged during the heating and cooling phases. Visualization with CCD cameras of droplets ejected by the tungsten melt layer detects fast particles with velocities of several hundred m/s. We apply also scattering of continuous wave laser (532 nm, 0.8 W) light for observation of dynamics of dust particles in the size range of 2–30 μ m ejected from the tungsten surface by the impact of transient heat load.

EX



Basic Studies of Blob Dynamics in X-Point Configurations and Interaction with Suprathermal Ions in the TORPEX Device

I. Furno¹, A. Fasoli¹, P. Ricci¹, M. Baquero¹, A. Bovet¹, F. Avino¹, C. Theiler¹, and M. Fabian¹

¹Swiss Plasma Center (SPC), École polytechnique fédérale de Lausanne (EPFL), 1015 Lausanne, Switzerland

Corresponding Author: I. Furno, ivo.furno@epfl.ch

TORPEX is a flexible basic plasma device in which plasmas are created and sustained by microwaves at 2.45 GHz using different gases. Different magnetic configurations of relevance for fusion are produced in TORPEX, including simple magnetized toroidal (SMT) configurations with a dominant toroidal field and a small vertical field component, or closed field-line configurations using a current-carrying toroidal conductor. This produces a poloidal magnetic field, which, combined with vertical field coils, allows configurations of increasing complexity, including X-points, and of more direct relevance to confined plasma experiments. Thanks to a continuously improving set of diagnostic techniques, of theoretical and modelling tools, together with a rigorous validation methodology, research on TORPEX today allows for quantitative comparisons between theory and experiment. In the past two years, most experiments have been conducted to investigate the interaction between suprathermal ions and intermittent turbulence associated with blobs and to study the propagation of turbulent structures in the presence of X-points. The experiments on suprathermal ion-turbulence interaction and the comparison with numerical simulations reveal different regimes for fast ion transport, resulting in the entire spectrum of suprathermal ion spreading: superdiffusive, diffusive, or subdiffusive, depending on particle energy and turbulence amplitude. Time-resolved conditionally sampled two-dimensional data demonstrate that superdiffusive suprathermal ions in TORPEX plasmas are subject to bursty displacement events, associated with blob propagation, resulting in highly intermittent time traces, not observed in the case of subdiffusion. The toroidal conductor system opens new research avenues on TORPEX. In present experiments, we investigate the blob dynamics in the presence of a first-order X-point. The blob motion is tracked and analyzed using multipoint data, showing an acceleration that is linked to the background radial flow and to the blob-induced electric potential dipole. The blob speed is quantitatively described by an analytical model that includes perpendicular and parallel currents. A crucial role is played by a geometrical parameter, expressing the length of the current path parallel to the magnetic field, along which the blob potential dipole is short-circuited.

EX

Experiments and Modelling towards Long Pulse High Confinement Operation with Radiofrequency Heating and Current Drive in EAST

Y. Peysson¹, X. Z. Gong², M. Goniche¹, L. Colas¹, B. J. Ding², A. Ekedahl¹, W. Helou¹, J. Hillairet¹, G. T. Hoang¹, M. H. Li², S. Lin², F. K. Liu², C. M. Qin², Y. T. Song², L. Valade¹, X. J. Zhang², B. Zhang², Y. P. Zhao², and X. L. Zou¹

The EAST Team

¹*Institut de Recherche sur la Fusion par confinement Magnétique (IRFM),*

Commissariat à l'énergie atomique (CEA/Cadarache), 13108 Saint-Paul-lès-Durance, France

²*Institute of Plasma Physics, Chinese Academy of Sciences, Hefei, Anhui, People's Republic of China*

Corresponding Author: Y. Peysson, yves.peysson@cea.fr

EX The radiofrequency (RF) heating and current drive systems play a crucial role in the mission of the experimental advanced superconducting tokamak (EAST) [1]. RF experiments and modelling were carried out on EAST in 2014–2015, within the framework of the Associated Laboratory ASIPP-IRFM, with the aim to optimize EAST long pulse high performance scenarios. H-mode plasmas have been sustained by LHCD+ICRH, in which most of the plasma current ($I_p = 0.4$ MA) is noninductively driven (loop voltage < 140 mV). In the density range considered, i.e., line averaged density $\langle n_e \rangle_{\text{lin}} = 2.4\text{--}3.2 \times 10^{19}/\text{m}^3$, it is found that ~50% of the power launched from the 2.45 GHz LHCD antenna may be damped at the plasma edge and not entering the plasma core. This interpretation is partially consistent with RF spectrum measurements in the scrape-off layer, which indicate broader pump width for the 2.45 GHz antenna.

First principle quantitative modelling has been carried out for various plasma conditions with the C3PO/LUKE codes [2]. The standard ray-tracing and Fokker–Planck calculations yield off-axis LH current density profile and hollow calculated hard X-ray profile, in disagreement with experimental observations. By introducing a fast-fluctuating power spectrum at the plasma edge [2], leading to a tail in the launched power spectrum at the separatrix, the calculated LH current density profile becomes more central and broad, more consistent with the toroidal MHD equilibrium one.

In addition to the experiment and modelling results obtained, EAST experiments in 2015 have revealed some operational issues important for long pulse operation. Arcing at the 4.6 GHz LHCD antenna, accompanied by emission of flakes near the antenna and divertor regions, was observed via visible cameras. Several corrective actions were therefore taken before the 2016 campaign, such as cleaning all plasma facing components from deposits and installing new LHCD guard limiters. The commissioning phase of EAST in early 2016 seemed to indicate improved power handling of the 4.6 GHz antenna, as well as improved plasma performance in general, such as facilitated access to H-mode.

References

- [1] B. Wan, *et al.*, Nucl. Fusion **55**, 104015 (2015).
- [2] Y. Peysson, *et al.*, Plasma Phys. Control. Fusion **58**, 044008 (2016).

Key Issues towards Long Pulse High β_N Operation on EAST Tokamak

X. Gao¹, Y. Yang¹, T. Zhang¹, H. Liu¹, T. Ming¹, Y. Wang¹, L. Zeng¹, X. Han¹, Q. Zang¹, Y. Yu¹, G. Li¹, D. Kong¹, and Z. Liu¹

¹*Institute of Plasma Physics, Chinese Academy of Sciences, Hefei, Anhui, People's Republic of China*

Corresponding Author: X. Gao, xgao@ipp.ac.cn

The ITER baseline scenario of the standard H-mode operation ($\beta_N = 1.8$) will be mainly sustained by inductive plasma current drive with the limited pulse duration. Two advanced scenarios of the hybrid scenario ($\beta_N = 2-2.5$) and steady-state scenario ($\beta_N > 2.6$) are being developed towards long pulse operation in present tokamak devices. A pulse duration of 32 s (about $20\tau_R$, where τ_R is the current diffusion time) H-mode plasma with small ELMs and lower normalized β ($\beta_N < 1$) was achieved on EAST superconducting tokamak in 2012. Long pulse H-mode with higher normalized β ($\beta_N = 1.8-2$) plasma scenario has also been suggested on EAST tokamak recently. In the 2015 campaign, long pulse high power heating discharges with the NBI system ($P_{\text{NBI}} < 4$ MW) and the 4.6 GHz LHW system ($P_{\text{LHW}} < 3$ MW) were carried out on EAST tokamak. Higher normalized beta ($\beta_N = 1.5-2$) plasmas were achieved on EAST experiments. Key issues towards long pulse high- β_N operation on EAST tokamak are discussed and summarized in this paper.

This work was supported by National Magnetic Confinement Fusion Program of China (No. 2014GB106000 and 2014GB106003) and the National Natural Science Foundation of China (No. 11275234, 11321092).

EX

ELM Suppression Using Resonant Magnetic Perturbation in EAST

Y. Sun¹, Y. Liang², Y. Q. Liu³, M. Jia¹, S. Gu¹, X. Yang⁴, Q. Zang¹, L. Wang¹, N. Chu¹, Y. Li¹, B. Lyu¹, C. Zhou⁵, H. Zhao¹, B. Zhang¹, T. Zhang¹, Y. Wang¹, G. Li¹, W. Guo¹, J. Qian¹, L. Xu¹, H. H. Wang¹, T. Shi¹, D. Chen¹, B. Shen¹, X. Ji¹, S. Wang¹, M. Qi¹, Z. Sheng¹, G. Gao¹, Y. Song¹, P. Fu¹, and B. N. Wan¹

¹*Institute of Plasma Physics, Chinese Academy of Sciences, Hefei, Anhui, People's Republic of China*

²*Forschungszentrum Jülich, Jülich, Germany*

³*Culham Centre for Fusion Energy (CCFE), Culham Science Centre, Abingdon, UK*

⁴*Dalian University of Technology, Liaoning, Dalian, Ganjingzi, People's Republic of China*

⁵*University of Science and Technology of China, Hefei, Anhui, People's Republic of China*

Corresponding Author: Y. Sun, ywsun@ipp.ac.cn

EX Big progress has been made in the type-I edge localized mode (ELM) control with resonant magnetic perturbation (RMP) on EAST in 2014 and 2015. A flexible in-vessel RMP coil system has been installed in 2014 for active MHD instabilities control to achieve long pulse steady state operation in the EAST tokamak. It can generate a variety range of spectrum covering most important configurations of the operating coil systems in present tokamaks and the designed one in future ITER. Complete suppression of ELM is observed during the application of $n = 1$ and 2 RMP in EAST, and ELM mitigation is observed for all of the $n = 1-4$ RMP in EAST. The transit peak flux on divertor is reduced during ELM suppression or mitigation. ELM control effect is sensitive to the RMP spectrum used. ELM suppression only happens in a limited resonant window during the scan of the phase difference between the upper and lower RMP coils. Plasma response plays an important role in the ELM control effect. The best spectrum of RMP for ELM suppression is consistent with the MARS-F modelling result. However, the transitions between ELM suppression and ELM mitigation are obviously nonlinear. Critical thresholds for the amplitude of the RMP and the plasma rotation for this transition are observed. Clear density pump-out is normally observed during the application of RMP, while magnetic braking effect depends on the plasma rotation. Magnetic braking is observed in the NBI heated relatively high rotation plasma case, while it is not obvious, when the plasma rotation is close to 0 in radio frequency wave dominated heating plasmas. Footprint splitting is also observed during the application of RMP and agrees well with vacuum modelling. The enhancement of transport of the tungsten has also been observed during ELM mitigation.



Recent Experimental and Modelling Advances in the Understanding of Lower Hybrid Current Drive in ITER-Relevant Regimes

B. J. Ding¹, P. T. Bonoli², A. A. Tuccillo³, M. Goniche⁴, K. Kirov⁵, M. Li¹, Y. Li¹, R. Cesario³, G. M. Wallace², Y. Peysson⁴, A. Ekedahl⁴, L. Amicucci³, R. R. Parker², S. Shiraiwa², I. Faust², S. G. Baek², A. Cardinali³, C. Castaldo³, J. Mailloux⁵, F. Liu¹, and B. N. Wan¹

¹*Institute of Plasma Physics, Chinese Academy of Sciences, Hefei, Anhui, People's Republic of China*

²*Plasma Science & Fusion Center, MIT, Cambridge, MA 02139, USA*

³*Associazione EURATOM-ENEA Unit  Tecnica Fusione, Frascati, Italy*

⁴*Institut de Recherche sur la Fusion par confinement Magn tique (IRFM),*

Commissariat   l' nergie atomique (CEA/Cadarache), 13108 Saint-Paul-l s-Durance, France

⁵*Culham Centre for Fusion Energy (CCFE), Culham Science Centre, Abingdon, UK*

Corresponding Author: B. J. Ding, bjding@ipp.ac.cn

To explore lower hybrid current drive at reactor relevant, high density is an important issue. Collisional absorption (CA), parametric instabilities (PI) and scattering from density fluctuations (SDF) are considered as possible candidates for the current drive (CD) efficiency decreasing faster than theory prediction. A multimachine assessment, including experiments and modelling in EAST, C-Mod and JET, has been continued under the ITPA-IOS coordination.

Experiments in EAST show that L-H waves (LHW) at 4.6 GHz have better CD capability than at 2.45 GHz. By means of 4.6 GHz/2.45 GHz LHCD, H-mode plasma obtained at relatively high density shows part of the current is driven by L-H waves. The role of the spectral broadening produced by PI at the plasma edge in affecting the LHCD efficiency will be further assessed. On Alcator C-Mod, the deposition of L-H wave power at high density was analyzed using power modulation techniques, showing that an increasing fraction of L-H power is absorbed in the edge with increasing density and reduced CD efficiency.

Modelling of PI, CA and SDF in EAST have shown that these mechanisms could be responsible for the reduction of CD efficiency at high density. PI modelling using the LHPI code and the code from MIT are nearly consistent with the measured RF spectra from a probe. The existence of a "tail" in the launched power spectrum due to SDF, considered in C3PO/LUKE, significantly improves consistency between modelling and experiments when the spectral gap is large in EAST and C-Mod. Using GENRAY/CQL3D, CA simulation results suggest that SOL plasmas could have impact on current drive. Results from the improved SOL plasma model in GENRAY/CQL3D taking into account more realistic geometry can reproduce the experimental trend in all range of LHCD densities on C-Mod. The effect of the L-H frequency (2.45 GHz and 4.60 GHz) on PI in EAST has been considered, showing that the ion sound quasi-mode growth rate is slightly smaller (~25%) with 4.60 GHz, hence producing a less pronounced broadening of the launched spectrum for the case of 4.60 GHz LHW. The driven current profile using LHstar code with different frequency will be presented.

In JET, a new Ray Tracing/Fokker-Planck package has been developed for the L-H power deposition analysis. Results are in a very good agreement with experimental data at lower density, whereas it is not at high density.



Experimental Study of Radio-Frequency Driven Spontaneous Rotation for High-Performance Plasmas on EAST

B. Lyu¹, F. D. Wang¹, Y. Y. Li¹, J. Fu¹, X. H. Yin¹, J. Chen¹, R. J. Hu¹, M. Wang¹, B. J. Ding¹, F. K. Liu¹, M. Bitter², K. W. Hill², L. F. Delgado-Aparicio², N. Pablant², S. G. Lee³, Y. J. Shi^{4,5}, and B. N. Wan¹

¹*Institute of Plasma Physics, Chinese Academy of Sciences, Hefei, Anhui, People's Republic of China*

²*Princeton Plasma Physics Laboratory (PPPL), Princeton, NJ 08540, USA*

³*National Fusion Research Institute (NFRI), Daejeon, Republic of Korea*

⁴*Seoul National University, Seoul, Republic of Korea*

⁵*University of Science and Technology of China, Hefei, Anhui, People's Republic of China*

Corresponding Author: B. Lyu, blu@ipp.ac.cn

EX Rotation driven by radio-frequency waves have been studied on EAST for plasmas heated by LHW, ICRF and ECRH. Understanding of momentum transport characteristics plays an important role in pushing towards RF-heating dominated high-performance plasma operations on EAST. Using newly developed diagnostics, studies on RF-heated plasma rotation and momentum transports have been further carried out. Efficient rotation increment has been observed and its effect on plasma confinement was seen. New observed plasma rotation behaviours in plasmas heated by newly commissioned LHCD and ECRH will be presented and parametric analysis were performed to study the dependence of rotation change on various plasma parameters to further understand the efficient rotation driving mechanisms on EAST. It was found that cocurrent rotation change increased with injected LHCD power and was closely related with internal inductance and safety factor, i.e., current density profile. Local rotation change induced by ECRH was also observed upon the commissioning of the ECRH system. For ohmic target plasmas, on-axis ECRH heating produced cocurrent increase in core rotation and elevated T_e/T_i ratio, consistent with cocurrent intrinsic torque with ECRH. Rotation increment upon RF injection was also linearly correlated with plasma β . Together with ICRF, a combination of various RF schemes provides good capability for efficient rotation drive in support of high-performance operations on EAST.



Heating and Confinements by the Waves in the Ion Cyclotron Range of Frequencies on EAST

X. J. Zhang¹, S. Yuan¹, Y. P. Zhao¹, B. N. Wan¹, Y. Z. Mao¹, X. Gong¹, C. M. Qin¹, Y. Chen¹, L. Wang¹, S. Q. Ju¹, Y. Lin², L. Hu¹, J. G. Li¹, Y. T. Song¹, S. Wukitch², G. Taylor³, J. C. Hosea³, J.-M. Noterdaeme⁴, R. Kumazawa⁵, T. Seki⁵, K. Saito⁵, and H. Kasahara⁵

¹*Institute of Plasma Physics, Chinese Academy of Sciences, Hefei, Anhui, People's Republic of China*

²*Plasma Science & Fusion Center, MIT, Cambridge, MA 02139, USA*

³*Princeton Plasma Physics Laboratory (PPPL), Princeton, NJ 08540, USA*

⁴*Max-Planck-Institut für Plasmaphysik, Garching, Germany*

⁵*National Institute for Fusion Science (NIFS), Toki, Gifu, Japan*

Corresponding Author: X. J. Zhang, xjzhang@ipp.ac.cn

The paper summarizes the recent experiments performed with ion cyclotron resonance heating (ICRH) on EAST. Heating and confinement studies using the hydrogen minority heating scheme have been investigated in Ohmic target plasma and in combination with low-hybrid waves. Energy confinement follows scaling law. The results show a typical L-mode behaviour, i.e., a power dependent confinement degradation. L-mode data agree with ITER89P scaling. The ICRF heating efficiency is $\sim 35\%$, rather low on EAST. One of the importance challenges for EAST is how to couple higher power into the core plasma. The experimental results show that local gas injection and reducing k_{\parallel} directly improves the coupling efficiency. Particular efforts have been devoted to investigations of the interaction of ICRF waves with fast ions injected by neutral beams. Third harmonic ion cyclotron resonance heating of D-beam ions have been achieved for the first time on EAST.

EX



Current Drive with Combined Electron Cyclotron Wave and High Harmonic Fast Wave in Tokamak Plasmas

X. Y. Gong¹, J. Q. Dong², J. Wang², N. Zhang¹, L. Yin¹, and C. Y. Yin¹

¹University of South China, Hengyang, Hunan, People's Republic of China

²Southwestern Institute of Physics, Chengdu, Sichuan, People's Republic of China

Corresponding Author: X. Y. Gong, gongxueyu0202@126.com

The current driven by combined electron cyclotron wave (ECW) and high harmonic fast wave (HHFW) is investigated with the GENRAY and CQL3D packages. It is shown that no significant synergetic current is found in a range of cases with combined ECW and FW. This result is consistent with the former study [1]. However, positive synergy effect does appear with the enhancement of the FW frequency. This positive synergy effect can be vividly explained with the picture of the electron distribution function induced by ECW and the very high harmonic fast wave (helicon). The dependence of the synergy effect on the wave power is also analyzed numerically and physically.

References

[1] R. W. Harvey, *et al.*, in Proceedings of IAEA TCM on Fast Wave Current Drive in Reactor Scale Tokamaks (Synergy and Complementarity with LHCD and ECRH), Arles, France, (IAEA, Vienna, 1991).



Evidence and Modelling of 3D Divertor Footprint Induced by Lower Hybrid Waves on EAST with Tungsten Divertor Operations

L. Wang¹, W. Feng¹, M. Rack², Y. Liang^{1,2}, H. Y. Guo^{1,3}, G. S. Xu¹, Z. D. Yang¹, J. C. Xu¹, B. Zhang¹, M. N. Jia¹, J. B. Liu¹, H. Liu¹, R. Chen¹, M. H. Li¹, B. J. Ding¹, A. Wingen⁴, X. L. Zou⁵, Y. W. Sun¹, X. Z. Gong¹, and B. N. Wan¹

¹*Institute of Plasma Physics, Chinese Academy of Sciences, Hefei, Anhui, People's Republic of China*

²*Institute of Energy and Climate Research, Forschungszentrum Jülich, Jülich, Germany*

³*General Atomics, San Diego, CA 92186, USA*

⁴*Oak Ridge National Laboratory (ORNL), Oak Ridge, TN 37831, USA*

⁵*Commissariat à l'énergie atomique (CEA), 91400 Gif-sur-Yvette, France*

Corresponding Author: L. Wang, wliang@ipp.ac.cn

Active control of high heat and particle fluxes deposited on the divertor targets is an essential issue for steady-state operations on the experimental advanced superconducting tokamak (EAST) and other future fusion devices, such as ITER. The change of edge magnetic topology is an effective method to exert positive influence on divertor heat and particle fluxes, which has been achieved by lower hybrid waves (LHW) on EAST, similar with the effect of resonant magnetic perturbations (RMP) coils. The 3D divertor footprint patterns induced by LHW have been systematically observed in the EAST 2016 January campaign. By comparing the particle fluxes deposited on the divertor targets in the same poloidal location while different toroidal locations, we find the secondary heat flux peak away from the strike point closely fits the pitch of the edge magnetic field line in different q_{95} , which has also been qualitatively modelled by a field line tracing code. In the simulation of this model, the same starting point and amplitude of the helical current filaments (HCFs) were assumed for each q_{95} case, with the total current of the group of four filaments taken as 1.5 kA. Steady-state discharges in various LHW power under low-confinement mode (L-mode) has also been carried out recently. As the LHW power increases to a threshold, the heat and particle fluxes in the strike point remain nearly constant while the secondary heat flux peak away from it turns out an significant enhancement, which is attributed to that more LHW power is absorbed in scrape-off layer (SOL) region as LHW power raises up, thus enhancing HCFs in the SOL. Furthermore, in comparison to purely 4.6 GHz-LHW heated experiments, we find an extra splitting area away from the main strike point at the toroidal angle of $19\pi/16$ (Port D) and an obvious decrease of particle fluxes at the toroidal angle of $31\pi/16$ (Port O) when 2.45 GHz LHW (Port N) are simultaneously added, which may provide a new means in spreading the wetted area and reducing the peak heat flux.

EX

Fishtail Divertor: A New Divertor Concept on EAST for Active Control of Heat Load on Divertor Plate

X. D. Zhang¹, J. P. Qian¹, J. X. Zheng¹, G. N. Luo¹, Q. Yu², S. J. Du¹, L. Wang¹, and B. J. Xiao¹

¹*Institute of Plasma Physics, Chinese Academy of Sciences, Hefei, Anhui, People's Republic of China*

²*Max-Planck-Institut für Plasmaphysik, Garching, Germany*

Corresponding Author: X. D. Zhang, xdzhang@ipp.ac.cn

A new divertor concept, the Fishtail divertor (FTD), is proposed and investigated on EAST, which can quickly move the strike point along the radial and poloidal direction like the swing of fishtail by additional alternating magnetic field. The maximum moving distance of the strike point is controlled by the alternating field amplitude. The wetted area of the heat flux is widened, so that the averaged heat load is reduced. Being different from the position swing of plasma on JET and for quasi-steady-state operation on EAST, the additional alternating magnetic field is to be generated by the AC current in the coil located behind the divertor target near the strike point. The maximum moving distance of the strike point is proportional to the coil current but inversely proportional to the plasma current. When EAST tokamak is operated at a plasma current 500 kA, 5 kA AC current in the coil is found to be required for a maximum moving distance of 10 cm on the divertor target. The numerical simulations show that the surface temperature of the divertor target plate is reduced significantly when the strike point swings. Without moving the strike point on EAST, the maximum surface temperatures of the carbon target plate are 1057°C and 1872°C, respectively, for a heat flux 10 MW/m² with a width of 1 cm and 2 cm. With a 10 Hz swing, the maximum surface temperatures are reduced to 525°C and 532°C, respectively. Based on the results from numerical simulations and preliminary engineering design, it is found that FTD has the following advantages compared with other divertor concepts:

1. The precise radial profile of the heat flux becomes unimportant;
2. Uniform distribution of the heat flux on the divertor target plate;
3. Reliable controls the heat load region on the divertor target plate;
4. Little effect on the plasma shape and X-point location;
5. Feasibility from the engineering and technology point of view;
6. Fast swing is possible and can be utilized for ELM mitigation.

Further analysis on the application of FTD or its combination with other concepts for a fusion reactor has also been carried out. A long divertor leg configuration together with a special divertor chamber is found to be attractive for reactors, since in this case the FTD coils can be located away from the core plasma to avoid neutron radiation.

Predictions of the Baseline Operation Scenario in Chinese Fusion Engineering Test Reactor

G. Li¹, V. Chan², J. Chen¹, H. Li¹, D. Kong¹, L. L. Lao³, Z. Li⁴, L. Liu², Z. Luo¹, X. Liu¹, X. Jian⁵, O. Meneghini³, P. B. Snyder³, G. M. Staebler³, S. Smith³, W. Yang¹, and D. Zhao³

¹*Institute of Plasma Physics, Chinese Academy of Sciences, Hefei, Anhui, People's Republic of China*

²*University of Science and Technology of China, Hefei, Anhui, People's Republic of China*

³*General Atomics, San Diego, CA 92186, USA*

⁴*Fusion Simulation Center (FSC), Peking University, Haidian, Beijing, People's Republic of China*

⁵*Huazhong University of Science and Technology, Hubei, People's Republic of China*

Corresponding Author: G. Li, ligq@ipp.ac.cn

The Chinese fusion engineering test reactor (CFETR) is under design. The machine aims to fill the gaps between ITER and DEMO. Recently, the physical design focusses on the so-called baseline scenario. It is a 10 MA steady state scenario to produce ~200 MW fusion power. With the integrated modelling of the equilibrium calculation, pedestal structures prediction, 1.5D core transport simulation, 2D divertor and scrape-off layer transport simulation and MHD instabilities analysis, the plasma performance of baseline scenario is predicted. Equilibrium calculations show that both the ITER-like configurations and the snowflake configurations could be achieved. The EPED1 model is used to predict the pedestal structure, gives the pedestal height 40 kPa and width 0.03 psi. 1.5D simulations are performed with coupled ONETWO/TGYRO codes under the framework of OMFIT, show that with 100 MW injected power, the temperature profiles could be sustained with $T_i(0) \sim 19$ keV and the fusion power is 192 MW. At the same time, the plasma current is fully noninductive, it is sustained by 4.65 MA bootstrap current and 5.39 MA driven current. The driven current is off-axis and the q profile is reversed. The heat flux on the divertor for the ITER-like configuration is simulated by the SOLPS (B2-EIRENE) code package. It shows that with Ar or Ne impurity seeding (a rate of $\sim 10^{21}$ particles/s) from the top of the machine, the peak heat flux is effectively reduced below 10 MW/m^2 , even at a relatively low edge density. MHD instabilities and its control methods are analyzed. The vertical instability could be controlled by the passive structure and the internal coils at the back of blanket. The global ideal MHD instability is stable since the baseline scenario is far below the ideal MHD limit. The neoclassical tearing modes (NTMs) could be controlled by 7 MW ECCD. The stability of toroidal Alfvén eigenmodes (TAEs) is analyzed with the linear code NOVA-K, shows that it is stable for the reversed shear equilibrium. The integrated modelling gives a set of relatively self-consistent parameters, shows that the target plasma parameters of the baseline operation scenario could be achieved.

EX



Current Transport and Density Fluctuations at L-H Transition on EAST

W. X. Ding¹, H. Q. Liu², J. P. Qian², S. B. Zhang², D. L. Brower¹, Z. Y. Zou², W. M. Li², Y. Yang², L. Zeng², J. L. Xie³, P. Zhu³, H. Cai³, C. X. Yu³, T. Lan³, S. X. Wang², X. C. Wei², Y. X. Jie², L. Q. Hu², and B. N. Wan²

¹University of California Los Angeles, CA 90095, USA

²Institute of Plasma Physics, Chinese Academy of Sciences, Hefei, Anhui, People's Republic of China

³University of Science and Technology of China, Hefei, Anhui, People's Republic of China

Corresponding Author: W. X. Ding, wding@ucla.edu

EX Plasma confinement and sustainment of a steady-state tokamak reactor depend on current density profile control to manage MHD instabilities. A number of operational scenarios have been identified for high-performance and high- β tokamak operation. In these high-temperature plasmas, current transport may occur on time scales much faster than resistive diffusion. Anomalous current transport can arise from magnetic reconnection, self-generated current (dynamo effect) through various MHD effects and magnetic flux pumping or kinetic effects such as fast particles loss in a stochastic magnetic field. Understanding and controlling current transport in a long-pulse tokamak using ITER relevant actuators (NBI, LHCD) and sensors (Faraday-effect polarimetry), as is being pursued on EAST, becomes increasingly important and will provide a strong physics base for ITER operation scenario development. In this paper, we report on current profile evolution in EAST NBI driven plasmas where two neutral beams are injected, one during the current ramp phase and the 2nd during flattop. At the end of the current ramp phase, it is found that a flat q profile with $q_0 \sim 1$ is achieved with low magnetic shear in the core. It is observed that plasma current and density both relax on a timescale much faster than resistive time, even in the absence of sawtooth activity when H-L transition happens. Density fluctuations associated with magnetic perturbations (3/2) are observed as a precursor to the H-L transition are observed. It is likely that these modes play a role in fast current transport.



Kinetic Alfvén-Ballooning Instabilities in Tokamak Plasmas with Weak Magnetic Shears and Low-Pressure Gradients

W. Chen¹, R. R. Ma¹, L. M. Yu¹, H. R. Du², X. T. Ding¹, M. Jiang¹, Z. B. Shi¹, X. Q. Ji¹, D. L. Yu¹, B. S. Yuan¹, Z. C. Yang³, Y. G. Li¹, W. L. Zhong¹, J. Q. Dong¹, M. Xu¹, Y. H. Xu¹, Q. W. Yang¹, Y. Liu¹, L. W. Yan¹, and X. R. Duan¹

¹Southwestern Institute of Physics, Chengdu, Sichuan, People's Republic of China

²Dalian University of Technology, Liaoning, Dalian, Ganjingzi, People's Republic of China

³Xihua University, Mianyang, Sichuan, People's Republic of China

Corresponding Author: W. Chen, chenw@swip.ac.cn

Kinetic Alfvén-ballooning instabilities (KABIs) are very common in magnetized plasmas both in space and laboratory. In present-day fusion and future burning plasmas, they are easily excited by fast particles and/or pressure gradients. They can not only cause the loss and redistribution of fast particles but also affect plasma confinement and transport. The physics associated with them is an intriguing but complex area of research. For weak magnetic shears and low pressure gradients, the study of KABIs, such as AITG/KBM, has not been paid enough attention.

In the present paper, we will report two experimental results in HL-2A Ohmic and NBI plasmas with weak magnetic shears and low pressure gradients. Firstly, low-frequency oscillations with $f = 15\text{--}40$ kHz and $n = 3\text{--}6$ were detected by many kind diagnostics in high-density Ohmic regimes. The LF oscillations appeared in the plasmas with the density peaking and weak magnetic shear, which indicates that corresponding instabilities were excited by the pressure gradients. Sometime these modes have the behaviours of the frequency jumping as the stairs or chirping-up. The analysis by the extended generalized fishbone-like dispersion relation (GFLDR-E) revealed that the frequency of the oscillations scaled with the ion temperature and η_i , and the frequency lies in the KBM-AITG-BAE ranges. This lets us to conclude that the LF oscillations were more like BAE instabilities although their some characteristics are like AITG. The minor disruption of bulk plasmas is potentially linked with the evolution of the instabilities. Secondly, the low- n AITG instabilities with $f_{\text{BAE}} < f < f_{\text{TAE}}$ and $n = 2\text{--}8$ are found to be unstable in the NBI plasmas with weak shears and low pressure gradients. The measured results are also consistent with the GFLDR-E, and the modes are more unstable $|s|$ is smaller in low pressure gradient regions. The calculation results from the HD7 code also suggest that AITG modes can be unstable for weak shears and low pressure gradients. These modes have possibly opposite effects on the ITB formation. The trapped electrons potentially enhance these modes unstable. It is worth emphasizing that the study of AITG/KBM with or without fast particles should be paid more attention because they link to the ITB and H-mode pedestal physics for weak magnetic shears.

EX



Experimental Investigation of Interaction between Turbulence and Large-Scale Mode Structures in HL-2A

X. Q. Ji¹, Y. Xu¹, Y. Liu¹, O. Pan¹, Z. B. Shi¹, D. L. Yu¹, B. B. Feng¹, Y. B. Dong¹, Y. Zhou¹, M. Jiang¹, J. Cheng¹, W. L. Zhong¹, W. Chen¹, L. W. Yan¹, and Q. W. Yang¹

¹*Southwestern Institute of Physics, Chengdu, Sichuan, People's Republic of China*

Corresponding Author: X. Q. Ji, jixq@swip.ac.cn

We present the first experimental observation of self-regulation of nonlocal transport events by NTMs generated during transient nonlocal transport events. The nonlocal effect is excited by edge cooling and propagates inward by avalanche events. These cause a local increase of the pressure gradient at the inversion surface, and thus the onset of the NTM in relatively low- β plasmas. The presence of the NTM, results in the development of sheared flows at the magnetic island. These then truncate the nonlocal transport due to suppression of avalanches by shearing. These results may have important implications for the understanding of multiscale transport dynamics, i.e., the intimate interplay between small and large scale structures.

Study of Impurity Transport in the HL-2A ECRH Plasmas with MHD Instabilities

Z. Y. Cui¹, K. Zhang¹, S. Morita², X. Q. Ji¹, Y. Xu¹, X. T. Ding¹, W. L. Zhong¹, L. M. Yu¹, P. Sun¹, C. F. Dong¹, B. Z. Fu¹, P. Lu¹, X. W. Cui¹, S. D. Song¹, Q. W. Yang¹, and X. R. Duan¹

¹Southwestern Institute of Physics, Chengdu, Sichuan, People's Republic of China

²National Institute for Fusion Science (NIFS), Toki, Gifu, Japan

Corresponding Author: Z. Y. Cui, cuizy@swip.ac.cn

In next-generation fusion devices the reduction of impurity concentration in core plasmas is of great importance not only for the decrease in the line radiation loss but also for mitigation of the fuel dilution and the bremsstrahlung radiation to achieve high-performance plasmas in the high density regime. In experiments, the electron cyclotron resonance heating (ECRH) has been widely applied as an effective tool to control impurity accumulation in the plasma core. An increase in the central impurity diffusivity and suppression of the convective pinch, sometimes even a reversal to the outward convection, has been observed. The possible interpretation for the strong increase of impurity diffusivity and positive (outward) convection could be due to an enhancement of turbulence. Recently, a long-lasting $m/n = 1/1$ MHD activity was observed in the AUG experiment when the ECRH was applied. The relation between the saturated MHD activity and the impurity density profile has also been discussed.

In the HL-2A tokamak ($R/a = 165/40$ cm), the impact of ECRH on the impurity transport has been studied with trace impurity injection and variation of the ECRH power deposition, whilst the MHD instabilities and density fluctuations are also measured. The experiment results show that the impurity transport has been strongly enhanced with inner-deposited ECRH than outer-deposited ECRH. The V is reversed to the outward direction (positive) with ECRH in comparison with ohmic discharges where the V normally directs inwards (negative). Both D and V are increased when the ECRH deposition position shifts toward the plasma centre. The calculated impurity density profile also confirms that the central peaked profile has been effectively flattened with central ECRH. Using the SXR measurement the MHD activities with relation to the ECRH (various deposition) and ohmic discharges are analyzed. The sawtooth oscillation is presented normally in the central channel for the outer-deposited ECRH discharge but becomes reversed for the inner-deposited ECRH. In case of inner-deposited ECRH a long-lasting $m/n = 1/1$ mode is observed in-between the sawtooth crashes. When this mode is presented an outward heat flux has been observed by the ECE measurement. The turbulent transport as density fluctuations measured by the reflectometer has also been discussed.

Role of SMBI Deposition in ELM Mitigation and the Underlying Turbulence Characteristics

Z. B. Shi¹, Z. C. Yang¹, W. L. Zhong¹, B. Y. Zhang¹, C. Y. Chen¹, M. Jiang¹, P. W. Shi¹,
W. Chen¹, Z. T. Liu¹, D. L. Yu¹, Y. Zhou¹, B. B. Feng¹, X. M. Song¹, X. T. Ding¹,
Q. W. Yang¹, and X. R. Duan¹

¹*Southwestern Institute of Physics, Chengdu, Sichuan, People's Republic of China*

Corresponding Author: Z. B. Shi, shizb@swip.ac.cn

In the next generation of large fusion device ITER, it has been accepted that the divertor could not endure the heat exhaust due to the edge localized modes (ELM), without any action to mitigate. The physical mechanism and controlling methods of ELM have become important tasks in physics of boundary plasmas. The supersonic molecular beam injection (SMBI), one of numerous approaches to mitigate ELMs, has been observed effective for some conditions. But the mechanism of mitigation even the key parameters of injection are not clear exactly. In this work, the relationship of ELM mitigation effect with SMBI deposition is researched experimentally, and simulated with the minimal self-organized criticality model. The underlying turbulence characteristics are observed highly correlated with ELM mitigation for the first time.

EX The deposition position is obtained from the radial position of the greatest growth of density due to SMBI pulses. The mitigation effect is identified by increase of ELM frequency and decrease of the energy loss caused by one ELM. We found when deposit to the bottom, even outside of pedestal, mitigation is hardly realized. When inject deeper, deposit ~20% into the pedestal, significant mitigation is achieved. But when inject further to the middle or deeper region, the mitigation effect decayed rapidly, till frequency and amplitude of ELM did not change obviously, just similar with condition of bottom deposition. The cellular-automata sand-pile model is used to simulate the ELM burst and explain the mitigation effect at different SMBI deposition. It is deemed that there is a threshold to trigger ELMs. The slightly shallower depositions trigger the crash in advance, and thus make the crash smaller and more frequently.

The relevant theoretical works point out that occurrence of ELM crashes does not only depend on the linear threshold, but also relies on nonlinear processes. The inward turbulence is found to be an important factor. The perturbation of electron density measured by multi-channel Doppler reflectometer is used to analyze the feature of turbulence spreading during ELM mitigation with SMBI. The inward spreading is observed during the unmitigated phase. The relation between the turbulence behaviours and ELM mitigation will also be presented.



Roles of an Inward Particle Flux Inducing Quasi-Mode in Pedestal Dynamics on HL-2A Tokamak

J. Dong¹, J. Cheng¹, K. Itoh², L. Yan¹, Z. Huang¹, Y. Shen¹, H. He¹, J. Xu¹, X. Ji¹, K. Zhao¹, W. Zhong¹, Y. Li¹, D. Yu¹, S.-I. Itoh³, S. Inagaki⁴, Z. Shi¹, X. L. Zou⁵, Q. Yang¹, X. Ding¹, and X. Duan¹

¹Southwestern Institute of Physics, Chengdu, Sichuan, People's Republic of China

²National Institute for Fusion Science (NIFS), Toki, Gifu, Japan

³Research Institute for Applied Mechanics (RIAM), Kyushu University, Kasuga, Japan

⁴Kyushu University, Kasuga, Japan

⁵Institut de Recherche sur la Fusion par confinement Magnétique (IREM), Commissariat à l'énergie atomique (CEA/Cadarache), 13108 Saint-Paul-lès-Durance, France

Corresponding Author: J. Dong, jiaqi@swip.ac.cn

Detailed analyses of the dynamic evolutions of the pedestal, including density, temperature, pressure and their gradients were performed in recent H-mode experiments on HL-2A tokamak. Dramatic increase of density gradient and decrease of electron temperature gradient were observed in the pedestal just prior to each burst in a series of ELM eruptions. An inward particle flux inducing quasi-coherent mode was found to be responsible for such changes, and triggering the ELM eruption. The results clearly show that the mode grows very rapidly 200 μ s before each ELM burst in the H-mode plasma. The auto-power spectrum analysis indicates that the mode peaks at $f = 50\text{--}60$ kHz. A higher harmonic at 120 kHz also appears in the density spectrum, but not in the floating potential. The poloidal and toroidal mode numbers are estimated as $m \approx 20\text{--}24$ and $n = m/q \approx 6\text{--}8$, respectively. The poloidal propagation velocity of the mode is estimated as 6.0–7.2 km/s at $\Delta r = -10.0$ mm. The radial wave vector of the mode is $k_r \approx 3.5\text{--}7.5$ cm⁻¹, propagating inward with a velocity of 400–850 m/s. The mode propagates in plasma current direction toroidally. The squared auto-bicoherence analyses of the floating potential and density fluctuations indicate that nonlinear three-wave coupling might be a plausible mechanism for the generation of the quasi-coherent mode. Decoupling of the mode induced density transport from energy transport, similar to that observed in I-mode discharges, was observed. A very interesting observation in the experiments is that the gradient scale length of electron density is always shorter than that of temperature at the starting point of the ELM burst and, therefore, the dominant role of density gradient over temperature gradient for ELM triggering is demonstrated. The results are consistent with I-mode discharges where high temperature gradient does not lead to ELM and in contrast with the previously reported quasi-coherent modes which play significant roles in sustaining H-mode discharges [1–3].

References

- [1] Z. Yan, *et al.*, Phys. Rev. Lett. **107**, 055004 (2011).
- [2] A. Diallo, *et al.*, Phys. Rev. Lett. **112**, 115001 (2014).
- [3] H. Q. Wang, *et al.*, Phys. Rev. Lett. **112**, 185004 (2014).



Direct Measurement of ELM Related Momentum Transport in the Edge of HL-2A H-Mode Plasmas

M. Xu¹, T. Long¹, L. Nie¹, Y. Wu¹, W. Zhong¹, X. L. Zou², and X. Duan¹

¹*Southwestern Institute of Physics, Chengdu, Sichuan, People's Republic of China*

²*Institut de Recherche sur la Fusion par confinement Magnétique (IRFM), Commissariat à l'énergie atomique (CEA/Cadarache), 13108 Saint-Paul-lès-Durance, France*

Corresponding Author: M. Xu, minxu.min@gmail.com

Turbulent momentum flux, including the Reynolds stress, convective flux, and the flux driven by nonlinear interactions, was experimentally measured in ELMy H-mode. It was found that net momentum in the electron diamagnetic direction was injected from the edge into the plasma during ELMs. This is a direct evidence that plasma is able to serve as a heat engine to convert heat into poloidal momentum and drive flows.

The experiments were conducted in ELMy H-mode deuterium discharges on the HL-2A tokamak. A special Langmuir probe array was positioned within millimetres around the separatrix and used for the measurement. It was found that during ELM eruptions electron density and temperature fluctuated violently, and their mean values indicated by their fluctuations envelopes increased dramatically. This is consistent with the idea that ELM bursts a pack of heat and particles from the pedestal into the SOL region. One pronounced feature is that the velocity measured by Mach probe increased towards the electron diamagnetic direction during the ELM eruption. This means that additional momentum in the electron diamagnetic direction was locally generated or transported and deposited into the region.

The measured total turbulent momentum flux is negative, which indicates that either momentum in the electron diamagnetic direction was transported towards the pedestal or momentum in the ion diamagnetic direction was transported towards the chamber wall. This immediately implies that net momentum in the electron diamagnetic direction was injected into the separatrix, and possibly drove the edge poloidal shear flow. It is worth noting that although the Reynolds stress term is the leading term, the other two terms including the nonlinear term are of the same order of magnitude and cannot be neglected. Particularly, the nonlinear term during the second ELM burst is significantly large, contrary to what people usually expect.

EX



Synchronization of GAMs and Magnetic Fluctuations on HL-2A Tokamak

L. W. Yan¹, K. J. Zhao¹, Y. Nagashima², P. H. Diamond³, J. Q. Dong¹, J. Cheng¹, K. Itoh⁴, S.-I. Itoh², A. Fujisawa², S. Inagaki², Y. Kosuga², M. Sasaki², Z. X. Wang⁵, L. Wei⁵, Z. H. Huang¹, Q. Li¹, X. Q. Ji¹, X. M. Song¹, Y. Huang¹, Y. Liu¹, Q. W. Yang¹, X. T. Ding¹, X. R. Duan¹, and Y. Liu¹

¹Southwestern Institute of Physics, Chengdu, Sichuan, People's Republic of China

²Research Institute for Applied Mechanics (RIAM), Kyushu University, Kasuga, Japan

³University of California San Diego, CA 92093, USA

⁴National Institute for Fusion Science (NIFS), Toki, Gifu, Japan

⁵Dalian University of Technology, Liaoning, Dalian, Ganjingzi, People's Republic of China

Corresponding Author: L. W. Yan, lwyang@swip.ac.cn

The synchronization of geodesic acoustic modes (GAMs) and magnetic fluctuations is identified in the edge plasmas of the HL-2A tokamak for the first time. The frequency entrainment and phase lock are elucidated. Meso-scale electrostatic fluctuations (MSEFs) with components of the dominant GAMs and the $m/n = 6/2$ potential fluctuations are found to have the same frequency as magnetic fluctuations of $m/n = 6/2$. The temporal evolutions of the MSEFs and magnetic fluctuations clearly show the frequency entrainment between the GAMs and the $m/n = 6/2$ magnetic fluctuations. The phase lock between GAMs and magnetic fluctuations is also demonstrated. The results suggest that the GAMs and magnetic fluctuations can transfer energy between each other through nonlinear synchronization. The nonlinear synchronization may contribute to the LFZF (low frequency zonal flow) formation, reduction of turbulent level, and thus confinement regime transitions.

EX

Investigation of Mechanisms for the Generation of Blobs/Holes at the Boundary of the HL-2A Tokamak

O. Pan¹, Y. Xu¹, J. Cheng¹, J. Q. Xu¹, L. W. Yan¹, K. Yao¹, M. Xu¹, Z. B. Shi¹, Y. Liu¹,
Q. W. Yang¹, X. R. Duan¹, and Y. Liu¹

¹*Southwestern Institute of Physics, Chengdu, Sichuan, People's Republic of China*

Corresponding Author: O. Pan, panou@swip.ac.cn

“Blob-filaments”, or simply “blobs”, denote radial convection of coherent plasma structures, which transport plasma mass and energy across the open magnetic field line region known as the scrape-off layer (SOL) and enhance the plasma interaction with the surrounding material boundaries. The generation mechanism for blobs has been investigated for many years. Experiments and theories/simulations have showed that the formation of blobs can be linked to a variety of mechanisms, such as the drift-wave turbulence, interchange instability, conducting wall instability and the turbulence spreading regime, etc. In this work, we have made an experimental survey on the spatial distribution of blobs (and holes) as well as their driving mechanism in the edge and SOL of the HL-2A tokamak. The results reveal that, depending on spatial locations at the plasma boundary, multiple mechanisms are responsible for the development of the blob and hole dynamics.

EX

Experimental Evaluation of Langmuir Probe Sheath Potential Coefficient

L. Nie¹, M. Xu¹, R. Ke¹, B. D. Yuan¹, J. Cheng¹, Y. Yu², T. Lan², H. G. Shen², R. J. Hong³, Y. B. Dong¹, D. Guo¹, Y. F. Wu¹, T. Long¹, X. Ji¹, J. Q. Xu¹, W. Chen¹, J. Wu², Y. H. Han¹, Y. X. Xu¹, L. W. Yan¹, and X. L. Zou⁴

¹Southwestern Institute of Physics, Chengdu, Sichuan, People's Republic of China

²University of Science and Technology of China, Hefei, Anhui, People's Republic of China

³University of California San Diego, CA 92093, USA

⁴Institut de Recherche sur la Fusion par confinement Magnétique (IRFM), Commissariat à l'énergie atomique (CEA/Cadarache), 13108 Saint-Paul-lès-Durance, France

Corresponding Author: L. Nie, nielin@swip.ac.cn

Sheath potential coefficient α is a very important parameter in Langmuir probe measurement. It is often used to estimate the plasma potential: $V_p = V_f + \alpha T_e$, where V_f and T_e are floating potential and electron temperature respectively. In magnetized high temperature fusion plasmas this coefficient is affected by many factors and may lead to large errors in the inferred electric field and fluid shear. Now a systematic calibration experiment of α were carried out in the HL-2A tokamak deuterium plasmas with the purpose to help to solve this issue. In this experiment, a multifunctional probe array was used in Ohmic and ECRH L-mode discharges to directly measure sheath potential coefficient. It is comprised of a triple probe array, a flat swept probe, and two poloidal separated V_f probes which can be used to estimate the location of the last-closed flux-surface (LCFS) by the reversal of turbulence propagation velocity in the poloidal direction.

At first, with the $V-I$ characteristic measured by swept probe and Druyesteyn method, the electron energy distribution function (EEDF) $F(\epsilon)$ can be inferred and the plasma potential V_p can be calculated where the second derivative equals 0 in the $V-I$ characteristic. Then, besides the traditional constant $\alpha_t = 2.8$ often used, there are another two methods to infer the α coefficient. We define them as: $\alpha_p = (V_p - V_f)/T_e$ and $\alpha_I = \ln(|I_{se}/I_{si}|)$. It should be noted that V_p and α_p , which are measured from $V-I$ characteristic directly, is the most credible as compared to the others. In our experiment, α_p and α_I are very different. The former increases from ~ 1.2 outside LCFS to ~ 2.1 inside LCFS while the latter increases from ~ 2.2 to ~ 2.8 . The potential estimated by α_I and α_t are both higher than V_p even if their trends are similar. This difference will cause an error ($> 20\%$) in electric field calculation and also will lead an ~ 5 mm error in the estimation of LCFS position where $E_r = 0$.

At last, there is another method consider that we should use the first derivative of $V-I$ characteristic, not the second derivative, to calculate EEDF and V_p while the probe is used in magnetic plasma. By using this method, we found that the plasma potential from the first derivative is larger than the one from second derivative but their profile are similar. The α increase from ~ 2.2 outside LCFS to ~ 2.8 inside LCFS. The details will be discuss in the further paper.



First Experiments in H-Mode Plasmas with the Passive-Active Multijunction LHCD Launcher in HL-2A and Impact on Pedestal Instabilities

A. Ekedahl¹, X. Bai², B. Lu², and R. Magne¹

¹*Institut de Recherche sur la Fusion par confinement Magnétique (IRFM),*

Commissariat à l'énergie atomique (CEA/Cadarache), 13108 Saint-Paul-lès-Durance, France

²*Southwestern Institute of Physics, Chengdu, Sichuan, People's Republic of China*

Corresponding Author: A. Ekedahl, annika.ekedahl@cea.fr

The passive-active multijunction (PAM), a relevant lower hybrid current drive (LHCD) launcher design, was developed in view of a LHCD system for the second phase of ITER [1]. PAM launchers have so far been successfully tested in L-mode plasmas on FTU [2] and Tore Supra [3]. This paper presents the first ever experiments with a PAM on H-mode plasmas, carried out on HL-2A tokamak [4] as a joint project between SWIP and CEA/IRFM. This paper gives an overview of the LHCD system on HL-2A, the design of the PAM launcher and the first experiments performed. This involves coupling experiments in L-mode and H-mode plasmas, ELM-mitigation studies and modification of the plasma turbulence at the pedestal. The coupling experiments in H-mode were carried out in lower single null plasmas with ~ 1 MW of neutral beam (NB) heating. If the NB power was less than 800 kW, the additional LHCD power (200–500 kW) triggered and sustained the H-mode. The LHCD power was coupled during type-I ELMs at large plasma-launcher gap (> 10 cm). Nonhomogeneous power reflection coefficients (RC) were observed along the poloidal rows on the launcher, which could partly be attributed to larger plasma-launcher gap for the top rows. Local gas injection from the near gas puffing system was found primordial to reduce RC at large plasma-launcher gaps. Increase in ELM frequency and decrease in ELM amplitude were observed during LHCD power modulations. This ELM mitigation effect was sensitive to electron density and LHCD power. Increase of the pedestal turbulence measured by Doppler reflectometry was also observed, suggesting that an enhancement of the particle transport due to pedestal turbulence could be the reason for the ELM mitigation. In summary, these first LHCD PAM experiments on HL-2A have shown that the PAM launcher is a viable concept for high performance scenarios. The LHCD power can be coupled at large plasma-launcher gap, assist in triggering and sustaining H-modes, as well as affect the ELM behaviour.

References

- [1] G. T. Hoang, *et al.*, Nucl. Fusion **49**, 075001 (2009).
- [2] V. Pericoli Ridolfini, *et al.*, Nucl. Fusion **45**, 1085 (2005).
- [3] A. Ekedahl *et al.*, Nucl. Fusion **50**, 112002 (2010).
- [4] M. Xu, X. R. Duan, *et al.*, Nucl. Fusion **55**, 104022 (2015).



Spectroscopic Studies on GLAST-III Tokamak by Varying the Inductance and Charging Voltage of Vertical Field Coils

F. Deeba¹, A. Qayyum¹, Z. Ahmad¹, S. Ahmad¹, R. Khan¹, and S. Hussain¹

¹National Tokamak Fusion Program (NTFP), Islamabad, Pakistan

Corresponding Author: F. Deeba, establish_87@hotmail.com

Optical emission spectroscopy is applied as a diagnostic tool to investigate the plasma in GLAST-III (glass spherical tokamak) at different scenarios. It is a small limiter device having aspect ratio ($R/a = 2$) with major radius $R = 20$ cm and minor radius $a = 10$ cm. Spectral analysis is performed to study the plasma induced optical emission and the electron temperature for different values of charging voltage, and inductance of vertical field (VF) coils. The inductance of the VF is changed by varying number of inductors in series systematically. HR-4000 spectrometer is used to record the spectrum in the visible range (280–750 nm). The electron temperature is determined from the emission intensity of argon (Ar is used as feed gas) lines by using Boltzmann plot method. The optical emission is also recorded using photodiode BPX65. H_{α} line impurity is monitored using a monochromator with fixed position of grating at 656.28 nm, and intensity follows the plasma current during discharge. The results indicate that the emission intensity decrease with increase of the inductance of VF coils. Consequently, with addition of inductors the plasma current, and electron temperature both are reduced. The effect of charging voltage of VF coils on the plasma current and hence electron temperature is also calculated. It is observed that with the increase of charging voltage of PF coils, the plasma current increases, attain a maximum value and then after a critical value of charging voltage the plasma current starts decreasing.

EX

Studies on ISTTOK during Edge Electrode Biasing Assisted AC Operation

A. Malaquias¹, R. B. Henriques¹, C. Silva¹, H. Figueiredo¹, I. S. Nedzelskiy¹, and H. Fernandes¹

¹*Instituto Superior Técnico (IST), Lisbon, Portugal*

Corresponding Author: A. Malaquias, artur.malaquias@ipfn.ist.utl.pt

It has been experimentally established in ISTTOK that edge electrode biasing under appropriated conditions improves confinement by reducing radial transport. In order to improve the repeatability and reproducibility of AC operation, edge electrode biasing was used to assist the transition of plasma current applied at different time lapses of the AC discharge. This paper presents the results of these studies. It has been observed that during ISTTOK AC discharges the restart of each plasma pulse depends on factors such as machine conditioning, operating background pressure, balanced external magnetic fields and on the level of current and plasma density just before the transition of the primary current. The control of the plasma density in the quiescent phase is made just before the AC transition by means of edge polarization leading to a transitory improved confinement that could be responsible to keep a more favourable quiescent plasma conditions. In addition, applying bias during the start-up of the following AC cycle, at proper time stamps, induces favourable modifications on the pressure-like profile as measured by the heavy ion beam diagnostic.

EX



Contribution of Joint Experiments on Small Tokamaks in the Framework of IAEA Coordinated Research Projects to Mainstream Fusion Research

J. Stockel¹, M. Gryaznevich², G. Van Oost³, and A. Melnikov⁴

¹*Institute of Plasma Physics AS CR v.v.i., Prague, Czech Republic*

²*Tokamak Energy Ltd, Abingdon, UK*

³*Ghent University, 9000 Ghent, Belgium*

⁴*National Research Centre "Kurchatov Institute", Moscow, Russian Federation*

Corresponding Author: J. Stockel, stockel@ipp.cas.cz

Small magnetic fusion devices continue to contribute to many areas of fusion research because of their compactness, flexibility, low operation costs and the high skill of their personnel. The concept of interactive coordinated joint research using small devices in the scope of IAEA Coordinated Research Projects (CRP) was started in 2004 with as overall objective to contribute to streamlining the contributions of small magnetic confinement fusion devices to mainstream fusion research by establishing a network of cooperation enabling coordinated investigations of topics of relevance to physics, diagnostics and technology issues of next step fusion devices such as ITER and DEMO.

In particular the Joint Host Laboratory Experiments (JE) have been very instrumental in coordinating the scientific investigations (their nature, contents, analyzes and outputs) as well as the development and application of novel diagnostics and technologies. In total, eight JEs have been carried out in the framework of the IAEA Coordinated Research Projects on "Joint Research Using Small Tokamaks" (2004–2008) and on "Utilization of a Network of Small Magnetic Confinement Fusion Devices for Mainstream Fusion Research" (2011–2015) on the tokamaks CASTOR, COMPASS and GOLEM (Czech Republic), T-10 (Russia), ISTTOK (Portugal), TCABR (Brazil) and STOR-M (Canada).

These JEs have been very instrumental in enabling collaborative studies of relevance to mainstream fusion research. Experimental, theoretical, and modelling activities conducted throughout the CRP lifetime have covered specific areas of physics, diagnostics and technology. Overall, the JEs have substantially contributed to capacity building and human resource development in various institutions in IAEA member states. This represents a significant asset in the provision of future skilled experts that will make possible the implementation of next steps in fusion energy development.

This work was partly funded by the IAEA technical contracts under IAEA Coordinated Research Projects (CRP) on "Joint Research Using Small Tokamaks" and on "Utilization of a Network of Small Magnetic Confinement Fusion Devices for Mainstream Fusion Research". Joint Experiments on the COMPASS tokamak were partly funded by the projects MSMT LM2011021.

Modification of Toroidal Flow Velocity through Momentum Injection by Compact Torus Injection into the STOR-M Tokamak Discharge

C. Xiao¹, A. Rohollahi¹, S. Elgriw¹, J. Adegun¹, D. Basu¹, M. Nakajima¹, T. Onchi², M. Patterson¹, J. Zhang¹, and A. Hirose¹

¹University of Saskatchewan, Saskatoon, SK S7N-5C9, Canada

²Kyushu University, Kasuga, Japan

Corresponding Author: C. Xiao, chijin.xiao@usask.ca

EX Plasma flow and its shear in tokamak discharges have many beneficial effects including suppression of turbulence, confinement improvement, control of the resistive wall modes, as well as enhanced tolerance to the error fields which may cause mode locking and even major disruptions. CT injection has also been considered not only as a candidate to directly fuel the core of a tokamak reactor, but also as a means to inject momentum leading to modification of plasma flow velocities. This paper reports on the first-ever evidence of modification of toroidal flow velocity by momentum injection by tangentially injecting a compact torus (CT) into the STOR-M tokamak discharge. In the previous experiments, the CT was injected into the tokamak discharge along the tokamak discharge current direction. It has been observed that CT injection suppressed magnetic fluctuations and also induced modification of the toroidal flow velocity towards the CT injection direction or cocurrent direction, similar to the flow velocity modification by resonant magnetic perturbations which also suppresses magnetic fluctuations. In order to clarify whether the flow modification after CT injection is due to suppression of magnetic fluctuations or due to momentum injection, the tokamak discharge direction was reversed and the CT was then injected in the countercurrent direction. Experimental observations reveal that modification is still in the CT injection or countercurrent direction although the intrinsic flow direction was reversed along with the discharge current. This observation strongly suggests that CT injection indeed injects momentum into the tokamak discharge and modifies the plasma flow. The experimental results demonstrate the additional benefit of CT fuelling for future tokamak reactors.



High Frequency Magnetic Oscillations in the TUMAN-3M Ohmically Heated Plasmas

S. Lebedev¹, L. Askinazi¹, A. Belokurov¹, V. Kornev¹, A. Tukachinsky¹, and N. Zhubr¹

¹*Ioffe Institute, St. Petersburg, Russian Federation*

Corresponding Author: S. Lebedev, sergei.lebedev@mail.ioffe.ru

Bursts of high frequency oscillations have been found in Ohmically heated plasmas in the TUMAN-3M using magnetic probes sited inside vacuum vessel. Typical frequencies of the oscillations are within 0.8–1.8 MHz range. It was found that the frequency of the oscillations followed the dependence of Alfvén velocity on toroidal magnetic field and density. This dependence allowed identifying the oscillations as Alfvén waves (AW). The observation is of interest since AWs are usually driven by energetic ions produced by strong auxiliary heating and thus are unexpected in Ohmic regime.

In the recent experiments isotope dependence of frequency measured in H and D plasmas has proved the Alfvén nature of the oscillations. Ratio of the oscillation frequency to Alfvén velocity is approximately constant in both working gases and at all velocities. In many cases bursts of AW oscillations are strongly linked to moments of magnetic reconnections arising due to sawtooth crashes or strong MHD events. Duration of bursts is typically in the range of 0.1–0.2 ms. The oscillations are quenched shortly after reconnection phases. Excitation of these AWs in Ohmic plasma without energetic ions could be understood in frames of the model of percussive magnetic perturbations arising due to reconnection events.

Besides the bursting modes, the patches of quasi-continuous oscillations were detected. The oscillations start 0.1–0.2 ms after reconnection event and persist 0.3–0.8 ms until next reconnection. Their spectra are by an order of magnitude narrower than in bursting cases: 20–40 kHz compared to 200–400 kHz. Coexistence of two quasi-continuous modes with different frequencies should be noticed. Frequency difference of these modes is up to 350 kHz. Trigger mechanism of quasi-continuous mode excitation is not evident and should be further analyzed. Energetic ions accelerated up to Alfvén velocity by electric field produced during reconnection process are candidate driver. Besides the energetic ions, runaway or subthermal electrons could be considered as a driver of the oscillations. Possible driving mechanism is the resonance interaction with precessional drift frequency of energetic particles or with diamagnetic drift frequency. Observation of correlation between quasi-continuous mode amplitude and amount of runaway electrons in TUMAN-3M plasma supports the hypothesis.

EX

Effect of the Transition to Improved Core Confinement Observed in the LHCD Experiment at FT-2 Tokamak

S. I. Lashkul¹, A. Altukhov¹, A. Gurchenko¹, E. Z. Gusakov¹, V. Dyachenko¹, L. Esipov¹, M. Irzak¹, M. Kantor¹, D. Kouprienko¹, A. Perevalov², A. Saveliev¹, and S. Shatalin²

¹Ioffe Institute, St. Petersburg, Russian Federation

²St. Petersburg State Polytechnical University, St. Petersburg, Russian Federation

Corresponding Author: S. I. Lashkul, serguey.lashkul@mail.ioffe.ru

To explain a relatively good efficiency of LHCD and improved core confinement transition obtained at the small FT-2 tokamak ($R = 0.55$ m, $a = 0.08$ m, $B_t \leq 3$ T, $I_p = 35$ kA, $f_0 = 920$ MHz, $\Delta t_{pl} = 50$ ms, $\Delta t_{RF} = 30\text{--}36$ ms) [1] a thorough modelling of experimental data has been performed. Effect of LHW on the transition into improved core confinement regime is discussed in the deuterium plasma experiment. It was observed, that in the LHCD experiment with initial OH density $\langle n_e \rangle = 1.6 \times 10^{19}/\text{m}^3$ the central electron temperature $T_e(r = 0$ cm) measured by TS diagnostics increases during RF pulse from 550 eV to 700 eV and that is accompanied by cooling of the plasma periphery and the density rise. This effect could not be explained by increase of working gas or impurity recycling because the D_β line intensity and radiation losses during RF pulse is not appreciably changed.

EX

According to GRILL3D, FRTC and ASTRA codes modelling the increase of the density and electron temperature T_e inside of $r < 3$ cm (despite the decrease of ohmic heating power P_{OH} at LHCD) happens due to strong reduction of the electron transport in this region where the magnetic shear vanishes, and the value of thermal diffusivity $\chi_{e,\text{eff}}$ decreases. Broadening of the plasma current profile by noninductive LHCD results in flattening of the safety factor q profile in the plasma column centre. As the result, the magnetic shear $s = (r/q)(dq/dr)$ in the centre became low, or even negative. In such a case the transport code (where the electron transport was described by the mixed Bohm and gyro-Bohm model) predicts a reduction of the transport [2].

This paper presents new experimental data and modelling results appropriate to the transition to improved core confinement during LHCD experiment. In particular, special attention one attends to the experimental periphery data and data of the threshold power for transition to improved core confinement in deuterium and hydrogen plasma.

References

[1] S. I. Lashkul, A. B. Altukhov, A. D. Gurchenko, *et al.*, Nucl. Fusion **55**, 073019 (2015).

[2] Y. Peysson and the TORE SUPRA Team., Plasma Phys. Control. Fusion **42**, B87-B114 (2000).

This work (for S. I. Lashkul and FT-2 team) was supported in part by the Russian Foundation for Basic Research project No. 14-08-00476.

Runaway Electrons Studies with Hard X-Ray and Microwave Diagnostics in the FT-2 Low-Hybrid Current Drive Discharges

A. Shevelev¹, E. Khilkevitch¹, S. I. Lashkul¹, V. Rozhdestvensky¹, A. Altukhov¹,
D. Kuprienko¹, I. Chugunov¹, D. Doinikov¹, L. Esipov¹, D. Gin¹, M. Iliasova¹,
V. Naidenov¹, N. Nersesyan¹, I. Polunovskiy¹, A. Sidorov¹, and V. Kiptily²

¹*Ioffe Institute, St. Petersburg, Russian Federation*

²*Culham Centre for Fusion Energy (CCFE), Culham Science Centre, Abingdon, UK*

Corresponding Author: A. Shevelev, shevelev@cycla.ioffe.ru

Analysis of the superthermal and runaway electrons behaviour in ohmic and low-hybrid current drive FT-2 tokamak ($R = 0.55$ m, $a = 0.08$ m, $B_t \leq 3$ T, $I_p = 32$ kA, $\langle n \rangle = 1.9 \times 10^{19}/\text{m}^3$, $f_0 = 920$ MHz) plasmas has been carried out using information obtained from measurements of hard X-ray spectra and nonthermal microwave synchrotron radiation intensity in the frequency range 53–78 GHz [1]. A gamma-ray spectrometer developed for gamma-ray diagnostics of ITER (Nuclear Facility INB-174) and based on $\text{LaBr}_3(\text{Ce})$ scintillator has been used in measurements of hard X-ray emission ($E > 0.1$ MeV) generated by runaway electrons. An advanced digital processing algorithm of the detector signal recorded with high sampling rate has provided a pulse height analysis at rates exceeding $10^7/\text{s}$. A spectrum deconvolution code DeGaSum has been used for reconstruction of the energy distribution of runaway electrons escaping from the plasma and interacting with materials of the FT-2 limiter in the vacuum vessel [2]. The developed digital signal processing technique for $\text{LaBr}_3(\text{Ce})$ spectrometer has allowed studying the evolution of runaways energy distribution in the FT-2 plasma discharges with time resolution of 1 ms. Superthermal electrons accelerated up to 2 MeV by the L-H waves at the high-frequency pumping of the plasma with low density $\langle n_e \rangle \sim 2 \times 10^{13}/\text{cm}^3$ and then up to 6 MeV by vortex electric field have been found. A correlation between the hard X-ray and synchrotron radiations as well as a role of MHD activity is discussed. Analysis of the runaway electron beam generation and evolution of their energy distribution in FT-2 plasmas has been presented in the report.

References

- [1] V. V. Rozhdestvensky, *et al.*, Energy Environ. Eng. **3**(3), 42-49, (2015).
- [2] A. E. Shevelev, *et al.*, Nucl. Fusion **53**, 123004 (2013).

This work was supported in part by the RF State Contract No. N.4k.52.9B.14.1002 and the Russian Foundation for Basic Research projects Nos. 13-08-00411 and 14-08-00476.



Control of Sawtooth Oscillation Dynamics Using Externally Applied Stellarator Transform

D. A. Maurer¹, M. Cianciosi², D. A. Ennis¹, J. D. Hanson¹, G. J. Hartwell¹, J. D. Hebert¹, J. L. Herfindal¹, S. F. Knowlton¹, X. Ma¹, M. Pandya¹, N. Roberts¹, and P. Traverso¹

¹Auburn University, Auburn, AL 36849, USA

²Oak Ridge National Laboratory (ORNL), Oak Ridge, TN 37831, USA

Corresponding Author: D. A. Maurer, dama0014@auburn.edu

The control of sawtooth oscillations is currently an active area of tokamak research. Large sawtooth oscillations need to be avoided in ITER, since these large sawteeth couple to neoclassical tearing modes and edge localized modes resulting in serious confinement degradation. Small sawtooth oscillations, however, may be beneficial in preventing impurity and helium ash accumulation in the centre of the plasma [1]. Sawtooth oscillations are observed in the Compact Toroidal Hybrid (CTH), a current-carrying stellarator/tokamak hybrid device. CTH has the unique ability to change the relative amount of vacuum transform from stellarator coils to that generated by plasma current to change sawtooth oscillation dynamics. The fractional transform, defined as the ratio of imposed vacuum transform to the total transform was systematically varied from 0.04 to 0.43 to observe changes in CTH sawtooth oscillation behaviour. We observe that the normalized inversion surface radius is proportional to the total transform as is found in tokamaks [2]. We also observe that the measured sawtooth period and amplitude decrease with increasing levels of 3D field, as quantified by the amount of vacuum transform imposed. In tokamaks, decrease in the observed sawtooth period has been attributed to a decrease in core electron temperature [3]. The decrease in sawtooth period observed on CTH appears to have no associated decrease in core electron temperature. Finally, the measured crash time of the sawtooth oscillation is independent of the amount of vacuum transform applied, indicating that the final reconnection dynamics of the $m = 1$ and $n = 1$ mode are not significantly affected by the 3D stellarator fields.

References

[1] T. C. Hender, *et al.*, Nucl. Fusion **47**, S128, (2007).

[2] R. T. Snider, Nucl. Fusion **30**, 11 (1990).

[3] P. de Vries, *et al.*, Proc. 28th EPS Conf. on Controlled Fusion and Plasma Physics **25A** (2001).

Work supported by the U.S. Department of Energy Grant No. DE-FG02-00ER54610.



On the Influence of ECRH on Neoclassical and Anomalous Mechanisms Using a Dual Heavy Ion Beam Probe Diagnostic in the TJ-II Stellarator

C. Hidalgo¹, A. Chmyga², L. Eliseev³, S. Khrebtov², A. Komarov², A. Kozachek², L. Krupnik², A. Melnikov³, J. de Pablos¹, S. Perfilov³, A. Zhezhera², V. Zenin³, and M. Ufimtsev⁴

¹*Centro de Investigaciones Energéticas, Medioambientales y Tecnológicas (CIEMAT), Madrid, Spain*

²*Institute of Plasma Physics, National Science Center, Kharkov Institute of Physics and Technology (KIPT), Kharkov, 61108, Ukraine*

³*National Research Centre "Kurchatov Institute", Moscow, Russian Federation*

⁴*Moscow State University, Russian Federation*

Corresponding Author: C. Hidalgo, carlos.hidalgo@ciemat.es

In the present paper we have investigated the influence of ECRH on neoclassical and anomalous mechanisms in the TJ-II stellarator. The results reported here were obtained by the use of a unique diagnostic which consists in two heavy ion beam probe (HIBP) systems located at two different toroidal ports separated by 90°. This dual HIBP was used to study the temporal and spatial evolution of density and plasma potential profiles and long range correlations (LRC) as proxy of zonal flows (ZFs) in the whole plasma cross-section. The unique possibilities of the dual HIBP system allow us to expand the investigation of multiscale mechanisms from the plasma edge to the plasma core. Experiments in plasmas with combined NBI and ECR heating in the TJ-II stellarator have shown direct experimental evidence of the influence of ECRH on turbulent mechanisms, increasing both the level of broadband fluctuation and the amplitude of ZFs, and neoclassical mean radial electric fields. Whereas the influence of ECRH on the level of fluctuations takes place in a wide range of plasma densities, the ECRH induced reversal of the neoclassical radial electric field has been observed only in low-density plasmas. These findings show that multiscale interactions are a crucial ingredient for understanding the influence of ECRH on anomalous and neoclassical transport mechanisms.

EX



Plasma Flow, Turbulence and Magnetic Islands in TJ-II

T. Estrada¹, F. Fernández-Marina¹, E. Ascasibar¹, E. Blanco¹, Á. Cappa¹, C. Hidalgo¹,
K. Ida², A. López-Fraguas¹, and B. van Milligen¹

¹Centro de Investigaciones Energéticas, Medioambientales y Tecnológicas (CIEMAT), Madrid, Spain

²National Institute for Fusion Science (NIFS), Toki, Gifu, Japan

Corresponding Author: T. Estrada, teresa.estrada@ciemat.es

The effect of magnetic islands on plasma flow and turbulence is experimentally investigated in ohmically induced magnetic configuration scans at TJ-II. This operational mode allows sweeping the radial position of a low order rational surface in a controlled way, what reveals effects that are difficult to notice in scans performed on a shot to shot basis. The main diagnostic used in the present work is a Doppler reflectometer (DR). A characteristic signature of the $n/m = 3/2$ magnetic island as it crosses the DR measurement position is clearly detected, showing a modulation in the perpendicular flow that changes twice its direction. This modulation allows the calculation of the radial propagation velocity of the magnetic island as well as an estimation of the island width, being close to 3 cm. As the magnetic island crosses the DR measurement position two peaks appear in the DR signal spectra. The double peak reflects the vortex around the magnetic island O-point. The consistency of the results is confirmed in five different magnetic configurations with slightly different rotational transform in combination with two different OH current intensities. TJ-II results resemble those found in LHD where the plasma flow is measured along the 1/1 magnetic island. Fluctuations of the perpendicular flow and density have been also measured along the 3/2 magnetic island. An increase in the low frequency flow oscillations is measured at the magnetic island boundaries together with a reduction in the density fluctuation level; the later being more pronounced at the inner island boundary. These observations could explain the link between magnetic islands and transport barriers observed in a number of fusion devices like TJ-II. Further studies have been performed to characterize the radial correlation properties of the density fluctuations in the presence of magnetic islands, both numerically and experimentally in TJ-II. The analysis of the density fluctuations simulated using a MHD code shows that in the presence of a magnetic island the coherence profile shows a characteristic asymmetry. This asymmetry is also detected by the Doppler reflectometer synthetic diagnostic. Experimentally, asymmetric coherence profiles have been eventually found which can be interpreted to be due to magnetic islands.

EX



Plasma Core Fuelling by Cryogenic Pellet Injection in the TJ-II Stellarator

K. J. McCarthy¹, N. Panadero¹, J. L. Velasco¹, J. Hernandez¹, R. Garcia¹, D. López-Bruna¹, J. Baldzuhn², A. Dinklage², R. Sakamoto³, and E. Ascasibar¹

¹Laboratorio Nacional de Fusión (LNF),

Centro de Investigaciones Energéticas, Medioambientales y Tecnológicas (CIEMAT), Madrid, Spain

²Max-Planck-Institut für Plasmaphysik, Greifswald, Germany

³National Institute for Fusion Science (NIFS), Toki, Gifu, Japan

Corresponding Author: K. J. McCarthy, kieran.mccarthy@ciemat.es

Core plasma fuelling is a critical issue on the pathway to developing steady-state scenarios in 3D magnetically confined plasma devices. Indeed, neoclassical theory predicts that on-axis electron cyclotron resonance heating (ECRH) requires a particle source situated at the same radial position as ECRH with an analogous deposition profile shape in order to mitigate potential core particle depletion [1]. A prime candidate for core fuelling is cryogenic pellet injection [2]. However, a detailed understanding of pellet ablation mechanisms, and subsequent particle transport, remains outstanding and is of paramount interest for stellarators.

A pellet injector (PI) is operating on the TJ-II stellarator [3]. It is a 4-pellet system, developed in conjunction with the Fusion Energy Division at Oak Ridge National Laboratory Tennessee [4] with in-situ pellet formation, fast propellant valves for pellet acceleration (800 to 1200 m/s), plus in-line diagnostics and optical access to the pellet path through the plasma (diodes and a fast frame camera collect the luminescence light emitted by the neutral, or partially ionized, cloud that surrounds an ablating pellet). On TJ-II, hydrogen pellets are injected into plasmas created using a range of magnetic configurations and heated by ECRH, neutral beam injection heating or by both. Studies are made of pellet ablation and penetration, neutral cloud evolution, particle transport and confinement, as well as fuelling efficiency. The findings can provide input for the W7-X pellet injection programme, this being of critical importance for neoclassical transport optimization in W7-X and the attainment of long-pulse high-power discharges with pure microwave heating.

References

- [1] H. Maaßberg, *et al.*, Plasma Phys. Control. Fusion **41**, 1135 (1999).
- [2] B. Pégourié, Plasma Phys. Control. Fusion **49**, R87 (2007).
- [3] K. J. McCarthy, *et al.*, Proc. of Science 134, (ECPD2015).
- [4] S. K. Combs, *et al.*, Fusion Sci. Technol. **64**, 513 (2013).

Work carried out within the framework of the EUROfusion Consortium with funding from the Euratom research and training programme 2014–2018 under grant agreement No. 633053. The views and opinions expressed herein do not necessarily reflect those of the European Commission. In addition, it is partially financed by a grant from the Spanish Ministerio de Ciencia y Innovación (Ref. ENE2013-48679-R).



Confinement Modes and Magnetic-Island Driven Modes in the TJ-II Stellarator

D. López-Bruna¹, M. A. Ochando¹, B. Sun¹, and M. A. Pedrosa¹

¹Centro de Investigaciones Energéticas, Medioambientales y Tecnológicas (CIEMAT), Madrid, Spain

Corresponding Author: D. López-Bruna, daniel.lopezbruna@ciemat.es

Magneto-hydrodynamic (MHD) activity is ubiquitous in magnetic confinement plasmas and is related with confinement states. Particularly, confinement quality in TJ-II plasmas is intimately linked to the location and behaviour of magnetic resonances in the plasma column, which often manifest themselves as magnetic islands. Two main physical processes have been identified that relate confinement and magnetic-island driven modes, always in the low-frequency range of magnetic spectra: magnetic-island-induced Alfvén eigenmodes (MIAE) with frequencies normally below helicity-induced but above β -induced eigenmodes (BAE, ~ 20 kHz) under NBI heating; and island rotation yielding frequencies generally below 100 kHz in both ECR and NBI heated plasmas.

MIAEs behave like shear-Alfvén waves. They are identified under the hypothesis that nonrotating islands add well-defined helicities to the B -field spectrum and, in presence of rotating islands, new modes at composed frequencies are also excited. This is a first link between magnetic islands and AEs in stellarators [1]. Island-AE couplings open the possibility of energy channelling between MHD scales [2], with such consequences as bridging fast-particle energy towards dissipation scales through wave energy cascading.

Island rotation modes are normally seen when the main magnetic resonances are located in the outer half of the plasma. Stable rotation can be found in ECR and NBI L-mode plasmas, both at a frequency compatible with $E \times B$ rotation [3]. In H-mode plasmas the rotation speed tends to increase but the mode dims noticeably or becomes undetectable. Unstable rotation with chirping-down frequencies is found at the threshold between L- and H-modes of confinement and can be ascribed to the diamagnetic rotation of the same islands chain in the $E \times B$ frame [3]. The chirping is due to a repetitive breaking of a transport barrier located at or by the magnetically resonant region, and it provokes typical I-mode phenomenology [4].

References

- [1] B. J. Sun, *et al.*, Nucl. Fusion **55**, 093023 (2015).
- [2] W. Chen, *et al.*, Europhys. Lett. **107**, 25001 (2014).
- [3] B. J. Sun, *et al.*, 41st EPS Conference Berlin **38**, P2.090 (Germany, 2014).
- [4] D. G. Whyte, *et al.*, Nucl. Fusion **50**, 105005 (2010).

Progress of Steady State Operation Using RF Heating in the LHD

Y. Yoshimura¹, H. Kasahara¹, S. Kamio¹, M. Tokitani¹, R. Sakamoto¹, Y. Ueda², S. Kubo¹, T. Shimozuma¹, H. Igami¹, H. Takahashi¹, T. I. Tsujimura¹, R. Makino¹, T. Seki¹, K. Saito¹, R. Seki¹, T. Akiyama¹, N. Ashikawa¹, S. Masuzaki¹, G. Motojima¹, M. Shoji¹, C. Suzuki¹, H. Tanaka¹, K. Tanaka¹, T. Tokuzawa¹, I. Yamada¹, Y. Goto³, H. Yamada¹, T. Mutoh¹, A. Komori¹, and Y. Takeiri¹

¹National Institute for Fusion Science (NIFS), Toki, Gifu, Japan

²Osaka University, Osaka, Japan

³Nagoya University, Nagoya, Japan

Corresponding Author: Y. Yoshimura, yoshimu@ms.nifs.ac.jp

Plasmas with the improved electron confinement state, electron internal transport barrier (e-ITB), have been investigated with short pulse discharges (< 1 s). Recent upgrade of ECH system enabled ECH power up to 0.6 MW at the pulse duration longer than a few minutes. Effective on-axis heating with the increased ECH power realized exploration of the possibility of long pulse sustainment of high performance plasmas having e-ITB, without negative effects of impurity accumulation and/or current diffusion. A plasma discharge #122257 (magnetic axis position $R_{ax} = 3.65$ m, average magnetic field on the magnetic axis $B_t = 2.712$ T) with the line average electron density $n_{e,ave} = 1.1 \times 10^{19} \text{ m}^{-3}$ and the central electron temperature $T_{e0} = 3.5$ keV was stably sustained for 330 s by ECH power of 340 kW. The T_e profile had fine ITB structure, and it was kept stably all over the discharge duration. The discharge #131054 ($R_{ax} = 3.6$ m, $B_t = 2.75$ T) was performed with nearly the same $n_{e,ave}$ and ECH power of ~ 350 kW, while there was no ITB, and T_{e0} was 2.7 keV. Calculation of ECH power deposition using TRAVIS code tells that the deposition power density at the plasma centre in #122257 (with ITB), 2 MWm^{-3} , is twice higher than that of #131054 (w/o ITB), 0.93 MWm^{-3} . Accumulation of the impurity and increase in radiation power are not recognized in these discharges.

Improvement of ICH system by an additional impedance transformer realized ICH power increment up to 1.5 MW. Keeping the minority hydrogen ion ratio H/(H+He) of plasmas not less than ~ 0.1 by repetitive H pellet injection mitigated the acceleration of risky fast hydrogen ions. Without the H pellets, the minority ion ratio tends to decrease by majority He gas fuelling. Modification of the structure of divertor plates contributed to the reduction of impurity influx events. In FY 2014, with these improvements, long pulse sustainment at higher density region over $2 \times 10^{19} \text{ m}^{-3}$ was investigated. About 2 MW in total of ICH and ECH powers sustained a plasma with $n_{e,ave}$ of $2.2 \times 10^{19} \text{ m}^{-3}$ for 8 min, while the former 48 min discharge with $n_{e,ave}$ of $1.2 \times 10^{19} \text{ m}^{-3}$ was sustained by ICH and ECH total power of 1.2 MW. So far, out-gas (density increase) and/or occurrence of sparks (intense impurity influx) at the plasma facing components are the main causes of the termination of the long pulse discharges in the LHD.



Impact of the LHD Peripheral Region and the Magnetic Axis Shift on Optimal On-Axis ECRH Injection for High-Electron-Temperature Plasmas

T. I. Tsujimura¹, S. Kubo¹, H. Igami¹, R. Makino¹, H. Takahashi¹, T. Shimozuma¹, Y. Yoshimura¹, R. Seki¹, M. Yokoyama¹, M. Osakabe¹, and T. Mutoh¹

¹National Institute for Fusion Science (NIFS), Toki, Gifu, Japan

Corresponding Author: T. I. Tsujimura, tsujimura.tohru@nifs.ac.jp

The central electron temperature of high-ion-temperature plasmas was successfully increased in the large helical device (LHD) up to 7.6 keV for the central ion temperature of 6 keV and a central electron density of $1.4 \times 10^{19} \text{ m}^{-3}$ by adding a new 154 GHz gyrotron and also by optimization of the ECRH (electron cyclotron resonance heating) injection. The optimization was carried out using the ray-tracing code "LHDGauss," upgraded to include three new features: 1) rapid postprocessing 3D equilibrium mapping, 2) refraction of rays in the peripheral region with the finite density gradient outside of the last closed flux surface, and 3) calculations of the ordinary/extraordinary (O/X) mode ratio. The absolute value of the power deposition profiles calculated at every shot enables feedback of the injection condition for the required deposition profile on a shot-by-shot basis, which resulted in the achievement of the high-temperature plasma. The impact of a plasma peripheral region not only on refraction of rays but also on pure excitation of the O/X mode is a common characteristic in magnetically confined plasmas with comparable scale lengths for the density and the magnetic shear angle, e.g., the stochastic region of LHD plasmas, or tokamak pedestal/SOL (scrape-off layer) plasmas. The adjustment of the ECRH injection settings using the ray-tracing code integrating the LHD peripheral region in 3D equilibrium mapping has contributed to the successful extension of the LHD operational regime.

EX

Global Particle Balance and its Relationship with the Plasma Wall Interaction Emerging in Long Pulse Discharges on the Large Helical Device

G. Motojima¹, M. Yajima¹, S. Masuzaki¹, M. Tokitani¹, N. Yoshida², Y. Ueda³, M. Oya³, H. Yamada¹, R. Sakamoto¹, H. Tanaka¹, T. Morisaki¹, M. Sakamoto⁴, and H. Kasahara¹

¹National Institute for Fusion Science (NIFS), Toki, Gifu, Japan

²Kyushu University, Kasuga, Japan

³Osaka University, Osaka, Japan

⁴Plasma Research Center, University of Tsukuba, Tsukuba, Ibaraki, Japan

Corresponding Author: G. Motojima, motojima.gen@lhd.nifs.ac.jp

We report the global particle balance analysis and its relationship with the plasma wall interaction emerging for the first time in long pulse helium discharges reaching 48 min on the Large Helical Device (LHD). Experimental observations show that i) the wall retention has dynamic characteristics and the differences of the plasma facing material, which are composed of the first wall with stainless steel and the divertor with graphite, is a possible candidate to explain the wall retention, and ii) the mixed-material deposition layer which plays an important role in the wall retention is quantified by the reflection measurement, suggesting that the deposition-dominant area of the outer torus side and near the divertor in the measured toroidal section is a possible sink of the wall retention on the first wall.

The understanding of the wall retention of the fuel particles is crucial from the viewpoint of the efficient fuelling and the inventory of tritium. In LHD, the wall retention has been investigated for steady-state long pulse discharges. Analysis of the global particle balance is conducted in the long-pulse helium discharge heated by ICH+ECH (1.2 MW × 48 min = 3.4×10^3 MJ). The wall inventory is separated into three phases. In the first phase, quite high wall inventory occurs. After the first phase, the wall inventory shows modest declination in the second phase. However, the high wall inventory appears again in the third phase. The physics of the phased retention is discussed based on an assumption that there are two kinds of helium reservoir, “first wall with stainless” and “divertor plate with graphite”.

An innovative measurement technique is employed for obtaining in broad spatial extent and in great detail the colour information, equivalent to the reflectivity, by a handy colour analyzer. The relation between the colour and the thickness of the deposition layer is revealed by the long-term exposed samples. Experimental observations show that the thickness decreases exponentially with the averaged RGB (Red, Green, and Blue) values. The RGB mainly of the stainless steel plates on the helically twisted coil in one of 10 toroidal sections of the vacuum vessel is measured. The results indicate that about 60% of the area on the measured helical coil, which is the outer torus side and near the divertor, suggests a sink of the wall retention.

Strong Suppression of Impurity Accumulation in Steady-State Hydrogen Discharges with High Power NBI Heating on LHD

Y. Nakamura¹, N. Tamura¹, M. Yoshinuma¹, C. Suzuki¹, S. Yoshimura¹, M. Kobayashi¹, M. Nakata¹, K. Nagaoka¹, K. Tanaka¹, B. Peterson¹, K. Ida¹, M. Osakabe¹, and T. Morisaki¹

¹National Institute for Fusion Science (NIFS), Toki, Gifu, Japan

Corresponding Author: Y. Nakamura, nakamura.yukio@nifs.ac.jp

EX Impurity behaviour in normal long pulse hydrogen discharges with a flat density profile is investigated in a wide operational range and steady state operational regimes providing stationary radiation loss conditions at an acceptable level are explored in LHD. As reported before, impurity transport studies in long pulse discharges provide two different physical pictures based on neoclassical impurity transport in the core plasma and on classical theory in the SOL region. For helical plasmas, impurity behaviour is generally dominated by the radial electric field (positive in the electron root and negative in the ion root) and impurity accumulation is always observed in the ion root with a large negative radial electric field. On the other hand, intrinsic impurities are shielded by friction force at high edge collisionality in the ergodic layer. Density scans with the same heating power reveal some impurity accumulation window. Recently, high NBI heating power of more than 10 MW is available to long pulse operation and strong suppression of impurity accumulative behaviour is observed. Density scan experiments show that there is no impurity accumulation even in a specific collisionality range (impurity accumulation window), where the intrinsic impurities (Fe, C) are always accumulated into the plasma core in the previous discharges. A new excellent operational regime without impurity accumulation is found in steady state hydrogen discharges. The high power heating plasmas in impurity accumulation window have a large negative radial electric field as well as that in low power discharges. A new contribution to impurity transport is required to explain the strong suppression of impurity accumulation. Studies on parameter dependence of carbon density profile show that core carbon density gradient decreases with increasing ion temperature gradient and carbon Mach number (toroidal rotation velocity). These similar correlations are also observed in the ASDEX-Upgrade tokamak plasmas and explained by the modelling as due to a combination of the turbulent regime and an impurity flux driven by rotation gradient, both of which are indirectly determined by the auxiliary heating power. Thus, the large outward contribution to impurity transport will be discussed with turbulent transport and toroidal rotation effect.

Formation of Impurity Transport Barrier in LHD Plasmas with Hollow Density Profile

X. Huang¹, T. Oishi¹, S. Morita¹, I. Murakami¹, M. Goto¹, H. Zhang², and Y. Liu²

¹National Institute for Fusion Science (NIFS), Toki, Gifu, Japan

²Graduate University for Advanced Studies (SOKENDAI), Hayama, Kanagawa, Japan

Corresponding Author: X. Huang, huang.xianli@nifs.ac.jp

In the Large Helical Device (LHD), the n_e profile can exhibit a peaked, flat or hollow shape. For the purpose of heavy impurity control, it is important to investigate the effect of n_e profile on the impurity transport.

Radial emissions profiles of Fe¹⁶⁺ through Fe²³⁺ ions have been simultaneously measured in the Fe L_α array. The total iron density ($N_{\text{Fe}}(\rho)$) profile is then calculated for peaked and hollow n_e profiles with $R_{ax} = 3.6$ m and $B_t = 2.75$ T. When the n_e profile is peaked (hollow), the N_{Fe} also exhibits a peaked (hollow) profile. The $N_{\text{Fe}}(\rho = 0)$ at the peaked n_e profile is at least one order of magnitude higher than that at the hollow n_e profile over a wide n_e range. The result strongly suggests the iron transport in the plasma core is entirely different between the two cases.

A one-dimensional impurity transport code is employed to simulate the time-dependent iron density profile. Minimization process of the error between measurement and simulation determines the transport coefficients. The convective velocity (V) is assumed to be proportional to the ion charge q . The iron transport is analyzed without assumption on the radial structure of transport coefficients because the Fe L_α transitions are distributed in a wide radial range.

The diffusion coefficient (D) profile is very similar between peaked and hollow n_e profiles, while the D gradually increases toward the plasma edge from the centre. On the other hand, the profile of V averaged among Fe¹⁶⁺ through Fe²³⁺, is entirely different. In the peaked n_e profile, the V is inward and increases from the centre to the edge. This indicates the impurity accumulation easily occurs with a peaked n_e profile. In the hollow n_e profile, an outward V is obviously observed inside $\rho = 0.8$. Near the edge, the V changes from outward to inward where the n_e gradient changes the sign from positive to negative. Due to this quick change in the V profile, the iron ions are pushed back outwards and concentrated near the edge. An impurity transport barrier is thus formed. As a result the large difference in the $N_{\text{Fe}}(\rho = 0)$ in the two cases can be well explained. Since hollow n_e profiles are usually observed in high-temperature and low-collision plasmas with high NBI power input, the present result demonstrates that the control of heavy impurities is possible in LHD by controlling the n_e profile.

EX

Experimental Observations and Modelling of Poloidal Asymmetries in Radiation Profiles during N₂ Seeding Compared with Ne Seeding in LHD

B. Peterson¹, G. Kawamura¹, K. Mukai¹, S. Dai², S. Masuzaki¹, T. Akiyama¹, M. Kobayashi¹, H. Tanaka¹, S. N. Pandya³, R. Sano¹, M. Goto¹, G. Motojima¹, R. Sakamoto¹, N. Ohno⁴, T. Morisaki¹, and J. Miyazawa¹

¹National Institute for Fusion Science (NIFS), Toki, Gifu, Japan

²Dalian University of Technology, Liaoning, Dalian, Ganjingzi, People's Republic of China

³Institute for Plasma Research (IPR), Bhat, Gandhinagar, India

⁴Graduate School of Engineering, Nagoya University, Nagoya, Japan

Corresponding Author: B. Peterson, peterson@lhd.nifs.ac.jp

EX Various noble gasses have been seeded in the Large Helical Device (LHD) to reduce the divertor heat load through enhanced radiation [1]. At the vertically elongated cross-section, in the case of N₂ seeding, bolometric images show additional outboard radiation, while in the case of Ne, only inboard radiation is observed. With N₂ seeding, radiation is observed by two imaging bolometers [2], viewing the same poloidal cross-section from top and bottom ports, respectively, at a location which is 36 degrees toroidally removed from the N₂ gas puff nozzle located at the bottom of the machine. These measurements both confirm that the additional radiation from the outboard side is coming exclusively from the top of the cross-section, indicating poloidal asymmetry. Triangulation between the two imaging bolometer signals indicates that the additional outboard radiation is coming from near the upper part of the last closed flux surface, and that the standard inboard radiation is coming from the upper X-point region. With N₂ seeding the radiation enhancement is observed to be from 20–100% depending on the discharge, while the reduction in divertor heat load indicated by I_{sat} was more than 50% in some locations but varied strongly toroidally, while in the case of Ne the I_{sat} signals are quite uniform toroidally. Modelling by EMC3-EIRENE [3] shows that the outboard radiation is enhanced with N₂ (versus Ne) seeding and with reduced recycling (0 versus 100%) indicating that the localized outboard radiation may be attributed to reduced recycling of N₂. Also, modelling with EMC3-EIRENE using a 90 degree (toroidally) model can reproduce the upper localization of the radiation at a cross-section which is 36 degrees toroidally separated from the N₂ source located at the bottom of the cross-section as is the case in the experiment.

References

- [1] K. Mukai, *et al.*, Nucl. Fusion **55**, 083016 (2015).
- [2] B. J. Peterson, *et al.*, Rev. Sci. Instrum. **74**, 2040 (2003).
- [3] G. Kawamura, *et al.*, Contrib. Plasma Phys. **54**, 437 (2014).

Flow Damping Due to the Stochastization of Magnetic Field in Large Helical Device

K. Ida¹, M. Yoshinuma¹, H. Tsuchiya¹, T. Kobayashi¹, C. Suzuki¹, M. Yokoyama¹,
A. Shimizu¹, K. Nagaoka¹, S. Inagaki², and K. Itoh¹

¹National Institute for Fusion Science (NIFS), Toki, Gifu, Japan

²Kyushu University, Kasuga, Japan

Corresponding Author: K. Ida, ida@nifs.ac.jp

Abrupt damping of toroidal flow associated with a transition from nested magnetic flux surface to a stochastic magnetic field is observed when the magnetic shear at the rational surface decreases to 0.5 in the Large Helical Device (LHD). 1) This flow damping and resulting profile flattening is much stronger than that expected from the Rechester–Rosenbluth model. 2) The stochastization starts from the rational surface and expands radially, and then propagates to the magnetic axis rapidly. 3) The toroidal flow shear shows a linear decay, while the ion temperature gradient shows an exponential decay, which suggests that the flow damping is due to the change in nondiffusive term of momentum transport [1].

The LHD is a heliotron-type device for magnetic confinement of high-temperature plasmas. When the direction of neutral beam injection (NBI) is switched from coinjection to counter-injection (parallel to antiparallel to the equivalent plasma current that gives the poloidal field produced by the external coil current), the edge rotational transform decreases due to the beam driven current and the central rotational transform increases due to the inductive current. Then the magnetic shear at the $q = 2$ rational surface decreases and finally the magnetic field becomes stochastic due to the overlapping of magnetic islands with higher modes [2].

After the stochastization of the magnetic field, the increase of χ_e is much larger than that of the ions ($\chi_e/\chi_i > 15$) because of the difference in thermal velocity, which is consistent with the Rechester–Rosenbluth model (~ 40). In contrast, the large effective Prandtl number observed during stochastization ($\mu_\phi/\chi_i = 3$) is inconsistent with the prediction of the Rechester–Rosenbluth model (~ 1). Furthermore, there are clear differences in the decay between ion temperature and toroidal flow velocity. The toroidal flow shear shows a linear decay, while the ion temperature gradient shows an exponential decay after the stochastization of the magnetic field. This result suggests that the damping of flow is due to the change in the nondiffusive term of momentum transport associated with the stochastization of the magnetic field.

References

- [1] K. Ida, *et al.*, Nature Com. **6**, 5816 (2015).
- [2] K. Ida, *et al.*, Plasma Phys. Control. Fusion **57**, 014036 (2015).

Observations of Sustained Phase Shifted Magnetic Islands from Externally Imposed $m/n = 1/1$ RMP in LHD

Y. Narushima¹, S. Sakakibara¹, Y. Suzuki¹, K. Watanabe¹, S. Ohdachi¹, Y. Takemura¹, M. Yoshinuma¹, K. Ida¹, F. Castejón², D. López-Bruna², C. C. Hegna³, M. Kobayashi¹, H. Tanaka¹, T. Akiyama¹, and N. Ohno⁴

¹National Institute for Fusion Science (NIFS), Toki, Gifu, Japan

²Centro de Investigaciones Energéticas, Medioambientales y Tecnológicas (CIEMAT), Madrid, Spain

³University of Wisconsin-Madison, Madison, WI 53706, USA

⁴Graduate School of Engineering, Nagoya University, Nagoya, Japan

Corresponding Author: Y. Narushima, narusima@lhd.nifs.ac.jp

New observations in LHD show that the magnetic islands externally imposed by $m/n = 1/1$ resonant magnetic perturbation (RMP) can be maintained in an intermediate state with a finite phase shift away from the value present in vacuum. The magnetic island is maintained with a deviated phase of around 0.3π rad from the imposed RMP. The experimental observation implies that the plasma response can provide plasma currents that produce deviations away from the RMP's designed position and can be maintained in the unfavourable phase. Given the previous experimental observation that the saturated magnetic islands show either growth or healing, the intermediate states are realized in the "healing region" in the β and collisionality space, which implies that the parameter except for β and collisionality should exist in order to determine the island state. Theories based on the competition between electromagnetic torques and poloidal flow-induced viscous torques provide a prediction for the intermediate state. These two kinds of torques might be balanced to realize the steadily maintained intermediate state whereas the islands are put in growth or healing state in the case in which the balance is broken. The new finding of the intermediate state brings a distinct paradigm shift in which the magnetic island can be moved and maintained in a partial position of the phase. If the poloidal flow can be externally varied, the phase of the magnetic island can be also arbitrarily controlled, which may permit continued utilization of the island divertor concept. The experimental observation shows that there is a possibility for the magnetic island phase to deviate from its designed position. If the parameters are controlled properly, it is possible to control the phase of the magnetic island, which may permit continued utilization of the island divertor concept.

EX

Magnetic Island Formation in Locked-Like Mode in Helical Plasmas

T. Tokuzawa¹, Y. Takemura¹, K. Watanabe¹, S. Sakakibara¹, Y. Narushima¹, H. Tsuchiya¹, Y. Nagayama¹, S. Inagaki², K. Ida¹, M. Yoshinuma¹, K. Tanaka¹, Y. Suzuki¹, and I. Yamada¹

¹National Institute for Fusion Science (NIFS), Toki, Gifu, Japan

²Kyushu University, Kasuga, Japan

Corresponding Author: T. Tokuzawa, tokuzawa@nifs.ac.jp

We report the discovery of the magnetic island formed in the locked-like mode in helical plasma. New analysis and observation techniques applied to the ECE signal and poloidal flow in LHD experiments show the following results. i) The magnetic island structure is present. This indicates that the resistive interchange mode can induce the rotating magnetic island in the locking phase. ii) The rotation speed of the island is not uniform in space. The toroidal structure of the island changes in the locking-phase, and the deformation increases till the mode is locked. These results are quite meaningful to understand the locked mode instability affecting the confinement.

The locked mode is well understood as the tearing mode in some tokamaks. In the LHD, a nonrotating $m/n = 1/1$ mode has been observed and it is identified as the resistive interchange mode. A minor collapse was observed with the damping of the magnetic fluctuation frequency and the lock of the mode. This is called "locked-like" mode. In the analogy of the tokamak locked tearing mode, the magnetic island existence has been implicated.

The clear indication of the magnetic island is obtained by ECE radiometer just before the locked phase that the strong $m/n = 1/1$ component of the radial magnetic field rises rapidly. The rotating $m/n = 1/1$ mode component included in the fluctuation amplitude and the phase difference of ECE intensity can be extracted. The odd radial structure and the flattened T_e profile clearly appear. It is also found that the inverse position is mostly the same as the $\nu/2\pi = 1$ surface.

The value of poloidal velocity V_p measured by toroidally-correlated microwave Doppler reflectometers is changed back and forth from around -4 to 0 km/s during the locking phase. It should be noted that $V_p \sim 0$ means that the O-point of the rotating magnetic island comes to the observation region. The staying time of the O-point of rotating island in the observation region is found to be different in the different toroidal locations. It suggests that the island structure is toroidally nonuniform. Also, the phase difference between two V_p measurements is changed in time. It is possible to explain as the distortion of the rotation structure that is the twisting rotating island structure disobeys the equilibrium magnetic structure. This distortion would lead to the damping of the rotation velocity.

Observation of the Ballooning Mode that Limits the Operation Space of the High-Density Superdense-Core Plasma in the LHD

S. Ohdachi¹, K. Watanabe¹, K. Tanaka¹, Y. Suzuki¹, S. Sakakibara¹, X. Du¹, T. Bando², Y. Narushima¹, R. Sakamoto¹, J. Miyazawa¹, G. Motojima¹, and T. Morisaki¹

¹National Institute for Fusion Science (NIFS), Toki, Gifu, Japan

²Graduate University for Advanced Studies (SOKENDAI), Hayama, Kanagawa, Japan

Corresponding Author: S. Ohdachi, ohdachi@nifs.ac.jp

The central β of the superdense-core (SDC) plasma in the Large Helical Device (LHD) is limited by a large scale MHD event called “core density collapse” (CDC). It is found that a new type of ballooning mode, quite localized in space and destabilized from the 3D nature of heliotron devices, is the cause of the CDC. It is the first observation that the ballooning mode is excited where the global magnetic shear is negative.

High-density operation is one possible reactor scenario of helical confinement system. In the SDC type discharges, the electron density higher than $10^{21}/\text{m}^3$ with $B_t = 2.5$ T is achieved in the LHD. The SDC plasma is characterized by the peaked density and pressure profiles. However, the central β of SDC plasma is strongly limited by the CDC. The ballooning instabilities related with the 3D nature of helical systems, referred to high- n ballooning mode, is considered to be the cause of collapse. In the heliotron devices, it was predicted that the local magnetic shear can be reduced around the local pressure gradient peak in the global negative magnetic shear region when the Shafranov-shift is large. The ballooning mode is driven by the pressure gradient in the bad curvature region when the local shear is reduced.

Just before the CDC events, precursor oscillations at around 8 kHz have been found only in the outboard side. If the mode structure of the precursor is localized around a flux tube connected to the outboard side of the horizontally elongated section (worst curvature region), two sharp peaks observed in the fluctuation profile can be understood. A newly developed 2D SX detector array reveals that this precursor like movement is aligned to the local magnetic field line.

In order to avoid the CDC for achieving higher central β , control of the ballooning mode by the reduction of the pressure gradient at the bad curvature region is experimentally performed. In the relatively low magnetic field experiment ($B_t = 1.5$ T), the pressure profile is broader than the profile with normal magnetic field $B_t = 2.5$ T. The operational boundary observed in the 2.5 T can be passed over and the central β has reached about 10% with $B_t = 1.5$ T. It is the highest central β achieved in the LHD. Therefore, the mitigation of the high- n ballooning mode is proved to be the key to achieve high central β in the SDC type operation of the LHD.

Improvements of Ion Energy Confinement in Helium Rich Plasma of LHD

K. Tanaka¹, K. Nagaoka¹, S. Murakami², M. Yokoyama¹, T. Hiromi¹, T. Tokuzawa¹, and M. Osakabe¹

¹National Institute for Fusion Science (NIFS), Toki, Gifu, Japan

²Kyoto University, Nishikyo-ku, Kyoto 615-8540, Japan

Corresponding Author: K. Tanaka, ktanaka@nifs.ac.jp

The improvement of the ion energy transport was observed in the He rich plasma of LHD. The ion thermal diffusivity around the edge pedestal region is lower than that of the gyro-Bohm prediction taking into account the effective ion mass and charge. The transport of different ion species is an important issue to predict the performance of ITER and the future reactor operation. In this paper, we report the results of a systematic study of effective ion mass and effective ion charge on ion energy transport of ion ITB plasma in LHD. With constant NB heating power (20–23 MW) at the same line averaged electron density ($1.35 \times 10^{19}/\text{m}^3$), clearly higher T_i was observed at higher He concentration plasma. The fuelling ratio R , which is defined as $R = n_{\text{H}}/(n_{\text{H}} + n_{\text{He}})$ were controlled by the discharge cleaning and external gas fuelling. R changed from 0.34 to 0.79. At lower R (with higher He concentration), total ion density n_i , which was consist of n_{H^+} , $n_{\text{He}^{2+}}$, $n_{\text{C}^{6+}}$, became lower. However, ion deposition powers per ion (P_i/n_i) were almost constant for different R . Thus, the achieved higher T_i at lower R is not due to the difference of P_i/n_i but due to the improvements of ion energy transport at lower R (He rich plasma). The T_i profiles shows edge pedestal formation both in He rich and H rich plasma. But T_i at pedestal top at $\rho \sim 0.9$ was higher in the He rich plasma. While in the inner region ($\rho < 0.9$), the normalized T_i gradients were almost constant for different R . At $\rho = 0.4\text{--}0.9$, ion scale turbulence ($k_{\perp}\rho_i \sim 0.4$) were observed. The linear gyrokinetic analysis showed ITG was the dominant instability. Thus, within the T_i pedestal ($\rho < 0.9$), it is likely that the normalized T_i gradient is limited by ITG threshold. The effective ion thermal diffusivities ($\chi_{i,\text{eff}}$), which is the representative ion thermal diffusivity of H^+ , He^{2+} and C^{6+} , were estimated from the power balance analysis. When $\chi_{i,\text{eff}}$ is normalized by the gyro-Bohm factor, which is $m_{\text{ieff}}^{0.5} T_i^{1.5} / (q_{\text{ieff}}^2)$, where m_{ieff} is effective ion mass, q_{ieff} is the effective ion charge, the normalized $\chi_{i,\text{eff}}$ is almost identical at $\rho < 0.8$ for different R , while the normalized $\chi_{i,\text{eff}}$ is clearly lower at lower R (larger He contamination). This suggests transport improvements in edge region and corresponds to the higher edge T_i pedestal in He rich plasma.

EX



Stabilization of the Helically Trapped Energetic Ions Driven Resistive Interchange Mode by On-Axis Electron-Cyclotron Heating in a Helical Plasma

X. D. Du¹, S. Ohdachi¹, M. Osakabe¹, T. Seki¹, T. Ozaki¹, K. Fujii², M. Goto¹, K. Nagaoka¹, K. Y. Watanabe¹, K. Tanaka¹, K. Ogawa¹, M. Isobe¹, S. Sakakibara¹, S. Nishimura³, T. Ido¹, T. Nicolas¹, and Y. Suzuki¹

¹National Institute for Fusion Science (NIFS), Toki, Gifu, Japan

²Graduate School of Engineering, Kyoto University, Nishikyo-ku, Kyoto 615-8540, Japan

³Kobe City College of Technology, Kobe, Hyogo, Japan

Corresponding Author: X. D. Du, du.xiaodi@nifs.ac.jp

A bursting resistive interchange mode destabilized by the resonant interaction with the helically trapped energetic ions (EIs), named as the helically trapped energetic-ion-driven resistive interchange modes, or "EIC", has been identified in Large Helical Device (LHD). It can induce the significant loss of the EIs in plasma peripheral region, therefore, the control of the EICs is important. It is found that when the electron-cyclotron-heating (ECH) near the magnetic axis is superimposed, the EIC locating in the plasma peripheral region is mitigated. The EIC can be further fully stabilized when the power of the ECH exceeds a certain threshold. The ratio of the gyro-radius of the trapped EIs to the radial width of the resistive interchange mode ($k_r \rho_{EI}$) is the key parameter to explain the observed stabilizing effect. That is, the FLR effect is thought to play an important role on the observed stabilization of the EIC in LHD.

EX



Abrupt Excitation of Intense Geodesic Acoustic Mode in the LHD

T. Ido¹, K. Itoh¹, M. Lesur², M. Osakabe¹, A. Shimizu¹, K. Ogawa¹, M. Nishiura³,
Y. Kosuga⁴, M. Sasaki⁵, K. Ida¹, S. Inagaki⁴, and S.-I. Itoh⁵

¹National Institute for Fusion Science (NIFS), Toki, Gifu, Japan

²Institut Jean Lamour, Université de Lorraine, CNRS, Nancy, France

³University of Tokyo, Tokyo, Japan

⁴Kyushu University, Kasuga, Japan

⁵Research Institute for Applied Mechanics (RIAM), Kyushu University, Kasuga, Japan

Corresponding Author: T. Ido, ido@lhd.nifs.ac.jp

Abrupt excitation of a geodesic acoustic mode (GAM) has been observed in the Large Helical Device (LHD), when the frequency of an up-chirping energetic-particle driven GAM (EGAM) approaches twice the ordinary GAM frequency. The abruptly excited GAM has larger amplitude and a lower frequency than the initially excited EGAM. The amplitude dependence of the growth rate of the abrupt GAM indicates that the GAM is excited through nonlinear processes. The observed specific phase relation between the GAM and the EGAM indicates the coupling between the GAM and the EGAM, and cannot be explained by well-known driving mechanisms such as nonlinear coupling of turbulence [1] or interaction between energetic particles and a GAM [2]. Thus, the observed phenomenon indicate the existence of a new excitation mechanism of the GAM.

A candidate mechanism of the abrupt excitation of the GAM is proposed in [3] and [4], in which a subcritical instability of the GAM is shown to be driven by a cooperative collaboration of fluid parametric coupling and kinetic nonlinearity. The model can reproduce the observed phase relation, amplitude, and time scale of the abrupt excitation.

References

[1] P. H. Diamond, *et al.*, Plasma Phys. Control. Fusion **47**, R35 (2005).

[2] G. Y. Fu, Phys. Rev. Lett. **101**, 185002 (2008).

[3] M. Lesur, *et al.*, Phys. Rev. Lett. **116**, 015003 (2016).

[4] K. Itoh, *et al.*, Plasma Phys. Reports, In Press, (2016).



Observation of Visible Forbidden Lines of Tungsten Highly Charged Ions in LHD Core Plasmas and its Application to Ion Distribution Analysis

D. Kato¹, I. Murakami¹, H. A. Sakaue¹, M. Goto¹, T. Oishi¹, S. Morita¹, K. Fujii², and N. Nakamura³

¹*National Institute for Fusion Science (NIFS), Toki, Gifu, Japan*

²*Kyoto University, Nishikyo-ku, Kyoto 615-8540, Japan*

³*The University of Electro-Communications, Chōfu, Tokyo, Japan*

Corresponding Author: D. Kato, kato.daiji@nifs.ac.jp

Visible emission lines of tungsten ions are useful for analysis of tungsten ion distributions at ITER because the radiation shielding of detectors is not basically necessary by using optical fibres. Here we report the result on observation of visible magnetic-dipole (M1) lines of highly-charged tungsten ions in the Large Helical Device (LHD) with tungsten pellet injection and its first application to the ion distribution analysis. Based on the measured spatial profile of the M1 line intensity, i) radial distributions of W^{27+} ions in LHD core plasmas are elucidated using an originally developed collisional-radiative model, and, ii) strong enhancement of the M1 line intensity due to proton collisions is predicted by the present calculation.

EX



Role of Magnetic Topology to Form Electron Internal Transport Barrier on Heliotron J

T. Minami¹, N. Kenmochi², C. Takahashi¹, K. Nishioka², S. Kobayashi¹, Y. Nakamura², H. Okada¹, S. Kado¹, S. Yamamoto¹, S. Ohshima¹, S. Konoshima¹, G. Weir¹, Y. Ohtani², K. Nagasaki¹, and T. Mizuuchi¹

¹*Institute of Advanced Energy, Kyoto University, Nishikyo-ku, Kyoto 615-8540, Japan*

²*Graduate School of Energy Science, Kyoto University, Nishikyo-ku, Kyoto 615-8540, Japan*

Corresponding Author: T. Minami, minami@iae.kyoto-u.ac.jp

A role of rational surface on electron internal transport barrier (eITB) formation of the helical plasma has been investigated in Heliotron J. The experiments have been performed on the standard magnetic configuration of $B_{ax} = 1.25$ T. The plasma with eITB is produced by a centrally focussed 70 GHz ECR heating ($P_{inj} \sim 270$ kW, absorption ratio is above $\sim 90\%$, $N_{\parallel} = 0.0$). When bootstrap plasma current increases up to 0.7 kA, a fast transitive increase of electron temperature due to an expansion of the improved confinement region has been observed. The eITB foot point moves from $r/a = 0.13$ to $r/a = 0.23$, and the rise time of the electron temperature is below $\sim 100 \mu\text{s}$, which is shorter than the confinement time. After the fast transition at 0.7 kA, the location of the eITB foot point moves to the outside of the plasma with the current increase. The current at the start of the expansion as a function of $\iota/2\pi(0)$ of the vacuum magnetic field shows that the required plasma current to the expansion decreases with the decrease of the difference between $4/7$ and the rotational transform values. The rotational transform profile including bootstrap current calculated by the Sugama–Nishimura moment method shows that the $n/m = 4/7$ rational surface is produced around $r/a \sim 0.37$ at ~ 1.5 kA. The timing of the $n/m = 4/7$ rational surface formation is consistent with the timing of the transitive increase of the electron temperature. The calculation also shows the movement of the eITB also synchronizes with the movement of the rational surface. Because the $4/7$ rational surface is a candidate on which the magnetic island can be formed due to the $n = 4$ toroidal periodicity of the Heliotron J vacuum magnetic field, and other rational surfaces have no contribution to the phenomena, the results show the possibility that the formation of the rational surface can expand the region of the improved confinement, and there is a synergy effect of the eITB and the magnetic island for the expansion of the improved confinement region.

EX



Study of H-Mode Transition Triggered by High-Intensity Gas Puffing in NBI Plasmas of Heliotron J

S. Kobayashi¹, S. Ohshima¹, K. Nagasaki¹, H. Okada¹, T. Minami¹, S. Kado¹, S. Yamamoto¹, G. Weir¹, M. Kirimoto², H. Matsuda², K. Ida³, T. Kobayashi³, Y. Nakamura², A. Ishizawa², N. Kenmochi², Y. Otani², X. Lu², Y. Nakashima⁴, K. Watanabe³, R. Seki³, S. Murakami⁵, Y. Suzuki³, S. Konoshima¹, and T. Mizuuchi¹

¹*Institute of Advanced Energy, Kyoto University, Nishikyo-ku, Kyoto 615-8540, Japan*

²*Graduate School of Energy Science, Kyoto University, Nishikyo-ku, Kyoto 615-8540, Japan*

³*National Institute for Fusion Science (NIFS), Toki, Gifu, Japan*

⁴*Plasma Research Center, University of Tsukuba, Tsukuba, Ibaraki, Japan*

⁵*Department of Nuclear Engineering, Kyoto University, Nishikyo-ku, Kyoto 615-8540, Japan*

Corresponding Author: S. Kobayashi, kobayashi@iae.kyoto-u.ac.jp

In this study, we report on the H-mode transition triggered by high-intensity gas puffing (HIGP) in NBI plasmas of Heliotron J. Heliotron J is a medium sized ($R/a = 1.2/0.17$ m) helical-axis heliotron device with an $L/M = 1/4$ helical coil, where L is the pole number of the helical coil and M is the pitch number. An H-mode transition has been observed in the high density NBI plasmas. In the H-mode phase, an improvement in the energy confinement time normalized to that of the international stellarator scaling law around 2 has been achieved.

In the case when the H-mode transition occurs, the recovery of the stored energy is found after the stop of HIGP. The recovery phenomenon is similar to that of so-called "reheat mode" observed in CHS. During the applying HIGP, a bursting $n = 2$ mode with $f = 5\text{--}30$ kHz appears until the occurrence of the H-mode transition. The density fluctuation with the burst frequency ($f = 0.8\text{--}3$ kHz), measured by beam emission spectroscopy (BES), propagates in the outward direction, which is synchronized with the H_α/D_α intensity. These observations indicate the particle exhaust phenomena. The time evolution of the density gradient in the peripheral region ($r/a = 0.9$) calculated by the BES signals suggests the repetition of the increase/decrease in the density gradient before the transition, indicating so-called "dithering" phenomena. At the timing of the H-mode transition, the density gradient increases along with the disappearance of the particle exhaust. After that, the formation of the steep density gradient is observed in the peripheral region ($r/a = 0.8\text{--}1$). In the case where the amount of HIGP is smaller than that when the H-mode transition occurs, the particle exhaust is not observed, although the reheat mode is found. In this case, the density gradient is smaller than that in the H-mode case.

This work was supported by JSPS Grant-in-Aid for Scientific Research (C) 15K06645.



Fast Ion Generation by Combination Heating of ICRF and NBI in Heliotron J

H. Okada¹, S. Kobayashi¹, S. Kado¹, K. Nagasaki¹, T. Minami¹, S. Yamamoto¹, S. Ohshima¹, T. Mutoh², H. Kasahara², T. Mizuuchi¹, Y. Nakamura³, K. Murakami³, Y. Jinno³, S. Konoshima¹, N. Kenmochi³, Y. Otani³, K. Hada³, X. Lu³, G. Weir¹, R. Tsukasaki³, D. Oda³, Y. Nakano³, H. Matsuda³, H. Kishikawa³, and A. Nuttarsart³

¹*Institute of Advanced Energy, Kyoto University, Nishikyo-ku, Kyoto 615-8540, Japan*

²*National Institute for Fusion Science (NIFS), Toki, Gifu, Japan*

³*Graduate School of Energy Science, Kyoto University, Nishikyo-ku, Kyoto 615-8540, Japan*

Corresponding Author: H. Okada, okada@iae.kyoto-u.ac.jp

The fast ion generation and confinement are studied by using ICRF minority heating (H minority and D majority) for the simulation study of alpha particles, whose heating is essential for fusion reactors. In a three dimensional magnetic field device, Heliotron J ($R_0 = 1.2$ m, $a = 0.1$ – 0.2 m, $B_0 \leq 1.5$ T), fast ion generation and confinement by ICRF minority heating are studied in combination with NBI heating. Fast ions are measured using a charge-exchange neutral particle analyzer with ten channels for hydrogen. The energy range is extended from the injection energy of the NBI beam, 25 keV, to 60 keV during the ICRF pulse in the newly attempted low- ϵ_t configuration and medium density operation ($1 \times 10^{19}/\text{m}^3$). This configuration is better in the fast ion generation and confinement than the high bumpiness configuration which is the best among the bumpiness scan. Here, the toroidicity and the bumpiness normalized by the helicity for the low- ϵ_t and the high bumpiness configurations are (0.77, -1.04) and (0.86, -1.16) in Boozer coordinates, respectively. They are key parameters in $1/\nu$ regime of helical devices. The low- ϵ_t configuration is expected to have good confinement from the neoclassical theory. The observed fast ions are limited up to 35 keV in the high bumpiness configuration for the same conditions. The Monte Carlo calculation is also performed for understanding the fast ions observed in the experiment. The test ions (protons), which represent the NBI particles, start at the middle point of the NB path in a plasma with the NB injection energy. The energy tail spread more toward the high energy region in the low- ϵ_t and its direction is relatively narrow in comparison with the high bumpiness. The experimental and calculation results are explained partially by the loss region of fast ions for these configurations.

EX



Suppression of Alfvén Eigenmodes by ECH/ECCD in Heliotron J

K. Nagasaki¹, S. Yamamoto¹, H. Matsuda², S. Kobayashi¹, H. Okada¹, T. Minami¹,
S. Kado¹, S. Ohshima¹, S. Konoshima¹, G. Weir³, K. Sakamoto¹, Y. Nakamura²,
N. Kenmochi², Y. Otani², X. Lu², H. Kishikawa², N. Inklin², N. Marushchenko³, and
T. Mizuuchi¹

¹*Institute of Advanced Energy, Kyoto University, Nishikyo-ku, Kyoto 615-8540, Japan*

²*Graduate School of Energy Science, Kyoto University, Nishikyo-ku, Kyoto 615-8540, Japan*

³*Max-Planck-Institut für Plasmaphysik, Garching, Germany*

Corresponding Author: K. Nagasaki, nagasaki@iae.kyoto-u.ac.jp

Experiments of suppressing Alfvén Eigenmodes (AE) have been made by using a second harmonic X-mode electron cyclotron current drive (ECCD) in the helical-axis heliotron device, Heliotron J. The weak magnetic shear under vacuum condition is modified into a positive magnetic shear when counter-ECCD is applied. The experiments show that global Alfvén eigenmodes (GAE) of around 130 kHz and 350 kHz are fully stabilized, and energetic particle modes (EPM) of around 100 kHz are weakened when the EC current of 0.7 kA is driven on axis. The mode amplitude is more reduced as the EC current is larger. These results indicate that the magnetic shear has an effective role in controlling GAEs as well as EPMs. This study extends the possibility of ECH/ECCD as a control knob for EP-driven MHD modes and give understanding of the excitation and damping mechanisms.

EX



Isotope Effects on Long Range Correlation and the Nonlinear Coupling with Turbulence in Heliotron J

S. Ohshima¹, S. Kobayashi¹, S. Yamamoto¹, K. Nagasaki¹, H. Okada¹, T. Minami¹, S. Kado¹, G. Weir¹, M. Motoshima², N. Kenmochi¹, Y. Ohtani², X. Lu², S. Konoshima¹, and T. Mizuuchi¹

¹*Institute of Advanced Energy, Kyoto University, Nishikyo-ku, Kyoto 615-8540, Japan*

²*Graduate School of Energy Science, Kyoto University, Nishikyo-ku, Kyoto 615-8540, Japan*

Corresponding Author: S. Ohshima, ohshima@iae.kyoto-u.ac.jp

The hydrogen/deuterium (H/D) isotope effects for long range correlation (LRC) and the nonlinear relationship with turbulence were observed for the first time in a helical device, Heliotron J. The fluctuation amplitude and the correlation in toroidal direction in the low frequency range < 4 kHz are enhanced as the D_2 gas becomes dominant during the shot-to-shot experiment. Turbulence scale size increases as D_2 gas is dominated in the discharge, which is consistent with the conventional turbulence theories and the past experimental works. Nonlinear coupling between the LRC and turbulence, which should relate to the generation of the LRC, is also enhanced along with the increase in the LRC. This observation gives an implication that the isotope effects on the confinement improvement and/or on the threshold in L-H transition are dominated by the increase of nonlinear coupling on turbulence and the resultant enhancement of the zonal flow activity in D plasmas.

EX



Liquid Metal Experiments on FTU

G. Mazzitelli¹, M. L. Apicella¹, M. Iafrati¹, G. Apruzzese¹, A. Buscarino², G. Calabrò¹, C. Corradino², F. Crescenzi¹, L. Fortuna², G. Maddaluno¹, T. W. Morgan³, G. Ramogida¹, and A. Vertkov⁴

¹Associazione EURATOM-ENEA Unità Tecnica Fusione, Frascati, Italy

²Dipartimento di Ingegneria Elettrica, Elettronica e Informatica (DIEEI), University of Catania, Catania, Italy

³FOM Institute DIFFER, Association EURATOM-FOM, Nieuwegein, Netherlands

⁴JSC "Red Star", Moscow, Russian Federation

Corresponding Author: G. Mazzitelli, giuseppe.mazzitelli@enea.it

The experiments on FTU with a cooled liquid lithium limiter (CLL) (2014&2015) and subsequently with a cooled liquid tin limiter (TLL) (2016) aim at testing liquid metals (LM) under reactor relevant thermal loads of up to 10 MW/m² in stationary conditions. In preparation of this programme, improvements of the FTU facility started in 2014 with: 1) the extension of the pulse duration from 1.5 s up to 5 s, and, 2) feasibility studies to achieve diverted plasmas with the X-point near the CLL. The additional aim is to get the H-mode in plasmas heated by electron cyclotron resonance heating (ECRH) to study the impact of edge localized modes (ELMs) on the CLL used as main target. The first CLL dedicated discharges were both ohmic and with auxiliary heating power ($P_{\text{ECRH}} = 500$ kW). Circular and elongated shape ($k \sim 1.2$) were tested as well as different CLL positions under the TZM toroidal limiter shadow up to 1.8 cm inside the last closed magnetic surface in elongated plasmas. Heat loads up to 2.3 MW/m² had been withstood by the limiter surface for all the duration of the plasma discharge (1.5 s) with temperatures below the threshold for acceptable Li evaporation ($\sim 500^\circ\text{C}$). Unfortunately, experiments with higher heat load values were prevented by the onset of hot spots on the joint points of the strips of CPS structure and by the poor control of the Li temperature that displayed large oscillations. To solve these problems, a new active CLL refrigeration head in Red Star Labs has been realized with a larger curvature radius and the CLL control system has been successfully implemented in ENEA in order to optimize the temperature monitoring and the control of the water circulation. An other important upgrade was the extension of FTU pulses to 4.5 s and $B_t = 2.5\text{--}4$ T. In the European framework of coordinated actions, a cooled sample of Sn CPS type envisaged for the TLL in FTU has been tested on Pilot-PSI linear device. A power handling of 26 MW/m² has been demonstrated under stationary conditions and without apparent damage of Sn sample, giving early indications the TLL will be effective. In this paper an overview of the main activities of the last two years will be presented followed by the experimental results obtained on FTU with the new CLL system. Then, the preliminary work with the tin liquid limiter (TLL) and the results on Pilot-PSI with liquid tin samples will be described.

EX



Analysis of Runaway Beam Suppression Experiments in FTU

D. Carnevale¹, B. Esposito², M. Gospodarczyk¹, A. Gabrielli¹, L. Boncagni², P. Buratti², F. Causa², S. Galeani¹, M. Sassano¹, G. Ferrò¹, C. Cianfarani², D. Marocco², G. Maddaluno², Z. Popovic³, J. R. Martín-Solís³, G. Pucella², and O. Tudisco²

¹Università di Tor Vergata, 00173 Rome, Italy

²ENEA C. R. Frascati, Dipartimento FSN, Frascati, Italy

³Universidad Carlos III de Madrid, Madrid, Spain

Corresponding Author: D. Carnevale, daniele.carnevale@uniroma2.it

The challenging task for a disruption mitigation system (DMS) is the implementation of reliable strategies in order to mitigate thermal, mechanical and electromagnetic loads at disruptions. Furthermore, the DMS has to cope with control and suppression of runaway electron beams, which are possibly generated during major disruptions, in order to avoid localized high-energy deposition causing deep melting of the structures. Strategies for runaway electron (RE) suppression are massive gas injection (MGI) or shattered pellet injection (SPI) although alternative or simultaneous strategies based on RE current dissipation via the central solenoid (ohmic coil) have been proposed. In ITER a preemptive strategy exploiting the central solenoid to deal with current quenches (CQ), yielding RE beam onset with current drop less than 5 MA, has been proposed. In the case the position control of the RE beam is not lost during the CQ, the maximum RE beam current decay rate has to remain below 0.5 MA/s, a limit that increases up to 1 MA/s for initial RE current of 12 MA.

In FTU a large database (650 pulses) of highly energetic postdisruption RE beams, produced spontaneously or with high- Z gas injection, have been analyzed. The study reveals that the decay rate during RE beam current ramp-down is an important parameter for runaway energy suppression. We have proposed a possible performance index to define suitable characteristics of the RE beam controller. Analysis of experimental data indicates that the reduction of the runaway current is possible when associated to small decay rate (longer confinement) of about 1 MA/s and a dedicated RE beam controller. Other important factors of RE beam premature final loss have been found to be: the large radial shift of the RE beam that potentially causes impacts on the low field side of the vessel during the plateau phase, MHD instabilities induced by large electrical field, VDE (elongated beams). The hysteretic behaviour of the runaway dynamics has been highlighted and experimentally quantified. Such nonlinearity affects runaway dynamics leading to increased density thresholds for runaway suppression once they have been previously formed.

Observation of Short Time-Scale Spectral Emissions at Millimetre Wavelengths with the New CTS Diagnostic on the FTU Tokamak

A. Bruschi¹, E. Alessi¹, W. Bin¹, O. D'Arcangelo², F. Belli², G. Calabrò², I. Casiraghi³, V. Cocolovo², L. Figini¹, C. Galperti⁴, S. Garavaglia¹, G. Granucci¹, G. Grosso¹, S. B. Korsholm⁵, M. Lontano¹, V. Mellera¹, A. Moro¹, S. K. Nielsen⁵, F. P. Orsitto⁶, M. S. Pedersen⁵, G. Ramogida², J. J. Rasmussen⁵, D. Ricci¹, and U. Tartari¹

¹Istituto di Fisica del Plasma (IFP), Consiglio Nazionale delle Ricerche (CNR), 20125 Milan, Italy

²Associazione EURATOM-ENEA Unità Tecnica Fusione, Frascati, Italy

³Università degli Studi di Milano Bicocca, Milano, Italy

⁴Swiss Plasma Center (SPC), École polytechnique fédérale de Lausanne (EPFL), 1015 Lausanne, Switzerland

⁵Technical University of Denmark (DTU), Lyngby, Denmark

⁶Consorzio CREATE, 80125 Napoli, Italy

Corresponding Author: A. Bruschi, bruschi@ifp.cnr.it

The collective Thomson scattering (CTS) diagnostic on FTU tokamak was renewed [1] for investigations on the excitation of parametric decay instabilities (PDI) by electron cyclotron (EC) beams in presence of magnetic islands and their effects on the EC absorption. Experiments were performed with a gyrotron probe (140 GHz, 400 kW) launched in symmetric and asymmetric configurations with respect to the equatorial plane, in different conditions of plasma density and magnetic field (with or without the EC resonance in the plasma), and with magnetic islands generated by Ne injection. The acquisition with a fast digitizer allowed observing spectral features with very high time and frequency resolution [2]. In the shots performed at 7.2 T, with the fundamental EC resonance out of the plasma region, a sequence of faint lines emitted with a fast temporal evolution have been observed in a range 0.5–1.1 GHz from the gyrotron frequency while at 4.7 T, with the resonance on the high field side of the plasma column, asynchronous “bursts” of continuous emissions were observed at a microsecond time scale.

In 2015 experiments were performed at 4.7 and 3.6 T, in this last case with the plasma between the first and the second EC harmonics. Different types of spectral features with a fast evolution were observed. Their correlation with magnetic probes and fast signals from the plasma has been investigated, to characterize the observations and exclude parasitic effects, as well as breakdown phenomena in front of the antennas. The variation in the stray radiation distribution in the vessel has been studied with the aid of a diffusive model, to characterize variations on the probe beam absorption associated to the observed phenomena. Further improvements of the diagnostic both in frequency band (up to ± 4.2 GHz from the probe) and with the addition of a second radiometer, will allow a clearer interpretation of the emissions.

References

[1] W. Bin, *et al.*, Fusion Eng. Des. **96–97**, 733–737 (2015).

[2] A. Bruschi, *et al.*, Proc. 42nd EPS Conference on Plasma Physics (2015).

Work carried out within the framework of the EUROfusion Consortium with funding from the Euratom research and training programme 2014–2018 under grant agreement No 633053. The views and opinions expressed herein do not necessarily reflect those of the European Commission.



Evidence of Thermo-Diffusive Pinch in Particle Transport

O. Tudisco¹, C. Meineri¹, G. Abruzzese¹, O. D'Arcangelo¹, E. Giovannozzi¹, C. Mazzotta¹,
G. Pucella¹, and V. Zanza¹

¹ENEA C. R. Frascati, Dipartimento FSN, Frascati, Italy

Corresponding Author: O. Tudisco, onofrio.tudisco@enea.it

Here is reported the simulation of density evolution in discharges performed at Frascati Tokamak upgrade (FTU) where a thermo-diffusion term have been used instead of the particle pinch. In these discharges a sensible density peaking is observed at high density, subsequent the formation of a strong MARFE thermal instability at plasma edge. They have been obtained in an experimental campaign dedicated to density limit studies, in which it has been found that, at high q , the Greenwald density limit can be exceeded, as a consequence of the density profile peaking. The presence of a strong MARFE seems to be the key to get density peaking and raise density above the Greenwald limit. Density profiles have been measured using the FTU scanning interferometer, with 32 independent chords of 1 cm separation. The density profile peaking is preceded by a drop of the edge temperature in a wide external region, caused by the thermal collapse at the edge which led to the MARFE formation. A neutral diffusion code has been used to evaluate neutral particle profiles, which has shown that the source term remains negligible in large part of the radius (up to $r/a = 0.8$) and in particular in the region where the change of density gradient is observed. In such region a sensible variation of the diffusion coefficients must occurs, while using a thermo-diffusive term, there is no need to change diffusion coefficients within the simulation. Boundary (at $r/a = 0.82$) and initial conditions have been taken from experimental density profile. The steepening of density gradient in confinement region is well described by the simulation, hence the whole variation of inward particle flux can be described considering the change in temperature characteristics length. The same simulation has been applied successfully to other discharges with similar phenomenology, and will be applied to other discharges where the density peaking is provoked by other effects, as impurity injection.

EX



The Physics of the Heat Flux Narrow Decay Length in the TCV Scrape-Off Layer: Experiments and Simulations

B. Labit¹, F. Nespoli¹, J. Horacek², C. Tsui³, J. A. Boedo³, C. Theiler¹, I. Furno¹,
F. Halpern¹, P. Ricci¹, and R. A. Pitts⁴

¹Swiss Plasma Center (SPC), École polytechnique fédérale de Lausanne (EPFL), 1015 Lausanne, Switzerland

²Institute of Plasma Physics AS CR v.v.i., Prague, Czech Republic

³University of California San Diego, CA 92093, USA

⁴International Thermonuclear Experimental Reactor (ITER),
Cadarache Centre, 13108 Saint-Paul-lès-Durance, France

Corresponding Author: B. Labit, benoit.labit@epfl.ch

EX Dedicated experiments have been performed in TCV to investigate the heat flux onto the first wall of inboard limited L-mode plasmas. An enhancement of the heat deposition, measured with an infrared (IR) camera, is observed in the vicinity of the contact point. Indeed, for all the discharges, the parallel heat flux profile exhibits a double decay length in the scrape-off layer (SOL), with a short decay length of about 3 mm and a longer one of about 18 mm. The enhanced heat load in the vicinity of the contact point could be a problem for ITER if it is too large therefore its first wall design has been recently revised. It is shown that the power deposited onto the inner wall due to the narrow feature increases mainly with the electron temperature, and decreases with plasma density, current and elongation. Dedicated numerical nonlinear simulations using the code GBS with realistic TCV parameters have been performed. The simulated parallel heat flux profiles on the limiter are in qualitative agreement with the experimental ones obtained by means of infrared thermography, showing a double scale length. Complementary experiments are currently being performed to better understand the physics of the narrow heat flux decay length. For D and He plasmas, inboard limited plasmas are investigated as a function of the plasma current, the plasma density and the plasma shape. In particular, TCV is well suited to investigate the effect of the elongation and the triangularity. The ion saturation current and the floating potential are measured with wall-embedded Langmuir probes and will complement the heat load measurements onto the inner wall with an upgraded IR thermography system. In addition, measurements of the ion saturation current, floating potential, Mach number and electron temperature and their fluctuations are done with a recently installed 10 tip reciprocating probe. While the narrow SOL width is clearly seen by the IR thermography on the inner wall, if it is present in the outboard midplane SOL, its measurement with the reciprocating probe strongly depends on the accuracy of the LCFS location. Different analysis methods, from the reciprocating probe data, are under evaluation to reduce the uncertainty of the LCFS position.



On Filamentary Transport in the TCV Tokamak: Addressing the Role of the Parallel Connection Length

N. Vianello¹, C. Tsui², C. Theiler³, S. Allan⁴, J. A. Boedo², B. Labit³, H. Reimerdes³, K. Verhaegh⁵, W. Vijvers⁶, N. Walkden⁴, S. Costea⁷, J. Kovacic⁸, C. Ionita⁷, V. Naulin⁸, A. H. Nielsen⁸, J. J. Rasmussen⁸, B. Schneider⁷, R. Schrittwieser⁷, M. Spolaore¹, D. Carralero⁹, and J. Madsen⁸

¹Consorzio RFX, Associazione EURATOM-ENEA sulla Fusione, Padova, Italy

²University of California San Diego, CA 92093, USA

³Swiss Plasma Center (SPC), École polytechnique fédérale de Lausanne (EPFL), 1015 Lausanne, Switzerland

⁴Culham Centre for Fusion Energy (CCFE), Culham Science Centre, Abingdon, UK

⁵York Plasma Institute, University of York, Heslington, UK

⁶FOM Institute DIFFER, Association EURATOM-FOM, Nieuwegein, Netherlands

⁸Technical University of Denmark (DTU), Lyngby, Denmark

⁸Jožef Stefan Institute, 1000 Ljubljana, Slovenia

⁹Max-Planck-Institut für Plasmaphysik, Garching, Germany

Corresponding Author: N. Vianello, nicola.vianello@igi.cnr.it

Addressing the role of scrape-off layer filamentary transport is presently a subject of intense studies in fusion science. Indeed, the broadening of the scrape-off layer profiles in high density discharges has been observed in a number of devices. The broadening has been attributed to an increase of the convective contribution to the perpendicular transport [1]. Recent observations in AUG and JET L-mode plasma [2] provide support to the idea that the profile broadening is caused by the transition of the filamentary dynamics from sheath-limited to inertial regime. The transition is then due to an increase of effective collisionality [3] and a consequential disconnection of the plasma filaments from the target. The experimental results from AUG and JET are not fully supported by observations on devices as MAST and DIII-D.

In this context experiments have been performed on the TCV tokamak [4], where the high flexibility in plasma shaping has been used to test the profile broadening against the dependence on the parallel connection length. In a set of L-Mode discharges the flux surface expansion at the outer target was progressively increased between shots, leading to an increase of the parallel connection length from the midplane to the outer target plates by almost a factor of two. In these shots identical density ramps were performed. A clear modification of the target profiles and a modest modification of upstream profiles have been observed. The investigation of profiles and turbulence, as observed from various diagnostics, is presented and correlated with the divertor conditions in terms of detachment and effective collisionality. The data obtained is compared with ASDEX-Upgrade results in terms of effective collisionality and dimensionless parameters.

References

- [1] B. LaBombard, *et al.*, Phys. Plasmas **8**, 2107 (2001).
- [2] D. Carralero, *et al.*, Phys. Rev. Lett. **115**, 215002 (2015).
- [3] J. R. Myra, *et al.*, Phys. Plasmas **13**, 112502 (2006).
- [4] S. Coda, *et al.*, Nucl. Fusion **53**, 104011 (2013).



First Experimental Results of Runaway Beam Control in TCV

B. Esposito¹, D. Carnevale², M. Gospodarczyk², M. Gobbin³, S. Galeani², C. Galperti⁴, J. Decker⁴, B. Duval⁴, H. Anand⁴, P. Buratti¹, F. Causa¹, G. Papp⁵, S. Coda⁴, and P. Martin³

¹ENEA C. R. Frascati, Dipartimento FSN, Frascati, Italy

²ENEA, Università di Tor Vergata, 00173 Rome, Italy

³Consorzio RFX, Associazione EURATOM-ENEA sulla Fusione, Padova, Italy

⁴École polytechnique fédérale de Lausanne (EPFL), 1015 Lausanne, Switzerland

⁵Max-Planck-Institut für Plasmaphysik, Garching, Germany

Corresponding Author: B. Esposito, basilio.esposito@enea.it

Runaway mitigation is one of the main concerns for safe ITER operation. The disruption mitigation system, still under development for ITER, will be designed to inject the correct amount of high- Z impurities in order to dissipate thermal and magnetic energy by radiation within the mechanical limits of the structure. During the ITER disruption phase and specifically during the current quench (CQ), significant production of high-energy runaway electrons (RE) is foreseen due to primary and secondary generation mechanisms. Present strategies to limit postdisruption runaway formation and suppression are based on massive gas injection (MGI) and shattered pellet injection. A different approach, more likely to be used simultaneously to MGI, exploits the ohmic coils to obtain a RE beam current ramp-down while its position is stabilized. This paper presents the first results of attempting RE beam suppression at TCV. In order to obtain a disruption-generated RE beam, small injections of high- Z impurities (Ar and Ne) have been performed in low-density inner limiter discharges with circular plasmas, $B_t = 1.43$ T and $I_p = 200$ kA. The gas injection is performed by means of the disruption mitigation valve system. A dedicated controller for RE suppression has been implemented in the digital plasma control system of TCV. The CQ and the RE plateau onset are detected by feeding I_p through an approximate derivative linear filter with specific logic. Once the RE plateau onset is detected at t_{CQ} , a new I_p reference is smoothly (via an exponential decay) substituted to the standard one. The new I_p reference, starting from the value at t_{CQ} , is ramped-down towards zero with a preselectable rate. To improve the ramp-down tracking performance, a further logic block, implementing a novel double integrator scheme, is paired with the standard plasma current controller to select the appropriate voltage for the amplifiers powering the ohmic coils. During the RE plateau, the beam has a slow outward (radially) and upward shift of the order of 0.15 m but the standard position control system is able to avoid RE interactions with the vessel before the final loss.

EX



Scattering of EC Waves by Edge Turbulence: Measurements and Modelling in TCV and TORPEX

T. P. Goodman¹, O. Chellai¹, S. Alberti¹, and I. Furno¹

¹Swiss Plasma Center (SPC), École polytechnique fédérale de Lausanne (EPFL), 1015 Lausanne, Switzerland

Corresponding Author: T. P. Goodman, timothy.goodman@epfl.ch

High power electron cyclotron (EC) waves are used worldwide to drive current locally in the magnetically confined plasmas in toroidal devices. Narrow beams are launched obliquely from antennas well outside the plasma, entering it through the scrape-off layer (SOL) and plasma edge to stabilize neoclassical tearing modes (NTMs).

In nearly all tokamaks, stellarators and reversed-field pinches, the SOL is an extremely turbulent region with frequent, large-density, poloidally-localized, field-aligned blobs propagating rapidly towards the walls of the device. In tokamaks, blobs are observed in L-mode discharges and between edge localized modes (ELMs) in H-mode plasmas. ELMs themselves cause rapid periodic changes in density and temperature in the edge pedestal region of the plasma.

In contrast to present day devices, the path length from edge-to-resonance in future devices, such as ITER, will be long enough that even small perturbations (scattering) of the beam near the edge may lead to significant beam spreading, resulting in a reduction of the peak EC driven current and thus an increase in the power required to stabilize NTMs.

This paper describes measurements made on two machines at SPC to quantify EC wave scattering by blobs; the small low-temperature, low-field, toroidally-magnetized device TORPEX and the medium sized tokamak TCV. In both, scattering of a transmitted radio-frequency (RF) beam is measured as opposed to localized plasma absorption, current drive, or associated plasma quantities. The transmission path length in TCV is similar to the edge-to-resonance length in ITER. Low power, low frequency waves are launched in TORPEX and high-power, high frequency waves in TCV. The received mm-wave signal is correlated with measurements of the blobs using conditional averaged sampling (CAS) of an extensive array of in-situ Langmuir probes in TORPEX and 2D modelling of the effect of blobs on the RF signal using the RF module of COMSOL shows good agreement with measurements. On TCV ex-plasma diagnostics — in particular a fast framing camera and an array of wall-mounted Langmuir probes — are used instead for CAS.

This work was partly supported by the Fonds National Suisse pour la Recherche Scientifique



Neutral Beam Heating on the TCV Tokamak

B. Duval¹, A. Karpushov¹

¹Swiss Plasma Center (SPC), École polytechnique fédérale de Lausanne (EPFL), 1015 Lausanne, Switzerland

Corresponding Author: B. Duval, basil.duval@epfl.ch

TCV's principal goal is to explore and develop the physics basis for ITER exploitation and to aid in the development of DEMO. In the initial design, a combination of X2 and X3 ECH power was planned and installed to provide precision auxiliary heating. With a nominal < 1.5 T toroidal field strength, X2 heating remains limited to electron densities $< \sim 4 \times 10^{19}/\text{m}^3$ and X3 to electron densities below $\sim 10^{20}/\text{m}^3$. Several realms of plasma operation, pertinent to our stated goals of ITER and DEMO relevance, remained, however, only marginally accessible. When ECH power alone heats the plasma, electron-ion collisional equipartition decreases resulting in extremely hot electrons with the ion temperature trailing, on TCV, by a factor that can exceed 30. For all these reasons, a phased upgrade programme [1] is underway on TCV that not only extends the power range of X2 and X3 heating but also introduces direct ion auxiliary heating using state-of-the-art neutral beam injection. In a first stage, (scheduled for final acceptance early in 2016), a 1 MW tangentially launched neutral beam of hydrogen or deuterium is installed and reported in this paper. By ion dominated heating at sufficient densities ($> 5 \times 10^{19}/\text{m}^3$) that increases collisional electron heating, efficient X3 power deposition also becomes possible. To harness this effect, part of the future upgrades, envisage some X3 power launched through the lateral launchers where, with sufficient electron temperature (> 2 keV), precision X3 deposition, similar to X2 heating today, becomes available, but at higher electron densities.

This paper concentrates on a comparison between the modelled and experimentally observed plasma behaviours and improved access to reactor relevant regimes. Models predict T_i/T_e ratios above 3 in L-mode and slightly less in H-mode with one beam and X2(L-mode) or X3(H-mode). With an eye to the future, with the planned increase in ECH power and the second counter injected beam, ion-electron temperature equalization with $\beta_N > 2.8$ is expected. This combination of a large electron heating power density and sufficient ion heating to achieve $T_i/T_e \sim 1$ will make TCV plasmas unique. Discharges with a highly nonthermal electron distribution together with those with a strong fast ion component, both relevant to reactor scenarios, become possible.

References

[1] A. Fasoli, FIP/P4-40, This Conference.

Study of the Fast-Ion Distribution Function in the TCV Tokamak Based on FIDA Spectroscopy and the TRANSP Code

B. Geiger¹, A. Karpushov¹, B. Duval¹, C. Marini¹, D. Testa¹, and R. Di Campi¹

¹Max-Planck-Institut für Plasmaphysik, Garching, Germany

²Swiss Plasma Center (SPC), École polytechnique fédérale de Lausanne (EPFL), 1015 Lausanne, Switzerland

Corresponding Author: B. Geiger, benedikt.geiger@ipp.mpg.de

The behaviour of fast particles in high temperature plasmas must be understood in view of future fusion devices. Fast particles result as a product of the fusion process and can be generated by neutral beam injection (NBI) or ion cyclotron heating. They heat the background plasma via collisions on electrons and ions and can, in case of an anisotropic velocity space distribution, drive noninductive currents. The corresponding heating and current drive profiles depend strongly on the fast-ion confinement properties which can be affected in presence of plasma instabilities, such as Alfvén eigenmodes or sawtooth crashes. Since a clear experimental quantification and reliable theoretical predictions of the instability-induced fast-ion transport are still missing, detailed studies of the fast-ion distribution function are required.

In the TCV tokamak, fast ions can be generated by a newly installed NBI source with 1 MW power, which started operation in January 2016. The beam has a tangential geometry and injects deuterium neutrals with a full energy of 25 keV. The fast-ion D_α (FIDA) technique is employed to study the corresponding fast-ion distribution function. Toroidal lines of sight that cross a diagnostic neutral beam collect strongly Doppler shifted Balmer alpha radiation from fast ions after charge exchange. Good signal to noise ratios are obtained due to the application of a $F/2$ spectrometer and due to the presence of very large fast-ion densities in TCV, explained by the high ratio of NBI heating power to plasma volume ($\sim 1 \text{ m}^3$).

For the interpretation of measured FIDA signals, the TRANSP [1] and FIDASIM [2] codes have been implemented at TCV. TRANSP predicts theoretical fast-ion distribution functions which are used as input for FIDASIM to calculate synthetic FIDA measurements. First comparisons between neoclassical predictions and measured FIDA spectra and profiles will be discussed. In addition, this contribution will present initial results on the effect of the fast-ion population on the loop voltage, internal inductance, normalized β and the neutron rate. These quantities change significantly when NBI is turned on and allow one to address the fast-ion transport properties and to validate theoretical models.

References

- [1] R. J. Hawryluk, Phys. Plasmas Close Thermonucl. Cond. **1**, 19 (1980).
- [2] W. W. Heidbrink, *et al.*, Commun. Comput. Phys. **10**, 716 (2011).

Development of Helium Electron Cyclotron Wall Conditioning on TCV for the Operation of JT-60SA

D. Douai¹, L. Figini², T. P. Goodman³, A. Isayama⁴, M. Fukumoto⁴, C. Sozzi², S. Garavaglia², Y. Miyata⁴, A. Moro², D. Ricci², P. Blanchard³, M. Silva³, C. Theiler³, S. Vartanian¹, K. Verhaegh³, S. Coda³, and T. Wauters⁵

¹*Institut de Recherche sur la Fusion par confinement Magnétique (IRFM),*

Commissariat à l'énergie atomique (CEA/Cadarache), 13108 Saint-Paul-lès-Durance, France

²*Istituto di Fisica del Plasma (IFP), Consiglio Nazionale delle Ricerche (CNR), 20125 Milan, Italy*

³*Swiss Plasma Center (SPC), École polytechnique fédérale de Lausanne (EPFL), 1015 Lausanne, Switzerland*

⁴*Japan Atomic Energy Agency (JAEA), Naka, Japan*

⁵*Laboratory for Plasma Physics, ERM/KMS, Brussels, Belgium*

Corresponding Author: D. Douai, david.douai@cea.fr

Wall conditioning will be required in JT-60SA to control fuel and impurity recycling and to improve plasma performance and reproducibility. In addition to glow discharge cleaning, operable only in the absence of toroidal field, electron cyclotron wall conditioning (ECWC) plasmas created with its ECRF launchers are envisioned. ECWC has been successfully operated in helium at the first harmonic in JT-60U, allowing recovering from disruptions. However, in JT-60SA ($R = 2.96$ m, $a = 1.18$ m, $B_t = 2.25$ T), with gyrotrons frequencies $f = 110$ or 138 GHz, ECWC discharges will have to be operated at the second harmonic of the EC wave.

This paper reports on helium ECWC experiments on TCV in support of JT-60SA operation. About forty discharges have been produced in TCV, at a toroidal field $B_t = 1.3$ – 1.54 T, with gyrotrons at 82.7 GHz in X2 mode. Hence, the cold ECR layer lies in TCV at $R = 0.78$ – 0.92 m, mimicking operation in JT-60SA. Helium pressures ranged between 0.5 and 2×10^{-2} Pa and ECRH powers up to 480 kW, using different launchers. Horizontal and vertical poloidal fields with amplitudes typically 0.1 to 2% of B_t have been used, aiming at extending the discharge vertically and radially. Discharge homogeneity was estimated from the electron density radial profile measured with far-infrared interferometry (FIR) and from visible CCD images, while wall coverage was assessed from the ion saturation current measured by the TCV array of wall-mounted Langmuir probes located at the high and low field sides, and at the bottom of the device. Electron densities of 5 – $15 \times 10^{18}/\text{m}^3$ and temperatures of 20 – 40 eV have been measured with the TCV FIR and Thomson Scattering systems. Typical edge temperatures were found to be 3 eV at the probes.

The efficiency of ECWC was assessed from the amount of released D_2 fuel, measured in the exhaust gas using optical Penning gauges connected to the vacuum vessel. About 2×10^{20} D_2 molecules could be removed with the forty He-ECWC discharges operated in TCV. Despite this, the initiation of a standard ohmic D_2 -plasma could not be sustained after conditioning. Thus, demonstration of the ability of ECWC, operated in X2 mode, to recover to normal operation still remains to be done. For this, a larger operational domain will need to be investigated, e.g., higher pressures, different field patterns, and longer ECWC operation will be needed.

Distributed Digital Real-Time Control System for the TCV Tokamak and its Applications

H. Anand¹, S. Coda¹, C. Galperti¹, B. Duval¹, F. Felici², T. Blanken², E. Maljaars², J.-M. Moret¹, O. Sauter¹, T. P. Goodman¹, H. B. Le¹, and D. Kim³

¹Swiss Plasma Center (SPC), École polytechnique fédérale de Lausanne (EPFL), 1015 Lausanne, Switzerland

²Eindhoven University of Technology, Eindhoven, Netherlands

³International Thermonuclear Experimental Reactor (ITER), Cadarache Centre, 13108 Saint-Paul-lès-Durance, France

Corresponding Author: H. Anand, himank.anand@epfl.ch

A key feature of the new digital plasma control system installed on the TCV tokamak is its possibility to rapidly design, test and deploy real-time algorithms. It accommodates hundreds of diagnostic inputs and actuator outputs, and offers the possibility to design advanced control algorithms with better knowledge of the plasma state and to coherently control all TCV actuators, including poloidal field coils, gas valves, the gyrotron powers and launcher angles of the electron cyclotron heating and current drive system together with diagnostic triggering signals. It encompasses plasma control applications ranging from basic experiments of coil current and density control to advanced experiments of MHD and plasma profile control. The system consists of multiple nodes, each of which may have a local ADC and/or DAC card; all nodes are connected to a memory network (reflective memory), providing a deterministic method of sharing memory between them. Recently, a generalized plasma position and shape controller based on the real time Grad-Shafranov solver RTLIUQE was developed and implemented, providing the basis for future high performance plasma operation with advanced plasma configurations. The controller design is based on an isoflux control scheme and utilizes singular value decomposition (SVD), to respect the limits on poloidal field coils currents by limiting the controlled parameters to the set that can be more easily controlled. The controller is capable in principle of providing improved equilibrium control especially for unconventional plasma scenarios, e.g., reliable control of “snowflake” equilibria with closely spaced X-points, i.e., the “exact” snowflake, and the development of negative triangularity plasmas in H-mode. An addition of a new node on the digital control system has enhanced the real time computational capacity and hosts the real-time transport code RAPTOR (rapid plasma transport simulator), an advanced density profile reconstruction algorithm including real-time fringe jump correction, as well as a plasma state monitoring, supervision and actuator management algorithm. In future, more signals from existing TCV diagnostics, including multiview pinhole X-ray diagnostics, Thomson scattering, visible image processing and magnetic signals for MHD mode analysis will be added to expand the capabilities of the digital control system.

EX



Real-Time Model-Based Plasma State Estimation, Monitoring and Integrated Control in TCV, ASDEX-Upgrade and ITER

F. Felici¹, T. Blanken¹, B. Maljaars¹, H. Van den Brand², J. Citrin², D. Hogewij², M. Scheffer¹, M. De Baar², M. Steinbuch¹, S. Coda³, C. Galperti³, J.-M. Moret³, O. Sauter³, A. Teplukhina³, T. Vu⁴, R. Nouailletas⁴, O. Kudlacek⁵, C. Piron⁵, P. Piovesan⁵, W. Treutterer⁶, C. Rapson⁶, L. Giannone⁶, and M. Willensdorfer⁶

¹Eindhoven University of Technology, Eindhoven, Netherlands

²FOM Institute DIFFER, Association EURATOM-FOM, Nieuwegein, Netherlands

³Swiss Plasma Center (SPC), École polytechnique fédérale de Lausanne (EPFL), 1015 Lausanne, Switzerland

⁴Institut de Recherche sur la Fusion par confinement Magnétique (IRFM),

Commissariat à l'énergie atomique (CEA/Cadarache), 13108 Saint-Paul-lès-Durance, France

⁵Consorzio RFX, Associazione EURATOM-ENEA sulla Fusione, Padova, Italy

⁶Max-Planck-Institut für Plasmaphysik, Garching, Germany

Corresponding Author: F. Felici, f.felici@tue.nl

To maintain a high-performance, long-duration tokamak plasma scenario, it is necessary to maintain desired profiles while respecting operational limits. This requires real-time estimation of the state of the profiles, monitoring of their evolution with respect to predictions and known limits, and their active control within a desired envelope. Model-based techniques are particularly suitable to tackle such problems due to the nonlinear nature of the processes and the tight coupling among the various physical variables. Control-oriented models required for such techniques have been recently developed for particle, temperature and current density profiles. These are implemented in the RAPTOR control-oriented physics-based tokamak simulation code. RAPTOR is capable of tokamak discharge plasma profile evolution in real-time. It includes the main nonlinear dependencies in the profiles, effects of sawteeth and NTMs, as well as all relevant sources, sinks, heating and current drive actuators.

We present various new applications of control-oriented profile evolution models for TCV, ASDEX-Upgrade and ITER. Real-time estimation of profiles is performed on TCV and ASDEX-Upgrade by combining diagnostic data with real-time model-based predictions in a dynamic state observer. By monitoring the differences between measurements and predictions, unexpected signals can be determined that may come from diagnostic faults, actuator failures or unexpected evolution of the plasma itself. These strategies for model-based real-time scenario monitoring are tested on TCV and ASDEX-Upgrade and can provide a first line of defence against easily predictable disruptions that have a clear origin, minimizing the use of last-resort disruption mitigation measures.

To maintain the plasma in the desired state for the duration of the discharge, profile controllers are designed that can deal with varying constraints in the plasma and actuators as well as provide ahead-of-time warning of constraint violations. At the same time, a real-time actuator allocation algorithm performs a prioritization of control objectives and assigns resources to each controller. Simulations of combined plasma q -profile, temperature, and NTM control for an ITER scenario are shown, representing a first example of a coupled, resource-aware control scheme that will benefit future tokamak operation.

Study of Interactions between GAMs and Broadband Turbulence in the T-10 Tokamak

A. Melnikov¹, L. Eliseev¹, S. Lysenko¹, S. Grashin¹, V. Lakhin¹, S. Perfilov¹,
A. Smolyakov¹, R. Solomatin¹, V. Zenin¹, and V. Vershkov¹

¹National Research Centre "Kurchatov Institute", Moscow, Russian Federation

Corresponding Author: A. Melnikov, melnikov_07@yahoo.com

The new finding in study of geodesic acoustic modes (GAMs) on the T-10 tokamak since the last IAEA FEC-2014 are described. The broadband oscillations of plasma electric potential and density in Ohmic and ECRH regimes are measured by heavy ion beam probe (HIBP) in the core plasma. At the periphery, at $r/a > 0.8$, the dominated GAM peak with frequency ~ 14 kHz and noticeable peak of quasi-coherent oscillations with frequency 40–100 kHz and HFHM ~ 30 kHz are observed. The noticeable GAM peak is also seen on the frequency resolved turbulent particle flux measured by HIBP and probes. It was found that in the high-density ($n_e \sim 4 \times 10^{19}/\text{m}^3$) discharges during ECRH pulse, causing the energy confinement degradation, the level of broadband fluctuations measured by correlation reflectometry and HIBP decreases. At the same time the amplitude of GAM oscillations of plasma potential increases. The bispectral analysis of potential oscillations shows the statistically significant auto-bicoherency at the GAM frequency at the periphery, $r/a > 0.8$, indicating existence of three-wave interaction between GAM and broadband turbulence up to the presently studied frequency band 250 kHz, that points to quadratic character of nonlinearity in GAM generation, e.g., owing to Reynolds stress. This also holds for the cross-bicoherency of potential with density and poloidal magnetic field. For the plasma periphery, the two-fluid model of nonlinear interplay between GAM and small-scale drift turbulence, excited by dissipative trapped electron mode is proposed. The model includes collisional damping of GAM due to parallel ion viscosity. The modelled GAM amplitude scales with density as $1/n$ that is consistent with the experimental observation.

EX



Disruptions and Runaway Mitigation Using ECRH and Inductive Power Supply Systems in the T-10 Tokamak

P. Savrukhin¹, E. Shestakov¹, and A. Ermolaeva¹

¹National Research Centre "Kurchatov Institute", Moscow, Russian Federation

Corresponding Author: P. Savrukhin, p.savrukhin@iterrf.ru

EX Experiments in the T-10 tokamak ($R = 1.5$ m, $a = 0.3$ m) have demonstrated possibility of control of the plasma current decay and prevention of formation of the nonthermal ($E_g > 150$ keV) electron beams after an energy quench at the density limit disruption using electron cyclotron heating (ECRH) and preprogrammed Ohmic (OH) power supply system. Quasi-stable plasma operation with repetitive sawtooth oscillations can be restored after an energy quench using high auxiliary power ($P_{EC} > 2-5P_{OH}$). Optimal conditions of the plasma discharge recovery after an energy quench using auxiliary heating are identified. A radial scan of the auxiliary power deposition location was provided by changing of the toroidal magnetic field. At high auxiliary power restoration of the plasma discharge can be provided with location of the EC resonance zone within the whole plasma cross section. The auxiliary power required for discharge restoration is minimal when the power is deposited around the $m = 2, n = 1$ magnetic island (close to the $q = 2$ surface). At low plasma current disruptions can be avoided only when auxiliary power is deposited inside the $q = 2$ surface. The threshold power increases linearly with plasma current. Numerical modelling has indicated that suppression of the nonthermal electrons can be connected with elimination of the bursting electric fields induced during periodic magnetic reconnections and reduction of the "equilibrium" electric field due to increase of the bulk plasma temperature due to ECRH. Possible strategy of the plasma discharge recovery after an energy quench in a tokamak reactor using auxiliary heating and controllable reduction of the plasma current is proposed.

Trigger conditions of the energy quench are studied in the T-10 tokamak using fast in-vessel movable magnetic probes. Experiments indicated that abrupt restructuring of the low- m MHD modes and inward plasma shift during an energy quench are accompanied by bursts of fast-scale (~ 0.5 MHz) magnetic fields perturbations. Analysis has revealed possible connection of the magnetic bursts with plasma arching phenomena and nonthermal electrons induced during disruption.

Work supported by ROSATOM (H.4f.45.90.11.1021).



Study of Light and Heavy Impurities Transport in OH and ECRH Plasmas on the T-10 Tokamak

M. Nurgaliev¹, V. Krupin¹, L. Klyuchnikov¹, A. Dnestrovskij¹, A. Nemets¹, K. Korobov¹, D. Sarychev¹, A. Borschevskij¹, S. Krylov¹, N. Naumenko², D. Ryzhakov¹, V. Trukhin¹, D. Sergeev¹, N. Mustafin¹, G. Tilinin¹, and S. Tugarinov¹

¹National Research Centre "Kurchatov Institute", Moscow, Russian Federation

²B.I. Stepanov Institute of Physics, NASB, Minsk, BY-220072, Belarus

Corresponding Author: M. Nurgaliev, maxim.nurgaliev@gmail.com

The results of impurity (C, O, Ar, K, Fe, and W) transport investigation in OH and ECRH discharges on the T-10 tokamak are presented in this paper. The main attention is paid to a study of the impurity removal from the plasma centre during ECRH. It is shown that in the ohmic discharges, neoclassical accumulation of impurities near the plasma axis occurs. This process enhances the effect of impurity removal during ECR heating. The investigation of impurities transport in OH plasmas allows determining a dependence of impurity confinement times τ_z and anomalous diffusion coefficient D_z^{an} on plasma parameters: $\tau_z \sim \gamma$ and $D_z^{an} \sim \gamma^{-1}$, where $\gamma = n_e Z_{eff} / I_{pi}^{1.5}$. Significant impurity accumulation followed by impurity density profile peaking relatively to the electron density is observed in ohmic discharges with high gamma.

The study of impurities behaviour at the ohmic stage is performed to define the influence of initial conditions on ECRH impurity removal process. The effect of the light atom (C and O) impurity removal during ECRH has been demonstrated on the T-10 previously. In the present paper, a removal efficiency from the plasma centre $K_{eff}(0)$ is introduced and it is shown that $K_{eff}(0)$ increases with gamma and ECRH power per particle.

In contrast to the OH stage, wherein impurity peaking phase follows the long accumulation of impurities, at the ECRH stage the fast elimination of enhanced peaking (the first phase: 20 to 40 ms after ECRH start) is followed by the slow phase of exponential impurity decay (the second phase: 100 to 150 ms after ECRH start). The analysis of the light and heavy impurities behaviour at the second phase shows that there are no significant differences of the transport coefficients for C, O, and Fe in the ECRH discharges on T-10.

Numerical simulation of impurity transport is performed in the transport code STRAHL, including neoclassical and anomalous transport. Anomalous transport coefficients and their dependences on plasma parameters and auxiliary heating power are determined by modelling of dynamic and balance characteristics of intrinsic impurities during ECR heating.

At the last experimental campaign, new tungsten limiter has been installed instead of a carbon one. It allows carrying out experiments for an investigation of tungsten transport on the T-10 in OH and ECRH discharges.

EX

Lithium and Tungsten Limiters for 3 MW of ECR Plasma Heating in T-10 Tokamak: Design, First Results

I. Lyublinski¹, A. Vertkov¹

¹JSC "Red Star", Moscow, Russian Federation

Corresponding Author: I. Lyublinski, lyublinski@yandex.ru

Application of powerful (up to 3 MW) ECR plasma heating in T-10 tokamak with graphite limiters is pulled down with a problem of the plasma pollution at power input more than 2 MW. The use of carbon based limiters leads to formation of carbon films on a surface of a tokamak chamber wall essentially increasing of impurity flux and hydrogen recycling. For the solution of these problems the new tungsten and lithium limiters are developed. As it is supposed, application of tungsten as a plasma facing material will allow excluding carbon influx into the vacuum chamber. An additional lithium limiter arranged in a shadow of tungsten one will be used as a lithium source for plasma periphery cooling due to a reradiation on lithium that will lead to decrease in power deposition on tungsten limiters.

Parameters and design of limiters are presented. Lithium limiter can move with respect to last closed magnetic surface that allows regulating of incoming power flux and, as consequence, a lithium influx into plasma. Plasma facing surface of a limiter is made of capillary-porous system (CPS) with lithium. Porous matrix of CPS (W felt) provides stability of liquid lithium surface under MHD force effect and an opportunity of its constant renewal due to capillary forces.

The necessary lithium flux from a lithium limiter surface is estimated for maintenance of normal operation mode of tungsten limiters at ECRH power of 3 MW during 400 ms. It is supposed, that Z_{eff} of plasma would not exceed 2 in this case and about 13 g of lithium deposit will be on the wall for the campaign of 1000 discharges. Thus, the upgrade of limiters in tokamak T-10 will allow providing of ECR plasma heating with power up to 3 MW at reasonable lithium flux. Results of first experiments with complex of lithium and tungsten limiters on T-10 tokamak are presented.



Reduction of CS Flux Consumption during Plasma Current Ramp-Up on DEMO Reactor

T. Wakatsuki¹, T. Suzuki¹, N. Hayashi¹, J. Shiraishi¹, S. Ide¹, H. Kubo¹, and Y. Kamada¹

¹*Japan Atomic Energy Agency (JAEA), Naka, Japan*

Corresponding Author: T. Wakatsuki, wakatsuki.takuma@jaea.go.jp

Reduction of magnetic flux consumption of a central solenoid (CS) during a plasma current ramp-up phase is investigated using an integrated modelling code suite (TOPICS). It is shown that 27% of the CS flux can be saved in DEMO reactor by 50 MW of EC heating at $\rho \sim 0.5$. The plasma β is kept low in this scenario. If a safety factor profile should not be a strongly reversed shear profile in order to avoid MHD instabilities, reduction of CS flux consumption is limited below 13% regardless of the electron density. This limitation can be relaxed if the heating profile becomes broad using multiple EC rays. Possibility of more advanced current ramp-up scenarios with no CS flux consumption has already been demonstrated for JT-60SA. As a result, requirement on heating and current drive sources, the plasma β , a safety factor profile and a pressure profile are clarified when CS flux consumption is reduced by 10–100%.

Development of a Real-Time Simulation Tool towards Self-Consistent Scenario of Plasma Startup and Sustainment on Helical Fusion Reactor FFHR-d1

T. Goto¹, J. Miyazawa¹, R. Sakamoto¹, C. Suzuki¹, R. Seki¹, S. Satake¹, B. Huang², M. Nunami¹, M. Yokoyama¹, and A. Sagara¹

¹National Institute for Fusion Science (NIFS), Toki, Gifu, Japan

²Graduate University for Advanced Studies (SOKENDAI), Hayama, Kanagawa, Japan

Corresponding Author: T. Goto, goto.takuya@lhd.nifs.ac.jp

EX In a heliotron type system like LHD, compatibility between MHD stability and good confinement is recognized as one of the crucial issues. This paper reports the world's first attempt of the close investigation of self-consistent solution of plasma operation scenario in view of MHD stability, anomalous transport, alpha energy loss and impurity effect in addition to MHD equilibrium and neoclassical transport. Using a 1D calculation model which can reproduce typical pellet discharges of LHD experiment, plasma operation regime of the LHD-type helical reactor FFHR-d1 was examined. It was found that a steady-state, subignition operation with fusion gain Q at least 5 can be attained with the plasma parameters established in the previous study: the same reference profile of gyro-Bohm normalized pressure, magnetic configuration with inward-shifted vacuum magnetic axis position (the ratio between the magnetic axis position and the major radius is 3.5/3.9) and alpha energy loss fraction of 15%. It is the first result to give the operation scenario of FFHR-d1 within the parameter regime that has already been confirmed in LHD experiment: edge electron density below Sudo density limit, Mercier index at the $m/n = 1/1$ rational surface below 0.25, the energy loss by anomalous transport twice larger than that by neoclassical transport. Operation with further larger fusion gain is achievable by optimization of the plasma and engineering design parameters. Because real time calculations are possible by utilizing the model or scaling established by the detailed analysis codes, systematic analysis of different design parameters can be easily obtained. This study clarified the effect of the plasma and engineering design parameters (e.g., magnetic field configuration and plasma radial profile) on self-consistent plasma operation regime of the helical reactor FFHR-d1. Although further detailed analysis including the effect of boot-strap current, temperature inequality, edge neutral particles and deposition profile of heating power is needed, this study provides the design conditions of the plasma control system and contributes to the plant system design of FFHR-d1. The developed calculation tool can be a base and guidelines of the real-time predictive simulation tool of the core plasma which aids the plasma operation control of future fusion power plants.

Physics and Operation Oriented Activities in Preparation of the JT-60SA Tokamak Exploitation

G. Giruzzi¹, E. Joffrin¹, J. Garcia¹, D. Douai¹, J.-F. Artaud¹, B. Pégourié¹, P. Maget¹, Y. Kamada², M. Yoshida², S. Ide², N. Hayashi², G. Matsunaga², T. Nakano², K. Shinohara², S. Sakurai², T. Suzuki², H. Urano², M. Enoeda², H. Kubo², K. Kamiya², M. Takechi², Y. Miyata², A. Isayama², T. Kobayashi², S. Moriyama², K. Shimizu², K. Hoshino², H. Kawashima², A. Bierwage², D. C. McDonald³, C. Sozzi⁴, L. Figini⁴, S. Nowak⁴, A. Moro⁴, P. Platania⁴, D. Ricci⁴, G. Granucci⁴, T. Bolzonella⁵, P. Bettini⁵, P. Innocente⁵, D. Terranova⁵, L. Pigatto⁵, F. Villone⁶, A. Pironti⁶, S. Mastrostefano⁶, G. De Tommasi⁶, M. Mattei⁶, A. Mele⁶, F. P. Orsitto⁶, D. Dunai⁷, T. Szepesi⁷, E. Barbato⁸, V. Vitale⁸, M. Romanelli⁹, L. Garzotti⁹, A. Boboc⁹, S. Saarelma⁹, M. Wischmeier¹⁰, P. Lauber¹⁰, P. Lang¹⁰, R. Neu¹⁰, C. Day¹¹, C. Gleason-Gonzalez¹¹, M. Scannapiego¹¹, R. Zagorski¹², K. Galazka¹², W. Stepniewski¹², N. Cruz¹³, E. de la Luna¹⁴, M. Garcia-Munoz¹⁴, J. Vega¹⁴, S. Clement-Lorenzo¹⁵, F. Sartori¹⁵, S. Coda¹⁶, T. P. Goodman¹⁶, and S. Soare¹⁷

¹*Institut de Recherche sur la Fusion par confinement Magnétique (IRFM), Commissariat à l'énergie atomique (CEA/Cadarache), 13108 Saint-Paul-lès-Durance, France*

²*Japan Atomic Energy Agency (JAEA), Naka, Japan*

³*EUROfusion Garching, 85748 Garching, Germany*

⁴*Istituto di Fisica del Plasma (IFP), Consiglio Nazionale delle Ricerche (CNR), 20125 Milan, Italy*

⁵*Consorzio RFX, Associazione EURATOM-ENEA sulla Fusione, Padova, Italy*

⁶*Consorzio CREATE, 80125 Napoli, Italy*

⁷*Wigner Research Center, Association EURATOM, Budapest, Hungary*

⁸*Agenzia nazionale per le nuove tecnologie, l'energia e lo sviluppo economico sostenibile (ENEA), Rome, Italy*

⁹*Culham Centre for Fusion Energy (CCFE), Culham Science Centre, Abingdon, UK*

¹⁰*Max-Planck-Institut für Plasmaphysik, Garching, Germany*

¹¹*Karlsruhe Institute of Technology (KIT), Karlsruhe, Germany*

¹²*Institute of Plasma Physics and Laser Microfusion, Warsaw, Poland*

¹³*Instituto Superior Técnico (IST), Lisbon, Portugal*

¹⁴*Centro de Investigaciones Energéticas, Medioambientales y Tecnológicas (CIEMAT), Madrid, Spain*

¹⁵*F4E: Fusion for Energy, ITER EU Centre, 08019 Barcelona, Spain*

¹⁶*Swiss Plasma Center (SPC), École polytechnique fédérale de Lausanne (EPFL), 1015 Lausanne, Switzerland*

¹⁷*Institute of Cryogenics and Isotopic Technologies (ICIT), Valcea, Romania*

Corresponding Author: G. Giruzzi, gerardo.giruzzi@cea.fr

JT-60SA is a large fully superconducting new tokamak device being built under the Broader Approach Satellite Tokamak Programme jointly by Europe and Japan, and under the Japanese national programme. The JT-60SA tokamak is due to start operation in 2019 and will be at the forefront of the international fusion programme for many years, both before and during the DT phase of ITER operation. It will support the ITER experimental programme as a satellite machine and at the same time provide key information for the design of DEMO scenarios. Efficient start-up of operation and scientific exploitation of such a large experimental device by an international team is a challenging enterprise, in many aspects similar to what is expected for ITER.

Continued...

In order to optimize such a start phase, a broad set of preparation activities has been carried out for years and are now significantly intensifying. They involve the elaboration of the JT-60SA Research Plan, advanced modelling in various domains (scenario, MHD and control, fast particles, edge, divertor, etc.), feasibility and conception studies of diagnostics and other subsystems (H&CD, matter injection and pumping, etc.) in connection with the priorities of the scientific programme, development and validation of operation tools (data and analysis system, remote participation, magnetic control, wall conditioning etc.). These activities are carried out in a coordinated way by a joint Japanese-EU JT-60SA Research Unit, with the EU team organized in the framework of the EUROfusion WPSA work package, in close interaction with the F4E JT-60SA home team. The logic and coherence of this approach, as well as the main results obtained so far, are presented and summarized in this work. A few examples only will be discussed in detail.

Preparation of PFCs for the Efficient Use in ITER and DEMO: Plasma-Wall Interaction Studies within the EUROfusion Consortium

S. Brezinsek¹, J. W. Coenen¹, T. Schwarz-Selinger², K. Schmid², A. Kirschner¹, A. Hakola³,
F. Tabares⁴, H. van der Meiden⁵, M.-L. Mayoral⁶, E. Tsitrone⁷, and M. Reinhart¹

¹Forschungszentrum Jülich, Jülich, Germany

²Max-Planck-Institut für Plasmaphysik, Garching, Germany

³VTT Technical Research Centre of Finland Ltd., Espoo, Finland

⁴Centro de Investigaciones Energéticas, Medioambientales y Tecnológicas (CIEMAT), Madrid, Spain

⁵FOM Institute DIFFER, Association EURATOM-FOM, Nieuwegein, Netherlands

⁶Culham Centre for Fusion Energy (CCFE), Culham Science Centre, Abingdon, UK

⁷Commissariat à l'énergie atomique (CEA), 91400 Gif-sur-Yvette, France

Corresponding Author: S. Brezinsek, s.brezinsek@fz-juelich.de

Particle and power exhaust compatible with first wall components and the edge plasma is a key area of research and mandatory for a successful operation of ITER and beyond. Within EUROfusion, the research includes tokamak (JET and Medium-Sized Tokamaks) research studies and dedicated laboratory experiments in linear plasma devices, electron and ion beam loading facilities. The connection of both research areas is done via common physics studies, qualification and specification of plasma-facing components (PFCs), and most importantly, by simulation of plasma exhaust and plasma-material interaction starting from basic process modelling by, e.g., molecular dynamics to integrated tokamak modelling by, e.g., erosion-deposition codes like ERO. Laboratory heat load facilities and linear plasmas are presently essential for predicting the PFC performance during long pulse operation at the high particle fluence ($> 10^{27} \text{ D}^+ / \text{m}^2$) and number of thermal cycles ($> 10^6$ ELMs), though WEST will be available soon for complementary tokamak studies.

The WP PFC is addressing these critical points in order to ensure reliable and efficient use of conventional, solid PFCs in ITER (Be and W) and DEMO (W) with respect to heat load capabilities (transient and steady-state heat and particle loads), lifetime estimates (erosion, material mixing, and surface morphology) and safety aspects (fuel retention, fuel removal, material migration, and dust formation) as well as to develop alternative scenarios and concepts (liquid Sn or Li PFCs) for DEMO if the conventional solution turns out not to be functional. The development of diagnostics to determine crucial physics quantities like, e.g., the fuel content and material composition in PFCs exposed to divertor-like plasma conditions (mixed fuel, helium, and seeding gas) by LIBS is covered in a supporting activity.

Here, an overview of results will be given with emphasis on i) the observed synergistic effects in particle and heat loading with the available set of exposition devices on material properties such as roughness, ductility and microstructure, ii) the progress in understanding of fuel retention, diffusion, and outgassing in W-based materials including the impact of damage and impurities like N, and iii) the preferential sputtering of Fe in EUROFER steel providing in-situ a W surface and a potential alternative first wall solution for DEMO.

Recent Progress of Divertor Simulation Research Using the GAMMA 10/PDX Tandem Mirror

Y. Nakashima¹, K. Ichimura¹, M. S. Islam¹, M. Sakamoto¹, N. Ezumi¹, M. Hirata¹, M. Ichimura¹, R. Ikezoe¹, T. Imai¹, T. Kariya¹, I. Katanuma², J. Kohagura¹, R. Minami¹, T. Numakura¹, M. Yoshikawa², M. M. Islam¹, K. Nojiri¹, K. Shimizu¹, A. Terakado¹, N. Asakura³, M. Fukumoto³, A. Hatayama⁴, Y. Hirooka⁵, S. Kado⁶, H. Kubo³, S. Masuzaki⁵, H. Matsuura⁷, T. Nakano³, S. Nagata⁸, N. Nishino⁹, N. Ohno¹⁰, A. Sagara⁵, K. Sawada¹¹, M. Shoji⁵, A. Tonegawa¹², and Y. Ueda¹³

¹Plasma Research Center, University of Tsukuba, Tsukuba, Ibaraki, Japan

²University of Tsukuba, Tsukuba, Ibaraki, Japan

³Japan Atomic Energy Agency (JAEA), Naka, Japan

⁴Faculty of Science and Technology, Keio University, Tokyo, Japan

⁵National Institute for Fusion Science (NIFS), Toki, Gifu, Japan

⁶Institute of Atomic Energy, Kyoto University, Nishikyo-ku, Kyoto 615-8540, Japan

⁷Radiation Research Center, Osaka University, Osaka, Japan

⁸Institute for Materials Research (IMR), Tohoku University, Sendai, Miyagi, Japan

⁹Graduate School of Engineering, Hiroshima University, Higashi-Hiroshima, Japan

¹⁰Graduate School of Engineering, Nagoya University, Nagoya 464-8603, Japan

¹¹Graduate School of Science and Technology, Shinshu University, Nagano, Japan

¹²Graduate School of Science, Tokai University, Tokyo, Japan

¹³Osaka University, Osaka, Japan

Corresponding Author: Y. Nakashima, nakashima@prc.tsukuba.ac.jp

This paper describes the characteristics of detached plasma produced by using hydrogen and noble gases together with the progress of high-heat and particle flux generation experiments in the GAMMA 10/PDX end-cell. In the Plasma Research Center, University of Tsukuba, divertor simulation experiments have been started at the end-cell of GAMMA 10/PDX (E-divertor) [1]. In the GAMMA 10/PDX end-cell, plasma flow with high temperature ($T_i = 100\text{--}400$ eV, $T_e = 30$ eV), heat and particle fluxes (> 10 MW/m², $> 10^{23}$ /m²s, respectively) have been produced under the high magnetic field (~ 1 T), which cannot be attained by conventional liner devices [2]. We have succeeded in achieving detachment of high temperature plasma equivalent to the SOL plasma of tokamaks in spite of using a linear device with short connection length of magnetic field line. Various gases (N₂, Ne, Ar, Xe) are examined to evaluate the effect of radiation cooling against the plasma flow of MW/m² level in a divertor simulation region and the following results are obtained: i) Xe gas was most effective on electron cooling (down to ~ 2 eV) and reduction of heat and particle fluxes (1%, 3%, respectively). ii) Ne gas was less effective. On the other hand, iii) N₂ gas showed more favourable effects than Ar. The above results are almost consistent with the observation from an absolutely calibrated visible spectrometer viewing the inside of D-module, such as i) stronger emission from Xe I and II, ii) significant molecular visible-emission from N₂, etc. Furthermore, in the case with a simultaneous injection of hydrogen and Xe gases, the ion flux was almost fully suppressed, which indicates the existence of molecular activated recombination in D-module.

Continued...

In plasma flow generation experiments, ICRF heating in anchor-cell successfully extended the particle flux up to $3.3 \times 10^{23}/\text{m}^2\text{s}$ in the end-cell. Superimposing the ECH pulse (380 kW \times 5 ms) into the ICRF plasma also succeeded in extending the highest heat flux of $\sim 15 \text{ MW}/\text{m}^2$ which exceeds the ITER divertor heat load in the steady state. These results will contribute to the progress in detached plasma operation and clarification of radiation cooling mechanism towards the development of the future divertor.

References

- [1] Y. Nakashima, *et al.*, Fusion Eng. Des. **85**, 6, 956–962 (2010).
- [2] Y. Nakashima, *et al.*, J. Nucl. Mater. **463** 537–540 (2015).



Spatial Structure of Spontaneously Excited ICRF Waves and Relevant High-Energy Ion Loss in the GAMMA 10 Tandem Mirror

R. Ikezoe¹, M. Ichimura¹, M. Hirata¹, T. Okada¹, S. Sumida¹, S. Jang¹, J. Itagaki¹, M. Yoshikawa¹, J. Kohagura¹, M. Sakamoto¹, and Y. Nakashima¹

¹*Plasma Research Center, University of Tsukuba, Tsukuba, Ibaraki, Japan*

Corresponding Author: R. Ikezoe, ikezoe@prc.tsukuba.ac.jp

High- β plasma confinement in a mirror field is subject to the influence of the temperature-anisotropy driven mode referred as Alfvén-ion-cyclotron (AIC) wave. The spatial structure of the AIC waves and the enhanced loss of high-energy ions owing to the AIC waves are simultaneously investigated in GAMMA 10 from a standpoint of wave-particle interaction. A clear correlation between the excitation of the AIC waves and the enhanced axial loss of high-energy ions is obtained and precise spatial structure of the AIC waves including those power and phase profiles, which is a key for the understanding of the temperature-anisotropy relaxation process, is clarified by using a reflectometer for the first time.



Investigation of Detached Recombining Plasmas in a Linear Device Pilot-PSI and its Impact on Plasma Detachment in Fusion Devices

Y. Hayashi¹, H. Nishikata¹, N. Ohno¹, S. Kajita¹, K. Ješko², H. Meiden³, J. Vernimmen³, T. W. Morgan³, T. Iijima⁴, A. Tonegawa⁴, A. Okamoto¹, and S. Kado⁵

¹Nagoya University, Nagoya, Japan

²Institut de Recherche sur la Fusion par confinement Magnétique (IRFM), Commissariat à l'énergie atomique (CEA/Cadarache), 13108 Saint-Paul-lès-Durance, France

³FOM Institute DIFFER, Association EURATOM-FOM, Nieuwegein, Netherlands

⁴Tokai University, Tokyo, Japan

⁵Institute of Advanced Energy, Kyoto University, Nishikyo-ku, Kyoto 615-8540, Japan

Corresponding Author: Y. Hayashi, hayashi-yuki13@ees.nagoya-u.ac.jp

Handling enormous plasma heat load to divertor is essential to the achievement of high fusion gain. The electron-ion recombination (EIR) process is required to reduce particle flux, leading to reduction of heat load due to the surface recombination. Further, in the ITER research plan, initial studies of H-modes are planned in helium plasmas because the predicted H-mode threshold power in helium plasma is lower than that of hydrogen [1]. Therefore, it is necessary to conduct plasma detachment experiments under the high density helium plasma condition that is relevant to detached divertor operations in ITER.

Electrostatic probe and Thomson scattering (TS) measurements were performed in detached recombining plasma (DRP) in a linear plasma device, Pilot-PSI. Pilot-PSI [2] can produce high density helium plasma above $10^{20}/\text{m}^3$ in steady state. The electron temperature (T_e) measured by using electrostatic probe showed a good agreement with TS measurement without any anomaly of probe characteristics, observed in other linear devices [3, 4].

The particle and heat fluxes at the target dramatically decreased with neutral pressure (P), while they were almost constant at the upstream. When $P \sim 15$ Pa, the peak particle flux decreased from 10^{24} to $10^{22}/\text{m}^2\text{s}$ and heat flux from $7 \text{ MW}/\text{m}^2$ to $0.1 \text{ MW}/\text{m}^2$ along the magnetic field in DRP region with a length of ~ 0.5 m. The EIR process contributed to the strong reduction of the particle and heat fluxes, due to the reduction of T_e from 3 eV to 0.2 eV. This experimental result indicates that narrow DRP region determines the heat load to the divertor plate associated with EIR process. It can be also said that the stable control of the DRP region is quite essential in future fusion devices.

References

- [1] D. J. Campbell, *et al.*, IAEA FEC-2012, (San Diego, CA, USA), [ITR/P1-18](#).
- [2] G. J. van Rooij, *et al.*, *Appl. Phys. Lett.* **90**, 121501 (2007).
- [3] N. Ohno, *et al.*, *Nucl. Fusion* **41**, 1055 (2001).
- [4] A. Okamoto, *et al.*, *Contrib. Plasma Phys.* **46**, 416 (2006).

This work was supported by JSPS KAKENHI Grant Number (25289337). This work is partially supported by NIFS/NINS under the project of Formation of International Network for Scientific Collaborations and NIFS Collaboration Research Programme (NIFS14KUGM094).



Development of Experiment on Multiple-Mirror Trap for Fusion in Budker INP

A. Burdakov¹, A. Avrorov¹, A. Arzhannikov¹, V. Astrelin¹, V. Batkin¹, A. Beklemishev¹, V. Burmasov¹, P. Bykov¹, L. Vyacheslavov¹, D. Gavrilenko¹, A. Gorbovsky¹, I. Ivanov¹, I. Kandaurov¹, A. Kasatov¹, V. Kurkuchekov¹, K. Kuklin¹, K. Mekler¹, S. Polosatkin¹, S. Popov¹, V. Postupaev¹, A. Rovenskikh¹, E. Sidorov¹, S. Sinitsky¹, V. Stepanov¹, A. Sudnikov¹, Y. Sulyaev¹, I. Timofeev¹, Y. Trunev¹, V. Sklyarov¹, N. Sorokina¹, A. Shoshin¹, and D. Yurov¹

¹*Budker Institute of Nuclear Physics (BINP), Novosibirsk, Russian Federation*

Corresponding Author: A. Burdakov, a.v.burdakov@inp.nsk.su

In 2015, the existing GOL-3 multiple-mirror trap has been converted into three specialized devices, each dedicated to a specific scientific problem. Experiments on studies of plasma mechanisms of sub-THz radiation generation use the GOL-3T device. A device with a sub-ms electron beam was isolated for further studies of ITER-grade transient heat loads to tungsten. Research of multiple-mirror physics will continue in a new GOL-NB device that will consist of a central trap with 0.3–0.6 T field, 2.5 m length and 1 m diameter and two attached multiple-mirror sections with 4.5 T field. The plasma will be heated by 1.5 MW NBI. Operation of the first stage of GOL-NB started in 2015. It includes 6 m-long 4.5 T solenoid of variable configuration with a plasma gun. The $1\text{--}4 \times 10^{20}/\text{m}^3$ plasma stream transport through the system was studied. We will also present other activity on the GOL-NB project. A new helical mirror confinement idea and the first concept exploration device SMOLA will be presented as well.

EX



Progress of Plasma Confinement Studies in the Gas Dynamic Trap

P. Bagryansky¹, A. Anikeev¹, M. Anikeev¹, G. Denisov², A. Dunaevsky³,
E. Gospodchikov², A. A. Ivanov¹, A. Lizunov¹, O. Korobeynikova¹, M. Korzhavina¹,
Y. Kovalenko¹, V. Maximov¹, S. Murakhtin¹, E. Pinzhenin¹, V. Prikhodko¹, V. Savkin¹,
A. Shalashov², E. Soldatkina¹, A. Solomakhin¹, D. Yakovlev⁴, P. Yushmanov³, and
K. Zaytsev¹

¹*Budker Institute of Nuclear Physics (BINP), Novosibirsk, Russian Federation*

²*Institute of Applied Physics (IAP), Russian Academy of Sciences (RAS), Nizhny Novgorod, Russian Federation*

³*Tri Alpha Energy, Foothill Ranch, CA 92688, USA*

⁴*Novosibirsk State University, Novosibirsk, Russian Federation*

Corresponding Author: P. Bagryansky, p.a.bagryansky@inp.nsk.su

Active and successful studies of plasma confinement in magnetic mirror traps stopped practically in the late 80's of the last century, despite a number of potential benefits of such systems as the basis for development a nuclear fusion reactor. The reason is that the mirror concept is thought to have three unattractive characteristics. The magnets are complex, the plasma is plagued with microinstabilities and the electron temperature would never approach required keV levels. Researches on the gas dynamic trap (GDT) device at the Budker Institute of Nuclear Physics demonstrated possibilities to overcome these three deficiencies. Stable high energy density plasma can be confined with simple circular magnets, microinstabilities can be tamed, and electron temperatures reaching a keV have been measured. These three accomplishments provide a basis to reconsider the mirror concept as a neutron source for materials development, nuclear fuel production, and fusion energy production. Furthermore, these three achievements unlocked the next level of tasks, aimed at support of the next generation of research facilities, as well as fusion reactors on the basis of mirror traps. List of the most important next-level problems includes: optimization of heating modes using neutral beam injection and auxiliary ECR heating and a detailed study of physical processes in the divertors (regions with an expanding magnetic field behind the magnetic mirrors), limiting longitudinal energy losses. The proposed report includes a brief overview of research on the stabilization of MHD instabilities, study of microinstabilities, and demonstration a tangible increase of the electron temperature with application of auxiliary ECR heating. According to Thomson scattering data, the electron temperature reaches 0.9 keV thus demonstrating threefold increase as compared with modes, where only neutral beams were applied. The main focus in the report made on the study a number of physical processes in the divertor, which define the longitudinal energy transport.

EX

TH: Magnetic Confinement Theory and Modeling

TH



Penetration and Amplification of Resonant Perturbations in 3D Ideal-MHD Equilibria

S. Hudson¹, J. Loizu²

¹Princeton Plasma Physics Laboratory (PPPL), Princeton, NJ 08540, USA

²Max-Planck-Institut für Plasmaphysik, Garching, Germany

Corresponding Author: S. Hudson, shudson@pppl.gov

The nature of ideal-MHD equilibria in three-dimensional geometry is profoundly affected by resonant surfaces, which beget a nonanalytic dependence of the equilibrium on the boundary. Furthermore, nonphysical currents arise in equilibria with continuously nested magnetic surfaces and smooth pressure and rotational-transform profiles.

We demonstrate that three-dimensional, ideal-MHD equilibria with nested surfaces and delta-function current densities that produce a discontinuous rotational transform are well defined and can be computed both perturbatively and using fully-nonlinear equilibrium calculations.

The results are of direct practical importance: we predict that resonant magnetic perturbations penetrate past the rational surface (i.e., “shielding” is incomplete, even in purely ideal-MHD) and that the perturbation is amplified by plasma pressure, increasingly so as stability limits are approached.



Gyrokinetic Projection of the Divertor Heat-flux Width from Present Tokamaks to ITER

C.-S. Chang¹, S.-H. Ku¹, R. Maingi¹, A. Loarte², V. Parail³, M. Romanelli³, and F. Koechl⁴

¹*Princeton Plasma Physics Laboratory (PPPL), Princeton, NJ 08540, USA*

²*International Thermonuclear Experimental Reactor (ITER),*

Cadarache Centre, 13108 Saint-Paul-lès-Durance, France

³*Culham Centre for Fusion Energy (CCFE), Culham Science Centre, Abingdon, UK*

⁴*Institute of Atomic and Subatomic Physics, Technische Universität Wien, 1040 Vienna, Austria*

Corresponding Author: C.-S. Chang, cschang@pppl.gov

The edge gyrokinetic code XGC1 shows that the divertor heat flux width λ_q in between ELMs of type-I ELMy H-modes in two representative types of present tokamaks (DIII-D type for conventional aspect ratio and NSTX type for tight aspect ratio) is set mostly by the ion neoclassical orbit spread, which is proportional to $1/I_p$, while the blobby turbulent spread plays a minor role. This explains the $1/I_p$ scaling of the heat flux width observed in present tokamaks. On the other hand, the XGC1 studies for ITER H-mode like plasmas show that λ_q is mostly set by the blobby turbulent spread, with the heat flux width being about $5\times$ wider than that extrapolated from the $1/I_p$ scaling. This result suggests that the achievement of cold divertor plasmas and partial detachment required for power load and W impurity source control may be more readily achieved and be of simpler control issue than predicted on the basis of the $1/I_p$ scaling. A systematic ongoing validation study of the XGC1 results on various existing tokamaks will also be presented, including JET that is the closest existing device to ITER.

Work supported by the U.S. Department of Energy, and computing resources supported by OLCF at ONRL.

TH/2



Study of Detached H-Modes in Full Tungsten ASDEX-Upgrade with N Seeding by SOLPS-ITER Modelling

I. Senichenkov¹, E. Kaveeva¹, E. Sytova¹, V. Rozhansky¹, S. Voskoboynikov¹, I. Veselova¹, A. S. Kukushkin², D. Coster³, F. Reimold⁴, and X. Bonnin²

¹St. Petersburg State Polytechnical University, St. Petersburg, Russian Federation

²International Thermonuclear Experimental Reactor (ITER),

Cadarache Centre, 13108 Saint-Paul-lès-Durance, France

³Max-Planck-Institut für Plasmaphysik, Garching, Germany

⁴Forschungszentrum Jülich, Jülich, Germany

Corresponding Author: I. Senichenkov, i.senichenkov@spbstu.ru

Our current understanding of divertor physics indicates that at least partial detachment will be a necessary condition for operation of future fusion power devices such as ITER, DEMO and beyond. In recent years a divertor operation with complete detachment was achieved in full tungsten ASDEX-Upgrade with nitrogen seeding [1–3]. Simultaneously, modelling with the SOLPS5.0 transport code reproduced the main features of these experiments [4], e.g., reduction of the target heat and particle fluxes, strong X-point radiation and moderate pedestal pressure loss. In parallel, additional modelling, aimed at understanding the transition to the detachment regime [5], and using the SOLPS-ITER version of the code [6], was performed, however assuming carbon walls, which corresponds to the ASDEX-Upgrade experimental condition before changing to full tungsten walls. This work demonstrated the key role played by the electric field near the X-point [7]. The possible effect of the detached divertor on the radial electric field in the confined region was reported [8].

In the present paper the SOLPS-ITER simulations and a modelling results analysis as from above are revisited, but now considering full tungsten ASDEX-Upgrade walls with nitrogen seeding. The main features observed earlier in the simulations with carbon as the (main) impurity are reproduced. They are in particular the development of strong electric field in the divertor region in the detached regime, cooling of the confined region near the X-point, reduction of the thermoelectric current between the divertor plates, redistribution of poloidal fluxes and reduction of the radial electric field (in absolute value) in the confined region. The influence of deuterium-impurity friction on the nitrogen impurity distribution in the SOL and in the confined region is also investigated.

References

- [1] S. Potzel, *et al.*, Nucl. Fusion **54**, 013001 (2014).
- [2] F. Reimold, *et al.*, Nucl. Fusion **55**, 033004 (2015).
- [3] A. Kallenbach, *et al.*, Nucl. Fusion **55**, 053026 (2015).
- [4] F. Reimold, *et al.*, J. Nucl. Mater. **463**, 128–134 (2015).
- [5] I. Senichenkov, *et al.*, submitted to Nucl. Fusion.
- [6] S. Wiesen, *et al.*, J. Nucl. Mater. **463**, 480–484 (2015).
- [7] I. Senichenkov, *et al.*, EPS conference 2015, Europhys. Conf. Abs. **39E**, P5.191 (2015).
- [8] E. Sytova, *et al.*, H-mode workshop, 2015.



Synergetic Effects of Collisions, Turbulence and Sawtooth Crashes on Impurity Transport

X. Garbet¹, J.-H. Ahn¹, S. Breton¹, P. Donnel¹, D. Esteve¹, R. Guirlet¹, H. Lütjens², T. Nicolas³, Y. Sarazin¹, C. Bourdelle¹, O. Février¹, G. Dif-Pradalier¹, P. Ghendrih¹, V. Grandgirard¹, G. Latu¹, J.-F. Luciani², P. Maget¹, A. Marx¹, and A. Smolyakov⁴

¹*Institut de Recherche sur la Fusion par confinement Magnétique (IRFM), Commissariat à l'énergie atomique (CEA/Cadarache), 13108 Saint-Paul-lès-Durance, France*

²*École Polytechnique, 91128 Palaiseau, France*

³*National Institute for Fusion Science (NIFS), Toki, Gifu, Japan*

⁴*University of Saskatchewan, Saskatoon, SK S7N-5C9, Canada*

Corresponding Author: X. Garbet, xavier.garbet@cea.fr

This paper investigates the interplay of neoclassical, turbulent and MHD processes, which are simultaneously at play when contributing to impurity transport. It is shown that these contributions are not additive, as assumed sometimes. The interaction between turbulence and neoclassical effects leads to less effective thermal screening, i.e., lowers the outward flux due to temperature gradient. This behaviour is attributed to poloidal asymmetries of the flow driven by turbulence. Moreover sawtooth crashes play an important role to determine fluxes across the $q = 1$ surface. It is found that the density profile of a heavy impurity differs significantly in sawtoothed plasmas from the one predicted by neoclassical theory when neglecting MHD events. Sawtooth crashes impede impurity accumulation, but also weaken the impurity outflux due to the temperature gradient when the latter is dominant. Hence the combination of turbulent and MHD effects tends to oppose the effect of neoclassical thermal screening.

THC



High Fidelity Simulations of Fast Ion Power Flux Driven by 3D Field Perturbations on ITER

R. Akers¹, S. Äkäslompolo², B. Colling¹, J. Hess¹, Y. Liu¹, S. D. Pinches³, M. Singh³, A. Turner¹, J. Varje², and K. Särkimäki²

¹United Kingdom Atomic Energy Authority, Culham Science Centre, Abingdon, UK

²Aalto University, Espoo, Finland

³International Thermonuclear Experimental Reactor (ITER), Cadarache Centre, 13108 Saint-Paul-lès-Durance, France

Corresponding Author: R. Akers, rob.akers@ukaea.uk

ITER will be the first tokamak to enter the burning plasma regime and approach ignition; plasma heating will be dominated by 3.5 MeV fusion-born alpha-particles and 1 MeV heating neutral beam (HNB) injected deuterons (together with a fast particle population resulting from ICRH). In this paper we describe a new Monte Carlo code, designed to simulate fast ion behaviour on ITER in the presence of 3D field perturbations. LOCUST-GPU (the Lorentz orbit code for use in stellarators and tokamaks) leverages modern graphics card technology in order to generate unprecedented high fidelity power and particle flux data using workstation-class hardware. We shall describe how the code delivers HPC (high performance computing) class performance to the desktop, the data ingestion part of the workflow (including the production of detailed first wall geometry using CATIA, SpaceClaim and ATTILA, and the generation of plasma response corrections using MARS-F) and ongoing detailed benchmarks and validation tests with the established ASCOT code. We shall also describe experimental validation using data from MAST and finally the results of extensive production runs that are being used to finalize the design of the ITER divertor substructure (where, in contrast to core-born alpha particles, peripherally born HNB ions impinge upon the divertor structure when ELM coil fields are applied). For the first time, it is possible to routinely use a fast-ion code as part of the virtual engineering process in order to design components that are compatible with H-mode operation and the required ELM coil currents for mitigating or controlling ELMs under burning plasma conditions. In the case of a 15 MA H-mode plasma with 33 MW of core HNB injection and a 3D field perturbation made up of toroidal field ripple, ferritic inserts and a 45 kAt ELM coil current for toroidal mode number $n = 3$, the total HNB power losses due to 3D fields are estimated using LOCUST to be $\sim 3.3\%$; the corresponding figure for ASCOT is $\sim 3.8\%$. Small differences are likely due to the fact that for the comparison, ASCOT deployed guiding centre trajectories whereas LOCUST-GPU resolved the full gyro-motion.

This work has been funded by the RCUK Energy Programme (grant number EP/I501045) and by ITER contract IO/13/RT/1-10006/AJB. The views herein do not necessarily reflect those of the ITER Organization.



Gyrokinetic Investigation of the Nonlinear Interplay of Alfvén Instabilities and Energetic Particles in Tokamaks

A. Biancalani¹, M. Cole², A. Bottino¹, A. Könies², P. Lauber¹, O. Mishchenko², B. D. Scott¹, and F. Zonca^{3,4}

¹Max-Planck-Institut für Plasmaphysik, Garching, Germany

²Max-Planck-Institut für Plasmaphysik, Greifswald, Germany

³Associazione EURATOM-ENEA Unitá Tecnica Fusione, Frascati, Italy

⁴Institute for Fusion Theory and Simulation (IFTS), Zhejiang University, Xihu, Hangzhou, Zhejiang, People's Republic of China

Corresponding Author: A. Biancalani, biancalani@ipp.mpg.de

Alfvén eigenmodes (AE) are global instabilities excited by energetic particles (EP) in magnetic fusion devices. AE can redistribute the EP population across flux surfaces, making the plasma heating less effective, and leading to additional loads on the walls. The interplay of AEs and EPs is investigated by means of gyrokinetic particle-in-cell simulations, with a nonperturbative approach. The global nonlinear codes ORB5 and EUTERPE are used for such studies. Both wave-particle and wave-wave nonlinearities are considered and various aspects of the nonlinear dynamics are addressed separately, by artificially switching off other nonlinearities. When concentrating on the wave-particle nonlinearity, a detailed study of the saturation is performed, as a consequence of the redistribution of the EP population in phase-space. A comparison with GK-MHD hybrid codes is also presented. When allowing wave-wave nonlinearities to occur with a zonal structure, the saturation level of the AE is observed to be drastically reduced. As a consequence, a much lower redistribution of EP is observed with respect to the case where only the wave-particle nonlinearity is allowed. Finally, numerical simulations of multiple modes with different toroidal mode number are also presented.

THW



First-Principle Simulations Reproduce Multiple Cycles of Abrupt Large Relaxation Events in Beam-Driven JT-60 Plasmas

A. Bierwage¹, K. Shinohara¹, Y. Todo², N. Aiba¹, G. Matsunaga¹, M. Takechi¹, M. Toma¹, and M. Yagi¹

¹*Japan Atomic Energy Agency (JAEA), Naka, Japan*

²*National Institute for Fusion Science (NIFS), Toki, Gifu, Japan*

Corresponding Author: A. Bierwage, bierwage.andreas@jaea.go.jp

Using the high-performance supercomputer Helios and advanced numerical methods, first-principle simulations of fast-ion-driven magnetohydrodynamic (MHD) modes have, for the first time, reproduced multiple cycles of so-called “Abrupt Large Events (ALE)” as observed in beam-driven high- β JT-60 tokamak experiments. This is a major milestone because, unlike experiments, such simulations can provide us with physical information at arbitrary levels of detail. This is required for clarifying the mechanism that triggers ALEs as well as for the development and verification of reduced models that are urgently needed for predictive simulations of fast ion dynamics in burning-plasma-relevant experiments (such as JT-60SA and ITER) and power plant design (DEMO). In this paper, we describe the numerical methods used, validate the results against experimental data from JT-60, and present first new physics insights that were obtained from the analysis of the simulation results. For instance, it is shown that ALEs occur when multiple fast-ion-driven modes with different toroidal wavelengths grow to large amplitudes while interacting nonlinearly. This multiwavelength nature of ALEs was subsequently confirmed experimentally, which demonstrates the predictive capability of these simulations. Moreover, it is shown that these long-time simulations yield more accurate and detailed predictions for the fast ion density profile and velocity distribution, even in the presence of strong Alfvén mode activity.

TH/4-3



Novel Reactor Relevant RF Actuator Schemes for the Lower Hybrid and the Ion Cyclotron Range of Frequencies

P. T. Bonoli¹, S. G. Baek¹, B. LaBombard¹, M. J. Greenwald¹, R. Leccacorvi¹, Y. Lin¹, E. S. Marmor¹, T. Palmer¹, R. R. Parker¹, M. Porkolab¹, S. Shiraiwa¹, B. M. Sorbom¹, R. Vieira¹, G. M. Wallace¹, A. White¹, D. G. Whyte¹, J. R. Wilson², J. C. Wright¹, and S. Wukitch¹

¹Plasma Science & Fusion Center, MIT, Cambridge, MA 02139, USA

²Princeton Plasma Physics Laboratory (PPPL), Princeton, NJ 08540, USA

Corresponding Author: P. T. Bonoli, bonoli@psfc.mit.edu

High field side (HFS) launch of RF power in the ion cyclotron range of frequencies (ICRF) and the lower hybrid range of frequencies (LHRF) in double null configurations in reactor grade plasmas is studied and found to represent an integrated solution that both mitigates PMI/coupling problems and at the same time opens up the possibilities of greatly improved core wave physics.

Power exhaust in a tokamak tends to send heat and particles to the low field side (LFS) scrape-off layer (SOL) of the tokamak forcing RF launchers to be placed farther away from the plasma on the LFS, which reduces wave coupling and increases the probability of parasitic absorption in the SOL. In contrast, the quiescent nature of the HFS SOL in double null configurations encourages placement of RF launchers closer to the plasma on the HFS making it possible to utilize a small antenna-plasma gap with good coupling. The HFS SOL also has been found to strongly screen impurities thus mitigating adverse effects of PMI on the core plasma that might arise from near and far field RF sheaths associated with ICRF launchers. In addition lower electron densities measured in the HFS SOL relative to the low field side, combined with a more quiescent SOL may help to reduce parasitic losses of LHRF power due to parametric decay instability, collisional losses, and scattering of LH waves from density fluctuations and blobs.

Significant improvements in core wave physics are also achievable with HFS launch of LHRF and ICRF power. Higher toroidal magnetic field on the HFS combined with careful poloidal positioning of the LH launcher makes it possible to couple faster LH waves resulting in improved core wave penetration and higher LH current drive efficiency. High field side launch of ICRF waves in a deuterium majority plasma with high minority hydrogen concentration (> 10%) makes it possible to couple fast waves directly to ion Bernstein waves (IBW) which damp strongly on bulk plasma electrons, thus avoiding the generation of fast ion tails and concomitant tail losses that can occur with the LFS minority ICRF absorption scheme.

Theoretical studies with advanced ray tracing, full-wave, and Fokker-Planck simulation tools (GENRAY, TORIC, TORLH, and CQL3D) will be presented for a range of configurations.

Work supported by the U.S. Department of Energy Contract Nos. DE-FC02-99ER54512 and DE-FC02-01ER54648.

THD



Role of Neutral Gas in Scrape-Off Layer of Tokamak Plasmas

N. K. Bisai¹, P. K. Kaw¹

¹*Institute for Plasma Research (IPR), Bhat, Gandhinagar, India*

Corresponding Author: N. K. Bisai, nirmal@ipr.res.in

The role of neutral gas in the scrape-off layer (SOL) of tokamak plasma is important as it modifies the plasma turbulence. This has been investigated using a simple two-dimensional (2D) model that consists of electron continuity, quasi-neutrality, electron energy and neutral gas continuity equations. Earlier the role of the neutral gas has been studied using uniform electron temperature [1]. However, in this study, a finite gradient of the electron temperature has been introduced using the electron energy equation, and the linear growth rate obtained from these equations has been studied. The neutral gas ionization rate is found to stabilize the linear growth rate. Neutral diffusion has an important role on the linear growth rates as it destabilizes the modes. The nonlinear equations are solved numerically. It is found that the neutral gas reduces (increases) fluctuations of the plasma density in the outer (inner) region of the SOL. Radial profiles of plasma density, electron temperature, and radial electric field have been studied. It is found that e-folding thickness of the plasma density, and electron temperature is reduced by the neutral gas. The neutral gas also reduces the radial electric field that agrees qualitatively with the ADITYA experimental observations.

References

- [1] N. K. Bisai, R. Jha, and P. K. Kaw, *Phys. Plasmas* **22**, 022517 (2015).



Demonstrating the Multiscale Nature of Electron Transport through Experimentally Validated Simulations

C. Holland¹, N. Howard², and B. A. Grierson³

¹University of California San Diego, CA 92093, USA

²Massachusetts Institute of Technology (MIT), Cambridge, MA 02139, USA

³Princeton Plasma Physics Laboratory (PPPL), Princeton, NJ 08540, USA

Corresponding Author: C. Holland, cholland@ucsd.edu

New experimentally validated simulations demonstrate for the first time that the turbulent transport that sets tokamak confinement is robustly multiscale across a variety of reactor-relevant regimes, with significant nonlinear cross-scale couplings that must be accurately described to correctly predict ITER performance. These gyrokinetic and gyrofluid simulations of electron transport dominated experiments performed on the Alcator C-Mod and DIII-D tokamaks consistently find that over half of the electron thermal transport arises from short-wavelength electron-scale ($k_{\theta} \rho_i > 1$) fluctuations not resolved by conventional ion-scale ($k_{\theta} \rho_i \leq 1$) microturbulence simulations. It is found that only by including these short-wavelength fluctuations can the turbulence simulations simultaneously match the measured temperature gradients, incremental electron thermal diffusivity, and independent power balance calculation energy fluxes within experimental uncertainties. Significant transport contributions from electron-scale streamers are found to persist even in discharges with low rotation and input torque, where they coexist with nonnegligible ion-scale eddies that drive the ion thermal transport. The multiscale simulations show complex nonlinear interactions between the electron- and ion-scale fluctuations, such that the intensity of electron-scale fluctuations can depend upon the ion-scale fluctuation intensity, and vice versa. Therefore, the resulting transport cannot be assumed to be a simple sum of separate ion- and electron-scale dynamics. Taken together, these simulations provide the clearest evidence to date that electron-scale turbulence will be prevalent in burning plasma conditions, and that the nonlinear multiscale dynamics and cross-scale couplings of this turbulence must be accurately described to confidently predict the performance of those regimes.

Work supported by the U.S. Department of Energy under DE-SC0006957, DE-FG02-06ER54871, DE-FC02-99ER54512, DE-AC02-05CH11231, and DE-AC02-09CH11466.

THC



Multimachine Analysis of Turbulent Transport in Helical Systems via Gyrokinetic Simulation

A. Ishizawa¹, Y. Nakamura¹, Y. Kishimoto¹, T. Watanabe², H. Sugama³, K. Tanaka³, S. Kobayashi⁴, and K. Nagasaki⁴

¹Graduate School of Energy Science, Kyoto University, Nishikyo-ku, Kyoto 615-8540, Japan

²Nagoya University, Nagoya, Japan

³National Institute for Fusion Science (NIFS), Toki, Gifu, Japan

⁴Institute of Advanced Energy, Kyoto University, Nishikyo-ku, Kyoto 615-8540, Japan

Corresponding Author: A. Ishizawa, ishizawa@energy.kyoto-u.ac.jp

As a trial in evaluating helical system designed with different concepts, we have compared two devices, the Large Helical Device (LHD) and the Heliotron J (HJ), with different magnetic field structure under two key parameters, i.e., the Mercier/interchange measure D_{well} and the magnetic shear \hat{s} , focussing on their linear drift wave instability and nonlinear evolution leading to turbulent transport. Here, the neoclassically optimized LHD is magnetically “hill” with moderate shear $(D_{\text{well}}, \hat{s}) = (-0.01, 1.2)$ while the HJ “well” with extremely small shear $(0.7, 0.02)$. We found a reciprocal relation between linear stability and nonlinear turbulence as that the device with smaller magnetic shear, which exhibits larger linear growth rate for the ITG mode, i.e., the HJ, provides smaller turbulent transport nonlinearly than that in the LHD due to larger production rate of zonal flows. The neoclassical optimization improves the turbulent transport in the HJ as well as the LHD. This suggests that the concept in optimizing Mercier/interchange mode and also neoclassical transport can be compatible with that in reducing turbulent transport.



Electromagnetic Gyrokinetic Analysis of the Isotope Effect

J. Garcia¹, T. Görler², F. Jenko², C. Challis³, and G. Giruzzi¹

¹*Institut de Recherche sur la Fusion par confinement Magnétique (IRFM), Commissariat à l'énergie atomique (CEA/Cadarache), 13108 Saint-Paul-lès-Durance, France*

²*Max-Planck-Institut für Plasmaphysik, Garching, Germany*

³*Culham Centre for Fusion Energy (CCFE), Culham Science Centre, Abingdon, UK*

Corresponding Author: J. Garcia, jeronimo.garcia@cea.fr

The thermal energy confinement time has been observed to largely vary with the exchange of the main isotope in broad experimental conditions in magnetically confined plasmas, leading to the so called isotope effect. Of particular interest is the isotope exchange between the fusion of deuterium-deuterium (DD) and deuterium-tritium (DT) nuclei, studied in dedicated experiments performed in the 1990's both in the Tokamak Fusion Test Reactor (TFTR) and in the Joint European Torus (JET), where a broad and unexpected variety of results including a clearly improved confinement in DT was obtained and a clear deviation from gyro-Bohm scaling.

In this paper, the isotope effect is analyzed by performing gyrokinetic simulations with the GENE code for the ITER hybrid scenario including kinetic electrons, collisions, electromagnetic effects and up to five species. The impact of the energetic particles has been also analyzed with two additional fast ion species.

It is found that the interplay between nonlinear microturbulence effects generate an isotope effect leading to an increase or decrease of ion heat fluxes from DD to DT plasmas in agreement with previous experimental findings and providing clues about how to proceed in the future for maximizing thermal energy confinement in the presence of DT mixture. In particular, at short plasma scales, the electrostatic potential radial correlation length always follows gyro-Bohm scaling, however, in the cases where the heat flux highly reduces from DD to DT, an anticorrelation region at longer (meso) scales appears due to the concomitant interplay of nonlinear multiscale interactions involving external $E \times B$ flow shear, magnetic geometry, zonal flow activity and electromagnetic effects. Extended analyzes show that the $E \times B$ flow shear quenches ion heat fluxes for DT more efficiently due to lower linear growth rates whereas a coupling between ion mass and zonal flow, which exists in any plasma condition, only becomes relevant at high- β leading to a deviation from gyro-Bohm scaling including a reduction of the ion heat flux by half.

THC



Assessment of the Runaway Electron Energy Dissipation in ITER

S. Konovalov¹, K. Aleynikova², R. Ismailov¹, A. A. Ivanov³, R. R. Khayrutdinov¹,
M. Lehnen⁴, S. Medvedev³, and P. Aleynikov⁵

¹National Research Centre "Kurchatov Institute", Moscow, Russian Federation

²Max-Planck-Institut für Plasmaphysik, Greifswald, Germany

³Keldysh Institute of Applied Mathematics, RAS, Moscow, Russian Federation

⁴International Thermonuclear Experimental Reactor (ITER),
Cadarache Centre, 13108 Saint-Paul-lès-Durance, France

⁵Max-Planck-Institut für Plasmaphysik, Garching, Germany

Corresponding Author: S. Konovalov, konovalov_sv@nrcki.ru

A substantial fraction of the plasma current can be converted into runaway electron (RE) current in ITER disruptions. During the RE plateau stage of the disruption, the kinetic energy of a runaway beam is expected to be much smaller than the magnetic one. However, at the following current termination phase, the electric field induced due to the RE loss to the wall causes the generation of new and acceleration of existing REs. Thus, some fraction of the initial plasma magnetic energy can be converted into RE kinetic energy. Preceding studies predicted significant, up to $\sim 100\%$, conversion of the magnetic energy into kinetic one during the RE current termination phase of disruptions, i.e., when the majority of REs are lost.

In the present report we assess the RE energy dissipation with the DINA disruption simulator appended with the new RE kinetic model based on the analytical solutions of the RE kinetic equation [1]. The new kinetic model allows for the direct evaluation of RE kinetic energy lost to the wall due to plasma scrapping off at final stage of vertical displacement event (VDE).

Generation of the halo currents was found to significantly reduce the conversion of RE magnetic into kinetic energy. Further suppression of RE regeneration at the plasma periphery is seen when an effective losses of REs are introduced in a narrow layer near the plasma boundary, mimicking the effect of external perturbations of the magnetic field. Sensitivity studies of the RE energy deposited to the wall are performed with variation of the amplitude and radial profile of the RE seed current at the beginning of the current quench (CQ). In addition, the simulations of the CQ with REs are accompanied by ideal and resistive MHD stability analysis, which allows identifying the RE plasma stability boundary and to estimate the value and radial profile of the RE loss time. Finally, the mitigation of RE by injection of impurity during RE plateau is simulated with various impurity quantity and delivery time dependence as expected for massive gas or shattered pellet injection techniques.

References

[1] P. Aleynikov and B. N. Breizman, Phys. Rev. Lett. **114**, 155001 (2015).



Effect of the Second X-Point on the Hot VDE for HL-2M

L. Xue¹, X. R. Duan¹, G. Y. Zheng¹, Y. O. Liu^{2,1}, S. L. Yan¹, V. N. Dokuka³, V. E. Lukash^{4,5},
and R. R. Khayrutdinov^{4,5}

¹Southwestern Institute of Physics, Chengdu, Sichuan, People's Republic of China

²Culham Centre for Fusion Energy (CCFE), Culham Science Centre, Abingdon, UK

³Troitsk Institute for Innovation and Fusion Research (TRINITI), Troitsk, Russian Federation

⁴National Research Centre "Kurchatov Institute", Moscow, Russian Federation

⁵National Research Nuclear University "MEPhI", Moscow, Russian Federation

Corresponding Author: L. Xue, xuelei@swip.ac.cn

The medium-sized copper-conductor tokamak HL-2M, is currently under construction and will be put into operation in the near future. The (up-down) symmetric poloidal field coil system inside the toroidal field coils of the machine has the capability of generating high vertically-elongated plasma. Thus the VDE is an unavoidable issue for HL-2M. Meanwhile, the opposite PF current in the middle of three divertor coils can generate two X-points, around which a poloidal weak field is existent. In this paper, effect of the second X-point on the hot VDE is investigated by the mature nonlinear time-dependent DINA code. During the investigation, variations of the distance between the two X-points are divided into two groups: I) exact snowflake-snowflake plus-standard divertor, and, II) exact snowflake-snowflake minus. Simulation result shows that, for group (I), as the distance increases, the poloidal weak field becomes long and thin in the vertical direction, causing the increase of the average VDE velocity before the thermal quench. Meanwhile, during the current quench, the halo current and the EM force on the vacuum vessel almost have the same decline trend along with the increase of the distance. Further, for group (II), the left minus and right minus cases are considered, respectively. The long and thin poloidal weak field, in the horizontal direction, seems to be beneficial for restraining the development of VDE. During the current quench, the halo current peak, as well as the maximum vertical EM force in VV becomes larger with increasing the distance of the second X-point. Through the comparison of the left minus and the right minus cases, it is found that the halo current peak in the left minus case becomes higher, meanwhile the maximum vertical EM force in VV increases slower. In the view of the EM loads, the stand divertor is better than the snowflake plus, which is better than the exact snowflake. The snowflake minus is the worst scenario.

THIS



Diamagnetic MHD Equations for Plasmas with Fast Flow and its Application to ELM Analysis in JT-60U and JET-ILW

N. Aiba¹, C. Giroud², M. Honda¹, E. Delabie³, S. Saarelma², L. Frassinetti⁴, S. Pamela², H. Urano¹, and C. Maggi²

¹Japan Atomic Energy Agency (JAEA), Naka, Japan

²Culham Centre for Fusion Energy (CCFE), Culham Science Centre, Abingdon, UK

³Oak Ridge National Laboratory (ORNL), Oak Ridge, TN 37831, USA

⁴KTH Royal Institute of Technology, Stockholm, Sweden

Corresponding Author: N. Aiba, aiba.nobuyuki@jaea.go.jp

Diamagnetic MHD equations for plasmas with fast flow were derived for the first time by introducing a suitable ordering parameter to two fluid equations. The extended Frieman-Rosenbluth (F-R) equation was obtained from the diamagnetic MHD equations by focussing on impacts of the ion diamagnetic drift effect on ideal MHD stability in rotating plasmas. The MINERVA-DI code was developed to solve the F-R equation, and was applied to analyze the edge localized mode (ELM) stability in JT-60U and JET with ITER like wall (ILW). The rotation profiles of deuterium in both toroidal and poloidal directions were estimated numerically based on the neoclassical theory with the measured impurity toroidal rotation by the CHARROT code. In static plasmas, the ion diamagnetic drift effect stabilizes the ELMs as discussed in past works. However, it is found that rotation in both toroidal and poloidal directions can destabilize ELMs, and this destabilizing effect can overcome the stabilizing effect due to the ion diamagnetic drift. In particular, the ion diamagnetic drift effect becomes negligible in a JT-60U type-I ELMy H-mode plasma rotating in the direction counter to the plasma current. In addition, the rotation makes the wavelength of ELMs shorter, and such a change of the wavelength is observed experimentally in JET when carbon wall was replaced with ILW. These results evince that rotation effects are indispensable for discussing the ELM stability in case the ELM wavelength is short as predicted in JT-60U and JET-ILW even when such ELMs are thought to be stabilized by the ion diamagnetic drift.



Multimachine Modelling of ELMs and Pedestal Confinement: From Validation to Prediction

S. Pamela^{1,2}, G. Huijsmans³, M. Hoelzl⁴, C. Giroud¹, S. Saarelma¹, S. Futatani⁵, H. Urano⁶,
M. Bécoulet³, I. Lupelli^{1,2}, C. Maggi¹, C. Roach¹, I. Chapman¹, A. Kirk¹, J. Harrison¹,
L. Frassinetti⁷, D. Dickinson⁸, N. Aiba⁶, T. Eich⁴, A. Lessig⁴, and F. Orain⁴

¹Culham Centre for Fusion Energy (CCFE), Culham Science Centre, Abingdon, UK

²United Kingdom Atomic Energy Authority, Culham Science Centre, Abingdon, UK

³Institut de Recherche sur la Fusion par confinement Magnétique (IRFM),

Commissariat à l'énergie atomique (CEA/Cadarache), 13108 Saint-Paul-lès-Durance, France

⁴Max-Planck-Institut für Plasmaphysik, Garching, Germany

⁵Centro Nacional de Supercomputación (BSC), Barcelona, Spain

⁶Japan Atomic Energy Agency (JAEA), Naka, Japan

⁷KTH Royal Institute of Technology, Stockholm, Sweden

⁸University of York, Heslington, UK

Corresponding Author: S. Pamela, stanislas.pamela@ukaea.uk

Future devices like JT-60SA, ITER and DEMO require quantitative predictions of pedestal density and temperature levels, as well as divertor heat fluxes, in order to improve global confinement capabilities while preventing divertor erosion/melting in the planning of future experiments. Such predictions can be obtained from dedicated pedestal models like EPED, and from nonlinear MHD codes like JOREK, for which systematic validation against current experiments is necessary. In this paper, we show progress in the validation of the JOREK code using MAST, AUG, JET-ILW and JT-60U simulations, with quantitative comparisons to experiments (including ELM energy losses and divertor heat fluxes), and we present the latest achievements of EUROPED as an extension of the EPED model, to clarify the pedestal width description based on kinetic ballooning modes (KBMs) and turbulence. In particular, we describe how JOREK and EUROPED have been coherently coupled to improve pedestal predictions in cases where ideal MHD fails to describe experimental observations, which is the case for many type-I ELMs in JET-ILW. EUROPED is used to provide JOREK with the pedestal width for a given pulse, and JOREK then evolves the pedestal height until the ELM-onset is reached. In ELM-onset simulations for JET pulse number #82630, the p_e^{ped} at the ELM-onset found by JOREK is lower than the linear ideal MHD peeling-ballooning limit, and close to the experimental value.

THS



Excitation of Zonal Flows and their Impact on Dynamics of Edge Pedestal Collapse

H. Jhang¹, H. H. Kaang¹, S. S. Kim¹, T. S. Hahm², R. Singh^{3,4}, and T. Rhee¹

¹*National Fusion Research Institute (NFRI), Daejeon, Republic of Korea*

²*Seoul National University, Seoul, Republic of Korea*

³*International Thermonuclear Experimental Reactor (ITER),
Cadarache Centre, 13108 Saint-Paul-lès-Durance, France*

⁴*Institute for Plasma Research (IPR), Bhat, Gandhinagar, India*

Corresponding Author: H. Jhang, hgjhang@nfri.re.kr

We study the role of zonal flows in edge pedestal collapse using a reduced magnetohydrodynamic (MHD) model. A dramatic change of dynamics happens when ideal ballooning modes are stabilized. A detailed analysis shows that a zonal flow driven instability is developed due to a strong excitation of zonal vorticity, resulting in secondary crashes. The presence of subsidiary bursts after a main crash increases the effective crash time and energy loss. These simulation results resemble the behaviour of compound edge localized modes (ELMs). Thus, our results indicate that a complete understanding of ELM crash dynamics requires the self-consistent inclusion of nonlinear zonal flows-MHD interaction and transport physics.



Development of a First-Principles Self-Consistent Core-Pedestal Model and its Application to ITER

O. Meneghini¹, P. B. Snyder¹, J. Park², S. Smith¹, B. A. Grierson³, J. Candy¹, D. Green²,
C. Holland⁴, W. Elwasif², G. M. Staebler¹, E. A. Belli¹, and L. L. Lao¹

¹General Atomics, San Diego, CA 92186, USA

²Oak Ridge National Laboratory (ORNL), Oak Ridge, TN 37831, USA

³Princeton Plasma Physics Laboratory (PPPL), Princeton, NJ 08540, USA

⁴University of California San Diego, CA 92093, USA

Corresponding Author: O. Meneghini, meneghini@fusion.gat.com

Accurate predictions of fusion performance requires including the strong interplay that exists between core transport, pedestal structure, current profile and plasma equilibrium. An integrated modelling workflow capable of finding the steady-state self-consistent solution to this strongly coupled problem has been developed. The workflow leverages first principles calculations and does not require prior knowledge of the kinetic profiles. Validation against DIII-D discharges shows that the workflow is capable of robustly predicting the kinetic profiles (electron and ion temperature and electron density) from the axis to the separatrix in agreement with the experiments. Results of a self-consistent optimization of the 15 MA DT ITER baseline scenario show that controlling the pedestal density and impurity content during ITER operations will be critical to achieve high fusion performance while satisfying the requirements imposed by the density-limit.

THC



Plasma Effects in Full-Field MHD-Equilibrium Calculations for W7-X

J. Geiger¹, C. D. Beidler¹, Y. Feng¹, P. Helander¹, Y. Suzuki^{2,3}, H. Hoelbe¹, H. Maaßberg¹, and Y. Turkin¹

¹Max-Planck-Institut für Plasmaphysik, Greifswald, Germany

²National Institute for Fusion Science (NIFS), Toki, Gifu, Japan

³Graduate University for Advanced Studies (SOKENDAI), Hayama, Kanagawa, Japan

Corresponding Author: J. Geiger, joachim.geiger@ipp.mpg.de

Wendelstein 7-X aims at quasi-steady-state operation to demonstrate the reactor viability of stellarators optimized with respect to MHD-equilibrium and -stability, low neoclassical transport, small bootstrap current and good fast-particle confinement. To reach this goal an island divertor is foreseen for particle and energy exhaust, which utilizes the naturally occurring boundary islands connected with the appearance of low-order rational values of the rotational transform at the plasma boundary. The island separatrix thus bounds the plasma, and the strike lines of the island fans determine the heat load distribution on the divertor structures.

Although the configuration of W7-X has been optimized to display a small impact of plasma currents on the configuration, these effects still persist and change the plasma shape and the boundary islands' width and location. From previous studies it is known, for example, that with growing plasma- β the island width increases, and the X- and O-point locations move poloidally, consistent with the effect of the Shafranov-shift. A net toroidal current is known to shift the island-generating resonance radially which, depending on the amount of plasma current, can lead to undesired deviations from proper island divertor operation, e.g., the shifting of the island structures away from the divertor plates resulting in a limiter magnetic configuration or in heat loads misdirected to critical components.

The contribution presents and discusses an approach for full-field calculations based on the VMEC-EXTENDER code combination. The effect of plasma- β and of net-toroidal currents on the width and location of the islands is investigated in configurations in which the bootstrap current is expected to be small enough (according to transport simulations) to allow high-performance, quasi-steady-state operation compatible with the island divertor. The calculated fields will be compared to calculations using the 3D MHD-equilibrium code HINT, whose numerical scheme does not rely on the existence of flux surfaces and allows the self-consistent treatment of islands and stochastic regions. The differences resulting from the two approaches will be discussed.



Physics of Flux Closure during Plasmoid-Mediated Reconnection in Coaxial Helicity Injection

F. Ebrahimi¹, R. Raman²

¹*Princeton Plasma Physics Laboratory (PPPL), Princeton, NJ 08540, USA*

²*University of Washington, Seattle, WA 98195, USA*

Corresponding Author: F. Ebrahimi, ebrahimi@princeton.edu

In a low-aspect-ratio spherical torus (ST), and in particular in an ST-based fusion reactor, due to the restricted space for a central solenoid, elimination of the central solenoid, and thus noninductive current-drive techniques, is necessary. Transient coaxial helicity injection (CHI) is a leading candidate for plasma start-up and current formation in NSTX-U. In NSTX, transient CHI has generated over 200 kA of toroidal current on closed flux surfaces without the use of the conventional central solenoid. To correctly model current generation and to better understand the physics of CHI start-up, comprehensive resistive MHD simulations have been conducted for the NSTX and NSTX-U geometries. It has been shown that magnetic reconnection has a fundamental role in the plasma start up and current formation in NSTX/NSTX-U. Here, we report two major findings from these CHI simulations: 1) formation of an elongated Sweet–Parker (S-P) current sheet and a transition to plasmoid instability has for the first time been demonstrated by simulations of CHI experiments and 2) a large-volume flux closure, and large fraction conversion of injected open flux to closed flux in the NSTX-U geometry have also now been demonstrated for the first time.

Work supported by the U.S. Department of Energy, Office of Science, Office of Fusion Energy Sciences under Award Numbers DE-SC0010565 and DE-FG02-99ER54519.

TH



Pressure Driven Currents Near Magnetic Islands in 3D MHD Equilibria: Effects of Pressure Variation within Flux Surfaces and of Symmetry

A. Reiman¹

¹*Princeton Plasma Physics Laboratory (PPPL), Princeton, NJ 08540, USA*

Corresponding Author: A. Reiman, reiman@pppl.gov

In toroidal MHD equilibria, pressure can generally be regarded as constant on the flux surfaces. The regions near small magnetic islands, and those near the X-lines of larger islands, are exceptions. We show that the variation of the pressure within the flux surfaces in those regions has significant consequences for the pressure driven current. We further show that the consequences are strongly affected by the symmetry of the magnetic field if the field is invariant under combined reflection in the poloidal and toroidal angles (“stellarator symmetry”). In nonstellarator-symmetric equilibria, the pressure-driven currents have logarithmic singularities at the X-lines. In stellarator-symmetric MHD equilibria, the singular components of the pressure-driven currents vanish. In contrast, in equilibria having p constant on the flux surfaces the singular components of the pressure-driven currents vanish regardless of the symmetry. In 3D MHD equilibria having simply nested flux surfaces, the pressure-driven current goes like $1/x$ near a rational surface, where x is the distance from the rational surface. To calculate the pressure-driven current near a magnetic island, we work with a closed subset of the MHD equilibrium equations that involves only perpendicular force balance, and is decoupled from parallel force balance. Two approaches are pursued to solve our equations for the pressure driven currents. First, the equilibrium equations are applied to an analytically tractable magnetic field with an island, obtaining explicit expressions for the rotational transform and magnetic coordinates, and for the pressure-driven current and its limiting behaviour near the X-line. The second approach utilizes an expansion about the X-line to provide a more general calculation of the pressure-driven current near an X-line and of the rotational transform near a separatrix. The calculations described here are motivated, in part, by tokamak experiments where significant differences are observed between the behaviour of stellarator-symmetric and nonstellarator-symmetric configurations with regard to stabilization of edge localized modes (ELMs) by resonant magnetic perturbations (RMPs). Implications for the coupling between neoclassical tearing modes (NTMs), and for magnetic island stability calculations, are also discussed.

Work supported by the U.S. Department of Energy contract DE-AC02-09CH11466.



Three-Dimensional Numerical Analysis of Interaction between Plasma Rotation and Interchange Modes

K. Ichiguchi¹, Y. Suzuki¹, Y. Takemura¹, S. Sakakibara¹, Y. Todo¹, M. Sato¹, S. Ohdachi¹, Y. Narushima¹, T. Nicolas¹, and B. Carreras²

¹National Institute for Fusion Science (NIFS), Toki, Gifu, Japan

²Universidad Carlos III de Madrid, Madrid, Spain

Corresponding Author: K. Ichiguchi, ichiguch@nifs.ac.jp

Effects of the poloidal shear rotation on the magnetohydrodynamic (MHD) stability of interchange modes in a large helical device (LHD) configuration are numerically studied. This simulation is the first three-dimensional (3D) full-MHD nonlinear analysis for heliotron plasmas including the flow. In LHD, the highest average β value of 5.1% is successfully obtained in the configuration where the plasma is predicted to be unstable with respect to the Mercier criterion. Thus, some stabilizing effects work on the plasma and it is crucial to identify the key physics of this stabilization for not only the understanding of the LHD plasmas but also the accurate design of the helical DEMO. Recently, it is observed in the experiments that the magnetic perturbation grows rapidly just after the mode rotation stops and causes a partial collapse of the electron temperature. This phenomenon indicates that the plasma rotation may suppress the growth of the mode

Thus, we numerically study the rotation effects on the MHD stability against the interchange modes in the LHD plasmas. As the numerical procedure, we employ a static equilibrium and incorporate a model shear flow as the rotation in the initial perturbation of the stability calculation. The 3D numerical codes of HINT and MIPS are utilized for the equilibrium and the stability calculations, respectively. We apply this method to an LHD equilibrium that is unstable for the interchange mode. In the no flow case, the pressure profile collapses and the magnetic field lines becomes stochastic in the nonlinear saturation phase. When a flow of which the kinetic energy is much larger than the saturation level in the no flow case is applied initially, such pressure collapse and field line stochasticity are not seen.

Hence, this simulation result shows that a large initially-applied poloidal flow can suppress the interchange modes. In this simulation, the flow needed for the suppression is much larger than the flow observed in LHD experiments. However, we expect that we can reduce the needed flow when we take it into account that the nonlinear relaxation of the mode continues in the β ramp-up phase. Therefore, the plasma rotation is considered as one of the candidates of the stabilization mechanism in LHD.

Two-Fluid Subgrid-Scale Viscosity in Nonlinear Simulation of Ballooning Modes in a Heliotron Device

H. Miura¹, F. Hamba², and I. Atsushi¹

¹National Institute for Fusion Science (NIFS), Toki, Gifu, Japan

²Institute of Industrial Science, University of Tokyo, Tokyo, Japan

Corresponding Author: H. Miura, miura.hideaki@nifs.ac.jp

Nonlinear growth of ballooning modes in a heliotron device is studied by means of two-fluid numerical simulations. A model to substitute an influence of the scales smaller than the grid size, subgrid-scale (SGS), on the scales larger than the grid scale (GS) is introduced. A simulation with the SGS model, a large eddy simulation (LES), of two-fluid MHD model successfully shows growth of the ballooning modes with a diamagnetic flow and nonlinear saturation, showing usefulness of the LES approach.

In order to enable two-fluid simulations of ballooning modes and clarify saturation mechanism of the modes in a heliotron device, we focus on influences of the SGS modes truncated because of the finite numerical resolution, instead of adopting an unphysically large viscosity. Since the truncation often contaminates nonlinear dynamics of the GS modes, compensating the influences of the SGS modes to the GS modes by a SGS model is essential. The SGS terms in two-fluid momentum equations can be modelled by the SGS viscosity and the resistivity which are composed of the rate of strain tensor, the fluctuation part of current density and two model constants.

Firstly the two model constants are calibrated by comparing a direct numerical simulation and LESes of homogeneous magnetized Hall MHD turbulence. A full 3D simulation of the ballooning modes in LHD with a small viscosity shows that the SGS viscosity can become locally considerably large. Secondly, it is shown in full-3D two-fluid MHD simulations that a diamagnetic flow generated by the two-fluid term is coupled with the ballooning modes and restricts the instability to relatively low modes. By the use of the SGS model, our LESes are carried out without numerical instability even though high modes grow in linear phase, and the computational cost is reduced to about 1/64 of a precise simulation with a large number of grid points.

In summary, our two-fluid MHD LESes achieve a nonlinear saturation of ballooning modes with a small viscosity. The LES approach enables a drastic reduction of the computational cost and better representation of dynamics in two-fluid simulations. The SGS-modelling in the pressure equation is left for future. Further results together with related subjects such as slab Rayleigh–Taylor instability will also be reported.



Self-Consistent Optimization of Neoclassical Toroidal Torque with Anisotropic Perturbed Equilibrium in Tokamaks

J.-K. Park¹, N. C. Logan¹, Z. R. Wang¹, A. H. Glasser², E. Kolemen³, and A. H. Boozer⁴

¹Princeton Plasma Physics Laboratory (PPPL), Princeton, NJ 08540, USA

²Fusion Theory and Computation Inc., Kingston, WA 98346, USA

³Princeton University, Princeton, NJ 08544, USA

⁴Columbia University, New York, NY 10027, USA

Corresponding Author: J.-K. Park, jpark@pppl.gov

Control of toroidal rotation is an important issue for tokamaks and ITER since the rotation and its shear can significantly modify plasma stability from microscopic to macroscopic scales. A potentially promising actuator for the rotation control is the nonaxisymmetric (3D) magnetic perturbation, as it can substantially alter toroidal rotation by neoclassical toroidal viscosity (NTV). The optimization of the 3D field distribution for the NTV and rotation control is however a highly complicated task, since NTV is mostly nonlinear in the magnitude of the applied field with a complex dependency on the 3D field distribution [1]. In this paper we present a new method that entirely redefines the optimizing process, using the new general perturbed equilibrium code (GPEC). GPEC solves a nonself-adjoint force operator and balance with the first-order change in pressure anisotropy by nonaxisymmetry, and integrates its second-order change for NTV under the force balance. This self-consistent calculation uniquely yields the torque response matrix function, and enables the NTV profile optimization by a single code run based on the full eigenmode structure of the matrix function. The code applications to nonaxisymmetric control coil (NCC) design in NSTX-U demonstrated the efficiency and accuracy of the new method, and in addition showed the importance of the backward helicity modes and self-shielding by torque [2] in local NTV control. The access to the optimized field distribution is limited in practice by available coils, but it is also straightforward to couple the coils to torque matrix and optimize the current distributions in the coils, as has been actively studied in KSTAR, NSTX-U, and ITER. A number of other GPEC applications will also be discussed, including the verification and validation of high- β 3D plasma response [3] and kinetic stabilization with the self-consistent eigenfunctions.

References

- [1] S. Lazerson, J.-K. Park *et al.*, Plasma Phys. Control. Fusion **57**, 104001 (2015).
- [2] A. H. Boozer, Phys. Rev. Lett. **86**, 5059 (2001).
- [3] Z. R. Wang, M. J. Lanctot, *et al.*, Phys. Rev. Lett. **114**, 145005 (2015).

Work supported by the U.S. Department of Energy, contract DE-AC02-09CH11466.



Nonlinear 3D M3D-C1 Simulations of Tokamak Plasmas Crossing a MHD Linear Stability Boundary

S. C. Jardin¹, N. M. Ferraro¹, J. Breslau¹, J. Chen¹, A. Fil¹, S. P. Gerhardt¹, S. Hudson¹,
E. Kolemen¹, I. Krebs^{2,1}, C. Myers¹, D. Pfefferle¹, S. Seol³, M. Shephard³, B. Tobias¹, and
F. Zhang³

¹Princeton Plasma Physics Laboratory (PPPL), Princeton, NJ 08540, USA

²Max-Planck-Institut für Plasmaphysik, Garching, Germany

³Rensselaer Polytechnic Institute, Troy, NY 12180, USA

Corresponding Author: S. C. Jardin, jardin@pppl.gov

The goal of the present work is to better understand and develop a predictive capability for when approaching and crossing a MHD linear instability boundary leads to a thermal quench and subsequent disruption (hard limit), and when it just leads to increased transport or small amplitude oscillations (soft limit). Understanding the difference between hard and soft limits is crucial for effective disruption prediction and avoidance. We present several examples of both hard and soft β limits. Recent advances in implicit numerical algorithms for solving the 3D extended magneto-hydrodynamic equations in strongly magnetized plasmas have enabled massively parallel simulations of the internal global dynamics of tokamaks that can use very large time steps which allow one to span the timescales of ideal MHD stability, magnetic reconnection, and particle, energy, and momentum transport. It is now possible and feasible to run these high-resolution time-dependent initial value simulations for 10^6 or more Alfvén times so as to span all relevant timescales in a single simulation. In addition, a new multiregion and adaptive meshing capability allows simulation of the self-consistent interaction of the plasma with a resistive wall. In the examples presented here, we begin the simulation with the plasma stable to all modes. During the simulation the plasma crosses a stability boundary due to evolving profiles, loss of control, or injection of mass, energy, and or flux. This can lead to saturation or disruption

TH



Nonlinear Extended-MHD Modelling by the NIMROD Code of Broadband-MHD Turbulence during DIII-D QH-Mode Discharges

J. R. King¹, K. K. Barada², K. H. Burrell³, X. Chen³, A. M. Garofalo³, R. J. Groebner³, S. E. Kruger¹, G. R. McKee⁴, A. Y. Pankin¹, P. B. Snyder³, M. Ono⁵, and T. L. Rhodes²

¹Tech-X Corporation, Boulder, CO 80303, USA

²University of California Los Angeles, CA 90095, USA

³General Atomics, San Diego, CA 92186, USA

⁴University of Wisconsin-Madison, Madison, WI 53706, USA

⁵Graduate University for Advanced Studies (SOKENDAI), Hayama, Kanagawa, Japan

Corresponding Author: J. R. King, jking@txcorp.com

It is desirable to have an ITER H-mode regime that is quiescent to edge-localized modes (ELMs). ELMs deposit large, localized and impulsive heat loads that can damage the divertor. A quiescent regime with edge harmonic oscillations (EHO) or broadband MHD activity is observed in some DIII-D, JET, JT-60U, and ASDEX-U discharge scenarios [1–3]. These ELM-free discharges have the pedestal-plasma confinement necessary for burning-plasma operation on ITER. The mode activity associated with the EHO or broadband MHD is characterized by small toroidal-mode numbers ($n \approx 1-5$) and is thus suitable for simulation with global MHD codes. The particle transport is enhanced during QH-mode, leading to essentially steady-state profiles in the pedestal region. Relative to QH-mode operation with EHO, operation with broadband MHD tends to occur at higher densities and lower rotation and thus may be more relevant to ITER. Nonlinear NIMROD simulations initialized from a reconstruction of a DIII-D QH-mode discharge with broadband MHD saturate into a turbulent state.

Results from a nonlinear NIMROD simulation of DIII-D QH-mode shot #145098 at 4250 ms with broadband MHD are presented. The measured toroidal and poloidal rotation profiles are included in the simulation as experimental observations indicate that the QH-mode operational regime is dependent on the rotation profile. The simulation develops into a saturated turbulent state and the $n = 1$ and 2 modes become dominant through an inverse cascade. Each toroidal mode in the range of $n = 1-5$ is dominant at a different time. The perturbations are advected and sheared apart in the counter-clockwise direction consistent with the direction of the poloidal flow inside the LCFS. Work towards validation through comparison to ECE, BES and Doppler reflectometry measurements is presented. Consistent with experimental observations during QH-mode, the simulated state leads to large particle transport relative to the thermal transport. A discussion of the transport assumptions built into our MHD modelling concludes that future QH-mode simulation studying the induced transport should run as a turbulence calculation where profiles are fixed and needs to include first-order FLR drift effects that stabilize high- n modes.

References

- [1] A. M. Garofalo, *et al.*, Phys. Plasmas **22**, 056116 (2015).
- [2] K. H. Burrell, *et al.*, Phys. Plasmas **19**, 056117 (2012).
- [3] A. M. Garofalo, *et al.*, Nucl. Fusion **51**, 083018 (2011).



Nonlinear MHD Simulations of Quiescent H-Mode Pedestal in DIII-D and Implications for ITER

F. Liu¹, G. Huijsmans², A. Loarte², A. M. Garofalo³, W. M. Solomon⁴, M. Hoelzl⁵, and S. Pamela^{6,7}

¹*Université Nice Sophia Antipolis, Nice, France*

²*International Thermonuclear Experimental Reactor (ITER),*

Cadarache Centre, 13108 Saint-Paul-lès-Durance, France

³*General Atomics, San Diego, CA 92186, USA*

⁴*Princeton Plasma Physics Laboratory (PPPL), Princeton, NJ 08540, USA*

⁵*Max-Planck-Institut für Plasmaphysik, Garching, Germany*

⁶*Culham Centre for Fusion Energy (CCFE), Culham Science Centre, Abingdon, UK*

⁷*United Kingdom Atomic Energy Authority, Culham Science Centre, Abingdon, UK*

Corresponding Author: F. Liu, feng.liu@iter.org

Nonlinear MHD simulations of DIII-D QH-mode plasmas have been performed with the nonlinear MHD code JOREK as a first step towards determining whether the physics mechanisms leading to the QH-mode behaviour would be at work in ITER plasmas and thus whether this confinement regime can be considered as an alternative to the controlled type-I ELMy H-mode for ITER high Q operation. In the nonlinear MHD simulations it is found that low- n kink-peeling modes (KPM) are unstable and grow to a saturated level, consistent with the physics picture put forward in linear study. The features of the dominant MHD modes found in the simulations of the KPM mode, which are due to its toroidal localization caused by the coupling of harmonics, are in good agreement with the observations of the EHO typically present in DIII-D QH-mode experiments. The influence of a realistic resistive wall in these DIII-D simulations shows that the inclusion of a resistive wall and plasma rotation has an effect on the nonlinear KPM evolution. In this work, the nonlinear evolution of MHD modes with toroidal mode numbers n from 0 to 20, including both kink-peeling modes and ballooning modes, will be investigated through MHD simulations starting from initial conditions either close to the ballooning or the kink-peeling mode limit in the edge stability diagram, both for DIII-D and ITER plasmas. The identification of the physics mechanisms that lead to the saturation of the KPM and to the appearance of the EHO in DIII-D QH-modes will allow us to evaluate whether this regime is an option for high fusion performance operation at the specific characteristics of ITER plasmas.

Modelling and Simulation of Pedestal Control Techniques for NSTX-U

A. Fil¹, E. Kolemen¹, N. M. Ferraro², S. C. Jardin², P. B. Parks³, R. Lunsford², and R. Maingi²

¹Princeton University, Princeton, NJ 08544, USA

²Princeton Plasma Physics Laboratory (PPPL), Princeton, NJ 08540, USA

³General Atomics, San Diego, CA 92186, USA

Corresponding Author: A. Fil, afil@pppl.gov

In this paper we present high level simulations and modelling of pedestal control for NSTX-U. Real-time pedestal control is a crucial topic for future fusion reactors and ITER where the pedestal has to be kept edge-localized-mode (or ELM) free. We developed and tested many different control schemes to adjust and regulate the pedestal at DIII-D and we plan to test them on NSTX-U. But to do this it is important to understand the physics bases for how the control actuators affect the pedestal. It has been observed many times that a control scheme that works for a specific machine or regime might not be applicable to other machines and regimes. This is especially the case for future reactors such as ITER.

We thus do high-level numerical simulations with the M3D-C1 code. M3D-C1 has been developed to study the plasma response when several actuators are triggered (gas puffing, 3D magnetic perturbations and LGI). The aim is to combine all these methods to get an adaptive and automatic pedestal control in tokamaks.

In this paper, we focus on the effect of each actuators on the ELM frequency and amplitude. First modelling results of ELM-triggering by LGI have been obtained with M3D-C1. Mesh adaptation techniques and high order 3D finite elements allow simulation of sub-mm granules, without constraints on the granule toroidal width. This unique capability of M3D-C1 allows the simulation of realistic pellet sizes. For this study, two models for LGI are implemented in M3D-C1. The first one is a neutral gas shielding model (NGS) calibrated on DIII-D experimental measurements of the lithium granule ablation rates. The second one is valid for small size granules (sub-mm) where the contribution of plasma ions to the ablation of the granule is not negligible. In the simulation, it takes about 100 μ s for total pellet ablation.

NSTX-U L-mode and H-mode simulations have been done and will be compared to available experimental data. Moreover, stability calculations from ELITE and M3D-C1 during the penetration process will be presented, as well as comparison with the EPED code. Among the granule parameters, it is found that the most important are the element in the pellet, its size and the angle of attack.

TH



First Principle Fluid Modelling of Neoclassical Tearing Modes and of their Control

P. Maget¹, O. Février¹, X. Garbet¹, G. Giruzzi¹, H. Lütjens², J.-F. Luciani², A. Marx², P. Beyer³, J. Decker⁴, O. Sauter⁴, E. Lazzaro⁵, S. Nowak⁵, and M. Reich⁶

¹*Institut de Recherche sur la Fusion par confinement Magnétique (IRFM),*

Commissariat à l'énergie atomique (CEA/Cadarache), 13108 Saint-Paul-lès-Durance, France

²*Centre de Physique Théorique (CPhT), École Polytechnique, 91128 Palaiseau, France*

³*Physique des Interactions Ioniques et Moléculaires (PIIM), CNRS, Aix-Marseille Université, France*

⁴*Swiss Plasma Center (SPC), École polytechnique fédérale de Lausanne (EPFL), 1015 Lausanne, Switzerland*

⁵*Istituto di Fisica del Plasma (IFP), Consiglio Nazionale delle Ricerche (CNR), 20125 Milan, Italy*

⁶*Max-Planck-Institut für Plasmaphysik, Garching, Germany*

Corresponding Author: P. Maget, patrick.maget@cea.fr

The confinement degradation of tokamak plasma by magnetic islands motivates numerous approaches to better understand their dynamics and possible suppression. We report here on nonlinear simulations using a consistent two-fluid implementation of neoclassical friction forces in the framework of the toroidal magneto-hydrodynamic model of the XTOR code, recently improved with the implementation of parallel heat fluxes that allows recovering a self-generated bootstrap current that compares well with analytical formulae. The island saturation width increases as expected with the bootstrap current fraction, but with a much weaker dependence than predicted by a Rutherford-type equation. We evidence the strong influence of diamagnetic rotations and to a lesser extent of neoclassical friction on the saturation size and shape of the island, by comparing with a pure resistive MHD simulation. In metastable plasmas, a seed is required for triggering a NTM. We find in a case taken from ASDEX-Upgrade that the shape of the seed has an influence on the island dynamics that follows.

The control of these magnetic islands by the coupling of RF waves is modelled by a source term in Ohm's law accounting for the propagation of accelerated electrons along field lines. This implementation is validated against analytical theory regarding the stabilization efficiency, and the 3D spatial localization of the RF source is shown to impact the island dynamics when the plasma is nearly static: the flip instability is recovered and described, and the possibility to create an island from the RF current filament is evidenced. For metastable modes, a control method allowing the island to go below the critical size is appropriate. A promising stabilization technique based on the radial sweeping of the ECCD source has been successfully demonstrated in TCV and ASDEX-Upgrade. Our numerical investigation shows that the effective stabilization efficiency of the sweep is better when remaining close to the resonance or when being decentred on the outside.

These developments on a fluid implementation of neoclassical physics and RF sources in a global MHD code allow further investigations on NTM triggering and saturation, on ECCD stabilization process, as well as on their possible characterizations thanks to density and temperature fluctuation signals.



Toroidal Gyrokinetic Studies of the Tearing Mode in Tokamak Plasmas

E. Poli¹, W. Hornsby¹, D. Zarzoso², F. J. Casson³, and A. Peeters⁴

¹Max-Planck-Institut für Plasmaphysik, Garching, Germany

²Physique des Interactions Ioniques et Moléculaires (PIIM), CNRS, Aix-Marseille Université, France

³Culham Centre for Fusion Energy (CCFE), Culham Science Centre, Abingdon, UK

⁴University of Bayreuth, 95447 Bayreuth, Germany

Corresponding Author: E. Poli, emanuele.poli@ipp.mpg.de

Our present understanding of the physics of the tearing mode (TM) still does not allow a quantitative prediction of TM evolution in fusion reactors. The early phase of a TM, in particular, is determined by a complex interplay of different processes. We investigate the physics of the TM via gyrokinetic (GK) simulations in toroidal geometry using the code GKW. Two routes are followed, namely simulating the response of the plasma to a prescribed magnetic island and addressing the complete problem of the growth of the TM in the presence of GK turbulence.

In simulations with prescribed magnetic perturbation, it is found that the density profile inside an island whose width does not exceed significantly the ion orbit width follows an adiabatic law (flattened for islands rotating at the ion diamagnetic frequency, unperturbed at the electron diamagnetic frequency) also in the presence of ITG turbulence, although the physics becomes more complex. The bootstrap current flowing in an island of this size is hence a function of the rotation frequency. Simulations performed to isolate the role of the island electric field show that for frequencies of the order of the parallel ion streaming the perpendicular fluxes exhibit a linear scaling with the island frequency ω and a complex radial pattern, confirming drift-kinetic results. A polarization signal (quadratic with ω) can be identified only in a narrow range at higher frequencies.

In linear, self-consistent simulations, the TM rotates at the electron diamagnetic frequency at low collisionalities, but reverses direction at higher collisionality. The growth rate scales with $1/7$ -power of the resistivity in the semicollisional regime. The growth of a TM embedded in GK electromagnetic turbulence shows, as in other (fluid) studies, that the turbulent fluctuations provide a seed for the magnetic island. They drive its growth at a rate significantly faster than the linear tearing growth rate. Depending on the value of the plasma β , the subsequent evolution exhibits a Rutherford behaviour largely independent of the turbulence, or a disruption of the Rutherford phase, with the TM growing at its linear growth rate even if the island width exceeds the singular layer width. The island rotation is also modified by the presence of the turbulence. Generally, the mode rotation slows as the island grows.

Active Control and Stabilization of Locked Mode in Tokamaks at High Magnetic Reynolds Number

S. Inoue¹, J. Shiraishi¹, G. Matsunaga¹, M. Takechi¹, A. Isayama¹, and S. Ide¹

¹*Japan Atomic Energy Agency (JAEA), Naka, Japan*

Corresponding Author: S. Inoue, inoue.shizuo@jaea.go.jp

We report a numerical study of mode locking in tokamaks, which reveals an active stabilization effect of the control field against the locking event. We developed the resistive MHD simulation code "AEOLUS-IT", which can simulate mode locking, where the magnetic island interacts with error/control field, under JT-60SA class high-magnetic Reynolds number condition. The developed code successfully simulates the stabilization effect of the control field against the error field, which reveals a frequency dependence of the control field for suppressing the island evolution. The obtained dependencies have different natures between high and low magnetic Reynolds number (large scale and medium size tokamaks), which agrees well with the theoretical prediction. Taking into account the successful calculation of the interaction between magnetic island and the error/control field under the high magnetic Reynolds number condition, as well as the adoption of the flux coordinate system, the developed code will enable us not only to check the agreement between our numerical studies and future JT-60SA experiments, but also to predict the error-field threshold in ITER.

Extension of Numerical Matching Method to Weakly Nonlinear Regime: Beyond the Rutherford Theory of Magnetic Island Evolution

M. Furukawa¹, S. Tokuda²

¹Graduate School of Engineering, Tottori University, Tottori, Japan

²Research Organization for Information Science and Technology (RIST), Japan

Corresponding Author: M. Furukawa, furukawa@damp.tottori-u.ac.jp

The theory of matched asymptotic expansion for resistive MHD is well established for linear modes [1] and for weakly nonlinear evolution [2]. Since then many applications of the Rutherford equation [2] have made much progress in fusion research, especially in the neoclassical tearing mode (NTM) studies [3–5]. However, the theoretical framework is still based on the Rutherford equation essentially.

We have recently developed a new framework for linear stability analysis of resistive MHD, the numerical matching method [6–8]. This method utilizes a finite-width inner region around a resonant surface, instead of an infinitely thin inner layer. We devised the boundary condition for the direct matching at interfaces between the inner and outer regions. Then we succeeded to remove difficulties that remain in the numerical applications of the traditional matched asymptotic expansion even though sophisticated theories were developed [9–12]. We developed both an eigenvalue and an initial-value approaches.

In this paper, we extend the initial-value approach of the numerical matching method to weakly nonlinear cases. In the presentation, we will explain the theory, and will show numerical results using reduced MHD in cylindrical plasmas that successfully reproduced Rutherford regime of magnetic island evolution. The computational cost is reduced, making inclusion of detailed physical effects easier because such a model requires more efficient solution method. Our new method will certainly aid understanding physics and will substantially contribute to the prediction of MHD activities such as NTMs in fusion plasmas.

References

- [1] H. P. Furth, J. Killeen and M. N. Rosenbluth, *Phys. Fluids* **6**, 459 (1963).
- [2] P. H. Rutherford, *Phys. Fluids* **16**, 1903 (1973).
- [3] A. I. Smolyakov, *Plasma Phys. Control. Fusion* **35**, 657 (1993).
- [4] O. Sauter, *et al.*, *Phys. Plasmas* **4**, 1654 (1997).
- [5] R. J. La Haye, *Phys. Plasmas* **13**, 055501 (2006).
- [6] M. Furukawa, S. Tokuda and L.-J. Zheng, *Phys. Plasmas* **17**, 052502 (2010).
- [7] M. Furukawa and S. Tokuda, *Phys. Plasmas* **18**, 062502 (2011).
- [8] M. Furukawa and S. Tokuda, *Phys. Plasmas* **19**, 102511 (2012).
- [9] A. Pletzer and R. L. Dewar, *J. Plasma Phys.* **45**, 427 (1991).
- [10] A. Pletzer, A. Bondeson and R. L. Dewar, *J. Comput. Phys.* **115**, 530 (1994).
- [11] S. Tokuda and T. Watanabe, *Phys. Plasmas* **6**, 3012 (1999).
- [12] S. Tokuda, *Nucl. Fusion* **41**, 1037 (2001).

This work was supported by KAKENHI Grant No. 23760805 and No. 15K06647.



Magnetic Island Behaviour under Nonaxisymmetric Halo Current at Vertical Displacement Event

N. Ivanov¹, A. Kakurin¹

¹National Research Centre "Kurchatov Institute", Moscow, Russian Federation

Corresponding Author: N. Ivanov, ivanov_nv@nrcki.ru

The nonaxisymmetric halo current arising due to loss of plasma vertical equilibrium, the so-called vertical displacement event (VDE), during plasma disruption in vertically elongated tokamak can be one of possible sources of helical magnetic perturbation. This perturbation penetrate into plasma producing magnetic islands in the vicinity of resonant magnetic surface with the same helicity. Results of simulation and analysis of magnetic island production by helical magnetic perturbation generated under nonaxisymmetric halo current are presented. Some predictions for ITER-like tokamak are presented with view of the disruption risk analysis. Calculations are carried out with the TEAR code based on the two-fluid MHD approximation. The radial distribution of the magnetic flux perturbation is calculated with account of the external helical field produced by halo current. The equations for the magnetic flux perturbation describe the dynamics of the tearing mode depending on plasma rotation. In sequence, this rotation is affected by electromagnetic forces depending on the tearing mode magnetic field and external magnetic perturbation. Numerically, the diffusion-type equations for the helical flux function and for the plasma rotation velocity are treated in a similar way. The magnetic island behaviour is analyzed for different plasma parameters and possible mode numbers. The width of the produced magnetic islands extends to a significant part of plasma minor radius. These magnetic islands can affect plasma stability, equilibrium and confinement, in particular the confinement of runaway electrons, thus affecting the development of the disruption and its impact on tokamak components.



Advances in Numerical Modelling of MGI Mitigated Disruptions in ITER

V. E. Lukash¹, Y. Gribov², M. Dubrov¹, R. R. Khayrutdinov¹, D. Kiramov¹, M. Lehnen², V. Leonov¹, V. Pustovitov¹, and V. Zhogolev¹

¹National Research Centre "Kurchatov Institute", Moscow, Russian Federation

²International Thermonuclear Experimental Reactor (ITER),
Cadarache Centre, 13108 Saint-Paul-lès-Durance, France

Corresponding Author: V. E. Lukash, lukash_ve@nrcki.ru

Disruption mitigation with use of the massive injection of noble gases (MGI) is widely used and experimentally validated on contemporary tokamaks. The disruption mitigation system (DMS) in ITER is aiming to subsequently or simultaneously achieve a solution for three main goals including mitigation of the heat loads on the plasma facing components during thermal quenches (TQs), keeping tolerable electro-mechanical loads on the conducting structures surrounding the plasma, and preventing the appearance of, or suppressing, the relativistic electron (RE) beams at the current quench (CQ) stage of the disruption. To assess the feasibility and operation domain of the ITER DMS, extended simulations are needed. The present report describes recent developments of the physical models for accurate and effective simulations of mitigated disruptions in ITER. The integrating core of these simulations is the disruption simulator based on the DINA code (DINA-DS). For specific conditions of impurity-dominated CQ plasmas, a special transport solver has been developed. Ionization of injected impurities due to interactions with REs is taken into account in the presented advanced transport model. MGI mitigated CQs are accompanied by fast vertical movement of the plasma column. A precise evaluation of the eddy currents induced in blanket modules and in the vacuum vessel has to take these dynamics into account. Representation of the ITER double wall vacuum vessel structure as two sets of 50 thin rings with rectangular cross-sections and relevant resistances for the inner and outer walls provides the necessary accuracy of the calculations. Recently, DINA has been updated to include parallel heat fluxes in the halo region for a complete energy balance. This provides the basis for a better estimate of the halo temperature and, therefore, plasma resistivity, affecting the resulting halo current amplitudes and CQ dynamics.

The evolution of the RE distribution function in DINA-DS is simulated with the use of a recently developed analytical model. Knowledge of the RE distribution function instead of just RE current is of principal importance in assessing the total kinetic energy deposited to the first wall due to the loss of REs. Representative scenarios of mitigated disruptions in ITER simulated with updated models are presented. The operation domain for the ITER DMS based on MGI is discussed.

Role of Explosive Instabilities in High- β Disruptions in Tokamaks

A. Y. Aydemir¹, H. Lee¹, S. G. Lee¹, J. Seol¹, B. Park¹, and Y. In¹

¹National Fusion Research Institute (NFRI), Daejeon, Republic of Korea

Corresponding Author: A. Y. Aydemir, aydemir@nfri.re.kr

Explosive growth of a ballooning finger is demonstrated in nonlinear magnetohydrodynamic calculations of high- β disruptions in tokamaks. The explosive finger is formed by an ideally unstable $n = 1$ mode, dominated by an $m/n = 2/1$ component. The quadrupole geometry of the $2/1$ perturbed pressure field provides a generic mechanism for the formation of the initial ballooning finger and its subsequent transition from exponential to explosive growth, without relying on secondary processes. The explosive ejection of the hot plasma from the core and stochastization of the magnetic field occur in Alfvénic time scales, accounting for the extremely fast growth of the precursor oscillations and the rapidity of the thermal quench in some high- β disruptions.



Securing High- β_N JT-60SA Operational Space by MHD Stability and Active Control Modelling

T. Bolzonella¹, P. Bettini¹, S. C. Guo¹, Y. Liu², G. Marchiori¹, G. Matsunaga³, S. Mastrostefano⁴, S. Nowak⁵, L. Pigatto¹, O. Sauter⁶, M. Takechi³, F. Villone⁴, X. Xu¹, N. Aiba³, J. Garcia⁷, L. Garzotti⁸, N. Hayashi³, P. Lauber⁹, M. Romanelli², J. Shiraishi³, and C. Sozzi⁵

¹Consorzio RFX, Associazione EURATOM-ENEA sulla Fusione, Padova, Italy

²Culham Centre for Fusion Energy (CCFE), Culham Science Centre, Abingdon, UK

³Japan Atomic Energy Agency (JAEA), Naka, Japan

⁴CREATE/ENEA/EURATOM Association, Università di Napoli, Naples, Italy

⁵Associazione EURATOM-ENEA, Istituto di Fisica del Plasma (IFP),

Consiglio Nazionale delle Ricerche (CNR), 20125 Milan, Italy

⁶Swiss Plasma Center (SPC), École polytechnique fédérale de Lausanne (EPFL), 1015 Lausanne, Switzerland

⁷Institut de Recherche sur la Fusion par confinement Magnétique (IRFM),

Commissariat à l'énergie atomique (CEA/Cadarache), 13108 Saint-Paul-lès-Durance, France

⁸United Kingdom Atomic Energy Authority, Culham Science Centre, Abingdon, UK

⁹Max-Planck-Institut für Plasmaphysik, Garching, Germany

Corresponding Author: T. Bolzonella, tommaso.bolzonella@igi.cnr.it

A careful numerical evaluation of MHD stability and of active control strategies is of paramount importance to reach one of the main goals of JT-60SA (Super Advanced) device, namely the development and qualification of high- β_N , steady-state regimes for future reactors like DEMO. Thanks to its powerful and flexible additional systems for heating and current drive, to its shaping capabilities and to several actuators for different kinds of real-time plasma control, JT-60SA aims at studying plasmas exceeding both the threshold for neoclassical tearing mode (NTM) destabilization and the so called Troyon no-wall β limit for external kink instabilities. This work reports on the latest results on key issues in MHD stability and control of JT-60SA advanced tokamak plasmas, with particular reference to Neoclassical Tearing modes (NTM) and Resistive Wall Mode (RWM) physics.

The amplitude evolution of NTM instabilities in the reference high- β_N scenarios is investigated by numerical tools developed in the framework of the European Integrated Tokamak Modelling effort. By solving the generalized Rutherford equation the role of different effects (such as bootstrap, curvature and polarization) is evaluated, including mode frequency evolution. Active NTM stabilization techniques are explored by modelling the action of the dual frequency (110 GHz and 138 GHz) electron cyclotron system.

JT-60SA steady state scenarios present also new challenges for RWM stability studies given their targets in terms of β_N (~ 4) and bootstrap current fraction ($\sim 70\%$). A further issue is given by the presence of a population of fast particles generated by high-power, high energy (10 MW at 500 keV) negative neutral beam injection system. The 2D stability code MARS-F/K is used to study plasma flow and drift kinetics stabilizing effects. Wall stabilization effects are estimated by the CarMa code that couples the 2D plasma stability to a 3D description of the passive boundaries surrounding the plasma. Feedback control of RWMs as provided by a set of 18 active coils is studied by the self-consistent inclusion in the model of a representation of the control system producing an overall dynamic model cast in the state variable space.



Plasma Disruption and VDE Modelling in Support of ITER

I. Bandyopadhyay^{1,2}, A. K. Singh^{1,2}, N. W. Eidietis³, D. A. Humphreys³, R. S. Granetz⁴,
G. Pautasso⁵, A. Isayama⁶, and S. C. Jardin⁷

¹International Thermonuclear Experimental Reactor (ITER), India Centre, Gujarat, India

²Institute for Plasma Research (IPR), Bhat, Gandhinagar, India

³General Atomics, San Diego, CA 92186, USA

⁴Massachusetts Institute of Technology (MIT), Cambridge, MA 02139, USA

⁵Max-Planck-Institut für Plasmaphysik, Garching, Germany

⁶Japan Atomic Energy Agency (JAEA), Naka, Japan

⁷Princeton Plasma Physics Laboratory (PPPL), Princeton, NJ 08540, USA

Corresponding Author: I. Bandyopadhyay, indranil.bandyopadhyay@iter-india.org

Accurate modelling of major disruption (MD) and vertical displacement events (VDEs) in ITER is necessary to determine the halo current amplitude during these events and hence the electromagnetic loads on the machine components. The modelling of these events were originally done by DINA code and the results were later validated by TSC simulations and they both agree remarkably well when similar code assumptions are made. However, in these simulations, the halo current amplitude depends critically on the choice of halo parameters, namely the temperature and width of the halo region. Due to lack of credible experimental data of these two parameters and absence of any sound physics-based model so far, these parameters are chosen rather ad-hoc. For validation simulations with existing experiments, these parameters, including their temporal profiles, are chosen carefully for each experimental discharge so as to give a good match between the experiments and simulations. But for predictive simulations for ITER, this creates a problem as to what parameters to be chosen. To resolve this issue, a concerted effort to validate the TSC model against a wider set of experiments in different machines are presently underway. We have selected a set of four shots each in DIII-D and C-Mod which are simulated in TSC. The halo parameters are set carefully only for one experiment in each machine and for the rest of the shots, they are kept unchanged. Thus the difference between the experimental and simulated halo current amplitude in these discharges would give an indication of the possible error in predictive modelling. We have already modelled three DIII-D discharges and we can reproduce the halo currents within about 10% of their experimental value. More discharges are being simulated at present both in DIII-D and C-Mod. Details of these simulations and their results will be presented in this paper. We shall also explore any possible scaling laws of the halo current amplitude on these two parameters in these discharges.



Impact of Kinetic Effects of Energetic Particles on Resistive Wall Mode Stability in Rotating High- β Plasmas

J. Shiraishi¹, N. Miyato¹, G. Matsunaga¹, M. Toma¹, M. Honda¹, T. Suzuki¹, M. Yoshida¹, N. Hayashi¹, and S. Ide¹

¹*Japan Atomic Energy Agency (JAEA), Naka, Japan*

Corresponding Author: J. Shiraishi, shiraishi.junya@jaea.go.jp

We found that inclusion of self-consistent rotation effect in the energetic particles' dynamics has significant impact on resistive wall mode (RWM) stability in tokamaks. For the first time, we apply the extended kinetic-magnetohydrodynamic (MHD) theory for rotating plasmas to energetic particles. The theory invokes an extended energy exchange term between the MHD mode and energetic particles' motion. In this study, the extended theory has been applied to RWM stability analysis in high- β JT-60SA plasmas. By using a new model equilibrium distribution function of energetic particles, it is found that extended energy exchange terms enhance the stabilization effect.



Nyquist Analysis of Kinetic Effects on the Plasma Response in NSTX and DIII-D Experiments

Z. R. Wang¹, M. J. Lanctot², Y. Liu³, J.-K. Park¹, and J. Menard¹

¹Princeton Plasma Physics Laboratory (PPPL), Princeton, NJ 08540, USA

²General Atomics, San Diego, CA 92186, USA

³Culham Centre for Fusion Energy (CCFE), Culham Science Centre, Abingdon, UK

Corresponding Author: Z. R. Wang, zwang@pppl.gov

Externally applied, nonaxisymmetric magnetic perturbations can strongly modify Tokamak plasmas, leading to the plasma response. Plasma response, often closely related to the resonant field amplification and to the ELM control using magnetic coils, has been systematically observed in Tokamak experiments. In particular, the importance of drift kinetic effects on modifying the plasma response has been demonstrated via quantitative modelling of NSTX and DIII-D high- β experiments [1, 2]. In this work, Nyquist analysis, as a very powerful tool in stability theory, is applied to analyze the plasma response with the intrinsically stable plasmas, where the technique, combined with Padé approximation, provides the deep physics understanding of the plasma behaviour. Based on the idea that the plasma response to externally applied 3D fields is often due to the linear combination of certain stable eigenmodes' response, Nyquist analysis clearly shows how the kinetic effects change the damping rate of these stable eigenmodes in the plasma, without resorting to direct stability computations. The capability of Nyquist analysis to infer the plasma stability for potential ELM mitigation or suppression, direct observation of so-called multimode response and identification of amplification associated with the preferred eigenmode is also presented in this work, where the multimode response is a phenomenon currently under extensive discussions [3]. The results suggest the application of Nyquist technique in 3D plasma response experiment since the plasma transfer function extracted from the experiments directly can be very useful to design the MHD control system and to better predict plasma behaviour in future experiments.

References

- [1] Z. R. Wang, M. J. Lanctot, *et al.*, 56th APS Conference, DPP.TI1.3 (2014).
- [2] Z. R. Wang, M. J. Lanctot, *et al.*, *Phys. Rev. Lett.* **114**, 145005 (2015).
- [3] C. Paz-Soldan, *et al.*, *Phys. Rev. Lett.* **114**, 105001 (2015).

Work supported by the U.S. Department of Energy contracts DE-AC02-09CH11466.

An Analytic Scaling Relation for the Maximum Tokamak Elongation against $n = 0$ MHD Resistive Wall Modes

J. P. Lee¹, J. P. Freidberg¹, A. Cerfon², and M. J. Greenwald¹

¹Plasma Science & Fusion Center, MIT, Cambridge, MA 02139, USA

²Courant Institute of Mathematical Science, New York University, New York, NY 10012, USA

Corresponding Author: J. P. Lee, jungpyo@psfc.mit.edu

In this study, the maximum achievable elongation in a tokamak against the $n = 0$ MHD resistive wall mode is investigated theoretically and compared with experimental observations. A highly elongated plasma is desirable to increase plasma pressure and confinement for high fusion power output. However, there is a limit on the maximum achievable elongation which is set by vertical instabilities driven by the $n = 0$ MHD mode. This limit can be increased by optimizing several parameters characterizing the plasma and the wall. The purpose of our study is to explore how and to which extent this can be done. Specifically, we extend many earlier calculations of the $n = 0$ mode to determine maximum elongation as a function of dimensionless parameters describing 1) the plasma profile (β_p and l_i), 2) the plasma shape (ϵ and δ), 3) the wall radius (b/a), and, 4) most importantly the feedback system capability parameter $\gamma\tau$. We make use of a new formulation of $n = 0$ MHD theory developed in our recent study [1, 2] that reduces the 2D stability problem into a 1D problem. This method includes all the physics of ideal MHD axisymmetric instability but it reduces the computation time significantly so that many parameters can be explored during the optimization process. We have explored a wide range of parameter space, and compared our results with data from tokamak experiments. Perhaps the most useful final result is a simple analytic fit to the simulations which gives the maximum elongation and corresponding optimized triangularity as functions $\kappa(\epsilon, \beta_p, l_i, b/a, \gamma\tau)$ and $\delta(\epsilon, \beta_p, l_i, b/a, \gamma\tau)$. These theoretically obtained scaling relations should be useful for determining optimum plasma shape in current experiments and future tokamak designs.

References

- [1] J. P. Freidberg, *et al.*, J. Plasma Phys. **81**, 515810607 (2015).
- [2] J. P. Lee, *et al.*, J. Plasma Phys. **81**, 515810608 (2015).

Pfirsch-Tasso Versus Standard Approaches in the Plasma Stability Theory

V. Pustovitov¹, A. Galyuzov²

¹National Research Centre "Kurchatov Institute", Moscow, Russian Federation

²Moscow Institute of Physics and Technology, Dolgoprudny, Moscow Region, Russian Federation

Corresponding Author: V. Pustovitov, pustovitov_vd@nrcki.ru

The paper is devoted to a theoretical description of plasma stability in toroidal fusion systems with a resistive wall. It aims to eliminate the contradictions between different approaches and between theory and experiment. The study is related to two predictions stated as theorems, see [1] and references therein. One is that an MHD-unstable configuration with a dissipationless plasma surrounded by vacuum and possibly superconducting walls cannot be stabilized by introducing walls of finite electrical conductivity. The other is that in the absence of dissipation in the plasma, such as viscosity, it is expected that the flow cannot stabilize the system. Both predictions forbid the experimentally demonstrated long-lasting wall stabilization of tokamak plasmas. In particular, they do not allow the rotational stabilization and the regimes with edge harmonic oscillations (EHOs) observed on the DIII-D tokamak. Besides, they cannot be reconciled with a number of theoretical studies on the plasma rotation effect on the stability. Situations when the results are incompatible with those theorems are not rare, but still remain unresolved compromising the conclusions of the both sides. The most known first theorem was published in 1971 [2], but since then it has never been analyzed, confirmed or corrected by independent researchers. This task is addressed here. A missing chain of derivations is restored and earlier unknown limitations that restrict the applicability of the Pfirsch–Tasso theorems are established. Thereby, the disagreements with the models of the rotational stabilization are explained and shown to be amendable. Replacement of the Pfirsch–Tasso energy principle is proposed. The new result is free from the constraints implicitly imposed in the Pfirsch–Tasso proofs. It eliminates the contradictions and can be used with any plasma model (not necessarily ideal) and for arbitrary perturbations. The proposed extensions allow applications for the cases of practical interest such as feedback stabilization of RWMs, analysis of the rotational stabilization and optimization of the ITER scenarios. Examples are presented and consequences are discussed.

References

- [1] H. Tasso and G. N. Throumoulopoulos, *Phys. Plasmas* **18**, 070702 (2011).
- [2] D. Pfirsch and H. Tasso, *Nucl. Fusion* **11**, 259 (1971).



Nonlinear MHD Modelling of Edge Localized Modes Dynamics

M. Bécoulet¹, G. Huijsmans¹, X. Garbet¹, C. Passeron¹, O. Février¹, J. Morales², M. Kim³,
G. Yun⁴, S. Pamela⁵, and A. Lessing⁶

¹*Institut de Recherche sur la Fusion par confinement Magnétique (IRFM),*

Commissariat à l'énergie atomique (CEA/Cadarache), 13108 Saint-Paul-lès-Durance, France

²*Swiss Plasma Center (SPC), École polytechnique fédérale de Lausanne (EPFL), 1015 Lausanne, Switzerland*

³*Ulsan National Institute of Science and Technology (UNIST), Ulsan, Republic of Korea*

⁴*Pohang University of Science and Technology (POSTECH), Pohang, Gyeongbuk 790-784, Republic of Korea*

⁵*Culham Centre for Fusion Energy (CCFE), Culham Science Centre, Abingdon, UK*

⁶*Max-Planck-Institut für Plasmaphysik, Garching, Germany*

Corresponding Author: M. Bécoulet, marina.becoulet@cea.fr

The nonlinear MHD modelling of full ELM crash dynamics was performed using JOEUK code for KSTAR pulse parameters and compared to the ECEI diagnostic observations. Some experimentally observed trends were reproduced in modelling. In particular the localization of the peeling-ballooning modes in the pedestal region inside the separatrix, the most unstable modes toroidal numbers and structures, poloidal velocity and the direction of the modes rotation are similar to the experimental observations on KSTAR. The rotation of the modes in electron diamagnetic direction is more common observation in many tokamaks due to the typically large negative radial electric field well in the pedestal region. However it was shown in JOEUK modelling that at relatively large toroidal plasma rotation, which was the case for the KSTAR pulse modelled in the paper, the modes can rotate in the ion diamagnetic direction before ELM crash similar to KSTAR ECEI observations. Multimodes ($n = 1-8$) modelling demonstrated the acceleration of growth of the peeling-ballooning modes and even destabilization of previously linearly stable modes approaching the ELM crash due to the strongly increasing nonlinear coupling at this stage of the instability. Moreover, a strongly sheared mean poloidal flow occurs on the nonlinear phase of an ELM leading to the filaments detachment from the main plasma in the form of "blobs" which propagate in the SOL mainly in the ion diamagnetic direction. In/out divertor heat flux asymmetry ($\sim 2:1$) due to ELM crash was obtained with two fluid diamagnetic drifts included in the modelling.

TH



Nonlinear MHD Simulations of Pellet Triggered ELMs

S. Futatani^{1,2}, G. Huijsmans³, A. Loarte⁴, S. Pamela⁵, M. Hoelzl⁶, P. Lang⁶, L. Garzotti⁵,
F. Orain⁶, and A. Lessig⁶

¹Centro Nacional de Supercomputación (BSC), Barcelona, Spain

²EUROfusion/JET, Culham Science Centre, Abingdon, Oxfordshire, OX14 3DB, UK

³Institut de Recherche sur la Fusion par confinement Magnétique (IRFM),
Commissariat à l'énergie atomique (CEA/Cadarache), 13108 Saint-Paul-lès-Durance, France

⁴International Thermonuclear Experimental Reactor (ITER),

Cadarache Centre, 13108 Saint-Paul-lès-Durance, France

⁵Culham Centre for Fusion Energy (CCFE), Culham Science Centre, Abingdon, UK

⁶Max-Planck-Institut für Plasmaphysik, Garching, Germany

Corresponding Author: S. Futatani, shimpei.futatani@gmail.com

ITER operation relies on the achievement of the H-mode confinement regime, which is expected to lead to the quasi-periodic triggering of ELMs (edge localized modes). The energy fluxes associated with natural ELMs will produce excessive erosion and/or damage on the plasma facing component. Controlled triggering of ELMs by the injection of small pellets at frequencies exceeding those of natural ELMs is one of the foreseen schemes to control ELMs in ITER. Although the technique has been demonstrated to decrease ELM size successfully in ASDEX-Upgrade [1], JET [2], and DIII-D [3], uncertainties still remain regarding the physics understanding as well as of the consequence of its application, such as localized power loads associated with this technique [4].

Modelling of ELM triggering by pellet injection for ASDEX-Upgrade, JET discharges, and the ITER 15 MA $Q = 10$ scenario has been carried out with the nonlinear MHD code JOREK [5, 6]. The JOREK code allows the simulation of a full pellet triggered ELM cycle, i.e., to study the nonlinear consequences of a pellet triggered instability and determine the ELM energy and particle losses. The dependence of the pellet injection geometry has been studied and it is found that pellet injection from high field side eases the pellet ELM triggering, consistent with the findings of DIII-D [5]. The dependence of the power deposition asymmetry on the injection geometry and the consequences for ITER with the JOREK simulation of JET which confirms the result will be presented. Detailed investigation of the particle and the energy loss during the full ELM cycle of pellet triggered ELM is will be presented.

References

- [1] P. Lang, *et al.*, Nucl. Fusion **44**, 665 (2004).
- [2] P. Lang, *et al.*, Nucl. Fusion **53**, 073010 (2013).
- [3] L. Baylor, *et al.*, Phys. Rev. Lett. **110**, (2013) 245001.
- [4] R. Wenninger, *et al.*, Plasma Phys. Control. Fusion **53**, 105002 (2011).
- [5] S. Futatani, *et al.*, Nucl. Fusion **54**, 073008 (2014).
- [6] G. T. A. Huysmans and O. Czarny, Nucl. Fusion **47**, 659 (2007).

This work has been carried out within the framework of the EUROfusion Consortium and has received funding from the Euratom research and training programme 2014–2018 under grant agreement No. 633053. The views and opinions expressed herein do not necessarily reflect either those of the European Commission or those of the ITER Organization.



Nonlinear Modelling of the Edge Localized Mode Control by Resonant Magnetic Perturbations in ASDEX-Upgrade

F. Orain¹, M. Hoelzl¹, E. Viezzer¹, M. Dunne¹, M. Bécoulet², P. Cahyna³, G. Huijsmans⁴, M. Willensdorfer¹, W. Suttrop¹, A. Kirk⁵, S. Pamela^{5,6}, S. Guenter¹, E. Strumberger¹, and A. Lessig¹

¹Max-Planck-Institut für Plasmaphysik, Garching, Germany

²Institut de Recherche sur la Fusion par confinement Magnétique (IRFM), Commissariat à l'énergie atomique (CEA/Cadarache), 13108 Saint-Paul-lès-Durance, France

³Institute of Plasma Physics AS CR v.v.i., Prague, Czech Republic

⁴International Thermonuclear Experimental Reactor (ITER), Cadarache Centre, 13108 Saint-Paul-lès-Durance, France

⁵Culham Centre for Fusion Energy (CCFE), Culham Science Centre, Abingdon, UK

⁶United Kingdom Atomic Energy Authority, Culham Science Centre, Abingdon, UK

Corresponding Author: F. Orain, forain@ipp.mpg.de

One of the foreseen methods to control the edge localized modes (ELMs) in ITER is the application of resonant magnetic perturbations (RMPs), proved capable to mitigate or suppress ELMs in existing tokamaks. However, the significant uncertainties that remain regarding the way plasma flows and ELMs interact with RMPs must be overcome to give reliable predictions for ITER. This work aims at assessing the impact of the different plasma responses (including resonant and kink components) on the ELM mitigation, in order to move towards more quantitative understanding of current experiments and better predictive capabilities for future experiments.

Nonlinear resistive MHD simulations were performed with the JOREK code, using input equilibrium profiles and $n = 2$ RMP spectrum closely matching the experimental data of ASDEX-Upgrade shots at low collisionality.

In a first step, the interaction between $n = 2$ RMPs and plasma flows is considered without ELMs. In experiments, a given RMP coil configuration was identified to lead to a stronger ELM mitigation: this is found to be correlated with the largest excitation of the kink response in the vicinity of the X-point observed in our modelling with JOREK (in good agreement with other modelling performed with MARS-F and VMFC). On the resonant surfaces $q = m/n$ located at the edge, the coupling between this excited kink component (poloidal mode $m+2$) and the resonant component m induces the amplification of the resonant component, resulting in an enhanced ergodicity at the edge. The ergodicity and the large displacement of temperature and density near the X-point therefore generate an increased radial transport.

In a second step, RMP effects on ELMs are considered in multiharmonic n simulations. First results on the ELM mitigation induced by nonlinear coupling of unstable modes with $n = 2$ RMPs depending on the plasma response are presented and compared to experiments.

Nonlinear Simulation of ELM Dynamics in the Presence of RMPs and Pellet Injection

D. Chandra¹, A. Thyagaraja², A. Sen¹, and P. K. Kaw¹

¹*Institute for Plasma Research (IPR), Bhat, Gandhinagar, India*

²*Astrophysics Group, University of Bristol, Bristol, BS8 1TL, UK*

Corresponding Author: D. Chandra, debasischandra@gmail.com

We report on nonlinear simulation studies on the dynamical behaviour of ELMs under the influence of RMPs and/or the presence of pellet injection using a two-fluid initial-value electromagnetic nonlinear global code (CUTIE). The full set of model fluid equations are solved for the so-called mesoscale, an intermediate scale between the device size and the ion gyroradius, incorporating approximations for the underlying classical and neoclassical transport effects. To simulate ELMs we introduce a particle source in the confinement region and a particle sink in the edge region. The code also incorporates turbulent transport effects and allows the development of profile-turbulence interactions thereby enabling a self-consistent description of the evolution of the mode. To study ELM control using RMPs we have applied an $n = 2$ static external magnetic perturbation at the edge and made numerous runs under varying conditions for the machine and plasma parameters typical of COMPASS-D. Our results show that ELM mitigation is possible for RMP powers beyond a specific threshold consistent with experimental observations of several tokamaks. The results also provide valuable insights into the RMP induced modifications of the complex nonlinear dynamics of the ELMs, in particular on the redistribution of mode energy and the cascading of energy to shorter scale lengths. We also observe a hysteresis in states as we increase the amplitude of RMPs and then decrease it to the same value. Preliminary simulations with pellet injection also show encouraging ELM mitigation results with corresponding changes in the ambient electromagnetic turbulence. Based on these results we have also used CUTIE in a predictive manner to map out parametric regions for safe operation of SST-1 by in terms of RMP thresholds and pellet pacing frequency for ELM control/mitigation in SST-1 H-mode scenarios.



Numerical Calculations of Plasma Response to External Magnetic Perturbations

J. Kim¹, S. S. Kim¹, and H. Jhang¹

¹*National Fusion Research Institute (NFRI), Daejeon, Republic of Korea*

Corresponding Author: J. Kim, yegakjh@nfri.re.kr

We investigate the effect of resistivity, mainly on pitch resonant responses induced by plasma rotation. As a confirmation of the newly developed code, we report that the detailed physics may not be important since the pitch resonant response is relatively weak at high resistivity and the penetration is strongly dependent on plasma rotation at low resistivity. At low resistivity, ion collisionality can affect the penetration of RMPs through poloidal flow. The preliminary quasilinear results with $n = 0$ parallel flow and radial electric field show that the torque induced by RMP may modify parallel flow significantly $t > 10^4 t_A \sim 1$ ms after RMP application. The detailed quasilinear responses will be presented with the possible implication on ELM suppression.

Drift-Alfvén Instabilities and Turbulence of Magnetic Field Aligned Shear Flows

V. S. Mykhaylenko¹, V. V. Mykhaylenko¹, and H. J. Lee¹

¹*Pusan National University, Pusan, Republic of Korea*

Corresponding Author: V. S. Mykhaylenko, vsmykhailenko@pusan.ac.kr

Numerous experimental observations from number of tokamaks and stellarators have found large nearly sonic magnetic field aligned (parallel) shear flows that are peaked at the last closed flux surfaces and extend for a few centimetres into the plasma and into the far SOL. The important consequence is that these plasma regions are unstable in the presence of shear flows. The shear flows along the magnetic field are the additional sources of free energy for the modification of the instabilities, existing in shearless plasma flows, as well as for the development of specific shear flow driven (SFD) instabilities, which are absent in the shearless plasma. It was reported recently, that in plasmas with ion temperature equal to — or even higher than — the electron temperature (the case relevant to tokamak plasma) the Kelvin–Helmholtz (or D’Angelo) driving mechanism of the excitation the hydrodynamic instabilities changes onto the combined effect of the velocity shear and ion Landau damping. It results in the development of a new set of the ion-kinetic SFD instabilities, which distinguish by strong interaction of waves with thermal ions. This is a striking difference between the instabilities of the parallel shear flows and the shearless plasma, where the ion Landau damping is, as a rule, a process that suppresses the development of the drift instabilities. It was found that in the parallel shear flow of plasmas with comparable ion and electron temperatures, two distinct drift–Alfvén instabilities (DAI) may develop: the shear flow modified DAI, which develops due to the inverse electron Landau damping and exists in the shearless plasma as well, and the SFD DAI, which develops due to the combined effect of the velocity shear and ion Landau damping and is absent in the shearless plasma flows. In this report, we present the results of the investigation of the nonlinear saturation of both these instabilities and the processes of the anomalous heating and transport of ions. The results of the analytical and numerical investigations of the SFD DAI and corresponding turbulence of the shear flow with inhomogeneous ion temperature, which develops due to the coupled reinforcing action of parallel flow shear, ion temperature gradient and ion Landau damping, will be given.

This work was supported by NRF of Korea (Grant No. NRF-2014M1A7A1A03029878) and BK21PLUS.



MHD Stability of ITER H-Mode Confinement with Pedestal Bootstrap Current and Diamagnetic Effects Taken into Account

L. Zheng¹, M. Kotschenreuther², P. Valanju¹, S. Mahajan¹, D. Hatch², and X. Liu¹

¹University of Texas at Austin, Austin, TX 78712, USA

²Institute for Fusion Studies (IFS), University of Texas at Austin, Austin, TX 78712, USA

Corresponding Author: L. Zheng, lzheng@mail.utexas.edu

MHD stability of ITER H-mode confinement is investigated with bootstrap current included for equilibrium, together with diamagnetic drift and rotation effects for stability. The ITER pedestal has high temperature, so the bootstrap current is large and diamagnetic effects are important. We construct numerically ITER equilibria with bootstrap current taken into account. Especially, we have considered a more realistic scenario in which density and temperature profiles can be different. The direct consequence of bootstrap current effects on equilibrium is the modification of local safety factor profile at pedestal, so that the magnetic shear can be reduced or reversed locally. This local q value is referred to as q_s . This q profile change results in a dramatic change of MHD mode behaviour. The stability of ITER numerical equilibria is investigated with AEGIS code. Both low- n and peeling-ballooning modes are investigated. Note that pressure gradient at pedestal is steep. High resolution computation is needed. Since AEGIS code is an adaptive code, it can well handle this problem. Also, the analytical continuation technique based on the Cauchy–Riemann condition of dispersion relation is applied, so that the marginal stability conditions can be determined. It is found that the pedestal stability depends not only on the edge current (J_{ped}) and pressure gradient (p'_{ped}), but also on the q_s value. This shows that the pedestal stability can be affected by the global current profile. The diamagnetic drift and rotation effects are also investigated. Both numerical scheme and results will be presented. The physical interpretation will be explained.



Equilibrium Solutions of MHD Equations for GAMs in the Edge Tokamak Plasma

R. Shurygin¹, A. Melnikov¹

¹National Research Centre "Kurchatov Institute", Moscow, Russian Federation

Corresponding Author: R. Shurygin, lysenksergej@yandex.ru

Numerical calculations of nonlinear MHD equations in frames of reduced two-fluid Braginskii equations for geodesic acoustic modes (GAM) with $n = 0, m = 0, \pm 1$ in high collisional edge tokamak plasma were performed. It was shown that with account of parallel dissipation (finite conductivity σ_{\parallel}) allows us to obtain the steady state equilibrium solutions for GAMs. The obtained 2D equilibrium includes the velocity of poloidal rotation and the equilibrium electric potential, which value is close to well-known Pfirsch-Schlüter potential. It was shown that the main role in formation of the equilibrium poloidal rotation plays two forces: the Stringer–Winsor force and the neoclassical force, linked with the parallel viscosity. Maximum values of GAM are located near the maximum of pressure gradient. Calculated radial profile of electric field E looks like the parabolic negative well ($E < 0$).



Excitation of Frequency Jump by Barely Passing Electrons

H. Feng¹, Z. Wang^{1,2}, and H. Li¹

¹*School of Science, Xihua University, People's Republic of China*

²*Southwestern Institute of Physics, Chengdu, Sichuan, People's Republic of China*

Corresponding Author: H. Feng, ddsteed@gmail.com

An e-fishbone frequency jump has been observed on Tore Supra, which is important for the redistribution of energetic electrons and energetic particle losses. E-fishbone periodic frequency jump phenomena are also observed on HL-2A. Soft X-ray tomography shows that the poloidal and toroidal mode numbers are 1/1 and 2/2 with the frequency jump. In this paper we present a theoretical base of the frequency jump in the e-fishbone experiments. It is identified that barely passing electrons are the drive of the e-fishbone, rather than the trapped electrons. The frequency jumps in HL-2A e-fishbone experiments are numerically reproduced. E-fishbone frequency increases with the hot electron energy which is consistent with the experiments. The growth rate of the mode ($m=2, n=2$) is greater than the one of the mode ($m=1, n=1$) in contrast to the pure MHD prediction. The calculated temporal evolutions of the hot electron energy and the kink mode amplitude are periodic which in good agreement with the observed e-fishbone jump cycle. The theory provides an insight on HL-2A and Tore Supra experiments.

Magneto-Thermal Reconnection Processes, Related Angular Momentum Transport Issues and Formation of High Energy Particle Populations

B. Coppi¹, B. Basu¹, A. Fletcher¹, R. L. White¹, and L. Sugiyama¹

¹Massachusetts Institute of Technology (MIT), Cambridge, MA 02139, USA

Corresponding Author: B. Coppi, coppi@mit.edu

In the context of a two-fluid theory of magnetic reconnection [1], when the longitudinal electron thermal conductivity is relatively large, the perturbed electron temperature tends to become singular [2] in the presence of a reconnected field component and an electron temperature gradient. A transverse thermal diffusivity is introduced in order to remove this singularity while a finite “inductivity” can remove the singularity of the corresponding transverse plasma displacement [1]. Then i) a new “magneto-thermal reconnection” producing mode, driven by the electron temperature gradient, and involving a considerable range of scale distances is found [3]; ii) the characteristic widths of the layers in which magnetic reconnections takes place remain significant even when the macroscopic distances involved in the process are very large; iii) the phase velocities of the modes that are found can be both in the direction of the electron diamagnetic velocity as well as those in the opposite (ion) direction. A numerical solution of the complete set of equations has been carried out and followed by a simplified analytical reformulation of the problem. The mode growth rate is related to the effects of a finite viscous diffusion coefficient or to those of a small electrical resistivity.

The features that can lead to a possible explanation of the fact that high energy particle populations are produced during reconnection events involve mode-particle resonances producing the transfer of energy to superthermal particle populations [4] and the spatial near-singularity of the electron temperature that can enhance the thermal energy of particles in one region while depleting that of particles in a contiguous region [3].

The low collisionality modes that produce magnetic reconnection can extract angular momentum from the plasma column and thereby sustain a “spontaneous rotation” [5] of it. This process is to be considered in addition to that associated with electrostatic modes excited at the edge of the plasma column [5].

References

- [1] B. Coppi, Phys. Fluids **8**, 2273 (1965).
- [2] B. Coppi, B. Basu, P. Montag, *et al.*, Nucl. Fusion **55**, 093018 (2015).
- [3] B. Coppi, MIT (LNS) Report HEP 15/06 (2015). In print for Fizika Plazmy.
- [4] B. Coppi, L. Sugiyama, J. Mark and G. Bertin, Ann. Phys. **119**, 370 (1979).
- [5] B. Coppi, Nucl. Fusion **42**, (2002).

Work supported by the U.S. Department of Energy, award DE-FG02-03ER54700.

Simulation Study of Interaction between Runaway Electron Generation and Resistive MHD Modes over Avalanche Timescale

A. Matsuyama¹, N. Aiba¹, and M. Yagi¹

¹Japan Atomic Energy Agency (JAEA), Naka, Japan

Corresponding Author: A. Matsuyama, matsuyama.akinobu@jaea.go.jp

Runaway electron (RE) generation after major disruptions is simulated over a full current quench (CQ) timescale, which covers both fast MHD events and slow RE avalanche amplification. A novel 3D RE analysis code EXTREM allows us to study 1) fast, global transport of REs with macroscopic MHD modes and 2) the RE generation triggered by electric fields induced owing to fast MHD dynamics (i.e., “mode-induced REs”). In the EXTREM code, slow CQ process ($n = 0$, for n the toroidal mode number) is described using the current diffusion model with a time varying resistivity, whereas RE transport and fast MHD dynamics ($n > 0$) are treated on the basis of reduced MHD models. The long-timescale simulations with the EXTREM code demonstrate their advantage for the analysis of net RE generation in a self-consistent manner with the anomalous transport and generation mechanisms due to resistive MHD modes. Effects of the resistive mode on the spatial profiles of generated REs can also be compared with a 1D diffusion model. These extensions of the model is a valuable step towards self-consistent treatments of the RE generation with thermal collapse, which is a highly complex task but is an important challenge for predictive simulations of the RE generation during mitigated disruptions in ITER. In this paper, particular attention has been paid to $m = 1$ resistive modes triggered with the current peaking resulting from massive RE generation (m is the poloidal mode number). It is shown that sawtooth-like events are triggered when the central safety factor $q(0)$ drops below unity, and the burst of Dreicer electrons is induced as a return current that compensates the expelled poloidal magnetic flux. In view of the global energy balance, the return current plays a role in converting the potential energy of the MHD instability to RE kinetic energies. It is still a small perturbation on a fast MHD timescale but can be amplified over the avalanche timescale. The scope of the paper will also be extended to the impact of tearing modes.

TH



Collisional Generation of Runaway Electron Seed Distributions Leading to Subcriticality, Avalanche, or Fast Transfer

D. Brennan¹, E. Hirvijoki¹, C. Liu¹, A. H. Boozer², and A. Bhattacharjee¹

¹Princeton Plasma Physics Laboratory (PPPL), Princeton, NJ 08540, USA

²Columbia University, New York, NY 10027, USA

Corresponding Author: D. Brennan, dbrennan@pppl.gov

Well before ITER operations begin, we must have a comprehensive understanding of the potential for runaway electron generation, as well as methods for their control and mitigation, as the destructive potential to the plasma facing components is severely intolerable. This makes for a unique situation in requiring an assessment based on plasma theory and computation well before validation experiments can be performed.

Among the most important questions given a thermal collapse event is that of how many seed electrons are available for runaway acceleration and the avalanche process. Seed electrons remain with a kinetic energy above the critical energy for runaway after a thermal quench, either natural or induced. The expected seed generation is a critical question that needs to be addressed, and new methods are now available to do so. The most important source of seed electrons is the high-energy tail of the pre-thermal-quench Maxwellian. This high energy tail can be lost in two ways: 1) collisional drag on cold electrons, or, 2) loss to the walls if all the magnetic surfaces within the plasma are destroyed.

In this study, we use the kinetic equation for electrons and ions to investigate how different cooling scenarios lead to different seed distributions. Given any initial distribution, we study their subsequent avalanche and acceleration to runaway with adjoint and test particle methods [1]. This method gives an accurate calculation of the runaway threshold by including the collisional drag of background electrons (assuming they are Maxwellian), pitch angle scattering, and synchrotron and Bremsstrahlung radiation. A resulting probability to runaway is determined in phase space, which has a sharp transition, such that electrons with energy above this transition become highly likely to runaway. Summing the electrons above this threshold determines the number of seed electrons N_s . When N_s exceeds the number of relativistic electrons needed to produce the entire equilibrium current, fast transfer to runaway current is possible. Alternatively, N_s can be small enough that the runaway process is too slow to cause any significant runaway population on the experimental timescale. Between these limits, the avalanche process determines the runaway population.

References

[1] C. Liu, *et al.*, Phys. Plasmas **23**, 010702 (2016).



Current Profile Shape Effects on the Formation and Termination of Runaway Beams in Tokamak Disruptions and Implications for ITER

J. R. Martín-Solís¹, A. Loarte², M. Lehnen², V. Riccardo³, and C. Reux⁴

¹Universidad Carlos III de Madrid, Madrid, Spain

²International Thermonuclear Experimental Reactor (ITER),
Cadarache Centre, 13108 Saint-Paul-lès-Durance, France

³Culham Centre for Fusion Energy (CCFE), Culham Science Centre, Abingdon, UK

⁴Institut de Recherche sur la Fusion par confinement Magnétique (IRFM),
Commissariat à l'énergie atomique (CEA/Cadarache), 13108 Saint-Paul-lès-Durance, France

Corresponding Author: J. R. Martín-Solís, solis@fis.uc3m.es

Runaway electrons (REs) generated during disruptions are usually found to deposit their energy in very short pulses and on localized areas of the plasma facing components (PFCs). In ITER, there is serious concern about the potential that large amounts of MeV REs generated during the disruption current quench (CQ) have for erosion or melting of the PFCs. Although zero-dimensional (0D) modelling has provided a rather complete physics picture of the CQ and termination phases of the disruption, there is evidence indicating that current profile shape effects could be important. In this work, a one dimensional model (1D) beyond the 0D model is used to evaluate effects associated with the evolution of the plasma and RE current profiles during the disruption. The model predictions are found to be in agreement with measurements of the plasma internal inductance for 2 MA JET disruptions with RE current plateau formation. The resulting runaway plasma is more peaked in the plasma centre than the predisruption plasma current. The peaking decreases when the RE current increases and is also found to be dependent on the runaway seed profile shape, increasing with the internal inductance of the seed current. These results can have important implications for ITER as: 1) due to the increase in the plasma internal inductance, for the same RE current magnitude, the magnetic energy of the RE plasma would be substantially larger; 2) the post-CQ plasma current profile might be MHD unstable as plasmas with peaked current profiles can be prone to the tearing-mode instability. Moreover, the magnetic energy does not scale linearly with the square of the RE current. In order to investigate these effects, an integrated 1D analysis of the runaway beam formation and termination during disruptions in ITER has been carried out, and including the essentials of the involved physical processes such as the main RE generation mechanisms expected in ITER as well as corrections to the RE dynamics to account for the collisions of the RE electrons with the partially stripped impurity ions.

This work was carried out within the framework of the EUROfusion Consortium and has received funding from the Euratom research and training programme 2014–2018 under grant agreement No 633053. The views and opinions expressed herein do not necessarily reflect those of the European Commission.

Simulations of Runaway Electron Generation including Hot-Tail Effect

H. Nuga¹, A. Matsuyama², M. Yagi², and A. Fukuyama¹

¹*Kyoto University, Nishikyo-ku, Kyoto 615-8540, Japan*

²*Japan Atomic Energy Agency (JAEA), Naka, Japan*

Corresponding Author: H. Nuga, nuga@p-grp.nucleng.kyoto-u.ac.jp

The suppression and mitigation of runaway electron (RE) is an urgent issue of large scale tokamak operation. The contribution of hot-tail effect, which arises from the fast thermal quench, is studied using Fokker–Planck simulation. It is found that if the thermal quench is fast enough to invoke the hot-tail effect, it may produce seed REs and enhance total RE current even in a high electron density plasma.



Phase Locking, Phase Slips and Turbulence: A New Approach to Mechanisms for Quiescent H-Mode

Z. Guo¹, P. H. Diamond¹

¹University of California San Diego, CA 92093, USA

Corresponding Author: Z. Guo, guozhipku@gmail.com

We demonstrate $E \times B$ shear governs the dynamics of the cross phase of the peeling-ballooning (PB) mode-driven heat flux, and so determines the evolution from the edge-localized (ELMy) H-mode to the quiescent, or QH-mode. A physics-based scaling of the $E \times B$ shearing rate for accessing the QH mode is predicted. The ELMy H-mode to the QH-mode evolution is shown to follow from the conversion from a phase locked state to a phase slip state. In the phase locked state, PB modes are pumped continuously, so bursts occur. In the slip state, the PB activity is a coherent oscillation. Strong $E \times B$ shearing implies a higher phase slip frequency. PB turbulence can degrade slip coherency. This model predicts a new state of cross phase dynamics and gives a new understanding of the mechanism for ELMy to QH-mode evolution.

Work supported by the U.S. Department of Energy, Office of Science, Office of Fusion Energy Sciences, under Award Numbers DE-FG02-04ER54738 and DE-SC0008378.



Gyrokinetic Analysis of the Effects of Electron-Scale Turbulence on Ion-Scale Microinstabilities

S. Maeyama¹, T.-H. Watanabe¹, A. Ishizawa², M. Nakata³, and M. Nunami³

¹*Nagoya University, Nagoya, Japan*

²*Kyoto University, Nishikyo-ku, Kyoto 615-8540, Japan*

³*National Institute for Fusion Science (NIFS), Toki, Gifu, Japan*

Corresponding Author: S. Maeyama, smaeyama@p.phys.nagoya-u.ac.jp

Most previous studies on plasma turbulence have assumed scale separation between electron-scale (\sim electron gyro-radius) and ion-scale turbulence (\sim ion gyro-radius). However, multiscale turbulence studies by using the latest supercomputers indicated existence of cross-scale interactions and its significant impact on turbulent transport, and are necessary for explaining experimental transport levels. Our recent work revealed a part of the cross-scale interactions: suppression of electron temperature gradient modes (ETG) by flow shears in ion temperature gradient mode (ITG) turbulence, and enhancement of ion-scale transport due to damping of the zonal modes by electron-scale turbulence. Since effects of electron-scale turbulence on ion-scale transport have not yet been fully revealed, it is important to explore the physical process in detail and to extend the analysis to other microinstabilities. Here, we report two analyzes: i) detailed investigation of the damping effects of ETG turbulence on zonal flows created by the ITG turbulence, and ii) effects of the ETG turbulence on linear growth of the microtearing mode (MTM).

First, we have analyzed the ITG/ETG turbulence simulation by using the gyrokinetic entropy transfer analysis. It is revealed that the zonal modes are mainly driven by the ion-scale modes, where relatively higher-wave-number modes are driven by the coupling with the twisted mode caused by kinetic electrons. Electron-scale turbulence effectively damps these higher-wave-number zonal modes. Second, we have investigated the effect of ETG turbulence on linear MTM growth. It is observed that the growth of MTM can be suppressed as ETG-driven turbulent fluctuations increase, which suggests that the ETG turbulence may interrupt the linear MTM growth. Our analyzes shed a light on the effects of electron-scale turbulence on ion-scale microinstabilities: i) ETG turbulence damps relatively higher-wave-number zonal flows created by ITG turbulence with twisted modes, and ii) ETG turbulence can distort the resonant mode structure of MTM and interrupt its linear growth. In both cases, kinetic electrons play important roles such as creation of the twisted mode and of the current sheet. This emphasizes the significance of intermediate-scale structures for the cross-scale interactions.



Multispecies ITG-TEM Driven Turbulent Transport of DT Ions and He-ash in ITER Burning Plasmas

M. Nakata¹, M. Honda², M. Nunami¹, T.-H. Watanabe³, and H. Sugama¹

¹National Institute for Fusion Science (NIFS), Toki, Gifu, Japan

²Japan Atomic Energy Agency (JAEA), Naka, Japan

³Nagoya University, Nagoya, Japan

Corresponding Author: M. Nakata, nakata.motoki@nifs.ac.jp

Burning plasmas are composed of multiple ion species such as fuel isotopes (D and T) and He-ash produced by the fusion reaction, and more complex turbulent transport processes are expected in comparison to the single-ion plasmas. Since simultaneous measurements of the kinetic profiles for all species are limited even in experiments, systematic studies on the particle and heat transport by the first-principle-based gyrokinetic simulations are indispensable for the prediction of the confinement performance and the optimization of the impurity exhausts and D/T fuelling. In this study, the ion-temperature-gradient and trapped-electron-mode (ITG-TEM) driven turbulent transport in realistic ITER plasmas is investigated by means of the multispecies electromagnetic gyrokinetic Vlasov simulation GKV [1] with D, T, He, and real-mass kinetic electrons including their interspecies collisions [2, 3], where a good prediction capability has been confirmed against the actual JT-60U tokamak experiment [4]. The GKV simulations reveal different saturation levels and spatial structures of the turbulent fluctuations in DT ions and He-ash. For the first time, gyrokinetic-simulation-based quantitative evaluation of a steady burning condition [5] with He-ash exhaust and fuel inward-pinch is realized by extensive nonlinear scans. Furthermore, the strong impacts of DT fuel ratio and He-ash accumulations on turbulent energy and particle fluxes are clarified. New findings in this study, which are crucial for the burning plasma performance, are i) imbalanced DT turbulent particle transport strongly influenced by He-ash accumulations, and ii) identification of the steady burning profile regimes with He-ash exhaust and DT fuel inward-pinch associated with the off-diagonal transport.

References

- [1] T.-H. Watanabe, *et al.*, Nucl. Fusion **46**, 24 (2006).
- [2] M. Nakata, *et al.*, Comput. Phys. Commun. **197**, 61 (2015).
- [3] M. Nunami *et al.*, Plasma Fusion. Res. **10**, 1403058 (2015).
- [4] M. Nakata, *et al.*, IAEA FEC-2014, TH/P7-38, (2014).
- [5] D. Reiter *et al.*, Nucl. Fusion **30**, 2141 (1990).



Anomalous and Neoclassical Transport of Hydrogen Isotope and Impurity Ions in LHD Plasmas

M. Nunami¹, M. Nakata¹, H. Sugama¹, M. Sato¹, J. L. Velasco², S. Satake¹, and M. Yokoyama¹

¹National Institute for Fusion Science (NIFS), Toki, Gifu, Japan

²Centro de Investigaciones Energéticas, Medioambientales y Tecnológicas (CIEMAT), Madrid, Spain

Corresponding Author: M. Nunami, nunami.masanori@nifs.ac.jp

Gyrokinetic and drift kinetic simulations are carried out to investigate anomalous and neoclassical transport of hydrogen isotope and impurity ions in large helical device (LHD) plasmas. Turbulent transport in high electron temperature regime, where the trapped electron mode (TEM) is dominant, is a critical issue for future burning plasmas. To clarify an impact of hydrogen isotope species on the turbulent transport in LHD system, TEM turbulence simulations in hydrogen and deuterium LHD plasmas with real-mass kinetic electrons have been carried out for the first time by gyrokinetic simulations with multispecies collision operator. The strong isotope dependence on the growth rate of collisionless TEM branch appears through the stabilization effect due to a mass dependence in the normalized electron-ion collision frequencies. Nonlinear simulations clarify the significant dependence of the isotope species in the reduction of the electron and ion energy fluxes in deuterium plasma. Here, stronger TEM stabilization in the deuterium plasma leads to the enhancement in the ratio of ZF energy to total energy.

Transport in high ion temperature (T_i) plasmas with extremely hollow impurity density profiles (impurity hole) is also a critical issue hole phenomena is also a critical issue for high-performance. In high- T_i LHD plasma, the simulation indicates the neoclassical particle fluxes of electron and bulk ion species are outward directed, although the flux of the impurity carbon is extremely small and its value and direction are sensitive to the radial electric field. On the other hand, the microinstability analyzes by gyrokinetic simulations show that the anomalous contributions of quasi-linear particle fluxes of all species are inward-directed which is consistent with the fact that the positive neoclassical particle fluxes and the negative turbulent fluxes should be balanced in a steady state. The ratio of each particle flux is almost consistent with the neoclassical contributions.



Direct Identification of Predator-Prey Dynamics in Gyrokinetic Simulations

S. Kobayashi^{1,2}, Ö. D. Gürçan¹, and P. H. Diamond²

¹*Laboratoire de Physique des Plasmas (LPP), CNRS/École Polytechnique, 91128 Palaiseau, France*

²*University of California San Diego, CA 92093, USA*

Corresponding Author: S. Kobayashi, sumire.kobayashi@lpp.polytechnique.fr

The interaction between spontaneously formed zonal flows and small-scale turbulence in nonlinear gyrokinetic simulations is explored in a shearless closed field line geometry. It is found that when clear limit cycle oscillations prevail, the observed turbulent dynamics can be quantitatively captured by a simple Lotka–Volterra type predator-prey model. Fitting the time traces of full gyrokinetic simulations by such a reduced model allows extraction of the model coefficients. Among other findings, it was observed that the effective growth rates of turbulence (i.e., the prey) remain roughly constant, in spite of the higher and varying level of primary mode linear growth rates. The effective growth rate that was extracted corresponds roughly to the zonal-flow-modified primary mode growth rate. The result also demonstrates that the effective damping of zonal flows (i.e., the predator) in the parameter range, where clear predator-prey dynamics is observed (i.e., near marginal stability), agrees with the collisional damping expected in these simulations. This implies when the tertiary instability plays a role the dynamics becomes more complex than a simple Lotka–Volterra predator prey model.

TH



Gyrokinetic Simulations of an Electron Temperature Gradient Turbulence-Driven Current in Tokamak Plasmas

S. Yi¹, H. Jhang¹, and J.-M. Kwon¹

¹*National Fusion Research Institute (NFRI), Daejeon, Republic of Korea*

Corresponding Author: S. Yi, yism@nfri.re.kr

The so-called “spontaneous” or “intrinsic” rotation driven by ion-scale turbulence has been widely observed in tokamaks. If we turn our attention to the electron parallel momentum balance, it is likely that electron-scale turbulence, e.g., electron temperature gradient (ETG) turbulence, can modify Ohm’s law, hence providing a current source. However, there has been no serious study of an ETG-driven current in self-consistent simulations using realistic tokamak geometry. In this work, we report results of a gyrokinetic simulation study elucidating the characteristics of an intrinsic current driven by ETG turbulence in toroidal geometry. We focus on effects of the normalized electron gyroradius ρ_e^* on the ETG-driven current. Our simulations demonstrate that the amount of the ETG-driven current increases with ρ_e^* , as expected from the gyro-Bohm scaling. In particular, a perturbation of a q -profile by the ETG-driven current becomes visible when $a < 4000\rho_e$. This finding suggests that a significant intrinsic current can be driven inside an H-mode pedestal where the steep gradient of an electron temperature pedestal can excite ETG turbulence in a narrow region.

Progress in the Theoretical Description and the Experimental Characterization of Tungsten Transport in Tokamaks

C. Angioni¹, E. A. Belli², R. Bilato¹, V. Bobkov¹, F. J. Casson³, E. Fable¹, A. Loarte⁴, P. Mantica⁵, R. Ochoukov¹, T. Odstřil¹, T. Pütterich¹, M. Sertoli¹, J. Stober¹, and M. Valisa⁶

¹Max-Planck-Institut für Plasmaphysik, Garching, Germany

²General Atomics, San Diego, CA 92186, USA

³Culham Centre for Fusion Energy (CCFE), Culham Science Centre, Abingdon, UK

⁴International Thermonuclear Experimental Reactor (ITER), Cadarache Centre, 13108 Saint-Paul-lès-Durance, France

⁵Istituto di Fisica del Plasma (IFP), Consiglio Nazionale delle Ricerche (CNR), 20125 Milan, Italy

⁶Consorzio RFX, Associazione EURATOM-ENEA sulla Fusione, Padova, Italy

Corresponding Author: C. Angioni, clemente.angioni@ipp.mpg.de

The validation of current models to predict the transport of a heavy impurity like tungsten in tokamaks is confronted with challenges from both the theoretical and experimental standpoints. Both neoclassical and turbulent transport mechanisms are involved, and have to take into account the impact of poloidal asymmetries, produced by both centrifugal effects and temperature anisotropies caused by auxiliary heating. These can significantly modify the neoclassical transport, affecting both its amplitude and the strength of the temperature screening. The size of turbulent impurity transport strongly depends on the ratio of the electron to the ion heat flux and is maximized when this ratio slightly exceeds unity. Moreover, in these conditions, subdominant modes can nonnegligibly impact the transport, and lead to turbulent convections which are in opposite direction with respect to the predictions based on the most unstable linear mode only. Theory validation benefits of experiments which are dedicated to testing detailed predictions. However, experiments on heavy impurity transport face limitations on the possibility of diagnosing the impurity density, the accessible domains of plasma parameters and the available heating systems in each device. Experiments have been performed in ASDEX-Upgrade to investigate the impact of central wave heating in the avoidance of W accumulation in H-mode plasmas with dominant neutral beam injection heating. Experiments show that ion cyclotron and electron cyclotron heating have similar effects on the W behaviour when similar power density profiles are produced with the two wave heating systems, consistent with dominant electron heating produced by ICRH in the H minority scheme in ASDEX-Upgrade. Theory-based modelling is performed by combining the GKW and NEO codes, and conditions under which the role of H minority becomes significant are highlighted. These results are compared with companion experimental and modelling research performed at JET. Finally the implications of the experimental and theoretical results on the prediction of the tungsten behaviour in ITER and a future reactor are presented. General parametric dependencies of confinement with increasing size of the device support the favourable expectation for impurities that in a reactor the impact of neoclassical transport is reduced with respect to present tokamaks.



Crucial Role of Zonal Flows and Electromagnetic Effects in ITER Turbulence Simulations Near Threshold

J. Candy¹, G. M. Staebler¹

¹General Atomics, San Diego, CA 92186, USA

Corresponding Author: J. Candy, candy@fusion.gat.com

Development of a validated integrated modelling framework is a fundamental research task within the US fusion energy programme. A primary component of this framework is an accurate transport model describing the small-scale, gradient-driven plasma microturbulence and its associated cross-field transport. Design and calibration of accurate transport models requires a database of well-converged nonlinear gyrokinetic simulations, which is a computationally very challenging undertaking. As early as 2008, GYRO simulations of ITER operating scenarios were observed to produce levels of nonlinear zonal-flow (ZF) activity large enough to quench turbulence inside the plasma core. This observation implied that modelling estimates of fusion power in ITER may have been pessimistic because turbulent transport was overestimated. The existence of flow-dominated, low-transport states persisted even as more accurate and comprehensive predictions of ITER profiles were made using the TGLF transport model. This was in stark contrast to GYRO-TGLF comparisons for modern-day tokamaks, for which GYRO and TGLF are typically in close agreement and transport is well-above threshold. It was speculated that closeness to threshold, ZF activity, and electromagnetic effects, could all play a key role in this discrepancy. Importantly, it became clear that TGLF must be generalized to include ZF stabilization for more accurate ITER simulations. The ongoing recalibration process also uncovered additional new concerns related to the accuracy of both the GYRO simulations as well as the TGLF saturation rule. Plaguing the workflow for the ZF recalibration effort is the intermittency of the near-threshold GYRO simulations. A second surprising result was that magnetic compression is strongly destabilizing in these plasmas, another effect not reproduced by TGLF. Exhaustive simulation and recalibration efforts are summarized, which represent an enormous undertaking carried out in stages over a period of years.

A Model of the Saturation of Coupled Electron and Ion Scale Gyrokinetic Turbulence

G. M. Staebler¹

¹General Atomics, San Diego, CA 92186, USA

Corresponding Author: G. M. Staebler, staebler@fusion.gat.com

Two important regimes, observed in nonlinear gyrokinetic turbulence simulations, are not well modelled by the TGLF quasilinear model. The first is the Dimits shift regime characterized by a nonlinear upshift in the effective critical ion temperature gradient above the linear threshold. The second is the electron temperature gradient (ETG) streamer regime characterized by high electron scale turbulence when the ion scale turbulence is weak or stable. The Dimits shift impacts the predicted temperature profile in the deep core. The streamer regime is important when the temperature gradient of the electrons exceed that of the ions. A new model of the saturated turbulence spectrum will be shown to be able to match the turbulence driven transport fluxes in both of these regimes when applied to the TGLF quasilinear model. Analysis of the spectrum of the saturated electric potential fluctuations from multiscale (both ion and electron scales) gyrokinetic turbulence simulations in tokamak geometry reveals that fluctuating zonal (axisymmetric) $E \times B$ flows couple the ion and electron scales. The zonal flows are driven by the ion scale instabilities but strongly regulate the amplitude of the electron scale turbulence. When the linear growth rate of the ETG modes exceeds the zonal flow mixing rate due to advection of the ETG modes, the electron scale turbulence can grow to large amplitude (streamer regime). The standard paradigm that the turbulence is saturated when the zonal flow shearing rate competes with linear growth cannot explain the saturation of the electron scale turbulence. Instead, it is the mixing rate of the zonal $E \times B$ velocity spectrum that competes with linear growth at both electron and ion scales. A model of the zonal flow mixing is shown to be able to capture the suppression of electron-scale turbulence by ion-scale turbulence and the threshold for the increase in electron scale turbulence when the ion-scale turbulence is reduced. The Dimits shift results from the impact of the zonal flow mixing on the ion scale turbulence amplitude.

Work supported by the U.S. Department of Energy under DE-FG02-95ER54309, DE-FC02-04ER54698 and DE-SC0006957.



New Nonlinear Microtearing Mode Transport Model for Tokamak Plasmas

T. Rafiq¹, J. Weiland², A. Kritiz¹, L. Luo³, and A. Y. Pankin⁴

¹Lehigh University, Bethlehem, PA 18015, USA

²Chalmers University of Technology, Göteborg, Sweden

³North Carolina State University, Raleigh, NC 27695, USA

⁴Tech-X Corporation, Boulder, CO 80303, USA

Corresponding Author: T. Rafiq, trafiqfusion@gmail.com

Microtearing modes (MTMs) have been identified as a source of significant electron thermal transport in high- β tokamak discharges. A model for MTMs that can be installed in integrated whole device predictive modelling codes is needed in order to improve the prediction of electron thermal transport and, consequently, the evolution of the plasma in devices in which MTMs have a significant role. A unified fluid/kinetic approach is used in the development of a nonlinear model for the transport driven by MTMs. The derivation of the model includes the effects of electrostatic and magnetic fluctuations (δB), collisionality, electron temperature and density gradients, magnetic curvature and the effects associated with the parallel propagation vector (k_{\parallel}). The electron momentum, electron density, Maxwell equations, Ampere's law and quasi-neutrality condition are used in the derivation of a nonlinear fluid microtearing dispersion relation. An iterative nonlinear approach is used to calculate distribution function employed in obtaining the nonlinear parallel current and the nonlinear dispersion relation. The third order nonlinear effects in δB are included in the development of microtearing mode model, and the influence of third order effects on a three wave system is considered. For the evolution of the nonlinear microtearing instability in time, the third order effects provide the possibility of saturation of the microtearing instability. In the limit of slab geometry, $k_{\parallel} = 0$ and strong collisionality, the fluid dispersion relation for nonlinear microtearing modes is found to agree with the kinetic dispersion relation in [1]. An envelope equation for the nonlinear microtearing modes in the collision dominant limit is introduced. The role of MTMs in driving electron transport in the midradius region of NSTX-U plasmas is examined, and the dependence of MTMs on plasma parameters including the magnetic shear length, safety factor, electron temperature gradient, electron density gradient, plasma β and collisionality is studied.

References

[1] J. F. Drake, *et al.*, Phys. Rev. Lett. **44**, 994 (1980).

Work supported by the U.S. Department of Energy, Office of Science, under Award Number DE-SC0013977 and DEFG02-92-ER54141 and DE-SC0012174.

Extending the Validation of Multimode Model for Anomalous Transport to High Poloidal β DIII-D Discharges

A. Y. Pankin¹, A. M. Garofalo², B. A. Grierson³, A. Kritiz⁴, T. Rafiq⁴, and J. Weiland⁵

¹Tech-X Corporation, Boulder, CO 80303, USA

²General Atomics, San Diego, CA 92186, USA

³Princeton Plasma Physics Laboratory (PPPL), Princeton, NJ 08540, USA

⁴Lehigh University, Bethlehem, PA 18015, USA

⁵Chalmers University of Technology, Göteborg, Sweden

Corresponding Author: A. Y. Pankin, pankin@txcorp.com

The multimode model (MMM7.1) for anomalous transport [1] is tested in predictive modelling of temperature profiles of high- β poloidal DIII-D discharges. This new H-mode plasma regime, with high- β poloidal and high plasma currents, has been studied in DIII-D tokamak discharges [2]. The MMM7.1 anomalous transport model includes a combination of contributions based on different transport theories. It includes the Weiland module for ion temperature gradient modes, trapped electron modes and collision dominated MHD modes, the Rafiq module for drift-resistive-inertial ballooning modes (DRIBM) and the Horton module with the Jenko threshold for anomalous transport driven by electron temperature gradient (ETG) modes.

The role of different modes described by MMM7.1 is investigated. In particular, the temperature profiles for a number of high- β poloidal DIII-D discharges are predicted using only the Weiland and ETG components of the MMM7.1 model. The magnitudes of the predicted temperature profiles are found to be in reasonable agreement with experimental profiles. However, the experimental profiles have an internal transport barrier in temperature profiles, due to strong off-axis ECR heating, which is not reproduced in the predictive MMM7.1 simulations due to significant electron thermal transport from both the Weiland component and from the ETG component of MMM7.1.

The effect of electron thermal transport due to the DRIBM model is also investigated. PTRANSP analysis of the DIII-D discharge #154406 shows that there is a significant transport predicted by DRIBM in the region from 0.34 to 0.7 of normalized minor radius. The electron temperature in this PTRANSP simulation is found to be below the experimental values. The DRIBM model includes contributions from other MHD modes in addition to the drift resistive ballooning modes that can be unstable in this region. This validation study suggests that the DRIBM predicts a significantly larger level of electron transport than expected. Possible effects that can contribute to stabilization of these modes, for example, effects associated with the large poloidal- β such as the Shafranov-shift stabilization in the MMM7.1 model, are discussed.

References

[1] T. Rafiq, *et al.*, Phys. Plasmas **20**, 032506 (2013).

[2] A. M. Garofalo, *et al.*, IAEA FEC-2014, PPC/P2-31, (2014).



Evaluation of Predictive Capability for Hydrogenic and Impurity Density in L- and H-Mode Tokamak Plasma Using Multimode Transport Model

S. Suwanna¹, T. Onjun², and W. Buangam²

¹*Department of Physics, Faculty of Science, Mahidol University, Bangkok, Thailand*

²*Sirindhorn International Institute of Technology, Pathum Thani, Thailand*

Corresponding Author: S. Suwanna, sujin.suw@mahidol.ac.th

Predictive capability of hydrogenic density and impurity density in L- and H-mode plasma is strongly desirable to fully understand behaviours of plasma in tokamak, which can exhibit many modes of transports depending on the plasma conditions. Combining many modes from turbulent transports, the multimode model version 1995 (MMM95) includes coefficients from the Weiland model for the ion temperature gradient (ITG) and trapped electron modes (TEM), the Guzdar–Drake model for drift-resistive ballooning (RB) modes, and modified kinetic ballooning (KB) modes. In this work, the hydrogenic and impurity density profiles in L- and H-mode plasma are investigated using self-consistent modelling of BALDUR integrated predictive modelling code in which theory-based models are used. In these simulations, a combination of NCLASS neoclassical transport and MMM95 anomalous transport model is used to compute a core transport. The boundary conditions for temperature and density are taken to be at the top of the pedestal, where the pedestal values are taken from experiments. The predictive capability is determined by comparing the predicted profiles with experimental data in 24 discharges from various tokamaks and plasma conditions. Statistical analysis such as the average relative root mean square (RMS) deviation and offsets are used to quantify the agreement. The multiparameters optimization technique is used to derive suitable coefficients for the MMM95 transport model. The simulation results show that even when the electron density and temperature profiles, and the ion temperature profiles agree well with experiments, yielding low RMS and correct trends, the impurity density profiles do not often agree with experiments, yielding much higher RMS and even opposite trends. The effects of KB and RB contribution are comparable on the impurity profiles. In addition, it is clear from the RMS optimization that a universal model with the same set of coefficients for all discharges is unlikely, but a range of each coefficient from each transport mode can be estimated for a given plasma regime.



Recent EUROfusion Achievements in Support to Computationally Demanding Multiscale Fusion Physics Simulations and Integrated Modelling

I. Voitsekhovitch¹, R. Hatzky², D. Coster², F. Imbeaux³, D. C. McDonald⁴, T. B. Fehér², K. S. Kang², H. Leggate⁵, M. Martone², S. Mochalsky², X. Sáez⁶, T. Ribeiro², T.-M. Tran⁷, A. Gutierrez-Milla⁶, S. Heuroux⁸, S. D. Pinches⁹, F. da Silva¹⁰, D. Tskhakaya¹¹, T. Aniel³, D. Figat¹², L. Fleury³, O. Hoenen², J. Hollocombe¹, D. Kaljun¹³, G. Manduchi¹⁴, M. Owsiak¹², V. Pais¹⁵, B. Palak¹², M. Plociennik¹², J. Signoret³, C. Vouland³, and D. Yadikin¹⁶

¹*Culham Centre for Fusion Energy (CCFE), Culham Science Centre, Abingdon, UK*

²*Max-Planck-Institut für Plasmaphysik, Garching, Germany*

³*Institut de Recherche sur la Fusion par confinement Magnétique (IRFM), Commissariat à l'énergie atomique (CEA/Cadarache), 13108 Saint-Paul-lès-Durance, France*

⁴*EUROfusion Garching, 85748 Garching, Germany*

⁵*Dublin City University, Dublin, Ireland*

⁶*Centro Nacional de Supercomputación (BSC), Barcelona, Spain*

⁷*Swiss Plasma Center (SPC), École polytechnique fédérale de Lausanne (EPFL), 1015 Lausanne, Switzerland*

⁸*Institut Jean Lamour, Université de Lorraine, CNRS, Nancy, France*

⁹*International Thermonuclear Experimental Reactor (ITER), Cadarache Centre, 13108 Saint-Paul-lès-Durance, France*

¹⁰*Institute of Plasmas and Nuclear Fusion (IPNF), Association EURATOM/IST, Lisbon, Portugal*

¹¹*Institute for Applied Physics, Technische Universität Wien, 1040 Vienna, Austria*

¹²*Poznan Supercomputing and Networking Center (PSNC), Poznań, Poland*

¹³*University of Ljubljana, 1000 Ljubljana, Slovenia*

¹⁴*Consorzio RFX, Associazione EURATOM-ENEA sulla Fusione, Padova, Italy*

¹⁵*National Institute of Laser, Plasma and Radiation Physics (INFLPR), Bucharest, Romania*

¹⁶*Chalmers University of Technology, Göteborg, Sweden*

Corresponding Author: I. Voitsekhovitch, irina.voitsekhovitch@euro-fusion.org

Integrated modelling (IM) of present experiments and future tokamak-reactor requires numerical tools which can describe spatially small-scale and large-scale phenomena as well as dynamically fast transient events and relatively slow plasma evolution within a reasonably fast computational time. The progress in the optimization and speed-up of the EU first-principle codes and in the development of a basis for their integration into a centrally maintained suite of IM tools achieved by the EUROfusion high level support team (HLST) and core programming team (CPT) is presented here. An overview of the physics phenomena which can be addressed in various areas (core turbulence and magnetic reconnection, collisional transport in nonaxisymmetric devices, edge and SOL physics, heating and current drive, pedestal physics, MHD and disruptions, reflectometry simulations) using the improved numerical tools is given.

Continued...

The optimization of physics codes performed by HLST achieved a six-fold speed-up of SOLPS-ITER simulations due to OpenMP parallelization of the B2 part of SOLPS; to investigate kinetic effects in SOL region using the realistic 3D geometry implemented in BIT2/BIT3; to perform the reflectometry simulations (REFMULX/REFMULF) for ASDEX-Upgrade or JET much more accurately and to preview with more reality the behaviour of reflectometry in ITER or DEMO; to resolve realistic wall structures enabling the simulation of the precise current patterns required for the prediction of asymmetric forces during disruption events (JOEK-STARWALL). The CPT development activities in support to integrated modelling including a support to local deployment of the IM infrastructure and experimental data access, to the management of releases for sophisticated IM workflows involving a large number of components and to the performance optimization of complex IM workflows are summarized.



- ²⁷Laboratory for Plasma Physics, ERM/KMS, Brussels, Belgium
- ²⁸Institute of Nuclear Techniques (INT), University of Technology and Economics (BME), Budapest, Hungary
- ²⁹Consorzio RFX, Associazione EURATOM-ENEA sulla Fusione, Padova, Italy
- ³⁰Catalan Institution for Research and Advanced Studies (ICREA)
- ³¹Centro Nacional de Supercomputación (BSC), Barcelona, Spain
- ³²Physique des Interactions Ioniques et Moléculaires (PIIM), CNRS, Aix-Marseille Université, France
- ³³Max-Planck-Institut für Plasmaphysik, Greifswald, Germany
- ³⁴Consorzio CREATE, Università degli Studi di Cassino e del Lazio Meridionale, Cassino, Italy
- ³⁵University College Cork, Cork, Republic of Ireland
- ³⁶Swiss Plasma Center (SPC), École polytechnique fédérale de Lausanne (EPFL), 1015 Lausanne, Switzerland
- ³⁷Université Libre de Bruxelles, Brussels, Belgium
- ³⁸University of Strathclyde, Glasgow, UK
- ³⁹Poznan Supercomputing and Networking Center (PSNC), Poznań, Poland
- ⁴⁰University of Cyprus, Nicosia, Cyprus
- ⁴¹Comenius University, Bratislava, Slovakia
- ⁴²Chalmers University of Technology, Göteborg, Sweden
- ⁴³Institute for Nuclear Research, Hungarian Academy of Sciences, Debrecen, Hungary
- ⁴⁴Institute for Applied Physics, Technische Universität Wien, 1040 Vienna, Austria
- ⁴⁵Institute of Plasma Physics AS CR v.v.i., Prague, Czech Republic

Corresponding Author: G. Falchetto, gloria.falchetto@cea.fr

Recent developments and achievements of the EUROfusion Code Development for Integrated Modelling project (WPCD, follow-up of EFDA-ITM-TF), which aims at providing a validated integrated modelling suite for the simulation and prediction of complete plasma discharges in any tokamak, are presented. WPCD develops generic complex integrated simulations, workflows, for physics applications, using the standardized EU Integrated Modelling (EU-IM) framework. The integration of codes in EU-IM workflows is besides accompanied by a thorough cross-verification and, recently, by the introduction of rigorous release procedures. Among the achievements, the European Transport Simulator (ETS), has now reached a capability equivalent to the state-of-the-art integrated modelling transport codes, including interchangeable physics modules for equilibrium (both fixed and free boundary), transport (interpretative analytical, neoclassical, anomalous), impurities (all ionization states), NTM, sawteeth, pellets, neutrals, heating and current drive (HCD) sources including all the heating schemes (EC, NBI, IC, nuclear) and synergy effects. The core ETS has been released and deployed at JET, offering a leading tool for both interpretive transport analysis and predictive modelling of complex scenarios. Selected physics applications are presented, in particular ETS simulations of plasma density control in reactor-scale plasmas fuelled with multiple pellets.

A MHD stability chain was developed for the analysis of equilibria from any tokamak in the EU-IM platform; it includes a pool of interoperable high-resolution equilibrium and linear MHD stability codes. Having passed a benchmark on core and global ideal kink instabilities, the chain has been released and applied to the predictive analysis of DEMO and JT60-SA scenarios and can be straightforwardly used for interpretive runs on present devices as JET and ASDEX-Upgrade. A predictive J-alpha MHD pedestal stability analysis workflow has also been developed. Routine application to sensitivity analysis of DEMO1 scenarios is performed. Furthermore, a workflow including a turbulence code and a synthetic probe was developed and applied to investigate the turbulent transport in the edge and scrape-off layer (SOL) of ASDEX-Upgrade. Finally, a prototype edge workflow integrating the interaction

with PFC was demonstrated.

TH



Progress in the ITER Integrated Modelling Programme and the Use and Validation of IMAS within the ITER Members

S. D. Pinches¹, R. Akers², R. Andre³, T. Aniel⁴, I. Bandyopadhyay^{5,6}, V. Basiuk⁴, E. A. Belli⁷, X. Bonnin¹, J. Candy⁷, A. K. Chattopadhyay^{5,6}, W. Dekeyser¹, L. T. H. van Dellen¹, B. Faugeras⁸, A. Fukuyama⁹, M. Gorelenkova³, M. Hosokawa¹, P. Huynh⁴, S. Ide¹⁰, F. Imbeaux⁴, H. Jhang¹¹, I. Johnson³, T. Johnson¹², L. Jung¹¹, R. R. Khayrutdinov¹³, S. H. Kim¹, S. Konovalov¹³, L. Kos¹⁴, L. L. Lao⁷, Y. Liu², L. LoDestro¹⁵, V. E. Lukash¹³, I. Lupelli², S. Medvedev¹⁶, O. Menghini⁷, W. H. Meyer¹⁵, D. Muir², O. Naito¹⁰, E. Nardon¹⁷, F. Poli³, A. Polevoi¹, O. Sauter¹⁸, M. B. Schneider¹, A. K. Singh^{5,6}, P. B. Snyder⁷, G. M. Staebler⁷, P. Strand¹⁹, M. Suzuki¹⁰, S. Wiesen²⁰, and D. Zhao²¹

¹International Thermonuclear Experimental Reactor (ITER),

Cadarache Centre, 13108 Saint-Paul-lès-Durance, France

²Culham Centre for Fusion Energy (CCFE), Culham Science Centre, Abingdon, UK

³Princeton Plasma Physics Laboratory (PPPL), Princeton, NJ 08540, USA

⁴Institut de Recherche sur la Fusion par confinement Magnétique (IRFM), Commissariat à l'énergie atomique (CEA/Cadarache), 13108 Saint-Paul-lès-Durance, France

⁵International Thermonuclear Experimental Reactor (ITER), India Centre, Gujarat, India

⁶Institute for Plasma Research (IPR), Bhat, Gandhinagar, India

⁷General Atomics, San Diego, CA 92186, USA

⁸Lab. J.A. Dieudonné, Université Nice Sophia Antipolis, Nice, France

⁹Kyoto University, Nishikyo-ku, Kyoto 615-8540, Japan

¹⁰Japan Atomic Energy Agency (JAEA), Naka, Japan

¹¹National Fusion Research Institute (NFRI), Daejeon, Republic of Korea

¹²KTH Royal Institute of Technology, Stockholm, Sweden

¹³National Research Centre "Kurchatov Institute", Moscow, Russian Federation

¹⁴University of Ljubljana, 1000 Ljubljana, Slovenia

¹⁵Lawrence Livermore National Laboratory (LLNL), Livermore, CA 94550, USA

¹⁶Keldysh Institute of Applied Mathematics, RAS, Moscow, Russian Federation

¹⁷Commissariat à l'énergie atomique (CEA), 91400 Gif-sur-Yvette, France

¹⁸Swiss Plasma Center (SPC), École polytechnique fédérale de Lausanne (EPFL), 1015 Lausanne, Switzerland

¹⁹Chalmers University of Technology, Göteborg, Sweden

²⁰Forschungszentrum Jülich, Jülich, Germany

²¹Oak Ridge Associated Universities (ORAU), Oak Ridge, TN 37831, USA

Corresponding Author: S. D. Pinches, simon.pinches@iter.org

The ITER integrated modelling (IM) programme will not only support the ITER Project in the development and execution of the ITER research plan (IRP) but also provide support for the design basis of the ITER facility during construction, in particular for diagnostics. Strategically, the ITER IM programme is implemented using expertise and technologies developed within the ITER members' research programmes with annual reviews by an integrated modelling expert group (IMEG) comprised of experts from all the ITER Parties.

Continued...

The integrated modelling and analysis suite (IMAS) is the software infrastructure that has been developed in response to the needs of the IM programme and which will support the requirements of both plasma operations and research activities. An agile approach is taken to the development of IMAS and a software management framework consisting of linked issue tracking, source code repositories and a continuous integration server to automatically build and regression test revisions has been established. It is essential that results generated for ITER are reproducible and so software hosting and rigorous version control are prerequisites and already ensured, whilst provenance tracking for handling inputs is still in development.

The unifying element of IMAS is its use of a standardized data model capable of describing both experimental and simulation data. This enables the development of workflows that can flexibly use different software components as well as being independent of the device being modelled. This makes IMAS an ideal framework for conducting code benchmarking exercises, such as that within the ITPA energetic particle physics topical group on the calculation of fast ion distributions. In this paper, some of the initial software adaptations are presented to indicate the use, and consequent validation, of IMAS within the ITER members. This has been facilitated by the release this year of a local installer for IMAS which has already allowed installation within the research facilities of the majority of the ITER Members including the EU, India, Japan, Korea and the US. For the most part, these workflows are predictive in nature with interpretive workflows expected to follow from the development of plugins to the IMAS data access tools to securely read and map remote experimental data from existing devices into the standardized data model.

The Development of SOL Transport Model for Integrated Core-SOL Simulation of L-Mode Plasma

A. Wisitsorasak¹, T. Onjun², and B. Chatthong³

¹King Mongkut's University of Technology Thonburi, Bangkok, Thailand

²Sirindhorn International Institute of Technology, Pathum Thani, Thailand

³Department of Physics, Prince of Songkla University, Songkla, Thailand

Corresponding Author: A. Wisitsorasak, apiwat.wis@kmutt.ac.th

Simulations of the plasma in the core and the scrape-off layer (SOL) region are carried out using 1.5D BALDUR integrated predictive modelling code to investigate tokamak plasmas in TFTR reactor operating in low confinement mode (L-mode). In each simulation, the plasma current, temperatures, and density profiles in both core and SOL regions are evolved self-consistently. The plasma profiles in the SOL region is simulated by integrating the fluid equations, including sources, along the field lines. The solutions in the SOL subsequently provide as the boundary conditions of the core plasma region. The core plasma transport model is described using a combination of anomalous transport by multimode-model version 1995 (MMM95) and neoclassical transport provided by NCLASS module. Furthermore the calculation of the toroidal velocity used in this work is based on the torque due to intrinsic neoclassical toroidal viscosity (NTV). While the transport coefficients in the SOL region are either determined by fixed constants or neoclassical transport based on NCLASS calculation. By comparing with eight L-mode discharges from TFTR, it was found that the simulations using the transport based on neoclassical theory for SOL transport yields better agreement to experimental results for both density and temperature profiles.



Alpha Heating and Isotopic Mass Scaling in JET DT Plasmas

R. Budny¹

¹Princeton University, Princeton, NJ 08544, USA

Corresponding Author: R. Budny, budny@princeton.edu

Experiments to detect alpha heating were performed in TFTR [1] and in JET DTE1 [2]. The TFTR results were claimed to be consistent with alpha particle heating of electrons. The JET results were claimed to show that alpha particle heating had been unambiguously observed. Recent papers [3, 4] reanalyzed the alpha heating and other discharges from the JET DTE1 using improved TRANSP analysis. One result [3] is that although alpha-electron heating most likely was occurring, thermal hydrogenic isotopic mass $\langle A \rangle$ effects could explain most of the effects attributed to alpha heating, and thus alpha heating was not clearly demonstrated. There are plans for new experiments in JET to investigate alpha heating and $\langle A \rangle$ effects. ITER plans to study these during the DT phase after 2034. To help prepare for these, further analysis including more discharges from the JET DTE1 campaign are studied. Examples are pairs studied in [5]. Correlations of sawtooth delay times and core temperatures with fast ion parameters are presented.

References

- [1] G. Taylor, *et al.*, Phys. Rev. Lett. **76**, 2722 (1996).
- [2] P. R. Thomas, *et al.*, Phys. Rev. Lett. **80**, 5548 (1998).
- [3] R. V. Budny, Nucl. Fusion **56**, 036013 (2016).
- [4] R. V. Budny, *et al.*, Submitted to Nucl. Fusion 2016.
- [5] J. G. Cordey, *et al.*, Nucl. Fusion **39**, 301 (1999).
- [6] F. Romanelli, *et al.*, IAEA FEC-2014, PPC/P3-22, (2014).

JET contributors are listed in the appendix of [6]. This work has been carried out within the framework of the EUROfusion Consortium, and has received funding from the Euratom research and training programme 2014-2018 under grant agreement No. 633053. The views and opinions expressed herein do not necessarily reflect those of the European Commission. This work was also supported in part by the U.S. Department of Energy contract No. DE-ACO2-76-CHO3073.

TH

Statistical Validation of Transport Models on Baseline Discharges in Preparation for the Extrapolation to JET DT

H.-T. Kim¹, M. Romanelli², X. Yuan³, S. Kaye³, R. Budny⁴, H. Weisen⁵, J. Buchanan², and I. Lupelli²

¹EUROfusion/JET, Culham Science Centre, Abingdon, Oxfordshire, OX14 3DB, UK

²Culham Centre for Fusion Energy (CCFE), Culham Science Centre, Abingdon, UK

³Princeton Plasma Physics Laboratory (PPPL), Princeton, NJ 08540, USA

⁴Princeton University, Princeton, NJ 08544, USA

⁵EUROFusion (EFDA), Max-Planck-Institut für Plasmaphysik, Garching, Germany

Corresponding Author: H.-T. Kim, hyun-tae.kim@euro-fusion.org

The EUROfusion Consortium is planning deuterium-tritium (DT) experimental campaigns in 2019 on JET with the ITER-like wall (ILW) to address physics issues which are important for ITER-DT experiments. To achieve the scientific objectives, JET operation should demonstrate 10–15 MW of fusion power for at least 5 s, a performance never attempted before in fusion-research history. The preparation of the DT campaign requires, therefore, reliable predictive simulations of this unprecedented JET operational scenarios, providing assessment of the impact of uncertainties resulting from operating with an ILW such as degraded edge confinement and core tungsten accumulation, and from operating with a DT mixture such as isotopic effects on stability and confinement and alpha heating.

Despite the remarkable improvements in present core transport models such as GLF23 and TGLF, the current ability to predict plasma temperature evolution and the resultant fusion power is still limited due to the incompleteness of first principles theories of energy and particle transport in turbulent thermonuclear plasmas and the uncertainty of input data required for predictive simulations such as pedestal temperature, Z_{eff} , and rotation profiles. Thus, for a quantitative assessment of the uncertainties in the DT performance with ILW, statistical validation of predictive simulations with a large database of DD discharges is of crucial importance.

Predictive TRANSP simulations with advanced transport models such as GLF23 and TGLF for JET experiments is now available using automated input data preparation routines, the JET-TRANSP scripts, which enables one to carry out a large number of predictive TRANSP simulations. In this paper, statistical assessment of the level of agreement of predictive TRANSP simulations with the GLF23 transport model carried out on a large set of well diagnosed JET baseline discharges will be presented, and sensitivity studies on uncertain parameters such as pedestal T_i , Z_{eff} , and rotation profiles will be discussed. The assumption used in the simulation is further investigated for a few representative discharges with the TGLF transport model, which is computationally expensive but more accurate than GLF23. This statistical validation with the assessment of uncertainty level will constitute the basis for TRANSP predictions of JET-ILW-DT experiments.



Simulation of Neoclassical Tearing Modes in JET

N. Poolyarat¹, W. Kanjanaput², B. Chatthong³, and T. Onjun²

¹*Department of Physics, Thammasat University, Thailand*

²*Sirindhorn International Institute of Technology, Pathum Thani, Thailand*

³*Department of Physics, Prince of Songkla University, Songkla, Thailand*

Corresponding Author: N. Poolyarat, nop096@gmail.com

In this work, a simulation of neoclassical tearing mode (NTM) in JET experiments is considered using a 1.5D BALDUR integrated predictive modelling code with an improved ISLAND. An original ISLAND module for calculating the saturated width of magnetic island caused by a magnetic reconnection is obtained from the NTCC Library. This ISLAND module is then modified to improve a consistency and reliability of island width prediction. The modified ISLAND module is still based on Rutherford equation and quasi-linear theory approach. With the improved ISLAND module integrated in 1.5D BALDUR, the effects of neoclassical tearing modes (NTM) can be considered. The effect of NTM is described using the model that both thermal and particle transport within the magnetic island is enhanced, resulting on the flattening of profiles within that region. The BALDUR code with a modified ISLAND module is then used to carry out the time evolution of plasma current, temperature, and density profiles, where the effects of NTM can be real time considered. For example, in JET discharge #33131, the simulations with magnetic islands mode (2, 1), or with magnetic island mode (3, 2), or with both magnetic island mode (2, 1) together with mode (3, 2), are carried out. It is found that when the magnetic island mode (2, 1) is considered, the ion and electron temperature profile, and also the total stored energy profile are decreased the most comparing to the other two scenarios.

TH



Core-Edge Coupled Predictive Modelling of JT-60SA High- β Steady-State Plasma with Impurity Accumulation

N. Hayashi¹, K. Shimizu¹, K. Hoshino¹, M. Honda¹, and S. Ide¹

¹*Japan Atomic Energy Agency (JAEA), Naka, Japan*

Corresponding Author: N. Hayashi, hayashi.nobuhiko@jaea.go.jp

The integrated modelling code TOPICS has been extended to couple impurity transports in core and scrape-off layer or divertor regions, and applied to predictive modelling of JT-60SA high- β steady-state plasma with the accumulation of impurity seeded to reduce divertor heat load. Consistent evaluation of impurity transport from the edge to the core clarified the compatibility of impurity seeding with the core plasma with high- β ($\beta_N > 3.5$) and full current drive condition, i.e., when the Ar seeding reduces the divertor heat load below 10 MW/m², its accumulation in the core is so moderate that the core plasma performance can be recovered by additional heating within the machine capability to compensate the Ar radiation. Validating anomalous heat transport models with JT-60U experiments and judging the applicability of models to the conservative prediction, which considers a lower bound of plasma performance, improved the above prediction reliability.

Investigation of Sustainable Reduced-Power Noninductive Scenarios on JT-60SA

M. Romanelli¹, L. Garzotti¹, S. Wiesen², M. Wischmeier³, R. Zagorski⁴, J. Garcia⁵, P. Mage⁵, E. de la Luna⁶, M. Yoshida⁷, H. Urano⁷, P. da Silva Arresta Belo¹, G. Corrigan¹, S. Saarela¹, T. Bolzonella⁸, and H. Derek¹

¹Culham Centre for Fusion Energy (CCFE), Culham Science Centre, Abingdon, UK

²Forschungszentrum Jülich, Jülich, Germany

³Max-Planck-Institut für Plasmaphysik, Garching, Germany

⁴Institute of Plasma Physics and Laser Microfusion, Warsaw, Poland

⁵Institut de Recherche sur la Fusion par confinement Magnétique (IRFM),

Commissariat à l'énergie atomique (CEA/Cadarache), 13108 Saint-Paul-lès-Durance, France

⁶Centro de Investigaciones Energéticas, Medioambientales y Tecnológicas (CIEMAT), Madrid, Spain

⁷Japan Atomic Energy Agency (JAEA), Naka, Japan

⁸Consorzio RFX, Associazione EURATOM-ENEA sulla Fusione, Padova, Italy

Corresponding Author: M. Romanelli, michele.romanelli@ukaea.uk

Along with the construction and operation of ITER, the design of a demonstration thermonuclear fusion reactor (DEMO) is the main goal of current international fusion research. New generation of tokamaks as JT-60SA are meant to provide important information to allow discriminating between different DEMO designs. In particular JT-60SA will explore the possibility of running steady state plasma scenarios characterized by high fraction of bootstrap current, low flux consumption and sustainable divertor heat-loads. The feasibility of the above scenarios will depend on the simultaneous control of core, divertor, and SOL conditions to maintain a peaked pressure profile, clean plasma while ensuring an acceptable heat load on the divertor targets. Preliminary investigations of the SOL and divertor conditions show that sustainment of the steady state scenario without impurity seeding will be challenging due to the large heat loads which are likely to appear when 30 MW of NBI power are employed. Before developing seeding schemes for the full power scenario it will be therefore necessary to prepare a reduced-power optimized scenario where both the fraction of noninductive current and β are maximized while the heat flux to the divertor is kept at a sustainable level. The above reduced-power scenario has been investigated with the integrated suite of core-divertor-SOL codes JINTRAC. A scan in NBI power and fuelling rate and location has been performed and found that acceptable levels of power-load on the outer divertor plate can be achieved in the absence of impurity seeding when the NBI power is lowered to 17 MW. The 0D plasma parameters of this lower-power high-fraction of bootstrap current scenario are discussed in this paper, along with the role on performance of the internal transport barrier, and the comparison against the reference values of the JT-60SA research plan.

This work has been carried out within the framework of the EUROfusion Consortium and has received funding from the Euratom research and training programme 2014–2018 under grant agreement No. 633053. The views and opinions expressed herein do not necessarily reflect those of the European Commission.



Integrated Simulation of Deuterium Experiment Plasma in LHD

S. Murakami¹, H. Yamaguchi¹, M. Homma¹, S. Maeta¹, A. Sakai¹, A. Fukuyama¹, K. Nagaoka², H. Takahashi², H. Nakano², M. Osakabe², M. Yokoyama², K. Tanaka², K. Ida², M. Yoshinuma², M. Isobe², H. Tomita³, and K. Ogawa²

¹Department of Nuclear Engineering, Kyoto University, Nishikyo-ku, Kyoto 615-8540, Japan

²National Institute for Fusion Science (NIFS), Toki, Gifu, Japan

³Department of Quantum Engineering, Nagoya University, Nagoya, Japan

Corresponding Author: S. Murakami, murakami@nucleng.kyoto-u.ac.jp

The deuterium experiment project from 2017 is planned in LHD, where deuterium NBI heating beams of power greater than 30 MW are injected into the deuterium plasma. The principal objects of this project are to clarify the isotope effect on the heat and particle transport in the helical plasma and to study energetic particle confinement in a helical magnetic configuration measuring triton burn-up neutrons. In this paper, the deuterium experiment plasma of LHD is investigated by applying the integrated simulation code TASK3D and the 5D drift kinetic equation solver GNET.

First, we perform the integrated transport simulation of deuterium plasma, $n_D/(n_H + n_D) = 0.8$, by TASK3D code assuming a typical flat density profiles. We evaluate the heat deposition profiles for the multi-ion species plasma (e, H, He, C) by using the multi-ion version of GNET, which can treat the D and H ion heatings precisely. The one-dimensional (1D) diffusive heat transport equation with multi-ion species (H, He, C) is solved using the heat deposition profiles by GNET. It is found that the deuterium ion temperature reaches more than 6 keV with the isotope effect in the deuterium experiment plasma. On the other hand, the ion temperature reaches about 5 keV if we assume a pure hydrogen plasma. This result indicates that we will obtain about 20% higher ion temperature than that of the hydrogen plasma in the deuterium experiment of LHD if we assume an isotope effect on the turbulent transport based on the He/H experiment results.

Next, we perform the triton burn-up simulation of the deuterium experiment of LHD and evaluate the DT fusion reaction rates to compare with the experimental results of the 14 MeV neutron diagnostic system. It is found that more than $7.0 \times 10^{11}/\text{m}^3\text{s}$ 14 MeV neutrons are generated by the DT fusion reaction at the plasma centre. We also find that the confinement of the 1 MeV tritons is improved by the strongly inward shifted configuration of LHD ($R_{ax} = 3.5$ m). and that the triton burn-up ratio, which is the ratio of 14 MeV to 2.5 MeV neutron production, is increased to about 0.1%, which is still smaller than that of the large tokamak experiment results.

Development of ITER Nonactivation Phase Operation Scenarios

S. H. Kim¹, R. Budny², T. Casper³, F. Koechl⁴, A. Loarte¹, T. C. Luce⁵, Y.-S. Na⁶,
A. Polevoi¹, F. Poli², M. Romanelli⁷, M. B. Schneider¹, J. A. Snipes¹, and P. de Vries¹

¹International Thermonuclear Experimental Reactor (ITER),
Cadarache Centre, 13108 Saint-Paul-lès-Durance, France

²Princeton Plasma Physics Laboratory (PPPL), Princeton, NJ 08540, USA
³1166 Bordeaux St Pleasanton, CA 94566, USA

⁴Institute of Atomic and Subatomic Physics, Technische Universität Wien, 1040 Vienna, Austria

⁵General Atomics, San Diego, CA 92186, USA

⁶Seoul National University, Seoul, Republic of Korea

⁷Culham Centre for Fusion Energy (CCFE), Culham Science Centre, Abingdon, UK

Corresponding Author: S. H. Kim, sunhee.kim@iter.org

Nonactivation phase H/He operations in ITER will be important for commissioning of tokamak systems, such as diagnostics, heating and current drive (HCD) systems, coils and plasma control systems, and for validation of techniques necessary for establishing feasible operations. The assessment of feasible HCD schemes at various toroidal fields (2.65–5.3 T) has revealed that the previously applied assumptions need to be refined for the ITER nonactive phase H/He operations. A study on the ranges of plasma density and profile shape using the JINTRAC suite of codes has indicated that the hydrogen pellet fuelling system should be carefully utilized in He operation to optimize IC power absorption, neutral beam shine-through density limit and H-mode access. The EPED estimation of the edge pedestal parameters has been extended to various H operation conditions, and the combined EPED and SOLPS estimation has provided a good guidance for modelling the edge pedestal in H/He operations. The availability of ITER HCD schemes, ranges of achievable plasma density and profile shape, and estimation of the edge pedestal parameters for H/He plasmas have been combined with the previous modelling efforts on studying the H-mode access and flat-top duration within the coil system constraints. Feasible ITER nonactivation phase H/He operation scenarios have been developed by performing integrated time-dependent tokamak discharge simulations using CORSICA.

TH



ITER Fuelling Requirements and Scenario Development for H, He and DT through JINTRAC Integrated Modelling

E. Militello Asp¹, G. Corrigan¹, P. da Silva Arresta Belo¹, L. Garzotti¹, D. Harting¹, F. Koechl², V. Parail¹, M. Cavinato³, A. Loarte⁴, M. Romanelli¹, and R. Sartori³

¹Culham Centre for Fusion Energy (CCFE), Culham Science Centre, Abingdon, UK

²Institute of Atomic and Subatomic Physics, Technische Universität Wien, 1040 Vienna, Austria

³F4E: Fusion for Energy, ITER EU Centre, 08019 Barcelona, Spain

⁴International Thermonuclear Experimental Reactor (ITER), Cadarache Centre, 13108 Saint-Paul-lès-Durance, France

Corresponding Author: E. Militello Asp, elina.militello.asp@ukaea.uk

The evolution from X-point formation of ITER H, He and DT plasmas with gas and/or pellet fuelling has been studied for the first time self-consistently with the integrated core and edge suite of codes JINTRAC developed at JET. Our results show that understanding how to optimize fuelling performance is vital to operate ITER and to achieve high fusion yield without exceeding operational limits for neutral beam (NB) shine-through and divertor power fluxes (10 MW/m²). In present devices, gas can fuel the core as the edge plasma is fairly transparent to neutrals. In contrast, the ITER edge plasma will be hotter and denser so more gas will be ionized in the far scrape-off layer (SOL) and not penetrate to the separatrix. We show that routine use of pellets in ITER is likely to reach the minimum density for safe NB operation in L-mode or for H-modes with Q equals 10. In L-mode with only gas fuelling, we reach a Greenwald density fraction less than 30% before the density build-up in the SOL leads to a MARFE. These can also be triggered by pellets and to avoid them in our simulations we had to fine tune the discrete pellet mass to the core density. To access ELMy H-mode in 15 MA, 5.3 T ITER DT plasmas, we show that alpha heating is crucial. Thus, during the L-H transition, fuelling will have to be kept low to allow the ion temperature to rise on-axis to boost the build-up of fusion power. Here, we prove the viability of heating (33 MW NB, 20 MW ICRH) and fuelling schemes to reach Q of 10, with no need for Ne seeding to ease the divertor power loads while Q is less than 5. For a 15 MA, 5.3 T ITER DT $Q = 10$ baseline scenario we show that if particle fuelling is too high during the H-L transition, the target power loads in our simulations may stay below the design limit, but a MARFE may occur.

In summary our results show that pellets may be crucial to obtain an L-mode density above the NB shine-through limit. We also prove that density control during the L-H and H-L transition is critical. Pellet fuelling should rather be turned off during the L-H transition to aid the access to ELMy H-mode by minimizing the density rise to boost the fusion power. Gas fuelling and Ne seeding can be used during the H-L transition to keep the power loads to the divertor tolerable, but precise feedback control over radiation is needed to keep the plasma within the permitted operational range.



On Benchmarking of Simulations of Particle Transport in ITER

Y.-S. Na¹, C. Kessel², D. H. Na¹, A. Fukuyama³, J. Garcia⁴, N. Hayashi⁵, K. Kim¹,
F. Koechl⁶, T. C. Luce⁷, A. Y. Pankin⁸, J. M. Park⁹, A. Polevoi¹⁰, F. Poli², A. Sips¹¹,
I. Voitsekhovitch¹², A. Wisitorsasak¹³, and X. Yuan²

¹Seoul National University, Seoul, Republic of Korea

²Princeton Plasma Physics Laboratory (PPPL), Princeton, NJ 08540, USA

³Kyoto University, Nishikyo-ku, Kyoto 615-8540, Japan

⁴Commissariat à l'énergie atomique (CEA/Cadarache), 13108 Saint-Paul-lès-Durance, France

⁵Japan Atomic Energy Agency (JAEA), Naka, Japan

⁶Institute of Atomic and Subatomic Physics, Technische Universität Wien, 1040 Vienna, Austria

⁷General Atomics, San Diego, CA 92186, USA

⁸Tech-X Corporation, Boulder, CO 80303, USA

⁹Oak Ridge National Laboratory (ORNL), Oak Ridge, TN 37831, USA

¹⁰International Thermonuclear Experimental Reactor (ITER),

Cadarache Centre, 13108 Saint-Paul-lès-Durance, France

¹¹JET Exploitation Unit, Culham Centre for Fusion Energy (CCFE), Culham Science Centre, Abingdon, UK

¹²EUROfusion Garching, 85748 Garching, Germany

¹⁴King Mongkut's University of Technology Thonburi, Bangkok, Thailand

Corresponding Author: Y.-S. Na, ysna@snu.ac.kr

We report present status and main results of the ITPA IOS topical group activity on the benchmarking of simulations of the core particle transport in ITER baseline ELMy H-mode scenario with the integrated codes which are presently used for the ITER scenario simulations. The ITPA IOS group is pursuing particle transport as an important component of integrated modelling, because the simulations have shown that dynamics of the particle transport plays a key role in the possibility to access and sustain the H-mode and stable burn conditions and to provide controllable shut-down of DT discharge in ITER. Optimization of the fuelling scenario for ITER requires sufficiently accurate numerical solvers with appropriate description of particle sources, sinks, boundary conditions and integration in the codes for simulations of self-consistent plasma evolutions. Core particle transport is being studied in the frame of code benchmarking within the ITPA IOS group with various integrated modelling codes used for the ITER scenario simulations. The purpose of the benchmark is to verify agreement among various integrated modelling codes by approximating closely the expected scenario on ITER and to predict ITER plasmas more accurately based on knowledge accumulated from the benchmark so to address the critical issues of ITER. It includes comparison of the particle transport solvers, description of the sources and sinks, as well as its implementation in the integrated codes. As a first step, the benchmark is carried out with identical prescribed particle sources, sinks, transport coefficients and boundary conditions for one time slice in the flat-top H-mode phase to compare and understand differences among the codes. As a next step, we pursue a series of sensitivity studies and model expansions and improvements. Finally, the impact of particle transport on ITER fusion performance is discussed in time evolution simulations. The results of our benchmarking can be used for the choice of the level of approximation of the particle transport description necessary and sufficient for simulations of the ITER and DEMO scenarios.



Physics-Based Integrated Modelling of the Energy Confinement Time Scaling Laws in Tokamaks

J. Y. Kim¹, H. S. Han¹, H. S. Kim¹, and L. Terzolo¹

¹*National Fusion Research Institute (NFRI), Daejeon, Republic of Korea*

Corresponding Author: J. Y. Kim, jykim@nfri.re.kr

As an effort to clarify the physics origin of the global scaling laws of energy confinement time, a new analysis scheme is first proposed in which the total stored energy is divided into the two parts, one being almost directly decided by the marginal stability property and edge boundary condition through profile stiffness and the other by the profile deviation from marginal one through turbulent dynamics under external heating. Initial application to the two parameter cases of plasma current and input power show this scheme is quite effective for identifying the relative role of various physics elements, such as the linear stability, nonlinear turbulent dynamics, pedestal boundary and core-edge coupling, in determining the global scaling law. Particularly, in the plasma current case it is found most of its scaling is originated from the marginal part with the significant role of the pedestal boundary. More detailed analysis results, including the other parameter cases, will be reported in the conference paper.



Predicted Fusion Performance for ITER and DEMO Plasmas Using a BALDUR Code with Predictive Tritium Influx Model

T. Onjun¹, S. Sangaroon², B. Chatthong³, A. Wisitsorasak⁴, B. Somjinda¹, and J. Promping¹

¹*Thailand Institute of Nuclear Technology, Bangkok, Thailand*

²*Maharakham University, Maha Sarakham, Thailand*

³*Department of Physics, Prince of Songkla University, Songkla, Thailand*

⁴*King Mongkut's University of Technology Thonburi, Bangkok, Thailand*

Corresponding Author: T. Onjun, thawatchai@siit.tu.ac.th

The deuterium and tritium are considered as a fuel for nuclear fusion reactors in the future fusion machine, like ITER and DEMOs. Generally, deuterium is applied by gas puffing or pellet injection; whereas tritium can be internally produced from a blanket of reactors, which relies on reactions between 14.1 MeV neutrons from nuclear fusion reactions and lithium as one composite of the blankets. In this work, a model for predicting tritium flux generated from lithium blanket is developed based on the Monte Carlo code MCNP5, and implemented in the BALDUR integrated predictive modelling code to provide the information of tritium flux coming to main plasma. This suite of code is then used to carry out an evolution of plasma current, densities and temperature in ITER and DEMOs under L-mode and type-I ELMy H-mode scenarios. Two designs of DEMOs considered are Chinese design and European design. In these simulations, a combination of NCLASS neoclassical transport and Multimode anomalous transport models (either MMM95 or MMM8_1 version) is used to compute a core transport. It is found that the wide range of fusion performance can be achieved, depending on designs and operation modes. The sensitivity of fusion performance due to the variation of plasma parameters, i.e., plasma current, toroidal magnetic field, plasma density, and auxiliary heating power, is also carried out. The ignition test for each design is also conducted. It is found that only plasmas in some of these designs can sustain the plasma and fusion reactions with slightly lower fusion performance after external heating is removed.

TH



A New Understanding of the Bootstrap Current in Steep Edge Pedestal and its Effect on the Pedestal Stability

R. Hager¹, C.-S. Chang^{1,2}

¹Princeton Plasma Physics Laboratory (PPPL), Princeton, NJ 08540, USA

²Korea Advanced Institute of Science and Technology (KAIST), Daejeon, Republic of Korea

Corresponding Author: R. Hager, rhager@pppl.gov

Based on the kinetic simulations with the new gyrokinetic neoclassical code XGCa in realistic magnetic separatrix geometry, we developed an improved bootstrap current formula [1] that is much more accurate in steep edge pedestal plasma than the widely used formula by Sauter, *et al.* [2], while being equally easy to use. The standard deviation of the Sauter formula from the XGCa result is about 24.8% while that from the new formula is only 5.4%. The XGCa-based bootstrap current formula is then applied to the electromagnetic stability analyzes in the hybrid gyrokinetic XGC1 code, which uses gyrokinetic ions and fluid electrons [3], together with a magnetic equilibrium code that takes the bootstrap current into account.

The improved formula is suitable for applications that require fast and accurate calculation of the bootstrap current, and it incorporates finite orbit-width effects and other nonlocal physics that are introduced by a magnetic separatrix and strong $E \times B$ shearing rate. The new formula was necessary because existing studies of the bootstrap current are often based on assumptions that are valid in the core plasma but easily violated in the plasma edge, and the accuracy of these conventional predictions become questionable.

Two significant findings from this XGCa study of the bootstrap current are the significant contribution of trapped electrons to the total current and the finite orbit-width effects that generally decrease the bootstrap current compared to the prediction from the conventional neoclassical theories and simulations.

References

- [1] R. Hager, C.S. Chang, submitted to *Phys. Plasmas*, (2015).
- [2] O. Sauter, *et al.*, *Phys. Plasmas* **6**, 2834 (1999).
- [3] S. Ku, *et al.*, *Phys. Plasmas* **16**, 056108 (2009).



Analysis of Weakly Coherent Mode in I-Mode with the BOUT++ Code

Z. Liu^{1,2}, X. Xu³, X. Gao², A. E. Hubbard³, J. W. Hughes³, J. R. Walk³, C. Theiler³, T. Y. Xia², S. G. Baek³, T. Golfopoulos³, D. G. Whyte³, T. Zhang², and J. Li²

¹Princeton Plasma Physics Laboratory (PPPL), Princeton, NJ 08540, USA

²Institute of Plasma Physics, Chinese Academy of Sciences, Hefei, Anhui, People's Republic of China

³Lawrence Livermore National Laboratory (LLNL), Livermore, CA 94550, USA

³Plasma Science & Fusion Center, MIT, Cambridge, MA 02139, USA

Corresponding Author: Z. Liu, zliu@pppl.gov

The weakly coherent mode (WCM) in I-mode has been studied by six-field two-fluid model based on the Braginskii equations under the BOUT++ framework. The calculations indicate that a tokamak pedestal exhibiting a WCM is unstable to drift Alfvén wave (DAW) instabilities and resistive ballooning mode. The nonlinear simulation shows promising agreement with the experimental measurements of WCM. The spectrum of the largest toroidal number mode $n = 20$ at the location of the reflectometry agrees with the experimental data. The mode propagating in electron diamagnetic direction is consistent with the results from the magnetic probes, a large ratio of particle to heat diffusivity is consistent with the distinctive experimental feature of I-mode, and the value of the electron thermal diffusivity from simulation is almost as same as the effective thermal diffusivity from the experiment. The prediction of the WCM shows that free energy is mainly provided by the electron pressure gradient, which gives a well guidance for pursuing future I-mode studies.

TH

Global 3D Braginskii Simulations of the Tokamak Edge Region

M. Francisquez¹, Z. Ben¹, and B. Rogers¹

¹*Dartmouth College, Hanover, NH 03755, USA*

Corresponding Author: M. Francisquez, mana@dartmouth.edu

A study of L- and H-mode-like plasma turbulence in the edge of tokamaks is presented, with an emphasis on characterization of these plasmas in numerical simulations with a new global drift-ballooning (GDB) model. This work employs drift-reduced Braginskii two-fluid equations for electromagnetic low-frequency turbulence and solves them in a global large-aspect ratio annulus centred on the last closed flux-surface (LCFS) as an approximation of small to medium-size tokamaks. The simulations include plasma sources at the inner edge of the pedestal region as well as a limiter region in the scrape-off layer (SOL) and evolves self-consistently the density, temperature, and $E \times B$ shear profiles on the transport time-scale. GDB is able to generate both L- and H-mode-like plasmas with realistic parameters. L-mode transport appears to be largely driven by resistive-ballooning structures, in the presence of a balance between $E \times B$ and the ion-diamagnetic drifts. Pressure profiles also appear to exhibit a near-SOL breakpoint that mirror Langmuir probes (MLP) detect in C-Mod, postulated to separate drift wave (DW) like and RB-like fluctuations. Separate simulations carried out with H-mode parameters develop improved confinement, E_r wells at the LCFS and spontaneous generation of temperature pedestals with density pedestals remaining absent up to times in the order of 0.2 ms. Candidate first-principles explanations to the modification of the electric field profile are discussed.

Work supported by the U.S. Department of Energy, Office of Science, Office of Fusion Energy Sciences, under Award Number DE-SC0010508.



Gyrokinetic Simulations of Tokamak Pedestals: Present Experiments and Extrapolation to Burning Plasmas

M. Kotschenreuther¹, D. Hatch¹, S. Mahajan², P. Valanju², L. Zheng², and X. Liu²

¹*Institute for Fusion Studies (IFS), University of Texas at Austin, Austin, TX 78712, USA*

²*University of Texas at Austin, Austin, TX 78712, USA*

Corresponding Author: M. Kotschenreuther, mtk@austin.utexas.edu

For the first time, electromagnetic gyrokinetic simulations of pedestal transport are reported (inter-ELM). For the JET-ILW (ITER-like wall) pedestal, nonlinear simulations show that microtearing mode (MTM) turbulence produces the bulk of the transport in the steep gradient region, and the combination of MTM, electron temperature gradient (ETG), ion-scale electrostatic turbulence and neoclassical transport reproduces experimental power balance across most of the pedestal. Pedestals with $\nu^* < 1$ are often well into the second stability region, so kinetic ballooning modes do not strongly affect pedestal transport, as indicated by previous linear analysis of JET-carbon cases [1]. A ρ^* scan of ITER-like pedestals is performed, keeping other dimensionless parameters constant. Simulations find gyro-Bohm scaling of transport in the range of ρ^* of ASDEX/DIII-D through low field JET. However, for high field JET and beyond, an insufficiency of velocity shear leads to strong ion scale electrostatic turbulence, and a strong departure from gyro-Bohm at lower ρ^* such as ITER. Inclusion of carbon or nitrogen greatly reduces this turbulence, so that gyro-Bohm scaling is reestablished through JET, and the departure at ITER is substantially reduced. Pedestal transport is also strongly affected by the separatrix density, which can be affected by gas puffing. These trends may account for observed differences in pedestal behaviour in JET-ILW and JET-carbon. Unstable electrostatic eigenmodes have an unusual structure in the pedestal, and localize where the velocity shear is low, near the top and bottom. In addition to including low- Z impurities, operation with a lower separatrix density can greatly reduce the problem, which may be possible with advanced divertor geometries of lithium. Finally, initial results indicate that low aspect ratio may have advantages for avoiding shear insufficiency.

References

[1] S. Saarelma *et al.*, Nucl. Fusion **53**, 123012 (2013).



Gyrokinetic Simulations of Microturbulence in DIII-D Pedestal

I. Holod¹, Z. Lin¹, S. Taimourzadeh¹, R. Nazikian², and A. Wingen³

¹University of California Irvine, CA 92697, USA

²Princeton Plasma Physics Laboratory (PPPL), Princeton, NJ 08540, USA

³Oak Ridge National Laboratory (ORNL), Oak Ridge, TN 37831, USA

Corresponding Author: I. Holod, iholod@uci.edu

Present understanding of ELM triggering mechanism is mostly based on the peeling-ballooning theory (PBT) often providing sufficiently good pedestal prediction. While PBT is rather empirical, the more comprehensive kinetic description is still required.

In this work we present recent gyrokinetic simulations aimed to identify electromagnetic microinstabilities in the H-mode pedestal region of DIII-D tokamak (discharge #131997 at 3011 ms) using global gyrokinetic code GTC. It was found that dominant instability at the top of the pedestal is the ion temperature gradient mode (ITG). In the middle of a pedestal the kinetic ballooning mode (KBM) becomes the most unstable for the intermediate range of toroidal mode number $n \sim 20$. For shorter wavelengths the dominant instability is TEM. We have demonstrated the ITG-KBM transition at the pedestal top and TEM-KBM transition in the steep pressure gradient region as plasma pressure increases.

One possibility to control drastic ELM activity during H-mode operation is applying resonant magnetic perturbations (RMP) however the detailed mechanism of RMP effect is not completely clear.

In our studies we address the direct effect of modified magnetic equilibrium geometry on microturbulence in DIII-D pedestal. By fixing the profiles, and excluding magnetic stochasticity effects, we examine the effect of various strength RMP on KBM stability, and turbulent transport. We have observed the increase of KBM growth rate when RMP is applied; however this change is only detectable for artificially amplified RMP strength. The direct effect of RMP geometry perturbation on zonal flow generation and turbulent transport is found to be insignificant.

Work supported by the U.S. Department of Energy theory grant DE-SC0010416, DE-SC0013804, and DOE SciDAC GSEP Center.

Gyrokinetic Simulation of Tokamak Edge Plasmas

Y. Xiao¹, H. Xie², C. Zhao¹, T. Zhang¹, and Z. Lin³

¹*Institute for Fusion Theory and Simulation, Zhejiang University, Xihu, Hangzhou, Zhejiang, People's Republic of China*

²*Fusion Simulation Center, Peking University, Beijing, People's Republic of China*

³*University of California Irvine, CA 92697, USA*

Corresponding Author: Y. Xiao, yxiao@zju.edu.cn

It has been recently discovered that the trapped electron mode (TEM) may play an important role in the H-mode edge plasma for domestic tokamaks such as EAST and HL-2A. The stability and transport for TEM for the edge parameters are studied using large scale gyrokinetic particle simulations. The gyrokinetic simulation reveals the parametric dependences on the wavelength, collisionality and the electron temperature gradients. The unconventional ballooning mode structure is found the H-mode edge parameters, which directly leads to a change in the transport characteristics in the edge. The zonal flow is found by the gyrokinetic simulation to be less important in the edge than in the core. In order to interpret the simulation results, a simplified analytic theory is developed to include both collisional and strong gradient edge characteristics.



Steep Gradients in Plasma Confined at Convex-Concave Magnetic Field Lines

M. M. Tsventoukh¹, G. Krashevskaya², and A. Kaziev²

¹*P. N. Lebedev Physical Institute, RAS, Moscow, Russian Federation*

²*National Research Nuclear University "MEPhI", Moscow, Russian Federation*

Corresponding Author: M. M. Tsventoukh, elley@list.ru

The formation of large stable plasma gradients, e.g., in form of internal transport barriers, is of both strong practical and fundamental interest. Normally the larger the gradient the larger the transport, and any deviation due to collective plasma behaviour is of great interest.

We have predicted theoretically that there is a strong stabilizing action against convective (flute-interchange) perturbations when plasma is confined by magnetic field of alternating-sign curvature, i.e., with convex-concave field lines [1]. The calculations that have been done for simple combinations of axisymmetric mirrors and cusps according to the kinetic stability criterion, give strongly centrally peaked stable plasma pressure profiles instead of shallow ones.

We have performed an experimental investigation of the plasma confinement at magnetic confinement device of the alternating-sign curvature [2]. For the experimental research of this effect, a compact magnetic confinement device has been modified by adding of the external current coil to fulfil the field-line curvature requirements. The critical convectively-stable plasma pressure profiles calculation in this experimental geometry and the probe measurements of the spatial plasma distribution in the new magnetic configuration of alternating-sign curvature have been performed.

The experimental results give some support for a conclusion that there is an increase in the ion saturation current at the region near the minimum of the specific volume $\int dl/B$. This region corresponds to the average minimum in the second adiabatic invariant, and the kinetic description predicts the stable pressure profile peaking here due to reduction of charge separation by particle drift in alternating-sign curvature.

For further experimental investigations, a stationary microwave device has been used. A mirror geometry has been created by axisymmetric coils, Langmuir and magnetic probes have been used for the measurements. For the theory, developing the effects of a finite plasma β has been analyzed in axisymmetric equilibrium, and plasma particle kinetics effect on the plasma transport.

References

[1] M. M. Tsventoukh, Nucl. Fusion **54**, 022004 (2014).

[2] M. M. Tsventoukh, *et al.*, Nucl. Fusion **55**, 062001 (2015).

Work was supported by RFBR grant 15-38-20617.



Full-f Gyrokinetic Simulation including Kinetic Electrons

Y. Idomura¹, Y. Asahi¹, N. Hayashi¹, and H. Urano¹

¹Japan Atomic Energy Agency (JAEA), Naka, Japan

Corresponding Author: Y. Idomura, idomura.yasuhiro@jaea.go.jp

A new hybrid kinetic trapped electron model [1] is developed for electrostatic full-f gyrokinetic simulations. The model is verified by computing the ion and electron neoclassical transport and the linear ion temperature gradient driven trapped electron mode (ITG-TEM) stability, in which collisional TEM stabilization shows an isotope effect. An impact of kinetic electrons on the ITG turbulence is investigated by comparing ITG turbulence simulations with adiabatic electrons and with kinetic electrons. It is found that in the kinetic electron case, resonant passing electrons transport at mode rational surfaces generates corrugated density profiles, and the resulting microscopic radial electric field E_r sustains nonlinear critical temperature gradients above linear ones. This is qualitatively different from the so-called Dimits shift sustained by turbulence driven zonal flows in the adiabatic electron case. In the toroidal angular momentum balance, kinetic trapped electrons enhance the field term stress, which is characterized by the phase difference between the perturbed distribution and the toroidal electric field, and thus reversed between the adiabatic and kinetic electron cases. It is also found that the field term stress and the resulting intrinsic rotation is reversed between the ITG turbulence and the TEM turbulence.

References

[1] Y. Idomura, *J. Comput. Phys.* **313**, 511 (2016).

Characteristics of Turbulent Transport in Flux-Driven Toroidal Plasmas

Y. Kishimoto¹, K. Imadera¹, H. Liu¹, W. Wang¹, K. Obrejan¹, and J. Q. Li¹

¹*Kyoto University, Nishikyo-ku, Kyoto 615-8540, Japan*

Corresponding Author: Y. Kishimoto, kishimoto@energy.kyoto-u.ac.jp

Profile stiffness and intermittent bursts are the basis in understanding L-mode plasmas. However, why and how these different processes coexist and regulate the transport have not been fully clarified. Here, we presented an overall picture of flux-driven ITG turbulent transport which reveals profile stiffness with self-similarity and SOC type intermittent bursts simultaneously using a flux-driven gyrokinetic code by incorporating with statistical analyzes.

We found that the transport is regulated by four nondiffusive processes: 1) radially localized fast time scale avalanches, 2) radially extended global bursts, 3) slow time scale avalanches with stair-case, and, 4) transport with long range time correlation. Among them, the process 2 is the key, which results from the instantaneous formation of radially extended ballooning-type structure with long radial correlation length from meso- to macro-scale. Such structures are disintegrated and damped by self-generated zonal flows while the repetitive occurrence of such structure provides a strong constraint on the profile causing stiffness.

Zonal flows produced by such global modes becomes the origin of the shear layer of radial electric field and associated pressure corrugation, referred to as $E \times B$ staircase. Since they are excited near both edges of global mode, the interspace is determined approximately by the size of the global mode. The staircase is found to evolve dynamically coupled with successive excitation of global mode. This process causes a long time scale breathing in transport and plays a role in sweeping out corrugations appeared on the self-organized stiff profile.

To obtain a unified view of transport, we study the spatiotemporal characteristics statistically. Quasi-steady baseline of transport is due to eddies from micro- to meso-scale, which follow a power law scaling, while the busty part to global eddies which release large amount of free energy as a non-power-law tail component. The spatiotemporal linkage of such different nondiffusive processes leads to a new turbulent state dominated by long range correlation in time and space.

Finally, we found that the magnetic shear is a key parameter, so that the profile stiffness with specific function form and intermittency have revealed in moderate magnetic shear plasmas while weaken in those with weak and reversed magnetic shear.



ITB Formation in Gyrokinetic Flux-Driven ITG Turbulence

K. Imadera¹, Y. Kishimoto¹, and J. Li¹

¹*Kyoto University, Nishikyo-ku, Kyoto 615-8540, Japan*

Corresponding Author: K. Imadera, imadera@center.iae.kyoto-u.ac.jp

Profile stiffness is a long standing problem, which may limit the overall performance of H-mode plasmas. In the JET experiment, while strong temperature profile stiffness is observed around the nonlinear threshold of ion temperature gradient, it can be greatly reduced by cocurrent toroidal rotation in weak magnetic shear plasma.

To understand such a mitigation mechanism of the stiffness, we investigate the impact of momentum injection on profile stiffness in flux-driven ion temperature gradient (ITG) turbulence by means of a newly developed toroidal full-f gyrokinetic code, GKNET. It is found that momentum injection can change the mean flow through the radial force balance, leading to internal transport barrier (ITB) formation in which the ion thermal diffusivity decreases to the neoclassical transport level. Only cocurrent toroidal rotation can benefit the ITB formation in weak magnetic shear plasma, showing a qualitative agreement with the observations in the JET experiment. Note that the established ITB is enough stable in the quasi-steady state.

The underlying mechanism is identified to originate from a resultant momentum flux. According to the nonlocal ballooning theory and momentum transport theory, the mean flow shear triggered by cocurrent toroidal rotation provides the momentum pinch, which can reduce the relaxation of both toroidal rotation and mean flow profiles. On the other hand, the role of counter rotation is opposite so that the relaxation is enhanced. Thus, there exists a positive feedback loop between the enhanced mean flow shear and resultant momentum pinch only in the cocurrent toroidal rotation case, signifying a favourite trend to ITB formation.

Such a momentum pinch effect is also essential for ITB formation around the q_{\min} surface in reversed magnetic shear plasma. We detect that the position of ITB is insensitive to the momentum source profile, which is determined only by the q_{\min} surface. These results show a qualitative agreement with the observations in the JT-60U reversed shear discharges.

TH



Gyrokinetic Simulations of Electrostatic Microinstabilities with Bounce-Averaged Kinetic Electrons for Shaped Tokamak Plasmas

L. Qi¹, J. Kwon¹, T. S. Hahm^{2,1}, and G. Jo^{1,3}

¹National Fusion Research Institute (NFRI), Daejeon, Republic of Korea

²Seoul National University, Seoul, Republic of Korea

³Yonsei University, Seoul, Republic of Korea

Corresponding Author: L. Qi, qileister@nfri.re.kr

Nonlinear bounce-averaged kinetic theory [1] is used for magnetically trapped electrons for the purpose of achieving efficient gyrokinetic simulations of trapped electron mode (TEM) and ion temperature gradient mode with trapped electrons (ITG-TEM) in shaped tokamak plasmas. Bounce-averaged kinetic equations are explicitly extended to shaped plasma equilibria from the previous ones for concentric circular plasmas, and implemented to a global nonlinear gyrokinetic code, gyro-kinetic plasma simulation program (gKPSP) [2]. Verification of gKPSP with bounce-averaged kinetic trapped electrons in shaped plasmas is successfully carried out for linear properties of ITG-TEM mode and Rosenbluth–Hinton residual zonal flow [3]. Physics responsible for stabilizing effects of elongation on both ITG mode and TEM is identified using global gKPSP simulations. These can be understood in terms of magnetic flux expansion leading to the effective temperature gradient $R/L_{T_i}(1 - E')$ [4] and poloidal wave length contraction at low field side resulting in the effective poloidal wave number $k_{\theta}\rho_i/\kappa$.

References

- [1] B. H. Fong and T. S. Hahm, *Phys. Plasmas* **6**, 188 (1999).
- [2] J. M. Kwon, *et al.*, *Phys. Plasmas* **21**, 013004 (2012).
- [3] M. N. Rosenbluth and F. L. Hinton, *Phys. Rev. Lett.* **80**, 724 (1998).
- [4] P. Angelino, *et al.*, *Phys. Rev. Lett.* **102**, 195002 (2009).

Validation of Self-Organization Dynamics in Fusion Plasmas

G. Dif-Pradalier¹, G. Hornung², F. Clairet¹, P. H. Diamond³, Y. Sarazin¹, V. Grandgirard¹, X. Garbet¹, P. Ghendrih¹, Ö. D. Gürçan⁴, G. Latu¹, P. Morel⁴, P. Hennequin⁴, R. Sabot¹, and L. Vermare⁴

¹Institut de Recherche sur la Fusion par confinement Magnétique (IRFM), Commissariat à l'énergie atomique (CEA/Cadarache), 13108 Saint-Paul-lès-Durance, France

²Ghent University, 9000 Ghent, Belgium

³University of California San Diego, CA 92093, USA

⁴École Polytechnique, 91128 Palaiseau, France

Corresponding Author: G. Dif-Pradalier, guilhem.dif-pradalier@cea.fr

Large-scale global organization of turbulence has attracted persistent interest in fusion plasmas as a means to control transport and access improved confinement. It has practical consequences on zonal flow formation and sustainment, on front propagation—a natural tendency in heat flux-driven turbulence—or on the spreading of turbulence in regions of quasi-linear stability.

In this paper we present novel results based on a careful confrontation between flux- and gradient-driven gyrokinetics using the GYSELA code and recent experimental data. We present the first experimental evidence of $E \times B$ staircase identification using state-of-the-art ultrafast sweeping reflectometry. The $E \times B$ staircase reconciles seemingly antagonistic trends in turbulence self-organization whilst spontaneously generating sets of weak transport barriers that organize transport on global scales. A large experimental database of several hundred-staircase signatures is analyzed. In addition to successfully confirming several of its numerically-predicted properties, interesting novel features are reported: i) an abrupt apparent disappearance of this structure at the LOC/SOC transition is observed, associated with a change in the nature of the turbulence (electron versus ion drift waves) that is still enigmatic at present, as well as ii) a possible route to gyro-Bohm breaking through staircase permeability, especially at low ρ^* and in the far-core, near-edge so-called “No Man’s Land” region.

This also led us to elucidating key aspects of the controversial “shortfall problem” there. The combination of flux drive and scrape-off layer-like boundary are key players of the No Man’s Land dynamics, especially as core turbulence spreads into the marginally stable edge, enhanced through a “beach effect”. A careful comparison within the same numerical framework between flux- and gradient-driven gyrokinetic computations of the same L-mode plasmas leads to the observation in certain plasma conditions of a shortfall in the gradient-driven case and not in the flux-driven case. Interpretation is given of this result in terms of an inhibition of spreading associated to a weakened staircase-avalanche interplay. An isotope effect on transport and on flow generation is also discussed.



Coupling Full-f Gyrokinetic Studies to Experimental Measurements of the Isotope Effect for FT-2 Tokamak Plasmas

S. Leerink¹, P. Niskala¹, A. Gurchenko², E. Z. Gusakov², A. Altukhov², T. Kiviniemi¹,
S. I. Lashkul², R. Rochford¹, and T. Korpilo¹

¹*Aalto University, Espoo, Finland*

²*Ioffe Institute, St. Petersburg, Russian Federation*

Corresponding Author: S. Leerink, susan.leerink@aalto.fi

Turbulent transport and flow dynamics in Ohmic FT-2 tokamak plasmas are investigated. Measurements utilize highly localized state-of-the-art backscattering while the turbulence simulations are performed with the global full-f nonlinear code ELMFIRE. The role of the geodesic acoustic mode in regulating turbulent transport is studied. Special emphasis is given to the isotope effect observed in tokamak anomalous transport scaling.

Effect of Magnetic Shear and Equilibrium Flows on Collisionless Microtearing and Mixed Parity Modes in Hot Tokamak Plasmas

D. Verma¹, A. K. Swamy¹, R. Ganesh¹, S. Brunner², and L. Villard²

¹*Institute for Plasma Research (IPR), Bhat, Gandhinagar, India*

²*Swiss Plasma Center (SPC), École polytechnique fédérale de Lausanne (EPFL), 1015 Lausanne, Switzerland*

Corresponding Author: D. Verma, deepak.verma@ipr.res.in

Turbulent transport of energy, particles and momentum is one of the important limiting factors for long time plasma confinement. Modern kinetic study using gyrokinetic formalism and simulation has progressed to identify several microinstabilities that cause ion and electron thermal transport. Typically, these have been ballooning parity modes such as the ITG, KBM and ETG modes which cause transport through fluctuations or tearing parity modes such as microtearing modes (MTM) which change the local magnetic topology and cause transport through stochastization of the magnetic field. Local gyrokinetic simulations have found collisional MTMs unstable in several magnetic confinement configurations such as spherical tokamaks, reverse field pinch and standard tokamaks. Global collisionless MTMs have been shown to be linearly unstable in regions of high positive magnetic shear [1, 2]. The collisionless MTM is found to be driven unstable by the magnetic drift resonance of passing electrons.

In this work, we address the complex multiscale problem of MTM stability in advanced tokamak scenarios which envisage reversed magnetic shear with observed strong sheared poloidal and toroidal flows in the internal transport barrier. In the first part of this work, safety factor profiles are continuously varied parametrically from standard shear profiles to weak and reverse shear profiles. Multiple MTM modes are found at finite positive shear. As the global safety factor profile is varied, novel mixed parity modes of MTMs are found to become unstable with weak shear. In the second part, the effect of equilibrium flows are studied for their effect on MTM and mixed parity (MP) instabilities and their global mode structures. These and several other characteristics of MTMs and mixed parity modes will be reported.

References

- [1] A. K. Aditya, *et al.*, Phys. Plasmas **21**, 082513 (2014).
- [2] A. K. Aditya, *et al.*, Phys. Plasmas **22**, 072512 (2015).



Neoclassical Toroidal Plasma Viscosity with Effects of Finite Banana Width in Finite Aspect Ratio Tokamaks

K. C. Shaing¹, S. A. Sabbagh²

¹University of Wisconsin-Madison, Madison, WI 53706, USA

²Columbia University, New York, NY 10027, USA

Corresponding Author: K. C. Shaing, kshaing@wisc.edu

Theory for neoclassical toroidal plasma viscosity is to describe the transport processes, including particle, momentum, and energy transport fluxes in real tokamaks with broken symmetry. The predictions of the theory are in agreement with the numerical results in all collisionality regimes in the large aspect ratio limit. The theory has since been extended to finite aspect ratio tokamaks. The extension is made possible because the perturbed distribution function is localized in the phase space in the low collisionality regimes. Thus, the theory can be used to model transport phenomena including toroidal momentum relaxation in real finite aspect ratio tokamaks. However, there are cases where self-consistent magnetic perturbations have radial variations that are comparable to the width of bananas. To model the transport phenomena, the theory for has to be extended further to include the effects of the finite banana width. To that end, an orbit averaged drift kinetic equation has been developed to describe the transport processes in the low collisionality regimes, when the effective collision frequency is much less than the bounce frequency of bananas. The equation is now solved to calculate the neoclassical toroidal plasma viscosity, and, thus, the corresponding transport fluxes through the flux-force relation, to include the effects of finite banana width in various asymptotic limits. The resultant radial profile for the neoclassical toroidal plasma viscosity varies on the equilibrium scale even though the magnetic perturbations vary rapidly. The reason is that the bounce motion of the finite width of the bananas naturally smoothes out the short scale variations. This result is consistent with the experimental measurements.

Predictions of Toroidal Rotation and Torque Sources Arising in Nonaxisymmetric Perturbed Magnetic Fields in Tokamaks

M. Honda¹, S. Satake², Y. Suzuki², K. Shinohara¹, M. Yoshida¹, N. Aiba¹, J. Shiraishi¹, N. Hayashi¹, G. Matsunaga¹, M. Nakata², A. Matsuyama¹, and S. Ide¹

¹Japan Atomic Energy Agency (JAEA), Naka, Japan

²National Institute for Fusion Science (NIFS), Toki, Gifu, Japan

Corresponding Author: M. Honda, honda.mitsuru@jaea.go.jp

Capabilities of the integrated framework consisting of TOPICS, OFMC, VMEC and FORTEC-3D, have been extended to calculate toroidal rotation in fully nonaxisymmetric perturbed magnetic fields, for demonstrating operation scenarios in actual tokamak geometry and conditions. It was found for the first time that the toroidally localized perturbed fields due to the test blanket modules (TBMs) and the heating and diagnostic ports in ITER augment the neoclassical toroidal viscosity (NTV) significantly, while they do not influence confinement of beam ions and alpha particles. The NTV takes up a large portion of total torque in ITER and fairly decelerates toroidal rotation. It was found that varying the numerical coefficient added to the intrinsic torque model by the residual stress within a factor of unity improves the reproducibility of toroidal rotation in JT-60U H-mode plasmas. This fact opens up access to reliable rotation predictions in H-mode plasmas.



Global Kinetic Effect on the Collisionality Dependence of the Neoclassical Toroidal Viscosity in the Superbanana-Plateau Regime

S. Matsuoka¹, Y. Idomura¹, and S. Satake²

¹Japan Atomic Energy Agency (JAEA), Naka, Japan

²National Institute for Fusion Science (NIFS), Toki, Gifu, Japan

Corresponding Author: S. Matsuoka, matsuoka.seikichi@jaea.go.jp

The neoclassical toroidal viscosity (NTV) caused by a nonaxisymmetric magnetic field perturbation is one of the key issues for the prediction and control of the plasma performance and/or stabilities, since it can play an important role in a momentum balance which determines a plasma rotation. However, there remains a severe discrepancy with regard to the NTV prediction; the so-called superbanana-plateau theory based on a simplified bounce-averaged model predicts collisionality-independent, or the resonant NTV [1], while a global drift-kinetic simulation by FORTEC-3D [2] shows a collisionality dependency of the NTV.

In this study, we investigate the cause of the discrepancy using two different types of global kinetic simulations; one is FORTEC-3D which is based on drift kinetic equation and solves it using the delta-f Monte Carlo approach, and the other is GT5D which solves the gyrokinetic equation based on the Eulerian full-f approach. We demonstrate that the two global kinetic simulations reproduce similar collisionality dependencies of the NTV over wide ranges of the collisionality, indicating that the collisionality dependency of the NTV is common in the global kinetic simulations. It is found that a theoretically predicted resonant structure in the velocity space, which generates the collisionality-independent NTV in the superbanana-plateau theory, vanishes in the global kinetic simulations. The following two mechanisms are discussed as possible causes for the loss of the resonant structure, which may lead to the nonresonant and collisionality dependent NTV: 1) the magnetic shear dependency of the toroidal precession drift frequency, and 2) trapping/detrapping processes of perturbed particle orbits.

References

[1] K. C. Shaing, *et al.*, Plasma Phys. Control. Fusion **51**, 035009 (2009).

[2] S. Satake, *et al.*, Phys. Rev. Lett. **107**, 055001 (2011).



Effects of Localized Neoclassical Toroidal Viscosity Effects on the Toroidal Rotation Profile in KSTAR

J. Seol¹, H. Lee¹, B. H. Park¹, and Y. In¹

¹*National Fusion Research Institute (NFRI), Daejeon, Republic of Korea*

Corresponding Author: J. Seol, jseol@nfri.re.kr

KSTAR provides a great environment to carry out the NTV study in that the intrinsic error fields and the toroidal field ripples are very small in magnitude, and asymmetric magnetic fields can be added by the in-vessel coil current on demand. In this paper, we report both theoretical and experimental studies on NTV in KSTAR. It is shown that the radial transport of the toroidal angular momentum is also proportional to the first order of gyro-radius. In this work, we introduce a different method of the NTV torque estimation, that includes the usual toroidal angular momentum transport besides the NTV torque. It may resolve some known discrepancies between theories and experiments and reveal unknown puzzles at the same time. We show that the inherent neoclassical toroidal viscosity induced by the intrinsic error fields and toroidal field ripple in KSTAR is small enough not to deform the pedestal structure in toroidal rotation profiles, always observed uniquely in H-mode KSTAR plasmas.



Understanding and Predicting Profile Structure and Parametric Scaling of Intrinsic Rotation

W. W. Wang¹, B. A. Grierson¹, S. Ethier¹, J. Chen¹, E. Startsev¹, P. H. Diamond², and Z. X. Lu²

¹Princeton Plasma Physics Laboratory (PPPL), Princeton, NJ 08540, USA

²University of California San Diego, CA 92093, USA

Corresponding Author: W. W. Wang, wwang@pppl.gov

The main focus of this paper is on developing physical understanding and a first-principles-based model for predicting intrinsic rotation profiles in magnetic fusion experiments, including ITER. It is shown for the first time that turbulent fluctuation-driven residual stress can account for both the shape and magnitude of the observed intrinsic toroidal rotation profile. Specifically, nonlinear, global gyrokinetic simulations of DIII-D ECH plasmas indicate a substantial ITG fluctuation-induced nondiffusive momentum flux generated around a midradius-peaked intrinsic toroidal rotation profile. The nondiffusive momentum flux is dominated by the residual stress with a negligible contribution from the momentum pinch. The residual stress profile shows a robust antigradient, dipole structure in a set of ECH discharges with varying ECH power. Such interesting features of nondiffusive momentum fluxes, in connection with edge momentum sources and sinks, are found to be critical to drive the nonmonotonic core rotation profiles in the experiments. Both turbulence intensity gradient and zonal flow $E \times B$ shear are identified as major contributors to the generation of the k_{\parallel} -asymmetry needed for the residual stress generation. By balancing the residual stress and the momentum diffusion, a self-organized, steady-state rotation profile is calculated. The predicted core rotation profiles agree well with the experimental measurements. The radial structure of residual stress profile and associated intrinsic rotation gradient are shown to have a complicated dependence on multiple physics parameters including turbulence type, q -profile structure, and collisionality, through which possible rotation profile optimization can be developed. Interesting results obtained include intrinsic rotation reversal induced by ITG-TEM transition and intrinsic rotation profile steepening in flat- q profile regime. Fluctuation-generated poloidal Reynolds stress is also shown to significantly modify the neoclassical poloidal rotation in a way consistent with experimental observations. Finally, the first-principles-based model is applied to ITER regime, attempting to predict intrinsic rotation in electron heated burning plasmas and to illuminate its ρ^* -scaling.



Residual Stress and Momentum Transport in Electromagnetic ITG Turbulence

H. H. Kaang¹, S. S. Kim¹, H. Jhang¹, R. Singh^{2,3}, and J. Kim¹

¹National Fusion Research Institute (NFRI), Daejeon, Republic of Korea

²International Thermonuclear Experimental Reactor (ITER),
Cadarache Centre, 13108 Saint-Paul-lès-Durance, France

³Institute for Plasma Research (IPR), Bhat, Gandhinagar, India

Corresponding Author: H. H. Kaang, hkaang@nfri.re.kr

We study how electromagnetic (EM) fluctuations impact on residual Reynolds stress in the context of the quasi-linear theory. Two-fluid model is employed to describe EM ion temperature gradient turbulence. Analyses show that not only the conventional parallel residual stress but also additional stress due to EM fluctuations strongly increase with plasma β (plasma thermal energy/magnetic energy), potentially leading to the strong enhancement of flow generation in high- β plasmas. We identify that this strong increase of residual stress originates from the reinforcement of radial k (the spectrally averaged parallel wavenumber) asymmetry due to the deformation of eigenfunctions near a rational surface.

Analysis and Prediction of Momentum Transport in Spherical Tokamaks

W. Guttenfelder¹, A. Field², I. Lupelli², J.-K. Park¹, T. Tala³, J. Candy⁴, S. Kaye¹, M. Peters⁵, Y. Ren¹, and W. M. Solomon¹

¹Princeton Plasma Physics Laboratory (PPPL), Princeton, NJ 08540, USA

²Culham Centre for Fusion Energy (CCFE), Culham Science Centre, Abingdon, UK

³VTT Technical Research Centre of Finland Ltd., Espoo, Finland

⁴General Atomics, San Diego, CA 92186, USA

⁵Indiana University, Bloomington, IN 47405, USA

Corresponding Author: W. Guttenfelder, wgutten@pppl.gov

The inward momentum convection or “pinch” observed in many tokamaks can be explained by the Coriolis drift mechanism, with relatively good quantitative agreement found with gyrokinetic predictions of the ion temperature gradient (ITG) instability. Here we attempt to validate this model over a broader range of β and aspect ratio by extending into the spherical tokamak (ST) plasma regime using data from NSTX and MAST. Previous perturbative measurements in NSTX H-modes have indicated the existence of an inward momentum pinch with a magnitude similar to that observed in conventional aspect ratio tokamaks. However, linear gyrokinetic simulations run for these cases predict the microtearing mode, which only transports electron energy, is the dominant microinstability in the region of interest due to the relatively large plasma β . Although weaker, there is also evidence of a variety of unstable electrostatic and electromagnetic ballooning modes. Quasi-linear calculations for all of these ballooning modes, assuming they contribute substantially to the momentum transport, predict a pinch that is small or directed outward, in contradiction to the experimental results. Additional scans show that the weak pinch is a consequence of how both electromagnetic effects (at relatively large β) and low aspect ratio influence symmetry-breaking of the instabilities. To minimize electromagnetic effects, similar experiments were performed in MAST L-mode plasmas at relatively low β using the time-dependent rotation response after the removal of a short $n = 3$ applied magnetic field perturbation. The inferred inward pinch is similar in magnitude to conventional tokamaks and the NSTX H-modes. However, linear gyrokinetic simulations indicate that even for low- β L-modes the predicted momentum pinch is relatively small and cannot reproduce the large experimentally inferred pinch. Based on the above observations and simulations, the Coriolis pinch mechanism predicted from local, linear gyrokinetic theory does not appear to explain perturbative momentum transport at low aspect ratio. Other mechanisms neglected thus far are being investigated as possible solutions to the apparent discrepancy, including nonlinear effects, perpendicular $E \times B$ shear driven transport, centrifugal effects and profile shearing.



Co- and Countercurrent Rotation in Tore Supra LHCD Plasmas: Neoclassical and Turbulent Transport Processes

C. Fenzi¹, B. Chouli¹, X. Garbet¹, C. Bourdelle¹, Y. Sarazin¹, J. E. Rice², T. Aniel¹, J.-F. Artaud¹, V. Basiuk¹, F. Clairet¹, G. Colledani¹, J. Decker¹, R. Dumont¹, D. Elbeze¹, C. Gil¹, P. Lotte¹, and D. Mazon¹

¹Institut de Recherche sur la Fusion par confinement Magnétique (IRFM), Commissariat à l'énergie atomique (CEA/Cadarache), 13108 Saint-Paul-lès-Durance, France

²Plasma Science & Fusion Center, MIT, Cambridge, MA 02139, USA

Corresponding Author: C. Fenzi, christel.fenzi@cea.fr

Lower hybrid (LH) wave effect on toroidal plasma rotation in L-mode Tore Supra plasmas has been analyzed in more than 50 plasma discharges, with LH input power P_{LH} up to 4.8 MW, plasma current I_p up to 1.4 MA, line integrated density n_l up to $6 \times 10^{19}/\text{m}^2$, $B_t = 3.8$ T, and a significant ripple amplitude (up to 5% at the plasma boundary) which makes ripple-induced momentum nonnegligible. At low plasma current ($I_p < 0.95$ MA), the rotation change is in the cocurrent direction and impacts the whole rotation profile. At higher plasma current, an opposite trend is observed, the core plasma rotation incrementing in the countercurrent direction, the profile being affected up to $r/a < 0.6$ only. In both low- and high- I_p cases, rotation increments are found to increase with P_{LH} . Moreover, when I_p increases, at fixed LH power ($P_{\text{LH}} = 4.8$ MW) and plasma density ($n_l = 3.8 \times 10^{19}/\text{m}^2$), the rotation increases in the countercurrent direction, switching from co- to countercurrent direction at $I_p \sim 0.95$ MA. Theoretical investigations show that the rotation evolution results from the competition of different contributions. At high plasma current, the rotation evolution in LHCD plasmas is controlled by the neoclassical friction force due to the trapped ions in banana trajectories through the toroidal diamagnetic velocity. This force results in a countercurrent rotation increment as observed in Tore Supra experiments. At low plasma current, the rotation is dominated by momentum turbulent transport when the LH waves are applied. The Reynolds stress grows strongly (through q profile effect) comparing to the high plasma current case, and acts as a cocurrent force through the residual stress contribution.



Effect of the EC Torque on Slow Plasma Rotation under Central ECH/ECCD for NTM Onset

S. Nowak¹, E. Lazzaro¹, O. Sauter², S. Fietz³, A. Karpushov², M. Maraschek³, M. Preynas², M. Reich³, D. Brunetti¹, P. Buratti⁴, B. Duval², E. Fable³, S. Garavaglia¹, C. Marini², R. McDermott³, A. Moro¹, G. Pucella⁴, H. Reimerdes², C. Sozzi¹, J. Stober³, and D. Testa²

¹*Istituto di Fisica del Plasma (IFP), Consiglio Nazionale delle Ricerche (CNR), 20125 Milan, Italy*

²*Swiss Plasma Center (SPC), École polytechnique fédérale de Lausanne (EPFL), 1015 Lausanne, Switzerland*

³*Max-Planck-Institut für Plasmaphysik, Garching, Germany*

⁴*Associazione EURATOM-ENEA Unità Tecnica Fusione, Frascati, Italy*

Corresponding Author: S. Nowak, nowak@ifp.cnr.it

The modification of low toroidal plasma rotation under application of central EC power injection with possible onset of neoclassical tearing modes (NTM) is an important issue for plasma confinement and for future devices (ITER will be characterized by a low rotation). In low collisionality regime and $P_{EC}/P_{oh} > 1$ TCV experiments central co-ECCD was observed to modify the toroidal plasma rotation both in absence and at the appearance of 3/2 and 2/1 modes, while no modes with counter-ECCD were observed.

The rotation profiles were promptly modified by the central EC power deposition and driven towards the plasma current direction as also observed in similar recent TCV experiments in the framework of the EUROfusion MST1 work package. Dedicated MST1 discharges for this study were also done on ASDEX-Upgrade and analysis is still ongoing.

The understanding of the physical mechanisms acting on the modification of the toroidal plasma rotation can allow the avoidance of the NTM onset and of the loss of confinement. The torques associated with the rotation changes have been generally not associated to a direct action of the EC power absorption, because the EC heating and current drive do not transfer momentum.

The toroidal rotation evolution under the effect of EC injection was simulated using a simplified model including an effective momentum diffusivity, scaled on the anomalous ion heat diffusivity, and an effective EC source term describing the effect of the torque due to possible different mechanisms. The physical origin of the torque associated with the EC power absorption in low collisionality regime for $P_{EC}/P_{oh} > 1$, can be associated to different causes such as driven turbulent effects or mechanisms of particles pump-out or based on the asymmetry in the power deposition.

In this work the change of rotation under the central EC power injection is investigated using the momentum balance equation and considering these different mechanisms for the interpretation of the experimental results.

We consider torque associated to the turbulent effects for the absorption of the EC power related to the enhancement of the turbulent Reynolds stress, torque related to the recycling phenomena at the edge and the occurrence of the EC pump-out and nonvanishing torque driving the toroidal rotation and provided by the surface-averaged displacement current.

Relation of Plasma Flow Structures to Particle Tracer Orbits

L. Garcia¹, B. Carreras², and I. Llerena³

¹*Universidad Carlos III de Madrid, Madrid, Spain*

²*BACV Solutions, Oak Ridge, TN 37830, USA*

³*Universitat de Barcelona, Barcelona, Spain*

Corresponding Author: L. Garcia, luis.garcia@uc3m.es

Turbulence induced transport is one of the outstanding physics problems in plasma physics. In the turbulence induced transport issue, we began with the identification of turbulent flow structures using topological and geometric techniques on the framework of resistive MHD. The structure of the flow is filamentary. The filaments are vortices that are linked to the rational surfaces. At a given time some filamentary vortices located at the lowest rational surfaces close on themselves forming toroidal knots, we characterize them by the time they remain close loops, that is their life. Other filaments are broken and we characterize them by their length. In the case that an averaged poloidal flow is self-consistently included in the calculation, there are some new structures associated with the transport barriers created by the shear in the mean flow.

Now, we want to relate these topological structures to properties of tracer particles within a framework of the continuous random walk (CTRW) approach. Vortices may cause some of the trapping of particles, while large scale flows may carry them from vortex to vortex. We focus on the relation between the trapping times and lifetimes of the flow structures and other detrapping mechanisms. The results indicate that most of the trappings that are completed during the calculation correspond to tracers trapped on broken filaments, including possible multiple trappings. The probability distribution function of the trapping times is then a function of the filament length, and has a log-normal character, like the distribution of filament lengths. In the case that an averaged poloidal flow is self-consistently included in the calculation, there is an increase in the tracer trapping due to the transport barriers created by the shear in the mean flow. The tracers trapped in the barriers do not follow the flow filaments linked to the magnetic field lines.

TH

Edge Flow from Momentum Transport by Neutrals

J. Omotani¹, I. Pusztai¹, and T. Fülöp¹

¹*Chalmers University of Technology, Göteborg, Sweden*

Corresponding Author: J. Omotani, omotani@chalmers.se

The accessibility and performance of the H-mode are critical to tokamak fusion reactors. While the physics of the pedestal is complicated and far from fully understood, it is clear that flow shear plays an important role. One of the mechanisms that may regulate flow velocity in the plasma edge is momentum transport by neutrals. Due to their high cross-field mobility they may be the most significant momentum transport channel even at low relative densities. There have also been experimental observations suggesting an important role for neutrals in determining pedestal properties and showing strong variation of confinement with the strike point position (as the target configuration changes). We have developed novel numerical tools to determine the radial electric field and plasma flows just inside the separatrix by coupling a kinetic, short mean-free-path model of neutrals to a neoclassical solver. This allows us to compute the momentum flux due to the neutrals that corresponds to specified plasma profiles. The flux must vanish in steady state and this constraint then determines the radial electric field given the density and temperature gradients. As an example we demonstrate the effect of X-point position on edge flow in ITER-like geometry. The major radius of the X-point has a strong effect both on the magnitude of the flow and its collisionality dependence, suggesting that altering the X-point position may offer a means to manipulate the edge flow shear. Beyond this particular scenario, it is clear that in the edge region of the plasma where neutral densities are relatively high the neutrals can have important effects on the radial momentum transport, flow and flow shear. Consequently they are likely to affect both the L-H transition and H-mode confinement, and they should be accounted for in the interpretation of current experiments and in the design of future machines.



New Results in Negative Viscosity Models for Fusion Plasma Dynamics

P. H. Diamond¹, A. Ashourvan¹, J. Li¹, M. Malkov¹, P.-C. Hsu¹, G. Tynan¹, and Ö. D. Gürcan²

¹University of California San Diego, CA 92093, USA

²École Polytechnique, 91128 Palaiseau, France

Corresponding Author: P. H. Diamond, pdiamond@ucsd.edu

Negative viscosity phenomena in which turbulence driven by the heat flux couples its energy to large scale structure, is a familiar and, in fact, necessary element in the success of magnetic fusion. Two prime examples of negative viscosity phenomena are zonal flow formation, where drift wave turbulence drives mesoscale shear flows which regulate large scale eddies, and intrinsic torque, where turbulence with broken symmetry drives toroidal rotation without momentum input. These two negative viscosity phenomena are essential for good confinement and MHD control. Here, we present new results in negative viscosity models, namely condensation of profile corrugations and intrinsic rotation due to dynamical symmetry breaking. These results yield new fundamental insights into zonal flow pattern structure and the origins of intrinsic torque, particularly in weak shear regimes.

Work supported by the U.S. Department of Energy, Office of Science, Office of Fusion Energy Sciences, under Award Numbers DE-FG02-04ER54738 and DE-SC0008378.



Transport of Parallel Momentum by the Triplet Correlation in Drift Wave Turbulence

Y. Kosuga^{1,2,3}, S.-I. Itoh^{2,3}, P. H. Diamond⁴, and K. Itoh^{3,5}

¹*Institute for Advanced Study, Kyushu University, Kasuga, Japan*

²*Institute for Applied Mechanics, Kyushu University, Kasuga, Japan*

³*Research Center for Plasma Turbulence, Kyushu University, Kasuga, Japan*

⁴*University of California San Diego, CA 92093, USA*

⁵*National Institute for Fusion Science (NIFS), Toki, Gifu, Japan*

Corresponding Author: Y. Kosuga, kosuga@riam.kyushu-u.ac.jp

Recent progress on the modelling of turbulent transport of parallel flow momentum is reported. Compared to the Reynolds stress or the convective term, the role of the triplet (nonlinear) flux is emphasized. The triplet term is calculated in the wave turbulence limit. The result indicates that the nonlinear flux becomes important compared to the stress term in the region with the steep intensity gradient, such as the tokamak edge. As an application, we demonstrate the impact of the nonlinear flux for the generation of intrinsic rotation in the H-mode plasmas.



Nonlocal Plasma Response to Edge Perturbation in Tokamak

M. Yagi¹, N. Miyato¹, A. Matsuyama¹, and T. Takizuka²

¹Japan Atomic Energy Agency (JAEA), Naka, Japan

²Graduate School of Engineering, Osaka University, Osaka, Japan

Corresponding Author: M. Yagi, yagi.masatoshi@jaea.go.jp

The transient transport events are observed in toroidally magnetic confinement devices. For example, the cold pulse experiment shows a rapid transient increase of electron temperature in the plasma core in response to an abrupt cooling at the edge. Understanding the nonlocal transport is important to control plasma core and/or fuel supply in ITER and DEMO. The nonlocal particle transport has been investigated based on 4-field reduced MHD model applying edge density source. It is shown that 0/0 and 1/0 modes play an important role for nonlocal transport. The edge cooling is also investigated based on 3-field gyro-fluid model, however, the nonlocal transport is found to be limited in the peripheral region [1]. To identify the effects of density source and temperature sink in the edge region, we have extended 4-field model [2] to 5-field model which consists of the vorticity equation, Ohm's law, parallel ion momentum equation, electron density equation and electron temperature equation. Simulation study on nonlocal plasma response in tokamak is performed using global fluid code based on the 5-field model. A nonlocal plasma response to edge perturbation is found. The simulation result shows that: i) the mean central electron temperature increases according to the edge cooling (it is shown for the first time); ii) the magnetic island located at $q = 2$ rational surface plays an important role (acting as internal transport barrier) as well as nonresonant modes such as 0/0 and 1/0 (here m/n implies Fourier mode with poloidal mode number m and toroidal mode number n); and, iii) redistribution of electron temperature occurs after switching off source and sink where meso-scale mode plays a major role.

References

- [1] N. Miyato, *et al.*, IAEA FEC-2014, TH/P2-12, (2014).
- [2] M. Yagi, *et al.*, Nucl. Fusion **45**, 900 (2005).



Modulated Heat Pulse Propagation and Partial Transport Barriers in 3D Chaotic Magnetic Fields

D. del-Castillo-Negrete¹, D. Blazevski¹

¹*Oak Ridge National Laboratory (ORNL), Oak Ridge, TN 37831, USA*

Corresponding Author: D. del-Castillo-Negrete, delcastillod@ornl.gov

The quantitative understanding of the role of magnetic field stochasticity on transport is critical for the confinement of fusion plasmas. Specific problems of interest include the control of ELMs by resonant magnetic perturbations and the assessment of heat fluxes at the divertor. Here we present direct numerical simulations of the time dependent parallel heat transport equation modelling heat pulses driven by power modulation in 3D chaotic magnetic fields. Understanding this problem is important because effective diffusivities, advection velocities, and damping rates are often inferred from local measurements of the amplitude and the phase of the propagation of harmonic temperature perturbations. Heat pulse propagation has also been recently used to study the connection between transport and magnetic field bifurcations in modulated electron cyclotron heating perturbative experiments in LHD and DIII-D. The numerical results presented here provide conclusive evidence that even in the absence of magnetic flux surfaces, chaotic magnetic field configurations exhibit partial barriers to modulated heat transport. In particular, it is shown that high-order islands and remnants of destroyed flux surfaces (Cantori) act as partial “leaky” barriers that slow down or even stop the inward propagation of heat waves where the connection length exhibits a strong gradient. Motivated by recent experimental studies in LHD and DIII-D we also present preliminary results on modulated heat pulse propagation across magnetic islands. The geometry used in this calculation is toroidal and the magnetic field was obtained using the MHD equilibrium code SIESTA. It is shown that magnetic islands, in particular the elliptic (O) and the hyperbolic (X) points, have a direct impact on the spatiotemporal dependence of modulated heat pulses. The main computational challenge in the work presented here stems from the strong asymmetry between the parallel and perpendicular conductivities. To address this problem, we use a Lagrangian Greene’s function (LG) method that bypasses known limitations of grid-based methods. To deal with time periodic sources, we present a novel reformulation of the LG method in Fourier space that is significantly more efficient than the original real space version of the method.

TH



L-H Transition Threshold Physics at Low Collisionality

M. Malkov¹, P. H. Diamond¹, P.-C. Hsu¹, J. E. Rice², K. Miki³, and G. Tynan¹

¹University of California San Diego, CA 92093, USA

²Plasma Science & Fusion Center, MIT, Cambridge, MA 02139, USA

³Japan Atomic Energy Agency (JAEA), Naka, Japan

Corresponding Author: M. Malkov, mmalkov@ucsd.edu

H-mode operation is the regime of choice for good confinement. Access to and sustainability of the H-mode requires understanding of the L-H transition power threshold and the related problem of hysteresis. To predict ITER transitions, one must also understand low collisionality, electron-heated regimes.

In this paper, we discuss a) L-H power threshold scaling including the minimum in $P_{th}(n)$ and elucidate an impact of interspecies energy transfer on threshold physics, b) transitions in collisionless, electron heated regimes where the electron-ion coupling is anomalous, due to the fluctuation of $\langle E \cdot J \rangle$ work on electrons and ions, and c) new transition scenarios, characterized by the sensitivity of transition evolution to preexisting L-mode profiles.

To study the above phenomena, we have developed a reduced model that independently evolves the collisionally coupled electron and ion temperatures, along with density, turbulence intensity and flow profiles. Our studies have revealed the physics of the power threshold minimum in density as a combined effect of the density dependence of collisionless electron-ion coupling and electron-ion heating mix. For collisionless regimes, we have included an anomalous power coupling between electrons and ions. Using a recently developed theory of minimum enstrophy relation which predicts a hyper-viscous turbulent flow damping we employ the nonlinear viscous heating of the ions. Our preliminary results on collisionless regimes suggest that L-H transition occurs as the endstate of an anomalous electron-ion thermal coupling front. The transition occurs when the front arrives at the edge and impulsively raises T_i there, thus building up the diamagnetic electric field shear. This study highlights the importance of collisionless energy transfer process to transitions in regimes of ITER relevance. Finally, we have explored transitions occurring in the absence of turbulence driven shear flow. The key here is the sensitivity of the transition to the preexisting L-mode density profile. Ongoing work focusses on elucidating this sensitivity and understanding how to exploit it to optimize the access to H-mode.

Work supported by the U.S. Department of Energy under Award No. DE-FG02-04ER54738.



Effects of Heat and Particle Sources Perturbations on L-H-L Transitions Based on Bifurcation Concept

B. Chatthong¹, T. Onjun²

¹*Department of Physics, Prince of Songkla University, Songkla, Thailand*

²*Sirindhorn International Institute of Technology, Pathum Thani, Thailand*

Corresponding Author: B. Chatthong, boonyarit.ch@psu.ac.th

This work aims to investigate the effects of perturbations of heat and particle sources on the formations of edge transport barrier (ETB) and on the hysteresis properties at the L-H-L transitions in the framework of bifurcation concept. The formation of transport barriers is studied via the combination of thermal and particle transport equations, which also includes neoclassical and anomalous effects. The suppression mechanism based on flow shear stabilization is assumed to affect only on the anomalous channel, where the flow shear is estimated from the force balance equation and couples both transport equations. The main thermal and particle sources are localized near plasma centre and edge, respectively. Experimental evidences and theoretical understanding reveal that the formation of an ETB, leading to an L-H transition, is related to the critical heating threshold. Analytical study reveals that the fluxes versus gradients space exhibits bifurcation behaviour with s-curve soft bifurcation type. Evidently, the backward H-L transition occurs at lower values than that of the forward transition, illustrating hysteresis behaviour. This work investigates perturbations effects of thermal and particle sources on the formations of both ETB and hysteresis properties. The focus is on the possibility of L-H transition triggering by the fluctuations in heating at marginal point and by pellet injection. It was shown that H-mode can be triggered and maintained so the central plasma pressure can be increased.



$E \times B$ Shear and Precession Shear Induced Turbulence Suppression

T. S. Hahm¹, G. J. Choi¹

¹Seoul National University, Seoul, Republic of Korea

Corresponding Author: T. S. Hahm, tshahm@snu.ac.kr

Starting from the modern bounce-kinetic formalism [1], a two-point equation which properly describes turbulent eddies associated with trapped electrons is systematically derived in general tokamak geometry. Trapped electron precession shear, as well as $E \times B$ shear, is naturally included in the derivation. Our two-point analysis, using moments of separation between the two points, reveals that both precession shear and $E \times B$ shear participate on suppressing trapped-electron-related turbulence and their synergism is determined by the relative sign. Our result provides explanations on broad range of experimental observation regarding electron thermal internal transport barrier observed in various tokamaks [2-4].

References

- [1] B. H. Fong and T. S. Hahm, *Phys. Plasmas* **6**, 188 (1999).
- [2] F. M. Levinton, *et al.*, *Phys. Rev. Lett.* **75**, 4417 (1995).
- [3] G. D. Conway, *et al.*, *Plasma Phys. Control. Fusion* **44**, 1167 (2002).
- [4] T. Fujita, *et al.*, *Plasma Phys. Control. Fusion* **46**, A35 (2004).



Zonal Flows and GAMs in Comparative Gyrokinetic and Two-Fluid Tokamak Turbulence Simulations

K. Hallatschek¹

¹*Max-Planck-Institut für Plasmaphysik, Garching, Germany*

Corresponding Author: K. Hallatschek, klaus.hallatschek@ipp.mpg.de

Fluid turbulence simulations cannot describe the kinetic effects due to the scarcity of collisions in tokamak plasmas but allow for much higher spatial resolution than kinetic simulations and become more reliable at large collision frequencies. Conversely, gyrokinetic simulations, the standard in current tokamak turbulence modelling, cannot be performed with the full set of nonlinearities that become relevant at the edge region of tokamaks, due to the high fluctuation amplitude. In addition the high collision numbers at the edge make gyrokinetic simulations numerically and physically challenging.

To allow a more reliable operation of both approaches in their respective fringe regions of validity and applicability, and to isolate special kinetic effects from the more robust fluid physics, results on ZF and geodesic acoustic modes (GAM) obtained with the nonlocal two-fluid Braginskii code NLET have been compared with gyrokinetic code simulations. The specific study of the global flows is of particular interest, with a view towards an eventual understanding of the L-H transition and the associated edge flows.

An important caveat raised by the comparisons is that particular care has to be taken with the physics and numerics of the collision operator used in the gyrokinetic codes, so that the proper fluid limit is eventually reached for high collisionalities. On the other hand, the gyrokinetic results can guide the proper renormalization of the fluid dissipative terms to account for the kinetic damping mechanisms (Landau-damping and phase-mixing) to prevent a partial break-down of the fluid description at the lower collisionalities.

The regions of validity and renormalizations of the fluid and gyrokinetic codes outlined by the present paper can be used to study regions close to the edge, where the gyrokinetic ordering breaks down, such as near the L-H transition or the density limit, and are a valuable sanity check for both approaches. Lastly, the presented results improve the understanding of the physics when kinetic phenomena can be reproduced in first principle fluid codes.

Helical Electric Potential Modulation via Zonal Flow Coupling to Resonant Magnetic Perturbations

M. Leconte¹

¹National Fusion Research Institute (NFRI), Daejeon, Republic of Korea

Corresponding Author: M. Leconte, mleconte@nfri.re.kr

Controlling edge localized modes (ELMs) is very important for ITER, and a well-tested way to achieve this is by using external coils to generate resonant magnetic perturbations (RMPs), demonstrated on several tokamaks [1-4]. The working hypothesis for the origin of ELM suppression is that RMPs increase transport in the pedestal, thus lowering the pressure-gradient below the ideal-MHD threshold. In this work, we show that — in presence of RMPs — zonal flows can drive a long-lived vortex-flow pattern. This finding clarifies the theory of RMP-induced zonal flow damping [5]. Note that evidence of such a vortex-flow pattern has been observed experimentally [6]. We obtain a dynamical system of coupled 1D equations for zonal flows and vortex-flow profiles, which we solve numerically (in our model, turbulence acts as a shear-dependent negative eddy-viscosity). As zonal flows are turbulence-driven, this shows that turbulence plays a major role in the plasma self-organization towards a 3D quasi-equilibrium. Contrary to zonal flows (which act as a benign reservoir of energy) the vortex flow pattern has a radial streamer-like flow associated to it and hence can drive convective transport. The associated enhancement in the particle transport, assuming the vortex flow has a density component, has a resonant character. This additional transport could act to limit the pressure-gradient, and is therefore a possible candidate to explain ELM suppression.

References

- [1] T. E. Evans, *et al.*, Nucl. Fusion **48**, 024002 (2008).
- [2] Y. Liang, *et al.*, Phys. Rev. Lett. **98**, 265004 (2007).
- [3] W. Suttrop, *et al.*, Phys. Rev. Lett. **106**, 225004 (2011).
- [4] Y. M. Jeon, *et al.*, Phys. Rev. Lett. **109**, 035004 (2012).
- [5] M. Leconte, P. H. Diamond and Y. Xu, Nucl. Fusion **54**, 013004 (2014).
- [6] N. Vianello, *et al.*, Plasma Phys. Control. Fusion **57**, 014027 (2015).



Tokamak Turbulence Simulations Using BOUT++ in Core Region

S. S. Kim¹, H. Jhang¹, X. Xu², T. Rhee¹, P. Xi², A. Dimits², and C. Ma²

¹*National Fusion Research Institute (NFRI), Daejeon, Republic of Korea*

²*Lawrence Livermore National Laboratory (LLNL), Livermore, CA 94550, USA*

Corresponding Author: S. S. Kim, sskim@nfri.re.kr

Development of a self-consistent, core-edge integrated simulation capability is a long standing problem in fusion simulation programme. Such capability would yield insight into questions related to global profile dynamics originating from L-H transition and internal transport barrier formation. Starting from a tokamak edge plasma simulation code, BOUT++ has evolved into a versatile framework that can be used to simulate a wide range of fluid models in complicated magnetic geometry. To realize self-consistent core-edge coupled simulations, we develop a core gyro-Landau-fluid code using the BOUT++ framework. Initial efforts focus on self-consistent simulations of core electrostatic ion temperature gradient (ITG) driven turbulence and code verification. Verification of the code is realized by comparing linear growth rates calculated from BOUT++ with those from gyrokinetic codes. To include a neoclassical poloidal flow and its effect on poloidal mean flow, we introduce an ad-hoc closure. Global nonlinear simulations are performed for ITG turbulence focussing on the role of zonal flows in turbulence suppression. Details of the code development and preliminary physics results will be presented.



Steady State Turbulent ITER-Like Plasmas with RF Drivers

W. Horton¹, L. Zheng¹, A. V. Arefiev¹, C. Michoski², P. Morrison¹, and F. Waelbroeck¹

¹*Institute for Fusion Studies (IFS), University of Texas at Austin, Austin, TX 78712, USA*

²*Institute for Computational Engineering and Sciences (ICES), University of Texas at Austin, Austin, TX 78712, USA*

Corresponding Author: W. Horton, wendell.horton@gmail.com

First stability and transport in RF driven plasmas in ITER-like geometries are investigated using new kinetically modified MHD stability equations analyzed with theory and advanced simulations. Extended MHD stability analysis describes in detail the outer most closed flux surfaces inside the magnetic separatrix where ions and electrons dynamics differ. The new physics includes the effect of charge separation in response functions used in MHD-ballooning modes with contributions from the anisotropic pressure tensor from the different ion and electron dynamics in this steep pedestal gradient region. Different responses of trapped and passing electron orbits just inside the magnetic separatrix gives rise to the I-mode confinement. Nonlinear dynamics is shown to be Hamiltonian, by Morrison *et al.*. New invariants are found that give rise to a new form of the energy principle and place constraints on turbulent cascades. Generalized helicities are associated with topological invariants. These invariants can be used to assess relaxed states akin to Taylor-relaxation. RF heating is investigated comparing results of mode conversion through upper-hybrid resonance layer where fast mode couples to the Bernstein slow waves. Fully kinetic particle-in-cell (PIC) simulations are performed with an open source code EPOCH. The code has been benchmarked at relatively low field amplitudes. Electron anisotropy in the ITG and ETG turbulence is analyzed with kinetic theory and used to describe the steady state response of the RF wave driven heating and current drive from RF waves in Tore Supra. Their extension to WEST plasmas is presented including the change in the heating across the magnetic separatrix. The turbulence in the electron density scatters direction and polarization of the current driving lower hybrid waves. The model is applied to experiments in Tore Supra and EAST and to the upcoming experiments in WEST. Scattering of the launched LHCD waves by the ETG turbulence gives the turbulent electron distribution functions. The RF wave scattering by the turbulence in the electron density is required to explain the broaden, anisotropic fast electron energy spectra measured deduced from the X-ray spectra in Tore Supra and EAST tokamak experiments [1, 2].

References

[1] W. Horton, M. Goniche, Y. Peysson, *et al.*, Phys. Plasmas **20**, 112508 (2013).

[1] J. Decker, Y. Peysson, *et al.*, Phys. Plasmas **21**, 092504 (2014).



Turbulent Current Drive Mechanisms

C. McDevitt¹, X. Tang¹, and Z. Guo¹

¹*Los Alamos National Laboratory (LANL), Los Alamos, NM 87545, USA*

Corresponding Author: C. McDevitt, mcdevitt@lanl.gov

In this work we discuss the efficiency of various turbulent mechanisms for modifying the plasma current. The first mechanism results from the establishment of an equilibrium between trapped and passing electrons due to resonant scattering by microturbulence. This mechanism is closely analogous to the familiar neoclassical bootstrap current except that it relies on wave-particle interactions to detrapp electrons rather than Coulomb collisions. In addition to the above mechanism, mean plasma current can be generated by either: 1) turbulent acceleration, 2) or a “residual stress” term in the electron momentum flux. The former mechanism relies on turbulence mediated exchange of momentum between ions and electrons, whereas the latter corresponds to a nondiffusive contribution to the momentum flux. The contributions from these mechanisms are quantified by employing a mean field formulation that incorporates phase space scattering by drift wave turbulence, turbulent acceleration, and nondiffusive contributions to the electron momentum flux. The impact of these mechanisms on the bootstrap current is assessed by the incorporation of a Coulomb collision operator such that turbulent and neoclassical effects are treated on an equal footing.

Work performed under the auspices of the U.S. Department of Energy by LANL under Contract No. DE-AC52-06NA25396.

TH

Effect of Energy-Nontransporting Nonlinear Flux on the Turbulent Plasma Transport

C.-B. Kim¹, C.-Y. An¹, and B. Min¹

¹Soongsil University, Seoul, Republic of Korea

Corresponding Author: C.-B. Kim, cbkim@ssu.ac.kr

Turbulent plasma transport is an important issue in the confinement of the fusion plasmas. $E \times B$ nonlinear flux plays a deciding role in redistributing the energy and the momentum. In the case of the isothermal plasma the particle flux Γ is the fundamental measure of the turbulent transport. In the fusion plasma where the particle collisions are relatively rare, the plasma is near the adiabatic state. The present work sets out to study Γ near adiabatic state of the electrostatic resistive fluid plasma fluctuations [1]. Simulations are performed in the BOUT++ frame [2] in two-dimensional slab $L_x = L_y = 80\pi$ perpendicular to the equilibrium magnetic field with grids 256×256 . The fixed equilibrium density gradient is in the negative x direction and the electron diamagnetic drift is along the y axis. Fluctuations at small scales $k\rho_s \gg 1$ are cut off by the hyper-dissipation.

At a quasi-steady state of the energy Γ , in contrast to the energy, is not quite steady exhibiting intermittent peaks as it changes between less than 10 to larger than 40. It is found that secondary broad peak $0.6 \leq k\rho_s \leq 1.0$ is present when Γ is large. The spectra of the $E \times B$ energy flux illustrate a similar distribution in the range $k\rho_s \geq 0.5$ that generally agrees with the difference of Γ 's. The $E \times B$ energy flux is divided into two parts: one directly involved in the energy redistribution, and the remainder [3, 4]. Preliminary results indicate the strong impact of the latter part on Γ by controlling the phases of the fluctuations. Similar process is believed to be working inside the fusion plasma. Detailed analyzes of the correlation between the energy flux and the phases as well as extension to the thermal flux of more realistic plasma models will be discussed at the conference.

References

- [1] A. Hasegawa and M. Wakatani, Phys. Rev. Lett. **50**, 682 (1985).
- [2] B. D.udson *et al.*, Comput. Phys. Commun. **180**, 1467 (2009).
- [3] B. Min, *et al.*, Plasma Phys. Control. Fusion **57**, 095009 (2015).
- [4] B. Min, *et al.*, J. Kor. Phys. Soc. **66**, 1226 (2015).



Numerical Diagnostics of Turbulent Transport in Three-Dimensional Magnetic Configurations

N. Kasuya¹, M. Nunami², and M. Yagi³

¹*Institute for Applied Mechanics, Kyushu University, Kasuga, Japan*

²*National Institute for Fusion Science (NIFS), Toki, Gifu, Japan*

³*Japan Atomic Energy Agency (JAEA), Naka, Japan*

Corresponding Author: N. Kasuya, kasuya@riam.kyushu-u.ac.jp

Recent simulations in three-dimensional (3D) magnetically confined plasmas show various aspects of plasma turbulence, and numerical diagnostics using 3D simulation data of helical plasmas have been carried out. Here we present results of turbulence analyzes i) in simplified geometry for detailed nonlinear mechanism of heat transport, and ii) in real 3D geometry for comprehensive understanding of experimental observations. The former topic is on the case with MHD modes with a rather long wavelength. Global nonlinear simulations of drift-interchange modes in helical plasmas are carried out using a reduced MHD model. The model includes various characteristic time-scales. A “nonlocal” effect has been studied in dynamical transport phenomena by the simulation of the heat source modulation. The nonlinear process plays the key role in the response, which takes a finite temporal duration for the energy redistribution. By conditional averaging the characteristic response can be extracted, such as a spiral 2D pattern of the heat flux, which is formed nonlinearly and sustained for longer duration than the turbulence decorrelation time. An electromagnetic oscillation also exists, which gives the other time-scale. The latter topic is on the case with 3D equilibrium and shorter wavelength perturbations. Gyrokinetic simulations of ion-temperature-gradient modes in the LHD configuration have been carried out, and the 3D data obtained from the simulations are analyzed taking into account of the line of sight of the experimental diagnostics. The method to resolve the local spectrum from the integrated signal (2D phase contrast imaging) is tested using the helical magnetic configuration. A vertical profile of the k spectrum can be obtained from the integrated signal. The analysis routine can give a fluctuation pattern at an arbitrary position, and comparison with it gives understanding of the observed integrated signals. The extracted component has a peak at a finite wavenumber in this case. A finite width in the local k spectrum deteriorates the spatial resolution. In this way, variety of the numerical diagnostics from several viewpoints can give physical understanding and quantitative comparison of turbulent plasmas.

The Effect of Shaping on Reversed Field Pinch Dynamics

R. Chahine¹, W. Bos^{1,2}, J. Morales³, and K. Schneider⁴

¹Laboratoire de Mécanique des Fluides et d'Acoustique (LMFA), École Centrale de Lyon, 69134 Écully, France

²Centre national de la recherche scientifique (CNRS), 75016 Paris, France

³Swiss Plasma Center (SPC), École polytechnique fédérale de Lausanne (EPFL), 1015 Lausanne, Switzerland

⁴Laboratoire de Mécanique, Modélisation & Procédés Propres (M2P2), Aix-Marseille Université, France

Corresponding Author: R. Chahine, robert.chahine@doctorant.ec-lyon.fr

A notable influence of the shape of the plasma on the dynamics of RFPs is clearly illustrated by simulations of fully nonlinear visco-resistive magnetohydrodynamics. The axial mode-spectrum is qualitatively changed in cylinders with elliptic cross-section. The results suggest that shaping will change, and possibly improve the confinement of RFPs.



Progress in Theoretical RFP Studies: New Stimulated Helical Regimes and Similarities with Tokamak and Stellarator

D. Bonfiglio¹, M. Veranda¹, M. Agostini¹, S. Cappello¹, D. Borgogno², L. Chacón³, D. Escande⁴, A. Fassina¹, P. Franz¹, M. Gobbin¹, D. Grasso⁵, P. Piovesan¹, I. Predebon¹, G. Rubino⁶, F. Sattin¹, and M. Zuin¹

¹*Consorzio RFX, Associazione EURATOM-ENEA sulla Fusione, Padova, Italy*

²*Université Côte d'Azur, CNRS, Observatoire de la Côte-d'azur, 06304 Nice, France*

³*Los Alamos National Laboratory (LANL), Los Alamos, NM 87545, USA*

⁴*Physique des Interactions Ioniques et Moléculaires (PIIM), CNRS, Aix-Marseille Université, France*

⁵*Istituto dei Sistemi Complessi-CNR, Politecnico di Torino, Torino, Italy*

⁶*Associazione EURATOM-ENEA Unitá Tecnica Fusione, Frascati, Italy*

Corresponding Author: D. Bonfiglio, daniele.bonfiglio@igi.cnr.it

Recent theoretical studies of the reversed-field pinch (RFP) have demonstrated the possibility of stimulating new quasi-single helicity (QSH) regimes by allowing a small helical deformation of the magnetic boundary. In particular, 3D nonlinear MHD modelling predicted QSH states based on nonresonant helicities are predicted to be more resilient to magnetic stochasticity induced by secondary modes. These theoretical predictions have motivated a series of experiments in the RFX-Mod device with applied magnetic perturbations (MPs).

We present here the current state of the art in research on nonlinear MHD modelling of helical RFP regimes, and we highlight similarities of the helical RFP with the tokamak and the stellarator. Helical RFP states with different helicities are compared in terms of their core confinement properties. We consider in particular stimulated helical configurations obtained by applying small $m = 1$ helical MPs with toroidal periodicity corresponding to nonresonant ($n = 6$) and resonant ($n = 7$ and $n = 8$) kink-tearing modes. The safety factor profile as a function of the helical magnetic flux decreases monotonically for the nonresonant case, whereas a region of flat or reversed magnetic shear appears in the core for resonant configurations. When secondary MHD modes are taken into account, a magnetic topology characterized by a conserved helical core enclosed by a stochastic region is typically observed. The width of the conserved core region turns out to be the largest for the nonresonant configuration, in qualitative agreement with RFX-Mod experiments suggesting that QSH regimes with $n = 6$ dominant mode are endowed with a larger hot core than spontaneous $n = 7$ QSH states. By using a finite-time Lyapunov exponent method applied for the first time to magnetic confinement configurations, barriers to the diffusion of magnetic field lines are diagnosed in the weakly stochastic region surrounding the conserved helical core in numerical QSH states. Similarly to what observed in the tokamak configuration, the sawtooth dynamics of RFP plasmas is mitigated with the application of helical MPs. The confinement properties of the RFP edge, characterized by $m = 0$ island chains at the $q = 0$ reversal surface playing a role similar to edge islands in tokamak and stellarator plasmas, are also discussed.



Solar Coronal Loops as Magnetically Confined Tori with Gravity

L. Sugiyama¹, M. Asgari-Targhi²

¹Laboratory for Nuclear Science, Massachusetts Institute of Technology (MIT), Cambridge, MA 02139, USA

²Harvard-Smithsonian Center for Astrophysics, Cambridge, MA 02138, USA

Corresponding Author: L. Sugiyama, sugiyama@mit.edu

A large amount of evidence suggests that the bright loops that are regularly observed in the sun's corona are magnetic flux ropes that confine plasma, tied at both ends to structures in the photosphere. Due to the difficulties of observation, their steady states have never been explained. Coronal loops resemble partial magnetic tori and ideas from the equilibrium and stability of toroidal magnetic fusion plasmas lead, for the first time, to 3D ideal MHD solutions for coronal loop steady states that take into account the complete force balance and geometry. The apparently weak solar gravity, previously ignored, is found to be the crucial factor that allows a loop steady state, and provides a unified observational picture. Gravity, combined with magnetic line-tying at the loop footpoints, stabilizes the intrinsic radial (major radius) expansion instability of a curved current-carrying loop, replacing the external fields used in laboratory plasmas. Normalized to the loop MHD parameters, the gravitational force parameter is $\hat{G} = Ga/v_A^2$, in terms of the acceleration due to gravity $G = 274.9 \text{ m/s}^2$, the loop minor radius a , and the shear Alfvén speed v_A . Analytical steady states exist at two orders in the loop inverse aspect ratio $\epsilon = a/R_o$, $\hat{G} = \epsilon^2$, and ϵ^3 . Comparison to observations shows good agreement. Short hot coronal loops and the shorter warm loops fit the ϵ^3 ordering, while long, lower density loops better fit ϵ^2 . Intermediate length loops fall in between. Small \hat{G} loops have an axisymmetric tokamak-like core, while large \hat{G} loops are strongly nonaxisymmetric and more closely related to high- β stellarators, modified by gravity. Sufficiently long loops will be metastable, since the gravitational force begins to decrease with height as $(R_o + R_s)^{-2}$, and may provide the seed state for large coronal mass ejections. The constraints imposed by the gravitational $N = 1$ nonaxisymmetry are related to fusion questions on the effects of small magnetic nonaxisymmetries on tokamaks, such as error fields and the density pump-out by RMPs.

Work supported in part by the U.S. Department of Energy OFES contract DE-SC0007883 and SCIDAC DE-FG02-04ER54802.



Studies of Magnetic Islands in the TJ-II Helic and the Related Transport

J. Martinell¹, S. Cancino¹, and D. López-Bruna²

¹*Instituto de Ciencias Nucleares, National Autonomous University of Mexico (UNAM), Mexico City, Mexico*

²*Laboratorio Nacional de Fusión (LNF),*

Centro de Investigaciones Energéticas, Medioambientales y Tecnológicas (CIEMAT), Madrid, Spain

Corresponding Author: J. Martinell, martinel@nucleares.unam.mx

In the first part we study the magnetic equilibrium of TJ-II using the VMEC code together SIESTA MHD code. The pressure profiles determine island geometry. For each island width we obtain the associated MHD energy in order to find a correlation between them and identify an island width that has better stability properties.

A dynamical analysis of magnetic islands is aimed at explaining the phenomenology in TJ-II showing a correlation between MHD activity and transport barriers. The nonlinear island growth is studied in presence of a plasma flow associated with the transport barrier. In previous works it has been found that the presence of a sheared flow reduces the growth rate of the island and is thus stabilizing. As mentioned before, the presence of flows near the island separatrix produces a polarization current which alters the dynamical properties related to diamagnetic effects. Based on these results we propose a model in which the polarization current, due to the oscillatory part of the parallel current, stabilizes an initial island. This coincides with the time after the MHD bursts are observed. As the current grows the associated sheared flow builds up a transport barrier. When the island size gets very small the effect of the transport barrier becomes more effective. Then the temperature around the island increases, which reduces collisional effects, and the boundary layer that shields the island from external flows gets reduced producing the island to get locked, i.e., the polarization current is ineffective in keeping the island stable and starts growing through magnetic reconnection. At this time there is particle acceleration and the MHD activity starts manifesting. The cause for the modification of the island state is that the magnetic torque acts on the island as the collisionality decreases.

At some point the island size becomes large enough to drive a polarization current, since large ripples outside the separatrix produce larger oscillations of the parallel current. This whole process is modelled using the Astra transport code in which we include a turbulence model based on the resistive ballooning mode. Three impurity species of carbon are also included in order to obtain the emitted radiation that is measured in the experiments by bolometers. In this way we can have a relatively good correlation with the experimental sequences.



Predicting Cross-Scale Self-Organization in Turbulent Magnetically Confined Plasmas

M. Rajković¹, M. Milovanović², and M. M. Škorić¹

¹*Vinča Nuclear Institute, University of Belgrade, Belgrade, Serbia*

²*Mathematical Institute of the Serbian Academy of Sciences and Arts, Belgrade, Serbia*

Corresponding Author: M. Rajković, milanr@vin.bg.ac.rs

Recently, we have developed a comprehensive mathematical and computational framework for the analysis and quantification of self-organization [1]. Application of this method may resolve some of the important issues of fusion plasmas such as prediction of changes in the pattern formation and transport properties, to name a few. We assume that the system self-organizes if its complexity (related to statistical prediction) increases with time.

The experimental data consists of the ion-saturation current measurements performed by a movable Langmuir probe located at the outboard midplane on the MAST device. Several different confinement regimes in MAST are analyzed: high-density L-Modes, dithering H-Modes with heating power close to the threshold for L-H transition with intermittent edge localized modes (ELMs) and H-Modes with ELMs present. We show how the method is used for predicting the occurrence of the particular Mode and we discuss the possible applications of this method for other issues relevant for fusion plasmas. Also, we illustrate how the method is used to predict ELM bursts in the edge plasma, in time and in the spatial location.

We further apply this framework in order to predict different bifurcations and dynamic regimes in the model of Stimulated Raman scattering (SRS) in plasma [2], a paradigm of three-wave interaction of great importance for inertial confinement fusion. This three-wave interaction is related to a nonlinear coupling of intense laser light (pump) to the electron plasma wave (EPW) and the scattered light, shifted in wavenumber and frequency. SRS belongs to a family of underdense plasma instabilities which can have a detrimental effect on efficiency of laser energy deposition into a fusion target. This particular SRS model has a very rich spatiotemporal dynamics and exhibits a paradigm of transition to spatiotemporal chaos via quasiperiodic and intermittent stages. We show that our self-organization framework predicts with great accuracy, pattern changes in time and space and occurrence of new dynamic regimes. In addition, the method quantifies each self-organizing state enabling precise characterization of self-organization process under change of different parameters of the system.

References

- [1] M. Milovanović and M. Rajković, *Europhy. Lett.* **102**, 40004 (2013).
- [2] M. M. Škorić, M. Jovanović and M. Rajković, *Phy. Rev. E.* **53**, 4056–66 (1996).



Diamagnetic Plasma Confinement in Linear Traps

A. Beklemishev¹

¹*Budker Institute of Nuclear Physics (BINP), Novosibirsk, Russian Federation*

Corresponding Author: A. Beklemishev, bekl@bk.ru

A new efficient method of magnetic confinement is suggested for use in linear traps with extremely high plasma pressure. While pressure grows, the equilibrium in a linear trap changes in such a way that the effective mirror ratio increases, and, as a result, the axial particle and energy confinement becomes gas-dynamic and improves linearly with mirror ratio. This effect is due to diamagnetic expulsion of the magnetic field from the plasma volume while β tends to one. The improved confinement could lead to construction of a compact fusion reactor based on a linear trap, if one could ensure suppression of pressure-driven instabilities, in particular, the ballooning instability. This paper shows how it can be done: one should use magnetic configuration with a stretch of uniform field at its minimum, and place external stabilizers near ends of that stretch. Equilibrium with anisotropic pressure, MHD stability, fast-ion confinement, startup, and the energy balance issues are considered for a linear trap in the diamagnetic-bubble regime. Such type of confinement is shown to be very promising for reactor perspectives.



Kinetic Modelling of Runaways in Fusion Plasmas

T. Fülöp¹, O. Embréus¹, A. Stahl¹, S. Newton¹, and I. Pusztai¹

¹*Chalmers University of Technology, Göteborg, Sweden*

Corresponding Author: T. Fülöp, tunde@chalmers.se

Runaway electrons (REs) are a pressing issue for ITER due to their significant potential to cause damage. Improved knowledge of RE formation mechanisms, their dynamics and characteristics, as well as transport or loss processes that may contribute to RE suppression and control, will benefit the fusion community and contribute to a safe and reliable operation of reactor-scale tokamaks.

In this work we discuss bremsstrahlung radiation emission and knock-on collisions, and describe an accurate theoretical framework for studying their effect on the RE distribution. These processes, together with synchrotron radiation reaction, have important implications for the understanding of many phenomena, such as the effective critical electric field for RE generation and the formation of nonmonotonic features in the RE tail. Starting from the Boltzmann transport equation, we derive a collision operator for bremsstrahlung radiation reaction, fully accounting for the finite energy and emission angle of the emitted photons. The Boltzmann bremsstrahlung operator allows the REs to reach energies several times higher than the previously used mean-force model, and the emission of soft photons shifts part of the momentum-space distribution function towards higher perpendicular momenta.

Avalanche runaway generation is the phenomenon whereby REs are generated due to large-angle collisions of already existing REs with thermal electrons, leading to an exponential growth of the runaway current. Here we describe a new large-angle collision operator, derived as the high-energy limit of the linearized relativistic Boltzmann collision integral. This operator generalizes previous models of large-angle collisions to account for the full momentum dependence of the primary distribution, and conserves particle number, momentum and energy, while also avoiding the double counting of small and large-angle collisions. We investigate the effect of the operator on the evolution of the RE distribution and find that the change to the RE growth rate can be large, especially during the early stages of the runaway acceleration process, and the likelihood of a given runaway seed transforming into a serious runaway beam can thus potentially be affected.

TH



Generation of Runaway Electrons during the Thermal Quench in Tokamaks

P. Aleynikov¹, B. N. Breizman²

¹*Max-Planck-Institut für Plasmaphysik, Garching, Germany*

²*University of Texas at Austin, Austin, TX 78712, USA*

Corresponding Author: P. Aleynikov, pavel.aleynikov@ipp.mpg.de

A consistent description of runaway electron (RE) generation in plasma disruptions remains an open physics issue. The possibility of the formation of high postdisruption RE currents raises safety-related concerns for large tokamaks, such as ITER. Although the avalanche mechanism of RE production is anticipated to be the dominant mechanism in ITER [1], the avalanche multiplication of the runaways after the thermal quench still requires a seed RE current. The need for reliable prediction of the RE generation in ITER calls for additional attention to the primary (seed) population of the RE.

We present an advanced description of electron kinetics during impurity-dominated thermal quenches in tokamaks. A 2D Fokker–Planck equation for the hot electrons and a power balance equation for the bulk plasma are solved self-consistently, with impurity radiation as the dominant energy loss mechanism. The post-thermal-quench (but pre-current-quench) RE density, energy and current are found for a broad range of initial plasma parameters (density, current density, temperature and impurity concentration), including those of interest for ITER.

We find that runaway formation is less efficient in plasmas with high pre-quench temperatures. In particular, we do not expect any significant runaway seed in a 10 keV plasma with a density of $10^{20}/\text{m}^3$ when the amount of injected argon is less than $5 \times 10^{19}/\text{m}^3$, while in a 2 keV plasma of the same density a significant RE population forms if $2 \times 10^{19}/\text{m}^3$ of argon is injected. We also find that runaway production increases for heavier injection of impurities up to prompt conversion of the total pre-quench current into the runaway current in the case of abundant impurities. The mean kinetic energy of RE population is in this case limited to rather moderate values (sub-MeV), asymptotically approaching those of the near-threshold regime [2].

We finally conclude that the nonuniformity of the plasma creates a possibility for the post-quench current to be carried by two distinct runaway populations (a sub-MeV and an ultrarelativistic).

References

- [1] M. N. Rosenbluth and S. V. Putvinski, *Nucl. Fusion* **37**, 1355 (1997).
 [2] P. Aleynikov and B. N. Breizman, *Phys. Rev. Lett.* **114**, 155001 (2015).

Work supported by ITER Contract No. ITER/CT/15/4300001178 and U.S. Department of Energy Contract No. DE-FG02-04ER54742.



The Effect of Plasma Response on Losses of Energetic Ions in the Presence of 3D Perturbations in Different ITER Scenarios

T. Kurki-Suonio¹, J. Varje¹, S. Äkäslompolo¹, K. Särkimäki¹, J. Terävä¹, S. K. Sipilä¹, G. Saibene², V. Parail³, and Y. Liu³

¹Aalto University, Espoo, Finland

²F4E: Fusion for Energy, ITER EU Centre, 08019 Barcelona, Spain

³Culham Centre for Fusion Energy (CCFE), Culham Science Centre, Abingdon, UK

Corresponding Author: T. Kurki-Suonio, taina.kurki-suonio@aalto.fi

The new physics introduced by ITER operation, of which there is very little prior experience, is related to the very energetic (3.5 MeV) alpha particles produced in large quantities in fusion reactions. These particles not only constitute a massive energy source inside the plasma, but also present a potential hazard to the material structures that provide the containment of the burning plasma. In addition, the negative neutral beam injection (NBI) produces 1 MeV deuterons and the application of ICRH produces minority ions in multi-MeV range, both of which have to be well confined to ensure successful operation of ITER.

Our past analyzes of the fast ion confinement have been restricted to vacuum approximation. This approach does not take into account the dynamic response of the plasma to the external perturbations produced by, e.g., ferritic inserts that are embedded in the ITER wall to reduce the TF ripple, the test blanket modules that also contain ferritic material, and ELM control coils. For long, neglecting plasma response has not been considered an issue because it was assumed that the plasma response simply shields the plasma from external perturbations. However, recent simulation results [1] suggest this is not generally the case. While hindering island formation deep inside the plasma, the plasma response can increase stochasticity at the very edge of the plasma. If the source of energetic ions does not vanish in this region, the stochastic field lines can transport these ions to the walls rapidly and, thus, with very high energy.

In this contribution we employ magnetic backgrounds where the plasma response has been included as calculated by the MARS-F code. The Monte Carlo orbit-following code ASCOT is used to simulate both thermonuclear fusion alphas and fast ions from ITER heating systems in the full 3D magnetic configuration with the plasma response and 3D wall. The analyzes covers all major operating scenarios of ITER. Comparing the present simulation results to the ones obtained in vacuum approximation shows that with only ferritic components, the plasma response increases the (small) total load by 10–15%. However, when the perturbation due to ELM control coils is included, the plasma response brings about significant changes in the power deposition and, in some cases, even increases it.

References

[1] D. Pfefferle, *et al.*, Nucl. Fusion **55**, 012001 (2015).



Diffusion of Energetic Particles Due to Charge Changes and Neoclassical Tearing Modes

R. Farengo¹, C. Clauser^{1,2}, I. Montellano¹, H. Ferrari^{1,2}, P. García-Martínez^{1,2}, and L. Lampugnani^{1,2}

¹*Instituto Balseiro, CNEA, Bariloche, Río Negro, Argentina*

²*Consejo Nacional de Investigaciones Científicas y Técnicas (CONICET), Buenos Aires, Argentina*

Corresponding Author: R. Farengo, farengo@cab.cnea.gov.ar

Theoretical calculations and particle simulations are used to show that charge changing processes (i.e., charge exchange) can significantly increase the diffusion of alpha particles in the pedestal-edge-SOL regions. The interaction of the alpha particles with the plasma species, He⁺ and neutral deuterium (both atomic and molecular) and helium are included. The numerical code calculates the exact alpha particles trajectories and introduces the probability of charge changing events via a Monte Carlo type method, where the probability of each process is taken proportional to the corresponding collision frequency. The cross sections of these processes were obtained from the existing databases. The code runs on a GPU, thus allowing calculations with a large number of particles in a short time using modest computational resources. The effect of neoclassical tearing modes on the confinement of energetic ions produced by NBI is also studied. The experimental information available about the perturbed current density and the displacement are employed. Ampere's law is used to calculate the perturbed poloidal magnetic flux and the resistive Ohm's law to calculate the perturbed electric field. The exact trajectories of the ions in the total fields (equilibrium plus perturbation) are calculated. The results show that the addition of the perturbed electric field produced by the rotation of the mode can greatly increase particle losses.

Improving Fast-Ion Confinement in High-Performance Discharges by Suppressing Alfvén Eigenmodes

G. J. Kramer¹, M. Podestá¹, C. T. Holcomb², L. Cui¹, N. N. Gorelenkov¹, B. A. Grierson¹, W. W. Heidbrink³, R. Nazikian¹, W. M. Solomon¹, M. A. Van Zeeland⁴, and Y. Zhu³

¹Princeton Plasma Physics Laboratory (PPPL), Princeton, NJ 08540, USA

²Lawrence Livermore National Laboratory (LLNL), Livermore, CA 94550, USA

³University of California Irvine, CA 92697, USA

⁴General Atomics, San Diego, CA 92186, USA

Corresponding Author: G. J. Kramer, gkramer@pppl.gov

The performance of steady-state DIII-D discharges is often reduced due to anomalous fast-ion transport that was observed to correlate with Alfvén eigenmode (AE) activity. Fast-ion transport modelling using the kick model [1] shows that the observed mode activity can account for the observed fast-ion confinement degradation. Therefore, suppressing the AE activity will improve the plasma performance through improved fast-ion confinement. This can be achieved by modifying the magnetic safety factor profile. In these discharges the q profile has a minimum near $r/a = 0.3$, in the same region where the fast-ion pressure gradient, which drives the AEs, has its maximum. By moving q_{\min} to a larger minor radius where the fast-ion pressure gradient is small, the drive for the reversed shear AEs weakens and conditions in the core become unfavourable for normal AEs. Experimental evidence will be presented that this solution is viable and that the fast-ion confinement can be restored to near classical levels.

References

[1] M. Podestá, *et al.*, Plasma Phys. Control. Fusion **56**, 055003 (2014).

Work supported by the U.S. Department of Energy under DE-AC02-09CH11466, DE-AC52-07NA27344, DE-FC02-04ER54698, and SC-G903402.



Linear and Nonlinear Dynamics of Electron Fishbones

G. Vlad¹, V. Fusco¹, S. Briguglio¹, C. Di Troia¹, G. Fogaccia¹, F. Zonca¹, and X. Wang²

¹Associazione EURATOM-ENEA Unitá Tecnica Fusione, Frascati, Italy

²Max-Planck-Institut für Plasmaphysik, Garching, Germany

Corresponding Author: G. Vlad, gregorio.vlad@enea.it

Internal kink instabilities exhibiting fishbone-like behaviour have been observed in a variety of experiments where a high energy electron population, generated by strong auxiliary heating and/or current drive systems, was present. Numerical simulations using XHMGC, a hybrid MHD-Gyrokinetic code, has been already applied successfully to analyzes of modes driven by energetic electrons. In particular, electron fishbones driven by an energetic particle population with on-axis peaked radial density profile were studied in some detail describing the linear and nonlinear mode dynamics using a strongly anisotropic distribution function, mainly constituted by deeply trapped particles. Deeply trapped energetic electrons were recognized to drive the mode, in this case, by precession resonance. In this paper we will further investigate electron fishbones driven by an energetic particle population with on-axis peaked radial density profile showing the relative importance of different driving and damping processes accounted for in the model, i.e., energetic electrons, thermal ion compressibility and diamagnetic effects, thermal electron compressibility. Numerical simulation results have shown that nonlinear fishbone dynamics is governed by frequency chirping due to phase-locking: transport of energetic electrons in phase space will be analyzed in detail using test particle Hamiltonian mapping (TPHM) techniques, and the saturation amplitude scaling will be compared with the theoretical predictions. After reviewing the on-axis peaked energetic electron density population, the case of off-axis peaked energetic electron density population will also be analyzed in detail. This case is closely related to the experimental set up of present experiments with off-axis ECRH heating, in particular for the case of high field side deposition, where barely trapped/circulating electrons will be preferentially heated with an inverted radial density profile of the energetic electrons close to the q_{\min} radial surface. It will be shown that, as expected from theory, unstable modes must propagate in the opposite direction with respect to that observed in the case of an energetic electron population with on-axis peaked radial density profile. Both the linear and nonlinear dynamics of an energetic electron population with off-axis peaked radial density profile will be presented.



Nonlinear Interactions of Low-Frequency Alfvén Eigenmodes

Z. Lin¹, Y. Liu², and H. Zhang²

¹University of California Irvine, CA 92697, USA

²Fusion Simulation Center (FSC), Peking University, Haidian, Beijing, People's Republic of China

Corresponding Author: Z. Lin, zhihongl@uci.edu

In this paper, we report gyrokinetic simulations of nonlinear interactions between β -induced Alfvén eigenmode (BAE) and β -induced Alfvén-acoustic eigenmode (BAAE), low frequency modes that have strong interactions with both thermal and energetic particles. When the ion temperature is comparable to the electron temperature, the unstable BAAE can be excited by realistic energetic particle density gradient, even though the damping rate of the BAAE (in the absence of energetic particles) is comparable to the real frequency. This is due to a smooth and broad radial mode structure of the unstable BAAE as compared to a singular mode structure of the damped BAAE. In the simulations with reversed magnetic shear, BAAE frequency sweeping is observed and poloidal mode structure has a triangle shape with a poloidal direction similar to that observed in tokamak experiments. By scanning the device size while keeping all other plasma parameters unchanged, we find that the BAAE dominates in the larger machine size (similar to ITER). For the smaller machine size, the dominant mode is BAE. At some machine size (similar to DIII-D tokamak), the BAE and BAAE can have the same growth rates, an interesting regime where BAE and BAAE can coexist and interact nonlinearly as demonstrated in the following nonlinear simulation.

The nonlinear simulation of the machine size where BAE and BAAE have the same growth rate has been carried out. Zonal fields are not included in this simulation. In the linear regime, BAAE and BAE coexist and have similar amplitudes. The mode structure is the superposition of BAE and BAAE. The BAE saturates first, followed by the saturation of the BAAE, which becomes dominant. The amplitudes of BAE and BAAE decrease significantly after saturation and various nonlinear modes including a very low frequency, a beat wave frequency, and its conjugate are successively excited. The BAE can later become dominant. In this long time simulation, the amplitudes of all these modes oscillate with certain phase shift, indicating energy exchanges between these linear and nonlinear modes. Furthermore, we have also performed nonlinear simulation with zonal fields included. Simulation results show that zonal flows reduce the saturation amplitudes of BAE, BAAE, and nonlinear modes.

TH



Gyrokinetic Particle Simulation of Fast-Electron Driven β -Induced Alfvén Eigenmodes

W. Zhang¹, J. Cheng^{1,2}, D. Li¹, W. Chen³, L. Yu³, and X. Ding³

¹*Institute of Physics, Chinese Academy of Sciences, Beijing 100190, People's Republic of China*

²*University of Science and Technology of China, Hefei, Anhui, People's Republic of China*

³*Southwestern Institute of Physics, Chengdu, Sichuan, People's Republic of China*

Corresponding Author: W. Zhang, wzhang@iphy.ac.cn

The fast electron driven β -induced Alfvén eigenmode (e-BAE) has been routinely observed in HL-2A tokamak. We study e-BAE for the first time using global gyrokinetic GTC simulation, where the fast electrons are described by the drift kinetic model. Frequency chirping is observed in nonlinear simulations in the absence of sources and sinks, which provide a new nonlinear paradigm beyond the standard “bump-on-tail” model. For weakly driven case, nonlinear frequency is observed to be in phase with particle flux, and nonlinear mode structure is almost the same as linear stage. In the strongly driven case, BAAE is also unstable and coexists with BAE after the BAE saturation. Analysis of nonlinear wave-particle interactions shows that the frequency chirping is induced by the nonlinear evolution of the coherent structures in the fast electron phase space, where the dynamics of the coherent structure is controlled by the formation and destruction of phase space islands in the canonical variables. Zonal fields are found to affect wave-particle resonance in the nonlinear BAE simulations through shearing effect to the structure of phase space islands. A verification and validation study is carried out for a sequence of fast-electron driven β -induced Alfvén eigenmode (e-BAE) in HL-2A tokamak plasma.

Global Gyrokinetic Simulation of Energetic Particle-Driven Instabilities in 3D Systems

D. Spong¹, I. Holod², Y. Todo³, and M. Osakabe³

¹*Oak Ridge National Laboratory (ORNL), Oak Ridge, TN 37831, USA*

²*University of California Irvine, CA 92697, USA*

³*National Institute for Fusion Science (NIFS), Toki, Gifu, Japan*

Corresponding Author: D. Spong, spongda@ornl.gov

Instabilities driven by energetic particle (EP) components are of interest to magnetic fusion concepts since they can lead to decreased heating efficiency, high heat fluxes on plasma-facing components, and decreased ignition margins in reactor systems. Since 3D magnetic field perturbations will be present to some extent in all toroidal configurations, the analysis of EP instabilities in 3D systems will be an important component of whole device modelling. To address this, the GTC global gyrokinetic PIC model has been adapted to the VMEC 3D equilibrium model, and 3D effects included in the field solvers and particle push. This model has been applied to several stellarators (LHD, W7-X, TJ-II) and tokamaks with 3D fields (NSTX with RWM). Also, a new code has been developed for the analysis of wave-particle resonance locations in phase space in 3D systems. The results indicate that Alfvén modes similar to those observed in LHD are obtained from the GTC simulations. The calculations also show a sensitivity as to which Alfvén gap mode is excited, depending on the shape of fast ion pressure profile. This feature allows diagnostic inferences for profiles, such as the fast ion pressure, that cannot be directly measured. Other parameter and profile sensitivities have been observed that are unique to 3D configurations. Initial nonlinear calculations have demonstrated the interplay between fast ion redistribution and zonal flows/currents in reaching a saturated state. Predicting the onset and effects of these instabilities is of significant importance due to their impact on heating efficiency, plasma-facing component heat loads, and possible diagnostic use. The importance of nonaxisymmetric effects in all toroidal devices motivates development of comprehensive new gyrokinetic simulation methods that can apply across the full range of symmetry-breaking perturbation levels.

Work supported by the U.S. Department of Energy under Contract DE-AC05-00OR22725 with UT-Battelle, LLC and the U.S. Department of Energy SciDAC GSEP Center. This research used the Oak Ridge Leadership Computing Facility at the Oak Ridge National Laboratory and the National Energy Research Scientific Computing Center which are supported by the U.S. Department of Energy Office of Science under Contract Numbers DE-AC05-00OR22725 and DE-AC02-05CH11231, respectively.



Simulations of Energetic Particle Driven Geodesic Acoustic Mode and Global Alfvén Eigenmode in 3D LHD Equilibrium

H. Wang¹, Y. Todo¹, and Y. Suzuki¹

¹*National Institute for Fusion Science (NIFS), Toki, Gifu, Japan*

Corresponding Author: H. Wang, wanghao@nifs.ac.jp

Energetic particle driven geodesic acoustic mode (EGAM) and Global Alfvén eigenmode (GAE) in a 3D Large Helical Device (LHD) equilibrium are investigated using MEGA code. MEGA is a hybrid simulation code for energetic particles interacting with a magnetohydrodynamic (MHD) fluid. It is found that the $n = 10$ harmonics of the 3D LHD equilibrium bring about the coupling between the $n = 0$ and 10 harmonics for the spatial profile of the EGAM. In addition to the EGAM with the frequency ~ 75 kHz, a GAE with the dominant harmonic $m/n = 1/0$ and the frequency ~ 480 kHz is discovered in the simulation. The emergence of the $n = 0$ GAE can be attributed to the avoidance of the continuum damping with the $n = 0$ shear Alfvén continua in the LHD plasma with the negative monotonic magnetic shear. In the nonlinear evolution, the frequency chirping of the EGAM, which is observed in the LHD experiments, and the frequency splitting of the GAE to the multiple peaks take place. The average of the poloidal flow takes a positive value, which indicates the generation of the negative radial electric field due to the redistribution of energetic ions.



A New Branch of Geodesic Acoustic Modes Driven by Fast Ions

M. Sasaki¹, N. Kasuya¹, Y. Kosuga², K. Itoh³, K. Hallatschek⁴, M. Lesur⁵, and S.-I. Itoh¹

¹*Research Institute for Applied Mechanics (RIAM), Kyushu University, Kasuga, Japan*

²*Institute for Advanced Study, Kyushu University, Kasuga, Japan*

³*National Institute for Fusion Science (NIFS), Toki, Gifu, Japan*

⁴*Max-Planck-Institut für Plasmaphysik, Garching, Germany*

⁵*Institut Jean Lamour, Université de Lorraine, CNRS, Nancy, France*

Corresponding Author: M. Sasaki, sasaki@riam.kyushu-u.ac.jp

A new branch of geodesic acoustic modes (GAMs) driven by the magnetic drift motion of fast ions is presented. An effective ion heating mediated by the new branch is expected. Strong ion Landau damping is attributed to the eigenfunction of the new branch, which has steep poloidal gradients. The analysis is based on a gyrokinetic model. The gyrokinetic equation for the fast ions has two kinds of resonances in accordance with the transit motion and the magnetic drift, which induces two unstable branches to appear. In a limit that the transit frequency is much larger than the magnetic drift frequency, a branch with the transit frequency of the fast ions appears, which has been investigated in previous studies. In this study, we focus on a limit that the magnetic drift resonance is dominant. The magnetic drift resonance is poloidally inhomogeneous, which is a typical feature. A dispersion relation of the GAMs that includes the magnetic drift resonance is derived, keeping the contributions from modes with arbitrary poloidal mode numbers. If one truncates the poloidal mode number at one, the previous theory is reproduced. The new branch is obtained, whose frequency is close to the magnetic drift frequency of the fast ions. The growth rate of the unstable branch takes the maximum when the magnetic drift frequency agrees with the ordinary GAM frequency. The poloidal eigenfunction has bump structures and phase shift, where the resonance is strong. The steep poloidal gradients, associated with the bump structure, increase the effective parallel wavenumber, which leads to an effective ion heating via Landau damping. The phase shift of the eigenfunction indicates particle and energy transfers.

TH



A Critical Gradient Model for Energetic Particle Transport from Alfvén Eigenmodes: GYRO Verification, DIII-D Validation, and ITER Projection

R. E. Waltz¹, E. M. Bass², and H. Sheng³

¹General Atomics, San Diego, CA 92186, USA

²University of California San Diego, CA 92093, USA

³Peking University, Haidian, Beijing, People's Republic of China

Corresponding Author: R. E. Waltz, waltz@fusion.gat.com

Local nonlinear gyrokinetic code GYRO simulations of energetic particle driven low- n Alfvén eigenmodes embedded in high- n microturbulence have motivated a local critical gradient model (CGM) for stiff energetic particle (EP) transport from Alfvén eigenmodes (AEs). The critical gradient in the EP density (or pressure) gradient identified by the local linear low- n AE growth exceeding the ion temperature gradient and trapped electron mode (ITG/TEM) linear rate at the same low- n was first found in GYRO simulations of ITER fusion alpha driven AEs. This recipe for the CGM has again been verified and made more precise by recent nonlinear GYRO simulations of a well studied neutral beam injected (NBI) DIII-D discharge (#146102) where about half the fast ions are lost from the inner half radius by AE induced transport. This CGM incorporated in the ALPHA EP density transport code, used in a previous ITER projection of AE fusion alpha losses, was validated by transported NBI pressure profile in good agreement with DIII-D experimental fast ion pressure profiles. Simulations using a recently developed kinetic (energy dependent) radial EP transport code EPtran illustrate the importance of EP drift orbit broadening of the critical gradient profile. A key focus of the new work to be presented is a generalization of the ALPHA code and the CGM to include simultaneous AE drive from (and transport of) fusion alphas and 1 MeV NBI EPs in a projection of ITER EP losses.

Work supported by the U.S. Department of Energy under Grants No. DE-FG02-95ER543091, DE-FC02-08ER549771,2.



Hybrid Simulations of Beam-Driven Fishbone and TAEs in NSTX

G. Fu¹, F. Wang¹, and D. Liu²

¹*Princeton Plasma Physics Laboratory (PPPL), Princeton, NJ 08540, USA*

²*University of California Irvine, CA 92697, USA*

Corresponding Author: G. Fu, fu@pppl.gov

Energetic particle modes and Alfvénic modes driven by super-Alfvénic beam ions were routinely observed in neutral beam heated plasmas on the National Spherical Torus Experiment (NSTX). These modes can significantly impact beam-ion transport, thus causing beam-ion redistribution and losses. In this paper we report on new self-consistent hybrid simulations of both fishbone instability and TAEs in NSTX plasmas using M3D-K code. First, linear simulations of beam-driven fishbone show that a new instability region appears for $q_{\min} > 1.35$ when plasma toroidal rotation is included. The corresponding fishbone mode structure has strong ballooning feature. Both passing and trapped beam particles contribute to the instability drive. Nonlinear simulation shows strong mode frequency chirping as beam ion distribute is substantially redistributed in radial direction. It is found that trapped particles are mainly responsible for the nonlinear frequency chirping although passing particles' instability drive is comparable to that of trapped particles. Second, nonlinear simulations of multiple beam-driven TAEs and the $n = 1$ fishbone have been carried out for the first time. The simulation results show strong interaction between multiple TAEs and fishbone that either enhances or reduces saturation level of individual modes due to overlap of wave particle resonances in phase space. Furthermore it is found that the mode saturation levels are very sensitive to q_{\min} . When q_{\min} drops below a critical value ~ 1.19 , the mode amplitudes increase sharply to large values. This result is similar to the observed transition to TAE avalanche as q_{\min} decreases in NSTX.

III



Coupling of Neutral-Beam-Driven Compressional Alfvén Eigenmodes to Kinetic Alfvén Waves in NSTX and Energy Channelling

E. Belova¹, N. N. Gorelenkov¹, N. Crocker², J. Lestz¹, E. Fredrickson¹, and K. Tritz³

¹*Princeton Plasma Physics Laboratory (PPPL), Princeton, NJ 08540, USA*

²*University of California Los Angeles, CA 90095, USA*

³*Johns Hopkins University, Baltimore, MD 21218, USA*

Corresponding Author: E. Belova, ebelova@pppl.gov

An energy channelling mechanism is proposed to explain flattening of the electron temperature profiles at high beam power in beam-heated National Spherical Torus Experiment (NSTX). High-frequency Alfvén eigenmodes are frequently observed in beam-heated NSTX plasmas, and have been linked to enhanced thermal electron transport and flattening of the electron temperature profiles. Results of 3D nonlinear self-consistent simulations of neutral-beam-driven compressional Alfvén eigenmodes (CAEs) in NSTX are presented that demonstrate strong coupling of CAE to kinetic Alfvén wave at the Alfvén resonance location. It is shown that CAE can channel significant fraction of the beam energy to the location of the resonant mode conversion at the edge of the beam density profile, modifying the energy deposition profile.



Nonlinear Excitation of Subcritical Fast Ion-Driven Modes

M. Lesur^{1,2}, K. Itoh^{3,4}, T. Ido³, S.-I. Itoh^{2,4}, Y. Kosuga^{2,3}, M. Sasaki², S. Inagaki^{2,3},
M. Osakabe^{3,5}, K. Ogawa^{3,5}, A. Shimizu³, and K. Ida^{3,5}

¹*Institut Jean Lamour, Université de Lorraine, CNRS, Nancy, France*

²*Research Institute for Applied Mechanics (RIAM), Kyushu University, Kasuga, Japan*

³*National Institute for Fusion Science (NIFS), Toki, Gifu, Japan*

⁴*Research Center for Plasma Turbulence, Kyushu University, Kasuga, Japan*

⁵*Graduate University for Advanced Studies (SOKENDAI), Hayama, Kanagawa, Japan*

Corresponding Author: M. Lesur, maxime.lesur@polytechnique.org

Energetic ions in fusion plasmas can excite the geodesic-acoustic mode (GAM), which is a finite-frequency counterpart of zonal flow. Depending on plasma conditions, GAMs can significantly enhance or mitigate transport. Therefore, understanding and controlling their excitation is of great interest. Recent observations on the LHD have revealed a new phenomenon of abrupt excitation of large-amplitude GAM, triggered by another, weaker GAM. In the present paper, we develop a theoretical model for the nonlinear interactions among fast ions and two coupled GAMs. The model is obtained by combining two descriptions: 1) the kinetic description of resonant interactions between fast ions and a GAM, and 2) the reduced description of modulational-parametric coupling between two GAMs. The model is able to recover key aspects of the experiment, with input parameters which are consistent with measured plasmas parameters and independent calculations. It provides a viable interpretation for the phenomenon of abrupt GAM excitation on LHD, as the result of a new kind of subcritical instability. This subcritical instability is a linearly stable mode which grows from a sustained collaboration between two kinds of nonlinearities: resonant particle trapping and wave-wave coupling. Our analysis suggests that a mechanism of synchronization between the periods of the two waves contributes to the abruptness of the subcritical growth. The model further predicts how this instability may be enhanced or mitigated. The abrupt GAM burst is important for fusion plasmas because of its increased amplitude and reduced frequency (compared to the triggering GAM), which should lead to a stronger coupling with thermal ions. The model can be straightforwardly adapted to other energetic particle-driven modes.

TH



On the Structure of Wave-Particle Interactions and Nonlinear Alfvénic Fluctuation Dynamics

X. Wang¹, S. Briguglio², M. Schneller³, P. Lauber¹, V. Fusco², C. Di Troia², G. Fogaccia², G. Vlad², and F. Zonca^{2,4}

¹Max-Planck-Institut für Plasmaphysik, Garching, Germany

²ENEA C. R. Frascati, Dipartimento FSN, Frascati, Italy

³Princeton Plasma Physics Laboratory (PPPL), Princeton, NJ 08540, USA

⁴Institute for Fusion Theory and Simulation (IFTS), Zhejiang University, Xihu, Hangzhou, Zhejiang, People's Republic of China

Corresponding Author: X. Wang, xwang@ipp.mpg.de

Shear-Alfvén modes can be driven unstable by energetic particles (EPs) produced by additional heating or nuclear fusion reactions. Alfvénic fluctuations can, in turn, be detrimental to EP confinement and lead large EP losses. Understanding the properties of EP confinement largely depends on the insights into Alfvén mode dynamics, with regard to both the linear stability properties; and the nonlinear dynamics, which have recently attracted significant interest both on theoretical and numerical analysis sides. In our work, nonlinear dynamics in intermediate regime between weakly driven AEs close to marginal stability and strongly driven energetic particle modes (EPMs) is investigated by means of the nonlinear hybrid magnetohydrodynamics gyrokinetic code (XHMGC) and compared to the hybrid LIGKA/HAGIS model. Saturation mechanism due to resonance detuning and/or radial decoupling are discussed. It will be shown that saturation field level exhibits a quadratic scaling with the growth rate, in the former case; a linear scaling, in the latter case. The dominance of one or the other mechanism depends on the linear properties of the mode. These fundamental results and scaling are crucial for any reduced or simplified EP transport model which is needed for fast and flexible predictive tools to be developed in the future. For EPMs, we analyze EPM saturation and the corresponding frequency chirping observed both in experiments and simulations (e.g., chirping electron-fishbone by XHMGC simulation). Phase locking has been proposed, within “fishbone” paradigm, to describe such chirping: the resonance condition with linearly resonant particles is maintained, while particles are radially displaced, through a continuous modification of the mode frequency. We show that an additional scenario is possible: mode radial localization and frequency appear to be locked to the shear Alfvén continuum; once the linear resonance population has exhausted its driving capability (because of local flattening of the phase-space distribution function), the mode is shifted to nonexhausted regions of the phase space. The effect is a succession of resonant excitations from different phase-space regions (each characterized by its own nonlinear evolution time), rather than mode adjustment to the evolution of the linearly-resonant particles.



On Excitation of Zonal Structures by Kinetic Alfvén Waves

L. Chen¹, F. Zonca², and Y. Lin³

¹Zhejiang University, Xihu, Hangzhou, Zhejiang, People's Republic of China

²Associazione EURATOM-ENEA Unitá Tecnica Fusione, Frascati, Italy

³Auburn University, Auburn, AL 36849, USA

Corresponding Author: L. Chen, liuchen@zju.edu.cn

Zonal flow (ZF) and zonal current (ZC) in fusion devices are manifestations of, respectively, electrostatic (ESCC) and magnetostatic (MSCC) convective cells in uniform plasmas. Similarly, kinetic Alfvén waves (KAW) appear as kinetic Alfvén eigenmodes (KAE) due to the presence of Alfvén continuum. Employing this paradigm, we have investigated the spontaneous excitation of CC via modulational instabilities induced by a finite-amplitude pump KAW both analytically and by numerical simulations. Our results demonstrate that kinetic finite ion Larmor radius (FILR) effects play crucially important roles in the excitation mechanism. More specifically, we have found that i) spontaneous excitation only sets in when both the pump KAW and the CC have perpendicular wavelengths comparable to the ion Larmor radius, and ii) both ESCC (ZF) and MSCC (ZC) are excited simultaneously. Results of fluid-electron and Vlasov-ion hybrid simulations show good agreements with analytical predictions. Implications to ZF/ZC excitations by KAEs in laboratory fusion devices will also be discussed.

Nonlinear Excitation of Fine-Structure Zonal Flow by Alfvén Eigenmodes

Z. Qiu¹, L. Chen^{1,2}, and F. Zonca^{3,1}

¹Zhejiang University, Xihu, Hangzhou, Zhejiang, People's Republic of China

¹University of California Irvine, CA 92697, USA

³ENEA C. R. Frascati, Dipartimento FSN, Frascati, Italy

Corresponding Author: Z. Qiu, zqiu@zju.edu.cn

Theory of low-frequency zonal structure (LFZS) generation as one mechanism for Alfvén eigenmode (AE) nonlinear saturation is presented, including 1) spontaneous excitation of LFZS by β -induced AE (BAE) via modulational instability, and 2) effects of energetic particles (EPs) on zonal flow (ZF) generation by toroidal AE (TAE). It is found that LFZS can be driven by a finite-amplitude BAE when the threshold condition due to frequency mismatch is exceeded, and the ZF growth rate depends on the BAE amplitude. Electrostatic ZF instead of zonal magnetic field is predominantly excited as the pump BAE is close to kinetic thermal ion induced shear Alfvén continuum gap. The excited ZF has both the usual meso-scale radial envelope structure, and a fine radial structure due to the BAE localization around mode rational surfaces. More significantly, the presence of the ZF fine structure significantly enhances the nonlinear couplings between ZF and BAE, leading to a much lower threshold condition on BAE amplitude. The obtained ZF radial electric field is an even function at the peak of radial envelope, consistent with numerical simulation. Effects of EPs on ZF generation by TAE have been investigated, showing that EP effects can qualitatively modify the process of ZF generation. It is found that nonlinear EP contribution in the ideal region dominates over the usual Reynolds and Maxwell stresses from thermal plasma contribution in the inertial layer. Due to the contribution of resonant EPs, ZF can be forced driven by TAE, with a growth rate being twice that of TAE. The ZF generation mechanism is shown to relate to EP quasilinear diffusion induced polarization. Similar to the BAE case, the driven ZF, has both the usual meso-scale radial envelope structure, as well as fine-scale structures due to the anti-Hermitian part of TAE mode structure associated with resonant EPs. This forced driven process is essentially thresholdless such that ZF can be generated in the linear growth stage of TAE, and may have important consequences on the nonlinear mode dynamics. A nonlinear model has been constructed to study TAE nonlinear saturation due to forced driven ZF, and different dynamics is observed in different parameter regimes.

Towards a Self Consistent Evaluation of the RF Wave-Field and the Ion Distribution Functions in Tokamak Plasmas

N. Bertelli¹, E. J. Valeo¹, J. Lee², P. T. Bonoli², M. Gorelenkova¹, D. Green³, E. F. Jaeger⁴, C. Phillips¹, and J. C. Wright²

¹Princeton Plasma Physics Laboratory (PPPL), Princeton, NJ 08540, USA

²Plasma Science & Fusion Center, MIT, Cambridge, MA 02139, USA

³Oak Ridge National Laboratory (ORNL), Oak Ridge, TN 37831, USA

⁴XCEL Engineering Inc., Oak Ridge, TN 37830, USA

Corresponding Author: N. Bertelli, nbertell@pppl.gov

The injection of fast waves (FW) in the ion cyclotron range of frequency (ICRF) is a well-established method of heating and driving current in magnetically confined toroidal plasma and it will play an important role in the ITER experiment. Taking into account self-consistently the interaction of FW with both the minority ion population and fast-ion/neutral-beam populations is a crucial aspect to more faithfully modelling and understanding of experimental results and to more accurately designing future devices. This paper examines precisely this aspect combining the evaluation of the wave-field, through a full wave solver, with the ion distribution function provided by either a Monte Carlo particle or Fokker-Planck codes. The recent extension of TORIC v.5 to include non-Maxwellian distribution functions (both in minority and high harmonic heating regimes) is employed in this work. First, for the case of the thermal distribution function, the extended TORIC v.5 has been verified against the standard TORIC v.5 showing an excellent agreement both in IC minority and high harmonic fast wave (HHFW) heating regimes. Second, an implementation of the bi-Maxwellian and slowing down analytical distributions has also been done. The application of such distributions shows different behaviour in the total absorbed power between the IC minority and HHFW heating regimes. In particular, for IC minority heating regime, the total absorbed power at the H fundamental is insensitive to variations in the perpendicular temperature, but varies with changes in parallel temperature, whereas for HHFW regime, the behaviour is the other way around, although power deposition profile varies with changes in the parallel temperature. Third, a comparison of the wave electric field and the power deposition profile with a slowing-down and a numerical distribution function obtained from the Monte Carlo NUBEAM module is presented and discussed. First attempts to apply the close iterative loop between the extension of TORIC v.5 in a self-consistent way and the NUBEAM module are also discussed and presented. Finally, for the IC minority regime, a self-consistent distribution function will be then obtained by iterating TORIC v.5 and the Fokker-Planck code QQL3D through the quasilinear diffusion coefficients, which has been recently derived and implemented in TORIC v.5, and the non-Maxwellian dielectric tensor.



A Fully-Neoclassical Finite-Orbit-Width Version of the CQL3D Fokker–Planck Code

Y. Petrov¹, R. W. Harvey¹

¹*CompX, Del Mar, CA 92014, USA*

Corresponding Author: Y. Petrov, petrov@compxco.com

The finite-difference bounce-average Fokker–Planck (FP) code CQL3D [1] has been upgraded to include the Finite-Orbit-Width (FOW) effects. This is achieved by transforming the FP equation written in canonical action variables to another set of constant-of-motion (COM) coordinates. A distinctive feature of our approach from that used by other authors is the selection of the major radius at the equatorial plane as one of the COM coordinates, i.e., we adopt $I = (R_0, u_0, \theta_0)$ as the COM coordinates. Here, R_0 is the major radius coordinate along the equatorial plane (the midplane of tokamak, in case of up-down symmetrical equilibrium). For each given R_0 point, the value of particle speed (momentum-per-mass) u_0 and value of the pitch-angle θ_0 at this point determine a unique orbit. The banana regime neoclassical radial transport appears naturally in the FOW version by averaging the local collision coefficients along guiding centre orbits, with a proper transformation matrix from local (R, Z) coordinates to the midplane computational coordinates, where the FP equation is solved. In a similar way, the local quasilinear RF diffusion terms give rise to additional radial transport of orbits. The FOW modifications are implemented in the formulation of the neutral beam source, collision operator, RF quasilinear diffusion operator, and in synthetic particle diagnostics. The CQL3D-FOW version is applied to simulation of ion heating in NSTX plasma. It is demonstrated that it can describe the physics of transport phenomena in plasma with auxiliary heating, in particular, the enhancement of the radial transport of fast ions by RF heating and the occurrence of the bootstrap current. Because of the bounce-averaging on the FPE, the results are obtained in a relatively short computational time. A typical run time is 30 min using 140 MPI cores. Due to an implicit solver, calculations with a large time step (tested up to $dt = 0.5$ s) remain stable.

References

[1] R. W. Harvey and M. McCoy, “The CQL3D Fokker–Planck Code”, General Atomics Report GA-A20978, (1992).



Nonlinear Particle Simulation of Radio Frequency Waves in Tokamak

J. Bao^{1,2}, A. Kulev^{2,3}, X. Wei⁴, Z. Lin², Y. Xiao⁴, and W. L. Zhang⁵

¹*Fusion Simulation Center, Peking University, Haidian, Beijing, People's Republic of China*

²*University of California Irvine, CA 92697, USA*

³*Xiamen University, Xiamen, People's Republic of China*

⁴*Institute for Fusion Theory and Simulation (IFTS), Zhejiang University, Xihu, Hangzhou, Zhejiang, People's Republic of China*

⁵*Institute of Physics, Chinese Academy of Sciences, Beijing 100190, People's Republic of China*

Corresponding Author: J. Bao, baojian@pku.edu.cn

In this work, we present a fully nonlinear electromagnetic particle simulation model for RF wave in the toroidal geometry, which has been successfully implemented in the gyrokinetic toroidal code (GTC). In this electromagnetic simulation model, the ion dynamics is described by 6D Vlasov equation and the electron dynamics is described by 5D drift kinetic equation. The ion cyclotron orbit is integrated by the Boris method, which has the advantage of energy conservation with long simulation time duration. Nonlinear particle simulations of radio frequency waves in tokamak have been carried out for the first time with a real electron-to-ion mass ratio. Linear simulation of the lower hybrid (LH) wave-packet in the tokamak shows that the wave propagates faster in the high field side than the low field side, in agreement with a ray tracing calculation. Global electromagnetic simulation confirms that the toroidicity induces an upshift of parallel reflective index when LH waves propagate from the tokamak edge toward the core, which modifies the radial position for the mode conversion between slow and fast LH waves. Furthermore, moving LH antenna launch position from low field side toward high field side leads to larger upshift of the parallel reflective index, which helps the slow LH wave penetration into the tokamak core. The broadening of the poloidal spectrum of the wave-packet due to wave diffraction is also verified in the simulation of the LH wave propagation. Both the upshift and broadening effects of the parallel spectrum of the wavepacket modify the parallel phase velocity and thus the linear absorption of LH waves by electrons Landau resonance. In the nonlinear simulation of ion Bernstein wave (IBW) in a tokamak, parametric decay instability (PDI) is observed where a large amplitude pump wave decays into an IBW sideband and an ion cyclotron quasimode (ICQM). The ICQM induces an ion perpendicular heating, with a heating rate proportional to the pump wave intensity. Finally, in the electromagnetic LH simulation, nonlinear wave trapping of electrons is verified and a plasma current is nonlinearly driven.

TH

Kinetic Simulations of the Full O-X-B Mode Conversion Process and the Deteriorating Effect of High Power Levels

A. V. Arefiev¹, E. Du Toit², A. Köhn³, E. Holzhauer⁴, V. Shevchenko⁵, and R. G. L. Vann²

¹Institute for Fusion Studies (IFS), University of Texas at Austin, Austin, TX 78712, USA

²University of York, Heslington, UK

³Max-Planck-Institut für Plasmaphysik, Garching, Germany

⁴Institut für Grenzflächenverfahrenstechnik und Plasmatechnologie (IGVP), Univ. Stuttgart, Germany

⁵Culham Centre for Fusion Energy (CCFE), Culham Science Centre, Abingdon, UK

Corresponding Author: A. V. Arefiev, alexey@austin.utexas.edu

High-performance spherical tokamaks are usually overdense, so regular electron cyclotron emission is blocked. However, electron Bernstein waves, generated at the local cyclotron frequency (and its harmonics) in the core may be observed outside the plasma via a mode conversion process that takes place typically in the plasma edge between an electromagnetic mode and the (electrostatic) electron Bernstein wave. Understanding the details of this mode conversion process is important in tokamaks with over-dense plasmas both for the interpretation of microwave diagnostic data and to assess the feasibility of EBW heating and/or current drive. To this end, we have performed the first ever 2D fully kinetic simulations of O-X-B mode conversion using the particle-in-cell code EPOCH. In addition to benchmarking these numerical results against the linear dispersion relation [1], we have also investigated nonlinearities associated with a larger incident intensity and the effect of a steeper (and more realistic) density gradient at the mode conversion layer. Simulations were performed on the HELIOS supercomputer at the IFERC-CSC, Rokkasho, Japan and on TACC supercomputers at the University of Texas at Austin, USA.

References

[1] A. V. Arefiev, *et al.*, AIP Conf. Proc. **1689**, 090003 (2015).



Integration of Core/Edge Plasmas in Fullwave RF Simulation

S. Shiraiwa¹, J. C. Wright¹, J. P. Lee¹, and P. T. Bonoli¹

¹*Plasma Science & Fusion Center, MIT, Cambridge, MA 02139, USA*

Corresponding Author: S. Shiraiwa, shiraiwa@psfc.mit.edu

A new efficient full wave simulation approach to solve a driven RF waves problem in hot core and edge SOL plasmas self-consistently is presented. Existing RF simulation codes are integrated to reconstruct self-consistent solutions from solutions obtained from each code. The approach allows for treating hot core plasma, SOL plasmas and launcher structure self-consistently, incorporating complicate 3D antenna structure, and potentially solving driven RF problem in ICRF waves, LH waves, HHFW/Helicon waves with a universal method.

Full wave modelling has been made significant progress in understanding both driven RF waves in core plasma and plasma-antenna coupling. However, in those simulations, the hot core plasma and edge SOL plasmas are solved as separate problems. In the core region, a spectral representation of wave field is used, which allows for accurate formulation of the dielectric plasma response but the region between the launcher and the separatrix was modelled poorly or not at all. In the edge, the simulation models often focusses on a small region in front of the launcher and the core plasma effects are introduced as perfectly radiating boundary or surface impedance. Extending an existing code to treat an entire simulation domain has not been straightforward mainly because, while in core plasma spectral decomposition of the wave field is required to properly treat hot dielectric tensor retaining complicated 3D geometry such as antenna structure and divertor is needed for accuracy which is incompatible with a spectral representation.

In our approach, we solved the core region and edge regions by TORIC spectral solver and COMSOL finite element package, respectively. The RF electric field on the boundary between core and edge regions is decomposed using spectral modes, and for each region we solve the RF field for all modes. A self-consistent solution is obtained from mode solutions in such a way that continuity of tangential RF fields at the core/edge boundary is satisfied. In this paper, details of formulation and numerical implementation/verification, a comparison of H minority heating and mode-conversion heating on C-Mod and 3D antenna simulation with hot plasma load are presented.

Work supported by the U.S. Department of Energy, Contract No. DE-FC02-99ER54512 on Alcator C-Mod, a Department of Energy Office of Science user facility, and DOE DE-FC02-01ER54648



Toroidal Electromagnetic Particle-in-Cell Code with Gyro-kinetic Election and Fully-kinetic Ion

J. Lin^{1,2}, P. Liu^{1,2}, W. Zhang^{1,2}, and D. Li²

¹University of Science and Technology of China, Hefei, Anhui, People's Republic of China

²Institute of Physics, Chinese Academy of Sciences, Beijing 100190, People's Republic of China

Corresponding Author: J. Lin, jblin@mail.ustc.edu.cn

Current drive and auxiliary heating is critical for fusion plasmas. A kinetic simulation model has been developed using gyro-kinetic electron and fully-kinetic ion by removing fast gyromotion of electrons using the Lie-transform perturbation theory. A particle-in-cell kinetic code is developed based on this model in general magnetic flux coordinate systems, which is particularly suitable for simulations of toroidally confined plasma. Single particle motion and field solver are successfully verified respectively. Integral electrostatic benchmark, for example the lower-hybrid wave (LHW) and ion Bernstein wave (IBW), shows a good agreement with theoretical results. Preliminary electromagnetic benchmark of fast wave at lower hybrid frequency range is also presented. This code could be a first-principal tool to investigate high frequency nonlinear phenomenon, such as parametric decay instability, during lower-hybrid current drive (LHCD) and ion cyclotron radio frequency heating (ICRF) with complex geometry effect included.



Scattering of Radio Frequency Waves by Density Fluctuations in Tokamak Plasmas

A. Ram¹, K. Hizanidis², Z. Ioannidis^{3,4}, and I. Tigelis³

¹*Plasma Science & Fusion Center, MIT, Cambridge, MA 02139, USA*

²*National Technical University of Athens, Greece*

³*National and Kapodistrian University of Athens, Greece*

⁴*Karlsruhe Institute of Technology (KIT), Karlsruhe, Germany*

Corresponding Author: A. Ram, abhay@mit.edu

In tokamak fusion plasmas, coherent, intermittent, fluctuations in the form of blobs or filaments and incoherent fluctuations due to turbulence are routinely observed in the scrape-off layer. Radio frequency (RF) electromagnetic waves, commonly used for heating the plasma and for providing noninductive plasma current, are excited by antenna structures placed near the wall of a tokamak. These waves have to propagate through the scrape-off layer before reaching the core of the plasma. While the effect of fluctuations on RF waves has not been quantified experimentally, there are telltale signs, arising from differences between results from simulations and from experiments, that fluctuations can modify the spectrum of RF waves. We have pursued pioneering theoretical studies and complementary computer simulations so as to elucidate the impact of fluctuations on RF waves. These studies, using the full complement of Maxwell's equations for cold, magnetized plasmas, show that the Poynting flux in the wake of a filament, or a blob, develops spatial structure due to diffraction and shadowing. The uniformity of power flow into the plasma is affected by modifications to the wave spectrum as a result of side-scattering, and the coupling of power to plasma waves different from the incident RF wave. For propagation through turbulent fluctuations, Snell's law and Fresnel equations have been formulated within the context of stratified, magnetized plasmas. The corresponding theory is distinctly different from its counterpart in scalar dielectric media, and reveals new and salient physical insight into the scattering of RF waves. All of these studies apply to the scattering of RF waves in any frequency range and for arbitrary variations in plasma density. In ITER, electron cyclotron waves will be used to stabilize the deleterious neoclassical tearing mode by providing current in the island region. In order to ensure that the waves provide plasma current with high efficiency within the appropriate spatial locations, it is imperative to understand the spatial and spectral effects of fluctuations on the propagation of electron cyclotron waves. The studies reported in this paper are a requisite and critical advances in that particular direction.

TH



Verification of a Configuration Space Method for Evaluating the All-Orders Linear Kinetic Plasma Response to RF Power

D. Green¹, E. F. Jaeger², and L. Berry²

¹*Oak Ridge National Laboratory (ORNL), Oak Ridge, TN 37831, USA*

²*XCEL Engineering Inc., Oak Ridge, TN 37830, USA*

Corresponding Author: D. Green, greendl1@ornl.gov

Linear kinetic solvers are the workhorse tools for predicting the core plasma response to applied radio-frequency (RF) power in magnetically confined fusion devices. These codes are typically frequency-domain spectral, or a combination of spectral and finite-element that require the inversion of a large, dense, or block-dense, ill-conditioned double complex matrix. On the engineering side of the RF system are the antenna codes used in designing the high power antennas. These linear cold-plasma solvers have a frequency (but not wave vector) dependent anisotropic dielectric, that is straight forward to implement in methods that allow geometry conforming meshes. To address the issues of designing RF launching structures that minimize plasma-material interactions, it has become evident that an antenna-to-core simulation capability that resolves both the geometric fidelity of the plasma facing components, and the kinetic physics of the confined plasma is required. Various couplings of antenna and core codes are being developed to allow prediction of the complete antenna-to-core problem. Such couplings are required due to the present lack of a solver that can support a geometry conforming mesh, kinetic physics where required, and is computationally tractable in 3D geometries. Here we present a verification of a computational kernel for evaluating the kinetic plasma current that will ultimately provide the kinetic plasma current operator, in an operator-split algorithm whose scaling properties will allow 3D kinetic calculations at both the high fidelity and on arbitrary meshes for the first time. The kernel is based on a configuration space evaluation of the solution to the linearized Vlasov equation, which not only removes the restrictions of the Fourier spectral method, but also includes additional physics such as violations of the stationary phase assumption. For verification of perpendicular ion kinetics, we choose the 1D fast-wave to ion-Bernstein-wave case. This problem requires the algorithm to resolve perpendicular ion kinetics; with parallel electron kinetics already being verified. We solve the problem with the AORSA for the reference solution. A successful verification for perpendicular ion kinetics is shown where the kernel reproduces the AORSA plasma current, given the AORSA wave-electric field as input.



An Improved RF-Sheath Boundary Condition and Implications for ICRF Modelling

J. Myra¹, H. Kohn²

¹*Lodestar Research Corporation, Boulder, CO 80301, USA*

²*Kyushu Institute of Technology, Kitakyushu, Fukuoka, Japan*

Corresponding Author: J. Myra, jmyra@lodestar.com

Heating and current drive by ion cyclotron range of frequency (ICRF) waves is expected to play an increasingly important role as tokamak research progresses towards the reactor regime. The basic heating and current drive interactions of ICRF waves with the core plasma are well understood, and sophisticated modelling tools are available. In contrast, the ability to understand, predict and control ICRF interactions with the scrape-off layer plasma is relatively poor. To improve the fidelity of global ICRF codes for this purpose, a newly improved sheath boundary condition has been formulated. Extending previous work, which employed a capacitive limit, the new boundary condition generalizes the formulation to a complex sheath impedance which additionally describes the effective sheath resistance at RF frequencies. The latter is important for modelling localized RF power deposition which could potentially cause damaging plasma material interactions. A generalized sheath model has been developed and is described by four dimensionless parameters: the degree of sheath magnetization, the magnetic field angle with the surface, the RF field strength and the degree of ion mobility set by the wave frequency. Complete characterization of the sheath impedance in this parameter space using fits and interpolations is in progress with the goal of a self-contained package that can be used in global RF codes to describe boundary interactions. The special case where the magnetic field is normal to the surface has been completed. The theory conserves energy between sheath dissipation and the waves. In the (low SOL density) case of propagating slow waves, the fraction of power absorbed by the sheath can be calculated. In the opposite regime of evanescent slow waves, the complex sheath impedance provides dissipation for the sheath-plasma wave resonance. Testing and verification of the boundary condition in slab geometry using numerical codes is in progress.

TH



Low-Threshold Two-UH-Plasmon Decay as a Reason for Anomalous Backscattering and Absorption in Second Harmonic ECRH Experiments

E. Z. Gusakov¹, A. Yu. Popov¹

¹*Ioffe Institute, St. Petersburg, Russian Federation*

Corresponding Author: E. Z. Gusakov, evgeniy.gusakov@mail.ioffe.ru

A model interpreting generation of the anomalous backscattering signal in the second harmonic X-mode ECRH experiments at TEXTOR as a secondary nonlinear process, which accompanies a primary low-threshold parametric decay instability (PDI) leading to excitation of two-upper hybrid (UH)-plasmon trapped in plasma is introduced. The primary absolute PDI enhancing the UH wave fluctuations from the thermal noise level is supposed to be saturated due cascade of secondary low-threshold decays of the daughter UH waves leading to excitation of the secondary UH waves down-shifted in frequency and the ion Bernstein waves. A set of equations describing the cascade is derived and solved numerically. The results of numerical modelling are shown to be in agreement with analytical estimations of the growth rates of the initial and secondary parametric decays and the saturation level. The generation of backscattering signal is explained by coupling of daughter UH waves. The fine details of the frequency spectrum of the anomalously reflected X-wave and the absolute value of the observed backscattering signal in 2nd harmonic X-mode ECRH experiments at TEXTOR are reproduced. The level of anomalous absorption due to the PDI is estimated as 25%. The mechanism as well explains the anomalous ion heating at TCV and TJ-II by the generation of the secondary IB waves which directly transfer the pump power to the ion component.



High-Performance Computational Modelling of Plasma-Surface Interactions and RF Antennas

T. Jenkins¹, D. Smithe¹

¹*Tech-X Corporation, Boulder, CO 80303, USA*

Corresponding Author: T. Jenkins, tjenkins@txcorp.com

The heating of confined tokamak plasma to fusion-relevant temperatures can cause sputtering of high- Z impurities from plasma-facing components, and such impurities radiatively cool the plasma, especially as transport effects carry them to the reactor core. The sputtering process is believed to be exacerbated by the large electromagnetic fields generated by RF antennas, since these fields alter the dynamics of sheaths that form on antenna components in contact with plasma. Recent advances in finite-difference time-domain (FDTD) modelling techniques [1] enable the physics of localized sheath potentials to be modelled concurrently with the physics of antenna near- and far-field behaviour and RF power flow. When implemented on high-performance computing platforms, such techniques enable the study of plasma-surface interactions in realistic experimental ion-cyclotron resonance heating scenarios at previously inaccessible levels of resolution. We will present results and 3D animations of high-performance (10k–100k core) FDTD simulations of Alcator C-Mod's field-aligned ICRF antenna on the Titan supercomputer, considering a) sputtering and impurity production, as driven by self-consistent sheath potentials at antenna surfaces; b) the use of localized dielectric coating material on antenna components, as a design-based impurity mitigation strategy, and c) the physics of slow wave excitation in the immediate vicinity of the antenna hardware and in the scrape-off layer for various edge densities.

References

[1] T. G. Jenkins and D. N. Smithe, *Plasma Sources Sci. Technol.* **24**, 015020 (2015).

Work supported by the U.S. Department of Energy, Office of Science, Office of Fusion Energy Sciences, under Award Numbers DE-FC02-08ER54953 and DE-SC0009501. This research used resources of the Oak Ridge Leadership Computing Facility at the Oak Ridge National Laboratory, which is supported by the Office of Science of the U.S. Department of Energy, Contract No. DE-AC05-00OR22725.



Parallel Momentum Transport Induced by RF Waves and by Plasma Turbulence

Z. Gao¹, J. Chen², and Y. Li^{1,3}

¹*Tsinghua University, Haidian, Beijing, People's Republic of China*

²*Institute of Plasma Physics, Chinese Academy of Sciences, Hefei, Anhui, People's Republic of China*

³*Southwestern Institute of Physics, Chengdu, Sichuan, People's Republic of China*

Corresponding Author: Z. Gao, gaozhe@tsinghua.edu.cn

Generation of plasma toroidal flow with or without low momentum input has been attracted much attention due to the key issue of plasma rotation on MHD stabilization and turbulence regulation. The general momentum equation is reached with a generalized ponderomotive force and then the drive and transport of parallel momentum are discussed in the case of RF injection and/or in the drift-wave turbulence background.

With the injection of RF waves, a generalized ponderomotive force exerts on the plasma, which includes three parts. Firstly, the inhomogeneity of RF field results in the conventional ponderomotive force, which is nonresonant, but only in the direction of the inhomogeneity. Secondly, the wave-particle resonant interaction produces a dissipative drive force (DDF), in which the wave deposits the momentum on resonant particles like the well-known process of photon absorption. Thirdly, the inhomogeneity of resonant wave-particle interaction can induce a resonant momentum redistribution, which is called resonant ponderomotive force (RPF). The DDF and its induced radial flux can be used to explain the flow drive during the injection of low hybrid waves; while the parallel RPF might be responsible to the strong rotation in the experiment of the ion-cyclotron-frequency mode-conversion flow drive.

The inhomogeneity of plasma profile can be integrated in the theory. For RF-driven case, this only contributes an additional factor in the local energy absorption rate without changing the expressions and the physical pictures of the RF forces. However, the theory can also be applied to study the momentum transport in turbulence background. By rearranging the terms, it is found that the residual stress is indeed the pinch effect of parallel resonant velocity. The ion parallel momentum source term is the resonant parallel momentum transfer rate between resonant ions and waves. Then the conservation of the parallel momentum of resonant ions and waves is clearly presented.

Work supported by NSFC, under Grant Nos. 11325524 and 11261140327, and MOST of China, under Contract Nos. 2013GB112001.



Isotopic Effect of Parametric Instabilities during Lower Hybrid Waves Injection into Hydrogen/Deuterium Plasmas

A. Zhao¹, Z. Gao¹

¹*Tsinghua University, Haidian, Beijing, People's Republic of China*

Corresponding Author: A. Zhao, zhaoaihui@sunist.org

The lower hybrid current drive (LHCD) is one of the most effective tools for driving current in present tokamak plasmas. However, for reactor-graded density plasmas, the efficiency of LHCD degrades dramatically. The dependence of LHCD efficiency on isotopic plasma content (hydrogen/deuterium) was studied in experiments. Although according to the linear dispersion theory, the deuterium plasma could increase the linear LH resonance density, but the observed density limit for LHCD generation in deuterium plasma experiments did not increase obviously as expected. Further experiments showed that parametric instabilities (PI) may play an important role in LHCD switch-off. So in this work, we will try to give a theoretical study of isotopic effect of parametric instabilities during lower hybrid waves injection into hydrogen/deuterium plasmas.

Based on the local dispersion relation of the PI, the numerical results are compared in hydrogen and deuterium plasmas under typical SOL parameters. The calculation results show that for isotopic plasmas the unstable regions of growth rates are close. The maximum growth rates corresponding to the ion sound quasimode (ISQM) have a little difference, while the second maximum growth rates corresponding to the ion cyclotron quasimode (ICQM) are nearly the same. These numerical results can be understood by the analytical approximation from the fluid model. For different parameters, such as density, temperature and magnetic field, the growth rates of the ICQM are calculated for isotopic plasmas. It shows that the ICQM growth rates increase with the increasing densities and the decreasing temperatures and magnetic fields for both hydrogen and deuterium plasmas.

TH



Temperature Anisotropy in Magnetized Fusion Plasma

A. Sid¹, A. Benahmed¹, and A. Ghezal²

¹*Batna University, Batna, Algeria*

²*Commissariat à l'Énergie Atomique (COMENA), Alger, Algeria*

Corresponding Author: A. Sid, a_sid@univ-batna.dz

In the present work, the electronic distribution function for high magnetized hot plasma, taking into account the electron ion collisions, is explicitly calculated. The basic equation in this investigation is the Fokker-Planck equation where some justified approximations for fusion and astrophysical magnetized plasmas are used. By computing the second moment of the distribution function, we have expressed the electrons temperatures in the parallel direction and in the perpendicular plane to the magnetic field. It has been shown that this temperature is anisotropic and this anisotropy is due to competition between magnetic field effect and collision effect.



Progress towards Self-Consistent Treatment of Turbulence in Edge Plasma Modelling Codes

P. Tamain¹, H. Bufferand¹, C. Baudoin¹, G. Ciraolo¹, C. Colin², D. Galassi², P. Ghendrih¹, Y. Marandet³, N. Nace¹, F. Schwander², and E. Serre²

¹*Institut de Recherche sur la Fusion par confinement Magnétique (IRFM),*

Commissariat à l'énergie atomique (CEA/Cadarache), 13108 Saint-Paul-lès-Durance, France

²*Laboratoire de Mécanique, Modélisation & Procédés Propres (M2P2), Aix-Marseille Université, France*

³*Physique des Interactions Ioniques et Moléculaires (PIIM), CNRS, Aix-Marseille Université, France*

Corresponding Author: P. Tamain, patrick.tamain@cea.fr

Mean-field transport codes are the key tools for the understanding of scrape-off layer and divertor regimes. They rely on models in which simple closures are used to model average fluxes and stresses due to fluctuations. In particular, turbulent transport is commonly described via a gradient-diffusion hypothesis and ad-hoc diffusion coefficients. However, these coefficients differ from one case to the other and must be considered as free parameters, which reduces drastically the predictive capabilities of these codes.

We here report progress made towards allowing a self-consistent treatment of turbulent transport in edge modelling codes. We consider two ways forward: on the one hand, direct numerical simulation of turbulence in 3D global simulations; on the other hand, innovative ideas to refine the description of transverse transport in mean-field transport codes and improve their predictive capabilities. This work is made possible by the joint exploitation of a 2D mean field code and a 3D global turbulence code, namely SOLEDGE2D and TOKAM3X

In a first part, we report the latest advances of these tools. We first present recent upgrades of the SOLEDGE2D-EIRENE plasma and neutrals solver. Multifluid equations for impurities as well as drifts have now been implemented. These new capabilities are illustrated by applications to the modelling of ASDEX, WEST and TCV in a snow-flake configuration. Concerning TOKAM3X, two major advances have been achieved: simulations in X-point geometry have been performed and the code has been successfully coupled to the EIRENE kinetic neutrals code. We will show how the X-point impacts the properties of edge turbulent transport while preserving the main features observed in limited simulations. We will also present first results on the mutual interaction between fluctuations and atomic physics.

We finally propose a novel approach to the modelling of transverse transport in mean field codes. The new model transposes to magnetized plasmas k-epsilon turbulence models long used in computational fluid dynamics. It depends on more universal parameters than gradient-diffusion closures and is able to capture key properties of edge turbulence physics. As a first step, we show how a simplified k-epsilon model allows one to recover self-consistently the ballooning properties of radial turbulence transport and the related asymmetric flows.



Scrape-Off-Layer Turbulence in Tokamaks Simulated with a Continuum Gyrokinetic Code

A. Hakim¹, E. Shi², I. Abel², G. Hammett¹, and T. Stoltzfus-Dueck²

¹Princeton Plasma Physics Laboratory (PPPL), Princeton, NJ 08540, USA

²Princeton University, Princeton, NJ 08544, USA

Corresponding Author: A. Hakim, ahakim@pppl.gov

We present a new gyrokinetic code, Gkeyll, for use in edge plasma simulations. The code implements energy conserving discontinuous Galerkin schemes, applicable to a general class of Hamiltonian equations. Several applications of our code to various test problems are presented. We compute the parallel heat-flux on divertor plates resulting from an ELM crash in JET, for a 1D/1V SOL scenario explored previously, where the ELM is modelled as a time-dependent intense upstream source, and walls modelled with using sheath boundary conditions. We simulate bad-curvature-driven ETG turbulence, running the full-F nonlocal code in a periodic local limit, illustrating $3x/2v$ capability. We will show results from simulating turbulence in an SOL in a simplified helical open-field-line geometry with the bad curvature drive, which is useful for demonstrating the feasibility of this approach and for initial physics studies of SOL turbulence. The inclusion of magnetic fluctuations with kinetic electrons has been challenging for many gyrokinetic algorithms in the past, requiring special treatment to reduce the Ampere cancellation problem. An important feature of this work is that we have developed novel versions of DG that can handle gyrokinetic magnetic fluctuations in an efficient way while preserving the energy invariant. We developed a novel version of DG that uses Maxwellian-weighted basis functions while still preserving exact particle and energy conservation. At a fixed error, the Maxwellian-weighted DG method achieves the same error with four times less computational cost, or 16 times lower cost in the two velocity dimensions of gyrokinetics (assuming memory bandwidth is the limiting factor). Finally, we have derived the adjoint of the gyrokinetic equation, which can be used for various purposes, including studying the fastest-growing instantaneous configuration due to non-normal modes (related to subcritical nonlinearly-sustained turbulence).

Growth Estimates, Control and Structures in a Two-Field Model of the Scrape-Off Layer

J. P. S. Bizarro¹, R. Vilela Mendes¹

¹*Institute of Plasmas and Nuclear Fusion (IPNF), Association EURATOM/IST, Lisbon, Portugal*

Corresponding Author: J. P. S. Bizarro, bizarro@ipfn.tecnico.ulisboa.pt

Anomalous transport, turbulence and generation of large-scale structures in the scrape-off layer (SOL) of tokamaks are some of the main issues that control machine performance (via impurity contamination) and the life expectancy of plasma-facing materials, and here one tries to achieve some understanding of these questions through the theoretical analysis of a reduced two-dimensional two fluid (density plus vorticity) model of the SOL. The model is built around a conservative system describing transport perpendicular to the magnetic field in a slab geometry, to which terms are added to account for diffusion and parallel losses (both for particles and current) and to mimic plasma flow from the core (in the form of a source). Nonlinear estimates for the growth rates are derived, which show the growth in the density gradient to be controlled by the vorticity gradient, and vice-versa, therefore suggesting a nonlinear instability in the model. The possibility of controlling fluctuations by means of a biasing potential is confirmed (negative polarizations being shown to be more effective in doing so, thus providing an explanation for what is seen in experiments), as well as the advantage in reducing the inhomogeneity of the magnetic field in the SOL to decrease plasma turbulence there. In addition, focussing on the conservative part of the equations, exact solutions in the form of travelling waves are obtained which might be the conservative ancestors of the collective structures (so-called blobs) that are observed in experiments as well as in numerical simulations.

TH



The Role of Statistical Noise in Edge Plasma Transport Codes Based on Kinetic Monte Carlo Solvers for Neutrals: an Analogy with Turbulent Fluctuations

Y. Marandet¹, M. Valentinuzzi², H. Bufferand², G. Ciraolo², P. Genesis¹, P. Meliga³, J. Rosato¹, P. Tamain², and E. Serre³

¹*Physique des Interactions Ioniques et Moléculaires (PIIM), CNRS, Aix-Marseille Université, France*

²*Institut de Recherche sur la Fusion par confinement Magnétique (IRFM),*

Commissariat à l'énergie atomique (CEA/Cadarache), 13108 Saint-Paul-lès-Durance, France

³*Laboratoire de Mécanique, Modélisation & Procédés Propres (M2P2), Aix-Marseille Université, France*

Corresponding Author: Y. Marandet, yannick.marandet@univ-amu.fr

Power exhaust is one of the major challenges that future devices such as ITER and DEMO will face. Because of the lack of identified scaling parameters, predictions for divertor plasma conditions in these devices have to rely on detailed modelling. Most plasma edge simulations carried out so far rely on transport codes, which consist of a fluid code for the plasma coupled to a kinetic Monte Carlo (MC) code for neutral particles (atoms, molecules). An example of such tools is the Soledge2D-EIRENE code developed by our team. One of the main difficulties in interpreting code results is the lack of a proper convergence criterion for the simulations, because of the statistical noise originating in the kinetic MC calculation. Here, we take a new look at these noise related issues. We argue that these two problems share strong similarities, and that what is usually referred to as the steady state reached by a transport code after convergence bears strong resemblance with the statistically stationary state (SSS) reached by a turbulence code. We argue, by analogy with turbulence related studies, that the proper choice for the solution of coupled fluid-kinetic Monte Carlo simulations is the time average of the SSS. In most of the cases, this quantity is time independent, and is solution of a well-defined set of equations. The latter exhibits additional terms compared to the initial system, originating from its parametric and/or statistical nonlinearities. The additional terms can be calculated from the SSS, and provide a physical picture of the effects of the noise. Numerical results show that if the spatial structure of the noise is frozen long enough for the plasma to adjust, then the mean solution can differ markedly from the noise free solution. We present cases for which noise leads to a lower recycling divertor. Nevertheless, the mean particle balance is satisfied even in those cases, highlighting the need to monitor the effects of noise closely, because usual sanity checks on the solution might not fail even in cases where the solution is strongly affected. The relative importance of the various noise-induced terms is discussed, in order to explain the mechanisms through which noise can push the mean solution towards less recycling conditions, at least in the simulations presented here.



Comparison of Divertor Heat Flux Splitting by 3D Fields with Field Line Tracing Simulation in KSTAR

W. Choe¹, K. Kim¹, J.-W. Ahn², H. Lee³, C. S. Kang³, J.-K. Park⁴, Y. In³, J.-G. Kwak³, and S.-W. Yoon³

¹*Korea Advanced Institute of Science and Technology (KAIST), Daejeon, Republic of Korea*

²*Oak Ridge National Laboratory (ORNL), Oak Ridge, TN 37831, USA*

³*National Fusion Research Institute (NFRI), Daejeon, Republic of Korea*

⁴*Princeton Plasma Physics Laboratory (PPPL), Princeton, NJ 08540, USA*

Corresponding Author: W. Choe, wchoe@kaist.ac.kr

Application of toroidally nonaxisymmetric (3D) magnetic fields has great impacts on the heat transport onto divertor target. The 3D magnetic fields form stochastic field layers by opening magnetic islands, leading to modifications of magnetic field structure and heat flux distribution on the divertor. The heat flux splitting pattern strongly depends on the applied field configuration, which is incorporated into 3D perturbed equilibrium. Understanding their physical relations can provide a new insight of divertor heat flux control under the 3D fields and clues for underlying physics of plasma response to the 3D fields. This presentation will describe simulations of magnetic field line splitting by 3D fields using field line tracing code POCA-FLT considering vacuum and ideal plasma response models, and compare them with heat flux striation patterns on the divertor target measured by IRTV in KSTAR. The measured striation patterns are well captured by distributions of magnetic field line connection length calculated by POCA-FLT code in the various 3D field configurations. Simulations reproduce the heat flux splitting on the target, while their agreement depends on the plasma response model used. Comparison results indicate that self-consistent inclusion of the plasma response physics is essentially required to achieve the best match to the heat flux measurement and better understanding of the edge 3D field structure.

TH



The Field Line Map Approach for Simulations of Plasma Edge/SOL Turbulence

A. Stegmeir¹, D. Coster¹, O. Maj¹, and A. Ross¹

¹Max-Planck-Institut für Plasmaphysik, Garching, Germany

Corresponding Author: A. Stegmeir, andreas.stegmeir@ipp.mpg.de

The complex geometry in the edge and scrape-off layer poses a challenge to simulations of magnetically confined plasmas, since the usually employed field/flux-aligned coordinates become singular on the separatrix/X-point. A field line map approach (see also flux-coordinate independent approach) offers a promising solution to these problems. The approach is based on a cylindrical grid, which is Cartesian within poloidal planes, and the characteristic flute mode property ($k_{\parallel} \ll k_{\perp}$) of structures is exploited computationally via grid sparsification in the toroidal direction. A field line following discretization for parallel operators is then required, which includes field line tracing and interpolation and/or discrete integration. Advanced numerical techniques were developed in order to overcome the critical issue of numerical diffusion and the treatment of boundaries. The whole concept is implemented in the code GRILLIX, which features flexibility in treating different and complex geometries, especially with separatrix and X-point(s). Simulations based on a simplified turbulence model (Hasegawa–Wakatani) elucidate the effect of the X-point on turbulent structures. Furthermore, a full-f drift reduced Braginskii model, where the Boussinesq approximation is dropped, is employed for studies on blob propagation in the scrape-off layer.

Neutral Recycling Effect on Edge ITG Turbulence and Transport

D. P. Stotler¹, J. Lang², S.-H. Ku¹, and C.-S. Chang^{1,3}

¹Princeton Plasma Physics Laboratory (PPPL), Princeton, NJ 08540, USA

²Intel Corporation, Santa Clara, CA 95054, USA

³Korea Advanced Institute of Science and Technology (KAIST), Daejeon, Republic of Korea

Corresponding Author: D. P. Stotler, dstotler@pppl.gov

Neutral particle recycling effect on the edge ITG (ion temperature gradient) turbulence has been studied in a realistic tokamak geometry with a steep edge pedestal, using a full-f edge gyrokinetic code XGC1. The ITG turbulence is chosen here because it is the most fundamental and robust form of tokamak plasma instability, with its long radial correlation length influencing other turbulence in the pedestal. It has been found that the charge exchange interaction of the neutral particles with the plasma ions enhance the edge ITG turbulence and transport through a) reduction of the $E \times B$ shearing rate and b) through cooling of the ion temperature near the magnetic separatrix, which leads to an enhanced ion temperature gradient in the extended edge region.

Work supported by the U.S. Department of Energy. Computing resources provided by OLCF, ALCF and NERSC.



Progress in First-Principles Simulation of SOL Plasma Turbulence and Neutral Atom Dynamics with the GBS Code

P. Ricci¹, F. Halpern¹, J. Loizu², S. Jolliet¹, R. Jorge¹, J. Morales¹, A. Masetto¹, P. Paruta¹, F. Riva¹, and C. Wersal¹

¹Swiss Plasma Center (SPC), École polytechnique fédérale de Lausanne (EPFL), 1015 Lausanne, Switzerland

²Max-Planck-Institut für Plasmaphysik, Greifswald, Germany

Corresponding Author: P. Ricci, paolo.ricci@epfl.ch

The GBS code has been developed in the last few years to simulate plasma turbulence and neutral atom dynamics in SOL conditions. GBS advances the drift-reduced Braginskii equations for low-frequency plasma turbulence, solving at the same time a kinetic equation of neutral atoms by the method of characteristics. In GBS the plasma dynamics is evolved as the interplay between plasma sources (due to the neutral ionization and the plasma outflow from the tokamak core), turbulent transport, and plasma losses (at the limiter or divertor plates or through recombination processes). Therefore, the simulations evolve self-consistently both the plasma profile and its fluctuations, with no separation between the equilibrium and fluctuation scale lengths. A detailed study of the interaction of the plasma with the solid wall was carried out and, based on the kinetic results, a set of boundary conditions was found that were implemented in GBS at the sheath edge, where the drift-reduced Braginskii model loses its validity. The neutral module implemented in GBS represents the first-ever successful implementation of a self-consistent neutral solver within a first-principles turbulence code. The interaction of the plasma with the neutrals is taken self-consistently into account, by evaluating plasma source and energy losses due to ionization events, the drag due to charge-exchange collisions, and the recombination processes. GBS was verified by using the method of manufactured solutions, and it was validated against experimental data from several tokamaks worldwide, showing good agreement. In the present work, we focus on our recent insights on the neutral atom dynamics. We first illustrate the model that allows us to evolve at the same time plasma turbulence and neutral atom dynamics. Second, we describe our recent progress in the study of the transition from the sheath- to the conduction-limited regimes that was simulated in GBS by increasing the plasma density in the system. Thanks to the simulation results, we expanded and refined the so-called two-point model that is used to estimate the drop of electron and ion temperature along the magnetic field lines in the SOL. Third, we discuss the role of neutrals in setting the long scale length, dubbed shoulder, that is observed in the far SOL in the high density regime.



Multiscale Modelling of Sheath Physics in Edge Transport Codes

N. Mellet¹, Y. Marandet¹, H. Bufferand², G. Ciruolo², P. Genesis¹, J. P. Gunn², P. Roubin³,
E. Serre⁴, and P. Tamain²

¹*Physique des Interactions Ioniques et Moléculaires (PIIM), CNRS, Aix-Marseille Université, France*

²*Institut de Recherche sur la Fusion par confinement Magnétique (IRFM),
Commissariat à l'énergie atomique (CEA/Cadarache), 13108 Saint-Paul-lès-Durance, France*

³*CNRS, Aix-Marseille Université, Marseille, France*

⁴*Laboratoire de Mécanique, Modélisation & Procédés Propres (M2P2), Aix-Marseille Université, France*

Corresponding Author: N. Mellet, nicolas.mellet@univ-amu.fr

Power exhaust constitutes one of the primary challenges for future fusion devices. Given the fact that scaling parameters have not been clearly identified, the prediction for divertor plasma conditions relies mainly on simulation with transport edge codes like Soledge2D-EIRENE that is used in the present work. For charged species, treated with a fluid model, the simulation domain does not extend all the way to the wall, because of the existence of the sheath. Even though it is very thin compared to the extension of the scrape-off layer (SOL), it plays an important role for the plasma wall interactions and SOL physics. By accelerating the ions towards the wall, it acts both on the energy and the angle of the impinging species, which affect the sputtering yield and reflection coefficients. The latter has a direct effect on the plasma parameters close to the surface. Additionally sheath physics has an important role in the prompt redeposition of eroded W ions, reducing considerably the erosion of plasma facing components and plasma contamination.

The work presented here is based on a multiscale approach where the sheath physics is simulated using a 1D PIC code. The latter provides in particular the distribution of incidence angle, twisting angle and energy at impact as a function of the plasma parameters in the vicinity of surface. This model, which is now fully implemented, exhibits incidence angles shallower than expected from simple models. A markedly higher temperature in the divertor is obtained for a flat surface and is due to reflection coefficients that increase with decreasing incidence angles. Additional effects are investigated like the surface roughness and the sensitivity of the model to the reflection database obtained by TRIM close to the physical sputtering threshold where it is known to be unreliable. In a first approximation, roughness is implemented as a probability density function (PDF) and tends to bring the divertor temperature down by increasing the incidence angle. A parametric study of the role of reflection coefficients in high recycling conditions, where most of edge transport code results rely on an assumed binding energy of 1 eV, is also conducted. This work shows the importance of a comprehensive sheath model and reliable reflection data on the way to predictive plasma edge modelling tools.

TH

Kinetic Understanding of Neoclassical Scrape-Off Layer Physics, Comparison with Fluid Modelling, and Experimental Validation

R. Churchill¹, J. Canik², C.-S. Chang^{1,3}, R. Hager¹, R. Maingi¹, A. W. Leonard⁴,
R. Nazikian¹, and D. P. Stotler¹

¹Princeton Plasma Physics Laboratory (PPPL), Princeton, NJ 08540, USA

²Oak Ridge National Laboratory (ORNL), Oak Ridge, TN 37831, USA

³Korea Advanced Institute of Science and Technology (KAIST), Daejeon, Republic of Korea

⁴General Atomics, San Diego, CA 92186, USA

Corresponding Author: R. Churchill, rchurchi@pppl.gov

Simulations using the fully kinetic code XGCa were undertaken to explore the impact of kinetic effects on scrape-off layer (SOL) physics in DIII-D H-mode plasmas. XGCa is a total-f, gyrokinetic code which self-consistently calculates the axisymmetric electrostatic potential and plasma dynamics, and includes modules for Monte Carlo neutral transport. Fluid simulations are normally used to simulate the SOL, due to its high collisionality. However, a number of discrepancies have been observed between experiment and leading SOL fluid codes (e.g., SOLPS) [1], including underestimating outer target temperatures, radial electric field in the SOL, parallel ion SOL flows at the low field side, and impurity radiation. Many of these discrepancies may be linked to the fluid treatment, and might be resolved by including kinetic effects in SOL simulations. Results presented here will address the SOL parallel ion flow discrepancy among other SOL kinetic effect findings from XGCa.

The XGCa simulation of the DIII-D tokamak in a nominally sheath-limited regime shows many noteworthy features in the SOL. The SOL ion Mach flows are at experimentally relevant levels ($M_i \sim 0.5$), with similar shapes and poloidal variation as observed in various tokamaks [2, 3]. Surprisingly, the ion Mach flows close to the sheath edge remain subsonic, in contrast to the typical fluid Bohm criterion requiring ion flows to be above sonic at the sheath edge. Related to this are the presence of elevated sheath potentials, $e\Delta\Phi/T_e \sim 3-3.6$, over most of the SOL, with regions in the near-SOL close to the separatrix having $e\Delta\Phi/T_e > 4$. These two results at the sheath edge are a consequence of non-Maxwellian features in the ions there.

Status of benchmarking efforts to compare XGCa with fluid models, in particular the fluid code SOLPS, will be presented in the sheath-limited and medium-recycling regimes, with future plans to compare results in the high-recycling and detached regimes.

References

- [1] A. V. Chankin, *et al.*, J. Nucl. Mater. **390-391**, 319-324 (2009).
- [2] J. A. Boedo, *et al.*, J. Nucl. Mater. **266-269**, 783-787 (1999).
- [3] S. K. Erents, *et al.*, Plasma Phys. Control. Fusion **46**, 1757-1780 (2004)

Work supported by the U.S. Department of Energy, Office of Science, Office of Fusion Energy Sciences under DE-AC02-09CH114661, DE-AC05-00OR227252, and DE-FC02-04ER546983.



Numerical Investigation of 3D Plasma Edge Transport and Heat Fluxes including Impurity Effects in Wendelstein 7-X Startup Plasmas with EMC3-EIRENE

F. Effenberg¹, Y. Feng², O. Schmitz¹, H. G. Frerichs¹, S. A. Bozhenkov², R. König², M. Krychowiak², T. Sunn Pedersen², and D. Reiter³

The W7-X Team

¹Department of Engineering Physics, University of Wisconsin-Madison, Madison, WI 53706, USA

²Max-Planck-Institut für Plasmaphysik, Greifswald, Germany

³Institute of Energy and Climate Research, Forschungszentrum Jülich, Jülich, Germany

Corresponding Author: F. Effenberg, effenberg@wisc.edu

Heat flux mitigation and power dissipation is a crucial and challenging topic in the 3D environment of stellarator devices foreseen for steady state operation. We show that the limiter startup configuration of the first quasi-isodynamic optimized stellarator Wendelstein 7-X features a complex helical scrape-off layer topology of helical scrape-off layer flux bundles of three different magnetic target-to-target-connection length scales L_C . This enables the study of the link between the scrape-off layer flux tube geometry and the eventual heat and particle deposition on target surfaces which is important for advanced stellarators as well as next generation tokamaks like ITER.

The plasma transport and the resulting limiter heat and particle loads are modelled with the fully 3D coupled plasma fluid and kinetic neutral edge transport Monte Carlo code EMC3-EIRENE. The helical 3D topology causes plasma pressure modulated with L_C and counter streaming flows. This leads in particular at low density and high heating power scenarios ($n_{LCFS} \sim 10^{18}/\text{m}^3$, $P_{in} = 4 \text{ MW}$) to a heterogeneous heat and particle load distribution on the limiter surfaces correlated to L_C .

Heat flux mitigation can be achieved by increasing the perpendicular transport, e.g., increasing the density at a fixed input power of $P_{in} = 4 \text{ MW}$ by an order of magnitude leads to a drop of the maximum peak heat loads $P_{peak} = 12 \text{ MW}/\text{m}^2$ by $\sim 24\%$, while the heat flux channel width, defined by the e-folding length $\lambda_{q\parallel}$ of the parallel heat flux deposited on the limiters, is increased by a factor of ~ 2 .

The impact of intrinsic and actively injected impurities on the limiter heat loads and radiative edge cooling performance is investigated as it is tested during the limiter operation phase as preparation for the later island divertor scenarios. It is shown that for sputtered carbon based on a yield of 2% of the recycling flux no significant power dissipation has to be expected. Fluxes are found that lead to a power dissipation of $\sim 40\%$ of the input power significantly reducing the maximum heat peak loads. Additionally seeded impurities tend to localize within the helical flux tubes. Radiative losses by nitrogen have the advantage to contribute as a carbon like species mainly to edge cooling while neon is a more effective radiator, but dissipates a significant power fraction within the confinement region.

Pedestal-to-Wall 3D Fluid Transport Simulations on DIII-D and NSTX

J. Lore¹, J.-W. Ahn¹, A. Briesemeister¹, J. Canik¹, N. M. Ferraro², H. G. Frerichs³,
 A. McLean⁴, J.-K. Park², M. Shafer¹, and R. S. Wilcox¹

¹Oak Ridge National Laboratory (ORNL), Oak Ridge, TN 37831, USA

²Princeton Plasma Physics Laboratory (PPPL), Princeton, NJ 08540, USA

³University of Wisconsin-Madison, Madison, WI 53706, USA

⁴Lawrence Livermore National Laboratory (LLNL), Livermore, CA 94550, USA

Corresponding Author: J. Lore, lorejd@ornl.gov

The 3D edge transport code EMC3-EIRENE is used to test magnetic field models with and without plasma response against experimental data on DIII-D and NSTX for a range of collisionalities, including the transition to detachment. None of the models tested can quantitatively reproduce the measured “lobe” structure in the scrape-off layer (SOL) temperature and density while maintaining the experimental pedestal pressure gradient. To make reliable predictions for future devices such as ITER, which will operate with applied and intrinsic 3D fields, transport simulations must be able to reproduce experimental observations in the edge, divertor, and pedestal. This “pedestal-to-wall” consistency depends strongly on the structure of the 3D magnetic field model in which EMC3-EIRENE [1] solves the fluid plasma and neutral particle transport equations. The magnetic fields used include axisymmetric equilibria, a superposition of 2D and 3D vacuum perturbation fields, and 3D MHD codes which include plasma response (VMEC [2], GPEC [3], M3D-C1 [4]).

In DIII-D plasmas, the divertor Thomson scattering system measures structure in the temperature and density that is not present in axisymmetric plasmas. These measurements are compared to EMC3-EIRENE simulations using vacuum and M3D-C1 fields. The two fluid M3D-C1 cases show lobes that are significantly larger than experimentally observed. These comparisons will be used to constrain inputs to the simulations such as the edge rotation profile that have large experimental uncertainty. In NSTX, 3D field application is observed to cause detached plasmas to reattach. As the density is increased, heat flux peaks at large major radius remain even as the primary peak is reduced. EMC3-EIRENE simulations reproduced these trends, with axisymmetric cases transitioning to detachment at a lower density than when 3D fields are included and the heat flux peaks caused by strike point splitting transitioning to detachment from the primary strike point outwards as the density is increased.

References

- [1] Y. Feng, *et al.*, J. Nucl. Mater. **241–243**, 930–934 (1997).
- [2] S. P. Hirshman, *et al.*, Phys. Fluids **26**, 3353 (1983).
- [3] J.-K. Park, *et al.*, Phys. Plasmas **14**, 052110 (2007).
- [4] S. Jardin, *et al.*, J. Phys. Conf. Series **125**, 012044 (2008).



Particle Simulation on Blob Formation and Propagation in an Open System

I. Katanuma¹, G. Oda¹, and T. Oi¹

¹University of Tsukuba, Tsukuba, Ibaraki, Japan

Corresponding Author: I. Katanuma, katanuma@prc.tsukuba.ac.jp

It is understood that plasma blobs produced near a separatrix are responsible for the most radial transport of plasma density in SOL. Particle simulation was first performed on a blob from its production to the propagation. The particle simulation uses the (2 and 1/2) dimensional electrostatic implicit code with 256×128 meshes. Ions (electrons) are distributed to have a $\tanh(x)$ density profile in x and the ions (electrons) flow in the y -direction with the $E \times B$ drift shear as an initial condition, where the conducting boundary condition in x and the periodic boundary condition in y are adopted. The effective gravitational acceleration force $g(x)$ is applied in the x -direction, where $g(x)$ changes its sign along x so that an interchange mode is stable in $x < 64$ and it is unstable in $x > 64$. A Kelvin–Helmholtz instability was driven by the drift velocity shear at first, so that ions and electrons in the high density region ($x < 64$) came into the unstable region ($x > 64$) to the interchange mode. The resultant interchange instabilities were localized around $x = 64$ and saturated at a low amplitude because of a small amount of ions and electrons contributing to an interchange instability. A blob was born after the saturation of an interchange instability under the $E \times B$ drift shear. Then the blob was found to propagate in x stably after it was born. This result indicates that the blob with a special initial condition can propagate stably. In fact it was shown that a blob produced from the initial three small charged-up clumps began to propagate stably in x . By the way, it is understood that a blob with an initial monopole structure is deformed into a characteristic mushroom shape, i.e., a blob receiving the charge separation is able to propagate but is deformed from a circular shape to a mushroom one, which means that a monopole shaped blob is unstable. The electron motion along a magnetic field line is considered to be a candidate for the stable propagation of blob. The line-tying, however, cancels the charge separation due to ∇B drift, which stops the blob propagation although it makes a blob stable. The line-tying effects on a monopole shaped blob propagation were studied also, that the line-tying was first found to inhibit the blob propagation by cancelling the charge separation caused by the ∇B drift before it made the blob propagation stable.

TH

Understanding the Blobby Turbulence in Edge Plasma from Gyrokinetic Simulation

S.-H. Ku¹, R. Churchill¹, C.-S. Chang^{1,2}, J. Myra³, and S. Parker⁴

¹Princeton Plasma Physics Laboratory (PPPL), Princeton, NJ 08540, USA

²Korea Advanced Institute of Science and Technology (KAIST), Daejeon, Republic of Korea

³Lodestar Research Corporation, Boulder, CO 80301, USA

⁴University of Colorado, Boulder, CO 80309, USA

Corresponding Author: S.-H. Ku, sku@pppl.gov

The importance of the nonlinear “blobby” turbulence (or “intermittent plasma objects”) in the scrape-off layer (SOL) of the tokamak plasma has been well known. Blobs are usually measured and discussed for L-mode edge/SOL plasmas and inter-ELM SOL plasmas. However, blobs are also known to exist in steep H-mode pedestals. From ITER’s perspective, understanding the H-mode blobs may be more important than the L-mode blobs for number of reasons: a) Strong blobby turbulence could limit the pedestal gradient before it reaches the kinetic ballooning mode or edge localized mode (ELM) limits, b) blobby turbulence may interact with ELMs and give rise to precursor activities, c) blobby turbulence can be responsible for expelling the fusion produced heat and helium ash particles across the last closed flux surface, d) it can play an important role in the impurity transport across the separatrix, e) it may contribute to the valuable inward momentum pinch from SOL to core, especially in interaction with the X-point orbit loss physics, and f) it may spread the divertor heat-load width. Here we present the first (to our knowledge) gyrokinetic study in realistic geometry. Importance of the full-function gyrokinetic study for the nonlinear edge blob physics cannot be emphasized enough since the blobs interact with the neoclassical kinetic physics and neutral particles in multiscale and since the edge plasma is in non-Maxwellian state in contact with material walls. Since blobs are mostly electrostatic fluctuations, as known from experiments, we use XGC1 in its more-established electrostatic mode for this study. The size of the blobs from XGC1 agrees qualitatively with experimental data. The radial and poloidal correlation length is on the same order as the radial width of the whole edge region from pedestal top to SOL. Blobs are born in the steep plasma gradient region just inside the separatrix surface and propagate radially outward into the SOL. Other important properties of the blobs that are relevant to extrapolation to ITER will be discussed. A systematic validation with the existing data will also be attempted and presented.

Work supported by the U.S. Department of Energy under DE-AC02-09CH11466. This work used computing resources of ORNL, supported by DE-AC05-00OR22725.

Impurity Transport Caused by Blob and Hole Propagations

H. Hasegawa¹, S. Ishiguro¹

¹National Institute for Fusion Science (NIFS), Toki, Gifu, Japan

Corresponding Author: H. Hasegawa, hasegawa.hiroki@nifs.ac.jp

It is firstly demonstrated that transport of impurity particles are caused by blob and hole propagations by means of the three dimensional (3D) electrostatic particle-in-cell (PIC) simulations. We have shown that 1) the impurity profile in the blob/hole structure becomes biased shape like a dipole, and 2) the biased density profile of impurity propagates with the blob/hole. The “blob” and “hole” are the intermittent filamentary coherent structures along the magnetic field line in peripheral plasmas of fusion magnetic confinement devices and the plasma densities in the blob and hole are higher and lower than that of background plasma, respectively. These structures are thought to be created from edge turbulences and play an important role in the radial convective plasma transport in the SOL. Furthermore, it has been pointed out that the blob and hole propagations can induce impurity transport. However, any numerical studies about the impurity transport with the blob and hole have not been conducted because of the difficulty in including minority ions, i.e., impurities in fluid models. Therefore, in this study, we have improved the 3D-PIC code and investigated dynamics between impurity and the blob and hole structures. In the PIC simulation, an external magnetic field is set as it is parallel to the z axis and has ∇B in the x direction. The initial ratio between impurity and background electron densities is given as 0.06 since it is $\sim 5\%$ in experiments for investigation of impurity transports. The impurity ions are uniformly distributed in the whole system at the initial stage. In the simulation, it is shown that impurity ions in the blob/hole are dragged from the higher to the lower potential sides (the dipole potential structure on the poloidal cross-section is created in a blob/hole) by the polarization drift and that the biased density profile of impurity is transported with the blob/hole by trapping impurity ions in the potential well of the blob/hole. The propagation speed of the blob/hole with impurity is nearly equal to that without impurity. Although the blob/hole propagation is hardly influenced by the impurity, the impurity ions in the blob/hole move with the blob/hole. The impurity averaged radial speed in the blob/hole is close to the blob/hole propagation speed.

TH



Nonlinear Dynamics of ELMs with E_r Shear and Collisionality Trends

X. Xu¹, D. Kong², N. Yan², J. Chen³, C. Ma³, A. Diallo⁴, R. Groebner⁵, P. B. Snyder⁵,
J. W. Hughes⁶, and P. H. Diamond⁷

¹Lawrence Livermore National Laboratory (LLNL), Livermore, CA 94550, USA

²Institute of Plasma Physics, Chinese Academy of Sciences, Hefei, Anhui, People's Republic of China

³Peking University, Haidian, Beijing, People's Republic of China

⁴Princeton Plasma Physics Laboratory (PPPL), Princeton, NJ 08540, USA

⁵General Atomics, San Diego, CA 92186, USA

⁶Plasma Science & Fusion Center, MIT, Cambridge, MA 02139, USA

⁷University of California San Diego, CA 92093, USA

Corresponding Author: X. Xu, xu2@llnl.gov

Simulations with the BOUT++ code have been used to study the energy loss for edge localized modes (ELMs) at different collisionality and electric field E_r shear and to investigate the controls of transition to different ELM and quiescent H-mode (QH-mode) regimes. The simulation results indicate that by development of a flexible E_r control capabilities, it is conceivable that tokamak operation regime access can be achieved through a control of edge fluctuation spectrum via the radial electric field and its shear. By decreasing collisionality with a increasing E_r for a narrow pedestal, nonlinear simulations show that 1) power spectrum becomes narrower and linear growth rate increases, the dominant mode decreasing from high- n ballooning modes to low- n peeling modes; 2) Bispectrum analysis shows that nonlinear mode coupling becomes weaker, resulting in the dominant filamentary structures and increasing ELM energy loss. The increasing E_r shear at high collisionality with a narrow pedestal leads to strong nonlinear coupling and reduced ELM energy loss. In contrast, the increasing E_r shear at low collisionality with a wide pedestal can modify the stability boundary to drive stable low- n peeling modes unstable, leading to enhanced pedestal transport due to either a saturated low- n peeling modes or a broadband turbulence, therefore leading to a reduced pedestal pressure gradient, allowing the development of a broader and thus higher transport barrier in QH mode without ELMs.

To validate BOUT++ simulations against experimental data for inter-ELM fluctuations, the BOUT++ simulations are performed based on a set of C-Mod and DIII-D experiment data, the overall signatures of simulation results for quasi-coherent fluctuations (QCF) show good agreement with C-Mod and DIII-D measurements. The simulation results show that 1) QCFs are localized in the pedestal region having a predominant frequency at $f \approx 300\text{--}400$ kHz and poloidal wavenumber at $k_\theta \approx 0.7/\text{cm}$, and propagate in the electron diamagnetic direction in the laboratory frame; 2) The pedestal profiles giving rise to QCFs are near the marginal instability threshold for ideal peeling-ballooning (P-B) modes for both C-Mod and DIII-D; and 3) Particle diffusivity is either smaller than the heat diffusivity for DIII-D or similar to the heat diffusivity for C-Mod.

Work performed for the U.S. Department of Energy by LLNL under Contract DE-AC52-07NA27344.LLNL-ABS-680566.

Divertor Heat Flux Simulations in ELMy H-Mode Discharges of EAST and Other Tokamaks

T. Y. Xia^{1,2}, B. Chen^{3,2}, B. Gui^{1,2}, X. T. Xiao^{1,2}, T. F. Tang^{4,2}, X. Q. Xu², D. H. Li¹, Z. Zheng¹, and J. B. Liu¹

¹*Institute of Plasma Physics, Chinese Academy of Sciences, Hefei, Anhui, People's Republic of China*

²*Lawrence Livermore National Laboratory (LLNL), Livermore, CA 94550, USA*

³*University of Science and Technology of China, Hefei, Anhui, People's Republic of China*

⁴*Dalian University of Technology, Liaoning, Dalian, Ganjingzi, People's Republic of China*

Corresponding Author: T. Y. Xia, xiaty@ipp.ac.cn

In this paper we report the simulations of the evolution of heat flux deposition and turbulence in edge plasma region for the ELMy H-mode discharges of EAST, C-Mod and DIII-D. The divertor sheath boundary conditions have been implemented into the BOUT++ six-field two-fluid model based on the Braginskii equations with nonideal physics effects. This module has shown the comparable transient heat flux distributions towards divertor targets during ELM crashes on DIII-D. In order to perform consistent scrape-off layer plasma transport calculations, the 2D fluid code SOLPS has been externally coupled to the 3D turbulence code BOUT++ for DIII-D and C-Mod. The radial profiles of turbulent transport coefficients have been calculated including the neoclassical transport and turbulent transport for the coupling. In order to study the effects of the different divertor materials of EAST on the transient heat fluxes in SOL induced by ELMs, the sheath energy transmission factors are calculated by full-PIC code PPSC within the secondary electron emission. The preliminary simulations show that if $T_e > 120$ eV, the energy transmission coefficients will show obvious differences between carbon and tungsten. The differences of ELM heat fluxes with carbon and tungsten divertors will be presented. The test particle module in BOUT++ framework will enhance the capability to understand the transport of the impurity and energetic particles during ELMs on EAST. The impurity particle loss under newly developed RF sheath induced equilibrium radial electric field will be reported in this paper.

TH

EMC3-EIRENE Simulations for the Impact of External Magnetic Perturbations on EAST Edge Plasma

J. Huang¹, Y. Feng², C. Wu¹, J. Chang¹, Y. Sun¹, M. Jia¹, Y. Liang¹, L. Wang¹, J. Xu¹, Z. Yang¹, W. Gao¹, Z. Xu¹, Y. Hou¹, Z. Jin¹, Y. Chen¹, X. Liu¹, P. Zhang¹, L. Zhang¹, W. Gao¹, Z. Wu¹, and B. N. Wan¹

¹*Institute of Plasma Physics, Chinese Academy of Sciences, Hefei, Anhui, People's Republic of China*

²*Max-Planck-Institut für Plasmaphysik, Greifswald, Germany*

Corresponding Author: J. Huang, juan.huang@ipp.ac.cn

On the EAST tokamak, resonant magnetic perturbations (RMPs) have been successfully applied to control edge localized mode (ELM) [1]. To quantify the impact of the resulting 3D magnetic field structure on the edge plasma transport, the EMC3-EIRENE code [2] is employed, which is a coupled code package of EMC3 for fluid ions and electrons and EIRENE for kinetic neutrals. The code had been applied to axisymmetric double null divertor plasmas for EAST before [3]. Recent progress has been made in the grid generator to allow for RMP fields to be taken into account using vacuum approximation [4], and a first 3D computational mesh is constructed for shot #52327. Field-line tracing based on the 3D mesh and the intrinsic field line integration procedure of the EMC3 code yields a field structure which agrees well with that produced by the MAPs code (magnetic perturbation spectrum analysis) [5]. First plasma transport simulations have shown a clear strike-line splitting effect which is also observed experimentally. This paper presents a systematic comparison in particle and energy deposition between the 3D simulation and experimental results. It is also attempted to identify possible plasma screening effects on the RMP fields, which are not yet taken into account in the computations.

References

- [1] B. Wan, *et al.*, Nucl. Fusion **55**, 104015 (2015).
- [2] Y. Feng, *et al.*, Contrib. Plasma Phys. **44**, 57–69 (2004).
- [3] J. Huang, *et al.*, Plasma Phys. Control. Fusion **56**, 075023 (2014).
- [4] T. Lunt, *et al.*, Nucl. Fusion **55**, 054013 (2012).
- [5] Y. Sun, *et al.*, Plasma Phys. Control. Fusion **57**, 045003 (2015).



Modelling of Prompt Deposition of Tungsten under Fusion Relevant Conditions

A. Kirschner¹, D. Tskhakaya², D. Borodin¹, S. Brezinsek¹, J. Romazanov¹, R. Ding³, and C. Linsmeier¹

¹*Institute of Energy and Climate Research, Forschungszentrum Jülich, Jülich, Germany*

²*Institute for Applied Physics, Technische Universität Wien, 1040 Vienna, Austria*

³*Institute of Plasma Physics, Chinese Academy of Sciences, Hefei, Anhui, People's Republic of China*

Corresponding Author: A. Kirschner, a.kirschner@fz-juelich.de

Tungsten is a promising first wall material in fusion devices. Though, due to its high atomic number, tungsten concentration levels in the plasma core have to be kept small. However, in addition to low sputtering yields, the high atomic number has the beneficial effect of prompt deposition, i.e., depending on the plasma parameters large amounts of sputtered tungsten can be deposited during the first gyration.

The deposition of sputtered tungsten is simulated with the 3D Monte Carlo impurity transport and plasma-wall interaction code ERO. No specific device geometry is used but constant plasma parameters along the surface. Variations of plasma density, temperature, flow velocity and sheath potential along the magnetic field are considered according to the simple two point model and PIC-simulated sheath characteristics. Simulations have been done for a magnetic field of 3 T with an angle of 2° relative to the surface. With an electron temperature $T_e = 20$ eV and density $n_e = 6 \times 10^{19}/\text{m}^3$ at the sheath entrance, the modelled amount of tungsten prompt deposition is 95%. Reducing T_e at the sheath entrance to 5 eV lowers the modelled deposition fraction to 65%. In both cases tungsten ionization occurs outside the sheath leading to mean deposition energies of about $3QT_e$ (with Q the mean charge of depositing tungsten ions), which are in accordance with the sheath potential drop.

Further parameter studies with T_e between 1 and 20 eV and n_e between 10^{18} and $10^{21}/\text{m}^3$ have been performed. At very high n_e and T_e , the tungsten ion trajectories do not describe clear gyration motions anymore as the movement is dominated by the large electric field near the surface. Therefore, the term "prompt deposition" is used for atoms, which after their ionization return to the surface within $t < t_{\text{gyro}}$. Whereas at the lowest T_e , n_e no prompt deposition occurs, all eroded tungsten is promptly deposited at the largest T_e , n_e . At high n_e in combination with low T_e , deposited tungsten ions can reach energies much larger than expected from the sheath potential. The energy excess comes from very effective entrainment of the tungsten ions with the plasma via friction.

The possible runaway sputtering due to an avalanche effect of tungsten self-sputtering will be studied. Also, the influence of ELMs on the prompt and overall deposition and resulting sputtering will be addressed.

Kinetic Modelling of Tungsten Impurity Transport Using the IMPGYRO Code

S. Yamoto¹, X. Bonnin², A. Hatayama¹, Y. Homma³, K. Hoshino³, H. Inoue¹, S. W. Lisgo², and R. A. Pitts²

¹Faculty of Science and Technology (Yagami Campus), Keio University, Yokohama, Japan

²International Thermonuclear Experimental Reactor (ITER),

Cadarache Centre, 13108 Saint-Paul-lès-Durance, France

³Japan Atomic Energy Agency (JAEA), Naka, Japan

Corresponding Author: S. Yamoto, yamoto@ppl.appi.keio.ac.jp

With the move in current and future fusion devices to all-metal walls, and particularly with tungsten (W) plasma-facing components, understanding heavy ion impurity transport processes in the scrape-off layer (SOL)/divertor region is becoming one of the most critical issues for tokamak operation. To improve this understanding, we are continuing to develop the kinetic SOL/divertor impurity transport code IMPGYRO (IG), which tracks the trajectory of impurity ions in the plasma, resolving their full gyro-orbits.

For the W transport in the SOL/divertor region, the friction force, the thermal force, the $E \times B$ drift and the anomalous radial transport are traditionally regarded as the dominant factors. In addition to these, it has recently been pointed out that neoclassical transport processes can have nonnegligible effects on transport in the SOL/divertor region. In this paper, we mainly focus on neoclassical transport processes associated with the parallel transport of W impurities in single null divertor configurations.

We focus the IG simulations using a plasma background obtained with the SOLPS5.0 plasma boundary code suite on the magnetic equilibrium of the JT-60U pulse #49540. When the background plasma is in a high recycling state, the W particles have been pushed upstream by the strong thermal force and transported to the top region of the SOL due to the existence of a steep parallel temperature gradient in front of the divertor plate. The W particles then stagnate near the top of the SOL where the parallel thermal force and the friction force are in balance. The W impurities then penetrate into the main plasma due to the ∇B drift and curvature drifts, which are automatically taken into account in the IG modelling, causing a net inward perpendicular flux. In order to better understand the W penetration process, we compare the IG model to a simpler guiding centre model with an anomalous transport. We find that in general the IG radial velocities tend to be larger than those from the guiding centre model. As a consequence, localized impurities have a larger radial flux in the IG calculation. The results suggest that not only the anomalous diffusion but also the drifts, specifically the ∇B drift and the curvature drift, should be taken into account in order to correctly predict the W core accumulation.



Numerical Analyses of Baseline JT-60SA Design Concepts with the COREDIV Code

R. Zagorski¹, I. Ivanova-Stanik¹, L. Garzotti², G. Giruzzi³, M. Romanelli², K. Galazka¹, W. Stepniewski¹, and N. Rudolf⁴

¹*Institute of Plasma Physics and Laser Microfusion, Warsaw, Poland*

²*Culham Centre for Fusion Energy (CCFE), Culham Science Centre, Abingdon, UK*

³*Institut de Recherche sur la Fusion par confinement Magnétique (IRFM),*

Commissariat à l'énergie atomique (CEA/Cadarache), 13108 Saint-Paul-lès-Durance, France

⁴*Max-Planck-Institut für Plasmaphysik, Garching, Germany*

Corresponding Author: R. Zagorski, roman.zagorski@ipplm.pl

JT-60SA is a superconducting tokamak supporting fusion research on the way towards realization of energy production in a DEMO reactor. The baseline JT-60SA design foresees full carbon wall, however feasibility studies have been initiated recently to assess the possibility of the transition to full W. In this paper, JT-60SA reference design scenarios at high (#3) and low (#2) density have been analyzed with the help of the self-consistent core-edge COREDIV code. Simulations results for standard carbon wall and the full W have been compared in terms of the influence of impurities, both intrinsic (C,W) and seeded (N, Ar, Ne, Kr) on the radiation losses and plasma parameters. In particular, the reduction of the divertor target power load due to radiation of sputtered and externally seeded impurities has been investigated. Simulations of plasmas with C wall have been performed for scenarios (#3) and (#2) assuming N as the reference seeding gas. However, for scenario (#2) seeding by other gasses (Ne, Ar, Kr) has been investigated as well. It has been found that the main plasma parameters of analyzed scenarios can be reasonably reproduced by COREDIV. For the considered scenarios, N and C radiates predominantly in the SOL region, Ne radiates also in the core, whereas Ar and Kr radiate mostly in the bulk plasma. For scenario #3 the regime of detachment on divertor plates can be achieved with N seeding whereas for high auxiliary power and scenario (#2), the carbon and seeding impurity radiation does not effectively reduce power to the targets. In this case only increase of neither average density or edge density together with Kr seeding might help to develop conditions with strong radiation losses and semidetached conditions in the divertor. First calculations done for scenario #3 with W divertor and Ne seeding show that for large enough Ne influx the divertor heat load is below the technological limit requirements. The energy losses are dominated by Ne and deuterium radiation and plasma contamination is tolerable with the energy losses approaching 70%. Simultaneously the target temperature is low indicating semidetached conditions. This result is further analyzed in terms of different transport assumptions and plasma edge parameters. Similar strategy is applied for analysis of scenario #2. In this case, however, in addition to the Ne also Kr seeding is considered.



Plasma Particle and Energy Exhaust to and Recycling at a Tungsten Surface

X. Tang¹, Z. Guo¹

¹*Los Alamos National Laboratory (LANL), Los Alamos, NM 87545, USA*

Corresponding Author: X. Tang, xtang@lanl.gov

The divertor and first wall surface not only recycles the plasma particles as returned neutrals but also returns a portion of the impacting ion kinetic energy to the plasma. Unlike carbon tiles, tungsten walls, for the much larger atomic mass, mostly reflect the impacting light ions and hence recycle a majority of the plasma ion kinetic energy. This hinders the plasma energy exhaust and affects the application of external controls for radiative cooling of the boundary plasma. We have carried out a combination of molecular dynamics simulations and plasma kinetic simulations, together with theoretical analysis, to understand how the plasma sheath and the tungsten recycling characteristics, determine the net plasma power exhaust in terms of the density the temperature of the boundary plasma. The new findings include insights on Bohm criterion which predicts a plasma exit speed that is robustly higher than local sound speed in conventional analysis, and on electron heat flux that is a major component of the plasma energy exhaust flux. More importantly, they point out ways for engineering control of the plasma power exhaust.

Retention and Release of Hydrogen Isotopes in Tungsten Plasma Facing Components: Understanding and Controlling with an Integrated Approach

R. Bisson¹, E. Hodille², F. Ghiorghiu¹, M. Minissale^{1,3}, Y. Addab¹, A. Založnik⁴, Z. Piazza^{1,5}, C. Martin¹, T. Angot¹, M.-F. Barthe⁶, S. Markelj⁴, L. Gallais³, C. Becquart⁵, J. Mougenot⁷, and C. Grisolia²

¹*Physique des Interactions Ioniques et Moléculaires (PIIM), CNRS, Aix-Marseille Université, France*

²*Institut de Recherche sur la Fusion par confinement Magnétique (IRFM),*

Commissariat à l'énergie atomique (CEA/Cadarache), 13108 Saint-Paul-lès-Durance, France

³*CNRS, Institut Fresnel UMR 7249, Aix-Marseille Université, Marseille, France*

⁴*Jožef Stefan Institute, 1000 Ljubljana, Slovenia*

⁵*CNRS, CEMHTI UPR 3079, Université d'Orléans, Orléans, France*

⁶*UMET UMR 8207, CNRS, Université de Lille 1, Villeneuve d'Ascq, France*

⁷*LSPM, CNRS, Université Paris 13, Sorbonne Paris Cité, Villetaneuse, France*

Corresponding Author: R. Bisson, regis.bisson@univ-amu.fr

Fusion fuel trapping (retention) and release from plasma facing components (PFC) is one of the critical issues for ITER and for any future industrial demonstration reactor such as DEMO. Therefore, understanding fundamental mechanisms behind hydrogen isotopes retention in first wall materials is necessary. We developed an approach that couples dedicated experimental studies with modelling at all relevant scales, from microscopic elementary steps to macroscopic observables, in order: 1) to gain insight in the fundamental interactions between fusion fuel and wall materials; 2) to build a reliable and predictive fusion reactor walls model. This integrated approach is applied to tungsten first wall materials with an additional goal in mind: addressing the efficiency of a laser-based method to release in a controlled manner the retained fuel from PFC. Indeed, it remains to assess if thermal gradients involved in laser induced desorption (LID) techniques could be beneficial or detrimental to the bulk distribution of trapped fuel.

In this contribution, a large set of complementary techniques (PAS, SEM, AES, NRA, TDS,...) is used to shed light on the origin of fuel trapping. The experimental dataset is exploited to initialize parameters of a fusion reactor walls model under development. This model based on macroscopic rate equations (MRE) includes all elementary steps: implantation of fusion fuel, defects creation, fuel diffusion in the bulk or towards the surface, fuel trapping on defects, release of trapped fuel during a thermal excursion of PFC. This MRE model is supported by a multiscale description thanks to density functional theory (DFT) and object kinetic Monte Carlo (OKMC) calculations.

Advances in the development of the MRE wall model are presented. In particular, we were able to unambiguously justify the use of a multitrapping site model for tungsten by showing that a single trap type–single trapping energy model was not able to reproduce an extended parameter space study of a well characterized samples exhibiting a single desorption peak. Microscopic identification of the trap type responsible for fuel retention in tungsten is thus on the right track. This new macroscopic model is used for developing a new LID method aiming at depositing locally a controlled amount of laser radiation in order to induce the release of trapped fuel without damaging PFC.



Particle Simulation of Plasma Heat-Flux Dissipation by Evaporated Wall Materials

K. Ibano¹, T. Takizuka¹, D. Nishijima², R. Doerner², H. T. Lee¹, Y. Ueda¹, M. Baldwin², and J. Yu²

¹*Osaka University, Osaka, Japan*

²*University of California San Diego, CA 92093, USA*

Corresponding Author: K. Ibano, kibano@eei.eng.osaka-u.ac.jp

Erosions of the wall materials via melting, sputtering, and vaporization caused by the intense pulsed heat loads during ELMs and disruptions in the fusion devices are the serious concern. At the same time, experimental observations have shown that the intense heat flux causes the formation of vapour layer which dissipates further incoming plasma heat-flux. Understandings on these vapour-shielding phenomena largely influence the lifetime estimation of the wall armours. Thus, experimental and computational approaches are being taken. In the computational approach, the MHD fluid plasma models have been used to simulate this phenomena. These fluids approaches well describe behaviours of low- Z walls such as carbon. However, these fluid models do not include the sheath and non-Maxwellian effects. Thus, in order to study these plasma-vapour-wall interactions including these effects, a 1D3V particle-in-cell (PIC) code has been developed by the authors. Here, we firstly demonstrate the consistency of the simulation results comparing with experimental observation from a linear plasma device; PISCES-B. Decay lengths of the BeI line intensity from the wall were compared as a function of ejected Be amounts and agreements were obtained between them. Then, the calculations of rates of the plasma heat-flux dissipation by the evaporated vapour (Be, W) in a fusion reactor condition were taken. Compared with Be and W, it was found that W shows less effective dissipation even for the vapour pressure larger than its melting point. A cause of this smaller dissipation of W is the prompt redeposition. The short ionization mean free path and redeposition due to its large gyro radius leads the smaller contribution to the plasma heat-flux dissipation. These kinetic effects simulated by the particle code well explain the behaviour of the high- Z wall materials. Compared with these shielding performance of W, the efficient shielding of Be wall can largely reduce the erosion due to the transient heat load events.

TH



Strong Electron Emission Could Enable a New Plasma-Surface Interaction Regime in Divertors

M. Campanell¹, M. Umansky¹

¹*Lawrence Livermore National Laboratory (LLNL), Livermore, CA 94550, USA*

Corresponding Author: M. Campanell, campanell1@llnl.gov

Electron emission from surfaces is important in many plasma applications. Recently, it was shown that a fundamentally distinct plasma-surface interaction regime denoted the “inverse regime” [1] occurs when the emission coefficient exceeds unity. An inverse regime might arise in divertors because secondary and thermionic emission from divertor plates are intense under certain operating conditions. Two characteristics of the inverse regime could offer compelling benefits. First, the sheath potential is positive, so the ions do not accelerate towards the wall. By comparison, ions gain an extra ~ 3 to $5T_e$ of energy in the conventional regime by acceleration in the Bohm presheath and negative sheath potential. A dramatic reduction of physical sputtering is therefore expected in the inverse regime. Secondly, in the inverse regime, an intense cloud of cold (< 1 eV) electrons dominates the quasineutral presheath region near the plasma edge. The cold electron cloud could thereby significantly cool the near-wall plasma, helping to achieve detachment conditions. Further analysis is needed to determine whether an inverse regime is really possible in a SOL and whether it would be beneficial or not.

References

[1] M. D. Campanell and M. V. Umansky, *Phys. Rev. Lett.* **116**, 085003 (2016).

Work performed under the auspices of the U.S. Department of Energy by LLNL under Contract No. DE-AC52-07NA27344.

TH

A Model for Predicting Tritium Flux from Blanket Mock-Up in Tokamak Fusion Reactors

S. Sangaroon¹, T. Onjun², R. Picha³, and J. Promping³

¹*Department of Physics, Mahasarakham University, Mahasarakham, Thailand*

²*Sirindhorn International Institute of Technology, Pathum Thani, Thailand*

³*Thailand Institute of Nuclear Technology, Bangkok, Thailand*

Corresponding Author: S. Sangaroon, siriyaporn.s@msu.ac.th

The tritium is considered as one of main fuels for DT nuclear fusion reactors, where it is planned to be produced from a blanket of reactors by using the interactions between 14.1 MeV neutrons from nuclear fusion reactions and lithium from the blankets. In this work, the simulations of the tritium production from mock-up breeding blanket due to interactions of neutrons and lithium in the blanket are carried out using the Monte Carlo n -particle transport code (MCNP) version MCNPX. Four designs of mock-up breeding blanket, including a design with a pure natural lithium, a design with lithium titanate (Li_2TiO_3) based compound, a design with a compound based on a combination of a pure natural lithium and thorium, and a design with a compound based on a combination of lithium titanate and thorium. It is found that the production of tritium significantly increases with the inclusion of thorium, where an increase of tritium production with a factor of 2 can be achieved.

Investigation of Neutral Particle Dynamics in ADITYA Tokamak Plasma with DEGAS2 Code

R. Dey¹, J. Ghosh¹, M. B. Chowdhuri¹, P. N. Maya¹, R. Manchanda¹, S. Banerjee¹,
N. K. Ramaiya¹, and D. P. Stotler²

The ADITYA Team

¹Institute for Plasma Research (IPR), Bhat, Gandhinagar, India

²Princeton Plasma Physics Laboratory (PPPL), Princeton, NJ 08540, USA

Corresponding Author: R. Dey, ritu.dey@ipr.res.in

Neutral particle behaviour in ADITYA tokamak, which has a circular poloidal ring limiter at one particular toroidal location, has been investigated using DEGAS2 code [1]. The code calculations are based on Monte Carlo algorithms and mainly used in the various tokamaks with divertor configuration. This code has been successfully implemented in ADITYA tokamak with limiter configuration and the simulated radial profile of the H_α emissivity is compared with the experimentally measured profile of H_α emissivity [2]. The simulated radial emissivity profile of H_α matches very well with the experimental one in the edge region up to $r/a \sim 0.8$. However, in the core region ($r/a < 0.8$), the simulated profile deviates substantially from the measured one. The total H_α emission is mainly dominated by atomic hydrogen process throughout the plasma ($r/a = 0$ to 1). The detail investigation of atomic and molecular processes, occurred predominantly at the tokamak plasma edge region, shows that the dissociation of molecular hydrogen ion (H_2^+) is responsible for a larger contribution to H_α emission compared to the dissociation of neutral molecular hydrogen (H_2) in the edge region of ADITYA tokamak. This is due to the higher reaction rate of H_2^+ dissociation at the prevailing edge temperature of ADITYA tokamak. The mismatch between the experimental and the simulated profiles towards the inner region of plasma is likely related to other processes, such as the charge exchange of hydrogen ions with different impurities present in the ADITYA plasma and also to the sputtering of H atoms from the wall [3], which are not included in the DEGAS2 code.

References

- [1] D. P. Stotler, C. F. F. Karney, *Contrib. Plasma Phys.* **34**, 392 (1994).
- [2] S. Banerjee, *et al.*, *J. Plasma Fusion Res. Series* **9**, 29 (2010).
- [3] D. P. Stotler, *et al.*, *Phys. Plasmas* **3**, 4084 (1996).



Plasma-Surface Interactions Leading to Self-Sustained Discharges at the First Wall

M. M. Tsventoukh¹, S. A. Barengolts², I. V. Uimanov³, D. L. Shmelev³, and G. A. Mesyats¹

¹*P. N. Lebedev Physical Institute, RAS, Moscow, Russian Federation*

²*A. M. Prokhorov General Physics Institute, RAS, Moscow, Russian Federation*

³*Institute of Electrophysics, RAS, Ekaterinburg, Russian Federation*

Corresponding Author: M. M. Tsventoukh, elley@list.ru

Intense plasma-surface interactions are accompanied not only by simple surface erosion and by the plasma pollution, but it also can lead to the intense collective phenomena of the electrical discharge that maintains at the first wall and derives the energy from the main plasma. As the fusion plasma typically contains a lot of energy and exhibits intense plasma splashes, e.g., in the ELM form, such a discharges can have a large intensity and duration. Furthermore, the modern first wall surface has a structure with microlayers — e.g., liquid metals (Li), or nanowires structure (*W-fuzz*), or layers that arises from the erosion/deposition pattern; this additionally is very favourable for the self-sustained electrical discharge burning.

We will consider the current theoretical approaches for the ignition and self-sustainment of the pulsed “vacuum discharge” at the first wall surface under external action. Vacuum discharge means the generation of the plasma from the erosion of the electrode materials that being initiated by explosive electron emission pulses from the cathode surface. Such a naturally nonstationary pulses that are responsible for the large current transfer through the system looks to be similar to the bubbles during the boiling. Both helps to emit from the surface a desirable value of matter in a form of portions. The portion of the dense explosive plasma formed within tens of ns within micron scale provides a portion of the current — the electron bunch — ecton.

Arcing phenomenon at the first wall seems to be unavoidable due to the intense plasma action and surface micro relief developed. The modern approaches for vacuum discharge physics under our consideration one allows to propose two general approaches for the arcing influence reduction; i.e., i) the control of the surface layer geometry (in particular the *W-fuzz* thickness), and ii) the control of the surface layer material properties (in particular the *W-fuzz* average density).

Work was supported by RFBR grant 15-38-20617.



Assessment of X-Point Target Divertor Configuration for Power Handling and Detachment Front Control

M. Umansky¹, M. Rensink¹, T. Rognlén¹, B. LaBombard², D. Brunner², J. Terry², and D. G. Whyte²

¹Lawrence Livermore National Laboratory (LLNL), Livermore, CA 94550, USA

²Massachusetts Institute of Technology (MIT), Cambridge, MA 02139, USA

Corresponding Author: M. Umansky, umansky1@llnl.gov

The challenges that will be facing the divertor in a tokamak-based fusion reactor prompt the search for innovative divertor configurations that use nonstandard magnetic geometry and additional X-points. Standard tokamak edge plasma transport codes such as UEDGE and SOLPS can be invaluable tools for exploration and evaluation of alternate divertor configurations for potential performance enhancements; however the presence of secondary X-points in the divertor has, up to now, hindered such application. A recent upgrade to UEDGE allows including a secondary X-point in the divertor, and in the present study UEDGE is used to analyze the recently proposed X-point target divertor that combines a radially extended outer leg with a secondary X-point placed in the outer leg volume. It is found in the modelling that as the input power into SOL is reduced to a threshold value, the outer divertor leg transitions to a fully detached state with the detachment front localized near the secondary X-point. Reducing the power further results in the front shifting upstream but remaining stable. As the power is reduced, the detachment front eventually moves to the primary X-point, which is associated with an X-point MARFE. However, for the X-point target divertor a fully detached divertor regime is maintained over a factor of 5–10 variation in the input power while for an otherwise similar parameter variation performed with a standard vertical plate divertor a much smaller detachment operational window is found. These results suggest that a stable, fully detached divertor operation over a wide parameter range may be realized for a tokamak with radially extended outer divertor legs.

TH

FIP: Fusion Engineering, Integration and Power Plant Design



Recent Progress of ITER Package in ASIPP

P. Fu¹, Y. T. Song¹, Y. Wu¹, J. Wei¹, and L. Q. Hu¹

¹*Institute of Plasma Physics, Chinese Academy of Sciences, Hefei, Anhui, People's Republic of China*

Corresponding Author: P. Fu, fupeng@ipp.ac.cn

ASIPP has taken the responsibility of most CN ITER package. All packages follow current ITER schedule.

The superconducting conductor package consists of 106 conductors with 6 kinds includes 7.5% TF conductor, total PF conductor from PF2 to PF5, total CC conductor, and MB and CB conductor of feeder. Now total CN TF conductor package has been completed in production, and delivered to IO; completed the production and acceptance test of CC and feeder conductor package; completed the production and acceptance test of 35 PF conductors and 4 dummy conductors.

The ITER feeder system consists of 31 units. They convey power and coolant to magnets, and hold the numerous instrumentation channels with the functioning of magnets system operation and monitoring. Now ASIPP has completed all qualification work and started manufacturing after PF4 CFT MRA meeting.

The ITER Correction Coils (CC) consists of three sets of six coils each. Each pair of coils located on opposite sides with respect to the plasma is series connected with polarity such to produce asymmetric fields. The CC PA was signed between IO and CN DA in 2010, now ASIPP has developed the manufacturing process including winding process, VPI technology, laser beam welding, helium inlet/outlet welding technology, and production qualification process is still on going.

CN power supply package consists of PF AC/DC converter, reactive power compensation and harmonic filter (RPC&HF), and pulsed power electrical network materials (PPEN). ASIPP takes responsibility of key technology R&D, all kind test, integration and technical support. ASIPP has completed AC/DC converter and RPC&HF prototype test and integration test, and started its manufacturing since 2015. Now first PF AC/DC converter unit manufacturing has been completed and qualified by IO, 15 kinds of PPEN equipment have been delivered to IO site.

ASIPP has two ITER diagnostic procurements, #12 horizontal port plug and radial X-ray camera (RXC). Port integration group has organized a system integration review meeting in July 2015 with mostly general issues be resolved or analyzed, most model clashes between tenants have been resolved. RXC's structure design is optimized and installation process is studied considering the simplification and easiness of maintenance. Remote handling skills and tools are designed for the system maintenance after being activated.



ITER Central Solenoid Module Fabrication

J. Smith¹, D. Norausky¹, D. Priddie¹, K. Schaubel¹, and A. Stephens¹

¹General Atomics, San Diego, CA 92186, USA

Corresponding Author: J. Smith, john.smith@ga.com

The fabrication of the modules for the ITER central solenoid (CS) has started in a dedicated production facility located in Poway, California, USA. The necessary tools have been designed, built, installed and tested in the facility to enable the start of production. The current schedule has first module fabrication completed in 2017, followed by testing and subsequent shipment to ITER.

The central solenoid is a key component of the ITER tokamak providing the inductive voltage to initiate and sustain the plasma current and to position and shape the plasma. The design of the CS has been a collaborative effort between the US ITER Project Office (US ITER), the international ITER Organization (IO) and General Atomics (GA). GA's responsibility includes completing the fabrication design, developing and qualifying the fabrication processes and tools, and then completing the fabrication of the seven 110 tonne CS modules. The modules will be shipped separately to the ITER site, stacked and aligned in the assembly hall prior to insertion in the core of the ITER tokamak.

A dedicated facility in Poway, California, USA has been established by GA to complete the fabrication of the seven modules. Infrastructure improvements included thick reinforced concrete floors, a diesel generator for backup power along with cranes for moving the tooling within the facility. The fabrication process for a single module requires approximately 22 months followed by 5 months of testing, which includes preliminary electrical testing followed by high current (48.5 kA) tests at 4.7 K. The production of the 7 modules is completed in a parallel fashion through ten process stations. The process stations have been designed and built with most stations having completed testing and qualification for carrying out the required fabrication processes.

The final qualification step for each process station is achieved by the successful production of a prototype coil. Fabrication of the first ITER module is in progress. The seven modules will be individually shipped to Cadarache upon their completion.

This paper describes the processes and status of the fabrication of the CS Modules for ITER.



Long-Pulse Acceleration of 1 MeV Negative Ion Beams toward ITER and JT-60SA Neutral Beam Injectors

J. Hiratsuka¹, A. Kojima¹, N. Umeda¹, M. Hanada¹, M. Kashiwagi¹, M. Yoshida¹, R. Nishikiori¹, M. Ichikawa¹, K. Watanabe¹, H. Tobar¹, M. Dairaku¹, H. Yamanaka¹, H. Abe¹, R. Kawamata¹, N. Shibata¹, T. Maejima¹, Y. Terunuma¹, Y. Oda¹, N. Akino¹, K. Mogaki¹, S. Sasaki¹, N. Seki¹, S. Nemoto¹, T. Shimizu¹, Y. Endo¹, K. Miyamoto², Y. Yamano³, and L. Grisham⁴

¹Japan Atomic Energy Agency (JAEA), Naka, Japan

²Naruto University, Japan

³Saitama University, Japan

⁴Princeton Plasma Physics Laboratory (PPPL), Princeton, NJ 08540, USA

Corresponding Author: J. Hiratsuka, hiratsuka.junichi@jaea.go.jp

In order to realize the negative-ion-based neutral beam (NB) systems for ITER and JT-60SA, development of the Multiaperture and Multigrad (MAMuG) electrostatic accelerator is one of common critical issues. For these NB injectors, 5- and 3-stage MAMuG accelerators are being developed to achieve the acceleration of negative ion beams up to 1 MeV, 40 A (200 A/m²) for 3600 s and 0.5 MeV, 22 A (130 A/m²) for 100 s, respectively. However, there were no experiments of long-pulse MeV-class beam acceleration. Though JAEA achieved the rated beam energy of 1 MeV, the pulse duration was limited to be less than 1 s [1] due to a low voltage holding capability and high grid power loads.

After the last FEC conference, the following issues were investigated, such as multigrad effect on the voltage holding capability and reduction of the grid power loads. New accelerators have been designed to realize stable voltage holding by taking into account the multigrad effect on voltage holding capability, which satisfies the requirement of beam energy for ITER and JT-60SA with 5-stage and 3-stage, respectively. The grid power load has been suppressed less than a half of the design values of the accelerators by modifying the geometry of the extractor and the acceleration grids to suppress generation of secondary electrons.

By applying the developed techniques based on the R&D results, the hydrogen negative ion beams of 0.97 MeV, 190 A/m² have been successfully accelerated up to 60 s from the ITER prototype accelerator. The pulse duration of such high power density negative ion beams (~184 MW/m²) has been extended from 0.4 to 60 s, which is currently the longest pulse length in the world. There is no limitation to extend the pulse duration, since no degradation of the voltage holding has been observed during the long-pulse operations neither by caesium accumulation nor by thermal damage of the acceleration grids. This achievement is one of the breakthroughs toward the realization of the high-energy NB systems.

References

[1] A. Kojima, *et al.*, Nucl. Fusion **55**, 063006 (2015).

Towards Powerful Negative Ion Beams at the Test Facility ELISE for the ITER and DEMO NBI System

U. Fantz¹, C. Hopf¹, D. Wunderlich¹, R. Friedl², M. Frösche¹, B. Heinemann¹, W. Kraus¹,
U. Kurutz², R. Riedl¹, R. Nocentini¹, and L. Schiesko¹

Rapporteured by: J. Hiratsuka

¹Max-Planck-Institut für Plasmaphysik, Garching, Germany

²Experimentelle Plasmaphysik (EPP), University of Augsburg, Augsburg, Germany

Corresponding Author: U. Fantz, fantz@ipp.mpg.de

The negative ion source test facility ELISE represents an important step in the European R&D roadmap towards the neutral beam injection (NBI) systems at ITER. ELISE provides early experience with operation of large RF-driven negative hydrogen ion sources. Its source area is $1 \times 0.9 \text{ m}^2$ and the net extraction area of 0.1 m^2 , formed by 640 apertures, corresponds to a half-size ITER source. The test facility aims at demonstrating large-scale extraction and acceleration of negative hydrogen ions (H^- , D^-) for pulses of up to 1 h with half the current required on ITER. Additionally, the ratio of coextracted electrons to ions must be kept below one, which is quite demanding in particular for deuterium operation. Starting with first plasma pulses in March 2013, ELISE has meanwhile demonstrated stable 1 h plasma discharges in hydrogen with repetitive 10 s extraction every 3 min with 9.3 A extracted current and an electron-to-ion ratio of 0.4 at the pressure required by ITER of 0.3 Pa but using only one quarter of the available RF power. At half of the available RF power a stable 400 s plasma discharge was achieved with 18.3 A beam pulses at an electron-to-ion ratio of 0.7. Linear scaling towards full RF power predicts that the target value of the negative ion current can be achieved or even exceeded. Issues in long pulse operation are the caesium dynamics and the stability of the coextracted electron current. Newly developed magnetic filter field configurations allowed achieving for the first time 1 h pulses in deuterium with an electron-to-ion ratio below one, however only at a quarter of the available RF power. Advanced beam diagnostics such as beam emission spectroscopy and a sophisticated diagnostic calorimeter reveal that the requirement on the uniformity of these large beams (deviations $< 10\%$) can be met.

For a DEMO fusion reactor, the requirements of a heating and current drive system will strongly depend on the DEMO scenario and are presently assessed within EUROfusion WPHCD. As NBI systems based on negative ions are regarded as one candidate, ELISE could serve in a later stage as a test bed for concepts concerning RF efficiency, operation without caesium or with largely reduced caesium consumption, and neutralization by a laser neutralizer in order to improve efficiency and reliability. IPP's present small scale experiments show promising results.



Progress of Experimental Study on Negative Hydrogen Ion Production and Extraction

M. Kisaki¹, K. Tsumori¹, K. Ikeda¹, H. Nakano¹, S. Geng², T. Tokuzawa¹, M. Osakabe¹, K. Nagaoka¹, P. Agostinetti³, M. Brombin³, A. Hatayama⁴, S. Nishioka⁴, E. Sartori³, G. Seriani³, P. Veltri³, O. Kaneko¹, and Y. Takeiri¹

¹National Institute for Fusion Science (NIFS), Toki, Gifu, Japan

²Graduate University for Advanced Studies (SOKENDAI), Hayama, Kanagawa, Japan

³Consorzio RFX, Associazione EURATOM-ENEA sulla Fusione, Padova, Italy

⁴Keio University, Yokohama, Japan

Corresponding Author: M. Kisaki, kisaki.masashi@lhd.nifs.ac.jp

Development of the high performance negative hydrogen ion source is a fundamental demand in realizing fusion reactor. In order to clarify the extraction mechanism of H^- , temporal and spatial variations of the negative ions and electrons in the extraction region are intensively surveyed at NIFS. In addition, the beam acceleration experiments have been performed by changing the accelerator configuration in order to improve the voltage holding capability and to study the negative ion beam optics.

In a caesiated hydrogen plasma, it was observed that the negative hydrogen ion density (n_{H^-}) becomes one order higher in magnitude than the electron density (n_e) in the vicinity of the plasma grid (PG). The response of negative-ion rich plasmas to the extraction field was investigated by measuring the plasma potential (V_p) profiles in the axis perpendicular to the PG before and during beam extraction. The V_p increases with applying the extraction field, and the influence of the extraction field on the V_p was observed at 30 mm from the PG. As for the n_{H^-} , it was also observed that the extraction field affects on the n_{H^-} at 30 mm from the PG, where the n_{H^-} decreases simultaneously with the beam extraction. These observations indicate that the extraction field affects the particle dynamics in the wide region extending over 30 mm from the PG. This feature is completely different from that of electron-ion plasmas.

We also found that the negative ion production efficiency becomes twice higher by changing the shape of grounded grid holes without any modification on the plasma chamber. We assumed that the behaviour of the back-streaming ion was affected by changing the GG. The back-streaming ion trajectory was analyzed with the beam trajectory simulation, and it was found that the back-streaming ion distributes in the larger area on the back plate with the slot GG. This implies that some part of condensed Cs on the back plate was more effectively evaporated by the back-streaming ion with the slot GG and that Cs flux onto the PG surface increased, which resulted in the enhancement of the negative ion production. This result suggests that the accelerator configuration is one of the key factors to determine the negative ion production efficiency and that the Cs consumption can be reduced by the Cs recycling from the wall of the ion source chamber.



Progress in High Power Test of R&D Source for ITER ICRF System

A. Mukherjee¹, R. Trivedi¹, R. Singh¹, R. Kumar¹, D. Soni¹, S. Verma¹, G. Suthar¹, A. Jha¹, P. A. Subbarao¹, M. Patel¹, R. Anand¹, R. Agarwal¹, K. Mohan¹, H. Jayanthi¹, H. Machchhar¹, P. Vasava¹, H. Patel¹, H. Dalicha¹, U. Baruah¹, A. Patel¹, N. Singh¹, N. S. Goswani¹, K. R. Mehta¹, D. V. Upadhyay¹, H. Dhola¹, F. Kazarian², B. Beaumont², A. Agharbi³, A. Boussaton³, P. Cacheux³, A. Debliche³, M. Grézaud³, N. Péneau³, F. Pompon³, C. Robert³, M. Savoie³, and S. Sierra³

¹Institute for Plasma Research (IPR), Bhat, Gandhinagar, India

²International Thermonuclear Experimental Reactor (ITER), Cadarache Centre, 13108 Saint-Paul-lès-Durance, France

³Thales Electron Devices S.A., Velizy, France

Corresponding Author: A. Mukherjee, aparajita.mukherjee@iter-india.org

The IC H&CD system is one of the major tools for achieving the plasma performances foreseen in ITER's operation scenario. This system is designed to provide 20 MW into the plasma, at frequencies included in the band 40 MHz to 55 MHz. For ensuring 20 MW power availability for plasma operation, 24 MW is required at the output of the RF sources. India is responsible to deliver nine numbers of RF Sources to the ITER system. Each source shall have the power handling capability of 2.5 MW/CW at VSWR 2 : 1 in the frequency range 35–65 MHz or 3.0 MW/CW at VSWR 1.5 : 1 in the frequency range 40–55 MHz, along with other stringent requirement. An urgent need for prequalification of final stage tube and few critical components is established through R&D programme to bridge the significant gap between demonstrated capability of RF source system at various worldwide fusion facilities versus ITER need, in terms of power level, pulse duration and bandwidth (BW) requirement.

In 2012, ITER-India has signed a contract with Thales Electron Devices (France) for establishing the technology in very high power RF amplifiers, using Diacrode tube. The contract is to design and develop driver and final stage amplifiers. Tubes and cavities are integrated in full amplifier chain developed by ITER-India. To test the performance of the amplifier chains at matched and mis-matched load condition, high power test rig (3 MW/CW capability) is developed at Indian test facility.

After successful assembly and integration of RF amplifier at Indian test facility, high power RF tests initiated. The objective for the tests is to confirm 1.5 MW output at 35–65 MHz for 2000 s with ~1 MHz BW (at 1 dB point) over central frequency and to check the reliability of both the tube and the amplifier with a mismatched load (up to VSWR 2 : 1) which simulates power transmission to an antenna coupled to the plasma.

This paper reports successful commissioning of RF amplifier and the achievement of 1.5 MW of RF power for more than 2000 s, confirming other extremely challenging specifications and describes the operating scenarios, dissipation limit, safety system and various infrastructure developed at Indian test facility to support such operation.



New Results of Development of Gyrotrons for Plasma Fusion Installations

G. Denisov¹, A. Litvak¹

¹*Institute of Applied Physics (IAP), Russian Academy of Sciences (RAS), Nizhny Novgorod, Russian Federation*

Corresponding Author: G. Denisov, den@appl.sci-nnov.ru

Gyrotrons for plasma fusion installations usually operate at frequencies 40–170 GHz. Requested output power of the tubes is about 1 MW and pulse duration is between seconds and thousands seconds. To provide operation with indicated parameters the gyrotrons have very large transverse cavity sizes, output barrier windows made of CVD diamond discs, effective collectors with particle energy recovery.

In ITER installation there will be 24 gyrotron systems with 1 MW power each. Russian contribution consists of 8 gyrotron systems. ITER requirements are: frequency 170 GHz, 1 MW power, 1000 s pulse duration, high efficiency of the gyrotrons over 50%, possibility of power modulation with frequency up to 5 kHz, compatibility of the gyrotron complex with ITER control system. In May, 2015 a prototype of ITER gyrotron system was completed and its operation was demonstrated. The system consists of gyrotron oscillator, liquid-free superconducting magnet, supplementary magnets, several electric power supplies, cooling systems control and protection systems, and other auxiliary units. The tests were performed in presents of ITER IO and ITER RF DA representatives. In October, 2015 final design procedure for the gyrotron system was successfully passed.

High-level parameters were also achieved with long-pulse 140 GHz gyrotrons developed for EAST and KSTAR installations. Significant results were shown on the way to 1.5–2 MW, CW gyrotrons. The development of higher frequency (230–700 GHz) gyrotrons for future plasma installations and for plasma diagnostics began. Novel ideas were proposed to enhance gyrotron operation



Development of Multifrequency Megawatt Gyrotrons for Fusion Devices in JAEA

R. Ikeda¹, T. Kobayashi¹, Y. Oda¹, K. Kajiwara¹, K. Takahashi¹, S. Moriyama¹, and K. Sakamoto¹

Rapporteured by: G. Denisov

¹*Japan Atomic Energy Agency (JAEA), Naka, Japan*

Corresponding Author: R. Ikeda, ikedar@iter.jp

Megawatt gyrotrons with frequency tuning have become essential devices in fusion science to perform effective EC H&CD. JAEA is developing two types of multifrequency gyrotrons equipped with a triode magnetron injection gun for ITER and JT-60SA. A TE_{31,11} mode, which is a candidate mode for 170 GHz oscillation, has sufficient margin for cavity heat-load in 1 MW operation, and it has a great advantage for multifrequency oscillation. In the JT-60SA project, EC H&CD by second harmonic EC waves are planned using nine sets of 110 GHz/138 GHz dual-frequency gyrotrons to broaden the experimental research area. In FEC-2014, demonstrations of 1 MW oscillations for 2 s at 170 GHz/137 GHz/104 GHz with the ITER gyrotron and achievement of 1 MW oscillations for 100 s at 110 GHz/138 GHz in the JT-60SA gyrotron were reported as world records. After FEC-2014, oscillation methods to improve the efficiency at 170 GHz for ITER requirements and higher frequency oscillation for the demo-class reactor were investigated. For the JT-60SA gyrotron, the operation area was expanded to surpass maximum performance (1.5 MW, 4 s) of the previous JT-60 110 GHz gyrotron. The TE_{31,11} mode oscillations were often prevented by adjacent counter-rotating (ctr-) modes such as TE_{29,12}, and TE_{28,12} modes. By introducing active anode-voltage control and beam-radius control to suppress adjacent counter-rotating modes, start-up of TE_{31,11} mode becomes stable and the overall efficiencies achieved ~50% up to 1.1 MW.

In looking ahead to a future gyrotron for the demo-class reactor, 203 GHz oscillation of higher-order volume mode (TE_{37,13}) was performed for the first time by taking advantage of the multifrequency gyrotron feature. In preliminary testing at 203 GHz, 0.9 MW for 0.3 ms and 0.42 MW for 5 s were demonstrated. ITER gyrotron having megawatt-class power at four frequencies in wide range over 100 GHz was developed. High power gyrotron development toward 1.5–2 MW oscillation for several seconds has been carried for further extension of the experiment regime of high performance plasma in JT-60SA. In a test conducted in 2015, achievements of 1.8 MW, 1.2 s at 110 GHz (TE_{22,8} mode) in noncoaxial type gyrotron and high-power oscillation of 1.3 MW, 1.3 s at 138 GHz (TE_{27,10} mode) and 1 MW, 1 s of 82 GHz (TE_{17,6} mode) have been demonstrated as a new world record.

Development of over-MW Gyrotrons for Fusion at Frequencies from 14 GHz to Sub-THz

T. Kariya¹, T. Imai¹, R. Minami¹, T. Numakura¹, K. Tsumura¹, Y. Ebashi¹, Y. Endo¹, R. Ikezoe¹, Y. Nakashima¹, K. Sakamoto², Y. Oda², R. Ikeda², K. Takahashi², T. Kobayashi², S. Moriyama², T. Shimozuma³, S. Kubo³, Y. Yoshimura³, H. Takahashi³, H. Igami³, S. Ito³, K. Okada³, S. Kobayashi³, T. Mutoh³, H. Idei⁴, K. Hanada⁴, K. Nagasaki⁵, M. Ono⁶, T. Eguchi⁷, and Y. Mitsunaka⁷

Rapporteur by: G. Denisov

¹Plasma Research Center, University of Tsukuba, Tsukuba, Ibaraki, Japan

²Japan Atomic Energy Agency (JAEA), Naka, Japan

³National Institute for Fusion Science (NIFS), Toki, Gifu, Japan

⁴Research Institute for Applied Mechanics (RIAM), Kyushu University, Kasuga, Japan

⁵Institute of Advanced Energy, Kyoto University, Nishikyo-ku, Kyoto 615-8540, Japan

⁶Princeton Plasma Physics Laboratory (PPPL), Princeton, NJ 08540, USA

⁷Toshiba Electron Tubes and Devices Co., Ltd, Tochigi, Japan

Corresponding Author: T. Kariya, kariya@prc.tsukuba.ac.jp

Megawatt (MW) gyrotrons with a wide frequency range from 14 to 300 GHz are being developed for the collaborative electron cyclotron heating (ECH) study of advanced fusion devices and DEMO reactor. 1) In the first experiment of 300 GHz gyrotron, an output power of over 0.5 MW with TE_{32,18} single-mode was achieved with a pulse width of 2 ms. This is the first report of MW level oscillation with the DEMO-relevant ECH gyrotron mode. It was also found that the reflection at the output window affects the oscillation mode determination. 2) A new record of the 28 GHz gyrotron output of 1.38 MW was obtained. The fabrication of a newly designed tube aimed at a dual-frequency output power of 2 MW at 28 GHz (0.4 MW CW) and 1 MW at 35 GHz has begun, with all components ready for assembly. Before installing a double-disk window in the dual-frequency gyrotron, we confirmed the dependence of reflective power on the coolant thickness including the reflective power less than 2% by the cold test using a Gunn diode power of 1 W and the hot test using the gyrotron output power of 600 kW. 3) Based on the successful results of 77 and 154 GHz LHD tubes, the new design of a 154/116 GHz dual-frequency gyrotron with output of over 1.5 MW has been presented.



Progress of Qualification Testing for Full-Scale Plasma-Facing Unit Prototype of Full Tungsten ITER Divertor in Japan

Y. Seki¹, K. Ezato², S. Suzuki², K. Yokoyama², H. Yamada², T. Hirayama², T. Hirai³,
F. Escourbiac³, A. Volodin⁴, and V. Kuznetsov⁴

¹National Institutes for Quantum and Radiological Science and Technology (QST), Naka Fusion Institute,
Naka-shi, Ibaraki-ken, Japan

²Japan Atomic Energy Agency (JAEA), Naka, Japan

³International Thermonuclear Experimental Reactor (ITER),
Cadarache Centre, 13108 Saint-Paul-lès-Durance, France

⁴D. V. Efremov Institute of Electrophysical Apparatus (JSC-NIIEFA), St. Petersburg, Russian Federation

Corresponding Author: Y. Seki, seki.yohji@qst.go.jp

R&D for starting operation with a full-tungsten (W) ITER (INB-174) divertor have been enhanced by recommendation of the ITER council since 2011. Japan Atomic Energy Agency (JAEA) as Japanese Domestic Agency (JADA) and the ITER organization (IO) have been actively working on the development and demonstration on the full-W ITER divertor under the framework of the task agreement. JAEA is in charge of technology development and demonstration for manufacturing the outer vertical target (OVT) together with Japanese industries. In 2013, as the first phase of the qualification programme, JAEA demonstrated the armour heat sink bonding technology with small-scale mock-ups. A high heat flux (HHF) testing for the mock-ups was carried out in the ITER divertor test facility in Efremov Institute, Russia. JAEA succeeded in demonstrating the durability of the W monoblock joint to the Cu-alloy cooling tube against the heat load of 10 MW/m² for 5000 cycles and 20 MW/m² for 1000 cycles, which are three times higher than a requirement (300 cycles). This result provided one of sufficient materials for the decision to start with the full-W ITER divertor in the baseline. Since 2014, as the second phase, the full-scale plasma-facing unit (PFU) prototypes have been manufactured to demonstrate the scale-up manufacturing technology.

In this paper, JAEA reports R&D progress on the full-scale PFU prototypes of a full-W ITER divertor OVT. Under a framework of a W divertor qualification programme, JAEA manufactured seven full-scale PFUs as prototypes. Through the manufacturing, i) all joint surfaces in four PFUs with a casting Cu interlayer successfully passed the ultrasonic testing, and, ii) the surface profile in target part of PFUs stayed within a tolerance. iii) Moreover, JAEA succeeded in demonstrating a durability for the HHF testing of the repetitive heat load of 10 MW/m² for 5000 cycles and 20 MW/m² for 1000 cycles under close collaboration with the IO and the Efremov Institute. These results demonstrated the ability of Japanese industries to produce the PFU of full-W ITER divertor enough to meet the technical requirements.



Progresses on WEST Platform Construction towards First Plasmas

J. Bucalossi¹, M. Missirlian¹, P. Moreau¹, F. Samaille¹, E. Tsitrone¹, T. Alarcon¹, S. Antusch², M.-H. Aumeunier¹, S. Balme¹, T. Batal¹, J. M. Bernard¹, F. Bouquety¹, C. Bourdelle¹, S. Bremond¹, S. Brezinsek³, C. Brun¹, H. Bufferand¹, Y. Camenen⁴, B. Cantone¹, M. Chantant¹, M. Chernyshova⁵, G. Ciraolo¹, G. Colledani¹, J. Colnel¹, E. Corbel¹, Y. Corre¹, X. Courtois¹, R. Daniel⁶, T. Daudel¹, R. Dejarnac⁷, E. Delmas¹, L. Delpéch¹, C. Desgranges¹, L. Doceul¹, D. Douai¹, H. Dognac¹, A. Ekedahl¹, D. Elbeze¹, A. Escarguel⁴, F. Escourbiac⁸, K. Ezato⁹, F. Faisse¹, C. Fenzi¹, F. Ferlay¹, M. Firdaoussi¹, J. L. Gardarein¹⁰, L. Gargiulo¹, J. Gaspar¹, P. Gavila¹¹, S. Gazzotti¹, J. C. Giacalone¹, C. Gil¹, E. Grigore¹², D. Guilhem¹, J. P. Gunn¹, A. Hakola¹³, J. C. Hatchressian¹, W. Helou¹, P. Hennequin¹⁴, C. Hernandez¹, M. Houry¹, M. Jouve¹, C. Klepper¹⁵, G. Laffont¹⁶, P. Languille¹, S. Larroque¹, Q. Li¹⁷, J. Linke³, M. Lipa¹, P. Lotte¹, G.-N. Luo¹⁷, Y. Marandet⁴, C. Martin⁴, A. Martinez¹, D. Mazon¹, O. Meyer¹, P. Mollard¹, E. Nardon¹, R. Nouailletas¹, H. K. Park¹⁸, J. Y. Pascal¹, B. Pégourie¹, R. A. Pitts⁸, C. Pocheau¹, S. Poli¹, N. Ravenel¹, B. Riccardi¹¹, M. Richou¹, M. Rieth², H. Roche¹, C. Ruset¹², F. Sabathier¹, A. Saille¹, F. Saint-Laurent¹, B. Santraine¹, Y. Seki⁹, D. Sestak⁷, J. Signoret¹, B. Soler¹, S. Suzuki⁹, D. Thouvenin¹, L. Toulouse¹, J.-M. Travere¹, W. Treutterer¹⁹, S. Vartanian¹, J.-M. Verger¹, L. Vermare¹⁴, N. Vignal¹, Y. Wang²⁰, Y. Wang¹⁷, A. Werner²¹, Q. Yang¹⁷, B. Zago¹, W. Zhao²⁰, and G.-W. Zhong²⁰

The WEST Team *Rapporteured by: Y. Seki*

¹Institut de Recherche sur la Fusion par confinement Magnétique (IRFM), Commissariat à l'énergie atomique (CEA/Cadarache), 13108 Saint-Paul-lès-Durance, France

²Institute for Applied Materials (IAM-KIT), 76344 Eggenstein-Leopoldshafen, Germany

³Forschungszentrum Jülich, Jülich, Germany

⁴Physique des Interactions Ioniques et Moléculaires (PIIM), CNRS, Aix-Marseille Université, France

⁵Institute of Plasma Physics and Laser Microfusion, Warsaw, Poland

⁶Institute for Plasma Research (IPR), Bhat, Gandhinagar, India

⁷Institute of Plasma Physics AS CR v.v.i., Prague, Czech Republic

⁸International Thermonuclear Experimental Reactor (ITER), Cadarache Centre, 13108 Saint-Paul-lès-Durance, France

⁹Japan Atomic Energy Agency (JAEA), Naka, Japan

¹⁰Institut Universitaire des Systèmes Thermiques Industriels (IUSTI), Aix-Marseille Université, France

¹¹F4E: Fusion for Energy, ITER EU Centre, 08019 Barcelona, Spain

¹²National Institute of Laser, Plasma and Radiation Physics (INFLPR), Bucharest, Romania

¹³VTT Technical Research Centre of Finland Ltd., Espoo, Finland

¹⁴École Polytechnique, 91128 Palaiseau, France

¹⁵Oak Ridge National Laboratory (ORNL), Oak Ridge, TN 37831, USA

¹⁶Commissariat à l'énergie atomique (CEA/LIST), 91120 Palaiseau, France

¹⁷Institute of Plasma Physics, Chinese Academy of Sciences, Hefei, Anhui, People's Republic of China

¹⁸Ulsan National Institute of Science and Technology (UNIST), Ulsan, Republic of Korea

¹⁹Max-Planck-Institut für Plasmaphysik, Garching, Germany

²⁰Southwestern Institute of Physics, Chengdu, Sichuan, People's Republic of China

²¹Max-Planck-Institut für Plasmaphysik, Greifswald, Germany

Corresponding Author: J. Bucalossi, jerome.bucalossi@cea.fr

Continued...

The WEST platform, which is a major evolution of Tore Supra towards a steady-state tungsten diverted tokamak, is targeted at minimizing risks for ITER divertor procurement and operation. This paper presents an overview of the status and relevant technical issues for the new platform. At the time of the writing, the 4 m diameter thick casing of the upper and lower divertor in-vessel coils has been manufactured, assembled inside the torus and accurately positioned. The in-situ winding of the water cooled copper conductor requiring about 140 brazings is underway. The complex assembly sequence as well as the resin epoxy impregnation has been simulated and validated on a full scale mock-up. The power supplies which will feed the divertor coils have been produced. Factory acceptance test have been performed and the two power supplies will be installed at Cadarache this summer.

The procurement of the ITER-like divertor plasma facing units (PFUs), using the ITER tungsten monoblock technology, is ongoing in collaboration with the European and Japanese Domestic Agencies in charge of providing ITER divertor vertical targets. Prototypes are in preparation and will be tested in WEST before launching series production. Tungsten-coated technologies have been developed and qualified on various substrates to cover the other high heat flux plasma facing components. In particular, inertial graphite PFUs with improved CMSII tungsten coating (15 μm) have been qualified and manufactured in order to complement the ITER-like prototypes of the WEST lower divertor for the first phase of operation. The new CW ELM-resilient ICRH antennas are in manufacturing and the first one will be assembled in spring 2016. The existing LHCD launcher front faces have been reshaped to match the new plasma geometry. The overall diagnostic layout is finalized. Key diagnostics are being upgraded to allow for a proper monitoring of the divertor plasma facing units, the tungsten sources and transport. A new plasma control system prototyping ITER requirements is being implemented. WEST is presently scheduled to be operational in late 2016.



Design and R&D Progress of Chinese HCCB TBS Programme

K. Feng¹, W. Xiaoyu¹

¹*Southwestern Institute of Physics, Chengdu, Sichuan, People's Republic of China*

Corresponding Author: K. Feng, fengkm@swip.ac.cn

The current design of the Chinese helium-cooled ceramic breeder test blanket module (HCCB TBM) with 1×4 configuration scheme, includes four independent breeding sub-modules with 10 mm gap (for thermal expansion) between each other along the poloidal direction. These submodules are connected to a big back plate containing auxiliary connection pipes for coolant and purge gas, shear keys and flexible supports forming a whole TBM. The TBM is connected to the helium cooling system (HCS) and tritium extraction system (TES) by means of pipes in the back plate. A 3D neutronics calculation for the updated TBM module design has been completed. Preliminarily, a simplified analysis model for the submodule of TBM is adopted.

In order to validate the design of CN HCCB TBS (module and system), much material R&D has been performed according to the technical requirements. The RAFM material of Chinese low-activation ferritic (CLF-1) steel has been developed and is scaled up to 5 ton ingot, which is used for the structure material certification. At the same time, 1 dpa neutron irradiation test in high flux test reactor and its PIE experiment has been performed. Based on the CLF-1 steel, some mock-ups have been fabricated by the different techniques and tested. A 1/3-size mock-up of the TBM module is under fabrication and will be tested soon.

The fabrication techniques for the functional materials, such as beryllium and Li_4SiO_4 , have also been developed and the related properties have been obtained. The fabrication of back plate system could be the current largest challenge for HCCB TBM. Several welding technologies and manufacture process are investigated on different size plates, including laser welding (LW) process for the BP and the FW, HIP welding for FW. The welding of the CLF-1 with the 316 L(N) IG (ITER Grade) is dissimilar welding process for assembling TBM module and shield block. For the manufacturing solution of FW, hot isostatic pressing (HIP) is a realistic process, and the base welding experimental researches for the HIP joining of RAFMs CLF-1 are being carried out to prepare for the next forming welding practices of FW at present.

A small-type helium gas testing loop (HGTL) is under construction, which will be used for the future component testing and operation testing. The design temperature is 300°C at a working He gas pressure of 8 MPa.



Lessons Learned for the Breeding Blanket Designers from the Design Development of the European Test Blanket Module Systems (He, Tritium, Liquid Metal Systems)

I. Ricapito¹, P. Calderoni¹, M. Ferrari¹, L. Giancarli², Y. Poitevin¹, and D. Panayotov¹

¹F4E: Fusion for Energy, ITER EU Centre, 08019 Barcelona, Spain

²International Thermonuclear Experimental Reactor (ITER),
Cadarache Centre, 13108 Saint-Paul-lès-Durance, France

Corresponding Author: I. Ricapito, italo.ricapito@f4e.europa.eu

The general objective of the ITER TBM Programme is to provide the first experimental data on the performance of the breeding blankets in the integrated fusion nuclear environment. Such data are essential to design and predict the performance of DEMO and future fusion reactors. To achieve this objective, the TBM programme will have to:

- test and validate technologies and materials in a fusion relevant environment in view of their further development for DEMO and power plants, and
- validate and qualify predictive tools for the design of the breeding blankets in DEMO and power plants.

To comply with this mission, the TBM programme will cover the full lifetime of ITER operation, with testing of series of TBM specifically instrumented for maximizing the ROX (return on experience) for each ITER operational phase in view of the DEMO breeding blanket design. The design of the European test blanket systems (TBS), helium cooled lithium lead (HCLL) and helium cooled pebble bed (HCPB), has concluded its conceptual phase. Particularly during the development of the design of the TBM systems (also known as “TBM ancillary systems”), several lessons learned can be already now considered very important for the designers of the DEMO breeding blanket. They deal with:

- the impact of the safety requirements on the design of systems and components;
- the impact of the licensing procedure on design requirements and implementation;
- the definition and implementation of the main safety functions;
- the compliance with the nuclear pressure equipment (ESPN) regulation;
- the functional analysis of the different systems and components;
- the selection of technological solutions for the TBM systems which appear relevant for the breeding blanket design; and,
- major integration issues, like the management of the tritium contamination due to permeation and leakage.

After a synthetic recall of the main design features of the HCLL and HCPB-TBS, all above mentioned topics are discussed in this paper, addressing the analysis onto the original inputs and ROX for the designers of a breeding blanket for DEMO from the current TBM systems design experience.



Development of Sensors for High-Temperature High-Pressure Liquid Pb/Pb-16Li Applications

A. Saraswat¹, S. Sahu¹, T. S. Rao¹, A. Prajapati¹, S. Verma¹, S. Gupta¹, M. Kumar¹,
R. Bhattacharyay¹, and P. Das²

¹*Institute for Plasma Research (IPR), Bhat, Gandhinagar, India*

²*Bhabha Atomic Research Centre, Mumbai, India*

Corresponding Author: A. Saraswat, asaraswat@ipr.res.in

Liquid lead lithium (Pb-16Li) is of primary interest as one of the candidate materials for coolant fluid and tritium breeder in liquid metal blanket concepts relevant to fusion power plants. For effective and reliable operation of such high temperature liquid metal coolant systems, monitoring and control of critical process parameters like pressure, level, temperature and flow is essential. However, high temperature operating conditions coupled with the corrosive nature of Pb-16Li severely limits the application of commercially available diagnostic tools. This paper illustrates indigenous test facility designs and experimental methods used to develop noncontact configuration radar level sensor and wetted configuration diaphragm seal pressure sensors for high temperature, high pressure liquid Pb and Pb-16Li. Calibration of these sensors at high temperature between 380–400°C and high pressure up to 10 bar was performed. Reliability and performance validation were achieved by continuous long duration testing of sensors in liquid Pb and liquid Pb-16Li environment for over 1000 hours. Estimated error for radar level sensor lies within ± 10 mm and estimated error for pressure sensors lies within 1.1% of calibrated span over the entire test duration. Results obtained and critical observations from these tests are presented in this paper.

Liquid Lithium Loop System to Solve Challenging Technology Issues for Fusion Power Plant

M. Ono¹, R. P. Majeski¹, M. A. Jaworski¹, Y. Hirooka², R. Kaita¹, T. K. Gray³, R. Maingi¹, and C. Skinner¹

¹Princeton Plasma Physics Laboratory (PPPL), Princeton, NJ 08540, USA

²National Institute for Fusion Science (NIFS), Toki, Gifu, Japan

³Oak Ridge National Laboratory (ORNL), Oak Ridge, TN 37831, USA

Corresponding Author: M. Ono, mono@pppl.gov

Steady-state fusion power plant designs present major divertor technology challenges, including high divertor heat flux both in steady-state and during transients. In addition to these concerns, there are the unresolved technology issues of long term dust accumulation and associated tritium inventory and safety issues. It has been suggested that radiation-based liquid lithium (LL) divertor concepts with a modest lithium-loop could provide a possible solution for these outstanding fusion reactor technology issues, while potentially improving the reactor plasma performance. The application of lithium (Li) in NSTX resulted in improved H-mode confinement, H-mode power threshold reduction, and reduction in the divertor peak heat flux while maintaining essentially Li-free core plasma operation even during H-modes. These promising results in NSTX and related modelling calculations motivated the radiative liquid lithium divertor (RLLD) concept and its variant, the active liquid lithium divertor concept (ARLLD), taking advantage of the enhanced Li radiation in relatively poorly confined divertor plasmas. To maintain the LL purity in a 1 GW-electric class fusion power plant, a closed LL loop system with a modest circulating capacity of ~ 1 ℓ/s is envisioned. We examined two key technology issues: 1) dust or solid particle removal, and, 2) real time recovery of tritium from LL while keeping the tritium inventory level to an acceptable level. By running the LL-loop continuously, it can carry the dust particles and impurities generated in the vacuum vessel to the outside where the dust and impurities can be removed by relatively simple dust filter, cold/hot trap and/or a centrifugal separation systems. With a 1 ℓ/s LL flow, even a small 0.1% dust content by weight (or 0.5 g/s) means that the LL-loop could carry away nearly 16 tons of dust per year. In a 1 GW-electric (or ~ 3 GW fusion power) fusion power plant, about 0.5 g/s of tritium is needed to maintain the fusion fuel cycle assuming $\sim 1\%$ fusion burn efficiency. It appears feasible to recover tritium (T) in real time from LL while maintaining an acceptable T inventory level. Laboratory tests are also planned to investigate the Li-T recover efficiency with the SCT concept and also to assess the viability of the centrifugal Li-T separator with consultation with the manufacturer.



Accomplishment of DEMO R&D Activity of IFERC Project in BA Activity and Strategy toward DEMO

H. Tanigawa¹, T. Nozawa¹, M. Nakamichi¹, T. Hoshino¹, K. Isobe¹, and K. Ochiai¹

¹*Japan Atomic Energy Agency (JAEA), Naka, Japan*

Corresponding Author: H. Tanigawa, tanigawa.hiroyasu@jaea.go.jp

International Fusion Energy Research Centre (IFERC) has implemented DEMO research and development activities for 10 years under the broader approach (BA) activity. Five common issues on blanket technologies were selected and corresponding R&D has been carried out. The accomplishments of R&D were; successful production of reduced activation ferritic/martensitic steel in DEMO scale production technology, preparation of SiC/SiC composite material property handbook as the functional structural material in the advanced blanket concept, a major technical breakthrough on the fabrication of beryllide pebbles as the advanced neutron multipliers, successful fabrication and demonstration of Li rich Li-titanate pebbles as the advanced tritium breeder, and the development of a new scintillation system as a tritium analysis tool and first analyzes of retained hydrogen isotope and beryllium on dust particles of JET ITER like wall. Interaction with DEMO design activity reveals the severe needs for further R&D to qualify these developed technologies as the concrete technical background of the DEMO design.



Progress of Conceptual Design Study on Japanese DEMO

R. Hiwatari¹, K. Tobita¹, and H. Takase¹

Rapporteured by: H. Tanigawa

¹*Japan Atomic Energy Agency (JAEA), Naka, Japan*

Corresponding Author: R. Hiwatari, hiwatari.ryoji@jaea.go.jp

This paper presents the recent progress of a conceptual DEMO design in Japan. First, the divertor concept is built under feasible engineering technology. Second, the circulating power in DEMO is precisely investigated as for the cooling power and the water detritiation system to ensure substantial net electric power. Then, 3D eddy current analysis shows the prospect for plasma elongation ~ 1.7 and increase the electric power output. Finally, safety analysis on an ex-vessel LOCA is carried out, and it is found that a vault of the tokamak cooling water system (TCWS) with a pressure suppression system (PSS) can mitigate it.



Dealing with Uncertainties in Fusion Power Plant Conceptual Development

R. Kemp¹, R. Kembleton¹, F. Maviglia², H. Zohm³, R. Wenninger², and T. Donne²

¹Culham Centre for Fusion Energy (CCFE), Culham Science Centre, Abingdon, UK

²EUROfusion Garching, 85748 Garching, Germany

³Max-Planck-Institut für Plasmaphysik, Garching, Germany

Corresponding Author: R. Kemp, richard.kemp@ukaea.uk

Although the ultimate goal of most current fusion research is to build an economically attractive power plant, the present status of physics and technology does not provide the performance necessary to achieve this goal. Therefore, in order to model how such plants may operate and what their output might be, extrapolations must be made from existing experimental data and technology. However, the expected performance of a plant built to the operating point specifications can only ever be a “best guess”. Extrapolations far beyond the current operating regimes are necessarily uncertain, and some important interactions, for example the coupling of conducted power from the scrape-off layer to the divertor surface, lack reliable predictive models. This means both that the demands on plant systems at the target operating point can vary significantly from the nominal value, and that the overall plant performance may potentially fall short of design targets.

Two questions must therefore be answered: what is it most important to know accurately? and, if we do build a power plant to a particular design, what is the expected performance as opposed to the design performance? Answering the first question leads to the ability to focus research in those particular areas of maximum leverage. Answering the second question allows the identification of a design point which can be robustly expected to meet performance requirements and thus provides a stable basis for further engineering design work. We can also explore additional operating scenarios within a fixed machine design which might restore performance, albeit at higher risk.

In this contribution we discuss tools and techniques that have been developed to assess the robustness of the operating points for the EU-DEMO tokamak-based demonstration power plant, and the consequences on its design. These tools fall into two main categories: ways of assessing the uncertainty of performance of a particular operating point, and a “risk register” which records the main potential issues and their consequences on design decisions or plant output. The consequences for plant design, if the uncertainties cannot be resolved and expected performance must be downgraded before the design is finalized, and plant output, if actual performance is not equal to that assumed at the final design stage, are included. The aim is to make explicit the design choices and areas where improved modelling and DEMO-relevant experiments will have the greatest impact on confidence in a successful DEMO design.

This work has been carried out within the framework of the EUROfusion Consortium and has received funding from the Euratom research and training programme 2014–2018 under grant agreement No. 633053 and from the RCUK Energy Programme (grant number EP/I501045). The views and opinions expressed herein do not necessarily reflect those of the European Commission.



Development of a Systematic, Self-Consistent Algorithm for K-DEMO Steady-State Operation Scenario

J. Kang¹, J. M. Park², L. Jung³, S. K. Kim¹, J. Wang¹, D. H. Na¹, C.-S. Byun¹, Y.-S. Na¹, and Y. S. Hwang¹

¹Seoul National University, Seoul, Republic of Korea

²Oak Ridge National Laboratory (ORNL), Oak Ridge, TN 37831, USA

³National Fusion Research Institute (NFRI), Daejeon, Republic of Korea

Corresponding Author: J. Kang, fatema@snu.ac.kr

A systematic, self-consistent process to find the K-DEMO operation scenario has been investigated. Recent progress on K-DEMO scenario study explored zero-dimensional operation regime and one-dimensional current density configurations with fixed safety factor profile [1]. However, previous research does not contain confinement optimization process for stable equilibria. In this study, an optimum plasma kinetic profile determination process is addressed simultaneously self-consistently with equilibrium, stability, confinement, and heating/current drive scheme. To consider the profile effect carefully, the inverse approach analyzes demo plasma performance starting from target plasma profile. Pressure profiles with pedestal structure are investigated by changing its height, slope, and flatness. Parallel current density profiles are composed of bootstrap current and centrally peaked external contribution. Formation of stable equilibria is evaluated by solving Grad-Shafranov equation and checking linear core MHD stability. For the case of stable equilibrium profiles, necessary external heating distribution is calculated from power balance equation considering the conduction energy loss, alpha particle heating, and radiation loss. The external current drive profile is obtained by subtracting the bootstrap current profile from the total current profile. The highest Q value plasma equilibrium is chosen to reference target. Relevant heating configuration matching both required external heating and current drive distribution is parametrically scanned by varying heating/current drive control knobs. As a final step, electron/ion temperature and poloidal flux evolution are solved with the derived heating configuration to find its time derivative zero solution and achieve self-consistent plasma kinetic profiles. An economic K-DEMO steady-state target operation scenario would finally be presented through the designed algorithm considering self-consistency with equilibrium, stability, confinement, and heating/current drive.

References

[1] J. S. Kang *et al.*, *Fusion Eng. Des.* (2016).



Two Conceptual Designs of Helical Fusion Reactor FFHR-d1A Based on ITER Technologies and Challenging Ideas

A. Sagara¹, J. Miyazawa¹, H. Tamura¹, T. Tanaka¹, T. Goto¹, N. Yanagi¹, R. Sakamoto¹, S. Masuzaki¹, and H. Ohtani¹

¹National Institute for Fusion Science (NIFS), Toki, Gifu, Japan

Corresponding Author: A. Sagara, sagara.akio@nifs.ac.jp

The fusion engineering research project (FERP) in NIFS is conducting the conceptual design activity of the LHD-type helical fusion reactor FFHR-d1A. Recently, two options of “basic” and “challenging” have been newly defined. Conservative technologies (including what will be demonstrated in ITER) are chosen in the basic option, while new ideas that would possibly be beneficial for making the reactor design more attractive are boldly included in the challenging option, aiming at “early construction, easy maintenance and high thermal efficiency”, in particular, for helical structure. In the basic option, the SC magnet coils adopt cable-in-conduit conductors with Nb₃Sn strands cooled by supercritical helium at 4.5 K. The helical coils are wound by the “react and winding” method using a large-scale winding machine. The divertor system is the water-cooled tungsten monoblock divertor with cooling pipes made of Cu alloy. The blanket system is the water-cooled ceramic breeder blanket. The key technologies needed for the basic option are already well established in LHD or will be established through the R&D activities for ITER. However, we need to develop maintenance schemes for these helical divertor and blanket with complicated 3D structures. In the challenging option, on the other hand, new technologies of high-temperature superconductor (HTS), liquid metal ergodic limiter/divertor, and molten salt (FLiNaBe mixed with metal powders) breeder blanket are adopted. The “joint winding” based on the mechanical lap joint technique are applied to fabricate the helical coils by connecting segmented HTS conductors. The cooling scheme is simplified using helium gas at 20 K. A new liquid metal limiter/divertor has been proposed, where ten units forming the molten tin shower jets stabilized by chains inside each jet are installed in the inboard side of the torus. Neutral particles are evacuated through the liquid metal shower. The blanket system using the metal powder mixed FLiNaBe is also the challenging option. The hydrogen solubility is effectively increased by adding powders of hydrogen storage metal such as Ti. Although the new technologies adopted in the challenging option can significantly ease the construction difficulties in the basic option, we have already started R&D arrangements to demonstrate them as fast as possible.

Development of Remountable Joints and Heat Removable Techniques for High-Temperature Superconducting Magnets

H. Hashizume¹, S. Ito¹, N. Yanagi², H. Tamura², and A. Sagara²

*Rapporteur*ed by: **A. Sagara**

¹Tohoku University, Sendai, Miyagi, Japan

²National Institute for Fusion Science (NIFS), Toki, Gifu, Japan

Corresponding Author: H. Hashizume, hidetoshi.hashizume@qse.tohoku.ac.jp

This study addresses development of mechanical joints and a heat removable technique for the remountable HTS magnet. We carried out i) Optimizing structure and fabrication procedure of mechanical joints, and ii) Analyzing heat transfer performance of metal porous media inserted channel to be applied to thermal analysis of joint. The developments and discussion will be taken into account in design of the remountable magnet.

The “remountable” HTS magnet has been proposed for both tokamak and heliotron-type fusion reactors, which is assembled from coil segments with mechanical joints. Our recent study successfully developed a bridge-type mechanical lap joint of 100-kA-class HTS conductors consisting of simple stacking of REBCO HTS tapes. The joint achieved a joint resistance of 1.8 nΩ at 100 kA, 4.2 K. For the local heat removal, we have proposed a metal porous media inserted channel and experimentally evaluated its heat transfer performance with liquid nitrogen (LN₂) to show heat transfer coefficient of 10 kW/m²K at low mass flow rate. However, it took over a half day to fabricate the joint because the joint piece was not integrated but just individual REBCO tapes. In addition, the fabricated joints all had straight geometry. Furthermore the joint resistance obtained with large-scale conductor joint was larger than predicted value based on small-scale conductor joint and varied largely due to nonuniform contact pressure distribution on the joint surfaces. Therefore, an integrated joint piece was newly introduced to shorten the fabrication process. Furthermore, we apply heat treatment during fabrication of the joint to reduce the joint resistivity from 25 pΩm² to 8 pΩm². This means the heat treatment is promising to be applied to large-scale conductor joints. For the local heat removal, we need to predict heat transfer coefficient of various cryogenic liquid coolants such as liquid helium (LHe), liquid hydrogen (LH₂) and liquid neon (LNe) with a metal porous media inserted channel, due to operating temperatures of < 30 K. At the constant pump power and each coolant’s saturated temperature, LH₂ and LNe show almost the same heat transfer coefficient and DNB point. The DNB point for LH₂ and LNe is about 10 times larger than that for LHe.



Lessons Learned from the Eighteen-Year Operation of the LHD Poloidal Coils Made from CIC Conductors

K. Takahata¹, S. Moriuchi¹, K. Ooba¹, S. Takami¹, A. Iwamoto¹, T. Mito¹, and S. Imagawa¹

Rapporteur by: A. Sagara

¹National Institute for Fusion Science (NIFS), Toki, Gifu, Japan

Corresponding Author: K. Takahata, takahata@lhd.nifs.ac.jp

The Large Helical Device (LHD) superconducting magnet system consists of two pairs of helical coils and three pairs of poloidal coils. The helical and poloidal coils use composite conductors with pool cooling by liquid helium, and cable-in-conduit (CIC) conductors with forced cooling by supercritical helium, respectively. The poloidal coils were first energized with the helical coils on March 27, 1998. Since that time, the coils have experienced 50 000 h of steady cooling, 10 000 h of excitation operation, and seventeen thermal cycles. During this period, no superconducting-to-normal transition of the conductors has been observed, even during fast current discharge. The subsequent experience gained from eighteen years of operation has also provided further useful information regarding preventive design and maintenance of peripheral equipment and long-term changes in electromagnetic and hydraulic characteristics. First, the poloidal coil system has experienced events that have interrupted plasma experiments due to the malfunction of a quench detection system and an insulating break used in cryogenic piping. The malfunction of the quench detection system was caused by the noise from the plasma heating devices and the coupling current, which is an intrinsic property of a composite superconductor. This suggested that the noise for quench detection should be estimated before magnet operation. During the sixteenth cool-down, one of the breaks suddenly leaked helium, which was caused by the cracking of a plastic adhesive material between the FPR and the stainless-steel pipes. Further investigation is needed to clarify the age degradation and the creep behaviour of plastic adhesive materials at cryogenic temperature. Second, the long-term monitoring of the electromagnetic and hydraulic characteristics of the coils has also been performed. Even though the AC losses slightly decreased during the first three years, the losses have remained unchanged in the fifteen years since. The pressure drops of coolant showed a tendency to decrease over the campaigns. The sudden increase in friction factor in the 15th campaign suggested that the compressor oil is a potential source of impurity gasses in helium coolant. These experiences would help in the design and maintenance of preventive measures for fusion magnets, including ITER and DEMO.

High Temperature Superconductors for Fusion at the Swiss Plasma Center

P. Bruzzone¹, R. Wesche¹, D. Uglietti¹, and N. Bykovsky¹

¹Swiss Plasma Center (SPC), École polytechnique fédérale de Lausanne (EPFL), 1015 Lausanne, Switzerland

Corresponding Author: P. Bruzzone, pierluigi.bruzzone@psi.ch

High temperature superconductors (HTS) may become in future an option for the superconducting magnets of commercial fusion plants. The general requirements for HTS conductors and coils are presented together with a tentative roadmap for the related R&D activity. The issue of the material cost and its evolution is also discussed in comparison to the low temperature superconductor (LTS) option.

At the Swiss Plasma Center (SPC) the R&D activity toward HTS high-current, high-field cable suitable for fusion magnets started in 2012 and led in 2015 to the assembly of the first 60 kA, 12 T prototype conductor. The basic component is a thin ceramic tape (0.1 mm thick, 4 mm wide) of coated conductor, generically named ReBCO and commercially available since about a decade. The main challenge for the design of high current cable is the assembly of a large number of brittle tapes in a mechanically stable configuration, able to withstand the large operating loads. The electrical requirements, tape transposition for balanced current distribution and moderate AC loss, set additional restrictions to the cable layout. The cable concept developed at SPC is based on the principle of “soldered, twisted stacks” of ReBCO tapes. The required number of stacks is then assembled in a cored flat cable, cooled by forced flow of supercritical helium.

The EDIPO facility at SPC, with 12.4 T background field, 100 kA test current and 1 m long high field section, is the ideal tool for qualification of high current HTS cables, where long cable pitches, in the range of 1 m, are mandatory to control the bending and torsion strain of the ceramic tapes. To test HTS cable samples at elevated temperature, the EDIPO test environment is upgraded with a low heat conduction “adapter”, inserted between the HTS sample and the NbTi based transformer. A counter-flow heat exchanger between inlet and outlet coolant allows cold gas return from the HTS sample to the cryoplant. The first test of a HTS high current sample was carried out in 2015.

The initial performance fulfilled the design target, but some degradation upon electromagnetic load cycles was observed and investigated after dismantling the cable. A new prototype HTS conductor is being now assembled at SPC with improved layout, based on the tentative spec for the high grade conductor of the DEMO central solenoid.



Assembly Technologies of the Superconducting Tokamak on JT-60SA

Y. Shibama¹, K. Masaki¹, A. Sakasai¹, F. Okano¹, J. Yagyu¹, H. Ichige¹, Y. Miyo¹, A. Kaminaga¹, T. Sasajima¹, T. Nishiyama¹, S. Sakurai¹, K. Hasegawa¹, K. Kizu¹, K. Tsuchiya¹, Y. Koide¹, K. Yoshida¹, J. Alonso², J. Botija², M. Medrano², E. Rincon², E. Dipietro³, S. Davis³, V. Tomarchio³, A. Hayakawa⁴, T. Morimoto⁴, T. Ogawa⁴, M. Ejiri⁴, S. Mizumaki⁴, T. Okuyama⁴, and S. Asano⁴

¹Japan Atomic Energy Agency (JAEA), Naka, Japan

²Association EURATOM, Centro de Investigaciones Energéticas, Medioambientales y Tecnológicas (CIEMAT), Madrid, Spain

³F4E: Fusion for Energy, ITER EU Centre, 08019 Barcelona, Spain

⁴Toshiba Corporation, Yokohama, Japan

Corresponding Author: Y. Shibama, shibama.yusuke@jaea.go.jp

The JT-60SA (JT-60 Super Advanced) project is a combined project of Japan's programme for national use and the Japan-EU Satellite Tokamak Program collaboration between Japan and the EU fusion community. The main objectives are to demonstrate steady-state high- β plasma and to support ITER through the optimization of ITER operation scenario. The JT-60SA tokamak device is designed as a superconducting tokamak, which is about half of ITER. This tokamak assembly must allow for the thermal deformations of the superconducting coils at 4 K and 473 K baking for the vacuum vessel (VV) in addition to withstanding electromagnetic and seismic forces. The rigid support method is not able to absorb the thermal contraction and expansion. On the other hand, a high accuracy, below several millimetres, control is required for the positioning of the superconducting coils to achieve a magnetic field error under $10^{-4} B_t$. Two types of gravity supports are employed for the superconducting coil system and the VV. Both gravity supports are characterized by their flexibility to absorb thermal deformation while maintaining their symmetry about the toroidal axis. In the onsite assembly work, it is important to install these components with high accuracy and adjust them to their design positions. Installation of the VV and pre-positioning of the lower equilibrium field coils have been achieved with high accuracy of a few millimetres using carefully planned assembly technologies, which are the combination of 3D CAD and real-time 3D position measurement by a laser tracker, customization of the joint structures derived from the measurement, and welds made while taking into account the predicted deformations. The assembly measurement precision due to spatial recognition is 0.5 mm in the tokamak hall of 40 metres square. The sector joints of the VV were completed up to 340°. The shrinkage of each weld was predicted from factory manufacturing results and this prediction was improved by the measurement of the shrinkage of each pass during the welding of the joints between sectors. The complete assembly of JT-60SA is expected to be achieved with high accuracy by applying these assembly technologies. The design and manufacturing of these components have been shared by the EU and Japan, and the assembly of these components started on the Naka site in 2013 aiming at the first plasma in 2019.



JT-60SA TF Coil Manufacture, Test and Preassembly by CEA

P. Decool¹, W. Abdel Maksoud², L. Genini², G. Disset², R. Gonde¹, C. Mayri², A. Torre¹, J.-C. Vallet¹, M. Nusbaum³, P. Eymard-Vernein⁴, and A. Tremoulu⁵

Rapporteur by: Y. Shibama

¹*Institut de Recherche sur la Fusion par confinement Magnétique (IRFM), Commissariat à l'énergie atomique (CEA/Cadarache), 13108 Saint-Paul-lès-Durance, France*

²*Institut de recherche sur les lois fondamentales de l'Univers (IRFU), Commissariat à l'énergie atomique (CEA/Saclay), 91191 Gif-sur-Yvette, France*

³*General Electric, F-90000 Belfort, France*

⁴*SDMS la chaudronnerie blanche, 38160 Saint Romans, France*

⁵*Alsyom, F-65000 Tarbes, France*

Corresponding Author: P. Decool, patrick.decool@cea.fr

In 2005, when the ITER site decision was made, the French Government decided to participate in the joint Europe-Japan implementation of the so-call "Broader Approach Activities" (BA) in support of the ITER project and DEMO activities. The BA comprises the ITER Satellite Tokamak Programme (STP) which consists in upgrading the JT-60U machine into the largest fully superconducting and actively cooled D shaped tokamak JT-60SA before ITER, and in the participation to its scientific exploitation. As collaboration with Fusion for Energy (F4E), the French commitments, in charge of CEA as voluntary contributor (VC), are described in the Agreement of Collaboration (AoC). The CEA contribution related to the toroidal field coil (TFC) procurement is 9+1 spare of the 18+2 spares TFCs, the whole supporting structures, the TFC cold test facility (CTF) and the TFC preassembly. The complementary contribution is in charge of Italy.

After the preparation and qualification phases, in these last two years, the industrial production for the procurement of the French contribution to the toroidal field coil manufacture is now well engaged. The first coils were wound and integrated into their casings. The first mechanical structures were produced. These coils were sent to the cold test facility and cold tested for final acceptance before to be assembled with their outer intercoil structures in a dedicated workstation. These assemblies are the first components of the TF magnet which were sent to JAEA. In parallel the following TFC production, qualification and preassembly are ongoing.

FIP

Conceptual Design of the Radial Gamma-Ray Spectrometers System for Alpha Particle and Runaway Electron Measurements at ITER

M. Nocente¹, R. Barnsley², L. Bertalot², B. Brichard³, G. Croci¹, G. Brolatti⁴, L. Di Pace⁴, A. Fernandes⁵, L. Giacomelli⁶, I. Lengar⁷, V. Krasilnikov², A. Muraro⁶, R. C. Pereira⁵, E. Perelli Cippo⁶, D. Rigamonti¹, M. Rebai¹, J. Rzakiewicz⁸, P. Santosh², J. Sousa⁵, I. Zychor⁸, and G. Gorini¹

¹Department of Physics, Università degli Studi di Milano-Bicocca, 20126 Milano, Italy

²International Thermonuclear Experimental Reactor (ITER), Cadarache Centre, 13108 Saint-Paul-lès-Durance, France

³F4E: Fusion for Energy, ITER EU Centre, 08019 Barcelona, Spain

⁴Associazione EURATOM-ENEA Unità Tecnica Fusione, Frascati, Italy

⁵Institute of Plasmas and Nuclear Fusion (IPNF), Association EURATOM/IST, Lisbon, Portugal

⁶Istituto di Fisica del Plasma (IFP), Consiglio Nazionale delle Ricerche (CNR), 20125 Milan, Italy

⁷Jozef Stefan Institute, 1000 Ljubljana, Slovenia

⁸National Centre for Nuclear Research (NCBJ), Świerk, Poland

Corresponding Author: M. Nocente, massimo.nocente@mib.infn.it

Among the key goals of ITER are the investigation of alpha particle physics in a burning plasma as well as the demonstration of the control of runaway electrons born in disruptions. The diagnostic needs to meet these goals are the determination of the alpha particle profile with a time resolution of < 0.1 s and the evaluation of the runaway electron beam current and end point energy with an estimated accuracy of 20%.

Spontaneous gamma-ray emission from nuclear reactions in the plasma can be exploited to satisfy both demands. Alpha particle studies rely on the observation of 4.44 MeV γ -rays born in ${}^9\text{Be}(\alpha, n\gamma){}^{12}\text{C}$ reactions. Spectral measurements of bremsstrahlung emission from runaway electrons, colliding either with plasma impurities during massive gas injection or with the machine first wall, are instead the way to determine properties of suprathermal electrons with projected energies up to 100 MeV.

Building on the successful experience of the Joint European Torus (JET), we here present the principles, requirements and corresponding solutions that have shaped the conceptual design of the ITER radial gamma-ray spectrometer (RGRS) system. The project aims at enabling gamma-ray measurements along a few of the collimated channels of the radial neutron camera by the design of a suitable set of detectors, collimators and attenuators. The grand challenge is to perform gamma-ray measurements in a neutron field of unprecedented intensity and to ensure the stability and reliability of the detectors. We show that we can combine the high energy resolution, fast time response and resilience to neutron damage of the most advanced, up to date gamma-ray spectrometers with the need of a multi-sightline system allowing for a spatial reconstruction of the alpha particle profile in the core plasma. The design starts from the calculated gamma-ray emission in the 15 MA $Q = 10$ ITER deuterium-tritium scenario delivering a projected fusion power of 500 MW, as well as bremsstrahlung emission from runaway electrons born in a disruption phase. By merging the most successful solutions adopted for similar measurements at JET and benefiting from cutting edge developments in nuclear detector technology, we demonstrate that RGRS successfully meets ITER requirements. Implications of our design for alpha particle and runaway electron physics investigations are finally discussed.

Conceptual Design of the Best TOF Neutron Spectrometer for Fuel-Ion Ratio Measurements at ITER

C. Hellesen¹

¹Uppsala University, Uppsala, Sweden

Corresponding Author: C. Hellesen, carl.hellesen@physics.uu.se

Measurements of the core plasma fuel ion density ratio (n_T/n_D) is required for safe and efficient burning plasma operations at ITER. However, this measurement is difficult and very few working techniques have been demonstrated. One candidate method to obtain the fuel-ion composition is neutron emission spectroscopy, specifically, measurement and analysis of the DT neutron spectrum of neutral beam heated plasmas. However, none of today's fully implemented neutron spectrometer techniques fulfils all requirements for such measurements at ITER and a suite of instruments will most probably be required.

In [1] the n_T/n_D measurement was demonstrated using data from the magnetic recoil proton (MPR) spectrometer acquired during JET DT operations in 1997. Due to size and weight constraints, the MPR is however not possible to interface at ITER. Instead, a back elastic scattering time-of-flight (BestTOF) spectrometer is presented here. The goal of the BestTOF design is to obtain a spectrometer that fulfils all requirements for fuel ion density measurements in a broad range of operational conditions at ITER. The technique takes advantage of the well-established (forward) time-of-flight method, while exploring the favourable conditions of (n, d) scattering in the backward direction (i.e., around 180°) regarding cross section and kinematics. This is achieved by introducing deuterium-based scintillators as first, in-beam scatterers in the design.

Aside of size and weight, the requirements of the instrument are a high efficiency and count rate capability to be able to acquire the counting statistics required for performing the analysis; to fulfil the ITER requirements on accuracy, precision and time resolution this means at least several 100 kHz rate of useful counts. The spectrometer also needs an energy resolution of 4% or better. Furthermore, the signal to background at the high-energy side of the DT emission ($E_n > 14$ MeV) must be at least 1000.

In this paper we show that the BestTOF design fulfils all of the above mentioned requirements while also being light and compact enough for installation at ITER. The BestTOF is also proposed to be a part of the complete high resolution neutron spectrometer system at ITER.

References

[1] C. Hellesen, *et al.*, Nucl. Fusion **55**, 023005 (2015).



Pellet Injection Technology and Application to Mitigate Transient Events on ITER

L. R. Baylor¹, S. Combs¹, S. Meitner¹, D. Rasmussen¹, S. Maruyama², and M. Lyttle¹

¹*Oak Ridge National Laboratory (ORNL), Oak Ridge, TN 37831, USA*

²*International Thermonuclear Experimental Reactor (ITER), Cadarache Centre, 13108 Saint-Paul-lès-Durance, France*

Corresponding Author: L. R. Baylor, baylorlr@ornl.gov

The formation and acceleration of cryogenically solidified pellets of hydrogen isotopes has long been under development for fuelling fusion plasmas. Injectors are being designed to provide this capability for fuelling ITER with DT pellets injected from the inner wall. In addition to the fuelling application, smaller pellets of D₂ are to be injected from the outer or inner wall to purposely trigger rapid small edge localized modes (ELMs) to limit transient heat flux damage from otherwise large naturally occurring ELMs. A further application of pellet injection technology that is planned for ITER is that of mitigating disruptions where large pellets of neon, argon, and deuterium mixtures are produced and shattered upon injection into disrupting plasmas to radiate the plasma energy in order to mitigate possible damage to in-vessel components [1].

The pellets for fuelling and ELM triggering are both to be formed by a twin-screw continuous extruder feeding that can produce either 5 mm fuelling size pellets or 3 mm ELM triggering pellets with a newly developed adjustable extrusion size control providing up to 50% variation in the pellet length. Acceleration of the pellets is accomplished with pressurized deuterium gas that will be captured and recirculated. The large shattered pellets for disruption mitigation are formed in-situ in a pipe gun device that is cooled with supercritical helium and held intact ready to fire until needed during a disruption. Pressurized gas is also used to accelerate these pellets, but the gas enters the vessel and is not captured. The pellets are shattered when they impinge on a bent guide tube in the port plug shield block that is optimized to produce a spray of solid fragments mixed with gas and liquid at speeds approaching the sound speed of the propellant gas. A prototype 3-barrel injector has been fabricated and tested with deuterium-neon mixture pellets of 25 mm size for thermal mitigation and for runaway electron suppression and dissipation [2]. The technology design and installation details and planned use on ITER will be presented.

References

[1] N. Commaux, *et al.*, Nucl. Fusion **50**, 112001 (2010).

[2] L. R. Baylor, *et al.*, Fusion Sci. Technol. **68**, 211 (2015).

This work was supported by the Oak Ridge National Laboratory managed by UT-Battelle, LLC for the U.S. Department of Energy under Contract No. DE-AC05-00OR22725.



Progress on Integrated Design of ITER Poloidal Polarimeter for Current Profile Measurement

R. Imazawa¹, Y. Kawano¹, and K. Itami¹

¹Japan Atomic Energy Agency (JAEA), Naka, Japan

Corresponding Author: R. Imazawa, imazawa.ryota@qst.go.jp

PoPola measures both orientation angle (θ) and ellipticity angle (ϵ) of polarization state of multiple probing far-infrared (FIR) laser beams (wavelength 119 μm). The change of θ and ϵ are mainly associated with the Faraday and the Cotton-Mouton effects, respectively, and provide information of electron density, electron temperature and magnetic field. Equilibrium reconstruction of PoPola measurement data together with other diagnostics data provides the current profile (or, equivalently, q profile). ITER organization and Japan domestic agency signed the procurement arrangement in 2013 and this paper provides the summary of the development activity during 2014–2015, which made an integrated design for the first time. The design study provides important knowledge for designing diagnostics of future reactors such as DEMO because long wavelength used by PoPola has potential for applicability to the reactors. All in-vessel components of PoPola are rigidly fixed, and laser beam alignment will be carried out by using ex-vessel mirrors. The alignment system can move the beam position at RR by 3 mm resolution and with a vertical range of approximately ± 3 cm even when the port plug moves by 40 mm in the vertical direction and rotates by 1° in the poloidal direction owing to thermal expansion. The authors developed a new analysis method for a rotating waveplate Stokes polarimeter, which is applicable to real-time calculation of FPGA. Experiments using a He–Ne laser showed that the achieved precision of θ and ϵ were 0.33° and 0.096° , respectively. Since the experimental condition using the He–Ne laser was worse than what is expected in ITER, the measurement error will be reduced by a factor of nine. As a result of the optical design, the measurement error of θ and ϵ were evaluated as 0.45° and 0.73° , respectively. A main error source is polarization change due to the optical transmission line of the zero-offset configuration. Error assessment of q profile measurement was carried out by using operation scenarios of both inductive and steady-state operations. The results suggest that a target accuracy of 10% is achievable.

Electron Cyclotron Power Management in ITER, the Path from the Commissioning Phase to Demonstration Discharges

F. Poli¹, E. Fredrickson¹, N. Bertelli¹, R. Andre¹, D. Farina², L. Figini², M. Henderson³, S. Nowak⁴, E. Poli⁵, and O. Sauter⁶

¹Princeton Plasma Physics Laboratory (PPPL), Princeton, NJ 08540, USA

²Istituto di Fisica del Plasma (IFP), Consiglio Nazionale delle Ricerche (CNR), 20125 Milan, Italy

³International Thermonuclear Experimental Reactor (ITER), Cadarache Centre, 13108 Saint-Paul-lès-Durance, France

⁴Associazione EURATOM-ENEA, Istituto di Fisica del Plasma (IFP), Consiglio Nazionale delle Ricerche (CNR), 20125 Milan, Italy

⁵Max-Planck-Institut für Plasmaphysik, Garching, Germany

⁶Swiss Plasma Center (SPC), École polytechnique fédérale de Lausanne (EPFL), 1015 Lausanne, Switzerland

Corresponding Author: F. Poli, fpoli@pppl.gov

Among the external heating systems planned in ITER, the electron cyclotron system has the highest flexibility. By combining the equatorial and the upper launcher, the EC can cover the whole plasma radius, from the axis to the edge, allowing for combined central heating, current profile tailoring and MHD stability control.

This work discusses how to best use the EC system in synergy with the other systems for MHD control and optimal plasma performance, by looking separately at the different phases of the discharge, moving from nonactive operation to the demonstration baseline. Time-dependent simulations with the TRANSP transport solver evolve self-consistently the plasma pressure and the heating and current drive profiles. Priority in the study is given to the power requirements for the stabilization of the neoclassical tearing modes (NTMs), because this sets constraints on the power that is available for the other applications, like active control of sawteeth and profile tailoring.

The evolution of the NTMs is calculated during the discharge and a real-time controller in TRANSP manages the steering of the upper launcher, calculates the power needed for stabilization and distributes the power between mirrors for combined applications. Simulations indicate that the NTMs evolve to their saturated size on time scales of a few seconds and that losing alignment with the NTM island, for example because of sawtooth crash, can be deleterious. This implies that preemptive control might be more effective than active control, especially in the case of the more dangerous (2, 1) mode. It is found that at half-field, an optimal steering of the neutral beams can change the sawtooth period by a factor three. Discharge design plays therefore an important role in the EC power management, by relaxing some of the requirements for MHD stability over central heating and profile tailoring.

High-Performance Data Transfer for Full Data Replication between ITER and the Remote Experimentation Centre

H. Nakanishi¹, K. Yamanaka², T. Ozeki³, N. Nakajima¹, J. Farthing⁴, G. Manduchi⁴, and F. Robin⁵

¹National Institute for Fusion Science (NIFS), Toki, Gifu, Japan

²National Institute for Informatics (NII), Tokyo, Japan

³Japan Atomic Energy Agency (JAEA), Naka, Japan

⁴F4E: Fusion for Energy, ITER EU Centre, 08019 Barcelona, Spain

⁵Commissariat à l'énergie atomique (CEA/Saclay), 91191 Gif-sur-Yvette, France

Corresponding Author: H. Nakanishi, nakanishi@nifs.ac.jp

A high-performance data transfer method has been developed for full data replication between ITER and the remote experimentation centre (REC) in Japan for the first time. Fast data transfer technology has been investigated as the crucial activity of REC with F4E, JAEA, NIFS, and NII collaboration. Full replication of ITER data will be expected to provide not only an equivalent research environment for the remote site but also data security against unexpected disasters. To realize the full replication, 1) A long-distance fast data transfer method, 2) high read/write throughputs on sender/receiver storage, and 3) 10–100 Gbit/s dedicated link, will be essential. The preliminary test result of MMCFTP, which is developed by NII, show 1.9 Gbit/s speeds on Japan-EU layer-3 (L3) internet. On a 10 Gbit/s layer-2 virtual private network (L2VPN) of SINET4, 8.5 Gbit/s speed was successfully sustained over 100 s.

The performance difference between L3 and L2VPN has been particularly tested between NIFS, NII, and REC sites. Internet L3 connections are obliged to use firewall and intrusion prevention systems (FW/IPS) for security; however they inevitably lower the packet forwarding rates. Tests on actual 10 Gbit/s FW/IPS show the performance limits around 2–4 Gbit/s. Hence, the international L2VPN is recommended between ITER and REC because it can provide more than 80% data transfer efficiency inside the closed network without any FW/IPS.

High-speed tests are also being prepared with ITER and other EU sites for after April 2016 to evaluate the improved efficiency using the 20 Gbit/s JA-EU direct link of SINET5. NII plans to upgrade the JA-EU link to 100 Gbit/s before the ITER experiment.

To make full use of 10–100 Gbit/s bandwidth, the read/write performance of the data storage must be improved correspondingly at both ends. A new double-layer storage structure has been developed in which high-speed frontend SSD arrays are added to the high-capacity main HDD ones. LHD's bulk data writing tests have demonstrated throughputs up to 2 GByte/s (roughly 20 Gbit/s).

The demonstrated technology would also be applicable to bidirectional data replication for ITER supporting machines in Japan, such as JT-60SA. It can change conventional remote participation and make local and remote sites equivalent regarding data accessibility.



Design Development of the ITER Divertor Diagnostic Systems in Japan

K. Itami¹, H. Ogawa¹, T. Sugie¹, M. Takeuchi¹, S.-I. Kitazawa¹, T. Maruyama¹, Y. Kawano¹,
E. Veshchev², P. Andrew², and M. Walsh²

¹Japan Atomic Energy Agency (JAEA), Naka, Japan

²International Thermonuclear Experimental Reactor (ITER),

Cadarache Centre, 13108 Saint-Paul-lès-Durance, France

Corresponding Author: K. Itami, itami.kiyoshi@qst.go.jp

Advanced design for Divertor Impurity Monitor (DIM) and IR Thermography (IRTh) is being developed in Japan to contribute to the divertor plasma control and research in ITER through the spectroscopic measurement with high spatial and spectral resolutions and accurate measurement of the target temperature.

DIM spectroscopically (200–1000 nm) measures two dimensional profiles of the emissions from metallic impurities (such as W, Be), injected impurity gas (Ar, Ne, Kr), fuel ions, helium in the divertor plasma. The DIM optical system consists of the upper port #1 system, the equatorial port #1 system and three optical systems in the lower port #2. The dome optics is expected to resolve the ionization and recombination of fuel ions to characterize the plasma detachment at the strike points with 20 mm resolution. Both the optical performance and neutron shielding performance is satisfied by labyrinth of optical path and nonspherical mirrors in the front-end optics. In the upper port #1 system, for example, the first mirror (M1) is inclined 45 degrees to enable the mirror cleaning discharge in the stationary toroidal field. The relay optics consists of six mirrors and two groups of chromatic corrections lenses.

This optics also has a function of optical axis alignment, so that the light flux is focussed to multichannel fibres by Cassegrain imaging optics in the port cell. UV light is measured by UV spectrometers in the port cell and visible light is transferred to the diagnostics room and is measured by visible spectrometers.

IR thermography (IRTh) is required to measure the target temperature of 200–1000 °C with the time resolution of 2 ms and that of 1000–3600 °C with the time resolution of 20 μs with the spatial resolution of 3 mm. Laboratory experiments were carried out to investigate characteristics of W samples for IRTh. It was found; i) Emissivity ε of the W sample increased from 0.2 to 0.6 when the surface roughness changed from 0.3 μm to 5.9 μm; ii) Back scattering of IR laser ($\lambda_{\text{IR}} = 3.22 \mu\text{m}$) on W samples was observable in the range of viewing angle by IRTh, if the surface roughness is 1 μm or larger than 1 μm; and iii) The formula, $\varepsilon(\lambda_{\text{IR}}) = 1 - f(\lambda_{\text{IR}})$, where f is reflectivity, was experimentally validated. Therefore, feasibility of in-situ calibration of by using IR laser light was demonstrated for the first time.



Development of ITER Poloidal Steering Equatorial EC Launcher Enhancing ECCD Performance

K. Takahashi¹, G. Abe¹, H. Shidara¹, Y. Oda¹, M. Isozaki¹, M. Komatsuzaki¹, T. Omori², M. Henderson², R. Ikeda¹, T. Kobayashi¹, S. Moriyama¹, and K. Sakamoto¹

¹Japan Atomic Energy Agency (JAEA), Naka, Japan

²International Thermonuclear Experimental Reactor (ITER),
Cadarache Centre, 13108 Saint-Paul-lès-Durance, France

Corresponding Author: K. Takahashi, takahashi.koji@jaea.go.jp

The ITER EC equatorial launcher (EL) has been newly designed to achieve an enhanced electron cyclotron current drive performance based on the dedicated calculations. The millimetre(mm)-wave beam design of EL optimized the mm-wave transmission capability and spatially limited beam path such as the mirrors' dimension and the plug mounted blanket shield module openings has implemented poloidal steering with fixed toroidal angle. The poloidal steering would reduce the Doppler shift broadening so that narrower deposition and full first pass absorption of mm-wave power could be achieved over the range of $0.4 < \rho < 0.6$. The new EL design allows doubling the current drive capabilities as required.

In the new EL design with poloidal steering capability, the beam path design was optimized with maximizing mm-wave beam propagation based on the calculated angular spectrum for both the near field and Fresnel diffraction for the far field. Multi-beams propagated through the beam path are superimposed and transmission efficiency and power profile of the superposed beams in the path were calculated to design the parameters such as the shape and size of both the fixed and steering mirrors, the waveguide set-up configuration, etc. The optimization resulted in power transmission efficiency of 97% was successfully attained assuming that beams in mixture of fundamental mode, HE11 (90%) and high order mode, HE21 (10%) were radiated from the waveguide. The peak heat load on M1 and M2 and the beam radius at plasma target were 4.95 MW/m^2 and 3.0 MW/m^2 , and 25 cm respectively, which compliant with ITER requirements.

The mock-up of the new EL design was fabricated. Only 4 out of the 8 beams (ones in each corner) were used to simulate the envelope of the 8-beam propagation. Beam profile measurement was performed and a good correlation between the design and measured radiation profile with agreement well within a few percent of error was obtained.

In conclusion, the optimized quasi-optical mm-wave beam design has resulted in transmission efficiency of 97%, a limited heat flux on both steering and fixed mirrors of less than 3.0 MW/m^2 and 5.0 MW/m^2 , respectively. A mock-up of the enhanced EL design has been constructed, followed by the validation of the quasi-optical design with mm-wave transmission. These results assure the doubled ECCD functionality for ITER.



Development of Ultrahigh Voltage Insulation Technology for the Power Supply Components in Neutral Beam System on ITER

N. Umeda¹, M. Kashiwagi¹, H. Tobari¹, A. Kojima¹, M. Dairaku¹, M. Hanada¹,
T. Maejima¹, N. Shibata¹, K. Watanabe¹, and H. Yamanaka¹

¹*Japan Atomic Energy Agency (JAEA), Naka, Japan*

Corresponding Author: N. Umeda, umeda.naotaka@jaea.go.jp

DC ultrahigh voltage insulation technologies in oil, gas and vacuum have been newly developed to fabricate DC 1 MV power supply components in the neutral beam (NB) system on ITER. In the ITER NB system, a 1 MV power supply with output pulse duration of 3600 s is required, which is twice higher in the voltage and two orders longer in the pulse than those of the existing NB systems in the world. To fulfil the requirements, R&D of the insulation technologies has been carried out for a DC 1 MV generator (step-up transformer and rectifier), a 1 MV transmission line and a 1 MV high voltage (HV) bushing. One of the issues for the DC generator is a long pulse DC high voltage insulation on the pressboard immersed in oil. Electric field on the pressboard is increased with time, and this could generate flashover. To lower the electric field strength in the pressboard, a new design with considering the DC long-pulse effect has been developed. A thickness of the pressboard has optimized to reduce the electric field concentration. Also barrier configuration for the pressboard at the connection points of the insulators has been adopted. For the 1 MV transmission line, an issue is to make a compact transmission line about 2 m in diameter since it penetrates tokamak building. To make the compact transmission line, all feeders at different voltages from 0.2 MV to 1 MV are designed within a single pressure vessel filled with SF₆ gas. The layout of the feeders is designed with 3D electrical analysis to reduce electric field to an allowable level. For a HV bushing, vacuum insulation in the multistage gaps has been found to be characterized by a total cathode area. On the basis of the result, a configuration of the five layered screens in the HV bushing was determined. Based on these insulation technologies, manufacturing three of five DC generators, the transmission line and the HV bushing has been completed. These components have showed the sufficient voltage holding to be required by ITER. They have been delivered to the site of NB test facility and installation has started since December, 2015, on schedule.



Overview of ITPA R&D Activities for Improvement of ITER Diagnostic Performance

Y. Kawano¹, D. L. Brower², and G. Vayakis³

¹Japan Atomic Energy Agency (JAEA), Naka, Japan

²University of California Los Angeles, CA 90095, USA

³International Thermonuclear Experimental Reactor (ITER),
Cadarache Centre, 13108 Saint-Paul-lès-Durance, France

Corresponding Author: Y. Kawano, kawano.yasunori@qst.go.jp

The International Tokamak Physics Activity (ITPA) Topical Group (TG) on diagnostics has been conducting R&D activities to support improved ITER diagnostic performance. Highlights of the TG activity focus on: 1) mitigating degradation of first mirrors in optical systems, development of techniques for removing impurity deposition on mirrors; 2) characterization of in-vessel stray-light to reduce impact on diagnostics; 3) diagnostics of escaping alpha particles, feasibility tests of the activation probe method under a multimachine joint experiment; 4) studies of real time diagnostics, measurement of surface temperature of in-vessel components using infrared thermography.



Electro-Mechanical Design and Experimental Validation of Post Insulators for Beam Source for ITER Diagnostic Neutral Beam

V. N. Muvvula^{1,2}, J. Joshi^{1,2}, S. Shah^{1,2}, D. Parmar^{1,2}, C. Rotti^{1,2}, M. Bandyopadhyay^{1,2}, and A. K. Chakraborty^{1,2}

¹International Thermonuclear Experimental Reactor (ITER), India Centre, Gujarat, India

²Institute for Plasma Research (IPR), Bhat, Gandhinagar, India

Corresponding Author: V. N. Muvvula, mvnraju@iter-india.org

The beam source (BS) for neutral beam injectors consists of two parts: “ion source” and “accelerator system”. For the ITER diagnostic neutral beam (DNB), the ion source is the plasma generator and consists of eight inductively coupled radio frequency (RF) plasma drivers. The accelerator system consists of three grids and accelerates the negative ion beam to 100 keV. The three grids: plasma grid (−100 kV), extraction grid (−90 kV) and grounded grid (ground potential) are sequentially arranged and coupled mechanically with the help of post insulators (PI).

These PIs are made of alumina and bolted with SS304L flanges on both ends. All the grids are joined by means of two sets, each consists of 18 number of PIs which provide not only the electric insulation between the grids but also work as a structural member as the BS is suspended vertically from an isolated frame. In this configuration, the total self-weight about seven tones acts on the PIs in cantilever fashion, and their specifications for load bearing capacity provides for this requirement. However, the mechanical behaviour of alumina depends on manufacturing procedures like sintering temperature, volume of the material, shape, etc., which are not addressed by the conventional standards. So it is essential that the design has to be supported with analysis and special tests that qualify.

In the present case, an integrated finite element (FE) assessment in ANSYS is performed where PIs experience combined axial and transverse loading conditions. The assessment determine the most severely loaded PI and its reaction forces and moments. This data becomes inputs for the experimental tests to be carried out for validation. Prior to experimental tests, the test configuration is assessed using FEA to ensure that the test configuration under the applied load condition simulates the realistic conditions.

Additionally, the PI design need to comply with a voltage holding requirement of 140 kV in vacuum. This compliance is established in the design by FE assessment, carried out in ANSYS, for the electrical field distributions, including the stress shields and localized stress field concentrations and subsequently verified by electrical tests.

The paper presents the analysis of BS and the results from the electrical and mechanical tests that have been carried out on 4 PIs manufactured as prototypes.



Concept Design of the Heavy Duty Multipurpose Deployer for ITER

K. K. Gotewal¹, N. Rastogi¹, S. M. Manoah¹, P. Dutta¹, and C.-H. Choi²

¹*Institute for Plasma Research (IPR), Bhat, Gandhinagar, India*

²*International Thermonuclear Experimental Reactor (ITER), Cadarache Centre, 13108 Saint-Paul-lès-Durance, France*

Corresponding Author: K. K. Gotewal, kgotewal@ipr.res.in

ITER presents the most demanding challenge to remote handling (RH) operations ever in terms of weight, complex geometry, limited space, required accuracy and task quality level. The ITER in-vessel components are to be maintained or replaced remotely since these components will be activated by high energy neutrons. In order to perform the in-vessel RH maintenance tasks, an RH system known as the multipurpose deployer (MPD) had been developed, hereafter, called as the light duty MPD (LD MPD). Based on the LD MPD design, an alternative version called as heavy duty MPD (HD MPD) is studied targeting to increase the payload capacity of the LD MPD. The HD MPD is based on the dual port operation that allows higher payload capacity than the LD MPD and prevents HD MPD equipment from contamination as the activated and contaminated in-vessel components are transferred from the nearby ports. The HD MPD transporter has multiple degrees of freedom with a payload capacity up to 5.8 tons for the short configuration, and 4.8 tons for long configuration. Attaching an extension arm can further extend the long configuration for the rescue of the failed LD MPD. A conceptual design of the HD MPD has been developed to provide heavy load handling capability inside the vacuum vessel, which can be used for blanket shield block (SB) handling. The different HD MPD configurations (short, long, long extended) are achieved by in-situ connection of the lower arm with the upper arm by means of an end-effector connector.

The work presented here includes the main design efforts for the development of conceptual envelope of the HD MPD as per the transfer cask and vacuum vessel constraints. The detailed feasibility and kinematic assessments have been carried out to determine the required degrees of freedom and HD MPD configurations for handling of the neutral beam region SB, the regular SB and rescue of the failed LD MPD. This paper summarizes the conceptual design of the HD MPD for various configurations and gives the recommendations for further design enhancements.

Effect of Wall Light Reflection in ITER Diagnostics

S. Kajita¹, M.-H. Aumeunier², A. B. Kukushkin³, E. Yatsuka⁴, M. Bassan⁵, E. Veshchev⁵,
R. Barnsley⁵, M. De Bock⁵, K. Andrei³, V. Neverov⁶, A. Alekseev⁶, E. Andreenko³,
R. Reichle⁵, and M. Walsh⁵

¹*Nagoya University, Nagoya, Japan*

²*Institut de Recherche sur la Fusion par confinement Magnétique (IRFM),
Commissariat à l'énergie atomique (CEA/Cadarache), 13108 Saint-Paul-lès-Durance, France*

³*National Research Centre "Kurchatov Institute", Moscow, Russian Federation*

⁴*Japan Atomic Energy Agency (JAEA), Naka, Japan*

⁵*International Thermonuclear Experimental Reactor (ITER),*

Cadarache Centre, 13108 Saint-Paul-lès-Durance, France

⁶*National Research Nuclear University "MEPhI", Moscow, Russian Federation*

Corresponding Author: S. Kajita, kajita@ees.nagoya-u.ac.jp

Reflection of light on walls will form parasitic signal on various diagnostics and be a serious issue in ITER. In this study, we show the recent progress in the assessment of the effects of the wall reflections in ITER on visible spectroscopy, Thomson scattering, active spectroscopy, and infrared thermography based on the ray-tracing simulation modelling. In this study, it is shown that the stray light becomes orders of magnitudes greater than the actual signal when the actual signal is significantly lower than the strong emission sources.

The line emission will be much stronger from the divertor region than from the scrape-off layer (SOL) in ITER. The emission from the divertor region is so strong that the stray light dominates the illuminance profile for SOL region when considering the wall reflections. It is shown that the stray light becomes significant even for visible spectroscopy measurement in divertor region if there are regions where original illuminance is much lower than the other parts. It is necessary to reduce the stray light level by using viewing dumps, etc. To estimate the error more accurately, the principles of synthetic diagnostics (SD) for ITER main chamber H α spectroscopy are formulated, and the developed algorithms are applied to evaluation of recovering the useful signal under a strong background from divertor stray light (DSL) in ITER.

In order to anticipate the IR measurements in such a metallic environment, a photonic simulation was performed using a Monte Carlo ray tracing based on SPEOS® CAA V5. The first step was done with the simulation of the wide-angle IR thermography system of the JET ITER-like wall, proving good agreement with the experimental data.

For the Thomson scattering diagnostic, to assess the background light reflection (bremsstrahlung and line emission), the emissivity profiles were obtained from the results of SOLPS4.3 modelling for the carbon-free ITER divertor with Ne seeding. The simulation indicates that the level of the reflected background from the divertor plasma, i.e., the bremsstrahlung and line emission, can be much greater than that from the core plasma. It was found that some lines were above the level of the bremsstrahlung, and should be rejected by the spectrometer filter for Thomson scattering systems in ITER.



On Fast Ions Diagnostics with Gamma-Ray Spectrometry in ITER

D. Gin¹, I. Chugunov¹, A. Shevelev¹, E. Khilkevitch¹, V. Naidenov¹, D. Doinikov¹,
A. Pasternak¹, I. Polunovskiy¹, N. Nersesyan¹, and M. Iliasova¹

¹*Ioffe Institute, St. Petersburg, Russian Federation*

Corresponding Author: D. Gin, pipha@mail.ru

Gamma ray spectrometry (GRS) is a mature technique implemented on many past and present tokamaks, including EAST, TFTR, JET etc., that can provide detailed data on the distribution functions (DF) of the plasma fast particles.

In several stages it was undertaken a fusion plasma gamma emission sources (GES) study. Firstly, data on main reactions relevant to alpha particles diagnostics were analyzed [1]. The key reactions for this case are $d(t, \gamma)^5\text{He}$ and $^9\text{Be}(\alpha, n\gamma)^{12}\text{C}$ which gives accordingly information on the source and confinement of mentioned plasma component. When the GRS project was suggested for the ITER neutral particles analyzer one of the main points of interests became ability to support complex measurements of the D to T density ratio with information derived from data on emission caused by reaction with the knock-on ions. Reactions with impurities, mainly ^9Be , were analyzed by modelling of the GES in the plasma and detection of generated quanta with detectors in order to obtain expected spectra and estimate performance of the spectrometer [2]. During preparation of the conceptual and preliminary designs of the ITER GRS further more detailed investigation of the emission was undertaken, particularly involving a complex n and γ background study. Later, another important GES was discussed for ITER and DEMO [3], which includes mechanisms of the consecutive reactions: $d(p, \gamma)^3\text{He}$, $d(t, \gamma)^5\text{He}$, $d(^3\text{He}, \gamma)^5\text{Li}$ and $t(p, \gamma)^4\text{He}$ where ongoing particles can be originated from another reaction (dd). The latter reactions are also suggested to be used for obtaining fuel ratio and the DFs of fast ions and the electron temperature. Uniting of the ITER GES most recent analysis results, comparison of the different GES impacts and application of these data for diagnostic tools development constitutes the main purpose of the current work and reflected in the report. Within the work data on nuclear reactions cross-sections were summarized, plasma emission models for different discharges scenarios suggested. Obtained results used in the MCNP calculations performed in order to estimate count rates of ITER GRS detectors and in the design optimization workflow.

References

- [1] I. N. Chugunov, *et al.*, Nucl. Fusion **51**, 083010 (2011).
- [2] D. Gin, *et al.*, AIP Conf. Proc. **1612**, 149–152 (2014).
- [3] V. G. Kiptily, Nucl. Fusion **55**, 023008 (2015).



System Level Design and Performances of the ITER Radial Neutron Camera

D. Marocco¹, B. Esposito¹, F. Moro¹, G. Brolatti¹, A. Mancini¹, S. Podda¹, F. Belli¹, L. Di Pace¹, D. N. Dongiovanni¹, G. Mazzone¹, M. Riva¹, M. Cecconello², S. Conroy², A. Hjalmarsson², J. Kotula³, D. Bocian³, R. Kantor³, C. P. Rita⁴, N. Cruz⁴, O. Ficker⁵, J. Mlynář⁵, A. Loarte⁶, A. Polevoi⁶, L. Bertalot⁶, R. Barnsley⁶, V. Krasilnikov⁶, S. D. Pinches⁶, A. Zimbal⁷, F. Crescenzi¹, D. Marzullo⁸, R. Miklaszewski⁹, and B. Brichard¹⁰

¹Associazione EURATOM-ENEA Unità Tecnica Fusione, Frascati, Italy

²Uppsala University, Uppsala, Sweden

³Henryk Niewodniczański Institute of Nuclear Physics, Polish Academy of Sciences, Kraków, Poland

⁴Institute of Plasmas and Nuclear Fusion (IPNF), Association EURATOM/IST, Lisbon, Portugal

⁵Institute of Plasma Physics AS CR v.v.i., Prague, Czech Republic

⁶International Thermonuclear Experimental Reactor (ITER),

Cadarache Centre, 13108 Saint-Paul-lès-Durance, France

⁷Physikalisch-Technische Bundesanstalt, Braunschweig, Germany

⁸Consorzio CREATE, 80125 Napoli, Italy

⁹Institute of Plasma Physics and Laser Microfusion, Warsaw, Poland

¹⁰F4E: Fusion for Energy, ITER EU Centre, 08019 Barcelona, Spain

Corresponding Author: D. Marocco, daniele.marocco@enea.it

We present the ongoing work performed by a consortium of European institutes on the design of the ITER radial neutron camera (RNC) within a framework contract placed by Fusion for Energy (F4E), the ITER European domestic agency. The RNC will measure the uncollided 14 MeV and 2.5 MeV neutrons from DT and DD fusion reactions via an array of flux monitors/spectrometers located in collimated lines of sight (LOS) viewing the plasma through equatorial port #1. The line-integrated neutron fluxes are used to evaluate, through reconstruction techniques, the radial profile of the neutron emissivity and therefore the neutron yield and alpha particles birth profile. The major operational role of the RNC is the plasma burn real-time control. The RNC is presently at the system level design (SLD) stage, whose final scope is the definition of an intermediate system architecture (ISA) for the diagnostic to be put under configuration control. The goal is achieved through a system engineering process in which different RNC architectural options are proposed and ultimately are ranked according to selection criteria. The paper concentrates on the part of the process that, starting from the diagnostic functions, leads to the analysis of the RNC measurement performances during DD and DT operations. Based on a set of top level RNC functions (“to provide plasma coverage”, “to provide field of view” and to “to detect particle/radiation”) six RNC global options have been identified and their performances studied by means of three different emissivity reconstruction algorithms: 1) 1D algorithm based on Tikhonov regularization with derivative objective functional; 2) tomography algorithm based on Tikhonov regularization with minimum Fisher information objective functional; 3) 1D algorithm based on neural networks. The analysis was carried out using a set of DT and DD ITER plasma scenarios covering the required neutron emissivity measurement range and including statistical and background errors. Results indicate that, considering only background and statistical uncertainties, the challenging requirements set for the use of the RNC for real-time plasma control operations (10% accuracy, 10 ms time resolution, $10^{14}-6 \times 10^{18}/\text{m}^3\text{s}$ measurement range) might be achieved.



CXRS-edge Diagnostic in the Harsh ITER Environment

A. Zvonkov¹, M. De Bock², S. Tugarinov¹, and V. Serov¹

¹*International Thermonuclear Experimental Reactor (ITER),
Project Centre "ITER", Moscow, Russian Federation*

²*International Thermonuclear Experimental Reactor (ITER),
Cadarache Centre, 13108 Saint-Paul-lès-Durance, France*

Corresponding Author: A. Zvonkov, a.zvonkov@iterrf.ru

CXRS diagnostics supply a set of important plasma parameters of fusion plasmas. According to the system requirements, the CXRS diagnostics in ITER should supply plasma velocity (poloidal and toroidal), impurity ion densities and ion temperatures. The ITER CXRS-edge diagnostic system must measure these parameters over the outer half of the plasma radius. The use of CXRS in ITER encounters serious challenges. In the paper the decisions made to overcome these difficulties for ITER CXRS-edge diagnostics system are described. Testing results of SC Mo prototypes of first mirror are presented. The results of image quality modelling of optical scheme, where the in-vacuum optics uses only mirrors and all lenses are in the air part rather far from plasma, are presented. The results of laboratory test of the device developed for CXRS-edge on the base of transmission holographic gratings are presented.



Progress on Design and R&D of ITER Diagnostic-Radial X-ray Camera

L. Hu¹, K. Chen¹, Y. Chen¹, H. Cao¹, S. Li¹, H. Yu¹, J. Zhan¹, J. Shen¹, S. G. Qin¹, X. Sheng¹, J. Zhao¹, L. Niu¹, C. Feng¹, J. Ge¹, S. Zhang¹, and B. Zhang¹

¹*Institute of Plasma Physics, Chinese Academy of Sciences, Hefei, Anhui, People's Republic of China*

Corresponding Author: L. Hu, lqhu@ipp.ac.cn

Great progress has been made to the design of ITER radial X-ray camera (RXC). The structure design is optimized and installation process is studied considering the simplification and easiness of maintenance. Remote handling skills and tools are designed for the system maintenance after being activated. For detector cooling against high environment temperature which can be up to 240°C, a dedicated gas cooling system using heat exchanger is designed. The structure analysis indicates that the maximum stress on main components is still less than allowable stress. Through putting B₄C material in the front part of DSM and around detectors for neutron shielding, the detectors are expected to survive the whole DD phase. As for electronics, preliminary design of highly integrated preamplifier and programme controllable mid-amplifier has been completed, both with bandwidth greater than 100 kHz to meet time resolution requirement of 20 kHz. To protect the electronics from intensive neutron and gamma irradiation, shielding cabinet capable of attenuating neutron flux down to 0.0001 and γ dose 0.01 is designed.

Based on EAST tokamak and technical experience from diagnostics development acquired on it, much R&D has been done to support the design. The tests of preamplifier and mid-amplifier indicated the electronics had no functional problem when debugging together and generally passed preliminary electromagnetic compatibility (EMC) test and nuclear test. The highly-integrated compact preamplifier has been used in EAST and proved useful. To test the feasibility of dedicated gas cooling system for detectors, a cooling test platform was built and preliminary cooling test has been done, indicating that during 250°C baking the detector temperature is promising to be cooled down to the detector temperature limit of 75°C. To increase signal-to-noise ratio, large area detector with dark current less than 2 nA has been manufactured and worked steadily in EAST experiments.

High Power Testing of Water-Cooled Waveguide for ITER ECH Transmission Lines

J. K. Anderson¹, J. Doane¹, H. Grunloh¹, R. O'Neill¹, R. Ikeda², Y. Oda², K. Takahashi², and K. Sakamoto²

¹General Atomics, San Diego, CA 92186, USA

²Japan Atomic Energy Agency (JAEA), Naka, Japan

Corresponding Author: J. K. Anderson, andersonjp@fusion.gat.com

ITER ECH transmission lines have challenging-to-meet transmitted waveguide mode purity requirements, pushing individual subcomponents towards strict manufacturing tolerances. In addition, most ECH components will require active cooling to remove heat generated by microwave losses, even those with very high transmission efficiencies. To meet these two particular challenges, several new components were built and tested under high power ITER-like conditions. One component is a 4.2 m water-cooled 63.5 mm diameter corrugated 170 GHz waveguide assembly, the straightest and longest corrugated waveguide built to date. The assembly consists of two sections of corrugated waveguide and a precision joint formed by aligning the sections using information from a scanning coordinate measurements machine. Other components include a short expansion joint capable of ± 5 mm change in length, and water-cooled waveguide sections which may be used for gyrotron commissioning transmission lines. The testing of these items occurred at the JAEA Gyrotron Test Facility using gyrotron pulses of 450 kW at 170 GHz for 300 s. A transmission line was constructed of the new components, with water cooling provided by JAEA. Overall power absorption per unit length of waveguide was measured for each water-cooled component by monitoring the temperature rise of the water. The maximum water temperature rise through all components is less than 4°C. The microwave losses are consistent with previous measurements taken of an uncooled transmission line using infrared camera data of waveguide exterior surfaces. Analysis shows that the power absorbed per unit length for the various waveguide components are dependent on location in the transmission line with respect to high-order mode generators, such as miter bends. Far from miter bends, the absorption is 250 W/m. The highest absorption, 700 W/m, occurs for a short section of waveguide between two bends, where both miters contribute decaying higher-order modes. The waveguide components demonstrate suitability for supporting ITER ECH transmission power levels of 1.5 MW at 170 GHz.



Research and Development Progress of the ITER PF Converter System

Z. Song¹, P. Fu¹, G. Gao¹, L. Xu¹, Y. Huang¹, J. Li¹, L. Huang¹, and L. Jiang¹

¹*Institute of Plasma Physics, Chinese Academy of Sciences, Hefei, Anhui, People's Republic of China*

Corresponding Author: Z. Song, zhquansong@ipp.ac.cn

This paper presents the research and development (R&D) progress of the ITER poloidal field (PF) converter for the coil power supply system applied in the ITER project. The PF converter system is composed of 14 PF converter units (PFCU), with a total apparent power of 1.2 GVA and a rated DC current of 55 kA. Due to the huge system power, unprecedented short circuit level, high reliability and availability requirements, special load characteristics and dynamic performance for the plasma control, so the special fault suppression capability (FSC) criterion, sequential control strategy and stringent short circuit test requirements should be adopted and implemented in the design and R&D of the PF converter system. In order to solve these technical challenges, the full scale prototype R&D work of PFCU, which including system analysis, structure design, manufacturing, components test, system integration and improvement, has been accomplished successfully by ASIPP on schedule, and the following final design review (FDR) and manufacturing readiness review (MRR) of PF converter procurement package have also been completed smoothly. At present, the series production of the PF converter system are going under control.



Technical Preparation for Series Production of ITER Enhance Heat Flux FW Panels

J. Chen¹, P. Wang¹, D. Liu¹, F. Jin¹, Q. Li¹, Y. Zhou¹, X. Liu¹, J. Wu¹, B. Yang¹, X. Zhu¹, X. Duan¹, E. Niu², and K. Wang²

¹*Southwestern Institute of Physics, Chengdu, Sichuan, People's Republic of China*

²*International Thermonuclear Experimental Reactor (ITER),
Chinese Domestic Agency, People's Republic of China*

Corresponding Author: J. Chen, chenjm@swip.ac.cn

China will manufacture 10% of the ITER FW panels, all in EHF type with heat load up to 4.7 MW/m². A hypervapotron (HVT) cooling channel was applied as heat sink to enhance heat transfer. Small scale mock-ups have been manufactured in China and successfully passed the thermal fatigue test at 4.7 and 5.9 MW/m² for 7500 cycles and 1500 cycles, respectively. Explosion bonding is used to make bi-metallic CuCrZr/316L(N) plates, while Be/CuCrZr is bonded by hot isostatic pressing (HIP) at 580°C and 150 MPa. Laser welding with 6~15 kW input power was used to close HVT cooling channel and the assembly of FW fingers to central beams. All these technologies were qualified according to specified requirements and standards, and will be used in FW series production. Finger pairs and a semiprototype were manufactured. The pairs will be subjected to the required thermal fatigue test for qualification, which is expected to be completed by July 2016.

To ensure the quality of the products, a number of inspections are performed in the manufacture route. That includes ultrasonic test, hydro-pressure test, helium leak test (HLT) and high heat flux test. The HLT is performed in vacuum with one temperature cycle between RT and 250°C. A hot-helium leak test system is under construction, for which the most challenges are the ultralow vacuum background leak rate and the heating/cooling efficiency requirements. For the purpose hot nitrogen gas with temperatures up to 270°C is designed to heat and cool FW panel by flowing in the FW cooling channels. Analysis showed that the FW panel temperature can be increased to 250°C in about 15 h by 4 MPa N₂ in a flow rate of 0.4 kg/s when the maximum temperature difference of the component is kept below 55°C. To prepare for the FW series production, a number of other large facilities have been equipped recently at SWIP, including a 16 kW YAG laser welding work station, a magnetosputtering equipment, a 200 MPa/1400°C hot isostatic pressing machine, two ultrasonic bath lines for pickling and cleaning, two vacuum baking furnaces, a hydro-pressure test facility with a limit pressure of 10 MPa, a phase-array ultrasonic nondestructive test system and a 400 kW electron beam scanning facility. This EB scanning system will be used to test the 1st FW prototype at 4.7 MW/m² for 1000 cycles and to test series FW fingers at 2 MW/m² for 100 cycles.



ITER Core Thomson Scattering: Objectives and Error Analysis

G. S. Kurskiev¹, E. E. Mukhin¹, A. B. Kukushkin², A. S. Kukushkin³, A. Z. Razdobarin¹, P. Sdvizhenskii², N. Ageorges⁴, A. Alekseev², P. Andrew³, M. Bassan³, P. V Chernakov⁵, A. Gorshkov², S. Gutruf⁴, D. Kampf⁴, M. Kochergin^{6,1}, A. Reutlinger⁴, D. S. Samsonov¹, A. Saveliev¹, S. Yu. Tolstyakov¹, and M. Walsh³

¹Ioffe Institute, St. Petersburg, Russian Federation

²National Research Centre "Kurchatov Institute", Moscow, Russian Federation

³International Thermonuclear Experimental Reactor (ITER), Cadarache Centre, 13108 Saint-Paul-lès-Durance, France

⁴Kampf Telescope Optics GmbH, Munich, Germany

⁵Spectral-Tech, ZAO, St. Petersburg, Russian Federation

⁶International Thermonuclear Experimental Reactor (ITER), Project Centre "ITER", Moscow, Russian Federation

Corresponding Author: G. S. Kurskiev, gleb.kurskiev@gmail.com

Measuring electron temperature and density profiles is a high priority task for tokamak diagnostics because the electron component is one of the main channels for the anomalous power loss and it is strongly sensitive to transient processes in the tokamak plasma. Measurements of the core Thompson scattering (TS) in ITER must cover the whole core region $r/a < 0.85$, $R > 6$ m with a spatial resolution of 67 mm or better and must be able to measure the electron temperature of $0.5 < T_e < 40$ keV and density of $0.3 \times 10^{20}/\text{m}^3 < n_e < 3 \times 10^{20}/\text{m}^3$.

In this paper we apply and extend the analytical approach for assessment of the measurement error and optimization of the ITER core TS system based on analyzes of the core plasma TS diagnostics for non-Maxwellian and Maxwellian plasmas via solving an inverse problem for error assessment. The extension of the approach includes:

- i) a comparative analysis of different ways of implementing the ITER core TS system, including the classical approach, for both the back and forward scattering geometry, and LIDAR (time-of-flight measurements along probing chords, performed with a single spectrometer);
- ii) simulations of the electron VDF under the conditions of the ECRH/ECCD in ITER, using the QQL3D and GENRAY codes;
- iii) analysis of possible advantages and limitations of the polarimetry for recovering T_e from measurements of the spectrum of the depolarized TS for $T_e \sim 40$ keV.

The ITER Neutral Beam Test Facility toward SPIDER Operation

V. Toigo¹, D. Boilson², T. Bonicelli³, A. K. Chakraborty^{4,5}, and U. Fantz⁶

¹*Consorzio RFX, Associazione EURATOM-ENEA sulla Fusione, Padova, Italy*

²*International Thermonuclear Experimental Reactor (ITER),
Cadarache Centre, 13108 Saint-Paul-lès-Durance, France*

³*F4E: Fusion for Energy, ITER EU Centre, 08019 Barcelona, Spain*

⁴*International Thermonuclear Experimental Reactor (ITER), India Centre, Gujarat, India*

⁵*Institute for Plasma Research (IPR), Bhat, Gandhinagar, India*

⁶*Max-Planck-Institut für Plasmaphysik, Garching, Germany*

Corresponding Author: V. Toigo, vanni.toigo@igi.cnr.it

In order to achieve thermonuclear-relevant plasma parameters in ITER, the auxiliary heating systems have to provide 50 MW, out of which 33 MW by two neutral beam injectors (NBI), each designed to operate at 1 MV, 40 A for one hour. The unprecedented parameters and the complexity of the NBI systems have led to recognize the need of a dedicated test facility to carry out an international R&D programme aimed at realizing, testing and optimizing the prototype of the NBI and to assist ITER during its operation. This facility is under construction in Padova Italy at Consorzio RFX premises and hosts two experiments: MITICA, a 1 MeV full-size prototype of the ITER NBI, and SPIDER, a full-size prototype of the ion source for ITER NBI.

The realization of the two experiments is carried out with the main contribution of the European Union, channelled through the Joint Undertaking for ITER (F4E), the ITER Organization and Consorzio RFX, with the Japanese and the Indian ITER Domestic Agencies (JADA and INDA) and European laboratories, such as IPP-Garching among others. The realization of MITICA and SPIDER progresses in parallel; presently, the installation phase of SPIDER is proceeding in good agreement with the general plan.

This paper mainly focusses on the integration issues and complementary research toward the SPIDER first operation, expected for next year. This is a very crucial phase, evolving along three main parallel paths: integration and testing of SPIDER components, completion and implementation of diagnostics and preparation of operation and research plan. The most interesting aspects of the wide set of activities, studies and further developments, all concurrent to determine the success of the SPIDER start of operation and exploitation will be described and discussed.



The Development of the European 1 MW, 170 GHz CW Gyrotron for the ITER Electron Cyclotron Heating System

F. Albajar¹, S. Alberti², K. Avramidis³, W. Bin⁴, T. Bonicelli¹, F. Braunmueller², A. Bruschi⁴, F. Cau¹, J. G. Chelis⁵, F. Cismondi¹, C. Darbos⁶, P.-E. Frigot¹, G. Gantenbein³, M. Henderson⁶, V. Hermann⁷, J.-P. Hogge², S. Illy³, Z. Ioannidis³, J. Jelonnek³, J. Jin³, W. Kasperek⁸, T. Kobarg³, G. P. Latsas⁹, L. Carsten⁸, M. Lontano⁴, M. Losert³, I. Pagonakis³, Y. Rozier⁷, T. Rzesnicki³, C. Schlatter², M. Schmid³, M. Thumm³, I. Tigelis⁹, M. Q. Tran², and J. L. Vomvoridis⁵

¹F4E: Fusion for Energy, ITER EU Centre, 08019 Barcelona, Spain

²Swiss Plasma Center (SPC), École polytechnique fédérale de Lausanne (EPFL), 1015 Lausanne, Switzerland

³Karlsruhe Institute of Technology (KIT), Karlsruhe, Germany

⁴Istituto di Fisica del Plasma (IFP), Consiglio Nazionale delle Ricerche (CNR), 20125 Milan, Italy

⁵National Technical University of Athens, Greece

⁶International Thermonuclear Experimental Reactor (ITER),

Cadarache Centre, 13108 Saint-Paul-lès-Durance, France

⁷Thales Electron Devices S.A., Velizy, France

⁸Institut für Grenzflächenverfahrenstechnik und Plasmatechnologie (IGVP), Univ. Stuttgart, Germany

⁹Faculty of Physics, National and Kapodistrian University of Athens, Greece

Corresponding Author: F. Albajar, ferran.albajar@f4e.europa.eu

The EU gyrotron for the ITER electron cyclotron heating system has been developed in coordinated efforts from several EU institutions (organized in the EGYC European Gyrotron Consortium, TED and F4E) and under the supervision of ITER Organization central team. The design of the ITER gyrotron is based on the EU expertise in the series production of high power and long pulse gyrotrons for the W7-X stellarator, and incorporates key improvements recently validated to enhance the quality of the electron beam at the cavity and the output RF beam at the window. Following a risk-reducing staged approach, the design was first verified in 2015 with tests on a short pulse prototype, showing > 1 MW of output RF power at the right frequency (~170.1 GHz) in stable and reproducible conditions. The electronic efficiency (~35%) obtained with the short pulse gyrotron was consistent with an ~50% output efficiency in voltage depression and in a CW electrostatic configuration. No parasitic oscillations were observed and a high quality of the output RF beam was measured (TEM₀₀ ~98%). A CW gyrotron prototype was then produced with the same design of the internal RF and electronic components. The CW prototype was delivered in November 2015 to the KIT gyrotron test facility, where it will be tested in 2016. This paper presents the main experimental results from the main prototyping and qualification activities aiming to demonstrate compliance with the ITER specifications and reduce the technical risks during the series production phase.



Synergy of Numerical Simulations and Experimental Measurements to Improve the Interpretation of Negative Ion Beam Properties

G. Serianni¹, P. Agostinetti¹, V. Antoni¹, D. Aprile¹, M. Brombin¹, M. Cavenago², G. Chitarin¹, R. S. Delogu¹, N. Marconato¹, R. Pasqualotto¹, A. Pimazzoni¹, E. Sartori¹, P. Veltri², O. Kaneko³, Y. Takeiri³, M. Osakabe³, K. Nagaoka³, K. Ikeda³, H. Nakano³, M. Kisaki³, and K. Tsumori³

¹*Consorzio RFX, Associazione EURATOM-ENEA sulla Fusione, Padova, Italy*

²*Istituto Nazionale di Fisica Nucleare (INFN), Italy*

³*National Institute for Fusion Science (NIFS), Toki, Gifu, Japan*

Corresponding Author: G. Serianni, gianluigi.serianni@igi.cnr.it

The ITER tokamak requires two heating neutral beam injectors (NBIs), based on the neutralization of 40 A of negative hydrogen ions accelerated to 1 MeV with a pulse length of one hour. As these simultaneous parameters were never experimentally achieved, in order to optimize source operation and to assess beam properties, a specific test facility (“PRIMA”) was established in Padova, comprising two experiments: SPIDER (full-size negative ion source with 40 A beam, 100 keV particle energy) and MITICA, the prototype of ITER NBIs.

A key NBI component is the particle accelerator, where electrostatic and magnetic fields produce the beam optics, which is modified by loss of additional electrons (stripping) and generation of secondary particles. The design of SPIDER and MITICA accelerators was based on the most advanced numerical codes available for the investigation of the expected beam properties and on the most up-to-date experience of various research groups. Several diagnostic systems will characterize source and beam during the experiments.

In view of the operation, effort is presently devoted (within bilateral collaboration frameworks between Italian and Japanese agencies) to the preparation for the synergistic employment of simulations and experiments. Specifically, the characterization of the beam properties is carried out in the NIFS-R&D multicusp negative ion source (NIFS-RNIS) by a sophisticated set of source and beam diagnostic systems. Simulations are mainly performed at Consorzio RFX, by a suite of numerical tools to compute or investigate various aspects of beam physics. Preliminary comparisons showed very good agreement between simulations and measured data regarding the basic features of the accelerator. Numerical codes allow also the investigation of extreme operational conditions, including phenomena not accessible to direct measurement, like the interception of grids by beam particles.

The present contribution describes the synergy between numerical codes and sophisticated diagnostic techniques. Both are applied to real-time characterization of the beam, with the main scopes of providing interpretation of the measured results and supplying data for successive choices during the operation. These activities allow also extensive validation of numerical models and the choice of the most useful set of codes to be used in future experiments like DEMO.



60 GHz–300 kW Gyrotron General Design for the Mexican Tokamak “T”

J. A. González Guevara¹, M. Salvador Hernández¹, O. A. Muñoz Ovalle¹,
A. Nieto Cuarenta¹, V. M. Arredondo Solís¹, J. González Marroquín¹,
J. R. Morones Ibarra¹, J. Martínez Torres², R. M. Chávez Rodríguez¹,
G. R. Cavazos Almaguer¹, M. A. Sanromán Reséndiz¹, C. U. Acosta Muñoz¹,
I. E. Morales Niño¹, J. V. Guzmán González¹, A. Acosta Pérez¹, C. A. Briseño Cárdenas¹,
and U. Aguilar Reyes¹

¹Universidad Autónoma de Nuevo León, San Nicolás de los Garza, Nuevo León, Mexico

²Comisión Federal de Electricidad, Mexico City, Mexico

Corresponding Author: J. A. González Guevara, sihigzzg@gmail.com

An important system into the magnetic confinement devices to obtain appropriate knowledge on plasma behaviour in nuclear fusion is the electron cyclotron resonance heating (ECRH). We present the preliminary design of our source for ECRH system applied in our Tokamak device, a gyrotron device 60 GHz–300 kW which is currently developed by the Fusion Research Group (GIF) at the Universidad Autónoma de Nuevo León (UANL) in Monterrey, Mexico.

It is present a gyrotron general design characterized with a magnetic intensity of 2.56 T, required into the cavity to arise 60 GHz high-power millimetre frequency in the fundamental harmonic and nominal beam parameters such as interaction region to cathode ratio of a magnetic compression of 13.68; a beam voltage of 100 kV, a beam current of 3 A, and transverse to axial velocity ratio of 1.5. From analytical adiabatic trade-off equations a triode type magnetron injection gun is designed. The mean radio of the emitter (7.3 mm), slant length of the emitting surface (8.8 mm), cathode modulating anode gap (11.5 mm), slope angle of emitter (40 degree) are obtained. These results are supported by 2D computer simulations performed by COMSOL Multiphysics and optimized using the electron optics finite element code EGUN.

Manufacturing and Commissioning of Large Size UHV Class Vacuum Vessel for Indian Test Facility (INTF) for Neutral Beams

J. Joshi^{1,2}, A. Yadav^{1,2}, K. Joshi^{1,2}, D. Singh^{1,2}, H. Patel^{1,2}, S. Ulahannan³, V. Abbavaram³, G. Hebbar⁴, M. Alaparthi⁴, M. Khan⁴, C. Rotti^{1,2}, M. Bandyopadhyay^{1,2}, and
A. K. Chakraborty^{1,2}

¹International Thermonuclear Experimental Reactor (ITER), India Centre, Gujarat, India

²Institute for Plasma Research (IPR), Bhat, Gandhinagar, India

³Airframe Aerodesigns Ltd., Murugeshpalya, Karnataka, India

⁴Vacuum Techniques Pvt. Ltd., Bengaluru, Karnataka, India

Corresponding Author: J. Joshi, jaydeep.joshi@iter-india.org

The Indian test facility (INTF) is designed for “Full characterization of the diagnostic neutral beam (DNB)” for ITER, to unveil the possible challenges in production, neutralization and transportation of neutral beam over the path length of ~ 20.67 m. This facility consist of a vacuum vessel (volume > 180 m³) which has been designed and manufactured as per ASME Sec. VIII Div. 1, to house and provide an ultrahigh vacuum (UHV) environment for DNB components, i.e, beam source, beam line components, high voltage bushing and cryopumps.

As per functional requirements, INTF vessel is fabricated from AISI 304L, in cylindrical shape (4.5 m D, 9 m L), with the unique attribute of “detachable top lid” to allow access for internal components during installation and maintenance. As per the best of authors’ knowledge, it is the biggest UHV vessel with this configuration ever realized, it was therefore essential to establish a systematic approach when moving from the “nonconventional design” to “nonconventional manufacturing”, while respecting all the UHV protocols. During this manufacturing, top lid is cut from the shell itself which demands controlling the deflection, arising due to stress relaxation caused by welding and shell rolling. Further, distortion monitoring during the welding of large flanges was carried out and following to that machining parameters was controlled to achieve the flatness ~ 1.2 mm over the area of $9\text{ m} \times 5\text{ m}$ for achieving leak rate of $< 10^{-9}$ mbar ℓ/s . In addition, methodology of stage machining was adopted to nullify the distortion caused by large amount of welding for top flange to collar welding and top lid flange to top lid welding.

Following fabrication, vacuum level of 8×10^{-6} was demonstrated with corresponding local and global leak rates as per the UHV requirements (better than 10^{-9} mbar ℓ/s and 10^{-7} mbar ℓ/s respectively).

This paper presents the experience, methodologies and learning generated in the establishing the manufacturing protocols and practices to achieve the distortion control, deflection requirements and vacuum demonstration for large size UHV vessel with detachable top lid configuration.

Fabrication of Divertor Mock-Up with ODS-Cu and W by Improved Brazing Technique

M. Tokitani¹, Y. Hamaji¹, Y. Hiraoka², S. Masuzaki¹, H. Tamura¹, H. Noto¹, T. Tanaka¹, T. Muroga¹, and A. Sagara¹

¹National Institute for Fusion Science (NIFS), Toki, Gifu, Japan

²Department of Applied Physics, Okayama University of Science, Okayama, Japan

Corresponding Author: M. Tokitani, tokitani.masayuki@lhd.nifs.ac.jp

It is considered that copper alloy could be used as a divertor cooling tube in not only helical reactor FFHR-d1 but also tokamak DEMO reactor, because of utilizing its high thermal conductivity. This study focussed on using an oxide dispersion strengthened copper alloy (ODS-Cu) of GlidCop® (Cu-0.3wt%Al₂O₃) as the divertor heat sink material of FFHR-d1. This alloy has superior high temperature strength over 300 MPa even after an annealing up to ~1000°C. This characteristic provides two important advantages. The first advantage ensures the redundancy of the temperature margin of the divertor operation even when an unexpected temperature excursion occurs. The second comes during the brazing procedures itself, since rapid cooling down phase is not needed at the final stage of the brazing heat treatment. The rapid cooling down phase would be give an undesired thermal stress to the material.

The changeable material properties of pure-Cu, GlidCop® and CuCrZr by neutron irradiation are summarized in this paper. A primary dose limit is the radiation induced hardening/softening (~0.2 dpa/1–2 dpa), and it has a temperature dependence. If the temperature of the GlidCop® is maintained at 300°C, radiation induced hardening/softening would be moderated. According to such an evaluation, GlidCop® can be selected as the current best candidate material in the commercial base of the divertor heat sink, and its temperature should be kept at 300°C when possible during operation.

Joining tungsten armour to the GlidCop® heat sink was successfully performed by using an improved brazing technique with BNi-6 (bal.%Ni, 11%P) filler material (W/BNi-6/GlidCop®). The joint strength was measured by three-point bending test, and was around 200 MPa. Surprisingly, several specimen showed obvious yield point. This means that BNi-6 brazing layer caused relaxation of the applied stress.

The small divertor mock-up of the W/BNi-6/GlidCop® was successfully fabricated by the improved brazing technique. The heat loading test was carried out by electron beam device ACT2 in NIFS. The highest temperature under 8 MW/m² is ~350°C in the tungsten plate. The temperature profile is quite reasonable by modelling calculation by a finite element method. The design of the W/BNi-6/GlidCop® showed an excellent heat removal capability for using in the FFHR-d1 divertor.

Liquid Metal Flow Control Simulation at Liquid Metal Experiment

M. Modestov^{1,2}, E. Kolemen³, E. P. Gilson³, J. A. Hinojosa¹, H. Ji³, R. P. Majeski³, and T. Kunugi³

¹Princeton University, Princeton, NJ 08544, USA

²Nordic Institute for Theoretical Physics (Nordita), 106 91 Stockholm, Sweden

³Princeton Plasma Physics Laboratory (PPPL), Princeton, NJ 08540, USA

Corresponding Author: M. Modestov, modestov@princeton.edu

Successful design of liquid metal wall or divertors for nuclear fusion reactors require the understanding of the behaviour of liquid metal flows. The liquid metal experiment (LMX) at PPPL has been designed in a form of a rectangular channel allowing investigation of major issues of heat transfer and magnetic field influence relevant to tokamak divertor operation. We present the numerical simulations of heat transfer in liquid metal flow and the comparison with the experimental data obtained on the LMX. Experiments with Reynolds number within 10^3 – 10^4 show temperature flux quadratic decay while laminar flow simulations predict exponential behaviour. This difference indicates that the boundary layer physics is dominant over the heat conduction mechanism in the studied liquid metal flow. When the Hartmann layer is formed in addition to viscous boundary layer, this may become more prominent. Also, the effects of various obstacles in the flow to enhance the advection of heat were simulated and show quantitative agreement with experiments.



Modelling the Lithium Loop in a Liquid Metal Divertor for Future Fusion Reactors

R. Zanino¹, D. Aquaro², G. Caruso³, F. Crisanti⁴, G. Mazzitelli⁴, and G. Vella⁵

¹*Dipartimento Energia, Polytechnic University of Turin, Turin, Italy*

²*Università di Pisa, 56126 Pisa, Italy*

³*Sapienza – Università di Roma, 00185 Rome, Italy*

⁴*Agenzia nazionale per le nuove tecnologie, l'energia e lo sviluppo economico sostenibile (ENEA), Rome, Italy*

⁵*Università degli Studi di Palermo, Palermo, Italy*

Corresponding Author: R. Zanino, roberto.zanino@polito.it

Solutions for the steady-state power exhaust problem in future fusion reactors (e.g, DEMO) are not automatically provided by present experiments or even ITER, because the expected heat fluxes, as well as the level of neutron irradiation, will be much higher. Dedicated work packages are being devoted to this problem within EUROfusion and even a dedicated facility (the divertor tokamak test, DTT) is being proposed by Italy. Among the possible innovative solutions, a liquid metal (LM) divertor had been proposed more than 20 years ago. The particularly attractive feature of this solution is obviously the absence of damage to the wall, even in the case of large heat fluxes, thanks to the high latent heat of evaporation and to the liquid nature of the wall, which can be constantly replenished.

The present work aims at developing a first model of the LM loop which will be the core of the tools to be developed and eventually applied, in a later phase of the project, to the conceptual design of an LM divertor for the DTT facility. The model will describe the transport of the LM in the evaporation chamber, including its interaction with the plasma.



TCV Divertor and Heating Upgrades for Contributing to DEMO Physics Basis

A. Fasoli¹

The TCV Team

¹*Swiss Plasma Center (SPC), École polytechnique fédérale de Lausanne (EPFL), 1015 Lausanne, Switzerland*

Corresponding Author: A. Fasoli, ambrogio.fasoli@epfl.ch

Major upgrades to the TCV infrastructure are implemented to increase the DEMO relevance of its research. A major component is the creation of an in-vessel divertor chamber of variable closure to contribute to the qualification of alternative divertor concepts, including the demonstration of advantageous plasma exhaust performance, combining detachment with particle control, He compression and impurity retention in the divertor, and ELM control. Options to implement mechanically extendable or replaceable baffles are studied. The present design consists of one set of 32 solid graphite tiles on the high field side and several sets of 64 tiles on the low field side. The latter vary in tile protrusion to change the divertor closure. Enhancements of existing diagnostics together with new systems are envisaged to characterize the divertor performance. A new high capacity pump and an extended set of gas valves will enhance the particle control. Finally, one to three additional poloidal field coils close to the divertor may be needed to increase the range of accessible divertor configurations and improve the relevant control capabilities. We intend to use high temperature superconductors, which permit over an order of magnitude larger current densities compared to water cooled copper coils, reducing space requirements and facilitating in-situ construction. The divertor upgrade completes a set of major improvements to the plasma heating systems, which are conducted in two steps, one presently under way and another foreseen in 2017–2020. The installation of a 1 MW 15–30 keV NBI has recently been completed. Ion temperatures of 2 keV and rotation velocities of 160 km/s have already been measured. The first step also includes the acquisition of two 0.75 MW gyrotrons for ECH/ECCD at the 2nd harmonic (X2, 87 GHz). The second step consists of the installation of a 1 MW, 50 keV beam, directed opposite to the first beam, for plasma rotation and fast ion physics studies, and two 1 MW dual frequency gyrotrons, (83 GHz, X2 and 126 GHz, X3). EMC3-EIRENE simulations indicate that realistic baffles together with the heating upgrade (designed to reach $T_i/T_e > 1$ and $\beta_N \sim 3$) allow for significantly higher neutral pressure, impurity compression and power dissipation in the divertor ($P_{sep}/R \sim 6$ MW/m).

This work was partly supported by the Fonds National Suisse pour la Recherche Scientifique.



Japan-US Joint Research Project PHENIX (2013–2018); Heat Transfer Tests, Neutron Irradiation and Postirradiation Examinations for Development of He-Cooled Tungsten Divertor

Y. Hatano¹, Y. Ueda², D. Clark³, Y. Takehiko⁴, A. Sabau⁵, M. Yoda⁶, T. Hinoki⁴, A. Hasegawa⁷, Y. Katoh⁵, L. Garrison⁵, Y. Oya⁸, M. Shimada⁹, D. Buchenauer¹⁰, M. Fukuda⁷, T. Tanaka¹¹, and T. Muroga¹¹

¹Hydrogen Isotope Research Center, University of Toyama, Toyama, Japan

²Osaka University, Osaka, Japan

³U.S. Department of Energy, Washington, DC 20585, USA

⁴Kyoto University, Nishikyo-ku, Kyoto 615-8540, Japan

⁵Oak Ridge National Laboratory (ORNL), Oak Ridge, TN 37831, USA

⁶Georgia Institute of Technology, Atlanta, GA, USA

⁷Tohoku University, Sendai, Miyagi, Japan

⁸Shizuoka University, Shizuoka, Japan

⁹Idaho National Laboratory (INL), Idaho Falls, ID 83415, USA

¹⁰Sandia National Laboratories (SNL), Albuquerque, NM 87185, USA

¹¹National Institute for Fusion Science (NIFS), Toki, Gifu, Japan

Corresponding Author: Y. Hatano, hatano@ctg.u-toyama.ac.jp

The goal of the Japan-US joint research project PHENIX (2013–2018) is to understand the feasibility of He-cooled W divertor for DEMO applications. To achieve this goal, the project has three major objectives: 1) to understand heat transfer in a divertor module cooled with high-temperature and high-pressure He gas, 2) to establish database on thermomechanical properties of W materials after high temperature (~500, ~800 and ~1200°C) neutron irradiation with fusion-relevant energy spectrum, and 3) to clarify tritium (T) trapping and permeation in neutron-irradiated W materials. Heat transfer tests for a He-cooled modular divertor with multi-jet (HEMJ) have been performed, and the problem of heat transfer degradation by relaminarization was identified. The irradiation capsule with thermal neutron shielding was designed for high temperature neutron irradiation in the High-Flux Isotope Reactor (HFIR), Oak Ridge National Laboratory (ORNL) with fusion-relevant transmutation. The expected damage level is 1–1.5 displacements per atom (dpa). Heat load resistance, thermal conductivity, mechanical properties and microstructures are examined in ORNL after the irradiation. Mechanical properties of W single-crystal samples irradiated with neutrons in HFIR at 90–850°C without thermal neutron shielding have been examined for comparison. Significant hardening was observed after irradiation to > 1 dpa. Microstructural examinations revealed that the hardening was mainly caused by formation of irradiation-induced precipitates consisting of W, Re and Os. Comparison with new samples irradiated in the capsule with thermal neutron shielding will show the effects of irradiation temperatures and transmutation elements. Retention and permeation of hydrogen isotopes including T in neutron-irradiated samples are examined in Idaho National Laboratory, and permeation of H and D in samples damaged with surrogate irradiations (heavy ions, electrons, etc.) is measured in Sandia National Laboratories, Livermore, to study hydrogen-defect interactions in wider conditions. High temperature D permeation tests performed for W damaged at 300°C with high energy Fe ions showed significant trapping of D at radiation-induced defects at temperatures as high as 900°C.



Assessment of the Operational Window for JT-60SA Divertor Pumping under Consideration of the Effects from Neutral-Neutral Collisions

C. Day¹, C. Gleason-Gonzalez¹, K. Shimizu², S. Varoutis¹, T. Nakano², K. Hoshino², H. Kawashima², M. Scannapiego¹, S. Sakurai², X. Luo¹, V. Hauer¹, N. Asakura², and F. Bonelli¹

¹Karlsruhe Institute of Technology (KIT), Karlsruhe, Germany

²Japan Atomic Energy Agency (JAEA), Naka, Japan

Corresponding Author: C. Day, christian.day@kit.edu

The JT-60SA device will start operation in 2019. One of the top research goals is to study high density plasma physics in view of a demonstration fusion power plant. In this context, this paper presents an integrated modelling of the divertor pumping system of JT-60SA.

The paper first presents a generic integrated workflow to assess the operational window of the pumping system. This approach is supposed to hold for any divertor pumping system, independent of the chosen magnetic configuration. Even today, to simulate such a system under consideration of all geometry details and through all collisionality regimes, is beyond the computational state-of-the-art. This is why such an assessment is usually done in a stepwise manner. The logical first step is a sensitivity study based on the ITERVAC code to identify the most relevant flow paths of the problem aiming for some sort of simplification. The next step is then to do a more accurate treatment of the subdivertor neutral gas flow using a collision-free approach (such as NEUT2D), a simplified collisional approach (EIRENE) or a complete collisional approach (DIVGAS). At this level, the simplified treatment of the plasma as black hole is being dropped, and the boundary is described with “real” particle flux and temperature profiles along the upper divertor region. This information is typical output from a plasma edge code (such as SONIC or SOLPS). Towards the pump side, a capture coefficient is introduced which translates the pumping speed of the installed pumps together with the conductance limiting effect of the port and its installations into an effective pumping speed at the edge of the subdivertor computational domain.

In the second part, the workflow is exemplified using JT-60SA in a challenging case for pumping, namely under the scenario #2 with moderate plasma density but strong gas puffing to result in collisional effects in the subdivertor. It is shown how the value of the capture coefficient influences the density contours and it is revealed that already for Knudsen numbers between 0.1 and 1, the macroscopic properties in the subdivertor deviate by more than factor two from the collision-free values.

FIP



Flow Characteristics in HyperVapotron Elements Operating with Nanofluids

A. Sergis^{1,2}, H. Yannis¹, and T. Barrett²

¹Imperial College, London, UK

²Culham Centre for Fusion Energy (CCFE), Culham Science Centre, Abingdon, UK

Corresponding Author: A. Sergis, a.sergis09@imperial.ac.uk

HyperVapotrons (HVs) are highly robust and efficient heat exchangers able to transfer high heat fluxes of the order of 10–20 MW/m². They employ the Vapotron effect, a complex two-phase heat transfer mechanism, which is strongly linked to the hydrodynamic structures present in the coolant flow inside the devices. HVs are currently used in the Jointed European Torus (JET) and the Mega-Amp Spherical Tokamak (MAST) fusion experiments and are planned to be used extensively in ITER. The heat transfer efficiency and component reliability of a fusion power plant are important factors to ensure its longevity and economical sustainability. Optimization of the heat transfer performance of these devices by the use of nanofluids is investigated in this paper. Nanofluids are advanced two-phase coolants that exhibit heat transfer augmentation phenomena. A cold isothermal nanofluid flow is established inside two HV models representing the geometries used at JET and MAST. A hybrid particle image velocimetry method is then employed to map in high spatial resolution (30 μm) the flow fields inside each replica. The instantaneous and mean flow structures of a nanofluid are compared to those present during the use of a traditional coolant (water) in order to detect any departure from the hydrodynamic design operational regime of the device. It was discovered that the flow field of the JET model is considerably affected when using nanofluids, while the flow in the MAST geometry does not change significantly by the introduction of nanofluids. This signifies a possible presence of a viscosity change mechanism inside nanofluids that is dominant for the JET geometry and insignificant for the MAST geometry. The finding goes against Einstein's effective viscosity equation (derived for spherical micron-sized suspensions) that is widely used in such applications.

Self-Consistent Coupling of DSMC Method and SOLPS Code for Modelling Tokamak Particle Exhaust

F. Bonelli¹, S. Varoutis¹, D. Coster², C. Day¹, and R. Zanino³

¹Karlsruhe Institute of Technology (KIT), Karlsruhe, Germany

²Max-Planck-Institut für Plasmaphysik, Garching, Germany

³Dipartimento Energia, Polytechnic University of Turin, Turin, Italy

Corresponding Author: F. Bonelli, flavia.bonelli@kit.edu

From both the physical and the technical point of view, the description of gas dynamics in the divertor and vacuum systems in tokamak fusion reactors poses a challenging task because of the wide range of regimes covered by the flow: from continuum and slip regimes in the plasma, to transition and free molecular flow in the subdivertor region. Nevertheless, over the past few years, significant progress has been made in modelling the complex system of the subdivertor region: a valid tool that has been proven able to describe such a range of gas rarefaction is the direct simulation Monte Carlo (DSMC) method. The present work aims to give a qualitative study of the neutral particle recirculation flows under different pumping conditions in the JET subdivertor. So far, investigations of the neutral gas flow in both ITER and JET subdivertor areas have been performed by successfully implementing DSMC using the input data from a SOL plasma modelling code, such as SOLPS and EDGE2D.

Nevertheless, until now there was a simple one-way coupling between a plasma and DSMC code, where the output information from the edge plasma code was imposed on the DSMC algorithm as inlet boundary condition. This paper will improve such a coupling by applying an iterative, but still manual, interaction between the two approaches. Specifically, the data containing the information on the recirculation flow towards the divertor, output of the first DSMC simulation, will be in turn used by the SOLPS code as neutral particle influx boundary condition in the private flux region. After performing the plasma edge calculation, the new estimated incoming flux to the subdivertor will be used as updated inlet boundary condition for the next DSMC simulation. Therefore, an iterative procedure will be established until convergence is achieved and a self-consistent solution is reached: this will lead to understand and quantify the mutual influence between the two regions via neutral particle recirculation.

The study will be performed for the case of a 2D symmetric and simplified geometry of the JET subdivertor, and will be focussed on plasma scenarios with high and medium electron density cases.



Computational Fluid Dynamic Analysis of Screw Tube Relevant for Fusion Applications

P. K. Domalapally¹, M. Dellabiancia¹

¹Research Center Řež, Husinec-Řež, Czech Republic

Corresponding Author: P. K. Domalapally, p_kumar.domalapally@cvrez.cz

Determination of the likely heat loads which may be expected on the first wall (FW) of the projected European fusion reactor DEMO is still underway. This uncertainty notwithstanding, the engineering design of the heat sink components must proceed, hence the scientific community is using the so called bottom-up approach to determine the maximum heat flux that the component could sustain given currently existing material limitations and forecast operating conditions. The European DEMO will most likely use a reduced activation ferritic martensitic steel called EUROFER 97 as the heat sink material for the FW. In terms of operating conditions one concept uses water as a coolant at PWR conditions i.e., 15.5 MPa and 285°C. The main challenge is that if the heat loads on the DEMO FW are extrapolated from ITER, they could be very high. Conversely the upper temperature limit of EUROFER is 550°C. Given also its low thermal conductivity ~ 30 W/mK (far lower than that of CuCrZr which is the heat sink material in ITER) and an operational coolant wall temperature of 285°C, the design of the heat-sink is difficult.

The current work attempts to study the heat absorption capability of the heat sink using a turbulence/critical heat flux enhancer inside the cooling channel known as a screw tube, by using computational fluid dynamics (CFD). A screw tube is a cooling tube with a helical triangular fin on its inner surface. The nut-like inner surface works as a combination of enhanced heat transfer area and turbulence promoter. In the literature, several experiments have been performed to determine the heat evacuation capability improvement from screw tubes but none has studied the fluid dynamics and heat transfer in detail. In this work, a commercial CFD code STAR-CCM+ is used to study the flow physics, in that several turbulence models were tested and the effect on flow dynamics is evaluated. In a second step, the most appropriate turbulence model was selected; the heat transfer from solid to fluid was studied (single phase heat transfer) and was then validated against the available experimental data in the literature. Thus the current work lays the foundations for a continuation of the work, for further optimization of the screw tube to be performed taking in to account the European DEMO conditions.

Upgrade of ADITYA Tokamak with Limiter Configuration to ADITYA Upgrade Tokamak with Divertor Configuration

J. Ghosh¹, R. Tanna¹, S. B. Bhatt¹, P. K. Chattopadhyay¹, K. Sathyanarayana¹, C. Chavda¹, C. Gupta¹, K. A. Jadeja¹, K. Patel¹, V. K. Panchal¹, V. Patel¹, K. Rathod¹, S. Patel¹, S. Jaiswal¹, P. K. Chauhan¹, V. Ranjan¹, R. Kumar¹, H. Raj¹, K. Kumari¹, D. Sadharakiya¹, M. Kalal¹, D. Varia¹, R. N. Panchal¹, K. Acharya¹, N. Patel¹, K. Chaudhary¹, M. N. Makwana¹, K. S. Shah¹, D. Raju¹, R. Srinivasan¹, D. K. Sharma¹, S. Dutta¹, B. Doshi¹, M. Gupta¹, U. Baruah¹, A. Varadharajulu¹, A. Das¹, Y. Saxena¹, D. Bora¹, R. Pal², S. Saha³, A. Apte⁴, and D. Patel⁴

¹Institute for Plasma Research (IPR), Bhat, Gandhinagar, India

²Saha Institute of Nuclear Physics, Kolkata, India

³Variable Energy Cyclotron Center, Bidhanagar, Kolkata, India

⁴Space Application Center, Ahmedabad, India

Corresponding Author: J. Ghosh, jghosh@ipr.res.in

It is a well-known fact that small and medium-sized tokamaks have enormously contributed in design and development of large size tokamaks such as ITER for building fusion reactors in terms of physics, engineering and diagnostics. Small and medium-sized tokamaks are very convenient to develop and test new ideas, technologies and materials, which, because of the risky nature, cannot be done in large machines without preliminary studies, such as disruption studies, runaway studies, etc. The worldwide effort on magnetic fusion is devoted to the present generations of large tokamaks like DIII-D, TCV, EAST, SST-1 etc., which are operational emphasizing on divertor and tungsten wall ITER-like operation. However, there are very few (2–3) small and medium-sized tokamaks operational around the world with divertor facility and technical capabilities to provide able support for operation and trouble shooting of these big tokamaks. Therefore, it has been planned to upgrade the existing ADITYA tokamak ($R_0 = 75$ cm, $a = 25$ cm) successfully operated over two decades with more than 30,000 discharges into a state-of-art machine with divertor operation and very good plasma control to support the future Indian Fusion programme.

The scientific objectives of ADITYA tokamak Upgrade include low loop voltage plasma start-up with strong pre-ionization having a good plasma control system. The upgrade is designed keeping in mind the experiments, disruption mitigation studies relevant to future fusion devices, runaway mitigation studies, demonstration of Radio-frequency heating and current drive, etc. This upgraded ADITYA tokamak will be used for basic studies on plasma confinement and scaling to larger devices, development and testing of new diagnostics and so on. This machine will be easily accessible and will be very useful for generation of technical and scientific expertise for future fusion devices.

The installation of ADITYA Upgrade tokamak is completed and plasma discharges will be initiated soon. In this paper, special features of the upgrade including various aspects of designing and fabrication of new components for ADITYA Upgrade tokamak along with preliminary results of plasma operations will be presented.



Development of a 3 m HTS FNSF Device and the Qualifying Design and Engineering R&D Needed to Meet the Low AR Design Point

T. Brown¹, J. Menard¹, R. P. Majeski¹, P. Titus¹, Y. Zhai¹, and L. El-Guebaly²

¹Princeton Plasma Physics Laboratory (PPPL), Princeton, NJ 08540, USA

²University of Wisconsin-Madison, Madison, WI 53706, USA

Corresponding Author: T. Brown, tbrown@pppl.gov

A Fusion Nuclear Science Facility (FNSF) study based on the spherical tokamak (ST) confinement option has progressed through a number of stages of development to understand the requirements to establish a self-consistent conceptual design of an ST-FNSF device. The objective has been to establish sufficient physics and engineering details needed to meet mission objectives centred on achieving tritium self-sufficiency and TF shielding protection within a configuration arrangement develop with a viable maintenance strategy that fosters high availability in the maintenance of the in-vessel components.

The ST physics is centred on lower aspect ratio designs that offer higher confinement times, improved stability and higher β operation when compared with the conventional high aspect ratio advanced tokamak. One disadvantage of the small major radius ST device is the machine geometry offers limited space on the plasma inboard side for shielding to protect the TF coils from neutron heating and material damage and space to locate inboard tritium breeding blankets. This is especially the case when working to define a small size FNSF device; greater inboard space is expected when an ST design is scaled to a larger DEMO device. The earlier copper ST-FNSF designs incorporated a copper centre stack of wedged TF plates with joints to the outer return legs and a maintenance approach that involved dismantling horizontal return legs of the TF coils to gain access to plasma components and replacing the TF coil centre stack after a few years of operation, due to neutron damage. In defining a superconducting ST-FNSF device sufficient inboard shielding is needed to protect against neutron heating and material damage condition for six FPY operations and a thin inboard breeding blanket is desired to augment the outboard blanket system. To accomplish this, two design features were pursued: incorporating HTS TF coils with a winding designed for high current density (reducing the dimensional build of the TF inboard leg) and reducing the size of the plasma by moving to a device with a slightly higher aspect ratio. This paper will provide the design details of the 3 m HTS ST-FNSF device — defining engineering R&D qualifying requirements, structural analysis results and any engineering defined limitations that may be imposed within a low aspect ratio tokamak environment.



REVOLVER-D: The Ergodic Limiter/Divertor Consisting of Molten Tin Shower Jets Stabilized by Chains

J. Miyazawa¹, T. Goto¹, T. Ohgo², T. Murase¹, N. Yanagi¹, Y. Hamaji¹, H. Tamura¹, S. Masuzaki¹, M. Tokitani¹, R. Sakamoto¹, and A. Sagara¹

¹National Institute for Fusion Science (NIFS), Toki, Gifu, Japan

²Department of Fusion Science, Graduate University for Advanced Studies (SOKENDAI), Toki, Gifu, Japan

Corresponding Author: J. Miyazawa, miyazawa@lhd.nifs.ac.jp

A new liquid metal divertor concept named the REVOLVER-D (reactor-oriented effectively volumetric vertical divertor) has been proposed for the helical fusion reactor FFHR-d1. The REVOLVER-D consists of molten tin shower jets stabilized by chains set inside each jet. These are installed in 10 inner ports of FFHR-d1 to intersect the ergodic layer surrounding the last-closed-flux-surface. The plasma heading for the divertor region hits the shower and disappears. Then the full-helical divertor as in LHD becomes less necessary. The majority of the heat load is absorbed inside the shower. At least half of the neutral particles generated inside the shower are pumped by the cryopump units installed in the centre of FFHR-d1. Maintenance of the REVOLVER-D is easy since it is localized in the inner port and its components are easily removed by simple up/down motion. Pure molten tin is the first candidate of the liquid metal for the REVOLVER-D, because of its low melting temperature, low vapour pressure, low material cost, low toxicity, no explosive reaction with water, and high nuclear stability. Both the amount and activation level of radioactive wastes emitted from the REVOLVER-D are small. Since tin is a high-Z material near Xe, the sputtered tin can be an efficient radiator for divertor heat load reduction. On the other hand, contamination of the main plasma by tin should be prevented. In the case of FFHR-d1 the impurity shielding effect of the ergodic layer as observed in LHD is beneficial for this. The permissible heat load of the REVOLVER-D is sufficiently high since it uses the flowing liquid metal as the plasma facing material. For example, in the case of a molten tin jet with 1.2 cm of diameter, 0.012 square metre of plasma wetted area, and 5 m/s of flow velocity, the vapour pressure is < 0.0001 Pa even at a high heat load of 40 MW per square metre. When a jet hits the plasma and connects two regions with different potentials, an electric current flows in the jet. The Lorentz force induced by this current and the toroidal magnetic field of ~ 2 T around the shower bend the jet in the radial direction. Since the electric current will be limited by the ion saturation current in the ergodic layer, plasma cooling by inserting the limiter in the ergodic layer and enhancing the radiation loss by tin is effective in mitigating the Lorentz force.



Progress in K-DEMO Heating/Current Drive and Tokamak Configuration Development

G. Neilson¹, D. Mikkelsen¹, C. Kessel¹, T. Brown¹, P. Titus¹, H. Zhang¹, K. Im², J. Park², and S. Kwon²

¹Princeton Plasma Physics Laboratory (PPPL), Princeton, NJ 08540, USA

²National Fusion Research Institute (NFRI), Daejeon, Republic of Korea

Corresponding Author: G. Neilson, hneilson@pppl.gov

A conceptual design study for a steady-state fusion demonstration reactor, K-DEMO, has been undertaken by the National Fusion Research Institute (NFRI) in the Republic of Korea. Analyses of the plasma heating and current drive configuration and of the tokamak configuration have continued in support of the study. It is assumed that a combination from among at least the standard heating and current drive technologies, i.e., lower hybrid waves (LH), neutral beams (NB), electron cyclotron waves (EC), and ion cyclotron conventional fast waves (IC) will be required to satisfy the requirements for startup, efficient overall current drive, and current profile optimization. A configuration optimized for physics performance and minimum adverse impact on tritium breeding and shielding must take advantage of the available design freedom in each system, e.g., (for wave systems) in frequency, phasing, and launcher location. Parameter scan calculations for each of the four technologies have quantified the dependence of key performance metrics, such as driven current per watt and radial profile, on these design variables. Tokamak configuration studies have investigated requirements on the in-vessel systems for maintainability, access for piping services, and structural support against magnetic forces. The blanket-shield system is segmented into a small number (48) of large modules, supported in part by a segmented semipermanent inboard shell. Structural loads due to disruption eddy currents are analyzed using a vertical-displacement event simulation in ANSYS. Methods to calculate the static forces due to the magnetic materials in the blanket structures are being developed using ANSYS. For a given segmentation scheme and assumed volume of RAFM steel in the module, it is estimated that the load on a blanket attachment is about 30% higher than eddy current loading alone.

DEMO Port Plug Design and Integration Studies

G. Grossetti¹, L. V. Boccaccini¹, F. Cisondi², U. Fischer¹, T. Franke², G. Granucci³,
F. Hernandez¹, D. Strauss¹, M. Q. Tran⁴, and A. Vaccaro¹

¹Karlsruhe Institute of Technology (KIT), Karlsruhe, Germany

³Istituto di Fisica del Plasma (IFP), Consiglio Nazionale delle Ricerche (CNR), 20125 Milan, Italy

²EUROfusion Programme Management Unit, EUROfusion Garching, 85748 Garching, Germany

⁴Swiss Plasma Center (SPC), École polytechnique fédérale de Lausanne (EPFL), 1015 Lausanne, Switzerland

Corresponding Author: G. Grossetti, giovanni.grossetti@kit.edu

The Power Plant Physics and Technology department (PPPT), being part of the EUROfusion Consortium established in 2014 and composed by European Fusion Laboratories (EFL), aims to develop a conceptual design for the fusion demonstration power plant. With respect to present experimental machines and ITER, the main goals of DEMO are to produce electricity continuously for a period of 2 to 4 hours, with a net electrical power output of the order of a few hundreds of MW, and to allow tritium self-sufficient breeding with an adequately high margin in order to guarantee its planned operational schedule, including all planned maintenance intervals. This will eliminate the need to import tritium fuel from external sources, except for plant start-up. In order to achieve these goals, extensive engineering efforts as well as physics studies are required to develop a design that can ensure a high level of plant reliability and availability. In particular, interfaces between systems must be addressed at a very early phase of the project, in order to proceed consistently.

In this paper we present a preliminary design and integration study, based on physics assessments for the EU DEMO1 Baseline 2015 with an aspect ratio = 3.1 and 18 toroidal field coils, for the DEMO port plugs. These aim to host systems like electron cyclotron heating (ECH) launchers currently developed within the PPPT work package "Heating and current drive" (WPHCD) that need an external radial access to the plasma that collides with in-vessel systems like the breeder blanket. A similar approach could be in principle followed by other systems, e.g., other heating and current drive systems or diagnostics.

The work addresses the interfaces between the port plug and the blanket on the specific example of the helium-cooled pebble bed (HCPB) which is one of four breeding blanket concepts under investigation in Europe within the PPPT programme: the required openings will be evaluated in terms of their impact onto the blanket segments thermo-mechanical and nuclear design considering mechanical integration aspects but also their impact on tritium breeding ratio (TBR). Since we are in a conceptual phase, the same methodology is applicable to the other three blanket concepts, as well.

Conceptual Design of the DEMO NBIs: Main Developments and R&D Achievements

P. Sonato¹, M. Q. Tran², U. Fantz³, I. Furno², P. Agostinetti¹, T. Franke⁴, A. Fassina¹,
L. Zanotto¹, E. Sartori¹, A. Simonin⁵, and C. Hopf³

¹Consorzio RFX, Associazione EURATOM-ENEA sulla Fusione, Padova, Italy

²Swiss Plasma Center (SPC), École polytechnique fédérale de Lausanne (EPFL), 1015 Lausanne, Switzerland

³Max-Planck-Institut für Plasmaphysik, Garching, Germany

⁴EUROfusion Garching, 85748 Garching, Germany

⁵Institut de Recherche sur la Fusion par confinement Magnétique (IRFM),

Commissariat à l'énergie atomique (CEA/Cadarache), 13108 Saint-Paul-lès-Durance, France

Corresponding Author: P. Sonato, piorgiorgio.sonato@igi.cnr.it

In the framework of the EUROfusion work package “Heating and current drive”, a conceptual design of the neutral beam injector (NBI) for DEMO, has been developed by Consorzio RFX in collaboration with other European institutes. High efficiency is a fundamental requirement for DEMO, this has been taken into great consideration for the DEMO NBI, as a fundamental part of the maximization of RAMI performance. To increase the efficiency of the system, innovative solutions have been introduced for the neutralizer and the vacuum pumping systems. In particular, the design of a neutralizer based on the “closed recirculating cavity with nonlinear gating” (RING) photoneutralizer concept, using the second harmonic of a laser trapped in cavity through which the beam passes, has been implemented in the DEMO NBI conceptual design. The DEMO NBI has been designed to be also compatible with a gas neutralizer. Non-evaporable getter (NEG) pumps are foreseen to provide the required vacuum pumping inside the vessel. Compared to cryopumps, NEG pumps present numerous advantages: they are more resistant to neutron radiation and they do not need any continuous energy supply system for the operation. In order to increase the reliability and availability of the beam source, the DEMO NBI features a beam source composed of 20 subsources (two adjacent columns of 10 subsources each), following a modular design concept. Each subsource features its radio frequency driver. Such a modular solution is capable to provide a better alignment among the corresponding apertures of the accelerator grids, because the modules have a significantly smaller size than the whole accelerator, hence the horizontal and vertical deformations are also reduced compared with a nonmodular solution. To increase the maintainability of the system, the DEMO NBI has been designed in such a way that all the main components can be substituted without removing other components. For example, the beam source can be removed from the lateral opening of the beam source vessel, the neutralizer and the residual ion dump from dedicated upper flanges, the duct from the equatorial port close to the NBI port. Several analyzes have been carried out to investigate and optimize this conceptual design, namely optics, electrostatics, magnetics, neutronics and thermo-mechanics assessments.



Smaller & Sooner: Exploiting High Magnetic Fields from New Superconductors for a More Attractive Fusion Energy Development Path

D. G. Whyte¹, J. Minervini¹, E. S. Marmor¹, M. J. Greenwald¹, B. LaBombard¹, L. Bromberg¹, and B. M. Sorbom¹

¹*Plasma Science & Fusion Center, MIT, Cambridge, MA 02139, USA*

Corresponding Author: D. G. Whyte, whyte@psfc.mit.edu

The recent industrial maturation of high-temperature, high-field superconductors opens up a faster and cheaper development path for fusion energy by enabling reactor-level performance at smaller scale. The current fusion energy development path, based on large-volume moderate magnetic B field devices is proving to be slow and expensive. A development effort is underway on new superconductor magnet technology development, and accompanying plasma physics research at high- B , that will open up a viable and attractive path for fusion energy development. This path would feature smaller volume, fusion capable devices that could be built more quickly than low-to-moderate field designs based on conventional superconductors. Fusion's worldwide development could be accelerated by using several small, flexible devices rather than relying solely on a single, very large device. These would be used to obtain the acknowledged science and technology knowledge necessary for fusion energy beyond achievement of high fusion plasma gain. Such a scenario would also permit the testing of multiple confinement configurations while distributing technical and scientific risk among smaller devices. Higher field and small size also allows operation away from well-known operational limits for plasma pressure, density and current. The advantages of this path have been long recognized — earlier U.S. plans for burning plasma experiments [Compact Ignition Tokamak (CIT), Burning Plasma Experiment (BPX), Fusion Ignition Research Experiment (FIRE)] featured compact high-field designs, but these were necessarily pulsed due to the use of copper coils. Underpinning this new approach is the recent industrial maturity of high-temperature, high-field superconductor tapes that would offer a truly “game changing” opportunity for magnetic fusion when developed into large-scale coils. The superconductor tape form and higher operating temperatures also open up the possibility of demountable superconducting magnets in a fusion system, providing a modularity that vastly improves simplicity in the construction, maintenance, and upgrade of the coils and the internal nuclear engineering components required for fusion's development.



EU DEMO Heating and Current Drive: Physics and Technology

M. Q. Tran¹, T. Franke², G. Granucci³, G. Grossetti⁴, J. Jelonnek⁴, I. Jenkins⁵,
J.-M. Noterdaeme⁶, A. Simonin⁷, P. Sonato⁸, R. Wenninger⁶, and H. Zohm⁶

¹Swiss Plasma Center (SPC), École polytechnique fédérale de Lausanne (EPFL), 1015 Lausanne, Switzerland

²EUROfusion Garching, 85748 Garching, Germany

³Istituto di Fisica del Plasma (IFP), Consiglio Nazionale delle Ricerche (CNR), 20125 Milan, Italy

⁴Karlsruhe Institute of Technology (KIT), Karlsruhe, Germany

⁵Culham Centre for Fusion Energy (CCFE), Culham Science Centre, Abingdon, UK

⁶Max-Planck-Institut für Plasmaphysik, Garching, Germany

⁷Institut de Recherche sur la Fusion par confinement Magnétique (IRFM),

Commissariat à l'énergie atomique (CEA/Cadarache), 13108 Saint-Paul-lès-Durance, France

⁸Consorzio RFX, Associazione EURATOM-ENEA sulla Fusione, Padova, Italy

Corresponding Author: M. Q. Tran, minhquang.tran@epfl.ch

In the frame of the European Fusion Roadmap and under the Power Plant Physics and Technology programme, the EUROfusion Consortium is conducting detailed studies on a tokamak demonstration power plant (DEMO). Scoping studies (e.g., scanning the aspect ratios and the toroidal magnetic field) are being performed. The EU DEMO1-2015 baseline is a 5.7 T reactor delivering electricity in long pulse (> 2 hours). Its operation relies on the use of external heating during plasma initiation, current ramp-up to H-mode, burn and instabilities control, and plasma ramp down phases. Extensive simulations of the power requirements during all plasma phases were conducted. It was found that about 150–170 MW are required during the different phases to fulfil the requirements described above. Since the DEMO1 is mainly an inductive tokamak, auxiliary current drive will contribute only weakly to the pulse duration (about 10%). System design based on the use of electron cyclotron (EC), ion cyclotron (IC) waves and neutral beam injection (NBI) and technical development in the fields of EC gyrotron sources and NB injector are performed. The HCD system must be fully integrated in the machine design and satisfy stringent criteria on safety, remote handling and impact on the tritium breeding ratio. The presentation will cover the physics requirements from scenarios modelling. It will highlight the requirements during the current ramp-up phase and the transition to H-mode. The technical part will be devoted to the design and R&D consideration for the three HCD systems and their integration in DEMO. For EC various options for the system from the gyrotrons to the launchers will be discussed. The integration of the launchers and the impact on the blanket design and TBR in the port plug will be outlined. Since the DEMO1 programme is still in a preconceptual phase, advanced high-frequency (240 GHz) high-power (up to 2 MW) gyrotrons are under development to avoid descoping of potentially interesting options. For IC, the focus is on a distributed antenna, which offers many advantages, such as low RF power density and minimum reduction in TBR. In the field of NBI, the main issues under consideration are Cs management or avoidance in the negative ion source and neutralization methods (photoneutralization), which would significantly increase both the neutral power and the wall plug efficiency ($\eta > 60\%$).

Conceptual Design of the DEMO EC-System: Main Developments and R&D Achievements

G. Granucci¹, J. Jelonnek², G. Aiello², S. Alberti³, K. Avramidis², F. Braunmueller³, A. Bruschi¹, J. G. Chelis⁴, J. Franck², G. Gantenbein², S. Garavaglia¹, G. Grossetti², S. Ily², Z. Ioannidis⁴, P. Kalaria², A. Moro¹, I. Pagonakis², E. Poli⁵, N. Rispoli¹, T. Rzesnicki², T. Scherer², D. Strauss², M. Thumm², C. Wu², I. Tigelis⁴, T. Franke⁶, and M. Q. Tran³

¹*Istituto di Fisica del Plasma (IFP), Consiglio Nazionale delle Ricerche (CNR), 20125 Milan, Italy*

²*Karlsruhe Institute of Technology (KIT), Karlsruhe, Germany*

³*Swiss Plasma Center (SPC), École polytechnique fédérale de Lausanne (EPFL), 1015 Lausanne, Switzerland*

⁴*NCSR/NKUA Faculty of Physics, & National Technical University of Athens, School of Electrical and Computer Engineering, Athens, Greece*

⁵*Max-Planck-Institut für Plasmaphysik, Garching, Germany*

⁶*EUROfusion Garching, 85748 Garching, Germany*

Corresponding Author: G. Granucci, granucci@ifp.cnr.it

For the development of a demonstration fusion power plant the design of auxiliary heating systems is a key activity to achieve a controlled burning plasma. The present heating mix considers electron cyclotron resonance heating (ECRH), neutral beam injection (NBI) and ion cyclotron resonance heating (ICRH) with a target power to the plasma of about 50 MW for each system. The main tasks assigned to the EC system are plasma startup assist, heating to L-H transition and current ramp up to burn, MHD stability and current ramp down control. These requirements are used as input for the conceptual design of the EC system, with an extensive R&D programme focussing on relevant technologies to be developed. Gyrotron: the R&D and Advanced Developments on RF generators are targeted on gyrotrons operating at 240 GHz, considered as optimum EC current drive frequency in case of higher magnetic field than for the 2015 DEMO1 baseline. Multipurpose (multifrequency) and frequency step-tunable gyrotrons are under investigation to increase the flexibility of the system. The principle feasibility of a 236 GHz, 1 MW CW conventional-cavity and, alternatively, of a 238 GHz, 2 MW CW coaxial-cavity gyrotron is under investigation together with the development of a Brewster-angle window. Transmission line (TL): Different options are under investigation and a preliminary study of an evacuated quasi-optical multiple-beam TL is presented and discussed in terms of layout, dimensions and theoretical losses. A list of the required components for broadband/double frequency and of a RF load is defined. Launcher: remote steering antennas and truncated waveguides have been considered under the constraints of a high neutron flux and to avoid movable mirrors close to the plasma. The deposition locations coverage and the wave absorption efficiency have been investigated, for a selection of frequencies, injection angles and launch points. A preliminary evaluation of the blanket apertures together with launching configurations and waveguide routing have been proposed. The proposed EC system is structured in cluster, in order to allow the necessary redundancy and flexibility to guarantee the required EC power in the different phases of the plasma pulse. Number and composition of the clusters are analyzed to have high availability and therefore maximum reliability with a minimum number of components.



Integrated Concept Development of Next-Step Helical-Axis Advanced Stellarators

F. Warmer¹, C. D. Beidler¹, A. Dinklage¹, and R. C. Wolf¹

¹*Max-Planck-Institut für Plasmaphysik, Greifswald, Germany*

Corresponding Author: F. Warmer, felix.warmer@ipp.mpg.de

One of the high-level missions of the European Roadmap for the realization of fusion energy is to bring the helical-axis advanced stellarator line (HELIAS) to maturity. The near-term focus is the scientific exploitation of the Wendelstein 7-X experiment in order to assess stellarator optimization in view of economic operation of a stellarator fusion power plant.

Meanwhile, the understanding of the physics and technology of stellarators has made significant progress in recent years. Essential contributions came from the design process of W7-X, from the construction experience itself, and from the ongoing theoretical work during the construction phase. However, even with the achieved progress it is not straightforward to extrapolate to a HELIAS power plant. Therefore, the need arises to study and develop concepts of next-step HELIAS devices.

In order to facilitate such an approach, HELIAS-specific systems-code models were developed and implemented in the European systems code PROCESS. Following this, systems studies have been carried out for HELIAS reactor concepts in order to assess the available design window. As the confinement properties have a great impact on such studies, transport simulations were included in this study and iterated back and forth with the systems studies.

Based on the definition of a HELIAS power plant design window, gaps in physics and engineering with respect to current understanding have been revealed. It turns out that the step from W7-X to a HELIAS power plant is significant for several important physics and engineering parameters (e.g., alpha-particle pressure, heating power, P/R, confinement time). This leads to the concern that a direct step from W7-X to a HELIAS reactor bears undue scientific and technological risks.

If W7-X demonstrates the success of stellarator optimization, the European strategy foresees a review point at which it should be decided if an intermediate-step stellarator is necessary to study the dynamics of a burning-plasma in 3D geometry. In preparation of this review-point, the properties of an intermediate-step stellarator are assessed. Following the integrated design analysis approach, different options for such a device have been studied. In particular, a fast-track, cost-efficient device without blanket and a DEMO-like machine requiring a full set of reactor systems were investigated.



Evolutions of EU DEMO Reactor Magnet System Design Along the Recent Years and Lessons Learned for the Future

L. Zani¹, M. Biancolini², R. Bonifetto³, P. Bruzzone⁴, C. Brutti², D. Ciazynski¹, M. Coleman⁵, G. Federici⁵, E. Gaio⁶, F. Giorgetti², P. Hertout¹, C. Hoa¹, B. Lacroix¹, M. Lewandowska⁷, A. Maistrello⁶, L. Muzzi⁸, A. Nijhuis⁹, F. Nunio¹⁰, A. Panin¹¹, J.-M. Poncet¹, L. Savoldi³, K. Sedlak⁴, B. Stepanov⁴, I. Tiseanu¹², A. Torre¹, S. Turtu⁸, R. Vallcorba¹⁰, R. Wesche⁴, K. Yagotintsev⁹, and R. Zanino³

¹*Institut de Recherche sur la Fusion par confinement Magnétique (IRFM), Commissariat à l'énergie atomique (CEA/Cadarache), 13108 Saint-Paul-lès-Durance, France*

²*Università di Tor Vergata, 00173 Rome, Italy*

³*Polytechnic University of Turin, Turin, Italy*

⁴*Swiss Plasma Center (SPC), École polytechnique fédérale de Lausanne (EPFL), 1015 Lausanne, Switzerland*

⁵*EUROfusion Garching, 85748 Garching, Germany*

⁶*Consorzio RFX, Associazione EURATOM-ENEA sulla Fusione, Padova, Italy*

⁷*West Pomeranian University of Technology, 70310 Szczecin, Poland*

⁸*Agenzia nazionale per le nuove tecnologie, l'energia e lo sviluppo economico sostenibile (ENEA), Rome, Italy*

⁹*University of Twente, 7522 Enschede, Netherlands*

¹⁰*Institut de recherche sur les lois fondamentales de l'Univers (IRFU),*

Commissariat à l'énergie atomique (CEA/Saclay), 91191 Gif-sur-Yvette, France

¹¹*Forschungszentrum Jülich, Jülich, Germany*

¹²*National Institute of Laser, Plasma and Radiation Physics (INFLPR), Bucharest, Romania*

Corresponding Author: L. Zani, louis.zani@cea.fr

The DEMO reactor is expected to be the first application of fusion for electricity generation in the near future. In DEMO, magnet system management is of central importance as the driver of many crucial aspects such as nominal performance (toroidal field scales the fusion power), overall investment budget ($\sim 1/3$ of the total construction cost), production efficiency (full-power total availability heavily impacted by magnet downtime). Therefore, a careful approach is requested for this kind of component to ensure a safe design compatible with a power plant production conditions, keeping control on the factors prone to degrade the economic model (cost, risk). The derivation of those considerations into practical activities results in a constant attempt to lead in parallel extensive design activities and the mastering of upstream knowledge in magnet behaviour. This enables to consolidate to the most extend crucial design choices (e.g., the operation temperature margin) by valorizing a maximum of breakthrough either in technological progresses or in knowledge of physics-related phenomena (e.g., instabilities in transient regimes).

To this end, DEMO magnet system design activities were continuously conducted in Europe, particularly evolving since 2011 in structured environments, always in collaboration with several laboratories. Since then, the actors underwent preparatory design phase and then the preconceptual design activity (CDA) phase, that led to design evolution in many aspects, from associated tools and methods to strategic considerations. Through 2011–2016, the DEMO magnet design was set for TF and CS systems but reinforced by ad-hoc tools (integrated and macroscopic mechanical design tools) developed to allow efficient predesign of TF and CS coils. R&D also provided assessed values of effective strain that strongly consolidates future design to come. Finally cross-fertilization between codes (at system and magnet scales) ensured alignment across the top-bottom flow of magnet functional features (e.g., TF allocated radial build). The results will be presented here.



Helical Coil Design and Development with 100 kA HTS STARS Conductor for FFHR-d1

N. Yanagi¹, Y. Terazaki², S. Ito³, S. Hamaguchi¹, H. Tamura¹, T. Tanaka¹, J. Miyazawa¹, T. Goto¹, T. Mito¹, H. Hashizume⁴, and A. Sagara¹

¹National Institute for Fusion Science (NIFS), Toki, Gifu, Japan

²Department of Fusion Science, Graduate University for Advanced Studies (SOKENDAI), Toki, Gifu, Japan

³Tohoku University, Sendai, Miyagi, Japan

⁴Graduate School of Engineering, Tohoku University, Sendai, Miyagi, Japan

Corresponding Author: N. Yanagi, yanagi@lhd.nifs.ac.jp

There is considerable progress in conceptual design studies of the helical fusion reactor FFHR-d1. The continuously wound helical coils (major radius 15.6 m) employ the 100 kA-class HTS (high-temperature superconducting) STARS (stacked tapes assembled in rigid structure) conductor using a simple-stacking technique of YBCO tapes. A prototype STARS conductor reached 100 kA at 5.3 T and 20 K. A bridge-type mechanical lap joint is developed to realize the “joint-winding” that connects and winds segmented conductors. The joint resistance measured in the sample assures that an additional electricity of < 3 MW is required in the cryoplant for cooling 3900 joints. 3D printing confirms that the unit length of a segmented conductor can be a helical pitch in maximum. If one joint is fabricated per day, the onsite winding would be completed in < 3 years. Vacuum pressure impregnation is skipped in the HTS option. High cryogenic stability of HTS intrinsically reduces the quench risk and the massive copper stabilizer further enhances the stability. The sample did not quench when the current density in the copper stabilizer was < 85 A/mm². Numerical analysis is being conducted to verify these characteristics. In case of a quench of the helical coils, a numerical simulation shows that the hot-spot temperature is < 200 K with a discharge time constant of 30 s and a ~ 20 s delay for a normal-zone to expand. When an emergency discharge starts, the voltage generation is < 3 kV if the two helical coils are divided into 30 blocks. A good organic or inorganic insulation should be installed between the stainless steel jacket and copper stabilizer. Helium gas flow through the four corners of the conductors is considered for the cooling scheme. The nuclear heating by fusion neutrons is more intense on the inboard side of the torus because of the thinner blanket space than on the outboard side. A pair of subhelical coils, named “NITA coils”, with opposite-directed currents, are used to enlarge the blanket space to 1.08 m. The maximum nuclear heating is ~ 3 W along the longitudinal cooling path of ~ 18 m on the inboard side. In contrast, the joule heating at a joint is ~ 9 W, which is cooled by ~ 0.3 g/s of helium gas flow through the outboard channels. Numerical simulation is conducted to examine the flow distribution in multipaths with nonuniform heat generation.

DTT: An Integrated Bulk and Edge Plasma Experiment to Tackle the Power Exhaust Problem in View of DEMO

F. Crisanti¹

¹*Agenzia nazionale per le nuove tecnologie, l'energia e lo sviluppo economico sostenibile (ENEA), Rome, Italy*
Corresponding Author: F. Crisanti, flavio.crisanti@enea.it

A DTT experiment should be capable of: 1) demonstrating a safe and robust power handling solution that can be extrapolated to DEMO; 2) achieving the previous goal without degrading the plasma core and pedestal performances, in a plasma regime as close as possible to a reactor one; and, 3) demonstrating the possibility to achieve points 1) and 2) by integrating as much as possible all the physics and technological aspects. The challenging task of integrating these three targets has been tackled by combining the approach of considering the divertor as a separated regions, as well as integrating the main adimensional physics aspects of the divertor and of the plasma bulk. A cost constraint of 500 M€ has been included among the scaling parameters. The integration of these aspects leads to a machine with $R \leq 2.3$ m. A reasonable minimum size with $R > 1.8$ m has been evaluated by: evaluating the necessity of varying the local divertor magnetic topology; considering the radiation load on the first wall; considering the necessity of long discharge to study the technical aspects of the divertor materials. An intermediate size of $R = 2.15$ m has been selected, with $a = 0.70$ m, $I_p = 6.0$ MA, $B_t = 6$ T, and elongation $k \approx 1.76$. The heating power will be $P_{ADD} = 45$ MW. The selected mix of heating is: ≈ 15 – 25 MW ECRH at 170 GHz; ≈ 15 – 25 MW ICRH at 60–90 MHz; ≈ 5 – 15 MW NBI at 300 keV. The main expected performances are an average density $\langle n_e \rangle = 1.7 \times 10^{20}/\text{m}^3$, an average temperature $\langle T \rangle = 6.2$ keV, $P_{SEP}/R = 15$ MW/m and a parallel flow $q_{\parallel} \sim P_{SEP}B/R = 125$. DTT will be equipped with a set of external poloidal coils able to guarantee a large set of different divertor magnetic configurations. The presence of a set of small internal coils will allow to locally modifying the magnetic configuration, so as to produce a very large set of quite different topologies. The possibility to use a liquid metal divertor has been included in the design. A double null standard X-point divertor scenario will be possible. All the external coils are designed by using superconductor technology, allowing discharges lasting around 100 s.



Ion Cyclotron Range of Frequency Power for DEMO

A. Bader¹, J.-M. Noterdaeme¹, G. Bosia², A. Garcia³, U. Fischer⁴, A. Messiaen⁵,
R. Ragona⁵, and D. Van Eester⁵

Research Units Participating in WP HCD

¹Max-Planck-Institut für Plasmaphysik, Garching, Germany

²University Torino, Turin, Italy

³Ghent University, 9000 Ghent, Belgium

⁴Karlsruhe Institute of Technology (KIT), Karlsruhe, Germany

⁵Laboratory for Plasma Physics, ERM/KMS, Brussels, Belgium

Corresponding Author: A. Bader, amro.bader@ipp.mpg.de

The paper summarizes the studies carried out on the use of an ion cyclotron range of frequency system on DEMO in the framework of the PPPT.

An ion cyclotron range of frequency (ICRF) heating system can contribute significantly to various plasma phases during an experimental cycle (“shot”). It can be used in the plasma start-up and current ramp-up phase, where election heating is beneficial. After this phase, various heating schemes that aim at direct or indirect bulk ion heating offer different paths to suitable operation points with a large power gain factor and large efficiencies.

Although mainly meant to heat the plasma, ICRF power can also contribute to current drive and plasma rotation and can help to control MHD instabilities. ICRF power can further be used to ensure a “soft” termination of the discharge. It was confirmed experimentally that the ICRF can be used for all those functions.

With the present emphasis on a pulsed DEMO machine (the EU DEMO1 2015 baseline) we studied in more detail the heating scenarios and a corresponding antenna. In DEMO, to reduce as much as possible the number and area of openings in the vessel, heating systems with high power density, using the smallest port area, would be expected to be favoured. An alternative is to integrate the heating system into the machine. ICRF antennas have been operating in machines like JET and ASDEX-Upgrade close to the plasma without using a large port for several tens of years without any problems. In DEMO, a distributed antenna, integrated in the blanket, covering the full 360° toroidal extend and of the travelling wave type would have a low power density, not use any port (except for the feeds) and be compatible with the tritium breeding. This new antenna type allows for an improved coupling by being able to work with low k_{\parallel} and conceptually avoids, with its 360° symmetry, the occurrence of sheaths and thus additional impurity production.

Such an integrated antenna needs to fulfil a number of conditions on compatibility with blanket function and remote handling, on modularity, level of safety and complexity. Scoping studies indicate that there are indeed no show-stoppers. A test of this type of antenna in a tokamak plasma is needed. It could be done in several steps, but a final proof of principle on a large machine will be essential.



Power Handling and Plasma Protection Aspects that Affect the Design of the DEMO Divertor and First Wall

R. Wenninger¹, G. Federici², R. Albanese³, R. Ambrosino⁴, C. Bachmann², L. Barbato³, T. Barrett⁵, W. Biel⁶, D. Coster¹, T. Eich¹, M. Firdaouss⁷, R. Kemp⁵, K. Lackner¹, C. Lowry⁸, M. Mattei⁹, F. Maviglia², R. Neu¹, M. Siccino¹, B. Sieglin¹, M. Turnyanskiy⁵, and H. Zohm¹

¹Max-Planck-Institut für Plasmaphysik, Garching, Germany

²EUROfusion Garching, 85748 Garching, Germany

³Università degli Studi di Napoli Federico II, 80138 Napoli, Italy

⁴Università di Napoli Parthenope, 80133 Napoli, Italy

⁵Culham Centre for Fusion Energy (CCFE), Culham Science Centre, Abingdon, UK

⁶Forschungszentrum Jülich, Jülich, Germany

⁷Institut de Recherche sur la Fusion par confinement Magnétique (IRFM), Commissariat à l'énergie atomique (CEA/Cadarache), 13108 Saint-Paul-lès-Durance, France

⁸European Commission, Brussels, Belgium

⁹DIII, Seconda Università di Napoli, Aversa (CE), Italy

Corresponding Author: R. Wenninger, ronald.wenninger@ipp.mpg.de

The development of a conceptual design for a demonstration fusion power plant (DEMO) is a key priority of the recent European fusion programme. The DEMO design R&D is expected to benefit largely from the experience gained with ITER construction and operation, but there are still outstanding gaps requiring a vigorous physics and technology R&D programme. The constraints coming from specific DEMO requirements bear a strong impact in the design and technology selection process of the components surrounding the plasma. This paper discusses some of the main risks related to the divertor and first wall configuration and the related benefits and shortcomings of alternative design options.

The recent pulsed “low extrapolation” DEMO baseline design includes a lower single null (LSN) configuration, a conventional X-point divertor (closed) and no high heat flux components outside the divertor. A number of weaknesses of this design are discussed:

- First wall protection: A low total heat load limit of $\sim 1 \text{ MW/m}^2$ for the first wall in DEMO and an increased SOL e-folding length for the steady state charged particle transport due to enhanced level of blob transport are expected for DEMO.
- Divertor protection: DEMO aspects like the high radiation requirement, high neutron exposure and the more challenging ELM problem lead to high divertor protection challenges than in ITER.
- Vertical stability: In addition to the large distance between plasma and conducting wall in DEMO, LSN suffer from a strong coupling between horizontal and vertical displacements.

Due to these DEMO baseline design issues, alternative design options will be investigated:

- Sacrificial limiters with high heat load capabilities in the first wall: For designs with poloidally elongated limiters a heat load analysis, impact on the tritium breeding ratio and several design integration aspects are discussed.
- Double null configuration (DN): The most recent findings on the potential of DN to simultaneously improve the situation at the first wall and divertor and also the vertical stability will be presented. Also drawbacks of DN (e.g., TBR reduction) will be discussed.



Nuclear Analysis of Structural Damage and Nuclear Heating on Enhanced K-DEMO Divertor Model

J. Park¹, K. Im¹, and S. Kwon¹

¹National Fusion Research Institute (NFRI), Daejeon, Republic of Korea

Corresponding Author: J. Park, jspark@nfri.re.kr

Studies to investigate the feasibility of the divertor system have been proceeding since the preconceptual design study on the Korean fusion demonstration reactor (K-DEMO) was initiated in 2012. The divertor is one of the main components and biggest challenges for a tokamak reactor. Its major function is the emission of the heat flux, helium and impurities from the plasma, and also the divertor should be able to endure the large plasma power and high radiation conditions inside the tokamak reactor. Previously, main parameter calculations were carried out to predict key neutronic parameters in an overall K-DEMO model, but the nuclear analysis for individual components such as the divertor was not yet demonstrated. In this paper, the enhanced K-DEMO divertor model was created by a commercial CAD programme with based on a preliminary developed K-DEMO. Then, the enhanced K-DEMO divertor was integrated into a previously developed K-DEMO neutronic analysis model by the help of the Monte Carlo automatic modelling (MCAM) programme, and a series of nuclear analyzes were performed by MCNP Monte Carlo simulations with FENDL-3.0 nuclear data library. The preliminary calculation results indicate that the maximum nuclear heating deposited over the tungsten armoured HHF units with values between 6–14 W/cm³, and the highest damage seems to be appeared in the support structures of the outboard target in reduced activation ferritic martensitic (RAFMs) materials with about 6 dpa.



Concept of Tritium Processing and Confinement in Fuel Cycle of Ignitor

M. Rozenkevich¹, A. Perevezentsev¹, and M. Subbotin²

¹*D. Mendeleev University of Chemical Technology of Russia, Moscow, Russian Federation*

²*National Research Centre "Kurchatov Institute", Moscow, Russian Federation*

Corresponding Author: M. Rozenkevich, rozenkev@mail.ru

One of the most important tasks among initial tasks for realization of the project is to determine different types of the engineering systems which will be required to support the engineering infrastructure of IGNITOR. One of the most important systems will be the tritium fuel cycle and detritiation systems which provides the scientific program of the research at the IGNITOR tokamak. This work presents further development of engineering assessment for the joint Italian and Russian project IGNITOR. The scope of work is engineering concept for tritium fuel cycle and detritiation systems for air and water in light of IGNITOR operation with tritium plasma at the TRINITY site, because a location for the IGNITOR tokamak the Russian Party suggested the TRINITY site, which is situated near Moscow (now it is the territory of "big Moscow").

Zero D and 1.5D Transport Analysis of SST-2

V. Menon¹, R. Daniel¹, R. Srinivasan¹, U. Prasad¹, C. Danani¹, A. L. Sharma¹, J. Agarwal¹, P. Dutta¹, N. Rastogi¹, R. Srivastava¹, S. Dutta¹, M. Himabindu¹, D. K. Sharma¹, K. K. Gotewal¹, A. K. Chakraborty¹, S. Khirwadkar¹, R. Kumar¹, S. Pradhan¹, S. P. Deshpande¹, and P. K. Kaw¹

¹*Institute for Plasma Research (IPR), Bhat, Gandhinagar, India*

Corresponding Author: V. Menon, vinay289@ipr.res.in

A key step towards a DEMO reactor and beyond is the development of key facilities addressing various engineering and physics issues. In the Indian plan, SST-2 is under consideration as a low fusion gain ($Q = 5$) reactor for realizing and qualifying technologies for DT fusion cycle and for the Indian DEMO programme [1, 2]. The 0D physics design of SST-2 is done using the 0D systems code SPECTRE that is used for the physics design of SST-2 [3]. The 100 MW baseline operation of SST-2 is a conservative design and assumes an ELMy H-mode operation. To supplement the 0D code, a 1.5D transport code simulation is done using METIS for the baseline parameters ($R_0 = 4.42$ m, $a = 1.47$ m, and $B_t = 5.42$ T, $I_p = 11.2$ MA). Various current drive schemes are simulated first for an auxiliary power of 20 MW NBI and then with a power sharing of 12 MW NBI and 8 MW ICRH for assessing the steady state operational regime for SST-2. The total volt-second used is checked with the available flux of the CS coils [4] to assess the pulse length of SST-2. A design sensitivity analysis using the 0D code is then carried out to assess the physics parameter space on the baseline operation. Particularly, the effect of varying the HH factor, aspect ratio and the Greenwald density ratio is checked for optimizing the fusion gain, pulse length and the fusion power. A performance assessment for the ignited domains and varying fusion power is done by the means of PoPCoN [5] representation. The accessible physics design space for the various operational scenarios of SST-2 are then presented.

References

- [1] R. Srinivasan, *et al.*, Fusion Eng. Des. **83**, 889–892 (2008).
- [2] R. Srinivasan, Fusion Eng. Des., In Press (2016).
- [3] V. Menon, *et al.*, FEC–2014 FIP/P7-19, (2014).
- [4] U. Prasad, *et al.*, IEEE Trans. Appl. Supercond. **26(4)**, (2016).
- [5] W. A. Houlberg, Nucl. Fusion **22**, 935 (1982).



Multiscale Integral Analysis of Tritium Leakages in Fusion Power Plants

M. Velarde¹, J. Fradera²

¹*Instituto de Fusión Nuclear (IFN), Universidad Politécnica de Madrid (UPM), Madrid, Spain*

²*Idom Nuclear Services, Gran Via Carlos III, Barcelona, Spain*

Corresponding Author: M. Velarde, marta.vmayol@upm.es

Tritium leakages are a major concern regarding nuclear power plants, not only in commercial fission power plants, but also in future fusion power plants. Future fusion reactors, as for example those studied in the ITER and NIF experiments, will breed tritium from other elements to use it as fuel. Hence, the need for preventing and containing tritium leakages, as is done with any other contaminant, turns out to be a key issue.

The present work presents an integral methodology towards a standard for safety analysis regarding tritium leakages to the environment. The methodology is based on a multiscale analysis covering the whole tritium cycle within a fusion power plant, from a micro scale, analyzing key components where tritium is leaked through permeation, to a macro scale, considering its atmospheric transport.

Advection, diffusion, recombination and deposition processes have to be considered in plant components as well as in the soil and vegetation to fully simulate the behaviour of different chemical forms of tritium, including their reactions. In addition, penetration in the underground, re-emission and later conversion to organic bound tritium (OBT) have to be taken into account. A final aspect of this work is the dosimetric analysis of the contamination through: inhalation, re-emission and ingestion. Early and chronic doses are also evaluated

An example of a multiscale integral analysis of a tritium leakage at a fusion power plant is presented, illustrating when, where and how different scale analysis interface with each other, in order to provide accurate and reliable results and give valuable insights from the design, operation and safety point of view.



Overview and Status of Construction of ST40

M. Gryaznevich¹, A. Sykes¹, P. Noonan¹, D. Kingham¹, P. Buxton¹, A. Dnestrovskij²,
A. Nicolai¹, J. B. Lister¹, A. Costley¹, V. Shevchenko¹, and A. McFarland¹

¹Tokamak Energy Ltd, Abingdon, UK

²National Research Centre "Kurchatov Institute", Moscow, Russian Federation

Corresponding Author: M. Gryaznevich, mikhail.gryaznevich@tokamakenergy.co.uk

Recent advances in the development of high temperature superconductors (HTS) and encouraging results on a favourable dependence of confinement on increase in toroidal field (TF) in spherical tokamaks (ST) open new prospects for a high field ST as a compact fusion reactor or a powerful neutron source [1]. The combination of the high- β (ratio of the plasma pressure to magnetic pressure), which has been achieved in STs, and high TF that can be produced by HTS TF magnets opens a path to lower volume fusion devices, in accordance with the fusion power scaling proportional to $\beta^2 B_t^4 V$.

Tokamak Energy Ltd's path to development of fusion power is based on the use of compact high-field spherical tokamaks. The feasibility of a low power compact ST reactor and the physics and engineering challenges of the ST path to fusion power will be outlined. Several advances addressing the main issues on the path to a compact fusion reactor include: development of superconducting magnets using 2nd generation HTS; optimization of the current drive for steady-state operation and heating and revision of requirements for alpha-particle confinement in a compact ST, based on full-orbit simulations; recent results of experiments on small tokamaks ST25 and fully superconducting ST25-HTS in support of the programme; and design of a new device, a high field spherical tokamak ST40 which aims to demonstrate the possibility of achieving burning plasma conditions in a compact device.

This new generation high field spherical tokamak, ST40, ($R_0 = 0.4\text{--}0.7$ m, $A = 1.7\text{--}2.0$, $I_p = 2$ MA, $B_t = 3$ T, $k = 2.5$, $\tau_{\text{pulse}} \in 1\text{--}5$ s, Cu LN₂ cooled magnets) is under construction with the first plasma expected in early 2017. An overview of the project will be presented. The main objectives of the project, parameters of the tokamak and the physics programme will be described. Physics and engineering challenges (mainly connected with the high toroidal field and high wall and divertor power loads) will be discussed. The device is aimed at demonstrating burning plasma parameters ($nT\tau_E$) and also is designed to be suitable for DT operations in future. The present status of the construction and commissioning will be reported. ST40 will be an important step in the commercial development of fusion energy as the project is funded mainly by private investments.

References

[1] M. Gryaznevich, *et al.*, Fusion Sci. Technol. **61**, 89 (2012).

Approaches for the Qualification of Exhaust Solutions for DEMO-Class Devices

W. Morris¹, L. Evans¹, B. Lipschultz², E. Surrey¹, and C. Waldon¹

¹*Culham Centre for Fusion Energy (CCFE), Culham Science Centre, Abingdon, UK*

²*York Plasma Institute, University of York, Heslington, UK*

Corresponding Author: W. Morris, william.morris@ukaea.uk

Plasma exhaust is a critical aspect of DEMO-class devices, so there needs to be confidence that it will work. This paper considers the methodology to establish confidence in potential solutions, drawing on approaches inside and outside fusion, including evolving high power computing tools — these approaches could also help find improved solutions, possibly where all the plasma and materials ingredients operate in known regimes, reducing uncertainty. Crucially, the elements need to be integrated into an overall solution that can meet the demanding performance requirements and constraints of a fusion plant yet also accommodate significant uncertainties in plasma, materials and component behaviour.

A prior full scale test of a DEMO exhaust solution is not feasible, almost by definition. The reference approach is to take the best available design, with various uncertainties and unknowns, and use margins and risk mitigation tools to address these. We explore a complementary approach based on models for the final step to give more confidence in the performance and uncertainty range of the design. The two approaches could be combined.

For the plasma aspects, qualification will be eased if solutions have resilience to uncertainties and variations, ideally with natural “springiness”, or damping of transients. These can be tested with integrated models containing all relevant mechanisms and interactions, suitably validated.

Materials and components have comparable modelling and integration challenges, in particular predicting the effects of combined loads (e.g., neutron, thermal, mechanical). A possible strategy is to combine measured and predicted materials properties and failure mechanisms (such as crack propagation, deformation) into a hierarchical multiscale model from atom-scale up. Such a modelling workflow would be well suited to high levels of parallelization and would improve over use of average material properties.

In-silico qualification of such a large and complex system is very challenging, but has large potential benefits in cost, time, flexibility and optimization. Fortunately essentially all science issues are being addressed in the community (e.g., in EUROfusion). The computational demands are excessive today, but the rapid development of both computing power and numerical techniques is likely to transform the situation in the next 10–20 years.



DEMO Design Using the SYCOMORE System Code: Conservative Designs and Pathways towards the Reactor

C. Reux¹, L. Di Gallo¹, F. Imbeaux¹, J.-F. Artaud¹, G. Aiello², J. Bucalossi¹, G. Ciraolo¹, S. Dardour³, J.-L. Duchateau¹, D. Galassi⁴, J.-C. Jaboulay², A. Li Puma², M. Owsiak⁵, B. Pégourié¹, J. Said¹, B. Saoutic¹, and L. Zani¹

¹*Institut de Recherche sur la Fusion par confinement Magnétique (IRFM),*

Commissariat à l'énergie atomique (CEA/Cadarache), 13108 Saint-Paul-lès-Durance, France

²*Commissariat à l'énergie atomique (CEA/Saclay), 91191 Gif-sur-Yvette, France*

³*Commissariat à l'énergie atomique (CEA/Cadarache), 13108 Saint-Paul-lès-Durance, France*

⁴*Laboratoire de Mécanique, Modélisation & Procédés Propres (M2P2), Aix-Marseille Université, France*

⁵*Poznan Supercomputing and Networking Center (PSNC), Poznań, Poland*

Corresponding Author: C. Reux, cedric.reux@cea.fr

A demonstration power plant is the next step for fusion energy following ITER. The design of such reactors is currently ongoing and still requires solving a number of issues regarding the models used for the different subsystems of the plant. System codes are able to address these questions as they model every major element of the fusion power plant and their interactions. This ensures that appropriate compromises between the different subsystems are handled correctly and enforces the global consistency of the design. The modular system code SYCOMORE has been used to propose a novel approach to DEMO design by starting the design process from present performance parameters and assessing the key variables to improve performances up to a reactor of reasonable size. The maximum allowed power on the divertor was found to be more critical in the range 5 to 10 MW/m² than the H-factor in the range 0.9–1.2 for pulsed DEMO1-like designs (400–500 MW net electric power, 2 hours burn duration). Multicriterion studies have also been carried out to find compromises between multiple figures of merit. Finally, sensitivity analyzes have been done to estimate the width of the operational domain around the design points. For the pulsed designs considered in the study, the net electric power was found to be more sensitive to small changes of the minor radius than the burn duration.



Physics and Engineering Design Studies on Power Exhaust and Divertor for a 1.5 GW Fusion Power DEMO

N. Asakura¹, K. Hoshino¹, H. Utoh¹, Y. Someya¹, S. Tokunaga¹, S. Suzuki², K. Ezato², Y. Seki², H. Kudou¹, K. Shimizu², Y. Sakamoto¹, R. Hiwatari¹, K. Tobita¹, N. Ohno³, and Y. Ueda⁴

¹Japan Atomic Energy Agency (JAEA), Rokkasho, Aomori, Japan

²Japan Atomic Energy Agency (JAEA), Naka, Japan

³Graduate School of Engineering, Nagoya University, Nagoya, Japan

⁴Graduate School of Engineering, Osaka University, Osaka, Japan

Corresponding Author: N. Asakura, asakura.nobuyuki@jaea.go.jp

Handling of a large exhausted power to the SOL and divertor is the most important issue for DEMO reactor design. The plasma concept ($I_p = 14$ MA, $R = 8.5$ m, $a = 2.5$ m) with the reduced fusion power of 1.5 GW and central solenoid coils sufficient for inductive start was proposed. Plasma simulation of the power exhaust and engineering design of tungsten (W) plasma-facing-component and water-cooling concept are developed. The divertor designs with the leg length of 1.6 m and 2.0 m are investigated to produce the plasma detachment. The peak heat loading both at the inner and outer divertor targets is reduced to 5 MW/m² level, even in the shorter divertor at the high radiation fraction ($f_{\text{rad}} = P_{\text{rad}}/P_{\text{out}}$, where P_{out} is the exhausted power to the plasma edge) of 0.8 and relatively low midplane density (n_i^{sep}) of 2.3×10^{19} /m³, corresponding to the Greenwald density fraction ($f_{\text{sep}}^{\text{GW}} = n_i^{\text{sep}}/n^{\text{GW}}$) of 0.33. Conceptual engineering design of the heat sink and the arrangement in a divertor cassette is proposed. ITER technology of W-monoblock and Cu-ally cooling pipe is applicable to the high heat flux area near the divertor strike point, where neutron flux is relatively low. Arrangements of two coolant routes for Cu-alloy pipe (200°C, 5 MPa) and reduced activation ferritic/martensitic steel (RAFMS) pipe (290°C, 15 MPa) and their flow velocities are determined to handle the peak target load of 10 MW/m² level. An integrated conceptual design of the DEMO divertor is presented.



Progress towards Achieving Large Pumping Speed for Exhaust from Fusion Grade Machines

R. Gangradey¹, S. Mukherjee¹, J. Agarwal¹, J. Mishra¹, P. N. Panchal¹, P. Nayak¹, S. Kasthurirengan², S. Udgata³, and V. S Tripathi³

¹Institute for Plasma Research (IPR), Bhat, Gandhinagar, India

²Centre for Cryogenic Technology, Indian Institute of Science, Bangalore, India

³I-Design Engineering Solutions Ltd., Ubale Nagar, Wagholi, Pune 412207, India

Corresponding Author: R. Gangradey, ranjana@ipr.res.in

The exhaust from a fusion grade machine comprises mainly isotopes of hydrogen gas and helium as the main content. The challenge lies in pumping voluminous amount of exhaust gases of the order of 200–400 Pa m³/s. At present, pumping such a large throughput of gas in a continuous way is a topic of primary focus in the field of vacuum science. Important requirement is of establishing technology at effective cost. In the Indian programme, a cryoadsorption cryopump (MPCP-08) offering pumping speeds as high as 50 000 to 70 000 ℓ/s for helium and 150 000 ℓ/s for hydrogen with 3.2 m² of sorbent panel area is developed at IPR, India. It took about seven years with initially establishing experimental set ups required for validation of the sorbents and its properties. It also included successful development of hydroformed cryopanel carrying liquid helium with leak-tight welds as a spin off technology. First laboratory scale pump integrating the developed technologies was a small scale cryopump (SSCP-01) with a pumping speed of 2 000 ℓ/s for helium. Subsequently, single panel cryopump (SPCP-01) with pumping speed 10 000 ℓ/s for helium was followed by multiple panel cryopump (MPCP-08).

Further works are in progress using different forms of activated carbon clothes, carbon fibres and tested at the various in-house experimental facilities to maximize the adsorption capacity of the porous materials, improve its thermal conductivity and provide enormous pumping speed. This paper describes India's contribution in realizing the studies carried out towards exploring carbon materials to provide large pumping speed for fusion grade machines.

Nuclear Design Analyses of SST-2

C. Danani¹, K. Chandrasekhar¹, B. J. Saikia², A. L. Sharma¹, D. K. Sharma¹, M. Himabindu¹, J. Agrawal¹, K. K. Gotewal¹, S. M. Manoh¹, N. Rastogi¹, P. Dutta¹, S. Dutta¹, U. Prasad¹, V. Menon¹, A. K. Chakraborty¹, S. Khirwadkar¹, R. Ellappan¹, S. Pradhan¹, S. P. Deshpande¹, and P. K. Kaw¹

¹*Institute for Plasma Research (IPR), Bhat, Gandhinagar, India*

²*Centre of Plasma Physics – Institute for Plasma Research (CPP-IPR), Nazirakhat, Assam, India*

Corresponding Author: C. Danani, chandanipr@gmail.com

SST-2 will be a medium size Indian fusion reactor to be built for realizing the reactor technologies and DT fuel cycle. It has a low fusion gain ($Q = 5$) and fusion power output can be from 100 to 300 MW. This work presents nuclear design analyzes for SST-2 employing the Indian LLCB (lead–lithium ceramic breeder) blanket for the tritium breeding. The nuclear design analyzes address the tritium breeding capability, the shielding performance and the nuclear power production taking into account various engineering design parameters. 1D radiation transport calculations have been performed to predict the neutronics performance of the SST-2 reactor with breeding blanket at only outboard side. A tritium breeding ratio (TBR) of 0.9 was obtained and the shield thickness (shield blanket + vacuum vessel) of ~80 cm at the inboard midplane was sufficient for keeping the radiation loads on TF coil under the limits. In order to achieve tritium self-sufficiency and to design a shield sufficient for five full power years of operations, a modified radial build with breeding blanket at inboard and outboard sides is being analyzed. The breeding and shielding performance is being investigated at the inboard torus midplane regarding the radiation load to the superconducting toroidal field coil. Nuclear responses such as TBR, fast neutron fluence, dpa and nuclear heating at TF coil will be calculated to obtain required breeding blanket and shielding thickness. Main results of the study with the new radial build will be presented in this paper.

Comparative Analysis of WCLL to Different European DEMO Blanket Concepts in Terms of Activation and Decay Heat after Exposure to Neutron Irradiation

G. Stankunas¹, A. Tidikas¹

¹Lithuanian Energy Institute, Laboratory of Nuclear Installation Safety, LT-44403 Kaunas, Lithuania

Corresponding Author: G. Stankunas, gediminas.stankunas@lei.lt

Activation inventories and decay heat are important nuclear quantities which need to be assessed on a reliable basis for fusion materials for the safe operation of a fusion nuclear power reactor and its final decommissioning. This comparative paper describes the activation and decay heat calculations for WCLL performed in the frame of the EUROfusion WPSAE programme and specifications in comparison to other European DEMO blanket concepts (i.e., DCLL, HCLL and HCPB) on the basis of using a three dimensional neutronics calculation model. Results are provided for a range of decay times of interest for maintenance activities, safety and waste management assessments. The study revealed that WCLL have the highest (~2–3 orders of magnitude) total decay heat at longer decay times in comparison to HCLL design which has the lowest total decay heat (17.5 MW) at short decay times. In addition, major nuclides were identified for WCLL in W armour (¹⁸⁷W and ¹⁸⁵W), EUROFER (⁵⁵Fe, ⁵⁶Mn, ⁵¹Cr, ¹⁸⁷W, ¹⁸²Ta) and LiPb excluding tritium (²⁰⁷Pb and ²⁰³Pb). In addition, focussed attention has been dedicated to the analysis of the decay heat and activity both from the different WCLL blanket modules for the entire reactor and from each WCLL blanket module separately.

How Tokamak Interface Requirements Are Driving the Design of TBM Systems in ITER towards Breeding Blanket Design in DEMO

M. Ferrari¹, L. V. Boccaccini², L. Giancarli³, Y. Poitevin¹, and J. van der Laan³

¹*Fusion for Energy, Test Blanket Module & Material Development Project Team, 13115 Saint-Paul-lès-Durance, France*

²*EUROfusion, Karlsruhe Institute of Technology (KIT), Karlsruhe, Germany*

³*International Thermonuclear Experimental Reactor (ITER), Cadarache Centre, 13108 Saint-Paul-lès-Durance, France*

Corresponding Author: M. Ferrari, marco.ferrari@f4e.europa.eu

The test blanket module (TBM) programme in ITER provides breeder units and related systems with all relevant technologies to test and validate design concepts of tritium breeding blankets for a power-producing reactor, specifically, DEMO. Three ports are allocated to the ITER Members (IM's) participating to the TBM program and six test blanket systems (TBS) are going to be installed and tested during ITER plasma operational phase. Port #16 has been assigned to the European IM hosting two types of TBM: a helium cooled lithium-lead and a helium cooled pebble-bed. Each of them belongs to the corresponding TBS which includes as well its own He cooling and tritium extraction and recovery systems. The TBS concern energy relevant systems in terms of thermodynamic and tritium fuel cycles and they qualify not only the TBM programme, but ensure also the fulfilment and completeness of the scientific mission of the ITER Project itself in view of the next generation of fusion reactors. The paper, taking into account the return of experience (RoX) gained in developing the two EU TBS, summarizes and discusses how, for the first time out of a mock-up based laboratory scale testing, the integration aspects and requirements impact and drive the design and the construction of this type of energy (power-production) systems in view of DEMO. Technological and fabrication solutions adopted for the EU TBS and their integration in ITER with more than 25 ITER interfacing systems implied a RoX gained on requirement management related to regulatory and licensing processes (TBS are under ESP/ESPN). Safety demonstration strategy, radioprotection and radwaste requirements are discussed on a system engineering basis, highlighting what applicable to DEMO. This effort is a key part of the scientific mission of the TBM Programme in ITER, providing to DEMO the maximum information on the TBS as technological objects operating in a real fusion reactor environment. The activity includes the RoX of the design, construction, installation, commissioning, operation, inspection and post-test analyzes, covering the complete consultation cycle with an agreed notified body and license oversight and endorsement by the French nuclear regulator. The integration of the safety demonstration for relevant tritium breeding blankets in DEMO is a key milestone along the pathway toward the future fusion power plant reactor.

Design of the Helium-Cooled Lithium-Lead Breeding Blanket in CEA: From TBM to DEMO

G. Aiello¹, L. V. Boccaccini², J. Aubert¹, J.-C. Jaboulay¹, L. Forest¹, and A. Li Puma¹

¹Commissariat à l'énergie atomique (CEA/Saclay), 91191 Gif-sur-Yvette, France

²Karlsruhe Institute of Technology (KIT), Karlsruhe, Germany

Corresponding Author: G. Aiello, giacomo.aiello@cea.fr

The helium-cooled lithium-lead (HCLL) blanket concept is based on the use of helium as coolant and the eutectic Pb-16Li as neutron multiplier and breeder material. This concept was originally developed in CEA at the beginning of 2000: it is one of the two EU blanket concepts to be tested in ITER in the form of a test blanket module (TBM) and one of the four blanket concepts currently being considered for DEMO.

The ITER HCLL-TBM was designed as representative of a DEMO blanket concept developed at the end of power plant reactor studies; its design is based on the same components and relevant geometries but intended to maximize the "DEMO relevancy" in the ITER environment, which is characterized by different plasma loads and the presence of other in-vessel components. It will allow studying the same physical phenomena that drive the design of DEMO, reproducing, e.g., similar temperature fields in structure and functional materials and typical velocities of liquid breeder and coolant in order to validate the numerical tools used for DEMO design. However, the TBM design must comply with ITER operational constraints, i.e., not jeopardize the safety and availability of the machine and account for specific issues of integration in an equatorial port. In short, the TBM is a highly optimized component for the ITER environment that will provide crucial information for the development of the DEMO blanket in several key areas, but the overall performances of the DEMO blanket will not be addressed in TBM. On the other hand, given the tight schedule for the construction of the DEMO reactor, CEA approach is to share as much as possible the technological solutions used on the HCLL-TBM for the DEMO BB design in order to profit from the ITER experience and reuse technologies with the highest technology readiness level (TRL). It is therefore essential to assess which technologies and design features could be transported from TBM to DEMO and which will instead need to be adapted, modified or replaced.

Overview of Indian LLCB TBM Programme and Status of R&D Activities

R. Bhattacharyay¹, A. Saraswat¹

The Indian TBM Team

¹*Institute for Plasma Research (IPR), Bhat, Gandhinagar, India*

Corresponding Author: R. Bhattacharyay, rbhattac@ipr.res.in

The lead-lithium ceramic breeder test blanket module (LLCB-TBM) is the Indian TBM representing the DEMO breeding blanket, to be installed in ITER radial port #2. The prime testing objective of LLCB TBM in ITER is to generate experimental data on the performance of tritium breeding blankets (such as tritium breeding and its extraction, nuclear heat extraction, neutron shielding) in an integrated fusion nuclear environment and validation of design tools. The LLCB TBM consists of lithium titanate (Li_2TiO_3), as ceramic breeder (CB) material, in the form of packed pebble beds, and a molten lead-lithium (Pb-Li) flow around the ceramic breeder cassette for extracting heat from the pebble bed zone. Apart from its role as coolant, Pb-Li also acts as a tritium breeder and neutron multiplier. The blanket module is in the shape of a box structure which is made of India-specific reduced activation ferritic martensitic steel (IN-RAFMS) and is cooled by high pressure gaseous helium. The box structure encloses the breeder cassettes and flowing lead-lithium. The tritium produced in the ceramic breeder zones is extracted in-situ by flowing low-pressure purge helium gas and the tritium produced in the Pb-Li circuit is extracted separately by an external detritiation column. The TBM shield is located behind the TBM to shield high-energy neutrons and radiation from plasma.

LLCB TBM has several ancillary systems, such as the helium cooling systems (HCS), lead-lithium cooling system (LLCS), tritium extraction system (TES), coolant purification system (CPS), etc. Their successful operation is highly desirable to achieve the desired testing objective of LLCB TBM. The conceptual design review (CDR) of LLCB TBS has recently been completed and design upgrade is currently under progress considering process optimization, fabrication feasibility and safety consideration.

TBM R&D activities are also under progress with a specific attention to blanket material qualification and database generation (IN-RAFMS, Pb-Li and Li_2TiO_3), technology development for LLCB TBS ancillary systems (in specific to Pb-Li and tritium) and fabrication technology development through fabrication and qualification of mock-ups.

This paper will provide a brief overview of the present status of the LLCB TBS design and various R&D activities.



DT Fuel System of DEMO-FNS Tokamak with Tritium Breeding Blanket

S. S. Ananyev¹, A. V. Spitsyn¹, and B. V. Kuteev¹

¹National Research Centre “Kurchatov Institute”, Moscow, Russian Federation

Corresponding Author: S. S. Ananyev, ananevss@gmail.com

As a part of the nuclear energy research centre “Kurchatov Institute” development a programme of creating a hybrid reactor combining nuclear and thermonuclear technologies was developed and proposed. The basis of a thermonuclear fusion reactor is neutron source (FNS) based on the tokamak [1]. The main difference from the FNS DEMO demonstration fusion reactor is that FNS is not necessary to achieve fusion plasma ignition conditions, and sufficient to obtain the neutron yield comparable to injected power auxiliary heating. The required power of thermonuclear reaction can be up to 100 times less due to the fact that most of the energy comes in a subcritical blanket due to fission reactions, which significantly reduces the requirements for the parameters of the tokamak plasma and materials.

FNS is a key system and hybrid reactor should provide steady flow of fusion neutrons with a capacity of 10–50 MW, which reached close to the pulse values of existing installations JET and JT-60U. Fuel cycle technologies (FC) is one of the key elements for the FNS. These technologies have to be developed significantly, because the technical solutions chosen ITER project can be used in FNS is only partially due to steady state operation of the plant, the higher neutron fluxes and fluxes of tritium fuel cycle elements.

To assess the distribution of tritium in fusion reactor systems and components “tritium plant” is necessary to carry out a dynamic simulation of all system elements allowing for the operation of the tokamak. Such calculations are now performed using the code “FC-FNS” [2]. The code allows the calculation of tritium flows and stocks in tokamak fusion systems. To close the FC processes of tritium in the hybrid blanket was considered.

The report is a conceptual diagram of a stationary fuel cycle FNS with 3–50 MW of fusion power, given current estimates of the distribution of tritium in fusion reactor systems and components “tritium plant”. The calculations for the neutral injection systems TC module and tritium breeding.

References

- [1] B. V. Kuteev, *et al.*, Nucl. Fusion **55**, 073035 (2015).
- [2] S. S. Anan’ev *et al.*, Fusion Sci. Technol. **67**, 241 (2015).

Remote Third Shift EAST Operation: A New Paradigm

D. Schissel¹, E. Coviello¹, N. W. Eidietis¹, S. Flanagan¹, F. Garcia¹, D. A. Humphreys¹, M. Kostuk¹, M. J. Lanctot¹, X. Lee¹, M. Margo¹, D. Miller¹, C. Parker¹, B. G. Penaflor¹, J. Qian², X. Sun², H. Tan², M. L. Walker², B. Xiao², and Q. Yuan²

¹General Atomics, San Diego, CA 92186, USA

²Institute of Plasma Physics, Chinese Academy of Sciences, Hefei, Anhui, People's Republic of China

Corresponding Author: D. Schissel, schissel@fusion.gat.com

Scientists at General Atomics (GA) have conducted in the United States remote experimental operation of the Experimental Advanced Superconducting Tokamak (EAST) in China during their third shift. These experiments were led by scientists in a dedicated remote control room that utilized a novel computer science hardware and software infrastructure to allow data movement, visualization, and communication on the time scale of EAST's shot cycle. This fusion science collaboration zone and the remote control room were used to conduct remote experiments on EAST on vertical controllability by triggering vertical displacement events to assess vertical growth rate and nonlinear evolution while a team at EAST provided scientific assistance and engineering operations oversight. The level of capability deployed to remotely operate EAST required the creation of an infrastructure that was a major advancement over what had previously been achieved in the fusion community. One component of the fusion science collaboration zone is data movement, where large amounts of data can be moved between continents in a short time scale and real-time data from control systems can be moved basically instantaneously. The large datasets are moved with a computer networking technique that does not use the traditional transmission protocol of the internet yielding a 300-fold increase in data transfer rate. Combining this speed with an event system tied to the EAST shot cycle allowed automatic initiation of data transfers, resulting in bulk EAST data to be transferred to GA within minutes. The real-time data transfer was accomplished by reading data directly from the EAST plasma control system memory through a networked, in-memory data structure server that received the data at GA to make it available to the scientific team. After the bulk data arrives at GA, it is served via MDSplus allowing an approved US client to securely and rapidly access EAST data. This architecture avoids multiple clients within the US from requesting data from EAST and competing for the long-haul network's bandwidth that is considerably slower than the network with the U.S. At present there are 35 approved scientists from seven U.S. research institutions.

This work was supported in part by GA Internal Research and Development Funds and by the U.S. Department of Energy under DE-SC0010685.

Extended Capability of the Integrated Transport Analysis Suite, TASK3D-a, for LHD Experiment, and its Impacts on Facilitating Stellarator-Heliotron Research

M. Yokoyama¹, R. Seki¹, C. Suzuki¹, M. Sato¹, A. Shimizu¹, M. Emoto¹, S. Murakami², M. Osakabe¹, T. I. Tsujimura¹, Y. Yoshimura¹, K. Ogawa¹, S. Satake¹, Y. Suzuki¹, T. Goto¹, K. Ida¹, N. Pablant³, D. Gates³, A. Y. Pankin⁴, F. Warmer⁵, and P. Vincenzi⁶

¹National Institute for Fusion Science (NIFS), Toki, Gifu, Japan

²Kyoto University, Nishikyo-ku, Kyoto 615-8540, Japan

³Princeton Plasma Physics Laboratory (PPPL), Princeton, NJ 08540, USA

⁴Tech-X Corporation, Boulder, CO 80303, USA

⁵Max-Planck-Institut für Plasmaphysik, Garching, Germany

⁶Consorzio RFX, Associazione EURATOM-ENEA sulla Fusione, Padova, Italy

Corresponding Author: M. Yokoyama, yokoyama@lhd.nifs.ac.jp

The integrated transport analysis suite, TASK3D-a (Analysis), has been developed to be capable for routine whole-discharge analyzes of plasmas confined in three-dimensional (3D) magnetic configuration such as the LHD. The routine dynamic energy balance analysis for NBI-heated plasmas was made possible in the first version released in September 2012, which consisted of four parts: LHD data interface, 3D equilibrium, heating, and energy balance analysis. The LHD data interface part automatically transfers experiment data registered on the LHD analyzed data server.

Recently, further extension has been conducted such as including ECH ray-tracing code, neo-classical transport code, and the module for creating data files to register in the International Stellarator-Heliotron Confinement and Profile Database. Inclusion of ECH ray-tracing code has significantly enhanced systematic energy transport analysis of ECH- (and NBI-) heated LHD plasmas. Neoclassical energy diffusion flux can also be routinely calculated by the implemented GSRAKE code, and thus, systematic comparison with experimental energy balance has been available. These kinds of data have been accumulated for elucidating turbulent transport contribution in a wide parameter space of LHD plasmas.

Utilizing the TASK3D-a development, the ISH-DB takes also an advantage from the LHD unified data that can be used verification and validation (V&V) studies of large simulation codes for stellarator-heliotrons. The TASK3D-a has already provided profiles and equilibrium data to several large-scale simulation codes such as gyrokinetic instability, energetic particles/Alfvén eigenmodes, and neoclassical plasma flows. The TASK3D-a data interface to ISH-DB has much simplified and enhanced V&V studies of large simulations.

Much further extensions should be pursued towards full-integration by incorporating modules for other physics process such as redistribution of energetic particles, particle transport issues. The architecture of TASK3D-a is modularized, and thus transferable to any other stellarator-heliotron (even tokamak) experiments. In this way, TASK3D-a will continue to give impacts on facilitating stellarator-heliotron research.

ELM Pacing with High Frequency Multispecies Impurity Granule Injection in NSTX-U H-Mode Discharges

R. Lunsford¹, A. Bortolon¹, R. Maingi¹, A. L. Roquemore¹, D. Mansfield¹, M. A. Jaworski¹, R. Kaita¹, and A. Nagy¹

¹Princeton Plasma Physics Laboratory (PPPL), Princeton, NJ 08540, USA

Corresponding Author: R. Lunsford, rlunsfor@pppl.gov

We report on ELM triggering and pacing experiments in NSTX-U, including comparisons to pellet ablation models. Multiple sizes and types of solid impurity granules are injected into the low field side of the plasma to determine their ELM triggering and pacing capability. Examining the penetration depths, mass deposition locations, and ELM triggering efficiencies of sub-millimetre lithium, boron carbide (B₄C) and carbon granules, we assess the optimal size and composition for minimally perturbative high frequency ELM pacing. By utilizing a neutral gas shielding model, benchmarked with lithium granule ablation experiments performed on DIII-D, the pedestal atomic deposition characteristics for the three different species of granule have been modelled for NSTX H-mode discharges with low natural ELM frequencies. Variations in the depositional barycentre can range from 5 cm for lithium to 17 cm for the same size and velocity carbon granule. We estimate that these penetration depths will be reduced by a factor proportional to $q_s \sim n_e T_e^{3/2}$ as the full NSTX-U capabilities are realized. In addition, by reducing the rotation speed of the impeller, the mass deposition location is translated closer to the top of the pedestal allowing further tuning of the pressure perturbation. At this location the pressure profile generated by the granule can be added to the preexisting pedestal pressure gradient, leading to a set of characteristics advantageous for ELM triggering while affecting a minimal perturbation to the core plasma. Using multiple high-speed cameras to precisely track the granule injections and monitor the ablation duration and penetration depths in NSTX-U, a fractional mass deposition location can be extrapolated. Fast infrared camera measurements are used to characterize the variations between triggered ELMs and the inter-ELM period. In addition, comparisons are also made between stimulated and spontaneously occurring ELMs. These measurements provide a comparison of the ELM peak heat flux mitigation factor, as well as variations in the ELM footprint due to the triggering mechanism. The results of ELM pacing and comparisons with the constructed ablation model in NSTX-U will be reported.

Work supported by the U.S. Department of Energy Contract No. DE-AC02-09CH11466



Towards the Completion of the CEA Contributions to the Broader Approach Projects

J.-C. Vallet¹, S. Chel², R. Gondé¹, F. Robin³, W. Abdel Maksoud², O. Baulaigue¹, N. Bazin², B. Bolzon², P. Bredy², N. Chauvin², J. David⁵, P. Decool¹, G. Disset², L. Genini², R. Gobin², F. Gougnaud², C. Hoa⁴, V. Lamaison¹, J. Marroncle², C. Mayri², J. Noé³, and B. Renard²

¹*Institut de Recherche sur la Fusion par confinement Magnétique (IRFM),*

Commissariat à l'énergie atomique (CEA/Cadarache), 13108 Saint-Paul-lès-Durance, France

²*Institut de recherche sur les lois fondamentales de l'Univers (IRFU),*

Commissariat à l'énergie atomique (CEA/Saclay), 91191 Gif-sur-Yvette, France

³*Commissariat à l'énergie atomique (CEA), 91400 Gif-sur-Yvette, France*

⁴*Commissariat à l'énergie atomique (CEA/Grenoble), 38054 Grenoble, France*

⁵*Commissariat à l'énergie atomique (CEA/Cadarache), 13108 Saint-Paul-lès-Durance, France*

Corresponding Author: J.-C. Vallet, jean-claude.vallet@cea.fr

The CEA contributions to the Broader Approach projects, IFERC, IFMIF and JT-60SA, which included the deliveries of components and services, are now approaching completion. For IFERC, the supercomputer Helios, provided by CEA, will perform until the end 2016 its last runs after 5 years of operation close to its nominal capabilities. For IFMIF, the CEA contributions include the deliveries and the commissioning of the prototype injector, of the beam diagnostics and beam control system which are now ready at Rokkasho and the prototype of the high energy SRF LINAC for which the manufacturing and delivery of most components will be completed end 2016. For JT-60SA, the firsts TF coils have been produced and are now being tested at the cold test facility at CEA Saclay. The JT-60SA cryogenic system is now being commissioned at Naka. The five superconducting magnet power supplies, in charge of CEA, have performed successfully the factory acceptance tests and will be delivered at Naka mid-2016. The first units of the mechanical structures of the JT-60SA magnetic field system, outer intercoil structures and gravity supports were manufactured in 2015. This report synthesizes the achieved performances for all of these components manufactured and starts to draw the manufacturing and operation feedback gained by CEA in association with its industrial subcontractors.



Techno-Economic Aspects of High Current Leads for Fusion Devices

V. L. Tanna¹, S. Pradhan¹

¹*Institute for Plasma Research (IPR), Bhat, Gandhinagar, India*

Corresponding Author: V. L. Tanna, vipul@ipr.res.in

The superconducting magnets system (SCMS) of the fusion devices, e.g., tokamak or stellarator, consists of complex superconducting magnetics. In order to supply such high currents from the power supplies to the SCMS, many numbers of current leads (CLs) are required in the temperature range of 4.5–300 K. As the studies revealed that based on the duty cycle of operation of fusion device, almost 25–30% of the total operation cost is just consumed by the CLs only. Therefore, optimum, reliable and low-loss CLs are essential for fusion devices. The studies include such CLs development using unitary (conventional heat exchanger) and binary (HTS or other superconductors module with metal or alloys heat exchanger) concepts.

The overall efficiency, energy flow and cryogen consumption as per operation duty cycle, analysis can predict the real operation cost of the device and can be compared with the capital investment to realize the massive savings by providing innovative solution. It would be possible if replacing the conventional CLs by innovative and techno-economically viable solution using MgB₂ and brass based overloaded CLs. This proposal has three folds benefits, the capital cost of the MgB₂ materials is cheaper compared to HTS materials. The critical temperature of MgB₂ is ~39 K where the thermodynamic efficiency of the helium cryo plant is maximum. The last but not least, significant cost can be reduced by designing the CLs in overloaded mode using brass. This type of engineering solution is quite unique and suitable for pulsed magnets of the fusion devices and till now not tried out. In this context a techno-economic comparative studies have been carried out for different types of CLs are being carried out for the fusion devices. As a part of specific case study has been carried out for 50 kA/30 pairs CLs in pulsed operation scenario. The cooling power required for the conventional CLs is 5–6 times higher than that of MgB₂ and brass based overloaded CLs and in case of HTS CLs the cooling power remains more or less same but there is significant saving in capital cost of factor of 2, if MgB₂ and brass based overloaded CLs will be used.

The Articulated Inspection Arm Development

E. Villedieu¹, V. Bruno¹, P. Pastor¹, B. Vincent¹, C. Dechelle¹, R. Nouailletas¹, R. Le¹,
L. Gargiulo¹, Y. Song², Y. Cheng², H. Feng², C. Liu², and S. Shi²

¹*Institut de Recherche sur la Fusion par confinement Magnétique (IRFM),*

Commissariat à l'énergie atomique (CEA/Cadarache), 13108 Saint-Paul-lès-Durance, France

²*Institute of Plasma Physics, Chinese Academy of Sciences, Hefei, Anhui, People's Republic of China*

Corresponding Author: E. Villedieu, eric.villedieu@cea.fr

Fusion Tokamaks are complex machines which require special conditions for their operation, in particular, high vacuum inside the vessel and high temperature of the vessel walls. During plasma phases, the first wall components are highly stressed and the control of their surface is necessary in case of doubt about their condition. To be able to make safely such an inspection in a short period of time is a great advantage. The articulated inspection arm (AIA) developed by the CEA provides the capabilities for fast inspections of the first wall overall surface keeping the vacuum and temperature conditions of the vessel. The robot prototype validated in Tore Supra in 2008 as followed an important upgrade programme in 2013 and 2014 in the view of using it routinely as a baseline diagnostic for the WEST programme. The upgrade mainly concerned the cabling, the controller electronics and the supervision system. The aim was to provide a user friendly control of the robot associated with high safety in term of automatic collision avoidance between robot and tokamak.

In the frame of the associated laboratory set between CEA/IRFM and CAS/ASIPP, it has been decided to validate the upgrades and qualify the routine usage of the robot in the ASIPP EAST tokamak. A dedicated vacuum cask for the robot and special adaptations for the EAST machine were developed. Extensive tests were made inside an EAST vessel mock-up. A first tokamak integration check was made in November 2014 in atmospheric condition. In 2015 the robot was connected to the EAST tokamak and used during the experimental campaign in 2016. In parallel a new robot, the EAST articulated maintenance arm (EAMA), was developed to be able to equip both the WEST and EAST tokamaks by the end of 2016. Details of the robot, the upgrades, the tests and the operation results are presented in the paper. Progress about the development of the new EAMA with its new functionalities will be sketched.



Status of Tokamak T-15MD

P. Khvostenko¹, I. Anashkin¹, V. Belyakov², E. Bondarchuk², O. Filatov², N. Injutin³,
V. Krylov², I. Levin¹, G. Notkin¹, M. Sokolov¹, and A. Sushkov¹

¹National Research Centre "Kurchatov Institute", Moscow, Russian Federation

²D. V. Efremov Institute of Electrophysical Apparatus (JSC-NIIEFA), St. Petersburg, Russian Federation

³GKMP group, Bryansk, Russian Federation

Corresponding Author: P. Khvostenko, ppkhvast@rambler.ru

Presently, the Tokamak T-15MD is being built. The magnet system of the Tokamak T-15MD will obtain and confine the hot plasma in the divertor configuration. Plasma parameters are a major radius of 1.48 m, a minor radius of 0.67 m, an elongation of 1.7–1.9 and a triangularity of 0.3–0.4. Tokamak T-15MD will be equipped with the auxiliary plasma heating and current drive ($P_{\text{aux}} = 15\text{--}20$ MW) systems. One of the main tasks of the experimental study programme on T-15MD is the obtaining of physical and technological data needed both for ITER project support and fusion neutron source creation. The manufacturing of the tokamak T-15MD magnet system and of vacuum chamber shell was completed. At present time, the preliminary assembly of the magnet system is conducted at the plant in Bryansk. The disassembly of the superconducting tokamak T-15 should be finished in middle of 2016 and T-15MD assembling must begin in NRC "Kurchatov Institute" in the end of 2016. Status of engineering systems modernization is presented too.



Spherical Tokamak Globus-M2: Design, Integration, Construction

V. Minaev¹, V. Gusev¹, N. Sakharov¹, N. Bakharev¹, V. Belyakov², E. Bondarchuk², F. Chernyshev¹, V. Dyachenko¹, A. Kavin², G. S. Kurskiev¹, A. Labusov², O. Leontev³, V. Mikov³, A. Mineev², M. Patrov¹, Y. Petrov¹, V. Rozhansky⁴, A. Saveliev¹, I. Senichenkov⁴, P. Shchegolev¹, O. Shcherbinin¹, V. Tanchuk², A. Telnova¹, S. Yu. Tolstyakov¹, V. Varfolomeev¹, and E. Zhilin⁵

¹Ioffe Institute, St. Petersburg, Russian Federation

²D. V. Efremov Institute of Electrophysical Apparatus (JSC-NIIEFA), St. Petersburg, Russian Federation

³Joint-Stock Company "INTEHMASH", St. Petersburg, Russian Federation

⁴St. Petersburg State Polytechnical University, St. Petersburg, Russian Federation

⁵Ioffe Fusion Technology Ltd., St. Petersburg, Russian Federation

Corresponding Author: V. Minaev, vladimir.minaev@mail.ioffe.ru

The Globus-M spherical tokamak has demonstrated practically all of the project objectives during the 15-year period of operation. The main factor limiting further enhancement of plasma parameters is a relatively low toroidal magnetic field. The increasing of the magnetic field up to 1.0 T together with the plasma current up to 0.5 MA will result in the significant extension of the operating parameters in the upgraded Globus-M2 machine. The experimental programme will be focussed on plasma heating and noninductive current drive and will serve creation of physical and technological base for the compact fusion neutron source development. In this presentation we describe the construction of new magnets and basic features of Globus-M2 experiment. The work current status and plans are outlined.



NSTX-U Contributions to Disruption Mitigation Studies in Support of ITER

R. Raman¹, W.-S. Lay¹, T. Jarboe¹, S. P. Gerhardt², S. C. Jardin², J. Menard², B. Nelson¹, M. Ono², and J. Schmitt²

¹University of Washington, Seattle, WA 98195, USA

²Princeton Plasma Physics Laboratory (PPPL), Princeton, NJ 08540, USA

Corresponding Author: R. Raman, raman@aa.washington.edu

Predicting and controlling disruptions is an important and urgent issue for ITER. In support of this activity, NSTX-U will employ three massive gas injection (MGI) valves that are similar to the double flyer plate design being developed for ITER [1]. NSTX-U will be the first device to operate this valve configuration in plasma discharges. NSTX-U experiments will offer new insight to the MGI database by studying gas assimilation efficiencies for MGI gas injection from different poloidal locations, with emphasis on injection into the private flux region [2]. These results are expected during Spring 2016. The valve has also been successfully operated in external magnetic fields of 1 T.

A limitation with the use of gases for pellet propulsion, whether they be solid refractory, shell, or cryogenic shatterable, is that the propellant gas limits the pellet velocity to about 300–400 m/s [1]. The electromagnetic particle injector (EPI) described here overcomes this limit by relying on an electromagnetic propulsion system for pellet acceleration [3]. In this system, $J \times B$ forces acting on the projectile, which is located between two linear electrodes, propel the projectile. The primary advantage of the EPI concept over gas-propelled injectors is its potential to meet short-warning time scale events. The system could also be located very close to the reactor vessel. The high levels of external magnetic fields that are present near the reactor vessel actually help to improve the efficiency of the system. The system has the potential to respond very rapidly by injecting impurities, into the plasma, within 3 ms after a command to inject is issued to the system. An offline, non-tokamak test, is underway with results expected during Spring 2016.

References

- [1] L. Baylor, *et al.*, Fusion Sci. Technol. **68**, 211 (2015).
- [2] R. Raman, *et al.*, Rev. Sci. Instrum. **85**, 11E801 (2014).
- [3] R. Raman, *et al.*, Fusion Sci. Technol. **68**, 797 (2015).

Work supported by the U.S. Department of Energy contracts DE-FG02-99ER54519 and DE-AC02-09CH11466.

Development of Regulators Synthesis Method for Magnetic Plasma Control System of the T-15 Tokamak

R. R. Khayrutdinov¹, M. Dubrov¹, V. E. Lukash¹, M. Sokolov¹, V. N. Dokuka¹, and P. Khvostenko¹

¹National Research Centre "Kurchatov Institute", Moscow, Russian Federation

Corresponding Author: R. R. Khayrutdinov, khayrutdinov_rr@nrcki.ru

In the present study a method of developing a magnetic control system of the plasma parameters (position, form, current) of the modernized now tokamak T-15 is described. According to the identification of the electromagnetic system and the plasma column of T-15 linear models are built for obtaining control regulators of the two types: 1) proportional-differential regulator to control of plasma parameters; 2) double-circuit system consisting of a regulator of control of the currents in the poloidal coils and a generator of settings of the currents in the poloidal coils that minimize the variance of the plasma parameters values. For the synthesis of regulators technique of linear-quadratic (LQ) control is used, in which providing of the specified quality of transient processes produced by adjusting the weighting coefficients for each controllable value and for each regulatory impact. A separate control system circuit is provided for the vertical stabilization of the plasma column using fast coil for the horizontal field. Stabilization is possible both using the proportional-differential regulator which provides the desired vertical coordinate, and using the differential damping controller in which the vertical position of the column is being stabilized by the outer circuit of the gaps control. Also a linear model was developed for the stationary phase on the basis of applying increments of currents in the coils of the poloidal system and every element of the vessel with the construction of the response matrix to the plasma parameters from the disturbance. A comparison of the results of calculations performed in various linear models with the T-15 plasma evolution calculations made by a nonlinear model based on the DINA code. Identification of linear models and synthesis of controllers performed at different temperatures of the plasma and for different points of a scenario of the discharge (for divertor and limiter configuration of the plasma equilibrium). A technique is developed to switching between the regulators created for different conditions. This makes it possible to carry out calculations of the entire scenario of discharge, including modes of the current ramp up, stationary stage and the current ramp down.

Reciprocating Langmuir Probes Set Design for the Mexican Tokamak "T"

O. A. Muñoz Ovalle¹, M. Salvador Hernández¹, J. A. González Guevara¹,
A. Nieto Cuarenta¹, V. M. Arredondo Solís¹, J. González Marroquín¹,
J. R. Morones Ibarra¹, J. Martínez Torres², R. M. Chávez Rodríguez¹,
G. R. Cavazos Almaguer¹, M. A. Sanromán Reséndiz¹, C. U. Acosta Muñoz¹,
I. E. Morales Niño¹, J. V. Guzmán González¹, A. Acosta Pérez¹, C. A. Briseño Cárdenas¹,
and U. Aguilar Reyes¹

¹Universidad Autónoma de Nuevo León, San Nicolás de los Garza, Nuevo León, Mexico

²Comisión Federal de Electricidad, Mexico-City, Mexico

Corresponding Author: O. A. Muñoz Ovalle, omar.munozov@uanl.edu.mx

A set of three reciprocating Langmuir probes has been designed to be part of the plasma diagnostics system in the tokamak "T", which will be based in Monterrey, Mexico. Due to the relatively short discharge times in a tokamak and to the widely well understood concept and accepted technology, a fast reciprocating probe system has been proposed to start studying the plasma properties in the scrape-off layer during the first season of campaigns in the Tokamak "T". Two configurations for the heads have been proposed. In the first configuration three Langmuir probes will be installed in the head of the reciprocating manipulators, while in a second configuration the head contains a ball-pen probe combined with a conventional triple Langmuir probe arrangement. While the triple probe concept has been extensively used and it is nowadays a current basic technology for different studies, the ball-pen probe concept is relatively new and it seems, even though it rises discussions, to deliver a fast and reliable measurement of the plasma potential. A test phase in a linear plasma device has been proposed due to the gap between the Tokamak "T" commissioning and the reciprocating probes commissioning. A single reciprocating manipulator will be built and tested together with the second head configuration mentioned before in order to ensure all design characteristics. Layouts and detailed arrangements are provided within this document for both the Tokamak stage and for the linear plasma device testing stage.

Upgrade and Operational Performance of EAST Cryogenic System

Q. Zhang¹, L. Hu¹

¹*Institute of Plasma Physics, Chinese Academy of Sciences, Hefei, Anhui, People's Republic of China*

Corresponding Author: Q. Zhang, zhangqy@ipp.ac.cn

Since the first commissioning in February 2006, EAST cryogenic system has been in operation for eleven plasma experiment campaigns with high reliability. However, ten years have passed from the beginning of system operations. With requirements of EAST physical experiment, new users of cryogenic system have been added such as cryopump, pellet inject and NBI. Some upgrades have been implemented to improve the reliability and availability of cryogenic system. New warm compressors, turbines and cryogenic distribution system have been constructed. EAST cryogenic control system has been upgraded in 2015 and put into operation the 11th campaign. This paper presents the upgrade solutions of cryogenic system in detail. At same time, the operational performance has been analyzed with further purpose to improve the cryogenic system reliability so as to guarantee the success of high performance plasma experiments in future.



India's Pellet Fuelling Programme

J. Mishra¹, S. Mukherjee¹, R. Gangradey¹, J. Agarwal¹, P. N. Panchal¹, and P. Nayak¹

¹*Cryo Pump and Pellet Injector Development Division, Institute for Plasma Research (IPR), Bhat, Gandhinagar, India*

Corresponding Author: J. Mishra, jsmishra@ipr.res.in

Fusion community worldwide is looking forward to an efficient pellet injection system catering to the requirements of fuelling high temperature and high density plasma. Various DEMO reactor design world over portray importance underlying development of this technology. The important characteristics being looked forward are operational flexibility, high reliability and remote operation with minimal maintenance. Fusion grade plasma machines find solution in pellet fuelling for ELM pacing by triggering small ELMs at higher frequency, disruption mitigation by injecting impurity pellets to handle the intense heat flux, the forces from halo currents, and the potential first wall damage from energetic runaway electrons.

In India, the IPR has initiated its domestic pellet fuelling programme. As a first step towards it, single pellet injector system (SPINS-IN) is successfully operating, producing pellets of size 2 mm and shooting them at velocity of 700 m/s. It is a cryogen-free system with pellet forming in a sleeve cooled to less than 10 K using GM cryocooler. The system is easy to handle, very flexible.

For a plasma temperature in the range of 1 to 3 keV and density $< 5 \times 10^{19} / \text{cm}^3$, a study was carried out using NGS model for penetration depth of pellet in plasma. Injector is now installed on SST-1 tokamak for pellet injection related experiments.

Advancing on the roadmap of pellet fuelling technology development of an extruder type pellet injection system (ETPIS) for continuous supply of hydrogen ice has been undertaken. ETPIS is a twin screw based cryogenic extruder. Its arrangement of precooler and liquefier is being studied. The DEMO machines will be requiring pellet fuelling in various forms, e.g., impurity pellets for radiative divertors, micropellets for ELM mitigation, massive pellet injection for controlled plasma disruption, etc. This paper describes India's contribution towards exploring the development in the field of pellet fuelling technology.

FIP

Design of Charge Exchange Recombination Spectroscopy (CXRS) on SST-1 Tokamak

M. B. Chowdhuri¹, G. Shukla¹, K. S. Shah¹, J. Ghosh¹, K. H. Burrell², B. A. Grierson³, V. Prahla¹, S. Sharma¹, P. Bharthi¹, R. Manchanda¹, S. Banerjee¹, and N. K. Ramaiya¹

¹Institute for Plasma Research (IPR), Bhat, Gandhinagar, India

²General Atomics, San Diego, CA 92186, USA

³Princeton Plasma Physics Laboratory (PPPL), Princeton, NJ 08540, USA

Corresponding Author: M. B. Chowdhuri, malay@ipr.res.in

SST-1 [1] is a medium sized tokamak with a minor radius of 0.2 m, magnetic field of 1.5 T and is equipped with heating hydrogen neutral beam capable of delivering 0.5–1.7 MW with a variable beam energy of 30–55 keV [2]. The beam parameters provide good candidate for CXRS on SST-1. Using this neutral beam, charge exchange recombination spectroscopy (CXRS) [3, 4] is proposed for SST-1 tokamak to obtain spatially and temporally resolved measurements of C VI line emission at 529 nm ($n = 8 \rightarrow 7$). The diagnostic is designed to provide profiles of impurity ion temperature, toroidal and poloidal plasma rotation using Doppler broadening and shift of charge-exchanged C VI spectral line respectively.

This diagnostic is designed to measure toroidal and poloidal rotation and impurity ion temperature with high temporal (~ 5 ms) and spatial resolution (~ 0.5 cm near the edge, \sim few cm near core). The diagnostic design comprises of a high resolution $f/8.7$, 1 m Czerny-Turner spectrometer along with a 2D fast ANDOR 1024×256 CCD. Line emission from plasma to spectrometer will be coupled using an array of fibres. This paper presents detailed design of the diagnostic including photon budget along with etendue budget for the spectrometer and CCD system. The paper also describes details of collection optics proposed for the diagnostic.

References

- [1] D. Bora, Braz. J. Phys. **32(1)**, (2002).
- [2] S. K. Sharma *et al.*, Rev. Sci. Instrum. **85**, 113504 (2014).
- [3] K. H. Burrell *et al.*, Rev. Sci. Instrum. **75(10)**, 3455–3457 (2004).
- [4] R. P. Seraydarian *et al.*, Rev. Sci. Instrum. **57(2)**, 155–163 (1986).

FNS: Fusion Nuclear Physics and Technology



Status of DEMO-FNS Development

Y. Shpanskiy¹, E. Azizov¹, and B. V. Kuteev¹

¹National Research Centre "Kurchatov Institute", Moscow, Russian Federation

Corresponding Author: Y. Shpanskiy, shpanski@mail.ru

Fusion-fission hybrid facility based on superconducting tokamak DEMO-FNS is developed in Russia for integrated commissioning of steady-state and nuclear fusion technologies at the power level up to 40 MW for fusion and 400 MW for fission reactions. The project status corresponds to transition from conceptual design to engineering one. This facility is considered in RF as the main source of technological and nuclear science information, which should complement the ITER research results in the fields of burning plasma physics and control. The new knowledge obtained on the device may accelerate implementation of fusion technologies as well as construction of demonstration and commercial fusion power plants in RF. Fusion-fission hybrid technologies tested on DEMO-FNS are capable to improve the neutron balance in the global nuclear energy system. Implementation of hybrid and molten-salt technologies should also accelerate the development of atomic energy reducing the radio-toxicity generated in nuclear fuel cycle and the level of pollution by fuel breeding and reprocessing. The development of fusion neutron source DEMO-FNS based on classical tokamak (CT) with a fusion power up to 40 MW was launched in the NRC "Kurchatov Institute" in 2013. The main goal of the 2015 activity was to determine the facility characteristics and to provide integration of the tokamak elements and hybrid blanket, operating in the subcritical regime with effective neutron multiplication factor $k_{\text{eff}} < 0.95$ and being designed for burning out minor actinoids from spent fuel of contemporary thermal nuclear reactors. During the work on the blanket in 2015, a variety of coolants were addressed including: water, eutectic Na-K (liquid metal coolant with $\sim -11^\circ\text{C}$ melting point), as well as helium gas coolant. The reasons for increasing the size of the tokamak and definition of geometric dimensions, structure and selection of hybrid blanket coolant with tritium breeding ratio greater than 1 will be presented in the report. Analyses of the interaction of DEMO-FNS facility with the nuclear fuel cycle of Russia's nuclear power industry is scheduled to be performed in 2016.



Activation, Decay Heat, and Waste Classification Studies of the European DEMO Concept

M. Gilbert¹, T. Eade¹, C. Bachmann², U. Fischer³, and N. Taylor¹

¹Culham Centre for Fusion Energy (CCFE), Culham Science Centre, Abingdon, UK

²EUROfusion Garching, 85748 Garching, Germany

³Karlsruhe Institute of Technology (KIT), Karlsruhe, Germany

Corresponding Author: M. Gilbert, mark.gilbert@ukaea.uk

Inventory calculations have a key role in designing future fusion power plants because, for a given irradiation field and material, they can predict the time evolution in chemical composition, activation, decay heat, gamma-dose, gas production, and even damage (dpa) dose. For conceptual designs of the European DEMO fusion reactor such calculations can provide information about the neutron shielding requirements, maintenance schedules, and waste disposal prospects; thereby guiding future development.

Extensive neutron-transport and inventory calculations have been performed for a reference DEMO reactor model with four different tritium-breeding blanket concepts. The results have been used to chart the poloidal variation in activity and decay heat from different regions of the same component, such as the vacuum vessel (VV) or divertor, and as a function of time since shutdown. Results demonstrate that the shielding performance of the four blanket concepts will differ significantly. The decay heat values can be summed across the cells (used to define the neutron-transport model) of the same component to produce time-evolving total decay heat, which can then be used to assess how long a component, such as a divertor cassette, will require active cooling after shutdown, or when it will become sufficiently cooled to be manipulated and removed from the vessel.

Detailed nuclide inventories for the VV and divertor, focussing on the dominant radionuclides, have been produced by averaging results across all relevant cells. They reveal which radionuclides are the most problematic, potentially suggesting how changes in material composition (including isotopic tailoring) could help to reduce activity. Minor impurities in the raw composition of W used in divertor tiles, for example, are shown to produce long-lived radionuclides.

Finally, using a simple waste classification, based on UK regulations, and a recycling potential limit, the simulations can be used estimate the time-evolution in waste masses for both the entire vessel and individual components, and also suggest when a particular component might be suitable for recycling. The results indicate that the large mass of the VV will not be classifiable as low level waste on the 100-year timescale, but the divertor will be, and that both components, on the other hand, will be potentially recyclable within that time.



Optimizing Full-coverage Free Surface Flow for Liquid Metal PFCs

Z. Xu¹, C. Pan¹, X. Zhang¹, and J. Chen¹

¹*Southwestern Institute of Physics, Chengdu, Sichuan, People's Republic of China*

Corresponding Author: Z. Xu, xuzy@swip.ac.cn

After obtaining a full-coverage free curve-surface flow by curve plate with three layer meshes, new experimental results showed that a full-coverage free surface flow can't be obtained by a flat plate with meshes. More were recently investigated on MHD effects of other free surface flows flowing on flat plate. Base on the experimental data and newly developed modelling method, another way is found to get a full-coverage free surface flow with wavy plate theoretically and experimentally, or to block "rivulet" flow formation by using new finding of the mechanism of secondary flow in free surface flow, or, to ensure the pressure is the same on surface of the free surface flow, the pressure profile in the cross section of the free surface flow will be reestablished once the flow becoming a free surface flow. How to change the pressure profile is dependent on inlet velocity profile and transverse magnetic field. The pressure changing in the cross section drives secondary flow to form "rivulet" flow.

Optimization Process for the Design of the DCLL Blanket for the European Demonstration Fusion Reactor According to its Nuclear Performances

I. Palermo¹, I. Fernández-Berqueruelo¹, D. Rapisarda¹, and A. Ibarra¹

¹*Centro de Investigaciones Energéticas, Medioambientales y Tecnológicas (CIEMAT), Madrid, Spain*

Corresponding Author: I. Palermo, iole.palermo@ciemat.es

The neutronic radiation coming from the fusion plasma of large machines as the foreseen DEMO could severely affect the stability and the lifetime of the components which constitute the reactor. Nevertheless neutrons are fundamental to allow the reactor to reach the tritium self-sufficiency and to generate and extract enough nuclear power. This means that in the nuclear design of a kind of facilities it is essential to achieve and keep the delicate balance among fuel sustainability and power efficiency versus radiation shielding.

The research study presented has focussed on the neutronic design optimization and analysis of one of the options for a fusion reactor designed as DCLL (dual coolant lithium-lead). The main objective has been to develop a new, reliable, efficient and technologically viable modular DCLL blanket using the DEMO generic design specifications and operational (pulsed) conditions established in the frame of the EUROfusion Programme.

By coupling the design tools with the neutronic transport Monte Carlo simulations, a 3D fully heterogeneous neutronic design has been developed and the behaviour of the components under the real operational conditions of a DEMO reactor have been determined from which performance improvements have been deduced.

The final neutronic design has to attend the requirements of: tritium self-sufficiency; BB thermal efficiency; preservation of plasma magnetic confinement; temperature limits imposed by the materials; and, furthermore, radiation limits to guarantee the largest operational life for all the components. Therefore, the neutronic assessments here presented have been specially focussed on: tritium breeding ratio; multiplication energy factor and power density distributions to give inputs for thermal-hydraulics and mechanical assessments; damage and shielding responses to determine if the components are keeping their structural integrity or their functionality as the case of the toroidal field coil superconductivity.

The paper describes the progress in the DCLL nuclear design in light of the observations and requirements explained above. New design choices to improve the BB performances are discussed. Moreover, the previous mentioned nuclear responses and their different distributions relevant for the global design choices have been also analyzed and are described in the paper.

Developing the Science and Technology for the Material Plasma Exposure Experiment (MPEX)

J. Rapp¹, T. Biewer¹, T. Bigelow¹, J. Caughman¹, R. Goulding¹, A. Lumsdaine¹, T. Bjorholm¹, C. Bradley¹, J. Canik¹, S. Diem¹, D. Donovan², R. Duckworth¹, R. Ellis¹, V. Graves¹, D. Giuliano¹, D. Green¹, D. Hillis¹, R. Howard¹, N. Kafle², Y. Katoh¹, A. Lasa¹, T. Lessard¹, E. Martin¹, S. Meitner¹, G. Luo³, W. McGinnis¹, L. Owen¹, H. Ray², G. Shaw², M. Showers², and V. Varma¹

¹Oak Ridge National Laboratory (ORNL), Oak Ridge, TN 37831, USA

²University of Tennessee, Knoxville, TN 37996, USA

³Institute of Plasma Physics, Chinese Academy of Sciences, Hefei, Anhui, People's Republic of China

Corresponding Author: J. Rapp, rappj@ornl.gov

Linear plasma generators are cost effective facilities to simulate divertor plasma conditions of present and future fusion reactors. They are used to address important R&D gaps in the science of plasma material interactions and towards viable plasma facing components for fusion reactors.

Next generation plasma generators have to be able to access the plasma conditions expected on the divertor targets in ITER and future devices. The steady-state linear plasma device MPEX will address this regime with electron temperatures of 1–10 eV and electron densities of 10^{21} – 10^{20} /m³. The resulting heat fluxes are about 10 MW/m². MPEX is designed to deliver those plasma conditions with a novel radio frequency plasma source able to produce high density plasmas and heat electron and ions separately with electron Bernstein wave (EBW) heating and ion cyclotron resonance heating (ICRH) with a total installed power of 800 kW.

The linear device Proto-MPEX, forerunner of MPEX consisting of 12 water-cooled copper coils, is operational since May 2014. Its helicon antenna (100 kW, 13.56 MHz) and EC heating systems (200 kW, 28 GHz) have been commissioned. The operational space was expanded considerably in the last year. 12 MW/m² was delivered on target. Electron temperatures of about 20 eV have been achieved in combined helicon and ECH/EBW heating schemes at low electron densities. Overdense heating with electron Bernstein waves was achieved at low heating powers. The operational space of the density production by the helicon antenna was pushed to 2×10^{19} /m³ at relatively high magnetic fields of 0.7 T, which would allow ECH absorption for 2nd harmonic X-mode overdense heating schemes. Proto-MPEX has been prepared to allow for first material sample exposures. The experimental results from Proto-MPEX will be used for code validation (B2-EIRENE, COMSOL, VORPAL, AORSA, GENRAY) to enable predictions of the source and heating performance for MPEX.

MPEX, in its last phase, will be capable to expose neutron-irradiated samples. In this concept, targets will be irradiated in ORNL's High Flux Isotope Reactor and then subsequently exposed to fusion reactor relevant plasmas in MPEX.

The current state of the MPEX preconceptual design and unique technologies already developed, including the concept of handling irradiated samples, will be presented.

First Wall Lifetime Extension with Flowing Liquid Zone for Fusion Reactors

S. Şahin¹

¹*Atılım University, Ankara, Turkey*

Corresponding Author: S. Şahin, sumer.sahin@atilim.edu.tr

In this work, different structural materials were subject of investigation. The calculations are conducted for a fusion power generation of 1 GW_{el} over thirty years of reactor operation with a thermos-dynamical conversion efficiency of 35% leading to 2.857 GW_{th} by a capacity factor of 100%. The structural material should have the properties given briefly as below:

- Low neutron absorption cross sections.
- Adequate mechanical properties before and after irradiation.
- Operation at a wide temperature window.
- Working at high temperatures.
- Resistant to atomic displacement and helium generation damage.
- Low activation property under 14 MeV neutrons.
- High thermal conductivity.

One of the candidates as structural material is the oxide dispersed steel (ODS). At first, a fusion-fission (hybrid) with a multilayered spherical blanket has been investigated, which is composed of a first wall made of oxide dispersed steel (ODS, 2 cm); neutron multiplier and coolant zone made of LiPb; ODS-separator (2 cm); a molten salt Flibe coolant and fission zone; ODS-separator (2 cm); graphite reflector. In the second phase, LiPb coolant zone behind the first wall has been removed. But instead, a flowing liquid protective first wall is included in front of the solid first wall in order to reduce material damage and residual radioactivity after final disposal of the latter. SS-304 type steel, SiC and graphite were also selected as structural materials of a magnetic fusion energy (MFE) reactor. Different types of liquid coolant with tritium breeding capabilities (FLIBE, Li17Pb83, natural lithium, all with natural lithium component) are investigated to protect the first wall from neutron- and bremsstrahlung radiation and fusion reaction debris.



New Integral Experiments for a Variety of Fusion Reactor Materials with DT Neutron Source at JAEA/FNS

S. Sato¹, S. Kwon¹, M. Ohta¹, K. Ochiai¹, and C. Konno¹

¹Japan Atomic Energy Agency (JAEA), Naka, Japan

Corresponding Author: S. Sato, sato.satoshi92@jaea.go.jp

In order to validate nuclear cross-section data, we performed integral experiments on tungsten, vanadium-alloy (V-4Cr-4Ti) and copper with the DT neutron source at JAEA/FNS over 20 years ago. The calculated results largely underestimated the measured ones sensitive to low energy neutrons. Background neutrons scattered in the concrete wall of the experimental room may cause these underestimations. In order to reduce the background neutrons and validate the nuclear data adequately, we perform new integral experiments with these materials covered with Li₂O blocks which effectively absorb background neutrons. In addition, we also perform new integral experiments on molybdenum and titanium. We measure the reaction rates of dosimetry reactions with activation foils and the fission rates of ²³⁵U and ²³⁸U with microfission chambers. We analyze these experiments by using the Monte Carlo code MCNP5-1.40 with the recent nuclear data libraries, ENDF/B-VII.1, JEFF-3.2, JENDL-4.0 and FENDL-3.0. The large underestimates observed in the previous studies are drastically improved in tungsten and vanadium-alloy experiments, and all the calculation results generally show good agreements with the measured ones. Although the underestimate is improved in copper experiment, the calculated results still underestimate the measured ones. It is demonstrated that the underestimation is drastically improved by applying the ⁶³Cu data in JEFF-3.2 and ⁶⁵Cu data in JENDL-4.0 with 10% larger elastic scattering cross section data and 10% smaller capture reaction cross-section data between 100 eV and 0.3 MeV. The calculated results generally underestimate the measured ones with increasing distance from the front surface of the assembly in the molybdenum experiment. From the detailed analysis with partly modified nuclear data based on the measured cross section data of Mo, it is found out that the (*n,2n*) cross section data for all the Mo stable isotopes in JEFF-3.2 are more suitable than those in JENDL-4.0 and the capture reaction cross section data of ⁹²Mo, ⁹⁴Mo, ⁹⁵Mo, ⁹⁶Mo, ⁹⁷Mo and ¹⁰⁰Mo in JENDL-4.0 should be decreased. The calculation results with ENDF/B-VII.1 agree with the measured ones the best in titanium experiment, because the (*n,2n*) and (*n,n'*_{cont}) reaction cross section data and resonance parameters are better than those in the other nuclear data libraries.

Optimization Study of Normal Conductor Tokamak for Commercial Neutron Source

T. Fujita¹, A. Okamoto¹, R. Sakai¹, and Y. Hayashi¹

¹*Nagoya University, Nagoya, Japan*

Corresponding Author: T. Fujita, fujita@ees.nagoya-u.ac.jp

The fast neutrons produced by DT fusion are able to burn the long-lived biologically hazardous transuranics (TRUs) in the spent fuel discharged from fission light water reactors more efficiently than other sources like fast fission reactors. Although a concept design of such a system employing a conventional tokamak (like ITER) with superconducting coils as the fusion core was proposed, the long pulse operation for more than several months is highly challenging. If a tokamak with demountable copper toroidal field coils is used, replacement of in-vessel components would be possible more frequently without reducing the plant availability and then technical difficulties would be mitigated. The resistive loss in the copper coils, however, is a great concern for its feasibility.

The optimum conceptual design of tokamak with normal conductor coils was studied for minimizing the circulating power and the cost for producing a given neutron flux (cost of neutrons, CON) in the range of plasma aspect ratio $A = 1.75\text{--}3$ by using a system code, PEC. The plasma performance was assumed to be moderate ones; normalized $\beta_N \sim 3\text{--}4$ in $A = 2\text{--}3$ and $H_{98}(y, 2) = 1$. It is also assumed that $q^* \geq 2.5$, considering the operation regimes of ST and of the conventional tokamak. We fix the nominal fusion power to 180 MW, the thermal power output, mainly generated in the blanket, to 3 GW, and the surface area of the blanket located on the low-field-side to $\sim 126 \text{ m}^2$. The fusion power is ramped up from 100 MW to 180 MW during the burn cycle.

The results are as follows. The circulating power decreases with A up to $A \sim 2.5$. This is due mainly to reduction of the toroidal field coil resistance by increase in the centre post radius. On the other hand, the capital cost (construction cost) increases with A . As a result, CON has its minimum around $A = 2.25$, namely, between ST and the conventional tokamak. At $A = 2.25$, the circulating power is 55% of the gross power in average during the cycle. The plasma major radius is 2.44 m, the toroidal field is 3.1 T, the plasma current is 9.4 MA, and the plasma energy gain is 1.04 at the end of the cycle.

Investigation on Irradiation Effects on Highly Integrated Leading Edge Electronic Components of Diagnostics and Control Systems for the LHD Deuterium Operation

K. Ogawa¹, T. Nishitani¹, M. Isobe¹, Y. Hatano², S. Matsuyama³, H. Nakanishi¹, K. Mukai¹, M. Sato¹, M. Yokota¹, T. Kobuchi¹, T. Nishimura¹, and M. Osakabe¹

¹National Institute for Fusion Science (NIFS), Toki, Gifu, Japan

²Hydrogen Isotope Research Center, University of Toyama, Japan

³Tohoku University, Sendai, Miyagi, Japan

Corresponding Author: K. Ogawa, kogawa@nifs.ac.jp

High-temperature and high-density plasmas are achieved by means of real time control, fast diagnostic, and high power heating systems. Those systems are precisely controlled by means of transmission and highly integrated electronic components. However, the radiation damage due to neutron and gamma-ray may lead to serious impact on those systems. Therefore, effects due to irradiation on electronic components being used currently should be investigated for control and measurement of LHD deuterium plasmas. For precise estimation of the radiation field in the LHD torus hall, MCNP-6 Monte Carlo neutronics code is used with the cross-section library of ENDF B-VI. The geometry is modelled based on the CAD drawing with some simplification. The dose on silicon, which is a major ingredient of electronics components, during the nine years of the LHD deuterium operation shows that the gamma-ray contributions are dominant in dose. To investigate the irradiation effect on electronic components used in LHD, neutron irradiation tests are performed in the Fast Neutron Laboratory at Tohoku University and gamma-ray irradiation tests are performed in the Nagoya University ⁶⁰Co irradiation facility. We found that most modules of the PLC are broken around the gamma-ray dose of 100 Gy. This is comparable with the dose in the LHD torus hall over nine years. Finally, if we consider the dose only, these components may survive more than nine years. However, the safety factor is low. For the safety of the LHD operation, electronic components placed on the torus hall have been rearranged.



Design and Analysis of SST-2 Vacuum Vessel

S. M. Manoah¹, P. Dutta¹, N. Rastogi¹, K. K. Gotewal¹, R. Srinivasan¹, C. Danani¹, V. Menon¹, A. L. Sharma¹, U. Prasad¹, M. Himabindu¹, D. K. Sharma¹, J. Agarwal¹, S. Dutta¹, R. Gangradey¹, R. Ellappan¹, S. Khirwadkar¹, A. K. Chakraborty¹, S. Pradhan¹, D. Shishir¹, and P. K. Kaw¹

¹*Institute for Plasma Research (IPR), Bhat, Gandhinagar, India*

Corresponding Author: S. M. Manoah, manoah@ipr.res.in

SST-2 is under design as an intermediate step before the Indian DEMO. The design provides a low fusion gain ($Q = 5$) for realizing the reactor technologies and serves as the test bed for qualifying reactor components and DT fuel cycle. The design is based on RCC-MR code. The vacuum vessel (VV) will be constructed out of SS316LN with control over cobalt content (in the range of 0.03%). The design incorporates provisions of fusion power output in the range of 100–300 MW with appropriate upgrade of in-vessel components.

In this design bulk thickness of the vessel takes into account the neutronic shielding requirements for the toroidal field coil. Optimum bulk thickness is taken into account by structural loads like dead weight, seismic events, off-normal events, coolant pressure and vacuum pressure loads and further electro-magnetic loads takes into account the magnetic discharge force. The parametric finite element model in ANSYS is used to arrive at the optimum shell thickness, rib thickness, rib spacing taking into account regular port size and special port size for neutral beam injectors. This design forms the basis to initiate the process of feasibility assessment for complex manufacturing aspects, the feedback from which in turn, would be incorporated in establishing a manufacturable engineering configuration. This paper gives an insight into the engineering requirements and design basis with the identified electromagnetic and structural loads on the double walled “D” shaped vacuum vessel for SST-2.



Advanced Neutronics Simulation Tools and Data for Fusion Applications

U. Fischer¹, A. Konobeev¹, D. Leichtle², L. Lu¹, P. Pereslavlsev¹, and Y. Qiu¹

¹Karlsruhe Institute of Technology (KIT), Karlsruhe, Germany

²F4E: Fusion for Energy, ITER EU Centre, 08019 Barcelona, Spain

Corresponding Author: U. Fischer, ulrich.fischer@kit.edu

Neutronics simulations play an important role for the design and optimization of the nuclear components of a fusion reactor and the related performance analyzes. Accurate data need to be provided to predict the tritium breeding capability, assess the shielding efficiency, estimate the nuclear power generated in all components, and produce activation and radiation damage data for the irradiated materials, as well as the resulting radiation dose loads to sensitive components and materials, or related biological dose rates.

Suitable computational approaches, tools and data need to be available to provide such data with sufficient accuracy. This includes a suitable method for the simulation of neutron transport in complex 3D geometries, high quality nuclear cross-section data to describe the nuclear interaction processes, and a simulation model which replicates the real geometry without severe restrictions. Such requirements are satisfied with the Monte Carlo particle transport technique which can handle any complex geometry and employ the nuclear cross-section data without any severe approximation. The simulations thus provide results limited only by the uncertainties of the nuclear cross-sections, the statistical uncertainty of the Monte Carlo calculation and the accuracy of the geometry model.

Key issues for reliable neutronics simulations are thus related to i) the reliability of the employed Monte Carlo particle transport code, to be validated with fusion relevant benchmark experiments, ii) the quality of the nuclear cross-section data evaluations for fusion applications, to be checked against integral experiments, and iii) the capability to describe in the simulation the real reactor geometry with high fidelity and sufficient detail. All of these key issues are addressed in R&D activities embedded in the European fusion programme with the objective to make available the tools and data which are required to ensure a sufficient prediction capability of the neutronic simulations for DEMO and power reactors.

This paper reports on the recent achievements of the tools developed for the high fidelity geometry representation in the Monte Carlo particle simulation and the provision of high quality nuclear cross-section data with uncertainty assessments.



Fusion Neutron Source Blanket: Requirements on Calculation Accuracy and Benchmark Experiment Precision

A. Zhirkin¹, P. Alekseev¹, V. Batyaev¹, M. Gurevich¹, A. Dudnikov¹, B. V. Kuteev¹,
K. Pavlov¹, Y. Titarenko¹, and A. Titarenko¹

¹National Research Centre "Kurchatov Institute", Moscow, Russian Federation

Corresponding Author: A. Zhirkin, aleksej-zhirkin@yandex.ru

In this report the requirements for the calculation accuracy of the main parameters of the fusion neutron source and the thermonuclear blankets with DT fusion power greater than 10 MW are formulated. To conduct the benchmark experiments the technical documentation and calculation models were developed for two blanket micromodels: the molten salt and heavy water solid-state blanket. The calculations of the neutron spectra and 37 dosimetric reaction rates that are widely used for the detection of thermal, resonance and threshold (0.25–13.45 MeV) neutrons were performed for each blanket micromodel. The MCNP code and the neutron data library ENDF/B-VII were used for the calculations. All the calculations were performed for two kinds of the neutron source: I is the fusion source, II is the source of neutrons generated by the ⁷Li target irradiated by protons with energy 24.6 MeV. The spectral index ratios were calculated to describe the spectrum variations from different neutron sources. The obtained results demonstrate the advantage of use of the fusion neutron source in future experiments.



Design and R&D Activities of Fusion Breeder Blankets in China

J. Yu¹

¹*Institute of Nuclear Energy Safety Technology, CAS, Anhui, People's Republic of China*

Corresponding Author: J. Yu, jie.yu@fds.org.cn

China has long been active in pushing forward fusion energy development to a demonstration of electricity generation. Two experts meetings were organized in 2014 by the Ministry of Science and Technology (MOST) to seriously discuss China's fusion roadmap and in particular the design and construction of magnetic confinement fusion reactor beyond ITER.

As one of the most challenging components in the fusion reactor, great efforts have been put on the development of breeder blanket which is the central part of fusion nuclear science and technology (FNST). Three blanket concepts have been mainly developed in China for China Fusion Engineering Test Reactor and DEMO, including dual functional lead lithium (DFLL), helium cooled ceramic breeder (HCCB), and water cooled ceramic breeder (WCCB). Moreover, there are also other options in the early stage of concept design.

In this paper, the blanket concept studies in China will be summarized, and the corresponding research and development activities will also be presented. The latest progress and technical challenges were emphasized in the fusion nuclear material development, the breeder and coolant technology and relevant test platforms, the tritium technology achievement, and fusion nuclear safeguard, which will form the very basis of FNST for fusion blanket.

Finally, the possible blanket development roadmap to DEMO in China will also be included as well as the international collaboration strategy.



Temperature Sensitivity Analysis of Nuclear Cross Section Using FENDL for Fusion-Fission System

C. Velasquez^{1,2,3}, G. Barros⁴, C. Pereira^{1,2,3}, M. A. F. Veloso^{1,2,3}, and A. L. Costa^{1,2,3}

¹*Universidade Federal de Minas Gerais, Belo Horizonte, MG, Brazil*

²*Instituto Nacional de Ciência e Tecnologia de Reatores Nucleares Inovadores, Conselho Nacional de Desenvolvimento Científico e Tecnológico (CNPq), Rio de Janeiro, Brazil*

³*Rede Nacional de Fusão (FINEP/CNPq), Conselho Nacional de Desenvolvimento Científico e Tecnológico (CNPq), Rio de Janeiro, Brazil*

⁴*Brazilian Nuclear Energy Commission (CNEN), Rio de Janeiro, Brazil*

Corresponding Author: C. Velasquez, carlosvelcab@ufmg.br

Fusion energy has been presented as a clean alternative way of energy source. Furthermore, the neutronics features from fusion reactors make favourable the fuel regeneration and actinoid transmutation due to the high-energy neutron flux. This work proposes a fusion-fission system (FFS) based on a tokamak at operating temperature for transmutation of MA using reprocessed fuel by UREX+ technique spiked with thorium. The purpose is to follow the burnup of the MA inventory at operating temperature. Thorium choice was due to the conversion from fertile to fissile nuclide and its abundance in crust earth. In this work, NJOY99.364 used to process the cross section at operating temperatures and the Monteburns, which links the ORIGEN2.1 and the MCNP to perform the depletion and modelling of the system. The results show a temperature sensitivity analysis of a FFS closest to its real material conditions at operating temperatures and one simulated at room temperature. The work establishes the neutronic modelling differences in the system, as well as, the temperature effect on the MA depletion and production nuclides for FFS.

IFE: Inertial Fusion Experiments and Theory



Overview of the Laser Megajoule First Experiments

J.-L. Miquel¹, E. Volant¹

¹CEA/DAM Île de France, Bruyères le Châtel, 91297 Arpaçon Cedex, France

Corresponding Author: J.-L. Miquel, jean-luc.miquel@cea.fr

Since the operational commissioning of the Laser Megajoule (LMJ) in October 2014, several experimental campaigns have been achieved, with the first eight beams, and demonstrated LMJ's aptitudes for the Simulation Programme.

The Simulation Programme of the Commissariat à l'Énergie Atomique et aux Énergies Alternatives (CEA) combines improvement of physics models, high performance numerical simulation, and experimental validation. The LMJ, designed to provide the experimental capabilities to study high energy density physics (HEDP), is a keystone of this programme. The 176 beams of the facility will deliver a total energy of 1.4 MJ of 0.35 μm (3ω) light and a maximum power of 400 TW. Using a variety of pulse shapes, it will be possible to bring material to extreme conditions with temperature of 100's MK and pressures of 100's Gbar. One of the LMJ's goals is to obtain ignition and burn of DT with the indirect drive approach. The experiments performed since the commissioning were dedicated to radiative transport, implosion hydrodynamics and hydrodynamic instabilities in order to validate radiative hydrodynamics simulations and prepare ignition.

LMJ will increase its capacities in the following years with the completion of other beams and a set of 25 diagnostics. A PW beam, the PETAL project, has been added to the LMJ. It is a short-pulse (ps) ultrahigh-power, high-energy beam (kJ). The first high energy test shots of PETAL have demonstrated the PW capabilities of PETAL with a record of 1.2 PW. Experiments combining LMJ and PETAL will then start in 2017, giving the possibility to address a new physics. LMJ-PETAL is open to the academic community. The academic access to LMJ-PETAL and the selection of the proposals for experiments is done through the Institut Laser & Plasmas (ILP) with the help of the PETAL international Scientific Advisory Committee. The LMJ-PETAL User guide provides the necessary technical references to researchers for the writing of Letter of Intent of experimental proposals to be performed on LMJ-PETAL. Regularly updated version of this LMJ-PETAL User guide is available on the LMJ website at <http://www-lmj.cea.fr/en/ForUsers.htm>.

The PETAL project is accomplished under the auspices of the Conseil Régional d'Aquitaine, of the French Ministry of Research and of the European Union.



Fast Ignition Inertial Confinement Fusion with Kilo-Tesla Magnetic Field

S. Fujioka¹, H. Nagatomo², Y. Arikawa¹, A. Morace¹, A. Sunahara³, T. Johzaki⁴, T. Ozaki⁵, Z. Zhang², T. Norimatsu¹, J. Kawanaka¹, H. Shiraga¹, H. Azechi¹, and K. F. F. Law¹

¹*Institute of Laser Engineering, Osaka University, Osaka, Japan*

²*Osaka University, Osaka, Japan*

³*Institute for Laser Technology, Suita, Osaka, Japan*

⁴*Graduate School of Engineering, Hiroshima University, Higashi-Hiroshima, Japan*

⁵*National Institute for Fusion Science (NIFS), Toki, Gifu, Japan*

Corresponding Author: S. Fujioka, sfujioka@ile.osaka-u.ac.jp

Here we report recent experimental results relevant to the fast ignition (FI) inertial confinement fusion assisted with external kilo-tesla magnetic field. We have experimentally observed generation of 0.6 kT magnetic field by using laser-driven capacitor-coil scheme, short diffusion time ($\ll 1$ ns) of laser-generated magnetic field into a target material, reduction of the REB beam diameter by the factor of two and additional acceleration of a fusion plasma hydrodynamics in the strong magnetic field. One of the critical problems facing the FI scheme is large divergence angle of the laser accelerated relativistic electron beam (REB). The application of a strong external magnetic field in the REB path to the fuel core is being investigated for controlling transport of the REB. Larmor radius of a 1 MeV electron, which heats efficiently the fuel core, is $6 \mu\text{m}$ in a 1 kT magnetic field. The radius is smaller than the typical radius of the REB at the generation point, thus a 1 kT magnetic field is enough for the REB guiding. Kilo-tesla magnetic field affects not only REB transport but also hydrodynamics of a fusion plasma by anisotropic thermal heat transport. Guidance of the REB using a 0.6 kT field in a planar geometry has been demonstrated. In this experiment, a $50 \mu\text{m}$ -thick plastic foil was put near the coil centre, and the foil was irradiated by a short pulse laser to generate REB. Spatial distribution of the REB was observed as a coherent transition radiation (CTR) image and spectrum from its rear side. CTR emission size and intensity become smaller and stronger in the magnetic field compared to those without the magnetic field. The CTR spectrum indicate reduction of divergence of REB at its generation point.



Observations of Residual Bulk-Fluid Motion and Low-Mode Areal-Density Asymmetries at Peak Convergence in NIF Implosions through Spectral Measurements of DD and DT Neutrons

J. Frenje¹, B. Appelbe², R. Bionta³, E. Bond³, D. K. Bradley³, J. Caggiano³, D. A. Callahan³, D. Casey³, C. Cerjan³, J. Chittenden², T. Döppner³, M. Eckart³, J. Edwards³, V. Glebov⁴, G. Grim³, E. Hartouni³, R. Hatarik³, D. E. Hinkel³, O. A. Hurricane³, W. W. Hsing³, M. Gatu Johnson¹, J. D. Kilkenny⁵, J. Knauer⁴, A. Kritcher³, D. Munro³, T. Murphy⁶, O. L. Landen³, S. LePape³, T. Ma³, A. Mackinnon⁷, N. Meezan³, P. Patel³, R. Petrasso¹, T. C. Sangster⁴, D. Sayre³, B. K. Spears³, P. Springer³, and C. Yeaman³

¹Massachusetts Institute of Technology (MIT), Cambridge, MA 02139, USA

²Imperial College, London, UK

³Lawrence Livermore National Laboratory (LLNL), Livermore, CA 94550, USA

⁴Laboratory for Laser Energetics, University of Rochester, Rochester, NY 14627, USA

⁵General Atomics, San Diego, CA 92186, USA

⁶Los Alamos National Laboratory (LANL), Los Alamos, NM 87545, USA

⁷SLAC National Accelerator Laboratory, Menlo Park, CA 94025, USA

Corresponding Author: J. Frenje, jfrenje@psfc.mit.edu

Hot-spot ignition planned at the National Ignition Facility (NIF) requires proper assembly of the DT fuel, as manifested by the evolution of areal density (ρR) symmetry and hot-spot ion temperature (T_i). Ideally, a spherically symmetric layer of cold dense fuel with $\rho R > 1 \text{ g/cm}^2$ surrounding a $\sim 5 \text{ keV}$ lower-density hot spot is obtained at peak convergence. To reach these conditions, the implosion must be 1D in nature and efficient conversion of implosion kinetic energy to hot-spot thermal energy must be obtained. If substantial 3D nonuniformities in the implosion exist, conversion efficiency is degraded and a significant fraction of implosion kinetic energy, in bulk-fluid motion form, remains at peak convergence. Experimentally, residual bulk-fluid motion is assessed from directional measurements of the primary DT and DD neutron spectrum. The width of the primary spectrum is characteristic of T_i as well as the variance of the bulk-fluid motion in the burning region. Energy shifts beyond T_i -induced shifts are also an indication of bulk-fluid motion. As well, ρR asymmetries are determined from directional yield measurements of scattered or unscattered neutrons. In recent high-foot-implosion experiments, directional measurements of the neutron spectrum illustrate the existence of substantial bulk-fluid motion and low-mode ρR asymmetries at peak convergence, which degrade the implosion performance. The measured DT-weighted apparent T_i is also consistently higher than the apparent DD-weighted T_i , a discrepancy that increases with increasing implosion drive. From a 1D perspective, the DD yields are also too high relative to DT yields. Effects due to profiles, reactivity differences, and bulk-fluid motion partly explain these observations, but none of them appear sufficient to explain the data. The observables are most likely caused by significant ρR asymmetries ($> 500 \text{ mg/cm}^2$) and substantial bulk-fluid motion of about 50–100 km/s. The hypothesis is that these observations are driven by radiation drive asymmetry, and instabilities seeded by the fill tube and thin tent holding the capsule in the hohlraum. These issues are currently being addressed by new engineering solutions, more refined implosion modelling, and implementation of new diagnostics.

Work supported by the U.S. Department of Energy (contract DE-AC52-07NA27344).



Laser-Driven Ion Acceleration on LFEX for Fast Ignition: State of the Art and Applications

A. Yogo¹, N. Iwata¹, K. Mima², A. Morace¹, S. Tosaki¹, S. Fujioka¹, Y. Arikawa¹, Y. Abe¹, S. Kojima¹, S. Sakata¹, S. Lee¹, K. F. F. Law¹, K. Matsuo¹, H. Nagatomo³, A. Sunahara⁴, T. Johzaki⁵, H. Sakagami⁶, T. Ozaki⁶, T. Sano¹, Y. Fujimoto¹, K. Yamanoi¹, T. Norimatsu¹, S. Tokita¹, Y. Nakata¹, J. Kawanaka¹, T. Jitsuno¹, N. Miyanaga¹, M. Nakai¹, H. Nishimura¹, H. Shiraga¹, S. Bulanov⁷, A. Sagisaka⁷, K. Ogura⁷, K. Kondo⁷, and H. Azechi¹

¹Institute of Laser Engineering, Osaka University, Osaka, Japan

²Graduate School for the Creation of New Photonics Industries, Hamamatsu, Shizuoka, Japan

³Osaka University, Osaka, Japan

⁴Institute for Laser Technology, Suita, Osaka, Japan

⁵Graduate School of Engineering, Hiroshima University, Higashi-Hiroshima, Japan

⁶National Institute for Fusion Science (NIFS), Toki, Gifu, Japan

⁷Japan Atomic Energy Agency (JAEA), Naka, Japan

Corresponding Author: A. Yogo, yogo-a@ile.osaka-u.ac.jp

Fusion fast ignition assisted by laser-driven ion beams requires 10 kJ energy deposition onto the fuel core having $\sim 500 \text{ g/cm}^3$ densities. Assuming 100 kJ as a technically manageable energy of the driving laser, the first milestone can be found on 10% conversion efficiency from the laser energy into ions having kinetic energies of 10–30 MeV/u.

In this paper, we experimentally investigate the ion acceleration mechanism using kilojoule picosecond laser LFEX. When we expand the pulse duration (FWHM) of the laser from 1.5 ps to 3 ps at the fixed laser intensity of $2.3 \times 10^{18} \text{ W/cm}^2$, the electron temperature measured by electron spectrometer (ESM) is drastically enhanced up to 1.2 MeV, which clearly exceeds the ponderomotive potential around 0.2 MeV for the laser intensity used in this measurement. At a duration of 6 ps, the electron temperature turns to decrease, indicating that an optimum duration can be found around 3 ps. In addition, the proton energy, analyzed simultaneously with the electron temperature, reaches 29 MeV at 3 ps and saturates around 30 MeV at 6 ps.

We also show that the energy conversion efficiency into the protons drastically grows from 0.2% to 5% when the laser duration is expanded from 1.5 to 6 ps. This fact is advantageous for the ion-driven fast ignition by ions from the viewpoint of the energy deposition onto the core plasma.

The efficient ion generation is attributed to the hot electrons anomalously heated by the laser beyond a typical scaling. The electron temperature enhanced via the anomalous mechanism is well reproduced by a particle-in-cell simulation. In the presentation, we will show that the enhanced proton energy is explained by newly introducing the anomalous heating effect into the conventional plasma expansion model.



Ion Kinetic Dynamics in Strongly-Shocked Plasmas Relevant to ICF

H. G. Rinderknecht¹, P. Amendt¹, J. Frenje², M. Gatu Johnson², V. Glebov³, N. Hoffman⁴, G. Kagan⁴, O. Larroche⁵, C. Li², R. Petrasso², M. Rosenberg³, C. Sangster³, F. Seguin², H. Sio², C. Stoeckl³, S. Wilks¹, and A. B. Zylstra⁴

¹Lawrence Livermore National Laboratory (LLNL), Livermore, CA 94550, USA

²Massachusetts Institute of Technology (MIT), Cambridge, MA 02139, USA

³Laboratory for Laser Energetics, University of Rochester, Rochester, NY 14627, USA

⁴Los Alamos National Laboratory (LANL), Los Alamos, NM 87545, USA

⁵Commissariat à l'énergie atomique (CEA), Bruyères-le-Châtel, France

Corresponding Author: H. G. Rinderknecht, rinderknecht1@llnl.gov

Implisions of thin-shell capsules produce strongly-shocked ($M > 10$), high-temperature ($T_i \sim \text{keV}$), low-density ($\rho \sim 1 \text{ mg/cm}^3$) plasmas, comparable to those produced in the strongly-shocked DT-vapour in inertial confinement fusion (ICF) experiments. A series of thin-glass targets was filled with mixtures of deuterium and ^3He gas ranging from 20% to 100% deuterium and imploded on the OMEGA laser at the Laboratory for Laser Energetics to investigate the impact of multispecies ion kinetic mechanisms on ICF-relevant plasmas. Anomalous trends in nuclear yields and burn-averaged ion temperatures, which have been interpreted as signatures of ion species separation and ion thermal decoupling [1], are found not to be consistent with single-species ion kinetic effects alone. Experimentally-inferred Knudsen numbers predict an opposite yield and temperature trend to those observed, confirming the dominance of multispecies physics in these experiments. Ion density is inferred to be half of the predicted value: models of undercompression and loss of ions at the fuel/ablator interface are considered. The impact of the observed kinetic physics mechanisms on the formation of the hotspot in ICF experiments is discussed.

References

[1] H. G. Rinderknecht, *et al.*, Phys. Rev. Lett. **114**, 025001 (2015).



LFEX-Laser: A Multi-Kilojoule, Multi-Petawatt Heating Laser for Fast Ignition

J. Kawanaka¹, N. Morio¹, S. Matsuo¹, K. Kawabata¹, Y. Kawakami¹, Y. Fujimura¹, K. Sawai¹, K. Tsuji¹, Y. Suzuki¹, Y. Matsuda¹, T. Kawasaki¹, H. Murakami¹, M. Ishida¹, H. Kitamura¹, H. Matsuo¹, T. Sakamoto¹, T. Sezaki¹, T. Yanagida¹, S. Tokita¹, Y. Nakada¹, K. Tsubakimoto¹, H. Shiraga¹, T. Jitsuno¹, and N. Miyanaga¹

¹*Institute of Laser Engineering, Osaka University, Osaka, Japan*

Corresponding Author: J. Kawanaka, kawanaka@ile.osaka-u.ac.jp

A new heating laser for fast ignition, called the LFEX-Laser, has been demonstrated with all four beams. The obtained total pulse energy was 2 kJ for a 1 ps pulse duration. The peak power of 2 PW is the highest of all kilojoule lasers in the world and was achieved with a high intensity contrast ratio of 1×10^{10} .

To increase the pulse energy to the kilojoule class in a short pulse of 1–2 ps, chirped-pulse amplification (CPA) was adopted. Recently, all four beams of this new LFEX-Laser were completed and high-power shots at kilojoule energies with a 1 ps pulse duration were demonstrated. In addition, a new pulse cleaner improved the pulse intensity contrast of the main pulse to suppress the pre-plasma, which significantly reduces the heating efficiency in fast ignition.

One of the key technologies enabling the realization of a kilojoule CPA system is the essential optics for CPA in a large enough size. In particular, the world's largest dielectric grating (92 cm \times 42 cm, 1740 grooves/mm) used in the pulse compressor has recently been developed through the collaboration of Okamoto Optics Works, Jovin Yvon, and Osaka University. Using the pulse compressor with the gratings, the typical pulse duration as short as about 1 ps was successfully obtained for all beams. The total pulse energy was 2 kJ, which corresponds to 2 PW. Deformable mirrors were used in the main amplifier to improve the focussing of the beams by compensating for wavefront distortions. About 70% of the pulse energy can be concentrated into a spot with a diameter of $5F\lambda$, where F is the F -number of the lens and λ is the laser wavelength of 1.053 μm .

Another key technology is our new pulse cleaner. Generally, amplified optical parametric fluorescence (AOPF) before the main pulse, which produces pre-plasmas, can be removed effectively with a saturable absorber (SA, Cr⁴⁺:YAG). In CPA, however, AOPF temporally overlaps with the chirped main pulse and is significant because the non-phase-locked AOPF is not compressed by the pulse compressor, making it difficult to remove it with an SA. Our new pulse cleaner combines the SA with the 4f optical layout, to remove the AOPF. By using two pulse cleaners in the front end, a high contrast ratio of 1×10^{10} , compared to 2×10^7 without the cleaners, was obtained.



Improvement of Characteristics of Laser Source of Ions by Changing the Parameters of the Target and External Parameters

R. Khaydarov¹, H. Besinbaeva¹, R. Khaydarov¹, and G. Berdiyrov¹

¹*Institute of Applied Physics, National University of Uzbekistan, Tashkent, Uzbekistan*

Corresponding Author: R. Khaydarov, rtkhaydarov@yahoo.com.ph

In recent years the ion components of the laser-produced plasmas has been intensively studied as an object to provide high-density and high-energy ion sources, which can be effectively used in the field of inertial confinement fusion. It is well known that processes taking place during the interaction of laser radiation with solid targets strongly depend on the target material leading to different erosion thresholds, etching rates, chemical yields, etc. In this work we discuss three methods to improve characteristics of laser source of ions, namely: i) effects of gamma radiations on the properties of glass materials, ii) influence of laser frequency on the parameters of plasma ions generated on the surface of porous targets, and iii) effect of light gas atom inclusions on the characteristics of laser-produced plasma ions. Our study will be based on the analysis of mass-charge spectrum of laser-produced plasma ions for different intensity of laser radiation.

The main impact of the radiation is observed in the charge state of the plasma ions: for small energy ions the charge increases with increasing the radiation dose, whereas the increase in the radiation dose results in the decrease of the charge of high-energy ions. The maximum energy of the ions also decreases with increasing the radiation dose.

Recent Advances in Theoretical and Numerical Studies of Z-Pinch Driven Inertial Confinement Fusion in the IAPCM

N. Ding¹, J. Wu¹, and Y. Zhang¹

¹*Institute of Applied Physics and Computational Mathematics, Beijing, People's Republic of China*

Corresponding Author: N. Ding, dingning580723@163.com

Fast Z-pinch has produced the most powerful X-ray radiation source in laboratory and also shows the possibility to drive inertial confinement fusion (ICF). The recent advances in the Z-pinch theoretical and numerical researches at the IAPCM are presented. We use a detailed circuit model to study the energy coupling between the generator and the Z-pinch process. With the full circuit model (FCL code) and MHD model (2D MARED code), the simulation of the propagation of electromagnetic wave pulse from the generator to the load is studied, the compression, the amplification and the transmission of the pulse has been observed. The simulation results could show about the information of the pulse at some locations of the generator. The experiments conducted on the PTS facility that is the most powerful pulsed-power generator for Z-pinch study in China recently validated our part simulation results. Specifically, the calculated electric parameters in front of the insulation stack, such as voltages and currents, show a quantitative agreement with the experimental results. The implosion parameters of wire-array Z-pinch, such as implosion velocities and convergence ratios agree qualitatively with the diagnosed results. Our codes can apply not only in optimal design of wire-array load, but also in the research of key issues of Z-pinch driven fusion. Recently, we are concentrating on the problems of Z-pinch driven ICF, such as quasi-spherical wire-array implosions, dynamic hohlraum and capsule implosions. When a quasi-spherical implosion (QSI) is used to drive a dynamic hohlraum system, the enhanced energy density helps to improve the energy-transport efficiency and increase the shock-induced radiation intensity of the foam convertor. We found that the quality of QSI can be enhanced by changing its initial shape to a prolate one, and it is more practical for wire array fabrication. The implosion dynamics of a tungsten wire-array Z-pinch embedded with a CH foam convertor, especially the impaction interaction of the wire-array plasma with the convertor plasma, is numerically investigated using a 1D nonequilibrium radiation MHD code. A suitable radius ratio of the wire array to the convertor, neither too large to induce strong MRT instability nor too small to gain a small kinetic energy of the wire array before impacting onto the convertor surface, should be selected.



Recent Activities on Heavy Ion Inertial Fusion in Japan

T. Kikuchi¹, J. Hasegawa², K. Horioka², Y. Iwata³, W. Jiang¹, S. Kawata⁴, K. Kondo², Y. Oguri², K. Okamura⁵, M. Okamura⁶, T. Sasaki¹, K. Takahashi¹, and K. Takayama⁵

¹Nagaoka University of Technology, Nagaoka, Niigata, Japan

²Tokyo Institute of Technology, Tokyo, Japan

³National Institute of Advanced Industrial Science and Technology (AIST), Tokyo, Japan

⁴Utsunomiya University, Utsunomiya, Tochigi, Japan

⁵High Energy Accelerator Research Organization (KEK), Tsukuba, Ibaraki, Japan

⁶Brookhaven National Laboratory (BNL), Upton, NY 11973, USA

Corresponding Author: T. Kikuchi, tkikuchi@vos.nagaokaut.ac.jp

Recent activities on heavy ion inertial fusion in Japan are reviewed in this paper. Particle accelerator development, beam dynamics research, interaction between heavy ions and target material, ion source development, and illumination scheme of heavy ion beams, for heavy ion inertial fusion, are reported.

Inertial confinement fusion scheme driven by intense heavy ion beams, so-called heavy ion inertial fusion (HIF), is a method to release nuclear energy by nuclear fusion reactions of prodigious proportions. When the intense heavy-ion beams illuminate a fuel target pellet, the target pellet is heated up due to interactions between the ion beams and the target material. As a result, implosion process is driven by ablation plasma in the target pellet.

In the HIF system, the related researches in particle accelerators and charged-particle beams including with the beam-material interaction are unique topics in comparison with other nuclear fusion systems. Also, common research topics such as properties of warm dense matter (WDM) are in the field of HIF studies. For this reason, the researches in Japanese HIF group are focussing to the related themes in the particle accelerator, the charged-particle beams, the interactions between the beam and the material with the solid, WDM, and plasma conditions.

The particle accelerator development is a crucial issue for HIF study, and the KEK digital accelerator brings a solution. The beam dynamics research, the interaction between heavy ions and target material, the ion source development, and illumination scheme of heavy ion beams are also unique research topics for HIF. Not only the above unique topic in HIF, but also the WDM research is an important problem for nuclear fusion system, and the studies were carried out by using the experimental setup based on pulsed power technique.



Adapting High Resolution X-ray Spectroscopy from MFE to Temperature and Density Measurements in ICF

K. W. Hill¹, M. Bitter¹, P. C. Efthimion¹, R. Ellis¹, L. Gao¹, M. B. Schneider², H. Chen², S. Ayers², M. A. Barrios², P. Beiersdorfer², P. M. Bell², R. Bettencourt², D. K. Bradley², D. Casey², M. J. Edwards², B. A. Hammel², M. C. Herrmann², W. W. Hsing², O. S. Jones², R. L. Kauffman², O. L. Landen², D. A. Liedahl², T. Ma², A. G. MacPhee², J. D. Moody², R. C. Nora², P. Patel², H. A. Scott², V. A. Smalyuk², B. K. Spears², D. B. Thorn², J. D. Kilkenny³, S. P. Regan⁴, and Y. Maron⁵

¹Princeton Plasma Physics Laboratory (PPPL), Princeton, NJ 08540, USA

²Lawrence Livermore National Laboratory (LLNL), Livermore, CA 94550, USA

³General Atomics, San Diego, CA 92186, USA

⁴Laboratory for Laser Energetics, University of Rochester, Rochester, NY 14627, USA

⁵Weizmann Institute of Science, Rehovot, Israel

Corresponding Author: K. W. Hill, khill@pppl.gov

X-ray spectroscopy will be used in indirect drive experiments at the National Ignition Facility (NIF) to diagnose plasma conditions and mix in ignition capsules near stagnation times, thus indicating the quality of the implosion, and at various positions in the hohlraum. The electron temperature, T_e , and density, n_e , will be measured from dielectronic satellites and Stark broadening, respectively, by doping a surrogate capsule ("symcap") with a small amount of Kr gas. These measurements will corroborate neutron based measurement of ion temperature, T_{ion} , assuming $T_e = T_{ion}$ due to quick equilibration at stagnation. This direct measurement of n_e will corroborate the inference of density from other measurements (T_{ion} , neutron yield, size of hotspot, duration of burn). The T_e measurement in Kr doped capsules will also benchmark other measurements from the X-ray continuum slope, which will then measure T_e in igniting capsules (without Kr). Mixing of capsule ablator material and fill tube material into the fuel quickly degrades performance. X-ray spectroscopy of doped elements in the ablator will diagnose the amount of mix into the hot spot, and other effects of mix. In the hohlraum, X-ray spectroscopy will measure plasma conditions in the hot plasma where laser energy is deposited, giving insight into the underlying physics that govern hohlraum behaviour, and processes that directly affect X-ray drive, symmetry and laser-hohlraum coupling. High resolution spectroscopy ($E/\Delta E \sim 5000-20000$) of impurity dopant X-ray is a mature technology that was developed on tokamaks for Doppler measurement of T_{ion} and plasma flow velocity. It has been deployed on tokamaks and stellarators world wide and will be used as a primary T_{ion} diagnostic on the international tokamak, ITER. The initial NIF instruments will be compact spectrometers mounted in positioners. The first experiments will field both von Hamos and conical crystal spectrometers to record time integrated and time resolved (> 30 ps) spectra of the He_α , Ly_α and He_β complexes of Kr. The spectrometer design and performance, based on photonics calculations using collisional radiative and atomic physics codes, will be presented.

Work performed under the auspices of the U.S. Department of Energy by LLNL under Contract DE-AC52-07NA27344 and PPPL under contract DE-AC02-09CH11466



The Role of Beryllium Ablators in Inertial Confinement Fusion

A. N. Simakov¹, J. L. Kline¹, S. A. Yi¹, D. C. Wilson¹, G. A. Kyrala¹, R. E. Olson¹, T. S. Perry¹, S. H. Batha¹, A. B. Zylstra¹, E. L. Dewald², R. Tommasini², J. E. Ralph², D. J. Strozzi², A. G. MacPhee², D. A. Callahan², D. E. Hinkel², O. A. Hurricane², J. L. Milovich², J. R. Rygg², S. F. Khan², S. W. Haan², P. M. Celliers², D. S. Clark², B. A. Hammel², B. Koziemski², M. B. Schneider², M. M. Marinak², H. G. Rinderknecht², H. F. Robey², J. D. Salmonson², P. K. Patel², T. Ma², M. J. Edwards², M. Stadermann², S. Baxamusa², C. Alford², Y.-M. Wang², A. Nikroo², N. Rice³, D. Hoover³, K. P. Youngblood³, H. Xu³, H. Huang³, and H. Sio⁴

¹Los Alamos National Laboratory (LANL), Los Alamos, NM 87545, USA

²Lawrence Livermore National Laboratory (LLNL), Livermore, CA 94550, USA

³General Atomics, San Diego, CA 92186, USA

⁴Massachusetts Institute of Technology (MIT), Cambridge, MA 02139, USA

Corresponding Author: A. N. Simakov, simakov@lanl.gov

Low-mode implosion asymmetry and hydrodynamic instabilities of the capsule are considered the main obstacles for achieving ignition in indirect drive inertial confinement fusion (ICF). Superior ablation properties of beryllium (Be) ablaters as compared with plastic and diamond ablaters may help overcome these obstacles. In particular, higher Be ablation pressure permits use of either thicker fuel layers and thereby lower ICF capsule convergence; or of lower radiation drive temperatures and thereby larger hohlraums and case-to-capsule ratios. Both effects are predicted to be beneficial for implosion symmetry. Higher ablation velocity can provide enhanced ablation front stabilization and reduce detrimental effects of hydrodynamic instabilities. "High-foot" plastic campaign on the National Ignition Facility (NIF) has demonstrated importance of the suppression of instabilities, in particular by reducing the perturbation induced by the capsule support membranes that hold the capsule in the hohlraum — a major factor degrading earlier implosions. Initial measurements using hydro-growth radiography have shown that Be ablaters are even more stable. In addition, high-adiabat Be implosions in 5.75 mm hohlraums with high-density (1.6 mg/cm³) helium gas fill showed that performances of Be and comparable plastic targets were similar. Difficult-to-model nonlinear plasma physics effects strongly degrade X-ray drive properties and the capsule implosion symmetry in such high-fill hohlraums. To fully test the predicted Be ablator advantages, hohlraums where such effects are suppressed need to be used. Beryllium integrated hohlraum experiments that started in the fall of 2015 have been using larger (6.72 mm) hohlraums with lower (< 0.6 mg/cm³) fill densities and purposely reduced radiation drive temperature, and have demonstrated significantly improved laser-capsule coupling and good Be ablator performance. This suggests a future possibility of using even larger hohlraums to control symmetry if necessary. We will next employ these well-performing hohlraums with the goal of obtaining Be capsule implosions with good in-flight and stagnation symmetry.

Spherical Convergent Plasma Fusion (SCPF) Neutron Generator by Laser Drive: Theory and Experiment

J. Liu¹, G. Ren¹, J. Yan¹, and L. Ke¹

¹*Institute of Applied Physics and Computational Mathematics, Beijing, People's Republic of China*

Corresponding Author: J. Liu, jliu2486@163.com

We propose a feasible scheme to acquire high ion temperature and high thermal nuclear fusion neutron yield with laser ablated spherical convergent plasmas fusion (SCPF). In our scheme, we use intense lasers (10^{14} – 10^{15} W/cm²) pulse of nanosecond duration to irradiate thermonuclear fuel (carbonized deuterium, CD) containing layer (~ 10 μ m) lined inside a spherical hohlraum, the fuel layer is ablated and then expands at high speed (~ 500 km/s) towards the sphere centre. The hot fuel plasmas eventually merge at the centre and convert most of their kinetic energy to the ion internal energy, raising the ion temperature to a high level of around 10 keV. We have done demonstrating experiment on SGIII-prototype facility. In the experiment, we use 6 kJ triple-frequency laser to irradiate a CD layer lined inside a 1.7 mm diameter spherical hohlraum with one laser entrance hole at each end, we have acquired a stable DD thermonuclear fusion neutron yield of 3×10^9 . The process is robust and neutron yield is insensitive to practical experimental environment and parameter fluctuation. The neutron ToF data shows that the ion temperature of the merged plasmas is around 7–8 keV. The experiment results agree with our theoretical scaling law and hydrodynamic simulation. The experiment has demonstrated the SCPF to be potentially a high laser fusion neutron generator in future. Improvement and further optimization of this scheme is undergoing.

Fast Heating of an Imploded Core under Counter Beam Irradiation by Using a Repetitive IFE Driver HAMA

Y. Mori¹, Y. Nishimura¹, R. Hanayama¹, S. Nakayama¹, K. Ishii¹, Y. Kitagawa¹, T. Sekine², N. Sato², T. Kurita², T. Kawashima², H. Kan², O. Komeda³, T. Nishi⁴, H. Azuma⁵, T. Hioki⁶, T. Motohiro⁶, A. Sunahara⁷, Y. Sentoku⁸, and E. Miura⁹

¹Graduate School for the Creation of New Photonics Industries,
Hamamatsu, Shizuoka, Japan

²Hamamatsu Photonics, K.K., Hamamatsu City, Shizuoka, Japan

³Toyota Technical Development Corp., Japan

⁴TOYOTA Central R&D Labs Inc., Nagakute, Aichi, Japan

⁵Aichi Synchrotron Radiation Center, Seto-shi, Aichi-ken, 489-0965 Japan

⁶Green Mobility Collaborative Research Center (GREMO), Nagoya University, Nagoya, Japan

⁷Institute for Laser Technology, Suita, Osaka, Japan

⁸University of Nevada, Reno, NV 89557, USA

⁹National Institute of Advanced Industrial Science and Technology (AIST), Tokyo, Japan

Corresponding Author: Y. Mori, ymori@gpi.ac.jp

Fast heating is a scheme to heat an imploded high density plasma into a hot state before the plasma hydrodynamically expands and dissolves. For a heating process driven by laser induced hot electron currents, the energy of hot electrons beyond MeV having a range of a few g/cm², therefore collisional coupling is inefficient until the core density reaches hundreds g/cm³. To improve the MeV electrons' coupling, an energy deposition via the anomalous resistivity in strong magnetic filaments induced by the electromagnetic tow-stream instability, so-called Weibel instability, was expected. However, this Weibel instability was found to be suppressed in the collisional dense plasma, namely, the heating by the fast electrons stays inefficient. In contrast, counter irradiating fast heating scheme we propose here can improve this insufficient coupling efficiency by introducing a magnetic field supposed to be contributing to trap hot electrons in the core. We report fast heating of a shock-imploded core under counter beam irradiation by using a repetitive IFE driver HAMA. Experimental results show that i) a shock-imploded core with 70 μm diameter, originally deuterated polystyrene (CD) spherical shell of 500 μm diameter, is flashed by counter irradiating 110 fs, 7 TW laser pulses. The coupling efficiency from the laser to the core emission was inferred to be 13%. A collisional particle-in-cell (PIC) simulation indicates a possibility that counter hot electron currents generate magnetic filaments in the imploded core. ii) Fast electrons with energy below a few MeV might be trapped by these filaments in the core region supposed to be contributing to the observed X-ray flash and the high coupling efficiency. These results indicate a possibility that counter irradiating fast heating scheme can improve the energy coupling into the core by hot electrons those are limited to less 10% for one-side irradiation fast heating conducted so far.

Unified Studies of Fast-Ignition Scheme Fusion with Counterbeam Configuration

Y. Kitagawa¹, Y. Mori¹, K. Ishii¹, R. Hanayama¹, Y. Nishimura¹, S. Nakayama¹, T. Sekine², T. Kurita², N. Satoh², T. Kawashima², H. Kan², O. Komeda³, T. Nishi³, T. Hioki⁴, T. Motohiro⁴, H. Azuma⁵, A. Sunahara⁶, Y. Sentoku⁷, E. Miura⁸, Y. Arikawa⁹, Y. Abe⁹, and S. Ozaki¹⁰

¹Graduate School for the Creation of New Photonics Industries,
Hamamatsu, Shizuoka, Japan

²Hamamatsu Photonics, K.K., Hamamatsu City, Shizuoka, Japan

³TOYOTA Central R&D Labs Inc., Nagakute, Aichi, Japan

⁴Green Mobility Collaborative Research Center (GREMO), Nagoya University, Nagoya, Japan

⁵Aichi Synchrotron Radiation Center, Seto-shi, Aichi-ken, 489-0965 Japan

⁶Institute for Laser Technology, Suita, Osaka, Japan

⁷University of Nevada, Reno, NV 89557, USA

⁸National Institute of Advanced Industrial Science and Technology (AIST), Tokyo, Japan

⁹Institute of Laser Engineering, Osaka University, Osaka, Japan

¹⁰National Institute for Fusion Science (NIFS), Toki, Gifu, Japan

Corresponding Author: Y. Kitagawa, kitagawa@gpi.ac.jp

The recent key physics of the laser fusion is how to make hot sparks for the alpha burning in the dense core. The fast ignition is expected to form a hot spark even with a nonuniform illumination configuration, such as with a counter-illumination one. By using both a high-repetition rate 10 J laser and a single-shot kJ laser, we have proposed and demonstrated a new concept for the fast-ignition scheme fusion, where main beams implode a shell target with counterbeam configuration and ultraintense lasers with the same configuration drive either hot electrons or ions or both, which has directly heated the core. Shock waves driven by ultraintense lasers are also powerful candidates for the core heating and are investigated. Combining these three fast-ignition schemes, we are demonstrating both the implosion and ignition to work well with counterbeam configuration.

Improvement in the Heating Efficiency of Fast Ignition Inertial Confinement Fusion by Suppressing the Preformed Plasma

Y. Arikawa¹, S. Kojima¹, A. Morace¹, M. Hata¹, S. Sakata¹, S. Fujioka¹, T. Kawashima¹, Y. Hironaka¹, K. Shigemori¹, Y. Abe¹, V. Xavier¹, L. Seungho¹, K. Matsuo¹, K. F. F. Law¹, Y. Kato¹, S. Matsubara¹, S. Tosaki¹, A. Yogo¹, H. Nagatomo¹, S. Tokita¹, Y. Nakata¹, T. Jitsuno¹, N. Miyanaga¹, J. Kawanaka¹, Y. Fujimoto¹, K. Yamanoi¹, T. Norimatsu¹, M. Nakai¹, H. Nishimura¹, H. Shiraga¹, H. Azechi¹, A. Sunahara², T. Johzaki³, T. Ozaki⁴, and H. Sakagami⁴

¹*Institute of Laser Engineering, Osaka University, Osaka, Japan*

²*Institute for Laser Technology, Suita, Osaka, Japan*

³*Graduate School of Engineering, Hiroshima University, Higashi-Hiroshima, Japan*

⁴*National Institute for Fusion Science (NIFS), Toki, Gifu, Japan*

Corresponding Author: Y. Arikawa, arikawa-y@ile.osaka-u.ac.jp

In the fast ignition scheme, a fusion fuel is compressed by implosion laser and then heating laser heats the core plasma to ignition temperature. The heating laser interacts with the cone target and fast electrons are accelerated, and the electrons are absorbed by the core plasma so that the core plasma is heated to ignition temperature. Since LFEX (heating laser) energy is limited to 10 kJ at maximum, the energy coupling efficiency from laser to the core plasma must be larger than 10%. In previous studies the energy coupling efficiency was limited up to 0.37% which was determined by the electron spectrum and the fuel core plasma density profile. The main reason of the low coupling efficiency was the electron spectrum was consisted with too much high energy.

The electron spectrum is strongly dependent on the scale length of the preplasma on laser interaction region, thus the suppression of the preplasma is key issue. We have two problems of preplasma creation, one is the prepulses of the LFEX laser, and second the preformed plasma originated by cone-target breaking by the implosion. In this paper especially the latter is discussed. If the cone target is not tough enough, it will be destroyed by implosion pressure before heating laser injection, then the heating laser interacts with the preformed plasma, and in this way too many high-energy electrons are generated. LFEX pulse contrast was improved up to 10^9 in 2015 from $\sim 10^8$ in 2013. In this study we directly observed the time when the cone target is broken by observing a reflected probe laser from cone tip by using an optical streak camera (VISAR diagnostics). The previous 7 μm thick cone was broken before the maximum core compression time. We modified it to 14 μm thickness (wall and tip are both 14 μm) so that cone-breaking time was delayed after the implosion laser peak. Electron spectra were measured under the improved condition. The colder electron spectrum was obtained in the condition. After the improvement the energy coupling efficiency from laser to the core plasma was resulted to be 2% with five times increment from 2013's experiment.

Compression and Electron Beam Heating of Solid Target under the External Magnetic Field for Fast Ignition

H. Nagatomo¹, T. Johzaki², T. Asahina³, K. Matsuo³, S. Lee³, A. Sunahara⁴, K. Mima⁵,
H. Sakagami⁶, S. Fujioka³, H. Shiraga³, and H. Azechi³

¹*Osaka University, Osaka, Japan*

²*Graduate School of Engineering, Hiroshima University, Higashi-Hiroshima, Japan*

³*Institute of Laser Engineering, Osaka University, Osaka, Japan*

⁴*Institute for Laser Technology, Suita, Osaka, Japan*

⁵*Graduate School for the Creation of New Photonics Industries,
Hamamatsu, Shizuoka, Japan*

⁶*National Institute for Fusion Science (NIFS), Toki, Gifu, Japan*

Corresponding Author: H. Nagatomo, naga@ile.osaka-u.ac.jp

Compression and heating of solid spherical target under the strong external magnetic field is studied using fast ignition integrated interconnecting simulation system (FI³). The simulation results show that i) a compression of a solid sphere target is stable, and it is possible to achieve a high areal density core plasma. Using GXII scale laser, it will be 60–80 mg/cm². ii) The magnetic mirror ratio is less than 4 which does not reflect most of the hot electrons for heating core, and iii) magnetic beam guiding enhances the heating efficiency and neutron yield which is enhanced to 300-fold compared with the case without magnetic field.

Plasma Mirror Implementation on LFEX Laser for Ion and Fast Electron Fast Ignition

A. Morace¹, S. Kojima¹, Y. Arikawa¹, S. Fujioka¹, A. Yogo¹, S. Tosaki¹, S. Sakata¹, Y. Abe¹, S. H. Lee¹, K. Matsuo¹, A. Sagisaka², K. Kondo², A. Pirozhkov², T. Norimatsu¹, T. Jitsuno¹, N. Miyanaga¹, H. Shiraga¹, M. Nakai¹, H. Nishimura¹, and H. Azechi¹

¹*Institute of Laser Engineering, Osaka University, Osaka, Japan*

²*Japan Atomic Energy Agency (JAEA), Naka, Japan*

Corresponding Author: A. Morace, morace@ile.osaka-u.ac.jp

Fast ignition (FI) is an alternative approach to inertial confinement fusion (ICF) based on the separation between compression and heating of the equimolar deuterium-tritium (DT) fuel capsule. In the FI scheme, the heating is produced by an energetic particle beam, either ions or electrons, generated by an ultrahigh intensity laser pulse.

Both in proton and fast electron fast ignition, a high contrast laser pulse is required in order to efficiently accelerate the particles, avoiding target foil explosion in case of target normal sheath acceleration (TNSA) of protons or by avoiding large scale preformed plasma which will increase the fast electron temperature in case of fast electron driven FI. In synthesis, both FI scenarios require high contrast laser pulses in order to be successful, therefore the laser pulse pedestal must be suppressed significantly.

In this work we show a method to reduce the laser pulse pedestal level, by implementing a plasma mirror (PM) device on LFEX laser. Very high shot-to-shot pointing and focussing reliability has been demonstrated during the experiment, obtaining stable experimental results in line with the theoretical expectations. In particular the pedestal reduction was demonstrated by transverse interferometry of the target surface, showing absence of preformed plasma even 140 ps before the main pulse arrival, while in absence of PM, underdense plasma expansion was observed as early as 1.3 ns before the main pulse arrival.

The fast electron spectrum generated by focussing the LFEX beam on an Au block target showed fast electron temperature reduction within the range of interest for fast ignition in presence of PM device. This further demonstrated that the fast electron spectrum is strongly determined by the presence of preformed plasma. Finally ion acceleration from sub- μm (100 nm) plastic (CH) foil, obtaining a proton beam with maximum energy of 20 MeV recorded on radio-chromic film (RCF) stack, unequivocally demonstrates the extremely high contrast achieved by implementation of the PM device and opens to a wide variety of acceleration mechanisms for fast ignition research.



Coherent Beam Combination for Laser Fusion Driver Design Using Rotation Wedge Self-Phase-Controlled Stimulated Brillouin Scattering Phase Conjugation Mirrors

H. J. Kong¹, S. Park¹, S. Cha¹, J. Oh¹, J. S. Kim², and K. Churn¹

¹*Korea Advanced Institute of Science and Technology (KAIST), Daejeon, Republic of Korea*

²*Laser Spectronix, Geumcheon-gu, Seoul, Republic of Korea*

Corresponding Author: H. J. Kong, hjkong@kaist.ac.kr

Laser fusion drivers requires a laser around 40 kJ at 10 ps for fast ignition. However, it is hard to produce such a high energy, high repetition rate laser because of the thermal problems. The output energy of current high repetition rate laser projects is at most 100 J, even with using the most advanced laser technologies. A coherent beam combining is one of the most promising technique to achieve such a high energy and high repetition rate laser. It has been shown experimentally that the coherent beam combination using self-phase-controlled SBS-PCMs is the simplest coherent beam combination method. Furthermore using a high energy and high repetition rate ns beam combination laser, a high energy, high repetition rate fs/ps laser can be generated by optical parametric chirped-pulse amplification (OPCPA). And so the laser fusion driver can be developed using the coherent beam combination laser.

The authors proposed a 0.54 MJ at 10 Hz practical LIFE (laser inertial fusion energy) driver. The LIFE driver is composed of 192 beamlines similar to NIF, a single beam line would have to produce at least 2.5 kJ at 10 Hz. It is suitably achieved by coherent 25 beams combination of 100 J double-pass amplifier modules having SBS-PCM. For 100 J modules, its SBS-cell focal spot load is over 100 W. Rotating wedge SBS-PCM should be used to relieve the thermal load in the SBS-cell focal spot. To reduce the thermal load in the SBS-cell focal spot, the rotating wedge self-phase-controlled SBS-PCM can be applied.

With the rotating wedge self-phase-controlled SBS-PCM, a real LIFE driver having a high energy, a high repetition rate can be developed through the coherent beam combination.



Present Operation Status of Target Injection System

K. Ishii¹, Y. Nishimura¹, Y. Mori¹, R. Hanayama¹, Y. Kitagawa¹, T. Sekine², T. Kurita²,
N. Sato², T. Kawashima², H. Kan², O. Komeda³, T. Nishi³, T. Hioki⁴, T. Motohiro⁴,
H. Azuma⁵, A. Sunahara⁶, Y. Sentoku⁷, and E. Miura⁸

¹Graduate School for the Creation of New Photonics Industries,
Hamamatsu, Shizuoka, Japan

²Hamamatsu Photonics, K.K., Hamamatsu City, Shizuoka, Japan

³TOYOTA Central R&D Labs Inc., Nagakute, Aichi, Japan

⁴Nagoya University, Nagoya, Japan

⁵Aichi Synchrotron Radiation Center, Seto-shi, Aichi-ken, 489-0965 Japan

⁶Institute for Laser Technology, Suita, Osaka, Japan

⁷University of Nevada, Reno, NV 89557, USA

⁸National Institute of Advanced Industrial Science and Technology (AIST), Tokyo, Japan

Corresponding Author: K. Ishii, ishii@gpi.ac.jp

The progress of the target injection system is reported, where deuterated polystyrene (CD) beads are injected and engaged by implosion and heating laser beams at the repetition rate of 1 Hz. Since the high repetition rate experiments require accurate positioning of the injected pellets, for two years we have continuously tested and improved the injected pellet positioning. Measuring the positions of the injected pellets is a required technology for target tracking and engagement. A newly developed shadowgraph system with two orthogonal probe beams has measured three-dimensional position of the flying targets for the first time. Using this shadowgraph system, we have evaluated the accuracy of the target injection, which will be useful for the future reactor system.

Suitability of Nano-Structured Materials for Inertial Fusion Reactor Inner Walls

R. C. Issac¹, T. Desai¹, and U. Cvelbar²

¹*Physics Department, Mar Athanasius College, Mahatma Gandhi University, Kerala, India*

²*Jožef Stefan Institute, 1000 Ljubljana, Slovenia*

Corresponding Author: R. C. Issac, rcisac@gmail.com

In this paper we present our experimental study for the development and investigation of suitable materials for protecting the IFE chamber wall from scattered laser light, energetic ions, electrons, neutrons, X-ray, etc., bombarding the chamber wall causing damage or activation in the wall material. We choose carbon nanotubes for the following reasons. Carbon nanotubes with its structural robustness, high thermal conductivity and promising mechanical properties are strong additives to various materials to attain enhanced tensile strength.

The purpose of our experiment is to study the effect of visible and IR laser radiation and energetic particles on carbon nanotube targets. Our present experimental facility include pulsed nanosecond lasers with energy up to 1 J per pulse and femtosecond Ti:Sa laser with intensity up to 10^{16} W/cm². In the first stage of experiments, we are measuring the optical limiting properties of the targets. We have irradiated planar 50–100 nm thick carbon nanotube films using a nanosecond laser beam at normal incidence. By measuring the transmitted intensity of the laser we explore the optical limiting behaviours of the material. In this series, results will be presented for carbon nanotube films with different thickness.

Carbon nanotube and other nano structured targets are prepared at the Jožef Stefan Institute, Slovenia. Details of the CNT target preparation and uniformity analysis using AFM will be presented. We are preparing ferromagnetic nanomaterials to be incorporated into metals like copper and tungsten. The idea is to incorporate magnetic nanoparticles into metals and study the residual magnetic field to check the possibility of reduced surface impact.

Initial target surface damage is recorded as a function of laser intensity using atomic force microscopy to establish optical damage threshold of these materials. Intensity on the target is varied from 10^{11} to 10^{13} W/cm². We analyze the optical damage caused on the surface of carbon and CNT targets from single to tens of multiple laser shots. Onset of laser induced damage on these targets is obtained using a Mach–Zehnder interferometer and optical emission diagnostics.

These analyzes explore the optical limiting behaviours of the materials. Details of the work will be presented.

Conceptual Design and Issue Analysis of Laser Fusion Experiment Reactor (LIFT)

T. Norimatsu¹, Y. Kozaki¹, H. Shiraga¹, H. Fujita¹, and K. Okano²

¹*Institute of Laser Engineering, Osaka University, Osaka, Japan*

²*Keio University, Yokohama, Japan*

Corresponding Author: T. Norimatsu, norimats@ile.osaka-u.ac.jp

In this work, we report a conceptual design of a laser fusion experimental reactor (LIFT) and an issue analysis of the design. After the demonstration of ignition and burn by a single shot in fast ignition experiment, construction of an experimental reactor will start. In order to bridge the technological gap between the single-shot experiment and a commercial reactor, an experimental reactor, LIFT, is conceptually designed based on a scheme of three phases. The full-scale laser will be constructed at the first phase and chambers will be constructed around the laser depending on the phase. The goal of phase I is to demonstrate repetitive fusion burns in a chamber without blankets. The goal of phase II is to show electric power generation in a dry-wall chamber with solid blankets. The goal of Phase III is long time operation with a wet-wall, and liquid LiPb blankets. Material test for commercial reactor is also important mission of this phase. Issues on the final optics and radiation safety will be also discussed.

MPT: Materials Physics and Technology



Recent Advances in Radiation Materials Science from the US Fusion Reactor Materials Programme

R. Stoller¹, C. Daniel², N. Ghoniem³, Y. Katoh¹, R. Kurtz⁴, J. Marian³, R. Odette⁵,
B. Wirth⁶, T. Yamamoto⁵, and S. Zinkle¹

¹*Oak Ridge National Laboratory (ORNL), Oak Ridge, TN 37831, USA*

²*Office of Fusion Energy Sciences, U.S. Department of Energy, Washington, DC 20585, USA*

³*University of California Los Angeles, CA 90095, USA*

⁴*Pacific Northwest National Laboratory (PNNL), Richland, WA 99354, USA*

⁵*University of California Santa Barbara, CA 93106, USA*

⁶*University of Tennessee, Knoxville, TN 37996, USA*

Corresponding Author: R. Stoller, rkn@ornl.gov

In addition to the engineering challenges associated with building and operating any complex facility, a range of critical materials issues must be addressed in order to make fusion power commercially viable. These include: 1) developing structural materials with suitably long lifetimes, 2) obtaining a plasma-facing material with sufficient ductility and low tritium retention, and 3) verifying the performance of functional materials such as electrical insulators, optical fibres, and tritium breeding materials. The US fusion reactor materials programme (FRM) has a well-developed focus on radiation effects in candidate structural materials and tungsten as a plasma-facing material. This includes both computational materials science and an extensive irradiation programme utilizing the High Flux Isotope Reactor at ORNL. Recent results from the US FRM programme will be discussed with an emphasis on advanced ferritic-martensitic steels, including the oxide-dispersion-strengthened and castable nanostructured alloy variants; SiC composites; and tungsten. The computational and experimental research is addressing the effects of helium produced by nuclear transmutation. In both the structural materials and tungsten, helium may increase tritium retention which has implications for operational safety in the event of an accident and for the successful recovery of tritium for use as fuel. In addition, it has been shown that low energy helium ions from the plasma may degrade the surface of tungsten components with the potential for increasing the amount of radioactive dust and plasma contamination.



Overview on Decade Development of Plasma-Facing Components at ASIPP

G.-N. Luo¹, G. H. Liu², Q. Li¹, S. G. Qin², W. J. Wang¹, Y. L. Shi², C. Y. Xie¹, Z. M. Chen³, M. Missirlian⁴, D. Guilhem⁴, M. Richou⁴, T. Hirai⁵, F. Escourbiac⁵, D. M. Yao¹, J. L. Chen¹, T. J. Wang², J. Bucalossi⁴, M. Merola⁵, and J. G. Li¹

¹*Institute of Plasma Physics, Chinese Academy of Sciences, Hefei, Anhui, People's Republic of China*

²*Advanced Technology & Materials Company, Haidian Beijing, People's Republic of China*

³*Xi'an Jiaotong University, Xi'an, Shanxi, People's Republic of China*

⁴*Commissariat à l'énergie atomique (CEA), 91400 Gif-sur-Yvette, France*

⁵*International Thermonuclear Experimental Reactor (ITER), Cadarache Centre, 13108 Saint-Paul-lès-Durance, France*

Corresponding Author: G.-N. Luo, gnyuo@ipp.ac.cn

The first EAST plasma was ignited in 2006 with nonactively-cooled steel plates as plasma-facing materials and components (PFMC) which was then upgraded into full graphite tiles bolted onto water-cooled copper heat sinks in 2008. The first wall was changed further into TZM in 2012, while keeping graphite for both of the upper and lower divertors. With rapid increase in H&CD power in EAST, the W/Cu divertor project was launched around the end of 2012, aiming at achieving actively-cooled full W/Cu-PFCs for the upper divertor, with heat removal capability up to 10 MW/m². The W/Cu upper divertor was finished in the spring of 2014, consisting of about 15 000 W monoblocks for 160 vertical targets, and 24 000 W flat tiles for 160 baffles and 80 domes, on 80 cassette bodies toroidally assembled.

Two different types of W/Cu actively-cooled PFCs for the project have been developed at ASIPP. The monoblock PFCs for vertical targets are manufactured by hot isostatic pressing (HIP) for cladding oxygen free Cu (OFC) to the inner surface of the W monoblocks, and then HIPing for the bonding between the clad monoblocks and CuCrZr cooling tube. The flat-tile PFCs for baffles and domes are manufactured by casting OFC onto the rear side of W tiles firstly, followed by HIPing of the W/OFC tiles onto CuCrZr heat sink plate. The nondestructive testing (NDT) quality control system has been established. In collaboration with IO and CEA teams, we have demonstrated our technology capability to remove heat loads of 5000 cycles at 10 MW/m² and 1000 cycles at 20 MW/m² for the small scale monoblock mockups, and surprisingly over 300 cycles at 20 MW/m² for the flat-tile ones.

Commissioning of the EAST upper W/Cu divertor in 2014 failed due mainly to leaks of e-beam welding between cooling tube and manifold box. After the campaign, we examined the leaking PFCs and reviewed the whole process, and then implemented several practical measures to improve connection design, component welding quality and installation welding reliability, which helped us achieve successful commissioning in 2015 campaigns.

Key technologies being developed at ASIPP for manufacturing W/Cu-PFCs have shown great performance against HHF testing. The experience and lessons we learned for batch production and commissioning are undoubtedly valuable for ITER engineering validation and tungsten-related plasma physics.

Advances in Understanding of High-Z Material Erosion and Redeposition in Low-Z Wall Environment in DIII-D

R. Ding¹, D. L. Rudakov², P. C. Stangeby³, W. R. Wampler⁴, T. Abrams¹, S. Brezinsek⁵, A. Briesemeister⁶, I. Bykov², V. S. Chan⁷, C. P. Chrobak⁷, J. D. Elder³, H. Guo⁸, J. Guterl¹, A. Kirschner⁵, C. J. Lasnier⁹, A. W. Leonard⁷, M. A. Makowski⁹, A. McLean⁹, P. B. Snyder⁷, D. M. Thomas⁷, D. Tskhakaya¹⁰, E. A. Unterberg⁶, H. Wang¹, and J. G. Watkins⁴

Rapporteured by: **G. N. Luo**

¹Oak Ridge Associated Universities (ORAU), Oak Ridge, TN 37831, USA

²University of California San Diego, CA 92093, USA

³Institute for Aerospace Studies, University of Toronto, Toronto, ON M5S-1A1, Canada

⁴Sandia National Laboratories (SNL), Albuquerque, NM 87185, USA

⁵Forschungszentrum Jülich, Jülich, Germany

⁶Oak Ridge National Laboratory (ORNL), Oak Ridge, TN 37831, USA

⁷General Atomics, San Diego, CA 92186, USA

⁸Institute of Plasma Physics, Chinese Academy of Sciences, Hefei, Anhui, People's Republic of China

⁹Lawrence Livermore National Laboratory (LLNL), Livermore, CA 94550, USA

¹⁰Institute for Applied Physics, Technische Universität Wien, 1040 Vienna, Austria

Corresponding Author: R. Ding, rding@ipp.ac.cn

Significant advances have recently been made in the understanding of erosion and redeposition of high-Z plasma facing components in a mixed materials environment, encouraging prospects on control of high-Z material erosion for future reactors. Dedicated DIII-D experiments, including modelling, reveal that the high-Z material net erosion rate is strongly affected by carbon concentration in the plasma and the magnetic pre-sheath, and is controllable with electrical biasing, or local gas puffing. Thin film tungsten (W) and molybdenum (Mo) samples of different diameters were exposed under well-diagnosed divertor plasma conditions in DIII-D using the divertor materials evaluation system (DiMES) to measure gross and net erosion rates by ion beam analysis. The net erosion rate of high-Z materials is strongly reduced by the high local redeposition ratio, itself mainly controlled by the electric field and plasma density within the magnetic pre-sheath. Modelling indicates a sheath potential decrease can suppress the erosion. Experiments have demonstrated the strong correlation of erosion with external biasing voltage. High carbon impurity concentration in the background plasma also reduces the net erosion rate of high-Z materials. Both DIII-D experiments and modelling show that local ¹³CH₄ injection creates a carbon coating on the metal surface. The ¹³C deposition provides quantitative information on radial transport from $E \times B$ drift and cross field diffusion. Moreover, new experiments show that local D₂ gas injection upstream of the W sample both reduced W net erosion rate by a factor 2 and increased the W redeposition ratio significantly, mainly by local plasma cooling. High-resolution measurements of the W erosion rate during and between ELM events near the outer strike point (OSP) demonstrate that peak W erosion during ELMs shifts away from the OSP radius, dramatically broadening the erosion profile at the divertor target. These new findings have significant implications for the understanding and active control of W divertor target operation in ITER with its low-Z beryllium first wall.

Work supported in part by the U.S. DOE under DE-AC05-06OR23100, DE-FG02-07ER54917, DE-AC04-94AL85000, DE-AC05-00OR22725, DE-FC02-04ER54698, & DE-AC52007NA27344.



Overview of Fuel Inventory in JET with the ITER-Like Wall

A. Widdowson¹, M. Rubel², G. Matthews³, E. Alves⁴, A. Baron-Wiechec¹, N. Barradas⁵, J. Beal¹, N. Catarino⁴, J. P. Coad¹, J. Likonen⁶, S. Koivuranta⁶, K. Heinola⁷, S. Krat⁸, M. Matej⁹, and P. Petersson²

¹United Kingdom Atomic Energy Authority, Culham Science Centre, Abingdon, UK

²KTH Royal Institute of Technology, Stockholm, Sweden

³Culham Centre for Fusion Energy (CCFE), Culham Science Centre, Abingdon, UK

⁴Institute of Plasmas and Nuclear Fusion (IPNF), Association EURATOM/IST, Lisbon, Portugal

⁵C2TN, Instituto Superior Técnico (IST), Lisbon, Portugal

⁶VTI Technical Research Centre of Finland Ltd., Espoo, Finland

⁷University of Helsinki, 00100 Helsinki, Finland

⁸National Research Nuclear University "MEPhI", Moscow, Russian Federation

⁹Max-Planck-Institut für Plasmaphysik, Garching, Germany

Corresponding Author: A. Widdowson, anna.widdowson@ukaea.uk

Post mortem analysis of components removed from the JET ITER-like wall (JET-ILW) provides an overall picture of long term fuel inventory. Results from the first 2011–'12 (ILW-1) and second 2013–'14 (ILW-2) JET-ILW campaigns are now available making a comprehensive overview possible. Overall plasma times for ILW-1 and ILW-2 are similar: ~6 h limiter plasma and ~14/~13 h divertor plasma; however variation in strike point distribution influences overall material migration and fuel retention.

Following ILW-1, the global long term fuel retention in JET-ILW is ~0.2% of injected fuel (deuterium, D) — at least an order of magnitude lower than the carbon wall configuration. Of this ~65% of the retained fuel is found in the divertor, with the remaining inventory located in the main chamber. Fuel retention at the inner divertor, 17×10^{22} D atoms, occurs predominantly by codeposition. The main deposition area is at the inner top horizontal surface where deposits $> 20 \mu\text{m}$ after ILW-2 are found. Overall the outer divertor surfaces remain a net erosion zone and have a lower fuel inventory, 3.9×10^{22} D atoms. Fuel retained on the bulk tungsten load bearing plate at the base of the divertor is $\sim 5 \times 10^{21}$ D atoms following ILW-1. This contributes only a small inventory to the divertor and is consistent with the surface being a net erosion zone. In the remote divertor corners deposition occurs by line of sight transport of neutrals sputtered from the SP; this demonstrates the influence of SP location on remote material migration. Analysis also shows that deposition and fuel retention is higher in the outer corner than the inner corner.

The total fuel inventory of plasma facing tiles in the main chamber contributes ~30%, 8.7×10^{22} D atoms, to the vessel inventory. Recessed areas, whilst having a relatively low concentration of fuel, can contribute significantly due to the large areas involved. Since the recessed areas do not interact with plasma ions, the fuel retention is due to implantation of charge exchange neutrals. Overall recessed areas and gaps in tiles contribute $> 30\%$ of the main chamber inventory, 4.6×10^{22} D atoms, with the recessed inner wall making the largest contribution.

MPT



Experimental Study of Deuterium Retention and Thermo-Mechanical Properties in Ion-Beam Displacement-Damaged Tungsten

G. Tynan¹, R. Doerner¹, J. E. Barton¹, R. Chen¹, S. Cui¹, M. Simmonds¹, Y. Wang², N. Mara², and S. Pathak²

¹University of California San Diego, CA 92093, USA

²Los Alamos National Laboratory (LANL), Los Alamos, NM 87545, USA

Corresponding Author: G. Tynan, gtynan@ucsd.edu

We present plasma-implanted D retention and thermo-mechanical properties in ion-beam displacement damaged tungsten targets. Cu ion beams with energies ranging from 0.5–5 MeV induce displacement damage of up to 1 dpa (displacement per atom) in the first micron of the surface in W samples held at a controlled temperature. Damaged samples are then exposed to D plasmas at 300–400 K to decorate damage sites with trapped D. Nuclear reaction analysis (NRA) and thermal desorption spectroscopy (TDS) are then used to characterize the effect of damage on D retention. Nano-indentation and nanoscale thermal diffusivity studies provide thermo-mechanical data localized to the near-surface damaged region in ion-beam damaged samples. In samples damaged at 300–400 K, NRA and TDS analyzes show the trapped D inventory increases in proportion to dpa^{0.65} for damage levels up to 0.1 dpa and begins to saturate as 1 dpa is approached. For W samples exposed to a D plasma ion fluence of 10²⁴/cm² with 0.2 dpa displacement damage at 300 K, the retained D retention inventory is 6 × 10²⁰ D/cm², about four times higher than in undamaged samples. The retained inventory drops to 2 × 10²⁰ D/cm² for samples damaged to 0.2 dpa at 1000 K, consistent with onset of vacancy annealing during the ion irradiation; at 1200 K damage temperature the D retention is reduced to 1 × 10²⁰ D/cm² and nearly equal to values seen in undamaged materials, suggesting that retention in high temperature radiation-damaged tungsten may not be affected as severely as might be expected at low temperatures. A 1D diffusion model with distributed trap sites reproduces the measured D spatial profiles in samples damaged at 300–400 K; work is underway to model to capture the reduced retention observed at higher damaging temperatures. The thermal conductivity of Cu ion-beam damaged surfaces drops from the unirradiated value of 182 W/mK to 53 ± 8 W/mK in W with 0.2 dpa damage at 770 K; slight further decreases occur at higher damage levels. The hardness increases from 5.3 GPa in undamaged W to 7.3 GPa for W damaged to 0.5 dpa with He ion beams, while no change in elastic modulus is found within the experimental uncertainties. We discuss the implications for the performance of W-based plasma-facing components, divertor heat flux management, tritium inventory management and fuel self-sufficiency in fusion energy systems.



ODS Steels: Nanostructure Evolution under Irradiation

S. Rogozhkin¹, A. Bogachev¹, O. Korchuganova¹, A. Nikitin¹, N. Orlov¹, A. Aleev¹, A. Zaluzhnyi¹, T. Kulevoy¹, B. Chalykh¹, R. Lindau², A. Möslang², P. Vladimirov², M. Klimenkov², M. Heilmaier², J. Wagner², and S. Seils²

¹National Research Centre "Kurchatov Institute", Moscow, Russian Federation

²Karlsruhe Institute of Technology (KIT), Karlsruhe, Germany

Corresponding Author: S. Rogozhkin, sergey.rogozhkin@itep.ru

Oxide dispersion strengthened steels providing exceptional high-temperature creep and irradiation resistance are presently being developed for fusion reactor. Excellent mechanical properties of ODS steels are directly related to the high density of homogeneously distributed, well-formed oxide particles (such as Y_2O_3 , or Y-Ti-O). However, atom probe tomography (APT) study of ODS steels revealed that they contain much higher amount of nanoclusters enriched in Y, O, V and Ti than of the oxide particles. The effect of these clusters on the mechanical properties and irradiation resistance of ODS steels and, especially, on the evolution of their chemical composition under irradiation has not been investigated in detail yet. Previous studies of the effect of irradiation on ODS EUROFER steel revealed an exchange of chemical elements between oxide particles and nanoclusters. For example, neutron irradiation at 300°C causes a significant change in nanocluster chemical composition: vanadium goes from clusters into the matrix, while yttrium and oxygen partially leave the oxide particles and enrich nanoclusters. A similar behaviour in ODS EUROFER was observed in APT samples irradiated with low energy Fe ions up to 30 dpa at room temperature.

In this work, we carried out atom probe tomography (APT) and transmission electron microscopy (TEM) studies of three different ODS steels produced by mechanical alloying: ODS EUROFER, 13.5Cr ODS and 13.5Cr-0.3Ti ODS. These materials were investigated after irradiation with Fe (5.6 MeV) or Ti (4.8 MeV) ions up to 10^{15} ion/cm² and part of them up to 3×10^{15} ion/cm². In all cases, areas for TEM investigation were cut at a depth of ~ 1.3 μ m from the irradiated surface corresponding to the peak of the radiation damage dose. It was shown that after irradiation at RT and at 300°C the number density of oxide particles in all the samples grew up. Meanwhile, the fraction of small particles in the size distribution has increased. APT revealed an essential increase in nanoclusters number and a change of their chemical composition at the same depth. The nanostructure was the most stable in 13.5Cr-0.3Ti ODS irradiated at 300°C: the increase of the fraction of small oxides was minimal and no change of nanocluster chemical composition was detected.



Tungsten Composite Materials for Fusion First Wall Applications

J. W. Coenen¹, J. Riesch², J.-H. You², H. Gietl², B. Jasper³, Y. Mao³, T. Hoeschen², A. Terra³, S. Sree⁴, C. Linsmeier³, C. Broeckmann⁴, and R. Neu²

¹Forschungszentrum Jülich, Jülich, Germany

²Max-Planck-Institut für Plasmaphysik, Garching, Germany

³Institute of Energy and Climate Research, Forschungszentrum Jülich, Jülich, Germany

⁴Lehrstuhl für Werkstoffanwendungen im Maschinenbau, RWTH Aachen, Aachen, Germany

Corresponding Author: J. W. Coenen, j.w.coenen@fz-juelich.de

The development of advanced materials is essential for sophisticated energy systems like a future fusion reactor, where multiple issues with respect to materials and components need to be evaluated. Brittle behaviour is the limiting factors when operating any W based plasma facing components (PFCs) in a tokamak. This is particularly crucial when considering material degradation from neutron-induced transmutation and embrittlement. Here tungsten fibre-reinforced tungsten composites (Wf/W) can mitigate these issues by utilizing extrinsic toughening mechanisms and therefore overcoming both intrinsic and neutron embrittlement. Extrinsic toughening for Wf/W is achieved similar to other composites by incorporating an interface between fibre and matrix allowing for additional energy dissipation without relying on intrinsic material properties such as ductility. The use of Wf/W could broaden the temperature window of W significantly and mitigate problems of cracking occurring typically in cyclic high heat flux loading. Wf/W as a material has been successfully produced and tested during the last years and the focus is now put on the technological realization for the use in PFCs as well as the further enhancement of production methods.

Here we present a way to utilize Wf/W composites for divertor applications by a fabrication route based on the both chemical vapour deposition or infiltration (CVD, CVI) of W and powder metallurgy (PM). Mock-ups based on the ITER typical design can be realized by the implementation of Wf/W-flat tiles or mono-block like approaches. In both cases, varying geometries for the introduction of fibres can be envisioned. For the CVD route, the furthest developed method is a concept based on a layered deposition approach allowing the production of flat tiles in the required geometry. One fibre layer after the other is positioned and ingrown into the W-matrix until the final sample size is reached. For the PM route development is progressing towards the use of pressure assisted sintering methods like field assisted sintering (FAST) and hot isostatic pressing (HIP). For multifibre PM-Wf/W special care needs to be taken developing a method for incorporating fibre and powder, while for the CVD Wf/W already large multifibre composites can be achieved. PM-Wf/W has only recently been shown to be able to achieve multifibre Wf/W.

Advanced Tungsten-Based Materials as an Option for a Fusion Reactor

C. Linsmeier¹, S. Brezinsek¹, M. Rieth², J.-H. You³, S. Antusch², J. W. Coenen⁴, R. Neu³, G. Pintsuk¹, and J. Riesch³

¹*Institute of Energy and Climate Research, Forschungszentrum Jülich, Jülich, Germany*

²*Karlsruhe Institute of Technology (KIT), Karlsruhe, Germany*

³*Max-Planck-Institut für Plasmaphysik, Garching, Germany*

⁴*Forschungszentrum Jülich, Jülich, Germany*

Corresponding Author: C. Linsmeier, ch.linsmeier@fz-juelich.de

Heat, particle and neutron loads are a significant challenge to first wall material lifetime when extrapolating from present devices to DEMO. For DEMO only, early design studies exist and detailed operational requirements are currently being developed. For a future fusion power plant, multiple issues with respect to materials and components need to be evaluated.

Tungsten is currently the main candidate material for the first wall of a fusion reactor as it is resilient against erosion, has the highest melting point of any metal and shows rather benign activation behaviour under neutron irradiation, as well as low tritium retention, which is beneficial to sustain the tritium fuel cycle. Despite its beneficial properties and its proposed use in ITER and DEMO as divertor material, W reveals various intrinsic problems when extrapolating to reactor conditions. Among those are the power handling capabilities and lifetime of the first wall and divertor plasma-facing components (PFCs). Crack formation by thermal shock and thermal fatigue, material modification due to neutrons as well as oxidation during accidental exposures are driving issues when deciding for new materials. Material solutions coping with neutron-induced effects such as transmutation, embrittlement and afterheat from are essential.

The development of advanced materials is essential for fusion, especially as for the next step devices, requirements on power exhaust, availability and lifetime are far more stringent, e.g., due to neutron irradiation. In particular, the PFCs can benefit from new approaches such as composites or new alloys. Here Wf/W composites as well as strengthened CuCrZr materials together with oxidation resilient W-alloys are promising solutions towards the realization of fusion reactor compatible materials. As part of the European strategy towards a first DEMO reactor, the development of advanced materials is addressed in several work packages, dealing with the divertor, the plasma-wall interface and the material development itself. When using materials in a fusion reactor environment a highly integrated approach is required.

This contribution highlights the progress for these advanced materials and composites. Focus is put on the materials roadmap of the EUROfusion consortium as a development line to enable construction and operation of a fusion reactor.



Overview of Recent Plasma-Material Interaction Studies in the Linear Plasma Device PSI-2

A. Kreter¹, M. Berger¹, D. Borodin¹, T. Dittmar¹, A. Eksaeva², A. Huber¹, S. Kraus¹, Y. Martynova¹, S. Möller¹, D. Nicolai¹, A. Pospieszczyk¹, M. Rasinski¹, M. Reinhart¹, B. Schweer¹, G. Sergienko¹, I. Sorokin², I. Steudel¹, A. Terra¹, B. Unterberg¹, M. Vogel¹, K. von Bover¹, M. Wirtz¹, Y. Yuan³, and C. Linsmeier¹

¹Forschungszentrum Jülich, Jülich, Germany

²National Research Nuclear University "MEPhI", Moscow, Russian Federation

³School of Physics and Nuclear Energy Engineering, Beihang University, 100191 Beijing, People's Republic of China

Corresponding Author: A. Kreter, a.kreter@fz-juelich.de

The fuel retention and the lifetime of plasma-facing components are critical plasma-material interaction factors potentially limiting the availability of a magnetic fusion reactor. Linear plasma devices are excellent test beds for investigating specific questions of plasma-material interaction. This contribution summarizes the recent plasma-material interaction studies on the linear plasma device PSI-2 focussing on the topics of fuel retention, erosion and evolution of surface morphology of metallic materials. The aim of these studies is the qualification of plasma-facing materials proposed for future fusion reactors: tungsten and reduced activation ferritic martensitic (RAFMs) steels. Depending on individual tasks, material samples were exposed either to pure deuterium or noble gas or mixed species plasma. The fraction of impurities such as helium, argon or nitrogen added to deuterium plasma was controlled by optical emission spectroscopy and in-situ mass analyzer. Exposure parameters were an electron density of $\sim 10^{17}$ – 10^{19} /m³, an electron temperature of 3–20 eV, an ion flux to the target of $\sim 10^{21}$ – 10^{23} /m²s and an incident ion energy of 20–300 eV, controlled by the target biasing. The sample temperature can be controlled in a range between 400–1400 K, covering the values for different first wall regions in a reactor. The incident ion fluence can be varied in a range between $\sim 10^{23}$ – 10^{27} /m² by extending the duration of exposure. A Nd:YAG laser ($\lambda = 1064$ nm) with a maximal energy per pulse of 32 J and a duration of 1 ms was used to apply repetitive heat loads for the ELM simulation on material samples. Optical emission spectroscopy (OES), target mass-loss technique and recently installed in-situ quartz microbalance (QMB) were employed to quantify the amount of eroded material. The deuterium retention was investigated by thermal desorption spectrometry (TDS) and nuclear reaction analysis (NRA). Scanning electron microscopy (SEM) including focussed ion beam (FIB) cross-sectioning and transmission electron microscopy (TEM) was used to observe the evolution of the surface morphology. The results and conclusions from the recent investigations on PSI-2 will be presented.

Smart Tungsten Alloys as First Wall Material for a Future Fusion Power Plant

A. Litnovsky¹, T. Wegener¹, F. Klein¹, C. Linsmeier¹, M. Rasinski¹, A. Kreter¹,
B. Unterberg¹, J. W. Coenen¹, C. Garcia-Rosales², A. Calvo², and N. Ordas²

¹Forschungszentrum Jülich, Jülich, Germany

²CEIT-IK4 Technology Center and Tecnun, Donostia – San Sebastián, Spain

Corresponding Author: A. Litnovsky, a.litnovsky@fz-juelich.de

Due to its low sputtering yield, excellent thermal conductivity and low tritium uptake, tungsten is currently deemed as most promising plasma facing material (PFM) for future power plant DEMO. However, in case of an accident the coolant supply may be damaged. The air can get into contact with PFMs during the air ingress. According to modelling, the temperature of PFMs can rise up to 1200°C due to nuclear decay heat. At this temperature, neutron-activated tungsten forms a volatile radioactive oxide which can be mobilized into the atmosphere. Therefore, tungsten oxidation must be avoided.

Self-passivating “smart” alloys are being developed to suppress tungsten oxidation. Smart alloys can adjust their properties to the environment. During plasma operation the preferential sputtering of lighter alloying elements will leave a pure tungsten surface facing the plasma. During an accident the alloying elements in the bulk form stable oxides thus protecting tungsten from mobilization.

The isothermal oxidation of thin film alloys produced by magnetron sputtering was carried out at 1000°C in the atmosphere containing 80 at.% of Ar and 20% of O₂. Oxidation resulted in the dramatic 6.4×10^6 fold reduction of the oxidation rate as compared to that of pure tungsten. Manufacture of bulk materials based on experience gained from the thin films is crucial. Bulk W-Cr-Ti samples were produced at CEIT (Spain) from mechanically alloyed powders treated by hot isostatic pressing at 1200°C at a pressure of 150 MPa.

Smart alloys and pure tungsten samples were exposed to a steady-state deuterium plasma under identical conditions in the linear plasma device PSI-2 at FZJ. The temperature of the samples was ~700°C, the energy of impinging ions was 210 eV matching well the conditions expected at the first wall of DEMO. The total fluence was 1.3×10^{26} ion/m². Weight loss measurements demonstrated similar mass decrease of smart alloys and of pure tungsten samples after exposure, implying that the sputtering rate of smart alloy is mostly defined by sputtering of its tungsten matrix. Investigations confirmed the preferential sputtering of alloying elements leaving almost pure tungsten facing the plasma as predicted with TRYDIN code. Plasma tests are followed by the oxidation of exposed samples comprising the first complete performance test of smart alloys in DEMO-relevant conditions.

Study of Properties of Tungsten Irradiated in Hydrogen Atmosphere

I. Tazhibayeva¹, M. Skakov¹, V. Baklanov¹, E. Koyanbaev¹, A. Miniyazov¹, T. Kulsartov¹,
Y. Ponkratov¹, Y. Gordienko¹, and Z. Zaurbekova¹

¹*Institute of Atomic Energy, National Nuclear Center, Kurchatov, Kazakhstan*

Corresponding Author: I. Tazhibayeva, tazhibayeva@ntsc.kz

The research goal is irradiation of tungsten samples in hydrogen and post irradiation studies of the samples for microstructure change after irradiation and comparison with nonirradiated samples. The tungsten samples of DF-grade, double forged pure, were manufactured in Jülich, Germany.

Irradiation of tungsten samples was carried out at the WWR-K reactor of Institute of Nuclear Physics, Almaty, Kazakhstan; irradiation time was 3255 hours or 135.6 days. Average temperature was 720°C. Tungsten samples were studied to obtain data on the extent of the changes in structure and physics-mechanical properties of the material as a result of reactor irradiation. Gamma spectrometric measurements to determine the isotopic composition and activity of the radioactive emitters in the tungsten samples were carried out using a spectrometric complex “InSpector” with scintillation detector, Canberra. Microstructural studies of tungsten samples irradiated in hydrogen and helium were carried out using the optical microscopes and scanning electron microscope. The experiments to study the parameters of hydrogen interaction with tungsten were carried out by thermo-desorption spectroscopy under linear heating with mass-spectrometer registration of the gases released during heating.

During the experiments we obtained the comparative characteristics of the microstructure and microhardness of tungsten samples, which were exposed to reactor irradiation in an atmosphere of hydrogen and helium; we determined hydrogen diffusion parameters in double forged pure tungsten, and W sorption characteristics towards hydrogen during reactor irradiation. The mechanism was proposed to describe the hydrogen interaction with tungsten during irradiation. Simulation experiments to study the effects of reactor irradiation on the characteristics of the hydrogen isotopes interaction with structural materials of fusion facilities will allow to establish correlation and synergistic effects between influence of fission and fusion reactors on the structural materials of fusion reactors.

This research has been performed in the framework of research project “Investigation of Changes in Structure and Properties of Tungsten Irradiated by Neutrons, Alpha-Particles and Heavy Ions within the Temperature Range up to 600° to Predict its Behaviour in Thermonuclear Fusion Reactors.”, CRP No. 17398, IAEA.



Structural Material Innovation for Advanced Blanket Design: Current Status and Future Prospect of ODS Steels R&D

A. Kimura¹, W. Han¹, H. Je¹, Y. Ha¹, R. Kasada¹, K. Yabuuchi¹, T. Takayama¹, D. Chen²,
T. Okuda³, S. Ukai⁴, S. Ohtsuka⁵, P. Dou⁶, and S. Noh⁷

¹*Institute of Advanced Energy, Kyoto University, Nishikyo-ku, Kyoto 615-8540, Japan*

²*Graduate School of Energy Science, Kyoto University, Nishikyo-ku, Kyoto 615-8540, Japan*

³*KOBELCO Research Institute, Kobe, Japan*

⁴*Hokkaido University, Sapporo, Hokkaido, Japan*

⁵*Japan Atomic Energy Agency (JAEA), Naka, Japan*

⁶*Chengqing University, Chongqing, People's Republic of China*

⁷*Korea Atomic Energy Research Institute (KAERI), Daejeon, Republic of Korea*

Corresponding Author: A. Kimura, kimura@iae.kyoto-u.ac.jp

Materials development is essential for realization of fusion DEMO reactor and beyond. High performance materials R&D has been conducted for the last several decades, and there have been made some remarkable technology innovations of fusion blanket structural material including first wall material. Among the several candidate blanket structural materials, oxide dispersion strengthened (ODS) steels, which have been produced by means of mechanical alloying, are considered to be promising for advanced nuclear systems with high thermal efficiency, because the ODS steels have high-strength at elevated temperatures and good resistance to corrosion and irradiation degradation.

There are several sorts of ODS steels with different Cr contents: (9–12)Cr-ODS ferritic/martensitic steels and (14–16)Cr-ODS ferritic steels with and without Al addition. The former two groups of ODS steels were developed for application to sodium cooled fast reactors and fusion reactors, and the last group of ODS steels were for so-called Generation IV nuclear systems. More recently, accident tolerant fuel R&D is progressing to apply high Cr/high Al ferritic ODS steels to fuel cladding of light water reactors because of “Fukushima Incident”. It has been considered that the replacement of zirconium alloys cladding with high-performance ferritic steels cladding may retard the hydrogen generation during a severe accident at a nuclear reactor, resulting in a large time lag up to hydrogen explosion.

In this presentation, current status of ODS steels R&D is summarized and the impacts of some material innovations on the safety issue of nuclear technologies are addressed. Radiation tolerance mechanism of ODS steels is introduced in terms of trapping capacity for radiation defects caused by nano-scaled ultrafine oxide particles dispersion. Furthermore, the recent experimental results on mechanical properties at elevated temperatures, aging effects, corrosion behaviour in super critical pressurized water and liquid lead alloy eutectics and phase stability under ion-irradiation of ODS steels are shown to demonstrate that the ODS steels with nano-scaled oxide particles in high number density are promising for radiation tolerant nuclear material.

Validation of Liquid Lithium Target Stability for Intense Neutron Source

H. Kondo¹, T. Kanemura¹, T. Furukawa¹, Y. Hirakawa¹, E. Wakai¹, and J. Knaster²

¹Japan Atomic Energy Agency (JAEA), Naka, Japan

²International Fusion Materials Irradiation Facility (IFMIF/EVEDA), Rokkasho, Aomori, Japan

Corresponding Author: H. Kondo, kondo.hiroo@jaea.go.jp

We report the validation results of liquid lithium target stability for an intense fusion neutron source, currently being planned as the International Fusion Materials Irradiation Facility (IFMIF), the advanced fusion neutron source (A-FNS), or the DEMO oriented neutron source (DONES). Thickness variation of the Li target must be suppressed to be within 1 mm inside a deuteron beam footprint to maintain the integrity of the Li target and guarantee the desired level of neutron flux. The engineering validation and engineering design activities (EVEDA) for the IFMIF are implemented under the broader approach (BA). As a major activity of the Li target facility, the EVEDA Li test loop (ELTL) was constructed by the Japan Atomic Energy Agency to validate the stability of the Li target envisaged in the IFMIF. Main validation results are 1) average target thickness variation was just 0.17 mm inside the beam footprint under the IFMIF conditions (target speed: 15 m/s, Vacuum pressure: 10^{-3} Pa, Li temperature: 250°C); 2) mean and maximum wave amplitudes were 0.26 mm and 1.46 mm, respectively, at the beam centre under the IFMIF conditions; 3) two-month long-term operation with one shutdown was performed, and the target stability was unchanged during the operation period; and, 4) all results satisfied the IFMIF requirements, and the Li target stability was successfully validated. From these results, we accomplished the engineering validation of the Li target stability for IFMIF, A-FNS and DONES, and achieved a significant milestone towards the next stage of those intense fusion neutron projects.



Design and Fabrication of the Active Cooling Divertor Components for HL-2M Tokamak

X. Liu¹, L. Cai¹, G. Zheng¹, and Y. Lian¹

¹*Southwestern Institute of Physics, Chengdu, Sichuan, People's Republic of China*

Corresponding Author: X. Liu, xliu@swip.ac.cn

HL-2M is a new tokamak machine under construction and advanced divertor configuration is one of the major targets. Snowflake and tripod divertor configurations can be performed with up to 3 MA plasma current and 25 MW heating power. The maximal wall load on divertor target plates will reach to 3–7 MW/m², depending on standard or advanced divertor configurations. Carbon fibre enhanced carbon (CFC) is selected as the armour materials, CuCrZr alloy and Inconel 625 are considered as heat sink and structural materials, respectively. Brazed CFC/CuCrZr flat plates with active cooling are designed as the divertor components.

Based on the database of CX-2002U and CuCrZr-IG, an open cassette divertor structure is designed for HL-2M. Thermal analysis of the target plates by ANSYS code indicated that the highest temperature under a wall load of maximal 10 MW/m² for 5 s loading time is lower than 1200°C at the cooling conditions of 4 Mpa inlet pressure and 4 m/s flux rate, this high temperature region located on a narrow region of the outboard target plates. When the wall load is reduced to 7 MW/m², the highest temperature will drop to 850°C. Mechanical analysis indicated that the stress is at an acceptable level of the materials and the bonding interface. Moreover, based on the maximal halo current an induced electromagnetic force was estimated and it is also in a safe range.

Two kinds of technologies of CFC joining with CuCrZr alloy are investigated. One is a slurry method and another is direct vacuum brazing method. Small scale samples have been prepared by both methods. Metallurgical observation identified a dense carbides layer formed on CFC surface. Shear tests indicated that the fracture took place within the CFC tiles, demonstrating the bonding strength was much higher than the shear strength of this CFC. Preliminary thermal fatigue experiments in a 60 kW electron-beam facility (EMS 60) showed that the small scale CFC/CuCrZr mockups can withstand 10 MW/m² heat flux. Further optimization of the CFC joining with CuCrZr techniques is under way. It is expected that one of the joining technologies will be used for the series production of HL-2M divertor components.



Progress on the Development of Linear IFMIF Prototype Accelerator and the Beam Commissioning

A. Kasugai¹, J.-M. Ayala², N. Bazin³, P.-Y. Beauvais⁴, L. Bellan⁵, B. Branas⁶, B. Bolzon³, P. Cara⁴, N. Chauvin³, S. Chel³, M. Comunian⁵, H. Dzitko⁴, A. Facco⁵, E. Fagotti⁵, D. Gex⁴, R. Gobin³, F. Harrault³, R. Heindinger⁴, R. Ichimiya¹, D. Jimenez-Rey⁶, J. Knaster², K. Kondo¹, A. Marqueta², J. Marroncle³, P. Mendez⁶, J. Molla⁶, S. Ohira¹, Y. Okumura², M. Perez², G. Phillips⁴, A. Pisent⁵, I. Podadera⁶, G. Pruneri², B. Renard³, K. Sakamoto¹, F. Scantamburlo², F. Senee³, K. Shinto¹, M. Sugimoto¹, H. Takahashi¹, and M. Valette³

¹National Institutes for Quantum and Radiological Science and Technology (QST), Rokkasho Fusion Institute, Rokkasho-mura, Aomori, Japan

²International Fusion Materials Irradiation Facility (IFMIF/EVEDA), Rokkasho, Aomori, Japan

³Commissariat à l'énergie atomique (CEA/Saclay), 91191 Gif-sur-Yvette, France

⁴F4E: Fusion for Energy, ITER EU Centre, 08019 Barcelona, Spain

⁵Istituto Nazionale di Fisica Nucleare (INFN), Laboratori Nazionali di Legnaro, Legnaro, Italy

⁶Centro de Investigaciones Energéticas, Medioambientales y Tecnológicas (CIEMAT), Madrid, Spain

Corresponding Author: A. Kasugai, kasugai.atsushi@qst.go.jp

In the beam commissioning of the injector of linear IFMIF prototype accelerator (LIPAc) at the International Fusion Energy Research Center in Rokkasho, Japan the initial target performances was accomplished for radio frequency quadrupole (RFQ) accelerator, of which assembling and commissioning will be started in 2016.

At present, 100 keV/120 mA at 20% duty cycle deuterium and 50 keV/74 mA at 10% duty cycle hydrogen ion beams have been extracted stably from a 12 mm diameter aperture and transported up to RFQ entrance point with a low beam emittance of 0.32π mm mrad (rms, normalized). Neutron production by DD reaction up to 2.4×10^9 n/s has been observed at the target of the emittance scanner whose front surface is covered by tungsten armour.

Hydrogen Isotope Retention in Tungsten Surface-Modified by Heavy Ion Irradiation, Helium Bubbles and Tungsten Deposition

M. Sakamoto¹, H. Tanaka¹, H. Watanabe², N. Yoshida², M. Tokitani³, S. Ino¹,
A. Terakado¹, N. Ezumi¹, and Y. Nakashima¹

¹Plasma Research Center, University of Tsukuba, Tsukuba, Ibaraki, Japan

²Research Institute for Applied Mechanics (RIAM), Kyushu University, Kasuga, Japan

³National Institute for Fusion Science (NIFS), Toki, Gifu, Japan

Corresponding Author: M. Sakamoto, sakamoto@prc.tsukuba.ac.jp

Tungsten is a candidate material for plasma facing components of DEMO as well as divertor plates of ITER, because it has favourable properties such as a very low solubility for hydrogen isotopes. However, surface condition of the plasma facing material is certainly changed by plasma-wall interaction (PWI). Such a surface modification could affect a property of H isotope retention which is a key concern for safety hazards as well as particle control. It is important to investigate relation between change in microstructure due to PWI and H isotope retention but such studies are few. In this paper, two kinds of experiments have been carried out to study H isotope retention in surface-modified W taking microstructure of the surface modification into account using a compact PWI simulator APSEDAS. One is damage level dependence for W irradiated by 2.4 MeV Cu²⁺ ions as surrogate of neutron irradiation. The other is D fluence dependence for W with a He bubble layer, W with a W deposited layer and pure W.

Hydrogen isotope retention in W irradiated by 2.4 MeV Cu²⁺ ions as surrogate of neutron irradiation increased significantly with the damage level up to 0.4 dpa and then saturated. A new desorption peak appeared at ~840 K in a thermal desorption spectra due to the heavy ion irradiation, which is attributed to nano-voids and vacancy clusters. On the other hand, the D retention in W with He bubbles became saturated for fluence over 1×10^{25} D/m², although retention in pure W increased with square-root dependence of the fluence. Retention in W with a W deposited layer with the thickness of ~30 nm was ~5 times lower than that of pure W. The surface modifications of He bubbles and W deposition seem to play a role of diffusion barrier for the mobile D atoms.

Material Properties and their Influence on the Behaviour of Tungsten as Plasma Facing Material

M. Wirtz¹, V. Barabash², F. Escourbiac², T. Hirai², J. Linke¹, T. Loewenhoff¹, S. Panayotis², G. Pintsuk¹, and I. Uytendhouwen³

¹Forschungszentrum Jülich, Jülich, Germany

²International Thermonuclear Experimental Reactor (ITER),
Cadarache Centre, 13108 Saint-Paul-lès-Durance, France

³SCK•CEN, Belgian Nuclear Research Centre, 2400 Mol, Belgium

Corresponding Author: M. Wirtz, m.wirtz@fz-juelich.de

Plasma facing materials (PFMs) for future fusion devices like ITER have to withstand severe environmental conditions such as steady state and transient thermal loads as well as high particle (H, He, n) fluxes. The design and the performance of plasma facing components (PFCs), such as the divertor targets, strongly depend on the selection of suitable PFMs, e.g., refractory metals, which meet certain predetermined specifications. For the ITER PFMs, material specifications have been set up in the past, which may need further refinement in order to select optimum candidates from a variety of commercially available products. This should help to mitigate material degradation during operation such as macro-crack formation in monoblock type PFCs, i.e., so called self-castellation, which extend from the plasma facing surface down to the W/Cu-interface.

For a possible improvement of the material specification, five different tungsten products manufactured by different companies and by different densification technologies, e.g., forging and rolling, are subject to a detailed microstructural and mechanical materials characterization programme. Additional material characterization for two of these tungsten products was performed to investigate the thermo-mechanical performance under intense transient thermal loads, which represent typical ELM or disruption like conditions. The thermal shock tests were performed by electron beam exposure in JUDITH 1 and 2 with different energy densities, base temperatures and pulse numbers in order to determine damage and cracking thresholds.

The obtained mechanical properties in combination with the thermal shock tests show that the thermal shock damage response strongly depends on the microstructure and hence the related mechanical properties of the tungsten product. High mechanical strength leads to less damage formation in terms of crack formation and plastic deformation. In contrast, recrystallized materials, providing the lowest mechanical strength, show severe surface damages such as thermal shock crack networks and surface roughening due to the reduced strength and cohesion between single grains. Accordingly, the materials were, amongst others, identified with respect to their recrystallization resistance and the related feature of a deferred material degradation, e.g., under slow transients up to 20 MW/m² during normal ITER operation.



Assessment of Corrosion Behaviour of Reduced Activation Ferritic/Martensitic Steel, F82H in High Temperature Water

M. Nakajima¹, T. Hirose¹, H. Tanigawa¹, H. Tanigawa², and Y. Kawamura¹

¹Japan Atomic Energy Agency (JAEA), Naka, Japan

²Japan Atomic Energy Agency (JAEA), Rokkasho, Aomori, Japan

Corresponding Author: M. Nakajima, nakajima.motoki@jaea.go.jp

Water cooled ceramic breeder concept is a primary candidates for ITER and DEMO blankets of Japan. In this blanket, the pressurized water of 15 MPa between 558 K to 598 K is used as the coolant. In such blanket, the structural material is required to be as thin as possible for tritium breeding. However, the pressure tightness is required to withstand 15 MPa of internal pressure. Therefore one of possible issues of such blanket concept is to understand the corrosion mechanism of structure materials in high temperature pressurized water in the operating temperature range. However, available data on the corrosion of reduced activation ferritic/martensitic steel (RAFM) in simulated PWR environment are limited. In this study, the temperature and DO dependencies of corrosion properties of RAFM, F82H were investigated using rotating disk specimen in autoclave. Based on the results obtained from corrosion test, all of the static corrosion test specimens demonstrate weight gain after the corrosion test in any temperature. The all of the rotated disk specimens of DO 0.02 mg/l showed weight loss after the corrosion test. In contrast, the results of rotated disk specimen tested at DO 8 mg/l were almost same as the static specimen. Additionally, the weight changes of static and rotated disk specimen tested at DO 8 mg/l were smaller than those of DO 0.02 mg/l specimen in any temperature. Based on the results of SEM observation and XRD measurement, the oxide particles were not observed on the surface of rotated disk specimen tested at DO 0.02 mg/l in any temperatures. On the other hand, the oxide particles were still observed on the DO 8 mg/l specimen even if the temperature changes. Based on the results of XRD measurement, the dominant oxides of static specimen in DO 0.02 mg/l condition and DO 8 mg/l condition were magnetite and hematite respectively. Considering these results, it can be concluded that the inhibition of flow accelerated corrosion at DO 8 mg/l was caused by the surface oxide which act as the diffusion barrier of Fe ion transport. In any events, it was desirable to control the DO concentration up to 8 mg/l, because the effects of temperature and water flow on corrosion behaviour were significantly suppressed. Based on these results, it was revealed that the high-DO operation is necessary to suppress the flow accelerated corrosion in the blanket system.



Investigation of W/Cu Functionally Graded Material with CMA Particles as Plasma Facing for First Wall Components

N. Nemati¹, S. M. Sadat Kiaii¹, and A. Sadighzadeh¹

¹*Nuclear Science and Technology Research Institute (NSTRI), Tehran, Islamic Republic of Iran*

Corresponding Author: N. Nemati, narguess.nemati@ut.ac.ir

Ten-layered (100 wt.%W 90 wt.%W / 10 wt.%Cu 80wt.%W / 2wt.%0Cu ... 100 wt.%Cu) W/Cu functionally graded material (FGM) with dispersion of Al₁₃Fe₄ CMA particles was synthesized by powder metallurgy technique at different temperatures for 1 h under a load of 650 MPa. The influences of different sintering processes on relative density, hardness, neutron irradiation resistance and microstructure at various layers of sintered samples were investigated. The experimental results indicated that the graded structure of the composite by addition of CMA nanoparticles could be well densified after the hot press process. The relative density increased with the increment of sintering temperature and it was up to 96.53% as sintered at 850°C. In addition, the coefficient of friction reached 0.1 at room temperature and 0.14 at 400°C, which could be ascribed to the specific heat resistant and heat sink properties of the CMA and Cu content respectively enwrapped by net-like Cu. And the Vickers hardness was converted from 5.2 to 5.68 GPa with in the different zones of the bulk graded material.



Investigation of Lanthanoid-Doped APLF Scintillators for Neutron Detection

T. Shimizu¹, Y. Arikawa¹, T. Murata², K. Yamanoi¹, M. J. F. Empizo¹, H. Shiraga¹, M. Nakai¹, N. Sarukura¹, T. Norimatsu¹, H. Nishimura¹, H. Azechi¹, S. Fujino³, H. Yoshida⁴, K. Kamada⁵, Y. Usuki⁵, A. Yoshikawa⁶, N. Izumi⁷, N. Satoh⁸, and H. Kan⁸

¹*Institute of Laser Engineering, Osaka University, Osaka, Japan*

²*Kumamoto University, Kurokami, Kumamoto, Japan*

³*Kyushu University, Kasuga, Japan*

⁴*Ceramic Research Center of Nagasaki, Hasami, Higashisonogi, Nagasaki, Japan*

⁵*Furukawa Co., Ltd, Kamondai, Tsukuba, Ibaraki, Japan*

⁶*Institute for Materials Research (IMR), Tohoku University, Sendai, Miyagi, Japan*

⁷*Lawrence Livermore National Laboratory (LLNL), Livermore, CA 94550, USA*

⁸*Hamamatsu Photonics, K.K., Hamamatsu City, Shizuoka, Japan*

Corresponding Author: T. Shimizu, shimizu-t@ile.osaka-u.ac.jp

Investigating the fusion plasma is necessary to control the fusion process and to understand the plasma dynamics. Down-scattered (DS) neutrons detection is much suitable for measurement of the areal-density. We have demonstrated that lanthanoid-doped $20\text{Al}(\text{PO}_3)_3\text{-}80\text{LiF}$ (APLF) has excellent characteristics as DS neutron scintillators. In this paper, the properties of lanthanoid-doped APLF scintillators for neutron detection was investigated.

Required temporal resolution of scintillators for DS neutron detection is less than 10 ns. The temporal resolution depends on fluorescence wavelength of luminescence centre ion. Different lanthanoid-doped APLF samples were prepared by melt-quench method for evaluation. Time-resolved spectroscopy using vacuum ultraviolet laser was used to assess the fluorescence decay times of each sample. Among all samples, the Nd-doped has the fastest time of 6.6 ns. When compared to the fluorescence decay time of a standard scintillator, GS2 with 38.1 ns, the lanthanoid doped APLFs exhibit better decay times by more than 10 ns.

The fluorescence decay time of a Pr-doped APLF was also evaluated using different radioactive sources. The Pr-doped APLF exhibits fast fluorescence lifetime compared to GS2 by one order of magnitude regardless of the excitation source. Nd-doped APLF exhibits the fastest decay time of 6.6 ns. The fluorescence of the Pr-doped and GS2 using three different radiation sources were also compared. Though the light output of the doped APLF is lower, the fluorescence intensity can still be detected. Lanthanoid-doped APLFs can be better alternatives to conventional scintillators for neutron detection. Further developments on lanthanoid-doped APLF based neutron scintillators are highly anticipated.

In addition, this Pr-doped APLF scintillator was applied to development of a multichannel low-energy neutron spectrometer, and was actually used to detect DS neutrons in the recent fusion experiment using GEKKO XII. As a result, DS neutrons were successfully detected. We are confident that our scintillator will be a powerful tool of fusion experiment.



Effects of Modified Surfaces Produced at Plasma-Facing Surface on Hydrogen Isotopes and Helium Release Behaviour in the LHD

Y. Nobuta¹, S. Masuzaki², M. Tokitani², D. Nagata², N. Ashikawa², N. Yoshida³, Y. Oya⁴, M. Yajima², G. Motojima², H. Kasahara², M. Miyamoto⁵, and N. Ohno⁶

¹*Hokkaido University, Sapporo, Hokkaido, Japan*

²*National Institute for Fusion Science (NIFS), Toki, Gifu, Japan*

³*Kyushu University, Kasuga, Japan*

⁴*Shizuoka University, Shizuoka, Japan*

⁵*Shimane University, Matsue, Shimane, Japan*

⁶*Graduate School of Engineering, Nagoya University, Nagoya, Japan*

Corresponding Author: Y. Nobuta, y-nobuta@eng.hokudai.ac.jp

In the present study, long-term samples made of stainless steel, which is the same material as the first wall panels in the LHD, were mounted at a lot of places on the plasma-facing surface in the LHD during the 17th experimental campaign (FY2013) and the surface modifications caused by plasma-surface interactions were evaluated. In addition, in order to investigate hydrogen isotopes release behaviour of the modified surface, a deuterium (D) ion beam irradiation against the long-term samples was performed after the experimental campaign and the desorption behaviour of D retained in the sample was investigated with thermal desorption spectroscopy (TDS). Since the samples were exposed to several months of hydrogen (H) plasma operation in the LHD, H retained in the sample should exist at much deeper regions compared to the additionally implanted D. Therefore, the H and D desorption behaviours could give useful information to understand release behaviour of hydrogen isotopes from the modified surface and deeper regions.

For most of the first wall samples, which were mounted far from graphite divertor tiles, little deposition was seen and helium (He) bubbles with diameter of 1–10 nm produced by He main and glow discharges were clearly observed within the depth of ~50 nm from the surface. On the other hand, for the divertor samples located in the vicinity of the divertor tiles, a thick (1–2 μm) carbon layer were observed. The desorption behaviour of D significantly depended on the surface conditions. For the first wall samples, D₂ desorbed at lower temperature of 350 K to 600 K, while H₂ desorbed mainly in the temperature range higher than 500 K. The D₂ desorption spectra for the divertor samples had a major peak at around 1050 K, which was similar to that of H₂. The present study revealed that D trapped at the modified surface in erosion dominant area desorbed at much lower temperatures than that in carbon deposition area. This suggests that H release from erosion dominant area could be more significant when the wall temperature increases during a long pulse discharge in the LHD. A He ion beam irradiation against the long-term samples is in progress and the difference of desorption behaviour between hydrogen isotopes and He at the modified surface will also be discussed.



Development of Dissimilar-Metals Joint of Oxide-Dispersion-Strengthened (ODS) and Non-ODS Reduced-Activation Ferritic Steels

T. Nagasaka¹, H. Fu¹, T. Muroga¹, W. Guan², S. Nogami², H. Serizawa³, A. Hasegawa²,
A. Kimura⁴, S. Ukai⁵, T. Tanaka¹, and A. Sagara¹

¹National Institute for Fusion Science (NIFS), Toki, Gifu, Japan

²Tohoku University, Sendai, Miyagi, Japan

³Joining and Welding Research Institute, Osaka University, Osaka, Japan

⁴Kyoto University, Nishikyo-ku, Kyoto 615-8540, Japan

⁵Graduate School of Engineering, Hokkaido University, Sapporo, Hokkaido, Japan

Corresponding Author: T. Nagasaka, nagasaka@nifs.ac.jp

Reduced-activation ferritic steels and their oxide-dispersion-strengthened (ODS) alloys are promising structural material for fusion blanket. The ODS steels are superior to the non-ODS steels in heat resistance and neutron irradiation resistance, however inferior in mass production. Since high temperature and high neutron dose area is limited at only the first wall section of the blanket, minimized application of ODS steels there is the most effective to utilize the advantage of ODS steels. In order to prove the feasibility of this advanced concept, dissimilar-metals joint of 9Cr-ODS steel and JLF-1 non-ODS steel were fabricated with electron-beam welding (EBW) and hot isostatic pressing (HIP) processes. Welding conditions were optimized based on systematic experiments with change in fabrication process parameters.

Hardening occurred in weld metal and heat-affected zones of EBW joint, and in base metals of HIP joint. The hardening is due to formation of quenched martensite phase. Since the hardening induces ductility loss, post-weld heat treatment (PWHT) was carried out for hardness recovery. In the case of EBW joints, the complete recovery of hardness was obtained by tempering at 780°C for 1 h. In the case of HIP joint, carbide coarsening in the base metals and decarburization around the bonding interface were observed, in addition to the formation of quenched martensite. In order to recover all these microstructural changes, normalizing at 1050°C for 1 h was required before the tempering. Tensile strength of the EBW joint was 580 MPa after the PWHT, and is equivalent to that of JLF-1 before EBW. Tensile strength of the HIP joint after the PWHT depends on HIP temperature. It was 370 MPa, 660 MPa and 580 MPa for 1000°C, 1050°C and 1100°C HIP specimens, respectively. The 1050°C and 1100°C HIP specimens fractured in JLF-1 base metal, while the 1000°C HIP specimen fractured at the bonding interface. Thus, 1050°C and 1100°C are suitable for HIP temperature to maintain the strength of joint.

Requirements for the dissimilar-metals joint in the structure design are the strength no less than that of JLF-1 base metal and no fracture at the bonding interface. These requirements are satisfied with proper welding conditions including PWHT. In conclusion, the advanced blanket utilizing ODS steels is feasible by using the bonding techniques developed in the present study.

BCA-KMC Hybrid Simulation with Meta-Modelling for Hydrogen Dynamic Retention in Tungsten Material

A. Ito¹, S. Kato², and H. Nakamura¹

¹National Institute for Fusion Science (NIFS), Toki, Gifu, Japan

²Doshisha University, Kyoto, Japan

Corresponding Author: A. Ito, ito.atsushi@nifs.ac.jp

To achieve the fuel balance and recycling in ITER and DEMO reactors, it is necessary to understand hydrogen behaviour in plasma facing materials. Because the plasma-wall interaction is determined by particle balance between the flux of plasma particles and the diffusivity in materials, the reproduction of realistic flux and fluence corresponding to experiments is a key issue in simulation. In the previous conference, the formation of the fuzzy nanostructure induced by helium plasma irradiation had been successfully represented by molecular dynamics and Monte Carlo (MD-MC) hybrid simulation which can treat the realistic flux, $10^{22}/\text{m}^2\text{s}$, and fluence, $0.5 \times 10^{22}/\text{m}^2$, corresponding to experimental conditions. In this paper, we further develop the hybrid simulation and propose multiscale meta-modelling (MSMM) as follows.

To estimate retained hydrogen amount in tungsten materials under the realistic flux and fluence condition, binary collision approximation and kinetic Monte Carlo (BCA-KMC) hybrid simulation has been developed. In the BCA-KMC hybrid simulation, the BCA part treats the collision cascade process of incident plasma particles and the KMC part treats the diffusion processes of hydrogen isotope atoms and vacancies in a tungsten material. The elapsed time can reach 10^{-2} s beyond 10^{10} times the gap of their time scales. By the BCA-KMC hybrid simulation, hydrogen retention amount at laboratory experiment flux, $10^{20}/\text{m}^2\text{s}$, to ITER divertor environment flux, $10^{24}/\text{m}^2\text{s}$ have been estimated. As a result, the retained hydrogen amount in the case of $10^{24}/\text{m}^2\text{s}$ is at least 10 times higher than that of $10^{22}/\text{m}^2\text{s}$.

Furthermore, we enhance the reproducibility of the KMC in terms of grain boundaries. In general, the KMC model is created by using the density functional theory (DFT) calculation. However, the calculation speed of the DFT is too slow to find many migration paths in grain boundaries. In the MSMM, the KMC model for the migration paths is automatically constructed by using the MD. The reliability of this automatic KMC modelling depends on the accuracy of the potential model of MD. The potential model of MD is improved by comparison with the DFT in terms of many sample structures. Thus, in the MSMM, almost all parameters are determined from the MD with the DFT level accuracy.

Status and Strategy of CLAM Steel for Fusion Application in China

Q. Huang¹

¹*Institute of Nuclear Energy Safety Technology, CAS, Anhui, People's Republic of China*

Corresponding Author: Q. Huang, qunying.huang@fds.org.cn

A programme for fusion reactor structural material, i.e., the China Low-Activation Martensitic (CLAM) programme, aims to satisfy the material requirements for test blanket module (TBM) for ITER, China fusion engineering test reactor (CFETR) and fusion demonstration reactor (C-DEMO) in China. It has been undertaken by INEST (Institute of Nuclear Energy Safety Technology), CAS (Chinese Academy of Science) since 2001 under support (among others) from the Ministry of Science and Technology of China, and with wide domestic and overseas collaborations. The status and strategy of the CLAM steel project are reviewed in this presentation.

CLAM steel has been chosen as the primary structural material for the Chinese helium cooled ceramic breeder (CN HCCB) TBM for ITER. Much progress of the CLAM project has been achieved with the efforts in the past fifteen years, including large scale fabrications, various physical and mechanical property tests, series of neutron irradiation experiments up to 21 dpa, long-term corrosion experiments in flowing liquid PbLi up to 20 000 h, different scaled TBM mockup fabrications, development and establishment of material database, and so on.

To license pressurized nuclear equipment, e.g., the ITER TBM and the blanket for DEMO, it needs to present the design and safety analyzes with sufficient data such as the consolidated materials data, design limits and qualified fabrication procedures specifications, etc., to the regulator (ESP/ESPN) and the agreed notified body (ANB) of France or nuclear safety agency of China. A lot of effort and work are being devoted to the R&D of CLAM steel to its final successful application in the fusion systems. Its properties database got basically meets the requirement of the qualification for ITER-TBM.

Small Specimen Test Technology Development towards Design of Fusion DEMO Reactors and Future Direction Plan

E. Wakai¹, S. Nogami², Y. Ito¹, A. Kimura³, H. Tanigawa¹, M. Sugimoto¹, M. Ando¹, A. Hasegawa², A. Nishimura⁴, R. Kasada³, M. Saito⁵, F. Arbeiter⁶, J. Knaster⁷, and S. M. González de Vicente⁸

¹Japan Atomic Energy Agency (JAEA), Naka, Japan

²Tohoku University, Sendai, Miyagi, Japan

³Kyoto University, Nishikyo-ku, Kyoto 615-8540, Japan

⁴National Institute for Fusion Science (NIFS), Toki, Gifu, Japan

⁵Hachinohe Institute of Technology, Hachinohe, Aomori-ken, Japan

⁶Karlsruhe Institute of Technology (KIT), Karlsruhe, Germany

⁷International Fusion Materials Irradiation Facility (IFMIF/EVEDA), Rokkasho, Aomori, Japan

⁸International Atomic Energy Agency (IAEA), Vienna, Austria

Corresponding Author: E. Wakai, wakai.eiichi@jaea.go.jp

Small specimen test technology or technique (SSTT) towards design of fusion DEMO reactors was investigated and evaluated in the related studies of the International Fusion Materials Irradiation Facility / Engineering Validation and Engineering Design Activities (IFMIF/EVEDA) project under the Broader Approach (BA) agreement between EURATOM and the Japanese Government. The main results are described as follows:

1. The master curve which is an evaluation method for the ductile-brittle transition temperature behaviour of the materials was found in the difference between F82H steel and EUROFER97 steel, and the optimization curve for F82H steel with sizes from 0.16CT (small size) to 1CT (standard size) was evaluated as an equation: $K_{JC-1T(\text{med})} = 30 + 70 \exp 0.05(T - T_o)$ in this study, where T is the test temperature, T_o is the reference fracture toughness transition temperature, using a random inhomogeneous model.
2. In the studies of the effects of size and shape on fatigue properties of F82H steel, a good correlation at room temperature was obtained between the small specimen with a diameter of 1 mm in the centre of round bar and the standard size with 10 mm. No size effect on the fatigue life was recognized in the test section with diameters ranging from 1 mm to 10 mm. In a hourglass specimen, the crack initiation life was shortened with a smaller diameter because of the influence of stress concentration, which result in a fatigue life shorter than that of standard specimens in the low strain condition without plastic strain.
3. The crack growth rate (CGR) of F82H steel using a wedge-opening load (WOL) type specimen with 1/4T (small size) and 3/4T (almost standard) in the water was examined, and the value was a slightly lower than that of 304 stainless steel.

SSTT standardization of RAFM steels and the other materials, which will be tested in the irradiation facilities, has to be established for design of fusion DEMO reactors, and it is desirable to establish firstly the test standard and the methodology for the nonirradiation materials of the fusion structural materials. Then, we also have to consider and establish the standardization for the irradiated materials containing transmutation atoms generated by the irradiation, such as helium.

Impact of Helium Ion Energy Modulation on Tungsten Surface Morphology and Nano-Tendrils Growth

K. B. Woller¹, D. G. Whyte¹, and G. M. Wright¹

¹*Plasma Science & Fusion Center, MIT, Cambridge, MA 02139, USA*

Corresponding Author: K. B. Woller, kbwoller@mit.edu

Helium (He) ion energy modulation is demonstrated, for the first time, to affect the development of the tungsten (W) nano-tendrils morphology that results from He irradiation. Dramatically isolated nano-tendrils bundles (NTBs) grow from the surface instead of a uniform nano-tendrils layer, or so called fuzz, leaving ~90% of the surface without nano-tendrils growth at all. The growth parameters for NTBs are the same as for fuzz except for the radiofrequency modulation of the ion energy. Analyses of the newly discovered NTB growth regime strongly support models of nano-tendrils growth that take adsorbed atom (adatom) kinetics as their basis. Additional modelling of the ion energy distribution function of the ITER divertor must take place in order to assess the scope of nano-tendrils growth that might occur, and of what type. Through mass loss measurements and electron microscopy, the minimally supported NTBs are shown to be a greater threat to plasma-facing component erosion and dust production than previously observed for uniform fuzz.



Deuterium Retention and Melting Behaviour in Toughened, Fine-Grained Recrystallized Tungsten

M. Oya¹, H. T. Lee¹, K. Imano¹, H. Kurishita², M. Oyaidzu³, T. Hayashi³, T. W. Morgan⁴, G. De Temmerman⁵, J. W. Coenen⁶, A. Kreter⁶, and Y. Ueda¹

¹Osaka University, Osaka, Japan

²International Research Center for Nuclear Materials Science, Institute for Materials Research (IMR), Tohoku University, Sendai, Miyagi, Japan

³International Fusion Energy Research Centre (IFERC), Rokkasho, Aomori, Japan

⁴FOM Institute DIFFER, Association EURATOM-FOM, Nieuwegein, Netherlands

⁵International Thermonuclear Experimental Reactor (ITER),

Cadarache Centre, 13108 Saint-Paul-lès-Durance, France

⁶Forschungszentrum Jülich, Jülich, Germany

Corresponding Author: M. Oya, ohya@st.eie.eng.osaka-u.ac.jp

Toughened, fine-grained recrystallized tungsten (TFGR W) has been developed at Tohoku Univ., Japan [1], in order to improve poor mechanical properties of W such as brittleness at low temperature and embrittlement following neutron irradiation. TFGR W has an average grain size of $\sim 1 \mu\text{m}$ with a small amount of TiC and TaC dispersoids. These features of the microstructure serve to improve ductility. Here we report the performance of TFGR W under hydrogen isotope irradiation conditions and its applicability as a plasma-facing material, with respect to hydrogen isotope retention and melting behaviour.

First, deuterium (D) retention was investigated. Two types of TFGR W specimens were prepared; TFGR W-1.1wt%TiC and TFGR W-3.3wt%TaC (referred to as W-TiC and W-TaC, respectively). For comparison, pure W specimens were also investigated. D irradiation was conducted using HiFIT at Osaka Univ. [2]. D fluence of $\sim 1 \times 10^{24}/\text{m}^2$ was implanted at temperatures of 473–873 K. The D retention was determined by TDS.

At temperatures above 473 K, D retention in TFGR W is systematically higher than in pure W. The difference is about one order of magnitude at ~ 573 K, which is close to the water coolant temperature of the W divertor of a recent DEMO concept [3], suggesting that the use of TFGR W could greatly increase tritium retention. At a temperature of 773 K, retained amount of W-TiC is higher than W-TaC. At ~ 800 K, which corresponds to about surface temperature of ferritic-martensitic steel blankets, W-TaC should be used for reduced retention.

Secondly, in order to study their melting behaviour, TFGR W specimens were exposed to TEXTOR edge plasmas at temperatures above the melting point. The D plasma parameters were $I_p = 350$ kA, $B_t = 2.25$ T and $n_e = 3.5 \times 10^{19}/\text{m}^3$. Specimen surfaces were molten at the roof limiter position of 46.4 cm. The resolidified layer of W-TiC has many small pores with size of $\sim 1 \mu\text{m}$, while that of W-TaC has a dome-like structure with a height of $\sim 500 \mu\text{m}$ and a few cracks with ~ 1 cm long. These rough layers could lead to increased erosion when loaded by repeated exposure. Therefore, TFGR W should be more improved to mitigate surface roughening under extreme heat flux conditions.

References

- [1] H. Kurishita, *et al.*, Phys. Scr. **T159**, 014032 (2014).
- [2] Y. Ueda, *et al.*, Fusion Eng. Des. **62**, 255-261 (2002).
- [3] K. Tobita, *et al.*, Nucl. Fusion **49**, 075029 (2009).

Modelling Fuel Retention in Tungsten Plasma-Facing Materials under Realistic Tokamak Operation including Plasma Impurities

H. T. Lee¹, Y. Ueda¹, and K. Ibano¹

¹Osaka University, Osaka, Japan

Corresponding Author: H. T. Lee, heunlee@wakate.frc.eng.osaka-u.ac.jp

To date, the primary method for fuel retention estimates in next step devices has been based on projection of laboratory data with input from gas balance and postmortem analysis. The use of a large database minimizes risk, but the static nature of the retention data is not amendable to making projections under varied conditions. One recent example would be the failure of predicting how the physicochemical changes incurred at W surfaces from N₂, Ne, and Ar impurity seeding would affect T-inventory. We present an alternative method by parameterizing the hydrogen trapping and release processes at the near surface by the solute hydrogen concentration. This solute concentration and the effects of various impurities on it are directly measured from laboratory ion driven permeation experiments with W. It allows extraction of key hydrogen transport parameters such as diffusivity or recombination coefficients, allowing physics-based modelling of hydrogen desorption or transport behaviour.

The data is summarized in the form of a solute concentration-temperature diagram. For the impurity-free case, the concentration is fixed by plasma parameters and scales linearly to the incident flux (i.e., diffusion limited) up to divertor relevant fluxes ($\sim 1 \times 10^{24}$ D/m²s). Noble gas impurities (He, Ne, Ar) result in a 20–50% reduction. With C impurities, the concentration at $T < 700$ K is controlled by precipitation effects effectively decoupling the concentration from changes in plasma parameters. For N impurities, co-deposition of D with N controls the solute concentration at $T < 650$ K while diffusion limited at $T > 650$ K. Extrapolating to divertor relevant fluxes predict a factor 10 difference in inward transport at 750 K, which is supported by a factor 10 difference in retention results from D and D+N exposures at Magnum-PSI.

The introduction of solute concentration as a physical parameter allows adopting a more physically sound model to improve our estimate and prediction of fuel retention in future burning plasma machines. The method lends itself to self-consistently model additional transport processes like recycling or steady state permeation to the coolant, which from an engineering point of view provides a necessary link for optimizing both plasma and material response in a fusion reactor.



High-Temperature, Liquid Metal Plasma-Facing Component Research and Development for the NSTX-U

M. A. Jaworski¹, A. Brooks¹, P. Rindt², K. Tresemer¹, J.-P. Allain³, R. J. Goldston¹, T. K. Gray⁴, R. Kaita¹, N. Lopes-Cardozo², J. Nichols¹, J. Menard¹, M. Ono¹, D. N. Ruzic³, and J. Schwartz¹

The NSTX-U Team

¹Princeton Plasma Physics Laboratory (PPPL), Princeton, NJ 08540, USA

²Eindhoven University of Technology, Eindhoven, Netherlands

³University of Illinois, Urbana-Champaign, IL 61820, USA

⁴Oak Ridge National Laboratory (ORNL), Oak Ridge, TN 37831, USA

Corresponding Author: M. A. Jaworski, mjaworsk@pppl.gov

Liquid metal plasma-facing components are actively studied as a possible plasma-facing component (PFC) material in current and future fusion experiments. Liquid metals provide a self-healing material that has the potential to eliminate net erosion and damage due to local melting of the plasma-facing surfaces, and separate neutron damage from the plasma-induced damage at the surface. The high vapour pressure of liquid lithium further raises the possibility of intercepting significant plasma-based heat flux into a gaseous target when operating at an elevated temperature ($T > 500^\circ\text{C}$). With the innovative use of multiple, differentially pumped chambers, the condensation of lithium vapour can be exploited to separate high-neutral pressure regions from the plasma main-chamber. These benefits would solve several issues associated with the leading solid material, tungsten.

The NSTX-U team has developed a programme for transitioning the machine from its current PFCs to surfaces that can provide a comparative assessment between the high- Z and low- Z , liquid approaches. The progressive steps include the implementation of high- Z divertor targets, prefilled liquid metal targets as an interim study and finally, the implementation of an integrated, flowing liquid metal divertor target. Each of the three steps described above represent significant technological challenges. The practical realization of experiments with prefilled targets and the development of porous substrates includes aspects such as the choice of porous substrate, methods of fabrication, and maintenance of the liquid and its chemical composition during and between experiments. Design of the NSTX-U high- Z divertor upgrade and laboratory testing of prefilled targets will be presented.

Work supported by the U.S. Department of Energy Contract No. DE-AC02-09CH11466.



Effect of Defect Concentration and Distribution on Hydrogen Isotope Retention and Diffusion in Damaged W for Fusion First Wall

Y. Oya¹, K. Katayama², O. Tepei², Y. Yamauchi³, Y. Nobuta³, M. Oya⁴, Y. Hamaji⁵, T. Chikada¹, M. Shimada⁶, D. Buchenauer⁷, C. N. Taylor⁶, R. Kolasinski⁷, D. Donovan⁸, S. Kondo⁹, T. Hinoki⁹, T. Toyama¹⁰, N. Yoshida², Y. Hatano¹¹, and Y. Ueda⁴

¹Shizuoka University, Shizuoka, Japan

²Kyushu University, Kasuga, Japan

³Hokkaido University, Sapporo, Hokkaido, Japan

⁴Osaka University, Osaka, Japan

⁵National Institute for Fusion Science (NIFS), Toki, Gifu, Japan

⁶Idaho National Laboratory (INL), Idaho Falls, ID 83415, USA

⁷Sandia National Laboratories (SNL), Albuquerque, NM 87185, USA

⁸University of Tennessee, Knoxville, TN 37996, USA

⁹Kyoto University, Nishikyo-ku, Kyoto 615-8540, Japan

¹⁰Tohoku University, Sendai, Miyagi, Japan

¹¹Hydrogen Isotope Research Center, University of Toyama, Japan

Corresponding Author: Y. Oya, oya.yasuhisa@shizuoka.ac.jp

Elucidation of tritium (T) dynamics is one of the key issues for sustainable DT fusion. Tungsten will be exposed to high T fluxes accompanied by various energetic particles. Therefore, T retention and its trapping states will be dramatically changed by the accumulation of ion and neutron-induced damage and recovery by heating. These facts motivate us to perform extensive hydrogen isotope retention experiments in damaged W under the framework of Japan/US joint project, PHENIX. This paper presents recent results, including an analysis of D retention by various methods over a range of defect concentrations.

Disks of stress-relieved W were irradiated using 6 MeV Fe²⁺ at room temperature in TIARA, JAEA or 6.4 MeV Fe³⁺ at higher temperature in DuET, Kyoto University, up to 1.0 dpa. These samples were then compared with neutron-damaged W (10⁻⁶ dpa for 14 MeV or 10⁻⁴ dpa for thermal neutrons). All the samples were exposed to 1 keV D₂⁺ up to a fluence of 1.0 × 10²² D/m² at room temperature. Thereafter, thermal desorption spectroscopy (TDS) was applied with the heating rate of 0.5 K/s up to 1173 K. The D₂ TDS spectra from Fe²⁺ damaged W showed that accumulation of damage shifted to higher desorption temperature, consistent with the formation of large voids. For W specimens damaged by 14 MeV fusion neutrons to 10⁻⁶ dpa, the D₂ desorption at 700 K was found even at low defect concentrations, suggesting that the collision cascades result in the formation of vacancies. The simulations showed that D accumulated within 0.5 μm of the exposed surface for W damaged by Fe²⁺ ions. The results of D permeation experiment showed that D permeability for damaged W was reduced by damage introduction. Furthermore, by heating above 1100 K, D permeability were completely consistent with that for undamaged W. The nature of the defects is critical, and their stability will strongly influence D permeability.

In summary, the accumulation of defects resulted in the formation of stable trapping sites. The D trapping by defects reduces the number of available D diffusion pathways through the lattice, a mechanism that could lead to a reduction of D permeability. Finally, we note that dynamic recovery of damages is enhanced by high temperature irradiation.



Novel Test Bed Facility for PSI Issues in Fusion Reactor Conditions on the Base of Next Generation QSPA Plasma Accelerator

I. E. Garkusha¹, V. Makhlai¹, D. Solyakov¹, V. Chebotarev¹, N. Kulik¹, S. Herashchenko¹,
V. Staltsov¹, and D. Yelisseyev¹

¹*Institute of Plasma Physics, National Science Center, Kharkov Institute of Physics and Technology (KIPT),
Kharkov, 61108, Ukraine*

Corresponding Author: I. E. Garkusha, garkusha@ipp.kharkov.ua

Understanding of plasma-surface interaction (PSI) effects during the transient events (disruptions, VDEs, ELMs) in tokamak reactor requires dedicated R&D activity in plasma simulators used in close connection with material characterization facilities as well as with theory and modelling activities. For such investigations different simulators of transient loads are now involved (quasistationary plasma accelerators QSPA, e-beams, pulsed plasma guns and, recently, PSI device), that are cost effective, flexible, able to provide faster results and important comparison of damage features from various machines.

In this report concept of new generation QSPA with external B-field up to 2 T has been developed and novel test bed facility has been constructed. It allows a new level of plasma stream parameters and its wide variation in new QSPA-M device, as well as possible combination of steady state and pulsed plasma loads to the materials during the exposures.

First plasma is recently obtained. Careful optimization of the operational regimes of the plasma accelerator's functional components and plasma dynamics in the magnetic system of QSPA-M device has been performed approaching step by step the necessary level of plasma parameters and their effective variation. The relevant results on plasma stream characterization are presented. Energy density distributions in plasma stream have been measured with calorimetry. Spectroscopy and probe technique have been also applied for plasma parameters measurements. The obtained results demonstrate ability of QSPA-M to reproduce the ELM impacts in fusion reactor both in term of heat load and particle flux to the surface. First results on plasma interaction with tungsten samples in QSPA-M are discussed.



Multiscale Modelling of Materials: Light Species Dynamics in Nano-W and EOS of Hydrogen

J. M. Perlado¹, C. Gonzalez², C. Guerrero¹, G. Valles¹, N. Gordillo¹, R. Iglesias², I. Martin-Bragado³, M. Panizo-Laiz¹, A. Prada¹, R. Gonzalez-Arrabal¹, and A. Rivera¹

¹*Instituto de Fusión Nuclear (IFN), Universidad Politécnica de Madrid (UPM), Madrid, Spain*

²*Universidad de Oviedo, Oviedo, Asturias, Spain*

³*IMDEA Materials Institute, 28906 Getafe, Madrid, Spain*

Corresponding Author: J. M. Perlado, josemanuel.perlado@upm.es

Multiscale modelling (MM) demonstrates its important role in the deep understanding of physics mechanisms involved in materials behaviour under extreme conditions. Damage of materials by neutrons and ion irradiation in fusion systems is progressively better characterized by using a combination of experiments and simulation. It is also possible to give the conditions of hydrogen (EOS) when cryogenic and under high pressures, such as happens in first states of fuel in inertial fusion targets. Benefits from MM are presented related to the diffusion of light species (H, He) in W and nanocolumnar W and EOS of H and H-Be.

A comparison between binary collision approximation (BCA) and molecular dynamics (MD) has been performed to conclude its influence in the defects formation and their diffusion in W depending on the type of irradiation. Ion and neutron irradiation show a very different behaviour. The H retention because of grain boundaries size and concentration has been modelled both with density functional theory (DFT) and object kinetic Monte Carlo (OKMC) (fed with parametrization from DFT), and compared with experiments in nano-W and coarse-grained W (CGW). Grain boundaries act as preferential paths for H diffusion; a combination of H and vacancies (more concentrated in nano-W than CGW) in HV are on the core of the explanation. When studying dependence of the hydrogen diffusion coefficient on grain size and hydrogen concentration by MD calculations, it is coherently demonstrated a smaller value for nano-W than CGW. Using OKMC (parametrization from DFT), we study the influence of a high grain boundary density on the amount, size and distribution of defects produced by pulsed helium irradiation in tungsten, in both monocrystalline and nanocrystalline tungsten. In nano-W the total elastic strain energy remains almost constant with the increasing number of pulses, contrary to its increase in monocrystalline tungsten.

Related to H and H-Be impurities under extreme conditions, ab initio, quantum molecular dynamic and mechanical properties calculations are performed to study the relation between the structural phase transitions and sound velocity in solid molecular hydrogen at 15 K pressures from 0.01 to 160 GPa. The structural difference of solid molecular hydrogen pure and solid molecular hydrogen with beryllium is remarked with differences in elastic constants.

MPT



Determination of Radiation Damage Limits to High-Temperature Superconductors in Reactor-Relevant Conditions to Inform Compact Fusion Reactor Design

B. M. Sorbom¹, Z. S. Hartwig¹, L. A. Kesler¹, D. G. Whyte¹, J. Minervini¹, M. Short², G. M. Wright¹, M. Takayasu¹, M. Ames³, and G. Kohse³

¹Plasma Science & Fusion Center, MIT, Cambridge, MA 02139, USA

²Department of Nuclear Science and Engineering, Massachusetts Institute of Technology (MIT), Cambridge, MA 02139, USA

³Reactor Lab, Massachusetts Institute of Technology (MIT), Cambridge, MA 02139, USA

Corresponding Author: B. M. Sorbom, bsorbom@mit.edu

The recent commercialization of high temperature superconductors (HTS) has opened up a new parameter space for the design of tokamak fusion pilot plants. The lack of significant critical current degradation at high magnetic fields of HTS allows tokamaks to be designed with much higher on-axis fields. The ARC reactor design study showed that the use of HTS to design a compact, high-field pilot plant enabled a 3.3 m major radius device to achieve a fusion power of 525 MW. A key finding of the ARC study was that the largest constraint to shrinking the size of a compact, high field reactor was radiation damage limits to the HTS coils. With this constraint in mind, it is critical to determine the absolute lifetime of modern HTS technology in a fast neutron environment as well as develop strategies to mitigate this damage. While previous HTS irradiation work using fission reactors has been performed, reactor studies are costly, require long cooldown times of samples due to activation, and make it difficult to emulate HTS operating conditions such as cryogenic temperature during the irradiation. In order to complement reactor irradiation studies of HTS, an experiment is in progress to develop similarity between neutron and charged particle irradiation damage to HTS. A recent body of work indicates that under certain conditions, charged particle irradiation can be used to emulate neutron damage. The use of accelerator-based, charged particle irradiation to emulate neutron damage of HTS tapes will allow for short turn-around time and experimental flexibility, enabling a large and varied set of HTS damage experiments to be performed to determine HTS lifetimes. HTS samples have been irradiated in the MIT research fission reactor and are currently cooling down. After the samples are safe to handle, critical current measurements and microstructure analysis will be performed and compared with other HTS samples which have undergone accelerator irradiation. Once a correlation between neutron and charged particle damage to HTS has been developed, further accelerator-based irradiation experiments will be performed to determine the HTS lifetime at reactor-relevant temperatures and strains. Results of the above testing and implications for future compact, high-field tokamak design will be presented.



Deuterium Permeation through Candidate Structural Materials for a Fusion Reactor

A. V. Spitsyn¹, D. I. Cherkez¹, A. V. Golubeva¹, and N. P. Bobyr¹

¹National Research Centre "Kurchatov Institute", Moscow, Russian Federation

Corresponding Author: A. V. Spitsyn, spitsyn_av@nrcki.ru

In the next step fusion devices, such as DEMO or fusion neutron sources high neutron fluxes and fluences are expected. In this case reduce activated (RA) and heat-resistant structural materials should be used.

In Russia V-(4–10) Ti-(4–10) Cr alloys, austenitic and RA ferritic-martensitic steels for fission applications are developed and manufactured in A. A. Bochvar High-technology Research Institute of Inorganic Materials. For using materials in next step fusion devices additional studies should be done. Interaction of hydrogen isotopes with structural material is one of the important factors, determining the possibility of using this material in fusion reactors. Permeation of hydrogen isotopes through structural material is one of the key characteristic as tritium is the component of fusion fuel available only in small quantities, expensive and radioactive.

In the present work gas-driven permeation (GDP) and plasma-driven permeation (PDP) through ferritic-martensitic steel RUSFER-EK-181 (Fe-12 Cr-2 W-V-Ta-BC), austenitic steel ChS-68 (used in fast breeder reactor BN-600 as cladding) and V-4 Ti-4 Cr were investigated using the PIM facility (at NRC "Kurchatov Institute"). In the experiments RUSFER-EK-181 and ChS-68 tubes of 250 mm length with diameter of 6.85 mm and wall thickness of 0.4 mm (effective area 50 cm²) and flat V-4Cr-4 Ti membrane with diameter of 50 mm and thickness of 0.1 mm (effective area 20 cm²) were used. The PIM facility is equipped with a distributed ECRH plasma source, which was used for cleaning the inlet sample surfaces by argon ions with ion energy 300 eV and for deuterium plasma irradiation in PDP measurements (typical ions flux density is 10 A/m² at accelerating potential of –300 V). Deuterium GDP measurements were performed in the pressure range of 5 × 10⁻²–100 Pa and in the temperature range of 600–900 K.

At GDP permeability coefficient of V-4Cr-4 Ti membrane is about four orders of magnitude higher than that of RUSFER-EK-181 while permeability coefficient of ChS-68 is higher than permeability coefficient of RUSFER-EK-181 at all pressures and temperatures. However V-Cr-Ti alloys are promising materials for a membrane pump as a superpermeable metal membranes that can be used for provide a significant compression for hydrogen and a 100% separation of fuel from He and other impurities.



Activities for Fusion Energy Functional and Plasma Facing Material Research at the University of Latvia

L. Avotina¹, M. Halitovs¹, A. Lescinskis¹, A. Zarins¹, D. Conka¹, I. Igaune¹, E. Pajuste¹, R. Kovaldins¹, A. Vitins¹, E. Piraga¹, O. Valtenbergs¹, R. Zarins¹, and G. Kizane¹

¹*University of Latvia, Riga, Latvia*

Corresponding Author: L. Avotina, liga.avotina@lu.lv

In the frame of EUROfusion consortium programme, the Institute of Chemical Physics and the Faculty of Chemistry, both of the University of Latvia, are performing investigations on plasma facing, neutron multiplying and self-sufficient tritium generating functional materials for the use of ITER and the DEMO power plant.

Beryllium is used as a plasma facing material in tile form and is considered for use as a neutron multiplier in pebble form in the He cooled pebble bed (HCPB) test blanket module (TBM) of ITER and DEMO. Tritium distribution was determined with dissolution method and release characteristics with thermal desorption spectroscopy (TDS). Tritium release from neutron irradiated pebbles shows the importance of material microstructure, irradiation temperature on the accumulated tritium amount and release characteristics and points to tile position as a determining factor for tritium accumulation and distribution.

Lithium based ceramics, lithium orthosilicate and metatitanate, are considered breeder materials in HCPB TBM. As formation of radiation-induced defects (RD) and radiolysis products (RP) may occur in tritium breeding ceramics during operating conditions, it can affect the tritium generated and may disturb its diffusion and release. Changes of RD and RP formation depending on absorbed dose were analyzed by electron spin resonance spectroscopy, thermally stimulated luminescence technique, and so on.

Carbon fibre composite (CFC) materials have been used as divertor and plasma facing materials in fusion devices, including the Joint European Torus (JET) until 2009. W-coated CFC tiles are used in the JET ITER-like wall divertor. During active operation, plasma-wall interactions (erosion, formation of dust — fullerenes and long-chain hydrocarbons, tritium retention) occur. Tritium distribution in the JET tiles and dust was determined with full combustion and liquid scintillation method, desorption process is analyzed by TDS to investigate tritium retention mechanisms.

This work has been carried out in collaboration with the Karlsruhe Institute of Technology, Institute for Applied Materials, within the framework of the EUROfusion Consortium and has received funding from the EURATOM research programme. The views and opinions expressed herein do not necessarily reflect those of the European Commission.

The Accomplishments of Lithium Target and Test Facility Validation Activities in the IFMIF/EVEDA Phase

F. Arbeiter¹, R. Heidinger², J. Knaster³, H. Kondo⁴, E. Wakai⁴, P. Favuzza⁵, F. Gröschel¹,
A. Ibarra⁶, V. Massaut⁷, F. Nitti⁸, G. Micciche⁸, S. O'hira⁴, T. Kanemura⁴, D. Rapisarda⁶,
and T. Yokomine⁹

¹Karlsruhe Institute of Technology (KIT), Karlsruhe, Germany

²F4E: Fusion for Energy, ITER EU Centre, 08019 Barcelona, Spain

³International Fusion Materials Irradiation Facility (IFMIF/EVEDA), Rokkasho, Aomori, Japan

⁴Japan Atomic Energy Agency (JAEA), Naka, Japan

⁵ENEA Firenze, Italy

⁶Centro de Investigaciones Energéticas, Medioambientales y Tecnológicas (CIEMAT), Madrid, Spain

⁷SCK•CEN, Belgian Nuclear Research Centre, 2400 Mol, Belgium

⁸Agenzia nazionale per le nuove tecnologie, l'energia e lo sviluppo economico sostenibile (ENEA), Rome, Italy

⁹Kyoto University, Nishikyo-ku, Kyoto 615-8540, Japan

Corresponding Author: F. Arbeiter, frederik.arbeiter@kit.edu

Validation activities for key systems of the lithium facility and the test facility of the International Fusion Materials Irradiation Facility (IFMIF) were performed during the Engineering Validation and Engineering Design Activities phase 2007–2015 by Japanese and EU Research Units. A fully functional lithium loop with a 1:3 scaled target were constructed and run in Oarai, Japan. The lithium target, which acts as neutron source together with the IFMIF 2×125 mA 40 MeV deuteron accelerators, has proven long term stability, and fulfilling the requirements on low surface waviness. Two types of high flux test modules were developed and tested in Japan and EU. Both types demonstrated a fulfilment of their thermal-hydraulic requirements and ability to keep the contained material specimens in low temperature spread conditions. Further research was done for the development of a small specimen test technique.

In conclusion, the validation activities for the IFMIF Lithium and Test Facilities were able to demonstrate major achievements for the design of critical components, and furthermore, give valuable impulses for the further development of IFMIF systems, which are currently ongoing in EU and Japanese R&D activities, aiming at the realization of an early neutron source for DEMO.



Investigations of Tungsten as Candidate Plasma Facing Material under High Repetition and Intense Fusion-Relevant Pulses

R. S. Rawat¹, I. E. Garkusha², R. Kamendje³, and G. Pintsuk⁴

¹National Institute of Education, Nanyang Technological University, Singapore

²Institute of Plasma Physics, National Science Center, Kharkov Institute of Physics and Technology (KIPT), Kharkov, 61108, Ukraine

³International Atomic Energy Agency (IAEA), Vienna, Austria

⁴Forschungszentrum Jülich, Jülich, Germany

Corresponding Author: R. S. Rawat, rajdeep.rawat@nie.edu.sg

For the purpose of investigating the damage processes of surface layers during transient heat loads, fuel retention and dust issues of tungsten as candidate plasma facing materials, the IAEA organized a dedicated Coordinated Research Project (CRP F1.30.13) from 2011–2015. The CRP involved 18 institutions from 15 member states. The activities concentrated on the irradiation and characterization of PLANSEE double-forged tungsten (PDF-W; tungsten forged in two orthogonal directions aiming to obtain a dense and nearly isotropic grain structure). These samples were provided by Forschungszentrum Jülich, Germany, to all participating research teams. More than 100 samples of 12 mm × 12 mm × 5 mm were investigated. All samples were expected to be identical, which was also demonstrated through microstructural and compositional investigations.

Round-robin tests were performed using different plasma and nuclear facilities and particle accelerators. A total of 25 different devices were used for irradiation during this CRP which included plasma accelerators, dense plasma focusses, a tokamak, a nuclear fission reactor, a cyclotron, and electron beam facilities. These facilities span a wide range of irradiation parameters thus allowing a meaningful contribution to the clarification of damage mechanisms under powerful heat loads and the dynamics of erosion products.

The mechanisms of plasma-material interaction and surface modifications were identified in different devices used. A database of surface damage, structural and compositional changes of tungsten materials irradiated under well-defined heat and particle load conditions in different plasma and particle accelerators was generated. It was established that the main factors affecting the performance and adequacy of double-forged tungsten during transient events are i) the base temperature of the material, ii) the heat flux factor ($W\sqrt{s}/\text{cm}^2$), iii) thermo-mechanical properties of the material, iv) the pulse duration, v) total fluence, and vi) the pulse frequency.

The investigations carried out within the framework of this IAEA CRP have gained insights into the issue of the adequacy of tungsten for fusion reactor environment.

PPC: Plasma Overall Performance and Control



Extension of Operational Regime in High-Temperature Plasmas and Effect of ECRH on Ion Thermal Transport in the LHD

H. Takahashi¹, K. Nagaoka¹, S. Murakami², M. Osakabe¹, H. Nakano¹, K. Ida¹, T. I. Tsujimura¹, S. Kubo¹, T. Kobayashi¹, K. Tanaka¹, R. Seki¹, Y. Takeiri¹, M. Yokoyama¹, M. Nakata¹, M. Yoshinuma¹, I. Yamada¹, R. Yasuhara¹, T. Ido¹, A. Shimizu¹, H. Tsuchiya¹, M. Goto¹, T. Oishi¹, S. Morita¹, C. Suzuki¹, M. Emoto¹, K. Tsumori¹, K. Ikeda¹, M. Kisaki¹, T. Shimozumata¹, Y. Yoshimura¹, H. Igami¹, R. Makino¹, T. Seki¹, H. Kasahara¹, K. Saito¹, S. Kamio¹, T. Mutoh¹, O. Kaneko¹, and T. Morisaki¹

¹National Institute for Fusion Science (NIFS), Toki, Gifu, Japan

²Department of Nuclear Engineering, Kyoto University, Nishikyo-ku, Kyoto 615-8540, Japan

Corresponding Author: H. Takahashi, takahashi.hiromi@lhd.nifs.ac.jp

In future reactors, the fusion reaction is expected to be sustained under the electron heating dominant condition, where both ion temperature and electron temperature are high. Thus the characterization of the thermal transport for the plasmas, of which ion temperature and electron temperature are simultaneously high, is necessary. In recent years, an integration of high ion temperature and high electron temperature has been successfully achieved in the LHD. In FY2014, one high power gyrotron (154 GHz, 1 MW) was newly installed, and since then five gyrotrons with 1 MW output power each have been under operation and the total ECRH power reached 5.4 MW. We finely adjusted the ECRH injection angle and the EC wave polarization taking account of the actual plasma profiles in real time. Simultaneous high ion temperature and high electron temperature regime was successfully extended due to the upgraded ECRH system and the optimization of the ECRH injection.

Such high-temperature plasmas were realized by the simultaneous formation of an ion ITB and an electron ITB by the combination of high power NBI and ECRH. In the heating condition, a seesaw-like behaviour of the ion thermal transport between core and edge has been observed. Both in the plasma core and the edge, the electron temperature and the gradient increased with increase in ECRH power. On the other hand, the ion thermal confinement was degraded in the plasma core with increase of the ratio of the electron temperature to the ion temperature by the on-axis ECRH@. In contrast, the ion thermal confinement was found to be improved at the plasma edge. The ion thermal diffusivity normalized by the gyro-Bohm factor was found to be reduced by 70% at the edge. Then the spatiotemporal coherence of the electron density fluctuations at the plasma edge clearly decreased. The improvement of the ion thermal confinement at the edge led to increase in the ion temperature in the entire plasma region even though the core transport was degraded.



Evaluation of Tungsten Transport and Concentration Control in ITER Scenarios

A. Loarte¹, M. Hosokawa¹, A. Polevoi¹, F. Koechl², V. Parail³, E. A. Belli⁴, J. Candy⁴,
R. Dumont⁵, and D. Zarzoso⁶

¹International Thermonuclear Experimental Reactor (ITER),
Cadarache Centre, 13108 Saint-Paul-lès-Durance, France

²Institute of Atomic and Subatomic Physics, Technische Universität Wien, 1040 Vienna, Austria

³Culham Centre for Fusion Energy (CCFE), Culham Science Centre, Abingdon, UK

⁴General Atomics, San Diego, CA 92186, USA

⁵Commissariat à l'énergie atomique (CEA), 91400 Gif-sur-Yvette, France

⁶Aix-Marseille Université, Marseille, France

Corresponding Author: A. Loarte, alberto.loarte@iter.org

In order to evaluate if W accumulation is expected in ITER plasma conditions and whether the available heating systems can provide the degree of control required for stable H-mode operation, we have applied integrated plasma models (ASTRA and JINTRAC) to a wide range of plasma conditions in ITER including confinement transients (i.e., L-H and H-L transitions). The studies find that, in agreement with present experiments, W transport is anomalous for most of the ITER plasma cross section except in the very central region (typically $r/a \leq 0.3$). In the central plasma region, W transport is neoclassical and for most stationary plasma conditions temperature screening is dominant over the inwards force originating from the density gradient. Main ion density gradients in the central plasma region are always found to be very moderate due to the low core fuelling rate provided by the ITER 1 MeV NBI system. This prevents strong W accumulation in ITER stationary H-modes, which is a result robust to assumptions on the level of particle and energy transport in the central region of the plasma. Modelling also shows that the application of central ECRH or ICRH heating at a level of 20 MW is sufficient to change the density and temperature gradients in the central region so as to modify the central W density profile and avoid strong peaking.

While the situation regarding core W control in stationary H-mode phases looks rather positive, core W control is found to be more complex in the termination phases of ITER H-modes. For optimum plasma radial position control, the plasma energy should decrease with timescales of 5–10 s in the termination phase of high- Q H-modes in ITER. The decrease of the plasma energy in such timescale can be achieved by a slow ramp-down of the auxiliary heating power, which together with alpha heating, extends the H-mode phase and the timescale of plasma energy decay over 5 s. Modelling of W transport for $Q = 10$ H-mode terminations shows that strong W accumulation (with timescales of ~ 5 s) can occur when the auxiliary heating power is gradually decreased. Further H-mode termination studies will be carried out to optimize the ramp-down of auxiliary heating power (as well as the type of heating scheme applied in this phase) and pellet fuelling so that the requirements regarding radial position and W control can be fulfilled simultaneously.

**SEE: Safety, Environmental and Economic
Aspects of Fusion**



Assessment of Potential and Breakeven Prices of Fusion Power Plants under Low-Carbon Development Scenarios

K. Gi¹, F. Sano¹, and K. Akimoto¹

¹Research Institute of Innovative Technology for the Earth (RITE), Kyoto, Japan

Corresponding Author: K. Gi, kgi@rite.or.jp

Climate change has become one of the most important issues to be tackled in the world. Deep emission reduction of greenhouse gas must be achieved in this century. In the COP21 of United Nations Framework Convention on Climate Change (UNFCCC) on December 2015 in Paris, a new mechanism of CO₂ emission reduction (Paris Agreement) was adopted based on the pledge-and-review approach. Fusion energy has outstanding characteristics of plentiful resources, no nuclear runaway, and zero-carbon emission. DEMO plant projects have begun in the participating parties of the ITER project. They aim at demonstration of not only electricity generation but also economy and social acceptability of commercial fusion power plants.

Roles and breakeven prices of nuclear fusion have been analyzed by using energy system models in the previous studies. However, their assumptions for fusion energy assessment are out of date, because new scenarios reflecting the latest data and storylines have been developed for the long-term energy system assessment. In this study, we assessed a role of fusion energy by using state-of-the-art model and scenarios.

We studied breakeven prices and potential capacity of fusion power plants under five low-carbon development scenarios using a state-of-the-art global energy system model: DNE21+. The DNE21+ model is a linear programming model which minimizes the world energy system cost. The model represents regional differences dividing world into 54 regions, and assesses energy technologies which are bottom-up modelled in detail.

A wide range of breakeven prices of capital costs per unit of 1–8 \$/W in the United States, EU, Japan, China, Korea, India, and Russia were revealed in the different condition of five CO₂ emission pathways and four types of innovativeness of fusion plant technology. A prospect of the capital costs less than 5 \$/W and/or enhancement of the plant availability are desired in the DEMO project. Fusion can play a significant role in the low-carbon development if it secures the economy, substituting fission and fossil fuel power plants with carbon dioxide capture and storage (CCS). Fusion energy development could be justified in economic meaning alone if their research and development (R&D) costs (\$) are less than the total installed capacity (W) to the power of 1.5, which correspond to the total energy system cost reduction in the world.

Proposal of the Confinement Strategy for EU DEMO

X. Z. Jin¹, D. Carloni¹, R. Stieglitz¹, S. Ciattaglia², J. Johnston³, and N. Taylor³

¹Karlsruhe Institute of Technology (KIT), Karlsruhe, Germany

²EUROfusion Garching, 85748 Garching, Germany

³Culham Centre for Fusion Energy (CCFE), Culham Science Centre, Abingdon, UK

Corresponding Author: X. Z. Jin, jin@kit.edu

Following the European roadmap to the realization of fusion energy, a demonstration fusion power plant (DEMO) is currently in preconceptual design phase until 2020. In this context an external stakeholder group formulated a nuclear licensed manufacturing and construction (M/C) as the top level requirement for a DEMO, translating essentially to the confinement of radioactive and hazardous materials as the most fundamental safety function in normal, abnormal and accidental situations. In a first step energy sources and radioactive source have been assessed for a conceptual DEMO configuration. Based on the European Plant Description Document (PDD) the main systems have been classified as active or passive systems with respect to their confinement functionality. By means of a bottom-up approach at system level, the major DEMO systems are analyzed regarding a potential confinement function. On the basis of those DEMO systems identified as having a confinement function a confinement strategy for EU DEMO has been proposed with respect to confinement barriers and confinement systems. In addition, confinement for the maintenance has been issued as well. The assignment of confinement barriers to the identified sources under abnormal and accidental conditions has been performed, and the DEMO main safety systems have been proposed as well. Confinement related open issues such as discharge of the huge magnet energy in an accidental case, confinement concerning plant states, investigation on further passive and active methods for the confinement, confinement during the procedure of removing and replacing in-vessel components, etc., need to be resolved in parallel with DEMO development.



Social Research on Fusion

A. Prades¹, A. Delicado², L. Schmidt², C. Turcanu³, G. Meskens³, T. Perko³, and D. Ward⁴

¹*Centro de Investigaciones Energéticas, Medioambientales y Tecnológicas (CIEMAT), Madrid, Spain*

²*Instituto de Ciências Sociais (ICS), Instituto Superior Técnico (IST), Lisbon, Portugal*

³*SCK•CEN, Belgian Nuclear Research Centre, 2400 Mol, Belgium*

⁴*Culham Centre for Fusion Energy (CCFE), Culham Science Centre, Abingdon, UK*

Corresponding Author: A. Prades, ana.prades@ciemat.es

Collecting scientific evidence on the human, social and ethical dimensions in energy systems is a fundamental tool for understanding (and intervening in) the acceptance of energy technologies, the siting of energy generation facilities, and the promotion of measures for risk mitigation and safety. Furthermore, this key role of social research in energy fully aligns with proposals for more open and responsive modes of research and science policy-making, as illustrated by contemporary EU-wide policy discourses on “Science with and for society” and “responsible research and innovation”. In the fusion domain, and since 1996, a specific research programme — currently known as Socio-economic Studies, or SES — has been dealing with the social and the socio-economic dimension of fusion. The SES social research has so far focussed on generating evidence regarding the conditions for social acceptance of fusion — currently as a research endeavour and in the future as an energy source — as well as the barriers and constraints for acceptance and suitable energy governance. Stakeholder engagement, lay attitudes and media analysis and media framing are our three main fields of research.

This paper presents the key challenges and findings from social research on fusion together with its very practical implications for the fusion community, such as promoting the engagement of the fusion community with stakeholders and the public, enhancing the communication strategies of fusion research, including additional variables in the economic model of the global energy system or making fusion research more responsive to societal concerns.



Exploration of Fusion Power Penetration under Different Global Energy Scenarios Using the EFDA Times Energy Optimization Model

H. Cabal¹, Y. Lechón¹, F. Gracceva², D. Ward³, M. Biberacher⁴, C. Bustreo⁵,
D. N. Dongiovanni², and P. E. Grohnheit⁶

¹Centro de Investigaciones Energéticas, Medioambientales y Tecnológicas (CIEMAT), Madrid, Spain

²Agenzia nazionale per le nuove tecnologie, l'energia e lo sviluppo economico sostenibile (ENEA), Rome, Italy

³Culham Centre for Fusion Energy (CCFE), Culham Science Centre, Abingdon, UK

⁴Research Studio Austria Forschungsgesellschaft (RSA FG), Salzburg, Austria

⁵Consorzio RFX, Associazione EURATOM-ENEA sulla Fusione, Padova, Italy

⁶Technical University of Denmark (DTU), Lyngby, Denmark

Corresponding Author: H. Cabal, helena.cabal@ciemat.es

The first commercial fusion power plants are expected to start operating from 2050. How the global energy system will be as for that time nobody knows, but future can be explored by means of scenarios. In this work, several scenarios have been formulated and represented by the EFDA Times model (ETM), a global optimization energy model developed within the framework of the Socio Economic Research of Fusion project (SERF) in EFDA. Some analyzes on the evolution of the global energy system in the long term under different scenarios have been carried out with especial focus on the future role of fusion technologies. Different issues related to fusion development have been analyzed for each scenario using the ETM model.

Results show that fusion technologies participation in the global electricity system by 2100 goes from 10% to 14% depending on the storyline. Using paternalism as a reference scenario, some additional analyzes have been done. Preliminary results show that the global rate of fusion technologies growth is 12% per year from 2070 to 2100. Besides, fusion penetration is very sensitive to investment cost variations going from 13% to 42% when investment costs are 30% lower than in the reference case and from 13% to 1% when those costs are 30% higher. Regarding the hypothetical case of fusion technologies anticipation, at the beginning, the penetration is low and similar in both scenarios, reference and anticipation, but at the end of the period it is much higher in anticipation, mainly due to the advanced reactors penetration.

Finally, sensitivity analyzes have been performed on key parameters such as the discount rate of each technology. The results show that the lower the discount rate, the higher the share of fusion in the global electricity system.



Safety and Waste Management Studies as Design Feedback for a Fusion DEMO Reactor in Japan

Y. Someya¹, M. Nakamura¹, A. Masui¹, K. Watanabe¹, H. Tanigawa¹, and K. Tobita¹

¹*Japan Atomic Energy Agency (JAEA), Naka, Japan*

Corresponding Author: Y. Someya, someya.yoji@jaea.go.jp

This paper presents safety and waste management studies for a fusion DEMO reactor. It was found that an impact of a large-scale ex-vessel loss-of-coolant accident (LOCA), i.e., a guillotine rupture of a main pipe of the primary cooling system with pressurized water reactor (PWR) condition (320°C, 16 MPa), can be mitigated by using a vault for the tokamak cooling water system (TCWS) with a pressure suppression system. A management scenario of radioactive waste generated in every replacement of in-vessel components was developed in consideration of residual heat, dose rate and tritium removal. An additional important finding is that all the radwaste will be disposed of in shallow land burial after the 10 year interim storage for cooling down the radioactivity.

Future Electric Market and Fusion Deployment Strategy with Electricity Storage Systems

S. Konishi¹, S. Takeda¹, and R. Kasada¹

¹*Kyoto University, Nishikyo-ku, Kyoto 615-8540, Japan*

Corresponding Author: S. Konishi, s-konishi@iae.kyoto-u.ac.jp

This paper points out one of the critical issue overlooked for fusion to become a viable energy source in the future, quantitatively analyzes the requirements, and suggests a possible solution. Future grids in possible markets and the impact of fusion introduction was analyzed with numerical model, and the limitation and requirements of the generation capacity of fusion plant is shown as the function of grid capacity, composition and stability. There are very limited opportunity of 1 GW or above for fusion in most of the emerging grids, and fusion will need smaller capacity, or better ancillary service including innovative storage.

Almost all the fusion reactor designs assume large and stable electricity grids to connect and expect unlimited large pulsed power supply for starting plants. Unlike in the grids in the countries where fusion research is currently pursued, majority of the future grids where fusion would be deployed are anticipated to be significantly different. Even in the large grids in advanced countries, future system will be rather unstable because of the larger renewable fraction and trends to free electricity markets. Majority of the electric grids in the world will be still far smaller than 50 GW at the middle of this century, where introduction of fusion electricity over 1 GW would be difficult.

This paper analyzes the impact of fusion electricity on small size grids. Fusion plants requires large electricity for startup, and in the case of disruption or other unexpected shut down, loss of electricity in a short time would disturb the stability of the grids. The authors established a simplified Heffron-Philips model constructed in Matlab/Simulink™. This model analyzes quantitative impacts of fusion on a given grid size and composition, and provides limits and requirements for fusion to be installed.

This concept suggests the possibility of faster and easier introduction of fusion energy in the future, with reduced difficulty and with larger and more attractive market possibility. Majority of sales of fusion, if it would be viable, is in the developing countries rather than the mature markets where growth is not expected, and thus encompassing such a business model could justify the investment for fusion development.

PD: Post-Deadline Contributions

Contributions exceptionally accepted post-deadline.

The following post-deadline contributions are currently unavailable:

PDP-01	Y.-M. Jeon	Korea, Rep. of	Robust RMP-ELM Control with a Distinctive Optimization of Plasma Shape in KSTAR
PDP-06	Z. Unterberg	USA	Characterization of Different Divertor Tungsten Sources, Migration and Impact on the Core in DIII-D ELM-y H-mode Conditions
PDP-17	A. Krasilnikov	Russian Fed.	Evidence of $p + {}^9\text{Be}$ Nuclear Reactions during High Power 2wch and Hydrogen Minority ICRH in JET-ILW Hydrogen and Deuterium Plasmas
PDP-20	H. Li	China	Laser Fusion and High-Energy Density Physics Studies in IAPCM
PDP-22	K. Kolacek	Czech Republic	Surface Modification of Some Perspective Plasma-Facing-Materials by Intense Nanosecond XUV Pulses



First Observation of ELM Suppression in ASDEX-Upgrade in a Similarity Experiment with DIII-D

R. Nazikian¹, W. Suttrop², A. Kirk³, T. Evans⁴, B. A. Grierson¹, R. McDermott²,
C. Paz-Soldan⁴, D. Orlov⁵, and M. Willensdorfer²

¹Princeton Plasma Physics Laboratory (PPPL), Princeton, NJ 08540, USA

²Max-Planck-Institut für Plasmaphysik, Garching, Germany

³Culham Centre for Fusion Energy (CCFE), Culham Science Centre, Abingdon, UK

⁴General Atomics, San Diego, CA 92186, USA

⁵University of California San Diego, CA 92093, USA

Corresponding Author: R. Nazikian, rnazikia@pppl.gov

ELM suppression with 3D magnetic perturbations (MPs) is obtained for the first time in low collisionality ASDEX Upgrade (AUG) plasmas following shape-matching experiments on DIII-D. These experiments demonstrate the importance of low pedestal collisionality and strong shaping to access ELM suppression, and reveal a remarkable similarity in the alignment of the $E \times B$ rotation profiles to edge rational surfaces for the two machines, relevant to models of ELM suppression based on resonant field penetration. The experiments also demonstrate the weak role played by the impurity species and main ion dilution in affecting the onset conditions for ELM suppression, strongly supporting a common physics basis for ELM suppression at ITER relevant collisionality in metal and carbon wall experiments, based on resonant magnetic field effects at the top of the pedestal.



Final Integration, Commissioning and Start of the Wendelstein 7-X Stellarator Operation

H.-S. Bosch¹, V. Bykov², R. Brakel², P. van Eeten², J.-H. Feist², M. Gasparotto¹, H. Grote², T. Klinger², M. Nagel², D. Naujoks², M. Otte², R. Konrad², T. Rummel², J. Schacht², T. Sunn Pedersen², R. Vilbrandt², L. Wegener², A. Werner², and R. Wolf¹

¹Max-Planck-Institut für Plasmaphysik, Garching, Germany

²Max-Planck-Institut für Plasmaphysik, Greifswald, Germany

Corresponding Author: H.-S. Bosch, claudia.schoenian@ipp.mpg.de

The main objective of the Wendelstein 7-X (W7-X) stellarator is to demonstrate the integrated reactor potential of the optimized stellarator line. An important element of this mission is the achievement of high heating power, high confinement in fully controlled steady-state operation. In March 2014, after the installation of the last current lead in the outer vessel, the cryostat was finished, and the commissioning of the W7-X device could start. The installation of the in-vessel components, diagnostic systems and of peripheral components was continued.

First, the cryostat vacuum system was commissioned and the cryostat was pumped for the first time. Movements and deformations of the outer vessel and the port bellows during this pumping agreed rather well with the corresponding FE modelling.

In the fall of 2014 the cryo-piping was finished, and leak-search and cleaning of the 2000 m piping started. In spring 2015 the magnetic coil set together with the support system, was cooled down to 4 K without any problem. In the next step, the superconducting magnet system consisting of 7 circuits with 10 coils each in serial connection was loaded with current for the first time. After integral commissioning of the magnet system, the magnetic flux surfaces were confirmed with an electron. Subsequently, the plasma vessel was baked to 150°C, and the central safety system was commissioned and validated. In December 2015, the first plasma was ignited in helium with ECRH, in February 2016 the working gas was switched to hydrogen.

The technical experiences of this commission process and the first operation phase will be discussed in this paper. The strong backing through numerical modelling and mechanical instrumentation monitoring has supported this process to guarantee structural integrity of W7-X main systems.



First Results from Recent JET Experiments in Hydrogen and Hydrogen–Deuterium Plasmas

I. M. Ferreira Nunes¹, S. Brezinsek², J. Buchanan³, K. Cave-Ayland³, C. Challis³, I. Carvalho⁴, E. Delabie⁶, D. Van Eester⁷, M. Faitsch⁸, F. Josep³, L. Garzotti⁹, M. Groth¹⁰, J. Hillesheim³, J. Hobirk⁸, A. Hubbard¹¹, A. Huber¹², E. Joffrin¹³, Y. Kazakov⁷, D. King³, A. Krasilnikov¹⁴, K. Krieger⁸, A. B. Kukushkin¹⁵, E. A. Lerche⁷, E. de la Luna¹⁶, C. Maggi³, P. Mantica¹⁷, M. Maslov³, V. Neverov¹⁵, M. Romanelli³, P. Siren¹⁸, E. R. Solano¹⁶, M. Stamp³, T. Tala¹⁹, M. Valisa²⁰, M. Valovic³, D. Valcarcel³, J. Varje¹⁰, E. Viezzer⁸, H. Weisen²¹, and S. Wiesen²

¹*Institute of Plasmas and Nuclear Fusion (IPNF), Association EURATOM/IST, Lisbon, Portugal*

²*Forschungszentrum Jülich, Jülich, Germany*

³*Culham Centre for Fusion Energy (CCFE), Culham Science Centre, Abingdon, UK*

⁵*Instituto Superior Técnico (IST), Lisbon, Portugal*

⁶*FOM Institute DIFFER, Association EURATOM-FOM, Nieuwegein, Netherlands*

⁷*Laboratory for Plasma Physics, ERM/KMS, Brussels, Belgium*

⁸*Max-Planck-Institut für Plasmaphysik, Garching, Germany*

⁹*United Kingdom Atomic Energy Authority, Culham Science Centre, Abingdon, UK*

¹⁰*Aalto University, Espoo, Finland*

¹¹*Plasma Science & Fusion Center, MIT, Cambridge, MA 02139, USA*

¹²*Institute of Energy and Climate Research, Forschungszentrum Jülich, Jülich, Germany*

¹³*Commissariat à l'énergie atomique (CEA), 91400 Gif-sur-Yvette, France*

¹⁴*International Thermonuclear Experimental Reactor (ITER), Project Centre "ITER", Moscow, Russian Federation*

¹⁵*National Research Centre "Kurchatov Institute", Moscow, Russian Federation*

¹⁶*Centro de Investigaciones Energéticas, Medioambientales y Tecnológicas (CIEMAT), Madrid, Spain*

¹⁷*Istituto di Fisica del Plasma (IFP), Consiglio Nazionale delle Ricerche (CNR), 20125 Milan, Italy*

¹⁸*Agenzia nazionale per le nuove tecnologie, l'energia e lo sviluppo economico sostenibile (ENEA), Rome, Italy*

¹⁹*VTT Technical Research Centre of Finland Ltd., Espoo, Finland*

²⁰*Consorzio RFX, Associazione EURATOM-ENEA sulla Fusione, Padova, Italy*

²¹*EUROFusion (EFDA), Max-Planck-Institut für Plasmaphysik, Garching, Germany*

Corresponding Author: I. M. Ferreira Nunes, inunes@ipfn.ist.utl.pt

The hydrogen campaign completed at JET in 2016 has demonstrated isotope ratio control in JET-ILW using gas puffing and pellets for fuelling, neutral beam injection alone or in combination, with D_{α}/H_{α} spectroscopy as a diagnostic. The plasma properties such as confinement, L-H threshold, density limit depend on the isotope composition. The L-H transition power increases with the hydrogen concentration with a wide plateau in the range 0.2.



Suppression of Alfvén modes through additional beam heating

N. Gorelenkov¹, E. Belova¹, E. Fredrickson¹, B. Le Blanc¹, A. Diallo¹, N. Crocker²,
D. Battaglia¹, D. Liu³, G. Hao⁴, M. Podesta¹, R. Bell¹, and D. Darrow¹

¹*Princeton Plasma Physics Laboratory (PPPL), Princeton, NJ 08540, USA*

²*University of California Los Angeles, CA 90095, USA*

³*University of California Irvine, CA 92697, USA*

⁴*Southwestern Institute of Physics, Chengdu, Sichuan, People's Republic of China*

Corresponding Author: N. Gorelenkov, ngorelen@pppl.gov

The International Tokamak Experimental Reactor (ITER) will have a large population of nonthermal, energetic ions consisting of fusion generated alphas and beam ions injected for current profile control. Potential redistribution and/or loss of those nonthermal ions is thus of concern as it will modify heating profiles, current profiles, and losses could lead to unacceptable local heating of plasma facing components. Redistribution and losses of fast ions have been documented as resulting from multiple Alfvénic modes, Toroidal Alfvén Eigenmodes and energetic particle modes (fishbones) on many smaller plasma devices. This paper presents experimental evidence that some fast ion driven instabilities can be suppressed by modifying the fast-ion distribution function. The experimental results were modelled using the HYM code and provide a valuable validation of our theoretical understand of fast-ion-driven instabilities. ITER will necessarily have a large population of fusion-generated super-Alfvénic alphas, and like the beam ions in NSTX-U, these alphas will excite a variety of beam-driven instabilities. Neither NSTX-U, nor any other operating tokamak can simultaneously match all relevant fast-ion parameters to those expected for ITER, so predictions of fast-ion driven modes on ITER will rely on well-developed and validated theory. NSTX-U, which sees a broad spectrum of modes excited by the neutral beam ions, provides a laboratory to improve our understanding of this physics and to develop tools to control these instabilities, or to predict their affect on ITER.



Advanced Tokamak Experiments in Full-W ASDEX Upgrade

J. Stober¹, A. Bock¹, R. Fischer¹, E. Fable¹, C. Angioni¹, A. Herrmann¹, J. Hobirk¹, C. Hopf¹, A. Kallenbach¹, A. Mlynek¹, R. Neu¹, T. Pütterich¹, M. Reich¹, D. Rittich¹, M. Schubert¹, D. Wagner¹, and H. Zohm¹

¹Max-Planck-Institut für Plasmaphysik, Garching, Germany

Corresponding Author: J. Stober, joerg.stober@ipp.mpg.de

Since 2007 the tokamak ASDEX Upgrade (AUG) successfully operates with fully W-coated plasma facing components. Operation in this environment is facilitated using high levels of deuterium puff to minimize W erosion of the out-board limiters by ELMs and by seeding impurities in order to control divertor temperature at a low level to protect especially the W-coatings of graphite tiles. These measures effectively mitigate W erosion and accumulation, but are incompatible with operation at collisionalities low enough to obtain significant global current drive with the available means, i.e., NBCD and ECCD at high power levels. As a consequence advanced tokamak studies relying on the modification of current profiles by external current drive made poor progress in the first years following full W coverage. Additionally, polarized reflections of H_α-light from W-coated surfaces distort the current profile measurement based on the motional Stark effect, as it turned out several years later. This contribution reports on how these multiple operational restrictions have been overcome in AUG with a variety of measures including optimization of shape and gas puff timing, change to a full-W divertor with better pumping and optimization of the heating schemes. In parallel current profile diagnostics have been significantly improved, including polarimetry. Equilibrium reconstruction has been included into the concept of integrated data analysis, allowing a direct analysis of the influence of stochastic and systematic errors in the data on the estimated current profiles. Improved H-mode operation at moderate collisionality could be recovered and studies of H-modes with centrally elevated q -profiles could be successfully extended making use of the extended ECRH capabilities. A noninductive scenario at $q_{95} = 5.5$ could be obtained, which does not depend on q -profile tailoring during the current ramp-up phase and its successive diffusion. These high- β plasmas are also compared to results with the TGLF model.

Fluid Models for Burning and 3D Plasmas: Challenging the Kinetic Paradigm

M. J. Hole¹, Z. Qu¹, M. Fitzgerald², B. Layden¹, G. Bowden¹, R. Dewar¹, T. Alexis¹, and S. Hudson³

¹Australian National University, Canberra, Australia

²Culham Centre for Fusion Energy (CCFE), Culham Science Centre, Abingdon, UK

³Princeton Plasma Physics Laboratory (PPPL), Princeton, NJ 08540, USA

Corresponding Author: M. J. Hole, matthew.hole@anu.edu.au

We highlight recent ANU-led research in energetic particle physics and multi-relaxed region MHD. Topics include 1) the inclusion of anisotropy and flow into tokamak equilibria, stability and wave-particle interaction studies, 2) the calculation of energetic geodesic acoustic modes (EGAMs) using fluid theory, 3) the development and implementation of continuum damping in 3D, 4) the application of these tools to KSTAR, MAST and DIII-D discharges, and 5) the ongoing development of multiple relaxed region MHD. A common feature of the approaches adopted is the use of fluid theory to capture the physics of energetic particles and fully 3D fields.

Our feature example is EGAMs: axisymmetric energetic particle modes found in toroidally confined plasmas resulting from the geodesic curvature of magnetic field lines. They are experimentally observed at half of the conventional GAM frequency and are localized at the core, where there is a significant fast particle population. Until recently, it was widely believed that EGAMs are driven unstable by a positive gradient of the fast particles in the velocity space. However, unlike previous studies which treat fast ions kinetically, we consider the thermal ions and fast ions as different type of fluids with a super thermal flow speed for the latter. Surprisingly, the frequency and growth rate predicted by our fluid mode agree well with the kinetic theory when the fast ion energy width is small, despite the absence of inverse Landau damping in the fluid model. This indicates the reactive nature of this instability. Further investigation reveals the similarity of our reactive EGAMs to the well-known two-stream instability. We demonstrate the consistency of reactive EGAMs with the early turn-on of EGAMs in DIII-D experiments.

We also report on progress in the modelling of fully 3D fields with multiple relaxed region MHD, or MR×MHD, a generalization of Taylor's theory, in which the plasma is partitioned into a finite number of nested regions that independently undergo Taylor relaxation. The plasma regions are separated by ideal transport barriers that are also assumed to be magnetic flux surfaces. We examine the relationship between flux surface irrationality, MR×MHD stability, and tearing mode stability, as well as report on extensions of MR×MHD to include field-aligned and toroidal flow, and pressure anisotropy.

Microwrinkle Structure on Refractory Metal Surfaces Irradiated by Noble Gas Plasma Species

S. Takamura¹

¹Aichi Institute of Technology, Toyota, Aichi, Japan

Corresponding Author: S. Takamura, takamura@aitech.ac.jp

In fusion reactor, the fusion output will be severely restricted by melting of divertor target plate made of W material. Therefore, the artificial impurities such as neon, argon, nitrogen would be injected into edge region to have a strong radiation to the whole plasma-facing surface to mitigate an overheating of a narrow divertor target surface area. Therefore, the divertor plasmas contain noble gas species, which have interactions with the divertor target surface. So-called “fuzz” formation [1, 2] is one of well-known phenomena. Another important surface modification, microwrinkle formation, has not yet been examined so far although the surface damage may be much influenced and would be triggered by this structure. The present paper clarified the structural formation experimentally, identified the formation mechanism, and concluded that the formation is not specific but very general phenomena in plasma-surface interactions. Microwrinkle structures with the pitch of less than 100 nm up to 600 nm on refractory metals, like tungsten (W) and molybdenum (Mo) irradiated by noble gas ions, like neon (Ne) and helium (He), have been identified systematically for the first time. The wrinkle formation mechanism is clarified to be a buckling of surface hard layer supported by a soft elastic substrate [3] induced by a penetration of noble gas species from the irradiated surface. Microwrinkle forms on this structure under lateral compressive strain/stress fields coming from thermal constriction on the way to substrate cooling. Such process would be anticipated when the wall in fusion reactor is attacked by the heat pulses like ELMs and/or vertical displacement events, and it might be an initial stage of W surface damage. Ne injection experiments into W [4] did not produce any fuzzy nanostructure on W. Recent molecular dynamic simulation on Ne implantation in W confirms the limitation of large bubble formation and the prevention of fibre-form nanostructure [5]. They did not touch upon wrinkle structure formation. However, Ne penetration into W lattice plays a role of pinning against geometrically necessary dislocation movement, bringing a surface hardness of W. The buckling process would occur during a cooling stage of substrate. At that period Ne atoms remain temporarily at the surface layer, maintaining a surface hardness of W although Ne atoms may go out from the surface on the way to cooling down to the room temperature, which was confirmed with TDS measurements. Such dynamic retention of Ne atoms associated by a thermal constriction strain would produce buckling.

References

- [1] S. Takamura, *et al.*, Plasma Fusion. Res. **1**, 051 (2006).
- [2] S. Takamura, *et al.*, Applied Surf. Sci. **356**, 888 (2015).
- [3] T. Ohzono and H. Manobe, J. Colloid Interface Sci. **368**, 1 (2012).
- [4] M. Yajima, *et al.*, Plasma Sci. Eng. **15**, 282 (2013).
- [5] M. Backman, *et al.*, Nucl. Fusion **56**, 046008 (2016).

The Effect of the Isotope on the H-Mode Density Limit

A. Huber¹, S. Wiesen¹, M. Bernert², S. Brezinsek³, A. Chankin², G. Sergienko³, V. Huber³, P. Abreu⁴, A. Boboc⁵, M. Brix⁵, D. Carralero², E. Delabie⁶, T. Eich², H. G. Esser¹, C. Guillemaut⁴, S. Jachmich⁷, E. Joffrin⁸, A. Kallenbach², U. Kruezi⁵, P. Lang², C. Linsmeier¹, C. Lowry⁹, C. Maggi⁵, G. Matthews⁵, A. Meigs⁵, P. Mertens³, F. Reimold³, J. Schweinzer², A. Sips¹⁰, M. Stamp⁵, M. Wischmeier², H. Zohm², and E. Viezzer²

¹Institute of Energy and Climate Research, Forschungszentrum Jülich, Jülich, Germany

²Max-Planck-Institut für Plasmaphysik, Garching, Germany

³Forschungszentrum Jülich, Jülich, Germany

⁴Institute of Plasmas and Nuclear Fusion (IPNF), Association EURATOM/IST, Lisbon, Portugal

⁵Culham Centre for Fusion Energy (CCFE), Culham Science Centre, Abingdon, UK

⁶FOM Institute DIFFER, Association EURATOM-FOM, Nieuwegein, Netherlands

⁷Laboratory for Plasma Physics, ERM/KMS, Brussels, Belgium

⁸Institut de Recherche sur la Fusion par confinement Magnétique (IRFM),

Commissariat à l'énergie atomique (CEA/Cadarache), 13108 Saint-Paul-lès-Durance, France

⁹European Commission, Brussels, Belgium

¹⁰EUROFusion (EFDA), Max-Planck-Institut für Plasmaphysik, Garching, Germany

Corresponding Author: A. Huber, a.huber@fz-juelich.de

Identification of the mechanisms for the H-mode density limit in machines with fully metallic walls, and their scaling to future devices is essential to find for these machines the optimal operational boundaries with the highest attainable density and confinement. Systematic investigations of H-mode density limit plasmas in experiments with deuterium and hydrogen external gas fuelling have been performed on JET machine with fully metallic walls, and results have been compared with one another. The observed H-mode density limit on JET in D- as well as in H-plasmas demonstrates similar operation phases: the stable H-mode phase, degrading H-mode, breakdown of the H-mode with energy confinement deterioration accompanied by a dithering cycling phase, followed by the L-mode phase. Independent of the isotopic effect, total radiated power as well as the radiation power in the main chamber (P_{rad} , bulk) stays almost constant during the H-mode phase until the H-L transition. The density limit is not related to an inward collapse of the hot discharge core induced by overcooling of the plasma periphery by radiation. It was observed in D- and H-plasmas that detachment, as well as the X-point MARFE itself, does not trigger the H-L transition and thus does not present a limit on the plasma density and that it is the plasma confinement, most likely determined by edge parameters, which is ultimately responsible for the H-mode DL. Independent of the isotopic mass of the main plasma, it has been observed that the transition from H-mode to L-mode is not always an abrupt event but may exhibit a series of H-L-H transitions ('dithering H-mode'), or a gradual transition (which is orders of magnitude longer than energy confinement time τ_E). Although the operation phases are identical for D- and H-plasmas, the DL shows strong dependency on the isotopic mass effect, the DL is up to 40% lower in the H-plasma than in the deuterium plasma. Basically, the density limit in H mode on JET-ILW is nearly independent of the power in the range of observed heating powers and the corresponding densities only approach in this configuration a Greenwald fraction of about $f_{GW} = 0.9$ and $f_{GW} = 0.84$ in D-plasma and in H-plasma correspondingly. The measured Greenwald fractions are found to be consistent with the predictions from theoretical model based on MHD instability theory in the near-SOL.

END

Recent Advances towards a Lithium Vapor Box Divertor

R. Goldston¹, A. Hakim¹, G. Hammett¹, M. Jaworski¹, and J. Schwartz¹

¹Princeton Plasma Physics Laboratory (PPPL), Princeton, NJ 08540, USA

Corresponding Author: R. Goldston, rgoldston@pppl.gov

We report here advances from earlier work [1] on a lithium vapor box divertor, in which a lithium vapor cloud is held in place by local evaporation and strong differential pumping, forming a target to dissipate the heat flux from the divertor. The lowest, hottest box contains lithium vapor with n_l calculated to extinguish the expected heat flux. Its bottom is wetted with a layer of lithium to handle transient heat fluxes. The upper boxes are much cooler than the bottom box, so lithium is condensed there, and recirculated, greatly limiting the lithium efflux to the plasma.

In recent work we have used Navier–Stokes calculations to confirm the estimates in [1] of the strong differential pumping capabilities of such systems. We have found, however, that reflecting surfaces must be included to induce standing shocks to slow the flow. The approximate condition for this is easily obtained if the reflecting surfaces are at the local stagnation temperature of the vapor.

We have also developed a simplified model for system design that assumes all dissipation occurs in the bottom box, and that E_{dis} of energy (in eV) is dissipated for each lithium atom entering the divertor plasma from the vapor target, by Langmuir flux. For example, for a fusion power plant dissipating $P_{\text{dis}} = 200$ MW in its outer divertor leg at $R = 6$ m, a bottom box length $l = 0.5$ m, and a conservative 10 eV per atom energy dissipation, the box temperature is 725°C , the vapor density in the box is $8 \times 10^{21}/\text{m}^3$, and the mass efflux, M_{dot} , through a slit of width $d = 0.1$ m is 228 g/s. Differential pumping, as shown in [1], Fig. 1, should reduce the resulting efflux to the plasma to < 1 g/s.

A small-scale similarity experiment is being designed to validate the Navier-Stokes calculations. It will match Knudsen number and use steam as the similarity fluid, employing thermocouples, pressure sensors and Schlieren imaging to study n_{vap} , T_{vap} , flows and shocks.

References

[1] R. J. Goldston, *et al.*, *Physica Scripta*, accepted for publication.

Work supported by the U.S. Department of Energy under contract No. DE-AC02-09CH11466.



Chirping in Plasmas; Test of Criterion for Chirping Onset and Simulation of Explosive Chirping

H. Berk¹, B. Breizman¹, M. Van Zeeland², W. Heidbrink³, L. Cheng¹, G. Wang¹, V. Duarte⁴, G. Kramer⁴, M. Podesta⁴, B. J. Tobias⁴, R. Nazikian⁴, and D. C. Pace²

¹University of Texas at Austin, Austin, TX 78712, USA

²General Atomics, San Diego, CA 92186, USA

³University of California Irvine, CA 92697, USA

⁴Princeton Plasma Physics Laboratory (PPPL), Princeton, NJ 08540, USA

Corresponding Author: H. Berk, hberk@austin.utexas.edu

When plasmas have a sufficient number of energetic particles to induce instability, such as may occur in burning plasmas, it is important to have a reliable method of predicting the nature of the unstable state that will arise. Two extreme scenarios for the TAE frequency, ω_{TAE} arises: relatively steady oscillations at one extreme and chirping oscillations at the other extreme. For the first case, this work uses the generalized form of a criterion found by [1] that indicates, whether marginally unstable Alfvénic modes destabilized by energetic particles are more likely to chirp or more likely to remain as steady oscillations. This criterion has been applied to data in NSTX and DIII-D to successfully predict the parameters that produce either chirping or steady Alfvénic oscillations. Chirping arises in DIII-D when background turbulence markedly decreases. In the second part of the paper we consider the case where the strength of the driving source of energetic particles increases. Then instability may emerge from the continuum to form what has been called energetic particle modes (EPM). Here we describe a new way of numerically simulating an EPM which enables a significantly increased time-step for the numerical simulations. This study simulates, we believe for the first time, a chirping avalanche that is triggered by an EPM excitation and explains the dynamics with a new analytic theory.

References

[1] M. K. Lilley, *et al.*, Phys. Rev. Lett. **102**, 195003 (2009)



Formation of Closed Flux Surfaces in Reconnection Current Layer by Accelerated Electrons during Merging Start-up of Spherical Tokamak

M. Inomoto¹, K. Yamasaki¹, T. Ushiki¹, X. Guo¹, S. Kamio², R. Yanai¹, T. Sugawara¹, Y. Fukai¹, H. Yamanaka¹, and R. Tamura¹

¹*University of Tokyo, Tokyo, Japan*

²*National Institute for Fusion Science (NIFS), Toki, Gifu, Japan*

Corresponding Author: M. Inomoto, inomoto@k.u-tokyo.ac.jp

Spherical tokamak (ST) concept provides a potential for high- β plasma confinement, however, it requires downsizing or removal of centre solenoid (CS) coil because of restricted room in the central region. As one of candidates for CS-free start-up methods, combination of torus discharge by using external poloidal field coils and axial merging technique has been developed in the UTST experiment to establish an ST target plasma for neutral beam injection. The merging method involves magnetic reconnection in which high-power energy conversion from magnetic to mostly ion kinetic/thermal energies takes place, but more efficient electron heating, which is supposed to be provided only inside the reconnection current layer, is required to apply the merging method to form an ST target plasma. In ST merging case, large toroidal magnetic field (TF) perpendicular to the reconnection magnetic field exists and changes the reconnection local and global behaviours. One of the unique features provided by the TF is electron direct acceleration along the TF by reconnection electric field. In the UTST experiment, soft X-ray emission burst was observed during the merging phase, indicating that energetic electrons were generated by the reconnection process with TF. Fast camera observation of reconnection region showed that ring-shaped emission regions where impurity ions were ionized/excited by accelerated electrons were formed near the reconnection X-point. The accelerated electrons are expected to flow out quickly from the reconnection region, but detailed analysis of the camera image indicated that the electrons with high parallel velocity stayed much longer duration inside the current layer and thus they would achieve higher energy than those predicted in the classical reconnection model. Magnetic field and current density profiles were obtained by an internal magnetic probe array inserted inside the current layer. Since the accelerated electrons had high parallel (toroidal) velocity, they locally enhanced the toroidal current density and finally made a reversal of magnetic field in the vicinity of the current channel, which improved the electron confinement and thus provided higher electron heating efficiency during merging start-up of ST plasma.

Overview of some key achievements on the route to IFE

S. Jacquemot¹

¹*Laboratoire pour l'Utilisation des Lasers Intenses (LULI), École Polytechnique, 91128 Palaiseau, France*

Corresponding Author: S. Jacquemot, sylvie.jacquemot@polytechnique.fr

The EUROfusion ToIFE project, launched in 2014 and gathering 14 European laboratories from 9 different countries, aims at achieving the fundamental understanding required to demonstrate the viability of laser-driven fusion as an alternative road towards sustainable, clean and secure energy source. It hinges on i) a programme of experiments and numerical simulations to understand underlying obstacles to central hot-spot ignition on MJ-scale laser facilities and to reduce uncertainties that input into all inertial fusion ignition schemes (focussing on studies related to the radiative properties of the ablator dopants, to multi-speckle—plasma interaction, to foam-induced imprint smoothing and hydrodynamic instabilities or to ion stopping in plasmas), ii) a programme of experiments and numerical simulations towards demonstration of shock ignition, currently the most promising scheme for fusion energy (including the building of an integrated simulation platform), iii) a programme of numerical simulations and experiments to test the viability of other alternative ignition schemes (electron- and ion-driven fast ignition or impact ignition) with emphasis on magnetic collimation of electron beams, improvement of the laser-to-ion conversion efficiency thanks to advanced acceleration schemes and demonstration of laser-induced p-B fusion reactions, and iv) the conceptual design of an Inertial Fusion Energy (IFE) reactor based on the development of key technologies, such as high-repetition-rate laser drivers or innovative materials, for fusion targets or first walls. Significant results have been achieved so far and part of them, obtained by the French partners, will be discussed here.



Statistical Description of Turbulent Transport for Flux Driven Toroidal Plasmas

J. Anderson¹

¹*Chalmers University of Technology, Göteborg, Sweden*

Corresponding Author: J. Anderson, anderson.johan@gmail.com

During recent years an overwhelming body of evidence shows that the overall transport of heat and particles is to a large part caused by intermittency (or bursty events) related to coherent structures. One of the main challenges in magnetic fusion research has been to predict the turbulent heat and particle transport originating from various microinstabilities. The ion-temperature-gradient (ITG) mode is one of the main candidates for causing the anomalous heat transport in core plasmas of tokamaks. Significant heat transport can however be mediated by coherent structures such as streamers and blobs through the formation of avalanche like events of large amplitude, as indicated by recent numerical studies. These events cause a deviation of the probability distribution functions (PDFs) from a Gaussian profile on which the traditional mean field theory (such as transport coefficients) is based.

A crucial question in plasma confinement is thus the prediction of the PDFs of the transport due to these structures and of their formation. This work provides a theoretical interpretation of numerically generated PDFs of intermittent plasma transport events as well as offering an explanation for elevated PDF tails of heat flux. Specifically, in this work we analyze time traces of heat flux generated by global nonlinear gyrokinetic simulations of ion-temperature-gradient turbulence by the GKNET software. The simulation framework is global, flux-driven and considers adiabatic electrons. In these simulations SOC type intermittent bursts are frequently observed and transport is often regulated by nondiffusive processes, thus the PDFs of, e.g., heat flux are in general non-Gaussian with enhanced tails.

Facing the Challenge of Power Exhaust on the way to a Future Power Plant with Experiments in the JET and ASDEX Upgrade Tokamaks

M. Wischmeier¹, M. Bernert¹, C. Lowry², G. Calabro³, S. Wiesen⁴, F. Reimold⁴, A. Huber⁴, M. Reinke⁵, D. Brida¹, R. Dux¹, G. Christophe⁶, L. Aho-Mantila⁷, S. Brezinsek⁴, P. Drewelow⁸, S. Glöggler¹, M. Groth⁹, D. Harting¹⁰, A. Kallenbach¹, B. Lipschultz¹¹, L. Tilmann¹, C. Maggi¹⁰, A. Meigs¹⁰, M. F. Nave⁶, S. Potzel¹, G. Sergienko⁴, A. Sips¹², M. Stamp¹⁰, and B. Viola¹³

¹Max-Planck-Institut für Plasmaphysik, Garching, Germany

²European Commission, Brussels, Belgium

³Agenzia nazionale per le nuove tecnologie, l'energia e lo sviluppo economico sostenibile (ENEA), Rome, Italy

⁴Forschungszentrum Jülich, Jülich, Germany

⁵Oak Ridge National Laboratory (ORNL), Oak Ridge, TN 37831, USA

⁶Institute of Plasmas and Nuclear Fusion (IPNF), Association EURATOM/IST, Lisbon, Portugal

⁷VTT Technical Research Centre of Finland Ltd., Espoo, Finland

⁸Max-Planck-Institut für Plasmaphysik, Greifswald, Germany

⁹Aalto University, Espoo, Finland

¹⁰Culham Centre for Fusion Energy (CCFE), Culham Science Centre, Abingdon, UK

¹¹University of York, Heslington, UK

¹²JET Exploitation Unit

¹³Agenzia nazionale per le nuove tecnologie, l'energia e lo sviluppo economico sostenibile (ENEA), Rome, Italy

Corresponding Author: M. Wischmeier, marco.wischmeier@ipp.mpg.de

Future fusion devices such as ITER and DEMO face a major challenge when limiting the thermal power load reaching the plasma-facing components, PFCs, to values below the engineering specifications. In the case of DEMO the combination of power load and erosion limitations require plasma operation at a high fraction of power dissipation, estimated to be well beyond 90%, while maintaining a sufficient energy confinement time to achieve an economically competitive gain in power. In the case of an ITER-like divertor geometry this leads to a radiative power fraction, f_{rad} , in the order of 70% in the region of closed flux surfaces.

In the all-metal devices ASDEX Upgrade (AUG) and JET high radiation is achieved by seeding impurities by gas injection. While AUG and JET have both operated with N, Ne and Ar, only AUG extended its operation to include Kr, which is expected to be included in the ongoing experimental campaign at JET. Nitrogen has been established in both devices for achieving stable highly radiative regimes with strong X-point radiation and complete detachment along the target plates. For both devices at the highest seeding levels the dominant radiation originates from the confined region. Higher- Z impurities increase the radiation in this region already at lower divertor radiative power fraction. A deterioration of the confinement is only observed when enhanced radiation is obtained for a ρ_{pol} smaller than the position of the pedestal top. Albeit this upper limit at JET for all demonstrated seeding species the highest f_{rad} obtained were consistently linked to complete detachment over the tested range of P/R . For both devices enhanced perpendicular transport is observed in the SOL that correlates with the establishment of a highly collisional divertor regime.

For both devices numerical efforts for interpretative studies using complex transport codes such as SOLPS and EMC3-EIRENE are ongoing. With increasing confidence additional

physics such as the role of drift terms are being studied, allowing for consistently better agreement with experimental observations. Cases exist for which it has been possible to numerically recover many of the experimentally observed features of the high recycling and the completely detached H-mode regimes for AUG.



Impurity Transport and Plasma Flow in a Mixed Collisionality Stellarator Plasma

S. Newton¹, P. Helander², A. Mollén², Y. Turkin², and H. Smith²

¹*Chalmers University of Technology, Göteborg, Sweden*

²*Max-Planck-Institut für Plasmaphysik, Greifswald, Germany*

Corresponding Author: S. Newton, sarahn@chalmers.se

Neoclassical accumulation of impurities in the core of hot stellarator plasmas is a known problem. The complexity of neoclassical transport in stellarators means that few analytic studies are available to support numerical modelling efforts, and a robust understanding of the parameter dependence of the impurity flux is still lacking. Therefore we present an extension of the existing analytic treatment for highly collisional plasmas, into the experimentally relevant mixed collisionality regime—where a dominant heavy, collisional, impurity is present in a collisionless bulk plasma, taken here to be in the $1/\nu$ regime. We find that temperature screening of the impurity flux by the bulk ion temperature gradient will arise. We also determine the bulk ion flow in the flux surface, and thus the effect of the impurity on the bulk ion contribution to the bootstrap current.



Advanced Fuelling in Spherical Tokamak by Compact Toroid Injection on QUEST

N. Fukumoto¹, K. Awajitani¹, K. Hanada², H. Togashi³, K. Toida³, M. Nagata¹, T. Onchi⁴, H. Idei², M. Hasegawa⁴, A. Fujisawa⁴, K. Nakamura⁴, H. Zushi², K. Aleksandrovich⁴, A. Ejiri⁵, Y. Takase³, Y. Nagashima⁴, O. Mitarai⁶, A. Higashijima⁴, T. Nagata⁴, and S. Kawasaki⁴

¹University of Hyogo, Kobe, Hyogo, Japan

²Research Institute for Applied Mechanics (RIAM), Kyushu University, Kasuga, Japan

³University of Tokyo, Tokyo, Japan

⁴Kyushu University, Kasuga, Japan

⁵Graduate School of Frontier Science, University of Tokyo, Tokyo, Japan

⁶University of Saskatchewan, Saskatoon, SK S7N-5C9, Canada

Corresponding Author: N. Fukumoto, fukumotn@eng.u-hyogo.ac.jp

Compact toroid (CT) injection was conducted on several middle-class tokamaks in the previous experiments for development of an advance fuelling method. We have carried out CT injection in a spherical tokamak (ST) plasma, for the first time, on QUEST equivalent to the tokamaks in facility size. The primary aim of the experiment is to produce a high-density ST plasma and control its density profile by CT fuelling. The QUEST is designed for a ST confinement at the toroidal field $B_t = 0.5$ T for a pulse mode. The UH-CTI injector has a sufficient performance to penetrate into a ST plasma at $B_t = 0.8$ T. However the CT travelling distance from the injector nozzle to the separatrix on QUEST is 1.525 m, which is longer by about 1 m than that in the previous experiment on JFT-2M. It is also our objective to investigate the long CT transport with a drift tube. In the experiment, a CT plasma with a high density up to the order of $10^{21}/\text{m}^3$ at more than 200 km/s was injected perpendicularly on the magnetic axis on the midplane. Plasma responses to CT injection was obtained in an OH-ST plasma at $V_{\text{form.}} = 17$ kV and $V_{\text{acc.}} = 25$ kV for the CT formation and acceleration banks respectively. Plasma current had no adverse effect of CT injection. A line averaged electron density increased just after CT injection. Thus the long CT transport and the nondisruptive CT injection are successfully made. Electron density profile was also measured by Thomson scattering. The trigger system is set up to observe electron density profile at any given timing in the order of microseconds after CT injection. At the rather fast time of 0.5 ms after CT injection, increment in electron density was observed on the peripheral channels. In this experimental research, we have successfully conducted CT injection in a ST plasma on QUEST. Nondisruptive CT fuelling in an OH-ST plasma is obtained. Peripheral fuel particle deposition is observed by Thomson scattering.

This work was performed with the support and under the auspices of the NIFS Collaboration Research Program (NIFS14KUTR102, NIFS15KUTR112).

Metal Hall Sensors for the New Generation Reactors of the DEMO Scale

N. Kargin¹, I. Bolshakova², M. Bulavin³, Y. Kost², T. Kuech⁴, S. Kulikov³, F. Shurygin²,
M. Strikhanov¹, I. Vasil'evskii¹, and A. Vasyliiev²

¹National Research Nuclear University "MEPhI", Moscow, Russian Federation

²Magnetic Sensor Laboratory, Lviv Polytechnic National University, Lviv Oblast, Ukraine

³Joint Institute for Nuclear Research (JINR), Dubna, Moscow Oblast, Russian Federation

⁴University of Wisconsin-Madison, Madison, WI 53706, USA

Corresponding Author: N. Kargin, krgn@yandex.ru

The testing experiments of the Hall sensors based on the gold nanofilms have been carried out in Joint Institute for Nuclear Research in Dubna at the JBR-2 research nuclear reactor in May 2015. The special test instrumentation has been developed to provide the investigation up to the high neutron fluences. The instrumentation permits to provide online measurements of the sensor parameters under irradiation in the nuclear reactors channels. The neutron energy spectrum in this reactor was similar to the assumed one for the steady-state sensors locations in ITER reactor. Earlier it was shown that the III-V semiconductor-based Hall sensors are successfully functioning under the ITER-relevant conditions of reactor neutron irradiation as high as the fluence 2×10^{18} n/cm². Stable long-term operation of the sensors was also demonstrated in a JET reactor during the five-year period. The neutron fluence achieved in this experiment on the testing of the gold sensors was 10 times greater and approximately equals 2×10^{19} n/cm², the neutron flux; 1.5×10^{13} n/cm² s; the irradiation temperature 140°C. The experiment showed that the sensors sensitivity to the magnetic field was practically unchanged for the all range of the researched fluences. Such great radiation stability of the golden sensors under the high fluences, which essentially exceeds the neutron fluences achieved in the ITER reactor during its life time (approximately 20 years), makes these sensors very useful for DEMO scale reactors of the next generation.



Effect of Divertor Performance on the Pumping Efficiency in DEMO

Y. Igitkhanov¹, S. Varoutis¹, C. Day¹, and R. Wenninger²

¹Karlsruhe Institute of Technology (KIT), Karlsruhe, Germany

²Max-Planck-Institut für Plasmaphysik, Garching, Germany

Corresponding Author: Y. Igitkhanov, juri.igitkhanov@partner.kit.edu

One of the important tasks of the DEMO divertor design optimization is to ensure a desirable divertor performance and high pumping efficiency by varying, for example, the divertor dome height and pumping port position. In this paper we analyse the latest European DEMO divertor design with the pumping port located at the bottom of the divertor plenum. Optimization of the dome height and its effect on neutral compression is made by using the DIVGAS code based on the direct simulation Monte Carlo (DSMC) method [1]. The numerical analysis includes the calculation of neutral density in the PFR region and the overall conductance of the subdivertor structure, which consequently affects the estimation of the effective pumping speed and the achievement of detachment. First results of density comparison in divertor operation with and without dome in divertor design with a lateral position of the pumping port were reported in [2]. It was shown that asymmetric position of pumping port relative to the gaps causes strong reflux of particles from high field side gap and in the configuration without dome from the low field side. Apart of that in the case without dome a strong neutral reflux from the private flux region was found. In the case of pumping port at the bottom of the divertor the neutral flow pattern exhibits more symmetrical distribution. It is shown that the divertor configuration with dome impedes the reflux of neutrals towards the plasma. Furthermore, in this configuration we investigate the achievements of detachment depending on the level of neutral pressure in the divertor private flux region and required throughput for actual pumping speed.

References

- [1] G. A. Bird, *Molecular Gas Dynamics and the Direct Simulation of Gas Flows*, Oxford University Press, Oxford, UK (1994).
- [2] C. Day, S. Varoutis, Y. Igitkhanov, "Initial Studies of the Divertor Dome Effect on Pumping Efficiency in DEMO", *Proc. of the 26th Symposium on Fusion Engineering (SOFE)*, IEEE, US, (2015).

Helium Ion Energy Threshold for Helium Retention and Nano-bubble Formation in Tungsten

C. Corr¹, M. Thompson¹, P. Kluth¹, and D. Riley²

¹*Australian National University, Canberra, Australia*

²*Australian Nuclear Science and Technology Organisation, Lucas Heights NSW 2234, Australia*

Corresponding Author: C. Corr, cormac.corr@anu.edu.au

Tungsten has been chosen as the material for the ITER divertor and is a contender for the wall of DEMO, which will experience temperatures in excess of 1000 K. The interaction between high-flux helium plasmas with tungsten can lead to plasma-induced surface modifications. In particular helium retention in tungsten is problematic, since helium is known to form nanoscale bubbles beneath the surface, and are thought to be responsible for the formation of nano-fuzz and surface pitting [1, 2].

Results from grazing incidence small angle X-ray scattering (GISAXS) measurements [3] performed at the Australian Synchrotron show that in tungsten exposed to pure helium plasmas in linear plasma devices, such as the magnetized plasma interaction experiment (MAGPIE) [4], nanosized bubbles of between 1.5–2.5 nm diameter are formed in near-surface layers of approximately 30 nm thickness. The findings are in excellent agreement with a direct observation by transmission electron microscopy. Depth distributions were estimated by taking successive measurements across a range of X-ray incidence angles. As an example, for tungsten at 700°C, the bubble layer is observed to be 31 ± 4 nm deep.

A helium ion energy threshold of approximately 9 eV has been identified, above which helium nano-bubbles are formed and is strongly correlated with an increase in helium retention. The effects of surface temperature and plasma fluence on nano-bubble formation will also be presented.

References

- [1] S. Kajita, *et al.*, *J. Nucl. Mater.* **418**, 152–158 (2011).
- [2] D. Nishijima, *et al.*, *J. Nucl. Mater.* **313–316**, 97 (2003).
- [3] M. Thompson, *et al.*, *Nucl. Fusion* **55**, 042001 (2015).
- [4] B. D. Blackwell, *et al.*, *Plasma Sources Sci. Technol.* **21**, 055033 (2012).



Active and Passive Stabilization of $n = 0$ RWMs in Future Tokamak Devices

A. Portone¹

¹F4E: Fusion for Energy, ITER EU Centre, 08019 Barcelona, Spain

Corresponding Author: A. Portone, alfredo.portone@f4e.europa.eu

In the design of next step tokamak devices, it will be of key importance to carefully optimize the plasma magnetic configuration, in particular its elongation, triangularity and aspect ratio. Indeed, the sharp dependence of the safety factor q upon plasma elongation and, as a consequence, of the maximum achievable plasma current in disruption-free operation mode is of paramount importance to achieve high plasma performances and high- Q .

The aim of this paper is to study the effects that plasma aspect ratio, plasma-wall normalized distance and plasma current profile have on passive plasma vertical stabilization, this being quantified by the plasma stability margin and instability growth time. Following this first step, the key aspects and figures of merit of plasma active vertical stabilization will be reviewed, with specific emphasis on the maximum disturbances that can be recovered by the plasma active control system with fixed current and voltage ratings. Both in-vessel as well as ex-vessel optimally placed stabilization coils will be considered. State of the art plasma models (as based on linear, MHD theory) and metallic structures (fully 3D structures) will be deployed in study.

The final goal is to derive the dependence of plasma elongation upon the parameters described above in order to achieve robust passive and active stabilization with and without internal coils.

Collisional Radiative Model Using the Fully Relativistic Cross-sections for the Hydrogen-cesium Plasma Relevant to ITER Negative Ion Based NBI System

R. Srivastava¹, P. Priti¹, and D. Dipti¹

¹*Indian Institute of Technology (IIT), Roorkee, India*

Corresponding Author: R. Srivastava, rajsrfph@iitr.ac.in

An improved collisional radiative (CR) model has been developed for hydrogen-cesium plasma for its application to the negative hydrogen ion sources where we used reliable cross sections. The required electron impact excitation cross-sections have been obtained using fully relativistic distorted wave theory for various fine-structure transitions from the ground as well as excited states. These are then incorporated in the CR model along with other processes such as radiative population transfer, electron impact ionization and mutual neutralization of Cs^+ ion with negative hydrogen ion along with their reverse processes. Results deduced from the present CR model have been compared with earlier experimental as well as the modelling results.

DD Neutron Emission Measurement in the Compact Tokamak TUMAN-3M

V. Kornev¹, L. Askinazi¹, A. Belokurov¹, S. Lebedev¹, F. Chernyshev¹, A. Melnik¹,
A. Shabelsky¹, A. Tukachinsky¹, and N. Zhubr¹

¹Ioffe Institute, St. Petersburg, Russian Federation

Corresponding Author: V. Kornev, vladimir.kornev@mail.ioffe.ru

Recent experiments on the TUMAN-3M compact tokamak were aimed at study of fast ion (FI) capture and confinement in co-current NBI heating scheme. Target plasma parameters in the experiments were as follows: $R_0 = 0.53$ m, $a_l = 0.22$ m, $B_t \leq 1$ T, $I_p \leq 180$ kA, $n_e \leq 4 \times 10^{19}/\text{m}^3$, $T_e(0) \leq 0.7$ keV, $T_i \leq 0.2$ keV. Maximum output power of deuterium neutral beam $P_{inj} = 700$ kW. Measurement of 2.45 MeV DD neutron flux was used to study of FI behaviour. The experiments allowed establishing of parametric dependencies of neutron rate and concluding absence of significant losses of FI during slowing down. Use of powerful ion source in second set of experiments allowed beam current by a factor of two higher than that with old one. This arrangement provided a possibility to alter output beam power at given beam energy. Losses of FI during slowing down were estimated using measurements of neutron rate decay time τ_n after NBI switch-off. Experimental R_n and τ_n measured at $E_b = 21.5$ keV indicate equal portions of FI power transferred to target electrons and ions during slowing down and small if any influence of anomalous losses on R_n magnitude. Numerical modelling of neutron rate in NBI experiment was performed using ASTRA transport code. Modelling of the influence of n_{av} , E_b , B_t and I_p on R_n in assumption of classical slowing down has shown good agreement with the experiment. Database of neutron rate measurements obtained with beam energy range of 14–20 keV was utilized to establish dependence of R_n on n_{av} , B_t , I_p and E_b : $R_n = 6 \times 10^5$, $n_{av} \sim 0.36$, $B_t = 1.29$, $I_p = 1.34$, $E_b = 4.69$. The scaling doesn't contain dependence of R_n on input power since the NBI module is unable to provide independent variation of E_b and P_{inj} . Replacement of ion source opened possibility to get another dataset in the same energy range but with approximately doubled power. Contrary to expectations increased input power does not result in an increase in the neutron rate. The deficit could be understood assuming significant dilution of target plasma in conditions of increased input power. Another option is substantial reduction of input beam intensity due to its attenuation in the input port. Further experiments are planned to clarify the reason of R_n deficit in conditions of increased input power.



Electron-Impact Ionization Cross Sections of Molecules and Ions in Fusion Plasma

M. Probst¹, I. Sukuba^{1,2}, J. Urban², A. Kaiser¹, T. Maihom^{3,4}, J. Limtrakul³,
K. Hermansson⁵, D. Borodin⁶, and S. Huber¹

¹University of Innsbruck, Innsbruck, Austria

²Comenius University, Bratislava, Slovakia

³Vidyasirimedhi Institute of Science and Technology, Rayong 21210, Thailand

⁴Kasetsart University, Kamphaeng Saen Campus, Chang Wat Nakhon Pathom 73140, Thailand

⁵Uppsala University, Uppsala, Sweden

⁶Institute of Energy and Climate Research, Forschungszentrum Jülich, Jülich, Germany

Corresponding Author: M. Probst, michael.probst@uibk.ac.at

Electron-impact cross sections yield the probability of an electron reacting with a particle—a molecule, an ion or an atom—as a function of the energy of that electron. At low energies so-called dissociative electron attachment (DEA) is the predominant reaction mechanism. At energies of the incoming electron higher than the ionization threshold of the particle, typically the particle loses one of its electrons. A rigorous treatment of such electron-molecule/atom reactions is difficult but certain approximate methods work well. Knowledge of the EICs for components occurring in plasma is crucial for obtaining the energy balance in the plasma which is influenced by the ionization of plasma components by plasma electrons. For example, the electron impact process can remove fast electrons and supply slow ones. It also leads to an abundance of cationic species that can, possibly at other locations, re-neutralize or become multiply charged cations. In our paper we describe the two most widely used methods for calculating the EICS, the binary-encounter-Bethe and the Deutsch-Maerk method. Then we apply these methods to calculate the electron-impact cross sections of neutral and ionized beryllium hydrides for the first time. Finally, we present a way to obtain partial, reaction-specific cross sections as opposed to the overall ones.

Indexes

Abstracts by Paper Number

EX/1-1	168	EX/P3-22	225	EX/P4-30	275
EX/1-2	169	EX/P3-23	226	EX/P4-31	276
EX/1-3	170	EX/P3-24	227	EX/P4-32	277
EX/1-4	171	EX/P3-25	228	EX/P4-33	278
EX/10-1	202	EX/P3-26	229	EX/P4-34	279
EX/10-2	203	EX/P3-27	230	EX/P4-35	280
EX/10-3	204	EX/P3-28	231	EX/P4-36	281
EX/11-1	205	EX/P3-29	232	EX/P4-38	282
EX/2-1	172	EX/P3-3	208	EX/P4-39	283
EX/2-2	173	EX/P3-30	233	EX/P4-4	250
EX/2-3	174	EX/P3-31	234	EX/P4-40	284
EX/3-1	175	EX/P3-32	235	EX/P4-41	285
EX/3-2	176	EX/P3-33	236	EX/P4-42	286
EX/3-3	177	EX/P3-34	237	EX/P4-43	287
EX/3-4	178	EX/P3-36	238	EX/P4-44	288
EX/3-5	179	EX/P3-37	239	EX/P4-45	289
EX/3-6	180	EX/P3-38	240	EX/P4-47	290
EX/4-1	181	EX/P3-39	241	EX/P4-48	291
EX/4-2	182	EX/P3-40	242	EX/P4-49	292
EX/4-3	183	EX/P3-41	243	EX/P4-5	251
EX/4-4	184	EX/P3-42	244	EX/P4-50	293
EX/4-5	185	EX/P3-46	245	EX/P4-51	294
EX/5-1	187	EX/P3-47	246	EX/P4-52	295
EX/5-2	188	EX/P3-5	209	EX/P4-53	296
EX/5-3	189	EX/P3-6	210	EX/P4-6	252
EX/6-1	190	EX/P3-7	211	EX/P4-7	253
EX/6-2	191	EX/P3-8	212	EX/P4-8	254
EX/7-1	192	EX/P3-9	213	EX/P4-9	255
EX/7-2	193	EX/P4-1	247	EX/P5-1	297
EX/7-3Ra	194	EX/P4-10	256	EX/P5-10	306
EX/7-3Rb	195	EX/P4-12	257	EX/P5-11	307
EX/8-1	196	EX/P4-13	258	EX/P5-12	308
EX/8-2	197	EX/P4-14	259	EX/P5-13	309
EX/9-1	198	EX/P4-15	260	EX/P5-14	310
EX/9-2	199	EX/P4-16	261	EX/P5-15	311
EX/9-3	200	EX/P4-17	262	EX/P5-16	312
EX/9-4	201	EX/P4-18	263	EX/P5-17	313
EX/P3-1	206	EX/P4-19	264	EX/P5-18	314
EX/P3-10	214	EX/P4-2	248	EX/P5-19	315
EX/P3-11	215	EX/P4-20	265	EX/P5-2	298
EX/P3-12	216	EX/P4-21	266	EX/P5-20	316
EX/P3-13	217	EX/P4-22	267	EX/P5-21	317
EX/P3-14	218	EX/P4-23	268	EX/P5-22	318
EX/P3-15	219	EX/P4-24	269	EX/P5-23	319
EX/P3-16	220	EX/P4-25	270	EX/P5-24	320
EX/P3-18	221	EX/P4-26	271	EX/P5-25	321
EX/P3-19	222	EX/P4-27	272	EX/P5-26	322
EX/P3-2	207	EX/P4-28	273	EX/P5-28	323
EX/P3-20	223	EX/P4-29	274	EX/P5-29	324
EX/P3-21	224	EX/P4-3	249	EX/P5-3	299

EX/P5-30	325	EX/P6-51	377	EX/P8-24	435
EX/P5-31	326	EX/P6-52	378	EX/P8-25	436
EX/P5-32	327	EX/P6-53	379	EX/P8-26	437
EX/P5-33	328	EX/P6-6	333	EX/P8-27	438
EX/P5-4	300	EX/P6-8	334	EX/P8-28	439
EX/P5-5	301	EX/P6-9	335	EX/P8-29	440
EX/P5-6	302	EX/P7-1	380	EX/P8-3	415
EX/P5-7	303	EX/P7-10	387	EX/P8-30	441
EX/P5-8	304	EX/P7-12	388	EX/P8-31	442
EX/P5-9	305	EX/P7-15	389	EX/P8-32	443
EX/P6-1	329	EX/P7-16	390	EX/P8-33	444
EX/P6-10	336	EX/P7-17	391	EX/P8-34	445
EX/P6-11	337	EX/P7-19	392	EX/P8-35	446
EX/P6-12	338	EX/P7-2	381	EX/P8-36	447
EX/P6-13	339	EX/P7-21	393	EX/P8-37	448
EX/P6-14	340	EX/P7-22	394	EX/P8-38	449
EX/P6-15	341	EX/P7-24	395	EX/P8-39	450
EX/P6-16	342	EX/P7-25	396	EX/P8-4	416
EX/P6-17	343	EX/P7-27	397	EX/P8-40	451
EX/P6-18	344	EX/P7-29	398	EX/P8-41	453
EX/P6-19	345	EX/P7-30	399	EX/P8-42	454
EX/P6-2	330	EX/P7-34	400	EX/P8-43	456
EX/P6-20	346	EX/P7-35	401	EX/P8-44	457
EX/P6-21	347	EX/P7-36	402	EX/P8-45	458
EX/P6-22	348	EX/P7-38	403	EX/P8-46	459
EX/P6-23	349	EX/P7-39	404	EX/P8-5	417
EX/P6-24	351	EX/P7-4	382	EX/P8-6	418
EX/P6-25	352	EX/P7-40	405	EX/P8-7	419
EX/P6-26	353	EX/P7-41	406	EX/P8-8	420
EX/P6-27	354	EX/P7-42	407	EX/P8-9	421
EX/P6-28	355	EX/P7-43	408	FIP/1-1	656
EX/P6-29	356	EX/P7-44	409	FIP/1-2	657
EX/P6-3	331	EX/P7-45	410	FIP/1-3Ra	658
EX/P6-30	357	EX/P7-47	411	FIP/1-3Rb	659
EX/P6-31	358	EX/P7-48	412	FIP/1-4	660
EX/P6-32	359	EX/P7-5	383	FIP/1-5	661
EX/P6-33	360	EX/P7-7	384	FIP/1-6Ra	662
EX/P6-34	361	EX/P7-8	385	FIP/1-6Rb	663
EX/P6-35	362	EX/P7-9	386	FIP/1-6Rc	664
EX/P6-36	363	EX/P8-1	413	FIP/2-1Ra	665
EX/P6-37	364	EX/P8-10	422	FIP/2-1Rb	666
EX/P6-38	365	EX/P8-11	423	FIP/2-2	668
EX/P6-39	366	EX/P8-12	424	FIP/2-3	669
EX/P6-40	367	EX/P8-13	425	FIP/2-4	670
EX/P6-41	368	EX/P8-14	426	FIP/2-5	671
EX/P6-42	369	EX/P8-16	427	FIP/3-1Ra	672
EX/P6-44	370	EX/P8-17	428	FIP/3-1Rb	673
EX/P6-45	371	EX/P8-18	429	FIP/3-2	674
EX/P6-46	372	EX/P8-19	430	FIP/3-3	675
EX/P6-47	373	EX/P8-2	414	FIP/3-4Ra	676
EX/P6-48	374	EX/P8-20	431	FIP/3-4Rb	677
EX/P6-49	375	EX/P8-21	432	FIP/3-4Rc	678
EX/P6-5	332	EX/P8-22	433	FIP/3-5	679
EX/P6-50	376	EX/P8-23	434		

FIP/4-1Ra.....	680	FIP/P7-24.....	740	IFE/P5-18.....	797
FIP/4-1Rb.....	681	FIP/P7-25.....	741	IFE/P5-19.....	798
FIP/7-7.....	724	FIP/P7-26.....	742	IFE/P5-2.....	784
FIP/P4-10.....	690	FIP/P7-27.....	743	IFE/P5-4.....	785
FIP/P4-11.....	691	FIP/P7-29.....	744	IFE/P5-5.....	786
FIP/P4-12.....	692	FIP/P7-3.....	720	IFE/P5-6.....	787
FIP/P4-13.....	693	FIP/P7-31.....	745	IFE/P5-7.....	788
FIP/P4-14.....	694	FIP/P7-33.....	746	IFE/P5-8.....	789
FIP/P4-15.....	695	FIP/P7-34.....	747	IFE/P5-9.....	790
FIP/P4-16.....	696	FIP/P7-35.....	748		
FIP/P4-17.....	697	FIP/P7-36.....	749	MPT/1-1.....	800
FIP/P4-18.....	698	FIP/P7-37.....	750	MPT/1-2Ra.....	801
FIP/P4-2.....	682	FIP/P7-38.....	751	MPT/1-2Rb.....	802
FIP/P4-20.....	699	FIP/P7-39.....	752	MPT/1-3.....	803
FIP/P4-21.....	700	FIP/P7-4.....	721	MPT/P5-1.....	804
FIP/P4-22.....	701	FIP/P7-40.....	753	MPT/P5-11.....	812
FIP/P4-27.....	702	FIP/P7-41.....	754	MPT/P5-12.....	813
FIP/P4-28.....	703	FIP/P7-42.....	755	MPT/P5-13.....	814
FIP/P4-29.....	704	FIP/P7-43.....	756	MPT/P5-14.....	815
FIP/P4-3.....	683	FIP/P7-44.....	757	MPT/P5-15.....	816
FIP/P4-31.....	705	FIP/P7-45.....	758	MPT/P5-16.....	817
FIP/P4-33.....	706	FIP/P7-46.....	759	MPT/P5-17.....	818
FIP/P4-36.....	707	FIP/P7-47.....	760	MPT/P5-18.....	819
FIP/P4-37.....	708	FIP/P7-5.....	722	MPT/P5-19.....	820
FIP/P4-38.....	709	FIP/P7-6.....	723	MPT/P5-2.....	805
FIP/P4-39.....	710	FIP/P7-8.....	725	MPT/P5-21.....	821
FIP/P4-4.....	684	FIP/P7-9.....	726	MPT/P5-23.....	822
FIP/P4-40.....	711	FNS/1-1.....	762	MPT/P5-24.....	823
FIP/P4-41.....	712	FNS/1-2.....	763	MPT/P5-25.....	824
FIP/P4-42.....	713	FNS/1-3.....	764	MPT/P5-26.....	825
FIP/P4-43.....	714	FNS/P5-1.....	765	MPT/P5-27.....	826
FIP/P4-44.....	715	FNS/P5-10.....	772	MPT/P5-29.....	827
FIP/P4-45.....	716	FNS/P5-11.....	773	MPT/P5-3.....	806
FIP/P4-46.....	717	FNS/P5-12.....	774	MPT/P5-30.....	828
FIP/P4-5.....	685	FNS/P5-13.....	775	MPT/P5-31.....	829
FIP/P4-6.....	686	FNS/P5-2.....	766	MPT/P5-32.....	830
FIP/P4-7.....	687	FNS/P5-3.....	767	MPT/P5-33.....	831
FIP/P4-8.....	688	FNS/P5-5.....	768	MPT/P5-35.....	832
FIP/P4-9.....	689	FNS/P5-6.....	769	MPT/P5-38.....	833
FIP/P7-1.....	718	FNS/P5-8.....	770	MPT/P5-39.....	834
FIP/P7-10.....	727	FNS/P5-9.....	771	MPT/P5-4.....	807
FIP/P7-11.....	728			MPT/P5-41.....	835
FIP/P7-12.....	729	IFE/1-1.....	778	MPT/P5-42.....	836
FIP/P7-13.....	730	IFE/1-2.....	779	MPT/P5-5.....	808
FIP/P7-14.....	731	IFE/1-3.....	780	MPT/P5-6.....	809
FIP/P7-15.....	732	IFE/1-4.....	781	MPT/P5-7.....	810
FIP/P7-16.....	733	IFE/1-5.....	782	MPT/P5-9.....	811
FIP/P7-17.....	734	IFE/1-6.....	783		
FIP/P7-18.....	735	IFE/P5-10.....	791	O/1-4.....	124
FIP/P7-19.....	736	IFE/P5-11.....	792	O/1-5.....	125
FIP/P7-2.....	719	IFE/P5-12.....	793	OV/1-1.....	128
FIP/P7-20.....	737	IFE/P5-13.....	794	OV/1-2.....	129
FIP/P7-21.....	738	IFE/P5-14.....	795	OV/1-3.....	130
FIP/P7-22.....	739	IFE/P5-17.....	796	OV/1-4.....	131

OV/2-1	132	PDP-25	872	TH/P1-31	510
OV/2-2	133	PDP-26	873	TH/P1-32	511
OV/2-3	134	PPC/1-1	838	TH/P1-33	512
OV/2-4	135	PPC/2-1	839	TH/P1-34	513
OV/2-5	136			TH/P1-35	514
OV/3-1	137	SEE/P7-1	842	TH/P1-36	515
OV/3-2	138	SEE/P7-2	843	TH/P1-37	516
OV/3-3	139	SEE/P7-3	844	TH/P1-38	517
OV/3-4	140	SEE/P7-4	845	TH/P1-4	483
OV/4-1	141	SEE/P7-5	846	TH/P1-5	484
OV/4-2	142	SEE/P7-6	847	TH/P1-6	485
OV/4-3Ra	143			TH/P1-7	486
OV/4-3Rb	145	TH/1-1	462	TH/P1-8	487
OV/4-4	146	TH/2-1	463	TH/P1-9	488
OV/4-5	147	TH/2-2	464	TH/P2-1	518
OV/5-1	148	TH/3-1	465	TH/P2-10	527
OV/5-2	149	TH/4-1	466	TH/P2-11	528
OV/5-3	150	TH/4-2	467	TH/P2-12	529
OV/5-4	151	TH/4-3	468	TH/P2-13	531
OV/5-5	152	TH/5-1	469	TH/P2-14	534
OV/P-1	153	TH/5-2	470	TH/P2-15	536
OV/P-10	163	TH/6-1	471	TH/P2-16	537
OV/P-11	164	TH/6-2	472	TH/P2-17	538
OV/P-12	165	TH/6-3	473	TH/P2-18	539
OV/P-2	154	TH/7-1	474	TH/P2-19	540
OV/P-3	155	TH/7-2	475	TH/P2-2	519
OV/P-4	156	TH/8-1	476	TH/P2-20	541
OV/P-5	157	TH/8-2	477	TH/P2-21	542
OV/P-6	159	TH/8-3	478	TH/P2-22	543
OV/P-7	160	TH/9-1	479	TH/P2-23	544
OV/P-8	161	TH/P1-1	480	TH/P2-24	545
OV/P-9	162	TH/P1-10	489	TH/P2-25	546
		TH/P1-11	490	TH/P2-26	547
PD/1-1	850	TH/P1-12	491	TH/P2-27	548
PD/1-2	851	TH/P1-13	492	TH/P2-28	549
PDP-02	852	TH/P1-14	493	TH/P2-29	550
PDP-03	853	TH/P1-15	494	TH/P2-3	520
PDP-04	854	TH/P1-16	495	TH/P2-30	551
PDP-05	855	TH/P1-17	496	TH/P2-31	552
PDP-07	856	TH/P1-18	497	TH/P2-32	553
PDP-08	857	TH/P1-19	498	TH/P2-33	554
PDP-09	858	TH/P1-2	481	TH/P2-4	521
PDP-10	859	TH/P1-20	499	TH/P2-5	522
PDP-11	860	TH/P1-21	500	TH/P2-6	523
PDP-12	861	TH/P1-22	501	TH/P2-7	524
PDP-13	862	TH/P1-23	502	TH/P2-8	525
PDP-14	863	TH/P1-24	503	TH/P2-9	526
PDP-15	865	TH/P1-25	504	TH/P3-1	555
PDP-16	866	TH/P1-26	505	TH/P3-10	564
PDP-18	867	TH/P1-27	506	TH/P3-11	565
PDP-19	868	TH/P1-28	507	TH/P3-12	566
PDP-21	869	TH/P1-29	508	TH/P3-13	567
PDP-23	870	TH/P1-3	482	TH/P3-14	568
PDP-24	871	TH/P1-30	509	TH/P3-15	569

TH/P3-16.....	570	TH/P4-1.....	593	TH/P4-8.....	600
TH/P3-17.....	571	TH/P4-10.....	601	TH/P6-1.....	625
TH/P3-18.....	572	TH/P4-11.....	602	TH/P6-10.....	634
TH/P3-19.....	573	TH/P4-12.....	603	TH/P6-11.....	635
TH/P3-2.....	556	TH/P4-14.....	604	TH/P6-12.....	636
TH/P3-20.....	574	TH/P4-16.....	605	TH/P6-15.....	637
TH/P3-21.....	575	TH/P4-17.....	606	TH/P6-16.....	638
TH/P3-22.....	576	TH/P4-18.....	607	TH/P6-17.....	639
TH/P3-23.....	577	TH/P4-19.....	608	TH/P6-18.....	640
TH/P3-24.....	578	TH/P4-2.....	594	TH/P6-19.....	641
TH/P3-25.....	579	TH/P4-20.....	609	TH/P6-2.....	626
TH/P3-26.....	580	TH/P4-21.....	610	TH/P6-20.....	642
TH/P3-27.....	581	TH/P4-23.....	611	TH/P6-22.....	643
TH/P3-29.....	582	TH/P4-24.....	612	TH/P6-23.....	644
TH/P3-3.....	557	TH/P4-25.....	613	TH/P6-24.....	645
TH/P3-30.....	583	TH/P4-26.....	614	TH/P6-25.....	646
TH/P3-31.....	584	TH/P4-27.....	615	TH/P6-26.....	647
TH/P3-32.....	585	TH/P4-28.....	616	TH/P6-27.....	648
TH/P3-33.....	586	TH/P4-29.....	617	TH/P6-28.....	649
TH/P3-34.....	587	TH/P4-3.....	595	TH/P6-29.....	650
TH/P3-35.....	588	TH/P4-30.....	618	TH/P6-3.....	627
TH/P3-36.....	589	TH/P4-31.....	619	TH/P6-30.....	651
TH/P3-37.....	590	TH/P4-32.....	620	TH/P6-31.....	652
TH/P3-38.....	591	TH/P4-34.....	621	TH/P6-32.....	653
TH/P3-39.....	592	TH/P4-35.....	622	TH/P6-4.....	628
TH/P3-4.....	558	TH/P4-36.....	623	TH/P6-5.....	629
TH/P3-5.....	559	TH/P4-37.....	624	TH/P6-6.....	630
TH/P3-6.....	560	TH/P4-4.....	596	TH/P6-7.....	631
TH/P3-7.....	561	TH/P4-5.....	597	TH/P6-8.....	632
TH/P3-8.....	562	TH/P4-6.....	598	TH/P6-9.....	633
TH/P3-9.....	563	TH/P4-7.....	599		

Contributions by Indico Submission Number

IAEA-CN-234-0001...765	IAEA-CN-234-0068...583	IAEA-CN-234-0120...419
IAEA-CN-234-0002...718	IAEA-CN-234-0069...748	IAEA-CN-234-0121...314
IAEA-CN-234-0003...246	IAEA-CN-234-0070...637	IAEA-CN-234-0122...587
IAEA-CN-234-0005...390	IAEA-CN-234-0071...575	IAEA-CN-234-0123...406
IAEA-CN-234-0006...780	IAEA-CN-234-0072...381	IAEA-CN-234-0124...721
IAEA-CN-234-0007...313	IAEA-CN-234-0073...493	IAEA-CN-234-0125...165
IAEA-CN-234-0008...526	IAEA-CN-234-0074...472	IAEA-CN-234-0126...722
IAEA-CN-234-0010...486	IAEA-CN-234-0075...484	IAEA-CN-234-0127...373
IAEA-CN-234-0011...766	IAEA-CN-234-0076...677	IAEA-CN-234-0128...227
IAEA-CN-234-0012...645	IAEA-CN-234-0077...184	IAEA-CN-234-0129...424
IAEA-CN-234-0013...601	IAEA-CN-234-0078...132	IAEA-CN-234-0130...483
IAEA-CN-234-0014...610	IAEA-CN-234-0079...763	IAEA-CN-234-0131...663
IAEA-CN-234-0015...609	IAEA-CN-234-0080...405	IAEA-CN-234-0132...513
IAEA-CN-234-0016...719	IAEA-CN-234-0082...574	IAEA-CN-234-0133...511
IAEA-CN-234-0017...207	IAEA-CN-234-0083...414	IAEA-CN-234-0134...322
IAEA-CN-234-0018...160	IAEA-CN-234-0084...842	IAEA-CN-234-0135...639
IAEA-CN-234-0019...634	IAEA-CN-234-0085...806	IAEA-CN-234-0137...457
IAEA-CN-234-0020...537	IAEA-CN-234-0086...807	IAEA-CN-234-0138...319
IAEA-CN-234-0021...619	IAEA-CN-234-0087...843	IAEA-CN-234-0139...430
IAEA-CN-234-0022...216	IAEA-CN-234-0088...156	IAEA-CN-234-0140...162
IAEA-CN-234-0023...235	IAEA-CN-234-0089...808	IAEA-CN-234-0143...329
IAEA-CN-234-0024...527	IAEA-CN-234-0090...790	IAEA-CN-234-0144...598
IAEA-CN-234-0025...311	IAEA-CN-234-0091...506	IAEA-CN-234-0145...525
IAEA-CN-234-0026...804	IAEA-CN-234-0092...333	IAEA-CN-234-0146...750
IAEA-CN-234-0028...767	IAEA-CN-234-0093...465	IAEA-CN-234-0147...709
IAEA-CN-234-0035...464	IAEA-CN-234-0094...306	IAEA-CN-234-0148...436
IAEA-CN-234-0036...220	IAEA-CN-234-0095...490	IAEA-CN-234-0149...710
IAEA-CN-234-0037...653	IAEA-CN-234-0096...305	IAEA-CN-234-0150...301
IAEA-CN-234-0039...708	IAEA-CN-234-0097...340	IAEA-CN-234-0151...723
IAEA-CN-234-0040...289	IAEA-CN-234-0098...643	IAEA-CN-234-0152...379
IAEA-CN-234-0041...420	IAEA-CN-234-0099...150	IAEA-CN-234-0153...361
IAEA-CN-234-0042...159	IAEA-CN-234-0100...541	IAEA-CN-234-0154...529
IAEA-CN-234-0043...476	IAEA-CN-234-0101...809	IAEA-CN-234-0157...792
IAEA-CN-234-0044...778	IAEA-CN-234-0102...471	IAEA-CN-234-0158...811
IAEA-CN-234-0045...805	IAEA-CN-234-0103...749	IAEA-CN-234-0160...624
IAEA-CN-234-0046...468	IAEA-CN-234-0104...618	IAEA-CN-234-0161...210
IAEA-CN-234-0047...642	IAEA-CN-234-0105...720	IAEA-CN-234-0163...620
IAEA-CN-234-0048...789	IAEA-CN-234-0106...604	IAEA-CN-234-0164...291
IAEA-CN-234-0050...785	IAEA-CN-234-0107...597	IAEA-CN-234-0165...521
IAEA-CN-234-0052...596	IAEA-CN-234-0108...230	IAEA-CN-234-0166...177
IAEA-CN-234-0053...417	IAEA-CN-234-0109...450	IAEA-CN-234-0167...317
IAEA-CN-234-0054...784	IAEA-CN-234-0110...664	IAEA-CN-234-0168...211
IAEA-CN-234-0055...747	IAEA-CN-234-0112...791	IAEA-CN-234-0169...705
IAEA-CN-234-0057...285	IAEA-CN-234-0113...796	IAEA-CN-234-0170...798
IAEA-CN-234-0059...397	IAEA-CN-234-0114...503	IAEA-CN-234-0171...518
IAEA-CN-234-0060...193	IAEA-CN-234-0115...429	IAEA-CN-234-0172...391
IAEA-CN-234-0061...236	IAEA-CN-234-0116...155	IAEA-CN-234-0173...416
IAEA-CN-234-0062...614	IAEA-CN-234-0117...810	IAEA-CN-234-0174...387
IAEA-CN-234-0065...627	IAEA-CN-234-0118...681	IAEA-CN-234-0175...724
IAEA-CN-234-0066...502	IAEA-CN-234-0119...362	IAEA-CN-234-0176...679

IAEA-CN-234-0177...161	IAEA-CN-234-0236...157	IAEA-CN-234-0294...226
IAEA-CN-234-0178...682	IAEA-CN-234-0237...499	IAEA-CN-234-0295...817
IAEA-CN-234-0179...344	IAEA-CN-234-0238...267	IAEA-CN-234-0296...178
IAEA-CN-234-0180...628	IAEA-CN-234-0240...426	IAEA-CN-234-0297...139
IAEA-CN-234-0182...180	IAEA-CN-234-0241...475	IAEA-CN-234-0298...540
IAEA-CN-234-0183...453	IAEA-CN-234-0242...152	IAEA-CN-234-0299...449
IAEA-CN-234-0184...803	IAEA-CN-234-0243...558	IAEA-CN-234-0300...392
IAEA-CN-234-0185...358	IAEA-CN-234-0244...668	IAEA-CN-234-0301...712
IAEA-CN-234-0186...504	IAEA-CN-234-0246...658	IAEA-CN-234-0302...672
IAEA-CN-234-0187...369	IAEA-CN-234-0248...393	IAEA-CN-234-0303...239
IAEA-CN-234-0189...607	IAEA-CN-234-0249...815	IAEA-CN-234-0304...603
IAEA-CN-234-0190...725	IAEA-CN-234-0250...768	IAEA-CN-234-0306...508
IAEA-CN-234-0191...348	IAEA-CN-234-0251...328	IAEA-CN-234-0309...781
IAEA-CN-234-0192...411	IAEA-CN-234-0252...751	IAEA-CN-234-0310...321
IAEA-CN-234-0193...605	IAEA-CN-234-0253...752	IAEA-CN-234-0311...818
IAEA-CN-234-0194...812	IAEA-CN-234-0254...659	IAEA-CN-234-0312...713
IAEA-CN-234-0195...680	IAEA-CN-234-0255...544	IAEA-CN-234-0313...413
IAEA-CN-234-0197...292	IAEA-CN-234-0256...331	IAEA-CN-234-0314...366
IAEA-CN-234-0198...563	IAEA-CN-234-0257...660	IAEA-CN-234-0315...318
IAEA-CN-234-0199...764	IAEA-CN-234-0258...374	IAEA-CN-234-0316...730
IAEA-CN-234-0200...456	IAEA-CN-234-0259...665	IAEA-CN-234-0317...258
IAEA-CN-234-0201...742	IAEA-CN-234-0260...412	IAEA-CN-234-0318...769
IAEA-CN-234-0202...813	IAEA-CN-234-0261...336	IAEA-CN-234-0319...346
IAEA-CN-234-0203...480	IAEA-CN-234-0262...600	IAEA-CN-234-0321...474
IAEA-CN-234-0204...676	IAEA-CN-234-0263...516	IAEA-CN-234-0322...731
IAEA-CN-234-0205...451	IAEA-CN-234-0264...616	IAEA-CN-234-0323...458
IAEA-CN-234-0206...711	IAEA-CN-234-0265...422	IAEA-CN-234-0325...437
IAEA-CN-234-0207...814	IAEA-CN-234-0266...407	IAEA-CN-234-0326...495
IAEA-CN-234-0208...523	IAEA-CN-234-0267...454	IAEA-CN-234-0327...669
IAEA-CN-234-0209...409	IAEA-CN-234-0269...368	IAEA-CN-234-0328...685
IAEA-CN-234-0211...554	IAEA-CN-234-0270...647	IAEA-CN-234-0329...632
IAEA-CN-234-0212...652	IAEA-CN-234-0271...143	IAEA-CN-234-0330...385
IAEA-CN-234-0213...559	IAEA-CN-234-0272...683	IAEA-CN-234-0331...491
IAEA-CN-234-0214...726	IAEA-CN-234-0273...684	IAEA-CN-234-0333...421
IAEA-CN-234-0215...630	IAEA-CN-234-0274...353	IAEA-CN-234-0334...360
IAEA-CN-234-0216...727	IAEA-CN-234-0275...434	IAEA-CN-234-0335...249
IAEA-CN-234-0217...400	IAEA-CN-234-0276...573	IAEA-CN-234-0336...410
IAEA-CN-234-0218...743	IAEA-CN-234-0277...548	IAEA-CN-234-0337...131
IAEA-CN-234-0220...591	IAEA-CN-234-0278...816	IAEA-CN-234-0338...501
IAEA-CN-234-0221...332	IAEA-CN-234-0279...435	IAEA-CN-234-0339...288
IAEA-CN-234-0222...625	IAEA-CN-234-0280...229	IAEA-CN-234-0340...245
IAEA-CN-234-0223...728	IAEA-CN-234-0281...279	IAEA-CN-234-0341...819
IAEA-CN-234-0224...432	IAEA-CN-234-0282...198	IAEA-CN-234-0342...168
IAEA-CN-234-0225...538	IAEA-CN-234-0283...192	IAEA-CN-234-0343...276
IAEA-CN-234-0226...729	IAEA-CN-234-0284...611	IAEA-CN-234-0344...339
IAEA-CN-234-0227...635	IAEA-CN-234-0285...517	IAEA-CN-234-0345...337
IAEA-CN-234-0228...744	IAEA-CN-234-0286...343	IAEA-CN-234-0346...633
IAEA-CN-234-0229...188	IAEA-CN-234-0287...631	IAEA-CN-234-0347...515
IAEA-CN-234-0230...171	IAEA-CN-234-0288...577	IAEA-CN-234-0348...363
IAEA-CN-234-0231...477	IAEA-CN-234-0289...753	IAEA-CN-234-0349...347
IAEA-CN-234-0232...617	IAEA-CN-234-0290...494	IAEA-CN-234-0350...754
IAEA-CN-234-0233...237	IAEA-CN-234-0291...462	IAEA-CN-234-0352...550
IAEA-CN-234-0234...308	IAEA-CN-234-0292...312	IAEA-CN-234-0353...380
IAEA-CN-234-0235...303	IAEA-CN-234-0293...568	IAEA-CN-234-0354...783

IAEA-CN-234-0355...282	IAEA-CN-234-0415...592	IAEA-CN-234-0475...263
IAEA-CN-234-0356...300	IAEA-CN-234-0416...688	IAEA-CN-234-0476...327
IAEA-CN-234-0357...148	IAEA-CN-234-0417...265	IAEA-CN-234-0477...297
IAEA-CN-234-0358...141	IAEA-CN-234-0418...324	IAEA-CN-234-0478...459
IAEA-CN-234-0359...320	IAEA-CN-234-0419...478	IAEA-CN-234-0479...691
IAEA-CN-234-0361...571	IAEA-CN-234-0420...388	IAEA-CN-234-0480...352
IAEA-CN-234-0362...531	IAEA-CN-234-0421...268	IAEA-CN-234-0482...762
IAEA-CN-234-0363...612	IAEA-CN-234-0422...732	IAEA-CN-234-0483...615
IAEA-CN-234-0364...489	IAEA-CN-234-0423...793	IAEA-CN-234-0485...569
IAEA-CN-234-0365...164	IAEA-CN-234-0424...259	IAEA-CN-234-0486...733
IAEA-CN-234-0366...175	IAEA-CN-234-0425...520	IAEA-CN-234-0487...154
IAEA-CN-234-0367...136	IAEA-CN-234-0426...821	IAEA-CN-234-0489...466
IAEA-CN-234-0368...199	IAEA-CN-234-0427...179	IAEA-CN-234-0490...692
IAEA-CN-234-0369...172	IAEA-CN-234-0428...252	IAEA-CN-234-0491...293
IAEA-CN-234-0370...714	IAEA-CN-234-0430...338	IAEA-CN-234-0492...734
IAEA-CN-234-0371...287	IAEA-CN-234-0432...689	IAEA-CN-234-0493...693
IAEA-CN-234-0372...686	IAEA-CN-234-0433...133	IAEA-CN-234-0494...439
IAEA-CN-234-0373...500	IAEA-CN-234-0435...674	IAEA-CN-234-0495...543
IAEA-CN-234-0374...512	IAEA-CN-234-0437...423	IAEA-CN-234-0496...771
IAEA-CN-234-0375...208	IAEA-CN-234-0438...582	IAEA-CN-234-0497...561
IAEA-CN-234-0376...233	IAEA-CN-234-0439...822	IAEA-CN-234-0498...824
IAEA-CN-234-0377...307	IAEA-CN-234-0440...203	IAEA-CN-234-0499...735
IAEA-CN-234-0378...636	IAEA-CN-234-0441...273	IAEA-CN-234-0500...694
IAEA-CN-234-0379...755	IAEA-CN-234-0442...418	IAEA-CN-234-0501...365
IAEA-CN-234-0380...219	IAEA-CN-234-0443...588	IAEA-CN-234-0502...201
IAEA-CN-234-0381...589	IAEA-CN-234-0444...555	IAEA-CN-234-0503...240
IAEA-CN-234-0382...272	IAEA-CN-234-0446...546	IAEA-CN-234-0504...756
IAEA-CN-234-0383...257	IAEA-CN-234-0448...355	IAEA-CN-234-0505...695
IAEA-CN-234-0384...349	IAEA-CN-234-0449...250	IAEA-CN-234-0506...839
IAEA-CN-234-0385...138	IAEA-CN-234-0450...441	IAEA-CN-234-0507...238
IAEA-CN-234-0386...196	IAEA-CN-234-0451...690	IAEA-CN-234-0509...736
IAEA-CN-234-0388...372	IAEA-CN-234-0452...586	IAEA-CN-234-0510...425
IAEA-CN-234-0389...576	IAEA-CN-234-0453...309	IAEA-CN-234-0511...205
IAEA-CN-234-0390...641	IAEA-CN-234-0454...376	IAEA-CN-234-0512...298
IAEA-CN-234-0391...820	IAEA-CN-234-0455...560	IAEA-CN-234-0513...241
IAEA-CN-234-0392...599	IAEA-CN-234-0456...448	IAEA-CN-234-0514...370
IAEA-CN-234-0393...315	IAEA-CN-234-0457...467	IAEA-CN-234-0515...147
IAEA-CN-234-0395...481	IAEA-CN-234-0458...394	IAEA-CN-234-0516...415
IAEA-CN-234-0396...585	IAEA-CN-234-0459...367	IAEA-CN-234-0517...772
IAEA-CN-234-0398...382	IAEA-CN-234-0460...823	IAEA-CN-234-0518...534
IAEA-CN-234-0399...564	IAEA-CN-234-0461...247	IAEA-CN-234-0519...444
IAEA-CN-234-0400...197	IAEA-CN-234-0462...594	IAEA-CN-234-0520...757
IAEA-CN-234-0401...134	IAEA-CN-234-0463...427	IAEA-CN-234-0521...737
IAEA-CN-234-0402...706	IAEA-CN-234-0464...567	IAEA-CN-234-0522...666
IAEA-CN-234-0403...507	IAEA-CN-234-0465...593	IAEA-CN-234-0524...696
IAEA-CN-234-0405...581	IAEA-CN-234-0466...565	IAEA-CN-234-0525...403
IAEA-CN-234-0406...687	IAEA-CN-234-0467...770	IAEA-CN-234-0527...433
IAEA-CN-234-0407...678	IAEA-CN-234-0468...497	IAEA-CN-234-0528...438
IAEA-CN-234-0408...326	IAEA-CN-234-0469...509	IAEA-CN-234-0529...364
IAEA-CN-234-0409...522	IAEA-CN-234-0470...844	IAEA-CN-234-0530...447
IAEA-CN-234-0410...170	IAEA-CN-234-0471...351	IAEA-CN-234-0531...217
IAEA-CN-234-0411...262	IAEA-CN-234-0472...174	IAEA-CN-234-0532...354
IAEA-CN-234-0412...261	IAEA-CN-234-0473...779	IAEA-CN-234-0533...715
IAEA-CN-234-0413...579	IAEA-CN-234-0474...845	IAEA-CN-234-0535...510

IAEA-CN-234-0536...222	IAEA-CN-234-0598...299	IAEA-CN-234-0665...570
IAEA-CN-234-0537...402	IAEA-CN-234-0599...698	IAEA-CN-234-0666...384
IAEA-CN-234-0538...825	IAEA-CN-234-0600...846	IAEA-CN-234-0667...149
IAEA-CN-234-0540...671	IAEA-CN-234-0601...556	IAEA-CN-234-0668...650
IAEA-CN-234-0541...302	IAEA-CN-234-0604...773	IAEA-CN-234-0669...244
IAEA-CN-234-0542...487	IAEA-CN-234-0605...357	IAEA-CN-234-0670...553
IAEA-CN-234-0543...277	IAEA-CN-234-0606...661	IAEA-CN-234-0671...209
IAEA-CN-234-0544...218	IAEA-CN-234-0610...829	IAEA-CN-234-0672...800
IAEA-CN-234-0545...482	IAEA-CN-234-0611...142	IAEA-CN-234-0673...182
IAEA-CN-234-0547...648	IAEA-CN-234-0612...830	IAEA-CN-234-0674...802
IAEA-CN-234-0548...181	IAEA-CN-234-0613...375	IAEA-CN-234-0676...578
IAEA-CN-234-0549...242	IAEA-CN-234-0615...128	IAEA-CN-234-0677...832
IAEA-CN-234-0550...787	IAEA-CN-234-0616...316	IAEA-CN-234-0678...200
IAEA-CN-234-0551...359	IAEA-CN-234-0617...572	IAEA-CN-234-0679...206
IAEA-CN-234-0552...342	IAEA-CN-234-0618...644	IAEA-CN-234-0680...700
IAEA-CN-234-0553...195	IAEA-CN-234-0621...536	IAEA-CN-234-0681...542
IAEA-CN-234-0554...224	IAEA-CN-234-0622...562	IAEA-CN-234-0682...623
IAEA-CN-234-0555...130	IAEA-CN-234-0623...838	IAEA-CN-234-0683...547
IAEA-CN-234-0556...445	IAEA-CN-234-0624...266	IAEA-CN-234-0684...701
IAEA-CN-234-0558...621	IAEA-CN-234-0625...253	IAEA-CN-234-0685...278
IAEA-CN-234-0559...183	IAEA-CN-234-0626...189	IAEA-CN-234-0686...248
IAEA-CN-234-0560...169	IAEA-CN-234-0627...528	IAEA-CN-234-0688...739
IAEA-CN-234-0562...223	IAEA-CN-234-0628...275	IAEA-CN-234-0689...254
IAEA-CN-234-0563...584	IAEA-CN-234-0629...383	IAEA-CN-234-0690...151
IAEA-CN-234-0564...479	IAEA-CN-234-0630...137	IAEA-CN-234-0691...163
IAEA-CN-234-0565...602	IAEA-CN-234-0631...831	IAEA-CN-234-0692...758
IAEA-CN-234-0566...782	IAEA-CN-234-0633...524	IAEA-CN-234-0695...673
IAEA-CN-234-0567...826	IAEA-CN-234-0634...214	IAEA-CN-234-0696...833
IAEA-CN-234-0568...580	IAEA-CN-234-0635...442	IAEA-CN-234-0697...255
IAEA-CN-234-0569...395	IAEA-CN-234-0636...738	IAEA-CN-234-0698...389
IAEA-CN-234-0570...140	IAEA-CN-234-0637...657	IAEA-CN-234-0700...651
IAEA-CN-234-0571...215	IAEA-CN-234-0638...745	IAEA-CN-234-0703...440
IAEA-CN-234-0572...519	IAEA-CN-234-0639...428	IAEA-CN-234-0704...485
IAEA-CN-234-0575...827	IAEA-CN-234-0642...176	IAEA-CN-234-0706...498
IAEA-CN-234-0576...606	IAEA-CN-234-0643...185	IAEA-CN-234-0707...834
IAEA-CN-234-0577...225	IAEA-CN-234-0644...243	IAEA-CN-234-0708...264
IAEA-CN-234-0578...640	IAEA-CN-234-0645...356	IAEA-CN-234-0709...716
IAEA-CN-234-0579...492	IAEA-CN-234-0646...304	IAEA-CN-234-0712...496
IAEA-CN-234-0580...398	IAEA-CN-234-0647...473	IAEA-CN-234-0713...251
IAEA-CN-234-0581...228	IAEA-CN-234-0648...488	IAEA-CN-234-0714...269
IAEA-CN-234-0582...828	IAEA-CN-234-0649...401	IAEA-CN-234-0715...545
IAEA-CN-234-0583...325	IAEA-CN-234-0650...566	IAEA-CN-234-0716...345
IAEA-CN-234-0584...788	IAEA-CN-234-0651...231	IAEA-CN-234-0718...551
IAEA-CN-234-0585...552	IAEA-CN-234-0652...232	IAEA-CN-234-0719...399
IAEA-CN-234-0586...557	IAEA-CN-234-0653...629	IAEA-CN-234-0720...717
IAEA-CN-234-0587...794	IAEA-CN-234-0654...191	IAEA-CN-234-0721...190
IAEA-CN-234-0589...697	IAEA-CN-234-0655...699	IAEA-CN-234-0724...740
IAEA-CN-234-0590...549	IAEA-CN-234-0656...404	IAEA-CN-234-0725...774
IAEA-CN-234-0591...146	IAEA-CN-234-0658...212	IAEA-CN-234-0727...335
IAEA-CN-234-0592...649	IAEA-CN-234-0659...256	IAEA-CN-234-0728...847
IAEA-CN-234-0593...670	IAEA-CN-234-0661...202	IAEA-CN-234-0729...396
IAEA-CN-234-0594...801	IAEA-CN-234-0662...221	IAEA-CN-234-0730...759
IAEA-CN-234-0595...622	IAEA-CN-234-0663...431	IAEA-CN-234-0731...707
IAEA-CN-234-0596...613	IAEA-CN-234-0664...187	IAEA-CN-234-0732...446

IAEA-CN-234-0734...786	IAEA-CN-234-0767...703	IAEA-CN-234-0797...836
IAEA-CN-234-0735...280	IAEA-CN-234-0768...675	IAEA-CN-234-0798...851
IAEA-CN-234-0736...294	IAEA-CN-234-0769...213	IAEA-CN-234-0799...854
IAEA-CN-234-0737...153	IAEA-CN-234-0770...296	IAEA-CN-234-0800...868
IAEA-CN-234-0738...330	IAEA-CN-234-0771...274	IAEA-CN-234-0801...863
IAEA-CN-234-0739...270	IAEA-CN-234-0772...656	IAEA-CN-234-0802...858
IAEA-CN-234-0740...290	IAEA-CN-234-0773...271	IAEA-CN-234-0803...869
IAEA-CN-234-0741...797	IAEA-CN-234-0774...323	IAEA-CN-234-0804...855
IAEA-CN-234-0743...377	IAEA-CN-234-0775...386	IAEA-CN-234-0805...871
IAEA-CN-234-0744...760	IAEA-CN-234-0776...590	IAEA-CN-234-0806...870
IAEA-CN-234-0745...135	IAEA-CN-234-0777...260	IAEA-CN-234-0852...145
IAEA-CN-234-0746...463	IAEA-CN-234-0778...295	IAEA-CN-234-0924...125
IAEA-CN-234-0747...283	IAEA-CN-234-0779...704	IAEA-CN-234-0925...124
IAEA-CN-234-0748...173	IAEA-CN-234-0780...371	IAEA-CN-234-0941...856
IAEA-CN-234-0749...443	IAEA-CN-234-0781...741	IAEA-CN-234-0942...862
IAEA-CN-234-0750...638	IAEA-CN-234-0782...835	IAEA-CN-234-0944...872
IAEA-CN-234-0751...626	IAEA-CN-234-0783...539	IAEA-CN-234-0945...857
IAEA-CN-234-0752...310	IAEA-CN-234-0784...470	IAEA-CN-234-0946...873
IAEA-CN-234-0753...286	IAEA-CN-234-0785...408	IAEA-CN-234-0947...860
IAEA-CN-234-0754...469	IAEA-CN-234-0786...646	IAEA-CN-234-0948...861
IAEA-CN-234-0755...334	IAEA-CN-234-0787...608	IAEA-CN-234-0950...865
IAEA-CN-234-0756...281	IAEA-CN-234-0788...775	IAEA-CN-234-0951...859
IAEA-CN-234-0757...702	IAEA-CN-234-0789...505	IAEA-CN-234-0952...850
IAEA-CN-234-0758...514	IAEA-CN-234-0790...595	IAEA-CN-234-0953...852
IAEA-CN-234-0759...234	IAEA-CN-234-0791...662	IAEA-CN-234-0954...866
IAEA-CN-234-0760...284	IAEA-CN-234-0792...795	IAEA-CN-234-0955...867
IAEA-CN-234-0762...129	IAEA-CN-234-0793...194	IAEA-CN-234-0956...853
IAEA-CN-234-0763...746	IAEA-CN-234-0794...378	
IAEA-CN-234-0764...204	IAEA-CN-234-0796...341	

Contributor Index

— A —

Abbavaram, V.	707
Abdel Maksoud, W.	681, 750
Abe, G.	689
Abe, H.	658
Abe, Y.	781, 791, 792, 794
Abel, I.	626
Abler, M. C.	242
Abramovic, I.	307
Abrams, T.	172, 802
Abreu, P.	857
Abruzzese, G.	435
Acharya, K.	717
Acosta Muñoz, C. U.	706, 757
Acosta Pérez, A.	706, 757
Acuña-Arias, E.	290
Adamek, J.	173
Addab, Y.	647
Adegun, J.	404
Adhiya, A. N.	143
Aftanas, M.	362
Agarwal, J.	59, 60, 734, 740, 759, 771
Agarwal, R.	661
Ageorges, N.	702
Agharbi, A.	661
Agostinetti, P.	660, 705, 722
Agostini, M.	41, 319, 321, 588
Agrawal, J.	741
Aguiam, D.	353
Aguilar Reyes, U.	706, 757
Ahlgren, T.	330
Ahmad, S.	401
Ahmad, Z.	401
Ahn, J.-H.	465
Ahn, J.-W.	32, 135, 195, 275, 286, 629, 636
Aho-Mantila, L.	173, 863
Aiba, N.	55, 61, 178, 339, 468, 476, 477, 497, 513, 563
Aiello, G.	59, 725, 738, 744
Airila, M. I.	531
Åkäslompolo, S.	466, 531, 595
Akers, R.	38, 47, 466, 534
Akimoto, K.	842
Akino, N.	658
Akiyama, T.	318, 335, 413, 418, 420
Alan, H.	363
Alaparthi, M.	707
Alarcon, T.	666
Albajar, F.	34, 704
Albanese, R.	363, 731
Alberti, S.	439, 704, 725
Alberto Morillas, A.	531
Aleev, A.	805
Alejaldre, C.	163
Aleksandrovich, K.	866
Alekseev, A.	694, 702
Alekseev, P.	773
Alessi, E.	434
Alexis, T.	855
Aleynikov, P.	35, 134, 366, 474, 594
Aleynikova, K.	474
Alford, C.	788
Allain, J.-P.	828
Allan, S.	276, 437
Allen, S.	172, 230, 233
Allfrey, I.	239
Almagri, A. F.	157, 311
Alonso, A.	185, 302
Alonso, J.	680
Alper, B.	360
Altukhov, A.	406, 407, 560
Alves, E.	803
Amano, Y.	10
Ambrosino, G.	363
Ambrosino, R.	363, 731
Ambulkar, K. K.	143
Amendt, P.	782
Ames, M.	832
Amicucci, L.	337, 343, 383
Amoskov, V.	363
An, C.-Y.	27, 585
An, Y.	259, 273
Anand, H.	438, 443
Anand, R.	661
Ananyev, S. S.	59, 746
Anashkin, I.	753

Anderson, J.....	67, 862
Anderson, J. K.	34, 40, 157, 225, 312, 699
Andersson Sundén, E.	531
Ando, M.	824
Andre, R.	287, 534, 686
Andreenko, E.	694
Andreeva, T.	185, 301
Andrei, K.	694
Andrew, P.	688, 702
Andrey, K.	363
Angioni, C.	19, 264, 343, 357, 523, 854
Angot, T.	647
Aniel, T.	371, 529, 531, 534, 569
Anikeev, A.	459
Anikeev, M.	459
Anja, G.	201
Antoni, V.	705
Antusch, S.	666, 807
Aoki, Y.	318
Apicella, M. L.	432
Appelbe, B.	780
Aprile, D.	705
Apruzzese, G.	432
Apte, A.	717
Aquaro, D.	710
Arakcheev, A.	50, 378
Araya-Solano, L. A.	290
Arbeiter, F.	45, 824, 835
Arefiev, A. V.	37, 583, 614
Arias-Brenes, J. M.	290
Arikawa, Y.	42, 779, 781, 791, 792, 794, 819
Arnichand, H.	358
Arredondo Solís, V. M.	706, 757
Artaud, J.-F.	451, 531, 569, 738
Artene, S.	173
Arzhannikov, A.	458
Asahi, Y.	555
Asahina, T.	793
Asai, T.	25, 239, 243
Asakura, N.	59, 345, 454, 713, 739
Asano, S.	680
Ascasibar, E.	410, 411
Asenjo Castillo, J.	377
Asgari-Targhi, M.	589
Ashikawa, N.	48, 345, 413, 820
Ashourvan, A.	573
Askinazi, L.	405, 872
Astrelin, V.	458
Asudani, K.	143
Asunta, O.	531
Atanasiu, C. V.	531
Atrey, P. K.	143, 145, 323
Atsushi, I.	484
Aubert, J.	744
Aumeunier, M.-H.	666, 694
Austin, M.	214, 221
Avino, F.	379
Avotina, L.	45, 834
Avramidis, K.	704, 725
Avrorov, A.	458
Awajitani, K.	866
Ayala, J.-M.	814
Aydemir, A. Y.	16, 256, 496
Ayers, S.	787
Azechi, H.	12, 18, 142, 779, 781, 792-794, 819
Azizov, E.	762
Azuma, H.	790, 791, 796
— B —	
Babu, G. R.	143, 328
Bachmann, C.	731, 763
Bader, A.	171, 730
Bae, M.-K.	31, 270
Bae, Y.-S.	247-249, 256, 258, 368
Baek, S. G.	192, 206, 211, 383, 469, 549
Baelmans, M.	531
Bagryansky, P.	66, 459
Bai, W.	315, 316
Bai, X.	400
Baiocchi, B.	371
Bairagi, N.	143
Bak, J. G.	30, 248, 254-257, 263, 269-271
Bakharev, N.	32, 288, 754
Baklanov, V.	810
Balboa, I.	332
Balden, M.	347
Baldwin, M.	648
Baldzuhn, J.	185, 297, 411
Ballinger, S.	211
Balme, S.	666
Banaudha, M.	143
Bando, T.	422

Bandyopadhyay, I.	16, 498, 534	Bécoulet, A.	69
Bandyopadhyay, M.	692, 707	Bécoulet, M.	16, 253, 477, 503, 505
Banerjee, S. 41, 60, 145, 189, 323, 651, 760		Becquart, C.	647
Bang, E.	266	Behr, W.	300
Bao, J.	37, 613	Beidler, C. D.	185, 480, 726
Baquero, M.	379	Beiersdorfer, P.	787
Barabaschi, P.	139	Beklemishev, A.	27, 458, 592
Barabash, V.	816	Bell, P. M.	787
Barada, K. K.	176, 487	Bell, R.	853
Barbato, E.	451	Bell, R. E.	233, 278–282, 285, 286
Barbato, L.	731	Bellan, L.	814
Bardoczi, L.	215	Belli, E. A.	479, 523, 534, 839
Barengolts, S. A.	652	Belli, F.	434, 696
Barhydt, J.	235	Belokurov, A.	405, 872
Barillas-Mora, L.	377	Belova, E.	36, 606, 853
Barnes, D.	243	Belyakov, V.	753, 754
Barnsley, R.	682, 694, 696	Belykh, V.	157, 312
Baron-Wiechec, A.	345, 346, 803	Ben, Z.	550
Barr, J.	151, 294	Benahmed, A.	624
Barradas, N.	803	Berdiyrov, G.	784
Barrett, T.	714, 731	Berger, M.	808
Barrios, M. A.	787	Berk, H.	859
Barros, G.	775	Berkery, J. W.	32, 248, 278, 279
Barruzo, M.	198	Bernard, J. M.	666
Barthe, M.-F.	647	Bernert, M.	179, 348, 857, 863
Barton, J. E.	226, 804	Berry, L.	618
Baruah, U.	661, 717	Berta, M.	362
Basiuk, V.	531, 534, 569	Bertalot, L.	682, 696
Bass, E. M.	604	Bertelli, N.	37, 192, 286, 611, 686
Bassan, M.	694, 702	Besinbaeva, H.	784
Basu, B.	512	Bettencourt, R.	787
Basu, D.	404	Bettini, P.	319, 351, 451, 497
Batal, T.	666	Beurskens, M.	165, 178, 179, 185, 298
Batha, S. H.	788	Beyer, P.	490
Batkin, V.	458	Bhandarkar, M. K.	143, 325, 326
Battaglia, D.	205, 853	Bharthi, P.	760
Batyaev, V.	773	Bhatt, S. B.	145, 717
Baudoin, C.	625	Bhattacharjee, A.	514
Baulaigue, O.	750	Bhattacharyay, R.	670, 745
Baxamusa, S.	788	Bialek, J.	242, 248
Baylor, L. R.	33, 199, 202, 223, 684	Biancalani, A.	38, 47, 467
Bazin, N.	750, 814	Biancolini, M.	727
Bazylev, B.	366	Biberacher, M.	845
Beal, J.	803	Biedermann, C.	185, 301, 303, 304
Beaumont, B.	661	Biel, W.	731
Beauvais, P.-Y.	814	Bierwage, A.	38, 47, 451, 468

Biewer, T.	766	Bonicelli, T.	703, 704
Bigelow, T.	766	Bonifetto, R.	727
Bigot, B.	10, 11, 129	Bonnin, X.	464, 531, 534, 644
Bilato, R.	354, 523, 531	Bonfiglio, P.	157, 312
Bilkova, P.	362	Bonoli, P. T.53, 63, 192, 207, 383, 469, 611, 615	
Bin, W.	434, 704	Boozer, A. H.	485, 514
Binderbauer, M.	239, 243	Bora, D.	143, 145, 717
Bionta, R.	780	Borba, D.	13, 162
Birkenmeier, G.	173, 356, 359	Borchardt, M.	157
Birus, D.	308	Borgogno, D.	588
Bisai, N. K.	53, 63, 323, 470	Borodin, D. ...	47, 331, 531, 643, 808, 873
Bisson, R.	52, 647	Borodkina, I.	331
Biswas, P.	143	Borschegovskij, A.	447
Bitter, M.	302, 384, 787	Borsuk, V.	308
Bizarro, J. P. S.	50, 627	Bortolon, A.	54, 61, 202, 224, 749
Bjorholm, T.	766	Bos, W.	587
Björkas, C.	331	Bosch, H.-S.	69, 185, 851
Blanchard, P.	442	Bosia, G.	730
Blanco, E.	185, 410	Botija, J.	680
Blanken, T.	349, 443, 444	Bottereau, C.	358
Blazewski, D.	576	Bottino, A.	467
Blommaert, M.	531	Boulbe, C.	531
Bobkov, V.	336, 342, 347, 353, 523	Bouquey, F.	666
Boboc, A.	451, 857	Bourdelle, C.	338, 371, 465, 569, 666
Boby, N. P.	833	Boussaton, A.	661
Boccaccini, L. V.	721, 743, 744	Bovet, A.	379
Bocian, D.	696	Bowden, G.	855
Bock, A.	355, 854	Boyer, M. D.	32, 226, 287
Bodner, G.	151	Boyle, D.	282
Boedo, J. A. ...	172, 174, 205, 214, 225, 436, 437	Bozhenkov, S. A. ...	40, 185, 298, 301, 303, 304, 635
Bogachev, A.	805	Bradley, C.	766
Bogar, O.	362	Bradley, D. K.	780, 787
Boguski, J.	157, 312	Brakel, R.	185, 851
Bohm, P.	362	Branas, B.	814
Boilson, D.	703	Braune, H.	307
Bolshakova, I.	867	Braunmueller, F.	704, 725
Bolzon, B.	750, 814	Bravenec, R.	214
Bolzonella, T.	16, 351, 451, 497, 541	Bredy, P.	750
Bonanomi, N.	340	Breizman, B.	67, 859
Boncagni, L.	433	Breizman, B. N.	10, 12, 134, 334, 594
Bond, E.	780	Bremond, S.	363, 666
Bondarchuk, E.	753, 754	Brennan, D.	17, 514
Bonelli, F.	35, 713, 715	Breslau, J.	241, 486
Bonfiglio, D.	27, 168, 588	Breton, S.	371, 465
Bongard, M.	33, 151, 294		

Brezinsek, S. 66, 171, 306, 329-331, 333,
 339, 342, 347, 453, 643, 666, 802,
 807, 852, 857, 863

Brichard, B. 682, 696

Brida, D. 352, 863

Briesemeister, A. 62, 172, 195, 275, 636,
 802

Briguglio, S. 531, 598, 608

Briseño Cárdenas, C. A. 706, 757

Brix, M. 173, 857

Broeckmann, C. 806

Brolatti, G. 682, 696

Bromberg, L. 723

Brombin, M. 660, 705

Brooks, A. 828

Brooks, J. W. 242

Brower, D. L. 40, 157, 313, 390, 691

Brown, T. 57, 241, 718, 720

Brun, C. 666

Brunetti, D. 570

Brunner, D. 23, 175, 210, 211, 223, 653

Brunner, S. 561

Bruno, V. 752

Brunsell, P. 157, 314

Bruschi, A. 65, 434, 704, 725

Brutti, C. 727

Bruzzo, P. 63, 68, 679, 727

Buangam, W. 528

Bucalossi, J. 29, 666, 738, 801

Buchanan, J. 344, 531, 538, 852

Buchenauer, D. 712, 829

Budny, R. 20, 537, 538, 543

Bufferand, H. 625, 628, 633, 666

Bulanov, S. 781

Bulavin, M. 867

Buldakov, M. 147

Bunting, P. 332

Buratti, P. 342, 433, 438, 570

Burckhart, A. 355

Burdakov, A. 66, 378, 458

Burhenn, R. 185

Burke, M. 151

Burke, W. 211

Burmasov, V. 458

Burrell, K. H. 176, 206, 215, 487, 760

Buscarino, A. 432

Bustreo, C. 845

Buttenschön, B. 185

Buxton, P. 238, 736

Bykov, I. 172, 223, 802

Bykov, P. 458

Bykov, V. 851

Bykovsky, N. 679

Byrne, P. J. 242

Byun, C.-S. 271, 675

— C —

Cabal, H. 60, 845

Cacheux, P. 661

Caggiano, J. 780

Cahyna, P. 505

Cai, H. 390

Cai, L. 813

Calabrò, G. 174, 432, 434

Calabro, G. 863

Calderoni, P. 669

Callahan, D. A. 780, 788

Callen, J. 169

Calvo, A. 809

Camenen, Y. 371, 666

Campanell, M. 52, 649

Campbell, D. J. 366

Campos Fernández, M. G. 377

Canal, G. 275

Cancino, S. 590

Candy, J. 19, 206, 479, 524, 534, 568, 839

Caniello, R. 347

Canik, J. 172, 195, 216, 221, 229, 275, 281,
 282, 634, 636, 766

Canizales, A. 290

Canton, A. 319

Cantone, B. 666

Cao, H. 698

Cao, J. 197

Capecchi, W. 157, 312

Cappa, Á. 185, 227, 307, 410

Cappello, S. 168, 588

Cara, P. 814

Cardinali, A. 383

Carloni, D. 843

Carmona, A. 377

Carnevale, D. 64, 349, 433, 438

Carpentier-Chouchana, S. 366

Carralero, D.	22, 29, 173, 347, 437, 857
Carraro, L.	343
Carreras, B.	483, 571
Carsten, L.	704
Caruso, G.	710
Carvalho, I.	852
Casey, D.	780, 787
Casiraghi, I.	434
Casper, T.	543
Casson, F. J.	177, 208, 342, 343, 491, 523, 531
Castaldo, C.	383
Castejón, F.	12, 18, 148, 420
Catarino, N.	803
Cats, S.	297
Cau, F.	704
Caudle, D.	235
Caughman, J.	766
Causa, F.	433, 438
Cavazos Almaguer, G. R.	706, 757
Cavazzana, R.	319
Cave-Ayland, K.	852
Cavedon, M.	179, 352, 356, 357
Cavenago, M.	705
Cavinato, M.	544
Cecconello, M.	696
Celliers, P. M.	788
Cerfon, A.	501
Cerjan, C.	780
Cesario, R.	180, 343, 383
Cha, S.	795
Chacón, L.	168, 588
Chahine, R.	27, 587
Chakraborty, A. K.	34, 35, 692, 703, 707, 734, 741, 771
Challis, C.	178, 342, 473, 852
Chalykh, B.	805
Chan, V.	140, 389
Chan, V. S.	802
Chandra, D.	323, 506
Chandrasekhar, K.	741
Chang, C.-S.	22, 30, 463, 548, 631, 634, 638
Chang, J.	642
Chankin, A.	339, 857
Chantant, M.	666
Chapman, B. E.	157, 313
Chapman, I.	28, 39, 178, 180, 477
Charl, A.	305
Chatthong, B.	536, 539, 547, 578
Chattopadhyay, A. K.	534
Chattopadhyay, P. K.	145, 323, 717
Chaudhari, B.	143
Chaudhari, V. K.	143
Chaudhary, K.	717
Chauhan, P. K.	143, 717
Chauvin, N.	750, 814
Chavda, C.	145, 717
Chávez Rodríguez, R. M.	706, 757
Chebotarev, V.	830
Chel, S.	750, 814
Chelis, J. G.	704, 725
Chellai, O.	439
Chen, B.	641
Chen, C. Y.	394
Chen, D.	382, 811
Chen, H.	787
Chen, J.	34, 384, 389, 486, 566, 622, 640, 701, 764
Chen, J. L.	801
Chen, K.	698
Chen, L.	36, 609, 610
Chen, R.	387, 804
Chen, W.	56, 197, 391, 392, 394, 399, 600
Chen, X.	28, 39, 169, 176, 181, 190, 225, 227, 229, 487
Chen, Y.	353, 385, 642, 698
Chen, Z.	163
Chen, Z. M.	801
Cheng, C.	271
Cheng, C.-Z.	240, 277
Cheng, J.	392, 395, 397-399, 600
Cheng, L.	859
Cheng, Y.	752
Cheon, M.	31, 267, 273
Cherkez, D. I.	833
Chernakov, P. V.	702
Chernyshev, F.	288, 754, 872
Chernyshova, M.	666
Chikada, T.	829
Chilenski, M.	208, 210
Chiocchio, S.	367
Chitarin, G.	705

Chittenden, J.....	780	Coelho, R.....	531
Chmyga, A.....	409	Coenen, J. W. . 43, 332, 453, 806, 807, 809, 826	
Choe, G. H.....	249, 256	Coffey, I.....	332, 343
Choe, W.....	51, 135, 255, 263, 269, 629	Colas, L.....	342, 353, 380
Choi, C.-H.....	693	Cole, M.....	467
Choi, D.....	201	Coleman, M.....	727
Choi, G. J.....	579	Colin, C.....	625
Choi, I.-S.....	254	Colledani, G.....	569, 666
Choi, J.....	373	Colling, B.....	466
Choi, M. J.204, 248, 251, 252, 255, 260, 265		Collins, C.....	38, 47, 191, 227
Chouli, B.....	569	Collins, C. M.....	196
Chowdhuri, M. B.....	145, 323, 651, 760	Colnel, J.....	666
Christian, D. R.....	143	Combs, S.....	199, 684
Christophe, G.....	863	Commaux, N.....	54, 61, 199, 202, 223
Chrobak, C. P.....	802	Comunian, M.....	814
Chrystal, C.....	168, 205, 213, 215	Conka, D.....	834
Chu, N.....	382	Connor, J.....	180, 238
Chu, Y.....	135	Conroy, S.....	531, 696
Chudasma, H. H.....	143	Conway, G.....	358, 359
Chugunov, I.....	407, 695	Conway, N.....	240, 277
Chung, J.....	272	Cook, C.....	157, 312
Chung, K.-S.....	270	Cooper, C. M.....	223
Chung, K. J.....	296	Coppi, B.....	17, 512
Churchill, R.....	51, 634, 638	Corbel, E.....	666
Churn, K.....	795	Corr, C.....	67, 869
Chuyanov, V.....	238	Corradino, C.....	432
Cianciosa, M.....	408	Corre, Y.....	47, 309, 332, 666
Cianfarani, C.....	433	Corrigan, G.....	541, 544
Ciattaglia, S.....	843	Costa, A. L.....	775
Ciazynski, D.....	727	Costea, S.....	437
Cinque, M.....	363	Coster, D.343, 464, 529, 531, 630, 715, 731	
Ciraolo, G.	531, 625, 628, 633, 666, 738	Costley, A.....	25, 238, 736
Cismondi, F.....	704, 721	Coto-Vílchez, F.....	377
Citrin, J.....	50, 340, 371, 444, 531	Courtois, X.....	666
Clairret, F.....	49, 358, 559, 569	Covele, B.....	24, 231
Clark, D.....	712	Coviello, E.....	747
Clark, D. S.....	788	Craig, B.....	297
Classen, I.....	351, 352	Craig, D.....	157, 311
Clauser, C.....	596	Crescenzi, F.....	432, 696
Claveau, E.....	235	Crisanti, F.....	58, 174, 710, 729
Clement-Lorenzo, S.....	451	Cristian, L.....	329
Coad, J. P.....	803	Croci, G.....	682
Coad, P.....	329	Crocker, N.....	606, 853
Cocilovo, V.....	434	Crombe, K.....	50, 353, 374
Coda, S.	12, 153, 165, 180, 201, 360, 361, 438, 442-444, 451	Crowley, B. J.....	240, 277

Crowley, T.	157	Debbiche, A.	661
Cruz, N.	451, 696	Dechelle, C.	752
Cui, L.	183, 597	Decker, J. 201, 349, 360, 361, 438, 490, 569	
Cui, S.	804	Decool, P.	63, 681, 750
Cui, X. W.	393	Deeba, F.	57, 401
Cui, Z. Y.	56, 393	deGrassie, J.	23, 205, 217, 225
Cvelbar, U.	797	Dejarnac, R.	13, 155, 332, 666
Czarnecka, A.	185, 336, 342	Dekeyser, W.	534
Cziegler, I.	175, 283	del-Castillo-Negrete, D.	26, 576
Czymek, G.	300	Delabie, E. ...	177, 188, 339, 476, 852, 857
— D —			
D’Arcangelo, O.	353, 434, 435	Delgado-Aparicio, L. F. 32, 207, 283, 302, 384	
D’Inca, R.	48, 335, 353, 374	Delicado, A.	844
da Silva Arresta Belo, P.	541, 544	Dellabiancia, M.	716
da Silva, F.	529	Delmas, E.	666
Dai, S.	193, 418	Delogu, R. S.	319, 705
Dairaku, M.	658, 690	Delpech, L.	666
Dal Bello, S.	154, 319	Demers, D.	157
Dalakoti, S.	143	Den Hartog, D.	40, 157, 311, 318
Dalicha, H.	661	Denisov, G.	11, 15, 459, 662–664
Dalla Palma, M.	319	Denk, S.	352
Damian, K.	344	Denner, P.	305, 306
Danani, C.	58, 59, 734, 741, 771	Derek, H.	541
Daniel, C.	800	Desai, T.	797
Daniel, R.	666, 734	Desgranges, C.	666
Darbos, C.	704	Deshpande, S. P.	734, 741
Dardour, S.	738	Dettrick, S.	243
Darrow, D.	853	Devaux, S.	374
Das, A.	143, 145, 717	Devynck, P.	343
Das, P.	670	Dewald, E. L.	788
Daudel, T.	666	Dewar, R.	855
David, J.	750	Dey, R.	651
Davis, E. M.	196, 206	Dhanani, K. R.	143, 328
Davis, S.	680	Dhola, H.	661
Davydenko, V.	157, 312	Dhongde, J. R.	41, 143, 325, 326
Day, C.	35, 451, 713, 715, 868	Dhyani, P.	145, 323
De Baar, M.	444	Di Campli, R.	441
De Bock, M.	694, 697	Di Gallo, L.	738
de la Luna, E. 48, 180, 333, 337, 341, 343, 368, 451, 541, 852		Di Pace, L.	682, 696
de Marne, P.	190	Di Troia, C.	598, 608
De Masi, G.	319	Diallo, A.	38, 47, 189, 233, 281, 282, 284–286, 640, 853
de Pablos, J.	409	Diamond, P. H. 26, 215, 397, 517, 521, 559, 566, 573, 574, 577, 640	
De Temmerman, G.	330, 347, 826	Dickinson, D.	477
De Tommasi, G.	363, 451	Diem, S.	766
de Vries, P. ...	50, 198, 363–366, 368, 543		

Dif-Pradalier, G.	25, 465, 559
Dimits, A.	582
Ding, B. J.	55, 133, 380, 383, 384, 387
Ding, F.	133
Ding, N.	42, 785
Ding, R.	55, 172, 643, 802
Ding, S.	133, 182, 183
Ding, W. X.	56, 157, 313, 315, 316, 390
Ding, X.	197, 395, 600
Ding, X. T.	391, 393, 394, 397
Dinklage, A.	39, 185, 297, 298, 308, 411, 726
Dipietro, E.	680
Dipti, D.	871
Disset, G.	681, 750
Dittmar, T.	808
Dmitry, K.	366
Dnestrovskij, A.	447, 736
Dnestrovskiy, Y.	147
Doane, J.	699
Doceul, L.	666
Doerner, R.	648, 804
Doinikov, D.	407, 695
Dokuka, V. N.	475, 756
Domalapally, P. K.	35, 716
Domier, C. W.	265, 280
Dong, C. F.	393
Dong, J.	56, 161, 197, 395
Dong, J. Q.	386, 391, 397
Dong, Y.	200
Dong, Y. B.	392, 399
Dongiovanni, D. N.	696, 845
Donne, T.	674
Donnel, P.	465
Donovan, D.	766, 829
Döppner, T.	780
Doriae, V.	531
Doshi, B.	717
Doshi, K. J.	143
Dou, P.	811
Douai, D.	65, 347, 442, 451, 666
Dougnac, H.	666
Doyle, E. J.	181, 213
Drewelow, P.	198, 337, 339, 343, 863
Drews, P.	40, 300, 305
Du Toit, E.	614
Du, H.	197
Du, H. R.	391
Du, S. J.	388
Du, X.	422
Du, X. D.	64, 424
Duan, X.	12, 18, 146, 197, 395, 396, 701
Duan, X. R.	391, 393, 394, 397, 398, 475
Duarte, V.	859
DuBois, A.	157
Dubrov, M.	495, 756
Duchateau, J.-L.	738
Duckworth, R.	766
Dudnikov, A.	773
Dudson, B.	276
Duff, J.	157, 313
Dumont, R.	336, 342, 531, 569, 839
Dunaevsky, A.	459
Dunai, D.	451
Dunne, M.	28, 39, 179, 180, 190, 351, 352, 505
Dutta, P.	693, 734, 741, 771
Dutta, S.	717, 734, 741, 771
Duval, B.	65, 174, 201, 349, 360, 438, 440, 441, 443, 570
Dux, R.	201, 356, 357, 360, 370, 863
Dyachenko, V.	406, 754
Dzitko, H.	814
— E —	
Eade, T.	763
Easy, L.	276
Ebashi, Y.	664
Ebrahimi, F.	15, 481
Eckart, M.	780
Edlund, E. M.	175, 206, 211, 283
Edo, T.	239
Edwards, J.	780
Edwards, M. J.	12, 14, 138, 787, 788
Effenberg, F.	51, 303, 635
Efthimion, P. C.	787
Egedal, J.	157
Eguchi, T.	664
Eich, T.	165, 194, 370, 477, 731, 857
Eidietis, N. W.	199, 223, 257, 363, 364, 372, 498, 747
Ejiri, A.	33, 152, 291, 293, 866
Ejiri, M.	680

Ekedahl, A.	56, 380, 383, 400, 666	Facco, A.	814
Eksaeva, A.	808	Fagotti, E.	814
El-Guebaly, L.	718	Faisse, F.	666
Elbeze, D.	569, 666	Faitsch, M.	194, 852
Elder, J. D.	172, 802	Falchetto, G.	20, 531
Eldon, D.	24, 169, 172, 187, 215, 224, 232	Fantz, U.	15, 659, 703, 722
Elgriw, S.	404	Farengo, R.	36, 596
Eliseev, L.	409, 445	Farina, D.	686
Ellappan, R.	741, 771	Farley, T.	276
Ellis, R.	766, 787	Farthing, J.	687
Elmore, S.	276	Fasoli, A.	35, 379, 711
Elwasif, W.	479	Fassina, A.	319, 588, 722
Embréus, O.	593	Faudot, E.	353, 374
Emoto, M.	748, 838	Faugel, H.	353, 374
Empizo, M. J. F.	819	Faugeras, B.	531, 534
Endler, M.	185	Faust, I.	192, 211, 383
Endo, Y.	658, 664	Favuzza, P.	835
Ennever, P. C.	206, 211	Federici, G.	727, 731
Ennis, D. A.	408	Fedorczak, N.	342
Enoeda, M.	451	Fehér, T. B.	529
Erdos, B.	201	Feibush, E.	373
Eriksson, J.	336	Feist, J.-H.	851
Ermolaeva, A.	446	Felici, F.	65, 349, 371, 443, 444
Ernst, D. R.	206	Felton, R.	363
Escande, D.	168, 588	Feng, B. B.	392, 394
Escarguel, A.	666	Feng, C.	698
Escourbiac, F.	366, 665, 666, 801, 816	Feng, H.	17, 511, 752
Esipov, L.	406, 407	Feng, K.	22, 29, 668
Esposito, B.	65, 349, 433, 438, 696	Feng, W.	387
Esquivel Sancho, R.	377	Feng, X.	157
Esser, H. G.	857	Feng, Y.	171, 480, 635, 642
Esteve, D.	465	Fenstermacher, M.	169, 172, 195, 224, 230, 231, 233
Estrada, T.	57, 185, 410	Fenzi, C.	26, 207, 569, 666
Ethier, S.	280, 566	Ferlay, F.	666
Evans, L.	737	Fernández Vega, J.	377
Evans, T.	850	Fernanda, R.	337
Evans, T. E.	161, 169, 171, 181, 221, 222, 224	Fernandes, A.	682
Everson, C.	244	Fernandes, H.	402
Eymard-Vernein, P.	681	Fernández-Berceruelo, I.	765
Ezato, K.	665, 666, 739	Fernández-Marina, F.	410
Ezumi, N.	454, 815	Ferrò, G.	433
— F —		Ferrari, H.	596
Fabian, M.	379	Ferrari, M.	59, 669, 743
Fable, E.	179, 349, 357, 370, 523, 531, 570, 854	Ferraro, N. M.	169, 176, 190, 216, 221, 222, 486, 489, 636

Ferreira Nunes, I. M.	66, 337, 341, 342, 368, 369, 373, 852	Friedl, R.	659
Ferreira, J.	334, 531	Frigot, P-E.	704
Ferron, J. R.	181, 196, 226, 230, 363, 364	Fröschle, M.	659
Février, O.	465, 490, 503	Fu, B. Z.	393
Ficker, O.	201, 361, 696	Fu, G.	36, 605
Field, A.	568	Fu, H.	821
Fietz, S.	352, 357, 570	Fu, J.	384
Figat, D.	529	Fu, P.	11, 14, 315, 316, 382, 656, 700
Figini, L.	434, 442, 451, 531, 686	Fuchert, G.	173, 185, 298
Figueiredo, A.	531	Fuchs, C.	201, 531
Figueiredo, H.	402	Fuenfelder, H.	353, 374
Fil, A.	16, 198, 349, 486, 489	Fujii, K.	424, 426
Filatov, O.	753	Fujimoto, Y.	781, 792
Fimognari, P.	157	Fujimura, Y.	783
Firdaouss, M.	666, 731	Fujino, S.	819
Fischer, R.	179, 352, 854	Fujioka, S.	46, 54, 779, 781, 792-794
Fischer, U.	42, 721, 730, 763, 772	Fujisawa, A.	292, 397, 866
Fisher, R.	180	Fujita, H.	798
Fitzgerald, I.	277	Fujita, T.	41, 152, 769
Fitzgerald, M.	334, 344, 855	Fukai, Y.	860
Flanagan, J.	337	Fukuda, M.	712
Flanagan, S.	747	Fukumoto, M.	442, 454
Fletcher, A.	512	Fukumoto, N.	67, 152, 866
Fleury, L.	529	Fukuyama, A.	152, 162, 245, 292, 293, 516, 534, 542, 545
Fogaccia, G.	531, 598, 608	Fülöp, T.	35, 572, 593
Fonck, R.	12, 18, 151, 284, 294	Funaba, H.	171, 184
Forbes, E.	235	Furlan, J.	164
Forest, C.	157	Furno, I.	50, 379, 436, 439, 722
Forest, L.	744	Furui, H.	291
Formisano, A.	363	Furukawa, M.	16, 493
Fornal, T.	185	Furukawa, T.	812
Fortuna, L.	432	Fusco, V.	598, 608
Fortuna-Zaleśna, E.	346	Futatani, S.	16, 477, 504
Fradera, J.	735		
Francisquez, M.	20, 550	— G —	
Franck, J.	725	Gabrielli, A.	433
Franke, T.	721, 722, 724, 725	Gaio, E.	727
Franz, P.	157, 168, 311, 588	Galante, M.	157, 311
Frassinetti, L.	40, 157, 177-179, 314, 337, 339, 343, 362, 476, 477	Galassi, D.	625, 738
Fredrickson, E.	32, 285, 606, 686, 853	Galazka, K.	451, 645
Freidberg, J. P.	501	Galdon, J.	190
Frenje, J.	46, 54, 780, 782	Galeani, S.	433, 438
Frerichs, H. G.	195, 269, 635, 636	Gallais, L.	647
Fridström, R.	157, 314	Galperti, C.	65, 434, 438, 443, 444
		Galyuzov, A.	502
		Ganesh, R.	26, 561

Gangradey, R.	740, 759, 771	Genesio, P.	628, 633
Gantenbein, G.	704, 725	Geng, S.	660
Gao, C.	207, 283	Genini, L.	681, 750
Gao, G.	382, 700	George, S.	143, 328
Gao, J. M.	197	Gerasimov, S.	198, 360
Gao, L.	787	Gergo, I. P.	201
Gao, W.	642	Gerhardt, S. P.	278
Gao, X.	55, 381, 549	Gerhardt, S. P.233, 279, 285-287, 372, 486,	755
Gao, Y.	305	Gex, D.	814
Gao, Z.	37, 295, 622, 623	Ghendrih, P.	465, 559, 625
Garate, E.	239, 243	Ghezal, A.	624
Garavaglia, S.	434, 442, 570, 725	Ghezzi, F.	347
Garbet, X.	38, 47, 465, 490, 503, 559, 569	Ghiorghiu, F.	647
Garcia Carrasco, A.	346, 347	Ghoniem, N.	800
Garcia, A.	730	Ghoos, K.	531
Garcia, F.	747	Ghosh, D.	143, 324
Garcia, J.	53, 63, 342, 451, 473, 497, 541,	Ghosh, J.	35, 52, 145, 323, 651, 717, 760
545		Gi, K.	60, 277, 842
Garcia, L.	26, 571	Giacalone, J. C.	666
Garcia, R.	411	Giacomelli, L.	336, 338, 344, 682
García-Martínez, P.	596	Giancarli, L.	669, 743
Garcia-Munoz, M.	38, 47, 190, 227, 451	Giannone, L.	201, 444
Garcia-Rosales, C.	809	Gietl, H.	806
Gardarein, J. L.	666	Gil, C.	569, 666
Garg, A.	143	Gilbert, M.	46, 54, 763
Gargiulo, L.	666, 752	Gilson, E. P.	709
Garkusha, I. E.	45, 830, 836	Gin, D.	34, 407, 695
Garofalo, A. M. 29, 39, 169, 176, 181-183,		Giorgetti, F.	727
196, 225, 487, 488, 527		Giovannozzi, E.	435, 531
Garrison, L.	712	Giroud, C.48, 178, 336, 338, 339, 342-344,	476, 477
Gary, T.	286	Giruzzi, G.	66, 451, 473, 490, 645
Garzotti, L.	276, 451, 497, 504, 541, 544,	Giuliano, D.	766
645, 852		Glasser, A. H.	485
Gaspar, J.	332, 666	Gleason-Gonzalez, C.	451, 531, 713
Gasparotto, M.	851	Glebov, V.	780, 782
Gates, D.	25, 241, 287, 299, 301, 302, 748	Glöggler, S.	863
Gatica Valle, O. A.	377	Gobbín, M.	201, 349, 438, 588
Gatu Johnson, M.	780, 782	Gobin, R.	750, 814
Gauthier, E.	332	Goetz, J.	157
Gavila, P.	666	Gohil, P.	187, 215
Gavrilenko, D.	458	Goldston, R.	67, 858
Gazzotti, S.	666	Goldston, R. J.	828
Ge, J.	698	Golfínopoulos, T.	211, 283, 549
Geiger, B.	65, 354, 355, 441	Golingo, R.	235
Geiger, J.	15, 185, 298, 301, 480		
Gellert, F.	307		

Goloborod'ko, V.	334, 531	Graves, J.	342
Golubeva, A. V.	833	Graves, V.	766
Gomes, R.	338	Gray, T. K.	275, 286, 671, 828
Goncharov, P.	288	Green, D.	37, 479, 611, 618, 766
Gondé, R.	681, 750	Greenwald, M. J. .	207, 283, 469, 501, 723
Gong, X.	133, 182, 183, 203, 368, 385	Greuner, H.	347
Gong, X. Y.	56, 386	Gribov, Y.	363, 366, 495
Gong, X. Z.	380, 387	Grierson, B. A. .	62, 68, 169, 176, 181, 182, 187, 196, 205, 206, 215, 224, 471, 479, 527, 566, 597, 760, 850
Goniche, M.	48, 336, 342, 380, 383	Grigore, E.	666
González de Vicente, S. M.	824	Grim, G.	780
González Guevara, J. A.	35, 706, 757	Grisham, L.	658
González Marroquín, J.	706, 757	Grisolia, C.	647
Gonzalez, C.	831	Groebner, R. .	169, 176, 202, 215, 228, 230, 233, 640
Gonzalez-Arrabal, R.	831	Groebner, R. J.	487
Goodman, T. P.	65, 439, 442, 443, 451	Grohnheit, P. E.	845
Gopalakrishna, M. V.	143, 145	Gröschel, F.	835
Gorbovsky, A.	458	Grossetti, G.	58, 721, 724, 725
Gordienko, Y.	810	Grosso, G.	434
Gordillo, N.	831	Grote, H.	851
Gorelenkov, N.	66, 853	Groth, M.	172, 173, 331, 333, 852, 863
Gorelenkov, N. N.	227, 597, 606	Grover, O.	362
Gorelenkova, M.	534, 611	Grulke, O.	40, 185, 300, 305, 310
Gorini, G.	682	Grunloh, H.	699
Görler, T.	340, 473	Gryaznevich, M. .	58, 238, 240, 277, 403, 736
Gorshkov, A.	702	Grzonka, J.	48, 345, 346
Gospodarczyk, M.	433, 438	Gu, S.	382
Gospodchikov, E.	459	Guan, W.	821
Goswami, N. S.	661	Gude, A.	351
Gota, H.	25, 239, 243	Guenter, S.	38, 505
Gotewal, K. K.	693, 734, 741, 771	Guerrero, C.	831
Goto, M. .	171, 193, 417, 418, 424, 426, 838	Gui, B.	641
Goto, T.	66, 450, 676, 719, 728, 748	Guilhem, D.	666, 801
Goto, Y.	413	Guillemaut, C.	857
Gougnaud, F.	750	Guirlet, R.	465
Goulding, R.	766	Gulati, H. K.	143
Grézaud, M.	661	Gunn, J. P.	633, 666
Gracceva, F.	845	Guo, D.	399
Graham, M.	342	Guo, H.	172, 203, 230, 231, 802
Grandgirard, V.	465, 559	Guo, H. Y.	387
Grando, L.	319	Guo, S. C.	497
Granetz, R. S. .	23, 207, 212, 223, 283, 372, 498	Guo, W.	182, 382
Granucci, G. .	58, 349, 434, 451, 721, 724, 725	Guo, X.	860
Grashin, S.	147, 445		
Grasso, D.	588		

Guo, Z.	17, 517, 584, 646
Gupta, C.	145, 717
Gupta, C. N.	143
Gupta, M.	717
Gupta, S.	143, 670
Gürcan, Ö. D.	521, 559, 573
Gurchenko, A.	406, 560
Gurevich, M.	773
Guruparan, S.	305
Gusakov, E. Z.	37, 406, 560, 620
Gusev, V.	288, 754
Guterl, J.	172, 802
Gutierrez-Milla, A.	529
Gutruf, S.	702
Guttenfelder, W.	26, 280, 568
Guzmán González, J. V.	706, 757
— H —	
Ha, Y.	811
Haan, S. W.	788
Hacek, P.	362
Hacquin, S.	358
Hada, K.	429
Hager, R.	20, 548, 634
Hahm, T. S.	27, 264, 478, 558, 579
Hahn, S.-H. ...	30, 248, 254, 257, 258, 278
Hakim, A.	50, 626, 858
Hakola, A.	48, 165, 347, 453, 666
Halitovs, M.	834
Hallatschek, K.	27, 580, 603
Halpern, F.	436, 632
Ham, C.	180
Hamada, Y.	50, 375
Hamaguchi, D.	345
Hamaguchi, S.	728
Hamaji, Y.	708, 719, 829
Hamba, F.	484
Hammel, B. A.	787, 788
Hammett, G.	626, 858
Han, H. S.	258, 546
Han, S. H.	247
Han, W.	811
Han, X.	381
Han, Y. H.	399
Hanada, K.	33, 152, 292, 293, 664, 866
Hanada, M.	658, 690
Hanayama, R.	790, 791, 796
Hansen, C. J.	242, 244
Hanson, J. D.	24, 219, 408
Hao, G.	853
Happel, T.	356, 359
Hara, H.	240
Hara, M.	345
Harrault, F.	814
Harris, J. H.	185, 303
Harrison, J.	174, 276, 277, 477
Hartfuss, H.-J.	298
Harting, D.	544, 863
Hartmann, D.	185, 308
Hartouni, E.	780
Hartwell, G. J.	408
Hartwig, Z. S.	832
Harvey, R. W.	157, 612
Hasegawa, A.	712, 821, 824
Hasegawa, H.	51, 639
Hasegawa, J.	786
Hasegawa, K.	680
Hasegawa, M.	293, 866
Hashizume, H.	62, 677, 728
Haskey, S.	169
Hasrgawa, M.	292
Hastie, J.	180
Hata, M.	792
Hatano, Y.	35, 345, 712, 770, 829
Hatarik, R.	780
Hatayama, A.	454, 644, 660
Hatch, D.	509, 551
Hatchressian, J. C.	666
Hatzky, R.	529
Hauer, V.	713
Havlicek, J.	361, 362
Havlickova, E.	276
Hawkes, N.	277, 340
Hawryluk, R.	68
Hayakawa, A.	680
Hayashi, N. ...	20, 449, 451, 497, 499, 540, 545, 555, 563
Hayashi, T.	826
Hayashi, Y.	66, 457, 769
He, H.	395
He, X.	197
Hebbar, G.	707
Hebert, J. D.	408

Hegna, C. C.	157, 169, 171, 312, 420
Heidbrink, W.	859
Heidbrink, W. W.	190, 191, 227, 597
Heidinger, R.	141, 814, 835
Heilmaier, M.	805
Heinemann, B.	659
Heinola, K.	47, 329, 330, 345, 803
Helander, P.	480, 865
Hellesen, C.	33, 336, 683
Helou, W.	380, 666
Hender, T.	198
Henderson, M.	686, 689, 704
Henderson, S.	263
Hennequin, P.	359, 559, 666
Henning, M.	297
Henriques, R. B.	402
Herashchenko, S.	830
Herfindal, J. L.	408
Hermann, V.	704
Hermansson, K.	873
Hernandez, C.	666
Hernandez, F.	721
Hernandez, J.	411
Herrmann, A.	194, 854
Herrmann, M. C.	787
Hertout, P.	727
Hess, J.	466
Hetzenecker, A.	359
Heuraux, S.	353, 374, 529
Hidalgo, C.	57, 161, 409, 410
Higashijima, A.	292, 293, 866
Higuchi, M.	318
Hill, D.	69, 172, 231
Hill, K. W.	42, 302, 384, 787
Hillairet, J.	380
Hillesheim, J.	38, 47, 188, 338, 339, 852
Hillis, D.	766
Himabindu, M.	734, 741, 771
Himura, H.	318
Hinkel, D. E.	780, 788
Hinojosa, J. A.	709
Hinoki, T.	712, 829
Hinson, E.	195
Hioki, T.	790, 791, 796
Hirai, T.	665, 801, 816
Hirakawa, Y.	812
Hiraoka, Y.	708
Hirata, M.	454, 456
Hirata, T.	292
Hiratsuka, J.	11, 14, 658, 659
Hirayama, T.	665
Hiroimi, T.	423
Hironaka, Y.	792
Hirooka, Y.	454, 671
Hirose, A.	404
Hirose, T.	817
Hirsch, M.	29, 39, 185, 298, 300
Hirshman, S.	157, 221, 312
Hirvijoki, E.	514
Hiwatari, R.	62, 673, 739
Hizanidis, K.	617
Hjalmarsson, A.	696
Hoa, C.	727, 750
Hoang, G. T.	380
Hobirk, J.	180, 369, 852, 854
Hodille, E.	487
Hoelbe, H.	480
Hoelzl, M.	190, 349, 477, 488, 504, 505
Hoenen, O.	529, 531
Hoeschen, T.	806
Höfel, U.	185, 298
Hoffman, N.	782
Hogeweyj, D.	444
Hogge, J.-P.	704
Holcomb, C. T.	168, 181-183, 196, 226, 230, 597
Hole, M. J.	66, 855
Holland, C.	53, 63, 214, 471, 479
Hollfeld, K. P.	305, 308
Hollmann, E. M.	199, 223
Hollocombe, J.	529
Holly, D.	157
Holod, I.	21, 552, 601
Holzhauser, E.	614
Homma, H.	291
Homma, M.	542
Homma, Y.	644
Honda, D.	289
Honda, M.	26, 476, 499, 519, 540, 563
Honda, T.	292
Hong, J.	31, 263
Hong, R. J.	399

- Hong, S.-H. 31, 135, 266, 269, 270
Honore, C. 359
Hoover, D. 788
Hopf, C. 49, 355, 659, 722, 854
Horacek, J. 436
Horioka, K. 786
Horiuchi, R. 38, 152, 240
Hornsby, W. 491
Hornung, G. 559
Horsten, N. 531
Horton, W. 27, 583
Horvath, L. 177
Höschen, D. 305
Hosea, J. C. 192, 286, 385
Hoshino, A. 289
Hoshino, K. 451, 540, 644, 713, 739
Hoshino, T. 672
Hosokawa, M. 363, 534, 839
Hossack, A. 25, 244
Hou, Y. 642
Houry, M. 666
Houshmandyar, S. 283
Howard, N. 208, 471
Howard, R. 766
Hronova, O. 361
Hsing, W. W. 780, 787
Hsu, P.-C. 573, 577
Hu, L. 34, 163, 385, 698, 758
Hu, L. Q. 390, 656
Hu, R. J. 384
Huang, B. 238, 450
Huang, H. 788
Huang, J. 51, 133, 642
Huang, L. 700
Huang, Q. 44, 823
Huang, X. 63, 193, 417
Huang, Y. 397, 700
Huang, Z. 395
Huang, Z. H. 397
Hubbard, A. 852
Hubbard, A. E. 28, 39, 175, 207, 208, 211,
283, 549
Huber, A. 808, 852, 857, 863
Huber, S. 873
Huber, V. 857
Hudson, S. 14, 18, 462, 486, 855
Hughes, J. W. 175, 206–208, 210, 211, 283,
549, 640
Hughes, M. 235
Hughes, P. E. 242
Hugill, J. 238
Huijsmans, G. 366, 477, 488, 503–505
Humphreys, D. A. 49, 135, 224, 226, 232,
257, 363–365, 368, 498, 747
Hurricane, O. A. 780, 788
Hussain, S. 401
Huynh, P. 531, 534
Hwang, Y. S. 259, 296, 675
Hyatt, A. W. 181, 183, 233, 257
- I —
- Iafrati, M. 432
Ibano, K. 52, 648, 826, 827
Ibarra, A. 765, 835
Iblyaminova, A. 288
Ichige, H. 680
Ichiguchi, K. 15, 483
Ichikawa, M. 658
Ichimiya, R. 814
Ichimura, K. 454
Ichimura, M. 454, 456
Ida, K. 64, 161, 171, 184, 197, 250, 297, 375,
410, 416, 419–421, 425, 428, 542,
607, 748, 838
Ide, S. 369, 449, 451, 492, 499, 534, 540, 563
Idei, H. 33, 152, 292, 293, 664, 866
Ido, T. 64, 375, 424, 425, 607, 838
Idomura, Y. 25, 555, 564
Igami, H. 413, 414, 664, 838
Igaune, I. 834
Igitkhanov, Y. 67, 868
Iglesias, D. 332
Iglesias, R. 831
Igochine, V. 49, 168, 351
Iijima, T. 457
Iiyoshi, A. 10, 124
Ikeda, K. 660, 705, 838
Ikeda, R. 15, 663, 664, 689, 699
Ikezoë, R. 66, 454, 456, 664
Iliasova, M. 407, 695
Illy, S. 704, 725
Im, K. 720, 732
Imadera, K. 25, 556, 557

Imagawa, S..... 678
 Imai, T..... 293, 454, 664
 Imazawa, R..... 33, 685
 Imbeau, F..... 371, 529, 531, 534, 738
 Imrisek, M..... 362
 In, Y.... 14, 19, 30, 135, 170, 248, 250, 252,
 255, 273, 275, 278, 496, 565, 629
 Inagaki, S.161, 395, 397, 419, 421, 425, 607
 Injutin, N..... 753
 Inklin, N..... 430
 Innocente, P..... 174, 319, 451
 Ino, S..... 815
 Inomoto, M..... 67, 240, 860
 Inoue, H..... 644
 Inoue, S..... 16, 240, 492
 Ioannidis, Z..... 617, 704, 725
 Ionita, C..... 437
 Irby, J. H..... 207, 211, 283
 Irzak, M..... 406
 Isayama, A..... 442, 451, 492, 498
 Ishida, A..... 291
 Ishida, M..... 783
 Ishiguro, S..... 639
 Ishii, K..... 43, 790, 791, 796
 Ishii, Y..... 162
 Ishizawa, A..... 53, 63, 428, 472, 518
 Islam, M. M..... 454
 Islan, M. S..... 454
 Ismailov, R..... 474
 Isobe, K..... 345, 672
 Isobe, M..... 424, 542, 770
 Isozaki, M..... 689
 Issac, R. C..... 43, 797
 Itagaki, J..... 456
 Itami, K..... 33, 685, 688
 Ito, A..... 44, 822
 Ito, S..... 664, 677, 728
 Ito, Y..... 824
 Itoh, K.... 13, 161, 197, 395, 397, 419, 425,
 574, 603, 607
 Itoh, S.-I. 161, 197, 395, 397, 425, 574, 603,
 607
 Ivanov, A. A. 157, 243, 246, 312, 459, 474
 Ivanov, I..... 458
 Ivanov, N..... 16, 494
 Ivanova-Stanik, I..... 531, 645

Iwamoto, A..... 678
 Iwata, N..... 781
 Iwata, Y..... 786
 Izumi, N..... 819
 Izzo, V..... 199

— J —

Jaboulay, J.-C..... 738, 744
 Jachmich, S..... 198, 332, 360, 857
 Jackson, D..... 163
 Jackson, G. L. 181, 202, 214, 363, 364, 369
 Jacobsen, A..... 354
 Jacobson, C..... 157, 311
 Jacquemot, S..... 45, 69, 861
 Jacquet, P..... 335, 336, 342
 Jacquot, J..... 353, 374
 Jadeja, K. A..... 145, 717
 Jaeger, E. F..... 611, 618
 Jaiswal, S..... 717
 Jakubowski, M..... 185, 301, 303, 304
 Jana, S..... 143, 324
 Janeschitz, G..... 367
 Jang, J..... 263
 Jang, S..... 456
 Jarboe, T..... 25, 236, 244, 755
 Jardin, S. C.... 15, 248, 249, 253, 486, 489,
 498, 755
 Järvinen, A. E..... 333, 338
 Jasper, B..... 806
 Jaworski, M..... 858
 Jaworski, M. A. 44, 286, 671, 749, 828
 Jayanthi, H..... 661
 Jayaswal, S. P..... 143
 Je, H..... 811
 Jelonnek, J..... 704, 724, 725
 Jenkins, I..... 724
 Jenkins, T..... 37, 621
 Jenko, F..... 473
 Jeon, Y. 135, 170, 248, 255, 257, 275
 Jeon, Y.-M..... 247, 251, 260
 Jeon, Y. M..... 250, 258, 278
 Jeong, J. H..... 263
 Jernigan, T..... 199
 Ješko, K..... 457
 Jha, A..... 661
 Jha, R..... 143, 145
 Jha, S. K..... 145

Jhang, H. 55, 61, 261, 264, 478, 507, 522,
534, 567, 582

Ji, H. 709

Ji, X. 197, 382, 395, 399

Ji, X. Q. 56, 391-393, 397

Jia, M. 203, 382, 642

Jia, M. N. 387

Jian, X. 389

Jiang, J. 163

Jiang, L. 700

Jiang, M. 391, 392, 394

Jiang, W. 786

Jiangang, J. 29

Jie, Y. X. 390

Jimenez-Ramos, C. 190

Jimenez-Rey, D. 814

Jin, F. 701

Jin, J. 704

Jin, M. 163

Jin, X. Z. 60, 843

Jin, Z. 642

Jinno, Y. 429

Jitsuno, T. 781, 783, 792, 794

Jo, G. 558

Jo, J. 267, 296

Joffrin, E. 54, 61, 198, 369, 451, 852, 857

Johnson, I. 534

Johnson, J. 157, 311

Johnson, R. D. 226

Johnson, T. 334, 531, 534

Johnston, J. 843

Johzaki, T. 779, 781, 792, 793

Joisa, Y. S. 143, 145

Jolliet, S. 632

Jones, O. S. 787

Jorge, R. 632

Josep, F. 852

Joshi, J. 692, 707

Joshi, K. 707

Joung, M. 258

Jouve, M. 666

Ju, S. Q. 385

Jucker, P. 164

Juhn, J.-W. 170, 268

Jung, L. 534, 675

— K —

Kaang, H. H. 26, 478, 567

Kado, S. 427-431, 454, 457

Kadowaki, K. 277

Kafle, N. 766

Kagan, G. 782

Kahn, M. W. M. 314

Kaiser, A. 873

Kaita, R. 233, 282, 671, 749, 828

Kajita, S. 34, 457, 694

Kajiwara, K. 663

Kakurin, A. 494

Kalal, M. 717

Kalaria, P. 725

Kalashnikov, A. 163

Kaljun, D. 529

Kallenbach, A. 10, 12, 132, 347, 854, 857,
863

Kallmeyer, J.-P. 308

Kalupin, D. 531

Kamada, K. 819

Kamada, Y. 69, 139, 152, 161, 449, 451

Kamendje, R. 836

Kaminaga, A. 680

Kamio, S. 413, 838, 860

Kamiya, K. 161, 178, 451

Kampf, D. 702

Kan, H. 790, 791, 796, 819

Kanabar, D. H. 143

Kandaurov, I. 378, 458

Kaneko, O. 660, 705, 838

Kanemura, T. 812, 835

Kang, C. S. 269, 275, 629

Kang, I. J. 270

Kang, J. 62, 68, 675

Kang, K. S. 529

Kanjanaput, W. 539

Kantor, M. 406

Kantor, R. 696

Kargin, N. 67, 867

Kariya, T. 15, 293, 454, 664

Karpushov, A. 440, 441, 570

Kasada, R. 811, 824, 847

Kasahara, H. 291, 385, 413, 415, 429, 820,
838

Kasatov, A. 378, 458

Kashiwagi, M.	658, 690	Khan, M.	707
Kashyap, A.	245	Khan, M. S.	143, 328
Kasperek, W.	307, 704	Khan, R.	401
Kasthurirengan, S.	740	Khan, S. F.	788
Kasugai, A.	43, 814	Khan, Z.	143, 328
Kasuya, N.	27, 161, 586, 603	Khaydarov, R.	42, 784
Katanuma, I.	51, 454, 637	Khayrutdinov, R. R.60, 363, 366, 368, 474, 475, 495, 534, 756	
Katayama, K.	829	Khilkevitch, E.	360, 407, 695
Kato, D.	64, 426	Khirwadkar, S.	734, 741, 771
Kato, S.	822	Khrebtov, S.	409
Kato, Y.	792	Khristi, Y. S.	143
Katoh, Y.	712, 766, 800	Khvostenko, P.	59, 753, 756
Kauffman, R. L.	787	Kikuchi, M.	246
Kaur, R.	143	Kikuchi, T.	42, 786
Kaveeva, E.	464	Kilkenny, J. D.	780, 787
Kavin, A.	368, 754	Kim, B.	235
Kaw, P. K. 10, 145, 323, 470, 506, 734, 741, 771		Kim, C.-B.	585
Kawabata, K.	783	Kim, D.	363, 443
Kawaharada, T.	289	Kim, H.	255, 269, 271
Kawakami, Y.	783	Kim, H.-S.	30, 254, 258, 270, 271
Kawamata, R.	658	Kim, H.-T.	20, 344, 538
Kawamura, G.	193, 418	Kim, H. S.	247, 250, 263, 546
Kawamura, Y.	817	Kim, J. . 17, 30, 31, 157, 170, 248, 251, 252, 254, 257, 259, 263, 271, 273, 275, 278, 312, 507, 567	
Kawanaka, J. 46, 55, 779, 781, 783, 792		Kim, J.-H.	345
Kawano, Y.	34, 685, 688, 691	Kim, J.-Y.	247
Kawasaki, S.	292, 293, 866	Kim, J. S.	795
Kawasaki, T.	783	Kim, J. Y.	20, 271, 546
Kawashima, H.	451, 713	Kim, K. . . 30, 163, 255, 263, 269, 275, 545, 629	
Kawashima, T.	790-792, 796	Kim, K.-W.	14
Kawasumi, Y.	375	Kim, M.	30, 253, 503
Kawata, S.	786	Kim, M. H.	204
Kawazura, Y.	245	Kim, S.	261
Kaye, S. 233, 280-282, 284, 538, 568		Kim, S.-H.	296
Kazakov, Y.	852	Kim, S. H. 20, 258, 363, 368, 534, 543	
Kazakov, Ye. O.	209, 308, 334, 336	Kim, S. K.	675
Kazarian, F.	661	Kim, S. S.	27, 478, 507, 567, 582
Kaziev, A.	554	Kim, T.-K.	265
Ke, L.	789	Kim, Y.	269
Ke, R.	399	Kimura, A.	43, 811, 821, 824
Keeling, D.	344	King, D.	852
Kembleton, R.	674	King, J. R.	15, 487
Kemp, R.	62, 68, 674, 731	Kingham, D.	238, 736
Kenmochi, N.	427-431		
Kesler, L. A.	832		
Kessel, C.	368, 369, 545, 720		

Kiptily, V.	336, 360, 407	Koechl, F. 48, 341, 343, 370, 463, 543-545, 839	
Kiptily, V. G.	334	Kohagura, J.	454, 456
Kiramov, D.	495	Köhn, A.	614
Kirimoto, M.	428	Kohno, H.	619
Kirk, A. 12, 18, 150, 180, 194, 276, 352, 477, 505, 850		Kohse, G.	832
Kirov, K.	383	Koide, Y.	680
Kirschner, A.	51, 329, 331, 453, 643, 802	Koivuranta, S.	803
Kisaki, M.	11, 15, 660, 705, 838	Kojima, A.	658, 690
Kishikawa, H.	429, 430	Kojima, S.	781, 792, 794
Kishimoto, Y.	25, 472, 556, 557	Kolasinski, R.	829
Kitagawa, Y.	42, 790, 791, 796	Kolemen, E.	24, 172, 181, 224, 232, 233, 485, 486, 489, 709
Kitamura, H.	783	Komarov, A.	409
Kitazawa, S.-I.	688	Komatsuzaki, M.	689
Kiviniemi, T.	560	Komeda, O.	790, 791, 796
Kizane, G.	834	Komm, M.	49, 362
Kizu, K.	680	Komori, A.	413
Klein, F.	809	Kondo, H.	43, 812, 835
Klepper, C.	666	Kondo, K.	781, 786, 794, 814
Klimenkov, M.	805	Kondo, S.	829
Kline, J. L.	788	Kong, D.	381, 389, 640
Klinger, T.	185, 851	Kong, H. J.	43, 795
Klose, S.	185, 303	Könies, A.	467
Kluth, P.	869	König, R.	185, 303, 304, 306, 635
Klyuchnikov, L.	447	Konishi, S.	60, 847
Knaster, J.	12, 18, 141, 812, 814, 824, 835	Konno, C.	768
Knauer, J.	185, 298, 780	Konobeev, A.	772
Knaup, M.	300	Konoshima, S.	427-431
Knowlton, S. F.	408	Konovalov, S. 55, 61, 69, 363, 366, 474, 534	
Ko, J.	31, 249, 252, 272, 278	Konrad, R.	851
Ko, J. S.	258	Korchuganova, O.	805
Ko, S.	31, 261	Korepanov, S.	243
Ko, S. H.	265	Kornejew, P.	185, 298
Ko, W.	262	Kornev, V.	67, 405, 872
Ko, W. H. 30, 161, 170, 247, 248, 250, 252, 255, 261, 263, 264, 275, 278		Korobeynikova, O.	459
Kobarg, T.	704	Korobov, K.	447
Kobayashi, M.	171, 193, 416, 418, 420	Korpilo, T.	560
Kobayashi, S.	19, 64, 427-431, 472, 521, 664	Korsholm, S. B.	434
Kobayashi, T. 161, 419, 428, 451, 663, 664, 689, 838		Korzhevina, M.	459
Kobuchi, T.	770	Kos, L.	531, 534
Kocan, M.	331	Koskela, T.	336, 344
Kochergin, M.	702	Kost, Y.	867
Kocsis, G.	185, 301, 304	Kostic, A.	374
		Kostuk, M.	747
		Kosuga, Y. 26, 161, 397, 425, 574, 603, 607	

Kotov, V.	531	Kudlacek, O.	319, 349, 444
Kotschenreuther, M.	21, 231, 509, 551	Kudou, H.	739
Kotula, J.	696	Kuech, T.	867
Kouprienko, D.	406	Kuklin, K.	458
Kovacic, J.	437	Kukushkin, A. B.	694, 702, 852
Kovaldins, R.	834	Kukushkin, A. S.	348, 464, 702
Kovalenko, Y.	459	Kulevoy, T.	805
Koyanbaev, E.	810	Kuley, A.	613
Kozachek, A.	409	Kulik, N.	830
Kozaki, Y.	798	Kulikov, S.	867
Kozioziemski, B.	788	Kulkarni, S. V.	143, 145
Kramer, G.	859	Kulsartov, T.	810
Kramer, G. J.	36, 191, 227, 286, 597	Kumar, A.	143, 145
Krämer-Flecken, A.	40, 185, 300, 305	Kumar, M.	143, 670
Krashennikov, S.	13, 160	Kumar, R.	661, 717, 734
Krashevskaya, G.	554	Kumar, S.	143
Krasilnikov, A.	22, 852	Kumari, K.	717
Krasilnikov, V.	682, 696	Kumazawa, R.	385
Krat, S.	803	Kunugi, T.	709
Kraus, S.	808	Kuprienko, D.	407
Kraus, W.	659	Kurc, T.	373
Krawczyk, N.	185	Kurihara, K.	10
Krbec, J.	362	Kurishita, H.	826
Krebs, I.	486	Kurita, T.	790, 791, 796
Krek, J.	531	Kurki-Suonio, T.	36, 595
Kreter, A.	43, 808, 809, 826	Kurkuchekov, V.	378, 458
Krieger, K.	332, 347, 852	Kuroda, K.	289
Kriete, D.	151, 294	Kurotaki, H.	345
Kritcher, A.	780	Kurskiev, G. S.	288, 702, 754
Kritz, A.	526, 527	Kurtz, R.	800
Krivchenkov, Y.	238	Kurutz, U.	659
Krivska, A.	308	Kurzan, B.	179
Kruezi, U.	198, 857	Kuteev, B.	69
Kruger, S. E.	487	Kuteev, B. V.	746, 762, 773
Krupin, V.	147, 447	Kuzmin, A.	292
Krupnik, L.	409	Kuznetsov, V.	665
Krychowiak, M.	185, 635	Kwak, J.-G.	31, 135, 248, 255, 267, 629
Krylov, S.	447	Kwon, J.	251, 261, 262, 558
Krylov, V.	753	Kwon, J.-M.	135, 260, 264, 522
Ksiazek, I.	185	Kwon, S.	720, 732, 768
Ku, S.-H.	51, 463, 631, 638	Kyrala, G. A.	788
Kuang, A.	210, 211, 223		
Kubala, S.	157	— L —	
Kubkowska, M.	185	La Haye, R. J.	181
Kubo, H.	449, 451, 454	Labit, B.	65, 174, 436, 437
Kubo, S.	161, 413, 414, 664, 838	LaBombard, B.	23, 52, 175, 210, 211, 469, 653, 723

Labusov, A.	754	Leconte, M.	27, 581
Lackner, K.	201, 731	Lee, H.31, 33, 170, 255, 266, 269, 296, 496, 565, 629	
Lacroix, B.	727	Lee, H. H.	247, 250, 256, 275
Laffont, G.	666	Lee, H. J.	508
Laguner, F.	179, 352, 356, 357	Lee, H. T.	44, 648, 826, 827
Lahtinen, A.	347	Lee, H. Y.	263
Lakhin, V.	445	Lee, J. 31, 204, 251, 253, 259, 260, 278, 611	
Lamaison, V.	750	Lee, J. A.	264
Lampert, M.	268	Lee, J. E.	204, 253
Lampugnani, L.	596	Lee, J. H.	250, 263, 268
Lamzin, E.	363	Lee, J. P.	16, 207, 501, 615
Lan, T.	41, 315, 316, 390, 399	Lee, K.	252
Lanctot, M. J. 169, 183, 247, 257, 364, 500, 747		Lee, K. C.	31, 268
Landen, O. L.	780, 787	Lee, K. D.	256, 258
Landreman, M.	241	Lee, S.	781, 793
Lang, J.	631	Lee, S. G. 30, 248, 256, 263, 264, 384, 496	
Lang, P.	451, 504, 857	Lee, S. H.	247, 263, 268, 794
Langenberg, A.	40, 185, 298, 299, 302	Lee, T. G.	258
Languille, P.	666	Lee, W.31, 160, 204, 249, 252, 253, 260, 265	
Lao, L. L.	389, 479, 534	Lee, X.	747
Laqua, H. P.	185, 298, 303, 307, 309	Lee, Y.	267
Larroche, O.	782	Leem, J.-E.	265
Larroque, S.	666	Leerink, S.	25, 560
Lasa, A.	766	Leggate, H.	529
Lashkul, S. I.	57, 406, 407, 560	Lehnen, M.49, 198, 363, 365-367, 474, 495, 515	
Lasnier, C. J. 169, 172, 181, 195, 199, 202, 223, 230, 233, 802		Leichtle, D.	772
Latsas, G. P.	704	Lengar, I.	682
Latu, G.	465, 559	Leonard, A. W.24, 172, 195, 228-233, 634, 802	
Lau, C.	225	Leonov, V.	495
Lauber, P.227, 351, 359, 451, 467, 497, 608		Leontev, O.	754
Law, K. F. F.	779, 781, 792	LePape, S.	780
Lay, W.-S.	755	Lerche, E. A.	336, 340, 342, 531, 852
Layden, B.	855	Lescinskis, A.	834
Lazerson, S.	40, 185, 241, 301, 302, 304	Lessard, T.	766
Lazzaro, E.	490, 570	Lessig, A.	477, 504, 505
Le Blanc, B.	853	Lessing, A.	503
Le Masurier, S.	69	Lestz, J.	606
Le, H. B.	443	Lesur, M.	36, 425, 603, 607
Le, R.	752	Levesque, J. P.	25, 242
Lebedev, S.	18, 57, 405, 872	Levin, I.	753
LeBlanc, B.	233, 278, 280-282, 284-286	Levinton, F.	285
Leccacorvi, R.	469	Lewandowska, M.	727
Lechón, Y.	845	Leyland, M.	177, 178, 339, 343
Lechte, C.	531		

Li Puma, A.	738, 744
Li, C.	782
Li, D.	600, 616
Li, D. H.	641
Li, G.	56, 133, 203, 381, 382, 389
Li, H.	315, 316, 389, 511
Li, J.	69, 140, 549, 557, 573, 700
Li, J. G.	385, 801
Li, J. Q.	556
Li, M.	133, 383
Li, M. H.	380, 387
Li, Q.	397, 666, 701, 801
Li, S.	698
Li, W. M.	390
Li, Y.	163, 197, 382, 383, 395, 622
Li, Y. G.	391
Li, Y. Y.	384
Li, Z.	389
Lian, Y.	813
Liang, Y.	10, 40, 133, 203, 300, 305, 306, 382, 387, 642
Liedahl, D. A.	787
Likonen, J.	330, 803
Limtrakul, J.	873
Lin, J.	37, 616
Lin, L.	157, 313
Lin, S.	380
Lin, Y.	175, 209, 210, 283, 385, 469, 609
Lin, Z.	36, 227, 243, 552, 553, 599, 613
Lindau, R.	805
Linke, J.	666, 816
Linsmeier, C.	43, 306, 331, 643, 806-809, 857
Lipa, M.	666
Lipschultz, B.	174, 211, 276, 737, 863
Lisgo, S. W.	331, 644
Lister, J. B.	736
Litaudon, X.	10, 11, 131
Litnovsky, A.	43, 809
Litvak, A.	662
Liu, A.	315, 316
Liu, C.	514, 752
Liu, D.	605, 701, 853
Liu, F.	15, 383, 488
Liu, F. K.	380, 384
Liu, G. H.	801
Liu, H.	133, 381, 387, 556
Liu, H. Q.	390
Liu, J.	42, 789
Liu, J. B.	387, 641
Liu, L.	197, 389
Liu, P.	616
Liu, S.	305
Liu, W.	40, 315, 316
Liu, X.	43, 389, 509, 551, 642, 701, 813
Liu, Y.	53, 54, 61, 140, 193, 197, 200, 295, 351, 352, 391, 392, 397, 398, 417, 466, 497, 500, 534, 595, 599
Liu, Y. O.	475
Liu, Y. Q.	382
Liu, Z.	20, 175, 381, 549
Liu, Z. T.	394
Lizunov, A.	459
Llerena, I.	571
Loarte, A.	38, 47, 208, 275, 341, 343, 366, 368, 370, 463, 488, 504, 515, 523, 543, 544, 696, 839
LoDestro, L.	534
Loewenhoff, T.	816
Logan, N. C.	169, 181, 485
Lohner, R.	531
Loizu, J.	462, 632
Lomas, P.	337, 360, 363, 369
Long, T.	396, 399
Lontano, M.	434, 704
Lópe-Fraguas, A.	410
Lopes-Cardozo, N.	828
López-Bruna, D.	57, 411, 412, 420, 590
Lore, J.	51, 195, 221, 229, 275, 636
Lorenzini, R.	41, 322
Losada, U.	333
Losert, M.	704
Lotte, P.	569, 666
Louche, F.	308, 374
Lowry, C.	731, 857, 863
Lu, B.	400
Lu, L.	772
Lu, P.	393
Lu, X.	428-431
Lu, Z. X.	566
Luce, T. C.	168, 169, 181, 214, 226, 230, 368, 369, 543, 545

Luciani, J.-F.	465, 490	Mahajan, S.	231, 509, 551
Luhmann, Jr., N. C.	176, 252, 260, 265	Mahsuria, G. I.	143
Lukash, V. E.	16, 363, 368, 475, 495, 534, 756	Maihom, T.	873
Lumsdaine, A.	766	Mailloux, J.	383
Lunniss, A.	177	Maingi, R.	32, 202, 233, 275, 282, 286, 463, 489, 634, 671, 749
Lunsford, R.	59, 202, 489, 749	Maisonnier, D.	163
Lunt, T.	174	Maistrello, A.	727
Luo, B.	315, 316	Maj, O.	531, 630
Luo, G.	766	Majeski, R. P.	25, 237, 671, 709, 718
Luo, G.-N.	46, 266, 666, 801	Makhlai, V.	830
Luo, G. N.	55, 388, 802	Makino, R.	161, 413, 414, 838
Luo, L.	526	Makowski, M. A.	172, 195, 202, 228, 230, 233, 802
Luo, X.	713	Makwana, A. R.	143
Luo, Z.	389	Makwana, M. N.	145, 717
Luo, Z. P.	212	Malaquias, A.	57, 402
Lupelli, I.	177, 178, 276, 477, 534, 538, 568	Maljaars, B.	444
Lütjens, H.	465, 490	Maljaars, E.	443
Lyons, B.	169, 222	Malkov, M.	27, 573, 577
Lysenko, S.	445	Manchanda, R.	143, 145, 323, 651, 760
Lyttle, M.	684	Mancini, A.	353, 696
Lyu, B.	55, 183, 382, 384	Manduchi, G.	529, 531, 687
Lyublinski, I.	65, 376, 448	Manoah, S. M.	34, 42, 693, 741, 771
— M —			
Ma, C.	582, 640	Mansfield, D.	202, 749
Ma, Q.	197	Mansuri, I. A.	143
Ma, R. R.	391	Mantica, P.	48, 338, 340, 342, 523, 852
Ma, T.	780, 787, 788	Mantsinen, M.	334, 531
Ma, X.	408	Manz, P.	49, 173, 356, 359
Maaßberg, H.	185, 298, 480	Mao, W.	315, 316
Machchhar, H.	661	Mao, Y.	806
Mackinnon, A.	780	Mao, Y. Z.	385
MacPhee, A. G.	787, 788	Mara, N.	804
Maddaluno, G.	432, 433	Marandet, Y.	51, 531, 625, 628, 633, 666
Madrigal Boza, G.	377	Maraschek, M.	201, 349, 351, 359, 570
Madsen, J.	173, 437, 531	Marchiori, G.	319, 497
Maejima, T.	658, 690	Marchuk, O.	299, 302
Maekawa, T.	289	Marconato, N.	351, 705
Maeta, S.	542	Marelli, L.	201, 351
Maeyama, S.	19, 518	Margo, M.	747
Maget, P.	16, 451, 465, 490, 541	Marian, J.	800
Maggi, C.	28, 39, 177, 178, 180, 188, 338, 339, 476, 477, 852, 857, 863	Marinak, M. M.	788
Maggiora, R.	353	Marini, C.	441, 570
Magne, R.	400	Marinoni, A.	206
Mahajan, K.	143	Marinucci, M.	343
		Markelj, S.	647

Markovic, T.	361	Matsuo, S.	783
Marmar, E. S. . . . 10, 12, 136, 175, 207, 210, 283, 469, 723		Matsuoka, S.	26, 564
Marocco, D.	34, 433, 696	Matsuura, H.	454
Maron, Y.	787	Matsuyama, A.	17, 513, 516, 563, 575
Marqueta, A.	814	Matsuyama, S.	770
Marrelli, L.	154, 168, 319, 349	Mattei, M.	363, 451, 731
Marroncle, J.	750, 814	Matthews, G.	198, 330, 332, 803, 857
Marsen, S.	40, 173, 185, 303, 307, 309	Matveev, D.	329
Martin, A.	333	Mauel, M. E.	242
Martin, C.	647, 666	Maurer, D. A.	57, 408
Martin, E.	766	Maurizio, R.	174
Martin, P. 48, 165, 198, 349, 360, 361, 438		Maviglia, F.	674, 731
Martin, Y. M.	360	Maximov, V.	459
Martin-Bragado, I.	831	Maya, P. N.	651
Martín-Solís, J. R.	17, 366, 433, 515	Mayo-Garcia, R.	531
Martinell, J.	27, 590	Mayoral, M.-L.	453
Martínez Torres, J.	706, 757	Mayri, C.	681, 750
Martinez, A.	666	Mazon, D.	569, 666
Martinez, J.-M.	366	Mazzitelli, G.	64, 432, 710
Martone, M.	529	Mazzone, C.	696
Martynov, A.	246	Mazzotta, C.	435
Martynova, Y.	808	Mazzucato, E.	280
Marushchenko, N.	185, 298, 430, 531	McCarthy, K. J.	57, 297, 411
Maruyama, S.	366, 370, 684	McCarthy, P. J.	201, 351, 531
Maruyama, T.	688	McClements, K.	277
Marx, A.	465, 490	McClenaghan, J.	182, 183
Marzullo, D.	696	McCollam, K.	157, 311, 312, 318
Masaki, K.	680	McCormack, O.	180
Masamune, S.	41, 318	McDermott, R. 179, 351, 355-357, 570, 850	
Masand, H.	143	McDevitt, C.	27, 584
Maslov, M.	338, 852	McDonald, D. C.	451, 529
Massaut, V.	835	McFarland, A.	736
Massidda, S.	302	McGarry, M.	157
Mastrostefano, S.	351, 451, 497, 531	McGinnis, W.	766
Masui, A.	846	McKee, G. R. . . . 23, 169, 176, 182, 187, 196, 206, 213-216, 284, 487	
Masuzaki, S. 345, 413, 415, 418, 454, 676, 708, 719, 820		McLean, A. 22, 29, 172, 195, 228, 230-233, 275, 286, 636, 802	
Matej, M.	803	McLean, H.	235
Matsubara, S.	792	Meakins, A.	277
Matsuda, H.	428-430	Medrano, M.	680
Matsuda, Y.	783	Medvedev, S.	25, 246, 370, 474, 534
Matsumoto, T.	239	Medvedeva, A.	358
Matsunaga, G. 451, 468, 492, 497, 499, 563		Meezan, N.	780
Matsuo, H.	783	Meghan, M.	311
Matsuo, K.	781, 792-794	Mehta, K. R.	661

Meiden, H.	457	Mima, K.	781, 793
Meigs, A.	857, 863	Min, B.	585
Meineri, C.	435	Minaev, V.	60, 288, 754
Meisl, G.	347	Minami, R.	454, 664
Meitner, S.	199, 684, 766	Minami, T.	64, 427-431
Mekler, K.	458	Mineev, A.	363, 754
Mele, A.	451	Minervini, J.	723, 832
Meliga, P.	628	Ming, T.	381
Mellera, V.	434	Minissale, M.	647
Mellet, N.	51, 633	Miniyazov, A.	810
Melnik, A.	288, 872	Miquel, J.-L.	46, 54, 778
Melnikov, A. . .	65, 147, 403, 409, 445, 510	Mirnov, V.	157
Mena Ceciliano, P.	377	Mironov, M.	288
Menard, J. . 12, 18, 149, 233, 287, 500, 718, 755, 828		Mishchenko, O.	467
Mendez, P.	814	Mishra, J.	740, 759
Meneghini, O.	63, 68, 224, 389, 479	Mishra, K.	293
Meneses, L.	188, 338	Mishra, P. K.	143
Menghini, O.	534	Missirlian, M.	666, 801
Menmuir, S.	338, 339	Mitarai, O.	171, 291, 292, 866
Menon, V.	734, 741, 771	Mito, T.	678, 728
Merle, A.	180, 246, 531	Mitsunaka, Y.	664
Merola, M.	801	Mitteau, R.	366
Mertens, P.	857	Miura, E.	790, 791, 796
Meskens, G.	844	Miura, H.	15, 484
Messiaen, A.	308, 353, 730	Miyamoto, K.	658
Messmer, M.	272	Miyamoto, M.	292, 345, 820
Mesyats, G. A.	652	Miyanaga, N.	781, 783, 792, 794
Meyer, H.	13, 165, 188	Miyata, Y.	442, 451
Meyer, O.	666	Miyato, N.	499, 575
Meyer, W. H.	172, 195, 534	Miyazawa, J. . . 57, 418, 422, 450, 676, 719, 728	
Micciche, G.	835	Miyo, Y.	680
Michael, C.	240, 277	Mizuguchi, N.	318
Michoski, C.	583	Mizumaki, S.	680
Miettunen, J.	331	Mizuuchi, T.	318, 427-431
Migliano, P.	340	Mlynář, J.	49, 349, 360, 361, 696
Miki, K.	577	Mlynek, A.	201, 355, 854
Mikkelsen, D.	720	Mochalskyy, S.	529
Miklaszewski, R.	696	Modestov, M.	35, 709
Mikov, V.	754	Moeller, C. P.	225, 291
Milanesio, D.	353	Mogaki, K.	658
Militello Asp, E.	20, 544	Mohan, K.	661
Militello, F.	32, 276	Molina, D.	358
Miller, D.	747	Mollén, A.	865
Milovanović, M.	591	Molla, J.	814
Milovich, J. L.	788	Mollard, P.	666

Möller, S.	808
Monakhov', I.	342
Moncada, V.	185, 309
Monge-Colepicolo, J. I.	290
Monier-Garbet, P.	342
Montellano, I.	596
Moody, J. D.	787
Moon, C.	161
Mora, J.	290
Mora-Meléndez, J.	50, 377
Morace, A.	43, 779, 781, 792, 794
Moradi, S.	338, 531
Morales Hidalgo, D.	377
Morales Niño, I. E.	706, 757
Morales, J.	503, 587, 632
Mordijck, S.	14, 23, 213, 338
Moreau, P.	363, 666
Morel, P.	559
Moreno, J.	374
Moreno, R.	198
Moret, J.-M.	443, 444
Morgan, G.	238
Morgan, K.	244
Morgan, T. W.	432, 457, 826
Mori, Y.	42, 790, 791, 796
Morimoto, T.	680
Morio, N.	783
Morisaki, T.	171, 415, 416, 418, 422, 838
Morita, S.	193, 393, 417, 426, 838
Moritz, J.	353, 374
Moriuchi, S.	678
Moriyama, S.	451, 663, 664, 689
Moro, A.	434, 442, 451, 570, 725
Moro, F.	696
Morones Ibarra, J. R.	706, 757
Morris, W.	59, 737
Morrison, P.	583
Morton, L.	157, 311
Moseev, D.	40, 185, 307, 309
Moser, A.	172, 228, 229, 232
Mosetto, A.	632
Möslang, A.	805
Motohiro, T.	790, 791, 796
Motojima, G.	63, 171, 297, 413, 415, 418, 422, 820
Motoshima, M.	431
Mougenot, J.	647
Moulton, D.	339
Moyer, R. A.	169, 199, 222, 223
Mueller, D.	257
Muir, D.	534
Mukai, K.	418, 770
Mukherjee, A.	11, 15, 661
Mukherjee, S.	740, 759
Mukhin, E. E.	34, 702
Müller, H. W.	173
Mumgaard, B.	210, 211
Mumgaard, R.	192, 207
Munaretto, S.	157
Muñoz Ovalle, O. A.	60, 706, 757
Munro, D.	780
Murakami, H.	783
Murakami, I.	417, 426
Murakami, K.	429
Murakami, M.	196, 229
Murakami, S.	20, 423, 428, 542, 748, 838
Murakhtin, S.	459
Murari, A.	198, 373
Muraro, A.	682
Murase, T.	719
Murata, T.	819
Muroga, T.	46, 708, 712, 821
Murphy, T.	780
Muscattello, C.	176
Mushiake, T.	245
Mustafin, N.	447
Mutoh, T.	291, 413, 414, 429, 664, 838
Muvvala, V. N.	692
Muzzi, L.	727
Myers, C.	50, 279, 372, 486
Mykhaylenko, V. S.	17, 508
Mykhaylenko, V. V.	508
Mynick, H.	241
Myra, J.	37, 619, 638
— N —	
N'Konga, B.	198
Na, D. H.	31, 262, 264, 545, 675
Na, Y.-S.	20, 135, 252, 258, 259, 264, 271, 543, 545, 675
Nace, N.	625
Nagano, T.	318

Nagaoka, K.	416, 419, 423, 424, 542, 660, 705, 838	Naulin, V.	338, 437
Nagasaka, T.	44, 821	Naumenko, N.	447
Nagasaki, K.	64, 427-431, 472, 664	Nave, M. F.	342, 863
Nagashima, Y.	161, 292, 397, 866	Navratil, G. A.	242
Nagata, D.	820	Nayak, P.	740, 759
Nagata, M.	41, 152, 317, 866	Nazikian, R.	69, 169, 176, 181, 202, 216, 552, 597, 634, 850, 859
Nagata, S.	454	Nedzelskiy, I. S.	402
Nagata, T.	292, 866	Neilson, G.	58, 241, 720
Nagatomo, H.	42, 779, 781, 792, 793	Neilson, G. H.	302
Nagayama, Y.	152, 421	Nelson, B.	235, 244, 755
Nagel, M.	851	Nemati, N.	44, 818
Nagora, U. C.	143, 145	Nemets, A.	447
Nagy, A.	202, 225, 749	Nemoto, S.	658
Naidenov, V.	407, 695	Nersesyan, N.	407, 695
Naito, O.	534	Nespoli, F.	436
Nakada, Y.	783	Neu, G.	363
Nakai, M.	781, 792, 794, 819	Neu, R.	451, 731, 806, 807, 854
Nakajima, M.	44, 404, 817	Neubauer, O.	300, 305, 306, 308
Nakajima, N.	162, 687	Neudatchin, S.	147
Nakamichi, M.	345, 672	Neverov, V.	694, 852
Nakamura, H.	822	Newton, S.	67, 593, 865
Nakamura, K.	291-293, 866	Nichols, J.	828
Nakamura, M.	846	Nicolai, A.	736
Nakamura, N.	426	Nicolai, D.	171, 305, 808
Nakamura, Y.	63, 416, 427-430, 472	Nicolas, T.	424, 465, 483
Nakanishi, H.	33, 375, 687, 770	Nie, L.	396, 399
Nakano, H.	542, 660, 705, 838	Nielsen, A. H.	437, 531
Nakano, S.	345	Nielsen, S. K.	354, 434
Nakano, T.	451, 454, 713	Niemann, H.	303, 304
Nakano, Y.	429	Nieto Cuarenta, A.	706, 757
Nakanobo, S.	318	Nijhuis, A.	727
Nakashima, H.	292, 293	Nikiforov, A.	374
Nakashima, Y.	66, 428, 454, 456, 664, 815	Nikitin, A.	805
Nakata, M.19, 196, 297, 416, 518-520, 563, 838		Nikoleava, V.	359
Nakata, Y.	781, 792	Nikroo, A.	788
Nakatsuka, M.	245	Nimavat, H. D.	143
Nakayama, S.	790, 791	Nishi, T.	790, 791, 796
Nam, Y.	249	Nishijima, D.	648
Nam, Y.-U.	135, 268	Nishikata, H.	457
Nardon, E.	198, 349, 361, 531, 534, 666	Nishikiori, R.	658
Narihara, K.	375	Nishimura, A.	824
Narushima, Y.	64, 171, 420-422, 483	Nishimura, H.	781, 792, 794, 819
Natorf, W.	531	Nishimura, S.	424
Naujoks, D.	185, 851	Nishimura, T.	770
		Nishimura, Y.	790, 791, 796

Nishino, N.	454
Nishioka, K.	427
Nishioka, S.	660
Nishitani, T.	770
Nishiura, M.	25, 245, 425
Nishiyama, T.	680
Nishizawa, A.	375
Nishizawa, T.	157
Niskala, P.	560
Nitti, F.	835
Niu, E.	701
Niu, L.	698
Nobuta, Y.	44, 820, 829
Nocente, M. ...	33, 190, 201, 336, 349, 360, 682
Nocentini, R.	659
Noé, J.	750
Nogami, S.	821, 824
Noh, S.	811
Nojiri, K.	454
Nonn, P.	157
Noonan, P.	238, 736
Nora, R. C.	787
Norausky, D.	657
Nordman, H.	338
Norimatsu, T. .	43, 779, 781, 792, 794, 798, 819
Nornberg, M.	157, 168, 311
Norval, R.	157
Noterdaeme, J.-M. .	49, 58, 217, 353, 374, 385, 724, 730
Notkin, G.	147, 753
Noto, H.	708
Nouailletas, R.	363, 444, 666, 752
Nowak, S. 26, 451, 490, 497, 531, 570, 686	
Nozawa, T.	672
Nozawa, Y.	289
Nuga, H.	17, 516
Numakura, T.	454, 664
Nunami, M. ...	19, 297, 450, 518-520, 586
Nunio, F.	727
Nurgaliev, M.	65, 447
Nusbaum, M.	681
Nuttasart, A.	429

— O —

O’Gorman, T.	277
O’hira, S.	141, 835
O’Mullane, M.	343, 531
O’Neill, R.	699
Oberkofler, M.	347
Obrejan, K.	556
Ochando, M. A.	412
Ochiai, K.	672, 768
Ochoukov, R.	353, 374, 523
Oda, D.	429
Oda, G.	637
Oda, Y.	658, 663, 664, 689, 699
Odette, R.	800
Odstrcil, T.	352, 357, 523
Offermans, G.	308
Ogawa, H.	688
Ogawa, K. 42, 424, 425, 542, 607, 748, 770	
Ogawa, T.	680
Ogura, K.	781
Oguri, Y.	786
Oh, J.	795
Oh, S.	269
Oh, Y.-K.	10, 12, 135, 247, 248, 255
Ohdachi, S. ...	64, 184, 420, 422, 424, 483
Ohgo, T.	719
Ohira, S.	814
Ohno, N.	418, 420, 454, 457, 739, 820
Ohshima, S.	64, 427-431
Ohta, M.	768
Ohtani, H.	676
Ohtani, Y.	427, 431
Ohtsuka, S.	811
Oi, T.	637
Oishi, T.	53, 62, 193, 417, 426, 838
Ojha, A.	143
Okabayashi, M.	24, 220
Okada, H.	64, 427-431
Okada, K.	664
Okada, T.	456
Okamoto, A.	457, 769
Okamura, K.	786
Okamura, M.	786
Okano, F.	680
Okano, K.	798
Okuda, T.	811

Okumura, Y.	814	Pal, R.	717
Okuyama, T.	680	Palak, B.	529, 531
Oliva, S.	157	Palermo, I.	41, 765
Oliver, H. J.	334	Palmer, T.	469
Olson, R. E.	788	Paméla, J.	11
Omori, T.	689	Pamela, S.	55, 61, 178, 339, 476, 477, 488, 503-505
Omotani, J.	26, 276, 572	Pan, C.	182, 764
Onchi, T.	292, 293, 404, 866	Pan, O.	392, 398
Ongena, J.	40, 209, 308	Panadero, N.	411
Onjun, T.	20, 27, 528, 536, 539, 547, 578, 650	Panayotis, S.	816
Ono, M.	22, 30, 176, 196, 487, 664, 671, 755, 828	Panayotov, D.	669
Ono, Y.	25, 152, 240	Panchal, A. G.	143
Ooba, K.	678	Panchal, P. N.	143, 740, 759
Oostebeek, J. W.	307	Panchal, R. N.	143, 717
Orain, F.	17, 352, 477, 504, 505	Panchal, V. K.	145, 717
Ordas, N.	809	Pandya, M.	408
Orlov, D.	24, 169, 181, 222, 850	Pandya, S. N.	143, 418
Orlov, N.	805	Panek, R.	361
Orsitto, F. P.	434, 451	Panin, A.	727
Osakabe, M.	414, 416, 423-425, 542, 601, 607, 660, 705, 748, 770, 838	Panizo-Laiz, M.	831
Osborne, T. H.	172, 176, 181, 202, 203, 228, 230, 233	Pankin, A. Y.	19, 487, 526, 527, 545, 748
Otárola Zuñiga, C.	377	Papp, G.	54, 61, 201, 349, 360, 361, 438
Otani, Y.	428-430	Paprok, R.	361
Otsuka, T.	345	Parail, V.	341, 343, 463, 544, 595, 839
Otte, M.	185, 301, 851	Paravastu, Y.	143, 328
Owen, L.	766	Parekh, T. J.	143
Owsiak, M.	529, 531, 738	Park, B.	252, 496
Oya, M.	44, 415, 826, 829	Park, B. H.	565
Oya, Y.	44, 292, 712, 820, 829	Park, G.	170, 222
Oyaidzu, M.	345, 826	Park, H.	30, 249, 265
Ozaki, S.	791	Park, H. K.	61, 135, 161, 170, 204, 248, 250, 252, 253, 260, 265, 666
Ozaki, T.	424, 779, 781, 792	Park, J.	58, 229, 479, 720, 732
Ozeki, T.	687	Park, J.-K.	15, 135, 170, 255, 269, 275, 485, 500, 568, 629, 636
— P —		Park, J. G.	268
Pütterich, T.	854	Park, J. M.	247, 545, 675
Pablant, N.	40, 185, 297-299, 302, 384, 748	Park, J. S.	263
Paccagnella, D.	198, 318, 349	Park, K.-R.	135
Pace, D. C.	181, 190, 191, 225, 227, 230, 335, 859	Park, S.	795
Pagonakis, I.	704, 725	Park, S.-A.	266
Pais, V.	529, 531	Park, Y.-S.	30, 248, 252, 265, 278, 279
Pajuste, E.	834	Parke, E.	157, 311, 313
		Parker, C.	747
		Parker, R. R.	192, 207, 383, 469

Parker, S.	638	Pégourié, B.	451, 666, 738
Parks, P. B.	202, 489	Pelka, G.	531
Parmar, D.	692	Penaflo, B. G.	226, 747
Parmar, N.	323	Péneau, N.	661
Parmar, P. R.	143	Peng, Q.	242
Parsons, M.	373	Pereira, A.	373
Paruta, P.	632	Pereira, C.	775
Pascal, J. Y.	666	Pereira, R. C.	682
Pasch, E.	185, 298	Perelli Cippo, E.	682
Pasqualotto, R.	705	Pereslavtsev, P.	772
Passeron, C.	503	Perevalov, A.	406
Pasternak, A.	695	Perevezentsev, A.	733
Pastor, P.	752	Perez Von Thun, C.	334
Patel, A.	661	Perez, M.	814
Patel, D.	717	Perfilov, S.	409, 445
Patel, H.	661, 707	Pericoli, V.	174
Patel, H. S.	143	Pericoli-Ridolfini, V.	531
Patel, J. C.	143	Perkins, R.	32, 192, 286
Patel, K.	327, 717	Perko, T.	844
Patel, K. B.	143	Perlado, J. M.	45, 46, 831
Patel, K. G.	143	Perry, J.	151
Patel, K. M.	143, 145	Perry, T. S.	788
Patel, M.	661	Peruzzo, S.	319
Patel, N.	319, 717	Pestchanyi, S.	366
Patel, N. C.	145	Peterka, M.	180
Patel, P.	780, 787	Peters, M.	568
Patel, P. J.	143	Peterson, B.	64, 416, 418
Patel, P. K.	788	Petersson, P.	329, 346, 347, 803
Patel, R. J.	143	Petrasso, R.	780, 782
Patel, S.	145, 717	Petrie, T. W.	24, 172, 181, 230, 233
Patel, V.	717	Petrov, Y.	37, 288, 612, 754
Pathak, S.	804	Petty, C. C. 29, 39, 176, 181, 187, 191, 196, 215, 225, 227, 229	
Pathak, S. K.	143, 145	Peysson, Y.	55, 380, 383
Pathan, F. S.	143, 328	Pfefferle, D.	486
Patrov, M.	288, 754	Phillips, C.	611
Patterson, M.	404	Phillips, G.	814
Pau, A.	198	Phillips, P.	283
Pautasso, G. . . 49, 198, 201, 349, 360, 363, 365, 372, 498		Piazza, Z.	647
Pavlov, K.	773	Picha, R.	650
Paz-Soldan, C. . 14, 19, 168, 169, 181, 216, 223, 224, 850		Piedra-Quesada, N.	290
Pedersen, M. S.	434	Pigarob, A.	160
Pedrosa, M. A.	412	Pigatto, L.	451, 497
Peebles, W.	215	Pimazzoni, A.	705
Peeters, A.	340, 491	Pinches, S. D.	20, 466, 529, 534, 696
		Pinsker, R. I.	24, 206, 225

Pintsuk, G.	807, 816, 836	Pospieszczyk, A.	808
Pinzhenin, E.	459	Postupaev, V.	458
Piovesan, P. 14, 18, 168, 201, 349, 351, 444, 588		Potzel, S.	179, 201, 863
Piraga, E.	834	Prada, A.	831
Piron, C.	349, 444	Prades, A.	60, 844
Piron, L.	168	Pradhan, S.	12, 18, 41, 59, 143, 145, 324-328, 734, 741, 751, 771
Pironti, A.	363, 451	Praghi, B. R.	143
Pirozhkov, A.	794	Prahlad, V.	760
Pisano, F.	185	Prajapati, A.	670
Pisent, A.	814	Prakash A, A.	143, 328
Pitts, R. A. ... 269, 270, 275, 330-332, 366, 436, 644, 666		Prasad, U.	143, 734, 741, 771
Platania, P.	451	Prater, R.	225
Plociennik, M.	529, 531	Praveenlal, E. V.	145
Plyusnin, V. V. 49, 201, 349, 360, 361		Predebon, I.	588
Pocheau, C.	666	Preynas, M.	309, 570
Podadera, I.	814	Priddie, D.	657
Podda, S.	696	Prikhodko, V.	459
Podestá, M. 191, 233, 281, 285, 597		Prisiazhniuk, D.	359
Podesta, M.	853, 859	Priti, P.	871
Poitevin, Y.	669, 743	Probst, M.	67, 331, 873
Pokol, G. I.	531	Proll, J. H.	297
Polevoi, A. 50, 370, 534, 543, 545, 696, 839		Prompting, J.	547, 650
Poli, E.	16, 491, 531, 686, 725	Pruneri, G.	814
Poli, F. 33, 287, 368, 534, 543, 545, 686		Pucella, G.	13, 156, 433, 435, 570
Poli, S.	666	Pueschel, M. J.	157, 313
Poljak, D.	531	Puiatti, M. E.	41, 154, 319, 343
Polosatkin, S.	157, 312, 458	Purohit, S.	143, 145
Poloskei, P. Z.	201	Pustovitov, V.	16, 495, 502
Polunovskiy, I.	407, 695	Pusztai, I.	572, 593
Pomphrey, N.	241	Pütterich, T. ... 49, 342, 356, 357, 369, 523	
Pompon, F.	661	Putvinski, S.	243
Poncet, J.-M.	727		
Ponkratov, Y.	810	— Q —	
Poolyarat, N.	20, 539	Qayyum, A.	401
Popov, A. Yu.	620	Qi, L.	25, 558
Popov, S.	458	Qi, M.	382
Popov, V.	378	Qian, J. 29, 39, 133, 182, 183, 368, 382, 747	
Popovic, Z.	433	Qian, J. P.	388, 390
Porkolab, M. 23, 206, 209, 225, 469		Qin, C. M.	380, 385
Porosnicu, C.	329	Qin, S. G.	698, 801
Porter, G.	172	Qiu, Y.	772
Portero, F.	10, 125	Qiu, Z.	36, 610
Portone, A.	67, 870	Qu, Z.	855
Poshekhonov, Y.	246		

— R —

Rack, M.	305, 306, 332, 387
Radhakrishnan, H.	531
Rafiq, T.	19, 526, 527
Ragona, R.	353, 730
Rahbarnia, K.	185
Raj, H.	145, 717
Rajković, M.	27, 591
Raju, D.	143, 145, 323, 717
Ralph, J. E.	788
Ram, A.	37, 617
Ramaiya, N. K. . . .	143, 145, 323, 651, 760
Raman, R.	60, 223, 233, 481, 755
Ramogida, G.	432, 434
Ranjan, V.	717
Rao, C. V. S.	145
Rao, T. S.	670
Rapisarda, D.	765, 835
Rapp, J.	41, 766
Rapson, C.	355, 363, 365, 444
Rasinski, M.	808, 809
Rasmussen, D.	684
Rasmussen, J. J.	338, 434, 437
Rastogi, N.	693, 734, 741, 771
Rathod, K.	717
Raupp, G.	363–365
Raval, D. C.	41, 143, 324, 328
Raval, J. V.	143, 145
Raval, T. Y.	143
Ravenel, N.	666
Ravensbergen, T.	363
Rawat, R. S.	45, 836
Ray, H.	766
Razdobarin, A. Z.	702
Rebai, M.	682
Redondo, J.	371
Regan, S. P.	787
Reich, M.	351, 355, 490, 570, 854
Reichle, R.	694
Reiman, A.	15, 482
Reimerdes, H. . . .	22, 29, 174, 437, 531, 570
Reimold, F.	48, 179, 348, 464, 857, 863
Reinhart, M.	453, 808
Reinke, M.	863
Reinke, M. L. . . .	23, 175, 206–208, 210, 211, 223
Reiser, D.	531
Reiter, D.	348, 635
Ren, G.	789
Ren, Q.	182, 183
Ren, X.	176
Ren, Y.	32, 280, 568
Renard, B.	750, 814
Rensink, M.	653
Reusch, J.	151, 157, 294, 311
Reusch, L.	157, 311
Reutlinger, A.	702
Reux, C. . . .	59, 198, 201, 341, 360, 361, 515, 738
Rhee, T.	271, 478, 582
Rhodes, D. J.	242
Rhodes, T. L.	169, 176, 187, 196, 206, 213–216, 487
Ribeiro, T.	529
Ricapito, I.	22, 29, 669
Riccardi, B.	666
Riccardo, V.	198, 360, 367, 515
Ricci, D.	434, 442, 451
Ricci, P.	51, 379, 436, 632
Rice, J. E. . . .	23, 175, 206–208, 217, 283, 569, 577
Rice, N.	788
Richou, M.	666, 801
Riedl, R.	659
Riesch, J.	806, 807
Rieth, M.	666, 807
Rigamonti, D.	682
Riley, D.	869
Rimini, F.	198, 334, 341, 342, 363, 369
Rincon, E.	680
Rinderknecht, H. G.	46, 54, 782, 788
Rindt, P.	828
Rispoli, N.	725
Rita, C. P.	696
Rittich, D.	355, 854
Riva, F.	632
Riva, M.	696
Rivera, A.	831
Rizvi, H.	274
Roach, C.	477
Robert, C.	661
Roberts, N.	408

Robey, H. F.	788	Ryutov, D.	233
Robin, F.	687, 750	Ryzhakov, D.	447
Roccella, M.	367	Rzadkiewicz, J.	682
Roccella, R.	49, 198, 366, 367	Rzesnicki, T.	704, 725
Rocchi, G.	353		
Roche, H.	666	— S —	
Roche, T.	239	Saarelma, S.	177, 178, 180, 337, 339, 451, 476, 477, 541
Rochford, R.	560	Sabathier, F.	666
Rodrigues, P.	334, 531	Sabau, A.	712
Rodriguez-Ramos, M.	190	Sabbagh, S. A. 32, 135, 248, 278, 279, 282, 284, 286, 562	
Rogers, B.	550	Sabot, R.	358, 559
Rognlien, T.	172, 653	Sadat Kiaii, S. M.	818
Rogozhkin, S.	43, 805	Sadharakiya, D.	717
Rohde, V.	347	Sadighzadeh, A.	818
Rohollahi, A.	404	Sáez, X.	529, 531
Roidl, B.	291	Sagara, A. . 62, 68, 450, 454, 676–678, 708, 719, 728, 821	
Rojas-Calderón, J.	290	Sagisaka, A.	781, 794
Rojas-Loaiza, A. M.	290	Saha, S.	717
Romanelli, M. . 20, 343, 451, 463, 497, 538, 541, 543, 544, 645, 852		Şahin, S.	41, 767
Romazanov, J.	331, 643	Sahu, S.	670
Roquemore, A. L.	202, 286, 749	Saibene, G.	366, 595
Rosato, J.	628	Said, J.	738
Rosenberg, M.	782	Saikia, B. J.	741
Ross, A.	630	Saille, A.	666
Ross, M.	235	Saint-Laurent, F.	361, 666
Rost, C. J.	176, 206	Saito, K.	291, 385, 413, 838
Rotti, C.	692, 707	Saito, M.	824
Roubin, P.	633	Saitoh, H.	245
Rovenskiikh, A.	458	Sakagami, H.	781, 792, 793
Rowan, W.	283	Sakai, A.	542
Rozenkevich, M.	58, 733	Sakai, R.	769
Rozhansky, V.	464, 754	Sakakibara, S. . . 29, 39, 184, 420–422, 424, 483	
Rozhdestvensky, V.	407	Sakamoto, K. . 430, 663, 664, 689, 699, 814	
Rozier, Y.	704	Sakamoto, M.	43, 415, 454, 456, 815
Rubel, M.	47, 329, 345, 346, 803	Sakamoto, R. 297, 411, 413, 415, 418, 422, 450, 676, 719	
Rubino, G.	588	Sakamoto, T.	783
Rudakov, D. L.	172, 214, 802	Sakamoto, Y.	739
Rudolf, N.	645	Sakasai, A.	680
Rummel, T.	851	Sakata, S.	781, 792, 794
Ruset, C.	666	Sakaue, H. A.	426
Ruzic, D. N.	828	Sakharov, N.	288, 754
Ryan, D.	351, 352	Sakurai, S.	451, 680, 713
Rygg, J. R.	788		
Ryter, F.	354–357, 359		
Ryu, C.-M.	31, 274		

Salewski, M.	334, 354	Sato, S.	41, 768
Salmi, A.	338	Satoh, N.	791, 819
Salmonson, J. D.	788	Sattin, F.	588
Salvador Hernández, M.	706, 757	Sauppe, J.	157, 311
Samaddar, D.	531	Sauter, O.180, 246, 443, 444, 490, 497, 531, 534, 570, 686	
Samaille, F.	666	Saveliev, A.	406, 702, 754
Samm, U.	171, 306	Savkin, V.	459
Samsonov, D. S.	702	Savoie, M.	661
Samuell, C.	172	Savoldi, L.	727
Sanchez-Castro, J.	377	Savrukhin, P.	65, 147, 446
Sanchis-Sanchez, L.	190	Sawada, K.	454
Sandri, N.	305	Sawai, K.	783
Sang, C.	172	Saxena, Y.	717
Sangaroon, S.	52, 547, 650	Saxena, Y. C.	145
Sangster, C.	782	Sayre, D.	780
Sangster, T. C.	138, 780	Scannapiego, M.	451, 713
Sangwan, D.	145	Scannell, R.	180, 240, 276, 277
Sannazzaro, G.	367	Scantamburlo, F.	814
Sano, F.	842	Scarabosio, A.	194
Sano, R.	418	Scarin, P.	321
Sano, T.	781	Schacht, J.	851
Sanpei, A.	318	Schaubel, K.	657
Sanromán Reséndiz, M. A.	706, 757	Scheffer, M.	444
Santala, M.	336	Schenkelaars, S.	272
Santosh, P.	682	Scherer, T.	725
Santra, P.	143	Schiesko, L.	659
Santraine, B.	666	Schissel, D.	59, 747
Saoutic, B.	738	Schlatter, C.	704
Saraswat, A.	22, 30, 59, 670, 745	Schlossberg, D.	151
Sarazin, Y.	465, 559, 569	Schmid, K.	453, 531
Sarff, J. S.	13, 157, 168, 311–313	Schmid, M.	704
Särkimäki, K.	466, 595	Schmidt, A.	235
Sartori, E.	660, 705, 722	Schmidt, L.	844
Sartori, F.	451	Schmitt, J.	755
Sartori, R.	544	Schmitz, L.	23, 196, 213, 215, 243
Sarukura, N.	819	Schmitz, O.14, 18, 157, 171, 195, 269, 275, 303, 635	
Sarychev, D.	12, 18, 147, 447	Schmuck, S.	298
Sasajima, T.	680	Schneider, B.	437
Sasaki, M.	36, 397, 425, 603, 607	Schneider, K.	587
Sasaki, S.	658	Schneider, M. B. ...	336, 531, 534, 543, 787, 788
Sasaki, T.	786	Schneider, P. A.	347, 354
Sassano, M.	433	Schneller, M.	351, 608
Satake, S.	302, 450, 520, 563, 564, 748	Schrittwiesser, R.	437
Sathyanarayana, K.	145, 717		
Sato, M.	483, 520, 748, 770		
Sato, N.	790, 796		

Schröder, T.	185	Sezaki, T.	783
Schubert, M.	854	Shabelsky, A.	872
Schuster, E.	24, 226	Shafer, M.	24, 169, 195, 216, 221, 636
Schwander, F.	625	Shah, K. S.	145, 717, 760
Schwartz, J.	828, 858	Shah, P.	143
Schwarz-Selinger, T.	453	Shah, S.	692
Schweer, B.	305, 308, 808	Shaing, K. C.	26, 278, 562
Schweitzer, J.	369, 857	Shalashov, A.	459
Scott, B. D.	467, 531	Shankar Joisa, Y.	323
Scott, H. A.	787	Sharapov, S. E.	48, 227, 334, 335
Scott, S. D.	192, 207, 344	Sharma, A. L.	143, 734, 741, 771
Scotti, F.	32, 233, 275, 281, 282	Sharma, A. N.	143
Sdvizhenskii, P.	702	Sharma, D. K.	143, 717, 734, 741, 771
Sears, S.	157, 312	Sharma, M.	143
Sedlak, K.	727	Sharma, P. K.	143, 145
Seguin, F.	782	Sharma, R.	143
Seils, S.	805	Sharma, S.	760
Seki, N.	658	Shatalin, S.	406
Seki, R.	413, 414, 428, 450, 748, 838	Shaw, G.	766
Seki, T.	291, 385, 413, 424, 838	Shchegolev, P.	288, 754
Seki, Y.	22, 29, 665, 666, 739	Shcherbinin, O.	754
Sekiguchi, J.	239	Sheikh, U.	174
Sekine, T.	790, 791, 796	Shelukhin, D.	147
Seltzman, A.	157	Shen, B.	382
Semwal, P.	143, 328	Shen, H. G.	399
Sen, A.	17, 61, 145, 323, 506	Shen, J.	698
Senee, F.	814	Shen, Y.	395
Senichenkov, I.	22, 30, 464, 754	Sheng, H.	604
Sentoku, Y.	790, 791, 796	Sheng, X.	698
Seo, D.	269	Sheng, Z.	382
Seol, J.	26, 250, 256, 496, 565	Shephard, M.	486
Seol, S.	486	Shestakov, E.	446
Seon, C. R.	263	Shevchenko, V.	238, 614, 736
Sergeev, D.	447	Shevelev, A.	57, 360, 407, 695
Sergienko, G.	808, 857, 863	Shi, E.	626
Sergis, A.	35, 714	Shi, P. W.	394
Serianni, G.	35, 660, 705	Shi, S.	752
Serizawa, H.	821	Shi, T.	382
Serov, V.	697	Shi, Y.	31, 262, 264
Serra, G.	164	Shi, Y. J.	384
Serre, E.	625, 628, 633	Shi, Y. L.	801
Sertoli, M.	523	Shi, Z.	197, 395
Šesnić, S.	531	Shi, Z. B.	56, 391, 392, 394, 398
Sestak, D.	666	Shibama, Y.	63, 69, 680, 681
Setiadi, A. C.	314	Shibata, N.	658, 690
Seungho, L.	792	Shidara, H.	689

Shigemori, K.	792	Singh, D.	707
Shimada, M.	712, 829	Singh, M.	466
Shimizu, A.	419, 425, 607, 748, 838	Singh, N.	661
Shimizu, K.	451, 454, 540, 713, 739	Singh, R.	478, 567, 661
Shimizu, T.	44, 658, 819	Sinitsky, S.	458
Shimozuma, T.	413, 414, 664, 838	Sio, H.	782, 788
Shinohara, K.	267, 271, 451, 468, 563	Sipilä, S. K.	531, 595
Shinto, K.	814	Sips, A.	50, 337, 338, 368, 369, 545, 857, 863
Shinya, T.	192, 291	Siragusa, M.	319
Shiraga, H. ...	779, 781, 783, 792-794, 798, 819	Siren, P.	852
Shirai, H.	12, 14, 139	Skakov, M.	810
Shiraishi, J.	16, 449, 492, 497, 499, 563	Skinner, C.	671
Shiraiwa, S.37,	192, 207, 211, 383, 469, 615	Sklyarov, V.	458
Shiraki, D.	199	Škorić, M. M.	591
Shirakid, D.	24, 202, 223	Skovorodin, D.	378
Shishir, D.	771	Smalyuk, V. A.	787
Shmelev, D. L.	652	Smirnov, A.	243
Shoji, M.	413, 454	Smirnov, R.	160
Short, M.	832	Smith, D.	32, 280, 284
Shoshin, A.	378, 458	Smith, G.	238
Showers, M.	766	Smith, H.	865
Shpanskiy, Y.	46, 54, 762	Smith, J.	11, 14, 657
Shukla, B. K.	143, 145	Smith, S.	389, 479
Shukla, G.	760	Smithe, D.	621
Shumlak, U.	24, 235	Smolyakov, A.	445, 465
Shurygin, F.	867	Snicker, A.	190, 357
Shurygin, R.	17, 510	Snipes, J. A.	49, 363-366, 368, 543
Siccinio, M.	731	Snyder, P. B. ...	28, 169, 176, 181, 389, 479, 487, 534, 640, 802
Sid, A.	37, 624	So, H. S.	266
Sidorov, A.	407	Soare, S.	451
Sidorov, E.	458	Sokolov, M.	753, 756
Sieglin, B.	53, 62, 194, 195, 201, 731	Solano Piedra, R.	377
Sierra, S.	661	Solano, E. R.	180, 852
Signoret, J.	529, 531, 666	Soldatkina, E.	459
Siju, V.	143	Soler, B.	666
Silburn, S.	332	Solomakhin, A.	459
Silva, A.	353	Solomatin, R.	445
Silva, C.	402	Solomon, W. M. ...	10, 11, 130, 169, 176, 181-183, 196, 205, 217, 226, 230, 488, 568, 597
Silva, M.	442	Solyakov, D.	830
Simakov, A. N.	42, 788	Someya, Y.	60, 739, 846
Simmonds, M.	804	Somjinda, B.	547
Simonin, A.	722, 724	Sommariva, C.	201, 349, 361
Simpson, J.	180		
Sinars, D. B.	138		
Singh, A. K.	143, 498, 534		

Sonara, D. P.	143	Stepanov, V.	458
Sonato, P. 58, 319, 722, 724		Stephens, A.	657
Sonehara, M.	291	Stephens, H.	157, 311
Song, I.	263	Stephey, L.	185, 303, 304
Song, S.	161	Stepniewski, W.	451, 645
Song, S. D.	393	Studel, I.	808
Song, X. M.	394, 397	Stevens, E.	163
Song, Y.	315, 316, 382, 752	Stieglitz, R.	843
Song, Y. T.	380, 385, 656	Stoafar, C. C.	242
Song, Z.	34, 700	Stober, J. 66, 368, 369, 523, 570, 854	
Soni, D.	661	Stockel, J.	57, 403
Sontag, A.	24, 229	Stoeckl, C.	782
Sorbom, B. M. 45, 175, 469, 723, 832		Stoller, R.	46, 55, 800
Sorokin, I.	808	Stoltzfus-Dueck, T.	189, 626
Sorokina, N.	458	Stotler, D. P.	51, 631, 634, 651
Soukhanovskii, V. 24, 233, 281, 282		Strachan, J.	344
Sousa, J.	682	Strait, E.	169
Sovinec, C.	151, 157, 311	Strand, P.	534
Sozzi, C. 198, 340, 349, 442, 451, 497, 570		Strauss, D.	721, 725
Spears, B. K.	780, 787	Strauss, H.	198
Spitsyn, A. V.	45, 746, 833	Strikhanov, M.	867
Spizzo, G.	171	Stroth, U.	22, 161, 173, 356, 358, 359
Spolaore, M.	41, 174, 319, 320, 437	Strozzi, D. J.	788
Spong, D.	36, 157, 227, 312, 601	Strumberger, E.	351, 352, 505
Springer, P.	780	Su, L.	235
Sree, S.	806	Subbarao, P. A.	661
Srikanth, G. L. N.	143	Subbotin, M.	733
Srinivasan, R.	143, 717, 734, 771	Suchkov, E.	531
Srivastava, R.	67, 734, 871	Sudnikov, A.	458
Stadermann, M.	788	Sugama, H.	472, 519, 520
Staebler, G. M. . 19, 53, 182, 205, 206, 389, 479, 524, 525, 534		Sugawara, T.	860
Stahl, A.	593	Sugie, T.	688
Staltsov, V.	830	Sugimoto, M.	814, 824
Stamp, M.	852, 857, 863	Sugiyama, L.	27, 222, 283, 512, 589
Stange, T.	185, 298, 307, 309	Sukuba, I.	873
Stangeby, P. C.	172, 228, 232, 802	Sulyaev, Y.	458
Stanislas, P.	177	Sumida, S.	456
Stankiewicz, R.	531	Sun, A.	197
Stankunas, G.	59, 742	Sun, B.	412
Startsev, E.	566	Sun, H. J.	173
Stefanikova, E.	343, 362	Sun, P.	393
Stegmeir, A.	51, 630	Sun, X.	747
Steinbuch, M.	444	Sun, Y.	55, 133, 278, 314, 382, 642
Stepanov, B.	727	Sun, Y. W.	387
Stepanov, I.	353	Sunahara, A.	779, 781, 790-793, 796
		Sung, C.	196

Sunn Pedersen, T. . 185, 301, 304, 635, 851
 Surrey, E. 68, 737
 Sushkov, A. 753
 Šušnjara, A. 531
 Suthar, G. 661
 Sutherland, D. 236, 244
 Suttrop, W. . . 190, 194, 201, 351, 352, 505,
 850
 Suwana, S. 19, 528
 Suzuki, C. . . . 413, 416, 419, 450, 748, 838
 Suzuki, M. 534
 Suzuki, S. 665, 666, 739
 Suzuki, T. 449, 451, 499
 Suzuki, Y. 184, 420-422, 424, 428, 480, 483,
 563, 602, 748, 783
 Svensson, J. 299, 302, 338
 Swamy, A. K. 561
 Sykes, A. 238, 736
 Sytova, E. 464
 Szepesi, G. 340, 531
 Szepesi, T. 185, 301, 304, 451

— T —

Tabares, F. 453
 Tahiliani, K. 145
 Taimourzadeh, S. 552
 Tajima, T. 239, 243
 Takagi, I. 292
 Takahashi, C. 427
 Takahashi, H. . . 29, 39, 413, 414, 542, 664,
 814, 838
 Takahashi, K. . . 34, 663, 664, 689, 699, 786
 Takahashi, N. 245
 Takahashi, T. 239
 Takahashi, W. 291
 Takahata, K. 63, 678
 Takamatsu, K. 289
 Takami, S. 678
 Takamura, S. 66, 856
 Takase, H. 673
 Takase, Y. 12, 18, 152, 291-293, 866
 Takayama, K. 786
 Takayama, T. 811
 Takayasu, M. 832
 Takechi, M. 451, 468, 492, 497
 Takeda, S. 847
 Takehiko, Y. 712

Takeiri, Y. . 10, 11, 128, 152, 413, 660, 705,
 838
 Takemura, Y. 420, 421, 483
 Takeuchi, M. 688
 Takeuchi, T. 291
 Takizuka, T. 575, 648
 Tala, T. 48, 338, 568, 852
 Tamain, P. 50, 625, 628, 633
 Tamura, H. 676, 677, 708, 719, 728
 Tamura, N. 416
 Tamura, R. 860
 Tan, H. 747
 Tan, M. 157, 315, 316
 Tan, Y. 33, 295
 Tanabe, H. 32, 277
 Tanaka, H. 33, 152, 171, 289, 413, 415, 418,
 420, 815
 Tanaka, K. 64, 184, 297, 413, 416, 421-424,
 472, 542, 838
 Tanaka, T. 676, 708, 712, 728, 821
 Tanchuk, V. 754
 Tang, T. F. 641
 Tang, W. 50, 373
 Tang, X. 52, 584, 646
 Tanigawa, H. . . . 62, 68, 345, 672, 673, 817,
 824, 846
 Tanna, R. 12, 145, 323, 717
 Tanna, V. L. 143, 751
 Tardini, G. 179, 201, 351, 354
 Tartari, U. 434
 Taylor, C. N. 829
 Taylor, G. 192, 385
 Taylor, N. 168, 763, 843
 Taylor, N. Z. 181
 Tazhibayeva, I. 43, 810
 Tegnered, D. 531
 Telnova, A. 288, 754
 Teplukhina, A. 444
 Teppei, O. 829
 Terakado, A. 454, 815
 Terävä, J. 595
 Terazaki, Y. 728
 Terra, A. 806, 808
 Terranova, D. 168, 451
 Terry, J. 175, 210, 211, 283, 653
 Terry, P. W. 157, 313

Terunuma, Y.	658	Tokuzawa, T.	64, 161, 184, 413, 421, 423, 660
Terzolo, L.	256, 261, 546	Tolstyakov, S. Yu.	288, 702, 754
Testa, D.	441, 570	Toma, M.	468, 499
Thakur, A. L.	143	Tomarchio, V.	680
Thankey, P. L.	143, 328	Tomita, H.	542
Thatipamula, S.	204	Tommasini, R.	788
Theiler, C.	174, 379, 436, 437, 442, 549	Tonegawa, A.	454, 457
Thomas, D. M.	172, 802	Tophøj, L.	531
Thomas, J.	143, 145	Torikai, Y.	345
Thome, K.	151, 294	Torre, A.	681, 727
Thompson, M.	869	Torreblanca, H.	225
Thompson, M. C.	243	Tosaki, S.	781, 792, 794
Thomsen, H.	185	Toulouse, L.	666
Thorn, D. B.	787	Townsend, R.	235
Thornton, A.	194, 276	Toyama, T.	829
Thouvenin, D.	666	Tran, M. Q.	58, 704, 721, 722, 724, 725
Thuecks, D.	157	Tran, T.-M.	529
Thumm, M.	704, 725	Travere, J.-M.	363, 666
Thyagaraja, A.	506	Traverso, P.	299, 302, 408
Tidikas, A.	742	Tremoulu, A.	681
Tigelis, I.	617, 704, 725	Tresemmer, K.	828
Tilinin, G.	447	Treutterer, W.	201, 363–365, 368, 444, 666
Tilmann, L.	863	Triana, J.	157, 311
Timofeev, I.	458	Trimino-Mora, H.	185
Tinguely, R. A.	212, 223	Tripathi, V. S.	740
Tiseanu, I.	727	Tritz, K.	606
Titarenko, A.	773	Trivedi, R.	661
Titarenko, Y.	773	Trukhin, V.	447
Titus, J.	157	Trunev, Y.	378, 458
Titus, P.	718, 720	Tsalas, M.	334, 338, 340
Tobari, H.	658, 690	Tsitrone, E.	453, 666
Tobias, B.	176, 486	Tskhakaya, D.	529, 531, 643, 802
Tobias, B. J.	859	Tsubakimoto, K.	783
Tobita, K.	163, 673, 739, 846	Tsuboi, R.	318
Todo, Y.	468, 483, 601, 602	Tsuchiya, H.	161, 185, 298, 419, 421, 838
Togashi, H.	291, 866	Tsuchiya, K.	680
Toi, K.	375	Tsui, C.	174, 436, 437
Toida, K.	291, 866	Tsuji, K.	783
Toigo, V.	34, 703	Tsuji-Iio, S.	152
Tókési, K.	531	Tsujii, N.	291
Tokita, S.	781, 783, 792	Tsujimura, T. I.	63, 161, 413, 414, 748, 838
Tokitani, M.	35, 345, 413, 415, 708, 719, 815, 820	Tsukasaki, R.	429
Tokuda, S.	493	Tsumori, K.	660, 705, 838
Tokunaga, K.	292	Tsumura, K.	664
Tokunaga, S.	739	Tsventoukh, M. M.	21, 52, 554, 652

Tu, C.	315, 316
Tuccillo, A. A.	353, 383
Tudisco, O.	65, 353, 433, 435
Tugarinov, S.	447, 697
Tukachinsky, A.	405, 872
Tummel, K.	235
Turcanu, C.	844
Turco, F.	23, 168, 181, 196, 218, 230
Turkin, Y.	185, 298, 480, 865
Turner, A.	466
Turnyanskiy, M.	731
Turtu, S.	727
Tuszewski, M.	243
Tynan, G.	43, 573, 577, 804
— U —	
Uchida, M.	289
Udgata, S.	740
Ueda, Y.	413, 415, 454, 648, 712, 739, 826, 827, 829
Ufimtsev, M.	409
Uglietti, D.	679
Uimanov, I. V.	652
Ukai, S.	811, 821
Ulahannan, S.	707
Umansky, M.	649, 653
Umeda, N.	34, 658, 690
Unterberg, B.	808, 809
Unterberg, E. A.	172, 195, 216, 224, 303, 802
Upadhyay, D. V.	661
Urano, H.	28, 39, 177, 178, 180, 339, 369, 451, 476, 477, 541, 555
Urban, J.	361, 531, 873
Usami, S.	240
Ushiki, T.	860
Usoltseva, M.	374
Usuki, Y.	819
Uto, H.	739
Uytendhouwen, I.	816
— V —	
Vaccaro, A.	721
Valade, L.	380
Valanju, P.	231, 509, 551
Valcarcel, D.	852
Valentinuzzi, M.	628
Valeo, E. J.	611
Valette, M.	814
Valisa, M.	48, 201, 319, 342, 343, 349, 523, 852
Vallcorba, R.	727
Vallejos, P.	531
Valles, G.	831
Vallet, J.-C.	59, 681, 750
Valovic, M.	852
Valson, P.	299, 302
Valtenbergs, O.	834
van Dellen, L. T. H.	534
Van den Brand, H.	444
van der Laan, J.	743
van der Meiden, H.	453
Van Eester, D.	48, 209, 308, 336, 340, 342, 353, 374, 531, 730, 852
van Eeten, P.	851
van Milligen, B.	410
Van Oost, G.	403
Van Schoor, M.	308
Van Zeeland, M.	859
Van Zeeland, M. A.	24, 181, 190, 191, 227, 230, 597
Vann, R. G. L.	614
Vanovac, B.	352
Varadharajulu, A.	143, 717
Varfolomeev, V.	754
Vargas-Blanco, I.	33, 290, 377
Varia, D.	717
Varje, J.	466, 595, 852
Varma, V.	766
Varmora, P.	143
Varoutis, S.	531, 713, 715, 868
Vartanian, S.	442, 666
Vasava, P.	661
Vasil'evskii, I.	867
Vasilyev, A.	378
Vasyliiev, A.	867
Vayakis, G.	691
Vega, J.	198, 373, 451
Velarde, M.	58, 735
Velasco, J. L.	411, 520
Velasquez, C.	42, 775
Vella, G.	710
Veloso, M. A. F.	775

Veltri, P.	660, 705	Voskoboynikov, S.	464
Venkatesh, M.	10	Vouland, C.	529
Veranda, M.	588	Vu, T.	444
Verdoolaege, G.	24, 234	Vyacheslavov, L.	378, 458
Vergara-Fernandez, A.	365		
Verger, J.-M.	666	— W —	
Verhaegh, K.	174, 437, 442	Waelbroeck, F.	583
Verma, D.	561	Wagner, D.	854
Verma, S.	661, 670	Wagner, J.	805
Vermare, L.	559, 666	Wakai, E.	44, 812, 824, 835
Vernimmen, J.	457	Wakatsuki, T.	66, 449
Vershkov, V.	147, 445	Waldon, C.	737
Vertkov, A.	50, 376, 432, 448	Walk, J. R.	175, 210, 211, 549
Vervier, M.	308	Walkden, N.	276, 437
Veselova, I.	464	Walker, M. L.	226, 257, 363, 364, 747
Veshchev, E.	688, 694	Wallace, G. M. .	53, 62, 192, 207, 210, 383, 469
Vianello, N.	65, 173, 174, 437	Walsh, M.	688, 694, 702
Victor, K.	366	Waltz, R. E.	36, 604
Vieira, R.	469	Wampler, W. R.	802
Vierle, T.	353	Wan, B. N.12, 133, 182, 203, 382–385, 387, 390, 642	
Viezzer, E.49, 352, 356, 357, 359, 505, 852, 857		Wan, S.	315, 316
Vignal, N.	666	Wan, Y.	12, 14, 140
Vijvers, W.	174, 437	Wang, B.	212
Vilbrandt, R.	851	Wang, F.	605
Vilela Mendes, R.	627	Wang, F. D.	384
Villalobos, E.	377	Wang, G.	214, 859
Villard, L.	246, 531, 561	Wang, H. .	36, 172, 203, 315, 316, 602, 802
Villedieu, E.	59, 752	Wang, H. H.	382
Villone, F.	198, 351, 363, 451, 497, 531	Wang, J.	197, 386, 675
Vincent, B.	752	Wang, K.	701
Vincenzi, P.	748	Wang, L. .	56, 133, 382, 385, 387, 388, 642
Viola, B.	531, 863	Wang, M.	203, 384
Virani, C. G.	143	Wang, N.	305
Vitale, V.	451	Wang, P.	701
Vitins, A.	834	Wang, Q.	353
Vlad, G.	36, 531, 598, 608	Wang, S.	135, 382
Vladimirov, P.	805	Wang, S. X.	390
Vlainic, M.	360, 361	Wang, T. J.	801
Vogel, M.	808	Wang, W.	556
Voitsekhovitch, I.	19, 368, 529, 545	Wang, W. J.	801
Volant, E.	778	Wang, W. W.	26, 280, 566
Volodin, A.	665	Wang, X.	36, 140, 205, 213, 598, 608
Vomvoridis, J. L.	704	Wang, Y.	203, 381, 382, 666, 804
von Bover, K.	808	Wang, Y.-M.	788
Vora, M. M.	143	Wang, Z.	197, 292, 511

Wang, Z. R.	16, 485, 500	Widdowson, A. 46, 55, 329, 330, 345, 346, 803
Wang, Z. X.	397	Wiesen, S. . 47, 66, 333, 339, 534, 541, 852, 857, 863
Ward, D.	844, 845	Wilcox, R. S. 23, 169, 195, 216, 636
Warmer, F.	58, 297, 726, 748	Wilks, S. 782
Watanabe, D.	289	Willensdorfer, M. . . 49, 179, 352, 355, 444, 505, 850
Watanabe, H.	292, 815	Williams, Z. 157, 313
Watanabe, K. 184, 420-422, 428, 658, 690, 846		Wilson, D. C. 788
Watanabe, K. Y.	424	Wilson, H. 177
Watanabe, O.	292, 293	Wilson, J. R. 192, 286, 469
Watanabe, T.	277, 472	Windisch, T. 300
Watanabe, T.-H.	518, 519	Windsor, C. 238
Watari, T.	375	Wingen, A. 169, 387, 552
Watkins, J. G. 172, 195, 225, 230, 231, 233, 802		Winter, A. 363, 364
Wauters, T. 185, 307, 308, 347, 442		Wirth, B. 800
Weber, T. 235		Wirtz, M. 44, 808, 816
Wegener, L. 851		Wischmeier, M. 67, 173, 179, 333, 348, 451, 541, 857, 863
Wegener, T. 809		Wisitorsasak, A. 20, 536, 545, 547
Wehner, W. P. 226		Wolf, R. 851
Wei, J. 656		Wolf, R. C. . 12, 14, 137, 185, 297-299, 302, 304, 308, 726
Wei, L. 397		Wolfe, S. M. . 175, 207, 208, 210, 211, 283, 368, 369
Wei, X. 613		Wolfrum, E. 173, 179, 356, 357
Wei, X. C. 390		Woller, K. B. 44, 825
Wei, Y. 197		Woo, M.-H. 247, 252, 258, 271, 368
Weiland, J. 526, 527		Wouters, P. 13, 164
Weiland, M. 49, 354		Wright, G. M. 825, 832
Weinzettl, V. 360, 361		Wright, J. C. 23, 209, 469, 611, 615
Weir, G. 298, 427-431		Wright, W. 180
Weisen, H. . . . 48, 336, 338, 344, 538, 852		Wu, C. 642, 725
Weisen, M. 344		Wu, J. 399, 701, 785
Welander, A. S. 363, 364		Wu, Y. 13, 163, 396, 656
Wen, X. 315, 316		Wu, Y. F. 399
Wenninger, R. 58, 674, 724, 731, 868		Wu, Z. 642
Wenzel, U. 185, 301, 304		Wukitch, S. . 175, 192, 208-211, 283, 385, 469
Werner, A. 185, 666, 851		Wunderlich, D. 659
Wersal, C. 632		Wurden, G. A. . . . 40, 185, 301, 303, 304
Wesche, R. 679, 727		
Westerhof, E. 531		
Whelan, G. 157		
White, A. 175, 469		
White, R. B. 191		
White, R. L. 512		
Whyte, D. G. . . . 18, 58, 175, 210, 469, 549, 653, 723, 825, 832		
Wi, H. 269		
		— X —
		Xanthopoulos, P. 241, 297
		Xavier, V. 792
		Xi, P. 582

Xia, T. Y.	51, 549, 641	Yamamoto, T.	800
Xiang, N.	133	Yamanaka, H.	658, 690, 860
Xiao, B.	315, 316, 747	Yamanaka, K.	687
Xiao, B. J.	212, 388	Yamanishi, T.	345
Xiao, C.	57, 315, 316, 404	Yamano, Y.	658
Xiao, X. T.	641	Yamanoi, K.	781, 792, 819
Xiao, Y.	21, 553, 613	Yamasaki, K.	860
Xiaoyu, W.	668	Yamasaki, M.	245
Xie, C. Y.	801	Yamauchi, Y.	829
Xie, H.	553	Yamazaki, H.	291
Xie, J.	315, 316	Yamoto, S.	52, 644
Xie, J. L.	390	Yan, J.	789
Xing, A.	157	Yan, L.	197, 395
Xu, G.	54, 61, 133, 182, 183, 203	Yan, L. W.	56, 391, 392, 397-399
Xu, G. S.	387	Yan, N.	640
Xu, H.	788	Yan, S. L.	475
Xu, J.	395, 642	Yan, Z.	38, 47, 176, 187, 213-215
Xu, J. C.	387	Yanagi, N.	58, 676, 677, 719, 728
Xu, J. Q.	399	Yanagida, T.	783
Xu, J. Q.	398	Yanai, R.	860
Xu, L.	382, 700	Yang, B.	701
Xu, M.	56, 391, 396, 398, 399	Yang, J.	296
Xu, Q.	266	Yang, L.	315, 316
Xu, X.	51, 175, 253, 497, 549, 582, 640	Yang, Q.	197, 203, 315, 316, 353, 395, 666
Xu, X. Q.	641	Yang, Q. W.	391-394, 397, 398
Xu, Y.	56, 171, 197, 392, 393, 398	Yang, S. M.	264
Xu, Y. H.	391	Yang, W.	389
Xu, Y. X.	399	Yang, X.	243, 382
Xu, Z.	46, 54, 642, 764	Yang, Y.	381, 390
Xue, L.	55, 61, 475	Yang, Z.	642
— Y —			
Yabuuchi, K.	811	Yang, Z. C.	391, 394
Yadav, A.	707	Yang, Z. D.	387
Yadikin, D.	351, 529, 531	Yannis, H.	714
Yagi, M.	26, 468, 513, 516, 575, 586	Yano, Y.	245
Yagotintsev, K.	727	Yao, D. M.	801
Yagyu, J.	680	Yao, K.	398
Yajima, M.	415, 820	Yasuhara, R.	838
Yajima, S.	291	Yatsuka, E.	694
Yakovenko, Yu. V.	334	Ye, M.	140
Yakovlev, D.	459	Ye, Y.	203
Yamada, H.	10, 297, 413, 415, 665	Yeamans, C.	780
Yamada, I.	184, 413, 421, 838	Yelisyeyev, D.	830
Yamada, T.	240, 277	Yi, S.	19, 522
Yamaguchi, H.	542	Yi, S. A.	788
Yamamoto, S.	427-431	Yin, C. Y.	386
		Yin, L.	386

Yin, X. H. 384
 Yoda, M. 712
 Yogo, A. 46, 54, 781, 792, 794
 Yokomine, T. 835
 Yokota, M. 770
 Yokoyama, K. 665
 Yokoyama, M. .59, 297, 302, 414, 419, 423,
 450, 520, 542, 748, 838
 Yoo, J. W. 256, 263
 Yoo, M.-G. 259
 Yoon, S.-W. 30, 135, 170, 247, 248, 250, 251,
 255, 258, 275, 629
 Yoshida, A. 289
 Yoshida, H. 819
 Yoshida, K. 680
 Yoshida, M. 53, 62, 196, 451, 499, 541, 563,
 658
 Yoshida, N. 292, 415, 815, 820, 829
 Yoshida, Y. 291
 Yoshida, Z. 245
 Yoshikawa, A. 819
 Yoshikawa, M. 454, 456
 Yoshimura, S. 416
 Yoshimura, Y. . 63, 413, 414, 664, 748, 838
 Yoshinuma, M. 161, 171, 297, 416,
 419-421, 542, 838
 You, J.-H. 806, 807
 You, W. 315
 Young, J. 276
 Youngblood, K. P. 788
 Yu, C. X. 390
 Yu, D. 53, 62, 197, 395
 Yu, D. L. 391, 392, 394
 Yu, H. 698
 Yu, J. 42, 648, 774
 Yu, L. 600
 Yu, L. M. 391, 393
 Yu, Q. 388
 Yu, Y. 381, 399
 Yuan, B. D. 399
 Yuan, B. S. 391
 Yuan, Q. 747
 Yuan, S. 385
 Yuan, X. 538, 545
 Yuan, Y. 808
 Yuh, H. 280, 285

Yun, G. 54, 135, 161, 248, 249, 252, 260,
 335, 503
 Yun, G. S. 61, 204, 253, 256, 265
 Yun, S. W. 258
 Yuriy, B. 344
 Yurov, D. 458
 Yushmanov, P. 459

— Z —

Zabeo, L. 363, 365
 Zadvitskiy, G. 288
 Zago, B. 666
 Zagorski, R. 52, 451, 531, 541, 645
 Zaitsev, F. 531
 Založnik, A. 647
 Zaluzhnyi, A. 805
 Zammuto, I. 353
 Zanca, P. 168, 319, 349
 Zang, Q. 133, 381, 382
 Zani, L. 58, 727, 738
 Zanino, R. 35, 710, 715, 727
 Zaniol, B. 168
 Zanotto, L. 319, 722
 Zanza, V. 435
 Zarins, A. 834
 Zarins, R. 834
 Zarzoso, D. 491, 839
 Zastrow, K.-D. 344
 Zaurbekova, Z. 810
 Zaytsev, K. 459
 Zeng, L. . 133, 176, 213-216, 225, 381, 390
 Zenin, V. 409, 445
 Zhai, Y. 718
 Zhan, J. 698
 Zhang, B. 380, 382, 387, 698
 Zhang, B. Y. 394
 Zhang, D. 185
 Zhang, F. 486
 Zhang, H. 193, 417, 599, 720
 Zhang, J. 404
 Zhang, K. 393
 Zhang, L. 133, 642
 Zhang, N. 386
 Zhang, P. 642
 Zhang, Q. 60, 758
 Zhang, S. 698
 Zhang, S. B. 390

Zhang, T.....	133, 381, 382, 549, 553	Zhong, G.-W.....	666
Zhang, W.....	36, 353, 600, 616	Zhong, W.....	197, 395, 396
Zhang, W. L.....	613	Zhong, W. L.....	391-394
Zhang, X.....	133, 764	Zhou, C.....	382
Zhang, X. D.....	56, 388	Zhou, H.....	315, 316
Zhang, X. J.....	55, 380, 385	Zhou, Y.....	197, 329, 392, 394, 701
Zhang, Y.....	133, 785	Zhu, P.....	390
Zhang, Z.....	779	Zhu, X.....	701
Zhao, A.....	37, 623	Zhu, Y.....	597
Zhao, C.....	553	Zhuang, G.....	13, 159
Zhao, D.....	389, 534	Zhubr, N.....	405, 872
Zhao, H.....	382	Zimbal, A.....	696
Zhao, J.....	698	Zinkle, S.....	800
Zhao, K.....	197, 395	Zohm, H.352, 354, 674, 724, 731, 854, 857	
Zhao, K. J.....	397	Zok, T.....	531
Zhao, W.....	666	Zoletnik, S.....	268
Zhao, Y.....	214	Zolfaghari, A.....	241
Zhao, Y. P.....	380, 385	Zonca, F.....	467, 598, 608-610
Zheng, G.....	813	Zou, X. L.....	380, 387, 395, 396, 399
Zheng, G. Y.....	475	Zou, Z. Y.....	390
Zheng, J. X.....	388	Zuin, M.....	12, 154, 588
Zheng, L.....	17, 509, 551, 583	Zushi, H.....	292, 293, 866
Zheng, Z.....	641	Zvonkov, A.....	34, 697
Zhezhera, A.....	409	Zweben, S.....	189
Zhilin, E.....	754	Zwingmann, W.....	531
Zhirkin, A.....	42, 773	Zychor, I.....	682
Zhogolev, V.....	370, 495	Zylstra, A. B.....	782, 788